

ANNUAL REVIEW OF NUCLEAR SCIENCE

EMILIO SEGRÈ, *Editor*
University of California

GERHART FRIEDLANDER, *Associate Editor*
Brookhaven National Laboratory

WALTER E. MEYERHOF, *Associate Editor*
Stanford University

VOLUME 10

1960

ANNUAL REVIEWS, INC.
PALO ALTO, CALIFORNIA, U.S.A.

Engine
QC
770
.A65
Y.10

ANNUAL REVIEWS, INC.
PALO ALTO, CALIFORNIA, U.S.A.

© 1960 BY ANNUAL REVIEWS, INC.
ALL RIGHTS RESERVED

Library of Congress Catalog Number: 53-995

FOREIGN AGENCY

Maruzen Company, Limited
6 Tori-Nichome Nihonbashi
Tokyo

PRINTED AND BOUND IN THE UNITED STATES OF AMERICA BY
THE GEORGE BANTA COMPANY, INC.

PREFACE

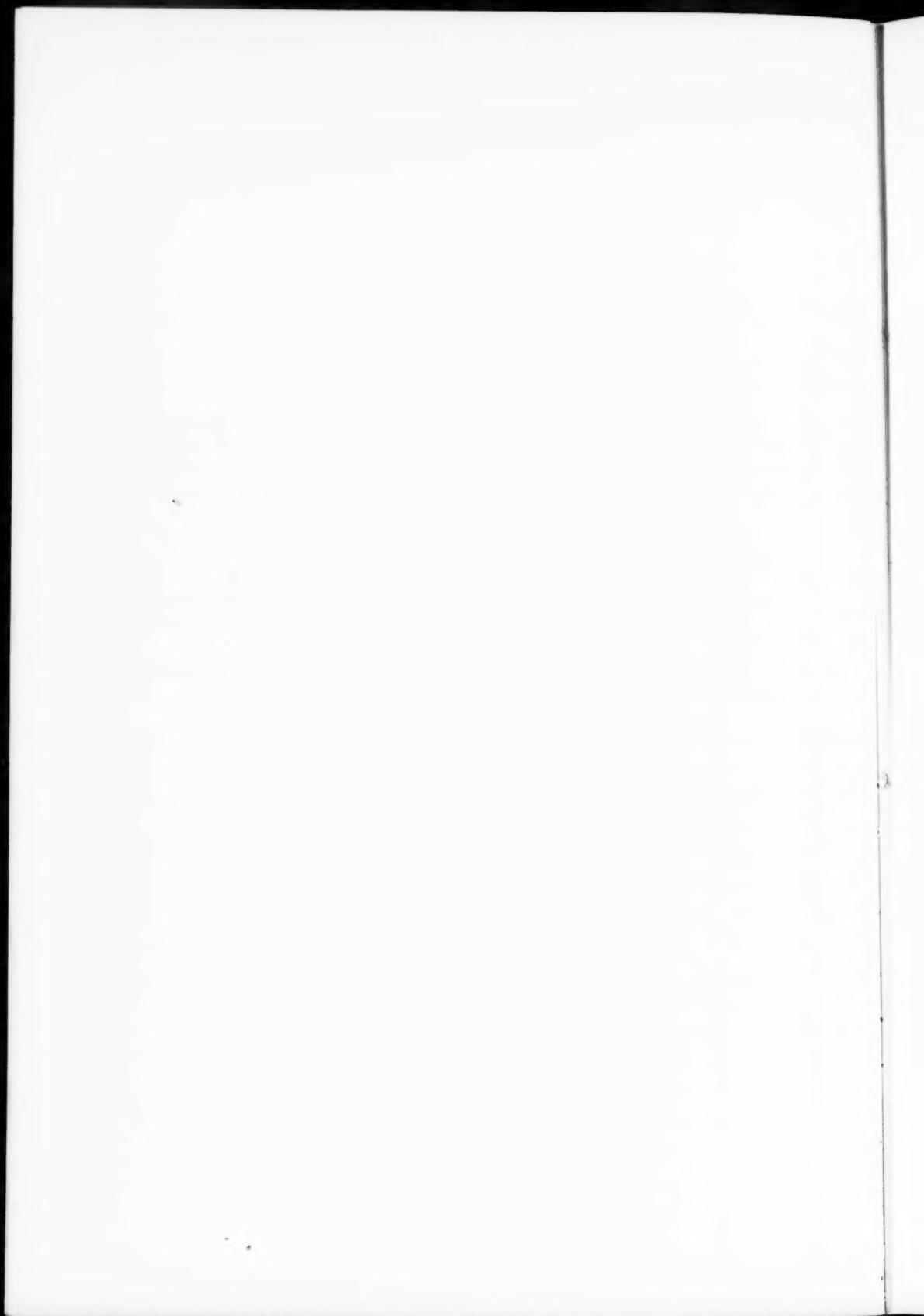
This volume marks the tenth anniversary of the *Annual Review of Nuclear Science*. The rapid progress of these studies is faithfully reflected in the series of volumes thus far published. We hope that they will continue to be as well received by our colleagues and fellow scientists in the future as they have been in the first ten years.

Thanks are again due to all our Authors, to the Editorial Staff and especially to Mrs. Joann Huddleston for their unremitting labors.

The Editorial Committee has suffered a grievous loss through the untimely death of Dr. Donald J. Hughes, a very active member of the Committee and a distinguished scientist. His unexpired term of office will be filled by Dr. C. S. Wu.

The Editorial Committee will welcome suggestions from our readers for topics to be reviewed in future volumes.

E. SEGRÈ



CONTENTS

	PAGE
NEUTRINO INTERACTIONS, <i>Frederick Reines</i>	1
NUCLEAR INTERACTIONS OF HEAVY IONS, <i>A. Zucker</i>	27
COSMIC RAY SHOWERS, <i>Kenneth Greisen</i>	63
BUBBLE CHAMBERS, <i>Hugh Bradner</i>	109
OPTICS OF HIGH-ENERGY BEAMS, <i>Owen Chamberlain</i>	161
NUCLEAR STRUCTURE EFFECTS IN INTERNAL CONVERSION, <i>E. L. Church and J. Weneser</i>	193
RECOIL TECHNIQUES IN NUCLEAR REACTION AND FISSION STUDIES, <i>B. G. Harvey</i>	235
LABELING OF ORGANIC COMPOUNDS BY RECOIL METHODS, <i>Alfred P. Wolf</i>	259
NUCLEON-NUCLEON SCATTERING EXPERIMENTS AND THEIR PHENOMENOLOGICAL ANALYSIS.	291
GENERAL FORMALISM, <i>H. P. Stapp</i>	292
EXPERIMENTAL DATA, <i>M. H. MacGregor</i>	313
PHENOMENOLOGICAL ANALYSIS, <i>M. J. Moravcsik</i>	324
THEORETICAL INTERPRETATION OF THE ENERGY LEVELS OF LIGHT NUCLEI, <i>I. Talmi and I. Unna</i>	353
APPENDIX: ENERGY LEVELS OF THE LIGHT NUCLEI, <i>F. Ajzenberg-Selove and T. Lauritsen</i>	409
NUCLEAR METHODS FOR SUBSURFACE PROSPECTING <i>J. G. Beckerley</i>	425
EXPERIMENTS ON COSMIC RAYS AND RELATED SUBJECTS DURING THE INTERNATIONAL GEOPHYSICAL YEAR, <i>E. P. Ney</i>	461
CELLULAR RADIOBIOLOGY, <i>Tikvah Alper</i>	489
VERTEBRATE RADIOBIOLOGY: METABOLISM OF INTERNAL EMITTERS, <i>Roy C. Thompson</i>	531
VERTEBRATE RADIOBIOLOGY: LATE EFFECTS, <i>J. B. Storer and D. Grahn</i>	561
AUTHOR INDEX	583
SUBJECT INDEX	597
CUMULATIVE INDEX OF CHAPTER TITLES, VOLUMES 1 TO 10	611
CUMULATIVE INDEX OF CONTRIBUTING AUTHORS, VOLUMES 1 TO 10	616

Annual Reviews, Inc., and the Editors of this publication assume no responsibility for the statements expressed by the contributors to this *Review*.

NEUTRINO INTERACTIONS¹

BY FREDERICK REINES²

Physics Department, Case Institute of Technology, Cleveland, Ohio

INTRODUCTION

As these words are written, the neutrino is being discussed in a new role, as a probe to study the structure of elementary particles, by Lee, Yang, Schwartz and others (1 to 4). Serious consideration is being given to the suggestion that high-energy machines be designed for the production of neutrino beams of sufficient intensity for the performance of experiments in which they are absorbed or scattered by nucleons or interact with electrons. Such experiments are particularly important because of the opportunity they offer to study the nature of the weak interaction. A most interesting point will be to check the identity of neutrinos produced in meson decay and those associated with nuclear beta decay. This topic of high-energy neutrinos, to which we shall return later in this review (which may have many aspects of a preview), is mentioned to indicate the continued emergence of the neutrino as a direct experimental tool in contrast to its long and more familiar role as a useful hypothesis.

It will be recalled that the neutrino was invented in 1930 by Pauli (5) as an artifice to save the energy-momentum conservation laws in face of the evidence presented by nuclear beta decay. Fermi's (6) quantitative formulation of beta-decay theory³ in 1933 employed the Pauli idea and indicated most of the peculiar properties that neutrinos should be expected to possess. Reasoning from the then known facts of beta decay, Fermi concluded that the neutrino had no electrical charge, little if any mass compared to that of an electron, spin equal to $\hbar/2$, and the ability to carry linear momentum and energy.⁴ Bethe & Peierls (9), using the Fermi theory, estimated the cross

¹ The survey of literature pertaining to this chapter was concluded May 1, 1960.

² Alfred P. Sloan Foundation Fellow. This work is supported in part by the United States Atomic Energy Commission.

³ A summary of the status of beta decay has been given by Konopinski in Vol. 9 of the present series (22). Wu has written on the neutrino as her contribution to the memorial volume to Wolfgang Pauli (7).

⁴ In addition to the evidence regarding the neutrino provided by beta-decay spectra, much detailed information about the beta interaction has resulted from a study of the angular correlation of the electron and recoiling nucleus associated with neutrino emission. In the simplest case, orbital electron capture, only two product particles result. The recoil energy even for this most favorable situation is in general rather low (<100 ev) and hence such experiments have necessitated the development of special techniques. These anticipated recoils have been measured in several cases, e.g. Be⁷, A³⁷, Cd¹⁰⁷, and are consistent with our ideas about the neutrino. It is important to point out that recoil experiments are observations of the products of neutrino emission and so, like the measurements of beta-decay spectra, do not constitute additional evidence for the neutrino hypothesis which is expressly formulated to

section of a neutrino inverting beta decay and concluded it would be 10^{-44} cm.² for 2.3-Mev neutrinos. This conclusion made it evident that the observation of such processes as:

$$\bar{\nu} + p \rightarrow \beta^+ + n \quad 1.$$

where $\bar{\nu}$, p , β^+ , and n designate antineutrino, proton, positron, and neutron respectively, was not possible with techniques of that era. Only in comparatively recent work has even this most readily observable interaction of free antineutrinos with matter been studied experimentally (10, 11). Theory had no useful comment to make as to neutrino interactions, other than simple inversion of nuclear beta decay, such as their interactions with electrons, until the recent work of Marshak & Sudarshan (12) and Feynman & Gell-Mann (13). Nonetheless, experimental searches were made for such an interaction, specifically in terms of a neutrino magnetic moment⁵ (14 to 17) which was determined to be $<10^{-9}$ electron Bohr magnetons (eh/mc). The same data have been interpreted by Rosendorff (18) to set an upper limit of the antineutrino electric dipole moment of $<2 \times 10^{-20} e \times \text{cm}$. where e is the electronic charge. These data allow also (18a) an upper limit on the electrical charge of a neutrino, but only an order of magnitude argument has been made, with the result $<10^{-5}e$. The electrical neutrality of matter could also be used to set a limit on the electrical charge of the neutrino through the reaction

$$n \rightarrow p + \beta^- + \bar{\nu} \quad 2.$$

According to the two-component theory of Lee & Yang (19), Landau (20), and Salam (16), the neutrino has strictly zero mass and no electrical or magnetic interaction. The theory also implies 100 per cent polarization with spin parallel (antineutrino) or antiparallel (neutrino) to its linear momentum.

In order to illuminate the more speculative discussion of the following sections concerned with the detection of free neutrino interactions other than reaction 1, we first consider the Los Alamos neutrino experiments in some detail (Sect. I). Next follows a discussion of the current low-energy program (Sect. II). As indicated, the neutrino has become of interest to high-energy physics; this is discussed in Section III. In a rather different vein we review the possibilities of studying cosmic rays via neutrinos (Sect. IV) and also comment briefly on the cosmic neutrino and its interest to cosmology in Section V.

I. THE LOS ALAMOS EXPERIMENTS

The primary object of the Los Alamos experiments was to show that the neutrino has an independent existence, that it can be detected away from

account for the apparent nonconservation of energy and momentum in such processes. However, if the expected recoils were not observed, the neutrino concept would be in trouble. A detailed discussion of recoil and angular correlation is given by Allen in his book, *The Neutrino* (8).

⁵ Salam (16) shows that the two-component theory requires a zero magnetic moment for the neutrino.

the site of creation by means of an effect it produces on a counter (10, 11). In the course of these investigations it became apparent that the value of the interaction cross section was also of interest, and some attention was given to that question once the main goal had been reached. The experiments which were made possible by the existence of intense sources of antineutrinos ($\sim 10^{13}$ $\bar{\nu}$ /cm.² sec.) embodied in fission reactors represent the first steps in the direct study of neutrino interactions.

THE ANTINEUTRINO ENERGY SPECTRUM FROM FISSION FRAGMENTS

Since a knowledge of the antineutrino spectrum incident on the detecting system is essential to an interpretation of the experiment, measurements were made to determine this spectrum. In principle two approaches are possible. One can measure the positron spectrum in reaction 1 and then infer the antineutrino spectrum (except for normalization). This is possible because in the few-Mev range the light positron takes very nearly all the kinetic energy. One can also measure the spectrum of electrons from fission fragments and deduce the antineutrino spectrum from this information. The normalization in terms of beta rays or antineutrinos per fission must be obtained in either case by a measurement of the fission beta rays. The first approach is to be preferred in principle because of the uncertainties associated with the complex beta spectrum resulting from a multitude of emitters. However, the primitive state of neutrino detection has thus far permitted only a crude direct spectral measurement (cf. below, Sect. II). Because of the energies of interest (> 1.8 Mev), the Coulomb distortion of each individual beta spectrum from the allowed shape is sufficiently small to allow a great simplification in the process of conversion without introducing large errors in the resulting antineutrino spectrum (21). The fission-fragment beta rays were measured by means of a plastic scintillator mounted on a photomultiplier tube. This detector viewed a fission counter placed in the thermal beam of the Los Alamos OWR reactor enabling the determination of the number of beta rays per fission in a given energy range. Gamma-ray background counts were much reduced by means of a coincidence requirement between the plastic detector and a gas proportional counter mounted in front of it.

Figure 1 shows the measured beta rays per fission per Mev and the antineutrino spectra derived for two limiting assumptions about the nuclear charge of the beta- (and antineutrino-) emitting fission fragments. The actual spectrum is bounded by the two dashed curves.

PREDICTED CROSS SECTION FOR REACTION 1

The cross section $\sigma(E_{\bar{\nu}})$ for the absorption of a monoenergetic antineutrino by a free proton (22)⁶ is given in the two-component neutrino theory

⁶ See Fermi (23) for a simple derivation which is correct except for the numerical factor.

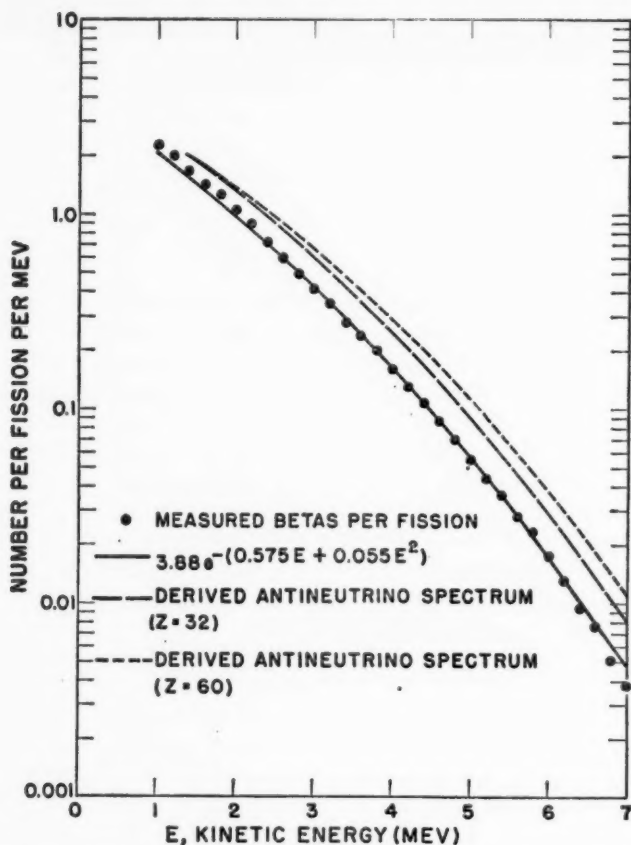


FIG. 1. Measured differential energy spectrum of beta rays in uranium fission and derived antineutrino spectra for nuclear charge $Z=32, 60$.

by the equation

$$\sigma(E_{\bar{\nu}}) = \frac{G^2}{\pi} \left(\frac{\hbar}{mc} \right)^2 \left[E_{\bar{\nu}} - \left(\frac{M_n - M_p}{m} \right) \right] \left[E_{\bar{\nu}} - \left(\frac{M_n - M_p}{m} \right)^2 - 1 \right]^{1/2} \quad 3.$$

where $M_n - M_p$ is the neutron-proton mass difference, $E_{\bar{\nu}}$ is the antineutrino energy in mc^2 units, and G^2 is the appropriate beta coupling constant.

Inserting numerical values,

$$\sigma(E_{\bar{\nu}}) = 2 \times (1.12 \pm 0.14) \times 10^{-44} (E_{\bar{\nu}} - 2.53) [(E_{\bar{\nu}} - 2.53)^2 - 1]^{1/2} (\text{cm}^2) \quad 4.$$

where

$$\left(\frac{\hbar}{mc} \right)^2 = 1.49 \times 10^{-21} \text{ cm}^2; \quad \frac{G^2}{2\pi} = g^2 \frac{m^2}{2\pi \hbar^4}$$

and g^2 is that constant customarily used in β -decay theory, assuming the nuclear matrix element to be unity for neutron decay. It is related to the neutron mean life τ_n by the expression (24)

$$\frac{1}{\tau_n} = \frac{g^2 m^5 c^4 F(\eta_0)}{2\pi^3 \hbar^7}$$

where $F(\eta_0)$ is the Fermi function, $\eta_0 = 2.324$, and $F(\eta_0) = 1.633$.

For

$$\tau_n = 17.3 \pm 2.2 \text{ min.}, \quad \frac{G^2}{2\pi} \left(\frac{\hbar}{mc} \right)^2 = (1.12 \pm 0.14) \times 10^{-44} \text{ cm.}^2$$

The energy dependence of the cross section in this low-energy range (< 10 Mev) is given by the familiar phase space argument. Other factors such as the effect of nucleon structure must be considered at high energies ($\sim \frac{1}{2}$ Bev) (cf. Sect. III).

Folding in the actual fission-fragment antineutrino spectrum of Figure 1, we find $N\bar{\sigma} = (6.1 \pm 1) \times 10^{-43} \text{ cm.}^2/\text{fission}$, where $N = 6.1$ (an accident), the number of antineutrinos per fission.

IDENTIFICATION EXPERIMENTS

As mentioned, the Los Alamos experiments were performed to demonstrate unambiguously a reaction caused in a target by a neutrino produced elsewhere. They were made possible by the development of large targets visible by means of a liquid scintillation detector and by the copious antineutrino source provided in powerful fission reactors. Figure 2 shows schematically the detection system employed. An antineutrino from fission products in a Savannah River Reactor is incident on a water target containing dissolved CdCl_2 . According to reaction 1, a positron and a neutron are produced. The positron slows down and annihilates with an electron producing two 0.5-Mev gamma rays which penetrate the target and are detected in coincidence by two scintillation detectors placed on opposite sides of the target. The neutron is moderated by the water and captured by the cadmium as signaled by the multiple capture gamma rays observed in coincidence by the two scintillation detectors. The antineutrino signature is, therefore, a delayed coincidence between the prompt pulses produced by positron annihilation and those produced microseconds later by the neutron captured in cadmium. The experiments consisted of a series of measurements in which the delayed coincidence events were studied in detail to show that: (a) The reactor-associated signal rate was consistent with theoretical expectations. (b) The first pulse of the delayed-coincidence signal was due to positron annihilation. (c) The second pulse of the delayed-coincidence signal was due to neutron capture. (d) The signal was a function of the number of target protons. (e) Radiation other than antineutrinos was ruled out as the cause of the signal by means of an absorption experiment.

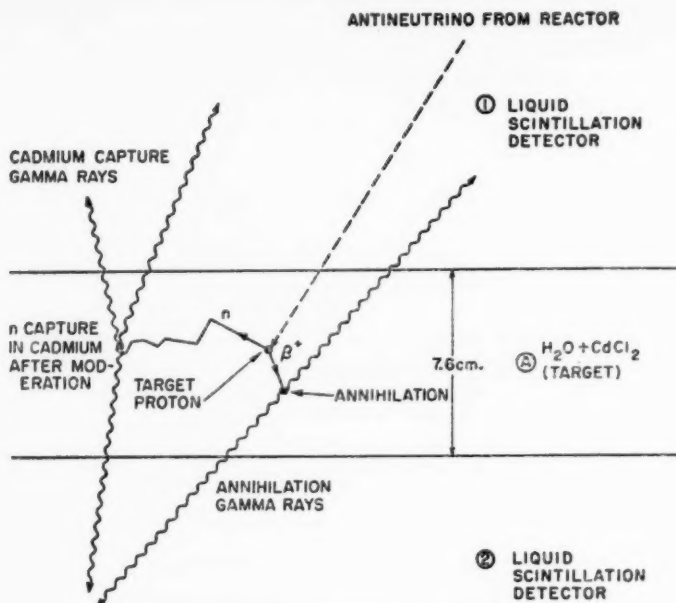


FIG. 2. Scheme of antineutrino detection experiment.

An idea of the detection system necessary to these experiments is given by the drawing of the detector assemblage shown in Figure 3. The small interaction cross section, together with the detailed nature of the experimental question posed, was primarily responsible for the size of the detector which, exclusive of the lead shield, weighed about 10 tons. In addition, because of the low counting rate and the many checks desired, the experiment was run for 2085 hours.

Signal rate.—A reactor-associated signal rate of $3.0 \pm 0.2 \text{ hr.}^{-1}$ was observed. This represented a signal to total accidental background ratio of 4/1; a signal to correlated (as in neutron capture) reactor independent background of 5/1; and a signal to reactor-associated increase of accidental background greater than 25/1. Measurements of positron and neutron detection efficiency and a knowledge of the reactor flux showed this signal rate to be consistent with a cross section of $\bar{\sigma} = (1.2^{+0.7}_{-0.4}) \times 10^{-43} \text{ cm.}^2$, a value in agreement with the theoretically expected $\bar{\sigma} = (1.0 \pm 0.16) \times 10^{-43} \text{ cm.}^2$

First pulse due to a positron.—The first pulse was tested by measuring the signal as a function of the thickness of lead sheet interposed between the water target and one detector. After correcting for the associated drop in neutron detection efficiency, the signal was observed to diminish as expected if the first pulse were due to positron annihilation radiation. Table I shows the expected and observed signal rates as a function of lead thickness. The agreement is believed to be acceptable in view of the uncertainties involved

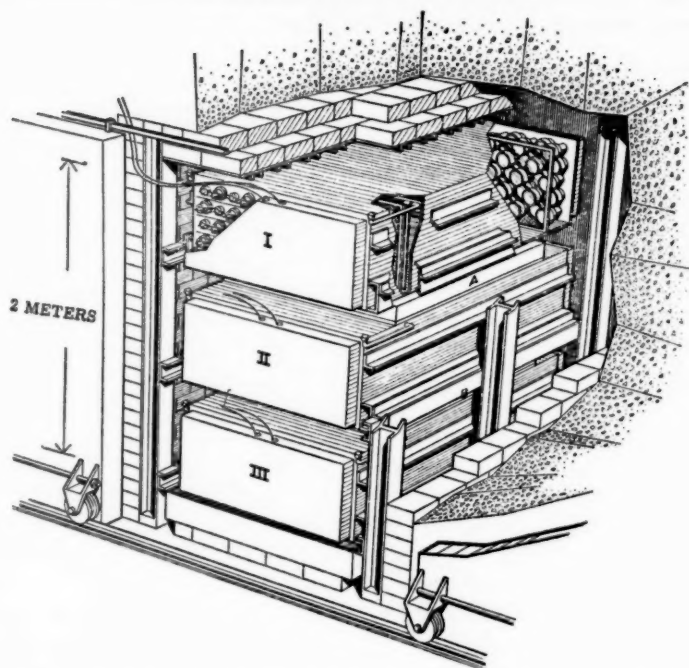


FIG. 3. Sketch of detectors inside their lead shield. The detector tanks marked I, II, and III contained 1400 l. of triethylbenzene (TEB) liquid scintillator solution which was viewed in each tank by 110 five-inch photomultiplier tubes. The TEB was made to scintillate by the addition of *p*-terphenyl (3 gm./l.) and POPOP wavelength shifter (0.2 gm./l.). The tubes were immersed in pure nonscintillating TEB which provided an optical match for the scintillation light. Tanks A and B were polystyrene and contained 200 l. of water in which were dissolved as much as 40 kg. of CdCl_2 . The sliding doors were made of lead.

in arriving at the predicted ratios. In addition, the pulse height spectrum of first pulses showed better agreement with that from a positron source than with the spectrum of the background. The total weight of experimental

TABLE I
LEAD ABSORPTION TEST OF SIGNAL

Pb thickness cm.	Signal predicted	Signal observed
0	1.00	1.00
0.16	0.40	0.50 ± 0.13
0.48	0.12	0.32 ± 0.14
0.95	0.02	0.03 ± 0.06

evidence on this point supports the statement that the first pulse was due to a positron.

Second pulse due to a neutron.—This point was clearly demonstrated by a series of experiments in which the cadmium concentration was varied. The most striking measurements were those with and without cadmium in the water target. As expected for neutrons, this totally removed the correlated count rate, giving a rate above accidentals of $0.02 \pm 0.07 \text{ hr.}^{-1}$. In addition, the distribution of intervals between the first and second pulses was found to be that expected for neutron capture, and the spectrum of second pulses was consistent with that expected for neutron-capture gamma rays.

Having proved that the second pulse of the reactor-associated pair was due to a neutron, it was believed necessary to show that the first pulse was not caused by a neutron. Such a false pulse sequence could conceivably arise from a complicated series of collisions in which a fast neutron makes collisions in both side detectors and is finally captured in the cadmium of the water target. This sequence was proved unlikely as a source of the signal by experiments with fast-neutron sources, which caused primarily an increase in the accidental rather than the correlated rate. As pointed out above, the reactor-associated rise in accidentals was less than $1/25$ of the antineutrino signal, ruling out neutrons from the reactor.

Signal as a function of target protons.—In this experiment, the number of protons in the target was reduced without drastically changing the detection efficiency of the system for events produced by antineutrinos. This was accomplished by replacing about one-half the protons by deuterons, i.e. mixing light and heavy water. The ratio of the observed to the expected rate is 0.7 ± 0.2 where the error listed is statistical. In estimating the expected rate an allowance was made for a small ($\sim 10\%$) contribution from antineutrino interactions with deuterons in the target due to the reaction.



The agreement with expectation leaves something to be desired, but it demonstrates in a semiquantitative way the dependence of the signal on the presence of protons in the target. It is to be noted that whereas the antineutrino signal changed significantly with dilution of the target by deuterons, the detection efficiency for background events was only slightly altered by this dilution, supporting the conclusion that the signal was in fact due to antineutrinos.

Absorption test.—Since the only known particles, other than antineutrinos, which are capable of being produced by the fission process can be heavily discriminated against by means of a gamma-ray and neutron shield, the signal was tested by such an experiment. The shield added in this experiment was placed between the reactor and the detector assembly. It was shown by separate measurements that the shield reduced gamma rays and neutrons penetrating to the detector by at least an order of magnitude. The signal, on the other hand, remained constant, i.e. was $1.74 \pm 0.12 \text{ hr.}^{-1}$ with the shield and $1.69 \pm 0.17 \text{ hr.}^{-1}$ without the shield.

MEASUREMENT OF CROSS SECTION FOR REACTION $\bar{\nu} + p \rightarrow \beta^+ + n$

After the demonstration of the antineutrino reaction, the next step was to measure the cross section more precisely. The scheme for this experiment is shown in Figure 4.

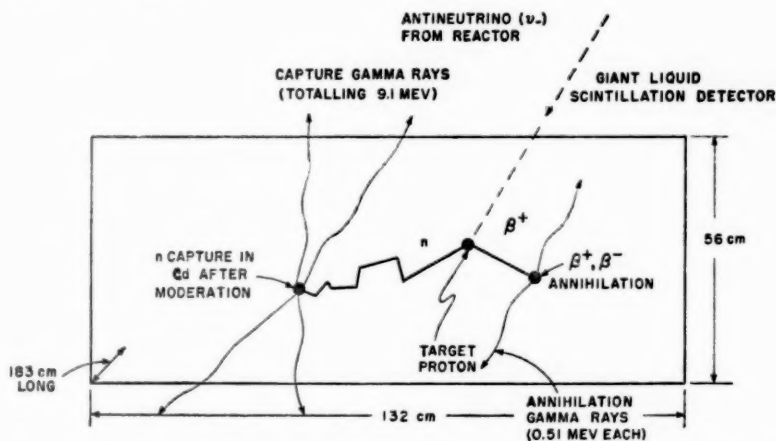


FIG. 4. Scheme of antineutrino detector. This 1.4×10^3 -l. detector is filled with a mixture which consists primarily of triethylbenzene (TEB) with small amounts of *p*-terphenyl (3 gm./l.), POPOP wavelength shifter (0.2 gm./l.) and cadmium (1.8 gm./l.) as cadmium octoate. An antineutrino is shown transmuting a proton to produce a neutron and positron. The positron slows down and annihilates, producing annihilation radiation. The neutron is moderated by the hydrogen of the scintillator and is captured by the cadmium, producing capture gamma rays.

Target protons were provided by a 1400-l. liquid scintillation detector—one of those used in the identification experiment—in which the scintillation solution was loaded with a cadmium compound (cadmium octoate) to allow use of the delayed-coincidence technique. Apart from technical improvements involving better shielding from the reactor and cosmic rays as well as improved circuitry, this experiment (25) was much like the early attempt (10) made in 1953.

The first pulse of the pair was caused by the positron slowing down and annihilating, the second by capture of the neutron in the cadmium of the scintillator solution. Except for the kinetic energy of the positron, less information is obtained per pulse than in the identification experiment, and hence it is reasonable that the detection efficiency and background should both rise. So, for example, the detection efficiency rose from ~ 2.5 per cent to ~ 8.5 per cent and the target size was changed from 400 l. (H_2O) to 1400 l. (TEB), giving an increase in the count rate from $\sim 3 \text{ hr.}^{-1}$ to $\sim 40 \text{ hr.}^{-1}$. The price paid for this increase in count rate was a decrease in the signal to noise ratio by two orders of magnitude, if we consider the noise as the accidental

background from the reactor. The background from cosmic rays rose relative to the signal by a factor of 10. These background increases are not surprising in view of the possibility that, as with an antineutrino, neutrons produced by the cosmic rays can also give a correlated delayed coincidence sequence the first pulse of which is due to a recoil proton (instead of a positron) and the second due to capture of the neutron. In addition, the reduction in the number of coincidences required in this experiment made accidentals much more likely. Despite the increased background, the rate was sufficiently great to enable statistical errors to be kept down, and the overall cross section was measured more accurately because the efficiency was better known.

The average cross section for antineutrinos from fission fragments is given by the equation

$$\bar{\sigma} = \frac{R}{3600fn\epsilon_{\beta^+}\epsilon_n} \text{ (cm.}^2\text{)} \quad 6.$$

where

R = observed signal rate in counts/hr.

$$= 36 \pm 4$$

n = number of target protons

$$= 8.3 \times 10^{28}$$

f = antineutrino flux near the reactor

$$= 1.3 \times 10^{13} \text{ } \bar{\nu}/\text{cm.}^2 \text{ sec.}$$

ϵ_{β^+} = positron detection efficiency

$$= 0.85 \pm 0.05$$

ϵ_n = neutron detection efficiency

$$= 0.10 \pm 0.02$$

and was measured to be $\bar{\sigma} = (1.10 \pm 0.25) \times 10^{-43} \text{ cm.}^2$

This is in agreement with the cross section predicted by the two-component theory and measurements of the fission beta spectrum and the neutron mean life as shown by the ratio $\bar{\sigma}/\bar{\sigma}_{\text{th}} = 1.1 \pm 0.3$.

The spectrum of first pulses (the positron spectrum) obtained in this experiment was used in conjunction with the conservation laws to deduce a rough antineutrino spectrum. It is shown in Figure 5.

II. CURRENT LOW-ENERGY PROGRAM

In view of the fundamental nature of reaction 1, it is of interest to obtain a more precise measurement of the cross section as well as a more precise prediction of the expected value. In addition, further experimentation with antineutrinos from fission reactors requires better information about their spectrum. The largest single uncertainty in the experiment described in the last section was the neutron detection efficiency. This uncertainty can be decreased by increasing the efficiency from the present 10 per cent to 80 per cent by adding more cadmium, with several concomitant advantages: the

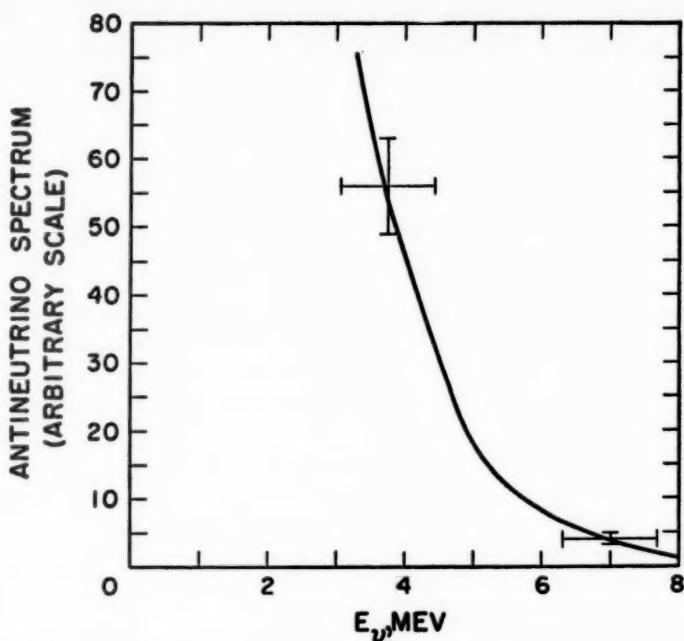


FIG. 5. Differential antineutrino spectrum from fission fragments deduced from β^+ spectrum in reaction $\bar{\nu}(p,n)\beta^+$. Crosses denote estimates of uncertainties. The curve is obtained from Fig. 1 and normalized appropriately. (*Note added in proof:* The curve shown is slightly in error. It should be somewhat lower at the high-energy end.)

signal rate per unit of detector volume would increase; the accidental background would drop sharply relative to the signal because the average time interval between the pulses of the delayed coincidence pair would decrease. A re-design of the detector in which an inner cadmium-bearing region is enclosed in a non-cadmium-bearing scintillator would minimize edge effects due to gamma-ray leakage from the detector. The energy resolution of such a detector would enable a much better positron and hence antineutrino spectrum determination. It also appears that cosmic ray background would be significantly reduced by the "uncadmiated" scintillator blanket. An illustrative scheme of such an improved system is shown in Figure 6. The signal rate with available antineutrino fluxes would be about 30 hr.^{-1} Such an improved experiment is well within present experimental knowledge and is under consideration by the group at Case Institute.

It should be remarked that a measurement of the less copious, higher energy, antineutrino from fission fragments is made less difficult by the increase in the cross section for reaction 1 with $\bar{\nu}$ energy ($\sim E_\nu^2$). This is to be compared with a deduction of the antineutrino spectrum from the direct measurement of fission betas that becomes relatively more difficult because

of the rapid drop in the number of beta rays (and antineutrinos) with energy. The present uncertainty in the spectrum at higher energies makes rather uncertain the prediction of a reaction rate for the antineutrino disintegration of deuterons, Equation 5, because of the high threshold involved (4.1 Mev as compared to 1.8 Mev for reaction 1). At present the ratio of the cross section for 5 to that for 1 is predicted to be about 1/30 (within a factor of 2) for fission antineutrinos.

Thus far only the antineutrino reaction 1 has been observed. An attempt was made to observe the antineutrino disintegration of the deuteron (26), reaction 5, but it was unsuccessful primarily because of the rather small cross section (relative to that for the reaction 1 for which the system was primarily designed) and the low neutron detection efficiency which op-

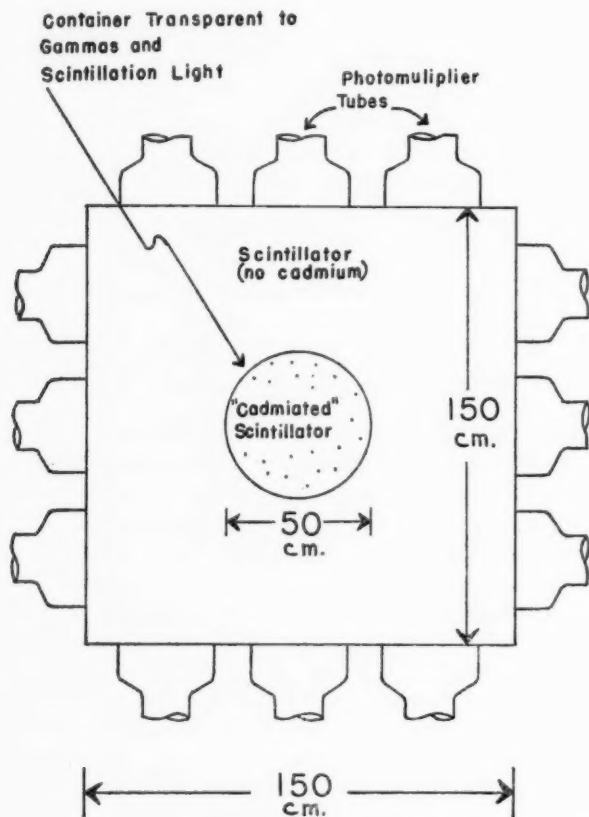


FIG. 6. Scheme of improved antineutrino detector to measure $\bar{\sigma}$ and the energy spectrum. Antineutrino events occurring in cadmiated regions release an energy of 9.1 Mev in Cd capture gammas and hence can be discriminated relative to those which occur in the outer, noncadmiated volume.

erated for each of the two product neutrons. These factors together with the low positron detection efficiency reduced the overall counting rate to about two per week, too low for effective study. This situation can be remedied by using substantially the experimental arrangement just described for an improved measurement of reaction 1 instead of that for the identification experiment which was previously employed. The only difference would be to replace the inner cadmiated detector with a deuterated scintillator. In this case the neutron detection efficiency would rise by a factor of four and the positron detection efficiency by a factor of six. Since there are two neutrons to be detected, the overall detection efficiency should rise by a factor of 100. On this basis and allowing for the differences in the numbers of deuteron targets, the rate should be expected to be about one per hour. It seems reasonable that the background would not rise as rapidly as the neutron detection efficiency squared because of the shielding provided the inner cadmiated target by the outer scintillator.

A second kind of experiment is the elastic scattering of antineutrinos by electrons.



This is distinct from the absorption type of experiment typified by reactions 1 and 5, which must occur independently of the precise form of the theory of weak interactions. The elastic scattering expectations depend very much on the theoretical structure employed. It is now generally believed that the conserved vector current theory (12, 13) is a good description of weak interactions at low energies. It is intriguing to contemplate the observation of a direct interaction between the two elementary particles and therefore to test the theory in this rather clean-cut and unambiguous case in which nucleons can play no direct role. For this reason a serious effort is now under way to study means of observing reaction 7 although it is an experimental problem of great difficulty.

The essential difficulties arise from two sources: the miniscule interaction cross section⁷ ($\sim 5 \times 10^{-46}$ cm.²/fission $\bar{\nu}$) coupled with the "nondescript" character of the event. For available antineutrino fluxes a sensitive volume of ~ 100 l. will give ~ 5 counts per hr., an acceptable rate in the absence of background. Since, for such a detector, backgrounds in the energy ranges in which most of the recoil electrons are expected (0.2 \rightarrow 1.5 Mev) are about 10^5 times this level, it follows that considerable background reduction is essential.

⁷ This cross section for fission antineutrinos is calculated from the antineutrino spectrum of Figure 1 and the cross section σ for monoenergetic antineutrinos given by Feynman & Gell-Mann (13):

$$\sigma = \sigma_0 \frac{\omega}{6} \left[1 - \frac{1}{(1 + 2\omega)^2} \right]$$

where $\omega = E_{\bar{\nu}}/mc^2$ and $\sigma_0 = 8.3 \times 10^{-46}$ cm.².

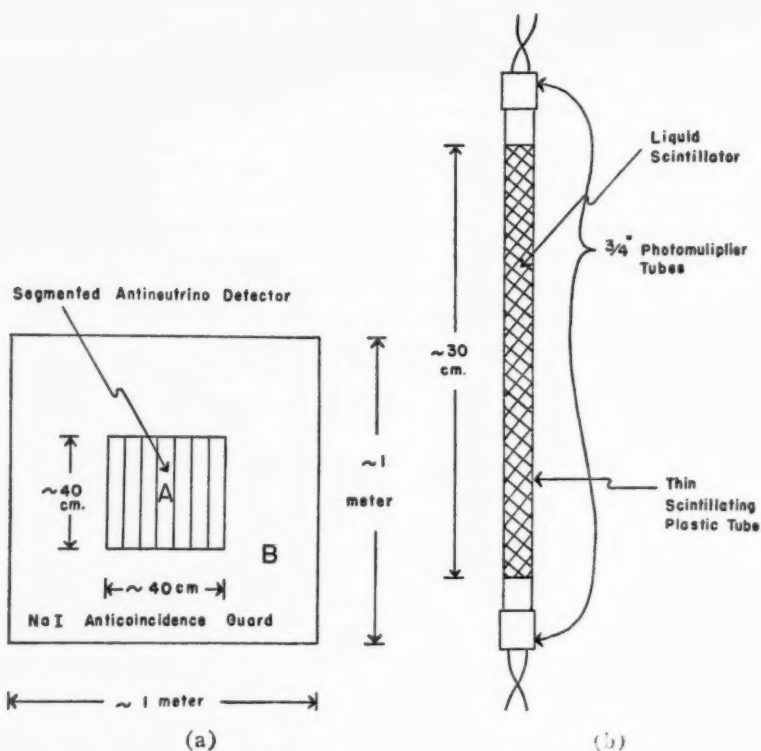


FIG. 7a. Possible antineutrino elastic-scattering experiment. The anticoincidence guard B consists of approximately 100 close packed NaI crystals each one viewed by a 5-in. photomultiplier tube. The segmented antineutrino detector A is made up of about 400 separate cylindrical detectors.

FIG. 7b. Details of proposed antineutrino detector segment.

It is believed that the backgrounds are caused by gamma rays from the environment and hence a discrimination scheme should take advantage of the differences between signals due to gamma rays and those due to electrons recoiling from antineutrinos. An experimental arrangement which shows promise of shielding against gammas and at the same time discriminating against gammas which penetrate the shield and enter the target volume is shown schematically in Figures 7 a and b.

The idea of the experiment is as follows: only events in A alone are acceptable; B or A + B are rejected; A events involving more than one cylindrical tube are rejected. Gamma rays produced externally are totally absorbed by B, produce a pulse in B enabling their rejection, or penetrate B without giving a B signal but give a signal in A alone. This last possibility can be made small by making any one of the A tubes of a diameter (~ 2 cm.),

which is much less than the Compton mean free path in the liquid scintillator (~ 10 cm.). Since Compton collisions, which are essentially the only kind that occur in hydrocarbons above >0.2 Mev, do not remove the gamma, it can escape to trigger either another tube of *A* or more likely the anticoincidence shield *B*.

It is too early to say how these ideas will work out although it appears that the construction of such a massive (2-ton) NaI detector is entirely feasible and that the radioactive contamination of the NaI can be kept within acceptable limits, e.g., <1 p.p.m. potassium. The electronic sorting system to classify and record the events looks manageable. The most serious problem may be the radioactivity of the small photomultiplier tubes (27) of detector *A*. It is already evident that some radioactively clean material such as quartz will have to be used instead of the customary glass. Experiments are now under way at the Case Institute to determine how far towards a solution of the background problem these ideas can lead.

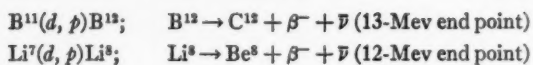
No discussion of low-energy neutrino interactions can be terminated without mentioning the extraordinary radiochemical experiments of Davis (28). It was suggested by Pontecorvo (29) and elaborated by Alvarez (30) that if the neutrino is identical with the antineutrino, neutrinos from fission reactors should be observable via the reaction



The idea, as developed and brought to fruition by Davis, was to irradiate a large volume of CCl_4 and then sweep out the product A^{37} with He gas, separate it from the He, and then count it in a small, low-background Geiger detector. Davis demonstrated that he can quantitatively sweep out A^{37} from a few thousand gallons of CCl_4 and then detect the A^{37} by observing its *K* capture. Thus far he has shown that the probability for the reaction to occur is less than $1/10$ of that expected for the assumption $\bar{\nu} \equiv \nu$. This demonstrates, in view of the observation of reaction 1, that the neutrino and antineutrino are not identical particles.

A word should perhaps be added as to other sources of man-made antineutrinos. The one most frequently mentioned is a nuclear explosion. It has been noted that it provides a pulsed source which reduces the background. An estimate of the total number of events seen with a one-ton detector located in a shielded underground chamber at a safe distance from a nuclear explosion (20 kilotons) shows this number to be $\gtrsim 10$ counts/explosion. This result would be difficult to interpret quantitatively in an air burst because of the fission product distribution in the rising cloud. The signal is predicted on the basis of a confined explosion. Since, as we have seen, the background is not a problem, a stationary reactor is a superior antineutrino source in every way.

Another source, a high-current low-energy electronuclear machine, has been suggested by Muehlhause & Oleksa (31). They propose using a pulsed beam of deuterons to make antineutrinos via the reactions:



No detailed study has been made of this suggestion.

LOW-ENERGY INTERACTIONS: CONCLUSIONS

We have discussed the two types of low-energy neutrino interactions: inverse beta (β^-) decay on which a successful start has been made, and the elastic scattering of *antineutrinos* by electrons, which it may be possible to study if one assumes certain refinements in experimental technique. Sufficiently strong man-made sources of low-energy *neutrinos* do not seem to be forthcoming in the foreseeable future, and hence experiments are believed to be unlikely in that direction. The theoretical structure has been tested at low energies in a positive manner using free antineutrinos and by negative experiments such as that of Davis. This experiment demonstrates that the neutrino and antineutrino are different by showing that an antineutrino does not invert positron decay. It is now generally believed that we have in hand most of the important checks on the nature of the low-energy interaction of free antineutrinos ($\bar{\nu}$) and that convincing theoretical arguments indicate we understand low-energy free neutrino (ν) interactions as well. With the completion of the experimental program outlined above, all the useful and interesting ideas thus far proposed for low-energy free neutrino work will have been tried.

III. HIGH-ENERGY INTERACTIONS

Low-energy neutrino interactions seem to be well described by theory. It is reasonable to ask, as have Pontecorvo, Lee, Yang (1, 2, 4) and others, whether the situation remains unchanged as the energy increases. Indeed one can even ask whether the various neutrino-like particles involved in the new processes which are characteristic of meson decay are in fact the same particle as the nuclear beta-decay neutrino. One can ask whether the conservation of leptons is valid at high energies; if the reaction between $\bar{\nu}$ and p is related to the reaction between ν and n (called S -symmetry by Lee & Yang); whether elastic interactions with proton and neutron exist; if, as at low energies, the high-energy neutrino interaction is properly described as a point interaction; if interactions involving β^\pm and μ^\pm are the same except for the difference in masses between β and μ ; if the conserved vector current of Feynman & Gell-Mann is related (e.g. proportional) to the electromagnetic current; if a weakly coupled or intermediate boson exists so that the neutrino reactions are strictly nonlocal, as in the meson theory of nuclear forces. One can also pose the question, to what energy is the first-order perturbation treatment valid from which Equation 3 is derived, and so be motivated to look for new detailed information in experiments at high energy?

The idea of an intermediate boson as the carrier of the weak interaction has been discussed by many authors (1, 2, 33, 35) from Yukawa (32) to Kinoshita (34).⁸ Glashow (35) has considered some consequences of an

⁸ Kinoshita's letter contains many references to the literature.

intermediate charged boson Z^\pm of mass equal to or greater than that of the K meson (because weak interactions can give rise to K mesons) which operates in the reaction

$$\bar{\nu} + \beta^- \rightarrow \bar{\nu} + \mu^-$$

to give

$$\bar{\nu} + \beta^- \rightarrow Z^- \rightarrow \bar{\nu} + \mu^- \quad 9.$$

Such a boson could mediate beta decay in the familiar Yukawa manner:

$$n \rightarrow p + Z^-; \quad Z^- \rightarrow \beta^- + \bar{\nu} \quad 10.$$

Glashow concludes that such a particle would raise the cross section for reaction 9 to detectable levels, using very high-energy cosmic ray neutrinos with large detectors deep underground (see Sect. IV).

Kinoshita gives an example of a different assumption

$$\nu + n \rightarrow B \rightarrow \beta^- + p \quad 11.$$

where the intermediate neutral boson B is assumed to carry a nucleonic and leptonic charge, so enabling 11 to be consistent with conservation of these quantities. According to Kinoshita the shape of nuclear β^- -decay spectra can be explained if $m_B \gtrsim 2300 m_e$ and the lifetime $\tau_B \lesssim 10^{-17}$ sec.

These questions regarding the nature of the weak interactions are not amenable to study at low energies. They could well have been formulated a long time ago but without much hope of stimulating experimentalists (with the possible exception of the Glashow suggestion) because appropriate high-energy machines were so far in the future.⁹ This may no longer be the case as pointed out by Pontecorvo (4, 36) and Schwartz (3). It is believed by these authors that high-energy machines can be built which will, in conjunction with large detectors, enable neutrino interactions to be pursued into these new and exciting ranges. The most plentiful targets for free neutrinos and antineutrinos are nucleons and negative electrons, and a list of direct reactions of interest with these targets is given in Table II. Low-energy reactions are included for completeness. The list of reactions can be extended by allowing for the possible production of K mesons, hyperons, electron pair creation in the nuclear field, etc. (1, 2, 4).

A clear test of the identity of the neutrinos from various processes would be provided by the absence of reaction 1a for neutrinos produced by pion decay. Lepton conservation, already shown at low energies by the observation of reaction 1a and the non-occurrence of 6a could in principle be tested at high energies by studying reactions 1a,b and then looking for a reaction such as 1a,b but induced by neutrinos. Reactions 1c and 3b, 2c and 3a represent a set similar to 4a,b; but, unlike the latter, such interactions are not predicted by any existing theory. Interest in the elastic scattering of neu-

⁹ During a discussion (1956) at Los Alamos in which a high-energy accelerator was being considered, C. L. Cowan made the suggestion that such machines be built for neutrino studies, specifically to test the identity of π , μ , and beta-decay neutrinos. At that time the idea seemed experimentally fanciful and no strong theoretical arguments had been mustered to support it.

TABLE II
REACTIONS OF FREE NEUTRINOS*

	Reaction	Remarks
1a,b,c	$\bar{\nu} + p \rightarrow \begin{cases} \beta^+ + n + \alpha\pi \\ \mu^+ + n + \alpha\pi \\ \bar{\nu} + p \end{cases}$	Observed at low $\bar{\nu}$ energies ($\sim 2-8$ Mev) with pion multiplicity $\alpha=0$.
2a,b,c	$\nu + n \rightarrow \begin{cases} \beta^- + p + \alpha\pi \\ \mu^- + p + \alpha\pi \\ \nu + n \end{cases}$	
3a,b	$\nu + p \rightarrow \nu + p$ $\bar{\nu} + n \rightarrow \bar{\nu} + n$	
4a,b	$\bar{\nu} + \beta^- \rightarrow \bar{\nu} + \beta^-$ $\nu + \beta^- \rightarrow \nu + \beta^-$	Not yet observed (see text).
5	$\nu + \beta^- \rightarrow \nu + \mu^-$	
6a,b	$\bar{\nu} + \text{Cl}^{37} \rightarrow \text{A}^{37} + \beta^-$	Not observed, so proving $\bar{\nu} \neq \nu$ for $\bar{\nu}$'s from nuclear beta decay.
	$\nu + \text{Cl}^{37} \rightarrow \text{A}^{37} + \beta^-$	Occasionally suggested as useful in measuring the solar ν flux but not if the p, p cycle has inappreciable higher-energy branches.†
7	$\bar{\nu} + d \rightarrow \beta^+ + n + n$	Not yet observed (see text).

* For simplicity in making the table, all neutrino-like particles are taken to be identical, e.g. those for π^+ decay, μ^- capture, and nuclear β decay. It can be argued that the first two must be the same because if this is true, a rearrangement of these reactions results in an observable (and observed) reaction, π^- capture by a proton. The identity between meson-associated neutrinos and nuclear beta-decay neutrinos is supported by the apparent equality of the interaction constant as noted independently by Tiomno & Wheeler (38) and Lee, Rosenbluth & Yang (37) [see also Fermi (39)].

† Discussed in Section V.

trinos by nucleons stems from the question, do neutral lepton currents exist in analogy with the electromagnetic field?

CROSS SECTION FOR REACTION $\bar{\nu} + p \rightarrow \beta^+ + n$ AT HIGH ENERGIES

In order to make some semiquantitative estimates of the experimental details we will consider reaction 1 at high energy. Assuming for the moment the identity of all classes of neutrinos (except that antineutrino may not be identical to the neutrino), how does the interaction cross section vary with

neutrino energy? This question has been considered by Lee & Yang (1, 2) and others. These authors conclude that the cross section does not continue to increase quadratically with energy as is the case at low energies, but saturates at value in the neighborhood of 0.8×10^{-38} cm.² for an antineutrino (lab.) energy in the vicinity of 7 Bev. The calculations referred to assume that the interaction is distributed throughout the nucleus as is the electrical charge distribution given by high-energy electron scattering. The fact of saturation itself follows, as shown by Lee (1), from the limitation in the number of final states resulting from the forward peaking of the reaction products. The approach to saturation is given by the distribution assumption. Figure 8 shows the cross sections predicted from these assumptions for reactions 1a as well as 2a (see Table II) but with no meson emission ($\alpha = 0$). Because of the high energies involved relative to nuclear binding, bound nucleons can be taken as free so that cross sections are additive over the number of nucleons in a nucleus.

If we do not restrict ourselves to these two reactions, then, as the neutrino energy increases, other reaction channels become available so that the total interaction cross section need not saturate as does the cross section for one channel. So, for example, multiple pion production ($\alpha > 0$ in reaction 1) can also contribute to the total cross section.

HIGH-ENERGY EXPERIMENTS

It is to be noted that all of the reactions listed in Table II give rise to extremely energetic light particles. This fact is of importance in planning since it makes use of the Cerenkov effect possible and so may simplify the detection problem, at least in the initial experiments. We shall return to this point.

An indication of how high-energy neutrino beams might be produced is given in Figure 9. A proton beam in the multi-Bev range is incident on a target in which it produces, among other particles, a multiplicity of pions. Because of the high energies involved the pions are well collimated about the direction of the proton beam. Some of these pions decay as they traverse the "decay space" l_1 , producing muons and neutrinos. These particles are also grouped about the direction of the parent pion so that a separation of muon and neutrino must be effected because of the overwhelming background produced by even a small muon contamination at the detector. Such a separation could in principle be made by magnetic fields (π^+ , π^- beams and so ν , $\bar{\nu}$ beams could be separated similarly); but because of the large distances (tens of meters) necessary, it is perhaps prudent at this stage to consider removing muons by means of a massive absorber as shown in the figure.

In view of the complexity of events in which the high-energy product particles are involved, it will take considerable ingenuity on the part of the experimentalist to disentangle and identify the reaction he wishes to study. So, for example, a high-energy antineutrino on a liquid scintillator will produce very much the same kind of signal as a neutrino and, as we have indi-

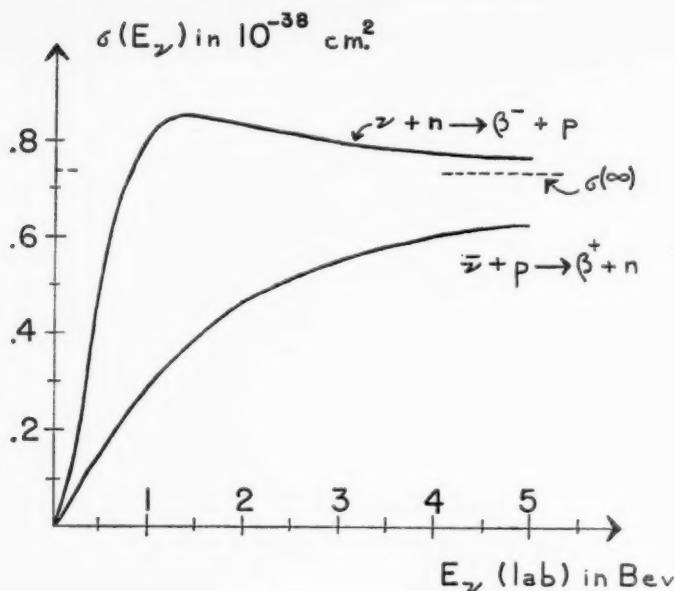


FIG. 8. Neutrino absorption cross sections after Lee & Yang (2).

cated, beam separation for antineutrino and neutrino is at best complicated to achieve.

As an example of the experimental conditions associated with high-energy neutrino experiments, we consider the simplest one in which the object is to demonstrate the existence of neutrino-like particles through an absorption process. If a total interaction cross-section measurement is also made, then the more complex problems listed above can be approached with greater confidence than is possible with theoretical guides alone. We esti-

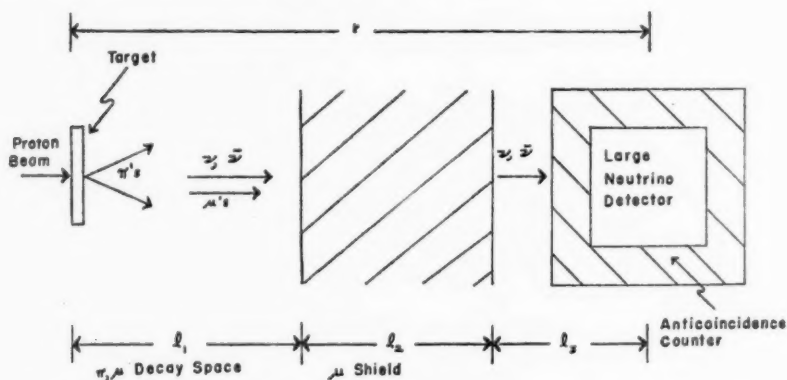


FIG. 9. Scheme of an experimental arrangement for high-energy neutrino experiments.

mate the neutrino, antineutrino flux presently expected from the CERN machine as follows: the number of 25-Bev protons per pulse is about 10^{11} and the pulse rate is about 10^3 per hr.¹⁰ Each proton interaction in a low- Z target is taken to produce a total of roughly 10 pions,¹¹ of which one-third are neutral and two-thirds are absorbed by the target itself. The average energy per pion is taken to be 2 Bev, and the half angle of the forward cone into which the product pions are projected is such that the intensity is increased over the isotropic inverse square intensity by a factor of about 40. The neutrinos (and antineutrinos) are emitted isotropically in the rest frame of the parent pions, and approximately one-half are within a cone of less than 10° about the pion direction so that the neutrino beam may be taken as approximately parallel to the pion beam. Combining these numbers and the relativistically time-dilated lifetime of the pion for π, μ decay, the neutrino plus antineutrino flux, F per hr. and cm^2 within the beam cone is approximately

$$F = 8 \times 10^{10} l_1 / r^2 \quad 12.$$

where l_1 is the decay distance and $r = l_1 + l_2 + l_3$ is the distance from the target to the center of the detector, all in centimeters, and we have replaced the exponential decay by its linear approximation.

The average neutrino (or antineutrino) energy is only a fraction of the pion energy, perhaps $\frac{1}{4}$, and so is ~ 500 Mev. The cross section for such a mixed neutrino-antineutrino beam on a water target is $\sim 7 \times 10^{-38} \text{ cm}^2/\text{H}_2\text{O}$ molecule, and the reaction rate $R(\text{hr}^{-1})$ in a mass $M(\text{gm.})$ is given by the equation

$$R = 1.6 \times 10^{-6} M l_1 / r^2 \quad (\text{hr}^{-1}) \quad 13.$$

If

$$R = 1 \text{ hr}^{-1}, \quad l_2 = 2 \times 10^3 \text{ cm. (limonite concrete to absorb 20-Bev muons)}$$

$$l_3 < 10^3 \text{ cm., so neglect here.}$$

$$M = \frac{1}{1.6} \times 10^4 (l_1 + 2000)^2 \frac{1}{l_1} (\text{gm.})$$

M is a minimum at $l_1 = l_2 = 2 \times 10^3 \text{ cm.}$, so that

$$M_{\min} = 5 \times 10^7 \text{ gm. or } 50 \text{ metric tons, a heroic size!}$$

A water cube of this mass is 3.7 m. on edge.¹²

The neutrino detector could consist of a water target in a white container at the end of which are located a few hundred 5-in. photomultiplier tubes. The detector would be completely surrounded by an anticoincidence counter to guard against cosmic rays and other charged particles. Neutral cosmic radiation could be discriminated against by burying the entire detector

¹⁰ The problem of neutrino detection is under active consideration by a group at CERN (40).

¹¹ For a brief discussion of pion multiplicities and angular distributions from nucleon-nucleon reactions, see Galbraith (41).

¹² If some other transparent but denser liquid such as CCl_4 were used, the size of the detector would drop inversely with the density ρ and the surface area as $\rho^{-2/3}$ so that fewer photomultiplier tubes would be required to collect the Cerenkov light.

under several meters of earth. The anticoincidence detector is necessary because the cosmic ray rate is $\sim 10^7$ times the expected signal. This situation can be greatly alleviated by synchronizing with the machine pulse, but even during the pulse¹³ the cosmic ray background is a thousand times the expected signal. It is conceivable that the detector design could be made more complicated to take advantage of the directional characteristic of the Cerenkov radiation in order to help discriminate against cosmic rays. Large area scintillation detectors are envisaged as constituting the elements of the guard detector.

Various assumptions have been made in arriving at these results; and although the conclusions are believed to be semiquantitatively correct, the assumptions should be checked by experiment. So, for example, the pion multiplicity and angular distribution can and should be measured for the energies available.

This is the present situation with respect to accelerator-produced high-energy neutrinos. It could be changed if an intermediate boson hypothesis is correct and the cross sections thereby increased. It will surely change when the ZGS (zero gradient synchrotron) now under construction at the Argonne National Laboratory is completed. It is estimated that this 12-Bev machine will produce an external beam of 10^{13} protons/pulse, and possibly greater, at the rate of one pulse every 4 sec. (42)¹⁴ and so should give a few counts/hr. in a detector weighing only a few tons.¹⁵ As the detector size decreases so do cosmic ray backgrounds and problems of analysis. So, given sufficient neutrino flux (and the anticipated 10^9 per hr. and cm.² may be enough), large bubble chambers can be constructed to study these interactions. This is especially important in this new and unknown field because of the enormous amount of information in even one bubble chamber picture. It is already possible to give serious consideration to NaI detectors weighing a few tons, and large liquid scintillation counters could easily be built in the 10-ton size range so that more traditional counting experiments might be used to study the details of high-energy neutrino interactions.

In summary, there is already the possibility of making a beginning in this new field, with the expectation that machines under construction and being planned will allow more detailed experimentation. The existence of an intermediate boson could raise the interaction cross section significantly and so simplify the detection problem, but we need not count on it to make an experimental study possible.

IV. COSMIC AND COSMIC RAY NEUTRINOS

As we have seen, interactions of high-energy particles with matter produce neutrinos (and antineutrinos). The question naturally arises whether

¹³ The pulse is assumed to be ~ 1 msec. in duration. If it can be shortened to a microsecond or less, cosmic ray backgrounds become much less important.

¹⁴ The Princeton-Pennsylvania high-intensity 3-Bev machine may also make neutrino studies possible.

¹⁵ It is amusing to realize that the detector tanks used in the original neutrino work (Fig. 3) could also be useful for the observation of high-energy neutrinos.

the neutrinos produced extraterrestrially (cosmic) and in the earth's atmosphere (cosmic ray) can be detected and studied. Interest in these possibilities stems from the weak interaction of neutrinos with matter, which means that they propagate essentially unchanged in direction and energy from their point of origin (except for the gravitational interaction with bulk matter, as in the case of light passing by a star) and so carry information which may be unique in character. For example, cosmic neutrinos can reach us from other galaxies whereas the charged cosmic ray primaries reaching us may be largely constrained by the galactic magnetic field and so must perforce be from our own galaxy. Our more usual source of astronomical information, the photon, can be absorbed by cosmic matter such as dust. At present no acceptable theory of the origin and extraterrestrial diffusion of cosmic rays exists so that the cosmic neutrino flux can not be usefully predicted. An observation of these neutrinos would provide new information as to what may be one of the principal carriers of energy in intergalactic space.

The situation is somewhat simpler in the case of cosmic-ray neutrinos: they are both more predictable and of less intrinsic interest. Cosmic-ray neutrinos can, in principle, be sampled at any point on the earth and so provide an overall picture of the interactions of cosmic-ray primaries and their charged progeny via the neutrino-producing reactions in the earth's atmosphere. First let us make a crude estimate of the flux and relevant cross sections. The flux (43) of primaries >5 Bev striking the earth's surface is $\sim 8 \times 10^{17}$ sec. $^{-1}$ or, assuming it to be uniform, $\sim 10^8$ hr. $^{-1}$ cm. $^{-2}$ Essentially all the primaries interact in the earth's atmosphere, producing pions, and then decay to produce a μ^\pm and $\nu, \bar{\nu}$. If the average pion multiplicity is taken as six we expect about four antineutrinos plus neutrinos per primary, allowing for the fraction of pions which is π^\pm . Allowing also for those which reach the detector by passing through the earth raises the flux by a factor of two giving $\sim 8 \times 10^8$ ($\nu + \bar{\nu}$)/hr. cm. 2 A reasonable average energy per neutrino is a few hundred Mev. The cross section per water molecule is, according to Figure 8, $\sim 3 \times 10^{-38}$ cm. 2 so that 1 event/day should be expected in 5000 cubic meters of H $_2$ O. These estimates could be modified by the existence of an intermediate boson. Even more sensitive to such a hypothesis is reaction 9. Glashow has estimated that a rate of from 0.1 to 2 muons might be produced per meter 2 per day depending on whether a boson of nucleon or kaon mass is the intermediate in the reaction. The cross section at resonance could in this event reach an unprecedented value (for neutrinos) of 10^{-32} cm. 2 ! If such a resonance exists, experimentalists can be expected to detect it. Aside from this possibility, the problem of detecting the cosmic ray neutrino appears to be a most formidable one.

V. NEUTRINOS AND COSMOLOGY

The lower-energy cosmic neutrino radiation may well hold a key to many questions of interest to cosmologists. For example, a measurement of the extraterrestrial flux of antineutrinos and neutrinos would bear on the presence or absence of antiworlds (44). A universe symmetric in this regard would be expected to produce equal numbers; and if despite local fluctuations in

favor of matter (as opposed to antimatter) some antineutrinos were detected, we could argue that somewhere in the universe the p, \bar{p} reaction and carbon cycles, etc., were operative, but with antimatter. Such reactions with matter produce neutrinos. Another interesting question has to do with the actual cosmic flux and direction of low-energy neutrinos and antineutrinos since this information would give the energy content of the ever increasing, noninteracting $\nu, \bar{\nu}$ reservoir.

Such low-energy cosmic neutrinos could arise in at least two ways: during the creation of the universe as given by the "big bang" theory, and as a result of current energy generation processes in stars. Attempts to describe the role of $\bar{\nu}, \nu$ in a big-bang evolutionary theory have been made by Alpher, Follin & Hermann (45). These authors indicate that such neutrinos have energies less than 100 kev because of the expansion of the universe and the associated adiabatic expansion of the neutrino "gas." Neutrinos of this low energy are undetectable by any known technique.

It is difficult to make estimates of the neutrino flux from all the current stellar energy sources, but it seems reasonable that it is significantly less than the solar flux because of the relative faintness of starlight compared with sunlight ($\sim 10^{-8}$). To elaborate, the fraction of energy escaping a star in the form of neutrinos relative to visible light may be taken as roughly constant. In the absence of obscuring matter, the neutrino flux could be calculated from the total intensity of starlight. It is estimated (45) that obscuration reduces the starlight by a factor of ~ 2.16 . Multiplying this by the intensity of starlight relative to solar light and by the solar neutrino flux ($4 \times 10^{10} \nu/\text{cm}^2 \text{ sec.}$, cf. below) we find an estimated cosmic neutrino flux of $\sim 10^3/\text{cm}^2 \text{ sec.}$

Experimental limits have been set on the $\nu, \bar{\nu}$ flux by the work of Davis (28) and by unpublished calculations of Cowan and Reines. If we assume the spectrum to be the same as that from fission fragments, then Davis' results can be interpreted to mean that the cosmic neutrino flux is $< 10^{12} \nu/\text{cm}^2 \text{ sec.}$ The antineutrino flux limit, again assuming the fission fragment spectrum, was determined from underground measurements to be $< 5 \times 10^{11} \bar{\nu}/\text{cm}^2 \text{ sec.}$ The flux figure stated is, of course, dependent on the spectrum assumed.¹⁷ For example, reaction 1 would not occur in an arbitrarily great flux of antineutrinos below the 1.8-Mev threshold energy.

Some improvement in sensitivity can be achieved by the simple expedient of going deep underground with current neutrino detecting techniques so as to reduce the flux of charged cosmic rays. An increase in sensitivity of

¹⁶ Information on the absorption of starlight within and between the galaxies may be found in Allen (46).

¹⁷ A more general way of expressing these limits is to quote the product of the flux F times the average cross section $\bar{\sigma}$ appropriate to the unknown spectrum:

$$\nu \text{ limit, } F\bar{\sigma} < 6 \times 10^{-33} \text{ sec.}^{-1}$$

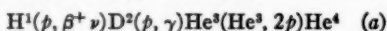
$$\bar{\nu} \text{ limit, } F\bar{\sigma} < 5 \times 10^{-33} \text{ sec.}^{-1}$$

an order of magnitude or greater can be expected for detectors so located.

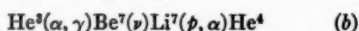
In view of the great uncertainties associated with the search for cosmic neutrinos, it is likely that the current upper limits on the flux will be reduced as a by-product of other work rather than as the result of a frontal assault on the problem.

SOLAR NEUTRINOS

The sun is a most copious source of neutrinos, $\sim 4 \times 10^{10} \nu/\text{cm}^2 \text{ sec.}$, and hence it is natural to inquire about the possibilities for their detection. These neutrinos arise from the thermonuclear reactions in the sun, currently believed to be described by the sequence (47)



or for the second and succeeding steps



where it is seen that these alternative routes all lead to the formation of He^4 from 4 H^1 and in process (a) 0.92 Mev, in (b) 1.4 Mev, and in (c) 14.1 Mev maximum-energy neutrinos are produced. The remote possibility that Li^4 might be particle stable (48) has been pointed out by Fowler (49) as a conceivable source $\sim 4 \times 10^{10}/\text{cm}^2 \text{ sec.}$ of higher-energy neutrinos. On the basis of measurements by Kavanagh (50) of the proton capture in Be^7 , Fowler (49) estimates the ν flux from (c) to be $\sim 10^7/\text{cm}^2 \text{ sec.}$

Because of the difference between ν and $\bar{\nu}$, solar neutrinos cannot be studied, whatever their energy, using reaction 1. The only direct counting approach which is hopeful in principle is one which uses the elastic-scattering reaction 7. This reaction could, for energetic neutrinos as given by (c), give events higher in energy than the background provided by natural radioactivity (e.g. gamma rays from K^{40}). However, a flux of $\sim 10^7/\text{cm}^2 \text{ sec.}$ is so ineffective that a detection volume in excess of 1000 cu. m. would be required for 10 counts/day. Detectors of this size are considered impractical for such low energies (a few Mev per event) as those involved.

The radiochemical technique of Davis could also be used in principle to rule against the presence in the sun of appreciable sources of higher-energy neutrinos. However, the probability of a negative result even with detectors of thousands or possibly hundreds of thousands of gallons of CCl_4 tends to dissuade experimentalists from making the attempt.

LITERATURE CITED

1. Lee, T. D., *Bull. Am. Phys. Soc.*, [II]5, 64 (1960)
2. Lee, T. D., and Yang, C. N., *Phys. Rev. Letters*, 4, 307 (1960)
3. Schwartz, M., *Phys. Rev. Letters*, 4, 306 (1960)
4. Pontecorvo, B., "Electron and Muon Neutrinos," *Rept. P-376 of Joint Inst. for Nuclear Research U.S.S.R.* (1959)
5. Pauli, W., Jr., Address to Group on Radioactivity (Tübingen, December 4, 1930) (Unpublished); *Rapports septièmes conseil phys. Solvay, Bruxelles, 1933* (Gautier-Villars, Paris, France, 1934)

6. Fermi, E., *Z. Physik*, **88**, 161 (1934)
7. Pauli, W., *Columbia Univ. Rept., CU-197* (1959) (Unpublished)
8. Allen, J., *The Neutrino* (Princeton Univ. Press, Princeton, N. J., 1958)
9. Bethe, H. A., and Peierls, R. E., *Nature*, **133**, 532 (1934)
10. Reines, F., and Cowan, C. L., Jr., *Phys. Rev.*, **92**, 830 (1953)
11. Reines, F., Cowan, C. L., Jr., Harrison, F. B., McGuire, A. D., and Kruse, H. W., *Phys. Rev.*, **117**, 159 (1960)
12. Marshak, R. E., and Sudarshan, G., *Padua-Venice Conf. Mesons & Newly Discovered Particles* (Italy, September 1957); *Phys. Rev.*, **109**, 1860 (1958)
13. Feynman, R. P., and Gell-Mann, M., *Phys. Rev.*, **109**, 193 (1958)
14. Nahmias, M. E., *Proc. Cambridge Phil. Soc.*, **31**, 99 (1935)
15. Bethe, H. A., *Proc. Cambridge Phil. Soc.*, **31**, 108 (1935)
16. Salam, A., *Nuovo cimento*, **5**, 299 (1957)
17. Cowan, C. L., Jr., and Reines, F., *Phys. Rev.*, **107**, 528 (1957)
18. Rosendorff, S. (Private communication, May 1960)
- 18a. Wightman, A. (Unpublished notes, 1951)
19. Lee, T. D., and Yang, C. N., *Phys. Rev.*, **105**, 1671 (1957)
20. Landau, L., *Nuclear Phys.*, **3**, 127 (1957)
21. Carter, R. E., Reines, F., Wagner, J. J., and Wyman, M. E., *Phys. Rev.*, **113**, 208 (1959)
22. Konopinski, E. J., *Ann. Rev. Nuclear Sci.*, **9**, 99-158 (1959)
23. Fermi, E., *Nuclear Physics* (Univ. of Chicago Press, Chicago, Ill., 1950)
24. Spivak, P. E., Sosnosky, A. N., Prokofiev, A. Y., and Sokoloff, V. S., *Proc. Intern. Conf. Peaceful Uses Atomic Energy, Geneva, 1955*, **2**, 33 (1956)
25. Reines, F., and Cowan, C. L., Jr., *Phys. Rev.*, **113**, 273 (1959)
26. Cowan, C. L., Jr., and Reines, F., *Phys. Rev.*, **107**, 1609 (1957)
27. Miller, C. E., Marinelli, L. D., Rowland, R. E., and Rose, J. E., *IRE Trans. Professional Group on Nuclear Sci.*, **NS-3**(4) (November 1956)
28. Davis, R., *Phys. Rev.*, **97**, 766 (1955); Davis, R., and Harmer, D. S., *Bull. Am. Phys. Soc.*, **[II]4**, 217 (1959); (Private communication, 1960)
29. Pontecorvo, B., *Natl. Research Council Canada Rept., P.D. 205* (November 20, 1946) (Unpublished)
30. Alvarez, L. W., *Univ. Calif. Radiation Lab. Rept., UCRL-328* (1949) (Unpublished)
31. Muehlhause, C. O., and Oleksa, S., *Phys. Rev.*, **105**, 1332 (1957)
32. Yukawa, H., *Proc. Phys.-Math. Soc. Japan*, **17**, 48 (1935)
33. Lee, T. D., and Yang, C. N., *Phys. Rev.*, **108**, 1611 (1957)
34. Kinoshita, T., *Phys. Rev. Letters*, **4**, 378 (1960)
35. Glashow, S., *Phys. Rev.*, **118**, 316 (1960)
36. Pontecorvo, B., *J. Exptl. Theoret. Phys. (U.S.S.R.)*, **37**, 1751 (1959)
37. Lee, T. D., Rosenbluth, M., and Yang, C. N., *Phys. Rev.*, **75**, 905 (1949)
38. Tiomno, J., and Wheeler, J. A., *Rev. Mod. Phys.*, **21**, 144 (1949)
39. Fermi, E., *Elementary Particles* (Yale Univ. Press, New Haven, Conn., 1951)
40. Cocconi, G. (Private communication, 1960)
41. Galbraith, W., *Extensive Air Showers* (Academic Press, Inc., New York, N. Y., 1958)
42. Hildebrand, R. H. (Private communication, 1960)
43. Leighton, R. B., *Principles of Modern Physics* (McGraw-Hill Book Co., New York, N. Y., 1956)
44. Goldhaber, M., *Science*, **124**, 218 (1956)
45. Alpher, R. A., Follin, J. W., and Hermann, R. C., *Phys. Rev.*, **92**, 1347 (1953)
46. Allen, C. W., *Astrophysical Quantities, Tables 121, 126* (Univ. of London Press, London, Engl., 1955)
47. Fowler, W. A., *Astrophys. J.*, **127**, 551 (1958)
48. Baskin, S., Kavanagh, R. W., and Parker, P. D. (Private communication, 1960)
49. Fowler, W. A. (Private communication, 1960)¹
50. Kavanagh, R. W. (Private communication, 1960)

¹ I am indebted to Professor Fowler for calling my attention to the work of Baskin, Kavanagh & Parker.

NUCLEAR INTERACTIONS OF HEAVY IONS¹

By A. ZUCKER

Oak Ridge National Laboratory, Oak Ridge, Tennessee²

INTRODUCTION

The field of heavy-ion reactions is a microcosm of nuclear reaction physics in general. Many types of experiments are performed: among them are studies of scattering, evaporation-type reactions, transfer reactions (called stripping or pickup in other fields), fission, Coulomb excitation, and the wide variety of work that is covered by the blanket heading of nuclear chemistry. This mélange of experimental work appears less disjointed when examined from an interpretive point of view. There are several underlying reasons for the use of heavy ions in nuclear investigations, as well as some common, if not yet realized, goals. A most important characteristic of a heavy ion (we limit the use of this word to ions of $Z > 2$) in a nuclear interaction is its classical character. By this we mean that the wave packet representing the ion extends over a distance which is small compared with some characteristic distance in a nuclear reaction. If we take for the characteristic distance that for the closest approach in a head-on collision, given by $Z_1 Z_2 e^2 / E$, and for the size of the wave packet the reduced wave length $\lambda = \hbar / \mu v$, then the collision may be considered classical if the ratio of these two distances $\eta = Z_1 Z_2 e^2 / \hbar v$ is large compared to unity. Here Z_1 and Z_2 are the atomic numbers of the nuclei involved, v is their relative velocity, and e the electron charge. By classical collision we mean one in which Coulomb orbits may be assumed for the colliding nuclei; this assumption simplifies calculations in many instances. A consequence of the classical collision picture is that information may be obtained about nuclear interaction distances and the diffuse nuclear surface.

A second basic property of heavy ions in their interactions with other nuclei is the possibility of obtaining very high values of angular momentum in the two-nucleus system. This is also related to the classical nature of the particles in that it is meaningful to localize in space a 160-Mev oxygen ion and state that in its interaction with gold, orbital angular momenta of $90\hbar$ may be important. These high angular momenta may be achieved with high-energy heavy ions, $E > 100$ Mev, and are expected to influence drastically the course of a nuclear reaction.

Finally, heavy ions are well suited for the investigation of compound nucleus reactions for two reasons. First, the low incident velocity favors amalgamation, rather than a knock-on process; and second, compound nucleus reactions are relatively easy to distinguish from direct processes. At energies less than about 50 Mev, heavy ions provide a useful tool for investigation of level densities and the statistical properties of nuclei in general.

¹ The survey of literature pertaining to this review was concluded in March 1960.

² Operated for USAEC by Union Carbide Corporation.

For higher energies, the interpretation of the experimental results in the light of some statistical model is chiefly concerned with the shapes of excitation functions and comparisons with other reactions going through the same compound nucleus.

We propose, in this article, to present principally experimental results and to show how they have been, or may be, interpreted theoretically. Our treatment of the theory will necessarily be sketchy, perhaps sufficient only to indicate its relation to the experimental results. The field of heavy-ion nuclear reactions is growing rapidly, and there exists a fairly large amount of tantalizing data whose significance is not yet clear. We are still in the discovery and classification stage in this field, and our fundamental understanding of the phenomena is incomplete.

In the limited space available, we can not possibly cover all the varied topics of heavy-ion physics. Chapters on scattering, transfer reactions and other direct processes, compound nucleus reactions, and fission are included. In making this choice we used two criteria. First, is the field clearly a province of heavy ions, i.e., does the use of heavy ions provide some new and in other ways unobtainable information? On this basis, we are not including the production of new isotopes by heavy ions or the study of energy levels by lithium bombardment of very light elements. In the second instance, it is true that these levels may not be found except via heavy-ion reactions, but the Li ion is here used as a projectile simply to make the levels experimentally observable, and not to elucidate the mechanism of heavy-ion reactions or to display those features of nuclear matter which become important when two complex nuclei collide. By the same reasoning we have excluded the discovery of new isotopes through heavy-ion reactions.

The second criterion is whether the subject forms an important portion of a much wider specialty and whether it would not be better to include it there. An example of this is the very interesting work on heavy-ion Coulomb excitation. It is our opinion that this material would gain a better and more interested audience if it were included in a review article on Coulomb excitation in general. Similarly, the subject of transuranium elements, their production and identification, is specialized and complicated enough to warrant a review of its own, which includes the heavy-ion experiments.

Finally, there is a whole class of atomic physics experiments with heavy ions which is not included here. These have to do with the energy loss of these ions as they pass through matter, the pickup and loss of orbital electrons, the response of scintillators to heavy ions, etc. As every nuclear physicist knows, the range-energy relations form the essential foundation on which sometimes fragile experimental results are built. There is no intention to slight this work, but it must be excluded on the grounds that it does not deal directly with the subject at hand. Table VI in the appendix lists those heavy-ion range-energy data which may prove useful to the nuclear physicist; Table VII in the appendix lists the work on the response of scintillators and surface barrier counters to heavy ions.

We will forego a historical introduction into the field of heavy-ion nuclear interactions, which may be obtained from Fremlin's (1) article. The interested reader may get a detailed picture of the state of the art as of 1958 from the *Proceedings of the Conference on Reactions Between Complex Nuclei* (2) and of its current state from a second conference on the same subject held in May 1960 (3). An outline, including a comprehensive bibliography, of the heavy-ion work in the U.S.S.R. was presented by Flerov in the Second United Nations Conference on the Peaceful Uses of Atomic Energy (4). A list of the laboratories at which heavy-ion experiments are now being performed is shown in Table I. To this list one should add every tandem Van

TABLE I
LABORATORIES ENGAGED IN HEAVY-ION WORK

Laboratory	Particles Available	Accelerator	Energy
Lawrence Radiation Laboratory	C, N, O, Ne	Linear accelerator	10 Mev/nucleon
Yale University	C, N, O, Ne	Linear accelerator	10 Mev/nucleon
Nobel Institute, Stockholm	C, N, O, Ne	Cyclotron	10 Mev/nucleon
Institute for Atomic Energy, Moscow	C, N, O	Cyclotron	60-130 Mev
Oak Ridge National Laboratory	N	Cyclotron	28 Mev
Physico Technical Institute, Leningrad	N, Ne	Cyclotron	1.1 Mev/nucleon
University of Minnesota	Li	Van de Graaff	3.2 Mev
University of Chicago	Li	Van de Graaff	2 Mev
Chalk River Laboratory	C, O	Tandem accelerator	up to 40 Mev

de Graaff accelerator as it comes into existence. The first such installation at Chalk River has already demonstrated its excellent performance as an accelerator of carbon and oxygen in the 10- to 40- Mev region. The cyclotrons at the University of Birmingham and at Saclay have also been used for the acceleration of heavy ions. At present, however, it appears that the nuclear research at these two cyclotrons is concerned chiefly with light-particle reactions.

Theoretical investigations into heavy-ion nuclear interactions are, of course, not predicated on the existence of large accelerators and may be done anywhere. We will only mention here that the whole field owes a great deal to G. Breit and his collaborators (5) who were the first to point out many of the characteristics of heavy-ion reactions and what may be learned from them.

In this section, we present some of the approaches to interpretation of the results of heavy-ion scattering experiments. We also present typical experimental results and compare them with theoretical predictions. A critical evaluation and exposition of scattering theory is beyond the scope of this article. We therefore outline a few of the theories and show how various authors attempt to analyze the experimental data with the aid of these theories. Comments will be made concerning the range of validity of different scattering theories.

Elastic scattering of heavy ions provides an excellent example of the validity of semiclassical approximations. It shows what information about nuclei can be obtained in this way, and it also shows the limitations of this approach. We shall see that alternative approaches such as optical model calculations and phase shift analysis can fit the data as well as semiclassical approaches do. In cases where the latter break down, the optical model was found to give satisfactory agreement.

A word now about the experimental techniques used in measuring elastic scattering. The simplest method is to use a detector such as a photographic emulsion, scintillation counter, or barrier counter to detect elastically scattered ions. These are distinguished by their range or pulse height from other reaction products such as protons or α particles; however, it is more difficult to distinguish them from inelastic events or transfer reactions. Ideally one may achieve this with a detector of very high resolution; but in practice, the detectors have only had moderate energy resolution, 2 per cent at best, and one had to rely on the assumption that elastic scattering has a much larger cross section than any other event that might be experimentally confused with it. This assumption is certainly valid at small angles where the ratio of the elastic-scattering cross section (σ) to the Coulomb scattering cross section (σ_c) is not much smaller than one. However, as the angle increases, and when σ/σ_c decreases to the order of 0.1, the elastic peak usually disappears or is difficult to resolve from other reactions.

To study the elastic-scattering cross section at relatively large angles, where $\sigma/\sigma_c < 0.1$, the Oak Ridge group used a coincidence scheme for identifying the elastic events and separating them from inelastic and transfer reactions. In this scheme one counter is used to detect the scattered particle, and a second counter, in coincidence, counts the recoiling nucleus. From the angles of the two counters and from pulse-height information in each, the nature of the scattering event may be determined. A detailed exposition of this technique appears in a paper by Halbert & Zucker (6).

THE SHARP-CUTOFF MODEL

The scattering cross section may be written quite generally as

$$\sigma(\theta) = |f(\theta)|^2 \quad 1.$$

where $f(\theta)$ is the scattering amplitude given by

$$f(\theta) = \frac{1}{2ik} \sum_{l=0}^{\infty} (2l+1)(e^{2i\delta_l} - 1)P_l(\cos \theta) \quad 2.$$

Here δ_l is the phase shift, and $P_l(\cos \theta)$ the Legendre polynomial of order l . Blair (7) has suggested a semiclassical approximation whereby the elastic-scattering amplitude is the amplitude for Coulomb scattering less the contribution to Coulomb scattering of all outgoing waves up to and including l' . The differential cross section is

$$\sigma(\theta) = \left| \frac{-\eta}{2k \sin^2 \theta/2} e^{-i\eta \log \sin^2 \theta/2} e^{2i\delta_0} - \frac{1}{2ik} \sum_{l=0}^{l'} (2l+1)e^{2i\delta_l} P_l(\cos \theta) \right|^2 \quad 3.$$

The δ_l 's here are the phase shifts for pure Coulomb scattering. In this view, a nucleus is completely absorbing up to a certain distance characterized by l' , beyond which there is no absorption. This is the sharp cutoff from which the model has its name. The model has but one parameter: only the value of l' is at our disposal to fit the data. If a fit with experimental data is achieved, one obtains an interaction distance R from the semiclassical turning point

$$l'(l' + 1)\hbar^2 = 2\mu R^2(E - E_B) \quad 4.$$

Here μ is the reduced mass of the incident ion, E its center-of-mass energy, and E_B the Coulomb barrier given by $E_B = Z_1 Z_2 e^2 / R$. The value of R may be related to the usual nuclear radius parameter r_0 by $R = r_0(A_1^{1/3} + A_2^{1/3})$. Thus one may obtain values of r_0 from elastic scattering of heavy ions and compare them with values of r_0 obtained from other sources.

A criterion for the validity of the Blair model is that $\eta > 1$. It is a peculiarity of this formalism that the cross section begins to oscillate if the ratio of the elastic cross section to the Coulomb cross section is so small that σ/σ_c approaches $1/\eta$. The experimental data usually depart from the theoretical prediction at this point; normally the data do not follow the oscillations but continue to fall off smoothly.

In heavy-ion scattering experiments, the targets employed are often relatively thick. Because of their short ranges, these ions experience considerable energy losses in targets which would be considered thin for protons or deuterons. At low energies, especially, intensity considerations have made it necessary to employ targets ~ 1 Mev thick. The effect of target thickness on comparisons with the Blair model is twofold: (a) the energy dependence of the cross section, i.e., dependence on k in Equation 3; and (b) the variation of l' through the target, from the dependence on E in Equation 4. In N-Al scattering (8), numerical investigations showed that the effect of (a) on the Blair calculation is minimal and may be neglected, while the effect of (b) is appreciable, should be taken into account, and usually results in a somewhat smoother cross section at large angles. This procedure is one in which cross sections are added and is not equivalent to the suggestion of Wall, Rees & Ford (9) that a rounded Blair model with weighted amplitudes might fit the data better than the sharp cutoff at l' .

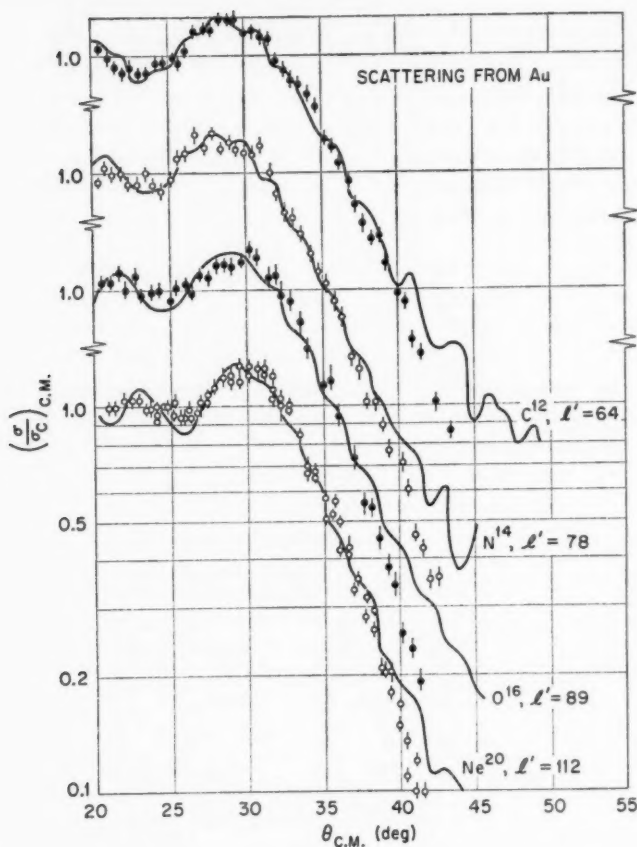


FIG. 1. The ratio of the elastic- to the Coulomb scattering cross section for C^{12} , N^{14} , O^{16} , and Ne^{20} scattered from gold at $\sim 10 \text{ Mev/nucleon}$. The solid lines are the results of sharp-cutoff calculations, with the appropriate l' values indicated in the figure (13).

The earliest work on elastic scattering of heavy ions was $\text{N}^{14} - \text{N}^{14}$ scattering measured by Reynolds & Zucker (10). They applied the then new Blair model to heavy-ion scattering and modified it for the case of identical particles. Very good agreement with the experimental results was obtained. Since then the Blair model has been used with more or less success to fit the elastic scattering of carbon on gold (11); nitrogen on beryllium (6), carbon (12), and aluminum (8); as well as carbon, nitrogen, oxygen, and neon on gold and bismuth (13). The last paper in particular reports on scattering of four projectiles by two heavy nuclei, and all Blair model fits are consistent with $r_0 = 1.46f$. Figure 1 shows the experimental results of this work on Au, along with the theoretical curves.

Table II lists elastic-scattering experiments which have been successfully analyzed with a sharp-cutoff calculation. The table also gives the relevant values of η and l' , as well as r_0 calculated from Equation 4 and the definition of r_0 as given. In general, it has been found that the Blair model provides a good fit to experimental data for heavy-ion scattering when $\sigma/\sigma_e > 1/\eta$. This confirms similar conclusions deduced from α -particle scattering (14). The N-Be, N-C, and N-Al experiments at low energies (~ 27 Mev) substantiate this conclusion. Particularly the N-Al scattering shows clearly how the

TABLE II
LIST OF EXPERIMENTAL INVESTIGATIONS OF HEAVY-ION ELASTIC
SCATTERING WHICH SHOW AGREEMENT WITH THE
SHARP-CUTOFF MODEL

Target	Projectile	Incident Energy (lab)	η	l'	r_0	Ref.
N ¹⁴	N ¹⁴	21.7	6.2	6	1.66	(10)
Al ²⁷	N ¹⁴	27.3	10.3	11	1.68	(8)
Au ¹⁹⁷	C ¹²	73.6 to 118.3	30.1 to 23.8	29 to 63	1.47	(11)
Au ¹⁹⁷	C ¹²	121.4	23.5	64	1.45	(13)
Au ¹⁹⁷	N ¹⁴	145.5	27.0	78	1.47	(13)
Au ¹⁹⁷	O ¹⁶	164.1	31.1	89	1.47	(13)
Au ¹⁹⁷	Ne ²⁰	207.6	38.6	112	1.47	(13)
Bi ²⁰⁹	C ¹²	124.0	24.4	64.5	1.45	(13)
Bi ²⁰⁹	N ¹⁴	145.4	28.4	77	1.45	(13)
Bi ²⁰⁹	O ¹⁶	164.0	32.6	89.5	1.48	(13)
Bi ²⁰⁹	Ne ²⁰	209.6	40.3	113	1.45	(13)

Blair model reproduces the data at small angles and then begins to oscillate. The elastic scattering of O¹⁶ from Au, Ni, Al, and C by McIntyre and collaborators (15) extends over too small an angular region for any comparison with the Blair model.

Another observation regarding the validity of a semiclassical approach was made by McIntyre *et al.* (15). They assume that a smooth dropoff in the elastic-scattering angular distribution characterizes a situation in which semiclassical approximations are valid, and contrariwise the appearance of diffraction patterns shows that they are not valid. Then they find that $\eta = 5$ seems to define the borderline: smooth curves are obtained if and only if $\eta > 5$. This seems to hold whether the projectile is an α particle or a heavy ion. On the other hand the criterion of "classically corresponding orbits" does not seem to be a good guide whether a particular scattering cross section will display diffraction patterns or not.

McIntyre, Wang & Becker (16) have extended the sharp-cutoff theory so as to include up to five adjustable parameters, depending on the demands

of the problem. In this way they have been able to fit 40-Mev α -particle scattering from Ag with four parameters. Their formulas have not been used to fit any heavy-ion scattering. One important property of this formalism is that it includes nuclear surface parameters as well as nuclear radius parameters.

RAINBOW SCATTERING

Recently, Ford & Wheeler (17) developed a semiclassical approach to elastic scattering which demonstrates the analogy between particles scattered from nuclei and light waves scattered from water droplets. In a classical rainbow scattering situation, the deflection function $\Theta(b)$ has a maximum or minimum and is therefore multiple-valued with respect to the impact parameter b . The deflection function $\Theta(b)$ is the angle of deflection, in a classical sense, which is a function of angular momentum (J) or of the impact parameter (b). The scattering cross section is then a sum of contributions from different branches and is given by

$$\sigma_{el}(\theta) = \sum_i (\sigma_{el})_i = (\sin \theta)^{-1} \sum_i b_i \left| \frac{d\Theta}{db} \right|_i \quad 5.$$

Here $b_i(\theta)$ is one of the impact parameters associated with the scattering angle θ , and $|d\Theta/db|_i$ is evaluated at $|\Theta| = \theta$ in the branch i . It can be seen from Equation 5 that $\sigma_{el}(\theta)$ has a singularity when $\partial|\Theta|/\partial b = 0$, i.e., at the rainbow angle $\theta = \theta_r$, corresponding to an extremum in Θ . It is precisely this singularity that is responsible for the appearance of rainbows in meteorological optics.

In the semiclassical treatment, Ford & Wheeler start with Equation 2 and make the following approximations: (a) The phase shifts δ_l are approximated by the JWKB phase shifts. In this approximation the classical deflection function Θ has the property $\Theta(l) = 2d\delta_l/dl$. (b) Every Legendre polynomial is replaced by its asymptotic expression for large l . (c) The sum is replaced by an integral. The resultant semiclassical cross section σ_{s-e} has a maximum rather than a singularity at θ_r .

For Θ close to θ_r the deflection function can be approximated by the expansion

$$\Theta(l) = \theta_r - q(l - l_r)^2 \quad 6.$$

where l_r is the angular momentum associated with the classical scattering angle θ_r . Evaluating the phase shifts from this relation, the semiclassical scattering cross section is

$$\sigma_{s-e}(\theta) = \lambda^2(l + 1/2)(2\pi/\sin \theta)(q^{-2/3})Ai^2(x) \quad 7.$$

Here $Ai(x)$ is the Airy integral, and $x = q^{-1/3}(\theta - \theta_r)$. The ratio of σ_{s-e} to the Coulomb cross section is

$$\sigma_{s-e}(\theta)/\sigma_c(\theta) = [2(\sin^3 \theta_r/2)/\eta q^{2/3}]2\pi Ai^2[q^{-1/3}(\theta - \theta_r)] \quad 8.$$

The rainbow scattering theory is a two-parameter model which assumes

that a nucleus has an attractive central region and a nonabsorbing refractive surface layer characterized by the parameter q . The nuclear radius is characterized by θ_r . For the semiclassical approximation to be valid, several conditions must be met. First, the value of the orbital angular momentum l for a grazing collision must be large compared to 1. The change in l and the change in the phase shift δ_l through the surface region must also be large compared to 1. The following quantities are useful in estimating the properties of l and δ_l :

$$\Delta l = \sqrt{\theta_r/q} \quad 9.$$

$$\Delta \delta_l = \theta_r/2\Delta l - \theta_r/2 \quad 10.$$

Figure 2 shows the N-Al data (8) as dots, the sharp-cutoff calculation as a dashed line, and the rainbow calculation as a solid line. It can be seen that the former fits the experimental results well to $\sim 90^\circ$ c.m., including a qualitative fit of the oscillations about $\sigma/\sigma_c = 1$ from 35° to 55° c.m. The rainbow theory, however, reproduces the data very well from 95° to 130° c.m.

A value of the interaction distance R (and subsequently r_0) is obtained from the rainbow angle $\theta_r = 94^\circ$ by using the equation of the Coulomb orbit,

$$R = \eta\lambda(1 + \csc \theta_r/2) \quad 11.$$

A "surface thickness" ΔR may be obtained from the second free parameter q and the relation $q = \theta_r/(k\Delta R)^2$. In the N-Al experiment the values thus obtained are $r_0 = 1.59f$ and $\Delta R = 0.83f$. The sharp-cutoff calculation yields a

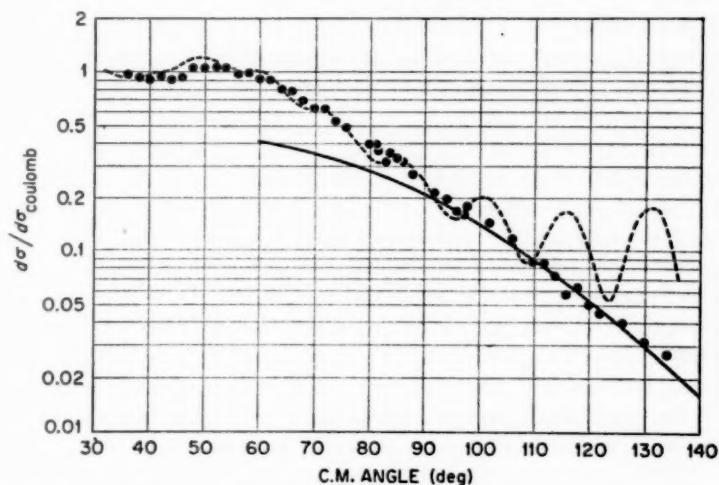


FIG. 2. The ratio of the elastic- to the Coulomb scattering cross section for N¹⁴ from Al²⁷ at 27.3 Mev. The dashed line is a sharp cutoff calculation (85% $l' = 11$, and 15% $l' = 10$). The solid line is the result of a rainbow scattering calculation $\theta_r = 94^\circ$ and $q = 0.30$ (8).

value of $r_0 = 1.68f$. It is noteworthy that the two values of r_0 are in fairly good agreement. Much more experimental evidence is needed before the physical significance of ΔR can be ascertained.

OPTICAL MODEL AND PHASE SHIFT ANALYSIS

In the past few years, the elastic scattering of protons and neutrons was successfully interpreted as scattering from complex potentials. The early potentials were square wells, but much better fits with the experimental data were obtained if the well was rounded by a so-called Saxon rounding factor. Recently, agreement with α -particle and deuteron elastic scattering was also found. The complex-potential view of the nucleus is now commonly referred to as the optical model.

The first attempt to fit heavy-ion scattering by the optical model was by Porter (18), who was able to fit the N-N scattering data (10) with a Saxon-type potential. He found that the real part of the nuclear phase shift contributes little to the scattering cross section, and the imaginary part serves to provide an absorptive mechanism for the process.

More recently, fairly good fits were obtained with Saxon-type potentials very similar to those used for nucleon scattering. In the N-C scattering (12), for example, such a fit was found with a real potential $V = 45$ Mev, an imaginary potential $W = 6$ Mev, a Saxon rounding factor $a = 0.65f$ and a nuclear radius parameter $r_0 = 1.32f$. Better fits (19) were obtained later, especially when volume absorption was replaced by a surface absorption in the form of a gaussian with the width b . Figure 3 shows the results of such an optical-model analysis. From these analyses it appears that the optical model provides a correction to the sharp-cutoff model whereby the step function in the absorption is replaced by a more gentle change and is equivalent to a rounding of the cutoff.

As in the case of rainbow scattering, the full significance of the optical-model calculations must await further developments, to see how the parameters change with particle energy or target nucleus. Even if our understanding is still incomplete, it is interesting that the optical model has found an application in heavy-ion scattering and that the potentials are not very different from those obtained from nucleon scattering.

Another method was used by Turner, McIntosh & Park (20) to fit N-N scattering at 21.7 Mev. They consider only two channels open: a scattering and a reaction channel. The magnitude of $S_l(R)$, the reaction matrix element of the scattering matrix, is estimated by interpolation from complete absorption at small l , to large l where $S_l(R)$ is proportional to the square of the regular Coulomb wave function. The unitary property of the S matrix is used to obtain the magnitude of the elastic part of the scattering matrix $S_l(sc)$. A set of phase shifts is then obtained which reproduces the differential elastic-scattering cross section. The errors in the data are sufficiently large, however, so that no clear-cut evidence exists on whether this point of view

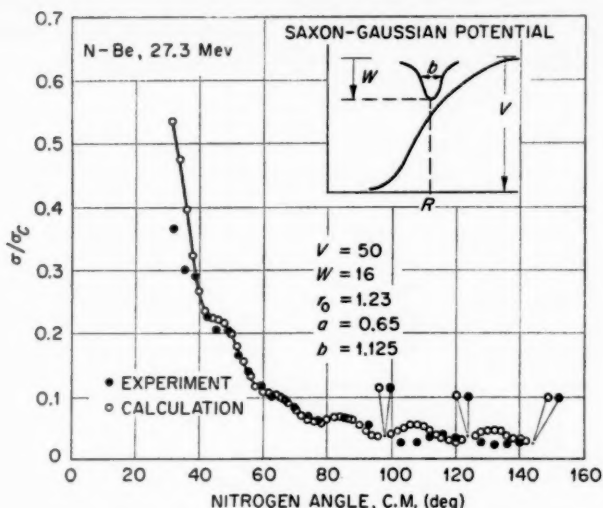


FIG. 3. The ratio of the elastic- to the Coulomb scattering cross section for N^{14} on Be^9 at 27.3 Mev. The black dots are experimental points and the open circles the results of an optical-model calculation. The optical parameters are given in the figure along with a pictorial representation of the complex potential.

gives better agreement than the Blair model. In any event the aim of this treatment is not really to compete in the "agreement with the data" race; rather it shows that phase-shift-type calculations can be used to interpret the results of collisions of strongly absorbing systems such as two nitrogen nuclei.

TRANSFER REACTIONS

TERMINOLOGY

In heavy-ion nuclear physics, the term "transfer reaction" is used for nuclear reactions where one or more particles are transferred from one nucleus to the other. The simplest such reaction is single transfer which implies that one particle, for example a neutron, was transferred. The terms neutron transfer and proton transfer are used as two varieties of single transfer. Double transfer means that two particles, e.g. two neutrons or two protons, have been transferred from one nucleus to the other. Multiple transfer is then the transfer of many particles, all in one direction. Exchange transfer is defined as a reaction in which a single particle transfers from nucleus a to nucleus b and at the same time another particle goes from b to a . Reactions in which more than one nucleon is exchanged we call complex transfer. Although many terms are defined here, they do not cover all possibilities unambiguously. The problem, perhaps only a semantic one, remains whether the transfer of a deuteron should be called a double transfer or a

single transfer. To avoid confusion we will use terms such as deuteron and alpha transfer to cover these cases.

SINGLE TRANSFER

The single-transfer reaction is the most thoroughly investigated of all heavy-ion reactions. It was first identified by Reynolds, Scott & Zucker (21), and at about the same time it was found by Chackett & Fremlin (22). The experimental material collected on these reactions consists chiefly of excitation functions and a few angular distributions. The principal experimental method is based on the fact that N^{14} , by losing a neutron in a transfer reaction, is transmuted into radioactive 10-min. N^{13} . This 10-min. activity is widely used to identify the reaction, and N^{13} recoil atoms are used for angular distribution studies. An example of a neutron-transfer reaction is



In most cases, only N^{13} is observed and the production of the residual nucleus merely inferred. In one case, however, $Mg^{26}(N^{14}, N^{13})Mg^{27}$, both residual nuclei are conveniently radioactive and it was shown (23) that near the barrier, at least, the reaction does proceed as indicated above. The reaction mechanism appears indeed to be the transfer of a neutron, rather than fission of a compound nucleus or evaporation of light fragments from it. The transfer mechanism was first proposed on general nuclear reaction considerations and has since been confirmed by studies of angular distributions and energy distributions (22; 24 to 26).

The neutron-transfer reaction has several fairly well established properties. Below the Coulomb barrier, the excitation function decreases more slowly with decreasing energy than the excitation functions for compound nucleus formation. This is to be expected for a reaction which takes place on the nuclear surface and does not require the formation of a compound system. Total cross sections for neutron-transfer reactions seem to level off at values of the order of tens of mb. Finally, it was somewhat unexpected to find that the cross sections were strongly Q dependent. A semblance of a systematic behavior of transfer reactions was presented by Halbert *et al.* (23) who plotted the total cross section as a function of E^* , which is defined by

$$E^* = E_{c.m.} - E_B + Q \quad 12.$$

Here Q has the usual meaning of the energy release in the reaction. The physical significance of E^* is that it represents the energy available to the two nuclei at the moment immediately after the transfer has occurred. As the authors point out, this implies a classical picture which takes into account neither the transfer mechanism nor the quantum mechanical nature of the orbits. Breit has suggested (27) that it may be more meaningful to plot σ vs. E^{**} , where $E^{**} = E^* - \frac{1}{2}Q$. As the energy of the incident ion is increased far above the barrier, the difference between E^* and E^{**} becomes insignificant.

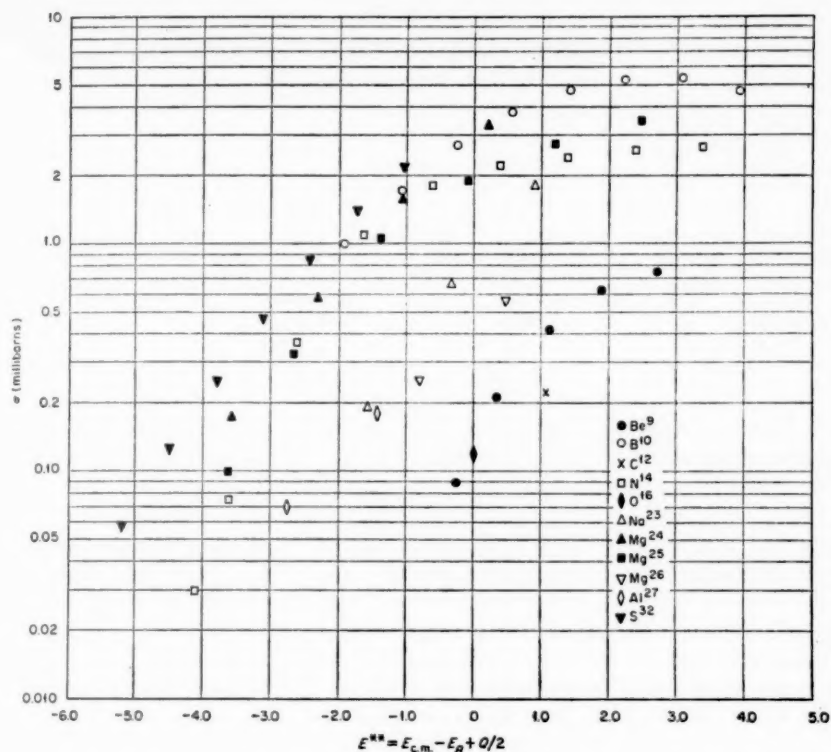


FIG. 4. Total neutron-transfer cross sections of the type (N^{14} , N^{13}) for 11 light elements plotted as a function of $E^{**} = E_{c.m.} - E_B + Q/2$, where $E_{c.m.}$ is the incident kinetic energy in the center-of-mass system and E_B is the barrier energy (28).

Figure 4 shows such a plot (28) of σ as a function of E^{**} . This, as well as a similar plot of σ vs. E^* (23), shows the general trends in neutron-transfer reaction excitation functions. It is evident that the nuclei fall into distinct groups; however, the significance of this behavior and its explanation are not obvious at this time.

The angular distributions of neutron-transfer reactions of the type (N^{14} , N^{13}) have been measured in several cases, listed in Table III. In all instances the recoil N^{13} was caught on strips placed to accept all or half the azimuthal angle at any polar angle. The amount of N^{13} was determined by beta counting or by measurement of positron annihilation radiation with a scintillation spectrometer. In all of these experiments, a peaked angular distribution was obtained. We may consider a transfer reaction to be an elastic-scattering event modified by the passage of a neutron from one nucleus to the other. In this view the appearance of the peak indicates that neutrons

TABLE III

SUMMARY OF ANGULAR DISTRIBUTION MEASUREMENTS FOR NEUTRON-TRANSFER REACTIONS OF THE TYPE (N^{14} , N^{13})

Target Nucleus	Incident Energy Mev(lab)	r_0 (fermis)*	Ref.
N^{14}	26	—	(29)
Mg^{25}	27.2	1.60	(24)
Ni	61	1.67	(25)
Ag	72	1.46	(25)
Ag	140	1.45	(2)
Sn	68	1.59	(25)
Au^{197}	74 to 142	1.54	(26)

* The value of r_0 is calculated from $r_0 = R'_{\max}/(A_1^{1/3} + A_2^{1/3})$, and where R'_{\max} is the value of R' for which the distribution $d\sigma/dR'$ is a maximum. N^{14} is the incident ion in all cases.

are not transferred for distant collisions (small angles) and that for very close collisions the compound nucleus formation competes successfully with the transfer process. The position of the maximum depends on the energy of the incident ion and can be most simply interpreted (26) by plotting the differential cross section $d\sigma/dR'$ as a function of the classical distance of closest approach $R' = (Z_1 Z_2 e^2 / 2E)(1 + \csc \theta/2)$. The maximum in the distribution will give the distance R at which most of the transfers occur. It should be noted that $d\sigma/dR' = (d\sigma/d\omega) \sin^3 \theta/2$ and that the effect of this way of analyzing the data is to push the peak of the angular distribution out to larger angles. Again we make tacit use of the premise that the orbits of heavy ions before and after transfer are sufficiently well described by classical Coulomb orbits and that the discontinuity produced by the act of neutron transfer does not influence the orbit appreciably. The net result of this interpretation is that one obtains a value of R' for which $d\sigma/dR'$ is a maximum, and one may interpret this R' as a nuclear interaction distance, from which r_0 may be calculated by $r_0 = R'_{\max}/(A_1^{1/3} + A_2^{1/3})$.

Table III lists the neutron-transfer reactions in which angular distributions were measured, as well as the values of r_0 deduced from replotting data, where necessary, as $d\sigma/dR'$ vs. R' . It would seem that above the barrier, at least, transfer reactions take place when nuclei are separated by distances corresponding to $r_0 \sim 1.5f$, the same value of r_0 which is obtained from nuclear reactions, and close to the one usually derived from neutron work. The differential cross section of the reaction $N^{14}(N^{14}, N^{13})N^{16}$, with both residual nuclei in the ground state, has a peak in the distribution $d\sigma/d\omega$ vs. $\theta_{c.m.}$ at $\theta_{c.m.} = 28^\circ$, as measured by Toth (29). On account of the identity of the two reacting nuclei, r_0 cannot be determined unambiguously, and no value for it is given in Table III.

A word now about the importance of excited states in the neutron-transfer reaction picture. One inherent advantage N^{13} has in these investigations is that all its excited states are unstable against proton emission, so that whenever N^{13} is observed it is sure to have been produced in the ground state. The extent to which the residual nucleus was left in an excited state is most readily determined from the range spectrum of N^{13} recoils. In the work of Halbert & Zucker (24) at 27 Mev, it was found that Mg^{26} was left excited to states as high as 7 Mev in an appreciable number of cases. Hubbard & Merkel (2) find that for 140-Mev N^{14} on Al^{27} , the residual nucleus is regularly excited to 20 or 30 Mev. With 123-Mev nitrogen on gold, McIntyre *et al.* (26) found that excited states in the residual nucleus are distributed around a most probable value of 5-Mev excitation, and contribute appreciably up to 14 Mev. Toth (29) in his experiments on the reaction $N^{14}(N^{14}, N^{13})N^{15}$ at lower energy was able to distinguish transitions to the ground state of N^{15} . He found that most of the reaction does indeed proceed to the ground states of both nuclei, and his angular distribution was measured for processes leading to these states only.

The theory of neutron-transfer reactions was first developed by Breit & Ebel (30), who consider a simple tunneling of the neutron from one nucleus to the other. They show that the angular distribution for this reaction should have the form

$$\sigma(\theta) \sim [1/\sin^3(\theta/2)] \exp(-\alpha R') \quad 13.$$

The quantity R' was defined before, and $\alpha = (2mI/\hbar^2)^{1/2}$, where I is the binding energy of the neutron being transferred, and m its mass. This expression for $\sigma(\theta)$ fits the leading edge of the angular distribution (24) for $Mg^{26}(N^{14}, N^{13})Mg^{26}$, and it agrees with the general trend of the data (26) for large R' in the distribution $d\sigma/dR'$ for $Au^{197}(N^{14}, N^{13})Au^{198}$ (large R' corresponds to small c.m. angles), especially at low energies.

The total cross section derived by Breit & Ebel is

$$\sigma_T = \frac{\pi^2}{2} \left(\frac{\hbar}{Mv} \right)^2 \left(\frac{1}{\alpha^2 \lambda_1 \lambda_2} \right) \left(\frac{\alpha a_1}{1 + \alpha a_1} \right)^2 \left(\frac{\alpha a_2}{1 + \alpha a_2} \right)^2 \cdot \exp[-2\alpha(2a' - a_1 - a_2)] \quad 14.$$

where a_1 and a_2 are the radii of the two nuclei, and λ_1 and λ_2 are related to the logarithmic derivatives of the radial part of the neutron wave function, and $a' = Z_1 Z_2 e^2 / (2E) = R' / [1 + \csc(\theta/2)]$. The exponential part of Equation 14 was derived for the neutron transfer between point nuclei by Lifshitz (31) as being

$$\sigma_T \sim \exp[-2a'2\alpha] \quad 15.$$

The exponential part of Equation 14 reduces to this if $a_1 = a_2 = 0$. Goldansky's (32) extension of Lifshitz's work for the case of an exchange transfer will be treated in the next section.

The cross section σ_T calculated according to Equation 14 does not agree with the measured values, and this induced Breit & Ebel to include the possibility of virtual Coulomb excitation as preceding the transfer process (33).

In this way the total cross sections are brought into reasonable agreement with experiment, but the calculated angular distributions do not reproduce the observed ones. On the whole, Breit (27) questions the possibility of deriving the values of reduced widths for states produced by transfer reactions. The reader is referred to Breit's article (27) for a thorough discussion of theoretical aspects of neutron-transfer reactions.

OTHER TRANSFER REACTIONS

After the early work at low energy in which single-transfer reactions were studied, higher-energy accelerators made possible the investigation of multiple- and complex-transfer reactions. These may occur also at low energies, where energetically possible, but their very negative Q values and consequently low cross sections make them difficult to observe with techniques currently used in this kind of research.

A two-neutron-transfer reaction to N^{14} produces 7.5-sec. N^{16} . The appearance of this isotope in nitrogen-induced reactions in LiF, Al, and Cu, and the fact that the N^{16} had much longer range than evaporation products could be expected to possess, led Karnaukhov *et al.* (34) to the conclusion that a two-neutron transfer was indeed taking place. They found quite small cross sections for this reaction in the energy interval from 92 to 55 Mev (the thickness of the targets caused this energy spread). They also found the yields proportional to the binding energy of the last two neutrons in the target nucleus. In this way they conclude that N^{16} produced in LiF is overwhelmingly due to the Li. Karnaukhov *et al.* give a cross section for the reaction in Li only. We have taken this cross section, multiplied it by the ratio of the yields per atom in Cu and Al to Li, and arrived at cross sections for these target elements which are included in Table IV.

Pinajian (35) investigated the (p, n) exchange-transfer reaction $Al^{27}(N^{14}, O^{14})Mg^{27}$ at 27-Mev incident energy. Actually the cross section for this reaction is so low that he was able to measure a thick-target yield only, but a fairly reliable estimate of the yield as a function of energy allowed him to conclude that the cross section is $2 \pm 1 \mu b$.

This reaction is very similar to the neutron-exchange reaction treated theoretically by Goldansky (32). He proposes that such reactions may lead to the population of levels with very high spin but with low excitation. Goldansky has extended Lifshitz's treatment (31) for point nuclei to take into account the exchange of two neutrons. He finds that the cross section for this process is proportional to

$$\exp [-2a'^2(\alpha_1 + \alpha_2)] \quad 16.$$

where $\alpha_1 = (2mI_1/\hbar^2)^{1/2}$ and similarly $\alpha_2 = (2mI_2/\hbar^2)^{1/2}$, and I_1 and I_2 are the binding energies of the neutrons in the two nuclei. Furthermore, Goldansky estimates that the cross section for a neutron-exchange reaction should be between 1 and 10 μb . The experimental result of 2 μb is in good agreement with this prediction.

TABLE IV

MEASURED CROSS SECTIONS FOR MULTIPLE- AND COMPLEX-TRANSFER REACTIONS

Reaction	Nature of Transfer	Incident Ion Energy (lab) (Mev)	Cross Section, mb	Ref.
Al ²⁷ (N ¹⁴ , N ¹⁶ *)	2n	55-92†	0.01	(34)
Cu(N ¹⁴ , N ¹⁶)	2n	55-92†	0.15	(34)
Al ²⁷ (N ¹⁴ , O ¹⁴)Mg ²⁷	p, n exchange	27	0.002	(35)
O ¹⁶ (N ¹⁴ , F ¹⁸)C ¹²	α or deuteron (or both)	26	1.5	(37)
Al ²⁷ (O ¹⁶ , N ¹³)	{ p2n or α , p exchange }	10/nucleon‡	4.0	(38)
Cu(O ¹⁶ , N ¹³)		10/nucleon‡	4.7	(38)
Sn(O ¹⁶ , N ¹³)		10/nucleon‡	1.4	(38)
Sn(N ¹⁴ , C ¹¹)		10/nucleon‡	4.2	(38)
Al ²⁷ (O ¹⁶ , C ¹¹)	{ 2p3n or αn }	10/nucleon‡	2.3	(38)
Cu(O ¹⁶ , C ¹¹)		10/nucleon‡	2.9	(38)
Sn(O ¹⁶ , C ¹¹)		10/nucleon‡	0.8	(38)

* No residual nucleus is given where its identity was not reasonably certain. In any case, the exact nature of the unobserved residual nucleus is not of primary concern here.

† Cross section integrated over this energy range.

‡ Thick-target cross sections obtained with 10 Mev/nucleon incident energy (cf. reference).

In the nitrogen bombardment of Li⁷ at 15.6 Mev (lab), Alkharov and collaborators (36) observed F¹⁸ and N¹⁶. They deduce from the high yield of F¹⁸ and from the yields of F¹⁸ in other nitrogen-induced reactions that the cross section for F¹⁸ production, at an energy equal to the Coulomb barrier, increases as the binding energy of the α particle in the target nucleus decreases, and they conclude that this indicates that F¹⁸ may be formed as a result of the capture of an α particle by the nitrogen ion. Because F¹⁸ in the nitrogen bombardment of Li and some other targets can be made by evaporation of light fragments from a compound nucleus, it is not clear what fraction of it, if any, should be ascribed to an alpha-transfer mechanism. In another case, that for N¹⁴ on O¹⁶, the formation of F¹⁸ by evaporation is most unlikely. It was pointed out by Reynolds *et al.* (37) that the reaction O¹⁶(N¹⁴, F¹⁸)C¹² may be an alpha transfer to the nitrogen, or a deuteron transfer to the oxygen, or both. They found its cross section to be appreciable, ~ 1.5 mb at 26 Mev.

The situation at low and medium energies, then, is that single transfers are quite likely, and above the Coulomb barrier they have total cross sec-

tions from 1 to 30 mb whereas the more exotic transfer reactions, such as (p, n) exchange or two-neutron transfer, have very low cross sections. In addition there are several cases for which the reaction mechanism is not clear.

At higher energies, ~ 10 Mev/nucleon, evidence for much more complicated transfer reactions was found by Kaufmann & Wolfgang (38). They found, for example, that N^{13} from the oxygen bombardment of Al, Cu, and Sn has cross sections of 4.0, 4.7, and 1.4 mb, respectively. The production of C^{11} from these same targets has cross sections of 2.3, 2.9, and .78 mb. These reactions are described by the authors as either being $p2n$ or $2p3n$ transfers from the oxygen, or perhaps (p, α) exchange transfers and (αn) double transfers. It is evident that these reactions have much higher cross sections than similar reactions at lower energies. The authors ascribe this to the fact that much higher angular momenta are associated with the higher energies. A qualitative classical description of the mechanism assumes that with large angular momenta available, the centripetal force prevents the two colliding nuclei from amalgamating; and during contact, nucleons and nuclear fragments may pass between the nuclei. The authors call this mechanism "contact transfer." The results of multiple- and complex-transfer reaction experiments are given in Table IV.

All the evidence cited so far concerning transfer reactions has been radiochemical. Various targets were bombarded with heavy ions, and the radioactive reaction products isolated chemically, by half life, by energy of the radiation, by recoil techniques, or by some combination of these methods. Recently an entirely new approach was used by Anderson *et al.* (39). They observed heavy reaction products from 160-Mev oxygen ions on aluminum. Various species of heavy fragments were distinguished and energy spectra obtained by the $dE/dx \cdot E$ method using a proportional counter-scintillation counter telescope. They find very large cross sections for heavy product elements from Li to F. Their results are shown in Table V. The fluorine production is compatible with other cross sections for single transfer reactions (in this case a proton transfer). The experimental method cannot differentiate

TABLE V
TOTAL CROSS SECTIONS IN MILLIBARNS FOR PRODUCTION OF NUCLEAR FRAGMENTS IN THE BOMBARDMENT OF Al^{27} BY 160-MEV OXYGEN IONS (39)

Product Element	Cross Section, mb
Fluorine	30
Oxygen (inelastic)	150-300
Nitrogen	170
Carbon	210
Boron	60
Beryllium	>20
Lithium	>30

between the various isotopes of the nuclei counted in the telescope, but comparison with Kaufmann & Wolfgang's data shows that only about 2 per cent of the total amount of nitrogen ions produced in the reaction is N^{13} and only 1 per cent of the carbon is C^{11} . In addition, Anderson *et al.* find that the angular distributions for the C, N, and O fragments are strongly peaked in the forward direction. The authors suggest that the reaction mechanism involves fragmentation of the projectile in the neighborhood of the target nucleus, and they add that comparison with radiochemical data indicates that the stability of the nuclide plays a large role in its production cross section. It should, however, be borne in mind that the radiochemical data (38) represent an integrated "thick-target" cross section (the thickness is not specified by the authors), while the counter telescope results (39) are from a thin target. A strong energy dependence for these reactions may explain at least part of this discrepancy. Further research in complex- and multiple-transfer reactions must be done before one can gain a more thorough understanding of the processes involved.

The "buckshot" mechanism proposed by Chackett *et al.* (40) is probably related to the kind of mechanism just described. The "buckshot" hypothesis states that in a close collision, N^{14} on Al^{27} , the incident nucleus disintegrates into fragments of α particles and nucleons and that some of these fragments are then absorbed by the target. The experiments were performed under very adverse circumstances, using a nitrogen beam with a very broad energy spectrum, and the evidence is therefore not clear cut. It was found by Webb *et al.* (41) that "buckshot" is not a probable reaction mechanism at energies near the Coulomb barrier, and Parfanovich *et al.* (42) and Baraboshkin *et al.* (43) conclude that the "buckshot" mechanism is not evident at higher energies in interactions with emulsion nuclei or with gold nuclei. There are indications that the cross section for fragmentation observed by Anderson *et al.* decreases with increasing atomic number of the target. This may be due to a larger radius of the target or the lower effective angular momentum caused by the larger Coulomb barrier. If so, there may be some connection between Chackett's "buckshot" hypothesis and the "fragmentation" mechanism proposed by Anderson *et al.*

Another factor makes the interpretation of high-energy transfer reactions difficult. It is the possibility that transfer reactions may leave the final nuclei excited sufficiently so that they may de-excite by emission of nucleons or α particles. The importance of this in two-neutron transfer was pointed out by Karnaukhov *et al.* (34) and for the complex transfers by Zucker (44). For example, the appearance of N^{13} in an oxygen-induced reaction may be the result of a two-step reaction: first the oxygen picks up a proton, thus forming F^{17} , which may, if excited, decay by α emission to N^{13} . Experimental evidence on this subject is very meager except, as described above, for the nucleus which has accepted a neutron; its excitation may be appreciable (of the order of 20–30 Mev at high energies). Whether the nucleus which loses a particle can also be left in an excited state has not been shown

in any experiment. Obviously this cannot be done so long as the (N^{14} , N^{13}) transfer reaction is used for the experiment. However, Kammuri has suggested (45) that, in accord with Cohen's (46) ideas, removal of a nucleon should not leave a nucleus highly excited since it is difficult to produce hole states of high excitation. Investigation of (C^{12} , C^{11}) or (O^{16} , O^{15}) transfer reactions may give important clues in this connection.

COMPOUND-NUCLEUS REACTIONS

In this section, we will treat those heavy-ion-induced reactions in which most of the nuclear matter fuses and the excited nuclear mass thus formed de-excites by emission of light particles such as nucleons, deuterons, tritons, α particles, and γ rays. The use of the phrase "compound nucleus" comes into question immediately. This expression was coined (47) to describe a compound system which lasts for a very long time compared to the time necessary for a nucleon to cross a nucleus. In slow-neutron absorption reactions, the narrow width of the resonances observed is taken as evidence that the compound nucleus does exist for a long time and that the excitation energy is therefore shared among many nucleons. This invention of the compound nucleus, and its formalization in the Breit-Wigner formula (48), were very successful in interpreting (p , γ) resonances and slow-neutron data. When other simple nuclear reaction theories were not available, the compound nucleus hypothesis was sometimes uncritically employed. In time it became a catch-all phrase denoting a situation of ignorance, whereas in fact the phrase had a definite meaning in its original form. Recently, many nuclear processes have been found to go by direct interaction and are not included in the compound-nucleus picture. Experimentally, reactions do not necessarily fall into neatly labelled categories and are still often referred to as having a "compound nucleus" part and a "direct part." Although this kind of nomenclature has some physical significance and is doubtless descriptive, it is by no means a rigorous way of looking at nuclear reactions. It has further served to lump all processes about which we know little under the convenient appellation "compound nucleus."

This situation is also encountered in heavy-ion reactions. Several authors have suggested other names to describe the situation when, for example, a nitrogen nucleus hits an aluminum or gold nucleus. Phrases such as "conglomerate nucleus" or "compound system" were put forth, but they have met with little acceptance. Therefore, the term "compound-nucleus reaction" will be taken to mean a heavy-ion reaction in which two nuclei have merged and small fragments are emitted as a means of de-excitation. Whether in fact the two nuclei produce a compound nucleus which lasts for a long time and achieves thermal equilibrium is a matter of conjecture and can not be ascertained by measuring widths of resonances, as in the slow-neutron case. In spite of these restrictions, useful information can be extracted from heavy-ion data by treating the reactions as if they did go through the stage of a compound nucleus in thermal equilibrium.

Other reaction mechanisms are, of course, possible and may confuse the thermal-equilibration hypothesis. One may speak of locally heated systems in which particles are emitted before the energy is shared between all nucleons. One may again speak of a "buckshot" mechanism which will produce light reaction products, in addition to forming a compound nucleus consisting of the target nucleus and a portion of the projectile. It can be seen that all of these mechanisms are much more complicated. They are more difficult to identify experimentally and investigate theoretically than is the compound-nucleus mechanism.

The compound nucleus in heavy-ion-induced reactions is very highly excited. Even at low incident energies, say with 25-Mev N^{14} , compound nuclei are excited to approximately 40 Mev. At these high excitations it is generally assumed that the energy levels of the compound nucleus overlap. Also, even a small spread in incident beam energy is sure to result in compound nuclei in many adjacent states of excitation. Overlapping levels and high excitation make the assumption of random phases in the decay channels plausible, so that some statistical model for the de-excitation of the compound nucleus should be applicable. As will be seen, this picture appears to be in accord with experimental results from 15 to 100 Mev incident energy; however, at the very highest energies available for heavy ions, ~ 10 Mev/nucleon, there is evidence that the very large angular momenta affect either the formation of a compound nucleus, or its decay, or both.

It is clear that at lower energies in heavy-ion reactions, so-called knock-on reaction products that are encountered with proton-induced reactions are not likely, because of the low velocity of the incident particle. Furthermore, the direct processes, equivalent to pickup or stripping, that may result in small fragments which can be confused with de-excitation products of a compound nucleus have small cross sections.

We assume then, always within the limits of the preceding discussion, that heavy ions do produce thermally equilibrated compound nuclei, and that the reaction has the following characteristics: a compound nucleus is formed at relatively high excitation (of the order of 50 Mev), its properties are independent of the method of formation on account of the random-phase character of overlapping levels, and the de-excitation of the compound nucleus can be treated by a statistical model (49).

The equation for the cross section of a nuclear reaction $A(a, b)B$ is

$$\sigma(a, b) = \sigma_c(a) \Gamma_b / \Gamma \quad 17.$$

$\sigma_c(a)$ is the cross section for capture of a by the nucleus A , and $\Gamma = \sum_i \Gamma_i$ is the sum over all open channels including Γ_b . The symbol Γ here is related to the mean lifetime of the compound nucleus by $\Gamma_i = \hbar / \tau_i$ and Γ_i / \hbar is a decay rate for the channel i . The value of $\sigma_c(a)$ for heavy ions can be computed, more or less approximately, but is usually eliminated in the analysis of experimental results. The problem of calculating the branching ratio Γ_b / Γ remains. This can be accomplished from (a) the statistical hypothesis

that the decay of a compound nucleus depends only on the angular momentum, energy, and parity of the system and is otherwise independent of its formation; and (b) the reciprocity theorem.

The probability of emission of particle b with wave number k_b from a compound nucleus is proportional to

$$k_b^2 \sigma_c(b) \mathcal{W}(\epsilon_{\max} - \epsilon) d\epsilon \quad 18.$$

The quantity σ_c is the capture cross section for particle b by the residual nucleus, ϵ is the channel energy, $\epsilon_{\max} - \epsilon \equiv E_B$ is the excitation energy in the residual nucleus and \mathcal{W} is the level density of the residual nucleus at E_B . Application of Expression 18 to energy spectra of light particles emitted in a nuclear reaction yields information about level densities and their energy dependence. The value of σ_c can be calculated with reasonable accuracy with optical model potentials, although in practice the energies of the emitted particles are sufficiently far above the Coulomb barrier so that a black-nucleus approximation (50) for σ_c is good enough.

For the analysis of excitation functions, Expression 18 must be integrated over the entire range of ϵ . The probability of finding the residual nucleus B is proportional to

$$\frac{2M_b}{\hbar^2} \int_0^{\epsilon_{\max}} \epsilon \sigma_c(b) \mathcal{W}(E_B) d\epsilon \quad 19.$$

To account for competing reactions, Expression 19 must be divided by the sum of similar expressions for all possible modes of de-excitation.

On the basis of a simple thermodynamic analogy, Weisskopf (51) has derived for the level density the formula

$$\mathcal{W} = C \exp 2\sqrt{aE_B} \quad 20.$$

The constant a determines the energy dependence of the level density while the constant C gives its absolute value, which is a function of the odd-even character of the nuclei and also of their shell structure. A nuclear temperature T is related to a by $E_B = aT^2$. More accurate and more complex expressions for the level density have been derived by Lang & Le Couteur (52 to 54) and Newton (55). However, the qualitative features of all of these expressions can be seen in the simplest representation in Equation 20.

INTERPRETATION OF EXPERIMENTAL RESULTS

Experimental results concerning compound-nucleus reactions have been treated in several ways in order to extract physical information from them. We list these here and give concrete examples. Because of lack of space we can present neither all the experimental data nor all the attempts to interpret them; rather we confine ourselves to typical cases.

Shapes of excitation functions.—Compound-nucleus reactions exhibit characteristic excitation function shapes. Experimental results may be compared with theoretical curves, and differences between them may provide some illuminating clues concerning the reaction mechanism. Excitation

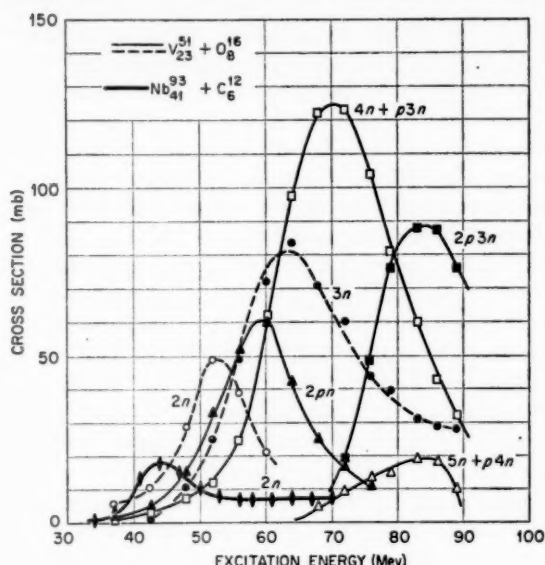


FIG. 5. Excitation functions for carbon- and oxygen-induced reactions in V^{51} and Nb^{93} . The curve for $Nb^{93}(C^{12}, 2n)Ag^{105}$ exhibits a characteristic flat shape beyond the peak at 45 Mev (56).

functions for heavy-ion-induced reactions may also be compared with those from proton and α -particle bombardments going through the same compound nucleus, and differences here may prove enlightening. Karamian & Plevé (56) reported characteristic excitation functions for reactions resulting from the system $O^{16} + V^{51}$, which are shown in Fig. 5, along with the reaction $Nb^{93}(C^{12}, 2n)Ag^{105}$. A given reaction cross section, say $V^{51}(O^{16}, 2n)Ga^{66}$, has a Coulomb barrier threshold at ~ 38 -Mev energy of excitation, rises slowly to a maximum of 50 mb around 52 Mev, and drops because competing reactions such as $(O^{16}, 2pn)$ and $(O^{16}, 3n)$ are taking over more and more of the available total cross section. From 40- to 90-Mev excitation energy, the most probable number of emitted particles changes from two to five. The authors compare the excitation function for $V^{51}(O^{16}, 2n)Ga^{66}$ with the excitation function $Cu^{63}(\alpha, 2n)Ga^{65}$ measured by Porges (57). Both reactions presumably go through the same compound nucleus, Ga^{67} . The two excitation functions are quite similar in shape, but Karamian & Plevé point out that the peak of the excitation function for the heavy-ion-induced reaction is about 15 Mev higher in excitation of the compound nucleus than for the α -induced reaction. They propose that this shift may be due to the much higher angular momentum available in the former ($\sim 23\hbar$, from Eq. 4) than in the latter ($\sim 12\hbar$). However, the shift in the peak may be at least partly due to the influence of the incoming Coulomb barrier in the heavy-ion case,

which tends to suppress the reaction cross section at low excitation energies. In the case of these two reactions, the excitation function is twice as wide for $(\alpha, 2n)$ as it is for $(O^{16}, 2n)$. This is probably a consequence of the higher excitation energy in the latter case. Similar excitation functions were obtained by Baraboshkin *et al.* (43) for the evaporation of $4n$, $5n$, and $6n$, following the nitrogen bombardment of gold. The authors state that the shapes of the curves are about what one expects from theoretical calculations (58) except that the peaks are shifted by ~ 10 – 15 Mev toward higher energies.

A peculiarity in the excitation functions found by Karamian & Plevé (56) in $C^{12} + Nb^{93}$, and also by Karamian, Gerlit & Myasoedov (59) in $C^{12} + V^{51}$, is the fact that the $(C^{12}, 2n)$ reaction cross section does not continue to decrease with increasing excitation energy. In fact, and quite surprisingly, the $(C^{12}, 2n)$ cross section levels off at ~ 25 mb in V^{51} and at ~ 7 mb in Nb^{93} . No such leveling off is observed for reactions in which more than two neutrons are evaporated, although the data are not too clear in this regard.

Compound-nucleus reactions induced in carbon by C^{12} , N^{14} , and O^{16} ions were studied by Tamers & Wolfgang (60), who compared them with proton-induced reactions leading to the same compound system. They do not find the shift in the peak of the excitation functions observed by Karamian & Plevé. If anything, the proton-induced reactions have peaks at higher excitation. Tamers & Wolfgang do find that α -particle emission seems to be favored in the heavy-ion-induced reactions as opposed to proton-induced reactions. This was found earlier at lower energies by Cohen, Reynolds & Zucker (61). Tamers & Wolfgang also note that the high-energy tail usually associated with direct processes in proton-induced reactions is absent in their work, although this conclusion can be reached unambiguously only for one excitation function, $C^{12}(C^{12}, pn)Na^{22}$. Their results contrast with the observation of the high-energy tail in the $2n$ evaporation.

One must conclude that many interesting clues concerning the heavy-ion reaction mechanism leading to a compound nucleus can be obtained from the comparison of excitation functions. However, it is difficult to draw definite conclusions because of great uncertainties concerning such factors as (a) penetrabilities in the incoming channel, (b) the effect of angular momentum, (c) the applicability of the compound-nucleus concept.

Comparison of calculated and measured cross-section magnitudes.—Besides testing the hypothesis that the decay of a compound nucleus is independent of its formation, the results of heavy-ion-induced reaction cross section measurements may be compared with the predictions of a statistical model such as the one proposed by Weisskopf (51) or by Jackson (58). The method of fitting excitation functions with such a model has been frequently described in connection with neutron- or proton-induced reactions and, more recently, for heavy-ion reactions by Nakasima *et al.* (62) and Halbert *et al.* (63). In these calculations one tries to fit entire excitation functions or cross sections at selected energies for several competing reactions from the same

nucleus, and since the capture cross-section calculation is fraught with uncertainty, it is sometimes advantageous to compare only ratios of reaction cross sections. Even the ratios are difficult to calculate unambiguously. Calculations of competing reactions depend strongly on the exit barrier encountered by charged particles emitted at low energies. Usually, penetrabilities based on a black-nucleus model are used (50) and are probably fairly good a few Mev above the barrier. The calculations are, however, very sensitive to penetrabilities near the barrier and below it, just where the penetrabilities are least valid. These low-energy transitions are the most probable because of the exponentially increasing level density in the residual nucleus. Near the barrier, if neutron competition is energetically forbidden, γ -ray transition probabilities must be included in the branching calculations, and very little theoretical work exists concerning such calculations. Furthermore, branching calculations have been performed on the basis of information about inverse reactions, which is limited to absorption of nucleons or γ rays by ground state nuclei. The physical situation is not necessarily the same for absorption by excited nuclei since these are almost surely deformed and in many other ways unlike nuclei in the ground state. This is especially true for γ de-excitation, where usually only the giant resonance is thought to be important in γ absorption, but the case may be quite different for emission from excited nuclei.

Uncertainties concerning the evaluation of the level density of the residual nucleus also enter, and they can be expressed essentially by uncertainties in the values of C and a in Equation 20. Additional difficulties appear when a more sophisticated level density formula is used. The value of the constants depends on shell effects, odd-even effects, and in general on details of nuclear structure. Indeed, the whole point of fitting reaction cross sections with the results of a statistical calculation is to obtain level density parameters which may be compared with those derived from other experiments and thus to gain some insight into the structure of nuclei. Unfortunately there are so many variables which are incompletely understood and, in many cases, difficult to handle mathematically that conclusions have remained tentative.

The most thorough set of calculations is that of Nakasima *et al.* (62) which fits the $C^{12}+N^{14}$ excitation functions (64) reasonably well. The theoretical prediction for 2α evaporation turns out to be too small, but this may be because the calculations use a value of $a = (0.1 + 0.01A)$ Mev $^{-1}$. This is much smaller than values of a which have since been deduced from energy spectra of protons and α particles in similar reactions. This and other similar calculations (28, 61, 64) indicate that heavy-ion reactions at low energies, $E \approx 30$ Mev, may be regarded as proceeding through a compound nucleus. Nakasima (65) reaches the conclusion that the "buckshot" process is probably not in evidence at these energies. Whether the compound nucleus is a thermally equilibrated one and whether it decays in a statistical manner are problems not solved at this time.

Recently, Monte Carlo type calculations have been performed (66) by means of which the evaporation of reaction products from compound nuclei in the region $45 < A < 75$ was computed for n , p , or α -particle-induced reactions. Although this appears to be a very promising approach, no calculations have been done for heavy-ion-induced reactions.

A remarkable, and as yet unexplained, fact was observed by Beydon *et al.* (67) in the bombardment of the copper isotopes by N^{14} and O^{16} , and by Pinajian & Halbert (68) in $K^{39} + N^{14}$ reactions. In both cases the observed residual nuclei have masses too close to the compound-nucleus mass. In other words, not as many particles are evaporated as would be expected from a statistical theory, or indeed from measured particle spectra in N-Al or N-O reactions. Two suggestions have been put forth: (a) that partial heating of the nuclear matter may create small regions of very high excitation which emit very energetic particles and (b) that γ -ray emission may be of much greater importance than has generally been considered. These phenomena may well be related to the flat (C^{12} , $2n$) excitation functions reported by Flerov (4).

Spectra and angular distributions of reaction products.—A different kind of information concerning the de-excitation of a compound nucleus may be obtained from energy spectra and angular distributions of light particles emitted in heavy-ion reactions. By light particles we mean protons, neutrons, α particles, deuterons, etc., and in some special cases γ rays.

The earliest work of this kind was done by Parfanovich, Rabin & Semchinova (42) who bombarded nuclear emulsions with nitrogen ions up to 130 Mev, and measured energy and angular distributions of protons and α particles from 198 stars. Seventy of these stars were from "heavy" constituents (Ag, Br) and 128 from "light" constituents (C, N, O) of the emulsion. These authors, and later Flerov (4), make several observations concerning this experiment: (a) There are 1.5 times more α particles than protons emitted from "heavy" stars, which shows that the process is not a simple de-excitation of a compound nucleus. (b) The α particles are strongly peaked in the forward direction from "heavy" stars. (c) Protons from "heavy" stars show a slight forward peaking, whereas protons from "light" stars are emitted isotropically. The authors conclude that this presents evidence that the "buckshot" mechanism does not appear to be valid, since the average energy of an α particle, according to this picture, is four times the energy of a proton, and the barrier for the α particle entering a nucleus is only twice that for a proton. Therefore, the "buckshot" theory would predict more protons than alphas, especially in the forward direction, whereas just the opposite effect is observed.

Fremelin & Lille (69) bombarded silver with a rather wide spectrum of nitrogen ions. They observe an excess of protons over α particles, by more than a factor of two, in the angular range from 45° to 170° c.m. The distributions of both protons and α particles show a peak in the forward direction, and neither is symmetric about 90° .

More recently, Knox *et al.* (70) have measured energy and angular distributions of α particles from Ni bombarded by 160-Mev oxygen ions. They find angular distributions which appear to be symmetric about 90° c.m., especially for lower α -particle energies. The angular distribution of α particles displays a $1/\sin \theta$ shape, which the authors attribute to the rapid rotation of the compound nucleus. The $1/\sin \theta$ distribution is just what one expects from random emission of particles from a rotating body. For high-energy particles there appears to be asymmetry: more alphas are emitted in the forward than in the backward direction.

It is obvious from the three experiments cited above that more extensive experimental investigations are needed before definite conclusions can be made. There seems to be good evidence for forward peaking of α particles from all observations, especially at high α energies. The questions of symmetry about 90° and of relative numbers of protons and α particles cannot be considered settled at this writing.

The experiments cited so far were performed to shed some light on the reaction mechanism involved when high-energy heavy ions impinge on nuclei. Experiments at relatively low energy by the Oak Ridge group were used chiefly to investigate level densities of nuclei, nuclear temperatures, and the details of the de-excitation process of nuclei excited to 30 or 40 Mev. The orbital angular momenta involved in these reactions calculated from a semiclassical turning point (Eq. 4) are not larger than about $10\hbar$, whereas for higher-energy heavy ions they go up to $50\hbar$. We will return to the question of the effect of angular momentum at the end of this section.

At low energies, spectra of protons, deuterons, and α particles from nitrogen-induced reactions in Li^6 , Li^7 , Be^9 , C^{12} , N^{14} , O^{16} , and Al^{27} have been measured (71 to 75). In the last two cases, angular distributions in the forward hemisphere were also obtained. The energy spectra in this series of measurements were analyzed on the basis of a simple statistical model, with the transition probability for a particle of channel energy ϵ given by Expression 18. If the level density is assumed to have $\sqrt{E_B}$ dependence as in Equation 20, then a plot of $\log N(\epsilon)/(\epsilon\sigma_\epsilon)$ vs. $\sqrt{E_B}$ should result in a straight line. Such straight lines have indeed been obtained as for example in Figure 6 for α particles from N on Al. A number of values of a (Eq. 20) were obtained in this way; they show approximately an $A/10$ dependence on the mass number of the residual nucleus (2).

The authors of this series of papers claim that good information about level densities and their energy dependence may be obtained in this way, since direct interactions which confuse the results of proton- or neutron-induced reactions are no problem here. The questions of "local heating" and "second-particle emission" do present serious obstacles to an unambiguous interpretation of the data. These two factors become increasingly important at higher energies of the incident heavy ions.

The experiments just cited also yield information about the relative emission probability of various particles, e.g. the ratio of protons to α particles

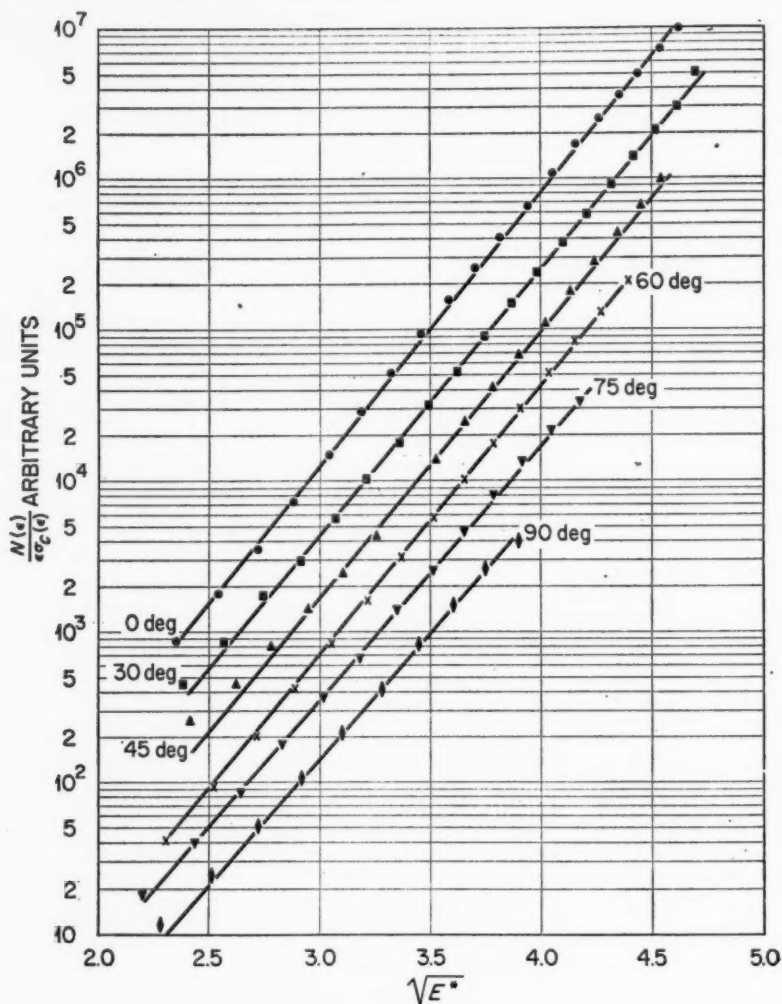


FIG. 6. The logarithm of the normalized energy distribution of alpha particles from 28-Mev N^{14} on Al^{27} , plotted as a function of the square root of the excitation energy of the residual nucleus. Measurements at various laboratory angles are displaced arbitrarily (75).

emitted from a compound nucleus. The proportionality constant for expression 18 is a product of several factors. In the simplest case, it can be seen that it depends on the mass of the particle, its spin, and perhaps some preformation coefficient which measures the probability that a particle is available to make the transition. In addition, the relative emission probability

will depend on the constants C and a in Equation 20. The value of a is obtained directly from the experiment, and the value of C may be estimated by means of Cameron's (76) calculations, probably to about 50 per cent. Within the uncertainty in estimating C and within the error introduced by the assumptions of the theory, the experimental results (73 to 75) give the value of the preformation coefficient as unity. In other words, protons, deuterons, and α particles are all evaporated with the same probability if one takes into account the Coulomb barrier, the phase space, and the level density of the residual nucleus. One may well be seeing, in this case, a compound nucleus which has come to thermal equilibrium and from which information about a statistical de-excitation mechanism may be deduced with a fair amount of confidence.

THE EFFECT OF HIGH ANGULAR MOMENTUM

At high energies, heavy ions may impart many units of orbital angular momentum to a compound nucleus. The effects of this have not been exhaustively studied, but certain interesting phenomena have been observed by the Moscow group (4). For example, the isomeric state of Mo^{93m} was produced (77) with a peak cross section of 250 mb with 70-Mev oxygen ions on Se^{80} . This is one hundred times larger than the cross section for the production of Mo^{93m} with 6.7-Mev protons on Nb^{93} . However, it should be kept in mind that the 6.7-Mev protons are well below the Coulomb barrier of Nb^{93} . In another experiment, it was found that in the O^{16} -induced fission of Au^{197} , the population of the spin 11/2 state of Cd^{115m} is 50 per cent greater relative to the ground state at 100 Mev than at 80 Mev. This ratio is 20 times larger in the oxygen-induced fission than in slow-neutron fission. Thus, one may consider heavy-ion-induced reactions as an excellent method for the production of high-spin metastable states.

When Sn was bombarded with C^{12} [Karanaukhov & Oganessian (4)], high-energy γ -ray cascades were observed. The authors explain this as an instance in which a large amount of angular momentum is deposited in the compound barium nucleus. After several neutrons are evaporated, the barium nucleus finds itself in a "neutron-metastable" state, still with many units of angular momentum but unable to de-excite by further neutron emission. It then decays to the ground state by a γ -ray cascade.

In another instance, a hypothesis was advanced by Anderson *et al.* (39) that in the case of heavy ions impinging on light targets, the formation of a compound nucleus may actually be forbidden because of the large angular momentum. This is based on the evidence that heavy fragments are emitted with such high probability in the reaction $\text{O}^{16} + \text{Al}^{27}$ that they account for a large fraction of the geometric cross section.

FISSION

The subject of fission may properly be regarded as part of the larger field of nuclear reactions proceeding through a compound-nucleus stage. We

reiterate that caution must be exercised in assuming the formation of a compound nucleus, but we will continue to make this assumption because it leads to some valuable results in the interpretation of fission experiments with heavy ions.

Study of the fission process itself constitutes a fertile domain of nuclear physics and, equally, of heavy-ion physics. There is also a practical side to the investigations of heavy-ion-induced fission. The production of very heavy elements, $Z > 100$, by means of heavy-ion bombardment has become an important, if very difficult, branch of nuclear chemistry. In this connection it is important to know how much of the total reaction cross section proceeds by way of fission and how much by spallation or some other mechanism by which very heavy elements may be made. This was one purpose of Sikkeland's (2) measurements of $U^{238} + C^{12}$ excitation functions.

In the study of high-energy fission of heavy nuclei, the use of heavy ions provides a definite advantage which can not be realized with energetic light projectiles. Druin, Polikanov & Flerov (78) state this case well, by noting that the probability of fission is strongly dependent on the parameter Z^2/A of the fissioning nucleus and that in fast-proton- or neutron-induced fission the value of Z^2/A is often subject to considerable doubt because direct interactions may produce nucleon cascades before the nucleus reaches thermal equilibrium. This effect then distorts the results of experiments where fission or competition of fission with spallation is investigated. When heavy ions are used to produce fission, there is no direct cascade and the evaporation-fission mechanism proceeds in a way which is more amenable to theoretical interpretation. In addition, because of the large angular momenta, one may obtain information concerning the fission of a rapidly rotating nucleus.

Experimentally, one observes in fission experiments: (a) excitation curves for fission and competing neutron evaporation reactions, (b) fission yields (the mass and charge distribution of fission fragments), and (c) the angular distribution of fission fragments. From this evidence one may obtain information concerning systematics of fission and details of the fission process.

Early in the investigation of heavy-ion-induced fission it was discovered that this process constitutes nearly the whole reaction cross section (85 to 100 per cent) for target elements heavier than bismuth. In fact, Druin *et al.* (79) and Polikanov & Druin (80) find that the excitation function for fission is very well approximated by the simple total reaction cross-section formula

$$\sigma_r = \pi r_0^2 (A_1^{1/3} + A_2^{1/3})^2 (1 - E_B/E) \quad 21.$$

for bismuth and uranium bombarded with carbon, nitrogen, and oxygen ions. A value of $r_0 \sim 1.5f$ fitted experimental data above the Coulomb barrier well. In fact, Equation 21 seems to be a very good formula for total cross sections measured this way. Similar observations were made by Goldberg &

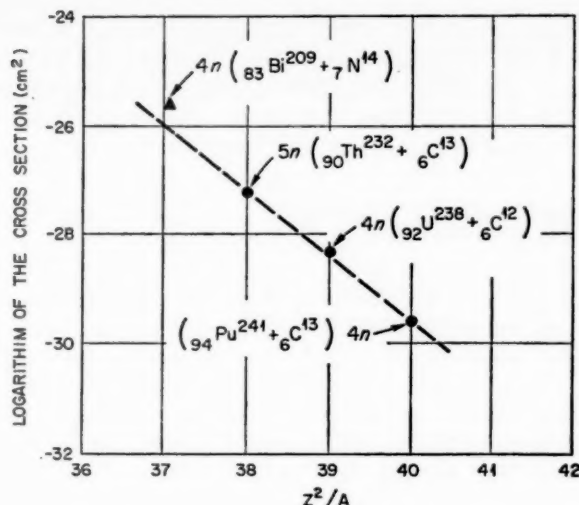


FIG. 7. Logarithm of the reaction cross section plotted as a function of Z^2/A (4).

Reynolds (2) from the carbon-induced fission in gold. Having once established fission as the most important process in this region of the periodic table, the measurement of the spallation cross section should give some evidence on the Z^2/A dependence of the fission process. This was the approach of the Moscow group who measured the cross section for $4n$ and $5n$ evaporations from the compound nuclei formed by heavy-ion bombardments of Bi, Th, U, and Pu. Figure 7 shows these cross sections plotted as a function of Z^2/A and is interpreted to show that the fissionability of heavy compound nuclei is related to this parameter.

Mass distributions of fission fragments were reported by Flerov (2) for irradiation of Au^{197} and U^{238} with 105-Mev nitrogen ions. In the former, the mass-yield curve has a full width at half maximum of about 20 mass units and has a peak at $A \sim 100$. In the latter case the mass distribution is much flatter, with a width of at least 50 mass units, centered about $A \sim 120$. The interpretation of these results is that the gold fission is symmetric whereas the uranium fission proceeds both by symmetric and asymmetric modes.

Measurements of angular distributions of fission fragments from heavy-ion-induced fission are beginning to be reported. Druin *et al.* (79) report coefficients of anisotropy ($141^\circ/102^\circ$) for $\text{Au}^{197}(\text{C}^{12}, f)$, $\text{Au}^{197}(\text{O}^{16}, f)$, and $\text{U}^{238}(\text{C}^{12}, f)$ with incident energies from 66 to 100 Mev. The coefficient of anisotropy increases with increasing energy and attains values as high as 1.62 for 111-Mev C^{12} -induced fission in gold. More recent results may be found in the *Proceedings of the Second Conference on Reactions Between Complex Nuclei* (3).

VERY RECENT RESULTS

A very recent result at the time this is written may well, in a rapidly growing field such as heavy-ion nuclear interactions, turn into a familiar phenomenon by the time of publication. We will list only two experimental results, not merely because they were recently obtained, but also because they do not fall into any class of phenomena so far discussed.

The first experiment is that of Bromley *et al.* (81) who measured the elastic-scattering cross section at 90° c.m. for C^{12} on carbon, O^{16} on oxygen, and O^{16} on carbon as a function of incident ion energy. The results are shown in Figure 8. It can be seen that the C-C system has a great deal of structure, the O-C system less so, and the O-O system is almost smooth. The authors suggest that the structure in the C-C system may be due to some sort of quasi-molecular states of the two carbon nuclei, accompanied by virtual nucleon transfers between the nuclei, and that the lack of structure in the O-O system is caused by the tight binding of the oxygen nucleus and the fact that transfers must occur between the p and d shell, thus inhibiting the process.

Another recent result reported by Hubbard & Merkel (82) indicates that in the neutron-transfer reaction $Ag(C^{12}, C^{11})Ag$, the C^{11} angular distribution

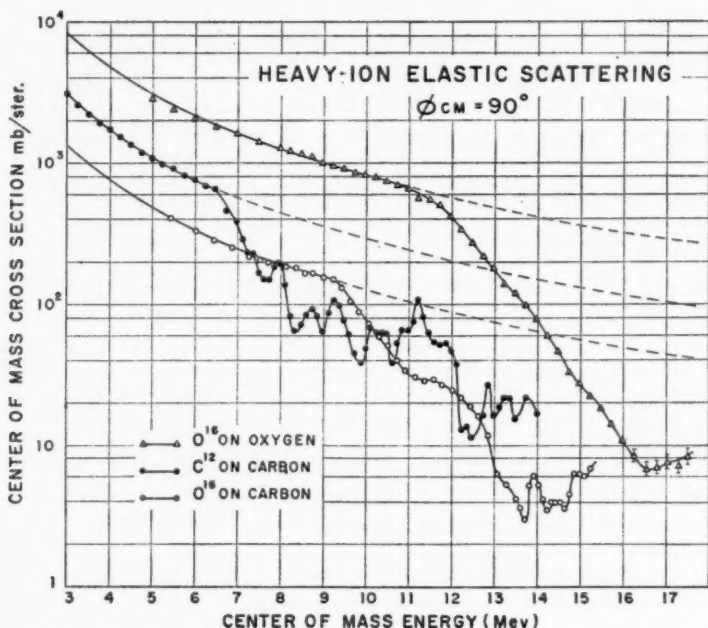


FIG. 8. Differential cross sections at 90° c.m. for the elastic scattering of O^{16} from oxygen, C^{12} from carbon, and O^{16} from carbon as a function of energy. The dashed lines are Coulomb scattering cross sections.

displays two peaks, the more prominent of which appears at zero degrees. A similar result was noted in the neutron transfer $\text{Rh}(\text{O}^{16}, \text{O}^{15})\text{Rh}$ by Wolfgang (83). These distributions stand in marked contrast to the (N^{14} , N^{13}) neutron transfers in which the peaks appear at angles which may be expected from classical collision considerations. No explanation has been proposed for the differences between these neutron-transfer angular distributions.

It is probable that with the rapid development of this field, many new and unusual results will be found. It should be pointed out, however, that a startling result is not necessarily one which most directly leads us to an understanding of nuclear phenomena. There is a need for systematic study as well as for new discoveries in heavy-ion reactions.

Heavy ions are a promising tool for the investigation of the nuclear surface, the behavior of highly excited nuclear matter, and the properties of nuclear systems possessing very large amounts of angular momentum. In some cases a coherent picture is beginning to emerge from the data currently available; in others, the vast amount of unexplored material provides a challenge both to the experimenter and the theorist.

ACKNOWLEDGMENTS

The author would like to thank E. C. Halbert and M. L. Halbert for many suggestions in the course of the preparation of this article.

APPENDIX

Table VI lists the measurements of range-vs.-energy for heavy ions in various materials. In some cases, several authors report results for the same particle, energy range, and stopping material. Only those results that are clearly superseded by more recent work have been left out of the table. Table VII lists the measurements of the response of scintillation and surface barrier counters to heavy ions.

TABLE VI
RANGE-ENERGY DATA FOR HEAVY IONS

Ion	Energy Range	Stopping Material	Ref.
N ¹⁴	8-27 Mev	Nickel	(84)
N ¹⁴	4-28 Mev	Emulsion	(85)
N ¹⁴	4-26 Mev	Aluminum	(86)
C ¹² , N ¹⁴ , O ¹⁶ Ne ²⁰ , Ar ⁴⁰	10 Mev to 10 Mev/nucleon	Emulsion	(87)
C ¹²	43-77* Mev	Al, Au, Cu	(88)
N ¹⁴	70-95 Mev	Al	(88)
O ¹⁶	55-108* Mev	Al, Au, Cu	(88)
N, O	3-120 Mev	Emulsion	(89)
He ⁴ , B ¹⁰ , B ¹¹	1-10 Mev/nucleon	Aluminum	(90)
C ¹² , N ¹⁴ , O ¹⁶ F ¹⁹ , Ne ²⁰	2-10 Mev/nucleon	Ni, O, Emulsion	(91)
C ¹² , O ¹⁶	1-10 Mev/nucleon	Mylar, Polyethylene	(92)
Ne ²⁰	1-10 Mev/nucleon	Mylar	(92)

* The energy range is the one for aluminum; it is somewhat different in the case of Cu and Au absorbers.

TABLE VII
MEASUREMENTS OF THE RESPONSE OF SCINTILLATION AND SURFACE BARRIER
COUNTERS TO HEAVY IONS

Detector	Particle	Energy Range	Ref.
NaI(Tl)	B ¹⁰ , B ¹¹ , C ¹² , N ¹⁴ O ¹⁶ , F ¹⁹ , Ne ²⁰	1 to 10 Mev/nucleon	(93)
KI(Tl)	C ¹²	15 to 110 Mev	(94)
CsI(Tl)	C, N, O	30 Mev to 10 Mev/nucleon	(95)
CsI(Tl)	N ¹⁴	3 to 24 Mev	(96)
CsI(Tl)	C ¹²	0.32-1.83 Mev	(97)
Si barrier Counter	N ¹⁴	2 to 26 Mev	(98)

LITERATURE CITED

1. Endt, P. M., and Demeur, M., Eds., *Nuclear Reactions*, I, Chap. III (North Holland Publishing Co., Amsterdam, Netherlands, 502 pp., 1959)
2. U. S. Atomic Energy Comm. Document, ORNL-2606 (Unpublished, 1958)
3. *Proc. Second Conf. Reactions Between Complex Nuclei* (In preparation)
4. *Proc. Intern. Conf. Peaceful Uses Atomic Energy*, 2nd, Geneva, 1958, 14, 151 (1958)
5. Breit, G., Hull, M. H., Jr., and Gluckstern, R. L., *Phys. Rev.*, **87**, 74 (1952)
6. Halbert, M. L., and Zucker, A., *Phys. Rev.*, **115**, 1635 (1959)
7. Blair, J. S., *Phys. Rev.*, **95**, 1218 (1954)
8. Halbert, M. L., and Zucker, A., *Nuclear Phys.*, **16**, 158 (1960)
9. Wall, N. S., Rees, J. R., and Ford, K. W., *Phys. Rev.*, **97**, 726 (1955)
10. Reynolds, H. L., and Zucker, A., *Phys. Rev.*, **102**, 1378 (1956)
11. Goldberg, E., and Reynolds, H. L., *Phys. Rev.*, **112**, 1981 (1958)
12. Halbert, M. L., Hunting, C. E., and Zucker, A., *Phys. Rev.*, **117**, 1545 (1960)
13. Reynolds, H. L., Goldberg, E., and Kerlee, D. D., *Phys. Rev.* (In press, 1960)
14. Wegner, H. E., Eisberg, R. M., and Igo, G., *Phys. Rev.*, **99**, 825 (1955)
15. McIntyre, J. A., Baker, S. D., and Watts, T. L., *Phys. Rev.*, **116**, 1212 (1959)
16. McIntyre, J. A., Wang, K. H., and Becker, L. C., *Phys. Rev.*, **117**, 1337 (1960)
17. Ford, K. W., and Wheeler, J. A., *Ann. Phys. (N. Y.)*, **7**, 259 (1959)
18. Porter, C. E., *Phys. Rev.*, **112**, 1722 (1958)
19. Bassel, R. H., Drisko, R. M., and Melkanoff, M. A., *Bull. Am. Phys. Soc.*, Ser. II, **5**, 67 (1960)
20. McIntosh, J. S., Park, S. C., and Turner, J. E., *Phys. Rev.*, **117**, 1284 (1960)
21. Reynolds, H. L., Scott, D. W., and Zucker, A., *Proc. Natl. Acad. Sci. U. S.*, **39**, 975 (1953)
22. Chackett, K. F., and Fremlin, J. H., *Phil. Mag.*, **45**, 735 (1954)
23. Halbert, M. L., Handley, T. H., Pinajian, J. J., Webb, W. H., and Zucker, A., *Phys. Rev.*, **106**, 251 (1957)
24. Halbert, M. L., and Zucker, A., *Phys. Rev.*, **108**, 336 (1957)
25. Volkov, V. V., Pasiuk, A. S., Flerov, G. N., *Zhur. Eksptl. i Teoret. Fiz.*, **33**, 595 (1957)
26. McIntyre, J. A., Watts, T. L., and Jobes, F. C., *Phys. Rev.* (In press, 1960)
27. Breit, G., *Encyclopedia of Physics*, **XLI/I**, Sect. 48, 367-406 (Springer Verlag, Berlin, Germany, 1959)
28. Fisher, D. E., Zucker, A., and Gropp, A., *Phys. Rev.*, **113**, 542 (1959)
29. Toth, K. S., *Phys. Rev.* (In press)
30. Breit, G., and Ebel, M. E., *Phys. Rev.*, **103**, 697 (1956)
31. Lifshitz, E., *Zhur. Eksptl. i Teoret. Fiz.*, **9**, 237 (1939)
32. Goldansky, V. I., *Nuclear Phys.*, **9**, 551 (1958)
33. Breit, G., and Ebel, M. E., *Phys. Rev.*, **104**, 1030 (1956)
34. Karnaukhov, V. A., Ter-Akopian, G. M., and Khalizov, V. L., *Zhur. Eksptl. i Teoret. Fiz.*, **36**, 748 (1959)
35. Pinajian, J. J., *Nuclear Phys.* (In press, 1960)
36. Alkhazov, D. G., Gangriskii, Iu. P., and Lemberg, I. Kh., *Zhur. Eksptl. i Teoret. Fiz.*, **33**, 1160 (1957)
37. Reynolds, H. L., Scott, D. W., and Zucker, A., *Phys. Rev.*, **102**, 237 (1956)
38. Kaufmann, R., and Wolfgang, R., *Phys. Rev. Letters*, **3**, 232 (1959)
39. Anderson, C. E., Knox, W. J., Quinton, A. R., and Bach, G. R., *Phys. Rev. Letters*, **3**, 557 (1959)
40. Chackett, K. F., Fremlin, J. H., and Walker, D., *Phil. Mag.*, **45**, 173 (1954)
41. Webb, W. H., Reynolds, H. L., and Zucker, A., *Phys. Rev.*, **102**, 749 (1956)
42. Parfanovich, D. M., Rabin, N. V., and Semchinova, A. M., *Zhur. Eksptl. i Teoret. Fiz.*, **31**, 188 (1956)
43. Baraboshkin, S. A., Karamian, A. S., and Flerov, G. N., *Zhur. Eksptl. i Teoret. Fiz.*, **32**, 1294 (1957)
44. Zucker, A., *Phys. Rev. Letters*, **4**, 21 (1960)
45. Kammuri, T. (Private communication)
46. Cohen, B. L., and Rubin, A. G., *Phys. Rev.*, **114**, 1143 (1959)
47. Bohr, N., *Nature*, **137**, 344 (1936)
48. Breit, G., and Wigner, E. P., *Phys. Rev.*, **519** (1936)
49. Blatt, J. M., and Weisskopf, V. F., *Theoretical Nuclear Physics*, Chap. VIII (John Wiley & Sons, Inc., New York, N. Y., 864 pp., 1952)

50. Shapiro, M. M., *Phys. Rev.*, **90**, 171 (1953)
51. Weisskopf, V. F., *Phys. Rev.*, **52**, 295 (1937)
52. Lang, J. M. B., and Le Couteur, K. J., *Proc. Phys. Soc. (London)*, **A67**, 586 (1954)
53. Le Couteur, K. J., and Lang, D. W., *Nuclear Phys.*, **13**, 32 (1959)
54. Lang, D. W., and Le Couteur, K. J., *Nuclear Phys.*, **14**, 21 (1959)
55. Newton, T. D., *Can. J. Phys.*, **34**, 804 (1956)
56. Karamian, A. S., and Plevé, A. A., *Zhur. Eksptl. i Teoret. Fiz.*, **37**, 654 (1959)
57. Porges, K. G., *Phys. Rev.*, **101**, 225 (1956)
58. Jackson, J. D., *Can. J. Phys.*, **34**, 767 (1956)
59. Karamian, A. S., Gerlit, Yu. B., and Myasoedov, B. F., *Zhur. Eksptl. i Teoret. Fiz.* (In press)
60. Tamers, M. A., and Wolfgang, R., *Phys. Rev.*, **117**, 812 (1960)
61. Cohen, B. L., Reynolds, H. L., and Zucker, A., *Phys. Rev.*, **96**, 1617 (1954)
62. Nakasima, R., Tanaka, Y., and Kikuchi, K., *Progr. Theoret. Phys. (Kyoto)*, **15**, 574 (1956)
63. Halbert, M. L., Handley, T. H., and Zucker, A., *Phys. Rev.*, **104**, 115 (1956)
64. Reynolds, H. L., and Zucker, A., *Phys. Rev.*, **96**, 1615 (1954)
65. Nakasima, R., *Proc. Intern. Conf. Nuclear Phys.*, 511 (Dunod, Paris, France, 1950 pp., 1959)
66. Dostrovsky, I., Fraenkel, Z., and Friedlander, G., *Phys. Rev.*, **116**, 683 (1959)
67. Beydon, J., Chaminade, R., Crut, M., Faraggi, H., Olkowsky, J., and Papineau, A., *Nuclear Phys.*, **2**, 593 (1956)
68. Pinajian, J. J., and Halbert, M. L., *Phys. Rev.*, **113**, 589 (1959)
69. Fremlin, J. H., and Lille, J. S., *Zhur. Eksptl. i Teoret. Fiz.*, **37**, 324 (1959)
70. Knox, W. J., Quinton, A. R., and Anderson, C. E., *Phys. Rev. Letters*, **2**, 402 (1959)
71. Goodman, C. D., *Bull. Am. Phys. Soc.*, Ser. II, **2**, 52 (1957)
72. Goodman, C. D., and Need, J. L., *Phys. Rev.*, **110**, 676 (1958)
73. Goodman, C. D., in *U. S. Atomic Energy Comm. Document, ORNL-2606* (Unpublished, 1958)
74. Halbert, M. L., and Zucker, A., *Phys. Rev.*, **114**, 132 (1959)
75. Zucker, A., *Nuclear Phys.*, **6**, 420 (1958)
76. Cameron, A. G. W., *Can. J. Phys.*, **36**, 1040 (1958)
77. Karamian, A. S., Rusinov, L. I., and Fomichev, V. A., *Zhur. Eksptl. i Teoret. Fiz.*, **36**, 1374 (1959)
78. Druin, V. A., Polikanov, S. M., and Flerov, G. N., *Zhur. Eksptl. i Teoret. Fiz.*, **32**, 1298 (1957)
79. Druin, V. A., Lobonov, Yu. V., and Polikanov, S. M., *Zhur. Eksptl. i Teoret. Fiz.*, **37**, 38 (1959)
80. Polikanov, S. M., and Druin, V. A., *Zhur. Eksptl. i Teoret. Fiz.*, **36**, 744 (1959)
81. Bromley, D. A., Kuehner, J. A., and Almqvist, E., *Phys. Rev. Letters*, **4**, 365 (1960)
82. Hubbard, E. L., and Merkel, G. (Private communication)
83. Wolfgang, R. (Private communication)
84. Reynolds, H. L., Scott, D. W., and Zucker, A., *Phys. Rev.*, **95**, 671 (1954)
85. Reynolds, H. L., and Zucker, A., *Phys. Rev.*, **96**, 393 (1954)
86. Webb, W. H., Reynolds, H. L., and Zucker, A., *Phys. Rev.*, **102**, 749 (1956)
87. Heckman, H. H., Perkins, B. L., Simon, W. G., Smith, F. M., and Barkas, W. H., *Phys. Rev.*, **117**, 544 (1960)
88. Oganessian, Yu. Ts., *Zhur. Eksptl. i Teoret. Fiz.*, **36**, 936 (1959)
89. Parfanovich, D. M., Semchinova, A. M., and Flerov, G. N., *Zhur. Eksptl. i Teoret. Fiz.*, **33**, 343 (1957)
90. Northcliffe, L. C., *Phys. Rev.* (In press, 1960)
91. Roll, P. G., and Steigert, F. E., *Nuclear Phys.*, **16**, 534 (1960)
92. Schambra, P. E., Rauth, A. M., and Northcliffe, L. C., *Phys. Rev.* (In press, 1960)
93. Newman, E., and Steigert, F. E., *Phys. Rev.*, **118**, 1575 (1960)
94. Burcham, W. E., *Proc. Phys. Soc. (London)*, **A70**, 309 (1957)
95. Quinton, A. R., Anderson, C. E., and Knox, W. J., *Phys. Rev.*, **115**, 886 (1959)
96. Halbert, M. L., *Phys. Rev.*, **107**, 647 (1957)
97. Bashkin, S., Carlson, R. R., Douglas, R. A., and Jacobs, J. A., *Phys. Rev.*, **109**, 434 (1958)
98. Halbert, M. L., and Blankenship, J. L., *Nuclear Instr.* (In press, 1960)

COSMIC RAY SHOWERS¹

BY KENNETH GREISEN

Laboratory of Nuclear Studies, Cornell University, Ithaca, N. Y.

I. SIGNIFICANCE OF EXTENSIVE AIR SHOWERS

1. EXPLORATION OF SPACE BY ANALYSIS OF RECEIVED RADIATION

Although bound to earth and its immediate vicinity, man has acquired a wealth of knowledge about a volume of space 10^{58} times that of the earth, almost entirely by interpretation of incoming radiation. The richest and clearest information has been conveyed by visible light. Recent years have witnessed a rapid advance in the detection and interpretation of radio signals. Rockets and satellites have opened up the fields of ultraviolet and x-ray astronomy. Gamma-ray astronomy is on the horizon. Each of these bands of radiation has its own peculiar potentialities for telling the story of special processes occurring in different parts of the universe, and about the conditions of matter and fields that make these processes possible.

That part of the incoming radiation which is distinguished by high specific energies has been known as cosmic radiation.² This radiation encompasses a very broad energy band from about 10^8 ev to an unknown upper limit, certainly large compared with 10^{10} ev. The comparatively high-energy cosmic rays, exceeding about 10^{10} ev, are distinguished by the capability of generating cascade showers containing thousands of secondary particles. This article concerns the analysis of such showers, which is carried on not only to reveal the behavior of high-energy particles, but also in the reasonable expectation that the radiation contains extractable information about its source and about the space through which it has propagated.

2. THE ATMOSPHERE: SHIELD, RADIATOR, MAGNIFIER, AND ANALYZER

The known primary cosmic rays are atomic nuclei, which interact strongly in the atmosphere. The longest interaction mean free path is that of protons, the most abundant primary component: about one-thirteenth of the vertical atmosphere. Hence the number of unaffected primary particles reaching sea level, or even mountain locations, is very small. This has made direct observation of the primaries difficult.

On the other hand, the way to identify high-energy particles, study their behavior, and measure their energies is to impose matter in their path and

¹ The survey of literature pertaining to this review was concluded in July 1960.

² Until the advent of rockets and satellites it has not been necessary to define the minimal energy of cosmic rays closely, since the atmosphere effectively cut man off from all radiation between 4 ev and one Bev in energy. To exclude from the present discussion particles and photons arising from ordinary nuclear reactions in stars, we here restrict the term cosmic radiation to radiation of specific energy large compared with 10 Mev. Thus we also exclude auroral particles and the Van Allen radiation.

observe the processes which ensue. In the case of ultra-energetic primaries, the atmosphere happens to be a singularly apt radiator for this purpose. Its low density permits the numerous secondaries to spread far enough apart to be resolved and counted. Its vertical thickness (27 radiation lengths) is sufficient to permit the largest showers yet detected to reach their maximum development, where a count of the number of particles affords a fairly direct measure of the total energy; but is also thin enough not to absorb fully the showers of more modest energy. At the base of the atmosphere, the denser earth permits the penetrating component among the secondary particles to be singled out and analyzed in terms of its range distribution in the ground.

The thickness of the atmospheric radiator has also been variable, permitting one to study the multiplication and absorption of the particles in the showers. The variation of thickness is achieved by making measurements at different elevations or, at a single elevation, by taking advantage of fluctuations in barometric pressure, and the dependence of the atmospheric thickness on the angle of the shower axis relative to the zenith.

The most helpful function of the atmosphere, however, is that of spreading out the secondary particles over a large area. This spreading leads to the name extensive air showers and is due to the low density and large geometrical thickness of the medium. Primary cosmic rays with many ergs of energy are so rare that to study them without taking advantage of the atmospheric magnification of their cross section would require prohibitively large detectors or excessive patience. The energy spectrum is very steep. With a detector of one square meter sensitive area and one steradian aperture, at the top of the atmosphere, primaries exceeding 100 ergs in energy can be detected about once an hour; but one would have to wait half a million years on the average before recording a primary with energy above one joule. Such a particle makes a sufficiently large shower in the air, however, to be easily detected 1000 m. from the path of the primary. An array of counters can therefore have a receptive area of 10^6 to 10^7 m.² and can register showers of total energy exceeding a joule on the order of once a month.

A price is paid for this magnification, of course, in the loss of some kinds of information. The ultra-energetic primary particle and its direct interactions are not recorded, but only the secondary particles resulting after many generations of cascade multiplication. Hence the nature of the primary particle and its behavior are well hidden and can only be revealed by subtle analysis of the observations.

3. SMALL-SCALE QUEST: STUDY OF THE RADIATION PROCESSES

The air showers have thus far been the only means for study of nuclear and electromagnetic interactions under the condition $E_c \gg Mc^2$, where E_c is the energy in the center-of-mass system of the interacting particles, and M is the rest mass of the heaviest elementary particle. In any such interaction, the number of possible final states is so great that all one can wish to deter-

mine by observation, besides the total cross sections, is the statistical distribution of the outgoing particles in number, type of particle, energy, and angle. It would not be very useful to specify the result of each interaction in detail, since no two interactions are alike. Thus, the limitations of the approach to this problem through the study of air showers may not be too important.

The condition $E_c \gg Mc^2$ can be rephrased as $\lambda \ll \lambda_0$, where λ is the wavelength of the interacting particles and λ_0 is the smallest known natural length. Thus, one is attempting the ultimate microscopy, observing an elementary interaction with particles of wavelength small compared with the suspected structural details of the interaction volume.

One cannot pretend that phenomenal success has attended this quest; yet the progress must at least be termed substantial. The altitude variation of the air showers permits one to set limits on the total cross section of the primaries and on the average elasticity of their interactions with air nuclei. The lateral distribution of the shower particles determines limits on the angular distribution of secondaries emerging from the early encounters. Measurements of the spectrum and lateral spread of the most highly energetic secondaries, both muons and nucleons, have been particularly informative in regard to the elasticity and angular distribution of the reactions. The types of particles produced in the early nuclear collisions are revealed by the relative numbers of electrons, muons, and nucleons present in later stages of the shower development. The statistical nature of the reactions is further illuminated by the fluctuations of individual showers as compared with the average behavior; i.e., by variations from one shower to another in composition, lateral distribution, and longitudinal development.

Progress along these lines has been halting and insecure, leading only to tentative and inexact conclusions, the essential difficulty being that each shower is extremely complex. Attempts to measure any property of the showers precisely, even a statistical property, have led to almost hopeless difficulty in defining what is being measured. What has been achieved thus far is therefore a collection of approximate determinations of vaguely defined statistical properties of the showers. In recent years, several experimental groups [notably in Moscow, Tokyo, Sydney, and at the Massachusetts Institute of Technology (MIT)] have recognized that in interpreting a complex phenomenon, possessing many variables, one needs the records of a complex detecting apparatus, incorporating many different kinds of counters. Such experiments are currently still in a stage of development but have already contributed substantially to the descriptive information to be presented in Part II of this article.

4. LARGE-SCALE QUEST: THE SOURCES AND MEDIUM OF PROPAGATION

As far as is yet known experimentally, the high-energy cosmic radiation arrives at the earth uniformly in time and direction, presumably because the primaries whose effects have been recorded thus far are charged particles

and have travelled for a long while in a medium occupied by irregular magnetic fields. The random deflections have robbed cosmic radiation of almost all information about where and when it originated. It is as though one were trying to do visible astronomy through an atmospheric haze that scattered the starlight equally in all directions.

Not quite all information about the sources is removed, however, and some about the medium is added. Indeed, the isotropy of the cosmic radiation was what led to the first suggestion (Fermi, 1949) that interstellar space contained magnetic fields, and the degree of isotropy of the radiation dictates some of the large-scale properties of the fields.

The size of the solar system and the strength of interplanetary fields are too small to have much effect on cosmic rays of $E > 10^{13}$ ev. The isotropy of this radiation therefore implies in the first place that it does not come in significant measure from the sun, nor from stars of like character on the main sequence. Other evidence suggests that the injection of cosmic rays into the interstellar medium is primarily accounted for by supernovae and other unusual stars which are strong sources of radio emission. Part of the acceleration of the cosmic radiation may occur in connection with its diffusion among the turbulent magnetic clouds in interstellar space.

There are many effects which can be expected to lead to anisotropy of the cosmic radiation: the sparsity of the strong cosmic ray injectors, the gradients of density and magnetic field strength in interstellar space, and the nonstatic character of the fields. The extreme isotropy of the cosmic radiation (to a few parts in a thousand at 10^{15} ev, and within a few per cent up to 10^{17} ev) is therefore not easily explained.

The stimulus to theoretical work in this area will of course become much greater when success is finally achieved in measuring the spatial asymmetry of the cosmic radiation, since this measurement will provide a quantitative effect to be accounted for.

The magnetic rigidity of the cosmic rays under investigation determines the distance scale of the field gradients and time variations to which the observations are sensitive. For instance, solar magnetic disturbances and plasma emission make themselves felt at the earth quite strongly in the cosmic radiation of energy under 20 Bev. In interstellar space, equipartition between magnetic energy and turbulent kinetic energy leads to the estimate of 10^{-5} to 10^{-6} gauss for typical field strengths. The cyclotron radius of a proton in such a field is one light-year at 10^{15} ev, 1000 light-years at 10^{18} ev—provided the field is coherent in direction over such a long distance. Thus, the isotropy of the primaries of comparatively small air showers depends on the uniformity of the region of space between the sun and the nearest neighboring stars, while the isotropy of the highest-energy primaries yet detected depends on the large-scale structure of the galaxy and on whether the cosmic ray density is as large outside as within it.

The dimension of time has a different aspect for the charged cosmic radiation from that which applies to electromagnetic radiation reaching the

earth. For instance, suppose that the supernova known as the Crab nebula has resulted in intense production of cosmic rays and that because of the intervening fields, these cosmic rays diffuse towards the earth with a mean scattering length of a few light-years. The nebula is several thousand light-years from the earth. Hence, although the brilliant visible light began arriving here about 900 years ago, we should not expect the cosmic rays until millions of years have elapsed. No supernova visible in human history has had time to signal us with charged particles. Conversely, if an imbalance of charged cosmic radiation is ever interpretable as an indication of unique sources, it will refer to activity in the distant past, and one should not expect to be able to see any longer a visible indication of the unusual activity, nor to detect it with radio waves.

There remain a couple of unexplored areas of cosmic ray measurement which may yield more easily interpretable astronomical information. It is difficult to conceive of processes that lead to the acceleration of cosmic rays without giving rise to a substantial production of mesons in the source region. Indeed, the abundant synchrotron radiation from the strong radio sources is most easily accounted for in terms of electrons arising from meson decay.³ Meson decay should also yield high-energy photons and neutrinos, which travel from the sources to the earth in straight lines and without delay relative to starlight.

The neutrinos are of course difficult to detect. The photons are few in number compared with the charged primaries; and there is a background problem, since they are also few in number compared with the photons of the same energy, produced in the atmosphere by the charged primary particles (again via meson production and decay). It is therefore easy to account for the lack of evidence for these components of the primary cosmic radiation up to the present. However, the detection problems do not seem insurmountable, and one may predict that these fields of high-energy quantum and neutrino astronomy will be opened up in the near future. Such radiations will be indicative of very unusual stellar atmospheres and will convey completely new types of astrophysical information.

II. DESCRIPTIVE INFORMATION

1. METHOD OF OBSERVATION

Early measurements of the properties of air showers, such as relative numbers and energy spectra of the different kinds of secondary particles, were made with crude methods of shower selection. For instance, coincidences among three or more counters not in a line were typically used to trigger a cloud chamber or hodoscope, of which the photographs were analyzed in order to identify the particles and measure the energies. Such a

³ The synchrotron radiation acts as a heavy drain on electron energies. Thus, the high-energy electrons are more economically obtainable as secondaries after proton acceleration than by direct acceleration of electrons in the source.

method of selection is far from specific. The counter coincidence selects showers on the basis of local density of the charged shower particles. But a given local density can be produced by small showers with centers landing near the apparatus, or by larger showers with axes farther away. The decrease of frequency with increasing shower size is compensated for to a high degree by the increase of area within which the large showers can produce the required density. Hence the sample includes a wide range of shower sizes (several orders of magnitude in the primary energy) and a large spread of distances from the axis. The shower properties measured under such a selection are weighted average properties, of which the variations from one experiment to another are difficult to interpret.

The most recent experiments have removed this objection by being developed around a basic apparatus which locates the center and measures the size (i.e., total number of charged particles) of each recorded shower. In some instances, the angular co-ordinates of the shower axes have been measured as well. An example of such a basic apparatus is the one that has been in use during 1957-59 at Cornell University. It contains 15 plastic scintillators, each of area 0.86 sq. m.: five of them in a central cluster of about 40-m. diameter, five on a surrounding circle of 300-m. diameter, and five on an outer circle of 900-m. diameter. The amplified pulses from the individual photomultiplier tubes are photographed whenever a multiple coincidence occurs. The amplitudes tell the local density of charged particles at the various counters, while the relative times of the pulses reveal the direction of the shower axis. The position of the axis is found by applying the assumption that the particle density (apart from statistical fluctuations) decreases smoothly with the perpendicular distance from the axis. Thus each shower is located in space, and its density is sampled at numerous points. Integration of the particle density over a plane normal to the axis yields the size of the shower.

In principle, this method yields as a by-product the lateral distribution of the particles in each shower. But in practice, because of the limited number of density samples and their statistical errors, an axis can only be located accurately with the aid of prior knowledge of the lateral distribution function. Given such a function, three density measurements are sufficient to locate an axis. The further measurements can then be used to test the consistency of the distribution function, to optimize a parameter in it, or to increase the precision of the core location.

The spacing of the counters in such an arrangement determines the minimum size of measurable showers and the maximum area within which showers can be analyzed. At Cornell, the minimum size is about 10^6 particles. The area within which axes can be located reliably increases with shower size to slightly more than 10^6 sq. m. for showers exceeding $2 \cdot 10^8$ particles. Larger showers can be detected when their axes are even farther away, but their particle numbers cannot be determined accurately because their axes cannot be well located.

Basic apparatus qualitatively similar to that at Cornell has also been

operated by the cosmic ray groups at MIT, Harwell, and the Universities of Sydney, Tokyo, and Moscow. An international co-operative enterprise along similar lines is now being set up at La Paz, Bolivia, with the assistance of scientists from Bolivia, Tokyo, MIT, and Michigan. The arrays of counters have varied in diameter, the stations vary in altitude, and sometimes hodoscoped Geiger counters have been used in place of scintillators to determine the particle density; but the main principles of the basic apparatus have been common. In some instances the equipment has not provided a determination of the direction of the shower axis; the showers have then been assumed to be vertical, since atmospheric absorption has a strong collimating effect, or else a statistical correction for the average distribution of inclinations has been applied.

The basic apparatus is supplemented in these experiments by a wide variety of other detectors having special functions. These detectors include shielded counters to measure the mu-meson component, thick Cherenkov counters to absorb the electronic component and thus measure its energy density, shielded ionization chambers or counter hodoscopes to observe the nuclear-interacting component, electron density detectors of high resolution to observe the structure of a shower near the axis, and photomultipliers to measure the Cherenkov light radiated by the electrons in the air. The basic apparatus provides a means of correlating such information with shower size, direction of the axis relative to the zenith, and distance of the special detector from the axis.

2. EVOLUTION OF EXTENSIVE AIR SHOWERS AND SELECTIVITY OF DETECTORS

The particles in extensive air showers are divided into three principal components: (a) the N component or nuclearactive component, which includes all kinds of particles that participate in strong nuclear interactions, (b) the electromagnetic or soft component, consisting of photons, electrons, and positrons, and (c) the mu-meson component.

The genetic relations between these components are well understood. The backbone of a shower consists of an N -component cascade, initiated by a primary nucleus and maintained by high-energy secondary nucleons, antinucleons, mesons, and hyperons. The decay of secondary K mesons and charged π mesons gives rise to the muon component, which is thereafter nonmultiplying and is very slowly absorbed by ionization and beta decay. The decay of secondary π^0 mesons (some of which are created directly, others by decay of K mesons and hyperons) transfers energy repeatedly to photons, each of which initiates an electromagnetic cascade. The overlapping photon-electron cascades rapidly grow to comprise the most numerous particles in the showers. The individual electromagnetic cascades have a small range compared with the thickness of the atmosphere, and the total soft component gradually dies out as the source of energy in the N -component cascade becomes depleted. Ultimately, the most numerous particles remaining in the shower are the muons.

There are minor cross-feeding processes between the muon and electro-

magnetic components, as follows. Through photonuclear reactions, the photons of energy larger than 2 Bev generate some π mesons, which decay into muons that are capable of surviving long enough to be detected. However, the number of muons generated in this way can be computed and is about one per 1000 electrons at the shower maximum, 10 to 100 times smaller than the observed numbers of muons in the extensive air showers. The muons, in turn, generate an electromagnetic component through beta-decay and knock-on processes. If this were the only source of electrons, they would be about half as numerous as the mesons instead of an order of magnitude more numerous. Therefore, in first order these cross-feeding processes may be ignored.

It is clear that the composition of a single air shower and the energy spectra of its components undergo major changes as the shower grows and dies down. But no apparatus has yet been constructed to follow the development of single showers; the experiments only sample each shower at one stage in its existence.

The nuclear cascade which is the backbone of a shower is dominated by a very few high-energy particles, sometimes only one, in the core of the shower; and the number of nucleon-nucleus mean interaction lengths in the vertical atmosphere is only about 13. Hence, fluctuations in the height of the first interaction and in the rate of shower growth are very large, and showers of a given size are encountered at a single altitude in all stages of development.

A dominant factor in determining the most probable condition of an observed shower is the steepness of the primary energy spectrum of cosmic rays. The least possible energy for a shower of a given size is the energy for which that shower would be at its maximum development, having undergone such fluctuations as lead to an unusually high maximum. Any shower that is very far from this condition will be rare among the other showers of the same size, because of the high energy required for its production.

As a consequence of this bias, the majority of the showers recorded at almost any elevation are in nearly the same stage of development, not very far from the stage at which the number of particles is a maximum. This selectivity of the detecting apparatus accounts for some of the uniformity in the shower properties that have been measured. In particular, it accounts for the observation that by far the most abundant charged particles in the recorded showers are the electrons. Indeed, physicists were long misled by the overwhelming abundance of electrons to interpret the showers as purely electromagnetic cascades.

3. AVERAGE LATERAL DISTRIBUTION AND ENERGY SPECTRUM OF THE ELECTROMAGNETIC COMPONENT

One of the most oft-repeated measurements of extensive air showers has been the average lateral distribution of the total charged particle density. A remarkable feature of the results has been their invariance, apart from small

discrepancies that are within the experimental errors—not only from one method of measurement to another, but also with respect to changes in the size of the selected showers and the altitude at which the observations were made. Furthermore, the form of the average distribution agrees with that computed for a pure electromagnetic cascade, in which the lateral distribution is entirely due to Coulomb scattering of the electrons.

According to the cascade theory, the local density of electrons can be written as

$$\rho = (N/r_1^2)f(s, r/r_1) \quad 3.1.$$

where N is the total number of electrons, r is the perpendicular distance from the shower axis, r_1 is the Molière unit, a characteristic unit of length in the scattering theory, and s is a parameter related to the energy spectrum of the photons and electrons.⁴ The geometrical value of r_1 is inversely proportional to the density of the medium, but because extensive air showers develop in a medium of varying density, one should evaluate r_1 with the air density about two radiation lengths (75 gm./cm.²) back from the observation level along the axis of the shower. For showers recorded at sea level, the appropriate value of r_1 is 79 m.

In Figure 1, $\rho(r)$ has been represented for a shower having 10^8 charged particles at sea level. The function drawn in this graph is an empirical analytic function which has been found (with appropriate adjustment of N for showers of different size, and of r_1 for the different elevations) to be indistinguishable from the average experimental distributions obtained by many workers in the United States, England, Russia, Japan, and Australia, for showers of size ranging from $2 \cdot 10^8$ to $2 \cdot 10^9$ charged particles, at atmospheric depths varying from 537 gm./cm.² (vertical showers at Chacaltaya, elevation 5200 m.) to 1800 gm./cm.² (at sea level with zenith angle 55°), and at distances from the shower axis running from 5 cm. to 1500 m. This function is

$$\rho(N, r) = \frac{0.4N}{r_1^2} \left(\frac{r_1}{r}\right)^{0.75} \left(\frac{r_1}{r+r_1}\right)^{3.25} \left(1 + \frac{r}{11.4r_1}\right) \quad 3.2.$$

Without the last factor on the right-hand side, Equation 3.2 is a close approximation to the complicated theoretical expression derived by Kamata & Nishimura (1) for electromagnetic cascades having an age parameter $s=1.25$. For $0.5 < s < 1.5$, the Nishimura-Kamata functions are in general well represented by

$$(s, r/r_1) = (r/r_1)^{s-2} (1 + r/r_1)^{s-4.5} \Gamma(4.5-s) / [2\pi\Gamma(s)\Gamma(4.5-2s)] \quad 3.3.$$

⁴ In showers begun by a single photon or electron, s increases as the shower progresses and the spectrum becomes softer, the form of the spectrum being approximately $E^{-(s+1)}dE$. The rate of growth and decay of the number of particles is also related to s , being described by $\partial \ln N / \partial t = \lambda(s)$, a decreasing function of s which is zero when $s=1$, at the shower maximum. Hence s is called the "age parameter," although in showers initiated by a power-law spectrum of photons or electrons [$n_0(E)dE \sim E^{-(\alpha+1)}dE$] s would be a constant, equal to α .

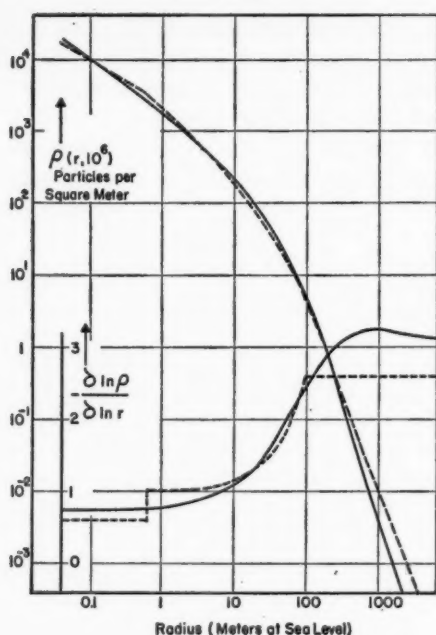


FIG. 1. Average lateral distribution of the density of charged particles in extensive air showers, represented for a shower of 10^6 particles at sea level. The solid curves give the density and its logarithmic derivative according to Equation 3.2 in the text; the dashed curves illustrate another approximate representation of the data, widely used in Russia.

The last factor in Equation 3.2 is empirically necessary to represent the experimental distribution of all charged particles, which varies about as r^{-3} at the largest distances from the axis. As will be shown below, one may interpret this factor as an approximate addition of the contribution of mu mesons and their secondary electrons to the total charged particle density.

Also shown in Figure 1 is the logarithmic derivative of $\rho(r)$, which is useful because the approximation $\rho(r) \sim r^{-n}$ is fairly accurate in certain intervals of radius and because the logarithmic derivative n is all that is directly determined in some of the experiments. One may see that n is equal to about 0.8 close to the axis, one at 10 m., two in the neighborhood of 50 m., and three for radii beyond 200 m.⁵

⁵ At these large radii, the Russian workers report a smaller exponent, $n=2.6$, but we believe that this discrepancy is due to their failure to measure the zenith angles of the showers. For small counter separations, most of the recorded showers are nearly vertical; but because $\rho(r)$ is so steep, many of the showers in which particles are recorded far from the center are strongly inclined relative to the vertical, and the distance of the particles from the axis is much less than the separation of the counters. This is an experimental observation at Cornell University, where all the zenith angles are measured, and the correct perpendicular distances are known in each case.

In the interval $1 < r < 200$ m. from the axis, the research groups at MIT, Moscow, and Sydney have found it convenient to approximate the lateral distribution with a function of the type

$$\rho(N, r) = (aN/r)e^{-r/b} \quad 3.4.$$

which is hardly distinguishable from Equation 3.2 in this range of r . For illustration, we have plotted with a dashed curve in Figure 1 the function adopted by the Moscow experimenters. For $0.6 < r < 96$ m., they have used Equation 3.4 with $a = 2 \cdot 10^{-3}$ and $b = 60$ m. For $0.05 < r < 0.6$ m., they find $\rho \sim r^{-0.6}$, and for $r > 96$ m. they have used $\rho \sim r^{-2.6}$. The MIT and Sydney groups have found that Equation 3.4 applies out to larger values of r (200 to 300 m.) if they adopt a larger value of b , about 74 m.

The choice of an approximating function is purely a matter of convenience for the analysis of experiments. In seeking significance in the results, one must resort to some physical model; and the outstanding fact is that all ways of approximating the average lateral distribution, if one discounts the mesons and their secondaries at very large radii, agree closely with the pure electronic cascade model incorporating a fixed age parameter s . Such close agreement cannot be accidental.

Some qualifications are necessary to the claim that a unique function fits the lateral distribution for all shower sizes from $N = 2 \cdot 10^5$ to $2 \cdot 10^9$ and at all radii from 5 cm. to 1500 m. A simple calculation shows that in a shower of 2000 particles, Equation 3.2 predicts only one particle within 10 cm. of the axis, and only 17 within 1 m. Hence the cores of such small showers cannot be located with sufficient precision to study the distribution at radii smaller than a meter. And the average density at 100 m. from the axis is only one particle per 120 sq. m.; hence the densities cannot be measured this far from the axis in such small showers. Indeed, to locate the axis to better than 10 cm. one needs showers containing several tens of thousands of particles. A second requirement is that the shower axis fall within an instrument of fine spatial resolution. Such devices have not yet been made larger than about 2 sq. m. in area. At sea level, showers containing more than 10^5 particles occur so rarely that their axes would traverse such a detector only about once in five days; for showers of 10^6 particles it would happen about twice a year. At mountain elevations an order of magnitude can be gained in frequency, but one normally loses in running time and the limitations imposed by the frequency of events are only slightly relieved.

For such reasons, within 1 m. of the axis the shower structure has only been measured for showers of size within a small range near $N = 10^5$. From 1 to 100 meters, showers of both smaller and larger sizes, from 10^5 to 10^7 particles, have been accessible to measurement. Beyond 100 m. from the axis, only showers of $N > 10^6$ have been measured. And for the largest recorded showers, containing around 10^9 particles, there are no measurements of the lateral distribution except beyond 100 m. from the shower axis.

Furthermore, small changes in the lateral distribution function with shower size and with altitude have actually been perceptible, although barely.

The few measurements on showers of more than 10^9 particles at sea level have been more consistent with $s=1.1$ in the distribution function represented by Equation 3.3 than with $s=1.25$; and some of the measurements on very small showers have been in better agreement with $s=1.4$. A direct test of the systematic variation of s with N has been made at Cornell (2), with the result that s decreases by 0.06 ± 0.09 for a factor 10^3 increase in N . The MIT group (3) has found that a 4100 m. elevation, showers containing more than 10^7 particles have a lateral distribution corresponding to $s=1.0$ or 1.1 ; although other groups, studying smaller showers, have found results fitting $s=1.2$ to 1.3 , as at sea level. At aeroplane elevations (on the order of 10 km.), the typical lateral distribution corresponds to a value of s less than one. And at all elevations, individual showers seem to exhibit substantial departures from the average distribution.

Thus, the shape of the distribution function is neither perfectly constant nor accurately known under all conditions; but all of the experiments reinforce the conclusion that systematic variations in shape with size of the shower and with elevation are extremely slow, as is also the change with r of the age parameter that characterizes the distribution function.

These results are contrary to predictions for electromagnetic cascades begun by a single photon or electron at the top of the atmosphere, or by a collection of π^0 mesons originating in a single nuclear collision at the origin of the shower. In a shower of finite energy with a single origin, the high-energy particles near the core reach their maximum development and begin to be absorbed sooner than the lower-energy particles farther from the axis; hence the value of the age parameter, s , that determines the slope of the lateral distribution, decreases with increasing radius (1, 4). Secondly, s should decrease more rapidly with altitude and with shower size than has been observed. On the other hand, the observations are just those that should be expected, after some distance from the origin, for showers that have a source of energy distributed along the axis according to $e^{\lambda t}$, where t is distance along the axis and $\lambda(s)$ is the cascade parameter related to the rate of change of particle number.⁴ For $s=1.25 \pm 0.05$, $(\lambda)^{-1}=4.2$ to 5.8 radiation lengths (160 to 220 gm./cm.²; or two to three nuclear interaction lengths). This is a plausible value for the absorption length of the nuclear cascade if high-energy collisions can be somewhat elastic, as is also inferred from individual interactions seen in emulsion stacks. Fluctuations of individual showers from the average form can be predicted, too, since in individual showers the source of energy would not be a smooth exponential function, but very bumpy.

Particular interest has centered on the lateral distribution in the immediate neighborhood of the axis, because of the possible implications regarding the energies and angles of the secondary particles from very-high-energy nuclear collisions. The search for complex structure near the axis has been carried out with cloud chambers and close-packed arrays of ionization chambers, especially by the cosmic ray groups at Moscow and the University of Michigan. For reasons given above, the data refer only to showers with $3 \cdot 10^4 \leq N \leq 3 \cdot 10^6$ and are rather sparse, less than 100 events having been

observed in all the reported investigations. On the whole, about two-thirds of the showers were found to have a single sharp peak in the density of particles. About half of the remainder exhibited flattened distributions within one-half meter of the axis, which may have been due to an unresolved core structure or simply to age of the shower: cores separated by less than 20 cm. were not resolvable. Ten to 20 per cent of the events had two or more resolved peaks in the distribution at separations of about one or two meters. Complex structure was more common in larger showers than in small ones.

The energy spectrum of the electromagnetic component of extensive air showers has been studied by examining the multiplication of particles in thin layers of lead, either within cloud chambers or placed above an array of ionization chambers. Many investigations of this sort have been performed in the United States, Japan, and Russia, both at sea level and at mountain elevations from 2800 to 3900 m.

As in the case of the lateral distribution, the shape of the energy spectrum has been found to be remarkably independent of the size of the showers and the elevation at which they were detected. In Figure 2, some typical results are shown for the combined energy spectrum of photons and electrons at several distances from the axis. It can be seen that the spectra grow steeper with increasing r , the showers being poorer in high-energy electrons and photons at larger radii.

In Figure 3, the average energy density in the electromagnetic component is shown as a function of r . From the energy density and the density of charged particles, the average energy per electron has been calculated and is graphed in the same figure. This combined energy of photons and electrons is around 4 Bev per electron at about 10 cm. from the axis, decreases with r about as $r^{-2/3}$ until r is about $0.5 r_1$, and is approximately constant for values of r exceeding r_1 , at a value a little less than the critical energy ϵ .⁶

By integrating the energy flux over the whole plane, one can calculate the total energy carried by the electromagnetic component. The result is about $0.2 N$ Bev, where N is the number of electrons.

The electromagnetic energy spectrum in the neighborhood of the axis is remarkably poor in high-energy particles, and the total electromagnetic energy in a typical shower is small. A purely electromagnetic shower with such a soft spectrum would be expected to have a much flatter lateral distribution than is observed for these extensive air showers, and it is easy to show that such a shower would be rapidly absorbed. Each electron dissipates by ionization an amount of energy equal to ϵ per radiation length; hence the absorption coefficient would be about $\epsilon/(0.2 \text{ Bev})$, which is 0.4 per radiation length. But measurements to be reported below show that the absorption coefficient is only half this large.

Thus, one can infer that the photon-electron component in an average shower is sustained not just by its original dowry of energy, but also by a

⁶ ϵ is the energy dissipated in ionization, per radiation length, by electrons of energy equal to ϵ . For air, $\epsilon = 84$ Mev [see (5) for definitions and survey of shower theory].

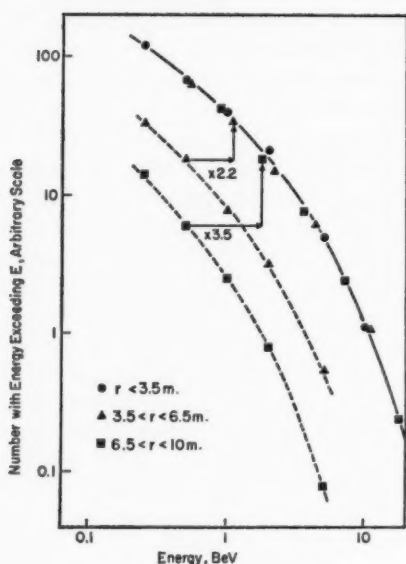


FIG. 2

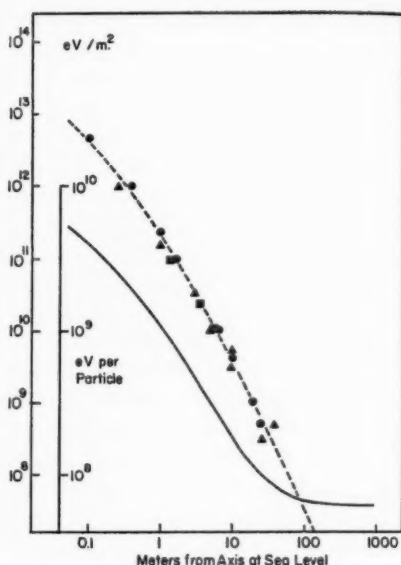


FIG. 3

FIG. 2. Energy spectra of photons plus electrons in three different intervals of distance from the axis or extensive air showers at 2770 m. elevation, as reported by Kameda, Maeda & Toyoda in (6). The average size of the showers was $4 \cdot 10^6$ charged particles. The points at the larger distances have been shifted in energy by a factor equal to the distance ratios, as indicated on the graph, to demonstrate that the shape of the spectrum is a function of the product Er , rather than of E and r separately, over the range of E and r encompassed by these data.

FIG. 3. The experimental points and dashed curve represent the average energy flux, carried by the photon-electron component in a shower of 10^6 charged particles. The squares represent the data of Kameda, Maeda & Toyoda (6) that are scaled down from 2770 m. elevation to sea level according to the change in the Molière unit r_1 . The triangles and circles represent data taken in two experiments at sea level, reported by Vernov, Goryunov and others (7). By dividing the energy flux by the average density of charged particles (Fig. 1), one obtains the solid curve in the present figure, which represents the average combined energy of the photons and electrons, per electron at the same location in the shower. The uncertainty at any point in the latter curve is at least 30 per cent, but the trend and the approximate level have been verified repeatedly.

repeated infusion of energy from the nuclear cascade; and one can infer the average rate at which such energy is injected, namely about $0.5 \epsilon N$ per radiation length, which for a shower of 10^6 electrons is 10^{13} ev per nuclear mean free path. In order to account for the continued steepness of the lateral distribution of the electrons, it is necessary that the nuclear cascade from which the energy is supplied have a well-defined core, smaller than a meter in diameter. Indeed, the fact that the lateral distribution has usually a single peak and continues to be steep even at 10 cm. from the center suggests that the core of a shower is usually dominated by a single nuclear particle of remarkably high energy, which generates π^0 mesons repeatedly in collisions of high elasticity.

How then should one interpret those showers that reveal multiple peaks in the density distribution at separations on the order of one or two meters? Two proposals are conceivable, and probably both are correct, the only question being which of the two mechanisms is dominant. One is that some of the showers are initiated by heavy nuclei, which are soon broken up by excitation received in a nuclear collision. Thereafter, each nucleon of the primary nucleus generates a shower through a succession of semielastic collisions, and all of these showers have nearly parallel axes. The succession of collisions, imparting transverse momenta on the order of 10^9 ev/c, would account for characteristic core separations of about one meter. Fluctuations in the development of the separate showers would account for the rather large differences in local particle density around the various cores.

The other proposal is that the elasticity of high-energy collisions is highly variable and subject to chance. This is indeed observed to be true at somewhat lower energies, where individual interactions have been studied in detail. Those primaries which undergo few collisions, or elastic collisions, in the high atmosphere would be the ones most likely to produce the showers observed near sea level; but some of the primaries would occasionally give up a large fraction of their energy to one or two secondary particles, which thereafter could produce distinct density peaks in the electron distribution.

As we consider other aspects of the extensive air showers, we shall see that there are further evidences of large fluctuations in the character of the nuclear interactions involving the most energetic particles in the showers.

4. THE MUON COMPONENT

The mu mesons are recognized by their ability to penetrate thick shields without interacting. Near the axis of an extensive air shower, the muon density is typically 50 to 100 times less than that of electrons, but with increasing radius muons grow comparatively more abundant, and beyond 1000 m. they are the dominant particles. Although most of the mesons are in areas where their density is small, integrated over the whole plane their number is very big. Furthermore, their average energy is much greater than that of the electrons. Thus the muons in a typical shower at sea level carry much more total energy than does the photon-electron component.

The energy spectrum of the mesons depends on the distance from the shower axis at which the mesons are detected. Figure 4 shows some measurements made with a magnetic spectrometer (8); at 475 m. from the axis the spectrum is as soft as that of the background mesons, but close to the axis it is much harder. The meson showers have been followed as far underground as 1600 m. of water equivalent (9), a range that requires a minimum energy of about 560 Bev. Of the mesons within 10 m. of the axis, several per cent penetrate at least that far, but practically none beyond 20 m. from the axis can do so.

Thus, the lateral distribution is dependent on the minimum energy required for detection of the mesons. The results shown in Figure 5 were obtained at sea level with an absorber requiring about a Bev—except for the three points at the largest distance (850 m.), for which the absorber thickness was somewhat less. For this reason the smooth curve is drawn a little below those points.

These data were taken at MIT with an apparatus that yielded knowledge of the shower size and axis inclination for each event. Showers were recorded of sizes from $2 \cdot 10^6$ to $2 \cdot 10^8$ charged particles, and it appeared that the number of mesons was not proportional to the shower size, but to N^α with $\alpha \approx \frac{3}{4}$. Adopting this proportionality, the data on showers of size between 10^6 and 10^8 particles have been normalized to $N = 10^6$. The consistency of the points indicates that the lateral distribution is not a strong function of N .

In the neighborhood of the axis, the data shown in Figure 5 are sparse, but several other experiments have revealed that the dependence on r in this range is approximately $r^{-3/4}$. The smooth curve in the figure is a function having the same general character as that which describes the total charged particle density (Eq. 3.2, drawn in Fig. 1): namely,

$$\rho_\mu(N, r) = 18(N/10^6)^{3/4} r^{-3/4} [1 + (r/320)]^{-2.5} \quad 4.1$$

with distances expressed in meters.

Integration of Equation 4.1 shows that half of the mesons are at distances exceeding 320 m. from the axis. The mean radius appears to be 1600 m. but is very sensitive to the assumed form of the distribution beyond where it has been measured. The total number of mesons above about one Bev in energy is

$$N_\mu(>1 \text{ Bev}) = 95,000(N/10^6)^{3/4}$$

Similar information on the density of mesons at various radii, in showers of known size, has been obtained underground by Andronikashvili and collaborators (11), at depths corresponding to minimal energies from 13 to 36 Bev. By integration over the plane and scaling according to the $N^{3/4}$ proportionality, the total numbers of such mesons have been found for an average shower of 10^6 particles. At 1600 m. water equivalent, corresponding to a minimal energy of about 560 Bev, Cornell experimenters (9) have measured the absolute frequency of showers as a function of the number of

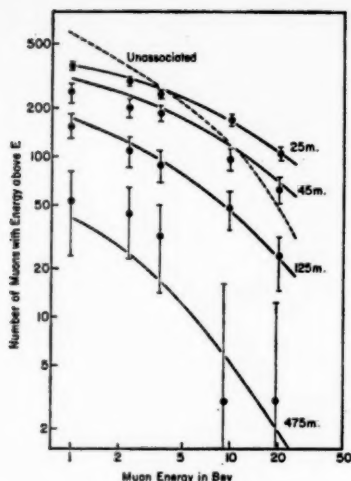


FIG. 4. Mu-meson energy spectra at various distances from extensive air-shower axes, measured by Bennett (8). The data cover a wide range of shower sizes, $10^3 < N < 10^7$, and each solid curve refers to a considerable interval of radius, with mean values indicated. The dashed curve refers to mesons that were not coincident with detected showers. The solid curves were computed with the following expression for the density of mesons (per sq. m.) with energy above E (Bev) at distance r (m.) from the axis of showers containing N charged particles:

$$= \frac{14.4 r^{-0.75}}{(1 + r/320)^{2.5}} \left(\frac{N}{10^6} \right)^{0.75} \left(\frac{51}{E + 50} \right) \left(\frac{3}{E + 2} \right)^{0.14r^{0.37}}$$

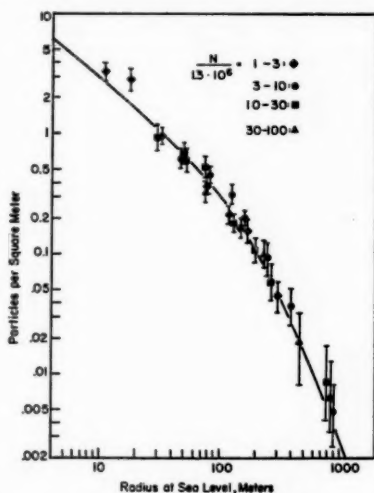


FIG. 5. Lateral distribution, at sea level, of mesons with energy exceeding about 1.0 bev; data reported by Clark, Earl, Kraushaar, Linsley, Rossi & Scherb (10). The results have been normalized to a shower of $N=10^6$ charged particles by assuming that the lateral distribution is independent of N but the total number of mesons is proportional to $N^{2/3}$.

mesons. By equating this to the frequency of extensive air showers at sea level with N charged particles, one finds that

$$N_{\mu}(>560 \text{ BeV}) \approx 75(N/10^6)^{\alpha}$$

with $\alpha \approx 0.7$ for large values of N and N_{μ} , decreasing towards 0.5 for N_{μ} in the neighborhood of one (i.e., showers of 500 to 1000 electrons contain on the average one such meson). With this information we have plotted in Figure 6 the energy spectrum of mu mesons integrated over the whole plane. The results fit the relation, with E expressed in BeV,

$$N_{\mu}(>E, N) = 1.7 \cdot 10^5 \left(\frac{2}{E+2} \right)^{1.37} \left(\frac{N}{10^6} \right)^{0.75} \quad 4.2.$$

Thus in an average shower of 10^6 charged particles at sea level, about 17 per cent are muons, and another 6 or 7 per cent must be electrons secondary to the muon component. The mean energy of these muons, computed from Equation 4.2, is 5.4 BeV, and their total energy is therefore $9 \cdot 10^{14}$ ev.⁷ As reported above, the mean photon-electron energy per electron in the shower is only 0.2 BeV; hence the energy carried by the electromagnetic component is $1.6 \cdot 10^{14}$ ev, five or six times less than that of the muons. In showers of less than 10^6 particles the imbalance can be considerably larger.

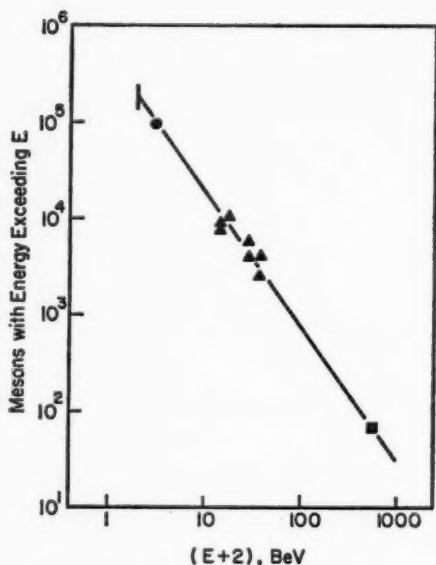


FIG. 6. Energy distribution of muons in extensive air showers, normalized to a shower of 10^6 charged particles at sea level, and integrated over the shower panel.

⁷ Bennett's data (8, Fig. 4) also fit the form of Eq. 4.2, but agree better with a numerical coefficient of 1.3×10^5 , and an exponent of 1.29 in the energy factor. Nevertheless, the total energy is the same as calculated above.

This situation is a consequence of the long range of muons and the comparatively rapid absorption of the other components. In an average shower at sea level the electromagnetic energy and that of the N component are much depleted, while that of the muons has only been reduced by about one-third through decay and ionization. But at the shower maxima high in the atmosphere, the electrons are an order of magnitude more numerous than at sea level and their average energy is also higher; therefore the energy balance between muons and electrons is reversed.

At high elevations there is not much information on the meson component. The meson densities seem higher than in the same showers at sea level. But since muons are absorbed very slowly, one must conclude that the higher densities are a consequence of compression of the lateral distribution. Indeed, the numbers are consistent with the crude picture that the mesons are produced near the axis at elevations mostly between 8 and 16 km., diverging from the axis in approximately straight lines as the shower approaches sea level. The widths of the lateral distributions for mesons of various energies are approximately consistent with this model if the mesons are produced with average transverse momenta of 0.2 to 0.7 Bev/c, in agreement with other experiments on meson production. It is reasonable to suppose that the comparatively low-energy mesons usually originate a little lower in the atmosphere (5 to 10 km.) and the most energetic ones a little higher (15 to 20 km.), because of energy degradation in the extensive air showers and the reduction of the π - μ decay probability with energy and atmospheric density.

The above picture of the distribution of meson origins in an extensive air shower is also supported by observations of meson directions relative to the axes [Cranshaw, deBeer & Parham (12)] and by measurements of the time delays of particles far from the axes of such showers [Greisen, Delvaille & Kendzioriski (13)].

The ratio of positive to negative muons in extensive air showers has been observed (8) to be close to 1.0. This value indicates that pion production continues to dominate heavily over K -meson production at an average secondary energy on the order of 10 Bev, since pions are charge symmetric, whereas the K^+/K^- ratio is large and the generation of muons through decay of Λ and Σ hyperons is comparatively inefficient in terms of energy.

From the numbers of muons reaching sea level, one can compute the amount of energy dissipated in the shower by transfer to neutrinos in π - μ and μ - e decay, and by the ionization loss of muons in the atmosphere. The result is 5 Bev per muon reaching sea level, about equal to the energy of the muons themselves.

5. THE NUCLEAR-INTERACTING COMPONENT

This component of extensive air showers requires different methods of study in different ranges of energy. Slow neutrons, from thermal energies up to one Mev, must be very abundant in the showers, but have not yet been measured. Moderately fast neutrons (1 to 20 Mev) have been found to be

10^{-2} to 10^{-3} times as numerous as electrons near the axis, but the measurements have been very few and quite crude. Neutrons in the range 50 Mev to 1 Bev have revealed their presence by delayed signals in scintillation counters and by occasional stars in cloud chambers in coincidence with extensive air showers. The density of these neutrons is about 1 per cent of the electron density near the shower axis, but increases relative to the electrons with distance, and is about 20 per cent of the electron density at 1 km. from the axis (according to unpublished Cornell data).

Most of the experimental attention has been devoted to the particles of higher energy, exceeding a few Bev, which can contribute to the shower development through production of energetic secondaries. In the energy range from about 3 to 100 Bev, 40 ± 5 per cent of the nuclearactive particles have been found to be neutral, indicating that π or K mesons constitute part of this component, but that most of the particles are protons and neutrons. Above 100 Bev no identification of the particles has been made.

Some of the studies have been pursued with cloud chambers containing lead plates, or with shielded counters in a hodoscope, detecting the N component by observation of the production of multiple penetrating particles and electron showers. Measurements of the energies of the incident particles from such observations are not precise, but the effective threshold for such events is a few Bev. Very high energies saturate such detectors, and a more appropriate apparatus has proved to be an array of shielded ionization chambers, with which nuclearactive particles have been measured up to 10^{14} ev. Through π^0 meson production, secondary electronic cascades are created in the shielding material, causing an ionization that on the average is proportional to the incident energy. The progress of individual nuclear cascades is subject to fluctuations, but the average behavior has been determined by measuring the response of many rows of ionization chambers under a succession of shielding layers. Unfortunately, the coefficient relating the ionization to the average incident energy still has an uncertainty of at least 30 per cent.

With a lattice of ionization chambers, as used in some of the Russian installations (14), one can distinguish and count the single nuclearactive particles. With simpler arrangements, it has only been possible to determine the average energy flux.

Out of a very large number of experiments, the following digest of information can be given about the high-energy N component.

Altitude variation.—For a shower of given size, the average spectrum and number of nuclearactive particles seem to be nearly the same at altitudes as high as 4000 m. as at sea level. This is illustrated in Figure 7.

Lateral distribution.—As expected, the particles of very high energy are closer to the axis than those of lower energy. Figure 8 illustrates this relationship with some measurements of spectra at various distances. Particles exceeding 10^{12} ev are usually found within 2 m. of the axis and have not been detected beyond 5 m. Those of 10^{11} ev are mostly closer than 10 m. and have not been detected beyond about 30 m.

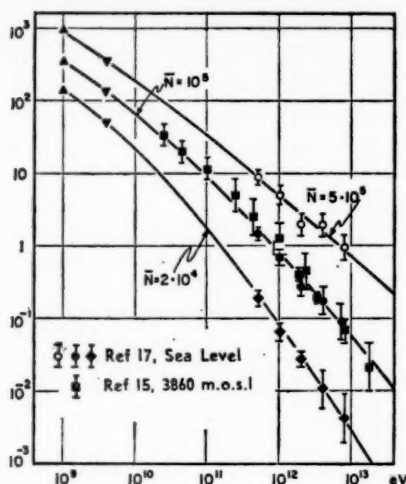


FIG. 7. Integral spectra of nuclearactive particles in extensive air showers of three different sizes. Systematic variations with elevation are less than the experimental errors. The low-energy points were estimated from numerous studies in the United States, England, and Japan at altitudes from 0 to 4300 m.

Thus, to make possible the study of the most energetic particles, the very center of the shower must strike the apparatus. For this reason, extensive air showers having more than 10^6 particles have been too low in frequency to permit such analysis. On the other hand, showers having less than 10^4 particles usually contain none of energy above 10^{11} ev. Therefore, the ion-chamber data on the high-energy N component are limited to showers of size between 10^4 and 10^6 particles.

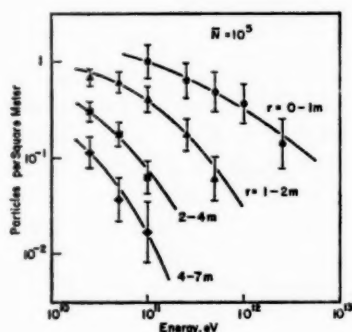


FIG. 8. Energy spectra of nuclear-interacting particles in various bands of distance from the axes of extensive air showers, at 3860 m. elevation; taken from (15). The densities were all scaled to represent a shower of 10^6 charged particles.

From the total ionization due to the N component at various distances from the axis, the energy density as a function of radius has been deduced. In Figure 9 this is compared with the energy density of the electron-photon component for a shower containing $3 \cdot 10^8$ charged particles.

Spectrum.—By integrating the lateral distributions, the total numbers of nuclearactive particles in extensive air showers can be obtained as a function of energy. The integral spectra for three shower sizes are shown in Figure 7. These numbers of N particles may be too low by a factor on the order of two, because of inadequate data in the tails of the lateral distribu-

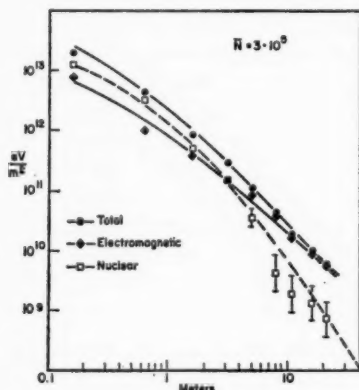


FIG. 9. Lateral distributions of the energy of the electromagnetic and nuclear-interacting components, in showers of average size $3 \cdot 10^8$ charged particles, at an elevation of 3860 m.: from Nikolsky & Tukung (16). The integrated energy of the electromagnetic and N components in a shower of this size is 10^{14} ev, approximately $6 \cdot 10^{13}$ ev being in the electromagnetic component.

tion, and because the energy conversion factor used by the Russian investigators was possibly too small; but one may be confident that the numbers and energies are not significantly too high. The curves represent statistical averages. Thus, when the number of particles is indicated to be less than one, it describes the probability of finding such a particle in a shower.

The spectra increase in steepness with increasing energy, having a logarithmic derivative less than one when the number of particles is large, and greater than one when the average number of N particles becomes less than one. The dependence of the number of nuclearactive particles on the size of the shower is therefore quite different at different minimal energies. If one approximates this dependence by $N_{na} \sim N^\alpha$, one finds that α increases from about 0.6 below 10^{10} ev to about 1.7 at 10^{13} ev, within the investigated range of shower size.

The unique feature of the nuclear-interacting component is the high value of the average energy per particle. Although the particle density near

the axis is typically less than 1 per cent of the electrons, the energy density exceeds that of the electronic component. With the aid of Figure 9, Figure 1 (with appropriate scaling), and measurements of the relative density of N component and electrons, one may evaluate mean particle energy at various distances from the shower axis, shown in Table I.

TABLE I
MEAN PARTICLE ENERGIES

[for shower of $N=3 \cdot 10^8$ at elevation of 3860 m. (pressure 650 gm./cm.²)]

Distance from axis		20 cm.	1 m.	10 m.
Energy density: (ev/m. ²)	Electrons plus photons	$0.7 \cdot 10^{13}$	$7.6 \cdot 10^{11}$	$2 \cdot 10^{10}$
	N component above 1 Bev	$1.1 \cdot 10^{13}$	$1.3 \cdot 10^{12}$	$7 \cdot 10^9$
Particle density: (m. ⁻²)	Electrons	910	270	39
	N component above 1 Bev	7.8	1.7	0.15
Mean energies: (Bev)	Electromagnetic energy per electron	7.7	2.8	0.52
	Nuclearactive particles above 1 Bev	1400	770	47

Integrated over the entire plane, the number of nuclearactive particles above one or two Bev in energy is

$$N_{na} \approx 0.35N^{0.6} \quad (10^4 \leq N \leq 10^9)$$

The total energy is approximately

$$(\Sigma E)_{na} \approx 0.8(\Sigma E)_{el} \approx 0.16N \text{ Bev}$$

Therefore the average energy of the nuclear-interacting particles is

$$\bar{E}_{na} \approx 0.45N^{0.4} \text{ Bev} \quad (10^4 \leq N \leq 10^9)$$

Thus, the mean energy is a function of shower size, as is clearly evident from Figure 7, but is on the order of 50 to 100 Bev for the showers which have been analyzed.

Energy balance.—By integrating over the energy spectrum, one obtains the average total energy of the N component. Within the accuracy of these calculations, the result is equal to the energy carried by the electronic component, $2N \cdot 10^8$ ev. This result seems to be independent of shower size and elevation, although it refers only to statistical averages: individual showers exhibit considerable fluctuations.

The constancy of the average result does not imply that the electromagnetic and nuclear energies are balanced throughout the whole history of an extensive air shower, but reflects the tendency for the most frequent

showers of a given size to be the ones that have reached the stage of development where the nuclear and electromagnetic energies are about equal. Nevertheless, this observation would not hold over such a large range of altitude and shower size, were the electronic component not in rather close equilibrium with the N component. This condition would not exist if the electronic component got its impetus in one or two catastrophic collisions near the shower origin; the energy transfer must usually be made in numerous, successive small proportions of the N -component energy. Such a picture fits well, also, with the sparsity of very-high-energy photons and electrons even in quite large showers.

Fluctuations.—As mentioned above, the individual showers exhibit large deviations from the statistical average, especially very near the axes. These deviations appear in the lateral distributions of the electrons and N component, and in the relative numbers and energy content of the electrons, muons, and nuclearactive particles—which may vary by an order of magnitude (i.e., a factor of three or more in either direction from the normal).

The spectrum of the N component is so flat that a rather large part of the total energy is carried by a small number of particles. The fluctuations are especially large in the part of the spectrum where the average number of particles is less than one. Indeed, in showers of $N=10^5$, there is usually only one particle of energy exceeding 10^{12} ev, which is equal to five per cent of the total electronic energy. But in some of these showers, a single nucleon has an energy as large as $2 \cdot 10^{13}$ ev, as much as the entire electronic component.

Since the interactions of the few nuclearactive particles carrying most of the energy are governed by chance, both in location and in distribution of energy among the secondary particles, it is only natural that large fluctuations in the energy balance should occur from one shower to another, particularly among the smaller showers, in which there is often only a single particle of very high energy in the core. And since the mean nuclear interaction length is long enough so that within one such length the electronic component can multiply or be absorbed by a factor exceeding two, one must expect even the course of a single shower to be rather bumpy—especially near the axis, where the response time is shortest.

6. CHERENKOV LIGHT

Many of the electrons in extensive air showers are sufficiently relativistic to emit visible Cherenkov radiation in the air. This light was first detected by Galbraith & Jelly in 1952 (18). The recent work of Chudakov and his collaborators in Russia (19) has demonstrated that the Cherenkov light conveys important information about the showers which can not be obtained by measurements on the particles themselves. We believe that the full value of this radiation has not yet been realized, and that its exploitation in the study of ultra-high-energy cosmic rays has great promise.

The experiments can only be carried out at night, and require a clear

moonless sky. One must also be in a remote location, far from city lights. The most effective detector has been a simple photomultiplier tube pointing upwards, housed in a box with the roof removed. Focussing mirrors have been used more often than not, but these make the signals much more difficult to interpret, and their advantage in noise level reduction is dubious. A single Cherenkov detector, of course, does not give enough information to analyze a shower; one must use a considerable number of them, spaced rather far apart. The relative times as well as the amplitudes of the signals are then of use in the analysis.

The unique aspect of the Cherenkov light is that it is not proportional to the local particle number, but to its integral over the previous history of the shower. The inverse square law of light intensity is compensated for by the increase, with height, of the area of sky from which each detector collects light.

The threshold energy of electrons for the Cherenkov process in air is 21 Mev at sea level. It increases slowly with elevation, as the inverse square root of the atmospheric density, and is 35 Mev at about 7.5 km., where extensive air showers typically have the largest number of electrons. The radiation by a particle of energy E is proportional to $1 - (E_0/E)^2$, where E_0 is the threshold energy. In first approximation one may assume the rate of radiation to be equal to its limiting value for all electrons of $E > \sqrt{2} E_0$ and neglect the radiation from the lower-energy particles. The limiting rate is about 200 photons (between 3750 and 6000 Å) per gm./cm.², or 7500 photons per radiation length. For each electron in a shower at sea level, there are on the order of 100 radiation lengths of electron track length in the atmosphere. Averaged over the whole shower [according to Richards and Nordheim (4)], 36 per cent of the electrons have energy above 50 Mev. Hence for each electron reaching sea level, there are about $3 \cdot 10^6$ Cherenkov quanta.

The background of starlight, according to Jelley, is $6.4 \cdot 10^7$ photons/(cm.² sec. sterad). If the photomultipliers are to detect showers with distant axes, the resolving time can be 0.5 μ sec. but should not be much less, because of straggling of the path lengths of the radiation. Thus a photomultiplier of 100 cm.² area, facing π steradians of the sky, receives per resolving time 10^4 photons and emits about 600 photoelectrons. The background fluctuation level is therefore 25 photoelectrons, and about 90 are required (1500 photons striking the tube) to make a pulse that stands out clearly from the noise. Thus, the threshold photon density is about $1.5 \cdot 10^6$ photons/m², whereas particle densities 10^4 to 10^5 times smaller can be measured equally easily, with a photomultiplier and large scintillator. However, the Cherenkov photons are so numerous that they still have a numerical advantage over particles of about 10 to 1, which is even greater far from the axis, because of the comparatively wide distribution of the radiation. The average scattering angle of 100-Mev electrons at the maximum of a shower is about 4°; hence the average distance of the Cherenkov

photons from the axes of extensive air showers at sea level is about 500 m.

Figure 10 shows some absolute measurements by Chudakov *et al.* of the photon density vs. radius in vertical showers of different sizes at mountain elevations and sea level. The ordinates are normalized to the local number of charged particles in the extensive showers, determined with associated counters of conventional types.

The smooth curves empirically fitted to the high-altitude data are represented by the following function:

$$\frac{\rho_\gamma}{N} = \frac{10^4}{(a + br + cr^2)^2} \left(\frac{1.4 \cdot 10^6}{N} \right)^{0.18}$$

with dimensions in meters, and $a = 16.5$, $b = 0.18$, and $c = 1.8 \cdot 10^{-4}$. At sea level the distribution is wider than in the mountains, as expected, but the data are inadequate to determine the lateral distribution accurately. It is interesting to note that at 200 m. from the axis at sea level, an extensive shower of $7 \cdot 10^5$ particles has a Cherenkov photon density two million times as great as the electron density.

Integration of the above function over radius yields a number of Cheren-

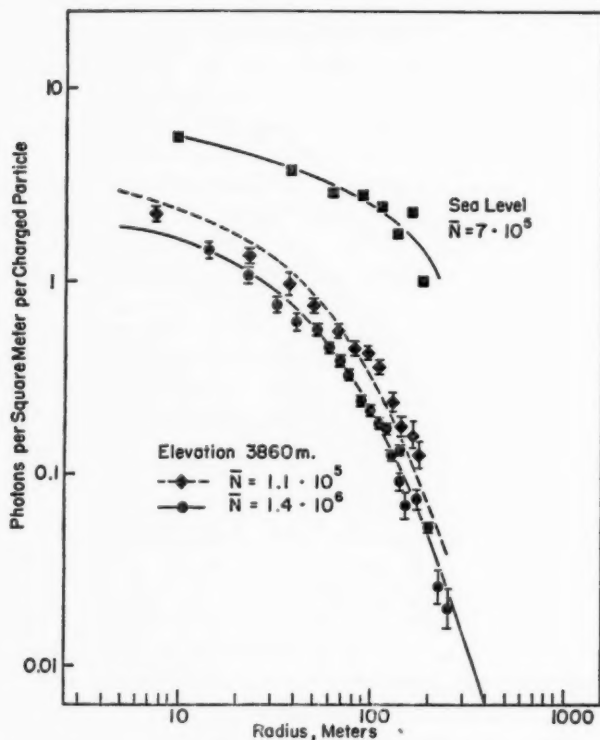


FIG. 10. Absolute densities of Cherenkov photons vs. distance from the axis, at sea level and mountain elevations; from data given in (19).

kov photons per electron equal to $1.2 \cdot 10^6$ at the mountain elevation, for $N = 1.4 \cdot 10^6$. Attempts to perform a similar integral of the sea level data yield a result an order of magnitude higher, but quite imprecise. From such integrals, one can find the total track length of electrons in the air above the apparatus, and hence the average primary energy of the extensive air showers. For instance, in order to yield $1.2 \cdot 10^6$ quanta the track length must be 45 radiation lengths, and the energy dissipation 3.8 Bev per electron, in the showers of $1.4 \cdot 10^6$ particles at 3860 m. elevation. The local energy, from Section II. 3-5 above, is about 0.4 Bev per electron in the electronic and nuclearactive components, and an equal amount in the muon and neutrino components (about five times less per electron than at sea level). Hence the average primary energy may be estimated as 4.6 Bev per electron or $6.5 \cdot 10^{16}$ ev.

Figure 10 shows that the average primary energy per local electron is greater in smaller showers, varying about as $N^{-0.15}$. Such an effect is expected because the smaller showers are farther beyond their maxima when detected locally. For the same reason, more light per electron accompanies inclined showers than vertical ones (15), and much more light per electron reaches sea level than mountain elevations. Equal primary energies yield approximately equal amounts of light, but the number of electrons diminishes with increasing atmospheric depth.

The data of Chudakov *et al.* demonstrate convincingly that most of the large showers seen at sea level are not events that begin low in the atmosphere and are observed near their cascade maxima; the number of electrons in these showers has been reduced beyond the maximum by a large factor. This demonstration sharpens up the question of why so many properties of the shower (lateral distribution and energy spectrum of the electrons, absorption coefficient, and balance of energy between electrons, and nuclearactive component) undergo very little change between mountain and sea levels.

The Cherenkov light provides a direct means of investigating the fluctuations in the local number of electrons arising from a primary particle of fixed energy and may offer a clue as to the distribution of high-energy primaries between protons and heavy nuclei. The Russian investigators found the fluctuations very small in large showers at mountain elevations, but the scope of such studies needs to be greatly extended.

7. DENSITY AND NUMBER SPECTRA OF SHOWERS

The integral density spectrum $H(\rho)$ is defined as the frequency with which the charged particle density at a fixed point in space exceeds the value ρ . Empirically, it is found that the logarithmic derivative $\beta = d(\log H)/d(\log \rho)$ is very nearly constant. Thus in first approximation

$$H(\rho) = c\rho^{-\beta} \quad 7.1.$$

This relation can be studied very precisely by measuring the frequency of coincidences among counters of area S , for different values of S . The probability of any counter being struck by a prescribed number of particles

is determined by the product $x = S\rho$; hence the counting rate is given by⁸

$$R = R_0 S^b \int_0^\infty g(x) x^{-b} dx \quad 7.2.$$

Thus, β can be determined from the derivative $\beta = \partial \log R / \partial \log S$, and the constant R_0 can be found by evaluating the definite integral. The integrand is typically peaked around a particular value of x , so each measurement relates to the spectrum in the neighborhood of a density $\propto 1/S$.

When such experiments were done carefully for a large range of values of S , the logarithmic derivative was found not to be perfectly constant. The slow variation was expressed adequately by

$$\partial \log R / \partial \log S = a + b \log \rho_m, \quad 1 < \rho_m < 10^4 m^{-2} \quad 7.3.$$

where ρ_m is the median value of x/S in the integral in Equation 7.2. Thus it was inferred that Equation 7.1 should be refined as follows:

$$\beta(\rho) = -\partial \log H / \partial \log \rho = a + b \log \rho \quad 7.4.$$

$$H(\rho) = H_1 \rho^{-(a+b \log \rho)}, \quad 1 < \rho < 10^4 m^{-2} \quad 7.5.$$

The following values of the constants were determined from the experiments: at sea level, $H_1 = 0.15$ per sec., $a = 1.30$, and $b \approx 0.11$ (for logarithms to the base 10); at 3260 m. elevation (705 gm./cm.²), $H_1 = 1.6$, $a = 1.25$, and $b \approx 0.13$. However, for most purposes it is adequate to use Equation 7.1 in the neighborhood of any density ρ_0 , with fixed values of c and β :

$$c = H_1 \rho_0^{0.5b \log \rho_0} \quad \text{and} \quad \beta = a + b \log \rho_0 \quad 7.6$$

If all extensive air showers have the same lateral distribution, i.e., if $\rho(r) = (N/r_1^2) f(r/r_1)$, the density spectrum represented by Equation 7.1 implies a similar number spectrum of showers. The integral number spectrum $F(N)$ is defined as the frequency of showers containing more than N charged particles, with axes crossing unit area. If F has the form

$$F(N) = KN^{-\gamma} \quad 7.7.$$

one may calculate the density spectrum as follows:

$$\begin{aligned} H(\rho) &= \int_0^\infty 2\pi r dr F[\rho r_1^2 f(r/r_1)] \\ &= \rho^{-\gamma} \frac{2\pi K}{r_1^{2(\gamma-1)}} \int_0^\infty [f(y)]^\gamma y dy \end{aligned} \quad 7.8.$$

By comparison of Equations 7.8 and 7.1 one may infer that $\gamma = \beta$, while the coefficient K can be computed from the lateral distribution $f(y)$ and the measured coefficient in the density spectrum. The result for vertical showers

⁸ Here $g(x)$ depends on counter geometry and on the number of particles that must strike each counter to satisfy requirements for recording an event; e.g., the probability of three adjacent counters each being struck by one or more particles would be $g(x) = (1 - e^{-x})^3$; or the probability of an ion chamber registering a pulse representative of n particles would be $g(x) = x^n e^{-x} / n!$

at sea level is

$$F_r(N) = 5.5 \cdot 10^{-8} (10^6/N)^{1.52+0.055 \log(N/10^6)} (\text{m.}^2 \text{ sec. sterad})^{-1} \quad 7.9.$$

while at an elevation of 3260 m. a similar analysis yields

$$F_r(N, 3260 \text{ m.}) = 60 \cdot 10^{-8} (10^6/N)^{1.48+0.055 \log(N/10^6)} \quad 7.10$$

Since 1955, large air shower experiments have been conducted, using many detectors, as described above in Section II.1. For each shower that meets the trigger requirements a size, direction, and core location are determined. At each value of N , one must determine, by computation or trial, within what area the axis must fall in order that the trigger requirement be met with known efficiency. For a spectrum determination, the only safe procedure is to restrict the area to that within which the efficiency is very nearly one; thus, after analysis, most of the events must be discarded because their axes lie outside of such areas. The accepted events are then normalized to unit area, and their distribution is found with respect to shower size and zenith angle.

Near sea level, the analysis is simplified by the observation that showers of all sizes have practically the same distribution in angle. Therefore in obtaining the distribution with respect to shower size, one may combine events at all angles.

By such methods, at sea level, in the range $10^6 < N < 10^9$ particles, workers at Harwell, Cornell, and MIT have consistently found that the number spectrum has a constant exponent, $\gamma = -\partial \log F / \partial \log N$, between 1.88 and 1.92 with experimental errors less than 0.10: a value of γ both larger and more constant than that derived from the density spectrum. The absolute frequencies reported at $N=10^6$ are consistently lower than that given in Equation 7.9, by factors from 1.4 to 2.1. For smaller showers, $8 \cdot 10^4 < N < 5 \cdot 10^5$, workers in Russia and Japan report a lower value of γ , 1.50 or 1.55, though both groups report values of γ near 2.0 for showers of $N > 5 \cdot 10^5$.

To bring the various experiments into harmony, one must refine the analysis by correcting for the systematic errors in both of the experimental methods, taking into account the effects of (a) the gradient of γ with respect to $\log N$ and hence also with $\log \rho$; (b) the slight variation of the average lateral distribution with size of the shower, characterized by the derivative of the age parameter, $ds/d(\log N)$; (c) the fluctuations in density close to the axis for fixed values of N and r (i.e., deviations of the lateral distribution of individual showers from the average); (d) the random errors in the "direct" measurements of N arising from errors in core location and from statistical fluctuations in number of detected particles (especially significant being the systematic decrease of these errors with N), and (e) the imperfect triggering efficiency of the large shower arrays.

Corrections a , b , and c raise the γ value derived from the density measurements and lower the numerical coefficient K . Effects b and d lower the value of γ derived from the "direct" measurements of the number spectrum with large counter arrays, and slightly lower the numerical coefficient. Harmony

among the experiments can be achieved by assuming a standard error of (e.g.) one-third in the shower size measurements at $N=10^6$ in the MIT experiments, and a natural standard deviation of a factor two in particle densities within 40 m. of the axis. The first assumption is supported by scrutiny of the experiment, and the second by direct observations in Tokyo and Moscow. For the average rate of change of the age parameter, $ds/d(\log N)$, the value 0.05 is consistent with measurements of the lateral distribution for showers of small and large sizes.

By applying all these corrections, one arrives at the following corrected number spectrum of extensive air showers in the vertical direction at sea level:

$$\gamma = -\partial \log F / \partial \log N = 1.66 + 0.12 \log (N/10^6) \quad 7.11.$$

$$F(N) = (3 \pm 0.6) 10^{-8} (N/10^6)^{-1.66-0.06 \log (N/10^6)} \quad 7.12.$$

The spectrum (7.12) is valid from $N=10^3$ up to the largest showers that have been recorded, $N \approx 4 \cdot 10^9$ particles, although the statistical accuracy grows weak beyond $N=10^9$. For $10^3 < N < 10^9$ the uncertainty in the exponent is probably not larger than 0.06.

8. GROWTH AND ABSORPTION OF THE SHOWERS

Direct observations of individual extensive air showers in different stages of growth have been rare and are not very precise. One method is that of Chudakov and collaborators, described in Section II.6, in which the amount of Cherenkov light from the sky is compared with the number of particles reaching the ground. A second method, attempted recently at Cornell, is based on the azimuthal asymmetry of the particle density in a horizontal plane in inclined showers, as illustrated in Figure 11. As yet, the latter method has only yielded the crude result that $(\mu)_{av} = (0.004 \pm 0.002)$ cm.²/gm. for the particles several hundred meters from the axis of large showers at sea level. A third approach lies in measuring (by time delay) the average radius of the shower front and in observing the directions of motion

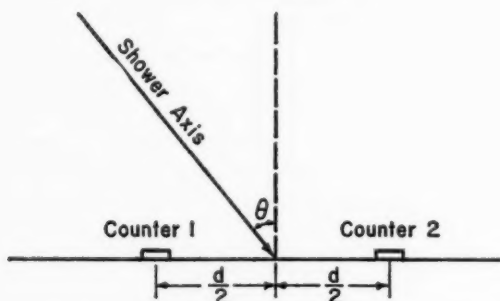


FIG. 11. Illustration of direct measurement of shower absorption. The densities of particles at counters 2 and 1 are related by $\rho_2/\rho_1 = \exp(-\mu d \sin \theta)$.

of the μ mesons, because these data are related to the distribution of particle production along the axis of the shower. The results of such studies and of the Cherenkov light measurements indicate that most of the showers observed at sea level originate very high in the atmosphere and attain substantial development at least 10 km. above the apparatus.

The Cherenkov light experiments have the potentiality of determining the total track length of electrons above the plane at which the shower is detected, and fluctuations in this track length relative to the number of particles there. As mentioned above, at 3860 m. elevation, for showers of about 10^6 particles, this track length is about 45 radiation lengths per particle and does not show large fluctuations; but corresponding data are not yet available at sea level.

Much more quantitative data are available of a statistical type. For instance, the counting rates of various extensive air shower detectors have been measured as a function of altitude, from which data one can in principle determine the differential vertical number spectrum as a function of altitude, $F'_v(N, t)$. Let this spectrum be composed of a continuous distribution of showers with different particle absorption coefficients μ : i.e., let

$$F'_v(N, t)dN = dN \int G'_v(N, \mu, t)d\mu$$

where $\mu = -\partial \ln N / \partial t$ for a shower of particle number N and absorption coefficient μ . Let the variation of G'_v with N be described by $\partial \ln G'_v(N, \mu, t) / \partial N = -[1 + \gamma(N, \mu, t)]$, which defines γ in such a way that its average is the usual exponent in the number spectrum. Then it is straightforward to show that

$$\frac{1}{\Lambda} = -\frac{1}{F'_v} \frac{\partial F'_v}{\partial t} = \frac{\int \mu \gamma G'_v d\mu}{\int G'_v d\mu} = (\mu \gamma)_{av} \quad 8.1.$$

Λ is called the absorption length of the number spectrum, and $\mu^{-1} = \lambda$ is called the absorption length of the particles. If $\gamma_{av}(N, t)$ varies slowly enough with N , as is the case, the value of Λ for the differential number spectrum does not need to be distinguished from the corresponding absorption length of the integral spectrum.

Measurements of the density spectrum at different elevations lead in a fairly straightforward way to knowledge of Λ and of γ_{av} (hereafter written without the subscript av). What is usually reported for the particle absorption length λ is the product $\Lambda \gamma$, which would have a simple interpretation if all showers of one size at one place were in the same stage of development; but which actually is a complicated average of absorption lengths over some showers that are still growing and others that are dying out at various rates.

Thus, if one attempts to reconstruct the history of a shower by performing the integral

$$\ln N(t) = \ln N(t_0) - \int_{t_0}^t dt' / \lambda(N, t') \quad 8.2.$$

one does not get a picture of the growth and absorption of any single shower. One is following the history of a changing population of showers, from which some members are continually dropping out and to which others are being added.

No satisfactory circumvention of this difficulty has yet been evolved, because there are too many unknowns involved. By adopting specific models for the initiation and development of air showers, one can simplify the problem enough to determine one or another unknown function or parameter in the model (e.g., the primary energy spectrum or mean primary interaction length, or some feature of the shower curve); but only by ignoring fluctuations entirely (in type of primary nucleus, distribution of points where interactions occur, and in the kinds and energies of the secondaries produced) can one determine the shower curve itself.

Nevertheless, there is value in the measurements of the parameters γ , Λ , and λ as functions of the thickness of atmosphere in the direction of the shower axis. With specific models of nuclear interactions, e.g., the Landau and Fermi statistical models (20 to 22), shower curves can be calculated and used as a basis for analysis. From such a model, an assumption about the nature of the primaries, and the number spectrum in the vertical direction at one altitude, one can compute the primary energy spectrum, and predict the average absorption lengths and number spectra of the extensive air showers in any direction, at all altitudes. By comparison with experiment, one can eliminate some models as unsatisfactory, and foresee essential features of any model that might achieve success. Chief among the conclusions that have emerged from such calculations is that the above statistical models of nuclear interactions do not fit the observations without incorporating the notion of partial elasticity, which is fundamentally out of character. Some version of the two-center or "fireball" model (23, 24) would be more satisfactory, although not the only possibility. As analytical ingenuity and experimental information increase, gradually a more and more specific and detailed picture of the shower process is emerging.

It has not been possible to operate very complicated air shower equipment at all altitudes. Typically, a comparatively simple array of counters is carried in an airplane to obtain the data at altitudes above the highest mountains. Such an apparatus records the density spectrum, not the number spectrum of the showers. To deduce the variations of the number spectrum one must correct for the change of the shower geometry with air density and with varying age of the showers. Also one must correct for the changing zenith-angle distribution of the showers: at higher elevations a larger and larger proportion of the showers appears at large angles.

As one carries a typical apparatus up in the atmosphere, from sea level to an altitude of about 4 km. (pressure 630 gm./cm.²), the counting rate

increases exponentially with diminishing pressure, a factor e in 135 gm./cm.² Thereafter it increases more slowly until a maximum about 40 to 70 times the sea-level rate is reached, at about 7.5 km. (350 to 400 gm./cm.²). At 12 km. (200 gm./cm.²), the rate is down to 60–70 per cent of the maximum. The exponent β in the density spectrum (hence also γ in the number spectrum) changes very slightly.

Application of the above-mentioned geometrical correction has been carried out in detail in (4, pp. 70–83). The result is that the coefficient of the number spectrum of vertical showers (of size in the neighborhood of 10^6 particles) rises from sea level, like the density spectrum, at a factor e per 135 gm./cm.², but reaches a maximum at a slightly lower elevation, 400 to 440 gm./cm.², the coefficient at the maximum being 25 to 30 times bigger than at sea level.

Ignoring fluctuations, one would conclude that vertical showers of $0.5 \cdot 10^6$ particles at sea level are the remains of showers that contained a maximum of $3.7 \cdot 10^6$ particles at 7 km. elevation and that the particle absorption length at sea level is 220 gm./cm.² (5.8 radiation lengths). The total track length of the shower in the atmosphere is 140 ± 30 radiation lengths per electron at sea level, implying a total energy dissipation by the electrons of 12 ± 2.5 Bev times the number of electrons at sea level. The Cherenkov light measurements by Chudakov indicate a track length equally high or higher; this fact, in addition to his observation that the fluctuations were not large, lends some credence to this energy evaluation. Inclusion of the energy content of the N component, muons, and neutrinos raises the estimate of the average primary energy of such showers to 15 ± 3 Bev per sea-level electron.

The slope of the absorption curve at various altitudes has been checked repeatedly by measurements of the barometric coefficient of the counting rate, which is about 10 per cent per cm. of mercury, in good agreement with the absorption length obtained by the altitude variation.

The absorption curve can be extended beyond sea level by measuring the number spectrum as a function of the zenith angle of the showers. Figure 12 shows some results obtained at Cornell for the quantity Λ , from both the zenith-angle distribution and the barometric effect.

A remarkable feature of all these measurements is their constancy. For showers of 10^4 to 10^8 particles, from an atmospheric depth of 600 gm./cm.² to 1500 gm./cm.², the absorption coefficient of the number spectrum seems almost perfectly constant. Between sea level and 1400 gm./cm.², at least, the absorption coefficient is practically independent of shower size between 10^4 and 10^8 particles. This constancy seems to demand that the electronic component of the showers be in equilibrium with a high-energy nuclearactive component that has a remarkable life expectancy, dying out at the rate of only a factor e in a length equal to $\gamma\Lambda$ or 200 to 250 gm./cm.², about three mean nuclear interaction lengths.

Another strange property of the results is that the maximum in the

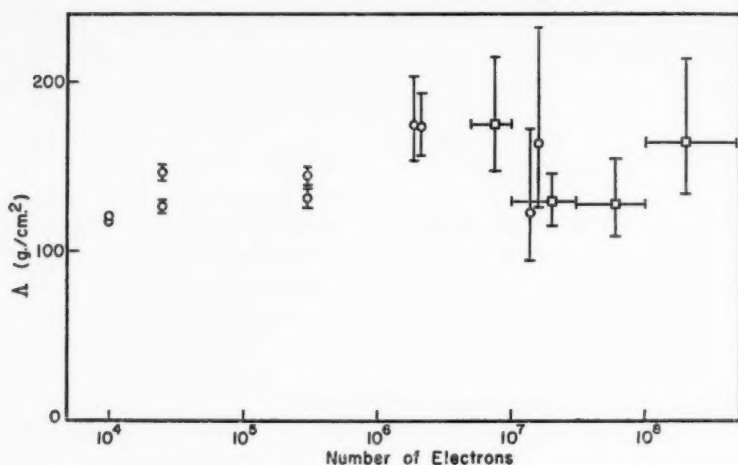


FIG. 12. Measurements at Cornell University of the absorption length of the number spectrum of extensive air showers, for different shower sizes. The circular points were obtained from barometric coefficients and the squares from the dependence of the frequency on zenith angle.

shower frequency occurs at a high altitude, even for very large showers. It appears that the extensive air showers grow to maximum size very quickly, seeming to require for this a rapid subdivision of the primary energy, and then die out very slowly, imposing a contradictory requirement that the energetic nuclear particles be very stingy about sharing their energy.

There are two considerations that offer promise to resolve this conflict. One is that some of the primary nuclei are light particles (protons and alpha particles) while others are heavy nuclei, up to at least iron. At high elevations one may be seeing showers that have developed rapidly because they were initiated by heavy nuclei, while at low elevations the most prominent showers may be those initiated by single protons.

The other explanation is purely in terms of fluctuations and would not apply to showers generated by heavy nuclei. Suppose it is equally possible for a primary proton to transfer any portion of its energy from 0 to 100 per cent in a nuclear collision, to a number of secondary particles that may vary widely in number and type. Collisions occurring near the top of the atmosphere, in which a large part of the energy happens to be transferred to numerous pions, would lead to rapid shower development and the big showers seen at high altitude. But since the interaction length is about 80 gm./cm.², an appreciable number of primaries will escape interactions for one-third of the atmosphere or more, and the lucky ones may in the first few interactions either transfer little energy to the secondaries, or transfer most of the energy

to a few particles that happen to be nucleons and antinucleons, which conserve the energy in the nuclear cascade. By such means some extensive air showers could conserve most of the original energy in the N component until they reach the lower part of the atmosphere, and thus account for the showers still flourishing after 1500 gm./cm.²

Both explanations fit qualitatively the observations (see Sect. II.5) of highly variable numbers of very energetic nuclear particles in the shower cores; sometimes only a single particle of extraordinary energy, comparable with that of all the particles in the shower, and at other times more numerous nuclear particles but none of the outstanding energy. Unfortunately, it is difficult to pin down either of these mechanisms of variation quantitatively.

In the case of very small showers that are far past their cascade maxima, the reason for the small absorption coefficient is at least partially that many of the particles are high-energy mu mesons.

9. DIRECTIONAL ASYMMETRY OF THE PRIMARIES

As the earth rotates, a directional asymmetry of high-energy primary cosmic rays would appear as a periodic time variation of air shower counting rates, with a period of one sidereal day. One might also observe such an asymmetry by transporting the detecting equipment in latitude. With detailed measurements of the angular co-ordinates of individual shower axes, one can see whether any particular sidereal co-ordinates are favored.

All of these methods have been tried. Invariably a finite asymmetry has been found, but never one that is far beyond expected deviations of an equivalent number of random events. Among the many experiments of this type, some authors have reported apparent asymmetries that represent rather improbable fluctuations, but repetition of the experiments has not confirmed the effects, and improbable fluctuations must be expected among numerous trials. Other apparently real asymmetries have been traced to atmospheric influences.

Of small showers with about 10^4 particles (primary energy around 10^{14} ev), many millions have been recorded; and by careful monitoring of pressure and temperature effects and periodic drifts of the efficiency of the apparatus, it has been possible to ascertain that the low-order harmonics of the diurnal variation are less than 0.1 per cent in amplitude. With increasing shower size the statistical precision diminishes, being about 3 per cent for showers exceeding 10^7 particles (10^{17} ev) and 30 per cent for showers exceeding 10^8 particles. Above $N=10^9$, the few showers that have been observed were distributed with apparent randomness in celestial co-ordinates. [Experiments to 1954 are summarized in (4), more recent work in (25 to 28).]

Directional asymmetry was expected to be present for two reasons. First, the sources of the particles must be very nonuniform if they are in our galaxy: the ordinary stars are ineffective at high energy, and the turbulent gas clouds in most of the galaxy are inadequate to produce such accelera-

tions by a Fermi-type mechanism. Secondly, the diffusing process would produce asymmetry because of the galactic structure and consequent field gradients and because of asymmetric leakage.

Besides, the diffusing process should fail at high energies. It is doubtful that a trapping mechanism is effective even for particles of moderate energy, because magnetic fields need special geometries to serve as effective traps; but as long as the scattering length is short, the mean velocity with which particles recede from their stellar and supernoval sources is small compared with the actual speed of the particles, and the directional intensity at a large number of scattering lengths from a source is nearly uniform. However, consider protons of about 10^{18} ev, primaries of showers that have about 10^8 particles at sea level (40 times smaller than the largest recorded showers). In the galactic disc the field strengths are estimated to be about $7 \cdot 10^{-6}$ gauss, and the diameter of the cyclotron orbit would be ~ 1000 light-years, comparable with the thickness of the disc itself. Since fields are not likely to be coherent over such a distance, these particles would not be contained and diffused within the spiral arms.

In the halo region of the galaxy, equipartition of energy suggests field strengths of about $4 \cdot 10^{-6}$ gauss. Even in a regular field, particles are not contained long when their gyration radius is several per cent of the trapping region radius. In irregular fields, the minimum scattering length for a 10^{18} -ev proton would be about 10^4 light years. Such protons coming from a source near the galactic center could scatter a few times before reaching the earth, but hardly enough to be made isotropic.

Thus, the directional symmetry suggests that the source of the high-energy particles is outside of the galaxy and that the density of such particles is as great in intergalactic space as near the earth. Such a conclusion seems probable, in retrospect, also because any acceleration mechanism of such particles requires a large volume. The acceleration cannot occur where the density of matter is high, because of collisions; hence it is restricted to regions of low field strength. The envelopes of supernovae are not big enough to contain such particles; nor are the coherent gas clouds in galactic interstellar space. It may be reasonable to seek the source mechanism in intergalactic plasma stirred up by the galactic rotations; or in traps of the closing-jaw type between pairs of approaching galaxies; or in unusual shock-wave phenomena such as that associated with the jet galaxy M87. In any case, it seems that the dimensions required are of galactic order.

In intergalactic space, the mean lifetime of the particles would be limited only by the general expansion, since nuclear collisions are unlikely to occur in the mean age of the universe. The degree of isotropy attained should then depend on whether the acceleration regions are few and localized, like the jet galaxy and colliding galaxies, or more generally distributed; and on the structure and nature of the intergalactic plasma.

III. CURRENT PROBLEMS

In this concluding section, we wish to mention some of the problems confronting research on extensive air showers, and areas in which progress will certainly be forthcoming.

1. NATURE OF THE PRIMARIES

It would shed light on astrophysics, the origin and acceleration of primary cosmic rays, and the nuclear cascade in the atmosphere to know whether the proportion of heavy nuclei among the primaries increases or decreases with energy. Between 10^9 and 10^{12} ev per nucleon, the number of nuclei with $Z \geq 6$ is about 1 per cent of the number of protons with the same velocity, but nearly equal to the number of protons with the same total energy. Heavy nuclei are comparatively abundant in supernovae as compared with average stars, and because of the extra nuclear charge they can be reflected by magnetic fields up to a higher limiting energy than can protons. On the other hand, they are more readily lost by nuclear collisions, and their average universal abundance is low.

Showers initiated by heavy nuclei should exhibit much less fluctuation than those initiated by protons. Because of the large cross section, the first interaction is sure to occur near the top of the atmosphere. Many of the nucleons would be only slightly affected in this collision, but the excitation would cause them to separate with low relative velocities. Thereafter, each shower would be the sum of a large number of independent cascades, and although individually (as in showers initiated by primary protons) these cascades might fluctuate widely, the overall extensive air shower would not deviate far from the average.

Evidence for initiation by heavy nuclei has been sought by looking for extensive air showers containing a collection of nucleons of equal energy in the core. But after 6 to 12 nuclear interaction lengths one should not expect much similarity among the original nucleons. Indeed, it should be common to find only one of them left with high energy.

Sitte and collaborators (29) and the Tokyo cosmic ray group (30) have attacked the problem by measuring the nuclear interaction length of the primaries, as follows. If one determines both the total number of particles in each shower and some property that changes with shower age (the mean energy of the electrons near the axis being used by Sitte, the relative number of muons and electrons by the Japanese group), and if one ignores fluctuations in the progress of showers after the first interaction (ascribing all variability to the distribution of depths where the first nuclear collision occurs), fixed values of N and the auxiliary property define both the primary energy and the atmospheric thickness through which the shower has developed. The rate of such events as a function of depth has been measured by observations at different elevations (Sitte) and zenith angles (Tokyo).

The interpretation assumes that all the primaries are of one type. The results for the mean interaction length were, respectively, 87 ± 7 and 85 ± 15 gm./cm.², values that are consistent only with proton primaries.

However, the recorded showers were rather small ($N \approx 10^5$), and it may be that such showers initiated by heavy nuclei are absorbed at high altitudes, leaving the proton-initiated showers to be dominant in the lower part of the atmosphere. Secondly, the variations in apparent age might not be associated with different points of initiation after all, but with fluctuations in the subsequent cascade processes, in which case it is not the primary interaction length that has been determined. Thirdly, protons might be the most abundant particles at 10^{14} to 10^{15} ev and still be virtually absent at 10^{18} ev, as proposed by Peters (31).

One gets at least the strong suggestion that protons are numerous among the primaries up to 10^{15} ev from the evidence, reported in various sections above, that large fluctuations are common in small air showers. And there is a hint that heavy nuclei may be dominant at higher energies, from the observations of Cherenkov light, radius of curvature of shower front, and directions of motion of mesons in showers of $N > 10^6$. These observations, discussed earlier, indicate small fluctuations and high points of initiation in the large showers. But the change with shower size, if real, can be explained in more ways than one. New methods need to be devised to gain more unambiguous information.

2. ANALYSIS OF FLUCTUATIONS

The importance of deviations from average behavior to the understanding of showers derives essentially from the steepness of the energy spectrum of cosmic rays. Thus, the most frequently observed phenomena may not represent the normal behavior of high-energy particles, but unusual behavior of more abundant particles of lower energy. Not until the fluctuations are understood can one associate primary energies reliably with showers of measured size, and thus obtain the primary energy spectrum accurately; nor can one derive the average features of the nuclear cascade from the experimental data.

We have emphasized in previous discussions the weaknesses of experimental information. But in the present matter, the greatest need is for development and application of analytical methods, to bridge the gap between theoretical models of elementary interactions and the experimental observations of the outcome of cascades of such events. Except for occasional Monte Carlo calculations, the existing theories of the nuclear cascade are essentially limited to predictions of average shower curves. The analytical difficulty of incorporating fluctuations is formidable, as illustrated by the calculations of oversimplified purely electromagnetic cascades. But recent years have witnessed development of mathematical methods for handling such problems, and this barrier between theory and experiment in air showers will doubtless be surmounted.

3. DESCRIPTION OF ULTRA-ENERGETIC INTERACTIONS

Out of the detailed measurements of composition of the extensive air showers, energy spectra of the secondaries, and their lateral distributions, one hopes to derive a picture of the interactions of ultra-energetic particles, which are accessible to study only in this frustratingly indirect way.

Before the last decade, essentially nothing was known about the nuclear cascade which forms the backbone of a shower. The over-all appearance of these showers was that of electromagnetic cascades initiated by primary electrons, and containing a few secondary mesons and nucleons. By now, the electromagnetic cascade has been shown to be a secondary aspect of the shower, and the primary role played by the nuclear-interacting particles has been revealed. It has been demonstrated that it is among the nuclear-interacting particles and mesons that the high individual energies are to be found, not among the electrons and photons. And some qualitative properties of the interactions of the few particles with high specific energies have been established.

The fact that the electron distribution retains a sharply defined core, in spite of the absence of very high energy in the electromagnetic component itself, implies that the nuclear cascade retains one or more particles of extremely high energy through a succession of collisions: i.e., that it is common in interactions at 10^{13} to 10^{16} ev for one or two nucleons to retain a large fraction of the entire energy. Direct detection of small numbers of energetic nuclearactive particles in the cores of highly developed showers substantiates this picture. That a large proportion of the interacting particles are neutral indicates that the high specific energies are retained preferentially by nucleons instead of going to mesons. But the detection of muons far underground, exhibiting a very flat energy spectrum (as flat as that of the N component), proves that it is also possible for large quantities of energy to be given to single mesons.

Indeed, the frequency of muons of energy exceeding 560 Bev (6) is the same as that of extensive air showers with more than only 400 charged particles at sea level and that of primary cosmic rays with energy above about $4 \cdot 10^{13}$ ev. In view of the π - μ decay probability, 11 charged and neutral pions of 700 Bev are produced, on the average, to yield one muon of 560 Bev. Therefore it must not be uncommon for single mesons to be given 5 to 10 per cent of the incident energy; though one or two nucleons may ordinarily emerge with an order of magnitude more energy than the individual mesons.

The observation that showers of 10^4 to 10^5 particles usually have a unique core containing one nuclearactive particle much more energetic than any other near-by particles suggests, indeed, that from a nucleon-nucleon collision one specific particle, which may be regarded as the incident nucleon, customarily emerges with most of the energy.

In larger showers there is apt to be more than one nuclearactive particle of energy exceeding 10^{12} ev, and the typical separation of such particles has

been found to be 1 m., with very few beyond 3 m. Since the nuclear interaction length is about 1 km. at mountain elevations, one learns from this that nuclearactive secondaries of 10^{12} ev are produced with a transverse momentum of about one Bev/c.

Similarly, the mu mesons of median energy $0.9 \cdot 10^{12}$ ev, detected far underground, are distributed at a mean radius of 9 m. from the center of the shower (6). The altitude at which most of these mesons are produced is 10 to 16 km. In this case a transverse momentum of about 0.6 Bev/c is implied.

Thus one gathers a little information about the angular distribution in high-energy interactions (since the subsequent Coulomb scattering produces comparatively small displacements). Studies of jets in emulsion stacks show that transverse momenta of about the same value, 0.4 to 1.0 Bev/c, are found almost independently of the energy of the incident particle and that of the secondary particle (in the high-energy region): i.e., the average angle at which the secondary particle emerges is inversely proportional to its energy. [Work reported by Cooperative Emulsion Group in Japan (32).]

A difficulty obstructing the derivation of new understanding from the study of extensive air showers, at present, is that there is no fundamental theory to serve as a framework for the observations, to give them coherence and provide predictions against which they can be compared. The old statistical models of high-energy interactions have had to be discarded because they did not fit the facts outlined above, nor the detailed observations of high-energy "jets" seen in nuclear emulsions.

The closest thing to a theoretical model that fits available data is an empirical one known as the two-center or "fireball" model (23, 24). According to this picture, after a high-energy nucleon-nucleon interaction the two nucleons proceed with only slightly reduced speed in the center-of-mass system, each one followed by a rapidly moving "fireball" from which new particles (both mesons and baryons) are evaporated with relative energies of about 1 Bev. A model of this type was predicated by the observed angular distribution of the secondaries, by the approximate constancy of their transverse momenta, and by the frequent observation that one of the emerging particles had much more energy than the others, implying that the collision was often rather elastic. But this model lacks a deep understanding or underlying explanation and has too many free parameters to be tested critically. Because the data create a need and need begets invention, we are optimistic that a fundamental theory of high-energy interactions will be forthcoming.

4. ASYMMETRY AND UPPER ENERGY LIMIT OF THE PRIMARY RADIATION

Extensive air shower experimenters have looked forward to the attainment of measurements of cosmic rays of high enough energy to travel in essentially straight lines and reveal the strange and rare places of their origin,

on the presumption that these places are not distributed uniformly around us. Also foreseen is an upper limit of energy which is not exceeded by the cosmic rays, because of the finite size and magnetic energy density of the sources. Neither expectation has shown any experimental sign of approaching fulfillment. It is only at low energy that asymmetry has appeared, related to cosmic ray production at a very weak but near source, the sun.

As for the upper energy limit, the largest showers reported thus far contained about $3 \cdot 10^9$ [MIT (28)] and $4 \cdot 10^9$ [Cornell (25)] secondary particles. Independent of specific models of the shower process, one can be sure that the primary energies of these events were at least 10^{19} ev (one ft.-lb). Possibly these showers were made by heavy nuclei. But a couple of showers exceeding 10^9 particles have been observed at Cornell with zenith angles near 60° (i.e., under an atmosphere of 2000 gm./cm.²). If these are assumed to be generated by heavy nuclei, the estimate of primary energy must be greatly raised, because large fluctuations in shower development would not be possible, and it is known experimentally (from the zenith-angle distribution) that showers of 10^8 particles reach maximum development in 800 gm./cm.² or less. Therefore one cannot avoid the conclusion that particles exist with energy up to about 10^{19} ev per nucleon.

Moreover, the number of observed showers above 10^9 particles is equal to the number predicted within the running time of the experiments only if it is assumed that the number spectrum continues in the range 10^9 to 10^{10} without change of form. Therefore there is no hint that 10^{19} ev is the upper limit.

Even if there is no increase in steepness of the spectrum, the expected number of showers greater than $4 \cdot 10^9$ particles is only 1/sq. km. in six years (in one steradian), and decreases as $N^{2.1}$. Therefore, if one wishes to know whether such showers are isotropic or to extend the knowledge of the spectrum much further, it will be necessary to adopt new methods of detection based on a type of radiation that permits the showers to be observed over a much wider radius than that reached by the charged particles. Use of Cherenkov light offers some improvement, but a more isotropic electromagnetic radiation in the visible or radio spectrum will ultimately provide the greatest area of reception.

At 10^{19} ev per proton, one might already think the regime of undeflectable particles had been reached. If the density of intergalactic gas is 10^{-5} atoms/cm³ and the rms velocity is 300 km./sec., equipartition of energy indicates field strengths of $4 \cdot 10^{-7}$ gauss. In such a field the cyclotron diameter of a 10^{19} ev proton would be $2 \cdot 10^6$ light-years. But if the fields are not coherent in direction over such large distances, the particle would only suffer small-angle scattering, and the transport mean free path would be much longer. The fallacy in this argument, of course, is that regions of space capable of deflecting such particles must exist in order to accelerate the particles to their observed energies.

However, it is probable that with increasing energy, the regions capable of accelerating and deflecting the particles become rare, and that both an asymmetry and an upper energy limit will be found in the neighborhood of 10^{19} to 10^{20} ev, not far beyond the limits of the present information. Either finding or failure to find such effects will be interesting.

5. PHOTON AND NEUTRINO COMPONENTS OF THE PRIMARY SPECTRUM

More than a decade ago, it was shown that among the primary cosmic rays with energy above a Bev, the number of photons is less than 1 per cent of the number of charged particles. No positive measurement of the primary photons has yet been made. Yet one can predict with confidence that such photons exist, in numbers large enough to measure. Similarly, one can predict the existence of primary neutrinos. For this component, detection is much more difficult, but we wish to suggest that it is not impossible. Since photons and neutrinos propagate in straight lines, success in their detection will open up broad new areas of astronomy. We will make some rough estimates of intensities that can be expected. The uncertainties in such calculations indicate things to be learned by making the actual measurements.

In stellar atmospheres, in spite of the low temperatures, there are indications of the occurrence of nuclear reactions. From these a line spectrum of gamma rays may be expected, including a line at 0.5 Mev from positron annihilation. The probable existence and intensity of such radiation has been discussed by Morrison (33). Here we wish to focus attention on the radiation of higher energy.

One source of such radiation is collisions of the cosmic rays with atoms of the interstellar gas. We assume the cosmic ray flux to be the same as that reaching the earth. By absorption in the atmosphere, it has been found to produce a charged pion spectrum given (34) by

$$n(E_\pi)dE_\pi = 0.156E_\pi^{-2.64}dE_\pi(\text{cm.}^2 \text{ sec. sterad})^{-1}(E_\pi \text{ in Bev})$$

We assume half as many neutral pions as charged pions. Analysis of the kinematics of π - μ , μ - e , and π^0 -(2γ) decays shows that the resulting spectra of photons, neutrinos, and electrons are similar to the pion spectrum but have coefficients respectively 0.059, 0.055, and 0.020. To compute the flux reaching the top of the atmosphere in any direction, one must multiply these spectra by the integral $x = \int \rho dr / \lambda$ along a line in that direction from the top of the atmosphere to the outer boundary of the source region. We assume both the gas and the primaries to be hydrogen, and take for λ the value 60 gm./cm.²

Now we consider different assumptions about the volume of the source.

(a) Let the cosmic ray density be equal to that at the earth throughout the disc of the galaxy, but zero outside. Then x varies with direction, being about $2.8 \cdot 10^{-5}$ normal to the disc, about 100 times greater towards the center of the galaxy, and about $1.4 \cdot 10^{-4}$ on the average over all directions. The density of the gas is assumed to be one atom per cm.³

(b) Let the cosmic ray density be the same in the galactic halo, where there are 10^{-2} atoms/cm.³, as in the disc, but zero outside the halo. Then the minimum value of x is raised to $4 \cdot 10^{-5}$ and the average to $1.5 \cdot 10^{-4}$ while the maximum value remains about $3 \cdot 10^{-3}$.

(c) Let the cosmic ray density be the same everywhere, and the density of hydrogen atoms in intergalactic space be 10^{-4} to 10^{-5} cm.⁻³. The Doppler shift caused by universal expansion is taken into account by cutting off the integral at the Hubble length, $2 \cdot 10^{28}$ cm. The integral outside the galaxy is then $6 \cdot 10^{-2}$ to $6 \cdot 10^{-3}$, as compared with $4 \cdot 10^{-5}$ to $3 \cdot 10^{-3}$ in different directions through the galaxy. The dominance of the extragalactic term is notable.

The predicted number of primary photons above a Bev varies with direction and from one of these assumptions to another, between 10^{-6} and $2 \cdot 10^{-3}$ (cm.² sec. sterad)⁻¹, compared with a primary proton flux (in the same units and above the same minimum energy) of $2 \cdot 10^{-1}$, and a secondary photon flux of $3.6 \cdot 10^{-2}$ created in the atmosphere. The estimated intensities of primary photons should be measurable in satellites without much difficulty.

Besides the diffuse source in interstellar space, it may be possible to detect unusual point sources, such as the colliding galaxies in Cygnus A, the "jet galaxy" M 87, and supernovae like Cassiopeia A and the Crab nebula. Let us consider the Crab nebula as the most promising example. It is estimated (35) that the energy being dissipated by electrons (almost all above 1 Bev) in synchrotron radiation in this nebula is $3 \cdot 10^{40}$ Bev/sec. The electrons are considered to be secondaries of a proton component which maintains the electron flux by pion production and decay. If so, the power emitted in photons from π^0 decay is $7 \cdot 10^{40}$ Bev/sec., creating a flux of $5 \cdot 10^{-4}$ Bev/cm.²/sec. at the earth, in photons above one Bev in energy.

If these photons can be detected at the equator with an instrument of moderate angular resolution, say 10^{-3} steradians, the photon energy flux from the Crab nebula (according to the above interpretation) will be almost as large in this aperture as the energy flux of all the charged cosmic rays. A photon flux 10 to 100 times smaller than this should be detectable.

At higher energies such as 10^{12} ev, the ratio of photon flux to the directional incoming flux of charged cosmic rays should be even more favorable, if the polarized light from the Crab nebula has been interpreted correctly, since many of the electrons and photons must have energies this high to account for the short wavelength synchrotron radiation. The absolute intensity is small, but if the photons are detected by means of the extensive air showers they create in the atmosphere, at the level of the highest mountains, the receptive area of the detector can be large and the showers can be counted at an estimated rate exceeding one a minute. The directional resolution required to distinguish these showers from ordinary air showers can be provided by the relative timing of the pulses in the various counters.

Such an experiment would provide a direct test of whether or not the fantastic deductions, drawn from the polarized light and radio waves emanating from the Crab nebula, are correct.

Let us now consider the feasibility of detecting the neutrino flux. As a detector, we propose a large Cherenkov counter, about 15 m. in diameter, located in a mine far underground. The counter should be surrounded with photomultipliers to detect the events, and enclosed in a shell of scintillating material to distinguish neutrino events from those caused by μ mesons. Such a detector would be rather expensive, but not as much as modern accelerators and large radio telescopes. The mass of sensitive detector could be about 3000 tons of inexpensive liquid. According to a straightforward extrapolation of the Fermi theory, the total cross section of high-energy neutrinos for all reactions leading to charged secondaries is about $10^{-35} E_\nu$, cm.² per nucleon, where E_ν is the laboratory neutrino energy in Bev, assumed to be larger than one (the cross section being proportional to E_ν^2 at lower energies). Therefore the reaction rate is proportional to the energy flux of the neutrinos. Other theoretical models of high-energy neutrino reactions, involving an intermediate boson propagator, lead to a cross section 10 to 100 times higher.

For example, from the Crab nebula the neutrino energy emission is expected to be three times the rate of energy dissipation by the electrons, leading to a flux of $6 \cdot 10^{-4}$ Bev/cm.²/sec. at the earth. In the detector described above, the counting rate would be one count every three years with the lower of the theoretical cross sections—rather marginal, though the background from other particles than neutrinos can be made just as small. The detector has the virtue of good angular resolution to assist in distinguishing rare events having unique directions.

The neutrinos from decay processes in interstellar space may be just as few or may be somewhat more numerous. If the cosmic ray density is everywhere the same, collisions in extragalactic space may yield an energy flux of $6 \cdot 10^{-3}$ to $6 \cdot 10^{-2}$ Bev/cm.²/sec. integrated over all directions, and a counting rate of 4 to 40 per year (estimated with the lower theoretical cross section).

These rates are admittedly low, but not more so than the rates that have been tolerated in the accumulation of some of the unusual air shower information: e.g., the observation of showers containing more than a billion particles; records of showers of 10^6 particles, in which the core is seen in a cloud chamber; and records of dense showers of mesons far underground. High frequencies are not absolutely essential if the events are sufficiently distinctive. And the estimate of the primary neutrino flux may be too low, since regions that produce neutrinos abundantly may not reveal themselves in the types of radiation yet detected.

Because of the energy dependence of the neutrino cross section, the rate of reactions with energy exceeding E is expected to diminish rather slowly with increasing energy, about as $E^{-2/3}$ for the neutrinos from interstellar

space, and even more slowly for the neutrinos from remarkable sources like the Crab nebula. About 500 reactions per year would be expected from neutrinos produced in the atmosphere, but these would have a steeper energy spectrum and a different angular distribution from that of the primary neutrinos, with a maximum in the horizontal direction, where the longer path length in the atmosphere permits more of the mesons to decay. The atmospheric neutrinos would serve to verify the neutrino cross section and calibrate the apparatus.

If the primary neutrino flux proves to be surprisingly large, it may ultimately be possible to detect their absorption in the earth. For the absorption to be appreciable, the cross section must be about 10^{-34} cm.²/nucleon; hence the neutrino energy must be close to 10^{13} ev.

Fanciful though this proposal seems, we suspect that within the next decade, cosmic ray neutrino detection will become one of the tools of both physics and astronomy.

LITERATURE CITED

1. Kamata, K., and Nishimura, J., *Progr. Theoret. Phys. (Kyoto)*, Suppl. 6, 93-100 (1958)
2. Delvaille, J., Kendzierski, F., and Greisen, K., *Proc. Moscow Cosmic Ray Conf.*, II, 101-3 (1960)
3. Rossi, B., *Proc. Moscow Cosmic Ray Conf.*, II, 18-29 (1960)
4. Greisen, K., in *Progr. in Cosmic Ray Phys.*, III, Chap. I (1956)
5. Rossi, B., *High-Energy Particles*, Chap. V (Prentice-Hall, New York, N. Y., 1952)
6. Kameda, T., Maeda, T., and Toyoda, Y., *Proc. Moscow Cosmic Ray Conf.*, II, 58-66 (1960)
7. Goryunov, N. N., Erlykin, A. D., Zatsepin, G. T., and Kamnev, A. B., *Proc. Moscow Cosmic Ray Conf.*, II, 70-78 (1960); Vernov, S. N., Goryunov, N. N., Dmitriyev, V. A., Kulikov, G. V., Nechin, Yu. A., Soloviera, V. I., Strugalsky, Z. S., and Khristiansen, G. B., *Proc. Moscow Cosmic Ray Conf.*, II, 109-14 (1960)
8. Bennett, S., *Energy Spectrum and Positive Excess of Muons in Cosmic Ray Air Showers* (Doctoral thesis, Cornell Univ., Ithaca, N. Y., 1960)
9. Barrett, P. H., Bollinger, L. M., Cocconi, G., Eisenberg, Y., and Greisen, K., *Revs. Mod. Phys.*, 24, 133-78 (1952)
10. Clark, G., Earl, J., Kraushaar, W., Linsley, J., Rossi, B., and Scherb, F., *Nuovo cimento*, 8, Suppl. 2, 623-52 (1958)
11. Andronikashvili, E. L., and Kasarov, R. E., *Proc. Moscow Cosmic Ray Conf.*, II, 149-51 (1960); Andronikashvili, E. L., and Bibilashvili, M. F., *Rept. 1956 Budapest Conf. Cosmic Radiation*, 63-72 (Hung. Acad. Sci., Budapest, Hungary, 1957)
12. Cranshaw, T. E., de Beer, J. F., and Parham, A. G., *Progr. in Cosmic Ray Phys.*, II, 152-54 (1956)
13. Greisen, K., Delvaille, J., and Kendzierski, F., *Progr. in Cosmic Ray Phys.*, II, 174-75 (1956)
14. *Proc. Moscow Cosmic Ray Conf.*, II (1960)
15. Dovzenko, O. I., Zatsepin, G. T., Murzina, E. A., Nikolsky, S. I., and Iakovlev, V. I., *Proc. Moscow Cosmic Ray Conf.*, II, 134-41 (1960)
16. Nikolsky, S. I., and Tukish, E. I., *Proc. Moscow Cosmic Ray Conf.*, II, 129-63 (1960)
17. Vernov, S. N., Goryunov, N. N., Dmitriyev, V. A., Kulikov, G. V., Nechin, Yu. A., and Khristiansen, G. B., *Proc. Moscow Cosmic Ray Conf.*, II, 115-21 (1960)
18. Galbraith, W., and Jelley, J. V., *Nature*, 171, 349-50 (1953)
19. Chudakov, A. E., Nesterova, N. M., Zatsepin, V. I., and Tukish, E. I., *Proc. Moscow Cosmic Ray Conf.*, II, 50-57 (1960)
20. Fermi, E., *Progr. Theoret. Phys. (Kyoto)*, 5, 570-83 (1950); *Phys. Rev.*, 81, 683-87 (1951)
21. Belenki, S. Z., and Landau, L. D.,

- Nuovo cimento*, 3, Suppl., 15-31 (1956)
22. Landau, L. D., *Izvest. Akad. Nauk S.S.S.R.*, 17, 57 (1953)
 23. Cocconi, G., *Phys. Rev.*, 111, 1699-1706 (1958)
 24. Ciok, P., Coghien, T., Gierula, J., Holynski, R., Jurak, A., Miesowicz, M., Saniewska, T., and Stanis, O., *Nuovo cimento*, 8, 166-69 (1958)
 25. Delvaille, J., Kendzierski, F., and Greisen, K., *Proc. Moscow Cosmic Ray Conf.*, III, 143-49 (1960)
 26. Daudin, J., Auger, P., Cachon, A., and Daudin, A., *Nuovo cimento*, 3, 1017-32 (1956)
 27. Citron, A., and Stiller, G., *Nuovo cimento*, 8, Suppl. 2, 675-80 (1958)
 28. Rossi, B., *Proc. Moscow Cosmic Ray Conf.*, II, 18-29 (1960); see also (10)
 29. Sitte, K., Kofsky, I. L., Stierwalt, D. L., Lehrer, S., Tausk, K., and Wataghin, A., *Nuovo cimento*, 8, Suppl. 2, 684-700 (1958); *Proc. Intern. Conf. Cosmic Rays* (Varenna, 1957)
 30. Fukui, S., Hasegawa, H., Matano, T., Miura, I., Oda, M., Ogita, N., Suga, K., Tanahashi, G., and Tanaka, Y., *Proc. Moscow Cosmic Ray Conf.*, II, 30-43 (1960)
 31. Peters, B., *Proc. Moscow Cosmic Ray Conf.*, III, 157-66 (1960)
 32. Hasegawa, S., Minakawa, O., Tsuzuki, M., Nishimura, Y., Yamanouchi, H., Aizu, H., Hasegawa, H., Ishii, Y., Tokunaga, S., Nishikawa, K., Imaeda, K., Kazuno, M., Mori, H., Fujimoto, Y., Nishimura, J., and Niu, K., *Nuovo cimento*, 8, Suppl. 2, 761-69 (1958)
 33. Morrison, P., *Nuovo cimento*, 7, 858-67 (1958)
 34. Pine, J., Davisson, R. J., and Greisen, K., *Nuovo cimento*, 14, 1181-1204 (1959)
 35. Oort, J. H., and Walraven, T., *Bull. Astron. Inst. Netherlands*, 12, 285-308 (1956)

BUBBLE CHAMBERS^{1,2}

BY HUGH BRADNER

Lawrence Radiation Laboratory, University of California, Berkeley, California

I. INTRODUCTION

It has been five years since an article by Fretter (1), in this publication, reviewed a new kind of nuclear particle detector called the bubble chamber. During these years, bubble chambers have become the foremost detectors of particles from high-energy accelerators. Many conference reports and review articles [e.g. (8, 20, 29, 35b, 43)] on chamber design and data processing have been published. Extensive bibliographies from CERN (2, 3) list work published before December 1958. The development and research effort in some laboratories has been extensive. The Alvarez group in Berkeley, for example, numbers more than one hundred people, including chamber operators, scientific assistants, engineers, and physicists, and costs about 2.5 million dollars per year.

The field has already grown too large to be covered fully in a single article. This article (a) indicates the great importance of bubble chambers and reviews the theory of their operation; (b) discusses chamber designs and the handling of data; (c) assembles some information useful to physicists in the planning of experiments. Emphasis in these latter sections will be on large bubble chambers, and especially on large hydrogen bubble chambers.

The standard detectors of ionizing particles eight years ago were cloud chambers, counters, and nuclear emulsions. Each of these detectors had many forms, and each had limitations for use in high-energy nuclear physics, where new particles were being studied, and where the number of particles leaving the point of an interaction frequently exceeded the number entering it.

Detectors that give images of charged-particle tracks are most valuable for investigating new or complex phenomena. High density is especially desirable if rare interesting events are to be produced frequently in the detector. High spatial resolution is important. Cycling rates should be at least 10 per min. if the detector is to be used at an accelerator like the Bevatron or the Cosmotron. Very short time resolution, such as 10^{-8} sec. would be desirable, so that many particles could be studied in a single accelerator pulse. The physicist often wants to determine velocity by ionization measurement, and momentum by track curvature in a magnetic field. He also needs to know the kind of nucleus in which a particle is produced or in which it interacts.

Nuclear emulsions afford high density and excellent spatial resolution,

¹ The survey of literature pertaining to this review was concluded in April 1960.

² This work was done under the auspices of the U. S. Atomic Energy Commission under Contract No. W-7405-eng-48.

but can not yield momentum of fast particles except by grain counting. Track curvature in magnetic fields of 20 kilogauss is not large enough to give even the sign of the charge. Emulsions contain such a mixture of complex nuclei that it usually is impossible to identify the interacting nucleus.

High-pressure hydrogen expansion cloud chambers, though presenting mostly simple nuclei, have a cycling time of many minutes; so Shutt and others developed high-pressure hydrogen diffusion cloud chambers. However, a 30 atm. diffusion chamber has a density of only ~ 0.003 gm./cm.³ Turbulence during the 200 msec. required for droplet growth can limit the accuracy of spatial measurements. Furthermore, the sensitive depth of diffusion chambers is limited to about three inches. Nuclei other than hydrogen are present in these chambers, because a condensible vapor must be used.

These shortcomings were widely recognized. It was also recognized that any detector of nuclear particles must operate by the triggering of some metastable energy source, since the particles passing through matter do not lose enough energy to be detected directly. But only Donald Glaser conceived that the localized effects of ionizing particles in a superheated liquid might give an imaging detector with the desired characteristics of sensitivity, rapid cycling, high density, and good spatial resolution. He developed a simple theory to describe the conditions under which a superheated liquid should be triggered into erupting upon the passage of an ionizing particle. This theory assumes that stable bubbles are formed when the net vapor pressure of the liquid, plus electrostatic repulsion of charge clusters, exceeds the surface tension of the liquid. Glaser tested his conclusions with a 1-cm.-diameter smooth glass vessel containing diethyl ether, which has a boiling point of 34.6°C. He raised the temperature of the liquid to 135°C. at a pressure of 300 p.s.i., and then released the pressure to leave the ether in a superheated condition. He reported (4) that "in the presence of a 12.6-mc. Co⁶⁰ source, the liquid in the tube always erupted as soon as the pressure was released, while when the source was removed, time delays between the time of pressure release and eruptive boiling ranged from 0 to 400 sec. with an average time of about 68 sec." The bubbles grew so rapidly that the ping of their shock wave striking the chamber walls could be heard. In 1953 Glaser reported success in photographing minimum-ionizing tracks of cosmic rays by triggering a flashlamp by a Geiger counter telescope (5). Good pictures in diethyl ether were obtained with flash delays of 10 μ sec. Counter-controlled expansion was apparently not possible, because the bubble nucleation centers de-excite too rapidly (6). Other physicists quickly realized the importance of this new detector and began designing chambers for use with a variety of liquids. All early chambers were made with careful attention to smoothness and cleanliness of internal surfaces, since it was believed that bubbles would form at any rough places as soon as the chamber pressure was reduced and that the expansion of these bubbles would repressurize the chamber and desensitize it before the ionizing particle could leave a track. Bubble chambers could not be made large enough to be really useful unless

this limitation could be overcome. Early liquid hydrogen experiments by the Alvarez group showed a way to solve the problem. A $1\frac{1}{2}$ -in.-diameter glass chamber was equipped with a fast pressure-release valve and a variable-delay light flash to attempt photography of proton recoil tracks from a Po-Be source (7). Tracks were observed, even when there was a large gas bubble in the chamber. Alvarez reasoned that the sudden release of pressure allowed bubbles to grow in the volume of the liquid before the large bubble at the wall could desensitize the chamber. Therefore, a large chamber could be made, without smooth clean surfaces, if the expansion was fast. The boldest and most important development of large chambers has certainly been the construction and use of a series of hydrogen chambers of increasing size, culminating in a $14 \times 20 \times 72$ -in. liquid hydrogen or deuterium chamber, under the direction of Alvarez at the Lawrence Radiation Laboratory.

The early history of the development of bubble chambers is very clearly described in Glaser's papers and in his review article in *Handbuch der Physik* (8). Comparisons of bubble chambers with other detectors can be found in Table I, taken from the Geneva Atoms-for-Peace Conference report on particle detectors by Bradner & Glaser (9). As Glaser says, "the bubble chamber was invented because a detector of its properties was needed for experiments in high-energy physics."

II. BASIC IDEAS OF BUBBLE CHAMBER OPERATION

A. THERMAL PROPERTIES

The operation of a bubble chamber can be understood with the aid of the pressure-volume plot diagram, Figure 1, which shows representative isotherms for a fluid in the region near the critical point. If the pressure on a liquid in a rough-surfaced container is lowered slowly, gas begins to form when the isotherm intersects the liquid saturation curve, as at A in the figure. Attempts to decrease the pressure further merely produce more gas. The volume can be increased along the constant pressure line ACE until all the liquid is vaporized. It has been found that if the experiment is repeated, but with a very smooth, clean container, the pressure may be reduced beyond the point A, toward the point B on the ideal Van der Waals curve. This region is unstable; the liquid begins boiling abruptly, raising the pressure, and establishing the liquid-gas equilibrium mixture. Further expansion proceeds along a constant pressure line, as with the rough surface.

The time during which a liquid can be held in the unstable superheated state depends, among other things, on the degree of the superheat. In the absence of ionizing radiation it is possible to hold a wide variety of liquids at temperatures about two-thirds of the way from the atmospheric pressure boiling point to the critical temperature, for several seconds.

B. BUBBLE FORMATION

The theories of liquid boiling consider whether small holes or vapor-filled bubbles tend to expand or collapse. The forces acting on an uncharged

TABLE I
COMPARATIVE CHARACTERISTICS OF DETECTORS

Type of detector	Characteristics (all quantities approximate)					Representative applications
	Time resolution* (sec.)	Space resolution (mm.)	Density (gm./cc.)	Velocity or momentum resolution	Nucleus unique (?)	
High-pressure cloud chamber						
H ₂	(1 pulse)†	0.5	0.03	2%	Almost	30 Interactions; particle production in chamber
Diffusion cloud chamber						
H ₂	(1 pulse)	0.5‡	0.002	2%	Almost	30 Interactions; particle production in chamber
Bubble chamber						
H ₂	10 ⁻³	0.1	0.05	2%	Yes	30 Interactions; particle production in chamber
Hydrocarbon	10 ⁻⁴	0.05	0.45	5%	No	30 } 30 }
Xenon	10 ⁻⁴	0.05	3.3	Poor	Almost	
Dissolved gas	10 ⁻³	0.1	0.5	5%	No	As above; also interactions involving γ rays
Scintillation chamber	10 ⁻⁶	1	1		No	100 Detection of fast particles; interactions in detector
NNuclear emulsion	(very slow)	0.001	4	Fair	No	No limit Detection of fast particles; interactions in detector
Scintillators						
Inorganic	10 ⁻⁴ §	10	4		No	10 ⁴ Beam studies
Organic	10 ⁻⁹	10	1		No	10 ⁴ Detection of fast particles
Cerenkov counters						
Liquid or solid	10 ⁻⁹	30	1	Good	No	10 ⁶ Detection of particles above critical velocity
Gas	10 ⁻¹⁰	30#	0.03	Good	No	10 ⁶ Detection of particles above critical velocity

* This figure refers to the possibility of distinguishing between two particles passing through the detector. Chambers can be used to resolve particle decay times of $\sim 10^{-11}$ sec., and nuclear emulsions can be used to resolve decay times of $\sim 10^{-12}$ sec.

† Can operate at only about 1 pulse per 10 min.

‡ Sensitive depth normally about 7 cm.

§ If scintillator is cooled, it may have resolution comparable to organic scintillator.

|| Time resolution is limited by available photomultipliers.

Figures apply to space resolution of "poor geometry" counter. Space and momentum resolution of "good geometry" counters is $\sim 1\%$.

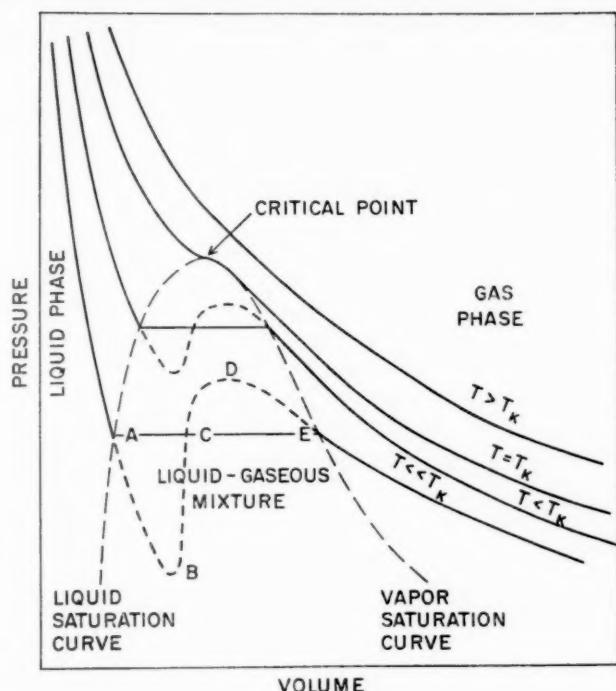


FIG. 1. Pressure-volume plot of representative isothermal curves for a real gas.

bubble in a liquid are the external pressure P and the surface tension σ trying to collapse the bubble, and the vapor pressure P_V trying to expand the bubble. It can be shown easily that bubbles smaller than a critical radius r_c collapse, whereas bubbles larger than the critical radius will grow. The critical radius is given by

$$P_V - P = \frac{2\sigma}{r_c} \quad 1.$$

We can think of the liquid as continually undergoing formation and collapse of tiny bubbles as a result of statistical thermal fluctuations. Increasing temperature increases the probability that a bubble exceeding critical size will be formed.

Glaser (10) reasoned that the passage of an ionizing particle could change the critical bubble size, since a cluster of charged ions with like sign may be trapped on the wall of a bubble, and may increase the expansion force by their mutual repulsion. He predicted that a bubble carrying n_q like charges would grow in a liquid of dielectric constant ϵ , if the saturated vapor pressure exceeds the applied pressure by an amount

$$P_V - P \geq \frac{3}{2} \left(\frac{4\pi\sigma^4\epsilon}{n_q^3 e^2} \right)^{1/3} \quad 2.$$

This formula has been successful in predicting the operating conditions for a wide range of bubble chamber liquids, if n_q is taken to be about 6. However, Glaser's *Handbuch* article gives several reasons for doubting the theory.

One of the most effective arguments results from observations of stopping α particles: The theory would require that 900 charges of the same sign must be deposited in a region 2×10^{-6} cm. in diameter. This charge concentration is greater than the maximum ionization density attained by a stopping α particle, even granting the possibility that all the opposite charges could separate. The total energy lost by the α particle is great enough to produce stable bubbles, but some other mechanism than charge clusters must be found for transferring the energy to the liquid.

Another serious argument against the charged-bubble theory comes from the observation that pure xenon does not produce bubble tracks, but works very well when 2 per cent of ethylene is added. The failure can be understood by noting that pure xenon is a good scintillator: Most of the energy lost by an ionizing particle is used in ionizing and exciting the atoms of the liquid. Xenon is monatomic, and hence can not have rotational or vibrational degrees of freedom to de-excite the atoms by collisions of the second kind before they radiate their energy away from the local region of ionization. The addition of ethylene or other quenching agent furnishes molecules with the necessary degrees of freedom to absorb the radiation and convert it locally to thermal energy.

We can consider that an ionizing particle acts like a hot needle plunged into the bubble chamber liquid. Viewed microscopically, there are, of course, local fluctuations in the heat delivered to the liquid, because of variations in the energies of ions and δ rays. A theory of bubble formation by local heating has been developed by Seitz (11), who concludes that δ rays of about 1 kev deposit their energy in a small region of about 10^{-6} cm. radius, to produce bubbles of larger than critical size explosively in 10^{-10} sec. The number of δ rays per cm. of path with energy between E_1 and E_2 kilovolts is given by

$$n_\delta = \frac{153Z\rho}{\beta^2 A} \left(\frac{1}{E_1} - \frac{1}{E_2} \right) \quad 3.$$

where ρ is the density, A the atomic mass, and Z the atomic number of the liquid, and β is the v/c of the particle. Hence Seitz' theory predicts that the bubble density at a given temperature should be proportional to β^{-2} rather than to specific ionization. Values of $\frac{1}{2}$ kev for E_1 and 1 kev for E_2 in Equation 3 give correct bubble densities for normal operating sensitivity, viz., about 8 bubbles per cm. for a minimum-ionizing particle in a hydrogen bubble chamber. The operating sensitivity of a bubble chamber can be adjusted by varying the degree of superheat so as to give anything from a few bubbles per cm. for heavily ionizing particles to saturated tracks for

minimum-ionizing particles. Increase of temperature reduces the minimum necessary δ -ray energy E_1 , but has little effect on E_2 . Since E_2 is probably several times as large as E_1 , the bubble density should be given approximately by $n_b \approx \beta^{-2} B(T)$, where $B(T)$ is a function only of temperature and expanded pressure for a given liquid.

C. NUMBER OF BUBBLES PER UNIT LENGTH OF TRACK

Glaser, Rahm & Dodd (12) found experimentally that the number of bubbles per cm. from π^+ mesons and protons of velocity βc in propane follows a relationship, $n_b = A\beta^{-2} + B(T)$, in which A is constant, 9.2 ± 0.2 , between temperatures of 55°C. and 59.5°C. Below 55°C. the value of A decreases rapidly. Here, B is a function of temperature only.

They found that bubble densities were not proportional to specific ionization or to β^{-2} . However, Willis *et al.* have re-examined Glaser's data, using gap counting instead of bubble counting, to avoid bias from overlapping bubble images (13). With this treatment they find that the data are in agreement with a β^{-2} proportionality; but they point out that the specific ionization in the measured energy region varies as $\beta^{-1.83}$, which can not be distinguished from β^{-2} within the accuracy of the experiment. Similar studies by Blinov *et al.* (14), Bassi *et al.* (15), and Birss (16) give results in agreement with a β^{-2} variation of bubble density vs. velocity; but their data are equally consistent with a bubble density proportional to specific ionization. Birss reports bubble densities proportional to β^{-2} for π mesons and protons, but the constants of proportionality differ from each other by a factor of about two. Blinov *et al.* report a small increase in bubble density for highly relativistic electrons in propane. However, unpublished work at CERN indicates that bubble densities do not show the expected relativistic increase.

D. RATE OF BUBBLE GROWTH

After a bubble has become larger than the critical size, its subsequent growth is governed by the evaporation rate of liquid from the bubble surface. The growth rate depends mainly upon the rate of heat transfer from the surrounding liquid, although the reduction of vapor pressure by evaporative cooling may not be negligible. Theoretical treatments have been given by Plessett & Zwick (17) and by Birkhoff, Margulies & Horning (18). In both studies the effects of surface tension and viscosity have been neglected, and applied pressure has been assumed constant. Theory and experiment both indicate that the relation between bubble diameter and time can be expressed as $d = F\sqrt{t}$, in which the value of F is strongly dependent on temperature and pressure. A disagreement between theory and experiment on the size of F has been reported (19), but there is doubt whether existing pressure measurements are accurate enough to provide a good test.

At Berkeley the hydrogen chambers are photographed 2 to 5 msec. after the particles enter the chamber. Bubbles are then about 0.3 mm. in diameter. The new 20-in. hydrogen chamber at Brookhaven, with a different kind of

expansion system, shows 0.3-mm.-diameter bubbles in as little as 0.1 msec. after the particles pass through the chamber. Characteristic times for propane and xenon are about 1 msec.

A bubble chamber review article by Bugg (20) contains an eight-page discussion of the theories of bubble formation and growth, with data on minimum temperatures, bubble energies, critical radii, surface tension, and heat capacities for hydrogen, deuterium, propane, and CF_3Br .

III. BUBBLE CHAMBER LIQUIDS

A. GENERAL

Bubble chambers have been made with any of a wide variety of pure liquids, liquid mixtures, and liquids containing dissolved gas. They range from hydrogen, with a density of 0.0586 and radiation length³ of 1100 cm., to xenon, with density 2.3 and radiation length 3.7 cm.

Many hydrogen chambers are described in technical literature (22a to f). Hydrogen is certainly the most significant liquid for use in high-energy physics, since it presents a target of pure protons in which most reactions can be unambiguously analyzed. This virtue is offset by serious cryogenic problems, since the operating temperature is about 28°K. The heat of vaporization of hydrogen is 7.5 cal./cc. Deuterium, the lightest element containing neutrons has an operating temperature of 32°K. and can be used in a chamber designed for hydrogen.

Helium bubble chamber designs have been described by Block and co-workers (23). Helium is the lightest atom that has nuclear spin 0. The cryogenic problems with helium are somewhat more severe than with hydrogen: the operating temperature is 3 to 4°K. Heat shielding must be better since the heat of vaporization of helium is only 0.73 cal./cc. The range of operating pressures for He is from $\frac{1}{4}$ atm. to just above atmospheric pressure, in contrast to the 5 to 7 atm. required for hydrogen. Furthermore, helium is nonflammable.

Propane (C_3H_8) is the most commonly used organic liquid (24). A propane chamber operates at a temperature of 58°C. and a pressure of 21 atm. Since the radiation length is about 110 cm., the characteristic length for gamma-ray conversion is less than that of pure hydrogen by a factor of 10. The amount of hydrogen per unit volume in a propane chamber is greater by a factor of 1.38 than in a hydrogen bubble chamber. However, unambiguous separation of hydrogen and carbon interactions in propane is often impossible.

³ Radiation length L_{rad} is calculated from Equation 1 in Rossi (21, p. 220). The quantity L_{rad} is a measure of the accuracy that can be obtained in momentum determinations, since multiple Coulomb scattering produces an uncertainty in track position proportional to $(L_{\text{rad}})^{-1/2}$. Also it is a measure of the efficiency that can be expected in pair production by gamma rays, since the mean conversion distance is proportional to L_{rad} .

Propane chambers are very much easier to build and operate than cryogenic chambers. However, the fire hazard with propane is at least as severe as with hydrogen. Both liquid vapors are highly flammable. Propane will sink into trenches and holes, while hydrogen will rise to the ceiling.

Liquids heavier than propane are used for experiments in which production of electron pairs by gamma rays is of primary importance. The shortest radiation lengths have been obtained with xenon (3.7 cm.) and tungsten hexafluoride (3.7 cm.). Xenon bubble chambers of approximately 25-liter capacity have been built in Russia (25) and the United States (26). A small chamber with tungsten hexafluoride has been constructed by Teem at California Institute of Technology (27). Since very short radiation lengths are not necessary with large bubble chambers, a number of people have investigated liquids with radiation lengths in the region of 10 to 20 cm. Today, the most satisfactory medium-heavy liquids appear to be the freons (28), especially CF_3Br . Several of the freons are inexpensive, nonflammable, and noncorrosive and have convenient working ranges of temperature and pressure. Williams (29) gives data on the properties of several practical heavy liquids and also discusses the problems of kinematic analysis in the heavy-liquid chambers in which multiple Coulomb scattering severely limits the precision of momentum determination by magnetic curvature. Williams emphasizes that one disadvantage of the freon chambers is their complete lack of hydrogen.

The insertion of lead plates in hydrogen bubble chambers has often been suggested as a way of combining short radiation length with the advantages of pure hydrogen. A single lead plate was installed for one Bevatron run of the Berkeley 10-in. hydrogen chamber, and provisions have been made for putting lead plates in the 72-in. hydrogen chamber.

Figures 2 to 6 show particle tracks in various kinds of bubble chambers.

B. DISSOLVED GAS IN BUBBLE CHAMBERS

Hildebrand has found that 1 per cent of helium, or small amounts of neon, can be dissolved into liquid hydrogen bubble chambers without significant changes in operating conditions (30). This technique may be useful in investigating the Panofsky effect. Hildebrand found that a concentration of one neon atom in 5000 hydrogen atoms made no change in bubble chamber operating conditions, but completely suppressed the μ -catalyzed hydrogen fusion, and gave a muon-capture rate characteristic of pure neon.

C. GAS BUBBLE CHAMBERS

Several experimenters have produced a different kind of chamber by using a supersaturated solution of gas in liquid (31). Two possible advantages of this type of chamber are a lengthening of the sensitive time, and operation at more convenient temperature. On the other hand, image distortions from liquid motion may be severe, since the evolution of gas is slow compared



FIG. 2. An event produced by 2.85-Bev protons in the Shutt 20-in. hydrogen bubble chamber. The interaction is $p+p \rightarrow \Lambda^0 + K^0 + \pi^+ + p$. The charged track to the left is the proton; the neutral decaying particle at the left side is the Λ^0 . (Courtesy of Dr. Ralph Shutt.)

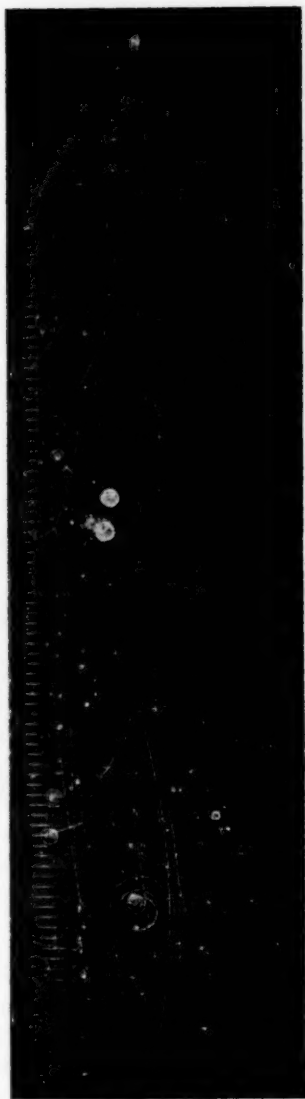


FIG. 3. 3.5-Bev/c π^- mesons in the 72-in. hydrogen bubble chamber. Two 4-prong events can be seen. The two large white spots are thermocouples on the window of the chamber. A small amount of "snow" on the coat hangers makes the illumination noticeably uneven.

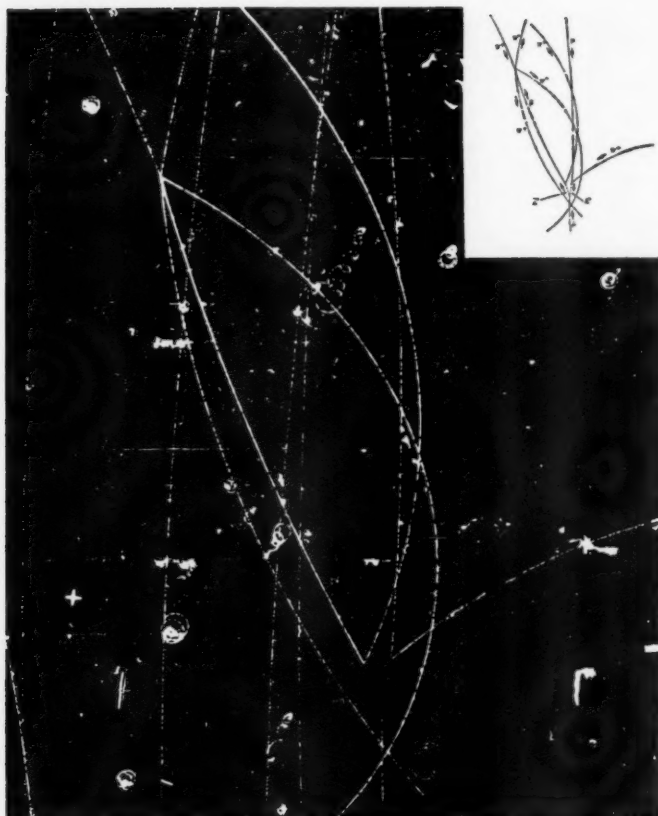


FIG. 4. Enlarged view of section of 72-in. hydrogen bubble chamber, showing production and decay of neutral lambda and anti-lambda hyperons. A fiducial mark on the glass can be seen near the lower left corner of the picture. The scale of this picture is approximately the same as that of Fig. 5 and Fig. 6.

with vapor bubble growth. Bugg (20) concludes that the dissolved-gas chamber is important only when the pure liquid would be chemically unstable at the temperature required for vapor bubble formation. Methyl iodide is an example of such a liquid. The pure liquid must be heated to 210°C. for normal bubble chamber operation, but it decomposes above 150°C. If an equal volume of propane is dissolved in methyl iodide, the mixture operates as a gas bubble chamber at 110°C.

D. PROPERTIES OF SOME BUBBLE CHAMBER LIQUIDS

Table II presents operating parameters of several common chamber liquids. The temperature and vapor pressure are given for the pre-expanded condition. The mean temperature is a normal operating value for "good

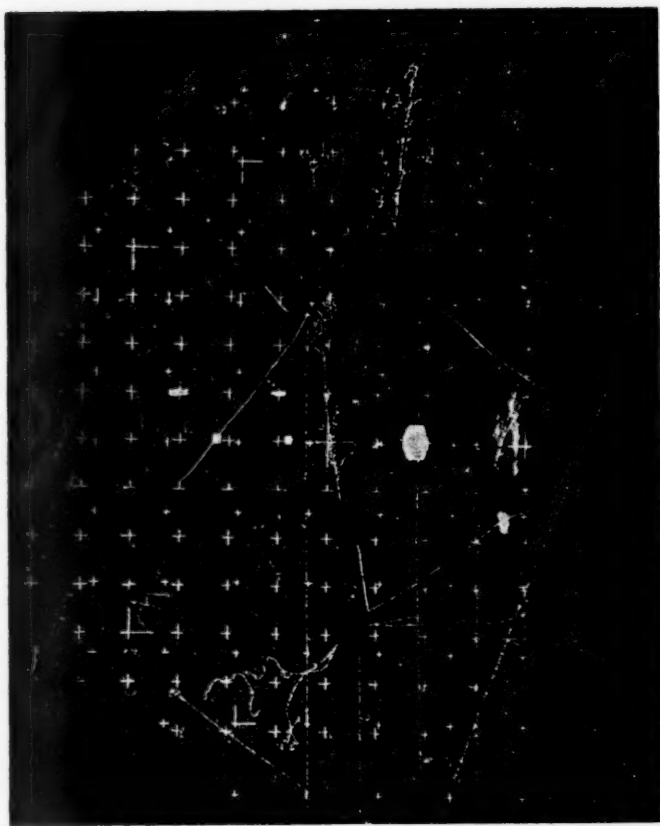


FIG. 5. 1.1 Bev/c π^- mesons in the 25-l. xenon bubble chamber. A Λ hyperon and 4 electron-positron pairs from K^0 decay in the neutral mode can be seen. There are also 2 inelastic collisions of π^- mesons in xenon. The scale of this picture is approximately the same as that of Fig. 4 and Fig. 6. Note the wander of the tracks in the high atomic number liquid. Glaser has put a large number of fiducial marks on the chamber glass, to facilitate interpolation in highest accuracy measurements.

tracks" of 10 to 20 bubbles per cm. from a minimum-ionizing particle. The range of temperature indicates approximate limits from first detection of tracks to spontaneous boiling. The density applies to the expanded liquid at the time that tracks are formed; numbers are given without \sim for quantities that have been measured, or computed accurately from π - μ - e range measurements.

The expansion ratios are drawn from actual operating experience, and may include some expansion due to initial rapid bubble formation. Hence the listed expansion ratios are generally larger than the thermodynamic values. The times listed for flash delay refer to the time between the passage

TABLE II
OPERATING PARAMETERS OF BUBBLE CHAMBERS

Liquid	Temp	Pressure, Expansion absolute (%)		Density	Radiation length (cm.)	Flash delay (msec.)	Index refraction 5300 Å	Source of data
H ₂ (Berkeley) (Brookhaven)	28 ± 2°K. 25–28°K.	~ 5.3 —	~2–4 0.6–0.8	0.0586 —	~1100 —	~2 0.1–0.2	1.093 —	Alvarez Shutt
D ₂	32 ± 2°K.	~ 7.3	~2–4	~0.13	~ 950	~2	~1.1	Alvarez
He	~3.4°K.	~ 1	≤1	~0.124	~ 900	~5	~1.03	Block (23)
Propane (C ₃ H ₈)	58°C.	~21	~3	~0.44	~ 110	~1	~1.22	Powell (42)
CF ₃ Br	28 ± 4°C.	~18	~3	~1.5	~ 11	~3	—	Bugg (28) Kalmus (34)
Xenon	–21°C.	~25	~3	~2.18	~3.8	~1	1.18	Glaser

of ionizing particles and the exposure of the photograph. The optimum flash delay is sensitively dependent on the pressure in the expanded chamber. Radiation lengths were computed according to Footnote 3 of this review paper. The data attributed to Alvarez, Shutt, and Glaser were obtained by private communication. Additional characteristics of *n*-pentane, isopentane, and diethyl ether are given by Bertanza, Martelli & Zacutti (32). Data for tungsten hexafluoride and for mixtures of methyl iodide with propane are given by Williams (29). Properties of several freons are given by Bugg (28), and by Hahn *et al.* (33). Extensive surveys of bubble chamber liquids were presented by Kalmus, and by Hahn during a 1959 CERN symposium on heavy-liquid chambers (34, 35a, b).

IV. DESIGN, CONSTRUCTION, AND OPERATION

A. GENERAL

A bubble chamber is merely a pressure vessel with glass windows, and a flash camera for photographing bubbles in the liquid after a pressure-release valve is operated. Usually a magnet surrounds the chamber so that particle momentum can be determined by measuring track curvature. The design of the chamber varies with the temperature and pressure characteristics of the liquid as well as the techniques chosen for illumination and pressure release. Photographs and diagrams of many chambers are given in a bubble chamber review article by Slätis (35b).

B. STEINBERGER 12-INCH PROPANE CHAMBER

A description of this chamber illustrates many of the design features of warm chambers. Some details of the design were given by Eisler *et al.*

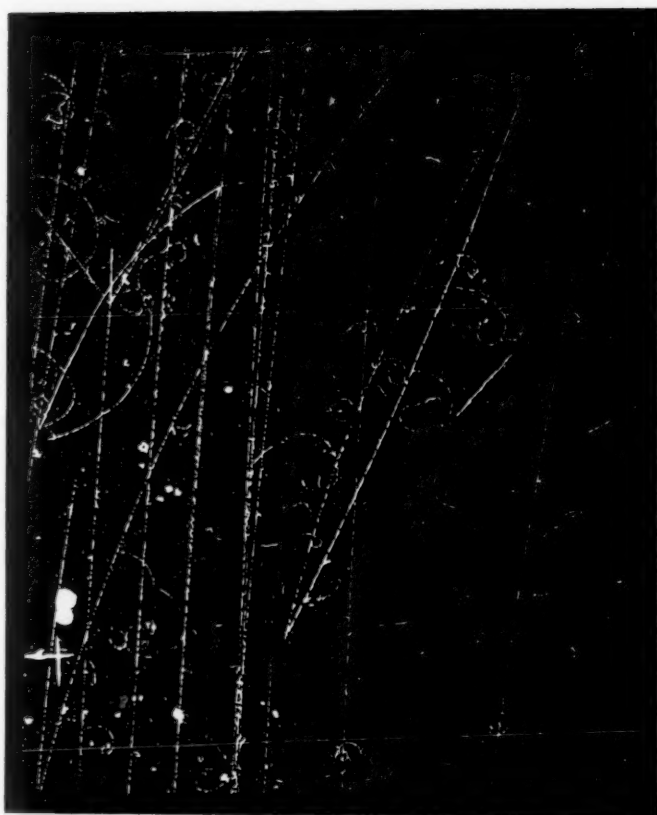


FIG. 6. Production and decay of a Λ hyperon by π^- mesons in the Steinberger 12-in. propane chamber. Note the difference in bubble density of the proton and the π meson from the Λ hyperon decay. Two 4-prong stars can also be seen from inelastic collisions of π^- mesons in propane. The scale of this picture is approximately the same as that of Fig. 4 and Fig. 5. (Courtesy of Prof. R. J. Plano.)

(22d); other information was obtained by private communication from Richard J. Plano (Columbia University). Figure 7 shows a schematic of the chamber, which is 12 in. in diameter and 8 in. deep. The cylindrical aluminum body is closed on both ends by herculite plate glass windows. The chamber is operated with these window surfaces vertical. Liquid propane is maintained at 57°C. and 21 atm. pressure by heating elements wrapped around the chamber. A commercial regulator, operated from a thermocouple attached to the chamber, maintains constant temperature. The chamber is expanded and recompressed by motion of a nylon-reinforced rubber diaphragm in the 5-in.-diameter neck of the opening below the chamber. The volume between this diaphragm and a second one, lower down, is filled with

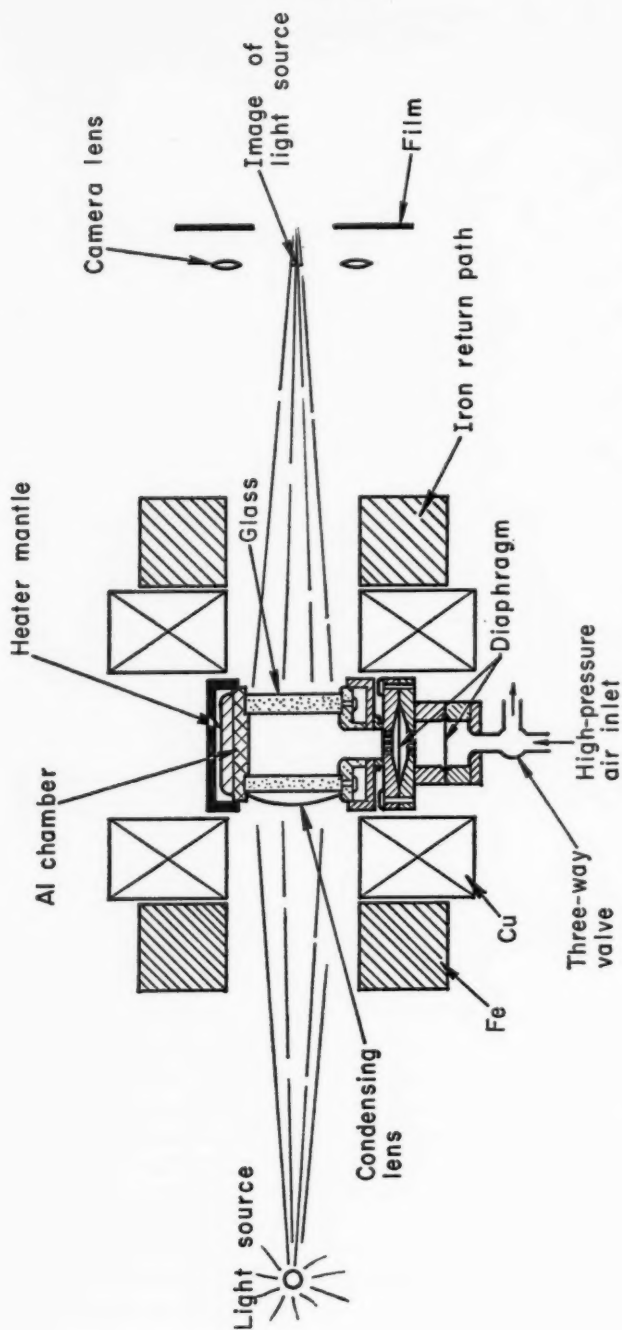


FIG. 7. Schematic assembly drawing of 12-in.-diameter propane chamber. (Courtesy of Prof. R. J. Plano.)

low-viscosity oil, which provides thermal insulation. Compressed air actuates the lower diaphragm. The operation proceeds as follows:

- (a) The chamber is held at a gauge pressure of 325 p.s.i.
- (b) An electronic time impulse from the Cosmotron initiates chamber expansion. Approximately 10 msec. are required for the chamber to come to equilibrium at the new pressure. Then the particle beam is introduced, and the lights are flashed approximately 1 msec. later in order to photograph the bubble tracks in the chamber.
- (c) Recompression of the chamber follows.

The complete cycle lasts for about 30 msec.

The chamber is usually operated in a horizontal magnetic field of 13.4 kgauss.

The illumination of the chamber is achieved by a single General Electric FT-220 flash lamp, 60 in. from the chamber. A 12.5-in.-diameter lens of 30-in. focal length, mounted just behind the chamber, converges the light through the chamber to a point equidistant between the three camera lenses, which are 40 in. from the inside surface of the front chamber glass. Thus, light is scattered from the bubbles to produce the track images on a dark-field background. The three lenses (Goerz-Artar of 100 mm. focal length) are mounted at the vertices of a 10-in. equilateral triangle, giving a stereo angle to the center of the chamber of 13 degrees for each pair of views. The images, on 35 mm. Linograph Ortho film, are one-tenth actual size.

C. LARGE NONHYDROGEN CHAMBERS

Although a number of groups are designing or building large non-hydrogen chambers, there is little literature available yet. Some data on these chambers are assembled in Table III.

D. HYDROGEN CHAMBERS

The range of normal operating temperatures and pressures for a number of hydrogen chambers (43) is shown in Figure 8. Two chambers are described here to illustrate techniques of hydrogen chamber design. Then alternative methods of illumination, expansion, temperature control, etc., are discussed.

Shutt 20-inch hydrogen chamber.—The recently completed 20-inch hydrogen chamber of Shutt's group at Brookhaven (44) is an example of an instrument whose size and cost still permit design decisions to be made primarily on the basis of technical considerations. We will see in a later section how factors of cost affect the design of large chambers.

The Shutt chamber is an aluminum forging, with internal dimensions of 20 by 9 in. normal to the magnetic field, and 10 in. parallel to the field. It must be suspended in an evacuated enclosure and surrounded by cold shields to minimize heat influx due to convection, conduction, and radiation. Shutt employs a conventional design of hydrogen chamber thermal

TABLE III

LARGE HEAVY LIQUID (FREON OR PROPANE) CHAMBERS COMPLETED OR UNDER CONSTRUCTION

Name	Size	Magnet	Windows	Ref.
Alichanyan-Lebedev, Moscow	90 cm. deep; 90 cm. diam. 570 l.	none	1	(36)
CERN, Geneva*	50 cm. deep; 100 cm. diam. 500 l.	≥ 18 kgauss 4.5 Mw.	1	(37)
Mass. Inst. Tech.*	15 in. deep; 40 in. diam. 310 l.	15 kgauss	1	(38)
Dodd-Univ. College,* London	40 cm. deep; 50 \times 140 cm. 300 l.	~ 15 kgauss 4 Mw.		(39)
Lagarrigue-Ecole Polytechnique, Paris	50 cm. deep; 50 \times 100 cm. 300 l.	20 kgauss 4.5 Mw.	3	(40)
Steinberger- Brookhaven	14 in. deep; 30 in. diam. 160 l.	15 kgauss	1	(41)
Powell-Lawrence Lab., Berkeley	6.5 in. deep; 18 \times 30 in. 57 l.	14.5 kgauss	1	(42)

* Data are tentative.

barrier: a shield at liquid hydrogen temperature surrounds the chamber, and is in turn surrounded by a shield at liquid nitrogen temperature. This arrangement minimizes the radiative heat loads on the hydrogen supplies. Most of the heat load is discharged by boiling off relatively inexpensive liquid nitrogen.

The chamber has two vertical windows of 1.25-in.-thick tempered glass. The illumination is similar to the Steinberger chamber arrangement. Two large glass lenses, cut to 20-in. by 9-in. dimensions, focus the light to a point between the cameras. Four separate 35-mm. cameras, mounted in a 9-in. square array about 40 in. from the middle of the chamber, take four photographs, one-ninth chamber size.

The straight-through illumination led Shutt to build his magnet without pole pieces. It requires 1.2 Mw. to produce a horizontal magnetic field of 17 kgauss uniform to ± 3 per cent throughout the chamber. The copper coils of the magnet weigh 3.5 tons, and the iron return yokes weigh 20 tons.

The chamber expansion is controlled by a helium-operated piston near the top of the chamber neck. The complete expansion-recompression cycle is adjustable in pressure, and in time down to 10 msec. The temperature of the chamber is controlled by a pressurized reservoir of hydrogen making thermal contact with the aluminum forging. Hydrogen boils off at a rate of 5 to 6 l. per hr. when the chamber is not pulsed. An additional 2 l. per hr. are lost when the chamber is pulsed 15 times a minute. The very rapid piston

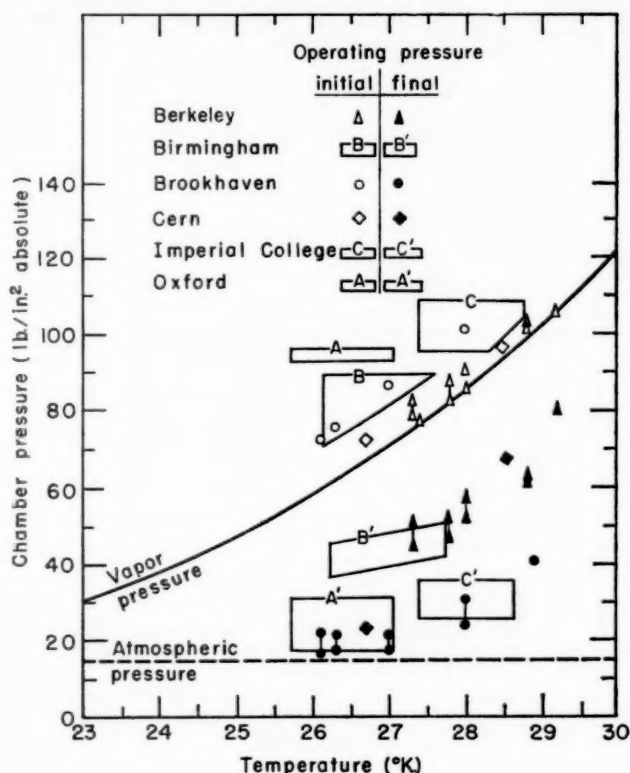


FIG. 8. Normal range of operating temperature and pressure for hydrogen bubble chambers. (Courtesy of Dr. N. C. Barford.)

expansion allows the liquid to reach a low final pressure, so that bubble growth is very fast. Good tracks have been obtained with expansion ratios as small as 0.8 per cent, compared with values of 2 to 4 per cent for most other hydrogen chambers. Flash delays are as short as 25 μ sec., compared with 2 to 5 msec. for most other hydrogen chambers. The low expansion ratio and short flash delay indicate that there is little boiling at the piston, and hence little repressurization of the chamber. It seems likely, from the short flash delays and the shape of the chamber, that track distortions will be very small. Preliminary measurements indicate that the accuracy of momentum determination on fast tracks may be limited only by multiple Coulomb scattering.

Alvarez 72-inch hydrogen chamber.—The large hydrogen bubble chamber at Berkeley was started in 1956, and first operated in March 1959. Details of construction are given in several hundred Radiation Laboratory Engineer-

ing Notes.⁴ The design is summarized in papers by Gow at the 1958 Geneva United Nations Conference on Peaceful Uses of Atomic Energy and the 1959 CERN Instrumentation Conference (22e, 45).

The total cost of engineering and construction was approximately \$2,100,000, including \$400,000 for a special bubble chamber building. About 65 man-years of effort were involved.

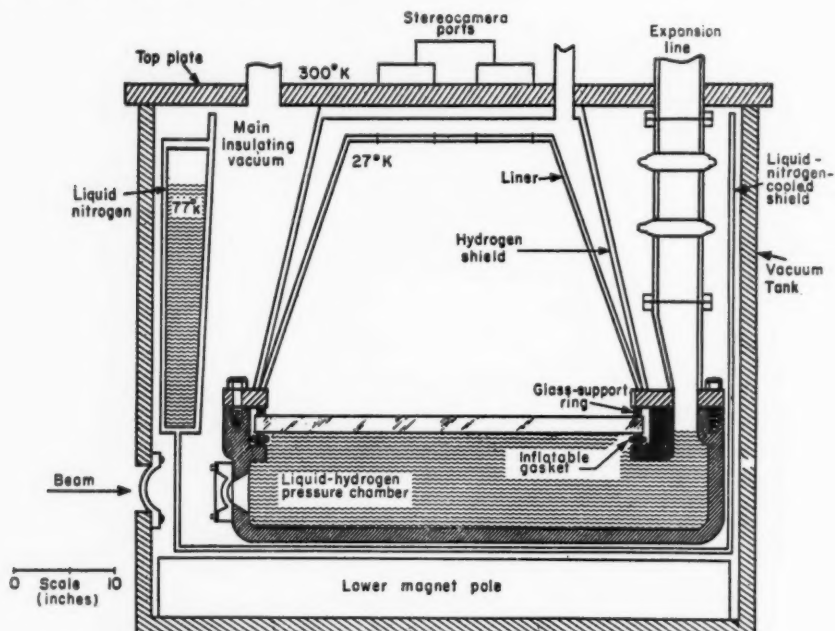


FIG. 9. Longitudinal cross section of 72-in. hydrogen bubble chamber.

Figure 9 is a longitudinal cross section of the chamber. The chamber is 72 in. long, 20 in. wide, and 14 in. deep. It has a single horizontal window on top, whose short axis is tilted 7.5° with respect to the horizontal. Hydrogen bubbles striking the top glass rise to the upper edge and are removed by a "gulper." The chamber body is a 6300-lb. casting of stainless steel. The material is an austenitic steel similar to Al SL-316, but with lower molyb-

⁴ A large part of the literature on bubble chambers exists in the form of laboratory reports. Notable among these are the Radiation Laboratory Notes, and reports of CERN meetings [see for instance (46, 34)]. These reports are widely circulated among people active in the field and are frequently referred to in published literature. The Radiation Laboratory Notes are called "Engineering Notes," or "Physics Notes," and are assigned UCID numbers. They are available from the Lawrence Radiation Laboratory Information Division. The most convenient bibliography of Radiation Laboratory Notes on hydrogen bubble chambers was published in a CERN report by Amiot & Ogden (3).

denum content. It was chosen for low permeability, high strength, and good ductility at liquid hydrogen temperature. The chamber has a refrigerated copper liner that also serves as an expansion-port plate. A large number of holes in the plate permit expansion and recompression over a large area without generating big vortices during recompression.

The chamber is supported from the top plate of the vacuum tank by means of a radiation shield of reinforced weldment at liquid hydrogen temperature. The shield has sufficient strength to contain the hydrogen that would be released if the window should fail. A liquid-nitrogen-temperature radiation shield surrounds both the chamber and the hydrogen shield.

Gasket seals of indium or lead are used throughout the low-temperature assembly. The 3/16-in. difference in expansion between glass and metal in cooling down to 28°K. makes it impossible to seal the top window onto the chamber permanently. Therefore, the indium seals in this region are mounted onto an inflatable gasket (46) of flattened stainless steel tubing, which is left deflated until the chamber has been cooled to below liquid nitrogen temperature. Finally, the seal is made by inflating the gasket with 500 p.s.i. of helium gas. Figure 10 is a cross section of the inflatable gasket. A vacuum

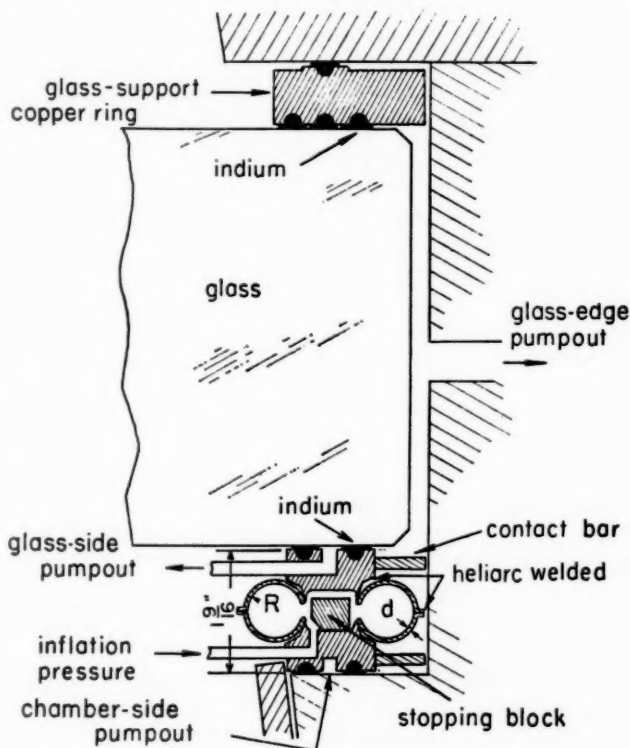


FIG. 10. Schematic cross section of inflatable gasket.

vessel of mild steel encloses the chamber and the two low-temperature shields. The entire chamber assembly, supported as a unit inside the vacuum vessel, is inserted into a hole in the top of the magnet structure. The bottom of the chamber lies close to the bottom pole piece of the magnet. There is no top pole piece. The 200-ton 2.5 Mw. magnet produces a field of 18 kgauss in the middle of the chamber. Low-conductivity water passing through the hollow square copper windings cools the magnet.

The complete structure can walk into different experimental areas on its feet. Parts of the refrigerator and vacuum equipment, most of the illumination power supply, extensive pressure-monitoring circuits, and the camera are mounted on the top platform of the magnet structure. Compressors and gas-purification system are in another room of the bubble chamber building. The refrigerator is a 1700-watt Joule-Thompson expansion unit. The temperature of the chamber is controlled by regulating the rate of flow of the refrigerating hydrogen around the chamber. A hydrogen vapor-pressure thermometer senses the temperature. The temperature regulation appears to be better than $\pm .05^\circ\text{K}$. at 28°K .

Approximately three days are required for cooling down from room temperature and filling with liquid hydrogen. The rate of temperature drop is limited by the allowed temperature gradient across the 5-in.-thick top window. Cooling starts with 20 p.s.i. absolute pressure of hydrogen in the chamber and the support shield, to produce convective cooling of the glass. When the temperature has dropped to 25°K ., very pure hydrogen is allowed to condense in the chamber. Impurities in the hydrogen must be kept below 1 part in 10^6 to prevent frost deposits which can spoil the quality of the pictures by condensing in visible amounts on the top glass and on reflectors at the bottom of the chamber.

The chamber is expanded through an 8-in. line by opening a modified Grove "flex-flow" boot valve into a 30 ft.³ expansion tank at 17 p.s.i. absolute pressure. The chamber is repressurized approximately 20 msec. later by closing the expansion valve and opening a recompression boot valve from a 10-ft.³ tank at 128 p.s.i.a.

Figure 11 is a schematic of the illumination system. Three special Edgerton Flash tubes of 50 watt-sec. each produce a flash lasting about $3/10$ msec. (Flash tubes can be replaced with only a few minutes' interruption of chamber operation.) Three plastic aspheric condensing lenses of $f/0.4$ direct the light into the chamber. Dark-field illumination is achieved by use of "retrodirective coat hangers," which are discussed in Section V. I., below. Three Schneider Super-Angulon lenses give pictures of the chamber on a single strip of 46-mm. film at $1/15$ chamber size. The camera lenses are placed directly above the chamber, at three corners of a 20-in. square. The lens axes are perpendicular to the top glass. The lenses are stopped down to $f/22$ to bring the whole chamber depth in focus with optimum resolution. A data board displaying chamber operating conditions, times, beam counts, and roll and frame number is photographed simultaneously with each cham-

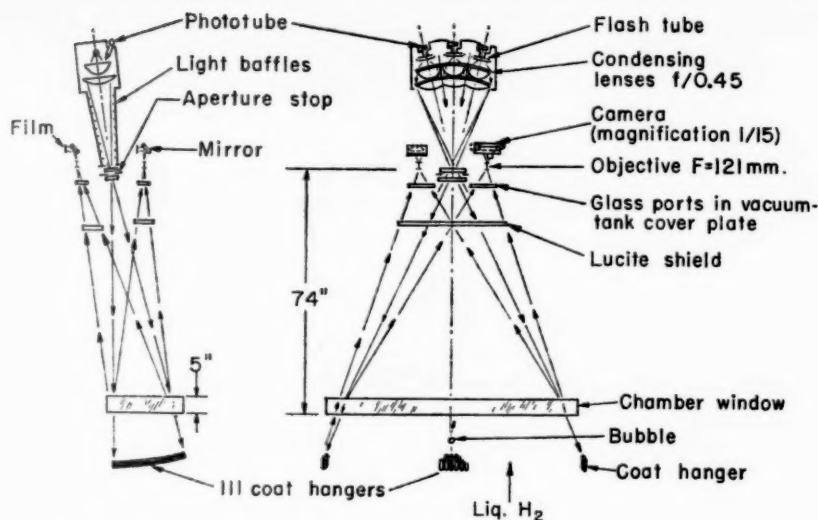


FIG. 11. Retrodirective illumination of 72-in. hydrogen bubble chamber.

ber exposure. A Polaroid Land camera, placed at the fourth corner of the 20-in. square, monitors the chamber operation. The light source and the camera box are maintained at a small positive pressure with clean air to prevent any escaping hydrogen from entering the regions of electrical contacts and high voltages.

A few measurements have been made on temperature gradients in the chamber and on the magnitude of turbulence and distortion. The temperature difference between bottom and top of the chamber can be held to less than 0.1°C . Measurements on the spurious curvature of 3.5-Bev/c π mesons with no magnetic field, and measurements on 1.6-Bev/c antiproton interactions at 18 kilogauss field, both showed a spurious radius of curvature of 160 to 200 m. The rms uncertainty in radius of curvature due to multiple Coulomb scattering is about 600 m. for these π mesons and 280 m. for these antiprotons.

V. DESIGN CONSIDERATIONS FOR LARGE HYDROGEN CHAMBERS

A. GENERAL

The only existing hydrogen chamber larger than 60 l. is the 520-l Alvarez chamber, described in the preceding section. Chambers of comparable size are being designed or constructed in Brookhaven (44), Great Britain (47), CERN (48), and the U.S.S.R. (49, 50). The British chamber and the Brookhaven chamber are shown schematically in Figure 12 and Figure 13.

The new designs differ in some significant respects from the 72-in.

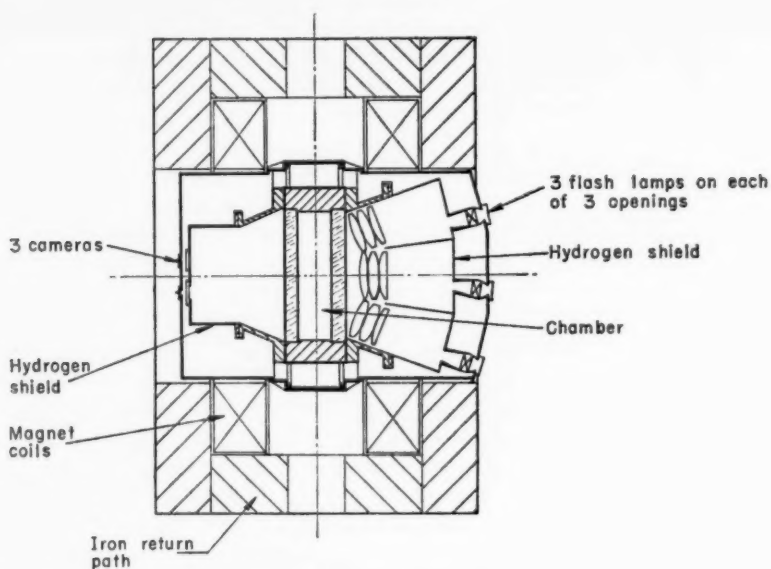


FIG. 12. Plan view of $18 \times 20 \times 59$ -in. British National hydrogen bubble chamber [schematically, Riddiford *et al.* (47)].

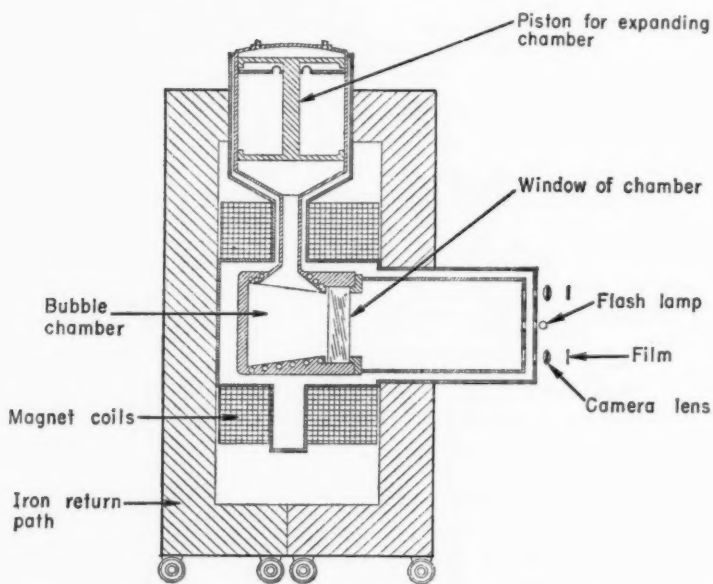


FIG. 13. Transverse cross-section of $28 \times 25 \times 80$ -in. Brookhaven hydrogen bubble chamber. (Courtesy of Dr. Ralph Shutt.)

chamber at Berkeley. Since large chambers are very expensive, it is worthwhile to discuss some of the design features and some of the reasons for their selection by the different groups.

Tables IV A and IV B show characteristics of various large chambers and of their associated magnets. Some of the features of these chambers are subject to change during development and construction, and should not be considered as definitely established.

TABLE IV A
TENTATIVE PARAMETERS OF SOME LARGE HYDROGEN BUBBLE CHAMBERS

Chambers	Dimension of illuminated volume (in.)	Volume of hydro- gen (l.)	Material	Number of windows	Window location	Expansion mechanism
Berkeley	14×20×72	520	Cast stainless steel	1	Top	Vapor
Brookhaven	28×25×80	1700	Cast or welded stainless steel	1	Side	Liquid (piston)
British Natl.	18×20×59	~ 500	Machined aluminum	2	Side	Vapor
CERN	20×24×78	~1000	Cast or welded stainless steel	2	Side	Liquid (piston)
U.S.S.R. (Nikitin)	18×27×79	~1000	Cast stainless steel	1	Top	Liquid (bellows?)

TABLE IV B
MAGNETS OF SOME LARGE HYDROGEN BUBBLE CHAMBERS

Magnet	Field (kgauss)	Power (Mw.)	Field homo- geneity	Pole pieces	Weight of Cu (tons)	Weight of Fe (tons)	Total wt. (tons)	Cost of magnet \$×10 ³
Berkeley	18	2.5	±12%	1	20	115	~200	200
Brookhaven	~18	4	± 3%	1	30	280	310	—
British Natl.	11.8	4	"few %"	0	40.2	240	300	—
CERN	~16.6	6	—	0	—	—	470	—
U.S.S.R. (Nikitin)	16-18	1.5	—	1	—	—	~350?	—

B. MAGNETS

It is generally agreed that magnetic fields should be as strong as is economically possible, since the attainable momentum accuracy for a given length of track is about proportional to the magnetic field strength. The cost of obtaining fields higher than 16 to 20 kgauss rises very rapidly because of the saturation of the iron. The field in the British chamber was originally planned to be 15 kgauss, but the value had to be lowered when the magnet dimensions were increased to accommodate the hydrogen shields (47).

Uniformity of magnetic field throughout the chamber was of great importance in cloud chambers, but is not usually considered significant in large bubble chambers, where the event analysis is to be carried out in high-speed digital computers. The cost of computing the corrections for the

nonuniform field in the analysis of 72-in. bubble chamber events is only \$300 per year.

Bugg (20) has summarized some of the economic factors of magnet design, and Eaton & Hernandez (51) have reported on detailed considerations regarding the Berkeley 72-in. magnet.

C. CHAMBER MATERIAL

Chambers must be made of a metal that is strong and ductile at low temperature, to withstand the large impact forces of fast expansion and recompression. It is desirable to use a material with high tensile strength so that the chamber can occupy a minimum volume of magnetic field. The metal also should remain nonmagnetic at liquid hydrogen temperature. The composition of stainless steel castings must be controlled with particular care to obtain low permeability. The British have chosen machined aluminum because it satisfies these requirements (except strength) and is easy to fabricate. At one time they also believed that the high thermal conductivity of aluminum would be important in obtaining uniform temperature distribution of hydrogen in the chamber, but subsequent experiments with other chambers indicated that high thermal conductivity is probably not important. The only serious drawback to aluminum appears to be the large wall thickness that is required, with the resultant increase in magnet cost.

D. CHAMBER WINDOWS

Borosilicate crown glass has been chosen for the Berkeley, Brookhaven, and British chambers. The thicknesses are 5 in., $6\frac{1}{2}$ in., and $6\frac{1}{4}$ in., respectively. Fiducial marks can safely be etched, scribed, or sandblasted on the inner surface, which is under compressional stress. Strength and fatigue tests on glass are reported by Kropschot (52). Half-tempered glass is specified for the Brookhaven hydrogen chamber. The others will use untempered glass.

E. GASKETS

The differential thermal expansion between glass and metal requires that the window must be sealed to the chamber after the system is cooled, and unsealed before the chamber is warmed up. The Berkeley design of inflatable gasket with indium sealing surfaces has been very satisfactory.

F. EXPANSION MECHANISMS

Ideally, chamber expansion should occur just early enough to make the chamber sensitive at the instant of beam arrival. Then recompression should take place as soon as the bubbles have been photographed. The expansion must start before the particles arrive, so that the reduced-pressure pulse can propagate at a rate of about 1000 m./sec. throughout the hydrogen. Accordingly, about 5 to 10 msec. are required to establish uniform sensitivity throughout the chamber. The time of arrival of the beam often has a jitter of 1 or 2 msec. In one mode of Bevatron operation, the beam particles can

all arrive in a pulse less than 1 msec. long. With other modes of accelerator operation the beam can dribble into the bubble chamber over an arbitrarily long period. The time for bubble growth requires up to a few additional milliseconds. All these times combine to give a total of about 20 msec., after which the pressure is reapplied rapidly. It is desirable to have the chamber pressure constant during the sensitive time, and reproducible from pulse to pulse, in order to get pictures with the same track sensitivity.

Barford (43) and Amiot *et al.* (53) have given extensive discussions of the existing expansion systems, and have suggested some improvements. Two basically different systems are used today. The liquid can be allowed to expand against a diaphragm or piston above the chamber at approximately 27°C. temperature, as is done in the Shutt 20-in. chamber and proposed for the large Brookhaven and CERN chambers; or alternatively, large pipes can lead from the chamber up to a fast-acting valve at room temperature. This system is used in the large Berkeley chamber and is proposed for the British chamber.

It is, of course, a very difficult problem to obtain a satisfactory seal between the piston and cylinder in a liquid-expansion system over the wide range of temperatures. Shutt uses graphite-impregnated teflon piston rings to make a reasonably tight seal, but there is some leakage. Also abrasion produces visible quantities of dust, which would seriously reduce picture quality if the chamber windows were horizontal. Peyrou (54) reports on a 30-cm.-diameter piston-expanded chamber, with similar excellent expansion ratios and similar amounts of abrasion.

Steinberger has used a bellows in the expansion system of his 30-cm. hydrogen chamber. This eliminates the problem of leakage and abrasion; but some workers believe that bellows can fatigue rapidly under conditions of pulse loading where high stresses may be concentrated in a few convolutions.

The outstanding consideration in liquid expansion for large chambers is the reliability of the mechanical design, since repair of the piston or bellows can be expected to require warming the whole chamber up to room temperature, thereby interrupting chamber operation for at least a week. Liquid expansion systems do, on the other hand, have modest refrigeration requirements after the chamber has been filled with liquid hydrogen. The cost of refrigeration must be judged according to the reliability of the system and weighed against possible interruptions of a bubble chamber run that costs \$10,000 per day.

All moving parts of the Alvarez chamber expansion system are at room temperature so that repairs can be made easily and quickly. The operation can be understood by referring to the schematic diagram of the 72-in. chamber, Figure 9. When the chamber is under pressure, the expansion valve is closed and the liquid extends a small distance up into the expansion line. The higher regions of the expansion line contain gas at progressively warmer temperatures. To expand the chamber, the valve is momentarily

opened to the expansion tank at 17 p.s.i.a. A few milliseconds later the valve is switched rapidly to the recompression tank at about 125 p.s.i.a. Finally the valve is closed, completing the cycle. Between expansions a recompressor re-establishes the appropriate pressure in the two tanks.

During the expansion, cold gas moves up the expansion line and gains heat, which it delivers to lower regions during recompression. This undesirable heat load can be reduced by proper choice of expansion-line dimensions. Further reduction has been attempted by introducing a heat exchanger of copper wire mesh or similar high-heat-capacity material in the cold part of the expansion line. The detailed design of expansion line and heat exchangers must be fixed by trial, since the heat load is strongly dependent on the amount of turbulent mixing of warm and cold gas. Static and dynamic heat loads for three Berkeley hydrogen chambers are given by Gow (22e). Gaseous expansion in large chambers requires a refrigerator that is larger by an order of magnitude than for liquid expansion, but a large refrigerator is usually wanted for initial cool-down of the chamber in either case.

G. LOCATION OF WINDOWS

A bubble chamber with a single window on the top affords the maximum safety if the glass should break. Also, a horizontal-window chamber can be rotated or moved easily to bring beams of various momenta through the fringing magnetic field into the chamber in the desired location. Horizontal-window chambers offer distinct advantages in experiments involving polarized particles, since the polarization is generally determined by left-right asymmetry in the second scattering of a particle whose first scattering lay in the horizontal plane. The geometry of separated beams introduces another consideration which may be very important for experiments on short-lived particles that require the bubble chamber to be put close to the accelerator: The angular separation between wanted and unwanted particles is characteristically a few milliradians. This produces such a small relative displacement of the particles that the separation is most effectively made in a vertical direction, while the fringing field of the accelerator focuses particles into a broad beam in the horizontal direction. Therefore, the beam entering the bubble chamber is broad in comparison with its height. Such proportions are appropriate to a bubble chamber with the window on the top. This rectangular-cross-section beam can be rotated 90 degrees at the cost of several additional feet of quadruple-type lenses. A disadvantage of horizontal windows is the possibility that dirt, or contaminating "frost" of solidified gas, can settle to the bottom of the chamber and deteriorate the quality of the image.

Chambers with windows on the side do not suffer from problems of cleanliness. Shutt has indicated, for example, that the dust from abrasion of his piston system does not affect the quality of the pictures in his 20-in. chamber although it might make pictures unusable if the windows were horizontal. For some time it was thought also that uniform temperature throughout a bubble chamber could be maintained only by having a good

heat conductor where the bubbles condensed at the top of the chamber. In the Berkeley chambers there was a great deal of difficulty in this respect, until automatic flap valves were installed to remove the bubbles and some liquid from the top of the chamber at each expansion. Both the Alvarez 72-in. chamber and the Shutt 20-in. chamber can be operated with less than 0.1° temperature difference throughout 90 per cent of the chamber. Under these conditions the number of bubbles per unit length of a relativistic track is the same to within statistical accuracy at all points in the chamber.

The fringing fields of bubble chamber magnets bend the incoming particle beams in a way that will be awkward for long chambers with vertical windows. Since the experimenter wants the beam to travel the full length of the chamber, it may be desirable to use external magnets that bend and displace the beam vertically before it reaches the chamber.

None of the points mentioned above appears to be of completely overriding importance. Even the problem of introducing the beam into a chamber with horizontal magnetic field has a number of solutions. Shutt plans to use a bending magnet to deflect the particles at upward angles, and then to raise the chamber as much as 2 ft. above beam height in order to get beams of momentum below 1 Bev/c into the chamber. The CERN chamber will incorporate a correcting coil placed directly in the side yoke and partly in the space between the main magnet coils, to allow beams of low momentum to enter the chamber undeviated.

H. MOVING THE CHAMBER

The entire structure of chamber and magnet must be provided with means for translation and rotation as required for the various particle beams. In addition, the Brookhaven chamber and the British chamber will need to be adjustable, about two feet in height. Translation and rotation of the Berkeley chamber is accomplished by four hydraulically actuated feet. The height of the chamber is determined by a central support structure on which the magnet rests between translations. The Brookhaven magnet will move on sliding pads or wheels, either as a unit, or in separate halves, for removing the chamber. The British magnet will be provided with a hydraulic jacking system for adjusting the height and will be moved horizontally on approximately 400 ball casters rolling on hard steel sheets. Peyrou reported that the CERN magnet will be moved on rails and rotated on a turntable (48). Recently, however, he has stated informally that the magnet may be actuated in the same way as the Berkeley chamber. Hernandez has suggested that magnets could be moved by the simple and elegant mechanism of floating the magnet on a pad of compressed air, if the floor is sufficiently level.

I. ILLUMINATION

General.—Bubble chambers must be illuminated with a short-duration high-intensity flash of well collimated light—intense enough to scatter a sufficient amount into the camera lens for photography.

Liquid hydrogen at chamber operating conditions has an index of refraction of 1.093 for light of 5300 Å (55). The intensity of light scattered at various angles from a spherical bubble can be calculated by geometrical optics, for bubbles that are large in diameter compared with the wavelength (49, 56). The light intensity for various values of the refractive index is shown in Figure 14, taken from Barford (43). The rapid decrease of light with scattering angle implies that intense light sources are required, for scattering angles around 10 degrees. Scattering the light through 90 degrees is feasible for cloud chambers and heavy liquid bubble chambers, but not for hydrogen bubble chambers. The task of illumination is made even more difficult since bubbles are photographed at as early a moment as possible, in order that the tracks will have suffered a minimum displacement due to motions of the liquid. In any case, it is important to take the photograph while the bubbles

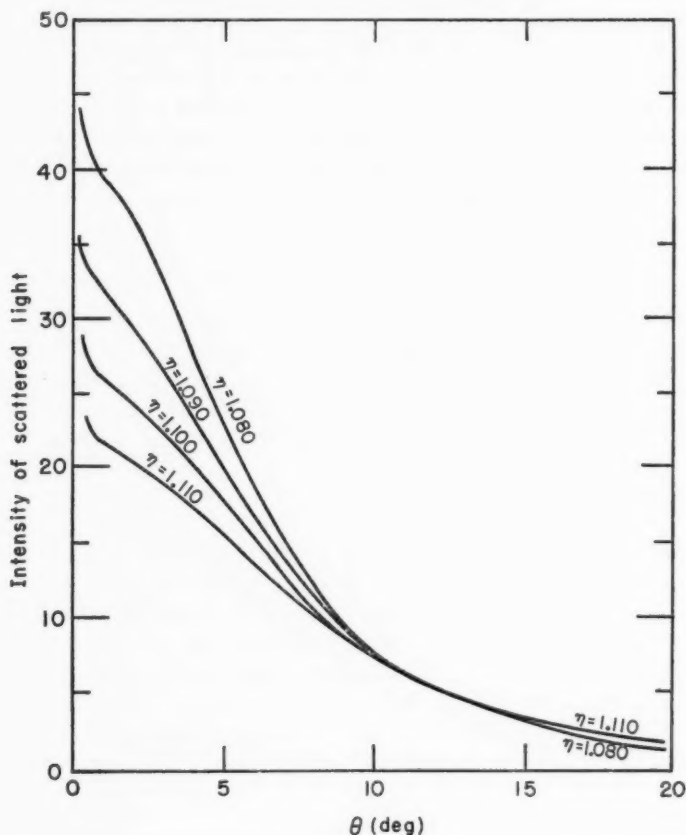


FIG. 14. Intensity of light scattered at angle θ for gas bubbles in liquids with different values of index of refraction. (Courtesy of Dr. N. C. Barford.)

are less than about $\frac{1}{2}$ mm. in diameter, so that bubble counting may be possible. Scattering angles as large as 10 degrees have been found to give satisfactory images with commercially available flashlamp sources.

Dark-field illumination, in which the only light reaching the cameras is scattered from the bubbles, produces pictures with satisfactory image contrast over a much wider range of illuminating intensity than the conventional light-field illumination.

Lighting is easy for very small chambers, but the possible designs of illumination and photography become progressively more restricted as the size of the chamber is increased. The ideal stereo system would use cameras pointing at the chamber on axes 90 degrees apart. Straight-through illumination with the light source on the side opposite the camera leads to a design like the $2.5 \times 2.5 \times 10$ -cm.³ chamber of Nagel, Hildebrand & Plano, with four glass walls (57). Such a system appears uneconomical with a chamber larger than about 6 in. Middle-sized chambers are normally illuminated by a single flash on one side and are photographed by two or more cameras, with axes parallel, on the opposite side of the chamber. The Steinberger propane chamber shown in Figure 7 is a representative example of this type of illumination.

The CERN chamber and the British chamber are planned for modified forms of straight-through illumination.

The CERN chamber will use one flash lamp per camera lens, and will photograph bubbles with approximately seven degrees deviation of the light (48). The Berkeley chamber operates with a similar scattering angle. The British have designed their illumination for a scattering angle of approximately two degrees, to minimize the variation in image intensity with changes of illuminating angle (47). Unfortunately, chromatic aberrations in the condenser system that could be designed for this illumination would give variations in angle of about three degrees across the condenser aperture. Therefore, the British will have to use monochromatic light and hence will not gain the intensity that would have been expected from such small-angle illumination. They expect, in fact, that it will be necessary to use 650 joules to produce good images with "fairly fast film." By comparison, the Berkeley 72-in. chamber flash of 150 joules produces good images on lino-graph shellburst film with ASA speed of about 100. The use of monochromatic light will, however, permit the British to eliminate reflection flares by applying a very-high-efficiency antireflection coating on the glass surfaces of the optical system and the chamber windows. Although straight-through illumination can be used with the largest chambers, considerations of magnet cost and of hydrogen safety in case of window breakage have led several groups to propose single-window designs for very large chambers, in which the cost of removing a pole piece or of adding an additional 10 in. of air gap can amount to \$100,000.

Single-window illumination.—The most direct way to illuminate a single-window chamber is to place a spherical Fresnel mirror in the bottom, and a

light source outside, midway between the lenses of the cameras. Such a system has the serious disadvantage that light going into the chamber can be scattered from bubbles and produce ghost images below the chamber thereby reducing the number of tracks permissible in the chamber on each expansion by a factor of two. One way to eliminate the ghost tracks is to cover the spherical mirror with small dimples or bumps a few millimeters in diameter and about one centimeter in radius of curvature. Bradner has made successful tests of this by pressing dimples into a polished aluminum plate with a polished steel ball (58). Plano (41) and Barford (43) have also proposed this system. In spite of the heat-transfer advantages of a metal

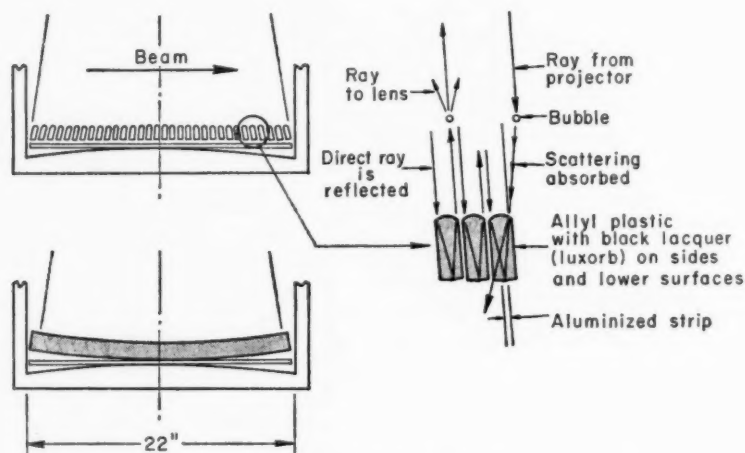


FIG. 15. Schematic view of "Coat hangers" for retrodirective illumination.

system, no one has undertaken to build a full-sized dimpled reflector, because of the difficulty of fabrication. Alvarez has proposed a one-window retrodirective illumination system, using a spherical Fresnel mirror in the bottom of the chamber, and Venetian blinds to eliminate ghost images (59). Other retrodirective materials—such as the Minnesota Mining Co. "Scotch-light," corner reflectors, and machined grooves of various shapes—have been tested and abandoned because of insufficient collimation, manufacturing difficulties, or cost.

The ghost images in the 72-in. Berkeley bubble chamber have been avoided by using an array of 111 transparent Homolite plastic "coat hanger" reflectors each 22 in. long by $\frac{3}{8}$ in. wide and $1\frac{1}{4}$ in. high, separated by 0.015 in. to allow heat transfer from the bottom of the chamber. Closer spacing causes spontaneous boiling at the edges of the reflectors. Figure 15 shows cross-section drawings of the coat hangers for the 72-in. Berkeley chamber. In side view the reflectors are curved, with the radius equal to the distance to the flash source. In end view they are shaped so that light

incident from the flash is focused onto an aluminized strip on the rear of the coat hanger and redirected back at the source. Light scattered from a bubble before reaching the coat hanger is absorbed in the Homolite walls, which have been coated with "Luxorb" black, a material having the same index of refraction as Homolite. The top surface of each coat hanger has been made elliptical to produce a more even illumination throughout the chamber from the finite-sized source (60).

Although the coat hanger retrodirective illumination is a satisfactory single-window illumination system, it does give nonuniform illumination of bubble tracks, especially in the bottom 2 in. of the chamber. There is also a flare of at least 1 in. diameter on the top glass. If the glass and the coat hanger surfaces are allowed to get dirty, the flare size increases and the photographic contrast decreases. However, careful attention to trapping of vacuum pumps and purifying of chamber hydrogen permits runs of several months' duration without significant deterioration of image quality.

Several other illumination schemes have been discussed for single-window chambers. The Venetian blind system could be used by putting the flash lamps inside the actual chamber volume. Powell has built his 30-in. propane chamber this way, but the scheme does not seem to have been considered seriously for large hydrogen chambers because of the long time that would be required in warming up the chamber in order to replace lights. Schwemin has considered getting around the flash lamp problem by using electroluminescent panels or phosphors with fast decay times, but has concluded that these approaches are impractical at present (61). Fiber optics lightpipes have also been proposed to carry the illumination from outside the chamber to the chamber bottom, but have been abandoned on considerations of cost and luminous intensity.

The ideal illumination system does not produce uniform intensity of light at the camera lens from all bubbles, since camera lenses reduce the intensity of images at an angle θ from the axis, by a factor as large as $\cos^4\theta$. This off-axis reduction is partially compensated in the Berkeley chamber, because the scattering angle of the light decreases as the position of the bubble gets farther off-axis. Additional compensation is made by adjusting the relative intensities of the three flash lamps that illuminate the separate regions of the chamber. Gray wedges and masks could be used to produce still greater image uniformity.

J. PHOTOGRAPHY

The parameters that must be considered in designing the photographic system for a bubble chamber include: (a) the dimensions and depth of the chamber that must be photographed with approximately uniform resolution; (b) the separation of the lenses; (c) the distance from the chamber to the camera lenses; (d) the focal lengths and resolution of available wide-angle camera lenses; and (e) the costs, speeds, resolutions, and distortions of photographic film.

Wilson has discussed the depth of field for lenses photographing very

small light sources in connection with design of cloud chamber optics (62). Good has carried out a somewhat similar but simplified discussion of the optimum camera lens (63). Good proposes that we adjust the camera lens aperture so that the maximum diameter of the circle of confusion is equal in size to the diameter of the first diffraction minimum. By geometrical optics, the apparent size in the chamber of a point source at a distance $h/2$ beyond the center of the chamber is a circle of confusion of diameter $c = ah p_0^{-1}$, as shown in Figure 16. By physical optics considerations, a point source at the center of the chamber is imaged as a series of diffraction rings. The diameter of the central diffraction disk, measured in the chamber, is $d = 1.22\lambda p_0 a^{-1}$. The diameter of the image from a point source should be approximately uniform

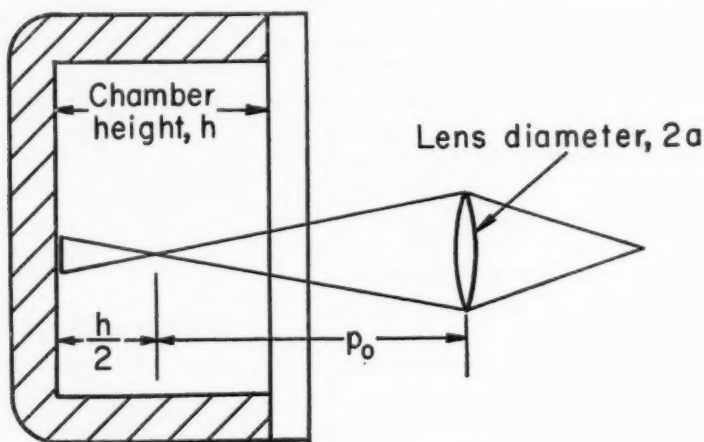


FIG. 16. Formation of bubble image by camera lens.

throughout the depth of the chamber when these two terms are equal, i.e., when $a^2 h$ equals $1.22\lambda p_0^2$. Then the apparent object diameter would be about equal to $\sqrt{c^2 + d^2}$, or $\sqrt{2.4\lambda h}$, quite independent of our choice of magnification or lens distance. In the Berkeley 72-in. bubble chamber, this equation predicts a limit of 0.7 mm. diameter to the apparent size of a bubble in the chamber, independent of the distance from lens to chamber or of the magnification chosen. Usual practice in bubble chambers is to take the photograph when the bubble is approximately 0.3 mm. diameter. Hence we would expect the apparent bubbles to be nearly 1 mm. in diameter. Experience has shown that the above treatment is considerably in error because of the assumption that the diameter of the diffraction image is equal to the diameter of the central diffraction disk. The image is smaller by a factor of about two, since bubble chamber photographs are taken on high-contrast film, which produces a black image only in the central part of the diffraction disk.

Although the simple theory indicates that the optimum lens opening for the 72-in. chamber cameras is $f/27$, the lenses can be opened up to $f/22$ be-

fore deterioration of the image anywhere in the chamber can be noticed. Normal film images in the 72-in. chamber are found to correspond to apparent bubble diameters of 0.5 mm. in the chamber instead of the size predicted by Good's treatment.

The British propose to use two different sizes of film for their large chamber. Initially they will use unperforated 35-mm. film in three separate cameras at demagnification of 16 with 3.25-in. focal length aerial survey lenses operated at aperture $f/27$. These cameras will be replaced later with units giving images at demagnification of 9 on 60-mm. unperforated film with 6-in. focal length aerial survey lenses operating at $f/45$.

It may be possible to increase the useful depth of field by employing a lens with large spherical aberration, since it can be shown that the annular zone of the lens that brings a point into proper focus on high-contrast film produces a darker image than the integrated effect of the out-of-focus zones (64a, b).

Welford (65) points out that the ratio of circle of confusion to diffraction-disk diameter can be improved by covering the center of the lens aperture with a disk. A disk whose diameter is a fraction b of the lens aperture increases the depth of field by a factor $1/(1-b^2)$.

Welford's suggestion of using annular apertures may make it possible to increase the aperture of the British 6-in. lenses to about $f/15$ and obtain images of size limited only by the grain resolution of the film.

It will be noted that the focal length of the lens and the magnification of the image did not enter the expression for the apparent size of a bubble in the chamber. If we had ultrafine-grain distortionless film and if all photographic lenses were equally good, then any convenient image size could be chosen, since all magnifications would allow the same precision of track reconstruction. A satisfactory expression for the resolution R of a picture taken on film with resolution F by a lens with resolution L appears to be $1/R^\alpha = 1/F^\alpha + 1/L^\alpha$, with a value of α between 1 and 2. Either exponent leads to the reasonable conclusion that 15-fold demagnification is acceptable for film with resolution of 70 to 90 lines per mm. Larger images would require less precise co-ordinate measurement for the data reduction and would decrease the errors from occasional serious distortions caused by film processing; but the difference in film cost between 10 diameters and 15 diameters demagnification on the 72-in. chamber was estimated to be \$100,000 per year.

The transverse resolution of the optical system is determined by the resolution of a single lens and film, but the depth resolution is determined also by the geometry of the stereoreconstruction, and hence depends also upon the ratio of the camera lens separations to the distance from lens to camera. The depth resolution is always poorer than the transverse resolution, if the lens axes are parallel. For perfect lenses it can be shown that the depth resolution improves as the lenses are moved closer to the chamber. A practical limit is set by the quality of the available wide-angle photographic lenses, in which the resolution is normally about 20 per cent less than the resolution of the theoretically perfect lens. The 72-in. chamber uses 121 mm. focal length

Schneider Super Angulon lenses operating out to a maximum angle of 34 degrees.

Although two lenses are sufficient to establish stereogeometry, a third lens is almost always added in order to speed up stereoreconstruction. A simplified explanation is as follows: Let us establish x , y , and z axes on each of two stereo images, with the z axis of each film perpendicular to its surface and passing through the optical axis of its lens, the x axis lying along the line between the two camera lenses. (See Fig. 17.) Then any arbitrarily chosen bubble will have the same y co-ordinate in both images. We do not have to identify the bubble on both images in order to make the geometrical recon-

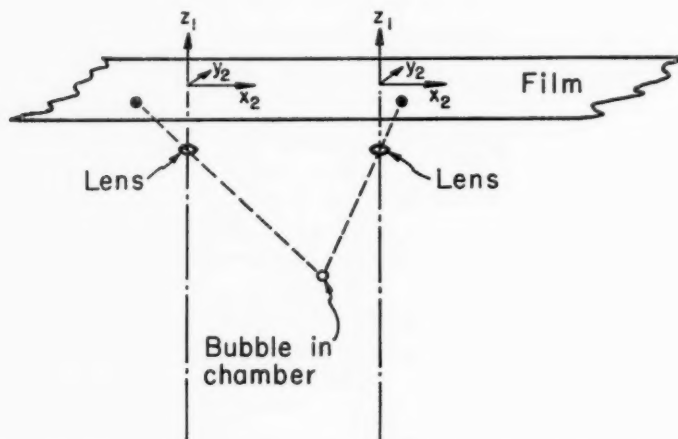


FIG. 17. Schematic perspective of stereo-optics used for 3-dimensional reconstruction of bubble position.

struction; we can make co-ordinate measurements on an arbitrary spot on the track in one view and can find the appropriate x co-ordinate in the other view by y interpolation between near-by track co-ordinates in that view. The accuracy of this interpolation decreases as the direction of the track approaches the x axis, and it would be necessary to make co-ordinate measurements on corresponding bubble images to get 10-micron accuracy for tracks that lie closer than about 15 degrees to the x axis. If a third lens is placed at the vertex of an equilateral triangle or a corner of a square, it is always possible to find two views in which a track makes a large enough angle to the axis so that bubble matching is unnecessary.

The use of four or more lenses would help eliminate occasional ambiguities in the photographs or would permit focusing more sharply in restricted regions of the chamber, but the cost of film argues strongly against using more than three images.

VI. PRESENT LIMITATIONS TO BUBBLE CHAMBER OPERATION

A. REPETITION RATE

The recycling rate of bubble chambers is limited purely by mechanical and thermal factors. The cycling rate of most bubble chambers has been chosen to match the pulse-repetition rate of the high-energy accelerators for which they were intended. Kuznetsov *et al.* have built a freon chamber to cycle 10 times per sec. for cosmic-ray research (66). At these very high rates there still appear to be some unsolved problems of removing the bubbles before the next expansion.

B. TRACK DISTORTION

A track image may be displaced from true track position by liquid motion subsequent to the bubble formation, or by index of refraction aberrations introduced by mixing warm and cold liquid. The actual displacement of the bubbles can be reduced by shortening the light delay or by reducing the magnitude of the liquid motions. Two counter-rotating eddies in hydrogen, 12 cm. in diameter and carrying liquid at the rate of 1 cm. per sec., can distort the track of a 1-Bev/c particle as much as the multiple Coulomb scattering. Donaldson & Watt point out that the half-time for decay of a vortex varies as the square of the vortex radius and is 13 min. for a 2-cm.-radius vortex in liquid hydrogen (67).

In addition to the gross distortions of track curvature mentioned above, there are short-wavelength wiggles which increase the root mean-square deviation of the measured points from a smooth curve. This deviation σ_{xy} , referred to the horizontal plane in the 72-in. bubble chamber, is characteristically 60 microns or 0.1 apparent bubble diameters, for 30-in.-long tracks. Preliminary measurements of sample film from Peyrou's 30-cm. hydrogen chamber and Shutt's 20-in. hydrogen chamber gave values of 30 to 50 microns for σ_{xy} . In all three cases, multiple Coulomb scattering would produce values of σ_{xy} nearly as large. Normal film distortions of ~ 3 microns, and measuring precision of ~ 2 microns give a σ_{xy} of 20 to 30 microns from a photograph of a ruled straight line.

C. NUMBER OF TRACKS PER PICTURE

The number of beam tracks that can be permitted to go through a bubble chamber for a single picture is limited by the danger of getting ambiguous events, in which it is not possible to say definitely which reaction products are associated. Although 100 or 200 tracks can be used in cloud chambers, the higher density of bubble chamber liquids ordinarily limits the number of tracks to 20 or 30. This number probably could be increased by dribbling a beam into bubble chambers over an extended period of time, and then distinguishing associated tracks by the differences in bubble size. However, it seems clear that the time required to look for events in a picture would in-

crease faster than the number of tracks; and hence, this technique is of questionable value as long as data analysis is slower than the rate of data accumulation.

D. TIME RESOLUTION

The time resolution of the bubble chamber as determined from bubble size is measured in tens or hundreds of microseconds. The time resolution as determined from the distance that particles travel before decaying is about 3 mm., or 10^{-11} sec. without relativistic time dilation.

E. MOMENTUM RESOLUTION

Momentum determination by measurements of track curvature in a magnetic field can never exceed the accuracy limit set by multiple Coulomb scattering (see Sec. VIII. B.). In several hydrogen chambers, momentum errors on relativistic tracks are less than twice this limit.

F. SPEED OF ANALYSIS

The steps in analysis of bubble chamber pictures are described in the following section. It does not appear likely that a group of experimenters can make accurate analysis at an average rate greater than 300 events per day, by improvement of the present system. Significantly higher rates can be achieved only by developing automatic character-recognition devices as well as fast measuring and computing techniques.

VII. ANALYSIS OF EVENTS

A. GENERAL

The analysis of bubble chamber events ordinarily requires stereoreconstruction of the trajectories of all particles involved, followed by a computation of the momentum balance and energy balance. Two-lens stereophotography permits this reconstruction if measurements are made on the same bubbles in the two views. Much more rapid stereoreconstruction can be done without bubble matching, on tracks that are at angles of more than about 15 degrees to the line between the camera lenses. For this reason three cameras are ordinarily located on the vertices of equilateral triangles or three of the corners of a square.

Analysis of picture measurements can yield a comprehensive description of the event: The curvature of the track in the magnetic field is a measure of momentum ÷ charge; the direction of the curvature indicates the sign of the charge; the range of a particle that stops in the liquid gives the energy, if the particle mass is known; the change of curvature with distance can establish mass if measurements are sufficiently accurate, and if multiple Coulomb scattering is small enough. Energetic delta rays can give some information on the velocity of the particles; the number of bubbles per unit length can give the velocity of the particle if its charge is known.

In addition to observing tracks of charged particles, it is also possible sometimes to detect neutral particles by energy-momentum balance, by ob-

serving charged decay fragments, or by observing secondary interactions that involve charged particles.

The frequent appearance of inelastic processes in high-energy physics usually demands that the trajectories of the particles be reconstructed with the highest possible accuracy. The geometrical problems of reconstructing an event in a bubble chamber are similar to the problems encountered in the analysis of cloud chamber photographs, but the reconstruction is complicated by the fact that the liquid has an index of refraction differing from unity. Furthermore, camera optics are usually wide-angle, and therefore corrections for the chamber windows are nonlinear. In addition, the magnetic fields in some chambers are very nonuniform.

The development of systems, apparatus, and computer programs for data reduction has been summarized in the reports of a number of conferences in Geneva (68 to 70). The largest effort has been made by the group under the direction of Bradner in connection with the hydrogen chambers at Berkeley. Their system is described in Lawrence Radiation Laboratory Engineering notes (3) and in papers by Bradner & Solmitz (71, 72).

B. NEED FOR RAPID ANALYSIS

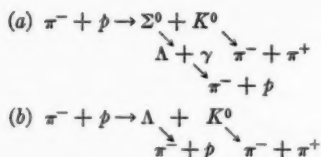
The article by Fretter (1) in this *Review* pointed out the difficulty of analyzing events with the necessary speed from high-pressure diffusion cloud chamber experiments at the Cosmotron. Physicists recognized that the number of interesting interactions in a bubble chamber would be even greater, by almost two orders of magnitude.

The following discussion is based largely on the work with hydrogen bubble chambers at Berkeley; the discussion is, however, broadly applicable to heavy-liquid chambers as well. The size of the problem can be appreciated by considering the 5-mo. run now under way with the 72-in. hydrogen chamber at the Bevatron. Twenty π^- mesons passing through the chamber per expansion are expected to produce 75,000 Λ hyperons, 200 Λ scatterings on hydrogen, 40 leptonic decays of Λ 's, and 3000 interesting Σ -hyperon events, plus many other interactions including 50,000 cases of π -production which can be used to investigate π - π interactions, plus 4,000,000 other interactions of π mesons without the production of strange particles. If analysis were at cloud chamber rates, each event would take nearly one man-day of effort. Now, with semi-automatic measuring microscopes and high-speed digital computer geometric reconstruction, the Berkeley Hydrogen Chamber Group can measure and analyze 200 events per day. Two measuring machines and a staff of 30 people are required. The cost of developing and carrying out the data reduction for bubble chambers has been comparable to the cost of developing and operating the chambers. Systems to handle data at even higher rates have been discussed; but these multimillion-dollar systems are several years in the future.

C. NEED FOR ACCURACY

The incident particle can undergo any one of several competing reactions, which sometimes look quite similar. These must be distinguished on the basis

of energy balance and momentum balance. An example is the pair of reactions



In case (a) the Σ^0 decays into a Λ plus a 70-Mev γ ray in a time $\ll 10^{-11}$ sec. In both cases, the Λ can decay to $\pi^- + p$ in a mean time of 2.8×10^{-10} sec. The incoming π^- in case (a) usually does not lie in the plane of the decaying Λ and K^0 particles, since momentum is carried off by the γ ray. However, the angle of non-coplanarity (in the laboratory system) is so small that it is difficult to separate the cases, even with the most accurate measurements.

Accurate measurements are not always required. For example, information on the polarization of a beam of low-energy antiprotons could be obtained without any measurement, simply by counting the frequencies of scatterings to the left and to the right. Generally, however, high-energy bubble chamber experiments have required a greater accuracy of analysis than can be obtained by template measurement or graphical reconstruction.

D. STEPS IN ANALYSIS

Nearly all research groups have separated their data reduction and data analysis into distinct steps of searching for events, measuring the film, reconstructing the event, and tabulating it. Goldschmidt-Clermont has summarized the equipment used at various laboratories (73). More detailed description of the individual components can be found in the *Proceedings of the International Meeting on Instruments for the Evaluating of Photographs* (69) held at CERN in September 1958.

Scanning.—The search for events is usually made on high-quality opaque projection tables. These instruments are used for initial scanning of the film and for the check scans that are required for determining event-finding efficiency. They are also used to prepare the "sketch" instructions for the operators of the measuring machines, and are used once more to re-examine any events in which the computer output has given an anomalous result. These scanning operations take more time than the measuring operation. It is desirable, therefore, that the instruments be easy to operate, and produce good images which can be superimposed, on events that need careful study. Fast and slow film transport and frame counters are desirable.

In the instrument for scanning film from the 72-in. Berkeley chamber, any one or more of the three images can be projected onto a white micarta surface at a magnification of 10 diameters, i.e., two-thirds the original bubble chamber size. The projection lenses are Schneider Componon, 200-mm. focal length, at f/5.6. It is necessary to use high-quality wide-angle lenses to keep the projection distance reasonably short. The mirrors are parallelplate, front-surface aluminized, with a silicon monoxide coating. A special mirror

suspension is required to keep the magnification sufficiently uniform throughout the picture. The three views are illuminated by three 500-watt motion picture projector lamps operating with $f/0.8$ Lucite condensers and Corning I-58 and I-69 heat-absorbing glasses. Film is clamped in an open-faced holder. The temperature rise of a piece of black film is no greater than 3°C .

We usually find it desirable to scan along the beam tracks, i.e., from the end of the table. It is not possible to magnify the image enough to see the necessary detail at the near end of the image without having the far end too distant from the observer. Hence, the film carriage is arranged to roll easily and thereby move the image toward or away from the operator by means of a hand lever. The film can be advanced from one frame to the next in approximately $\frac{1}{4}$ sec. It can run at slew speed of 800 ft. per min., and can be started and stopped with a minimum film tension of less than 3 lb. A frame counter automatically indicates the picture number.

Measuring.—Special instruments have been developed by a number of laboratories for making measurements on the film to accuracies of about two microns. The usual instrument is a projection microscope with which the operator views the image on a translucent screen at sufficient magnification for him to position marks on the film to ± 2 micron accuracy. The film is moved to bring the point of interest on the image in coincidence with a mark fixed on the screen at the optical axis of the system. The co-ordinates of the stage carrying the film are measured by rotary encoders on the screws driving the stage, or by a scaler that counts fringes on gratings attached to the stage. The co-ordinate measurements are entered automatically on IBM cards or punched tape.

Many of the instruments are equipped with photoelectric sensing devices and tight servo loops which automatically hold the instrument centered on a track. In some instruments careful attention has been paid to designing components for high reliability and to utilizing techniques of "human engineering" so as to minimize errors and operator fatigue.

Figure 18 is a schematic diagram of one of the "Franckenstein MP-II" machines used for measuring film from the 72-in. bubble chamber (74). Light from a 2500-watt mercury lamp is filtered by water and heat-absorbing glass before passing through the three images on the film. These images are 1.4 by 4.9 in. After leaving the film, the light is divided by a partially silvered mirror, and passes through two lenses to give images at different magnifications. A Schneider Xenotar lens of 10.5 mm. focal length produces an image at magnification of 33 on an 18-in.-square transmission screen, for making co-ordinate measurements. A Dallmeyer Serrac lens of 18-in. focal length projects an image of the entire chamber at a magnification of 7.5, i.e., one-half life size, onto an opaque screen. An illuminated reticle projected onto the half-scale view shows the region displayed on the highly magnified view. Co-ordinate measurements are made on the optical axis to 2.5 microns least count by using *moiré* fringe gratings. The sensing element for the automatic track-following servo is a photomultiplier mounted behind an opaque disk with 24 radial slits, spinning at 3600 rpm. The co-ordinates of 10 to 20

arbitrary locations on each track are recorded on perforated tape. These data are subsequently transferred to magnetic tape and put into an IBM 704 machine for computation. The cost of manufacturing one of these measuring projectors is about \$140,000.

Computing.—Most research groups have divided the computation into two separate stages of geometrical and kinematic reconstruction, although their detailed philosophies in each stage may differ. In the geometrical stage, each track of an event is reconstructed in space. The CERN program searches for the best helix passing close to the optical rays through the center of the camera lens from each measured point on the stereoscopic views (73). In the Berkeley program, developed primarily by Rosenfeld and Solmitz, a repre-

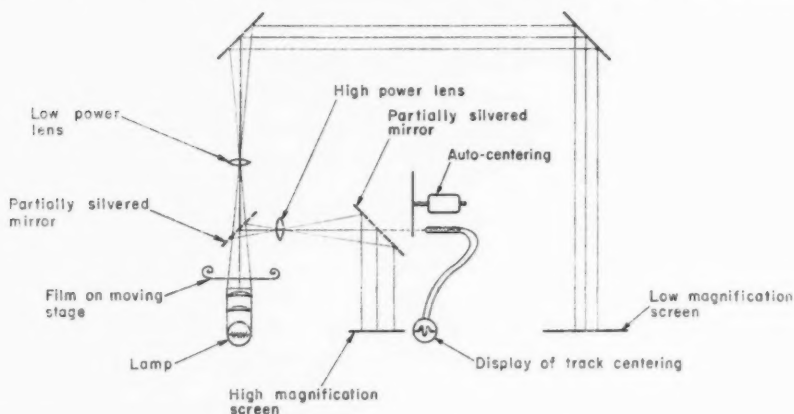


FIG. 18. Schematic drawing of "Frankenstein" measuring projector for film from the 72-in. hydrogen bubble chamber.

sentative set of points in space is computed from the co-ordinates measured in the stereo views. These points are fitted to trajectories for different assumed particles, taking into account optical and magnetic-field corrections and the rate of momentum loss of the particle in hydrogen. The final fit is a fourth-order polynomial in the horizontal projection and a third-order polynomial in the vertical. The program calculates dip, azimuth, and momentum for both ends of the track, plus uncertainties and correlation coefficients between all the output quantities. The Berkeley programs are described in several physics notes and are summarized in Rosenfeld's paper at the 1959 CERN conference (75).

For the kinematical stage, the most powerful and versatile program has been developed by Rosenfeld and his associates. It was summarized at the 1959 CERN Symposium, and is described in a series of articles by Rosenfeld, Solmitz, Snyder, Taft, and others (76). The equations of energy balance and momentum balance impose constraints on the interrelations between the momentum components of the observed tracks. The program calculates the constrained momentum components which approximate the measured values, and prints out the relative goodness of fit for the different possible

interpretations together with all fitted information specified by the physicist.

The time required for the complete computation in the IBM 704 is approximately one minute, representing a computing cost per event that is about equal to the total cost per pulse of operating the bubble chamber plus the bevatron. Interesting events occur as often as one per pulse, or as rarely as one per 10,000 pulses, depending on the experiment.

The output from the computing machine must be examined and tabulated, or remeasured if an error is evident. The task of bookkeeping is becoming increasingly large and will require complicated computer programs. Apparently the most sophisticated effort in this direction up to the present has been made by White, in connection with analysis of propane bubble chamber film at Berkeley (77). The steps in the analysis operation and the required times are summarized in Table V.

TABLE V
OPERATIONS IN DATA PROCESSING
(Berkeley hydrogen chambers)

	Equipment	Output	Comments	Approximate time/event
<i>Operation</i>				
Run experiment	Bubble chamber	Film	Typical reactions, e.g. $\pi^- + p \rightarrow \Lambda + K^0$ may occur once every	5 min.
Scan	Scan table	Handwritten scan form	Physicist or skilled assistant searches for interesting reactions	Typical 10 min.
Sketch	Scan table	Sketch card	Physicist designates event type, numbers tracks, and specifies which views to be measured	5 min.
Measure	Franckenstein	Track coordinates (15-in.: IBM cards)	(1) Technician advances film, sets in fixed data, measures fiducials, etc.	5 min.
		(72-in.: paper tape)	(2) Then he measures about 10 x-y-coordinates on two views of each track	5 min.
Card-to-tape or Tape-to-tape	IBM Card-to-tape or our own tape-to-tape			
<i>IBM Program</i>				
PANG (P and ANGLE)	IBM 704	Track \vec{p} , $\delta\vec{p}$, etc. (*Printouts + binary tape)	(1) Computes space-synthesis of points and makes zero-order fit (2) Makes one final fit for each mass assignment	$\frac{1}{2}$ sec./track $\frac{1}{2}$ sec./track
KICK K-interaction Coplanarization and Kinematics	IBM 704	X^2 -fitted data with errors (*binary tape)	(1) Computes kinematic fit of each vertex to assigned hypotheses (2) Combines successful vertex fits into multivertex events	3 sec. 3 sec. X number of vertex fits
EXAMIN (and print) KICK output	IBM 704	*Printouts	Prints, selects event with special criteria, makes histograms, keeps books	3 sec. to write a vertex fit
DRIVEL	IBM 704	*Magnetic tape	TOTAL 704 time for average event Merges and sorts KICK-format tape	$\frac{1}{2}$ min.

* All our data come out of the 704 on magnetic tape, except for lists of mistakes, printed by the on-line printer; binary tape if the output is to be used as input for later programs, plus additional BCD (Binary Coded Decimal) tape to feed to our off-line printer if desired.

VIII. SUPPLEMENTARY DATA FOR EXPERIMENTERS

This section presents a compilation of data to aid physicists in planning experiments. The data are not intended to be a basis for precise computation. The limits of their applicability are not discussed at length, and assumptions made in the development of equations are not detailed. The reader should refer to the cited literature for more information.

A. COMPARISON OF BUBBLE CHAMBER LIQUIDS

Table VI shows comparative characteristics of a number of bubble chamber liquids. Density and radiation length are taken from Table II. Values of dE/dx at minimum for H_2 and propane are taken from Barkas & Rosenfeld (78). The value for propane was changed by a factor of 44/41, to compensate for the different density used. Other values of dE/dx , and stopping power, were obtained from the high-energy particle data of Atkinson & Willis (79). Values for $SnCl_4$ and CF_3Br were assumed to be the linear sums of the values for the atomic constituents of the compounds. Scattering sagitta and required magnetic field are computed from the formulas in Section B, below. The number of events per day is based on present average running conditions of 30 tracks per expansion, and 6000 expansions per day.

The following conversions are useful for order-of-magnitude planning with the 72-in. hydrogen bubble chamber:

- A cross-section of 1 barn gives one event per ft. of track,
- A cross-section of 1 m barn gives one event per min. of running,
- A cross-section of 1μ barn gives one event per day of running.

B. MULTIPLE COULOMB SCATTERING FORMULAE

The accuracy with which momentum can be obtained by measuring track curvature in a magnetic field is limited by multiple Coulomb scattering of the charged particles. A convenient expression for the root mean square curvature due to multiple Coulomb scattering is

$$K_{sc} = \sqrt{\frac{2}{3}} \frac{21}{p\beta} \sqrt{\frac{1}{LX}} \text{ cm.}^{-1}$$

where p = momentum in Mev/c, β = velocity divided by velocity of light, L = length of track in cm. X = radiation length in cm.

The root mean square value of the sagitta, δ , due to multiple Coulomb scattering curvature is given by

$$\delta = \frac{2.14L^{3/2}}{p\beta X^{1/2}} \text{ cm.}$$

The curvature of a singly charged particle of momentum p in a magnetic field of H kilogauss is

$$K_H = 0.3H/p \text{ cm.}^{-1}$$

TABLE VI
COMPARISON OF VARIOUS BUBBLE CHAMBER LIQUIDS

Liquid	Density (gm./cm. ³)	Radiation length (cm.)	dE/dx at minimum (Mev/cm.)	Scattering sagitta for 2 Bev/c track 20 cm. long (microns)	Magnetic field required for 5% momentum uncertainty in 20 cm. rela- tivistic track (kgauss)	Stopping power of 50 cm. chamber (gm./cm. ²)	Events per day in 50 cm. chamber at σ per nu- cleon = 1μ Barn	Collision mean free path for $\sigma = 10$ mb/ nucleon	Collision mfp in hydrogen for $\sigma = 10$ mb/ nucleus
H ₂	0.059	1100	0.24	20	8	2.5	0.27	2800	2800
D ₂	0.13	950	0.22	22	8.5	2.6	0.28	1270	—
He	0.124	900	0.21	23	8.7	5.0	0.54	1330	—
Propane (C ₃ H ₈)	0.44	110	1.0	65	25	22	2.3	370	2040
SnCl ₄	1.5	8.6	2.2	230	90	75	8	110	—
CF ₃ Br	1.5	11	2.5	200	80	80	8	110	—
Xenon	2.18	3.7	2.8	350	135	110	11	76	—

hence the fractional uncertainty in momentum is

$$K_{\text{sc}}/K_{\text{H}} = \sqrt{\frac{2}{3}} \frac{21}{0.3\beta H} \sqrt{\frac{1}{LX}}$$

For the particular case of a hydrogen bubble chamber this reduces to

$$K_{\text{sc}}/K_{\text{H}} \doteq 1.2/(\beta H \sqrt{L}) \quad \text{for hydrogen.}$$

More accurate values of multiple Coulomb scattering are given by Barkas & Rosenfeld (78). Kim (80) has given a more complete treatment of the momentum accuracy obtainable under the combined influence of the magnetic field and multiple Coulomb scattering. Williams (29) discusses this point and also considers the uncertainty of angle measurements under the combined influence of multiple Coulomb scattering and measurement errors.

C. DELTA RAYS

The collision of an energetic particle with a stationary electron ejects the electron at an angle and energy dependent only on the center of mass velocity of the incident particle. Crawford (81) describes a method of obtaining the mass by measuring angle and energy of δ rays from an incident particle whose momentum is known. There is, of course, a lower limit to the length of δ ray for which satisfactory measurements can be made. Figure 19 shows the cross section and mean free path in liquid hydrogen for producing δ rays, 2.2 mm. long, 5 mm. long, and 10 mm. long, by particles of various incident momentum \div mass. The length of a δ ray can sometimes permit a mass determination without measurement of angles, since the maximum possible δ -ray energy is a function of both the momentum of the particle and its mass. Figure 20 shows the regions of momenta in which δ -ray measurements and gap counts are useful for distinguishing various particles in liquid hydrogen. Shaded regions at the bottom of each section show the momenta for which different methods are applicable. Curvature versus residual range on stopping tracks allows particles to be distinguished, in the crosshatched region. Bubble counting is most valuable in the solid black area. Delta rays furnish the best identification in the dotted region. Protons, for example, stop in a 20-in. chamber if their momentum is less than about 0.3 Bev/c. If we assume that gap counting is satisfactory for ionization of $0.9 I_{\text{min}}$, we conclude that gap counting is useful for proton momentum up to about 3 Bev/c. At higher momentum the ionization is too close to minimum. At the other end of the scale, the probability of having a δ ray long enough to measure is too small for proton momentum less than about 1 Bev/c. The appearance of a δ ray longer than 10 cm. on a 1.5-Bev/c track would immediately rule out the possibility that the particle is a proton.

D. RANGE-ENERGY AND RANGE-MOMENTUM RELATIONS

Figure 21 shows range as a function of energy for various particles in hydrogen bubble chambers (82) and in propane chambers (83). Figure 22

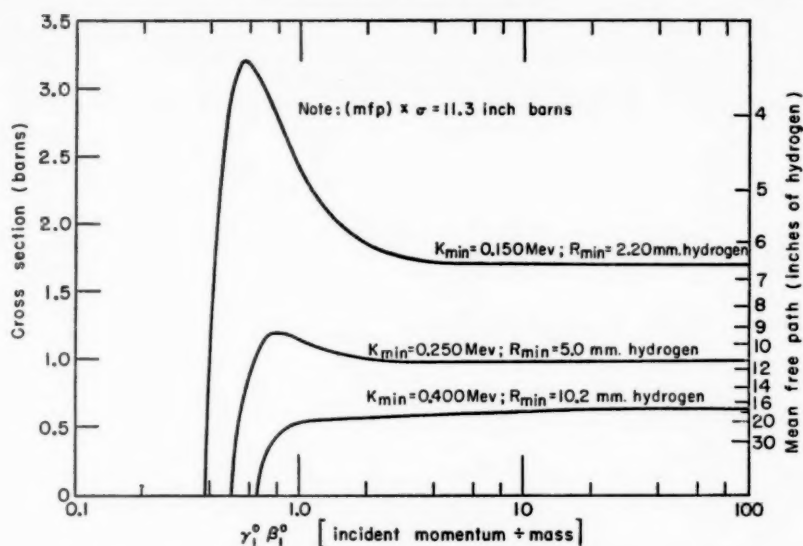


FIG. 19. Cross section and mean free path in liquid hydrogen chamber for producing δ rays of greater range than R_{\min} , vs. $\beta\gamma$ for three different values of minimum range.

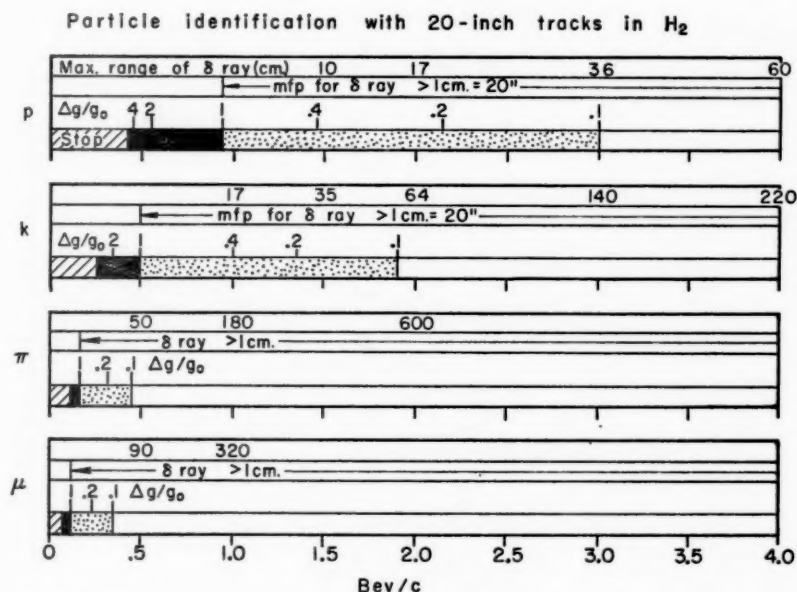


FIG. 20. Values of momentum for which particle identification can be made by δ rays, by gap counting, or by range.

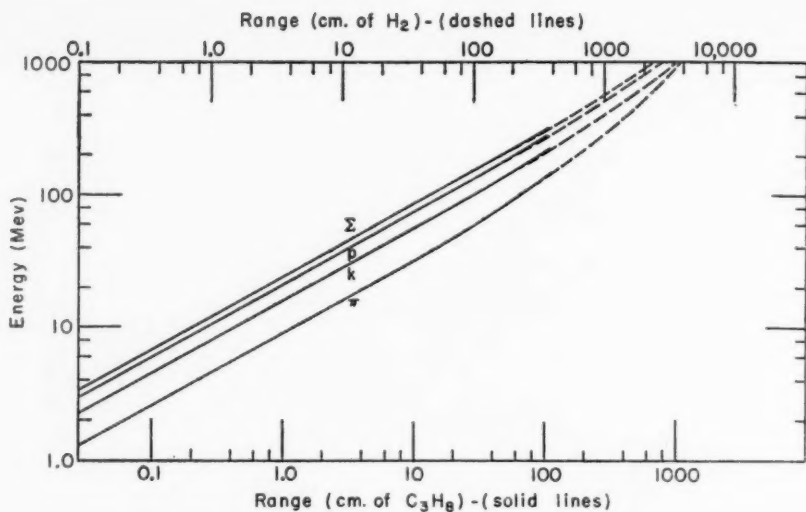


FIG. 21. Energy vs. range in hydrogen bubble chamber and in propane bubble chamber.

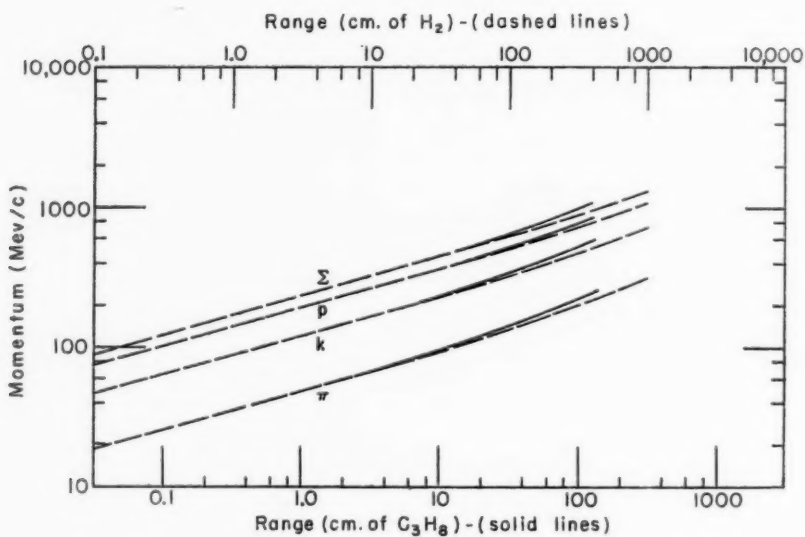


FIG. 22. Momentum vs. range in hydrogen bubble chamber and in propane bubble chamber.

gives range as a function of momentum for the same particles. The data for hydrogen and propane are plotted on the same graph, to make comparison easy. The curves are valid to the accuracy that can be read from these graphs, but the literature references should be consulted for more precise data.

E. EFFORT REQUIRED IN AN EXPERIMENT

The following information was compiled at the end of the recent anti-proton run at the Bevatron with the 72-in. hydrogen bubble chamber (84).

The experiment ran for a period of 17 weeks in July–October 1959. The manpower used, exclusive of Bevatron operation and maintenance, averaged over the whole period of the run, amounted to 4 man-years of physicists plus 20 man-years of technicians and scientific assistants. This is equivalent to 13 full-time physicists and 60 full-time support people during the 17 weeks of the run.

Five physicists worked on the experiment during the whole run, and about eight others worked on it for some period of the run. There should probably be about twice as many physicists on an experiment of this complexity.

During this time, 255 rolls of film were exposed, each containing about 600 stereo triads. The chamber was operated 24 hr. a day, at a repetition rate of about 3 per min. Under these conditions the Bevatron is capable of about 10^5 pulses per week; the chamber was able to accept about 3×10^4 pulses per week. About 10^4 pictures per week were taken. This one third efficiency is a measure of the difficulty of keeping such complicated equipment running, since the Bevatron beam spectrometers and bubble chamber ran "pretty well."

Physics with large bubble chambers has indeed become a big effort. It can be expected to become bigger as scientists develop ways to handle a larger proportion of the interesting events that exist in bubble chamber pictures. However, there is not yet any other tool combining the important characteristics of hydrogen bubble chambers for high-energy nuclear physics investigations. The trends with other existing types of detectors, such as counters, are toward large counter arrays and digital-computer data processing that do not equal the 72-in. hydrogen chamber operation costs, but may become comparable in cost and complexity to other bubble chamber operations.

LITERATURE CITED

1. Fretter, W. B., *Ann. Rev. Nuclear Sci.*, **5**, 145-78 (1955)
2. Ogden, B. K., *CERN Bibl.* **2** (1958)
3. Amiot, P., and Ogden, B. K., *CERN Bibl.* **3** (1959)
4. Glaser, D. A., *Phys. Rev.*, **87**, 665 (1952)
5. Glaser, D. A., *Phys. Rev.*, **91**, 762-63 (1953)
6. Glaser, D. A., and Rahm, D. C., *Phys. Rev.*, **97**, 474-79 (1955)
7. Wood, J. G., *Phys. Rev.*, **94**, 731 (1954)
8. Glaser, D. A., *Handbuch der Physik*, **45**, 314-41 (Springer-Verlag, Berlin, Germany, 1958)
9. Bradner, H., and Glaser, D. A., *Proc. Intern. Conf. Peaceful Uses Atomic Energy*, 2nd, Geneva, 1958, **14**, 412-22 (1958)
10. Glaser, D. A., *Nuovo cimento*, **11**, Suppl. 2, 361-68 (1954)
11. Seitz, F., *Phys. Fluids* **1**, 2-13 (1958)
12. Glaser, D. A., Rahm, D. C., and Dodd, C., *Phys. Rev.*, **102**, 1653-58 (1956)
13. Willis, W. J., Fowler, E. C., and Rahm, D. C., *Phys. Rev.*, **108**, 1046-47 (1957)
14. Blinov, G. A., Krestnikov, Iu. S., and Lomanov, M. F., *Zhur. Ekspil. i. Teoret. Fiz.*, **31**, 762-70 (1956) (Russian); *Soviet Phys. JETP*, **4**, 661-70 (1957) (Engl.)
15. Bassi, P., Loria, A., Meyer, J. A., Mittner, P., and Scotoni, I., *CERN Symposium High-Energy Accelerators and Pion Phys.*, Geneva, 1956, *Proc.*, **2**, 28 (1956)
16. Birss, I. R., *Nature*, **184**, Suppl. 19, 1474 (Nov. 7, 1959)
17. Plessett, M. S., and Zwick, S. A., *J. Appl. Phys.*, **25**, 493-500 (1954)
18. Birkhoff, G., Margulies, R. S., and Horning, W. A., *Phys. Fluids*, **1**, 201-4 (1958)
19. Bassi, P., Loria, A., Meyer, J. A., Mittner, P., and Scotoni, I., *Nuovo cimento*, **4**, 491-500 (1956)
20. Bugg, D. V., *Progr. in Nuclear Phys.*, **7**, 1-52 (1959)
21. Rossi, B., *High Energy Particles*, 220 (Prentice-Hall Inc., New York, N. Y., 1952)
- 22a. Hildebrand, R. H., and Nagel, D. E., *Phys. Rev.*, **92**, 517-18 (1953)
- 22b. Alvarez, L. W., *Proc. Ann. Rochester Conf. High-Energy Nuclear Phys.*, 5th, Chap. VII, 181-82 (1955)
- 22c. Alvarez, L. W., *Proc. Intern. Conf. Peaceful Uses of Atomic Energy*, 2nd, Geneva, 1958, **30**, 164-65 (1958)
- 22d. Eisler, F., Plano, R., Prodell, A., Samios, N. P., Schwartz, M., Steinberger, J., Bassi, P., Borelli, V., Puppi, G., Tanaka, H., Waloschek, P., Zobeli, V., Conversi, M., Franzini, P., Manelli, I., Santangelo, R., and Silvestrini, V., *Nuovo cimento*, **10**, 468-89 (1958)
- 22e. Gow, J. D., *Proc. Intern. Conf. Peaceful Uses of Atomic Energy*, 2nd, Geneva, 1958, **30**, 166-73 (1958)
- 22f. *Intern. Conf. High-Energy Accelerators and Instrumentation* (CERN, 1959), 435-60
23. Block, M. M., Fairbank, W. M., Harth, E. M., Kikuchi, T., Meltzer, C., and Leitner, J., *Intern. Conf. High-Energy Accelerators and Instrumentation* (CERN, 1959), 461-65; *CERN Bibl.* **2**, Refs. 130-35 (1958)
24. Block, M., Lagarrigue, A., Musset, P., Rancon, P., Rousset, A., Sauteron, X., and Six, J., *Intern. Conf. High-Energy Accelerators and Instrumentation* (CERN, 1959), 499-502; (*CERN Bibl.* **2**, Refs. 146-63 (1958))
25. Kamarek, T. I., Maltsev, E. I., Nagy, T., Nagy, J., Prokes, A., Stashkov, G. M., Ustenko, E. P., Chuvilo, I. V., and Skhobin, U. N., *Intern. Conf. High-Energy Accelerators and Instrumentation* (CERN, 1959), 506-8
26. Brown, J. L., Bryant, H. C., Burnstein, R. A., Hartung, R. W., Glaser, D. A., Kadyk, J. A., Sinclair, D., Trilling, G. H., Vande Velde, J. C., and van Putten, J. D., *Phys. Rev. Letters*, **3**, 51 (1959)
27. Alyea, E. D., Gallagher, L. R., Mullins, J. H., and Teem, J. M., *Nuovo cimento*, **6**, 1480-88 (1957)
28. Bugg, D. V., *Rev. Sci. Instr.*, **29**, 587-89 (1958)
29. Williams, R. W., *Can. J. Phys.*, **37**, 1085-99 (1959)
30. Hildebrand, R. H. (Univ. of Chicago, Enrico Fermi Inst., private communication)
31. *CERN Bibl.* **2**, Refs. 115-29 (1958)
32. Bertanza, L., Martelli, G., and Zacutti, A., *Nuovo cimento*, **2**, 487-94 (1955).
33. Hahn, B., Riepe, G., and Knudsen, A. W., *Rev. Sci. Instr.*, **30**, 654-55 (1959)
34. Kalmus, G. E., *Meeting Heavy Liquid Bubble Chambers*, CERN 59-24, 33-39 (CERN, Geneva, Switzerland, July 1959)

- 35a. Hahn, B., *Meeting Heavy Liquid Bubble Chambers*, CERN 59-24, 39-55 (CERN, Geneva, Switzerland, July 1959)
- 35b. Slätis, H., *Nuclear Instruments and Methods*, 5, 1-25 (1959)
36. Alichanyan, A. I., Veremeev, M. M., Galper, A. M., Kirillov-Ugrumov, W. G., Kotenko, L. P., Kusun, L. A., Kuznetsov, E. P., and Popov, U.S., *Intern. Conf. High-Energy Accelerators and Instrumentation* (CERN, 1959), 512-14
37. Resegott, L., *Meeting Heavy Liquid Bubble Chambers*, CERN 59-24, 31-32 (CERN, Geneva, Switzerland, July 1959)
38. Pless, I. (Mass. Inst. Tech., private communication)
39. Henderson, C., *Meeting Heavy Liquid Bubble Chambers*, CERN 59-24, 26-30 (Geneva, Switzerland, July 1959)
40. Rousset, A., *Meeting Heavy Liquid Bubble Chambers*, CERN 59-24, 17-24 (Geneva, Switzerland, July 1959) and *Intern. Conf. High-Energy Accelerators and Instrumentation* (CERN, 1959), 499-503
41. Plano, R. (Columbia Univ., New York, private communication)
42. Powell, W. M., *Rev. Sci. Instr.*, 29, 874-79 (1958); and private communication.
43. Barford, N. C., *Progr. in Cryogenics*, 2 (1960)
44. Rahm, D. C., *Intern. Conf. High-Energy Accelerators and Instrumentation* (CERN, 1959) 440-41.
45. Gow, J. D., and Rosenfeld, A. H., *Intern. Conf. High-Energy Accelerators and Instrumentation* (CERN, 1959), 435-39
46. Franck, J. V., *Univ. Calif. Radiation Lab. Rept.*, UCID-71 (March 1956)
47. Riddiford, L., Van de Raay, H. B., Barford, N. C., Butler, C. C., McMullan, D., Thetford, A., Thomas, D. B., Welford, W. T., Amery, A., Evans, W. H., Moore, M. J., Polak, P., Skinner, H. W. B., Williams, P. R., Shaw, D., Ashburn, A. G., and Snowden, M., *Intern. Conf. High-Energy Accelerators and Instrumentation* (CERN, 1959), 445-53.
48. Peyrou, C., *Intern. Conf. High-Energy Accelerators and Instrumentation* (CERN, 1959), 454-59
49. Belonogov, A. V., Zeldovich, A. G., Kolganov, V. Z., Landsberg, L. G., Lebedev, A. V., Nikitin, S. Ia., Smoliankin, V. I., and Sokolev, A. P., *Pribory i Tekh. Ekspt.*, 1, 38-41 (1958); or *Atomic Energy Commission Transl.*, 3664
50. Nikitin, S. Ia. (U.S.S.R., private communication)
51. Eaton, W., and Hernandez, H. P., *Univ. California Radiation Lab. Rept.*, UCRL-8134 (Oct. 1955)
52. Kropschot, R. H., and Mikesell, R. P., *Natl. Bur. Standards Rept.*, 3590 (June 22, 1956)
53. Amiot, P., Nullens, G., and Spondlin, R., CERN 59-20 (CERN, Geneva, Switzerland, 1959)
54. Peyrou, C. (CERN, private communication)
55. Ross, R., *Univ. Calif. Radiation Lab. Rept.*, UCID-146 (May 1958)
56. Davies, G. E., *J. Opt. Soc. Am.*, 45, 572 (1955)
57. Nagel, D. E., Hildebrand, R. H., and Plano, R. J., *Rev. Sci. Instr.*, 27, 203-7 (1956)
58. Bradner, H. (Lawrence Radiation Lab., Berkeley, unpublished work)
59. Alvarez, L. W., *Univ. Calif. Lawrence Radiation Lab. Rept.*, UCID-977 (April 1960)
60. Rosenfeld, A. H., and Solmitz, F. T., *Univ. Calif. Radiation Lab. Rept.*, UCID-186 (May 1958)
61. Schwemin, A. J., (Lawrence Radiation Lab., Berkeley, private communication)
62. Wilson, J. G., *Principles of Cloud Chamber Techniques* (Cambridge Univ. Press, London, Engl., 1951)
63. Good, M. L., *Univ. Calif. Radiation Lab. Rept.*, UCID-29 (April 1955)
- 64a. Bradner, H. (Lawrence Radiation Lab., Berkeley, unpublished work)
- 64b. Rasetti, F. (Johns Hopkins University, Baltimore, unpublished work)
65. Welford, W. T. (Imperial College, London, unpublished work)
66. Kuznetsov, E. V., Lomanov, M. F., Blinov, G. A., Chuan Chen-Niang, and Khwan Shen-Nian, *Zhur. Eksptl. i Teoret. Fiz.*, 31, 911 (1956) (Russian); and *Soviet Phys.-JETP*, 4, 773-74 (1957) (Engl.)
67. Donaldson, R., and Watt, R., *Univ. Calif. Radiation Lab. Rept.*, UCID-117 (Feb. 1956)
68. CERN Symposium High-Energy Accelerators and Pion Phys., Geneva, 1956, *Proc.*, 2 (1956)
69. *Intern. Meeting Instruments for Evalu-*

- ation of Photographs, CERN 58-24 (1958)
70. *Intern. Conf. High-Energy Accelerators and Instrumentation (CERN, 1959)*
 71. Bradner, H., and Solmitz, F., *Intern. Conf. Peaceful Uses Atomic Energy, 2nd, Geneva, 1958*, 14, 423-26 (1958)
 72. Bradner, H., *Univ. California Lawrence Radiation Lab. Rept., UCRL- 9104* (Jan. 1960)
 73. Goldschmidt-Clermont, Y., *Intern. Conf. High-Energy Accelerators and Instrumentation (CERN, 1959)*, 523-32
 74. Franck, J. F., et al., *Rev. Sci. Instr.* (To be published)
 75. Rosenfeld, A. H., *Intern. Conf. High-Energy Accelerators and Instrumentation (CERN, 1959)*, 533-41
 76. Rosenfeld, A. H., and others, to be submitted to *Rev. Sci. Instr.*
 77. White, H., *Univ. California Lawrence Radiation Lab. Rept.* (To be published)
 78. Barkas, W. H., and Rosenfeld, A. H., *Univ. Calif. Radiation Lab. Rept., UCRL-8030* (March 1958)
 79. Atkinson, J. H., and Willis, B. H., *Univ. Calif. Radiation Lab. Rept., UCRL-2426*, revised II (June 1957)
 80. Kim, Y. B., *Rev. Sci. Instr.*, 29, 680-88 (1958)
 81. Crawford, F. S., *Univ. Calif. Radiation Lab. Rept., UCID-241* (Nov. 1957)
 82. Rosenfeld, A. H., *Univ. Calif. Radiation Lab. Eng. Note, 4310-03-M6* (Feb. 1956)
 83. Birge, R. W., *Univ. Calif. Lawrence Radiation Lab. Rept., UCID-1052* (Sept. 1959)
 84. Alston, M., and Blumberg, R., *Univ. Calif. Lawrence Radiation Lab. Rept., UCID-1054* (Nov. 1959)

OPTICS OF HIGH-ENERGY BEAMS^{1,2}

BY OWEN CHAMBERLAIN

Physics Department University of California, Berkeley, California

INTRODUCTION

Many of the experiments now being conducted on high-energy accelerators require the use of beams of charged secondary particles. It is worth while at this time to attempt to summarize information about some of the most useful methods of setting up such beams.

We are not concerned here with the primary beam of the accelerator. Rather, we assume that a target is struck by the primary beam and that it is desired to form a beam from the secondary charged particles that emerge from collisions within the target.

The simplest system of forming this beam of secondary particles involves the use of magnetic fields only. In most cases it is desirable to obtain a beam of particles of known magnetic rigidity, or momentum. The bulk of this article is addressed to this problem. Some comments are also made about the use of electric fields in conjunction with magnetic fields. The inclusion of electric fields allows the separation of a beam of known momentum into its various components according to the velocities of the particles, hence according to the masses of the particles. These are referred to as "separated beams."

The curvature K of a charged particle moving in a magnetic field is given by

$$K = (eB)/(pc)$$

where e is the charge in electrostatic units, B is the magnetic induction in gauss, p is the momentum in cgs units, and c is the velocity of light in cm./sec. The curvature K is given in cm.⁻¹, and is the reciprocal of the radius of curvature. In the above expression, it has been assumed that the particle moves in a direction perpendicular to the direction of the field B . If the velocity and field are not perpendicular, the curvature vector may be given as

$$K = (d\hat{p}/ds)/p = (e\mathbf{v} \times \mathbf{B})/(pvc)$$

where v is the particle velocity in cm./sec. and ds is an increment of distance along the trajectory of the particle. The curvature is perpendicular to the field B (and by definition perpendicular to the velocity v). The magnitude of the curvature clearly depends upon the component of B perpendicular to v .

In most cases the momentum of beam particles is given in the unit Mev/c. (Momentum in Mev/c is numerically equal to pc in Mev.) If we restrict our attention to particles of single charge (4.8×10^{-10} esu) and meas-

¹ The survey of literature pertaining to this chapter was concluded in May 1960.

² Among the abbreviations used in this review is: r.f. (radio frequency).

ure the momentum in Mev/c, then our expression for the curvature in a magnetic field reduces to

$$K = 3.00 \times 10^{-4} B/\rho, \quad B\rho = [\rho(\text{in Mev/c})]/[3.00 \times 10^{-4}]$$

ρ being the radius of curvature in field B . This form is the most convenient for our discussion. It resembles closely the well-known form

$$B\rho = p(\text{in ev/c})/300$$

Nearly all the arrangements in use for forming beams of secondary particles have B field patterns with a plane of symmetry. We therefore restrict our attention to systems with such symmetry, and for convenience in explanation we speak as though this plane is always a horizontal plane. With respect to this plane of symmetry, which we call the "central plane," the system should have the following characteristics.

- (a) The magnetic field in the central plane is perpendicular to the central plane.
- (b) Every north magnetic pole above the central plane is accompanied by a south pole of equal magnitude at the mirror point below the central plane.
- (c) To every current element above the plane there is a corresponding current element of equal magnitude whose position and direction are obtained by mirror reflection in the central plane.
- (d) A drawing of the magnetic field lines will exhibit reflection symmetry with respect to the central plane; however, the direction of the magnetic field below the plane is opposite to that given by simple reflection.

This symmetry should be obvious in all the systems to be discussed. Of course, we want to make occasional use of further symmetry properties in special cases.

Because of the reflection symmetry assumed, the field in the central plane is perpendicular to the central plane. We choose this upward direction as the z direction, so that we have B_z as the only field component in the central plane. In principle the field is everywhere known once B_z is known throughout the central plane because the conditions

$$\nabla \times \mathbf{B} = 0$$

and

$$\nabla \cdot \mathbf{B} = 0$$

allow all derivatives of the field components with respect to z to be computed in terms of derivatives of B_z in the central plane. In practice this usually means the field is completely known only fairly close to the central plane, since it is not feasible to obtain such accurate data in the central plane that high-order derivatives can be evaluated with good accuracy.

BASIC COMPONENTS OF PURELY MAGNETIC SYSTEMS

For experiments conducted in connection with magnetic accelerators such as cyclotrons and synchrotrons, the first magnetic component is frequently the field of the accelerator itself. The magnetic field of the accelera-

tor is usually available in the form of a plan view showing contours of equal B_z in the central plane.

For most applications it is essential to perform a momentum analysis in the process of forming a charged-particle beam. This is frequently accomplished by the use of deflecting magnets such as that shown in Figure 1. This magnet has been designed to approximate a uniform field within a rectangular region in the central plane. However, other field distributions are frequently used and can be made by using tapered pole pieces.

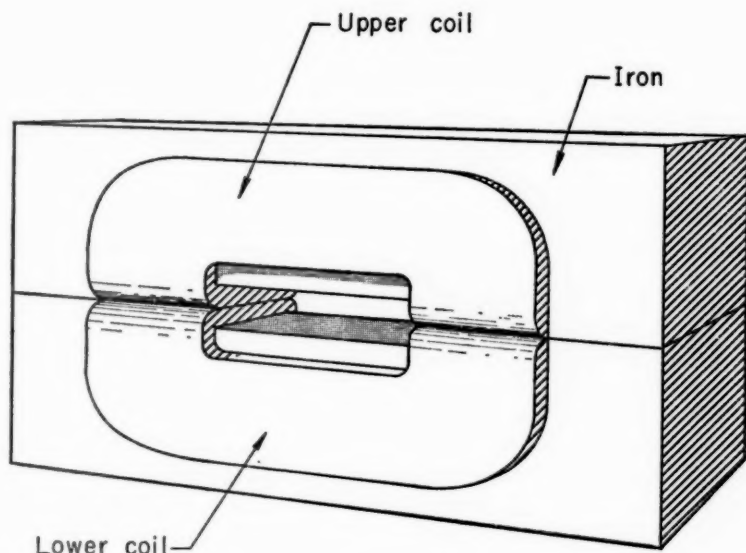


FIG. 1. General-purpose deflecting magnet. This arrangement, with so-called "window-frame" construction, has proved very useful because it gives a very uniform field even close to the coils and may be used at high magnetic flux densities.

For the formation of the most useful beams some focusing properties are essential. Most deflecting magnets have some focusing action, but it is usually too weak to accomplish the desired effect. An important and valuable component is a magnetic lens made of quadrupole magnets. The field pattern of a quadrupole magnet is shown in Figure 2. Quadrupole magnets were introduced in 1952 by Courant, Livingston & Snyder (1) along with the strong-focusing synchrotron. A single quadrupole magnet has a focusing action for motion in one plane (either horizontal or vertical) and a defocusing action in the other plane. However, two or more quadrupole magnets may be used to give a net focusing action in both planes and, in fact, to produce a magnetic lens that closely approximates a simple thin lens of the type used in optics for visible light. Notice that quadrupole magnets, if oriented

in the way shown in Figure 2, have the desired symmetry property with respect to a central (horizontal) plane.

DETERMINATION OF A TRAJECTORY IN THE CENTRAL PLANE

In designing a magnet system, one of the first steps is to determine one trajectory through the system, which may involve the magnetic field of an accelerator. We may call this trajectory the central ray or central orbit. On

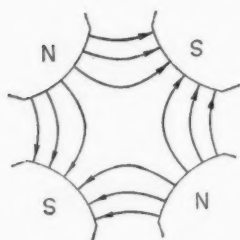


FIG. 2. Field pattern of a quadrupole magnet.

the basis of a contour map of B_z in the central plane, it is a simple matter to construct trajectories (orbits) in the central plane for particles of given momentum. One usually starts from a specified point, which may be the location of a target, and computes an orbit for a particle that leaves the target in some specified direction. Alternatively, one may trace the orbit in reverse, computing back from a known point toward which the desired particles are aimed; for example, one may compute backward from an existing collimator to determine where a target should be placed.

A trajectory may be determined by numerical integration, perhaps with the help of an electronic computer, with the use of a mechanical orbit plotter such as that described by Rankin (2), or by a graphical method. An example of the graphical tracing of a trajectory is shown in Figure 3, for a hypothetical case. The orbit is approximated piecewise by circular arcs. In the figure the first arc extends from the target center on the contour of 12,000 gauss to the contour of 8000 gauss, being drawn with the radius of curvature appropriate to 10,000 gauss. Through the end-point of the first arc and through the center C_1 of the first arc, the radius line can be extended to the new center C_2 , whose position is such as to give a new radius appropriate to the average field over the next circular arc, in this example 6000 gauss. The second arc can then be drawn about C_2 as center and extending to the 4000 gauss contour. The third arc is drawn similarly, extending to the 2000 gauss contour. Finally, a straight line (at right angles to the line through the end of the last arc and C_3) is used to carry the orbit into the weak-field region with a deflection at point D to take account of the total field beyond the 2000 gauss contour. The angle of deflection (in radians) at D is $\theta_D = (\int B ds) / (B \rho)$. The position of the point D may be fixed as $\bar{s} = (\int B s ds) / (\int B ds)$. The integrals are carried along the approximate orbit from the end of the last arc. It should be emphasized that the example shown in Figure 3 is done in exceptionally coarse steps to make the diagram clear. In practice, it appears that each arc should cover only about a 20-per cent range of field values if the final orbit is to correspond to the proper momentum to within about 1 per cent. (If the field plot is not drawn to actual size, the radii of curvature must obviously be scaled to correspond to the scale of the drawing.)

Clearly, other magnets, such as deflecting magnets, may be treated in the same way to obtain orbits. However, if the deflecting magnets are con-

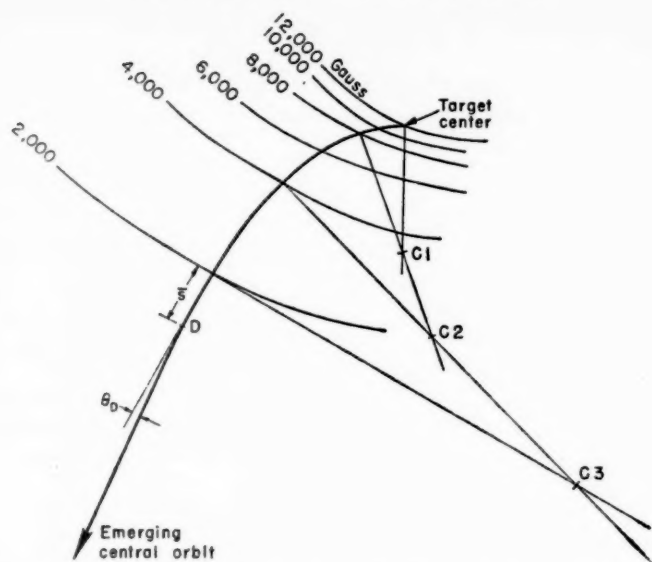


FIG. 3. Example of the graphical tracing of the orbit of a charged particle in the central plane. The orbit is approximated by a succession of circular arcs. This example is carried out in unusually coarse steps. See text for details.

structed like that shown in Figure 1, the field contours are very nearly straight lines and it is usually satisfactory to make the simplifying assumption that the region of field is rectangular, being full field within that rectangle and zero outside. The length of the rectangle is the so-called effective length of the field defined by

$$L_{\text{eff}} = \left(\int B ds \right) / B_{\text{max}}$$

Here B_{max} is the maximum field and the integral is to be taken over a straight line through the magnet aperture perpendicular to the entrance edge of the pole face. The effective length usually exceeds the physical length of the iron pole face by about one gap width (being one-half gap width at each end). The advantage of the proposed simplification is that it allows the trajectory within the deflecting magnet to be constructed as one circular arc.

A quadrupole magnet has zero field along its center line so that the central orbit is usually, in the vicinity of the quadrupole, a straight line coincident with the quadrupole axis. The focusing properties are discussed in another section.

FOCUSING PROPERTIES OF MAGNETIC FIELDS

It is usually quite important to know the focusing properties of a magnetic field and to adjust the focusing properties to achieve the desired result.

We consider separately the focusing in the horizontal plane and in the vertical plane.

In the horizontal plane, we may first study two orbits that leave the target center in slightly different directions, perhaps tracing the two rays by the graphical method mentioned in connection with Figure 3. An example is shown in Figure 4 of a target within the magnetic field of an accelerator

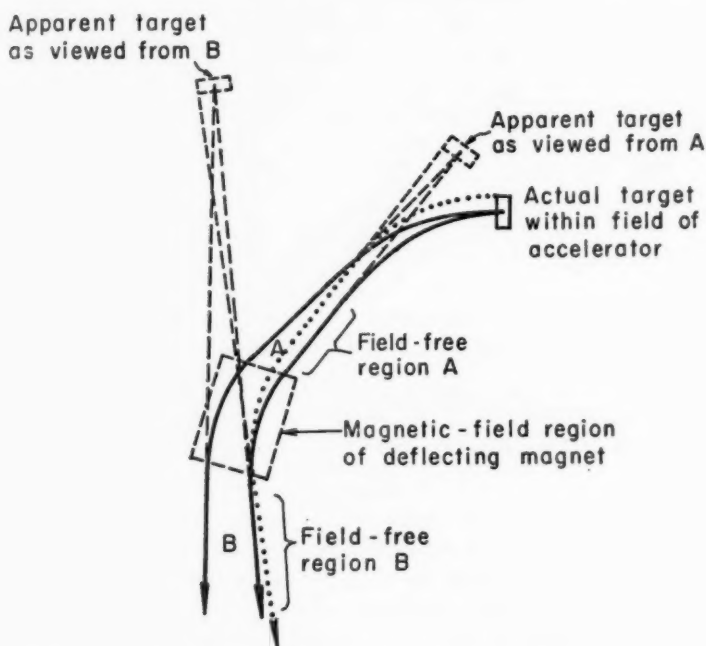


FIG. 4. Diagram of orbits illustrating the determination of position and horizontal size of the apparent target. Solid lines are used to represent orbits originating at the target center. The dotted line shows an orbit from the edge of the target. Dashed lines show extrapolation back to the apparent target. In some cases the apparent target may be quite different in size from the actual target.

and with one deflection magnet in the system. It is usually assumed that the system is linear enough for two adjacent orbits that interpolation may be used to determine positions and directions of intermediate orbits. Figure 4 shows the apparent target positions, as viewed from certain points along the beam for particles of the particular momentum for which the orbits have been calculated. The figure shows as dashed lines the straight lines extended backwards to their intersection to determine the apparent target positions.

It is also valuable to know the apparent magnification of the target as viewed through the system. This may be accomplished by tracing an orbit that starts at one edge, rather than the center, of the target. One such orbit

is shown as a series of dots in Figure 4. Again dashed lines are used to show straight lines extended backward to determine the size of the apparent target. Usually an unrealistically large target must be assumed so that graphical errors may be minimized.

There is an alternative method for finding the behavior of orbits close to the central orbit. Once a central orbit has been determined graphically, a simple differential equation may be solved numerically to find the focusing properties. The theory given here is a linear theory, adequate providing the orbits under consideration do not deviate too much from the central orbit.

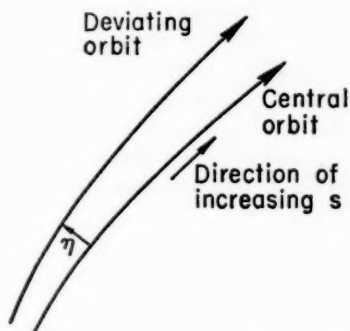


FIG. 5. Diagram illustrating the parameter η , the lateral displacement of an orbit from the central orbit. Here η is positive as drawn if the z axis is directed up out of the plane of the figure.

Figure 5 illustrates the terminology used here. The deviation (in the central plane) of some orbit from the central orbit is called η and is measured perpendicular to the central orbit. Figure 5 is drawn for a positively charged particle moving in a field directed out of the plane of the figure with η taking a positive value. The differential equation for η as a function of s , the distance along the central orbit, is

$$\frac{d^2\eta}{ds^2} = - \left[\frac{1}{B\rho} \frac{dB_z}{d\eta} + \frac{B_z^2}{(B\rho)^2} \right] \eta$$

Here, B_z is the magnetic flux density along the central orbit, and $dB_z/d\eta$ is the space rate of change of B_z along a line perpendicular to the orbit (and in the direction of positive η as indicated in Fig. 5) evaluated at the central orbit.

The differential equation can be used to determine the same properties for which we have used the construction shown in Figure 4, once a suitable central orbit has been determined. To determine the apparent source positions we would use starting values at the target of perhaps $\eta=0$, $d\eta/ds \neq 0$. Then, to determine the apparent source sizes we would use as initial values $\eta \neq 0$, $d\eta/ds=0$. In each case the differential equation would be integrated numerically along the trajectory from the target point. The results would be

interpreted as suggested by Figure 4 to determine the (horizontal-plane) apparent target position and size.

The same theory may also be constructed for a deviating orbit of a particle that differs slightly in momentum from the momentum corresponding to the central orbit. There is then an additional term.

$$\frac{d^2\eta}{ds^2} = - \left[\frac{1}{B\rho} \frac{dB_z}{d\eta} + \frac{B_z^2}{(B\rho)^2} \right] \eta + \frac{B_z}{B\rho} \frac{\delta p}{p}$$

Here $\delta p/p$ is the fractional change in momentum with respect to the central momentum. The equation is, in the author's experience, ascribable to Fermi (3). Here B_z is to be taken as positive if the field is directed out of the plane of the figure. The quantity $B\rho$ is to be given a positive sign for a positively charged particle and a negative sign for a negative particle.

The focusing properties for orbits that deviate vertically from the central orbit can also be handled in a similar way. Because of the zero divergence and zero curl of the flux density B the vertical focusing may be related to the same normal derivative $dB_z/d\eta$ that has been used for the horizontal focusing. The differential equation is

$$\frac{d^2\zeta}{ds^2} = \frac{1}{B\rho} \frac{dB_z}{d\eta} \zeta$$

Here ζ is the vertical displacement of the deviating orbit as measured from the central plane or from the central orbit. Again, the expression is linear in the displacement. The sign conventions are the same as those given above. This differential equation can be used for all cases for which the central orbit lies in the central plane.

For deflecting magnets with uniform field B_0 (or that can be approximated by a region of uniform field), some simple expressions are useful. Vertical focusing occurs only where the central orbit enters or leaves the magnetic field region, and then only when the orbit is other than normal to the boundary line of the field region. The vertical focusing acts like a thin lens at the entrance point and another thin lens at the exit point, the focal length F_v being in either case given by

$$1/F_v = (1/\rho) \tan \theta \quad (\text{entrance or exit of deflecting magnet with uniform field})$$

where ρ is the radius of curvature in the field, or $(B\rho)/B_0$, and θ is the angle between the central orbit and the normal to the boundary line of the field region. Figure 6 shows θ_1 at entrance and θ_2 at exit, for positive θ_1 and θ_2 . For the horizontal focusing it is convenient to measure the object distance p'_H from the entrance boundary and the image distance q'_H from the exit boundary. The expression relating object and image distances is

$$\arctan [(\rho/p'_H) + \tan \theta_1] + \arctan [(\rho/q'_H) + \tan \theta_2] = \alpha$$

for horizontal focusing, uniform field, where α is the bending angle of the central orbit in the magnet. Notice p'_H and q'_H are measured from entrance and exit points of the effective region of uniform field. Extensive discussions

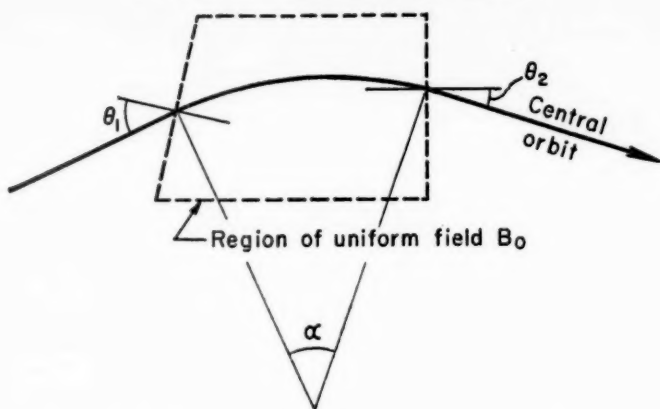


FIG. 6. Definition of the angles θ_1 , θ_2 , and α used in the text. The angles are considered positive as drawn.

of magnets with uniform field have been given by Cross (4), by Bainbridge (5), and by Buechner (6). Judd (7), and Sternheimer (8) have analyzed instruments involving non-uniform fields.

The methods discussed above should be adequate for almost all magnetic components except quadrupole magnets (or strong-focusing magnets). A typical quadrupole magnet is shown in end view in Figure 7. Figure 8 shows side and top views in cross section, with typical deviating orbits. The central orbit is assumed to lie on the center line. Notice that a single quadrupole is focusing for deviations in one plane and defocusing for deviations in the other plane.

The field within the poles of the quadrupole is intended to conform to the following expressions. We take the x axis to be along the orbit in the forward direction, the z axis to be vertically upward out of the central (horizontal) plane, and the y axis to be fixed to make a right-handed co-ordinate system.

$$B_x = \alpha y$$

$$B_y = \alpha z$$

The simplest treatment of quadrupole focusing involves assuming that the magnetic flux density is given by these expressions throughout the length of the pole pieces and a short distance beyond at each end. The full length over which the field is assumed to be of the given form is then called the effective length l . To fair approximation the effective length is given by

$$l = l_p + a$$

where l_p is the length of the iron poles and a is the aperture radius shown in Figure 7. The field is then assumed to be zero beyond the region of the effective length. Unfortunately this field, as given, does not satisfy Maxwell's equations because the curl of the field does not vanish near the ends of the

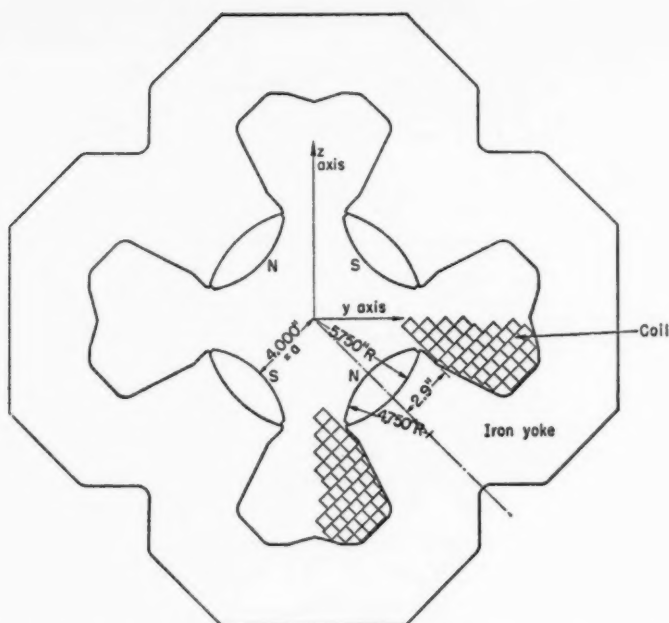


FIG. 7. Quadrupole magnet, showing the cross section, to scale, of one of the most satisfactory quadrupole varieties. Important dimensions are indicated.

quadrupole. Nevertheless, very useful calculations of orbits can be made with this assumed field, neglecting the effects of the fringing field that must inevitably be present.

Within the quadrupole field, the curvature of the orbit that deviates in the y direction from the central orbit along the center line is

$$-\frac{\frac{d^2y}{dx^2}}{\left(1 + \left(\frac{dy}{dx}\right)^2\right)^{3/2}} = \frac{B_z}{B\rho} = \frac{\alpha y}{B\rho}$$

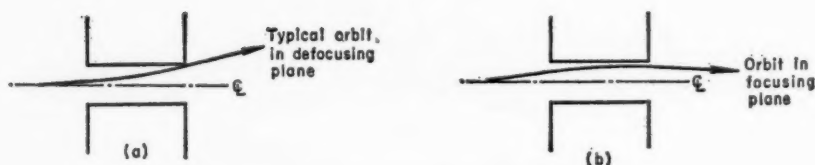


FIG. 8. Side and top views of quadrupole aperture showing a typical orbit that is off the axis.

By assuming $dy/dx \ll 1$ we may justify neglect of the second-order correction in dy/dx and use

$$\frac{d^2y}{dx^2} = -\frac{\alpha}{B\rho}y = -k^2y \quad (\text{focusing plane})$$

where we have defined $k^2 \equiv \alpha/B\rho$. This set of approximations (and its consequences) is termed the "linear" theory. The resulting linear equation may be solved to give the focal length

$$f = 1/[k \sin(kl)]$$

The principal plane, from which the image distance is to be measured, is located inside the effective quadrupole a distance

$$x_p = [1 - \cos(kl)]/[k \sin(kl)] \cong \frac{l}{2} [1 + (kl)^2/12] \cong l/2;$$

The last approximation is somewhat more crude than necessary.

In the defocusing plane the corresponding expressions are

$$\frac{d^2z}{dx^2} = \frac{\alpha}{B\rho}z = k^2z \quad (\text{defocusing plane})$$

where $k^2 = \alpha/B\rho$, as before. The focal length is

$$f = -1/[k \sinh(kl)] \quad (\text{defocusing plane}),$$

and the principal plane is inside the quadrupole a distance

$$x_p = [\cosh(kl) - 1]/[k \sinh(kl)] \quad (\text{defocusing plane})$$

where x_p is measured from the effective end of the quadrupole.

This linear theory is extremely useful and is for many purposes adequate. A computationally convenient form of this theory, given by Stork (9), is reproduced here.

We use l to indicate the effective length of a quadrupole. The object distance, measured from the entrance effective end of a quadrupole magnet, is designated p' . The image distance q' is measured from the exit effective end. (The similarity to a simple lens is lost here because the object and image distances are not measured from either the magnet center or principal planes; however, the method presented here is very useful in practice.) The expression for the image distance q' and magnification m are given by

$$q' = [p' \cos(kl) + (1/k) \sin(kl)]/[p'k \sin(kl) - \cos(kl)] \quad (\text{focusing plane})$$

$$m = -1/[p'k \sin(kl) - \cos(kl)]$$

in the focusing plane. By expressing lengths in terms of the effective length l of the quadrupole we may simplify further. We use

$$P' = p'/l, \quad Q' = q'/l, \quad L = kl$$

Then,

$$Q' = [P' \cos L + (1/L) \sin L]/[P' L \sin L - \cos L]$$

$$m = -1/[P' L \sin L - \cos L] \quad (\text{focusing plane})$$

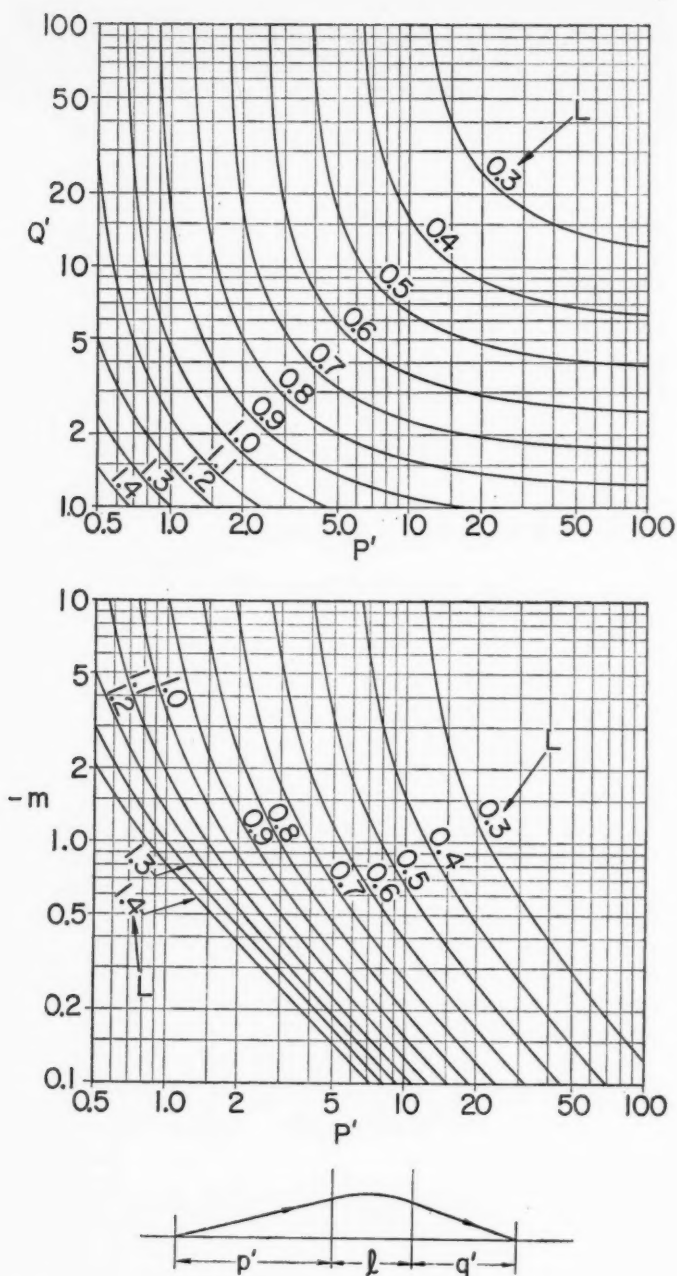


FIG. 9. Graphical presentation of quadrupole optics. The reduced image distance Q' and magnification m are given as functions of reduced object distance P' for various values of the reduced strength parameter L . This graph is to be used for the convergent plane of a quadrupole with real object and real image. Distances are measured from the effective ends of the quadrupole. $P' = p'/l$, $Q' = q'/l$, $L = kl$.

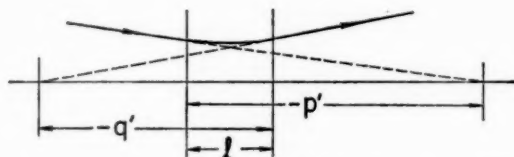
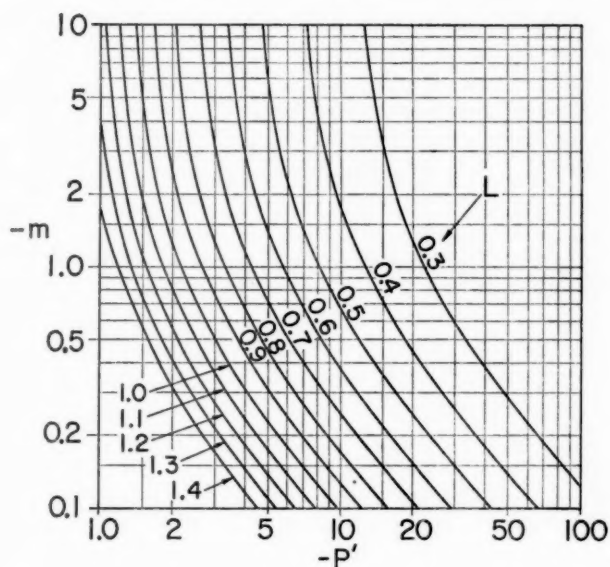
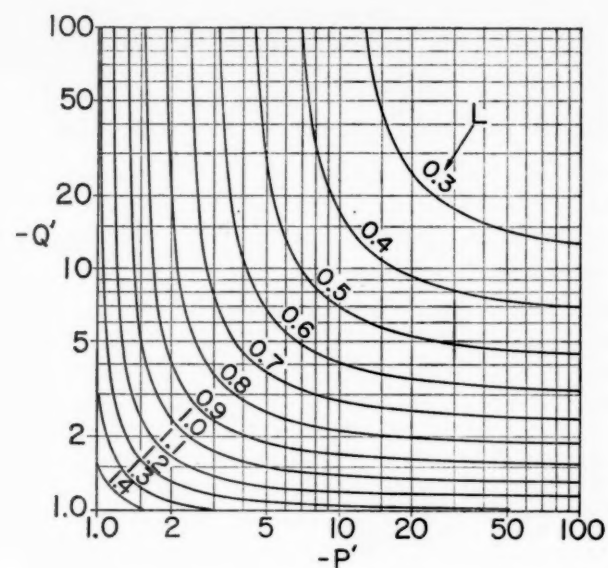


FIG. 10. Graphical presentation of Q' and m for various P' and L ; Divergent plane of quadrupole, virtual object, and virtual image. Notice negative P' implies a virtual object and negative Q' has a similar implication. $P' = p'/l$, $Q' = q'/l$, $L = kl$.

or

$$Q' = [P' + (1/L) \tan L] / [P'L \tan L - 1] \quad (\text{focusing plane})$$

The corresponding expressions for reduced image distance (from the effective end of the quadrupole) and magnification m in the defocusing plane are

$$Q' = - [P' + (1/L) \tanh L] / [P'L \tanh L + 1] \quad (\text{defocusing plane})$$

$$m = 1 / [P'L \sinh L + \cosh L]$$

The relations above are sufficient to describe any quadrupole in first-order theory. For convenience in use, these relations are summarized graphically in figures 9, 10, and 11. Usually the graphs are used to obtain approximate values of L that are appropriate to a given problem, and the final calculations are performed numerically through the use of the algebraic expressions above. (The necessary field measurements can be made with a rotating-coil gaussmeter such as the Rawson Model 720.)

Two or three quadrupoles may frequently be combined to make a lens. Figure 12(a) shows two quadrupoles of equal length (and opposite polarity) assembled to form a "doublet" lens. Figure 12(b) shows what is known as a quadrupole "triplet," each quadrupole being of opposite polarity to the next quadrupole.

Whether a lens should be a doublet or a triplet is a question about which there has been some difference of opinion. Each has advantages and disadvantages. Doublets are less expensive for a given lens strength at a given particle momentum. Doublets have somewhat peculiar focusing properties, in that even if they are adjusted to be without astigmatism they give different magnifications in the horizontal and vertical planes. In some problems this is a great advantage for doublets, but it makes them somewhat harder to think about. Triplets, on the other hand, behave rather like a simple thin lens located at the center of the triplet and, therefore, are relatively easy to deal with. Triplets have also the advantage that their focal length (focal length of the combined lens) changes somewhat less rapidly with beam particle momentum. Probably the novice is better off using triplets, but the best design frequently involves using some doublet lenses.

The expressions given above for the image distance q' , measured from the effective end of the quadrupole, can very readily be applied twice to give the net result of the two quadrupoles of a doublet lens. The object distance from the effective entrance end of the first quadrupole would be indicated by p'_1 . The image distance from the effective exit end of the first quadrupole q'^1 would be related to the object distance p'_2 for the second quadrupole by

$$q'_1 + p'_2 = g$$

where g is the effective gap between quadrupoles as indicated in Figure 12. Usually the two quadrupoles of a doublet are of the same effective length l , so that it is convenient to use the normalized forms in which distances are measured in terms of l . With the definition

$$G = g/l$$

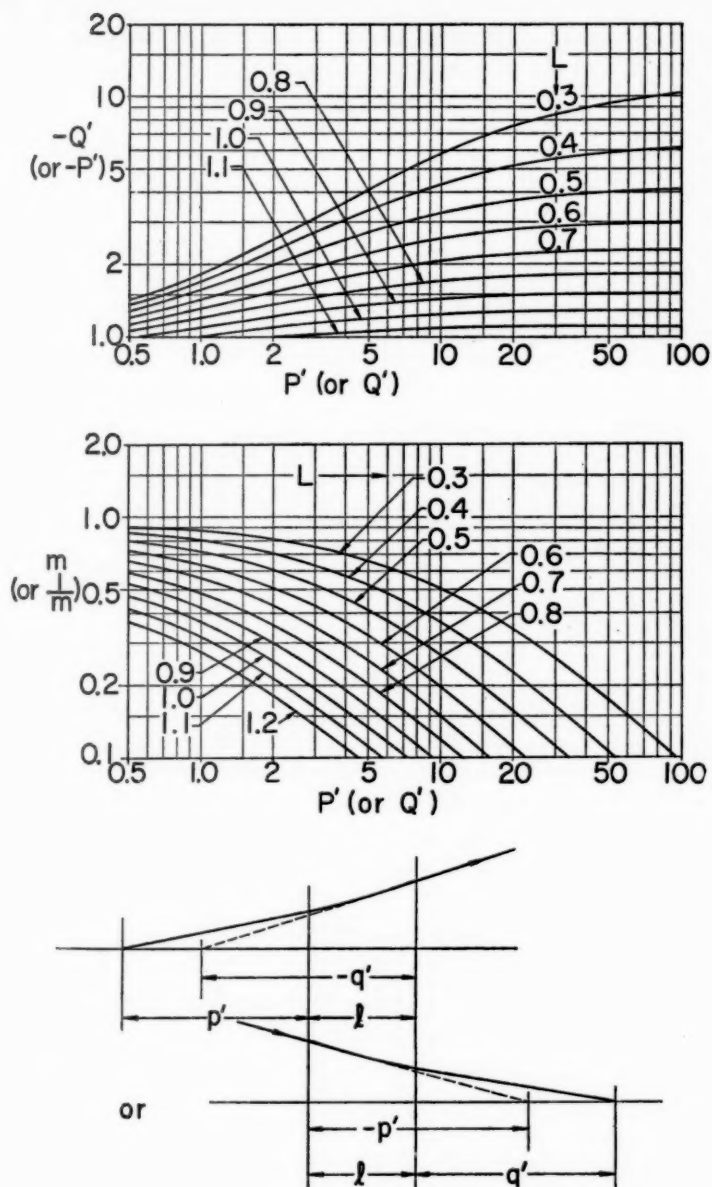


FIG. 11. Graphical presentation of Q' and m for various P' and L ; divergent plane of quadrupole, real object, and virtual image, or virtual object and real image. We use the relations $P' = p'/l$, $Q' = q'/l$, $L = kl$.

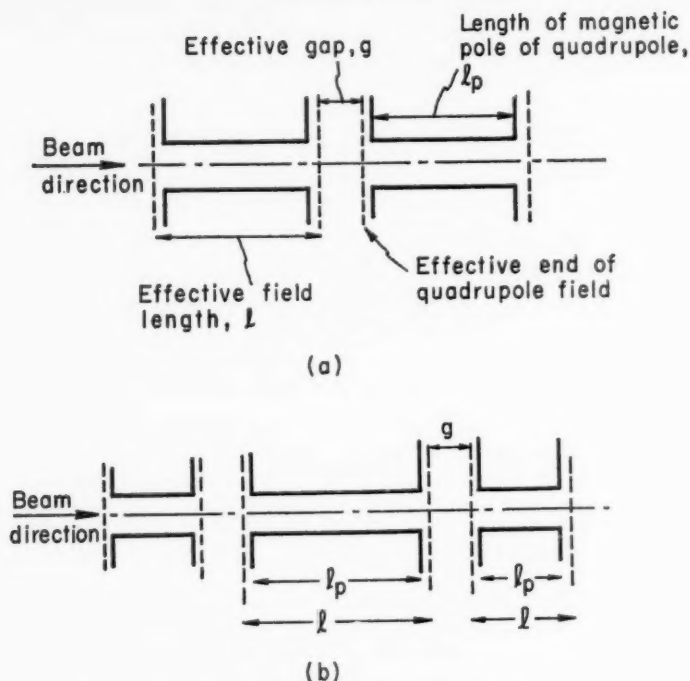


FIG. 12. Quadrupole lenses. (a) Doublet lens. (b) Triplet lens.

we have, for the plane in which the first quadrupole is focusing and the second is defocusing,

$$Q'_1 = [P'_1 + (1/L_1) \tan L_1] / [P'_1 L_1 \tan L_1 - 1]$$

$$m_1 = -1 / [P'_1 L_1 \sin L_1 - \cos L_1]$$

$$P'_2 = G - Q'_1$$

$$Q'_2 = -[P'_2 + (1/L_2) \tanh L_2] / [P'_2 L_2 \tanh L_2 + 1]$$

$$m_2 = 1 / [P'_2 L_2 \sinh L_2 + \cosh L_2]$$

$$m = m_1 m_2 = -1 / ([P'_1 L_1 \sin L_1 - \cos L_1] [P'_2 L_2 \sinh L_2 + \cosh L_2])$$

For the other plane (for which the first quadrupole is defocusing) we have

$$Q'_1 = -[P'_1 + (1/L_1) \tanh L_1] / [P'_1 L_1 \tanh L_1 + 1]$$

$$m_1 = 1 / [P'_1 L_1 \sinh L_1 + \cosh L_1]$$

$$P'_2 = G - Q'_1$$

$$Q'_2 = [P'_2 + (1/L_2) \tan L_2] / [P'_2 L_2 \tan L_2 - 1]$$

$$m_2 = -1 / [P'_2 L_2 \sin L_2 - \cos L_2]$$

$$m = m_1 m_2 = -1 / ([P'_1 L_1 \sinh L_1 + \cosh L_1] [P'_2 L_2 \sin L_2 - \cos L_2])$$

Notice that in the above expressions $L_1 = k_1 l$ is usually different from $L_2 = k_2 l$, corresponding to different magnetizations of the two quadrupoles.

Notice also that the same notation is used for the reduced object and image distances, such as Q'_1 , whether they refer to focal properties in the horizontal or vertical plane, even though the distances involved may be different for the two planes.

We have here a prescription for determining the focal properties of a given combination of quadrupoles. The experimenter is usually faced with the opposite problem, how to find the quadrupole strengths that will accomplish a given focusing. In practice this is usually accomplished by a process of trial and error. The graphs shown in Figures 9, 10, and 11 may be used for rapid rough calculations for both planes of focusing. To describe the method of reaching the desired values of L_1 and L_2 for specified object and image distances in each plane, we call plane I the plane in which quadrupole 1 is focusing, and plane II that in which quadrupole 2 is focusing. For plane I a value of L_2 is assumed (usually about 0.8) and the graphs are used to calculate backward through quadrupole 2 from the desired image distance so that L_1 may be chosen for the desired object distance. In plane II the calculation is carried forward through the system, keeping L_1 as previously determined but adjusting L_2 to give the desired image distance. The calculation is then again carried backward in plane I, L_1 being adjusted to the proper object distance, and the cycle carried on until adequate accuracy is achieved. The recommended order of calculations is chosen to take advantage of the fact that in a given plane the focusing lens has a much more dominant effect than the defocusing lens. Thus, the suggested order gives a rapid convergence to the desired conditions. The use of the graphs usually allows obtaining L_1 and L_2 to within less than 10 per cent. Actual computation, again by trial, should allow determining the quadrupole characteristics for a given problem to 1 per cent.

For quadrupole triplets the procedure is not much different except that it is less convenient to use the reduced object and image distance P' and Q' because the effective lengths l of the quadrupole components are not usually equal for all elements of the triplet. The expressions involving p' and q' are more convenient. The first and last quadrupoles of a triplet are frequently identical and are often operated at the same magnetization.

Hand & Panofsky (10) have developed a rectangular quadrupole, on the basis of a suggestion by O. Piccioni. The field pattern is the same as that of the conventional quadrupoles already discussed, but it is available in rectangular, rather than square or round, cross section. The rectangular quadrupole is suggested because conventional quadrupoles cannot usually be used to full aperture except in the focusing plane. By using a rectangular quadrupole, with larger aperture in the focusing plane, one avoids producing some unused region of field. Whether rectangular quadrupoles have economic advantages over conventional quadrupoles is difficult to determine at this time.

Sternheimer (11) has made extensive calculations for a double-focusing magnet system that combined, in the same components, the functions of

deflecting magnet and quadrupoles. Non-uniform fields are used. Instruments of this type may be expected to be extremely useful in the future, especially for short-lived particles; however, they are somewhat less flexible than instruments in which the deflecting and focusing functions are separated.

MATRIX METHOD FOR COMBINING COMPONENTS

Matrices may also be used to advantage, especially if the computation is to be adapted to a digital computer. The y and z co-ordinates of an orbit with respect to the lens axis (x axis) may be treated separately. Taking, for example, the y co-ordinates, one can represent the position and slope of an orbit as a column symbol

$$\begin{pmatrix} y \\ \frac{dy}{dx} \end{pmatrix}_{x=0}$$

at a given point in the system, here taken as $x=0$. A field-free region of length b is represented by the matrix

$$\begin{pmatrix} 1 & b \\ 0 & 1 \end{pmatrix} \quad (\text{field-free length } b)$$

in that the new y co-ordinate and slope dy/dx are given by the matrix equation

$$\begin{pmatrix} y \\ \frac{dy}{dx} \end{pmatrix}_{x=b} = \begin{pmatrix} 1 & b \\ 0 & 1 \end{pmatrix} \begin{pmatrix} y \\ \frac{dy}{dx} \end{pmatrix}_{x=0}$$

Similarly, the matrix giving the values of y and dy/dx at the exit effective end of a quadrupole in terms of the corresponding values at the entrance-effective end is, for the focusing plane,

$$\begin{pmatrix} \cos(kl) & (1/k) \sin(kl) \\ -k \sin(kl) & \cos(kl) \end{pmatrix}$$

and, for the defocusing plane,

$$\begin{pmatrix} \cosh(kl) & (1/k) \sinh(kl) \\ k \sinh(kl) & \cosh(kl) \end{pmatrix}$$

As an example of the use of these matrices, we give the matrix applicable to the following situation: from the starting point there is first a field-free region of length b to the entrance-effective end of a focusing quadrupole of effective length l and strength parameter k_1 , followed by effective gap g , and finally by a defocusing quadrupole of the same effective length l and strength parameter k_2 . The combined matrix is

$$\begin{pmatrix} \cosh(k_2 l) & (1/k_2) \sinh(k_2 l) \\ k_2 \sinh(k_2 l) & \cosh(k_2 l) \end{pmatrix} \begin{pmatrix} 1 & g \\ 0 & 1 \end{pmatrix} \begin{pmatrix} \cos(k_1 l) & (1/k_1) \sin(k_1 l) \\ -k_1 \sin(k_1 l) & \cos(k_1 l) \end{pmatrix} \begin{pmatrix} 1 & b \\ 0 & 1 \end{pmatrix}$$

with

$$k = (\alpha/B\rho)^{1/2} = [(dB/dr)/B\rho]^{1/2}$$

The matrix above will be taken to have the form

$$\begin{pmatrix} a_1 & a_2 \\ a_3 & a_4 \end{pmatrix}$$

If we assume the object is at the original starting point, this matrix has the form

$$\begin{pmatrix} m + (q'/f) & -(q'/m) \\ -(1/f) & (1/m) \end{pmatrix}$$

where m is the magnification of the image formed, q' is the distance to this image, and f is the focal length of the combined lens. Therefore, the distance q' from the exit-effective end to the image is

$$q' = -(a_2/a_4)$$

and the magnification is

$$m = (1/a_4)$$

The form of the matrix relating the column symbol at image position to the column symbol at object position must be

$$\begin{pmatrix} m & 0 \\ -(1/f) & (1/m) \end{pmatrix}$$

In general, when quadrupoles are to be adjusted to perform a desired focusing operation in both the y co-ordinate and the z co-ordinate, a method of successive approximations must be used.

USE OF WIRE ORBITS TO TEST COMPONENTS

A current-carrying wire that is under tension takes up a position coincident with the orbit of a charged particle in a magnetic field, provided the current and tension of the wire are adjusted to correspond to the momentum of the particle in question. The current I (amps) in the wire and tension T (grams of force) must satisfy the condition

$$I(\text{in amp.})/T(\text{in gm.}) = 2.94/p(\text{in Mev/c})$$

and the current I must flow in the direction opposite to the beam current represented by the charged particles moving along the orbit. The outline of a brief derivation follows.

Using Gaussian cgs units, one finds the force $d\mathbf{F}$ on a small length $d\mathbf{s}$ of a wire carrying current I in magnetic flux density \mathbf{B} is

$$d\mathbf{F} = -I d\mathbf{s} \times \mathbf{B}$$

The minus sign in the expression above reflects the opposite sense of I and \mathbf{s} . Using \mathbf{t} as a unit vector tangent to the wire, we readily obtain

$$d\mathbf{t}/ds = (I/T)\mathbf{t} \times \mathbf{B}$$

A similar equation may be derived for the orbit of a charged particle if t is now used to represent the unit vector tangent to the orbit. Again in Gaussian units, the force \mathbf{F} on a particle with charge e and velocity \mathbf{v} is

$$\mathbf{F} = (e/c)\mathbf{v} \times \mathbf{B} = d\mathbf{p}/dt$$

The following expressions outline the steps:

$$\begin{aligned} |\mathbf{p}| &= p = \text{const. magnitude of momentum} \\ ds &= v dt \\ t &= \mathbf{p}/p = \mathbf{v}/v \\ (e/c)\mathbf{v} \times \mathbf{B} &= (ev/c)t \times \mathbf{B} = v d\mathbf{p}/ds = v p dt/ds \\ dt/ds &= (e/p c)t \times \mathbf{B} \quad (\text{Gaussian units}) \end{aligned}$$

The equations for wire and orbit are identical provided we have

$$I/T = e/p c \quad (\text{in Gaussian units})$$

Measuring wire current I in amperes, tension T in grams of force ($g=980$ cm./sec.²), taking e as one (positive) electron charge, and measuring p in Mev/c give the expression at the beginning of this section. The weight of the wire is neglected here.

The current-carrying wire allows easy visualization of particle trajectories through a magnetic system. With measuring microscopes, accurate information about focusing properties may be obtained. Using a carefully balanced pulley wheel located at the source or apparent source of particles, with weights to give the desired wire tension, one may use the wire to find accurate data on the focal length of a magnet system. It is not feasible to extend the wire all the way to the focus point because the wire then becomes unstable. The wire is held fixed at some movable support short of the focus point, and wire positions are recorded at two points along the wire in the field-free region outside the magnet system. A number of wire positions must be used to determine the focus point to which the orbits converge.

Figure 13 shows the arrangement for measuring the focal properties of a pair of quadrupoles, showing two positions of the current-carrying wire. In some cases two wires carrying the same current in the same direction may be used to advantage. The focus point is determined by straight-line extrapolation of the orbits in the field-free region.

Careful measurements with wire orbits can give valuable information about aberrations, especially in arrangements such as those involving electric deflection to separate particles of differing mass. A suitable current regulator has been described by Lutz & Pike (12).

EXAMPLES OF PURELY MAGNETIC SYSTEMS

A simple system for obtaining a negative pion beam at 1.4 Bev/c has been used by Chretien, Leitner, Samios, Schwartz & Steinberger (13). Their focusing and momentum selection were provided by the magnetic field of the

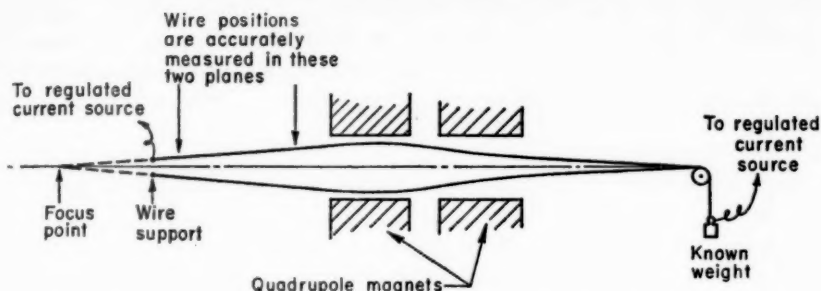


FIG. 13. Arrangement for measuring focal properties of a pair of quadrupoles.

Cosmotron. Where an image of the target was formed they inserted a collimator to provide momentum selection. No great intensity was needed for their bubble chamber; but they required, and obtained, momentum selection within about 1 per cent accuracy. The arrangement is shown in Figure 14.

A single spectrograph magnet of very considerable usefulness has been made by Crewe (14). It uses a uniform field, and can be used up to about 19,000 gauss, with focusing provided purely by sloping and curving the pole edge at entrance and exit. It provides a focus only in the central plane (which we refer to as horizontal even though it is not horizontal in the Crewe design). In the vertical plane it does not focus, but because of some vertical focusing

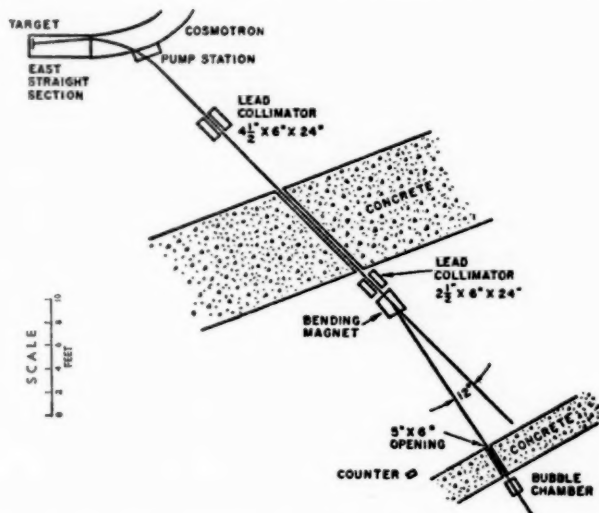


FIG. 14. Experimental apparatus of Chretien, Leitner, Samios, Schwartz & Steinberger for providing a π^- beam at 1.4 Bev/c.

at the entrance to the magnet it preserves a good effective solid angle for particles leaving the target. The magnet involves bending by 60 degrees. Reference (14) gives a worthwhile discussion of the design considerations. Similar principles have been used by Meier, Fletcher, Wisseman & Williamson (15).

A very useful spectrometer based on uniform magnetic field has been constructed by Lovati & Tyrén (16). Their instrument has focusing in both planes.

Browne & Buechner (17) have discussed the use of a magnet with uniform field and round pole pieces to allow focusing, as a spectrograph, for a wide band of momenta. A refinement of the same type of instrument is described by Enge (18), in which a single quadrupole is introduced to give a greatly increased effective solid angle.

A series of important experiments has been done by Hofstadter and others with a magnetic spectrograph based on a non-uniform field and 180-degree bending. A brief description of one model has been given by Hofstadter, Fechter & McIntyre (19). A more complete description of this general type of magnet may be seen in the article of Snyder, Rubin, Fowler & Lauritsen (20).

A double spectrograph, essentially one spectrograph followed by a second spectrograph, has been used in the antiproton work of Chamberlain, Segrè, Wiegand & Ypsilantis (21) and discussed previously in this *Review* (22). A later version utilizing the same principles was described by Elioff, Agnew, Chamberlain, Steiner, Wiegand & Ypsilantis (23) and is shown in Figure 15. The magnetic analysis is provided by the deflecting magnets $M1$ and $M2$, and the focusing by quadrupole triplet lenses $Q1$, $Q2$, and $Q3$. The target T is first focused at the position of the scintillation counter $S1$, where there is considerable dispersion, so that the counter acts to select a narrow momentum band about the central momentum near 1.5 Bev/c. The second spectrograph, involving $Q2$ and $M2$, forms a second focus at the counters $S2$, VSC II, and \bar{C} . The momentum dispersion of the first spectrograph is compensated by that of the second spectrograph so that all particles accepted by the first spectrograph fall into a reasonably small image at $S2$. The momentum was defined to ± 3 per cent, and the image size at $S2$ was 4.5 cm. high by 7 cm. wide. The final lens $Q3$ focused the beam into the experimental area A . Helium-filled plastic bags were inserted in the spectrograph over most of its length, to reduce the multiple scattering that would otherwise be caused by air. Antiprotons were selected (from the beam that was mostly composed of mesons and electrons) by both a Cerenkov counter and time-of-flight measurement.

Owing to finite size of target and deviation of the momentum from the central momentum, there is a loss of particles that fail to enter the aperture of the second spectrograph in the arrangement of Figure 15, even for particles within the desired band of momenta. Piccioni (24) has pointed out that the

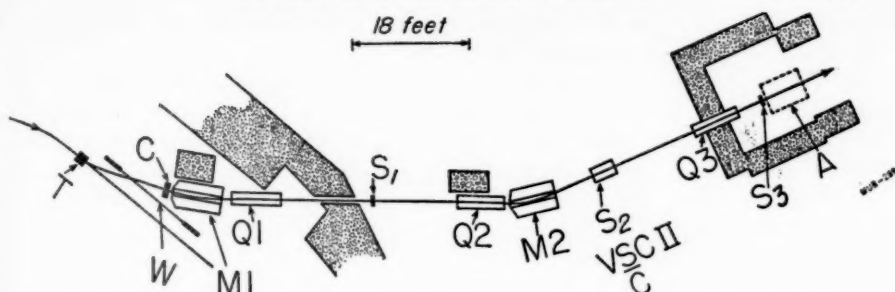


FIG. 15. Double spectrograph used for antiproton experiments by Elioff, Agnew, Chamberlain, Steiner, Wiegand & Ypsilantis. Deflecting magnets are indicated as $M1$ and $M2$. Triplet quadrupole lenses are $Q1$, $Q2$, and $Q3$. The initial bending of the orbit near the target T is due to the field of the Bevatron.

loss may be reduced by installing a field lens close to $S1$. Such a lens would be arranged to focus the aperture of $Q1$ onto the aperture of $Q2$. In the apparatus of Figure 15 there was so much multiple scattering by $S1$ at the first focus that the field lens would not be expected to help the transmission of

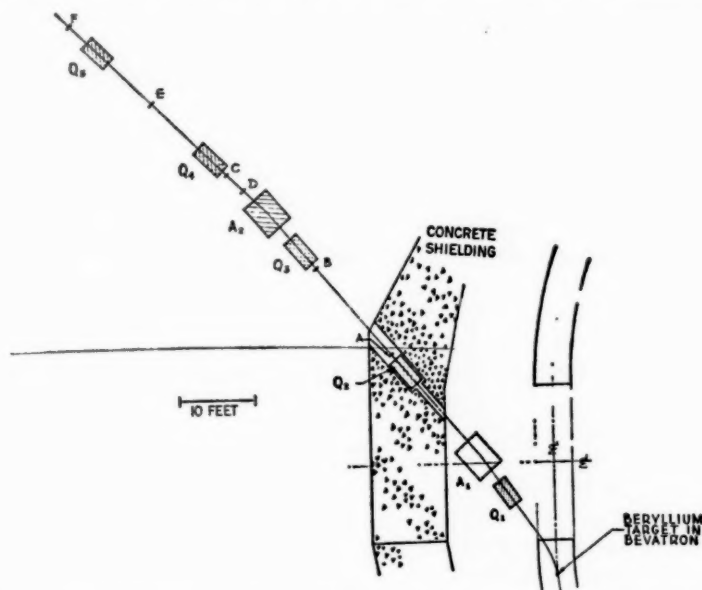


FIG. 16. Arrangement of Cork, Lambertson, Piccioni & Wenzel for antiproton experiments. The second and fourth quadrupole lenses $Q2$ and $Q4$ act as field lenses. The quadrupole system, if used without the deflecting magnets $A1$ and $A2$, could pass a wide band of momenta.

the system materially. However, the concept of the field lens has been used to great advantage in other arrangements.

The use of field lenses can be extended to give a series of lenses that successively focus and refocus the beam even if the beam includes a fairly broad band of momenta. Such a system, used in connection with antiproton experiments, is shown in Figure 16. It is taken from the work of Cork, Lambertson, Piccioni & Wenzel (25), who have given a readable description of their arrangement of magnets. Antiprotons were selected purely on the basis of time-of-flight measurements.

For the handling of the beam from a linear electron accelerator, Panofsky & McIntyre (26) have devised a useful system for providing momentum analysis without introducing dispersion in the final image. Their paper is recommended reading because of the insight it gives into their design considerations.

MEASUREMENT OF TRANSMISSION OF A MAGNETIC BEAM-FORMING SYSTEM

The typical magnetic system we are discussing is intended to form a secondary beam of particles from the particles emerging from a target. The number of particles in the secondary beam is usually proportional to what we will call the acceptance A , which may be written as the product of a solid angle Ω , referring to the solid angle in which particles may leave the target and still be contained in the secondary beam, and a momentum Δp , loosely called "momentum bite":

$$A \cong \Omega \Delta p$$

In most cases the acceptance A is not simply the product of the maximum solid angle and the momentum spread of the resultant beam. Rather, the solid angle in which particles may be accepted is a function of the momentum p of the particles, and the acceptance is defined as

$$A = \int_{p_{\min}}^{p_{\max}} \Omega(p) dp$$

It is frequently unnecessary to measure or calculate the solid angle function $\Omega(p)$, but it is important to know the acceptance A . One example is the early antiproton experiment, in which it was desired to have some estimate of the absolute antiproton yield. This involved knowing the acceptance of the system and the number of antiprotons passing through the system for a given number of high-energy protons hitting the (primary) target.

If the system is very simple and involves only one focus point of the particles, then the problem is relatively simple. Figure 17 shows such an example. It is assumed that the target represents a "white" source because a broad band of momenta is emitted by the target into a solid angle large compared to the solid angle subtended by the lens aperture. Then the rate at which particles pass through the system (i.e., the counting rate) is proportional to

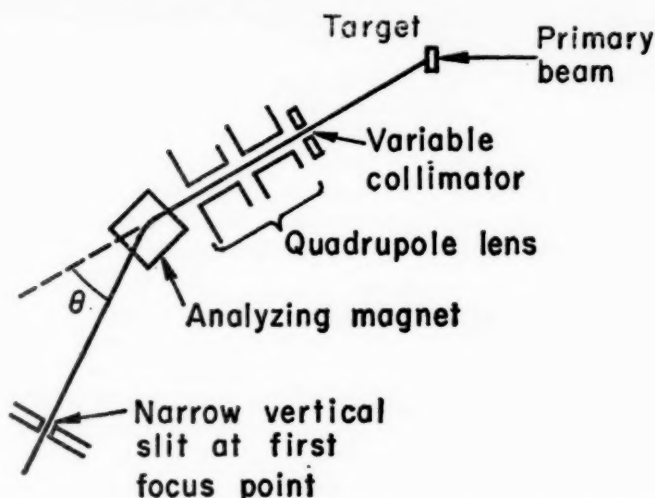


FIG. 17. Insertion of a variable collimator and narrow vertical slit for the determination of beam intensity under conditions of known acceptance A . A necessary condition is that the observed beam intensity be proportional to collimator area and to slit width.

the acceptance of the system. By temporarily installing a variable collimator and a narrow slit (or narrow counter) at or near the first focus point, one may measure the counting rate under conditions for which the acceptance is

$$A = \Omega_{\text{coll}} \Delta p_{\text{slit}}$$

where Ω_{coll} is the solid angle subtended at the target by the collimator aperture and Δp_{slit} is the momentum interval corresponding to the slit width for a ray that is initially a central ray (passing through target center and collimator center). For the example in Figure 17, where the analyzing magnet is used near minimum deviation one may use the expression

$$\Delta p_{\text{slit}} = p(\Delta\theta/\theta)$$

where p is the particle momentum for which the system is adjusted, θ is the bending angle at the analyzing magnet, and $\Delta\theta$ is the interval of θ determined by the edges of the vertical slit at the focus point.

Once the counting rate has been determined for conditions of known acceptance (i.e., with collimator and slit, as discussed above), the acceptance of the system with collimator and slit removed may be known simply by measuring the counting rate, for the acceptance is directly proportional to the counting rate of particles through the system.

More complicated systems are frequently used, in which the secondary

beam may be focused and refocused at several points along the system. Usually the acceptance is a function of how well the various components are matched to one another. In measuring the over-all acceptance it is good practice to compare the counting rate through the complete system with the

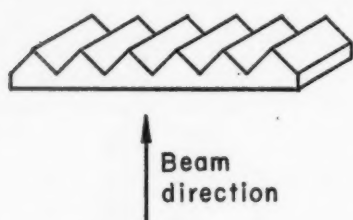


FIG. 18. Ribbed absorber for converting a monoenergetic beam into a "white" beam suitable for evaluating the acceptance of a magnet system.

rate at which particles reach the first focus when the collimator and slit are in place as described above. This simple procedure should be adequate even for complicated systems with aperture stops at many points along the system.

When a monochromatic initial beam is to be used in evaluating the acceptance of a magnetic system, a ribbed absorber can frequently be used at the position usually occupied by the target to give a "white" spectrum and to give sufficient multiple scattering to cause the entrance to the magnetic system to be rather uniformly illuminated. One form of ribbed absorber is shown in Figure 18. The ribs must be deep enough to give a momentum spread to the emerging particles that is guaranteed to be greater than the momentum spread of the beam that normally would pass through the system. Each rib should be quite narrow compared with the width of the incident beam.

ABERRATIONS

Chromatic aberration tends to be present in any system of quadrupole lenses. For a single lens, a given fractional change of momentum is usually reflected in a fractional change of effective focal length 1.5 to 4 times as great, i.e., $\Delta f/f \cong (1.5 \text{ to } 4)(\Delta p/p)$. Of course, chromatic aberrations can be calculated by the procedures previously described, providing a particle momentum slightly different from the central momentum is used in the calculation.

Geometrical aberrations are failures of focus related to finite object size and finite angular aperture. For bending magnets aberrations may appear in second order, while for a pure quadrupole system the third-order aberrations should be the lowest order to appear.

For bending magnets the second-order spherical aberration can be eliminated for the horizontal plane (27), and, in fact, perfect focusing may be achieved in the horizontal plane—as was pointed out for example, by Kerwin (28) and by Kerwin & Geoffrion (29). However, it is not possible to eliminate all second-order aberrations simultaneously, including those in the vertical plane.

For purely quadrupole components, second-order aberrations should be absent to the extent that quadrupole symmetry is maintained. The third-

order aberrations are extremely complicated, involving some 20 Seidel coefficients.

SEPARATED BEAMS

Given a magnetic system that provides a charged-particle beam of well defined momentum, one may separate out particles of a particular mass by sorting the particles on the basis of their velocities. A number of methods have been suggested. We describe here one of the most successful forms of apparatus for achieving the separation, the parallel-plate electrostatic separator. It was first used for particles of high energy by Coombes, Cork, Galbraith, Lambertson & Wenzel (30). Whereas deflection in a magnetic field depends on particle momentum, being proportional to $1/p$, deflection in an electric field depends upon momentum times velocity, and is proportional to $1/pv$.

The magnetic selection of momenta involves deflection in the horizontal plane, as in the systems described previously. The electric deflection occurs in the vertical plane, with a vertical electric field obtained by applying high voltage to electrodes above and below the beam of secondary particles. In its simplest form such a system is shown in Figure 19. Figure 19a shows the plan view. Figure 19b shows the focal properties of the system for deviations in the horizontal plane and for the central momentum only. In that plane the separator has no effect. Figure 19c shows the focusing properties in the vertical plane. The vertical electric field between the parallel plates of the separator causes a deflection, usually very small, in the vertical plane. The curvature (in cm.^{-1}) of the trajectory in the transverse electric field is given by the expression

$$K = \frac{E(\text{in } v/\text{cm.})}{p(\text{in Mev}/c)\beta} \times 10^{-6}$$

As a result of the electric field, particles of differing velocity have different vertical focus positions at the final slit, and a narrow slit may be used to exclude all except the particles of a chosen velocity.

So far, we have described the separated beam only in a rudimentary form. A number of refinements are necessary if one is to achieve the best available performance:

(a) Since it is important to get considerable separation of particles of differing masses on the basis of a small electric deflection, the target is made extremely small in the vertical dimension, perhaps 2 mm.

(b) To avoid the multiple scattering involved in passing the beam through vacuum windows, the whole system may be made with a vacuum system common to the accelerator.

(c) The focusing properties are chosen to eliminate, as much as possible, the particles that have scattered from the walls of the vacuum system.

(d) In the region of the separator (where there is a vertical electric field), a small horizontal magnetic field is also applied. This makes the arrangement into a

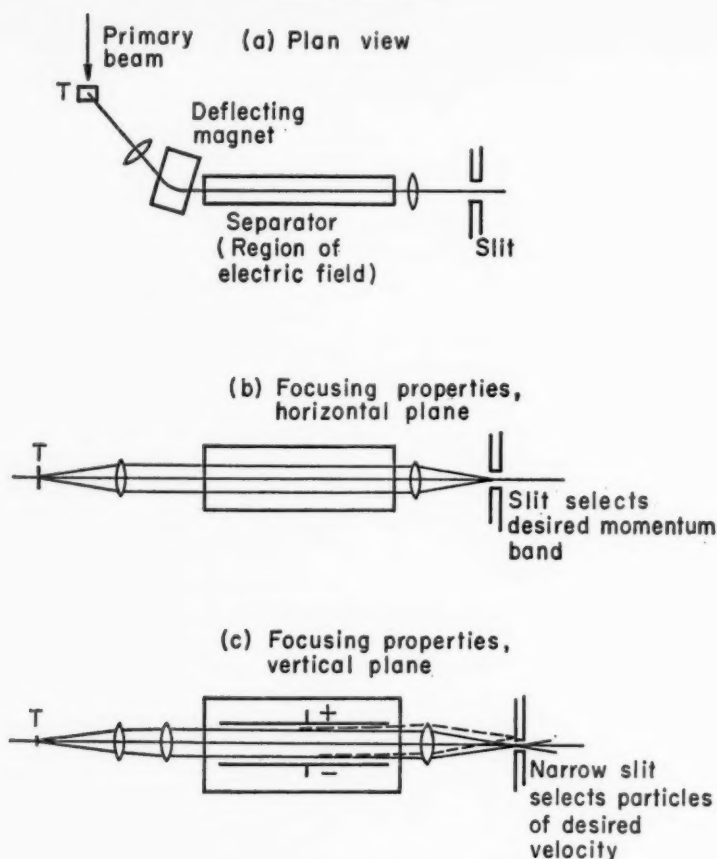


FIG. 19. Schematic presentation of a one-stage separated-beam apparatus with parallel-plate separator.

Wien filter. In the resulting system there is no deflection due to the separator for particles of the desired velocity, but faster or slower particles are deflected upward or downward. This choice allows all the magnet components except the separator to be adjusted before the separator is turned on.

(e) Care is given to the shaping and spacing of the "parallel-plate" electrodes to give a strictly uniform vertical component of electric field, at least to a few per cent.

(f) One of the magnets, usually the deflecting magnet, is carefully shimmed for the purpose of making the vertical focus as good as possible, particularly with respect to chromatic aberrations. This process usually involves great care in the use of wire orbits to measure the aberrations. The vertical focusing properties are improved at the sacrifice of the properties in the horizontal plane, which need not be nearly as good.

(g) A small series of counters is located close to the slit but above or below the

desired beam to show the spatial shape and position of the focus of one of the undesired (but copious) components of the beam. This series of counters allows constant checks on the adjustment of the separator and on the focusing properties of the magnetic system.

(h) Frequently two or more stages of separation are used to obtain better over-all separation and to prevent the system's being "fooled" by particles that suffer a decay process while passing through the system.

An extraordinarily good separated beam with parallel-plate separators has been set up by Eberhard, Good & Ticho (31). It was designed to give a separated beam of K^- mesons of momentum 1.2 Bev/c for a liquid-hydrogen bubble chamber. Two successive stages of separation were used to reject negative pions by a factor of 10^5 . The vertical dimension of the target was 3 mm. The spacing between parallel-plate electrodes was 6.3 cm. and the potential difference between electrodes was 380 kv. Reference (31) describes many of their design considerations, some of which have been outlined above. The quality of the beam may be summarized by stating the relative numbers of K^- , π^- , and μ^- as 1:0.06:1, whereas at the target there was a ratio $K:\pi$ of 1:140.

A coaxial Wien-filter separator has been used by Horwitz, Miller, Murray & Tripp (32). The separator has been described in an unpublished report by Murray (33). At present, it appears that the parallel-plate separators may be more useful than the coaxial separators simply because the parallel-plate construction is simpler.

A new form of separator, called a septum separator, has been proposed by Murray (34). It involves many plane electrodes spaced very closely in vacuum, with alternate electrodes connected to high positive and negative voltage supplies. As with the other separators, a transverse magnetic field would be applied to make a Wien filter. Unwanted particles would be stopped by absorption in the plates of the separator. The advantage of the septum separator is that high electric fields (200 kv./cm. over 0.16 cm. gap) can be used, making shorter separators possible. The disadvantage is its inherently poor geometrical transmission. It is not yet fully evaluated experimentally.

Preliminary work by Murray (35) shows that higher fields can be maintained in a parallel-plate separator if the negative electrode is coated with slightly conducting glass. The glass serves to quench sparks locally before a strong discharge can develop. The glass surface has not yet been tested in a full-size separator.

Radio-frequency fields can be used, instead of d.c. fields, to achieve separation of particles of different mass. A number of distinct modes of operation have been proposed. One method involves using a primary beam, from an accelerator, that is modulated rapidly and periodically in time, such as the beam from an electron accelerator that uses microwave acceleration. By passing the magnetically analyzed secondary beam through a synchronized radio-frequency (r.f.) field, one may achieve a separation of the

components of the beam of different velocities because the different-speed components of the secondary beam have different times of flight between the target and the r.f. field region. Such a system has been described by Panofsky (36). In the same paper the focusing properties of an interesting spectrograph are illustrated.

Another mode of operation of an r.f. separator involves using a long r.f. cavity. The field in the cavity is visualized in terms of traveling waves reflecting from the ends of the cavity. The phase velocity of the cavity is adjusted to match the velocity of some unwanted component in the beam, such as the pions in an antiproton beam. The pions then suffer a deflection due to the r.f. field. The length of the cavity is chosen so that there is no net deflection of the desired (antiproton) beam component, by arranging the length so that the desired component falls behind (or ahead of) the r.f. traveling wave by an integral number of full wavelengths during the transit through the cavity. A recent proposal of this type has been made by Blewett (37).

The simplest use of an r.f. cavity would seem to be in a TE mode, with the electric field transverse to the beam direction. However, Panofsky & Wenzel (38) have pointed out that in such a mode the magnetic field cancels the deflection due to the electric field. Either a TM mode must be used, or a special cavity configuration such as that discussed by Blewett (37).

Until now the r.f. separators have not been thoroughly tried in practice; therefore, no complete analysis is attempted here.

EXTREMELY CLEANLY COLLIMATED BEAMS

In some experiments it is of no consequence if there is a very small fraction of the beam spread rather widely in space, but in other experiments it is quite crucial that the beam be very well confined to a given region. In general, strong focusing has been a great help toward clean beams but special precautions are still necessary in special cases, such as separated beams.

Considerable care was given to the problem of a clean beam by Eberhard. Good & Ticho (31). Another very elegant example is the so-called pencil beam of protons from the Cosmotron used by Cool, Morris, Rau, Thorndike & Whittemore (39) to produce strange particles within a diffusion cloud chamber while leaving most of the chamber free from unwanted tracks. Both these papers give some description of design methods.

No attempt is made in this article to give a complete description of methods of producing very clean beams. However, a few comments can be made. It is very helpful to be able to use a geometrically small target, since the desired beam can then be passed, with careful focusing, through relatively narrow slits. It pays to place the important collimators fairly early in the system. Particles that have been degraded in energy in passing through the walls of a collimator can be effectively rejected if one of the last components of the beam-forming system is a deflecting magnet with large pole separation. It is frequently important to use collimators that are rather thin

in the beam direction to reduce the number of particles that scatter from the inside collimator wall. A collimator need not be very thick, if it is followed by considerable magnetic bending, to reject particles that have lost appreciable energy in the collimator material.

ACKNOWLEDGMENTS

The author expresses thanks to a number of colleagues who have discussed with him various phases of the subject matter, but who should not be held responsible for shortcomings of the article. Dr. David Judd has been of help, especially on the subject of aberrations. Dr. Leroy Kerth has contributed a number of ideas concerning systems with quadrupoles. Dr. Harold Ticho has pointed out problems in connection with separated beams. It is a pleasure to thank Dr. Donald Stork for permission to publish his useful curves.

LITERATURE CITED

1. Courant, E. D., Livingston, M. S., and Snyder, H. S., *Phys. Rev.*, **88**, 1190 (1952)
2. Rankin, B., *Rev. Sci. Instr.*, **25**, 675 (1954)
3. Fermi, E. (Personal communication, 1949)
4. Cross, W. G., *Rev. Sci. Instr.*, **22**, 717 (1951)
5. Bainbridge, K. T., *Experimental Nuclear Physics*, Part V, **I**, 559 (Segrè, E., Ed., John Wiley & Sons, Inc., New York, N. Y., 789 pp., 1953)
6. Buechner, W. W., *Progr. in Nuclear Phys.*, **5**, 1 (1956)
7. Judd, D. L., *Rev. Sci. Instr.*, **21**, 213 (1950)
8. Sternheimer, R. M., *Rev. Sci. Instr.*, **23**, 629 (1952)
9. Stork, D. H. (Personal communication, 1959)
10. Hand, L. N., and Panofsky, W. K. H., *Rev. Sci. Instr.*, **30**, 927 (1959)
11. Sternheimer, R. M., *Rev. Sci. Instr.*, **24**, 573 (1953)
12. Lutz, I., and Pike, C., *Rev. Sci. Instr.*, **30**, 841 (1959)
13. Chretien, M., Leitner, J., Samios, N. P., Schwartz, M., and Steinberger, J., *Phys. Rev.*, **108**, 383 (1957)
14. Crewe, A. V., *Rev. Sci. Instr.*, **29**, 880 (1958)
15. Meier, O., Jr., Fletcher, N. R., Wiseman, W. R., and Williamson, R. M., *Rev. Sci. Instr.*, **29**, 1004 (1958)
16. Lovati, A., and Tyrén, H., *J. Sci. Instr.*, **33**, 151 (1956)
17. Browne, C. P., and Buechner, W. W., *Rev. Sci. Instr.*, **27**, 899 (1956)
18. Enge, H. A., *Rev. Sci. Instr.*, **29**, 885 (1958)
19. Hofstadter, R., Fechter, H. R., and McIntyre, J. A., *Phys. Rev.*, **92**, 978 (1953)
20. Snyder, C. W., Rubin, S., Fowler, W. A., and Lauritsen, C. C., *Rev. Sci. Instr.*, **21**, 852 (1950)
21. Chamberlain, O., Segrè, E., Wiegand, C., and Ypsilantis, T. J., *Phys. Rev.*, **100**, 947 (1955)
22. Segrè, E., *Ann. Rev. Nuclear Sci.*, **8**, 127 (1958)
23. Elioff, T., Agnew, L., Chamberlain, O., Steiner, H., Wiegand, C., and Ypsilantis, T., *Phys. Rev. Letters*, **3**, 285 (1959)
24. Piccioni, O. (Personal communication, 1956)
25. Cork, B., Lambertson, G. R., Piccioni, O., and Wenzel, W. A., *Phys. Rev.*, **107**, 248 (1957)
26. Panofsky, W. K. H., and McIntyre, J. A., *Rev. Sci. Instr.*, **25**, 287 (1954)
27. Bainbridge, K. T., *Proceedings of the Seventh Solvay Conference*, 55 (Stoops, R., Ed., Brussels, Belgium, 411 pp., 1948)
28. Kerwin, L., *Rev. Sci. Instr.*, **20**, 36 (1949)
29. Kerwin, L., and Geoffrion, C., *Rev. Sci. Instr.*, **20**, 381 (1949)
30. Coombes, C. A., Cork, B., Galbraith, W., Lambertson, G. R., and Wenzel, W. A., *Phys. Rev.*, **112**, 1303 (1958)
31. Eberhard, P., Good, M. L., and Ticho, H. K., *U. S. Atomic Energy Commission Doc., UCRL-8878 Rev.*, 25 pp. (1959); or *Rev. Sci. Instr.* (To be published)
32. Horwitz, N., Miller, D., Murray, J. J., and Tripp, R. D., *Phys. Rev.*, **115**, 472 (1959)
33. Murray, J. J., *U. S. Atomic Energy Commission Doc., UCRL-3492*, May 1957 (Unpublished)
34. Murray, J. J. (Personal communication, 1958)
35. Murray, J. J. (Personal communication, 1959)
36. Panofsky, W. K. H., *Proc. Intern. Conf. High-Energy Accelerators and Instrumentation, CERN, 1959*, 428 (Kowarski, L., Ed., CERN, Geneva, Switzerland, 705 pp., 1959)
37. Blewett, J. P., *Proc. Intern. Conf. High-Energy Accelerators and Instrumentation, CERN, 1959*, 422 (Kowarski, L., Ed., CERN, Geneva, Switzerland, 705 pp., 1959)
38. Panofsky, W. K. H., and Wenzel, W. A., *Rev. Sci. Instr.*, **27**, 967 (1956)
39. Cool, R. L., Morris, T. W., Rau, R. R., Thorndike, A. M., and Whittemore, W. L., *Phys. Rev.*, **108**, 1048 (1957)

NUCLEAR STRUCTURE EFFECTS IN INTERNAL CONVERSION¹

By E. L. CHURCH

Pitman-Dunn Laboratories, Frankford Arsenal, Philadelphia, Pennsylvania²

AND

J. WENESER

Brookhaven National Laboratory, Upton, New York³

CONTENTS

INTRODUCTION	194
FORMULATION OF THE INTERACTION	196
<i>Magnetic multipoles</i>	198
<i>Electric multipoles</i>	199
<i>Electric monopole</i>	202
STATIC EFFECTS OF NUCLEAR STRUCTURE	203
<i>Nuclear size and charge distribution</i>	203
<i>Static nuclear moments</i>	208
<i>Summary</i>	209
DYNAMICAL EFFECTS IN MAGNETIC TRANSITIONS	210
<i>The function c_{ij}</i>	211
<i>Magnetic penetration matrix elements and nuclear models</i>	213
<i>Analysis of the 480-kev transition in Ta^{181}—an l-forbidden transition</i>	215
<i>Rotational transitions—accidental cancellation</i>	219
<i>Analysis of Ti^{202}—a puzzle</i>	220
DYNAMICAL EFFECTS IN ELECTRIC TRANSITIONS	222
<i>The functions Φ and Θ</i>	223
<i>Electric penetration matrix elements and nuclear models</i>	228
<i>Experimental results</i>	229
ELECTRIC MONOPOLE TRANSITIONS	230
<i>Harmonic nuclei</i>	231
<i>Deformed nuclei</i>	232
SUMMARY	232
ACKNOWLEDGMENTS	233
LITERATURE CITED	233
Table I	212
Table II	224
Table III	227

¹ The general survey of literature pertaining to this review was concluded in March 1960.

² Guest Scientist at Brookhaven National Laboratory, Upton, New York. Presently at UITP, Copenhagen, Denmark, supported by a Secretary of the Army Research and Study Fellowship.

³ Under the auspices of the United States Atomic Energy Commission.

INTRODUCTION

Internal conversion of nuclear radiation has long been used as a means for determining the angular-momentum and parity properties of nuclear transitions (1 to 5). In recent years the dependence of internal conversion on the details of nuclear structure has been made clear. As a result, internal conversion can no longer be considered a passive tool, but now provides a means for determining detailed information about nuclear structure.

In making a transition from one level to another, the atomic nucleus can give up energy k , angular momentum L , and parity π , in the form of a gamma ray. One speaks of the emission of a gamma ray of a particular multipole; electric 2^L , EL , if the parity change is $(-1)^L$, and magnetic 2^L , ML , if the parity change is $(-1)^{L+1}$. Alternatively, the nuclear transition can take place by transferring the energy, angular momentum, and parity to one of the orbital atomic electrons, K , L_I , L_{II} , L_{III} . . . ⁴ This is spoken of as the internal conversion of the electric or magnetic multipole. The ratio of the rate of electron ejection \mathcal{W}_e to the rate of gamma-ray emission \mathcal{W}_γ is defined as the *internal-conversion coefficient* α

$$\alpha = \mathcal{W}_e / \mathcal{W}_\gamma$$

The ejection of the atomic electron occurs through the interaction of the electron and nuclear currents and charges via the electromagnetic field. Outside the region of the nuclear transition currents and charges, the form of the electromagnetic field can depend only on the gross properties k , L , and π , not on the details of the nuclear current and charge distribution. The probability of ejection of an electron that does not penetrate this distribution depends only on the form and strength of the field and on the relevant electron wave functions. However, the strength of the field of a given multipole is measured by the probability of gamma-ray emission. For a nonpenetrating electron, the internal conversion coefficient, defined as the ratio of the rates, is independent of the field strength and so depends only on k , L , π , and the electron functions. Since the probability of penetration is finite but small, one expects the internal-conversion coefficient to be reasonably independent of the detailed features of the nuclear transition, except for a class of interesting transitions whose study forms the main subject of this article.

Calculations of the internal-conversion coefficients based on a point- and on a finite-size nucleus exist in the literature. The earliest tabulations were based on the Dirac wave functions for an electron in the atomic field of a point nucleus (5, 6). However, the nucleus does have a finite extent, and this affects the electron wave functions, particularly at small distances, and, hence, the computed conversion coefficients. For those cases in which the region of small distances is importantly weighted, the modifications of the coefficients are considerable. However, this is a static effect which leaves the internal-conversion coefficient independent of the dynamics of the particular

⁴ For nuclear transition energies greater than $2m_e c^2$, pair production is also possible.

transition. The importance of this static effect of the nuclear charge size was pointed out by Sliv (7, 8, 9) and has been incorporated in the most recent tabulations of internal-conversion coefficients by Sliv *et al.* (10, 11) and by Rose (12).

Of course, the electron does penetrate the nuclear region a small fraction of the time. While there, it probes the transition charges and currents, and weights them differently from a nonpenetrating electron, which sees them as in the gamma-ray matrix element. This difference leads to so-called dynamical penetration effects in internal conversion, which have important consequences.

First, the whole $E0$ mode of nuclear de-excitation occurs only through penetration effects, since there is no parallel gamma-ray mode. An $E0$ transition occurs between two states of the same spin and parity by transferring the energy, zero units of angular momentum, and no parity change to an orbital electron. While it had long been known that $0+ \rightarrow 0+$ transitions proceeded via the $E0$ mode, the possibility had been overlooked until recently in $I \rightarrow I$ transitions for $I \neq 0$ (13 to 15), even though the $E0$ mode of de-excitation is of practical importance for such transitions in heavier nuclei. Further, the $E0$ nuclear matrix element which determines this monopole rate is characteristically different from those of all other multipoles. In other words, the rate of electron ejection in an $I \rightarrow I$ nuclear transition cannot be predicted from a knowledge of the competing gamma-ray modes and a table of internal-conversion coefficients. Instead, observation of the $E0$ mode and deduction of the $E0$ matrix element provide new information about the nuclear levels involved.

There is a second, less obvious, penetration effect in the internal conversion of higher multipoles, which do have corresponding gamma-ray modes. This arises because the penetrating electron sees a weighting of the nuclear transition charges and currents different from that appearing in the usual gamma-ray matrix element (16). Formally, this means that an additional nuclear matrix element appears in the expression for the conversion-electron transition probability that is characteristically different from the gamma-ray matrix element. Since this penetration matrix element appears with a small weighting, the contribution of penetration effects to the total conversion probability is generally small. However, there are transitions for which the gamma-ray matrix element is greatly inhibited, while the penetration matrix elements may have their uninhibited values. For such transitions, penetration effects may be important and may produce sizable deviations from the tabulated internal-conversion coefficients. Such conversion "anomalies" are direct consequences of the dynamical effects of nuclear structure. In turn, the interpretation of such anomalies provides new types of nuclear information, which may be used to test models proposed to explain other nuclear phenomena.

The dynamic-penetration matrix elements in internal conversion are the transition analogues of static penetration effects. The $E0$ transition mode is

related to the isotope shift. The penetration effects in magnetic-dipole transitions are the analogues of the matrix elements introduced by Bohr & Weisskopf (17, 18) to explain anomalies in magnetic hyperfine structure.

The current interest in internal conversion lies in the observation and study of dynamical penetration effects, with the object of uncovering a new body of nuclear information. The purpose of the present paper is to review the current status of this developing field and to illustrate the methods of analysis.

FORMULATION OF THE INTERACTION

The interaction between the electron and nuclear transition currents and charges occurs via the electromagnetic field. This interaction can be written in the retarded form:⁵

$$H' = - \int d\tau_n d\tau_e (j_n \cdot j_e - \rho_n \rho_e) \frac{\exp [ik|\mathbf{r}_n - \mathbf{r}_e|]}{|\mathbf{r}_n - \mathbf{r}_e|} \quad 1.$$

when the nucleus undergoes a transition from state n_i to n_f giving up energy $\hbar = E_i - E_f$, while one of the atomic electrons is lifted from state e_i to e_f . The quantities ρ_e and j_e are the usual Dirac electron transition charge and current densities

$$\begin{aligned} \rho_e &= -e\psi_{e_f}^*(\mathbf{r}_e)\psi_{e_i}(\mathbf{r}_e) \\ j_e &= -e\psi_{e_f}^*(\mathbf{r}_e)\boldsymbol{\alpha}\psi_{e_i}(\mathbf{r}_e) \end{aligned}$$

The explicit forms of the nuclear transition charge ρ_n and current j_n will be discussed later. The rate of electron ejection is proportional to the square of H' .

In a quantum-mechanical theory, the interaction, Equation 1, is only correct to lowest order in e^2 . Of course, there are higher-order terms which would be expected to make small contributions. These have not yet been worked out, although parts have been considered (3; 19 to 21). All of the fairly elaborate computations of internal conversion carried out during the past 30 years have been based on the lowest-order interaction, Equation 1, as is the work described here.

Since classification according to the multipolarity (angular-momentum and parity representation) is vital to the nuclear physicist, a multipole expansion of the electron-nuclear interaction is required. The expansion of the classical electrostatic Coulomb interaction in Legendre polynomials or spherical harmonics is a familiar example of such a multipole expansion. The multipole expansion of Equation 1 is outlined below. A more complete treatment is found in standard textbooks (22, 23).

⁵ We use relativistic units, $\hbar = c = m_e = 1$. In other words, energies are measured in units of the electron rest mass, lengths in units of the electron Compton wavelength, and time in units of the electron Compton wavelength divided by the velocity of light. The quantity e is positive, and in these units $e^2 = \alpha \approx 1/137$.

The expansion of the scalar part of the retarded interaction, Equation 1, is most directly analogous to the Coulomb decomposition and is⁶

$$\begin{aligned} \rho_n(r_n)\rho_e(r_e) \frac{\exp[ik|\mathbf{r}_n - \mathbf{r}_e|]}{|\mathbf{r}_n - \mathbf{r}_e|} \\ = 4\pi ik \sum_{\substack{L=0 \\ L,M}}^{\infty} [\rho_n(r_n)j_L(kr_n)Y_L^{M*}(\hat{\mathbf{r}}_n)][\rho_e(r_e)h_L^{(1)}(kr_e)Y_L^M(\hat{\mathbf{r}}_e)] \quad r_n \leq r_e \\ = 4\pi ik \sum_{\substack{L=0 \\ L,M}}^{\infty} [\rho_n(r_n)h_L^{(1)}(kr_n)Y_L^{M*}(\hat{\mathbf{r}}_n)][\rho_e(r_e)j_L(kr_e)Y_L^M(\hat{\mathbf{r}}_e)] \quad r_n \geq r_e \quad 3. \end{aligned}$$

The only effect of the retardation is the replacement of the Coulomb radial dependences r^L and $1/r^{L+1}$ by the spherical Bessel j_L and Hankel $h_L^{(1)}$ functions. The expansion of the current part of the interaction is further complicated by its vector nature and requires the use of vector spherical harmonics.⁷ Using these we have

$$\begin{aligned} \mathbf{j}_n(r_n) \cdot \mathbf{j}_e(r_e) \frac{\exp[ik|\mathbf{r}_n - \mathbf{r}_e|]}{|\mathbf{r}_n - \mathbf{r}_e|} \\ = 4\pi ik \sum_{\substack{L,M,i}}^{\infty} [j_n(r_n) \cdot \mathbf{A}_{LM}^{(i)*}(kr_n)][j_e(r_e) \cdot \mathbf{B}_{LM}^{(i)}(kr_e)] \quad r_n \leq r_e \\ = 4\pi ik \sum_{\substack{L,M,i}}^{\infty} [j_n(r_n) \cdot \mathbf{B}_{LM}^{(i)*}(kr_n)][j_e(r_e) \cdot \mathbf{A}_{LM}^{(i)}(kr_e)] \quad r_n \geq r_e \quad 4. \end{aligned}$$

The $\mathbf{A}_{LM}^{(i)}$, $\mathbf{B}_{LM}^{(i)}$ are the magnetic $i=m$, transverse electric $i=e$, and longitudinal $i=l$, vector potentials corresponding to total angular momentum L and Z -component M . They can be written in operator form:

$$\mathbf{A}_{LM}^{(m)}(kr) = \frac{r \times \nabla j_L(kr) Y_L^M(\hat{\mathbf{r}})}{[L(L+1)]^{1/2}} \quad \mathbf{B}_{LM}^{(m)}(kr) = \frac{\hat{\mathbf{r}} \times \nabla h_L^{(1)}(kr) Y_L^M(\hat{\mathbf{r}})}{[L(L+1)]^{1/2}} \quad 5.$$

$$\mathbf{A}_{LM}^{(e)}(kr) = -\frac{\nabla \times (r \times \nabla) j_L(kr) Y_L^M(\hat{\mathbf{r}})}{k[L(L+1)]^{1/2}} \quad \mathbf{B}_{LM}^{(e)}(kr) = -\frac{\nabla \times (r \times \nabla) h_L^{(1)}(kr) Y_L^M(\hat{\mathbf{r}})}{k[L(L+1)]^{1/2}} \quad 6.$$

$$\mathbf{A}_{LM}^{(l)}(kr) = \frac{\nabla j_L(kr) Y_L^M(\hat{\mathbf{r}})}{k} \quad \mathbf{B}_{LM}^{(l)}(kr) = \frac{\nabla h_L^{(1)}(kr) Y_L^M(\hat{\mathbf{r}})}{k} \quad 7.$$

For a given L and M , the scalar, the electric, and the longitudinal parts of the interaction have the same parity and angular-momentum selection rules. The magnetic part has the opposite parity behavior. It is therefore useful to split up the interaction along these lines into magnetic and electric terms,

$$H' = \sum_{\substack{L=1 \\ L,M}}^{\infty} H_{\text{mag}}'(L, M) + \sum_{\substack{L=1 \\ L,M}}^{\infty} H_{\text{el}}'(L, M) + H_{\text{el}}'(L=0) \quad 8.$$

and to discuss them separately.

⁶ The symbol $\hat{\mathbf{r}}$ denotes a unit vector in the radial direction.

⁷ As employed here, the star in $\mathbf{B}_{LM}^{(i)*}$ is understood not to operate on the complex Hankel function $h_L^{(1)}$.

Magnetic multipoles.—The magnetic part of the interaction is the easiest to handle, and we consider it first. Because of the change in the form, Equation 4, in going from the region $r_e \geq r_n$ to $r_e \leq r_n$, the interaction appears as the sum of two terms

$$H_{\text{mag}}'(L, M) = -4\pi ik \left[\int_0^\infty d\tau_n j_n \cdot A_{LM}^{(m)*}(k\tau_n) \int_{r_n}^\infty d\tau_e j_e \cdot B_{LM}^{(m)}(k\tau_e) + \int_0^\infty d\tau_n j_n \cdot B_{LM}^{(m)*}(k\tau_n) \int_0^{r_n} d\tau_e j_e \cdot A_{LM}^{(m)}(k\tau_e) \right] \quad 9.$$

These two terms correspond to the electron outside and inside the nuclear current. As written, there is complete symmetry between the nuclear and electron variables since we have not used the physical fact that the electron is outside the nuclear region most of the time. In order to exhibit this situation, we rewrite Equation 9 in the form

$$H_{\text{mag}}'(L, M) = -4\pi ik \left[\int_0^\infty d\tau_n j_n \cdot A_{LM}^{(m)*}(k\tau_n) \int_0^\infty d\tau_e j_e \cdot B_{LM}^{(m)}(k\tau_e) \right] + 4\pi ik \left[\int_0^\infty d\tau_n j_n \cdot A_{LM}^{(m)*}(k\tau_n) \int_0^{r_n} d\tau_e j_e \cdot B_{LM}^{(m)}(k\tau_e) - \int_0^\infty d\tau_n j_n \cdot B_{LM}^{(m)*}(k\tau_n) \int_0^{r_n} d\tau_e j_e \cdot A_{LM}^{(m)}(k\tau_e) \right] \quad 10.$$

The first term in Equation 10 is the product of two factors, the first depending only on the nuclear variables, and the second depending only on the electron variables. The nuclear factor is just the ML gamma-ray matrix element. This factorability has the simple interpretation (already seen on physical grounds) that for a nonpenetrating electron the internal-conversion coefficient is independent of any nuclear transition matrix elements.

The final two terms in Equation 10 are penetration terms and would vanish if the electron current j_e vanished inside nuclear dimensions $r_e \leq r_n$. It is obvious that the dependence on the nuclear variables in the penetration terms is not as in the first, the factorable term. To make this important point clearer, we put the penetration terms in a form as close as possible to that of the first term by combining them in the form

$$4\pi ik \int_0^\infty d\tau_n j_n \cdot A_{LM}^{(m)*}(k\tau_n) \left\{ \int_0^{r_n} d\tau_e j_e \cdot B_{LM}^{(m)}(k\tau_e) - \frac{k_L^{(1)}(k\tau_n)}{j_L(k\tau_n)} \int_0^{r_n} d\tau_e j_e \cdot A_{LM}^{(m)}(k\tau_e) \right\} \quad 11.$$

The nuclear dependence differs from that appearing in the gamma-ray matrix element by the radial factor in the curly brackets. The consequences of this difference cannot be taken into account without invoking an explicit nuclear model.

Three major tabulations of internal-conversion coefficients now exist in the literature. The earliest of these is based on the "point-nucleus" approx-

imation (5, 6), which uses electron wave functions appropriate for a point nuclear charge distribution. Further, the confinement of the nuclear currents to the origin results in the vanishing of all penetration terms.

The computations for a nucleus of finite extent were first carried out by Sliv (7 to 11), who evaluated the finite penetration terms by assuming the very simple nuclear model in which the nuclear transition current lies on the spherical nuclear surface $r_n = R$. In this case, the penetration term itself

$$4\pi ik \int_0^\infty d\tau_n j_n \cdot A_{LM}^{(m)*}(kr_n) \left\{ \int_0^R d\tau_s j_s \cdot B_{LM}^{(m)}(kr_s) - \frac{h_L^{(1)}(kR)}{j_L(kR)} \int_0^R d\tau_s j_s \cdot A_{LM}^{(m)}(kr_s) \right\} \quad 12.$$

is also separable, since the factor in brackets is now a constant. Thus for this "surface-current" model it is also possible to calculate an internal-conversion *coefficient*, which is apparently independent of nuclear matrix elements. The electron wave functions are those appropriate for a finite static nuclear charge distribution.

An alternative procedure is to set the penetration terms equal to zero, while evaluating the principal term in Equation 10 using electron wave functions appropriate to a finite charge distribution. Since the principal term is factorable, an internal conversion *coefficient* is again calculable. This "no-penetration" model is the one used by Rose in his most recent computations, which include finite-size effects (12).

In the "surface-current" approximation, the penetration terms are found to be only a few per cent of the principal term, so that one might expect the details of the models used in the evaluation of the penetration terms to be relatively unimportant. This is not necessarily the case and the penetration terms may be very important, or even dominant, in the conversion process. This would occur when the gamma-ray matrix element is anomalously small, while the penetration matrix element has its dimensional value. There is experimental and theoretical evidence for the existence of such phenomena. These points will be discussed later in detail.

Electric multipoles.—Electric multipoles require more complicated considerations in order to exhibit their penetration terms explicitly. Omitting the electric monopole ($L=0$), which will be considered separately, the electric interaction in Equation 8 has the rather cumbersome form:

$$\begin{aligned} H_{01}'(L, M) = 4\pi ik \left[\int_0^\infty d\tau_n \rho_n j_L(kr_n) Y_L^{M*}(\hat{r}_n) \int_{r_n}^\infty d\tau_s \rho_s h_L^{(1)}(kr_s) Y_L^M(\hat{r}_s) \right. \\ \left. + \int_0^\infty d\tau_n \rho_n h_L^{(1)}(kr_n) Y_L^{M*}(\hat{r}_n) \int_0^{r_n} d\tau_s \rho_s j_L(kr_s) Y_L^M(\hat{r}_s) \right. \\ \left. - \int_0^\infty d\tau_n j_n \cdot A_{LM}^{(1)*}(kr_n) \int_{r_n}^\infty d\tau_s j_s \cdot B_{LM}^{(1)}(kr_s) \right] \end{aligned}$$

$$\begin{aligned}
& - \int_0^\infty d\tau_n j_n \cdot B_{LM}^{(l)*}(k\tau_n) \int_0^{\tau_n} d\tau_e j_e \cdot A_{LM}^{(l)}(k\tau_e) \\
& - \int_0^\infty d\tau_n j_n \cdot A_{LM}^{(e)*}(k\tau_n) \int_{\tau_n}^\infty d\tau_e j_e \cdot B_{LM}^{(e)}(k\tau_e) \\
& - \int_0^\infty d\tau_n j_n \cdot B_{LM}^{(e)*}(k\tau_n) \int_0^{\tau_n} d\tau_e j_e \cdot A_{LM}^{(e)}(k\tau_e) \Big] \quad 13.
\end{aligned}$$

There are a number of related difficulties with the above form. First, the expected overall factorability into a pure electron part and the *EL* nuclear gamma-ray matrix element,

$$\int d\tau_n j_n \cdot A_{LM}^{(e)*}(k\tau_n) \quad 14.$$

is not apparent in the point-nucleus limit because the scalar and longitudinal terms have different nuclear matrix elements. Second, in the point-nucleus limit, the transverse and longitudinal electron integrals diverge at their lower limit. The resolution of these related difficulties was given long ago by Dancoff & Morrison (24). Their solution has recently been re-examined in detail by Kramer (25) in order to extract the penetration terms. The key is the use of the continuity equations

$$\nabla \cdot j_e + ik\rho_e = 0, \quad \nabla \cdot j_n - ik\rho_n = 0 \quad 15.$$

which connect the three rather differently appearing terms in Equation 13. To show this we first rewrite $B_{LM}^{(e)}$, $A_{LM}^{(e)}$ in the equivalent forms:

$$\begin{aligned}
B_{LM}^{(e)}(kr) &= \frac{1}{k[L(L+1)]^{1/2}} \left\{ \nabla \frac{d}{dr} + k^2 \hat{r} \right\} r h_L^{(1)}(kr) Y_L^M(\hat{r}) \\
A_{LM}^{(e)}(kr) &= \frac{1}{k[L(L+1)]^{1/2}} \left\{ \nabla \frac{d}{dr} + k^2 \hat{r} \right\} r j_L(kr) Y_L^M(\hat{r}) \quad 16.
\end{aligned}$$

and indicate that it is the gradient term in $B_{LM}^{(e)}$ that causes the divergence difficulty.

The Dancoff-Morrison solution consisted of replacing the transverse interaction by one which differs from it by a "gauge-transformation" designed to remove the offending part:

$$j_e \cdot B_{LM}^{(e)} \rightarrow j_e \cdot B_{LM}^{(e)} - [j_e \cdot \nabla \Delta_{LM} - ik\rho_e \Delta_{LM}] \quad 17.$$

where

$$\Delta_{LM}(kr) = \frac{1}{k[L(L+1)]^{1/2}} \frac{d}{dr} r h_L^{(1)}(kr) Y_L^M(\hat{r}) \quad 18.$$

Although the added term in Equation 17 has the appearance of a gauge transformation, it would give a nonvanishing contribution to the incomplete integral in which it appears in Equation 13. Instead, the transverse electric term can be rewritten by explicitly adding in and subtracting out the "gauge" terms:

$$\begin{aligned}
& -4\pi i k \left\{ \int_0^\infty d\tau_n j_n \cdot A_{LM}^{(*)}(k\tau_n) \int_{\tau_n}^\infty d\tau_e [j_e \cdot (B_{LM}^{(*)}(k\tau_e) - \nabla \Lambda_{LM}(k\tau_e)) + ik\rho_e \Lambda_{LM}(k\tau_e)] \right. \\
& - \int_0^\infty d\tau_n j_n \cdot B_{LM}^{(*)}(k\tau_n) \int_0^{\tau_n} d\tau_e [j_e \cdot (A_{LM}^{(*)}(k\tau_e) - \nabla \lambda_{LM}(k\tau_e) + ik\rho_e \lambda_{LM}(k\tau_e)] \\
& + \int_0^\infty d\tau_n j_n \cdot A_{LM}^{(*)}(k\tau_n) \int_{\tau_n}^\infty d\tau_e [j_e \cdot \nabla \Lambda_{LM}(k\tau_e) - ik\rho_e \Lambda_{LM}(k\tau_e)] \\
& \left. - \int_0^\infty d\tau_n j_n \cdot B_{LM}^{(*)}(k\tau_n) \int_0^{\tau_n} d\tau_e [j_e \cdot \nabla \lambda_{LM}(k\tau_e) - ik\rho_e \lambda_{LM}(k\tau_e)] \right\} \quad 19.
\end{aligned}$$

where λ_{LM} differs from Λ_{LM} only in the replacement of $h_L^{(1)}$ by j_L . These last two, the "gauge" terms, can be shown to cancel exactly the sum of the longitudinal and scalar terms which complete the electric interaction in Equation 13. The demonstration of this remarkable result can be achieved by straightforward manipulation, using the continuity equations for the electron and nuclear currents. We do not repeat the details, which are given in the paper of Kramer (25).

The electric interaction may now be put in a form strictly analogous to that already achieved for magnetic transitions, Equation 10:

$$\begin{aligned}
H_{el}'(L, M) &= \frac{-4\pi i}{[L(L+1)]^{1/2}} \int_0^\infty d\tau_n j_n \cdot A_{LM}^{(*)}(k\tau_n) \int_0^\infty d\tau_e \left[j_e \cdot k^2 \hat{r}_e + \rho_e i k \frac{d}{d\tau_e} \right] r_e h_L^{(1)}(k\tau_e) Y_{LM}(\hat{r}_e) \\
&+ \frac{4\pi i}{[L(L+1)]^{1/2}} \left\{ \int_0^\infty d\tau_n j_n \cdot A_{LM}^{(*)}(k\tau_n) \int_0^{\tau_n} d\tau_e \left[j_e \cdot k^2 \hat{r}_e + \rho_e i k \frac{d}{d\tau_e} \right] r_e h_L^{(1)}(k\tau_e) Y_{LM}(\hat{r}_e) \right. \\
&\left. - \int_0^\infty d\tau_n j_n \cdot B_{LM}^{(*)}(k\tau_n) \int_0^{\tau_n} d\tau_e \left[j_e \cdot k^2 \hat{r}_e + \rho_e i k \frac{d}{d\tau_e} \right] r_e j_L(k\tau_e) Y_{LM}(\hat{r}_e) \right\} \quad 20.
\end{aligned}$$

The first term is separable and finite. It is just this term which is the basis of the early "point-nucleus" calculations (5, 6).

Sliv, in his finite-nucleus computations for electric transitions (10, 11), includes the penetration terms, as for the magnetic transitions, by invoking the "surface-current" nuclear model, for which

$$\frac{\int_0^\infty d\tau_n j_n \cdot B_{LM}^{(*)}(k\tau_n)}{\int_0^\infty d\tau_n j_n \cdot A_{LM}^{(*)}(k\tau_n)} \simeq -\frac{L}{L+1} \frac{h_L^{(1)}(kR)}{j_L(kR)} \quad 21.$$

The electric interaction is then:

$$\begin{aligned}
H_{el}'(L, M) &= \frac{-4\pi i}{[L(L+1)]^{1/2}} \int_0^\infty d\tau_n j_n \cdot A_{LM}^{(*)}(k\tau_n) \left\{ \int_0^\infty d\tau_e \left[j_e \cdot k^2 \hat{r}_e + \rho_e i k \frac{d}{d\tau_e} \right] r_e h_L^{(1)}(k\tau_e) Y_{LM}(\hat{r}_e) \right. \\
&\quad \left. - \int_0^R d\tau_e \left[j_e \cdot k^2 \hat{r}_e + \rho_e i k \frac{d}{d\tau_e} \right] r_e h_L^{(1)}(k\tau_e) Y_{LM}(\hat{r}_e) \right. \\
&\quad \left. - \frac{L}{L+1} \frac{h_L^{(1)}(kR)}{j_L(kR)} \int_0^R d\tau_e \left[j_e \cdot k^2 \hat{r}_e + \rho_e i k \frac{d}{d\tau_e} \right] r_e j_L(k\tau_e) Y_{LM}(\hat{r}_e) \right\} \quad 22.
\end{aligned}$$

This expression is in the factorable form necessary for the computation of a conversion coefficient. Rose (12) carries through his finite-size computations for electric transitions with a "no-penetration" model, in which the penetration terms in Equation 20 are set equal to zero.

As in the magnetic case, both of these tabulations of conversion coefficients are based on the assumption of convenient values for the dynamical nuclear effects contained in the penetration terms. In reality, there may be very large deviations from these values. The investigation of these effects constitutes the main part of the rest of the present article.

Electric monopole.—The electric monopole ($L=0$, no parity change) is different from all other electric multipoles in that there is no transverse part, and so no corresponding $E0$ gamma-ray matrix element. The $L=0$ scalar and longitudinal terms can be combined into the monopole part of the Coulomb interaction:

$$H_{e1}'(L=0) = \int_0^\infty d\tau_n \int_r^\infty d\tau_a \rho_n \rho_a \frac{1}{r_a} + \int_0^\infty d\tau_n \int_0^r d\tau_a \rho_n \rho_a \frac{1}{r_n} \quad 23.$$

This simple form can also be derived directly. One can choose any gauge for the form of the electromagnetic interaction, and this choice can be made separately for each multipole. We are, then, free to use the gauge that results in an instantaneous Coulomb interaction plus a transverse retarded interaction. Since there is no $L=0$ transverse term, all of the electric monopole comes from the Coulomb interaction, given in Equation 23. It follows immediately that there is no corresponding magnetic monopole ($L=0$ yes), since any $L=0$ mode must come from the electrostatic interaction, which has no negative-parity monopole part.

That the electric-monopole interaction is entirely a penetration effect is obvious if Equation 23 is first recast in the form:

$$H_{e1}'(L=0) = \left(\int_0^\infty d\tau_n \rho_n \right) \left(\int_0^\infty d\tau_a \rho_a \frac{1}{r_a} \right) + \int_0^\infty d\tau_n \rho_n \int_0^r d\tau_a \rho_a \left(\frac{1}{r_n} - \frac{1}{r_a} \right) \quad 24.$$

and it is noted that since the total nuclear charge is a constant it can have no off-diagonal matrix elements:

$$\int d\tau_n \rho_n = 0 \quad 25.$$

Therefore,

$$H_{e1}'(L=0) = \int_0^\infty d\tau_n \rho_n \int_0^r d\tau_a \rho_a \left(\frac{1}{r_n} - \frac{1}{r_a} \right) \quad 26.$$

The $E0$ mode of electron ejection arises entirely from dynamical nuclear structure effects. There are no monopole gamma rays, and so it is meaningless to speak of an $E0$ conversion coefficient. The rate of $E0$ conversion may be written in the customary form of an electron factor times the square of a nuclear matrix element. Computations of the electron factor for various

electron shells, atomic numbers, and transition energies are available in graphical form in the literature (13, 15, 26, 27).

STATIC EFFECTS OF NUCLEAR STRUCTURE

The computations of Sliv *et al.* (10, 11) and of Rose (12) include the static effect of the finite extent of the nuclear charge distribution. These results are easily available in tabular form. Both computations consider the nuclear charge as uniformly distributed in a sphere of conventional radius, $R = 1.2 A^{1/3} \times 10^{-13}$ cm. They do deal differently with the penetration terms, however; but since these are at most only a few per cent of the principal term, the two sets of coefficients ought to be in agreement within a few per cent. Unfortunately, there appear to be unexplained residual disagreements between the two tabulations.

Nuclear size and charge distribution.—Going from a point nucleus to one of finite extent brings about a large change in the internal-conversion coefficients for the lower magnetic and the higher electric multipoles in heavy elements. For example, the $M1$ internal-conversion coefficient is decreased by 30 to 40 per cent. From this it might be thought that the conversion coefficients are particularly sensitive to the assumed nuclear radius or charge distribution. They are not.

To see why, we examine the internal conversion of an $M1$ transition in the K shell. In nonrelativistic language,⁸ the K shell is an $s_{1/2}$ state, and the addition of one unit of angular momentum and no parity change leads to either an $s_{1/2}$ or $d_{3/2}$ final continuum state. In relativistic notation the K shell is a $\kappa = -1$ state, and an $M1$ transition leads to either a final continuum $\kappa = -1$ or $\kappa = +2$ state.

The K -shell internal-conversion coefficient is the sum of two partial conversion coefficients, one for each of the two final states:

$$\alpha_{M1}^K = \alpha_{M1}^{K \rightarrow s_{1/2}} + \alpha_{M1}^{K \rightarrow d_{3/2}} = \frac{1}{12k} \sum_M \left\{ \frac{|\langle e_f = s_{1/2} | H_{\text{mag}}'(1, M) | e_i = K \rangle|^2}{\left| \int d\tau_n j_n \cdot A_{LM}^{(m)*}(kr_n) \right|^2} + \frac{|\langle e_f = d_{3/2} | H_{\text{mag}}'(1, M) | e_i = K \rangle|^2}{\left| \int d\tau_n j_n \cdot A_{LM}^{(m)*}(kr_n) \right|^2} \right\} \quad 27.$$

The first term, which corresponds to a final electron $s_{1/2}$ continuum state, is by far the largest and most strongly affected by finite-size effects. The $d_{3/2}$ final state is small in the region of the origin and so is relatively unaffected by a change in the potential extending over nuclear dimensions. It is sufficient to discuss the $s_{1/2}$ partial conversion coefficient only.

The quantity H' in Equation 27 contains both radial and angular integrations over the electron variables. As already seen, the radial dependence

⁸ We use the descriptive nonrelativistic language for indicating the corresponding relativistic states.

breaks up the interaction into a principal term plus penetration terms. The principal and penetration terms have a common electron angular dependence, characteristic of the transition considered. After carrying out the trivial angular integrations, the expression for the partial conversion coefficient of interest here may be written:

$$\alpha_{M1K \rightarrow s_{1/2}} = \frac{4\pi\alpha k}{3} |R_{s_{1/2}}|^2$$

$$R_{s_{1/2}} = \int_0^\infty dr r^2 (f_{s_{1/2}} g_K + g_{s_{1/2}} f_K) h_1^{(1)}(kr) \\ - \frac{h_1^{(1)}(kR)}{j_1(kR)} \int_0^R dr r^2 (f_{s_{1/2}} g_K + g_{s_{1/2}} f_K) j_1(kr) \quad 28.$$

The radial factor $R_{s_{1/2}}$ consists of a main term plus a penetration term which is written here for the "surface-current" model. In the "no-penetration" model, the penetration term in Equation 28 is simply omitted. The quantities f_K and g_K are the usual "small" and "large" radial Dirac amplitudes of the bound K -shell wave functions, and $f_{s_{1/2}}$ and $g_{s_{1/2}}$ are the corresponding continuum functions. Both the bound and continuum functions are understood to be those appropriate for a nuclear charge distribution of finite extent.

In the computations of Sliv *et al.* (10, 11) and of Rose (12), these electron wave functions were obtained by numerical integration for the particular case of a uniformly charged spherical nucleus of radius R . However, to gain insight into the effects of variation of the radius and charge distribution, we follow a simpler but approximate, analytic procedure (7, 8; 28 to 30). A brief outline is given below.

Outside the nuclear charge distribution, the electron wave functions are linear combinations of regular and irregular Coulomb solutions of the appropriate energies. Only such small distances—defined by $(p_{ef}r) \ll 1$, $(\alpha Zr) \ll 1$ —will be of interest that the asymptotic forms of these functions are adequate. For the bound and continuum states, which are both $\kappa = -1$ in this case, the radial functions are in the region $r \geq R$:

$$f \simeq - \left(\frac{1 - \gamma_1}{1 + \gamma_1} \right)^{1/2} N r^{\gamma_1 - 1} - \left(\frac{1 + \gamma_1}{1 - \gamma_1} \right)^{1/2} \bar{N} r^{-\gamma_1 - 1} \\ g \simeq N r^{\gamma_1 - 1} + \bar{N} r^{-\gamma_1 - 1} \\ \gamma_1 = (1 - (\alpha Z)^2)^{1/2} \quad 29.$$

The constants N, \bar{N} , weighting the regular and irregular functions, are determined by matching these external solutions to the internal solutions at $r = R$ and by the requirement of overall normalization. However, since the irregular solution dies off rather quickly relative to the regular, its contribution to the normalization is small. A useful simplifying approximation consists of taking the weighting factor of the regular solution N to be the same as in the point nucleus case, and determining \bar{N} by matching at the nuclear surface.

The internal solutions, $r \leq R$, have the approximate form:

$$\begin{aligned}
&= \mathcal{K}r\phi(r) \\
g &= \mathcal{K}J(r) \\
J(r) &= 1 - \int_0^r dr' \frac{V(r')}{r'^2} \int_0^{r'} dr'' r''^{1/2} V(r'') J(r'') \\
\phi(r) &= \frac{1}{r^3} \int_0^r dr' r'^{1/2} V(r') J(r')
\end{aligned} \tag{30}$$

where \mathcal{K} is the internal constant to be determined by matching. These forms neglect small terms of order $(\alpha Z r)^2$, but have the virtue of exhibiting the dependence on the potential $V(r)$ in a simple, direct fashion. Very roughly, for $r \leq R$

$$\begin{aligned}
f &\sim 1 & \phi &\sim -\frac{\alpha Z}{2R} \\
f &\sim -\frac{\alpha Z}{2R} \frac{r}{R} \mathcal{K} & g &\sim \mathcal{K}
\end{aligned} \tag{31}$$

These results are in sharp contrast to the point Coulomb solutions, which blow up at small distances because of the r^{γ_1-1} . It is this striking difference that is responsible for the large modification in the internal-conversion coefficients due to the finite nuclear size.

Putting the results of these analyses together, the $\kappa = -1$ wave functions for a nucleus of finite extent can be written for small distances as

$$\begin{aligned}
f &= -\left(\frac{1-\gamma_1}{1+\gamma_1}\right)^{1/2} N r^{\gamma_1-1} \left[1 + S \left(\frac{1+\gamma_1}{1-\gamma_1}\right) \left(\frac{R}{r}\right)^{2\gamma_1} \right] \Bigg|_{r \geq R} \\
&= N r^{\gamma_1-1} \left[1 + S \left(\frac{R}{r}\right)^{2\gamma_1} \right] \\
f &= \mathcal{K}r\phi(r) \Bigg\{ \\
&= \mathcal{K}J(r) \Bigg\} \quad r \leq R
\end{aligned} \tag{32}$$

where

$$S = -\frac{\left(\frac{1-\gamma_1}{1+\gamma_1}\right)^{1/2} + \frac{R\phi(R)}{J(R)}}{\left(\frac{1+\gamma_1}{1-\gamma_1}\right)^{1/2} + \frac{R\phi(R)}{J(R)}} \tag{33}$$

$$\mathcal{K} = \frac{N R^{\gamma_1-1}}{J(R)} \frac{\left(\frac{1+\gamma_1}{1-\gamma_1}\right)^{1/2} - \left(\frac{1-\gamma_1}{1+\gamma_1}\right)^{1/2}}{\left(\frac{1+\gamma_1}{1-\gamma_1}\right)^{1/2} + \frac{R\phi(R)}{J(R)}} \tag{34}$$

and N is the appropriate point-nucleus normalization coefficient for either the bound K shell or the continuum $s_{1/2}$ state. Inside the charge distribution, $r \leq R$, the wave functions are very different from point-charge functions at the same radius. Outside, $r \geq R$, the difference between the two is only in the small term involving the factor S . These simple expressions for the radial wave functions, Equation 32, are valid at small distances, say $r < \xi$, where ξ

is of the order $10R$. Fortunately, it is only within this region that there is an important difference between the finite-size and point-nucleus wave functions. For $r > \xi$ the differences may be neglected.

The difference between the radial factors $R_{s_{1/2}}$ for a finite nucleus and a point nucleus may now be rearranged and written as:

$$R_{s_{1/2}} - R_{s_{1/2} \text{ point}} = \left[\int_R^\xi dr r^2 \{ (f_{s_{1/2}} g_K + g_{s_{1/2}} f_K) - (f_{s_{1/2}} g_K + g_{s_{1/2}} f_K)_{\text{point}} \} h_1^{(1)}(kr) \right] \\ + \left[\frac{h_1^{(1)}(kR)}{j_1(kR)} \int_0^R dr r^2 (f_{s_{1/2}} g_K + g_{s_{1/2}} f_K) j_1(kr) \right. \\ \left. - \int_0^R dr r^2 (f_{s_{1/2}} g_K + g_{s_{1/2}} f_K)_{\text{point}} h_1^{(1)}(kr) \right] \quad 35.$$

The first term is the outside contribution to the difference, where the upper limit has been taken as ξ , since point and finite functions are the same beyond this point. The second term is the difference between the inside contributions. Inserting the wave functions of Equations 32 to 34, we find to lowest order:

$$R_{s_{1/2}} - R_{s_{1/2} \text{ point}} \\ \approx - \frac{2i}{k^2} \left(\frac{1 - \gamma_1}{1 + \gamma_1} \right)^{1/2} N_K N_{s_{1/2}} R^{2\gamma_1-1} \left[\frac{-2}{1 - \gamma_1} S + \left(-\frac{1}{5} + \frac{1}{2\gamma_1 - 1} \right) \right] \quad 36.$$

The largest term in the square bracket in Equation 36 is $1/(2\gamma_1 - 1)$, which is just the point-nucleus contribution in the region $0 \leq r \leq R$. In the finite-size case this large term is replaced by the much smaller value, $\frac{1}{5}$. The term proportional to S is the small difference arising from the region outside the nucleus. It should be emphasized that the important change in going from the point nucleus to the finite nucleus is in dropping the singular Dirac Coulomb wave functions in the region where they make no physical sense, namely within the nuclear charge. Once this singular contribution is removed, the contribution from the nuclear region is no longer very important. This accounts for the insensitivity of the finite-size conversion coefficients to variations of the description of the static nuclear charge distribution.

With the above machinery, it is easy to compute the effects of variations of the nuclear charge distribution. Using the very adequate approximation of ignoring the $d_{3/2}$ contribution to the total conversion, and taking the phase of the $s_{1/2}$ contribution from a study of its behavior in the important region of small r , we have

$$R_{s_{1/2}} \approx i \left[\frac{3}{4\pi\alpha k} \alpha_{M1^K} \right]^{1/2} \\ \frac{\alpha_{M1^K} (\text{Sliv})}{\alpha_{M1^K} (\text{point})} \approx \left[1 - \frac{2}{k^2} \left(\frac{1 - \gamma_1}{1 + \gamma_1} \right)^{1/2} N_K N_{s_{1/2}} R^{2\gamma_1-1} \right. \\ \left. \cdot \left(\frac{4\pi\alpha k}{3\alpha_{M1^K} (\text{point})} \right)^{1/2} \left(-\frac{2}{1 - \gamma_1} S - \frac{1}{5} + \frac{1}{2\gamma_1 - 1} \right) \right]^2 \quad 37.$$

For example, for $Z \simeq 82$, $\gamma_1 = 0.8$, and for a uniform charge distribution of radius $R = 1.2 A^{1/3} \times 10^{-13}$, $S = -0.030$. Equation 37 then indicates that the finite nuclear size reduces the $M1$ K -conversion coefficient to about 70 per cent of its point-nucleus value. Increasing the radius by 10 per cent results in a further decrease of only about 2 per cent.

One might be concerned about the use of a uniform charge distribution with a sharp cutoff, which is known from high-energy electron scattering data (31) to be unrealistic. A charge distribution more in line with these results, but still simple enough for our purpose, is:

$$\rho(r) = \frac{21}{16\pi} \frac{Z}{R'^3} \left[1 - \left(\frac{r}{R'} \right)^4 \right] \quad r \leq R'$$

$$= 0 \quad r \geq R' \quad 38.$$

The parameter R' is chosen to be $(9/7)^{1/2}R$ in order that this distribution shall have the same mean-square charge radius as does the uniform distribution. In this case, $S = -0.025$. The $M1$ K -shell coefficient changes by less than 0.5 per cent when this more realistic charge distribution is substituted for the uniform one.

The above considerations indicate the degree of validity of the computed $M1$ K -shell internal-conversion coefficients. The uncertainties in nuclear radius and shape reflect themselves as an uncertainty of only a few per cent in the conversion coefficients. Similar analyses may be carried through for higher magnetic multipoles. Conversion of higher multipoles means that higher values of angular momentum are transferred to the electron. The effects of finite size and shape are decreasingly important for these higher-angular-momentum waves. The net effect on the magnetic conversion coefficient and its sensitivity to nuclear size and shape, therefore, decreases with increasing multipole order. Similar remarks are expected to apply to conversion in the L and higher atomic shells.

Effects of the nuclear charge distribution are generally less for electric conversion than for magnetic, and the coefficients are correspondingly even less sensitive to variations in the physical assumptions used in their computation. The K -shell conversion of EL transitions leads to two final electron states: $j = L + \frac{1}{2}$ and $j = L - \frac{1}{2}$, both of orbital angular momentum L . The state of lower j , as in the magnetic case, leads to radial electron matrix elements which are strongly affected by finite-size effects. However, in contrast with the magnetic case, the state of higher j involves electron matrix elements of the same order of magnitude, since the $j = L \pm \frac{1}{2}$ electron wave functions are comparable at moderate distances. Further, cancellation occurs among the radial electron matrix elements for the state of lower j , so that its net contribution to the total conversion coefficient is small in cases of practical interest. The finite size produces moderate effects on this small quantity. The total EL conversion coefficient is therefore insensitive to the static effects of the nuclear charge distribution. It should be emphasized that we have so far used convenience definitions of the penetration matrix elements

and have not yet included the range of dynamical effects that can arise from these matrix elements.

Static nuclear moments.—We have so far considered only a spherically symmetric static nuclear charge distribution. However, it is well known that there are nuclei which have large static deformations and correspondingly large static electric-quadrupole moments. One can also ask about the effect of static magnetic-dipole moments on the electron wave functions and so on the conversion process. These matters have not been very deeply explored, and we have only the results of a first-order perturbation calculation on the K -shell wave functions to guide us (32).

The effect of a nuclear magnetic moment μ is to add to the electron energy the usual spin interaction, which has the form

$$-e\mathbf{u} \cdot \frac{\boldsymbol{\alpha} \times \mathbf{r}}{r^3} \quad 39.$$

outside the nuclear structure, and is some finite function, depending on the distribution of magnetism, inside. The effect of this perturbation on the bound K -shell wave functions, which can be written symbolically as $(1s_{1/2}^2, J=0)$, is to add in $(s_{1/2}', 1s_{1/2}, J=1)$ and $(d_{3/2}', 1s_{1/2}, J=1)$ components. If we confine ourselves to the point-nuclear problem, the relativistic first-order wave functions can be obtained in closed form. For present purposes, it is sufficient to note that at small distances, where the perturbation has its maximum importance, the orders of magnitude of the perturbation amplitudes are given by

$$\left| \frac{f'}{f_{K \text{ point}}} \right| \sim \left| \frac{g'}{g_{K \text{ point}}} \right| \sim \mu e \frac{\alpha Z}{r} \quad 40.$$

The finite size of the nuclear-charge and static-magnetic-moment distributions would change this divergent result into a finite one within nuclear dimensions. However, since the perturbation wave function, Equation 40, is only 10^{-3} – 10^{-4} of the unperturbed K -shell wave function at $r=R$, the effect of a static magnetic-dipole moment is negligible. If we can extrapolate from these results for the K shell to the assumption of similar behavior for the continuum states, the effects of the magnetic moment on the K -conversion coefficients themselves should also be negligible. Similar results are expected for conversion in higher atomic shells.

A static nuclear quadrupole moment can be considered in quite an analogous manner. In first order, the quadrupole perturbation adds $(d_{3/2}', 1s_{1/2}, J=2)$ and $(d_{5/2}', 1s_{1/2}, J=2)$ components to the K -shell wave function. Again it is possible to solve the relativistic first-order equation in closed form. The orders of magnitude of the perturbation amplitudes at small distances are found to be

$$\left| \frac{f'}{f_{K \text{ point}}} \right| \sim \frac{1}{10\alpha Z} \frac{\alpha Q}{r^2} \quad \left| \frac{g'}{g_{K \text{ point}}} \right| \sim \frac{\alpha Z}{10} \frac{\alpha Q}{r^2} \quad 41.$$

where Q is the quadrupole moment of the nucleus. The divergent behavior

as $r \rightarrow 0$ is again characteristic of the assumed point-moment interaction, and for a finite nucleus there is no real divergence. For present purposes, we use Equation 41 for $r \geq R$ only and neglect the inside region. For a large static quadrupole moment ($Q \sim 10R^2$) the perturbation amplitude is only a few per cent of the unperturbed point-nucleus wave function value at $r = R$ and drops off very rapidly at larger distances.

For nuclear transitions ending in a spin 0 or $\frac{1}{2}$ state, there is no quadrupole effect on the continuum state. In this case the effect of the quadrupole moment on the conversion coefficient comes only via the perturbation of the initial, bound state and may be estimated. For $M1$ and $E2$ K conversion, for example, the quadrupole perturbation of the K shell affects the K -conversion coefficients by only a per cent or so in practical cases.

The static quadrupole perturbation can produce a large effect in EL conversion, but only in cases of no immediate practical importance. As an example, consider $E3$ conversion in the K shell. An electron initially in an $s_{1/2}$ state is ejected as a final $f_{5/2}$ or $f_{7/2}$ wave. Because the quadrupole perturbation adds a ($d_{5/2}'$, $1s_{1/2}$, $J=2$) component into the initial ($1s_{1/2}^2$, $J=0$) configuration, it is possible to have a very strong transition from this component to the ($p_{1/2}$, $1s_{1/2}$, $J=1, 0$) final electron state. However, since the total angular momentum of nucleus and electron system must be conserved, this can only be the case if the initial and final nuclear spins add vectorially to 1 or 0. However, in these cases competing $E1$ and $M2$ transitions are also possible, and would presumably so dominate the transition that any aspect of the $E3$ component would be only academic.

The effects of the static nuclear moments are actually parts of the contributions to the electron-nuclear interaction of the next higher order in α . There are many types of perturbation terms describing these higher-order interactions which involve electron and nuclear intermediate states. The static moments have been considered here because they suggest themselves on a different physical basis.

Summary.—Tabulations of internal-conversion coefficients computed on a reasonable basis exist in the literature. They are insensitive to specific assumptions about the static nuclear charge distribution made in their computation. However, these results are expected to be realistic only when special penetration effects are not important.

How good is the agreement with experiment? In a recent review, Listengarten (33) indicated that the data are in agreement with the conversion coefficients computed taking the finite extent of the nuclear charge into account. Nevertheless, there is some disturbing evidence. Some of the most accurate measurements of pure $E2$ internal-conversion coefficients, of $2+ \rightarrow 0+$ transitions in several rare-earth nuclei (34), are reported to be about 20 per cent higher than the tabulated values. Dynamical effects are expected to be very small for these fast transitions. No theoretical or experimental explanation has yet been given for this discrepancy.

The establishment of agreement or disagreement between experiment

and tabulation at this stage is critical, since it is only by reference to these tabulations that the dynamical conversion effects can be exhibited.

DYNAMICAL EFFECTS IN MAGNETIC TRANSITIONS

In this section, we turn to a closer examination of the penetration matrix elements and the different model-dependent selection rules which they and the gamma-ray matrix element obey. First, however, we must display these penetration matrix elements in their most useful form.

The interaction for ML conversion has already been written in the form

$$H_{\text{mag}}'(L, M) = -4\pi i k \int_0^\infty d\tau_n j_n \cdot A_{LM}^{(m)*}(k\tau_n) \int_0^\infty d\tau_s j_s \cdot B_{LM}^{(m)}(k\tau_s) \\ + 4\pi i k \int_0^\infty d\tau_n j_n \cdot A_{LM}^{(m)*}(k\tau_n) \left\{ \int_0^\tau d\tau_s j_s \cdot B_{LM}^{(m)}(k\tau_s) \right. \\ \left. - \frac{h_L^{(1)}(k\tau_n)}{j_L(k\tau_n)} \int_0^\tau d\tau_s j_s \cdot A_{LM}^{(m)}(k\tau_s) \right\} \quad 42.$$

After carrying out the electron angular integration common to all terms,

$$H_{\text{mag}}'(L, M) \\ = B(ML, M; e_i, e_f) \left[\int_0^\infty d\tau_n j_n \cdot A_{LM}^{(m)*}(k\tau_n) \int_0^\infty d\tau_s e^2 (g_{ef} f_{e_i} + f_{e_j} g_{e_i}) h_L^{(1)}(k\tau_s) \right. \\ \left. - \int_0^\infty d\tau_n j_n \cdot A_{LM}^{(m)*}(k\tau_n) \left\{ \int_0^\tau d\tau_s e^2 (g_{ef} f_{e_i} + f_{e_j} g_{e_i}) h_L^{(1)}(k\tau_s) \right. \right. \\ \left. \left. - \frac{h_L^{(1)}(k\tau_s)}{j_L(k\tau_s)} \int_0^\tau d\tau_s e^2 (g_{ef} f_{e_i} + f_{e_j} g_{e_i}) j_L(k\tau_s) \right\} \right] \quad 43.$$

The factor $B(ML, M; e_i, e_f)$ is the result of the angular integrations and depends on the initial and final, total and orbital angular momenta, symbolically represented by e_i, e_f .

In the numerical tabulations of Sliv *et al.* (10, 11), the penetration terms of Equation 43 are evaluated for the "surface-current" model. The exact general expression may be written as the product of these tabulated values and a correction factor containing the dynamical effects. It is easily seen that each partial conversion coefficient is then precisely

$$\alpha_{ML}^{e_i \rightarrow e_f} = \alpha_{ML}^{e_i \rightarrow e_f}(\text{Sliv}) \left| 1 - \frac{\int_0^\infty d\tau_n j_n \cdot A_{LM}^{(m)*}(k\tau_n) [c_{j_f}(r_n) - c_{j_f}(R)]}{\int_0^\infty d\tau_n j_n \cdot A_{LM}^{(m)*}(k\tau_n)} \right|^2 \\ = \alpha_{ML}^{e_i \rightarrow e_f}(\text{Sliv}) \left| 1 - c_{j_f}(R) \left[\frac{\int_0^\infty d\tau_n j_n \cdot A_{LM}^{(m)*}(k\tau_n) c_{j_f}(r_n) / c_{j_f}(R)}{\int_0^\infty d\tau_n j_n \cdot A_{LM}^{(m)*}(k\tau_n)} - 1 \right] \right|^2 \quad 44.$$

The radial weighting function $c_{jf}(r)$ is the ratio of the coefficient of $j_n \cdot A_{LM}^{(m)*}$ in the penetration term of Equation 43 to the sum of all of the coefficients of $j_n \cdot A_{LM}^{(m)*}$ evaluated for the "surface-current" model. A form similar to Equation 44, but based on the Rose tabulations, is obtained by letting $R \rightarrow 0$ everywhere. The function $c_{jf}(r)$ represents the additional radial weighting of the nuclear currents in the penetration matrix elements relative to that in the gamma-ray matrix element. It is this different radial weighting that makes the penetration terms characteristically different from the gamma-ray matrix element.

The ML conversion coefficient is determined by the important penetration parameter appearing in Equation 44.

$$\lambda = \frac{\int d\tau_n j_n \cdot A_{LM}^{(m)*}(kr_n) c_{jf}(r) / c_j(R)}{\int d\tau_n j_n \cdot A_{LM}^{(m)*}(kr_n)} = \frac{M_e}{M_\gamma} \quad 45.$$

In the "surface-current" model employed by Sliv *et al.*, $\lambda = +1$.

The function c_{jf} .—The weighting function $c_{jf}(r)$ depends on the electron wave functions in the vicinity of the nucleus. Following the procedure outlined in Equations 29 to 34, it is fortunately simple to calculate, for each of the possible final states, the Dirac electron wave functions at small distances, of the order of nuclear dimensions.

Analogously to $M1$, ML conversion in the K shell leads to two final electron states, $j_f = L - \frac{1}{2}$ ($\kappa = -L$), and $j_f = L + \frac{1}{2}$ ($\kappa = L + 1$). The first, corresponding to a much higher electron density at the nucleus, leads to a much stronger weighting of its penetration matrix element. It is also this transition to the $j_f = L - \frac{1}{2}$ state which dominates the total conversion. In the region of practical interest, $Z > 50$, $k < 1.5 m_e c^2$, the partial conversion coefficient to the $j_f = L - \frac{1}{2}$ final state is always more than 10 times that to the $j_f = L + \frac{1}{2}$ state. It is then a reasonable and useful simplification to ignore penetration effects in the $j = L + \frac{1}{2}$ part and to consider dynamic effects only in the dominant $j_f = L - \frac{1}{2}$ partial conversion coefficient.

The total ML conversion coefficient is, then,

$$\alpha_{ML}^K(\lambda) = \alpha_{ML}^{K \rightarrow L-1/2}(\text{Sliv}) |1 - c_{L-1/2}(R)(\lambda - 1)|^2 + \alpha_{ML}^{K \rightarrow L+1/2}(\text{Sliv}) \quad 46.$$

A very useful approximation to this expression is the simpler one

$$\alpha_{ML}^K(\lambda) = \alpha_{ML}^K(\text{Sliv}) |1 - (\lambda - 1)C_S|^2$$

$$C_S = c_{L-1/2}(R) \frac{\alpha_{ML}^{K \rightarrow L-1/2}(\text{Sliv})}{\alpha_{ML}^K(\text{Sliv})} \quad 47.$$

which is good enough to determine λ to better than 10 per cent. Formulae very similar to these, but based on the Rose tabulation (12), are:

$$\alpha_{ML}^K(\lambda) = \alpha_{ML}^K(\text{Rose}) |1 - \lambda C_R|^2$$

$$C_R \simeq C_S(1 - C_S) \quad 48.$$

The penetration coefficients have been computed in the paper of Green & Rose (35), on the assumption of a uniform nuclear charge distribution of radius $R = 1.2 A^{1/3} \times 10^{-13}$ cm. Values of C_S have been derived from this work and are presented in Table I. These coefficients are always very nearly real, and we explicitly neglect the small imaginary part. As expected for a penetration effect, C_S is greatest for heavy elements, where it becomes of the order of a few per cent.

The form of the weighting factor appearing in λ , Equation 45, is given as a power series, of which only the first two terms need be considered:

$$c_{L-1/2}(r)/c_{L-1/2}(R) = \frac{1}{1 + \sigma_{L-1/2}} \left(\frac{r}{R}\right)^2 + \frac{\sigma_{L-1/2}}{1 + \sigma_{L-1/2}} \left(\frac{r}{R}\right) \quad 49.$$

In practice, the second term is not very important, since $\sigma_{L-1/2}$ is always between $\frac{1}{10}$ and $\frac{1}{5}$. This quantity is also given in Table I.

TABLE I
MAGNETIC PENETRATION COEFFICIENTS

Z	k	M1		M2	
		C_S	$\sigma_{1/2}$	C_S	$\sigma_{3/2}$
64	0.5	0.011	-0.12	0.0083	-0.13
	1.8	0.013	-0.12	0.0089	-0.13
	5.0	0.016	-0.12	0.010	-0.13
78	0.5	0.019	-0.14	0.014	-0.15
	1.8	0.023	-0.15	0.015	-0.15
	5.0	0.031	-0.15	0.019	-0.15
96	0.5	0.038	-0.18	0.027	-0.18
	1.8	0.046	-0.18	0.029	-0.18
	5.0	0.063	-0.19	0.037	-0.18

These results have been derived from those of Green & Rose (35) using the relations $C_S = X(1 + X - y_L)$, $X = \rho_{-L}(1 + \sigma_{L-1/2})$, $\sigma_{L-1/2} = a_1(-L)/a_0(-L)$.

The combination of quantities appearing in Equation 47 which determines the penetration effect is then

$$\lambda C_S = \left[\frac{C_S}{1 + \sigma_{L-1/2}} \frac{1}{R^2} \right] \frac{\int d\tau_n j_n \cdot A_{LM}^{(m)*}(k\tau_n) r_n^2}{\int d\tau_n j_n \cdot A_{LM}^{(m)*}(k\tau_n)} + \left[\frac{C_S \sigma_{L-1/2}}{1 + \sigma_{L-1/2}} \frac{1}{R^4} \right] \frac{\int d\tau_n j_n \cdot A_{LM}^{(m)*}(k\tau_n) r_n}{\int d\tau_n j_n \cdot A_{LM}^{(m)*}(k\tau_n)} \quad 50.$$

The weighting factors in square brackets are moderately dependent on assumptions about the static nuclear charge distribution. For example, if we increase R by 10 per cent, the coefficient

$$\frac{C_S}{1 + \sigma_{L-1/2}} \frac{1}{R^2}$$

would decrease by 14 per cent for an $M1$ transition and 11 per cent for an $M4$, for $Z=82$. The second, less important coefficient,

$$\frac{C_S \sigma_{L-1/2}}{1 + \sigma_{L-1/2}} \frac{1}{R^4}$$

would decrease correspondingly by 38 per cent for an $M1$ and 37 per cent for an $M4$. A change from the uniform charge distribution to the more realistic distribution, Equation 38, increases the first coefficient by 5 per cent for an $M1$, and 4 per cent for an $M4$. The second coefficient is correspondingly increased by 18 per cent and 17 per cent, respectively.

The above calculations are based on the assumption that the radiating nucleon is always inside the nuclear charge distribution. This is, of course, not the case. However, the simple polynomial expressions already employed for the electron wave functions inside the charge distribution are good extrapolations for $r > R$. For example, they are less than the true functions by only 3 per cent at $r = 1.25R$, and 10 per cent at $r = 1.50R$, and are quite adequate for the present purposes.

Magnetic penetration matrix elements and nuclear models.—Results of the previous section can be summarized by the statement that the ML conversion coefficient depends on the quantity λ , which is the ratio of a new nuclear matrix element, the penetration electron matrix element, and the usual gamma-ray matrix element. Approximately

$$\lambda \sim \frac{\int d\tau_n j_n \cdot A_{LM}^{(m)*} \left(\frac{r_n}{R} \right)^2}{\int d\tau_n j_n \cdot A_{LM}^{(m)*}} \quad 51.$$

This ratio λ is weighted by a factor of a few per cent, and the effects of this quantity are significant whenever λ is large—for example when the gamma-

ray matrix element M_γ is inhibited, while the penetration matrix element M_e has its dimensional value.

To see when this may happen, we consider an explicit form for the nuclear current j_n , namely, the usual independent-particle convection plus spin currents,

$$j_n = \frac{e}{2iM} [\phi_{nj}^* \nabla \phi_{ni} - (\nabla \phi_{nj}^*) \phi_{ni}] + \mu \nabla \times \phi_{nj}^* \phi_{ni} \quad 52.$$

Although similar results occur in all magnetic multipoles, for purposes of illustration we limit ourselves to the simple case of an $M1$ transition. In the usual long-wavelength approximation,

$$A_{1M}^{(m)} \simeq \frac{k}{\sqrt{24\pi}} r \times \hat{e}_M \quad 53.$$

where the \hat{e}_M are unit vectors. In this approximation the gamma-ray matrix element is

$$M_\gamma = \int d\tau j_n \cdot A_{1M}^{(m)*} \simeq \frac{k}{\sqrt{6\pi}} \hat{e}_M^* \cdot \int d\tau \phi_{nj}^* \left[\frac{e}{2M} 1 + \mu \sigma \right] \phi_{ni} \quad 54.$$

which exhibits the familiar form of the magnetic-dipole operator, with the usual weighting of orbital and spin contributions. For a many-nucleon system, the generalization of Equation 54 is obvious:

$$\frac{k}{\sqrt{6\pi}} \hat{e}_M^* \cdot \int d\tau \phi_{nj}^* \sum_i \left[\frac{e_i}{2M} 1_i + \mu_i \sigma_i \right] \phi_{ni} \quad 55.$$

A similar treatment reduces the penetration matrix element, in the numerator of Equation 51, to

$$M_e \simeq \frac{k}{\sqrt{6\pi}} \hat{e}_M^* \cdot \int d\tau \phi_{nj}^* \sum_i \left(\frac{r_i}{R} \right)^2 \left[\frac{e_i}{2M} 1_i + 2\mu_i \sigma_i - \mu_i \hat{r}_i (\sigma_i \cdot \hat{r}_i) \right] \phi_{ni} \quad 56.$$

There are several important differences between these two matrix elements. Besides the expected appearance of the overall radial factor $(r/R)^2$, the spin contribution is now weighted by an additional factor of two relative to the orbital contribution. In addition to these expected forms, there is an entirely new spin-dependent term, $\hat{r}(\sigma \cdot \hat{r})$. In this form, the penetration matrix element M_e is distinctly different from the gamma-ray matrix element M_γ , and it is obvious that they may exhibit different model-dependent selection rules.

We now list the more obvious conditions under which M_γ vanishes, while M_e need not.

(a) A radial selection rule. If M_γ vanishes because of a radial selection rule, the extra factor of r^2 in M_e would prevent the same orthogonality from applying.

(b) An accidental cancellation. If M_γ vanishes because of a cancellation between the orbital and spin contributions, this cancellation could be upset in M_e because of the different weighting of orbital and spin parts.

(c) "*l*-Forbiddenness." If the orbital angular momentum of the transition nucleon changes, M_γ vanishes. For example, a nuclear

$$d_{3/2} \xrightarrow{M1} s_{1/2}$$

transition is allowed by the parity and total angular momentum selection rules, but is forbidden since $\Delta l = 2$ (36). However, the third term in M_e , Equation 56, would make a nonvanishing contribution for this $\Delta l = 2$ transition, since, using Clebsch-Gordanry,

$$(\hat{e}_M^* \cdot \hat{r})(\hat{d} \cdot \hat{r}) = \frac{1}{3} \hat{e}_M^* \cdot \hat{d} - \frac{1}{3} \sqrt{2\pi} \sum_{\mu, \nu} (-1)^\mu C(2, 1, 1; \mu, \nu, -M) Y_2^\mu \sigma_\nu, \quad 57.$$

and the Y_2 factor connects $\Delta l = 2$ states.

In this discussion, only the conventional spin and convection currents have been considered, without mentioning possible currents arising from exchange or velocity-dependent forces. These additional currents must be considered when any detailed model is employed. These small contributions to the current are expected to be very important in the evaluation of the forbidden gamma-ray matrix element M_γ , but not in the evaluation of the allowed penetration matrix element M_e . It is in part for this reason that we shall take M_γ from experiment and only use the model to calculate M_e .

Analysis of the 480-kev transition in Ta¹⁸¹—an l-forbidden transition.—We now illustrate the analysis of a case of an $M1$ transition in which a penetration effect has definitely been seen. This is done in some detail to demonstrate both the experimental and theoretical techniques involved. In doing so, we follow the original discussion of Snyder & Frankel (37).

The level scheme of Ta¹⁸¹ is shown in Figure 1. The $M1$ component of the 480-kev transition is known to be very slow—its gamma-ray transition probability is only 5×10^{-6} (38) of its dimensional single-particle, or "Weisskopf," value. The levels have been interpreted in terms of rotational bands in the Bohr-Mottelson unified model (39 to 41). In this picture, the 480-kev transition occurs between the bottom of the $K = 5/2+$ band, the particle substructure of which is roughly describable as $d_{5/2}$, and the bottom of the $K = 7/2+$ band, with substructure which is roughly $g_{7/2}$. The 480-kev transition is interpreted as a "*l*-forbidden transition" (essentially $d_{5/2} \rightarrow g_{7/2}$).

As usual in transitions involving an *l*-forbidden $M1$ component, the 480-kev transition is a mixture of $M1$ and $E2$. To extract the properties of the $M1$ component from those observed for the mixed transition, the $M1$ - $E2$ mixing ratio must be determined, as may be done from the analysis of a gamma-gamma directional-correlation experiment involving the mixed transition. Such a result, plus a measurement of the net conversion coefficient of the mixed transition, yields the conversion coefficient of the $M1$ component alone, assuming that the conversion properties of the (uninhibited) $E2$ component are known. In all that follows it is assumed that the $E2$ conversion properties are given by their tabulated values.

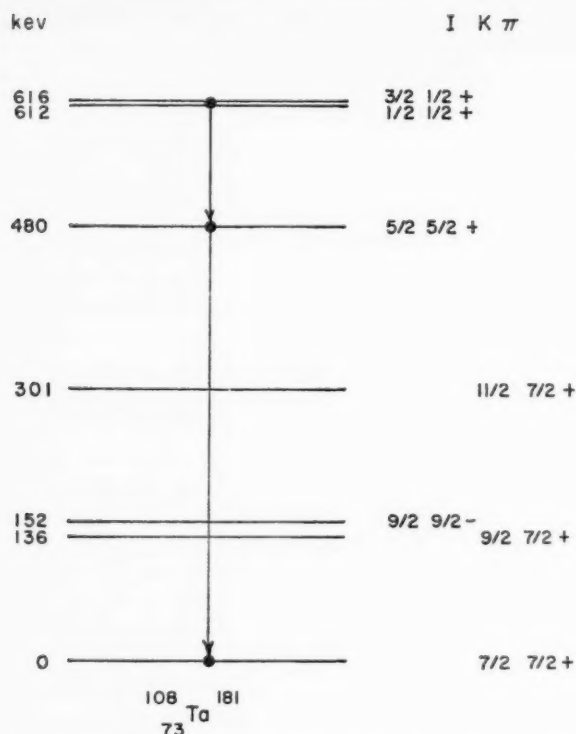


Fig. 1. The level scheme for Ta^{181} . The energies of the levels above the ground state are given in keV on the left. The Mottelson-Nilsson (41) level assignments are given on the right. The ground, first, and third levels have been interpreted as members of a single rotational band. Only those gamma transitions discussed in the text are indicated in the figure.

Gamma-gamma directional-correlation experiments result in a value for the amplitude mixing ratio δ .

$$\delta = \frac{E2 \text{ gamma-ray amplitude}}{M1 \text{ gamma-ray amplitude}} = +6 \pm 2 \quad 58.$$

The net K -conversion coefficient of this transition is taken to be

$$\alpha_{480}^K = 0.025 \pm 0.005 \quad 59.$$

These two experimental quantities are connected by the relation:

$$\alpha^K = \frac{\alpha_{M1}^K + \delta^2 \alpha_{E2}^K}{1 + \delta^2} \quad 60.$$

where α_{M1}^K , α_{E2}^K are the K -shell conversion coefficients of the pure multi-

pole components. With the tabulated value, $\alpha_{E2}^K = 0.0171$ (37), we find

$$0.856 \geq \alpha_{M1}^K \geq 0.066 \quad 61.$$

which is to be compared with its tabulated value, $\alpha_{M1}^{K(\text{Sliv})} = 0.0481$ (37). The large range of the experimental value of α_{M1}^K comes from the fact that the $M1$ component is only a small fraction of the 480-keV transition, but carries the cumulative experimental error. These results are sensitive to the value of the $E2$ conversion coefficient. If this $E2$ coefficient were 7 per cent higher, the range of possible values for the $M1$ coefficient would extend down to its tabulated value. We assume the correctness of the above $E2$ conversion coefficient for the present discussion and also omit the possibility of enhanced higher multipoles.

The value of α_{M1}^K , Equation 61, indicates a definite deviation from its tabulated value, and hence a value of λ appreciably different from 1. To determine λ we make use of the approximate relation, Equation 47,

$$\alpha_{M1}^K(\lambda) = \alpha_{M1}^K(\text{Sliv}) |1 - 0.021(\lambda - 1)|^2 \quad 62.$$

which is analyzed graphically in Figure 2.

Data on $\gamma - e^-$ directional-correlations involving the K -conversion electrons of the 480-keV transition are available (37, 37a). The $M1$ contribution to the correlation function is determined by the relative amounts of $s_{1/2}$ and $d_{3/2}$ waves in the final electron state (42). In turn, the $s_{1/2}$ partial wave depends on λ through the factor $[1 - 0.021(\lambda - 1)]$. The analysis of this correlation experiment is also given in Figure 2. The experimental correlation data have large errors, but do serve to exclude the region of negative values of the quantity $[1 - 0.021(\lambda - 1)]$.

Taking all the available data together, the range of permissible λ 's is:

$$-7 \geq \lambda \geq -150 \quad 63.$$

depending on the value of δ . The permitted ranges of λ , δ are replotted in Figure 3 for future reference.

It is of interest to compare the experimental values of λ with the predictions of a nuclear model. To predict λ we must consider the two nuclear matrix elements M_γ and M_e . The value of M_γ is deduced from the $M1$ gamma-ray lifetime, and is known, then, except for a sign. Since M_e is allowed, we compute it from the model. If the usual convection and spin currents are used,

$$M_e = \frac{1}{1 + \sigma_{1/2}} \hat{e}_M^* \cdot \int d\tau \phi_{n_f}^* \sum_i \left(\frac{r_i}{R} \right)^2 \left[\frac{e_i}{2M} l_i + 2\mu_i \sigma_i - \mu_i \hat{r}_i (\sigma_i \cdot \hat{r}_i) \right] \phi_{n_i} \\ + \frac{\sigma_{1/2}}{1 + \sigma_{1/2}} \hat{e}_M^* \cdot \int d\tau \phi_{n_f}^* \sum_i \left(\frac{r_i}{R} \right)^4 \left[\frac{e_i}{2M} l_i + 3\mu_i \sigma_i - 2\mu_i \hat{r}_i (\sigma_i \cdot \hat{r}_i) \right] \phi_{n_i} \quad 64.$$

where the different numerical coefficients originate from the different radial weightings in Equation 50.

Mottelson & Nilsson (41) have interpreted the levels in Ta^{181} in terms of the unified model. With the wave functions of that model, the value of

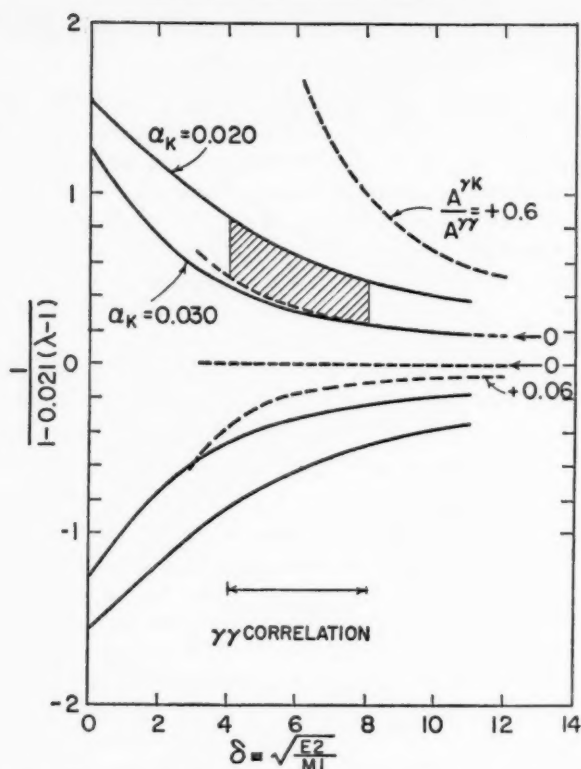


Fig. 2. Graphical analysis of the available experimental data for the 480-keV transition in Ta^{181} . The abscissa is the amplitude mixing ratio δ , which gamma-gamma directional-correlation experiments fix as $+6 \pm 2$ [reanalysis of (37)]. The ordinate is the quantity $[1 - 0.021(\lambda - 1)]^{-1}$, the magnitude of which is $[\alpha_{M1}^K(\text{Sliv})/\alpha_{M1}^K(\lambda)]^{1/2}$. The two sets of solid curves correspond to the extreme values of the observed net K -conversion coefficient for this transition [reanalysis of the data of Snyder & Frankel (37)]. The two sets of dashed curves correspond to the extreme values of the correlation coefficient ratio $A_2^{\gamma K}/A_2^{\gamma\gamma} = 0.3 \pm 0.3$ for the (132+136)-480 keV cascade [(37a) and reanalysis of the data in (37)]. The region compatible with all three sets of experimental data is shaded.

M_e is obtained by straightforward computation. This value, taken with the experimental value of M_γ , which depends on the mixing ratio δ , gives:

$$\lambda \simeq \pm 86[1 + \delta^2]^{1/2} \quad 65.$$

This predicted λ is plotted in Figure 3 for comparison with the empirical results obtained earlier. There is *no* area of agreement. The predicted λ is at least five times larger than the empirical one for the permissible range of δ . This discrepancy in λ implies a corresponding discrepancy in the calcu-

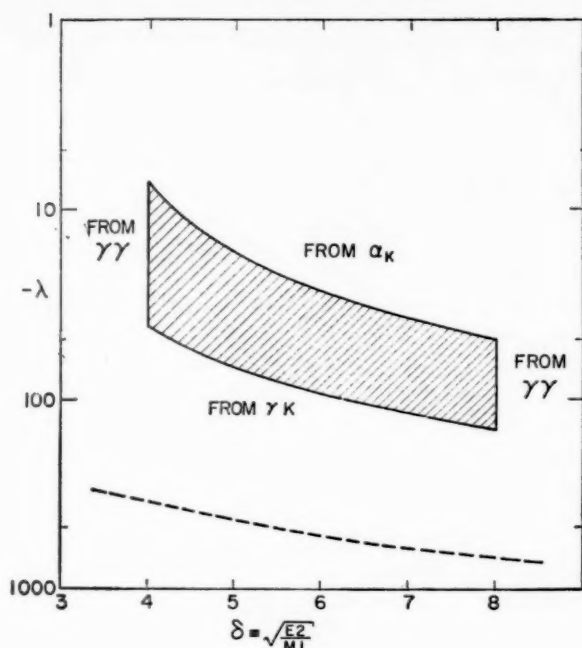


FIG. 3. Comparison of the experimental (shaded) and the calculated (dashed) results for the properties of the 480-keV transition in Ta^{181} . The horizontal axis is the amplitude mixing ratio δ , and the vertical axis is $(-\lambda)$, where λ is the ratio of the $M1$ penetration matrix element to the $M1$ gamma-ray matrix element. The shaded area has been taken from the analysis of the experimental data shown in Fig. 2. The dashed line has been computed for the Nilsson model assignments shown in Fig. 1 and is essentially independent of the assumed nuclear deformation. It is seen that the magnitude of the calculated value of λ is always at least 5 times greater than the values allowed by experiment.

lated value of M_e . Since M_e is the transition matrix element of a magnetic-dipole penetration operator, we may compare this discrepancy with those for the related static magnetic-dipole moments. The calculated magnetic-dipole moments of both the initial and final states deviate by ~ 0.3 nuclear magneton from the experimental values (41), and deviations of ~ 0.5 nuclear magneton are not unusual in nearby nuclei. The discrepancy in M_e indicated above is also of about this magnitude. The present result may, therefore, be taken as additional evidence for significant deviations from the Nilsson model.

Rotational transitions—accidental cancellation.—The low-lying levels of odd-A deformed nuclei have been interpreted as forming a rotational band (39). All members of a given band have a common particle substructure. Successive levels of the band have spins differing by one unit, and since they

have the same parity, the transitions between these levels are mixed $M1$ and $E2$.

The $M1$ gamma-ray matrix element is proportional to

$$(g_0 - g_R) \quad 66.$$

where g_0 and g_R are the particle and core gyromagnetic ratios (39). Slow $M1$ transitions between rotational levels are, then, interpreted as cancellation or near-cancellation between the particle and core g factors. However, the penetration matrix element M_e is characteristically different and need not simultaneously suffer such a cancellation.

The details of the calculation of λ in the rotational region have been exhaustively discussed by Reiner (43), who lists a number of experimental cases for which 10 to 50 per cent changes in the $M1$ K -shell conversion coefficient may be expected. Unfortunately, in practical cases, the near-cancellation necessary to give the large change in the $M1$ conversion coefficient also reduces the $M1$ transition probability to the point where it only weakly competes with the very strong $E2$. Strong enhancement of the rotational $E2$ is fundamental to the collective model. This is unlike the case of the 480-kev transition in Ta^{181} just discussed, which is a particle transition between bands. The optimum case for observation of conversion anomalies of this type would occur when the $M1$ component is inhibited so that its rate of conversion equals that of the $E2$ component. Then, quite sizable effects, say 15 per cent, in the net conversion coefficient might be observed.

Since an accidental cancellation is unlikely, large effects on the conversion coefficients in retarded $M1$ rotational transitions would not generally be expected. They have not yet been observed.

Analysis of Tl^{203} —a puzzle.—The low-lying part of the level scheme of Tl^{203} is particularly simple (Fig. 4), and the ground, first, and second excited states have long been interpreted in terms of the shell-model assignments $s_{1/2}$, $d_{3/2}$, and $d_{5/2}$. The $M1$ component of the 279-kev ($d_{3/2} \rightarrow s_{1/2}$) transition is known to be slow. Its transition probability is of the order of 10^{-4} of its "Weisskopf" value, which supports its assignment as an l -forbidden transition. The $M1$ - $E2$ mixing ratio (44) and the K -conversion (45) coefficient have been measured, and a value of λ can be obtained from these. The acceptable ranges are found to be

$$3.9 \geq \lambda \geq 0.46 \quad 67.$$

or

$$77 \geq \lambda \geq 73 \quad 68.$$

depending on whether the factor determining the electron $s_{1/2}$ amplitude, $[1 - 0.026(\lambda - 1)]$, is positive or negative. On the other hand, if we take the shell model seriously, compute a value for M_e , and take the magnitude of M_γ from experiment, $|\lambda| \sim 12$ is obtained. This is in substantial disagreement with the empirical values indicated in Equations 67, 68. Attempts to modify the shell model by including configuration mixing fail to change M_e

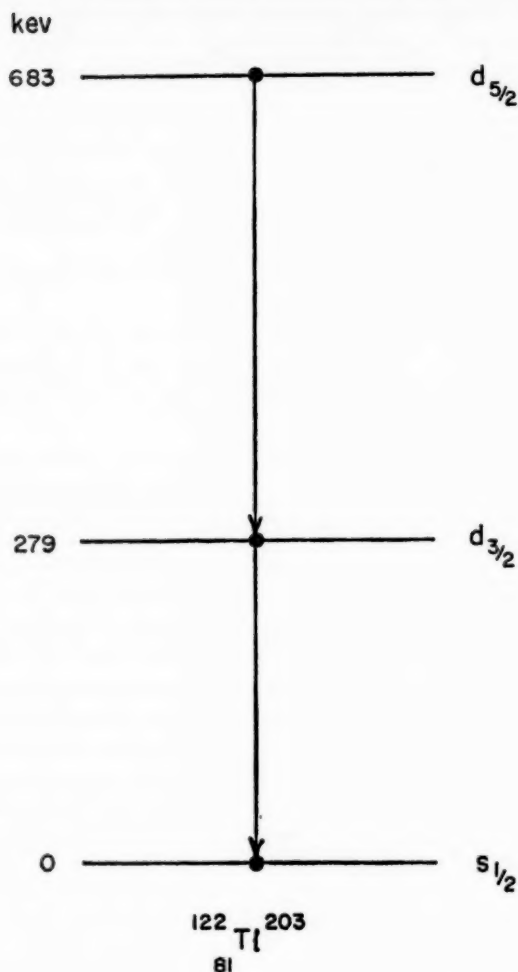


FIG. 4. The level scheme for Tl^{203} . The energies of the levels above the ground state are given in keV on the left. The assumed spin-orbit assignments are given on the right. Only those gamma transitions discussed in the text are indicated in the figure.

appreciably, and no agreement with the experimental λ is possible if we use an M_γ compatible with the experimental lifetime (46).

Further, there appear to be deeper troubles. The 404-keV ($d_{5/2} \rightarrow d_{3/2}$) transition, which is allowed by all other criteria, seems to show a K -conversion coefficient which is anomalously low by 15 per cent (45a). Further, reported $e^{K_{404}} - \gamma_{279}$ and $\gamma_{404} - e^{K_{279}}$ directional-correlation experiments seem

inconsistent, no matter what $M1$ -penetration effects are allowed in either or both transitions (47). Large $E2$ penetration effects would produce enough flexibility to explain these results, but the magnitude of the required penetration terms seems unreasonably large for these uninhibited $E2$ transitions.

DYNAMICAL EFFECTS IN ELECTRIC TRANSITIONS

The exhibition of the penetration terms for electric conversion follows the tactics used for the magnetic conversion. The interaction for EL conversion has already been written in Equation 20:

$$\begin{aligned}
 H_{el}'(L, M) = & \frac{-4\pi i}{[L(L+1)]^{1/2}} \int_0^\infty d\tau_n j_n \cdot A_{LM}^{(e)*}(k\tau_n) \\
 & \cdot \int_0^\infty d\tau_e \left[j_e \cdot k^2 \hat{r}_e + \rho_e i k \frac{d}{d\tau_e} \right] r_e h_L^{(1)}(k\tau_e) Y_{LM}(\hat{r}_e) \\
 & \frac{+4\pi i}{[L(L+1)]^{1/2}} \left\{ \int_0^\infty d\tau_n j_n \cdot A_{LM}^{(e)*}(k\tau_n) \right. \\
 & \cdot \int_0^\infty d\tau_e \left[j_e \cdot k^2 \hat{r}_e + \rho_e i k \frac{d}{d\tau_e} \right] r_e h_L^{(1)}(k\tau_e) Y_{LM}(\hat{r}_e) \\
 & - \int_0^\infty d\tau_n j_n \cdot B_{LM}^{(e)*}(k\tau_n) \\
 & \cdot \left. \int_0^\infty d\tau_e \left[j_e \cdot k^2 \hat{r}_e + \rho_e i k \frac{d}{d\tau_e} \right] r_e j_L(k\tau_e) Y_{LM}(\hat{r}_e) \right\} \quad 69.
 \end{aligned}$$

The penetration terms in the curly brackets contain the new nuclear matrix elements. In contrast to the magnetic case, there are two characteristically different electric penetration matrix elements (35). This can be seen immediately from the expanded form of the electric vector potential, Equation 16, which contains both a gradient and a radial part. The penetration matrix elements chosen may be any two linearly independent linear combinations of these two forms. Green & Rose chose forms based on irreducible tensors (35), while we use below a pair which is more convenient for specific calculations.

Carrying out of the angular integration for the electron results again in a common angular factor B . After grouping the two penetration terms

$$\begin{aligned}
 H_{el}'(L, M) = & B(EL, M; e_i, e_f) \left\{ \int_0^\infty d\tau_n j_n \cdot A_{LM}^{(e)*}(k\tau_n) \right. \\
 & \cdot \int_0^\infty d\tau r^2 \left[(g_e f_{e_i} - f_e g_{e_i}) k - (f_e f_{e_i} + g_e g_{e_i}) \frac{d}{d\tau} \right] r h_L^{(1)}(kr) \\
 & + \int_0^\infty d\tau_n j_n \cdot \nabla \Phi(r_n) Y_{LM}^*(\hat{r}_n) \\
 & \left. + \int_0^\infty d\tau_n j_n \cdot \frac{r_n}{r_n} \Theta(r_n) Y_{LM}^*(\hat{r}_n) \right\} \quad 70.
 \end{aligned}$$

The penetration weighting functions Φ and Θ are given by the imposing expressions:

$$\Phi(r) = \frac{1}{k[L(L+1)]^{1/2}} \left\{ \left[\frac{d}{dr} r h_L^{(1)}(kr) \right] \int_0^r dr' r'^2 \left[(g_j f_{e_i} - f_j g_{e_i}) k - (f_j f_{e_i} + g_j g_{e_i}) \frac{d}{dr'} \right] r' j_L(kr') \right. \\ \left. - \left[\frac{d}{dr} r j_L(kr) \right] \int_0^r dr' r'^2 \left[(g_j f_{e_i} - f_j g_{e_i}) k - (f_j f_{e_i} + g_j g_{e_i}) \frac{d}{dr'} \right] r' h_L^{(1)}(kr') \right\}$$

and

$$\Theta(r) = \frac{1}{k[L(L+1)]^{1/2}} \left\{ -i(g_j f_{e_i} - f_j g_{e_i}) r^2 \right. \\ \left. + k^2 r h_L^{(1)}(kr) \int_0^r dr' r'^2 \left[(g_j f_{e_i} - f_j g_{e_i}) k - (f_j f_{e_i} + g_j g_{e_i}) \frac{d}{dr'} \right] r' j_L(kr') \right. \\ \left. - k^2 r j_L(kr) \int_0^r dr' r'^2 \left[(g_j f_{e_i} - f_j g_{e_i}) k - (f_j f_{e_i} + g_j g_{e_i}) \frac{d}{dr'} \right] r' h_L^{(1)}(kr') \right\} \quad 71.$$

An examination of the orders of magnitude of these functions in the long-wavelength region $kr_n \ll 1$ indicates

$$\Theta/\Phi \sim kr_n \quad 72.$$

so that the first of the two types of penetration matrix elements in Equation 70 is strongly weighted relative to the second. However, because of a cancellation in Φ , this is not so for $\kappa_i = -\kappa_f$ electron transitions. Examples are the $s_{1/2} \rightarrow p_{1/2}$ or $p_{1/2} \rightarrow s_{1/2}$ electron transitions prominent in $E1$ conversion. We return to this important point in a moment.

The functions Φ and Θ .—The radial weighting functions $\Phi(r)$ and $\Theta(r)$ depend on the initial and final electron wave functions in the vicinity of the nucleus and can be computed in the same way as the function c_j in the magnetic case. As in the magnetic case, an expansion in r^2 is obtained for these weighting functions, of which only the two lowest terms are of interest. The formulation for the electric conversion has been carried out by Green & Rose (35), Nilsson & Rasmussen (48), and Tang (49). Green & Rose also carried out a very complete numerical evaluation for the K -shell penetration coefficients, and the numerical coefficients used here are derived from their work.

As we have already seen, the final electron states of EL conversion in the K shell are $j = L - \frac{1}{2}$ ($\kappa = L$) and $j = L + \frac{1}{2}$ ($\kappa = -L - 1$), and the K -conversion coefficient is the sum of the two corresponding partial coefficients. The total internal conversion coefficient, including penetration effects, takes the form

$$\alpha_{EL}^K = \alpha_{EL}^K(\text{Rose}) \left\{ \frac{1}{1+U^2} \left| 1 - e^{i\pi L+1/2} (c_{L+1/2}' \lambda_{L+1/2}' + c_{L+1/2}'' \lambda_{L+1/2}'') \right|^2 \right. \\ \left. + \frac{1}{1+U^2} \left| U - e^{i\pi L-1/2} (c_{L-1/2}' \lambda_{L-1/2}' + c_{L-1/2}'' \lambda_{L-1/2}'') \right|^2 \right\} \quad 73.$$

The quantity α_{EL}^K (Rose) is Rose's tabulated value of the EL K -conversion coefficient, in which the penetration terms have been taken as zero

TABLE II
ELECTRIC PENETRATION COEFFICIENTS

E1

Z	k	$p_{1/2}$					$p_{1/2}$				
		$\epsilon_{1/2}'$	$\epsilon_{1/2}''$	$\sigma_{1/2}'$	$\sigma_{1/2}''$	$\cos \tau_{1/2}$	$\epsilon_{1/2}'$	$\epsilon_{1/2}''$	$\sigma_{1/2}'$	$\sigma_{1/2}''$	$\cos \tau_{1/2}$
64	0.3	-0.000053	-0.00043	-0.0056	-0.11	-1.0	+0.00025	+0.0000019	-0.038	∞	+1.0
	0.5	+0.000053	-0.00083	-0.15	-0.11	-0.99	+0.00033	+0.0000030	-0.039	∞	+0.99
	1.8	+0.0012	-0.0045	-0.080	-0.12	+0.93	+0.00080	+0.0000016	-0.042	∞	+0.98
78	0.3	-0.00027	-0.00032	-0.0029	-0.37	-0.99	+0.00051	+0.0000016	-0.055	∞	+1.0
	0.5	-0.000017	-0.0012	-2.13	-0.24	-0.98	+0.00065	+0.0000036	-0.056	∞	+0.99
	1.8	+0.0024	-0.0087	-0.11	-0.17	+0.92	+0.0015	+0.0000031	-0.060	∞	+0.98
96	0.5	+0.00033	-0.0055	-0.33	-0.25	-0.88	+0.0016	+0.0000011	-0.084	∞	+0.99
	1.8	+0.0062	-0.021	-0.17	-0.26	+0.92	+0.0034	+0.0000094	-0.089	∞	+0.96

E2

Z	k	$d_{1/2}$					$d_{1/2}$				
		$\epsilon_{1/2}'$	$\epsilon_{1/2}''$	$\sigma_{1/2}'$	$\sigma_{1/2}''$	$\cos \tau_{1/2}$	$\epsilon_{1/2}'$	$\epsilon_{1/2}''$	$\sigma_{1/2}'$	$\sigma_{1/2}''$	$\cos \tau_{1/2}$
64	0.3	+0.0017	-0.00023	-0.086	-0.089	-1.0	+0.00017	+3 $\times 10^{-7}$	-0.039	∞	+1.0
	0.5	+0.0021	-0.00044	-0.086	-0.099	-0.98	+0.00021	+6 $\times 10^{-7}$	-0.039	∞	+1.0
	1.8	+0.0035	-0.0022	-0.085	-0.11	+1.0	+0.00049	+2 $\times 10^{-6}$	-0.040	∞	+0.99
78	0.3	+0.0046	-0.00052	-0.099	-0.13	-0.99	+0.00036	+6 $\times 10^{-7}$	-0.057	∞	+1.0
	0.5	+0.0051	-0.00091	-0.10	-0.15	+0.96	+0.00043	+1 $\times 10^{-6}$	-0.057	∞	+1.0
	1.8	+0.0076	-0.0042	-0.10	-0.16	+1.0	+0.00091	+1 $\times 10^{-5}$	-0.060	∞	+0.99
96	0.5	+0.017	-0.0025	-0.12	-0.22	+1.0	+0.0011	+6 $\times 10^{-6}$	-0.086	∞	+1.0
	1.8	+0.021	-0.0097	-0.13	-0.24	+1.0	+0.0021	+4 $\times 10^{-5}$	-0.090	∞	+0.99

The penetration coefficients for $E1$ and $E2$ K -shell conversion are derived from Green & Rose (35). The general connection between the forms used here and those of Green & Rose is given by the relations:

$$\begin{aligned}
 C_{L-1/2}' &= +\omega_L \left[\left(\frac{L+1}{L} \right)^{1/2} (\bar{b}_0(L) + \bar{b}_1(L)) + \bar{c}_0(L) + \bar{c}_1(L) \right] \\
 C_{L-1/2}'' &= -\omega_L \left[\left(\frac{L+1}{L} \right)^{1/2} (2\bar{b}_0(L) + 4\bar{b}_1(L)) + (2L+3)\bar{c}_0(L) + (2L+5)\bar{c}_1(L) \right] \\
 \sigma_{L-1/2}' &= \frac{\left(\frac{L+1}{L} \right)^{1/2} \bar{b}_1(L) + \bar{c}_1(L)}{\left(\frac{L+1}{L} \right)^{1/2} \bar{b}_0(L) + \bar{c}_0(L)} \\
 \sigma_{L-1/2}'' &= \frac{4 \left(\frac{L+1}{L} \right)^{1/2} \bar{b}_1(L) + (2L+5)\bar{c}_1(L)}{2 \left(\frac{L+1}{L} \right)^{1/2} \bar{b}_0(L) + (2L+3)\bar{c}_0(L)} \\
 c_{L+1/2}' &= +\omega_{-L-1} \left[\left(\frac{L+1}{L} \right)^{1/2} (1 + \bar{b}_1(-L-1)) + \bar{c}_0(-L-1) + \bar{c}_1(-L-1) \right] \\
 c_{L+1/2}'' &= -\omega_{-L-1} \left[4 \left(\frac{L+1}{L} \right)^{1/2} \bar{b}_1(-L-1) + (2L+5)\bar{c}_1(-L-1) \right] \\
 \sigma_{L+1/2}' &= \frac{\left(\frac{L+1}{L} \right)^{1/2} \bar{b}_1(-L-1) + \bar{c}_1(-L-1)}{\left(\frac{L+1}{L} \right)^{1/2} + \bar{c}_0(-L-1)} \\
 \sigma_{L+1/2}'' &= \infty
 \end{aligned}$$

The quantities ω , \bar{b} , \bar{c} , U and τ are given in (35). Note that when U passes through zero there is a corresponding change in the sign of $\cos \tau$.

(12), and U is the relative conversion amplitude for the $j = L - \frac{1}{2}$ final electron state. The τ_j 's are the phases with which the penetration terms appear relative to the principal contributions, and the c_j , c_j'' are their weighting factors. The penetration matrix elements themselves, λ_j' and λ_j'' , are explicitly:

$$\begin{aligned} \lambda_j' = & \frac{1}{1 + \sigma_j'} \frac{1}{kR^2} \frac{\int d\tau_n j_n \cdot \nabla_n j_L^0(kr_n) r_n^2 Y_L^{M*}(\hat{r}_n)}{\int d\tau_n j_n \cdot A_{LM}^{(*)}(kr_n)} \\ & + \frac{\sigma_j'}{1 + \sigma_j'} \frac{1}{kR^4} \frac{\int d\tau_n j_n \cdot \nabla_n j_L^0(kr_n) r_n^4 Y_L^{M*}(\hat{r}_n)}{\int d\tau_n j_n \cdot A_{LM}^{(*)}(kr_n)} \end{aligned} \quad 74.$$

and

$$\begin{aligned} \lambda_j'' = & \frac{1}{1 + \sigma_j''} \frac{1}{kR^2} \frac{\int d\tau_n j_n \cdot (\hat{r}_n/r_n) j_L^0(kr_n) r_n^2 Y_L^{M*}(\hat{r}_n)}{\int d\tau_n j_n \cdot A_{LM}^{(*)}(kr_n)} \\ & + \frac{\sigma_j''}{1 + \sigma_j''} \frac{1}{kR^4} \frac{\int d\tau_n j_n \cdot (\hat{r}_n/r_n) j_L^0(kr_n) r_n^4 Y_L^{M*}(\hat{r}_n)}{\int d\tau_n j_n \cdot A_{LM}^{(*)}(kr_n)} \end{aligned} \quad 75.$$

The various quantities c_j' , c_j'' , σ_j' , σ_j'' , τ_j , and U , derived from the work of Green & Rose, are given in Table II. The symbol $j_L^0(kr)$ denotes the value of $j_L(kr)$ in the long-wavelength limit,

$$j_L^0(kr) = k^L r^L / (2L + 1)!! \quad 76.$$

and is introduced to simplify comparisons between matrix elements. An expression similar to Equation 73 can also be written in terms of Sliv's conversion coefficients. However, values of the partial conversion amplitudes and their phases are not yet available for the "surface-current" model.

The nuclear matrix element appearing in the denominators of Equations 74 and 75 is the EL gamma-ray matrix element. Substituting the explicit form for the vector potential, Equation 16, this is

$$\int d\tau_n j_n \cdot A_{LM}^{(*)}(kr_n) = \frac{1}{k[L(L+1)]^{1/2}} \int d\tau_n j_n \cdot \left[\nabla_n \frac{d}{dr_n} + \hat{r}_n k^2 \right] r_n j_L(kr_n) Y_L^{M*}(\hat{r}_n) \quad 77.$$

In this form the comparison with the corresponding penetration terms is obvious. In order to obtain the textbook form of the gamma-ray matrix element, we first make use of the long-wavelength approximation, and then the continuity equation. The final result for M_γ is

$$\begin{aligned}
\frac{1}{k[L(L+1)]^{1/2}} \int d\tau_n j_n \cdot \nabla_n \frac{d}{d\tau_n} r_n j_L^0(kr_n) Y_L^M(\hat{r}_n) \\
= -i \left(\frac{L+1}{L} \right)^{1/2} \int d\tau_n \rho_n j_L^0(kr_n) Y_L^{M*}(\hat{r}_n) \\
= -i \left(\frac{L+1}{L} \right)^{1/2} \frac{k^L}{(2L+1)!!} \int d\tau_n \rho_n r_n^L Y_L^{M*}(\hat{r}_n)
\end{aligned} \quad 78.$$

It should be emphasized, though, that when discussing highly forbidden gamma-ray transitions, use of this simple long-wavelength form may be completely inappropriate, since it neglects higher-order terms which need not be negligible.

The dependences of the various coefficients on the size and shape of the static nuclear charge distribution are similar to those of the corresponding magnetic penetration coefficients. The details are given in Table III. As in the magnetic case, the results indicate a moderate dependence on the assumed gross features of the nuclear charge distribution.

Before we can turn to consideration of nuclear models and experimental results, there is an important feature of $E1$ conversion yet to be discussed. For K conversion there are the two electron transitions: $s_{1/2} \rightarrow p_{1/2}$ and

TABLE III

DEPENDENCE OF THE ELECTRIC PENETRATION COEFFICIENTS ON THE STATIC NUCLEAR CHARGE DISTRIBUTION

	Effect of increasing R by 10%		Effect of changing to a $\left[1 - \left(\frac{r}{R'}\right)^4\right]$ charge distribution	
	$j=L-\frac{1}{2}$	$j=L+\frac{1}{2}$	$j=L-\frac{1}{2}$	$j=L+\frac{1}{2}$
$\frac{1}{1+\sigma'} \frac{c'}{R^2}$	$E1 \quad \sim -4\%$ $EL > 1 \quad \sim -13\%$	$\sim -3\%$	$E1 \quad \sim +1\%$ $EL > 1 \quad \sim +4\%$	$< +1\%$
$\frac{\sigma'}{1+\sigma'} \frac{c'}{R^4}$	$E1 \quad \sim -2\%$ $EL > 1 \quad \sim -36\%$	$\sim -24\%$	$E1 \quad \sim +8\%$ $EL > 1 \quad \sim +17\%$	$\sim +10\%$
$\frac{1}{1+\sigma''} \frac{c''}{R^2}$	$EL \quad \sim -3\%$	—	$E1 \quad \sim +1\%$ $EL > 1 \quad < +1\%$	—
$\frac{\sigma''}{1+\sigma''} \frac{c''}{R^4}$	$EL \quad \sim -25\%$	$\sim -13\%$	$EL \quad \sim +11\%$	$\sim +4\%$

$s_{1/2} \rightarrow p_{3/2}$. Since the $p_{1/2}$ electron wave function is large in the vicinity of the origin, it is expected that the penetration terms would be by far largest in the $s_{1/2} \rightarrow p_{1/2}$ electron transition. However, there is a near-cancellation in the dominant term for this transition which greatly reduces the penetration coefficient $\Phi(r)$. The leading term in $\Phi(r)$ involves the electron wave functions in the combination

$$(f_{p_{1/2}} f_{s_{1/2}} + g_{p_{1/2}} g_{s_{1/2}}) \quad 79.$$

To understand the origin of the cancellation, we note that if the electron mass m_e were zero, the Dirac equation would imply

$$\frac{f_{s_{1/2}}(r)}{g_{s_{1/2}}(r)} = - \frac{g_{p_{1/2}}(r)}{f_{p_{1/2}}(r)} \quad 80.$$

and the expression in Equation 79 would vanish. It is interesting to note that it is just this invariance of the neutrino wave functions which hid parity violation for so long. For a finite-mass particle, this result is modified to an expansion

$$\frac{f_{s_{1/2}}(r)}{g_{s_{1/2}}(r)} = - \frac{g_{p_{1/2}}(r)}{f_{p_{1/2}}(r)} \left[1 + \mathcal{O} \left(\frac{m_e c^2}{E + V(r)} \right) \right] \quad 81.$$

and the cancellation is no longer complete.

In the study of penetration effects we are interested only in distances of the order of nuclear dimensions where

$$V(r) \sim -\alpha Z \left(\frac{\hbar/m_e c}{R} \right) \gg m_e c^2 \quad 82.$$

$\gg E$

Because of this near-cancellation, the weighting function Φ is reduced by the factor of $2R/\alpha Z \approx 1/20$ for $s_{1/2} \rightarrow p_{1/2}$ transitions. There is no such cancellation in Φ for the $s_{1/2} \rightarrow p_{3/2}$ electron transition. This situation is reflected in the more nearly comparable values of the coefficients $c_{1/2}'$ and $c_{3/2}'$ in Table II.

There is no cancellation in Θ , and the coefficient $c_{1/2}''$ has its expected value, which is quite comparable with, or even larger than, $c_{1/2}'$. In other words, the coefficient $c_{1/2}'$, instead of being of relative order 1, is of order R , while the coefficient $c_{1/2}''$ is of order kR . In detail, the ratio of the $c_{1/2}''$ and $c_{1/2}'$ turns out to be of order $(5 \text{ to } 10)k$, a considerable quantity. The coefficient $c_{3/2}''$ is, as expected from Equation 72, of order kr relative to the already small coefficient $c_{3/2}'$.

Nilsson & Rasmussen (48), in their early discussion of electric penetration effects, neglected terms of order kr from the beginning, so that all λ'' were dropped, including the importantly weighted $\lambda_{1/2}''$.

Electric penetration matrix elements and nuclear models.—Nilsson & Rasmussen (48) pointed out that there is an interesting class of highly inhibited $E1$ gamma-ray transitions in some heavy deformed nuclei that would be expected to exhibit penetration effects. The inhibition of these transitions has been interpreted in terms of the Nilsson wave functions (40).

We can illustrate this easily by an example based on the asymptotic

limit of the model for large nuclear deformations. In a spheroidal harmonic oscillator potential, states are specified by the oscillator number of the motion along the symmetry axis n_z , the value of the angular momentum about that symmetry axis Λ , and the energy of the oscillator motion in the x - y plane $n_{xy}(\hbar\omega)$. Since we are interested only in low-energy transitions between states of opposite parity, the only transitions we need consider are those for which $\Delta N = \pm 1$, where $N = n_{xy} + n_z$. The long-wavelength approximation of the $E1$ gamma-ray matrix element, Equation 78, is proportional to

$$\int d\tau \rho_n r Y_1^{m*}(\hat{r}_n) = e \int d\tau \phi_{n_f}^* r Y_1^{m*}(\hat{r}_n) \phi_{n_i} \quad 83.$$

This form implies definite selection rules. For example, if $\Lambda_{n_i} - \Lambda_{n_f} = \pm 1$, then $m = \pm 1$, and so $r Y_1^{m*} = \mp [(3/(8\pi))^{1/2}(x \mp iy)]$. The oscillator selection rules are obviously $\Delta n_{xy} = \pm 1$ and $\Delta n_z = 0$, $\Delta N = \pm 1$. A transition with $\Delta N = +1$, $\Delta n_z = +2$, for example, would be forbidden. On the other hand, for this forbidden gamma-ray transition, the penetration matrix elements have an additional factor containing z^2 and so would be allowed. This is an example of the relaxation of a radial selection rule.

The above discussion concerns the asymptotic limit of the Nilsson model: the "knitting-needle nucleus" (40). Reflections of this extreme behavior are seen in detailed calculations at finite deformations. For such highly inhibited gamma-ray transitions sizable penetration effects may be expected.

Experimental results.—Nilsson & Rasmussen (48) also pointed out a number of experimental examples for which the $E1$ internal-conversion coefficients strongly deviate from their tabulated values. These were later systematically studied by Asaro, Stephens, Hollander & Perlman (50). All of these transitions are below the threshold for K conversion, but information is available on their L_I , L_{II} , and L_{III} conversion properties.

The results of Asaro *et al.* (50) may be summarized as follows: (a) The deviation from tabulated values of the conversion coefficients is correlated with the inhibition of the gamma-ray matrix element. (b) Anomalies are observed only in L_I and L_{II} conversion, but L_{III} is compatible with the tabulated values in all cases. (c) Qualitatively similar results are observed in higher atomic shells. The most spectacular example is the 85-kev transition in Pa^{231} , for which the observed L_I and L_{II} conversion is 10 to 20 times the tabulated values, while L_{III} is normal. The normal L_{III} conversion excludes an explanation based only on an admixture of $M2$.

Unfortunately, a complete set of numerical penetration coefficients is not yet available for the L shell. However, an extension of rough results of Nilsson & Rasmussen to include the radial-current penetration matrix elements, Equation 75, provides enough information for this preliminary study. The coefficients c_j' of the $\mathbf{j} \cdot \nabla$ type of penetration matrix elements are roughly the same for the following electron transitions:

$$\begin{aligned} L_I: & 2s_{1/2} \rightarrow p_{1/2} \quad \text{and} \quad 2s_{1/2} \rightarrow p_{3/2} \\ L_{II}: & 2p_{1/2} \rightarrow s_{1/2} \\ L_{III}: & 2p_{3/2} \rightarrow s_{1/2} \end{aligned} \quad 84.$$

while the coefficient c_j'' of the $\mathbf{j} \cdot \hat{\mathbf{r}}$ type of penetration matrix elements is comparable with the c_j' , or even larger, for the transitions:

$$\begin{aligned} L_I: 2s_{1/2} &\rightarrow p_{1/2} \\ L_{II}: 2p_{1/2} &\rightarrow s_{1/2} \end{aligned} \quad 85.$$

The penetration coefficients for all the other electron transitions are very small. In other words, the $\mathbf{j} \cdot \nabla$ type of penetration term appears equally in L_I , L_{II} , and L_{III} conversion. The $\mathbf{j} \cdot \hat{\mathbf{r}}$ type, on the other hand, is importantly weighted in L_I and L_{II} conversion but not in L_{III} .

The experimental observation that L_{III} conversion is normal, while L_I and L_{II} show large anomalies, would be understood if the $\mathbf{j} \cdot \hat{\mathbf{r}}$ matrix element is the important one, i.e. much larger than the $\mathbf{j} \cdot \nabla$ type (51, 52). The ratio of the two is

$$\frac{\int d\tau \mathbf{j}_n \cdot \hat{\mathbf{r}} r^2 Y_1^{m*}}{\int d\tau \mathbf{j}_n \cdot \nabla r^3 Y_1^{m*}} = \frac{\int d\tau \mathbf{j}_n \cdot \hat{\mathbf{r}} r^2 Y_1^{m*}}{-ik \int d\tau \rho_n r^3 Y_1^{m*}} \quad 86.$$

Exact calculations of this ratio require the use of specific and consistent nuclear wave functions and currents. However, on dimensional grounds it can be seen that

$$\int d\tau \mathbf{j}_n \cdot \hat{\mathbf{r}} r^2 Y_1^{m*} = iE \int d\tau \rho_n r^3 Y_1^{m*} \quad 87.$$

where E is some energy characteristic of the nuclear model. In general, this characteristic energy would be of the order of nuclear shell spacing rather than the small transition energy k , introduced by the continuity equation. For the Nilsson model, E is of the order of the oscillator spacing, $\hbar\omega \sim 6-7$ Mev. The ratio of the two penetration matrix elements is then:

$$\sim \frac{\hbar\omega}{k} \sim 10^2 \quad 88.$$

This argument indicates the dominance of the $\mathbf{j} \cdot \hat{\mathbf{r}}$ penetration matrix elements and makes it plausible that the existing formalism can describe the observed $E1$ conversion anomalies in a natural way.

When detailed penetration coefficients for L conversion become available, the observed conversion anomalies will lead to specific values of the various penetration nuclear matrix elements that must then be accounted for by any successful nuclear model. These matrix elements as computed from the Nilsson model (40, 41) appear to be of the right order of magnitude (52).

ELECTRIC MONOPOLE TRANSITIONS

Electric-monopole transitions between spin zero states have long been known. However, until recently the possibility of an $E0$ mode in $I \rightarrow I$ (no parity change) transitions had been overlooked when $I \neq 0$. The monopole mode is not inherently slow. For high- Z elements its rate would be compar-

able with that of $M1$ conversion and considerably faster than $E2$ conversion, or even $E2$ gamma-ray emission—if the $E0$, $M1$, and $E2$ matrix elements all have their dimensional, or “Weisskopf” values (13, 15). There is, of course, no $E0$ gamma-ray mode, and monopole conversion is entirely a dynamical penetration effect.

The $E0$ interaction is, as in Equation 26,

$$H_{el}'(L=0) = -e \int_0^\infty d\tau \rho_n \int_0^\tau d\tau' \psi_{n_i}^* \left(\frac{1}{r_n} - \frac{1}{r_{n'}} \right) \psi_{n_i} \quad 89.$$

The part depending on the electron functions, ψ_n , is evaluated in the same way as in the discussion of the other penetration matrix elements. The resultant $E0$ transition probability can then be written as the product of an electron factor Ω and the square of a nuclear matrix element or strength parameter ρ ,

$$\rho = \frac{1}{e} \int d\tau \rho_n \left[\left(\frac{r}{R} \right)^2 + \dots \right] \quad 90.$$

where we have omitted small terms involving higher powers of $(r/R)^2$. Computations of Ω and the coefficients of higher-order terms in the nuclear matrix element have been carried through for K - and L -shell conversion and are available in the literature (13, 15, 26, 27). As is characteristic of all penetration effects, the factor Ω increases strongly with Z , and weakly with energy. We briefly mention several applications.

A classic example of a “hidden” $E0$ transition has been noted by Peker & Sliv (53). The 191-kev $\frac{1}{2}^+ \rightarrow \frac{1}{2}^+$ transition in Au^{197} apparently exhibits a K -shell conversion coefficient significantly greater than that expected for a normal $M1$ transition. In principle, this anomaly could be attributed to a very large penetration effect in the $M1$ conversion, but it seems more reasonable to interpret the result in terms of a moderate $E0$ contribution.

Harmonic nuclei.—There is a large, well-defined class of even-even nuclei where the ground, first, and second excited states are uniformly spaced. The first excited state is 2^+ , and the second is 0^+ , 2^+ , or 4^+ . These have been called harmonic or vibrational nuclei (54, 55).

Sufficient data are available to determine the $E0$ component of the $2^+ \rightarrow 2^+$ transitions in three such nuclei; Pt^{192} , Pt^{196} , and Hg^{198} . A careful analysis of the gamma-ray modes and the measured K -shell internal-conversion coefficients discloses no measurable $E0$ component in these $2^+ \rightarrow 2^+$ transitions (13 to 15). This corresponds to an inhibition of the $E0$ transition probability by a factor of $\sim 10^3$. Such a strong inhibition is of interest for testing of the nuclear models designed to explain other features of these nuclei. The monopole mode implies a zero angular dependence of the operator, and the $E0$ operator is purely radial. For the two proposed models of the harmonic nuclei (54, 56), the two 2^+ states differ in their angular dependence and so have forbidden $E0$ matrix elements, in accord with experiment (15).

In a directional-correlation experiment, the $E0$ conversion interferes with the $E2$ conversion (42), and since the $E2$ is dominant in these transi-

tions, the interference term provides a sensitive means of measuring small $E0$ components. In this way Gerholm & Pettersson (57) established the presence of the $E0$ component in the $2+ \rightarrow 2+$ transition in Pt^{196} , along with a possible penetration effect in the inhibited $M1$ component. The magnitude of the $E0$ matrix element which they deduced is compatible with theoretical estimates (15).

Deformed nuclei.—Deformed even-even nuclei exhibit a rotational band built on their spin-zero ground state. There are high-lying levels in some of these nuclei which have been interpreted as similar members of a rotational band built on a β -vibrational level. A β -vibrational level corresponds to the oscillation of the amount of deformation about its equilibrium value, while preserving axial symmetry. Since the addition of this vibrational quantum does not change the angular properties of the levels, the $E0$ transitions between the two sets of rotational levels are allowed. Specific models of the β -vibrational levels lead to predictions of the allowed monopole transition probabilities. A more model-independent prediction, and one which is more readily checked experimentally, is the ratio of the $E0$ transition probability to the rate of $E2$ gamma-ray emission between levels of the two bands (58).

Levels which have been interpreted as members of β -vibrational bands located ~ 1 Mev above the ground state have been reported in Sm^{152} (59, 60), Er^{166} (60), Os^{188} (60), Th^{232} (61), U^{240} (62), U^{234} (63), and Pu^{238} (64). Monopole transitions have been variously reported in the $2+ \rightarrow 2+$ transitions and the $0+ \rightarrow 0+$ transitions in these nuclei. Unfortunately, there is not yet enough quantitative information for detailed analysis but it is becoming increasingly available. Further study of the $E0$ transitions in these nuclei will provide important information for perfecting the understanding of the higher levels in deformed nuclei.

SUMMARY

Nuclear matrix elements which differ from gamma-ray matrix elements are available from internal-conversion data. These penetration matrix elements are weighted weakly in the conversion process, and so are determined most accurately when the gamma-ray matrix element is inhibited, while the penetration matrix elements are allowed.

Since it is only by comparison with tabulated values of conversion coefficients that the additional penetration effects are known, it is first necessary to make comparison between tabulated and accurately measured coefficients for transitions where penetration effects are expected to be negligible. Once the reliability of tabulated coefficients has been established, obtaining the additional nuclear information, the penetration matrix elements, is a natural goal.

At the moment, penetration effects have been measured in relatively few transitions. However, as more accurate measurements of internal-conversion coefficients become available, information on penetration matrix elements should become more and more abundant.

Penetration matrix elements are related to transition matrix elements in high-energy inelastic-electron scattering (31, 55), where, for momentum transfers appreciably greater than $\sim 1/R$, penetration effects should appear importantly in all transitions, inhibited or not. Thus, both omnipresent orbital atomic electrons and artificially accelerated electrons will provide nuclear-transition matrix elements supplementing the familiar gamma-ray matrix elements as raw material for extending our knowledge of nuclear structure.

ACKNOWLEDGMENTS

We thank Dr. M. Goldhaber and other colleagues at Brookhaven National Laboratory for many helpful discussions, and for their constant encouragement during the early stages of our work and the preparation of this review.

During this period, one of us (ELC) was a guest at Brookhaven and later at the Institute for Theoretical Physics, Copenhagen, as a recipient of a Secretary of the Army Research and Study Fellowship. The indispensable hospitality and generosity of these institutions are gratefully acknowledged.

LITERATURE CITED

1. Hulme, H. R., *Proc. Roy. Soc. (London)*, **A138**, 643 (1932)
2. Taylor, H. M., and Mott, N. F., *Proc. Roy. Soc. (London)*, **A138**, 665 (1932)
3. Taylor, H. M., and Mott, N. F., *Proc. Roy. Soc. (London)*, **A142**, 215 (1933)
4. Fisk, J. B., and Taylor, H. M., *Proc. Roy. Soc. (London)*, **A146**, 178 (1934)
5. Rose, M. E., Goertzel, G. H., Spinrad, B. I., Harr, J., and Strong, P., *Phys. Rev.*, **83**, 79 (1951)
6. Rose, M. E., *Beta- and Gamma-Ray Spectroscopy* (Siegbahn, K., Ed., North Holland Publishing Co., Amsterdam, Netherlands, 1955)
7. Sliv, L. A., *Zhur. Eksptl. i Teoret. Fiz.*, **21**, 770 (1951)
8. Sliv, L. A., and Listengarten, M. A., *Zhur. Eksptl. i Teoret. Fiz.*, **22**, 29 (1952)
9. Sliv, L. A., *J. phys., radium*, **16**, 523 (1955)
10. Sliv, L. A., and Band, I. M., *Coefficients of Internal Conversion of Gamma Radiation, Part I—K Shell* (Physico-Technical Institute, Academy of Science, Leningrad, U.S.S.R., 1956); issued in U. S. as *Rept. 57ICC K1*, Physics Dept., Univ. of Illinois, Urbana, Ill.)
11. Sliv, L. A., and Band, I. M., *Tables of Gamma-ray Conversion Coefficients Part II—L Shell* (Physico-Technical Institute, Academy of Science, Leningrad, U.S.S.R., 1958; issued in U. S. as *Rept. 58ICC L1*, Physics Dept., Univ. of Illinois, Urbana, Ill.)
12. Rose, M. E., *Internal Conversion Coefficients* (North Holland Publishing Co., Amsterdam, Netherlands; Interscience Publishers, Inc., New York, N. Y., 1958)
13. Church, E. L., and Weneser, J., *Phys. Rev.*, **100**, 943, 1241(A) (1955)
14. Thieme, M. T., and Bleuler, E., *Phys. Rev.*, **101**, 1031 (1956)
15. Church, E. L., and Weneser, J., *Phys. Rev.*, **103**, 1035 (1956)
16. Church, E. L., and Weneser, J., *Phys. Rev.*, **104**, 1382 (1956)
17. Bohr, A., and Weisskopf, V. F., *Phys. Rev.*, **77**, 94 (1950)
18. Eisinger, J., and Jaccarino, V., *Revs. Mod. Phys.*, **30**, 528 (1958)
19. Tralli, N., and Goertzel, G., *Phys. Rev.*, **83**, 399 (1951)
20. Coish, H. R., *Phys. Rev.*, **84**, 164 (1951)
21. Krutov, V. A., and Muller, K., *Bull. Acad. Sci. U.S.S.R., Phys. Ser. (Engl. Transl.)*, **22**, 159, 168 (1958)
22. Morse, P. M., and Feshbach, H., *Methods of Theoretical Physics* (McGraw-Hill Book Co., New York, N. Y., 1953)
23. Rose, M. E., *Multipole Fields* (John

- Wiley & Sons, Inc., New York, N. Y., 1955)
24. Dancoff, S., and Morrison, P., *Phys. Rev.*, **55**, 122 (1939)
 25. Kramer, G., *Z. Physik*, **146**, 187 (1956); **147**, 628 (1957)
 26. Reiner, A. S., *Physica*, **23**, 338 (1957)
 27. Listengarten, M. A., and Band, I. M., *Bull. Acad. Sci. U.S.S.R., Phys. Ser. (Engl. Transl.)*, **23**, 225 (1959)
 28. Matumoto, Z., and Yamada, M., *Progr. Theoret. Phys. (Kyoto)*, **19**, 285 (1958)
 29. Brysk, N., and Rose, M. E., *U. S. Atomic Energy Comm. Rept., ORNL-1830* (1955)
 30. Rose, M. E., and Holmes, D. K., *U. S. Atomic Energy Comm. Rept., ORNL-1022* (1951); Rose, M. E., *Phys. Rev.*, **82**, 389 (1951)
 31. Hofstadter, R., *Ann. Rev. Nuclear Sci.*, **7**, 231 (1957)
 32. Church, E. L., and Weneser, J., *Bull. Am. Phys. Soc.*, **3**, 184 (1958)
 33. Listengarten, M. A., *Bull. Acad. Sci. U.S.S.R., Phys. Ser. (Engl. Transl.)*, **22**, 755 (1958)
 34. McGowan, F. K., and Stelson, P. H., *Phys. Rev.*, **107**, 1674 (1957)
 35. Green, T. A., and Rose, M. E., *Phys. Rev.*, **110**, 105 (1958)
 36. Sachs, R. G., and Ross, M., *Phys. Rev.*, **84**, 379 (1951)
 37. Snyder, E. S., and Frankel, S., *Phys. Rev.*, **106**, 755 (1957)
 - 37a. Gimmi, F., Heer, E., and Scherrer, P., *Helv. Phys. Acta*, **29**, 147 (1956)
 38. Strominger, D., Hollander, J. M., and Seaborg, G. T., *Revs. Mod. Phys.*, **30**, 585 (1958)
 39. Bohr, A., and Mottelson, B. R., *Kgl. Danske Videnskab. Selskab, Mat.-fys. Medd.*, **27**, No. 16 (1953)
 40. Nilsson, S. G., *Kgl. Danske Videnskab. Selskab., Mat.-fys. Medd.*, **29**, No. 16 (1955)
 41. Mottelson, B. R., and Nilsson, S. G., *Kgl. Danske Videnskab. Selskab., Mat.-fys. Skrifter*, **1**, No. 8 (1959)
 42. Church, E. L., Rose, M. E., and Weneser, J., *Phys. Rev.*, **109**, 1299 (1958)
 43. Reiner, A. S., *Nuclear Phys.*, **5**, 544 (1958)
 44. McGowan, F. K., and Stelson, P. H., *Phys. Rev.*, **109**, 901 (1958)
 45. Nijgh, G. J., and Wapstra, A. H., *Nuclear Phys.*, **9**, 545 (1959)
 - 45a. Nijgh, G. J., Wapstra, A. H., Ornstein, L. Th. M., Salomons-Grobbe, N., and Huizenga, J. R., *Nuclear Phys.*, **9**, 528 (1959)
 46. Kisslinger, L. S., *Phys. Rev.*, **114**, 292 (1959)
 47. Deutch, B. I., and Goldberg, N., *Phys. Rev.*, **117**, 818 (1960)
 48. Nilsson, S. G., and Rasmussen, J. O., *Nuclear Phys.*, **5**, 617 (1958)
 49. Tang, Y. C., *Nuclear Structure Effect on the Electric K-Conversion Coefficients* (Doctoral thesis, Physics Dept., Univ. of Illinois, Urbana, Ill., 1958)
 50. Asaro, F., Stephens, F. S., Hollander, J. M., and Perlman, I., *Phys. Rev.*, **117**, 492 (1960)
 51. Voikhanskii, M. E., and Listengarten, M. A., *Bull. Acad. Sci. U.S.S.R., Phys. Ser. (Engl. Transl.)*, **23**, 228 (1959)
 52. Church, E. L., and Weneser, J., *Bull. Am. Phys. Soc.*, **5**, 231 (1960)
 53. Peker, L. K., and Sliv, L. A., *J. Exptl. Theoret. Phys. (U.S.S.R.)*, **5**, 515 (1957)
 54. Scharff-Goldhaber, G., and Weneser, J., *Phys. Rev.*, **98**, 212 (1955)
 55. Alaga, G., Alder, K., Bohr, A., Stech, B., and Winther, A., *Revs. Mod. Phys.*, **28**, 432 (1956)
 56. Wilets, L., and Jean, M., *Phys. Rev.*, **102**, 788 (1956)
 57. Gerholm, T. R., and Pettersson, B. G., *Phys. Rev.*, **110**, 1119 (1958)
 58. Reiner, A. S., *Structure Effects in the Interaction Between Nuclei and Atomic Electrons* (Doctoral thesis, Univ. of Amsterdam, Amsterdam, the Netherlands, 1958)
 59. Nathan, O., and Hultberg, S., *Nuclear Phys.*, **10**, 118 (1959); and private communication (1960)
 60. Marklund, I., Van Nooijen, B., and Grabowski, Z., *Nuclear Phys.*, **15**, 533 (1960)
 61. Durham, F. E., Rester, D. H., and Class, C. M., *Bull. Am. Phys. Soc.*, **5**, 110 (1960)
 62. Bunker, M. E., Dropesky, B. J., Knight, J. D., Starner, J. W., and Warren, B., *Phys. Rev.*, **116**, 143 (1959)
 63. Gallagher, C. J., Jr., and Thomas, T. D., *Nuclear Phys.*, **14**, 1 (1959)
 64. Perlman, I., and Rasmussen, J. O., *Handbuch der Physik*, **42**, 109 (Springer-Verlag, Berlin, Germany, 1957)

RECOIL TECHNIQUES IN NUCLEAR REACTION AND FISSION STUDIES¹

By B. G. HARVEY

*University of California, Lawrence Radiation Laboratory,
Berkeley, California²*

INTRODUCTION

Nuclear reactions are traditionally studied by measurement of reaction cross sections; differential cross sections, angular distributions, and energy spectra of emitted particles or gamma rays; and more recently by measurements of the polarization of emitted particles and angular correlations. Except for radiochemical determinations of reaction cross sections, all these techniques involve the observation of emitted light particles. The momenta and angular distributions of the recoiling product nuclei are connected to the momenta and angular distributions of the emitted particles by the requirements of momentum and energy conservation. Thus the study of the recoiling nuclei may in some cases be an excellent method for obtaining information about a nuclear reaction.

The vector representing the direction and momentum of a recoiling nucleus must be equal to the vector sum of the momenta of the incident and emitted particles. If a compound nucleus is formed, the total momentum of the incident particle is transferred to the struck nucleus. The evaporation of a few low-energy nucleons subsequently modifies the momentum vector of the recoil, but the average recoil momentum should be very nearly equal to the momenta of the incident particles. If the reaction takes place by a direct mechanism (e.g. stripping or cascade), then only a part of the momentum of the incident particle may be transferred to the struck nucleus. Reconstruction of the kinematics from the observed angles and momenta of the recoils is then much more difficult. The most promising approach seems to be to compare the experimental results with calculations based on a detailed model of the reaction.

In special cases, the average forward component of the momenta of recoils may be greater than the momenta of the incident particles. This can happen only when secondary particles are emitted preferentially in the backward direction. In spite of the existence of this possibility, the discovery that recoil nuclei have momenta nearly equal to those of the incident particle over a range of incident-particle energies creates a strong presumption that a compound nucleus is formed.

Because of their low velocities, the recoil nuclei have short ranges and scatter very strongly. Thus, measurements based on emitted light fragments and particles are usually more accurate, but some kinds of information

¹ The survey of literature pertaining to this review was concluded March 15, 1960.

² This article was written under Atomic Energy Commission Contract No-7405-eng-48.

cannot be obtained in this way. Such cases arise when the nature of the nuclear reaction leading to a specific product is the subject of interest. For example, measurement of the spectrum and angular distribution of neutrons emitted from Au^{197} under bombardment with 50-Mev helium ions would not easily yield information about the reaction $\text{Au}^{197}(\alpha, 2n)\text{Tl}^{199}$, because only an insignificant fraction of the total yield of neutrons would arise from this reaction. However, it is possible that the information could be obtained by studying the kinetic energy and angular distribution of the recoiling Tl^{199} atoms. The essential point is that the Tl^{199} could be distinguished from the other products by its chemical and radioactive decay properties, whereas the neutrons from the $(\alpha, 2n)$ reaction are of course indistinguishable from those of the $(\alpha, 3n)$, $(\alpha, 4n)$, etc., reactions.

Recoil studies are particularly useful when a large number of different nuclear reaction products is formed simultaneously, for example in the study of fission and of high-energy spallation reactions. The results obtained are usually only semiquantitative, for a variety of reasons. First, the formation of a wide range of products in a single bombardment necessarily implies a low cross section for each individual species. Second, the high-energy accelerators produce beams of small intensity, and long bombardment periods are not easily obtained. It has therefore been necessary for most workers to use thick targets in order to obtain measurable yields of the products of interest, and the interpretation of thick-target results is far from straightforward. Third, the fundamental processes of scattering and stopping of heavy recoils are understood only semiquantitatively. In particular, the conversion of experimental ranges into kinetic energies has often been accomplished with the crudest of range-energy relationships, and the effects of scattering have been neglected. Fourth, scattering becomes particularly severe when the recoil energies are low. Hence the advantages of the high beam intensities which are available from low-energy accelerators are offset by the necessity of using extremely thin targets to minimize scattering. An ideal application of recoil methods seems to be in the study of nuclear reactions in which many particles are emitted, since coincidence counter measurements of the light particles are limited by low counting rates.

This review will be restricted to a discussion of techniques that have been used in experiments involving measurement of angular distributions and ranges of recoils, identified by their chemical and radioactive properties. The behavior of recoiling fission fragments was reviewed in 1957 by Walton (1); the fission process was discussed from a less specialized point of view in 1959 by Halpern (2); high-energy nuclear reactions were reviewed in 1959 by Miller & Hudis (3) and Harvey (4).

EXPERIMENTAL METHODS IN FISSION AND SPALLATION STUDIES

The quantities which can be measured are the angular distributions and ranges of recoil atoms. Detailed angular distributions of fission fragments

have been obtained in several experiments, but such distributions have rarely been measured in spallation reactions because of the intensity problems discussed above. More commonly, the fractions of the recoils escaping from a thick target into the forward, backward, and perpendicular directions were measured. Kinetic energies were almost invariably measured by range determinations. Measurements of momenta by magnetic analysis are possible, but they are complicated by the difficulty that a given nuclear reaction product is usually formed in a wide range of charge states. For example, the most probable charge carried by atoms of mass 97 formed in the fission of U^{235} was found to be +21 (5), but charge states +20 and +22 were also present in sufficient abundance to interfere seriously with the momentum analysis.

The different experimental methods may be roughly divided into two categories. In the first, the target layer is made very thin with respect to the range of the recoils of interest. The emerging recoils therefore preserve the range distribution and angular distribution with which they were formed, and these can be measured. The disadvantage of this method is that very thin targets produce very small yields of recoils, and hence radiochemical identification of the products may be difficult. In practice, the thin-target method is most suitable for the study of products which are very easily identified, especially α emitters, for which accurate yield measurements may be made even with low counting rates.

In the second method, the target is of a thickness which is large with respect to the range of the recoils. By measuring the fractions of a given product which recoil from the front and back faces of the target, it is possible to measure an average recoil range in the target material, and the quantity η , defined as the ratio v/V ; here v is the average velocity (in the laboratory system) imparted to the recoil by the impact of the incident particle, and V is the average velocity (in the system of the moving recoil) imparted to the struck nucleus by the particles which are emitted. Figure 1 shows the relationship between η and the vectors v and V . The results obtained by the thick-target method are less direct, but many experimental difficulties are avoided.

THIN TARGET METHOD

Ranges.—For heavy-element targets bombarded with low-energy particles, such as 20-Mev deuterons, ranges of recoils may be as low as $20 \mu\text{g./cm.}^2$ (6). Hence "thin" targets must be $1 \mu\text{g./cm.}^2$ or less, which corresponds to a monatomic layer of a heavy element. Suitable targets may be prepared by standard methods of vacuum evaporation or by electrodeposition. Under bombardment with charged particles, thin targets deteriorate rather rapidly. Yellow or brown deposits form on the target surface; they appear to be caused by radiation decomposition of vacuum pump oil deposits. Clean vacuum techniques minimize this difficulty.

Ranges of recoils have been measured in stacks of metallic catcher foils

or plastic films, or in gases. The plastic films suffer severe radiation damage and become extremely fragile; their only advantage is that they can be made as thin as $1 \mu\text{g./cm.}^2$. Films of the plastic known as VYNS were used by Harvey, Wade & Donovan (7). [Methods for making VYNS films and for measuring their thickness have been described by Pate & Yaffe (8).] Such films withstood bombardment with a few tenths of a microampere of helium ions for several hours, provided that the beam area was small compared with the area of the films. A beam spot of $\frac{1}{4}$ -in. diameter on films 1 in. in diameter was found satisfactory. After a bombardment long enough to generate a sufficient number of recoil nuclei, differential range curves were obtained by analysis of the catcher foils for the required nuclear reaction products. The

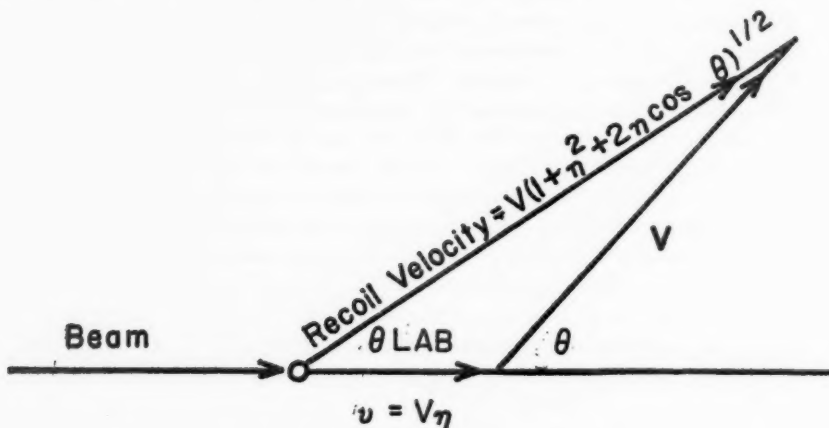


FIG. 1. Relationship between vectors v and V and the quantity η used in analysis of thick target experiments.

ranges were, however, not very reproducible. When the ranges to be measured are sufficiently great, metal foils (usually aluminum) are preferred by most workers.

If a thin source which is emitting recoils isotropically is pressed close to a stack of absorber foils, then the range of the recoils in the material of the foils may be measured by analysis of the foils in the stack. The number of recoils A_t penetrating the stack to a depth t is given by $A_t = \text{const.} \times (R - t)$ where R is the range. This method was first used by Segrè & Wiegand (9) and later by Finkle, Hoagland, Katcoff & Sugarman (10), Douthett & Templeton (11), and many others, to measure the ranges of fission fragments. The advantages of the method are that collimation of the beam of recoils is not required and that the source may be of any area.

Katcoff, Miskel & Stanley (12) measured the ranges in air of several products from the fission of Pu^{239} with slow neutrons. The recoiling fission prod-

ucts passed through a stack of very thin ($15 \mu\text{g./cm.}^2$) plastic films, between which there were air gaps. Virtually all the energy loss occurred in the air gaps, but the fragments were caught in or on the plastic film closest to the end of their range. Analysis of the films gave excellent differential range curves. The method was found not suitable for the study of any fission product with a rare gas of half life greater than 20 sec. among its precursors; diffusion of the gas before decay distorted the differential range curve. The results given by these authors are ranges in air at 760 mm. pressure and 15°C

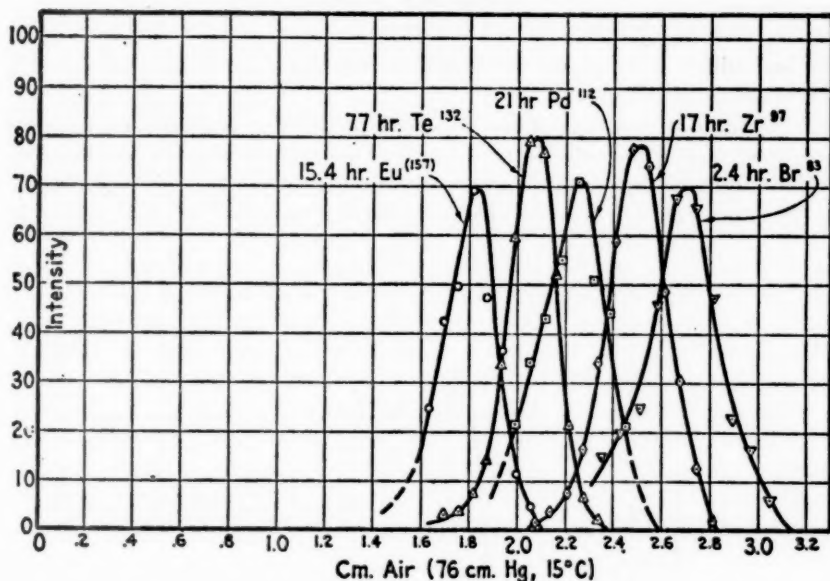


Fig. 2. Differential range curves for fission products stopping in air [Katcoff, Miskel & Stanley (12)].

temperature, and not at standard temperature and pressure. Some of their data are shown in Figure 2.

Integral range curves in gases have been measured by placing a source of recoils at a fixed distance from a "catcher" and varying the gas pressure, or by keeping the gas pressure constant and varying the distance (13, 14).

Another method for the measurement of differential ranges in gases was developed by Ghiorso & Sikkeland (15). A collimated beam of recoils passes through a gas, and the stopped ions are collected on a catcher plate by the application of a small electrostatic field normal to the recoil direction. The apparatus is represented schematically in Figure 3. After a suitable period of collection, the catcher plate may be cut into strips and the pieces analyzed

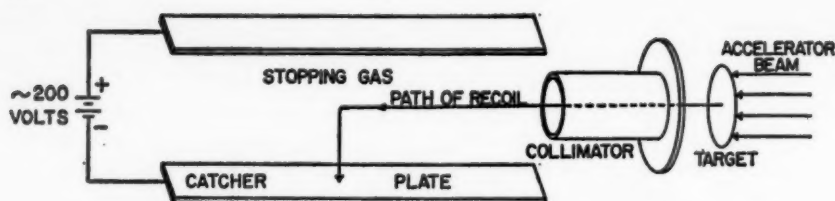


FIG. 3. Apparatus for differential range measurements by electrostatic collection.

for individual recoil products. A differential range curve obtained in this way is shown in Figure 4.

The recoil atoms must remain ionized to the very end of their range if they are to be collected electrostatically. Ghiorso was able to collect gross fission fragments from the spontaneous fission of Cf^{252} in high yields, using air as the stopping gas. Valyocsik (16) collected Th^{226} and Ra^{224} recoils stopped in

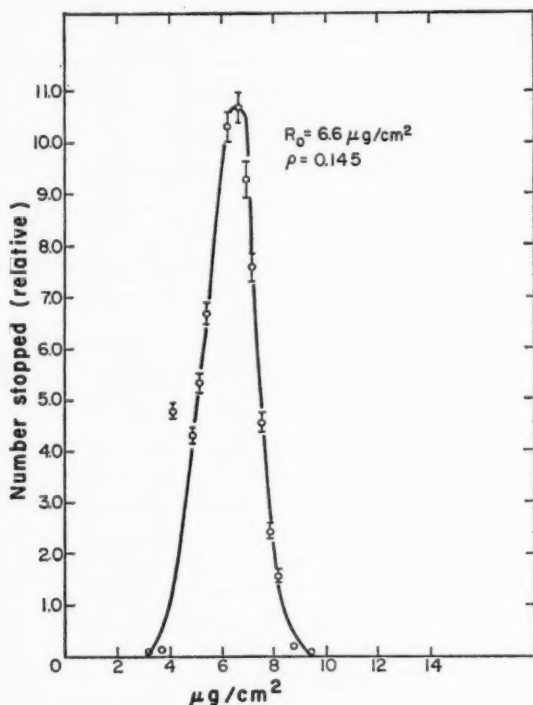


FIG. 4. Differential range curve for 96.8-keV Ra^{224} recoils stopping in deuterium [Valyocsik (16)].

H₂, D₂, He, N₂, Ne, or Ar, but Valyocsik, Donovan & Morton (17) were unable to obtain high yields of At or Po stopped in He. Collecting fields of about 100 v./cm. were used in all cases.

Using ~ 0.1 -Mev Ra²²⁴ recoils arising from the α decay of Th²²⁸, Valyocsik found that, when the collimator (Fig. 3) was made of polystyrene, all the recoils appeared on the leading edge of the catcher plate regardless of the gas pressure. Substitution of a metal collimator removed the difficulty. It appears that the polystyrene acquired surface charges at a sufficiently high potential (10⁵ v. or more) to stop the recoil ions.

The electric collecting potential will have little effect upon the trajectory of the recoils until their kinetic energies are extremely low. The path of the recoils should, therefore, break sharply downwards, and the final position of a recoil on the catcher plate should be vertically below the end of its range. Valyocsik (16) considered the possibility that the differential range curve is broadened by diffusion of the ions in their relatively slow drift down the electric field lines. On the assumption that the recoil atoms are always charged, he was able to show that range straggling introduced in this way should be negligible by comparison with true range straggling even in hydrogen (where range straggling should be minimal). However, if the drifting ions spend an appreciable part of the time in an uncharged state, then the diffusion might be much greater. In this case, however, it seems unlikely that a high collection efficiency would be achieved.

The electrostatic collection method shows great promise, but further experiments are needed to establish it as a reliable technique. The ranges of Ra²²⁴ recoils measured by Valyocsik agree reasonably well with the integral range measurements in gases of Baulch & Duncan (13), but the range stragglings which he obtained do not agree with theoretical estimates in the lighter gases (see below), and it is possible that the electrostatic method introduced some constant broadening to the differential range curves.

Alexander & Gazdik (18) used targets that were not of negligible thickness, but they were able to obtain accurate ranges of fission fragments. Most workers have added on to the measured ranges a correction for the energy loss in the target material and have tried to minimize the correction by keeping the targets as thin as possible while still obtaining a measurable yield of recoils. Alexander & Gazdik showed that the fraction F_t of the total yield of a given recoil species which succeeds in passing through a thickness t of external absorber is given by

$$F_t = 1/2(1 - t/\bar{R} - cW/2\bar{R}) \quad 1.$$

where W is the target thickness and $1/\bar{R}$ is the average reciprocal range in the external absorbers [i.e., $\bar{R} = (\langle 1/R \rangle)^{-1}$]. Equation 1 assumes that the recoils are emitted isotropically from a stationary nucleus, that the target is in close contact with the external absorber stack (50% geometry), and that the rate of velocity loss in the target material is proportional to the rate of velocity loss in the external absorbers: $-(dv/dR)_{\text{absorber}} = c(dV/dR)_{\text{target}}$.

From Equation 1, $(\partial F_t / \partial W)_t = -c/4\bar{R}$, and the constant c can be evaluated by measuring the change of F_t with respect to the target thickness W . This method is equivalent to measuring a range as a function of target thickness and extrapolating the results to zero thickness.

Suzor (19) measured ranges of individual fission products in aluminum and gold foils, using an external absorber stack. He found that the effective thickness of a uranium oxide layer formed by electrodeposition on a copper surface was substantially greater than corresponded to the weight of the oxide layer; presumably the electrodeposition process attacked the copper. Layers deposited on nickel were more satisfactory.

Alexander & Gazdik (18) made measurements in which one of the aluminum foils adjacent to the target was replaced by a gold foil. They found that some backscattering of the recoils occurred in the gold foil, but they were able to make a correction for this effect and to obtain the ranges of selected fission fragments in gold. Serious backscattering will undoubtedly occur in the target material, especially when it is a heavy element. Until this problem is more completely understood, figures quoted for the accuracy of range measurements should be viewed skeptically.

Angular distributions.—Detailed angular distributions of the products of spallation reactions have been obtained by only two groups of investigators (6, 7, 20). Donovan *et al.* (6) found that scattering of the recoils in the target material was a severe problem. To obtain accurate angular distributions of At^{211} recoils generated by the reaction $\text{Bi}^{209}(\alpha, 2n)\text{At}^{211}$ with helium ions between 20 and 48 Mev, it was necessary to use bismuth targets with a surface density of only about $1 \mu\text{g./cm.}^2$, which is approximately a monolayer of bismuth. Ball, Fairhall & Halpern (20) studied the reactions $\text{Ni}^{58}(\alpha, \gamma)\text{Zn}^{62}$ and $\text{Co}^{59}(\alpha, 2n)\text{Cu}^{61}$ at 30 Mev. Since their targets were of lower atomic number, the recoil products were of higher velocity, and scattering was less severe; they were able to use target thicknesses as high as $200 \mu\text{g./cm.}^2$. Further, they were mainly interested in recoils emitted almost normal to the target surface, and these should scatter less than those emitted obliquely, since they travel through a smaller thickness of target material. Both groups allowed the recoils to travel through an evacuated space until they were intercepted by a plane aluminum foil normal to the cyclotron beam and thick enough to stop all the recoils. The foil was subsequently cut into concentric rings that were analyzed for the various radioactive products of the nuclear reactions.

THICK TARGET METHODS

In many nuclear reactions, especially those induced by heavy incident particles, the momentum imparted to the target nucleus by the incident particle is greater than the combined momenta of all the emitted secondary particles. No matter in what direction the secondary particles are emitted, the final recoiling nucleus will always have a momentum component in the direction of the incident particle. Thus, all recoil nuclei will leave a target

from the front (down beam) face. If the target is thick, only those product nuclei formed sufficiently close to its front face will be able to escape; nuclei formed at greater depths will come to rest within the target. An average range $\langle R \rangle$ of a particular reaction product in the material of the target is obtained from

$$\langle R \rangle = N_e T / (N_e + N_t) \quad 2.$$

where N_e is the number of recoils which escape from the target, N_t is the number which remain in the target, and T is the target thickness.

In other reactions, the combined momentum of the emitted particles may exceed the momentum imparted by the incident particle, so that recoil nuclei may leave a target from both the front and back faces, depending on the relative orientation of the two momenta. By sandwiching a target of thickness W between two catcher foils thick enough to stop the recoil nuclei, the fractions of the total number of product nuclei which recoil in the forward and backward directions may be measured. Measurements of this kind have been made by Sugarman, Campos & Wielgoz (21), Porile & Sugarman (22), Fung & Perlman (23), and Porile (24). Sugarman, Campos & Wielgoz showed that the fractions R_f and R_b of the total number of product nuclei recoiling in the forward and backward directions, respectively, were related to the average range of the recoils in the target material by the equation

$$\begin{aligned} \langle R \rangle &= 4WR_f / (1 + \eta)^2 \\ &= 4WR_b / (1 - \eta)^2 \end{aligned} \quad 3.$$

The quantity η was defined on p. 237 above. It can now be related to R_f and R_b by the equation

$$\eta = \frac{(R_f/R_b)^{1/2} - 1}{(R_f/R_b)^{1/2} + 1} \quad 4.$$

In the derivation of these equations, it was assumed that the momentum resulting from the emission of secondary particles is isotropic, that the range of recoil atoms is proportional to their velocity, that the recoil paths are straight, and that the velocities involved are nonrelativistic. Porile & Sugarman (22) and Winsberg (25) discussed the effects of distributions of momentum of secondary particles of the forms $(a + b \cos^2 \theta)$ and $(a + b \sin^2 \theta)$. Winsberg also derived the equations which arise when the range of the recoil atoms is proportional to their energy rather than to their velocity; this situation may arise when the velocities are below about 2×10^8 cm./sec.

Porile & Sugarman (22) measured the amounts of various fission products (from the bombardment of bismuth and tantalum with 450-Mev protons) that were projected in the forward, backward, and perpendicular directions relative to the incident particles. From these measurements, they were able to extract the average kinetic energies of the various fragments (using an approximate range-energy relationship), the average energy deposited in the struck nucleus by the incident particle for formation of the various products, and the ratio of the parameters b/a in the angular distributions. It was pos-

sible to distinguish between the $(a+b \cos^2 \theta)$ and $(a+b \sin^2 \theta)$ distributions by comparison of the average forward-backward ranges $R_{fb} [= \frac{1}{2}(R_f + R_b)]$ with the perpendicular ranges R_p . The former distribution gives $R_{fb} > R_p$, and the latter $R_{fb} < R_p$. Experiments of this kind require the greatest possible accuracy in the estimation of the yields of recoils stopped in the various foils, and it is not clear to which co-ordinate system the angular distributions belong.

Wolke & Gutmann (26) bombarded with 450-Mev protons a brass sphere coated with a layer of bismuth 15 mg./cm.² thick and caught the recoiling fission fragments on a conical catcher that was subsequently sectioned and analyzed for the individual species. A section of the cone was cut away to permit passage of the beam. They were able to obtain the angular distribution of each species in the center-of-mass system, making the assumption that the fissioning nucleus was moving in the direction of the incident beam at the moment of fission. (There was some evidence in their work that this was not a good assumption.) Ramaniah & Sugarman (31) reinvestigated the method used by Wolke & Gutmann and found that it gave incorrect results when the intensity of the cyclotron beam at the target varied radially, because the missing sector of the catcher prevented proper averaging of the yield of recoils over the azimuthal angle. Angular distributions of fission fragments have been measured by means of catcher foils placed at a few angles around the target by Cohen and co-workers (27a to c), Winhold & Halpern (28), Coffin & Halpern (29), and Meadows (30).

RANGE-ENERGY RELATIONS

THEORY

The theory of the penetration of atomic particles into matter has been studied by several workers (32 to 39), but especially by Bohr (39), and the main features of the various types of interaction are reasonably well understood. At sufficiently high velocities, the charged moving particle interacts with the atomic electrons of the stopping medium, causing ionization and excitation. Collisions with electrons cause the moving particle to lose those electrons whose orbital velocities are less than the velocity of the particle. Its ionization, and hence rate of energy loss, will therefore be greater at the beginning of its range when its velocity is greatest (40). Very roughly, the charge of the recoil, Z^* , is related to its velocity V and atomic number Z by $Z^* = Z^{1/3} V / V_0$, where $V_0 = e^2 / \hbar^2 = 2.2 \times 10^8$ cm. per sec. [Bohr (39)]. The equation predicts charges of about +20 for fission fragments at the beginning of their range, and experimental values in agreement with this estimate have been obtained by Perfilov (41), Lassen (42), and Cohen, Cohen & Coley (5). No reliable theoretical estimates have been made for the total range of particles as a function of their initial velocity; but very approximately, the

range should be a linear function of the initial velocity (39).

At velocities below V_0 , ionization and excitation become a relatively small part of the energy loss mechanism, and energy loss by elastic collisions (so-called nuclear stopping) becomes increasingly important. This does not mean that slow particles produce no ionization. In fact the density of ionization remains high, as cloud chamber, counter, and nuclear emulsion studies show [Bøggild, Brostrøm & Lauritsen (43), Lassen (44), Demers (45), Mathieu & Demers (46)]. However, the average energy loss per ion pair formed is greater for slow than for fast particles (47).

In the nuclear stopping region, the behavior of the recoils is dependent on the ratio of the masses of the moving and stopping atoms, M_1/M_2 . If the ratio is large, then the average energy loss per collision will be small, and the recoils will follow a path which does not deviate seriously from a straight line. However, if the ratio is unity or less, the moving particles can be deflected through large angles; if the ratio is close to unity, the particles can lose a large fraction of their energy in a single encounter. It therefore becomes rather meaningless to use the concept of a range; when $M_1 < M_2$ the process should be discussed in terms of diffusion theory (37).

Bohr (39) assumed that the interaction of two atoms in the nuclear stopping region was governed by a potential of the form $P(r) = Z_1 Z_2 e^2 a / e r^2$, where Z_1 and Z_2 are the atomic numbers of the moving and stopping atoms, e is the electronic charge, e is the base of natural logarithms, and r is the distance between the two atoms. The screening parameter a is equal to $a_0 / (Z_1^{1/3} + Z_2^{1/3})^{1/2}$ where a_0 is the "radius" of the hydrogen atom, $\hbar^2 / \mu e$. With this potential, the relationship between the velocity of a particle and its mean range R_0 was found to be given by:

$$R_0 = \frac{e^2}{\pi^2 a_0^2} \cdot \frac{M_1 + M_2}{2\mu N} \cdot \frac{V^2}{V_0^2} \cdot \frac{\sqrt{Z_1^{2/3} + Z_2^{2/3}}}{Z_1 Z_2} \quad 5.$$

where N is the volume density of the atoms of the stopping medium. The equation reduces to the form

$$R_0 (\mu\text{g./cm.}^2) = kE \cdot \frac{M_2(M_1 + M_2)}{M_1} \cdot \frac{\sqrt{Z_1^{2/3} + Z_2^{2/3}}}{Z_1 Z_2} \quad 6.$$

where E is the kinetic energy of the recoil and k is a constant whose value is 602 when E is expressed in Mev.

The distribution of ranges about the mean range R_0 is expected to be given by the Gaussian expression

$$W(R) = \frac{1}{(2\pi)^{1/2} \rho R_0} \cdot \exp [-(R_0 - R)^2 / 2\rho^2 R_0^2] \quad 7.$$

TABLE I

RANGES OF MONOENERGETIC IONS IN THE NUCLEAR STOPPING REGION

Moving Ion	Energy (Mev)	Stopping Medium	Mean Range ($\mu\text{g./cm.}^2$)	Straggling Parameter		k	M_1/M_2	Ref.
				Exp.	Calc.			
Cs^{137}	0.004	Ge	1.5	—	—	1200	1.89	(50)
	0.020	Ge	8.0	—	—	1280	1.89	(50)
	0.040	Ge	11	—	—	882	1.89	(50)
Na^{24}	0.030	Al	15.0	—	—	386	0.89	(50)
Rb^{86}	0.030	Al	8.4	—	—	930	3.18	(50)
Cs^{137}	0.030	Al	7.6	—	—	1250	5.07	(50)
Ra^{224}	0.097	H_2	3.9	0.136	0.0543	725	224	(16)
	0.097	D_2	6.6	0.145	0.0765	656	112	(16)
	0.097	He	6.6	0.162	0.107	644	56	(16)
	0.097	N_2	7.0	0.238	0.192	619	16	(16)
	0.097	Ne	7.3	0.264	0.224	624	11.2	(16)
	0.097	Ar	9.4	0.315	0.293	624	5.6	(16)
Po^{218}	0.101	Air	8.27	—	—	674	15.2	(13)
Tl^{208}	0.116	H_2	5.0	—	—	777	208	(13)
	0.116	Air	8.66	—	—	598	14.5	(13)
	0.116	Ar	10.5	—	—	547	5.2	(13)
At^{210}	0.676	Bi	100	—	—	382	1.00	(7)
At^{209}	0.676	Bi	121	—	—	380	1.00	(7)
Th^{220}	0.725	D_2	32	—	—	429	113	(16)
	0.725	He	30	—	—	394	56.5	(16)
	0.725	N_2	38	—	—	456	16.2	(16)
	0.725	Ar	40	—	—	365	5.65	(16)
At^{203}	2.80	Ag	476	0.40	0.389	382	1.88	(49)
At^{205}	2.20	Ag	434	0.39	0.389	448	1.88	(49)
Tb^{140}	4.0	Al	340	0.28	0.294	484	5.52	(48)
At^{203}	4.0	Al	280	0.28	0.263	506	7.53	(48)
	4.0	Au	500	0.43	0.408	351	1.04	(48)
Au^{196}	0.014*	Au	5.8	—	—	1100	0.99	(51)
Ag^{109m}	0.022*	Ag	7.7	—	—	690	0.98	(51)
Mo^{91}	0.026*	Mo	7.3	—	—	540	0.95	(51)
Cu^{62}	0.040*	Cu	12.6	—	—	482	0.98	(51)
Cu^{64}	0.040*	Cu	13.6	—	—	510	1.01	(51)
Zn^{63}	0.040*	Zn	9.1	—	—	364	0.97	(51)
Ti^{45}	0.053*	Ti	14.7	—	—	353	0.94	(51)

* These recoils were not monoenergetic. They are included because there are so few data in this energy range.

and Lindhard & Scharff (38) gave the following expression for ρ , the range-straggling parameter:

$$\rho^2 = 2M_1M_2/[3(M_1 + M_2)^2] \quad 8.$$

A similar expression, differing only by a factor of two, was obtained by Bohr (39). Gaussian range distributions were indeed observed in several experiments (16, 48, 49) but not in others (12, 50). Range-straggling parameters measured by Valyocsik (16) in argon and by Alexander & Winsberg (48) are in better agreement with Equation 8 than with the equation given by Bohr.

The mean range given by Equations 5 and 6 is in fact the total distance travelled by a moving particle in coming to rest, but the experimental ranges are the vector sums of the projections on a fixed direction of the paths of the moving particle between collisions. For $M_1 \gg M_2$, the path should be nearly straight, so that the true range and the experimental range should be nearly identical. However, for $M_1 \approx M_2$, the projected (experimental) range should be less than the true range and, if Equation 6 is used for the experimental range, the constant k should be some function of M_1 and M_2 .

In the high-energy (electronic stopping) region, Bohr (39) discussed range straggling. He concluded that the observed straggling should arise almost entirely from the elastic collision processes occurring at the end of the range of the particle. The straggling will therefore depend on M_1 and M_2 through Equation 8, and on the fraction of the range which lies in the nuclear stopping region.

In the following sections, the more reliable range-energy and straggling measurements are discussed, first those in which the recoil energies lie in the elastic collision region and then those at higher energies. The results of the low-energy experiments are summarized in Table I, those of the high-energy experiments in Tables II and III.

EXPERIMENTAL RESULTS

Low-energy region.—Davies (50) has reported preliminary values for the ranges of 30-kev Na^{24} , Rb^{86} , and Cs^{137} ions in aluminum and for Cs^{137} ions in germanium. He allowed the electrostatically accelerated ions to fall upon an aluminum surface and then obtained differential range curves by anodic oxidation of the surface to a known depth, after which the oxide film was stripped and analyzed. Repeated application of this step gave the differential range curves. The curves were not symmetrical about the most probable range. Ranges in germanium were measured by allowing the ions to fall upon a thin germanium layer on an aluminum backing. The germanium was subsequently dissolved off and analyzed.

Recoil atoms resulting from the formation and decay of a compound nucleus should have an average momentum nearly equal to the momentum of the incident particle. The evaporation of particles will cause the recoil momentum to be modified; but close to the reaction threshold, the particles must be emitted with very low energies. Thus, the recoils should be almost

TABLE II
RANGES OF FISSION PRODUCTS IN THE ELECTRONIC STOPPING REGION

Mass Number	Energy (Mev)	Range (mg./cm. ²)	Ref.	Mass Number	Energy (Mev)	Range (mg./cm. ²)	Ref.
U²³⁵ + THERMAL NEUTRONS				U²³⁵ + THERMAL NEUTRONS			
<i>Ranges in Aluminum</i>				<i>Ranges in Zirconium*</i>			
87	96.9	3.98	(52)	89	96.6	6.88	(54)
89	96.6	4.05	(52)	99	98.5	6.12	(54)
		4.12	(18)	138	67.5	5.51	(54)
91	96.5	4.02	(18)	140	64.9	4.78	(54)
97	97.8	4.16	(19)	141, 144	64.0, 61.0	4.20	(54)
		3.99					
99	98.5	4.16	(19)				
111	—	3.51	(18)	Pu²³⁹ + THERMAL NEUTRONS			
115	—	3.33	(18)	<i>Ranges in Air</i>			
131	85.6	3.37	(18)	83	—	3.25	(12)
132	75.2	3.49	(19)	91	101	3.12	(12)
137	68.8	3.21	(52)	92	101	3.12	(12)
140	64.9	2.98	(18)	93	101	3.10	(12)
				94	101	3.09	(12)
<i>Ranges in Uranium</i>				97	99.2	3.06	(12)
77	—	12.9	(53)	99	98.8	3.04	(12)
86	97.2	10.5	(53)	105	99.0	2.96	(12)
89	96.6	11.5	(53)	109	96.6	2.88	(12)
90	96.5	11.9	(53)	112	91.4	2.74	(12)
91	96.5	11.5	(53)	117	—	2.55	(12)
93	96.7	11.3	(53)	127	82.9	2.56	(12)
95	97.1	11.4	(53)	129	81.9	2.56	(12)
97	97.8	11.4	(53)	132	79.2	2.51	(12)
99	98.5	11.2	(53)	133	78.1	2.50	(12)
103	95.7	11.2	(53)	134	76.5	2.50	(12)
106	91.5	10.9	(53)	140	69.8	2.35	(12)
109	—	10.1	(53)	143	66.8	2.32	(12)
111	—	9.74	(53)	149	60.8	2.23	(12)
112	—	9.61	(53)	157	—	2.20	(12)
115	—	9.52	(53)				
125	—	9.14	(53)	SPONTANEOUS FISSION Cf²⁵²			
127	76.6	9.58	(53)	<i>Ranges in Air</i>			
129	76.4	9.75	(53)	91	104.5	3.13	(55)
132	75.2	9.63	(53)	97	104.3	2.99	(55)
136	70.2	8.36	(53)	99	104.0	2.99	(55)
137	68.8	9.18	(53)	111	100.5	2.84	(55)
140	64.9	8.74	(53)	112	100.0	2.83	(55)
141	64.0	8.55	(53)	115	98.8	2.77	(55)
143	62.1	8.42	(53)	121	95.6†	2.69	(55)
144	61.1	8.37	(53)	127	91.4†	2.56	(55)
147	58.1	8.07	(53)	132	87.0	2.54	(55)
153	—	7.43	(53)	139	80.0	2.47	(55)
156	—	7.1	(53)	140	79.0	2.43	(55)
				141	78.0	2.38	(55)
<i>Ranges in Gold</i>				143	76.0	2.33	(55)
89	96.6	10.8	(18)	147	71.7	2.34	(55)
97	97.8	10.6	(19)	153	65.4	2.30	(55)
111	—	9.0	(18)	156	62.4	2.28	(55)
115	—	8.6	(18)	160	58.3	1.99	(55)
131	75.6	8.6	(18)				
140	64.9	8.0	(18)				

* Containing 0.05 per cent uranium.

† Only at these two energies do (68) and (69) differ by more than 3 per cent.

TABLE III
RANGES OF SPALLATION PRODUCTS FROM HEAVY-ION REACTIONS
IN THE ELECTRONIC STOPPING REGION

Energy (Mev)	Range (mg./cm. ²)	Energy (Mev)	Range (mg./cm. ²)	Energy (Mev)	Range (mg./cm. ²)*
Tb¹⁴⁹		At²⁰³		At²⁰³	
<i>Ranges in Aluminum (48)</i>		<i>Ranges in Aluminum (48)</i>		<i>Ranges in Gold (48)</i>	
4.21	0.367	3.99	0.281	4	0.50
4.50	0.371	4.77	0.318	5	0.65
6.08	0.459	4.91	0.318	6	0.79
8.61	0.657	6.36	0.411	7	0.95
9.59	0.708	6.06	0.410	8	1.12
9.43	0.730	9.27	0.598	9	1.32
10.36	0.765	10.69	0.670		
13.27	0.921	10.80	0.635		
21.32	1.323	12.10	0.732		
23.80	1.421	12.68	0.735		
26.25	1.510	13.37	0.771		
28.59	1.557	14.75	0.807		

* Values read from smooth curve.

monoenergetic, with well-known energies. Valyocsik (16) measured differential range curves in various gases for 0.725-Mev Th²²⁶ recoils produced by the reaction Ra²²⁶ (α , 4n)Th²²⁶. In these experiments, the straggling in range was partly caused by the momentum carried away by the four neutrons, but if the neutrons were emitted isotropically, then the most probable range should have been very little affected. Valyocsik also studied the ranges of monoenergetic Ra²²⁴ atoms produced by the α decay of Th²²⁸.

Ranges of (monoenergetic) recoils generated by the α -decay process have been measured by a large number of workers. The results have been summarized by Baulch & Duncan (13), who also measured integral range curves for Tl²⁰³ and Po²¹⁸ recoils in various gases.

Harvey, Wade & Donovan (7) measured the ranges in bismuth of At²⁰⁹ and At²¹⁰ recoils from the reactions Bi²⁰⁹ (α , 3n)At²¹⁰ and Bi²⁰⁹ (α , 4n)At²⁰⁹, using the thick-target method. Near the reaction thresholds, where the neutrons must be emitted with low energies, the recoils should have been monoenergetic.

Alexander & Winsberg (48) generated recoils from heavy-ion-induced compound nucleus reactions such as Pr¹⁴¹(C¹², 4n)Tb¹⁴⁹ and Au¹⁹⁷(C¹², 6n)At²⁰³. They were able to measure both ranges and range straggling in aluminum and gold foils at several energies. The emission of the neutrons was shown to cause only a negligible increase in the measured range straggling of

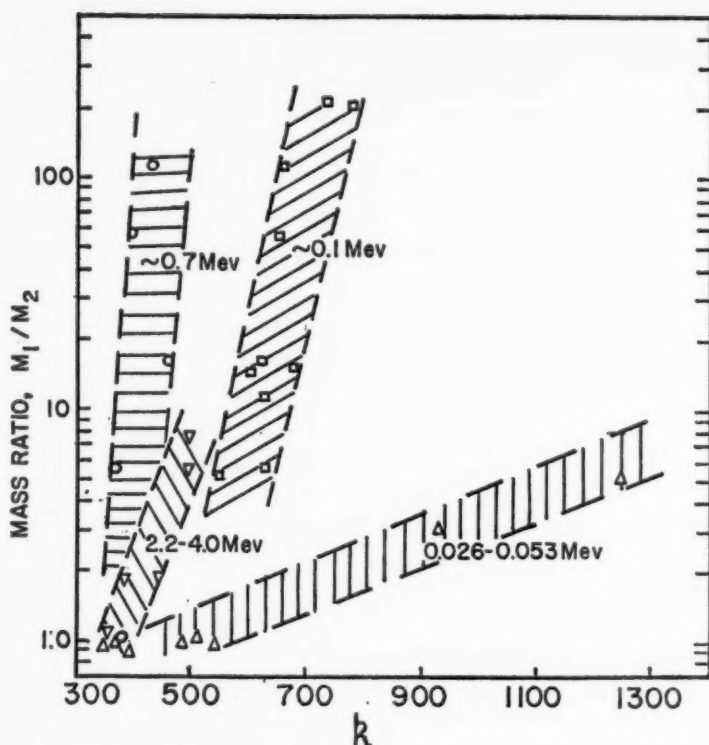


FIG. 5. Variation of k (Eq. 6) with mass ratio M_1/M_2 in the nuclear stopping region. Δ 0.026–0.053 Mev; \square ~ 0.1 Mev; \circ ~ 0.7 Mev; ∇ 2.2–4.0 Mev.

recoils from heavy-ion-induced reactions, and the straggling parameters are in good agreement with Equation 8. Their results for 4-Mev recoils are shown in Table I. Similar results were obtained by Leachman & Atterling (49) for the ranges of At^{203} and At^{205} recoils in aluminum and silver. However, their bombardments were made with a continuous energy spectrum of C^{12} ions, and the actual particle energies responsible for the formation of the astatine products were not accurately known. The energy of Leachman & Atterling's recoils may be obtained from their ranges in aluminum combined with Winsberg & Alexander's range-energy curve for astatine recoils in aluminum. The energies and ranges in silver may then be used to define two points on a range-energy curve for At^{203} or At^{205} in silver. Again the range-straggling parameters agree well with Equation 8.

Schmitt & Sharp (51) studied the ranges of several recoil species resulting from (γ, n) reactions. The momentum of the recoils derived almost entirely from the evaporated neutrons, and neither the neutrons nor the recoils were

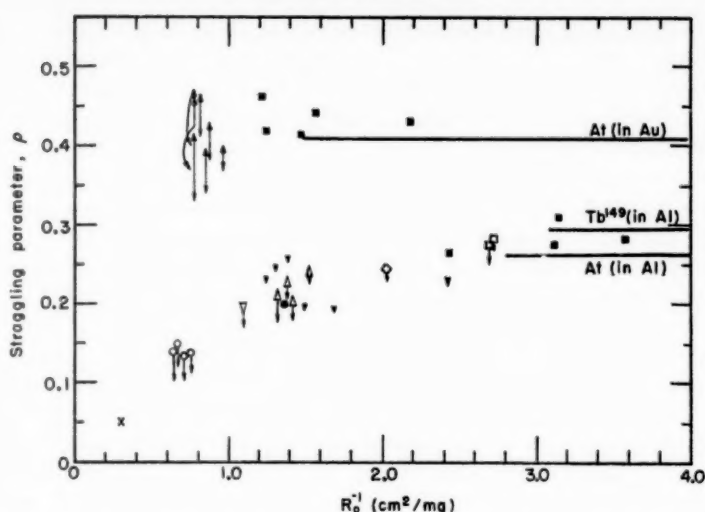


FIG. 6. Variation of range-straggling parameter ρ with reciprocal of range (R_0^{-1}) (48). Closed points are for At and Po recoils, open points for Tb^{149} . The recoils were made by heavy-ion bombardment as follows: C^{12} \square , N^{14} \diamond , O^{16} \triangle , O^{18} ∇ , Ne^{20} \odot . The symbol \times represents the range straggling of fission product Te^{132} (19). The horizontal bars are theoretical estimates from Equation 8, terminating on the left at the Bohr velocity.

monoenergetic. The results which they obtained for recoils moving in elementary matrices are shown in Table I.

All the ranges shown in Table I are in the energy region for which range is expected to be proportional to energy, and Equations 6 and 8 should apply, at least when $M_1 \gg M_2$. Column 7 of Table I shows the values of k (Eq. 6) calculated from the experimental ranges; they lie within the interval 320 to 1280, and many of them are close to the value 600. Column 8 of Table I shows the values of M_1/M_2 , and Figure 5 shows the variation of k with the mass ratio. As expected, k increases with increasing mass ratio, but it is also a function of the initial energy of the moving particles. At the lowest energies, k exceeds the theoretical value; at higher energies, k is substantially less than the theoretical value, even for large values of M_1/M_2 . This effect is perhaps caused by the greater contribution of electronic stopping at the higher energies. Unfortunately, there are not yet sufficient data on ranges as a function of E , M_1 , and M_2 to establish a universal empirical range-energy relationship.

Except for the results obtained by Valyocsik for the light gases, Table I shows that there is good agreement between the experimental range-straggling parameters and the values calculated from Equation 8. Alexander & Winsberg (48) studied the variation of ρ with recoil energy. Figure 6 shows

their results; ρ is plotted against the reciprocal of the range of the recoil expressed in mgm./cm.^2 . In the nuclear stopping region at the right of the figure, where Equation 8 is expected to apply, ρ is independent of recoil range.

High-energy region.—As the velocity of the recoils approaches V_0 , gradually increasing departures from Equation 5 should be observed, and the ranges should become more nearly proportional to velocity than to energy (velocity squared). For recoils of mass 200, the velocity V_0 corresponds to a kinetic energy of 5 Mev. Except for a few recent experiments in which recoils were generated by bombardment with heavy ions, all the experimental results in the high-energy region were obtained from the fission process, and the velocities of the recoils were very far above the critical value V_0 . The ranges of gross fission products or of the light and heavy groups have been measured many times (9; 44 to 46, 56 to 66). In several cases, the ranges of individual fission products were obtained (12, 18, 19; 52 to 55, 62, 67), and the results of some of these experiments are summarized in Table II. The only fission experiments included in the Table are those for which the energy of the fragment can be obtained from measurements independent of range measurements, in practice from velocity measurements. The kinetic energies of the fragments shown in the table were obtained from the velocity measurements of Stein (68) (U^{235} and Pu^{239}) and of Milton & Fraser (69) (Cf^{252} spontaneous fission). The Cf^{252} spontaneous fission fragment velocities were also measured by Stein & Whetstone (70), but their measurements do not agree with Milton & Fraser's in the region of symmetrical fission. Here Stein & Whetstone found a large decrease in the total kinetic energy (which is well established in the thermal-neutron fission of U^{235} , Pu^{239} , and U^{233}). The preliminary range measurements of Miskel (55), which were made by the method of Katcoff, Miskel & Stanley (12) described earlier, appear to support the results of Milton & Fraser, so that the energies shown in Table II were calculated from the velocity measurements of these authors. Actually, with the exception of the two points indicated in the table, the results of Stein & Whetstone agree within 3 per cent with the results of Milton & Fraser. In Table II, the kinetic energies are the kinetic energies of the fragments after the evaporation of neutrons. It was assumed that the average velocity is not altered by the neutron evaporation process, but that the kinetic energy decreases in proportion to the mass decrease.

Alexander & Gazdik (18) used their own results and the more reliable published data to obtain range-velocity curves for the median-light and median-heavy fission product groups in air, aluminum, and gold. The experimental ranges were obtained from their own results and from the experiments of Katcoff, Miskel & Stanley (12), Leachman & Schmitt (63), Fulmer (66), and Suzor (19). Rates of velocity loss were obtained from the papers of Leachman & Schmitt, and Fulmer. The resulting range-velocity curves could be fitted equally well with the empirical equations $R = kV - \Delta$ and $R = KE^{2/3}$, where the quantities k , Δ , and K are functions of the mass numbers of the recoil atoms and the atoms of the stopping medium. The following relations

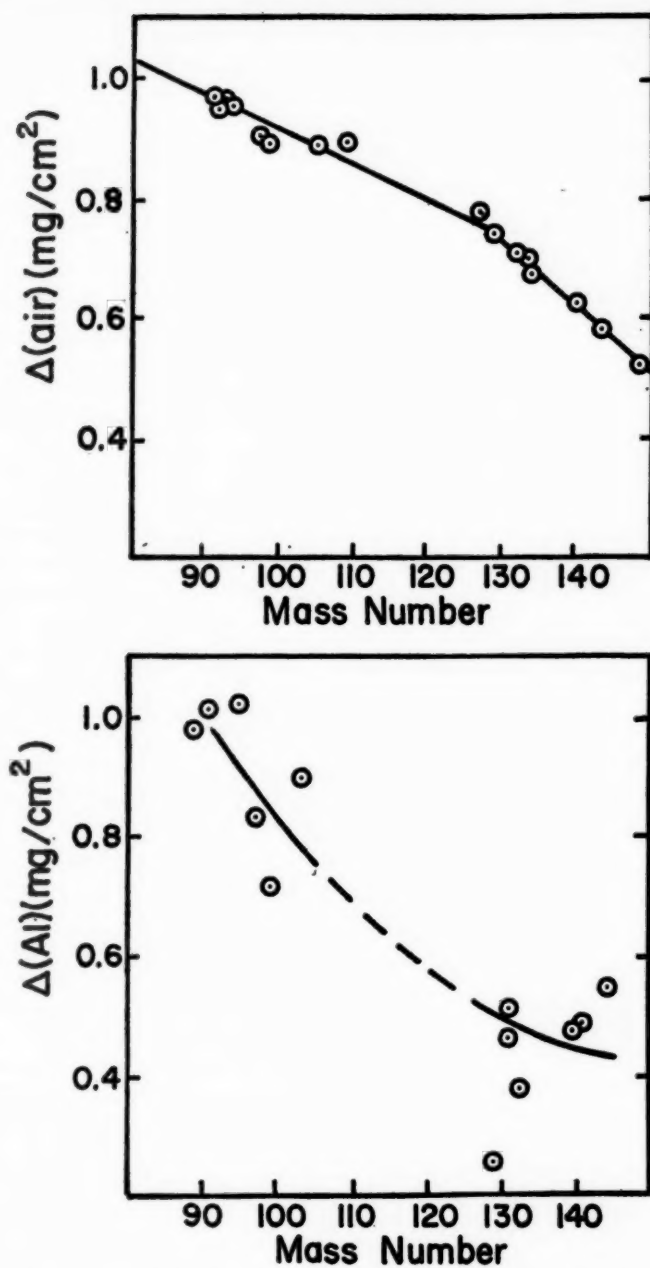


FIG. 7. The quantities $\Delta(\text{air})$ and $\Delta(\text{Al})$ of Equations 9 and 10, as functions of mass number M_1 (18).

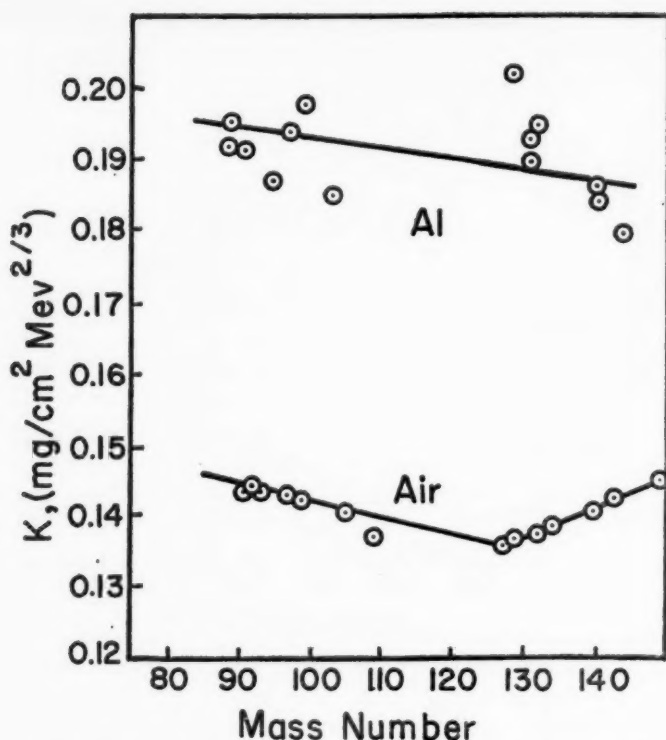


FIG. 8. The parameter K of the range-energy equation $R(\text{mg./cm.}^2) = KE^{2/3}$, as a function of mass number M_1 , for stopping in aluminum (upper curve) and air (lower curve) (18).

between range and velocity and energy were found to agree with the experimental results to within 0.5 Mev, but these equations should not be used for fragment energies below about 25 Mev, or for fragments whose mass-to-charge ratio is very different from that of a fission product.

$$R(\text{air}) = (5.44 \times 10^{-3} M_1 + 2.253)V - \Delta(\text{air}) \quad 9.$$

$$R(\text{Al}) = (2.84 \times 10^{-3} M_1 + 3.206)V - \Delta(\text{Al}) \quad 10.$$

In these equations, the velocity V is equal to $[2E(\text{Mev})/M_1]^{1/2}$, where M_1 is the mass number of the fission product. Values of $\Delta(\text{air})$ and $\Delta(\text{Al})$ as a function of M_1 are given in Figure 7. Values of K for aluminum and air are given as a function of M_1 in Figure 8, in units of $\text{mgm.}/(\text{cm.}^2 \text{Mev}^{2/3})$.

Unfortunately, calculation of the kinetic energies of fragments from the spontaneous fission of Cf^{252} , using Equation 9 and the ranges quoted in Table II, gives results which differ by an average of 8.3 per cent from the kinetic energies calculated from Milton & Fraser's velocity measurements. Obviously more range-velocity measurements are badly needed.

In the transition region between nuclear and electronic stopping, the ranges of Tb^{149} in aluminum and At^{203} in aluminum and gold were measured by Alexander & Winsberg (48), with both differential and integral methods. Measurements were made over a wide range of energies by generating the recoils in different nuclear reactions, for example $\text{Pr}^{141}(\text{C}^{12}, 4n)\text{Tb}^{149}$, $\text{La}^{139}(\text{O}^{18}, 8n)\text{Tb}^{149}$ and so on. There are too many points in their range-energy curve for At^{203} stopping in gold to make it possible to include them all in Table III. Therefore, the table contains a few values read from the smooth range-energy curve. Application of Equation 10 to the Tb^{149} data in Table III gives calculated ranges which are about 15 per cent greater than the experimental values, but Tb^{149} is on the neutron-deficient side of stability, while Equation 10 was established for neutron-excess fission products. The charge carried by Tb^{149} atoms is likely to be different from the charge carried by a fission fragment of the same mass, so that it is not surprising that somewhat different stopping properties are observed.

CALCULATIONS

Conversion into the center-of-mass system of a recoil kinetic energy or angular distribution measured in the laboratory system requires a knowledge of the reaction Q values. Since recoil measurements are invariably made with nuclear reactions in which particles are emitted with a continuous distribution of kinetic energies, it is clear that conversion to the center-of-mass system is not straightforward. There is no unique Q value for such reactions, but rather an unknown distribution of values. The problem would be no simpler if the emitted light particles were studied instead of the recoiling nuclei. However, there are many reactions in which the velocities of the light particles are much greater than the center-of-mass velocity, and then their kinetic energies and angular distributions are nearly the same in both systems of co-ordinates. Except in fission studies, such a circumstance is not likely to occur for the heavy recoil fragments.

If, from some model of the nuclear reaction, it is possible to construct a probability distribution of Q , then the problem of conversion can be solved. Gonzalez-Vidal (71) attempted an analytical conversion from laboratory to center-of-mass system for angular distributions of recoil nuclei from reactions in which one or two neutrons were evaporated with an energy spectrum of the form $P(E) = Ee^{-E/T}$, where T is a nuclear temperature, but he found that the two-neutron problem involved equations which required computer programming. An alternative approach was made by Donovan, Harvey & Wade (6, 7), who applied the Monte Carlo method to reactions in which up to four neutrons were evaporated with the (assumed) energy spectrum mentioned above. Angular distributions and kinetic energies of light particles have been calculated by the Monte Carlo method for high-energy cascade processes (72, 73). Kinetic-energy spectra of particles emitted in evaporation processes have also been computed by the Monte Carlo method (74 to 78). Results of these various computations may be used to calculate recoil kinetic energies and angular distributions which can then be compared with experimental

results. The high-energy cascade calculations were used in this way by Porile (79). The disadvantage of this approach is that when calculation and experiment fail to agree, it is necessary to repeat the calculations with a modified model, and it may not be clear in which way the model requires changing. Even when agreement is achieved, it is not obvious that the chosen model is the only one which would lead to agreement.

The precise meaning of ranges and values of η obtained by the forward-backward ratio method with the aid of Equations 3 and 4 has been discussed by Porile & Sugarman (22) and Winsberg (25). Regardless of the form of the range-energy relationship, these equations yield, in the limit for small values of η , $\langle 1/R \rangle^{-1}$, and $\langle \eta \rangle$ when the target is thin; but when the target thickness exceeds W_{\max} the measured quantities become $\langle R \rangle$ and $\langle R\eta \rangle / \langle R \rangle$. The quantity W_{\max} depends on the range-velocity relationship: if this can be expressed in the form $R = kV^N$, then $W_{\max} = R(1 \pm \eta)^N$. Naturally, it is important to remember the kind of averaging which has taken place when ranges are converted into energies subsequently used in dynamical calculations.

SUMMARY

The study of recoiling nuclei is likely to be of increasing importance in the nuclear reaction field. The techniques are improving very rapidly, but it is clear from the discussion above that better range-energy relationships and a better understanding of scattering are urgently needed. Until this has been accomplished, the most promising applications will perhaps be in uncovering new phenomena and making semiquantitative measurements in relatively unexplored fields such as the study of complex nuclear reactions in which many particles are emitted, or of reactions for which the cross sections are small.

ACKNOWLEDGMENTS

Many studies of recoil ranges were in process of completion as this review was compiled. At the risk of including data which may not stand the test of time, the author has persuaded several authors to permit him to quote information which is about to be published. For this co-operation, thanks are due to Drs. Davies, Schmitt, Niday, Miskel, Alexander, and Winsberg, and Mrs. Gazdik. Particular thanks are due to Drs. Alexander and Winsberg for many valuable discussions.

LITERATURE CITED

1. Walton, G. N., *Progr. in Nuclear Phys.*, **6**, 192 (1957)
2. Halpern, I., *Ann. Rev. Nuclear Sci.*, **9**, 245 (1959)
3. Miller, J. M., and Hudis, J., *Ann. Rev. Nuclear Sci.*, **9**, 159 (1959)
4. Harvey, B. G., *Progr. in Nuclear Phys.*, **7**, 89 (1959)
5. Cohen, B. L., Cohen, A. F., and Coley, C. D., *Phys. Rev.*, **104**, 1046 (1956)
6. Donovan, P. F., Harvey, B. G., and Wade, W. H., *U. S. Atomic Energy Commission Document, UCRL-9060* (1960); *Phys. Rev.* (In press)
7. Harvey, B. G., Wade, W. H., and Donovan, P. F., *U. S. Atomic Energy Commission Document, UCRL-9061* (1960); *Phys. Rev.* (In press)
8. Pate, B. D., and Yaffe, L., *Can. J. Chem.*, **33**, 15 (1954)
9. Segrè, E., and Wiegand, C., *Phys. Rev.*, **70**, 808 (1946)
10. Finkle, B., Hoagland, E. J., Katcoff, S., and Sugarman, N., *Natl. Nuclear Energy Ser., Div. IV*, **9**, Book 1, 463, 471 (1951)
11. Douthett, E. M., and Templeton, D. H., *Phys. Rev.*, **94**, 128 (1954)
12. Katcoff, S., Miskel, J. A., and Stanley, C. W., *Phys. Rev.*, **74**, 631 (1948)
13. Baulch, D. L., and Duncan, J. F., *Australian J. Chem.*, **10**, 112 (1957)
14. Good, W. M., and Wollan, E. O., *Phys. Rev.*, **101**, 249 (1956)
15. Ghiorso, A., and Sikkeland, T. (Private communication)
16. Valyocsik, E. W., *U. S. Atomic Energy Commission Document, UCRL-8855* (1959)
17. Valyocsik, E. W., Donovan, P. F., and Morton, J. R. (Unpublished work, 1958)
18. Alexander, J. M., and Gazdik, M. F., *U. S. Atomic Energy Commission Document, UCRL-8978-Revised* (1960); *Phys. Rev.* (To be published)
19. Suzor, F., *Compt. rend.*, **224**, 1155 (1947); *Compt. rend.*, **226**, 1081 (1948); *Ann. phys.*, **4**, 269 (1949)
20. Ball, J. B., Fairhall, A. W., and Halpern, I., *Phys. Rev.*, **114**, 305 (1959)
21. Sugarman, N., Campos, M., and Wielgoz, K., *Phys. Rev.*, **101**, 388 (1956)
22. Porile, N. T., and Sugarman, N., *Phys. Rev.*, **107**, 1410 (1957); with corrections, in *Phys. Rev.*, **111**, 1747 (1958)
23. Fung, S.-C., and Perlman, I., *Phys. Rev.*, **87**, 623 (1952)
24. Porile, N. T., *Phys. Rev.*, **108**, 1526 (1957)
25. Winsberg, L., *U. S. Atomic Energy Commission Document, UCRL-8618*, **44** (1959)
26. Wolke, R. L., and Gutmann, J. R., *Phys. Rev.*, **107**, 850 (1957)
- 27a. Cohen, B. L., Jones, W. H., McCormick, G. M., and Ferrell, B. L., *Phys. Rev.*, **94**, 625 (1954)
- 27b. Cohen, B. L., and Neidigh, R. V., *Rev. Sci. Instr.*, **25**, 255 (1954)
- 27c. Cohen, B. L., Ferrell-Bryan, B. L., Coombe, D. J., and Hullings, M. K., *Phys. Rev.*, **98**, 685 (1955)
28. Winhold, E. J., and Halpern, I., *Phys. Rev.*, **103**, 990 (1956)
29. Coffin, C. T., and Halpern, I., *Phys. Rev.*, **112**, 536 (1958)
30. Meadows, J. W., *Phys. Rev.*, **110**, 1109 (1958)
31. Ramaniah, M. V., and Sugarman, N., *Phys. Rev.*, **118**, 562 (1960)
32. Brunnings, J. H. M., Knipp, J. K., and Teller, E., *Phys. Rev.*, **60**, 657 (1941)
33. Knipp, J. K., and Teller, E., *Phys. Rev.*, **59**, 659 (1941)
34. Lamb, W. E., *Phys. Rev.*, **58**, 696 (1940)
35. Bell, G. I., *Phys. Rev.*, **90**, 548 (1953)
36. Bohr, N., and Lindhard, J., *Kgl. Danske Videnskab. Selskab, Mat.-fys. Medd.*, **28**, No. 7 (1954)
37. Nielsen, K. O., *Electromagnetically Enriched Isotopes and Mass Spectrometry*, 68 (Smith, M. L., Ed., Academic Press, Inc., New York, N. Y.; Butterworth and Company, London, England, 272 pp., 1956)
38. Lindhard, J., and Scharff, M., in Leachman, R. B., and Atterling, H., *Arkiv Fysik*, **13**, 101 (1957)
39. Bohr, N., *Kgl. Danske Videnskab. Selskab, Mat.-fys. Medd.*, **18**, No. 8 (1948)
40. Lassen, N. O., *Phys. Rev.*, **69**, 137 (1946)
41. Perfilov, N. A., *Compt. rend. acad. sci. U.R.S.S.*, **28**, 426 (1940)
42. Lassen, N. O., *Kgl. Danske Videnskab. Selskab, Mat.-fys. Medd.*, **23**, No. 2, (1945); *Phys. Rev.*, **68**, 142 (1945); *Kgl. Danske Videnskab. Selskab, Mat.-fys. Medd.*, **26**, No. 5 (1951); *Kgl. Danske Videnskab. Selskab, Mat.-fys. Medd.*, **26**, No. 12 (1951)
43. Bøggild, J. K., Brostrøm, K. J., and Lauritsen, T., *Kgl. Danske Videnskab. Mat.-fys. Medd.*, **18**, No. 4 (1940)
44. Lassen, N. O., *Kgl. Danske Videnskab.*

- Selskab, Mat.-fys. Medd.*, 25, No. 11 (1949); *Phys. Rev.*, 69, 137 (1946); *Phys. Rev.*, 70, 577 (1946)
45. Demers, P., *Can. J. Phys.*, 31, 78 (1953)
46. Mathieu, R., and Demers, P., *Can. J. Phys.*, 31, 97 (1953)
47. Madsen, B. S., *Kgl. Danske Videnskab. Selskab, Mat.-fys. Medd.*, 23, No. 8 (1945)
48. Alexander, J. M., and Winsberg, L., *U. S. Atomic Energy Commission Document, UCRL-8997* (1960); *Phys. Rev.* (To be published)
49. Leachman, R. B., and Atterling, H., *Arkiv Fysik*, 13, 101 (1957)
50. Davies, J. A. (Private communication, March 1960); *Can. J. Chem.* (To be published)
51. Schmitt, R. A., and Sharp, R. A., *Phys. Rev. Letters*, 1, 445 (1958); Schmitt, R. A., and van Lint, V. A. J., *General Atomic Company Rept., GA-1193* (San Diego, Calif., 1960)
52. Sugarman, N., *J. Chem. Phys.*, 15, 544 (1947)
53. Niday, J. B. (Private communication, March 1960)
54. Smith, E. R., and Frank, P. W., *Bettis Atomic Power Lab. Rept., WAPD-TM-198* (Pittsburgh, Pa., November 1959)
55. Miskel, J. A. (Private communication, March 1960)
56. Booth, E. T., Dunning, J. R., and Slack, F., *Phys. Rev.*, 55, 982 (1939)
57. Corson, D. R., and Thornton, R. L., *Phys. Rev.*, 55, 509 (1939)
58. McMillan, E. M., *Phys. Rev.*, 55, 510 (1939)
59. Green, L. L., and Livesey, D. L., *Nature*, 158, 272 (1946)
60. San-Tsiang, T., Zah-Wei, H., Chastel, R., and Vigneron, L., *J. Phys., radium*, 8, 165 (1947)
61. Bøggild, J. K., Arrøe, O. H., and Sigurgeirsson, T., *Phys. Rev.*, 71, 281 (1947)
62. Bøggild, J. K., Minhagen, L., and Nielsen, O. B., *Phys. Rev.*, 76, 988 (1949)
63. Leachman, R. B., and Schmitt, H. W., *Phys. Rev.*, 96, 1366 (1954)
64. Shamov, V. P., and Lozhkin, O. V., *J. Exptl. Theoret. Phys. (U.S.S.R.)*, 29, 286 (1955); *J. Exptl. Theoret. Phys. (Engl. Transl.)* 2, 111 (1956)
65. Lozhkin, O. V., Perfilov, N. A., and Shamov, V. P., *J. Exptl. Theoret. Phys. (U.S.S.R.)*, 29, 292 (1955); *J. Exptl. Theoret. Phys. (Engl. Transl.)*, 2, 116 (1956)
66. Fulmer, C. B., *Phys. Rev.*, 108, 1113 (1957)
67. Freedman, M. S., Metcalf, R. P., and Sugarman, N., *Natl. Nuclear Energy Ser., Div. IV*, 9, Book 1, 459 (1951)
68. Stein, W. E., *Phys. Rev.*, 108, 94 (1957)
69. Milton, J. C. D., and Fraser, J. S., *Phys. Rev.*, 111, 877 (1958)
70. Stein, W. E., and Whetstone, S. L., *Phys. Rev.*, 110, 476 (1957)
71. Gonzalez-Vidal, J. (Private communication, 1958)
72. Metropolis, N., Bivins, R., Storm, M., Miller, J. M., Friedlander, G., and Turkevich, A., *Phys. Rev.*, 110, 204 (1958)
73. Metropolis, N., Bivins, R., Storm, M., Turkevich, A., Miller, J. M., and Friedlander, G., *Phys. Rev.*, 110, 185 (1958)
74. Dostrovsky, I., Fraenkel, Z., and Rabinowitz, P., *Proc. Intern. Conf. Peaceful Uses Atomic Energy, 2nd, Geneva, 1958*, Paper 1615 (1958)
75. Dostrovsky, I., Rabinowitz, P., and Bivins, R., *Phys. Rev.*, 111, 1659 (1958)
76. Dostrovsky, I., Fraenkel, Z., and Friedlander, G., *Phys. Rev.*, 116, 683 (1959)
77. Dostrovsky, I., Fraenkel, Z., and Winsberg, L., *Phys. Rev.*, 118, 781 (1960)
78. Dostrovsky, I., Fraenkel, Z., and Rabinowitz, P., *Phys. Rev.*, 118, 791 (1960)
79. Porile, N. T. (Private communication, May 1960, to be submitted to *Phys. Rev.*)

LABELING OF ORGANIC COMPOUNDS BY RECOIL METHODS^{1,2}

BY ALFRED P. WOLF

Department of Chemistry, Brookhaven National Laboratory, Upton, Long Island, N. Y.

Atoms undergoing nuclear transformation frequently suffer some significant displacement in the matrix they find themselves in at the time the nuclear process occurs. The law of the conservation of momentum requires that an atom produced in a nuclear process have a recoil energy; this fact was recognized early in the history of radiochemistry [Brooks (1)] and was later made use of by Hahn & Meitner (2) and others. The first study of the chemical consequences of nuclear recoil was done by Lind & Bardwell (3). Attention was not centered on the fate of the recoiling atom until the now classical work of Szilard & Chalmers (4). The observation that only part of the I^{128} formed by the $I^{127}(\gamma\gamma)I^{128}$ reaction on iodine in ethyl iodide could be extracted as inorganic iodine clearly indicated that some of the radioactive iodine was held in organic combination.

The use of nuclear recoil in labeling organic molecules was not explicitly investigated until 1946 when Reid (5) studied the formation of labeled amyloid iodides by recoil methods. This study did not involve the isolation of radiochemically pure materials. The elegant work of Glueckauf, Jacobi & Kitt (6) in preparing nearly carrier-free methyl bromide-82 is the first reported example of the successful application of recoil techniques to labeling organic compounds.

INTRODUCTION

The proper application of nuclear recoil to labeling procedures requires some background in the general field of nuclear recoil chemistry, more popularly called "Hot-Atom Chemistry." Numerous worthwhile reviews of this subject have appeared in journals and books (7 to 22). The comprehensive reviews by Willard (20, 21) and the more up-to-date chapter in Haissinsky's book (22) can serve as an introduction to the field. The reader's attention is also drawn to a collection of papers (23 to 31) published as a result of a symposium on the chemical effects of nuclear transformations given at the 132nd meeting of the American Chemical Society in New York, September 1957. These papers, in addition to another paper by Willard and his co-workers (32), can serve as an up-to-date survey of many of the aspects of

¹ The survey of literature pertaining to this review was concluded in January 1960. It is the author's hope that the survey is complete with regard to recoil carbon and recoil tritium work. Recoil studies on other elements and work on ion acceleration methods, insofar as they apply to labeling processes, were also exhaustively surveyed. Any oversight on the author's part was purely accidental; he would be most grateful if such oversights were brought to his attention.

² Review prepared under the auspices of the U. S. Atomic Energy Commission

this field of research. Purely theoretical approaches to hot-atom chemistry have been presented by Libby (33); Miller, Gryder & Dodson (34); Capron and Oshima (35); Yankwich (36); and Monchick, Funabashi & Magee (37). The point of view of physicists on the problem of recoil and knock-on displacements in solids, notably the work of Seitz & Koehler (38) and Kinchin & Pease (39), has further stimulated the chemist's theoretical and mechanistic approach to hot-atom chemistry. This aspect of the field is reflected in the work of Yankwich (36) and of Harbottle & Sutin (24, 40).

Articles on recoil labeling with carbon-14 have been written by Muxart (41) and Wolf (42). Tritium recoil labeling has been discussed by Rowland & Wolfgang (43). The more general aspects of recoil labeling of organic substances have been presented by Wolf (44).

THEORETICAL AND MECHANISTIC APPROACH

In order to make use of nuclear recoil as a labeling technique, it is useful to have some physical or conceptual picture of the physical and chemical processes going on. Ideas on the mechanisms involved in the process are continually undergoing change. As yet there seems to be no satisfactory theoretical or phenomenological explanation consistent with all the reported data. In considering this problem the reader must be aware that the organic chemist concerns himself with molecular species containing atoms bound by covalent bonds. The vast body of excellent work on inorganic crystals and conventional Szilard-Chalmers reactions will not be considered in this review.

The formation of labeled species as a result of nuclear recoil in the liquid or solid state can be described as a stepwise process (45). The initial step involves the birth and then the slowing down of the recoil fragment until it becomes localized in a reactive site where it finally enters chemical combination. In the second step, intermediate chemical species are formed depending on the nature of the chemical surroundings in which the attenuated fragment finds itself. In the third step, the intermediate or excited species collapse to stable isolable compounds or at least collapse to fragments which are converted to stable compounds during the subsequent chemical operations carried out in order to isolate specific compounds. Each step can be further described in operational terms (45). A purely physical picture of the process can be seen in Figure 1 with recoiling carbon-14 as the example. At the moment of its birth, carbon-14 receives a recoil energy of about 45,000 electron volts. There seems to be little disagreement, today, that this results in complete rupture of the bonds attached to the nitrogen from whence the carbon was born. The charge state of this energetic fragment has been discussed by Yankwich (36). It initially loses energy by electronic excitation (39). Below 15,000 eV, energy loss by Rutherford scattering becomes important. Around 5000–6000 eV, hard-sphere scattering takes over as the major energy degradation process. By this time the fragment has moved 200–500 Å from its birthplace. How far it travels from this point on is quite difficult to estimate. The major portion of the energy loss in this region occurs by collisions with atoms

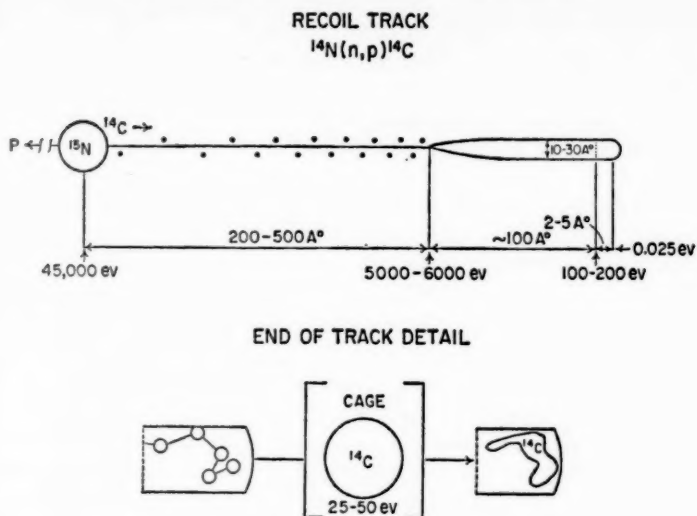


FIG. 1. Attenuation of recoil fragment.

of roughly equal mass, with an average value of one-half the kinetic energy of the fragment being lost per collision. The last few hundred eV are lost in a very small volume, with about 25 to 50 eV being associated with the terminal hot spot. Since these last few hundred eV are released in a relatively small volume, the hot spots or molten zones may overlap and provide additional reactive sites for the attenuated fragment. It is in this region that the value of this purely physical approach becomes nebulous. Recoil products formed in high-energy reactions (i.e., before the recoil fragment is thermalized) in the gas phase, sometimes in high yield, do not depend on caging effects. One can, of course, say that the nature of the de-excitation is a factor in product formation and that this is analogous to the operation of a cage.

It is also interesting to consider the consequences of the direct replacement of an atom in the lattice by a recoiling carbon-14. Such a collision was called a billiard-ball collision by Libby (33) who connected with it certain product-determining concepts (46). Kinchin & Pease (39) called this a replacement collision and did not attach any mechanistic significance to it. As these authors (39) have pointed out, if the energy of displacement of an atom in the lattice (which they take to be about 25 eV) is of the same order of magnitude as the energy required to replace an atom in the lattice (which energy can be taken to be at least the sum of the energies of the bonds binding that atom in a molecular compound), then the number of replacement collisions begins to compare favorably with the displacement collisions. This sort of process becomes more probable in the lower-energy regions. In a replacement collision the carbon-14 transfers a large amount of its kinetic

energy to the struck atom which then leaves the site of the event. The carbon-14 is left with only 25 to 50 eV and is now trapped in a volume element in which it finally becomes bound. Again, overlapping of the hot zones (36) or spikes (24) can be involved. In this picture the end of the track is defined by the distance the replaced and displaced secondaries move before the kinetic energy has been degraded. A most significant problem which has received very little attention in considering the nature of the recoil fragment and, indeed, those highly excited molecules which lead to isolable products has been the question of high-energy de-excitation. More specifically, this concerns the part played by conversion of translational to vibrational and electronic energy either in a precursor or in the hot product itself as it relates to the probability that a stable entity will be formed. The values given in Figure 1 are estimates based on the work of Yankwich (36), Seitz & Koehler (38), Kinchin & Pease (39), and Primak (47). An attempt to measure the distance traveled by carbon-14 in a nuclear emulsion gave a value of 3000 Å which is probably too high [Faraggi (48)]. It must be emphasized that this physical picture does not imply product-determining factors. Other recoil fragments, such as tritium, the halogens, sulfur, and phosphorus, must be considered independently; details such as recoil energy and charge state at the end of the track will vary. Phosphorus and other recoil fragments emitting numerous gammas present a complicated picture in which the question of complete bond rupture has not been definitively answered. Others such as N^{14} produced by β decay of carbon-14 may not rupture their bonds at all.

The two most widely quoted product-determining hypotheses are those of Libby (33, 46) and Willard (20). The model suggested by Libby involves a hot or high-energy range and an epithermal range. Hot reactions are defined as those in which nearly complete momentum transfer takes place and the recoiling atom is nearly thermalized. It was suggested that only atoms of equal or nearly equal mass can undergo these reactions, and therefore the major product resulting from a complete momentum transfer step would be the parent compounds, e.g., *n*-propyl bromide-82 from *n*-propyl bromide. In the epithermal range where inelastic collisions of the recoil atom with its surroundings are the important energy degrading processes, fragmentation of molecules and scission of carbon-carbon and carbon-hydrogen bonds take place. Here, it is suggested, the energies involved are low enough so that caging effects become important. Substitution and addition products are said to be formed in this region. Willard has suggested that the recoil atom, in striking a particular atom, is in reality transferring energy not only to the struck atom but to all the atoms attached to it and backing it up in any condensed phase. The result is a "nest" or "brush heap" of radicals surrounding the hot atom. The nature of this molecular debris is then product determining. Recombination may take place before or after the atom has a chance to diffuse in this system. Reaction after diffusion has taken place is called a thermal process. Further work in Willard's laboratory has modified this picture.

The phase effect and the radical scavenging effect have been used as

operational criteria for distinguishing between high-energy and low-energy reactions. It has been assumed that high-energy reactions should be relatively insensitive to phase and that total organic retention³ should be higher in the solid than in the liquid. The addition of scavengers to the system

TABLE I
RADIOCHEMICAL YIELDS IN ALKYL HALIDE IRRADIATIONS

Halide	Total Organic Retention		Retention as Parent		Scavenger Present		Retention as Isomer of Parent		Reference
					Tot. Org. Ret.	Ret. as Parent			
	L*	S*	L	S	L	L	L	S	
Chlorine									
Ethyl chloride	22.9	62							(51)
<i>n</i> -Propyl chloride	22.3	62			23.2				(51)
<i>i</i> -Propyl chloride	21.8				19.6				(51)
<i>n</i> -Butyl chloride	21.3	35.3			19.2				(51)
Bromine									
Ethyl bromide	31.5	84	22.6	45.5	9.0	3.6			(52)
<i>n</i> -Propyl bromide	32.4	81.6	18.0	26.0	21.0	7.6	1.9	3.4	(46)(S), (49)(L)
<i>i</i> -Propyl bromide	23.6	91.2	10.06	11.3	16.9	5.7	1.03	30.9	(46)(S), (49)(L)
Iodine									
Ethyl iodide	42.6	40.2	35.2	27.2					
<i>n</i> -Propyl iodide	54.6	61.5	42.2	21.3	34.1	24.7	2.3	18.8	(53)
<i>i</i> -Propyl iodide	31.6	51.5	23.8	39.2	23.3	16.0	1.6	3.3	(53)

* L and S in the column headings stand for liquid and solid, respectively.

(either before or after the nuclear transformations have taken place) should affect only the yields of thermal or "diffusive" (32, 49, 50) products.

The application of these criteria to a wide variety of systems has been notably inconsistent with the original hypotheses. Data in Table I on some

³ Generally speaking, the word "retention" has been taken to mean that fraction of the activity produced which is not extractable by a particular method. For example, inorganic active halide in the elemental form or in ionic form is extracted (with or without carrier present) from an alkyl halide. The activity remaining in the organic phase is assumed to be organically bound. Organic retention is then that fraction of the total activity produced which is organically bound. Retention as parent is the amount of activity in the parent molecule expressed as a fraction of the total activity produced, and so forth. Yield does not have the same context as yield in a chemical reaction. The percentage of the total radioactivity produced that is found as a particular chemical entity is defined as "yield." A more proper term would be "radiochemical yield." It must be remembered that in all nuclear recoil work the number of active atoms produced is many powers of ten smaller than the total number of molecules which were in the sample.

alkyl halides are illuminating in this regard (46, 49; 51 to 53). Total organic retention usually goes up in the solid phase except for ethyl and *n*-propyl iodide. Retention as the parent goes up for ethyl bromide, *n*-propyl bromide, and *i*-propyl iodide; it goes down for ethyl iodide and *n*-propyl iodide. The effect of scavenger is equally striking. Chloride retentions are insensitive to scavenger. Bromide and iodide retentions go down. What is perhaps more striking is that the presence of scavenger decreases parent retentions in all cases investigated. Finally, the effect of isomerization processes in the solid is curious. In the case of the bromides, the normal propyl halide is favored but in the case of the iodides, the isopropyl halide is favored.

The replacement of atoms and groups of mass smaller than that of the recoiling atom has been studied. Products which seemingly result from fragmentation and recombination might also be included in this class. Some data on these systems are presented in Table II.

TABLE II
RADIOCHEMICAL YIELDS IN HYDROGEN AND CARBON REPLACEMENT

Product Halide	Radiochemical Yield	Radiochemical Yield with Scavenger	Starting Halide	Entity Lost	Ref.
C ₂ H ₄ Br ₂	1.65	1.39	<i>n</i> -Propyl bromide	CH ₃	(49)
1,2-Dibromopropane	2.4	2.3	<i>n</i> -Propyl bromide	H	(49)
1,3-Dibromopropane	2.4	2.2	<i>n</i> -Propyl bromide	H	(49)
	Radiochemical Yield, Liquid	Radiochemical Yield, Solid			
Ethyl iodide	0.9	1.8	<i>n</i> -Propyl iodide	CH ₂ I	(53)
Ethyl iodide	0.9	0.9	<i>i</i> -Propyl iodide	CH ₂ I	(53)
<i>n</i> -Propyl iodide	0.4	0.6	<i>n</i> -Butyl iodide	CH ₂ I	(53)
<i>n</i> -Propyl iodide	0.2	0.3	<i>s</i> -Butyl iodide	CH ₂ I	(53)

The substitution of Br⁸² for hydrogen and methyl is unaffected by radical scavenger in the pertinent products from *n*-propyl bromide. Correspondingly, the gross loss of CH₂I by whatever mechanism seems to be relatively insensitive to phase. The effect of the extraneous radiation during any neutron bombardment must also be considered, as was done by Chien & Willard (54) and by Alimarin & Svoboda (55) among others.

The contention that the labeled parent compound is the product of a billiard-ball or elastic collision involving complete momentum transfer of the incoming heavy atom with the replaced atom, followed by the rapid recombination of the two fragments left behind, is not valid if the operational criteria have any validity. Clearly the yields of parent compounds are affected by both change in phase and, more drastically, by radical scavenger.

In addition, hydrogen substitution and group substitution are not affected either by change in phase or by radical scavenger.

These effects are also observed in a system involving carbon recoil (28). The yield of benzene- C_1^{11} goes down in going from liquid to solid benzene ($C^{12}(n,2n)C^{11}$ in benzene). Added scavenger reduces the yield of benzene- C_1^{11} in the liquid phase. On the other hand, the yield of toluene- C_1^{11} from benzene (substitution of H by CH_3) is unaffected by radical scavenger and by change in phase.

An increasing amount of work is being done on gas phase reactions. It was assumed during the early studies on Szilard-Chalmers reactions that recoil events in the gas phase would not lead to organic recombination. Hornig, Levey & Willard (56) showed this assumption to be wrong. The yield of CH_3I^{128} was as high as 50 per cent when the $I^{127}(n\gamma)I^{128}$ process was carried out in the gas phase. Later work showed that this was independent of the source of the iodine (e.g., I_2 , RI, HI) (25).

The virtue of the earlier theories lies in the stimulation they afforded to experimentalists in their attempt to correlate theory with fact. The great importance of a proper mechanistic hypothesis lies in the power that such a hypothesis has in directing the person using the recoil phenomenon for labeling purposes. It is self evident that a generally applicable hypothesis would aid in choosing the proper conditions for obtaining maximum yield and purity in a desired product.

The trend in the field of hot-atom chemistry has been to get away from a purely physical picture and to emphasize more strongly the chemical environment in which the recoil fragment finds itself. This attitude can be seen in the papers of Willard *et al.* (25); Milman *et al.* (50; 57 to 59); McCauley & Schuler (27); Wolf *et al.* (28, 45); Harbottle & Sutin (24); Keller & Rowland (29); and El Sayed, Estrup & Wolfgang (26). In this regard, it has become increasingly useful to describe products as being formed in the hot region or in the thermal region. The hot region is described as that region where the recoil atom still has energy in excess of 0.025 ev and is probably not in thermal equilibrium with its surroundings. A hot reaction, then, is one which occurs at energies in excess of thermal energies. The thermal region is defined as containing a recoil atom with an energy of about 0.025 ev and probably in thermal equilibrium with its surroundings. Here the atom can diffuse and react with the fragments in its vicinity. The energy of 0.025 ev should not be taken as a rigid dividing line between hot and thermal reactions.

This picture does not depend on the previous history of the atom, nor does it depend on the mode in which the recoil atom is slowed down. If the recoil atom, for example carbon-14, undergoes a replacement collision (39) while its energy is of the order of 300 ev, the actual energy left behind may be as little as a few ev or perhaps 50 or 60 ev. The reaction taking place following this event may be a hot reaction or a thermal reaction. This depends entirely on the lifetime and surroundings of that excited atom. The 200-odd ev of kinetic energy carried by the replaced carbon-12 are degraded in fur-

ther collision, and the debris left in the wake of the carbon-12 may or may not interact with the trapped carbon-14, depending again on the lifetime and energy of the recoil fragment and whether or not the hot spots overlap. If a carbon-14 atom is finally trapped at the end of its range where perhaps only a few eV are left, it can again undergo a hot reaction or a thermal reaction. It may be true that the nature of the fragments surrounding a replacement event is different from those found at the end of a track, but we have as yet no criteria for relating the observed products to the exact nature of the entrapping event.

If we accept this division into hot reactions and thermal reactions as useful, we can ask what criteria may be used to distinguish between them. It seems reasonable that a thermal radical would be affected by appropriate radical scavengers. Since radical reactions frequently are diffusion dependent, change of phase might also affect their yield. Whether a particular hot reaction is affected by change in phase or added radical trap is a debatable point. If the energies involved are very high, then most reactions will proceed with essentially zero activation energy. The question of concentration dependence (as it pertains to scavengers) becomes quite involved. It has also been pointed out (24) that since liquids are better thermal conductors than solids, the lifetimes of hot zones will be longer in solids. High-energy reactions are given a greater probability of occurring. The added cage energy will also cut down on diffusive reactions. This is meaningful only insofar as the radical, thermal or hot, has a low probability of reacting with the cage wall.

Willard *et al.* (25, 60) have presented evidence that some reactions of recoil fragments may proceed through ionic or ion-molecule reactions. Evaluation of the phase and scavenger criteria in this regard is certainly difficult.

Miller & Dodson [(61), cf. (51)] have studied the concentration dependence of the yield of cyclohexyl chloride-38 in varying mol fractions of carbon tetrachloride in cyclohexane. The constancy of the yield of alkyl halide over a wide range of carbon tetrachloride concentrations was taken to mean that the first reaction chlorine can undergo with appreciable probability is the reaction with the alkane. Further, their work indicates that this reaction occurs while the chlorine is still hot. They point out that, in principle, information of this sort may allow the calculation of the width of the energy interval in which the reaction can occur. Concentration dependence of this kind may well provide us with another clue to the nature and energy of the reactive intermediates.

It is probably valid to say that if the yield of product is sensitive to both added scavenger and change in phase, the reaction may be termed a thermal one. Hot reactions, on the other hand, may or may not be sensitive to phase. It seems less plausible that hot reactions be sensitive to scavenger. Finally, if a reaction is insensitive to phase and scavenger, it is probably a hot reaction. It can not be overemphasized that these criteria are limited in their applicability. The possibility of ionic reactions and the chemical details of the system must also be considered.

RECOIL LABELING WITH CARBON-14

LABELING PROCEDURES

The methodology involved in recoil labeling is one of its virtues. By comparison with many procedures used in organic synthesis, it is simplicity itself. The next several sections will describe carbon-14 recoil labeling, tritium recoil labeling, and labeling with other elements.

Carbon-14 recoil labeling requires thermal neutron fluxes of at least 10^{11} n cm^{-2} sec^{-1} . The cross section for the (n,p) reaction of N^{14} with thermal neutrons is about 1.75 barns; consequently, smaller fluxes will not produce sufficient activity in a reasonable time. A high thermal flux with minimal gamma and fast fluxes is desirable. Unfortunately, as the thermal flux goes up, the gamma and fast fluxes increase proportionately in currently available reactors. Proper reactor design might alleviate this situation. The author's current work is being done at fluxes of 1.2×10^{13} n cm^{-2} sec^{-1} with an accompanying gamma flux of about 3×10^8 r/sec. The cadmium ratio in the facility is about 50. The use of thermal columns (fluxes range from 10^7 – 10^9) requires excessively long irradiations although radiation damage is minimized. Facilities for carrying out the irradiation of organic compounds range in temperature from $-195^\circ C$. to $150^\circ C$. Higher temperatures are not practical because of the thermal instability of most organic compounds.

With the current high fluxes available, gamma heating becomes a problem. Sample temperatures will usually not be at the ambient air temperature or water temperature (i.e., if the sample container is immersed in H_2O) when high fluxes (e.g. 10^{13}) are being taken advantage of. Poor heat conduction in the sample and the removal of heat by diffusional processes are at fault here.⁴

The carbon-14 yield may be calculated from Equation 1

$$N^* = N\sigma\phi t \quad 1.$$

where N^* is the number of active atoms formed, N is the number of nitrogen-14 atoms being irradiated, σ is the thermal capture cross section in cm^2 , ϕ is the neutron flux per cm^2 per sec., and t is the length of the irradiation in seconds. Fluctuations in neutron flux can be most troublesome. It is sometimes possible to relate an integrated power level to the average flux, but in experimental reactors these flux levels are rarely kept constant unless special provisions are made. If simple labeling is all that is desired, this is of little consequence; if accurate radiochemical yields are desired, these should always be based on the experimentally determined carbon-14 yield. Where gaseous carbon-14 products are obtained, the found total carbon-14 yield is usually lower than the calculated yield because of losses occurring before assay is accomplished. Reasonable agreement between observed and calculated yields

⁴ The facilities at Brookhaven are being converted to forced-air cooling where the air is *circa* $-30^\circ C$. At fluxes of 10^{13} n cm^{-2} sec^{-1} with the concomitant high γ flux, samples of organic substances with masses of about 100 g. will heat to a steady temperature of about $70^\circ C$. when the ambient air temperature is about $35^\circ C$.

is found in most cases. It is sometimes advantageous to include monitoring foils as a check on the flux; aluminum foils containing 0.08 per cent manganese are convenient for this purpose. The samples are packaged in quartz or in containers made of metals certified for reactor use. The activities produced in Pyrex by capture processes make irradiation in Pyrex containers troublesome. A few of the designs used at Brookhaven are shown in Figure 2. A top view of the most commonly used vessel is pictured in A. The tube on top of the vessel is to allow for release of gases from radiation decomposition and to serve as an infinite capillary, thereby cutting down contact with oxy-

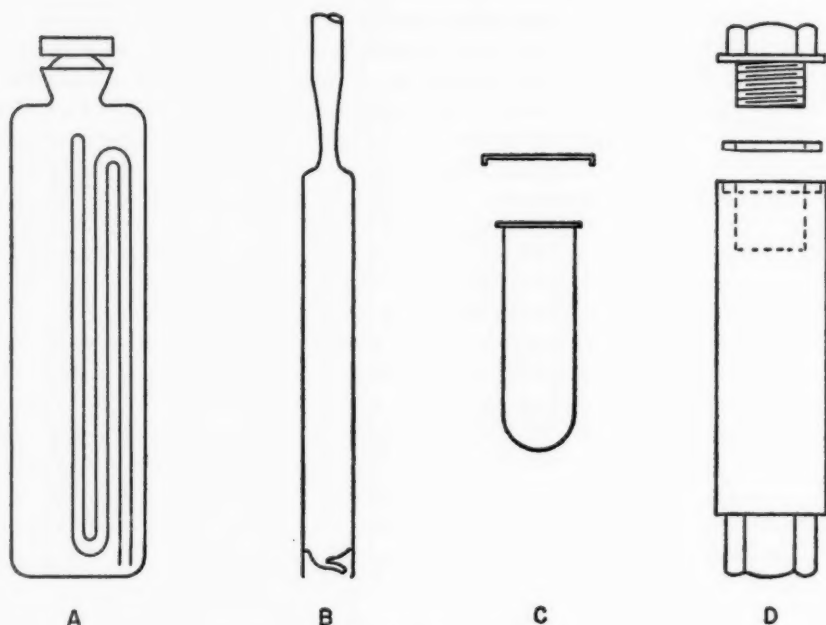


FIG. 2. Irradiation vessels.

gen. If the compound (either liquid or solid) is relatively stable, a sealed quartz container such as B may be used. The presence of a breakseal is not necessary except when subsequent assay of gaseous fragments is required. In practice, we find that quartz vessels having internal pressures below 15 atm. have essentially zero mortality in the pile. These sealed tubes are set in quartz wool and irradiated in protective aluminum containers. Container C is a standard Brookhaven National Laboratory reactor irradiation capsule well suited for the irradiation of reactor-stable solids. Container D is made of 61ST aluminum and is designed to withstand 5000 psi. A device for opening this vessel after irradiation has been described by Wolf & Oltman (62).

At the present time, an irradiation of about 200 g. of liquid or 500 g. of solid can be carried out in any of the water-cooled facilities at Brookhaven. Packaging and provision for temperature control of the sample must of course be tailored to the reactor being used.

Optimum irradiation time depends to a large extent on the material in question; its thermal and its radiation stability must be considered. Estimates of radiation stability can be made from information in a review on the radiation chemistry of organic substances by Collinson & Swallow (63). In general, most aromatic substances are less prone to damage than aliphatic compounds. Acridine is 76 per cent recoverable after three weeks of pile irradiation at a flux of 5×10^{12} thermal neutrons. On the other hand, L(+)-alanine is only 22 per cent recoverable after six days under the same conditions. The effect of radiation damage on product distribution has not as yet been studied in organic systems involving carbon-14 recoil [cf. (54, 55)]. This problem may be a most serious one not only because of the gross damage which results but, more significantly, because of the effect it may have on the product distribution (i.e., how it affects and effects the types of products that are observed). The effect of radiation damage in tritium recoil reactions has received some study and is noted in the section on tritium.

In many cases the compound can serve as its own nitrogen source (e.g., pyridine or acridine) to give a variety of labeled substances. If no nitrogen is present in the compound, it may be derivatized with a suitable nitrogen source (e.g., hydrazide or amide formation of acids or salt formation with an amine, cf. Table III). Systems in which solid solution formation is possible can be used. Yang & Wolf (64) have successfully labeled stilbene by using the stilbene-azobenzene solid solution system; clathrates (65, 66) and addition complexes (67) have also been used. Homogeneous solutions of liquids with nitrogen-containing compounds can also be used. The mole ratios of substances can affect product yield and should be considered when this procedure is used.

The nitrogenous substance should have a high nitrogen-to-carbon ratio, it should be radiation stable, and it should be easy to remove after the irradiation of such a mixture either by virtue of its boiling point, being isolable in a different phase, or because of its basic character. The general problem of maximization of the nitrogen-to-carbon ratio in order to provide optimum specific activities has been considered by Santoro & Minozzi (68, 69).

The use of liquid ammonia has proven to be disappointing to date because of solubility difficulties; heterogeneous mixtures have proven equally fruitless. This is to be expected since the pathlength of the recoil fragment is too short to allow a reasonable percentage of fragments to escape from the nitrogen source, e.g., powdered ammonium carbonate or melamine. Zifferero & Cieri (70) have reported no labeling of naphthalene from a mixture of naphthalene and hydrazine oxalate.

TABLE III
 CARBON 14 RECOIL-LABELED COMPOUNDS

Irradiated Compound	Nitrogen Source	Labeled Product	Radiochemical Yield (Per cent)	Specific Activity $\mu\text{c./mg. C}$	Reference
ALIPHATIC COMPOUNDS (and Nitrogen-containing ionic compounds)					
Acetamide	Self	Acetic acid	6.4-8.1	0.7	(45)
		Propionic acid	4.8-6.5	2.2	(45)
		Acetone	0.13	0.068	(45)
L(+)-Alanine	Self	L(+)-Alanine	0.2	0.06	(42)
Ammonia (g)	Self	Methane	90-100		(64)
Ammonium bromide	Self	Methylamine	79.1		(98)
		Methylbromide	1.8		(98)
Ammonium oxalate	Self	Oxalic acid	11.5		(86)
Butane	2-Methyl pyrazine	n-Butane	~3.0		(104)
		n-Pentane	~5.0		(104)
		i-Pentane	~5.0		(104)
i-Caproic acid anilide	Self	i-Caproic acid	<1.0		(103a)
		Aniline	2.0	0.17	(103a)
Carbon tetrachloride	Aniline	Carbon tetrachloride	31.0		(83)
1,1-Dimethylcyclopentane	2-Methylpyrazine	1,1-Dimethylcyclopentane	0.1		(104)
Trans-1,2-dimethylcyclopentane	2-Methylpyrazine	Trans-1,2-dimethylcyclopentane	0.3		(104)
Trans-1,3-dimethylcyclopentane	2-Methylpyrazine	Trans-1,3-dimethylcyclopentane	0.4		(104)
Ethylamine hydrofluoride	2-Methylpyrazine	Ethylamine	16.1		(81)
		n-Propylamine	14.7		(81)
Methanol	Aniline	Methanol	15.9		(81)
		Ethanol	8.4		(81)
Methanol	NH ₃ (liquid homogeneous)	Methanol	1.0	0.049	(103b)
		Ethanol	5.5	0.24	(103b)
		n-Propanol	3.0	0.014	(103b)
Methylamine hydrofluoride	Self	Methylamine	15.8		(81)
		Ethylamine	16.0		(81)
i-Pentane	Aniline	i-Pentane	3.8		(82)
		n-Pentane	1.3		(82)
		2-Methylpentane	6.7		(82)
		3-Methylpentane	8.7		(82)
		Neopentane	3.2		(82)
n-Pentane	Aniline	n-Pentane	2.3		(82 cf. 80)
		n-Hexane	13.4		(82 cf. 80)
		2-Methylpentane	4.9		(82 cf. 80)
		3-Methylpentane	9.1		(82 cf. 80)
n-Pentane	2-Methylpyrazine	n-Pentane	2.8	0.04	(76)
		n-Hexane	6.5	0.09	(76)
		2-Methylpentane	4.3	0.03	(76)
		3-Methylpentane	2.1	0.03	(76)
AROMATIC COMPOUNDS					
Aniline	Self	Aniline	3.0		(81)
		Benzene	0.1		(81)
		Toluene	0.7		(81)
Aniline	Self	Aniline	2.8	0.10	(103c)
		Benzene	0.35	0.03	(103c)
		Toluene	0.074	0.006	(103c)
Aniline oxalate	Self	Aniline	8.0		(88)
Anthracene	NH ₃ (liquid, heterogeneous)	Anthracene	0.009	0.010	(103c)
Azobenzene	Self	Azobenzene	2.3	0.05	(64a)
Benzamide	Self	Benzoic acid	3.8	0.5	(64)
Benzamide	Self	Benzamide	4.1		(90)
		Acetophenone	0.7		(90)
		Benzanilide	1.5		(91)
		Benzene	4.0		(87)
Benzene	Clathrate of ammoniacal nickel cyanide	Benzene			
Benzene	Clathrate of ammoniacal nickel cyanide	Benzene	1.44	0.63	(70)
Benzene	Aliphatic amine	Benzene	2.6		(105)
		Toluene	2.25-3.3		(105)
4-Ethylpyridine	Self	4-Ethylpyridine	1.0		(103c)
Naphthalene	Hydrazine oxalate	Naphthalene	0.0		(64)
Phenylalanine	Self	Phenylalanine	2.8		(93)
		Aspartic acid	4.7		(93)
		Glutamic acid	2.9		(93)
		Serine	1.0		(93)

TABLE III (Continued)

Irradiated Compound	Nitrogen Source	Labeled Product	Radiochemical Yield (Per cent)	Specific Activity $\mu\text{c./mg. C}$	Reference
Stilbene Toluene	Azobenzene 2-Methylpyrazine	Lysine	1.4		(93)
		α -Aminobutyric acid	1.2		(93)
		α -Aminovaleric acid	2.0		(93)
		Formic acid	4.2		(93)
		Propionic acid	1.8		(93)
		Malonic acid	2.9		(93)
		Succinic acid	1.4		(93)
		Glutaric acid	3.6		(93)
		Phenylpropionic acid	3.7		(93)
		Stilbene	1.3	0.05	(64)
		Toluene	1.6	0.1	(103c, e; 104)
			<i>o</i> -Xylene	0.33	0.04
	<i>m</i> -Xylene	0.37	0.02		
	<i>p</i> -Xylene	0.16	0.04		
	Ethylbenzene	0.50	0.06		
HETEROCYCLIC COMPOUNDS					
Acridine	Self	Acridine	3.5	0.22	(73)
Ammonium nicotinate	Self	Anthracene	0.2	0.32	(73)
		Nicotinic acid	4.1		(94)
		Benzoic acid	1.5		(94)
		Propionic acid	2.3		(94)
		Valeric acid	1.5		(94)
		Malonic acid	16.3		(94)
		Glutaric acid	3.2		(94)
5,6-Benzacridine	Self	5,6-Benzacridine	4.0		(78)
Isoquinoline oxalate	Self	5,6-Benzanthracene	0.2		(78)
		Isoquinoline	10.0		(88 cf. 96)
Nicotinamide	Self	Nicotinamide	3.4	0.93	(75)
Nicotinic acid hydrazide	Self	Benzoic acid	0.4	1.81	(75)
		Benzoic acid		0.43	(75)
Pyridine oxalate	Self	Pyridine	2.0		(88)
Quinoline oxalate	Self	Quinoline	1.6, 6.9		(92 cf. 86 and 96)
		Naphthalene	8.4, 0.7		(92 cf. 86 and 96)
Reserpine	Aminotetrazole complex	Reserpine		0.16	(67)
Tetrazole 1-butyl-5-amino	Self	Tetrazole 1-butyl-5-amino		14.4	(69)
Tetrazole 1-decyl-5-amino	Self	Tetrazole 1-decyl-5-amino		1.6	(69)
Tetrazole 1-ethyl-5-amino	Self	Tetrazole 1-ethyl-5-amino		5.5	(69)
Tetrazole 1-hexyl-5-amino	Self	Tetrazole 1-hexyl-5-amino		7.7	(69)
Tetrazole 1-phenyl-5-amino	Self	Tetrazole 1-phenyl-5-amino		1.0	(69)

RESULTS OF THE LABELING PROCESS

The chemical consequences of carbon-14 nuclear recoil in organic systems have been the subject of an increasing number of studies (41, 42, 44, 45; 64 to 96). A few studies on carbon-14 recoil in inorganic compounds have also appeared (97 to 100). It was pointed out by Yankwich, Rollefson & Norris (71) that recoil labeling might be possible in organic systems. They irradiated glycine, pyridine, and aniline but could not isolate the parent labeled species. It was not until the work of Edwards (72) that demonstrable activities were isolated and identified in the parent compounds irradiated, i.e., pyridine and aniline.

It is clear from the discussion in the theory section that considerable fragmentation and general molecular disruption is brought about by the

moderation of the recoil fragments' kinetic energy. In any organic system undergoing such severe local damage, it would seem that an almost infinite number of products can be formed. It is therefore perhaps somewhat surprising that sensible amounts of recognizable organic compounds can be isolated. These products result from carbon, hydrogen, nitrogen and other atom replacement, ring enlargement, deep seated structural changes, fragmentation, and polymerization processes. They can perhaps best be described in terms of some of the types of products that can be obtained. Nicotinic acid as pictured in Figure 3 is used as an example. Re-entry⁵ products are those resulting from the replacement of any carbon or nitrogen in the original irradiated compound. Synthesis products are those formed

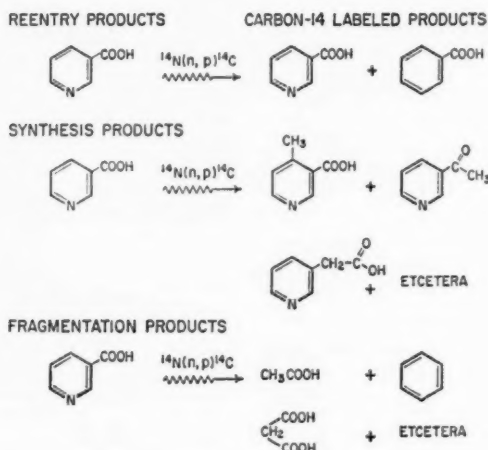


FIG. 3. Product types obtained by recoil processes.

with one carbon more than the parent compound exclusive of the carbon analogue of the parent. These products result from hydrogen, oxygen, sulfur, etc., replacement in the original compound. Compounds undergoing ring expansion or other structural changes are also included in this category. Fragmentation products are those which must arise by complex degradation, oxidation, and reduction of the original molecule. In this regard it is interesting to consider the chemical consequences of allowing active nitrogen to react with organic compounds. A complex system of compounds has been reported to result [cf. Aronovich *et al.* (101, 102)].

It must again be emphasized at this point that precursors and products are formed while the material is in an intense radiation field. Just how prod-

⁵ The division described here is artificial. Objection to the word "re-entry" can easily be raised.

uct distribution varies as a result (if at all significantly) is as yet unknown. Polymerization products are not considered in this review.

NATURE OF PRODUCTS AND ACTIVITY DISTRIBUTION IN THESE PRODUCTS

Data on a large number of compounds are collected in Table III: some conflicting data are listed where these are available in the literature; not all the data listed are truly representative of the radiochemically pure compounds. Concepts of a general nature as they apply to labeling can be derived from presently available information. These apply in particular to re-entry and synthesis products. While the yields of fragmentation products are sometimes unusually high (cf. Table III, malonic acid from ammonium nicotinate), there is as yet no reasonable a priori basis for predicting what fragmentation products might be expected in good yield or, indeed, expected in a particular system.

When one wishes to use tracers in organic molecules, it is frequently necessary to know the exact nature of the labeling, whether random or specific. In no instance reported to date has there been either true uniformly random or specific labeling. Uniformly random labeling might be expected to apply when re-entry products are formed; Figure 4 gives a number of examples of such compounds (103). It is immediately apparent that wide discrepancies exist between the theoretical values (i.e., those expected for uniformly random labeling) and the actual values. It would be presumptuous to generalize from these few cases. For example, in toluene replacement the replacement of ring carbons is favored; the reverse is true when stilbene is re-entered. The alanine case underlines the rather drastic deviation from

ACETIC ACID FROM ACETAMIDE			D-ALANINE		
	$\begin{array}{c} \text{CH}_3 - \text{COOH} \\ \\ \text{---} \end{array}$			$\begin{array}{c} \text{NH}_2 \\ \\ \text{CH}_3 - \text{CH} - \text{COOH} \\ \\ \text{---} \end{array}$	
THEORETICAL	50%	50%	33.3%	33.3%	33.3%
FOUND	38%	62%	14%	7%	79%

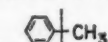
TOLUENE [2-METHYL PYRAZINE AS N SOURCE]			TRANS STILBENE [AZOBENZENE AS N SOURCE]			
	$\begin{array}{c} \text{C}_6\text{H}_5 - \text{CH}_3 \\ \\ \text{---} \end{array}$			$\begin{array}{c} \text{C}_6\text{H}_5 - \text{CH} = \text{CH} - \text{C}_6\text{H}_5 \\ \quad \quad \\ \text{---} \quad \quad \text{---} \end{array}$		
THEORETICAL	85.7%	14.3%	42.9%	7.1%	7.1%	42.9%
FOUND	89%	11%	37.5%	12.5%	12.5%	37.5%

FIG. 4. Activity distribution where random and uniform labeling might apply.

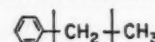
random labeling that can occur when statistical replacement might be expected.

Figures 5 and 6 give examples where specific labeling might be expected (103). The examples are synthesis compounds resulting from hydrogen or nitrogen replacement. It can be seen, for example, that specific methyl-labeled toluene results neither from the replacement of hydrogen in benzene nor from the replacement of nitrogen in aniline. It is also noteworthy that

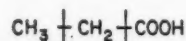
TOLUENE FROM BENZENE
2-METHYL PYRAZINE AS N SOURCE

		
THEORETICAL	0%	100%
FOUND	12%	88%

ETHYL BENZENE FROM TOLUENE
2-METHYL PYRAZINE AS N SOURCE

		
THEORETICAL	0%	100%
FOUND	5%	86%

PROPIONIC ACID FROM ACETAMIDE

			
THEORETICAL	100%	0%	0%
FOUND	52%	24%	24%

ETHANOL FROM METHANOL
NH₃ AS N SOURCE

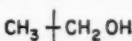
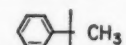
		
THEORETICAL	100%	0%
FOUND	95%	5%

FIG. 5. Activity distribution where specific labeling might apply. Hydrogen substitution.

TOLUENE FROM ANILINE

		
THEORETICAL	0%	100%
FOUND	14%	86%

BENZALANILINE FROM AZOBENZENE
STILBENE MIXTURES

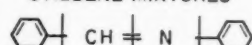
				
THEORETICAL	0%	100%	0%	0%
FOUND	15%	85%	NOT MEASURED	

FIG. 6. Activity distribution where specific labeling might apply. Nitrogen substitution.

the activities to be found in the ring are comparable. The extent of the rearranged activity can also vary widely in synthesis compounds, from the extensive rearrangement observed in the propionic acid case to the minor rearrangement observed in ethanol from methanol.⁶ The opportunity for rearrangement may be dependent on the stabilization the intermediate can get from functional groups within the molecule. Such stabilization is possible in benzene (e.g., ring resonance and low-lying excited states) and acetamide

⁶ Preliminary studies in the author's laboratory (using the Kuhn-Roth oxidation) on synthesis compounds from pentane, i.e., *n*-hexane and 3-methyl pentane, indicate that about 95 per cent of the activity is in the methyl groups in these compounds.

(e.g., carbonyl resonance stabilization) but not in intermediates leading to ethanol and hexane formation from methanol and pentane, respectively. If these generalizations have any validity, then one might expect little rearranged activity in synthesis compounds where the point of attachment is removed from functional groups (i.e., groups with π -electron systems, etc.) which might interact. In this way judicious guesses as to the degree of specificity may be made.

The radiochemical yields of synthesis products are generally higher than those of the corresponding re-entry products (cf. Table III). The yields of aliphatic synthesis products are considerably higher than the yields of aromatic synthesis products (cf., the hexanes from pentane vs. the xylenes from toluene). Re-entry products vary greatly in yield [e.g. pentane 2%, benzene 2.6%, L(+)-alanine 0.2%, acetic acid (from acetamide) 6-8%]. Santoro (69) has implied even higher yields for some re-entry products.

Yields of re-entry and synthesis products can be affected by changes in the "chemical" variables in a particular system. The specific activities of re-entry products as a function of the ratio of the number of carbons to the number of nitrogens (ρ) in particular compounds have been investigated by Santoro (68, 69). Maximum specific activities in re-entry products seem to be obtained when ρ equals 1. The yield of synthesis products has been related to the availability of hydrogen in the mixture being irradiated. Wolf and co-workers showed that with equimolar concentrations of amines as nitrogen sources, synthesis yields (e.g., toluene from benzene) will be enhanced in those solutions where the amines have the greatest number of hydrogens per mole of amine (e.g., 3,3'-diaminodipropylamine vs. 2-methylpyrazine) (105). An equation allowing the calculation of maximum yield as a function of hydrogen availability in the amine was derived. The yield may also be dependent on the chemical nature of the amine used. Atomic volume in crystals has also been suggested as a possible yield-determining influence (88, 95). The effect of phase on the yield of re-entry and synthesis products in comparable systems has not been extensively studied [cf. (28, 96)]. The results from the $C^{12}(n, 2n)C^{11}$ recoil work (28) indicate that in the benzene system the yield of benzene, a re-entry product, is decreased in going from the liquid to the solid phase and the yield of toluene, a synthesis product, is unchanged.

The statistical nature of the replacement process must be carefully considered. It was shown (73) that the radiochemical yield of anthracene from acridine was roughly in the ratio of the number of nitrogens to the number of carbons in acridine. The radiochemical yield of benzanthracene from benzacridine also followed this statistical behavior (77, 78). An early report on replacement in quinoline oxalate seemed anomalous (86). A closely related experiment (92) seemed to show that statistical behavior was followed in this system also. The yield of acetone from acetamide (45) did not follow this statistical behavior. Conditions where statistical replacement of atoms of mass comparable to carbon-14 in organic molecules might obtain have

been discussed (45). A formalism describing statistical versus nonstatistical re-entry using quinoline, quinoline oxalate, and isoquinoline as examples has been described by Brunello & Muxart (96). These authors find a deviation from statistical behavior for quinoline and for isoquinoline. The results reported for this system are contradictory and in need of clarification [cf. (86, 88, 92)].

Investigation of the statistical nature of hydrogen replacement indicates that for simple aliphatic and aromatic compounds the yields of synthesis products are in the ratio of the number of available positions. In pentane, for example, the ratio of 3:2:1 for the replaceable hydrogens is closely paralleled by the ratio of yields of *n*-hexane to 2-methyl pentane to 3-methyl pentane (106). Lack of radiochemical purity in the isolated products was responsible for the nonstatistical behavior reported in the literature at an earlier date (80, 82). The formation of ortho-, meta-, and para-xylenes from toluene also closely follows statistical behavior (107).

The stereochemical result for the replacement of an asymmetric carbon by carbon-14 has been reported for one compound, L(+)-alanine (42). Re-investigation of this system indicates that the extent of racemization (or inversion) obtained is less than that initially reported but the equivalence of activity distribution in the two enantiomers is correct (42).

The effect of chemical "working up" of irradiated materials has not been the subject of direct investigation [cf. (45, 93, 94)]. This might well prove a fertile field. For example, the yields of saturated compounds might be enhanced by thorough hydrogenation of the irradiated mixture before isolation of the compounds desired. The yield of oxygenated compounds such as acids might be enhanced by chemical oxidation of the crude materials in which the acids might be found. (For example, if $\text{CH}_3\text{CH}_2\text{OH}$, CH_3CHO , and CH_3COOH are products in the irradiation of CH_3OH , then oxidation of appropriate fractions to CH_3COOH would enhance the radiochemical yield of CH_3COOH .)

The effect of gross radiation damage to the system during irradiation on product type and yield is as yet not understood. Some work has been done which purports to show no, or only minor, effects (81, 96). It may be that the radiation effects in the systems studied were saturation effects and the variation in radiation intensity in the separate experiments was not sufficiently large in magnitude to be below the range where saturation effects exist. It must certainly be remembered that the accompanying radiation field in reactor irradiations is high.

To the author's knowledge no investigation concerning itself with post-irradiation or annealing effects for carbon-14 recoil has been reported in the literature to date.

ISOLATION AND PURIFICATION OF RECOIL PRODUCTS

To the uninitiated chemist, the appalling appearance of reactor-irradiated organic substances is usually sufficient to raise grave doubts about the usefulness of such a method. Surprisingly enough, the usual black or brown

solids and liquids one gets are frequently brought to chemical purity with relative ease. Gross contaminants such as polymeric material and decomposition products are readily removed by conventional physical and chemical methods; isolating specific compounds and bringing them to radiochemical purity is quite another matter.

Isolation of synthesis products has been done mainly by carrier methods. The parent substance acts as its own carrier for the re-entry products. Fragmentation products may result from radiation damage to the bulk material with the activity in these products being a result of labeling of the source compound or of labeling of the radiation damage fragments by recoil. These products may or may not require carriers for their isolation. Labeled fragmentation products produced as a direct result of nuclear recoil may be isolated by the usual carrier methods. Carriers are usually necessary as the concentration of labeled molecules will vary from 10^{-8} to 10^{-9} g./g. of irradiated material in the majority of cases. The specific activity of the isolable compounds is directly dependent on the amount of carrier used. The use of paper chromatography (76) and gas-liquid chromatographic techniques may allow the isolation of nearly carrier-free species.

The question of radiochemical purity has been discussed (41, 44, 45). The great multitude of synthesis and fragmentation products formed during most irradiations makes bringing any particular compound to radiochemical purity a frequently tedious task. Examples of the requisite extensive purifications can be readily found (42, 44, 45, 73, 78, 93, 94).

In re-entry compound purification, careful attention must be given to the presence of synthesis products whose properties, both physical and chemical, may be only slightly different from those of the parent substance. This becomes especially true as the molecular weight of the parent increases since the percentage difference in physical properties usually decreases concurrently. Synthesis compounds formed by nitrogen replacement are somewhat easier to isolate since their chemical properties can differ markedly from the parent substance. The ease of isolating a synthesis product from the mixture usually depends on how many isomers are produced along with it, e.g., there are seven methyl quinolines produced from quinoline but only one 2-carbon alcohol from methanol. Fragmentation products pose the same general problems.

Achievement of radiochemical purity of recoil products depends firstly on consideration of all conceivable impurities in any particular system, secondly on removal of gross impurities, and lastly on final removal of all radiochemical contaminants. The task is clearly defined when one considers that the contaminant is usually noticeable only because of its radioactivity and not because of its mass. The use of such powerful separative tools as gas liquid chromatography and column chromatography is often necessary to provide confidence in any given result. Erroneous data resulting from lack of radiochemical purity are not the exclusive province of the early work on organic halogen compounds but can be readily found in carbon-14 work also.

MECHANISMS AND APPLICATIONS

An understanding of the mechanisms involved in product formation from carbon-14 recoils is not as advanced as it is for halogen recoils and for tritium recoils. Considerable data of an empirical nature are available. Numerous postulates have been put forth, but none of these are compelling in their delineation of a specific mechanism, nor has any suggested specific mechanism been proven.

The specificity of the carbon-14 label in re-entry and synthesis products has been investigated in numerous cases. The extent of rearrangement in re-entry compounds seems to be greater for simple compounds where reactive functional groups are near the site of replacement.

It has been found that replacement of hydrogen is statistical in simple molecules such as toluene and pentane where no functional groups such as carbonyl are present. This is what one would expect of the reactions of a highly energetic fragment. Statistical replacement of hydrogen in pentane by energetic methylene produced from diazomethane has been reported by Doering *et al.* (108). It is tempting to suggest that an energetic methylene- C^{14} [$C^{14}H_2$] may be responsible for the statistical distribution found in the recoil-labeled molecules. However, the statistical distribution observed in the recoil-labeling cases does not a priori define the fragment as having been methylene- C^{14} . The distribution of activity in toluene from benzene may be a reflection of the probability of collapse from a common intermediate to give ring labeling or methyl labeling; on the other hand, the assumption of two different reaction paths is equally valid at this point.

Work in the $C^{12}(n, 2n)C^{11}$ system (if applicable to carbon-14 recoil systems) would indicate that the replacement of hydrogens in aromatic systems goes via a highly energetic fragment or intermediate and not via radical recombination. This work also clearly indicates at least two pathways for heavy-atom replacement, one occurring at thermal or near thermal energies, the other above thermal energies.

Recent gas phase work (64b) favors a collision complex as being an intermediate in high-energy C^{14} reactions. This approach may prove fruitful, but it does not as yet yield a clearly delineated and detailed mechanistic picture for any particular product.

Reasonable guesses can be made about product constitution based on information currently available (cf. Table III); one must, however, keep in mind the dangers inherent in generalizing from the results on one particular compound or system of compounds. Essentially four questions need to be answered in applying compounds labeled by the recoil method to any particular study. First and foremost: Is the compound radiochemically pure? Then: Is absolute radiochemical purity necessary? What is the specificity of the label? Is the level of activity high enough for the purpose for which it is intended?

Recoil-labeled compounds have been prepared in a pure state; applications in the oil industry and in biogenesis studies have been described (44). The implementation of the new food and drug laws may require large num-

bers of labeled compounds some of which may be conveniently prepared by the recoil method. In this regard it is significant that the labeling of reserpine by recoil has been reported. If it becomes possible to prove unequivocally that the activity reported can be attributed solely to labeled reserpine rather than to impurities from homologues (of which there are many, if hydrogen substitution is significant in this system), then the recoil labeling technique indeed opens the door to the labeling of many complex molecules which heretofore have not been considered for carbon-14 labeling because of the difficulty of introducing such a label by standard synthetic procedures.

The deficiencies of recoil labeling have been amply explored. The greatest virtue of recoil labeling is that laborious synthetic procedures are often replaced by a simple irradiation followed by isolation and adequate purification. Bulk quantities of material can be readily produced once the isolation and purification techniques have been developed (e.g., the labeling of benzene). The extent of the application of this technique remains to be seen. Certainly the surface has hardly been scratched.

RECOIL LABELING WITH TRITIUM

Labeling with recoil tritons has been discussed in several reviews (43, 44, 109). The majority of the papers in the literature have been published by Rowland and co-workers (29; 110 to 117) and by Wolfgang and his associates (26; 118 to 121). Some papers from other laboratories concerning mechanism (25, 122), mechanism and distribution (123), and use in labeling (124) have also appeared.

Recoil tritons can be produced by the $\text{Li}^6(n, \alpha)\text{H}^3$ reaction or by the $\text{He}^3(n, p)\text{H}^3$ reaction. Labeling of solids and liquids is usually effected by making use of the $\text{Li}^6(n, \alpha)\text{H}^3$ reaction. The high cross section, 945 barns, of lithium-6 compensates for the fact that the natural abundance of the isotope is only 7.3 per cent. This large cross section in conjunction with the shorter half life of tritium allows one to obtain much higher specific activities than with carbon-14. Lithium in the form of Li_2CO_3 (29, 43, 110, 114; 117 to 119) has been the usual source of tritium although Li_2SO_4 (43, 118), LiNO_3 (111), Li_2S (119), LiF (119), and LiCl (29, 111, 114) have also been used. Lithium chloride, for example, has limited solubility in some organic liquids. Activities other than tritium are produced by nuclear reactions in each of these salts except in the carbonate; this must be kept in mind during assay and purification procedures. The use of gels involving lithium myristate (123) has been described and holds promise for a wide variety of organic compounds. Optimum lithium concentrations lie between 1 and 15 per cent by weight. The radiation damage to the compounds during irradiation comes mainly from the nuclear process itself. The total energy deposition from the triton and the alpha particle amounts to 4.8 Mev; this is to be contrasted with 0.6 Mev from carbon-14 formation. In addition, the number of events per unit time is much greater in tritium production than in carbon-14 production. The specific activities attainable are limited by the radiation damage to the compound and by the concentration of lithium that can be used.

These factors are at present the most serious drawback to triton recoil labeling. The high recoil energy of the triton, combined with its low mass, results in a rather long path for the recoil fragment. This allows the use of finely ground salts, in admixture with the compound to be labeled, as a source of tritons; it also makes feasible the use of slurries and other heterogeneous mixtures.

A representative list of compounds is to be found in Table IV. It should be indicated that labile tritium (i.e., tritium which can be easily exchanged, such as hydroxyl tritium, tritium attached to nitrogen, and tritium attached to carbon alpha to carbonyl or other activating groups) is generally removed before the specific activity is considered constant. What constitutes stably bound tritium is not always as clear as what constitutes stably bound carbon since the former depends on the chemical surroundings of the molecule in question. Even tritium in the methyl groups of isobutane can be exchanged if the material is heated with concentrated H_2SO_4 .

TABLE IV
TRITIUM RECOIL-LABELED COMPOUNDS

Irradiated Compound	Lithium Source	Radiochemical	Specific	Reference
		Yield as Parent	Activity $\mu\text{c./mg. H}$	
Acetone	$LiNO_3$ —3%	24	0.03	(111)
L(+)—Alanine	Li_2CO_3 —3%	12 (dl)	4.2	(114)
Benzoic acid	Li_2CO_3 —17%	—	18.2	(43)
Cholestane	Li_2CO_3 —10%	19	1.4	(43)
Ethanol	$LiCl$ —12%	23	0.27	(43)
Galactose	Li_2CO_3 —10%	12	1.2	(43 cf. 110, 29)
Glucose	Li_2CO_3 —50%	10	0.04	(43 cf. 110, 29)
Nicotinic acid	Li_2SO_4 —10%	6	3.3	(43)
β -Phenylacetic acid	Li_2CO_3 —3%	31	0.15	(43)
Reserpine	Li_2CO_3 —3%	18	1.4	(43)

Again, as in carbon-14 labeling, neither uniquely random nor uniquely specific labeling is observed. Work on sugars has indicated that distributions within the molecule may be a function of crystal structure, irradiation conditions, and method of isolation and purification (29, 110). Group replacement in a large number of substituted benzoic acids indicates most of the T activity to be in the position initially occupied by the leaving group (117). Variation of the amount of rearranged activity was also noted. Brown & Garnett have shown that, in isopropyl benzoate, replacement of aromatic ring hydrogens is preferred (123). These authors indicate also that secondary hydrogens may be replaced more readily than primary hydrogens. Distribution in steroids has been described (124). Retention of configuration is observed when replacement at an asymmetric carbon occurs (114).

Gas phase work (25, 26, 115, 116; 120 to 122) has been primarily concerned with mechanism studies. The helium-3 isotope is the usual source of tritium although vessels coated with LiNO_3 have also been described (26, 120). A general review of work with the helium isotope is available (125). The purification of helium-3 for recoil work was described by Lee & Rowland (126). Even though only small quantities of labeled species may be prepared in this way, greater specificity of label and uniqueness of product may make gas phase work useful in synthesis. The work of Wolfgang (121) and Rowland (116) indicates that reduction of double bonds can take place. This may give alkanes with relatively high specific activity and perhaps with relatively high specificity of label. Wolfgang (121) has also shown that compounds analogous to those observed in thermal decompositions of radicals are formed by addition of T followed by bond cleavage. By judicious choice of an appropriate system, it might be possible to produce desired compounds, again with relatively high specific activity.

Wolfgang & Rowland (127) reported the application of radioassay by gas chromatography to these systems. The counters used were described by Wolfgang & MacKay (128). The achievement of radiochemical purity presents problems quite similar to those for carbon-14. In addition the problem of exchangeable hydrogens (not encountered with carbon-14-labeled compounds) must be considered. In general, however, the achievement of constancy of specific activity and radiochemical purity is somewhat easier with tritium-labeled compounds. The powerful tool of gas liquid chromatography has been used to good advantage in studies of the chemistry of the recoil triton.

Tritium recoil labeling can be profitably used where large amounts of tritium-labeled materials are required. The scope of the method is somewhat restricted because of a lack of adequate lithium sources for a wide variety of liquids.

Labeling of organic compounds by exposure to tritium gas deserves some mention here. The technique was first described by Wilzbach (129): the compound to be labeled is sealed in a small container with 1 to 20 curies of tritium gas; exposure varies from several hours to several days. This process can be used in labeling liquids, solids, or gases. High specific activities are readily attained. The subject has been considered in general terms (109, 130). There are numerous specific articles dealing with techniques (131, 132) and the labeling of natural products such as proteins (133), fatty acids (134), and morphine (135). The labeling of *p*-aminosalicylic acid (136) and some hydrocarbons (137) has also been reported.

The connection between this method and the recoil method seemed remote, and evidence was presented to indicate that recoil labeling was probably not involved (137). It may well be that a fragment with excess kinetic energy is not involved in liquid- or solid-phase labeling. However, the implication by Willard *et al.* (138) that a recoil HeT^+ fragment from T_2 might be involved (even though this work favored ionization of the methane as the most likely step prior to labeling) has found some experimental justification

in the work of Gant & Yang (139, 140) who presented evidence that labeling of the parent compound is brought about at least in part by the HeT^+ recoil fragment when labeling is done in the gas phase. The recent work of Dorfman & Wilzbach (141) and Lemmon *et al.* (142), using electric discharge as an adjunct to labeling by exposure to tritium gas, has served to underline the complexity of this labeling process. While labeling by recoil tritons from $\text{Li}^6(n, \alpha)\text{H}^3$ probably involves tritium atoms (16), and some of the labeling occurring during exposure of a compound to tritium gas may be caused by a recoiling HeT^+ fragment, the fact that some of the energy needed to bring about chemical reaction results from the excess kinetic energy of the fragment is a factor common to both methods. How much acceleration is involved in discharge methods (141, 142) is at present not clear. Since it is likely that many recoil reactions involving tritons occur at energies not too far removed from thermal [cf. (116, 121)], it can be proposed that recoil reactions, in the formal sense, may be involved.

The discharge method gives incorporations equal to or better than those obtained by exposure to tritium gas alone. In addition, the exposure times are cut from days to minutes. Unfortunately the accompanying molecular disruption is considerably greater. Whether the discharge method changes the spectrum of products appreciably has not been investigated in detail.

The question of distribution of isotope involves considerations similar to those discussed in previous sections [cf. (130)]. It is interesting that no parent substitution products are found in fatty acid labeling (134), addition to the double bond being observed as the main reaction. This contrasts with the observation that, in the exposure of cyclohexene to tritium, labeled cyclohexene and cyclohexane are formed (137). In recoil labeling, addition and substitution occur concurrently in all reported cases.

The products obtained by exposure to tritium gas also must be subjected to extensive purification before radiochemical purity is obtained. Wilzbach & Riesz (143) have pointed out that, because of the high percentage of hydrogens replaced, use of gas liquid chromatography sometimes results in isotope effects being observed during the separation of compounds (e.g., tritiated parent species having a retention time differing from the remaining untritiated parent molecules). The simplicity of the method and of its electric-discharge modification, coupled with the high specific activities attainable, is greatly in its favor.

Two mechanisms (26, 121) have been suggested as being operative in gas phase reactions of recoil tritons. A direct "hot" displacement [(26), cf. (25)] is postulated for the formation of CH_3T in $\text{CH}_4\text{-He}^3$ systems. In addition, evidence from the careful fractionation of the many products produced in gaseous alkenes supports an "addition reaction" mechanism (121) in which the addition of T to a double bond is followed by decomposition of the hot radical in a manner similar to thermal decomposition at high temperatures. It is difficult at this stage to assess the more subtle question of whether the "displacement" involves front side attack, attack from the rear, or attack on the bond itself. Rowland (114) has shown that T substitution,

by what must be defined as a hot reaction, occurs with retention of configuration in the case of L(+)-alanine. If this result is applicable to the CH_4 gas phase reaction, it must presuppose front side attack as being the only mode of formation of CH_3T . Rowland (116) prefers to describe the displacement reaction in terms of the formation of a true (high-energy) intermediate which can then degrade its energy or decompose to give the labeled parent or some fragmentation product thereof. White & Rowland (117) have also pointed out the lack of correlation between the mass of a replaced group and the mass of the triton. They have suggested a correlation between bond strength and ease of replacement in the formation of tritiated benzoic acid formed from a variety of substituted benzoic acids. The position (*o*, *m*, or *p*) of the group being replaced also has some effect on the yield of tritiated benzoic acid, implying possible electronic effects affecting the nature of the excited intermediate. It has been emphasized that these reactions are occurring at the lower end of the energy range of the recoil fragment. The focusing of attention on a few systems, combined with the careful investigation of numerous parameters, has provided some valuable working hypotheses for the elucidation of the detailed mechanisms involved. It is clear from this work that more than one mechanism is operative and that much work needs to be done. Its value to labeling is clear, being comparable to the effect that the elucidation of organic reaction mechanisms has had on the field of organic synthesis. While the empirical approach is still very much in evidence in recoil triton work, the mechanistic postulates discussed are invaluable in assessing the reaction of a particular organic compound to recoil triton labeling.

LABELING BY ELEMENTS OTHER THAN CARBON-14 OR TRITIUM

Labeling by elements other than carbon and tritium has been considered by Willard *et al.* (144). The vast majority of the work with other elements has been done with a view towards understanding the mechanisms involved (20, 21).

Isotopes of interest to the organic chemist which might be useful in recoil labeling are Cl^{38} , Br^{82} , I^{128} , P^{32} , As^{76} , Se^{76} , Fe^{59} , and Co^{60} , all produced by n, γ reactions, and S^{35} , from either S^{34} (n, γ) or Cl^{35} (n, p). A convenient table for calculating isotope yields from given neutron bombardments has been prepared by Senftle & Champion (145). The formation of carbon-14 and tritium is uncomplicated by other significant nuclear processes. This is unfortunately not the case with most other elements. Bromine-82 is a case in point. Allowance must be made for the bromine-80 which is formed from the bromine-79 since both bromine-79 and bromine-81 have appreciable cross sections for thermal neutrons. Sufficient time must be allowed for the bromine-80 content to be essentially zero. Similar problems arise with other elements.

The preparation of carrierless methylbromide- Br^{82} has been described by Glueckauf, Jacobi & Kitt (6). These authors investigated a number of

compounds as precursors, finding that a mixture of 90 per cent acetic acid and 10 per cent dibromobenzene gave the best results in the preparation of CH_3Br . A number of iodides were also studied.

The reported preparation (146) of vitamin B^{12} with Co^{60} in good yield by recoil methods was later shown to be improbable (147, 148). At best, yields of 1 to 2 per cent can be expected (149).

The preparation of sulfur-35-labeled cystine by recoil methods was reported by Ball, Solomon & Cooper (150). Later work by Lipp & Weigel (151) indicated that the activity reported was an impurity. A novel approach to recoil labeling by preparing an intermediate in a synthesis by recoil methods has been suggested by the author (44). The recoil labeling of methyl mercaptan from either $\text{CH}_3\text{Cl}^{35}$ or $\text{CH}_3\text{S}^{34}\text{H}$ should be feasible. This labeled intermediate could then be used in a synthesis of *dl*-methionine as described by Livak *et al.* (152), thus circumventing the elegant but laborious method of Schlüssel *et al.* (153). Simple organic halides have been extensively investigated (cf., references given in Introduction) with regard to the mechanism of the Szilard-Chalmers reaction.

Most of the halogen isotopes are relatively short-lived but the rapid purifications and separations possible with gas-liquid chromatography have put many halogen-labeled organic compounds within easy reach (28, 60; 154 to 156).

Radiochemical yields of the parent molecule are generally much higher than is found for carbon-14- or tritium-recoil-labeled parents. Herr, Stöcklin & Schmidt (156) have shown how the radiochemical yield of *n*-propylbromide- Br^{82} can be increased by the presence of tertiary amines during irradiation. Product distribution in aromatic systems has been investigated. The competitive labeling of benzene and naphthalene with bromine-80 from ethylbromide reportedly gives labeled bromonaphthalenes with seven times the activity of labeled bromobenzene (157). Gavoret & Ivanoff [(158 to 162), cf. (163)] have investigated substitution ratios in some benzoates, in nitrobenzene, and in toluene substituted by recoil bromine-82.

Numerous studies have been carried out on other elements covalently bound in organic molecules or in the presence of organic compounds. It must again be emphasized that none of this work was reported with the production of labeled organic compounds in mind. A few representative cases are, however, instructive. Campbell *et al.* (164) have studied the organic products from the neutron irradiation of tributylphosphate. Active phenyl, diphenyl, and triphenylarsine can be isolated from the neutron irradiation of triphenylarsine (165). A more recent study on the activation of AsCl_3 in benzene has yielded similar products (166). A radiochemical yield as high as 21 per cent of iron-59-labeled ferrocene can be obtained by irradiating ferrocene (167). Herr (168), while investigating the production of carrier-free elements by recoil from metal phthalocyanine complexes, noticed that platinum and iridium isotopes gave relatively high yields of organically bound entities. Successful purification of these organic fractions could lead

to usefully labeled compounds. Many of the problems with regard to specificity, purity, etc., discussed in the sections on carbon-14 and tritium apply here also. Application of the organic mechanistic point of view could easily increase our knowledge in this area. For example, the question of inversion or retention of configuration about a carbon halogen bond after replacement has not been studied. This whole field needs to be investigated and exploited.

ACCELERATED IONS AND IONIZATION METHODS IN LABELING STUDIES

Labeling of organic compounds with carbon-14 by exposure of the organic compound, to a source of carbon-14 in conjunction with a radiation source,⁷ either internal or external, has been reported. Turton (169) has reported the preparation of labeled benzoic acid and benzaldehyde by exposing benzene to a mixture of $C^{14}O_2$ (1.3 mc.) and Kr^{85} (2 curies). The benzoic acid was reported to have 98 per cent of the activity in the carboxyl group; the benzaldehyde showed a larger proportion of ring-incorporation. Cacace *et al.* (170) have reported preliminary results on a number of approaches. Exposure of benzene to $C^{14}O_2$ in a discharge tube gave benzoic acid with most of the activity in the carboxyl group. These workers also irradiated thin paraffin deposits with Tl^{204} , using $C^{14}O_2$ as the carbon-14 source. A homogeneous irradiation using pentane, Kr^{85} , and $C^{14}O_2$ kept in a vessel for 40 to 50 days was also described. The formation of carboxylic acids by irradiation of *n*-pentane and $C^{14}O_2$ by x rays has been recorded by Cacace *et al.* (171). The types of compounds producible by these methods seem limited to carboxylic acids and aldehydes although Turton (169) reported the preparation of derivatives of pyridine (structure unidentified), using $HC^{14}\equiv CH$ rather than $C^{14}O_2$. It does not seem likely that these methods will find general applicability in synthesizing a wide variety of compounds.

The acceleration of ions into organic targets is receiving an increasing amount of interest, primarily for the purpose of studying the mechanisms of these reactions. Wolfgang *et al.* (172) first reported the preparation of labeled organic compounds using accelerated tritium ions. Magnac-Valette & Liess (173) reported on a method for accelerating T^+ with a Van de Graaff generator which might find interesting applicability in this regard. An acceleration device somewhat similar to Wolfgang's has been described by Guillaume (174), who labeled a variety of compounds by accelerating $C^{14}O_2^+$ onto a cathode on which the materials were plated.

Aliprandi, Cacace & Giacomello (175) first reported using a C^{14+} ion beam in an isotope separator for labeling purposes. A sample of sodium benzoate irradiated in this way produced labeled benzoic acid. A later paper describes the labeling of cholesterol (176) in a similar manner. The device used has been described by Aliprandi *et al.* (177). A communication by

⁷ Carbon-14 is not suitable as its own radiation source.

Lemmon *et al.* (178) reported the formation of labeled benzene and toluene by focusing a C^{14+} beam on solid benzene covering the collector plate in a mass spectrometer, with yields similar to those reported for nuclear recoil work. It was later found (179) that the distribution of activity was similar to that found in recoil-labeled toluene from benzene.

The ion acceleration methods are of considerable interest from the mechanistic point of view, but are of questionable value for synthetic purposes at the present time. The sizable cost of a suitable accelerator, coupled with the rather wasteful use of C^{14} (recoil labeling uses N^{14} as its carbon-14 source whereas carbon-14 as such must be supplied to the accelerators), necessitating devices for recovering unused carbon-14, makes the method economically unattractive at the present time. Its prime advantage is the ability, in principle, to control the energy of the impinging ion. The work reported to date has involved the use of ions in the 2-keV to 7-keV range so that considerable attenuation occurs in the irradiated material before chemical reactions take place. The distribution of energies at any nominal energy also needs to be known. The effect on re-entry, synthesis and fragmentation as a function of particle energy is of primary interest. In this regard the results from use of low-energy beams, i.e., less than 200 eV, will prove particularly interesting. The question of lack of radiation damage in the accelerators is a more complex one. In an ion accelerator, there is essentially no secondary radiation, and one is not bothered by track interaction except from the tracks made by the ions themselves. Whether product type and distribution are affected by secondary radiation or are primarily functions of the "damage" within the track itself is an open question. The nature of the gross damage and its effect on product distribution may be quite different from that observed in recoil work. Ion acceleration should prove a fertile tool for exploring the mechanisms of these high-energy reactions.

CONCLUSION

The purpose of this review has been to detail the specific work done on recoil carbon-14 and recoil tritium with emphasis on how these processes can be applied to the labeling of organic compounds. It is clear that much work remains to be done before broad generalizations can be made; many questions of mechanism remain unanswered or have not been investigated. Allied fields have been mentioned insofar as they may have some application to the use of recoil fragments for labeling or to the understanding of the processes involved.

The study of high-energy reactions in general should provide the clue to a greater understanding of recoil reactions. It will be interesting to see how studies on reactions in flames, reactions in shock tubes, and reactions of molecules and molecular fragments in highly excited states will help in understanding "hot-atom chemistry" in organic systems.

LITERATURE CITED

1. Brooks, H., *Nature*, **70**, 270 (1904)
2. Hahn, O., and Meitner, L., *Phys. Z.*, **10**, 697-703 (1909)
3. Lind, S. C., and Bardwell, D. C., *J. Am. Chem. Soc.*, **46**, 2003-9 (1924)
4. Szilard, L., and Chalmers, T. A., *Nature*, **134**, 462 (1934)
5. Reid, A. F., *Phys. Rev.*, **69**, 530-31 (1946)
6. Glueckauf, E., Jacobi, R. B., and Kitt, G. P., *J. Chem. Soc.*, S330-35 (1949)
7. Edwards, R. R., and Davies, T. H., *Nucleonics*, **2**, No. 6, 44-56 (1948)
8. Daudel, P., Daudel, R., May, S., Muxart, R., and Chalvet, O., *J. chim. phys.*, **45**, 182-87 (1948)
9. Maddock, A. G., *Research*, **2**, 556-63 (1949)
10. Broda, E., *Österr. Chemiker-Z.*, **51**, 32-35 (1950)
11. Knie, J., *Rev. fac. quim. ind. y agr. (Univ. nac. litoral, Santa Fe, Arg.)*, **19**, #32, 21-29 (1950)
12. Green, J. H., *Revs. Pure and Appl. Chem. (Australia)*, **1**, 235-56 (1951)
13. Haissinsky, M., *Scientia*, **88**, 191-96 (1953)
14. Maddock, A. G., *Endeavor*, **12**, 95-100 (1953)
15. Nesmeyanov, A. N., Sazonov, L. A., and Sazonova, I. S., *Russ. Progr. of Chem.*, **22**, 133-78 (1953)
16. McKay, H. A. C., *Progr. in Nuclear Phys.*, **1**, Chap. 7 (1950)
17. Williams, R. R., Jr., *Principles of Nuclear Chemistry*, Chap. 7 (D. Van Nostrand Co., Inc., New York, N. Y., 307 pp., 1950)
18. Broda, E., *Advances in Radiochemistry* (Cambridge Univ. Press, London, England, 152 pp., 1950)
19. Wahl, A. C., and Bonner, N. A., *Radioactivity Applied to Chemistry*, Chap. 8 (John Wiley & Sons, Inc., New York, N. Y., 604 pp., 1951)
20. Willard, J. E., *Ann. Rev. Nuclear Sci.*, **3**, 193-220 (1953)
21. Willard, J. E., *Ann. Rev. Phys. Chem.*, **6**, 141-70 (1955)
22. Haissinsky, M., *La chimie nucleaire et ses applications*, Chap. 17 (Masson et Cie, Paris, France, 651 pp., 1957)
23. Schuler, R. H., *J. Phys. Chem.*, **62**, 1343-44 (1958)
24. Harbottle, G., and Sutin, N., *J. Phys. Chem.*, **62**, 1344-51 (1958)
25. Evans, J. B., Quinlan, J. E., Sauer, M. C., Jr., and Willard, J. E., *J. Phys. Chem.*, **62**, 1351-55 (1958)
26. El Sayed, M. A., Estrup, P. J., and Wolfgang, R., *J. Phys. Chem.*, **62**, 1356-63 (1958)
27. McCauley, C. E., and Schuler, R. H., *J. Phys. Chem.*, **62**, 1364-68 (1958)
28. Suryanarayana, B., and Wolf, A. P., *J. Phys. Chem.*, **62**, 1369-73 (1958)
29. Keller, H., and Rowland, F. S., *J. Phys. Chem.*, **62**, 1373-77 (1958)
30. Snell, A. H., and Pleasonton, F., *J. Phys. Chem.*, **62**, 1377-82 (1958)
31. Wexler, S., and Hess, D. C., *J. Phys. Chem.*, **62**, 1382-89 (1958)
32. Jones, T. O., Luebke, R. H., Jr., Wilson, J. R., and Willard, J. E., *J. Phys. Chem.*, **62**, 9-15 (1958)
33. Libby, W. F., *J. Am. Chem. Soc.*, **69**, 2523-34 (1947)
34. Miller, J. M., Gryder, J. W., and Dodson, R. W., *J. Chem. Phys.*, **18**, 579-83 (1950)
35. Capron, P. C., and Oshima, Y., *J. Chem. Phys.*, **20**, 1403-10 (1952)
36. Yankwich, P. E., *Can. J. Chem.*, **34**, 301-9 (1956)
37. Monchick, L., Funabashi, K., and Magee, J. L., *J. Chem. Phys.*, **27**, 734-39 (1957)
38. Seitz, F., and Koehler, J. S., *Solid State Physics*, 305-448 (Seitz, F., and Turnbull, D., Eds., Academic Press, Inc., New York, N. Y., 468 pp., 1956)
39. Kinchin, G. H., and Pease, R. S., *Repts. Progr. in Phys.*, **18**, 1-51 (The Physical Soc., London, England, 1955)
40. Harbottle, G., and Sutin, N., *Advances in Inorganic Chemistry and Radiochemistry*, **1**, 267-314 (Academic Press, Inc., New York, N. Y., 449 pp., 1959)
41. Muxart, R., *Bull. soc. chim. France*, 1857-61 (1956)
42. Wolf, A. P., *Radioisotopes in Sci. Research, Proc. Intern. Conf. Paris, Sept. 1957*, **2**, 114-35 (1958)
43. Rowland, F. S., and Wolfgang, R., *Nucleonics*, **14**, No. 8, 58-61 (1956)
45. Wolf, A. P., *Angew. Chem.*, **71**, 237-43 (1959)
45. Wolf, A. P., Redvanly, C. S., and Anderson, R. C., *J. Am. Chem. Soc.*, **79**, 3717-24 (1957)
46. Fox, M. S., and Libby, W. F., *J. Chem. Phys.*, **20**, 487-97 (1952)
47. Primak, W., *Phys. Rev.*, **103**, 1681-92 (1956)
48. Faraggi, H., *Ann. Physik*, **6**, 325-400 (1951)

49. Chien, J. C. W., and Willard, J. E., *J. Am. Chem. Soc.*, **79**, 4872-76 (1957)
50. Milman, M., and Shaw, P. F. D., *J. Chem. Soc.*, 1303-10 (1957)
51. Chien, J. C. W., and Willard, J. E., *J. Am. Chem. Soc.*, **75**, 6160-65 (1953)
- 52a. Milman, M., *J. Am. Chem. Soc.*, **80**, 5592-95 (1958)
- 52b. Roy, J. C., Williams, R. R., Jr., and Hamill, W. H., *J. Am. Chem. Soc.*, **76**, 3274-78 (1954)
53. McCauley, C. E., Hilsdorf, G. J., Geissler, P. R., and Schuler, R. H., *J. Am. Chem. Soc.*, **78**, 3246-52 (1956)
54. Chien, J. C. W., and Willard, J. E., *J. Am. Chem. Soc.*, **77**, 3441-44 (1955)
55. Alimarin, I. P., and Svoboda, K. F., *Soviet J. Atomic Energy (Engl. Transl.)*, **4**, 888-90 (1958)
56. Hornig, J. F., Levey, G., and Willard, J. E., *J. Chem. Phys.*, **20**, 1556-60 (1952)
57. Milman, M., Shaw, P. F. D., and Simpson, I. B., *J. Chem. Soc.*, 1310-17 (1957)
58. Milman, M., and Shaw, P. F. D., *J. Chem. Soc.*, 1317-25 (1957)
59. Milman, M., and Shaw, P. F. D., *J. Chem. Soc.*, 1325-32 (1957)
60. Gordus, A. A., and Willard, J. E., *J. Am. Chem. Soc.*, **79**, 4609-16 (1957)
61. Miller, J. M., and Dodson, R. W., *J. Chem. Phys.*, **18**, 865-75 (1950)
62. Wolf, A. P., and Oltman, A., *Intern. J. Appl. Radiation and Isotopes*, **3**, 169-72 (1958)
63. Collinson, E., and Swallow, A. J., *Chem. Revs.*, **56**, 471-568 (1956)
64. Yang, J., and Wolf, A. P., *J. Am. Chem. Soc.* (In press, 1960)
65. Zifferero, M., *Ann. chim. (Rome)*, **44**, 563-68 (1954)
66. Wolf, A. P., Redvanly, C. S., and Anderson, R. C., *Nature*, **176**, 831-32 (1955)
67. Santoro, V., and Minozzi, G., *Ricerca sci.*, **29**, 2243-47 (1959)
68. Santoro V., and Minozzi, G., *Ricerca sci.*, **29**, 1950-56 (1959)
69. Santoro, V., *Ricerca sci.*, **29**, 2237-42 (1959)
70. Zifferero, M., and Cieri, L., *Ann. chim. (Rome)*, **46**, 105-11 (1956)
71. Yankwich, P. E., Rollefson, G. K., and Norris, T. H., *J. Chem. Phys.*, **14**, 131-40 (1946)
72. Edwards, R., *Am. Chem. Soc., Southwest Regional Meeting, 6th, San Antonio, Texas* (1949)
73. Wolf, A. P., and Anderson, R. C., *J. Am. Chem. Soc.*, **77**, 1608-12 (1955)
74. Wolf, A. P., Gordon, B., and Anderson, R. C., *J. Am. Chem. Soc.*, **78**, 2657-58 (1956)
75. Anderson, R. C., Penna-Franca, E., and Wolf, A. P., *Brookhaven Natl. Lab. Quart. Progr. Rept.*, BNL 326(S-24), 15 (Oct.-Dec. 1954)
76. Wolf, A. P., Gordon, B., and Redvanly, C. S., *Brookhaven Natl. Lab. Ann. Rept.*, BNL 462(AS-11), 47 (July 1957)
77. Muxart, R., *Compt. rend.*, **242**, 2457-58 (1956)
78. Muxart, R., and Pinte, G., *Bull. soc. chim. France*, 1675-79 (1956)
79. Muxart, R., *Bull. soc. chim. France*, 314-15 (1958)
80. Schrodt, A. G., and Libby, W. F., *J. Am. Chem. Soc.*, **76**, 3100 (1954)
81. Schrodt, A. G., and Libby, W. F., *J. Am. Chem. Soc.*, **78**, 1267-73 (1956)
82. MacKay, C. F., and Libby, W. F., *J. Am. Chem. Soc.*, **79**, 6366-69 (1957)
83. Hein, R. E., Setser, D. W., Terhaar, C. J., Chang, S. C., McFarland, R. H., and Hansen, M. F., *Science*, **125**, 195 (1957)
84. Giacomello, G., *Ricerca sci.*, **21**, 1211-12 (1951)
85. Giacomello, G., *Il Farmeco*, **6** (1951)
86. Croatto, U., Giacomello, G., and Maddock, A. G., *Ricerca sci.*, **21**, 1598-1601 (1951)
87. Zifferero, M., and Masi, I., *Ann. chim. (Rome)*, **44**, 551-54 (1954)
88. Zifferero, M., *Ann. chim. (Rome)*, **44**, 555-57 (1954)
89. Giacomello, G., and Zifferero, M., *Ann. chim. (Rome)*, **44**, 558-62 (1954)
90. Zifferero, M., and Sordelli, D., *Ricerca sci.*, **26**, 1194-98 (1956)
91. Cacace, F., Cieri, L., and Zifferero, M., *Ann. chim. (Rome)*, **47**, 892-95 (1957)
92. Cacace, F., and Cieri, L., *Ricerca sci.*, **28**, 1174-77 (1958)
93. Barbieri, R., Belluco, U., and Bruno, M., *Gazz. chim. ital.*, **87**, 1377-92 (1957)
94. Belluco, U., Barbieri, R., and Schiavon, G., *Gazz. chim. ital.*, **88**, 78-88 (1958)
95. Cacace, F., Giacomello, G., and Montefinale, S., *Gazz. chim. ital.*, **89**, 1829-30 (1959)
96. Brunello, C., and Muxart, R., *Bull. soc. chim. France*, 16-21 (1960)

97. Yankwich, P. E., *J. Chem. Phys.*, **15**, 374-75 (1947)
98. Yankwich, P. E., and Vaughan, J. D., *J. Am. Chem. Soc.*, **76**, 5851-53 (1954)
99. Yankwich, P. E., and Cornman, W. R., Jr., *J. Am. Chem. Soc.*, **77**, 2096-98 (1955)
100. Yankwich, P. E., and Cornman, W. R., Jr., *J. Am. Chem. Soc.*, **78**, 1560-62 (1956)
101. Aronovich, P. M., and Mikhailov, B. M., *Izvest. Akad. Nauk. S.S.S.R., Otdel Khim. Nauk*, 541-46 (1956)
102. Aronovich, P. M., Belsky, N. K., and Mikhailov, B. M., *Bull. Acad. Sci. U.S.S.R., Div. Chem. Sci. S.S.R. (Engl. Transl.)*, 707-12 (1956)
103. Work done at Brookhaven Natl. Lab.: a. Wald, M.; b. Oae, S.; c. Wolf, A. P.; d. Anderson, R. C.; e. Suryanarayana, B.
104. Gordon, B., Shell Oil Company (Unpublished work)
105. *Brookhaven Natl. Lab. Ann. Rept., BNL 560(AS-13)*, 48 (July 1, 1959)
106. *Brookhaven Natl. Lab. Ann. Rept., BNL 523(AS-12)*, 51 (July 1, 1958)
107. *Brookhaven Natl. Lab. Ann. Rept., BNL 426(AS-11)*, 47 (July 1, 1957) (The numbers quoted in this report have been revised.)
108. Doering, W. von E., Buttery, R. G., Laughlin, R. G., and Chandhuri, N., *J. Am. Chem. Soc.*, **78**, 3224 (1956)
109. Scharpenseel, H. W., *Angew. Chem.*, **71**, 640-46 (1959)
110. Rowland, F. S., Turton, C. N., and Wolfgang, R., *J. Am. Chem. Soc.*, **78**, 2354-58 (1956)
111. Hoff, W. J., Jr., and Rowland, F. S., *J. Am. Chem. Soc.*, **79**, 4867-72 (1957)
112. Hoff, W. J., Jr., and Rowland, F. S., *J. Inorg. & Nuclear Chem.*, **5**, 164-69 (1958)
113. Lee, J. K., Musgrave, B., and Rowland, F. S., *J. Am. Chem. Soc.*, **81**, 3803 (1959)
114. Kay, J. G., Malsan, R. P., and Rowland, F. S., *J. Am. Chem. Soc.*, **81**, 5050-53 (1959)
115. Lee, J. K., Musgrave, B., and Rowland, F. S., *J. Chem. Phys.*, **32**, 1266 (1960)
116. Lee, J. K., Musgrave, B., and Rowland, F. S., *J. Am. Chem. Soc. (In press)*, 1960
117. White, R. M., and Rowland, F. S., *J. Am. Chem. Soc. (In press)*, 1960
118. Wolfgang, R. L., Rowland, F. S., and Turton, C. N., *Science*, **121**, 715-17 (1955)
119. Wolfgang, R., Eigner, J., and Rowland, F. S., *J. Phys. Chem.*, **60**, 1137-38 (1956)
120. El Sayed, M. A., and Wolfgang, R., *J. Am. Chem. Soc.*, **79**, 3286 (1957)
121. Wolfgang, R. L., and Urch, D. S., *J. Am. Chem. Soc.*, **81**, 2025-26 (1959)
122. Gordus, A. A., Sauer, M. C., Jr., and Willard, J. E., *J. Am. Chem. Soc.*, **79**, 3284-85 (1957)
123. Brown, W. G., and Garnett, J. L., *Intern. J. Appl. Radiation and Isotopes*, **5**, 114-20 (1959)
124. Bradlow, H. L., Fukushima, D. K., and Tsutsui, M., *Chem. & Ind. (London)*, No. 36, 1124 (1959)
125. Tumanov, K. A., *Uspekhi Fiz. Nauk*, **37**, 405-13 (1949)
126. Lee, J. K., and Rowland, F. S., *J. Inorg. & Nuclear Chem.*, **10**, 336-37 (1959)
127. Wolfgang, R., and Rowland, F. S., *Anal. Chem.*, **30**, 903-6 (1958)
128. Wolfgang, R., and MacKay, C. F., *Nucleonics*, **16**, No. 10, 69-73 (1958)
129. Wilzbach, K. E., *J. Am. Chem. Soc.*, **79**, 1013 (1957)
130. Rosenblum, C., *Nucleonics*, **17**, No. 12, 80-83 (1959)
131. Pany, J., *Naturwissenschaften*, **46**, 515 (1959)
132. Bergström, S., and Lindstedt, S., *Acta Chem. Scand.*, **11**, 1275 (1957)
133. Steinberg, D., Vaughan, M., Anfinsen, C. B., and Gorry, J., *Science*, **126**, 447-48 (1957)
134. Dutton, H. J., Jones, E. P., Mason, L. H., and Nystrom, R. F., *Chem. & Ind. (London)*, No. 36, 1176-77 (1958)
135. Misra, A. L., and Woods, L. A., *Nature*, **185**, 304-5 (1960)
136. Rydberg, J., and Hanngren, A., *Acta Chem. Scand.*, **12**, 332-39 (1958)
137. Riesz, P., and Wilzbach, K. E., *J. Phys. Chem.*, **62**, 6-9 (1958)
138. Ahrens, R. W., Sauer, M. C., Jr., and Willard, J. E., *J. Am. Chem. Soc.*, **79**, 3285-86 (1957)
139. Gant, P. L., and Yang, K., *J. Chem. Phys.*, **30**, 1108-9 (1959)
140. Yang, K., and Gant, P. L., *J. Chem. Phys.*, **31**, 1589-94 (1959)
141. Dorfman, L. M., and Wilzbach, K. E., *J. Phys. Chem.*, **63**, 799-801 (1959)
142. Lemmon, R. M., Tolbert, B. M., Strohmeier, W., and Whittemore, I. M., *Science*, **129**, 1740-41 (1959)
143. Wilzbach, K. E., and Riesz, P., *Science*, **126**, 748 (1957)

144. Evans, J. B., Quinlan, J. E., and Willard, J. E., *Ind. Eng. Chem.*, **50**, 192-95 (1958)
145. Seftle, F. E., and Champion, W. R., *Nuovo Cimento Suppl.* **12**, 549-54 (1954)
146. Anderson, R. C., and Delabarre, Y., *J. Am. chem. Soc.*, **73**, 4051-52 (1951)
147. Numerof, P., and Kowald, J., *J. Am. Chem. Soc.*, **75**, 4350-52 (1953)
148. Woodbury, D. T., and Rosenblum, C., *J. Am. Chem. Soc.*, **75**, 4364-65 (1953)
149. Maddock, A. G., and Coelho, F. P., *J. Chem. Soc.*, 4702-4 (1954)
150. Ball, E. G., Solomon, A. K., and Cooper, O., *J. Biol. Chem.*, **177**, 81-89 (1949)
151. Lipp, M., and Weigel, H., *Naturwissenschaften*, **39**, 189-90 (1952)
152. Livak, J. E., Britton, E. C., Vander Weele, J. C., and Murray, M. F., *J. Am. Chem. Soc.*, **67**, 2218-20 (1945)
153. Schlüssel, H., Maurer, W., Hock, A., and Hummel, O., *Biochem. Z.*, **322**, 226-29 (1951)
154. Herr, W., Schmidt, F., and Stöcklin, G., *Z. anal. Chem.*, **170**, 301-10 (1959)
155. Herr, W., Schmidt, F., and Stöcklin, G., *Z. Electrochem.*, **63**, 1006-7 (1959)
156. Herr, W., Stöcklin, G., and Schmidt, F., *Z. Naturforsch.*, **14b**, 693-99 (1959)
157. May, S., Roux, M., Buu Hoi, Ng. Ph., and Daudel, R., *Compt. rend.*, **228**, 1865-66 (1949)
158. Gavoret, G., *J. chim. phys.*, **50**, 183-85 (1953)
159. Ivanoff, N., and Gavoret, G., *J. chim. phys.*, **50**, 524-26 (1953)
160. Ivanoff, M., *Bull. soc. chim. France*, 266-69 (1953)
161. Gavoret, G., *J. chim. phys.*, **50**, 434 (1953)
162. Gavoret, G., and Ivanoff, N., *Bull. soc. chim. France*, 166-69 (1952)
163. Carlson, T. A., and Koski, W. S., *J. Chem. Phys.*, **23**, 2410-14 (1955)
164. Campbell, I. G., Poczynajlo, A., and Siuda, A., *J. Inorg. & Nuclear Chem.*, **10**, 225-37 (1959)
165. Maddock, A. G., and Sutin, N., *Trans. Faraday Soc.*, **51**, 184-96 (1955)
166. Siekierska, K. E., Sokolowska, A., and Campbell, I. G., *J. Inorg. & Nuclear Chem.*, **12**, 18-29 (1959)
167. Sutin, N., and Dodson, R. W., *J. Inorg. & Nuclear Chem.*, **6**, 91-98 (1958)
168. Herr, W., *Z. Naturforsch.*, **7b**, 201-7 (1952)
169. Turton, C. N., *Proc. Intern. Conf. Peaceful Uses Atomic Energy*, 2nd, Geneva, 1958, Paper 284 (1959); Cf. *Nucleonics*, **16**, No. 9, 86 (1958)
170. Cacace, F., Ciranni, G., Giacomello, G., and Zifferero, M., *Ricerca sci.*, **28**, 2131-34 (1958)
171. Cacace, F., Guarino, A., and Possagno, E., *Gazz. chim. ital.*, **89**, 1837-42 (1959)
172. Wolfgang, R., Pratt, T., and Rowland, F. S., *J. Am. Chem. Soc.*, **78**, 5132 (1956)
173. Magnac-Valette, D., and Liess, M., *J. Phys. Radium*, **17**, 449-50 (1956)
174. Guillaume, M., *Nature*, **182**, 1592 (1958)
175. Aliprandi, B., Cacace, F., and Giacomello, G., *Ricerca sci.*, **26**, 3029-34 (1956)
176. Aliprandi, B., and Cacace, F., *Ann. chim. (Rome)*, **46**, 1204-7 (1956)
177. Aliprandi, B., Cacace, F., Cieri, L., Giranni, G., Masironi, R., and Zifferero, M., *Radioisotopes in Sci. Research, Proc. Intern. Conf., Paris, Sept. 1957*, **2**, 146-53 (1958)
178. Lemmon, R. M., Mazzetti, F., Reynolds, F. L., and Calvin, M., *J. Am. Chem. Soc.*, **78**, 6414-15 (1956)
179. Mullen, R., Lemmon, R. M., and Reynolds, F. L., *Bio-organic Chem. Quart. Rept., Radiation Lab., Univ. of Calif., UCRL 8575*, 8-10 (1958)

NUCLEON-NUCLEON SCATTERING EXPERIMENTS AND THEIR PHENOMENOLOGICAL ANALYSIS¹

BY M. H. MACGREGOR, M. J. MORAVCSIK, AND H. P. STAPP

*Lawrence Radiation Laboratory, University of California, Livermore and
Berkeley, California*

INTRODUCTION

The last treatment of the nucleon-nucleon interaction in the *Annual Review of Nuclear Science* was the article of Breit & Gluckstern (30) in 1953. Since that time several major advances have occurred, the most important being the development of experimental techniques to the degree where polarization, triple-scattering, and correlation experiments are possible.

Largely because of these new experiments, phenomenological phase-shift analyses have become considerably more meaningful and now provide a fair idea of the energy dependence of the proton-proton phase shifts up to 400 Mev. Also, phenomenological potentials have developed from their rudimentary forms of 1953 to the point where reasonably accurate fits to the available data are provided over wide energy ranges.

On the theoretical side the amount of work is also considerable but the progress less apparent. Many meson-theoretical calculations of contributions to the nucleon-nucleon interaction have been carried out, but unfortunately the results for all but the familiar Yukawa one-meson tail seem to depend critically on the precise method of approximation. Newer methods, based on dispersion-theoretic arguments, hold out the hope that an unambiguous practicable procedure for attacking the problem of strong interactions can be developed, but these methods have not yet reached fruition in the area of the nucleon-nucleon interaction.

Because of the ambiguities in the theoretical situation and because of the space limitations the present article has been confined to the experiments themselves and to their direct phenomenological analysis; theoretical attempts to understand the nucleon-nucleon interaction will be deferred to a later article. The present article is divided into three parts. In the first the general formalism for the description and analysis of the nucleon-nucleon scattering experiments, and in particular of the polarization, triple-scattering, and correlation experiments, is described. The aim here is not a survey of contributions but rather a unified, self-contained development of the basic machinery. In Part II, the experimental data are collected, chiefly in the form of graphs and references. Part III contains a survey of recent phenomenological analyses. Potential models and related subjects are expressly excluded here, these being reserved for the later article.

Review articles dealing with the nucleon-nucleon system written by Hulthén & Sugawara (174), by Gammel & Thaler (173), and by Phillips

¹ The survey of literature pertaining to this review was concluded in May 1960.

(254) have recently appeared. Our aims, however, are rather different from those of the above authors. In the present article the emphasis is, as mentioned, on the experiments themselves and their phenomenological analysis, and the forthcoming theoretical article will emphasize what we believe to be the more satisfactory dispersion-theoretic approach. The area covered is therefore complementary in the main to that of Gammel & Thaler, who emphasize potential models, and to that of Phillips, who emphasizes the conventional meson-theoretic calculations. The Hulthén & Sugawara article was written before the important triple-scattering experiments and devoted chiefly to description of low-energy phenomena in terms of static potentials.

I. GENERAL FORMALISM

BY HENRY P. STAPP

1. INTRODUCTION

The outstanding feature in the development of nucleon-nucleon scattering experiments since 1953 is the use of polarized beams. Initial nucleon-nucleon polarization experiments were reported in 1954 by Oxley, Cartwright & Rouvina (112), and two years later triple-scattering experiments were performed by Chamberlain, Segrè, Tripp, Wiegand, and Ypsilantis (10). These, and subsequent similar experiments, have been the decisive factors in the comparative successes of recent phenomenological analyses and will accordingly receive a major emphasis in this article.

In typical polarization experiments the internal proton beam of a cyclotron is scattered from a target such as carbon, and the scattered protons are found to have their spins partially aligned in a direction normal to the scattering plane, with generally more protons having spin up than down for a left scattering. A beam such as this, in which the spins are partially aligned, is said to be polarized, and if it is caused to strike a (second) target of, say, liquid hydrogen, the second scattering cross section generally exhibits an azimuthal asymmetry. The measurement of this asymmetry is the object of the so-called double-scattering polarization experiments. In the more complicated triple-scattering experiments the protons emerging from the second collision are allowed to scatter again and the asymmetry after this third scattering process is measured. In variations of the experiment magnetic fields may be interposed between the various scatterings.

In these experiments the final measured asymmetry depends upon the properties of the various interactions involved and upon the geometric configuration. It is the object of the formalism discussed in this part to exhibit in a simple way the dependence of the observed quantities on the characteristic parameters describing these two factors. A nonrelativistic treatment is given first, but this is later extended to the relativistic case. At the outset the two nucleons are considered distinguishable, with the effects of undistinguishability being brought in later.

The discussion is based upon the use of the density matrix, which was introduced in this connection by Wolfenstein & Ashkin (1) and by Dalitz (2). This device greatly simplifies the analysis, both mathematically and conceptually, and is the basis of all contemporary work in the field. The next section describes the use of the density matrix formalism in nucleon-nucleon scattering.

2. STATISTICAL MIXTURES AND THE DENSITY MATRIX

The spin vector of a Pauli particle is defined here as the expectation value of the Pauli spin operator $\sigma = i\sigma_x + j\sigma_y + k\sigma_z$. Thus if an arbitrary normalized spin wave function is written in the form $[\cos \theta/2 \exp(i\alpha/2), \sin \theta/2 \exp(i\beta/2)]$ the spin vector is a unit vector with polar angle θ and azimuthal angle $\phi = (\alpha - \beta)/2$. It is important, however, that the particles injected into or emerging from a cyclotron are not usually all in the same quantum state. The various individual spin vectors generally have different directions and the expectation value of the spin operator averaged over the particles of the beam is usually a vector of length less than unity. This average over the particles of the beam of the individual unit spin vectors is called the polarization vector of the beam; it is the central object in polarization experiments, the measured quantities being directly related to it. Although it is possible to carry out calculations for each individual quantum state and then to perform (classical) averages over the various particles, it is much easier to deal directly with statistical averages over the particles of the beam.

If the fraction of beam particles in the pure quantum state $|\psi_i\rangle$ is f_i , the beam expectation value of an operator A is

$$\langle A \rangle = \sum f_i \langle \psi_i | A | \psi_i \rangle \quad 2.1$$

Often a bar is placed over the quantity on the left-hand side to signify that it is an average over individual quantum states. It is convenient to re-express 2.1 in the form

$$\langle A \rangle = \text{Tr} \rho A \quad 2.2$$

where Tr means trace and ρ is a Hermitian matrix called the density matrix. One sees immediately from 2.1 and 2.2 that the density matrix ρ can be represented in the form

$$= \sum f_i P_i$$

where P_i is a projection operator which is unity when acting on the state $|\psi_i\rangle$ and zero when acting on states orthogonal to $|\psi_i\rangle$.

From a more abstract point of view, the fact that 2.1 can be cast in the form 2.2 can be deduced as follows: The physical state of a system is determined by the expectation values of a complete set of Hermitian operators. In an N -dimensional space there are N^2 independent Hermitian operators. The corresponding N^2 equations of the form 2.2 determine completely the

Hermitian matrix ρ , and by linearity this equation then determines the expectation values of all other operators.

In treating scattering experiments it is important that the density matrix can be used to characterize not only a collection of particles but also a single particle. For example, in a system of two particles the wave function may take the form

$$\psi(x_1, x_2) = a_1 \phi_1(x_1) \psi_1(x_2) + a_2 \phi_2(x_1) \psi_2(x_2) + \dots$$

If the states $\psi_i(x_2)$ are nonoverlapping (i.e., orthogonal), the contributions from the various $\phi_i(x_1)$ cannot interfere and must be combined according to classical statistics. The density matrix is therefore appropriate for describing the first particle alone if information regarding the second particle is unavailable. If the states of the second particle are partially overlapping, the situation is more complex, but the first particle is still characterized by some density matrix, as the abstract argument shows.

The density matrix defined above characterizes a system at a given time. As time proceeds the density matrix changes—at least in the Schrodinger representation, which is used throughout. In particular, if the states before and after a scattering process are related by $\psi_f = S\psi_i$, the density matrices characterizing the system before and after the scattering are related by

$$\rho_f = S\rho_i S^* \quad 2.3.$$

as is seen from Equations 2.1 and 2.2. For scattering experiments in which the final particles are counted outside the unscattered beam, the incident beam must be subtracted out and one uses, instead of 2.3,

$$\rho_{so} = R\rho_i R^* \quad 2.4.$$

where $R = S - 1$. The ρ_{so} defined in this way describes the scattered wave. Equations 2.2 and 2.4 are the two fundamental equations for treating the scattering of statistical mixtures: 2.2, applied to both ρ_i and ρ_{so} , determines the connection to experiment; and 2.4 gives the dynamical content.

In scattering experiments the momentum can usually be considered well defined. Consequently, the operators A used in Equation 2.2 can be considered the product of an operator A_s in spin-space times an operator $P(\mathbf{k})$ that projects onto a state of relative momentum \mathbf{k} . According to 2.2, the expectation value of a spin operator A_s in this momentum state is

$$\langle A_s \rangle_{\mathbf{k}} = \frac{\langle P(\mathbf{k}) A_s \rangle}{\langle P(\mathbf{k}) \rangle} = \frac{\text{Tr} \rho(\mathbf{k}) A_s}{\text{Tr} \rho(\mathbf{k})} \quad 2.2'.$$

where the denominator $\langle P(\mathbf{k}) \rangle$ is the probability that the particle is in the momentum state \mathbf{k} , and the spin-space density matrix $\rho(\mathbf{k})$ is some as yet arbitrary multiple of $\langle \mathbf{k} | \rho | \mathbf{k} \rangle$, the diagonal momentum-space matrix element of ρ . In 2.2' the trace is over spin states only, the sum over momentum states present in 2.2 having been cancelled by the momentum-state projection operator $P(\mathbf{k})$.

Aside from the undetermined normalization, Equation 2.2' can be considered the definition of the spin density matrix $\rho(\mathbf{k})$. Indeed, if one introduces in the four-dimensional spin-space of the two Pauli particles the 16 independent matrices $\sigma_\mu^{(1)} \sigma_\nu^{(2)}$ defined by

$$\langle m, n | \sigma_\mu^{(1)} \sigma_\nu^{(2)} | m', n' \rangle = (\sigma_\mu)_{mm'} (\sigma_\nu)_{nn'} \quad 2.5.$$

where m and n specify the spin states of the first and second particles, respectively, and $\sigma_1, \sigma_2, \sigma_3$, and σ_0 are the Pauli spin matrices and the Pauli unit matrix, one obtains, using the orthogonality relations

$$\frac{1}{4} \text{Tr} \sigma_\mu^{(1)} \sigma_\nu^{(2)} \sigma_\lambda^{(1)} \sigma_\rho^{(2)} = \delta_{\mu\lambda} \delta_{\nu\rho} \quad 2.6.$$

the inverse of 2.2':

$$\rho(\mathbf{k}) = \frac{1}{4} \text{Tr} \rho(\mathbf{k}) \sum_{\mu, \nu} \langle \sigma_\mu^{(1)} \sigma_\nu^{(2)} \rangle_{\mathbf{k}} \sigma_\mu^{(1)} \sigma_\nu^{(2)} \quad 2.7.$$

In this form the spin density matrix is expressed directly in terms of $\text{Tr} \rho(\mathbf{k})$ and the 16 expectation values $\langle \sigma_\mu^{(1)} \sigma_\nu^{(2)} \rangle_{\mathbf{k}}$. Six of these, the quantities

$$\langle \sigma_i^{(1)} \sigma_0^{(2)} \rangle_{\mathbf{k}} = \langle \sigma_i^{(1)} \rangle_{\mathbf{k}} \quad \text{and} \quad \langle \sigma_0^{(1)} \sigma_j^{(2)} \rangle_{\mathbf{k}} = \langle \sigma_j^{(2)} \rangle_{\mathbf{k}},$$

are the components of the polarization vectors for the first and second particles, respectively; and $\langle \sigma_i^{(1)} \sigma_j^{(2)} \rangle_{\mathbf{k}} \equiv C_{ij}(\mathbf{k})$ are nine parameters related to a correlation between spin expectations in the two beams. These 15 parameters can be considered as specifying the spin state of the combined two-particle system.

On the dynamical side, the momentum-space matrix element $\langle \mathbf{k} | \mathbf{R} | \mathbf{k}' \rangle$ is a matrix in spin-space whose elements, aside from a normalization factor, are the scattering amplitudes for individual initial and final spin states. In the description of polarization phenomena, it is convenient to incorporate this normalization factor and to deal also with the spin matrix $M(\mathbf{k}, \mathbf{k}')$ whose matrix elements are exactly the scattering amplitudes in various final spin states for fixed initial spin states. In terms of $M(\mathbf{k}, \mathbf{k}')$ and the $\rho(\mathbf{k})$ defined in 2.2' Equation 2.4 becomes

$$\rho_{\text{sc}}(\mathbf{k}) = M(\mathbf{k}, \mathbf{k}') \rho_i(\mathbf{k}') M^*(\mathbf{k}, \mathbf{k}') \quad 2.4'.$$

where the freedom in the normalization of the $\rho(\mathbf{k})$ has been exploited. With this choice of normalization the differential cross section becomes simply

$$\frac{d\sigma}{d\Omega} = I(\theta, \phi) = \frac{\text{Tr} \rho_{\text{sc}}}{\text{Tr} \rho_i} = \frac{\text{Tr} M(\mathbf{k}, \mathbf{k}') \rho_i M^*(\mathbf{k}, \mathbf{k}')}{\text{Tr} \rho_i} \quad 2.8.$$

which is the straightforward generalization to the case of polarized initial particles of the usual rule of summing over the final states and averaging over the initial states.

The operator $M(\mathbf{k}, \mathbf{k}')$ is a matrix in the spin-space of the two particles and, like $\rho(\mathbf{k})$, it can be expanded in terms of the $\sigma_\mu^{(1)} \sigma_\nu^{(2)}$:

$$M(\mathbf{k}, \mathbf{k}') = \sum M^{\mu\nu}(\mathbf{k}, \mathbf{k}') \sigma_\mu^{(1)} \sigma_\nu^{(2)} \quad 2.9.$$

In the center-of-mass frame, where \mathbf{k} and \mathbf{k}' are the only vectors upon which the $M^{\mu,\nu}(\mathbf{k}, \mathbf{k}')$ can depend, the most general function of the form 2.9 invariant under rotations and spatial reflections is

$$\begin{aligned} M(\mathbf{k}, \mathbf{k}') = & a + b(\sigma^{(1)} \cdot \mathbf{N} - \sigma^{(2)} \cdot \mathbf{N}) + c(\sigma^{(1)} \cdot \mathbf{N} + \sigma^{(2)} \cdot \mathbf{N}) \\ & + m(\sigma^{(1)} \cdot \mathbf{N}\sigma^{(2)} \cdot \mathbf{N}) + g(\sigma^{(1)} \cdot \mathbf{P}\sigma^{(2)} \cdot \mathbf{P} + \sigma^{(1)} \cdot \mathbf{K}\sigma^{(2)} \cdot \mathbf{K}) \\ & + h(\sigma^{(1)} \cdot \mathbf{P}\sigma^{(2)} \cdot \mathbf{P} - \sigma^{(1)} \cdot \mathbf{K}\sigma^{(2)} \cdot \mathbf{K}) \\ & + j(\sigma^{(1)} \cdot \mathbf{P}\sigma^{(2)} \cdot \mathbf{K}) + l(\sigma^{(1)} \cdot \mathbf{K}\sigma^{(2)} \cdot \mathbf{P}) \end{aligned} \quad 2.10.$$

Here vectors \mathbf{N} , \mathbf{P} , and \mathbf{K} are unit orthogonal vectors in the directions $\mathbf{k} \times \mathbf{k}$, $\mathbf{k}' + \mathbf{k}$, and $\mathbf{k} - \mathbf{k}'$ respectively, and the coefficients a, b, \dots, l are scalar functions of the vectors \mathbf{k} and \mathbf{k}' .

For proton-proton (p - p) scattering, in which the two particles are identical, $b=0$ and $j=l$, since M must be symmetric under interchange of the two particles. The same conditions would be satisfied also for neutron-proton (n - p) scattering if charge independence were strictly maintained.

It was pointed out by Wolfenstein & Ashkin (1) that the requirement of time-reversal invariance implies the vanishing of the coefficients j and l . As is shown later, this requirement directly implies the invariance of $M(\mathbf{k}, \mathbf{k}')$ under the simultaneous substitutions $\mathbf{k} \leftrightarrow -\mathbf{k}'$ and $\sigma \leftrightarrow -\sigma$. Since the terms multiplying j and l change sign under this transformation while j and l , like the available scalars $\mathbf{k} \cdot \mathbf{k}$, $\mathbf{k}' \cdot \mathbf{k}'$ and $\mathbf{k} \cdot \mathbf{k}'$, are invariant, j and l must vanish. Thus the combined requirements of invariance under rotation, spatial reflection, and time reversal imply that the scattering matrix M can be expressed in terms of the six (five for p - p) remaining complex scalar parameters in Equation 2.10. These parameters are called the Wolfenstein parameters. For fixed energy, they are functions of the single scalar variable $\mathbf{k} \cdot \mathbf{k}'$ or, equivalently, of the polar scattering angle θ . They are, of course, independent of the initial and final polarizations; these latter quantities enter the theory only through the initial and final density matrices $\rho_i(\mathbf{k}')$ and $\rho_{ac}(\mathbf{k})$.

An alternative way of writing the M matrix has been given by Wolfenstein (3):

$$\begin{aligned} M(\mathbf{k}, \mathbf{k}') = & BS + C(\sigma^{(1)} + \sigma^{(2)}) \cdot \mathbf{N} \\ & + \frac{1}{2}G(\sigma^{(1)} \cdot \mathbf{K}\sigma^{(2)} \cdot \mathbf{K} + \sigma^{(1)} \cdot \mathbf{P}\sigma^{(2)} \cdot \mathbf{P})T \\ & + \frac{1}{2}H(\sigma^{(1)} \cdot \mathbf{K}\sigma^{(2)} \cdot \mathbf{K} - \sigma^{(1)} \cdot \mathbf{P}\sigma^{(2)} \cdot \mathbf{P})T \\ & + N(\sigma^{(1)} \cdot \mathbf{N}\sigma^{(2)} \cdot \mathbf{N})T \end{aligned} \quad 2.10'.$$

The quantities S and T in this equation are the singlet and triplet projection operators, $\frac{1}{4}(1 - \sigma^{(1)} \cdot \sigma^{(2)})$ and $\frac{1}{4}(3 + \sigma^{(1)} \cdot \sigma^{(2)})$, respectively; and the coefficients B, C, G, H , and N are again functions of the scattering angle θ , but these have the symmetry properties $B(\theta) = B(\pi - \theta)$, $C(\theta) = C(\pi - \theta)$, $G(\theta) = -G(\pi - \theta)$, $H(\theta) = H(\pi - \theta)$, and $N(\theta) = -N(\pi - \theta)$ for the isotopic triplet case. The isotopic singlet amplitudes have the opposite symmetries.

The formalism described above is the basis of the discussions in the following sections and, indeed, of all contemporary discussions of polarization phenomena.

3. POSSIBLE EXPERIMENTS

In principle 256 experiments can be performed on the nucleon-nucleon system at a single scattering angle. The final spin-space density matrix depends on 16 independent real scalar parameters, and each of these depends linearly through Equation 2.4' on each of the 16 real scalar parameters that determine the initial density matrix. In terms of the 256 scalar coefficients

$$Z_{\mu,\nu;\lambda,\rho}(\mathbf{k}, \mathbf{k}') = \frac{1}{4} \text{Tr} \sigma_{\mu}^{(1)} \sigma_{\nu}^{(2)} M(\mathbf{k}, \mathbf{k}') \sigma_{\lambda}^{(1)} \sigma_{\rho}^{(2)} M^*(\mathbf{k}, \mathbf{k}') \quad 3.1.$$

the relation between initial and final expectation values is simply

$$I(\theta, \phi) \langle \sigma_{\mu}^{(1)} \sigma_{\nu}^{(2)} \rangle_{\mathbf{k}} = Z_{\mu,\nu;\lambda,\rho}(\mathbf{k}, \mathbf{k}') \langle \sigma_{\lambda}^{(1)} \sigma_{\rho}^{(2)} \rangle_{\mathbf{k}'} \quad 3.2.$$

The experimental problem is to fix the initial expectation values and measure the final ones. This determines the Z 's, which in turn give information on the nucleon-nucleon interaction through Equation 3.1.

The initial polarization is fixed and the final ones measured, generally, by making auxiliary scatterings before and after the principal nucleon-nucleon scattering. These auxiliary scatterings can be treated by using a formalism analogous to the one described above. If, for simplicity, the initial auxiliary scatterer is taken to have spin zero and if invariance under spatial reflection is assumed, this initial scattering is described by a two-by-two spin matrix of the form

$$M_1 = a_1 + b_1 \sigma \cdot N \quad 3.3.$$

as discussed by Wolfenstein (4) in an earlier volume. Inserting this into 2.4' and using 2.2', one obtains for the polarization vector after the scattering of an initially unpolarized beam the expression

$$\langle \sigma \rangle_{\mathbf{k}'} = [2 \text{Re} a_1 b_1^* / (|a_1|^2 + |b_1|^2)] N_1 \equiv P_1 N_1 \quad 3.4.$$

Here N_1 is the normal to the first scattering plane; and the quantity P_1 , which gives the magnitude of the polarization vector, is called the polarizing power of the reaction. The subscripts 1 identify the quantities as pertaining to the initial scattering.

A possible third scattering acts as an analyzer. If the final target is also taken to have spin zero, the final scattering will be represented by a matrix like that in Equation 3.3, but now with subscripts 3 to denote the third scattering. Inserting this matrix into 2.4', one obtains, for the differential cross section 2.8,

$$I_3 = I_{03} [1 + \alpha_3 N_3 \cdot \langle \sigma \rangle_{\mathbf{k}}] \quad 3.5.$$

where

$$I_{03} = |a_3|^2 + |b_3|^2 \quad 3.6.$$

and

$$\alpha_3 I_{03} = 2 \text{Re} a_3 b_3^* \quad 3.7.$$

Here I_{03} is the differential cross section for the third scattering when the incident beam is unpolarized, and α_3 is called the analyzing power of the reaction. According to 3.5 the deviation from azimuthal symmetry after

the final scattering is a measure of $\langle \sigma \rangle_k \cdot N_3$, the component perpendicular to the final-scattering plane of the polarization vector of the incident beam of the final reaction.

That the vectors appearing in Equations 3.4 and 3.5 are the normals to the scattering plane is a consequence of the assumed invariance of the interaction under spatial reflection; the normal is the only axial vector that can be formed from the initial and final relative momentum vectors. The equality of polarizing and analyzing powers for a given reaction, which is seen from Equations 3.4 to 3.7, was shown by Wolfenstein & Ashkin (1) to be a general consequence of the assumed invariances under rotation, reflection, and time reversal, true even for targets of nonzero spin. This equality is often tacitly assumed, and the polarizing and analyzing powers, undifferentiated, are called the polarization function of the reaction.

According to Equation 3.4 the polarization vector after the scattering of an initially unpolarized beam is normal to the line of flight of the nucleon. To obtain polarization components along the line of flight, the beam can be passed through a magnetic field. Relativistic formulas for the precession rate are given by Bargmann, Michel & Telegdi (5). Magnetic fields may also be used to rotate a longitudinal component of the final polarization vector into a measurable transverse component.

At present, no experiments in which the target nucleon is polarized have been performed. When polarized targets become available the dependence on the initial correlation parameters can be investigated. Since there can be no correlation between the orientations of individual target and beam nucleons, the initial correlation parameter is simply the product of the individual polarizations:

$$\langle \sigma_\mu^{(1)} \sigma_\nu^{(2)} \rangle_{k'} = \langle \sigma_\mu^{(1)} \rangle_{k'} \langle \sigma_\nu^{(2)} \rangle_{k'}$$

The dependence of final expectation values on this term may be isolated by performing experiments with various combinations of the signs of $\langle \sigma_\mu^{(1)} \rangle_{k'}$ and $\langle \sigma_\nu^{(2)} \rangle_{k'}$ and then averaging with an appropriately signed weighting factor to eliminate the unwanted terms. As in many of these experiments, however, it must be remembered that the differential cross section appearing on the left of 3.2 generally depends on the initial spin expectation values, so that the relation between the initial and final spin expectation values, unlike that between the two density matrices, is not linear.

To measure the final correlation parameters $\langle \sigma_i \sigma_j \rangle_k$, one can rescatter both outgoing nucleons. Contrary to the case for the initial state, the orientations of the two nucleons can now possess correlations, and the correlation parameter is expected to differ from the product of the individual polarizations. It is therefore necessary to consider simultaneously the scattering of both particles.

If the two particles are considered a single system, the final scattering process is described by the product scattering matrix

$$M_3 = (a_3^{(1)} + b_3^{(1)} \sigma^{(1)} \cdot N^{(1)}) (a_3^{(2)} + b_3^{(2)} \sigma^{(2)} \cdot N^{(2)})$$

where for simplicity the final targets are again assumed spinless. Substituting this expression into 2.8 and identifying the ρ_i of that equation with $\rho(\mathbf{k})$, the final density matrix of the nucleon-nucleon collision, one obtains (6), after some rearrangement, the coincidence cross section

$$I_3^{(1)(2)} = I_{03}^{(1)} I_{03}^{(2)} [1 + \alpha_3^{(1)} \langle \sigma^{(1)} \rangle_{\mathbf{k}} \cdot \mathbf{N}_3^{(1)} + \alpha_3^{(2)} \langle \sigma^{(2)} \rangle_{\mathbf{k}} \cdot \mathbf{N}_3^{(2)} + \alpha_3^{(1)} \alpha_3^{(2)} \langle \sigma^{(1)} \cdot \mathbf{N}_3^{(1)} \sigma^{(2)} \cdot \mathbf{N}_3^{(2)} \rangle_{\mathbf{k}}] \quad 3.8.$$

Here the analyzing powers $\alpha_3^{(i)}$ are $2\text{Re } a_3^{(i)} b_3^{(i)*} / (|a_3^{(i)}|^2 + |b_3^{(i)}|^2)$, as before. The final correlation parameter $\langle \sigma_i^{(1)} \sigma_j^{(2)} \rangle_{\mathbf{k}} = C_{ij}(\mathbf{k})$ can again be isolated by averaging appropriate combinations of the senses of $\mathbf{N}_3^{(1)}$ and $\mathbf{N}_3^{(2)}$. For example,

$$C_{NN} = \frac{(L, L) + (R, R) - (L, R) - (R, L)}{(L, L) + (R, R) + (L, R) + (R, L)} \times [\alpha_3^{(1)} \alpha_3^{(2)}]^{-1}$$

where (L, R) represents the number of times that the first of the nucleons from the nucleon-nucleon collision scatters left at its subsequent final scattering and the other nucleon scatters right, etc. To establish that the two nucleons come from a single nucleon-nucleon scattering event, high-speed coincidence circuits are used.

Certain of the more common experimental quantities have been given names which are now fairly standard in the field. In terms of the Z 's defined in 3.1 and 4.1, the simplest of the 256 observables is $Z(\mathbf{k}, \mathbf{k}'; 0, 0; 0, 0) \equiv I_0(\theta)$, which is the differential cross section for an initially unpolarized beam. If particle 2 is considered to be the target particle, the quantities next in order of experimental simplicity are $Z(\mathbf{k}, \mathbf{k}'; N, 0; 0, 0)/I_0(\theta)$ and $Z(\mathbf{k}, \mathbf{k}'; 0, 0; N, 0)/I_0(\theta)$, the polarizing and analyzing powers, respectively. As mentioned before, these are the magnitude of the polarization vector after the scattering of an initially unpolarized beam and the coefficient of azimuthal asymmetry after the scattering of a completely polarized beam. The simplest of the triple-scattering experiment measures, $Z(\mathbf{k}, \mathbf{k}'; N, 0; N, 0)/I_0(\theta)$, which determines the dependence of the normal component of the polarization vector after the nucleon-nucleon scattering on the normal component before scattering, where the normal is defined relative to the nucleon-nucleon scattering plane. This observable is denoted by D and called depolarization; in the D experiment all three scattering planes are evidently coplanar. The quantities $Z(\mathbf{k}, \mathbf{k}'; \mathbf{K}, 0; N \times \mathbf{K}_{\text{in}}, 0)/I_0(\theta)$ and $Z(\mathbf{k}, \mathbf{k}'; \mathbf{K}, 0; \mathbf{K}_{\text{in}}, 0)/I_0(\theta)$ are denoted by R , for rotation, and A , respectively, where \mathbf{K}_{in} is a unit vector in the direction \mathbf{k}' . In the experiment that measures R , the nucleon-nucleon scattering plane is perpendicular to the first scattering plane and hence contains the initial polarization vector. The third scattering plane contains the final laboratory momentum, of course, and is perpendicular to the nucleon-nucleon scattering plane. The normal to this third plane is then \mathbf{K} , the unit vector along $\mathbf{k} - \mathbf{k}'$, provided small relativistic corrections are neglected. In the " A " triple-scattering experiment a magnetic field is used to precess the spin of the incident particle in order to give it a component

along the line of flight. The final scattering plane is perpendicular to the nucleon-nucleon scattering plane as in the R experiment.

The only other experiments yet performed are the correlation experiments which measure $Z(\mathbf{k}, \mathbf{k}'; N, N; 0, 0)/I_0(\theta) = C_{NN}$ and $Z(\mathbf{k}, \mathbf{k}'; \mathbf{K}, \mathbf{P}; 0, 0)/I_0(\theta) = C_{KP}$. In the former the two final scattering planes are parallel to the nucleon-nucleon scattering plane, and in the latter they are perpendicular to it. The vector \mathbf{P} appearing in C_{KP} specifies the direction perpendicular to the laboratory velocity of the recoil target nucleon, provided relativistic corrections are neglected. For identical particles the final momentum \mathbf{k} refers, of course, to the particle identified as the scattered incident particle.

Correlation experiments in which the initial nucleon is polarized appear feasible although none have yet been carried out. The symbol C_{ABC} has been used for the relevant quantity $Z(\mathbf{k}, \mathbf{k}'; \mathbf{B}, \mathbf{C}; \mathbf{A}, 0)/I_0(\theta)$.

The quantities obtained by replacing the vector \mathbf{K} by \mathbf{P} in the above expressions for A and R are called A' and R' , respectively. The vector \mathbf{P} is a unit vector along the laboratory velocity of the scattered nucleon, with relativistic corrections again neglected. Thus in order to measure A' or R' the scattered beam from the nucleon-nucleon reaction can be passed through a magnetic field.

The experimental quantities defined above can be expressed in terms of the Wolfenstein parameters by inserting 2.10 or 2.10' into 3.1 and performing the matrix multiplication. Results have been given by many authors (3, 6 to 12). A list is given in Table I on page 301.

4. THEORETICAL RELATIONS BETWEEN EXPERIMENTS

Although the 256 experiments are experimentally independent, there are theoretical relationships between them. The results of presumably related experiments would be useful as checks on either the theoretical assumptions or the experimental results.

The theoretical assumptions, aside from basic quantum mechanics, are the invariances under rotations, reflections, and time reversal. The basic principles of quantum mechanics already imply 224 relations among the 256 observables, for the 256 observables are functions of the 16 complex M -matrix elements, as one sees by Equation 3.1. The specific consequences following from these relations alone have apparently not been examined.

The requirement of invariance under space reflection implies the vanishing of half of the 256 Z coefficients, since half are pseudoscalars. A nonzero value of any one of the 128 pseudoscalar Z coefficients would constitute unambiguous proof that parity is not conserved in the interaction that produces the scattering.

The consequences of time-reversal invariance may be expressed in a simple form if one introduces the definition

$$Z(\mathbf{k}, \mathbf{k}'; A, B; C, D) = \sum_{\substack{\mu, \nu \\ \lambda, \rho}} Z_{\mu, \nu; \lambda, \rho}(\mathbf{k}, \mathbf{k}') A_{\mu} B_{\nu} C_{\lambda} D_{\rho} \quad 4.1.$$

TABLE I

EXPERIMENTAL OBSERVABLES IN TERMS OF WOLFENSTEIN PARAMETERS

The Wolfenstein parameters are as defined in Equations 2.10 and 2.10' with b of the former set to zero. The observables are defined in Section 3. Complete lists are given in (9) and (12). Expressions for the general case where space reflection and time-reversal invariances are not imposed are given by the author in the *Lawrence Radiation Laboratory Report, UCRL-8859* (unpublished). The consequences of these invariances are discussed there in some detail.

$$\begin{aligned}
 I_0 &= \frac{1}{4} |B|^2 + 2 |C|^2 + \frac{1}{4} |G - N|^2 + \frac{1}{4} |N|^2 + \frac{1}{4} |H|^2 \\
 &= |a|^2 + |m|^2 + 2 |c|^2 + 2 |g|^2 + 2 |h|^2 \\
 I_0 P &= 2 \operatorname{Re} C^* N = 2 \operatorname{Re} c^* (a + m) \\
 I_0 (1 - D) &= \frac{1}{4} |G - N - B|^2 + |H|^2 \\
 &= 4 |g|^2 + 4 |h|^2 \\
 I_0 R &= \frac{1}{2} \operatorname{Re} [(G - N)^*(N + H) + B^*(N - H)] \cos \theta / 2 \\
 &\quad + \operatorname{Im} [C^*(B + G - N)] \sin \theta / 2 \\
 &= [|a|^2 - |m|^2 - 4 \operatorname{Re} h g^*] \cos \theta / 2 + 2 \operatorname{Re} i c (a^* - m^*) \sin \theta / 2 \\
 I_0 A &= -\frac{1}{2} \operatorname{Re} [(G - N)^*(N + H) + B^*(N - H)] \sin \theta / 2 \\
 &\quad + \operatorname{Im} [C^*(B + G - N)] \cos \theta / 2 \\
 &= -[|a|^2 - |m|^2 - 4 \operatorname{Re} h g^*] \sin \theta / 2 + 2 \operatorname{Re} i c (a^* - m^*) \cos \theta / 2 \\
 R' &= -\operatorname{Im} [C^*(B + G - N)] \cos \theta / 2 \\
 &\quad + \frac{1}{2} \operatorname{Re} \{ (G - N)^*(N - H) + B^*(N + H) \} \sin \theta / 2 \\
 &= -2 \operatorname{Re} i c (a - m)^* \cos \theta / 2 + (|a|^2 - |m|^2 + 4 \operatorname{Re} g h^*) \sin \theta / 2 \\
 I_0 A &= \frac{1}{2} \operatorname{Re} \{ (G - N)^*(N - H) + B^*(N + H) \} \cos \theta / 2 \\
 &\quad + \operatorname{Im} C^*(B + G - N) \sin \theta / 2 \\
 &= (|a|^2 - |m|^2 + 4 \operatorname{Re} g h^*) \cos \theta / 2 + 2 \operatorname{Re} i c (a - m)^* \sin \theta / 2 \\
 I_0 C_{KP} &= -2 \operatorname{Re} i C H^* = 4 \operatorname{Re} i c h^* \\
 I_0 (1 - C_{NN}) &= \frac{1}{4} |G - N + B|^2 + \frac{1}{4} |G - N - B|^2 \\
 &= |a - m|^2 + 4 |g|^2 \\
 I_0 C_{NNN} &= 2 \operatorname{Im} i C N^* = 2 \operatorname{Im} i c (a + m)^* \\
 I_0 C_{NKP} &= -\frac{1}{4} \operatorname{Im} [(G - N + B)(G - N - B)^* - 4 N H^*] \\
 &= -2 \operatorname{Im} [(a - m) g^* + (a + m) h^*] \\
 I_0 C_{N \times K 1 \text{ in } NP} &= \frac{1}{2} \cos (\theta / 2) \operatorname{Im} [N(G - N - B)^* - (G - N + B) H^*] \\
 &\quad + \sin (\theta / 2) \operatorname{Im} [i C (G - N - B)^*] \\
 &= 2 \cos (\theta / 2) \operatorname{Im} [(a + m) g^* + (a - m) h^*] + 4 \sin (\theta / 2) \operatorname{Im} [i c g^*]
 \end{aligned}$$

In this expression, if A, B, C or D is replaced by a zero the corresponding index of $Z_{\mu, \nu; \lambda, \rho}$ is to be taken as zero. Then invariance under time reversal implies

$$Z(k, k'; A, B; C, D) = Z(-k', -k; -C, -D; -A, -B) \quad 4.2.$$

where plus and minus zero are considered equivalent. Equation 4.2 gives 128 conditions, the simplest of which is the equality of polarizing and analyzing power mentioned before. To derive this equality, notice first that the analyzing power $A(\mathbf{k}, \mathbf{k}'; 0, 0; N, 0)/I_0$, being a scalar linear in N , must, by rotation and space-reflection invariance, be of the form $\mathbf{k} \times \mathbf{k}' \cdot \mathbf{N}$ times a function of the scalar products of \mathbf{k}' and \mathbf{k} . It is therefore equal to $Z(-\mathbf{k}', -\mathbf{k}; 0, 0; -N, 0)/I_0$ which, by 4.2, is equal to the polarizing power $Z(\mathbf{k}, \mathbf{k}'; N, 0; 0, 0)$. Another consequence of the same three invariances is a relationship between A , R , A' , and R' , also first deduced by Wolfenstein (3). To derive this relation one takes from 4.1 the relation

$$Z(\mathbf{k}, \mathbf{k}'; \mathbf{K}, 0; \mathbf{P}, 0) = Z(-\mathbf{k}', -\mathbf{k}; \mathbf{P}, 0; \mathbf{K}, 0) \quad 4.3.$$

where the linearity in the last four variables has been used. The right-hand side, being a scalar linear in both \mathbf{P} and \mathbf{K} , must change sign when the first two arguments are changed to \mathbf{k} and \mathbf{k}' , respectively, as one sees by enumerating the possible forms. Both sides of 4.3 can then be expressed in terms of A , R , A' , and R' , and the relation $(A + R')/(A' - R) = \tan(\theta/2)$ follows immediately.

If rotation, space-reflection, and time-reversal invariances are all maintained, there are for the p - p system at one scattering angle only nine independent scattering experiments; the M matrix and hence also the observables are determined by the five complex Wolfenstein parameters, and the over-all phase of M is irrelevant. For the n - p system there are also nine independent experiments if charge independence is assumed—otherwise eleven.

At a scattering angle of 90 degrees, two of the Wolfenstein parameters of 2.10' vanish for p - p scattering, and five experiments are sufficient to fix M up to the over-all phase. Also, at this angle the combination $I_0(1 - C_{nn})$ is determined completely by the absolute value of singlet scattering amplitude and therefore measures this quantity. Details are given in (6). For n - p scattering at 90° the situation is also very favorable, since there are only two nonvanishing isotopic singlet amplitudes.

By virtue of the symmetry properties of the Wolfenstein parameters appearing in Equation 2.10', experimental observables at θ and $\pi - \theta$ can both be expressed in terms of the scattering amplitudes at θ . For some types of experiments, such as p - p differential cross sections and polarizations, the two experiments do not give independent information. However, for others, such as p - p triple-scattering experiments, the observables at the two scattering angles are given by different expressions in terms of the Wolfenstein parameters and furnish independent conditions on the latter. In n - p scattering the symmetries involve the isotopic singlet and triplet parts of the Wolfenstein parameters separately which, in effect, doubles the number of unknowns and renders the experiments at θ and $\pi - \theta$ essentially independent unless isotopic spin invariance is assumed. In this latter case, n - p and p - p

experiments can be analyzed simultaneously, and 19 experiments at the two angles are sufficient to determine the five isotopic singlet and five isotopic triplet parts of the Wolfenstein parameters up to a single over-all phase. This is discussed in detail by Golovin, Dzhelepov, Nadezhdin & Satarov (11).

Some relations between experimental observables imposed by unitarity are discussed in the next section.

5. UNITARITY AND PHASE SHIFTS

The important fact that S matrix is unitary has not been incorporated into the formalism developed above. A standard way of including unitarity is to decompose the scattering amplitudes into partial waves. Unitarity is then easily expressed by using phase shifts, as discussed below. The partial-wave expansion is also useful because only the lower partial waves contribute significantly to the scattering, and the reaction can be approximately described by a small finite number of parameters.

The S matrix, by its definition, depends only on the asymptotic form of the wave function; it is a transformation in the spin-angle variables, the radial dependence being essentially known. To simplify the writing it is convenient, therefore, to suppress the radial factor $i^L j_L(kr)$, where $j_L(kr)$ is the spherical Bessel function. Specifically, the symbol $|L, m; S_1, m_1; S_2, m_2\rangle$ will represent the state having spin quantum numbers (S_1, m_1) and (S_2, m_2) for the first and second particles, respectively, and a spatial dependence $Y_L^m(\theta, \phi)$ ($i^L j_L(kr)$), where $Y_L^m(\theta, \phi)$ is the spherical Bessel function as defined in Blatt & Weisskopf (13). The symbol $\langle L, m; S_1, m_1; S_2, m_2 | \psi \rangle$ will represent the amplitude of this state. Since the asymptotic outgoing part of ($i^L j_L(kr)$) is $e^{ikr}/2ikr$, the scattering amplitude becomes, using these conventions,

$$\begin{aligned} f_{S_1 S_2 m_1 m_2}(\theta, \phi) &= \frac{1}{2ik} \sum_{L, m} Y_L^m(\theta, \phi) \langle L, m; S_1, m_1; S_2, m_2 | R | \text{in} \rangle \\ &\equiv \frac{1}{2ik} \langle \theta, \phi | L, m \rangle \langle L, m; S_1, m_1; S_2, m_2 | R | \text{in} \rangle \\ &\equiv \frac{1}{2ik} \langle \theta, \phi; S_1, m_1; S_2, m_2 | R | \text{in} \rangle \end{aligned} \quad 5.1.$$

where the symbol $\langle \theta, \phi | L, m \rangle \equiv Y_L^m(\theta, \phi)$, the summation convention, and the completeness relation $|L, m\rangle \langle L, m| = 1$ have been used.

According to the above conventions, the state represented by $|\theta', \phi'\rangle$ is $(4\pi)^{-1}$ times a plane wave moving in the direction (θ', ϕ') as one sees from the Gegenbauer expansion (13),

$$\sum_{L, m} i^L j_L(kr) Y_L^m(\theta, \phi) (Y_L^m(\theta', \phi'))^* = \exp i\mathbf{k}' \cdot \mathbf{r} / 4\pi \quad 5.2.$$

Combining this fact with Equation 5.1 and the definition of the M matrix, one obtains the important relationship

$$M(\mathbf{k}, \mathbf{k}') = \frac{4\pi}{2ik} \langle \theta, \phi | R | \theta', \phi' \rangle \quad 5.3.$$

The most convenient phase shifts are related to the matrix elements of R in the representation where J , the total angular momentum, is diagonal. These states are characterized by quantum numbers J, L, S, M , where S is 0 or 1 for the singlet or triplet states, respectively, and M is the Z component of the total angular momentum J . Transforming from this representation, one obtains for the matrix elements of $M(\mathbf{k}, \mathbf{k}')$ in the singlet-triplet representation

$$\begin{aligned} \langle S, m_S | M(\mathbf{k}; \mathbf{k}') | S', m_{S'} \rangle &= \frac{4\pi}{2ik} \langle \theta, \phi; S, m_S | R | \theta', \phi'; S', m_{S'} \rangle \\ &= \frac{4\pi}{2ik} \langle \theta, \phi; S, m_S | L, S'', J, M \rangle \langle L, S'', J, M | R | L', S''', J', M' \rangle \\ &\quad \langle L', S''', J', M' | \theta', \phi'; S', m_{S'} \rangle \end{aligned} \quad 5.4.$$

The transformation functions occurring in 5.4 are sums of products of spherical harmonics and Clebsch-Gordan coefficients:

$$\begin{aligned} \langle \theta, \phi; S, m_S | L, S'', J, M \rangle &= \langle \theta, \phi | L, m \rangle \langle L, m; S, m_S | L, S'', J, M \rangle \\ &= \sum_m Y_L^m(\theta, \phi) C_{LS}(J, M; m, m_S) \delta_{SS''} \end{aligned} \quad 5.5.$$

where $C_{LS}(J, M; j, m_S) \equiv \langle L, m; S, m_S | L, S, J, M \rangle$ is the Clebsch-Gordan coefficient as defined in Blatt & Weisskopf (13).

Equations 5.4 and 5.5 allow the M -matrix elements to be expressed in terms of the R -matrix elements $\langle L, S, J, M | R | L', S', J', M' \rangle$. Because total angular momentum and its Z component are conserved, these R -matrix elements must vanish unless $J=J'$ and $M=M'$. Moreover, because of rotational invariance the matrix elements are independent of M . For a fixed angular momentum J , the possible values of L are $L=J$ and $L=J \pm 1$, where the second class can occur only in the triplet case. Also, the two classes cannot be coupled because of conservation of parity.

For brevity, we introduce for the nonvanishing matrix elements of the class $L=J \pm 1$ the definitions

$$\langle J \pm 1, 1, J, M | R | J \pm 1, 1, J, M \rangle = R_{J \pm 1, J} \quad 5.6.$$

$$\langle J \pm 1, 1, J, M | R | J \mp 1, 1, J, M \rangle = R_{\pm}^J = R^J \quad 5.7.$$

and, for the class $L=J$,

$$\langle J, 1, J, M | R | J, 1, J, M \rangle = R_{JJ}, \quad 5.8a$$

$$\langle J, 0, J, M | R | J, 0, J, M \rangle = R_J, \quad 5.8b$$

$$\langle J, \frac{1}{2} \pm \frac{1}{2}, J, M | R | J, \frac{1}{2} \mp \frac{1}{2}, J, M \rangle = R_{\pm}^J = R^J \quad 5.9.$$

The equalities $R_+^J = R_-^J = R^J$ and $R_+^{J'} = R_-^{J'} = R^{J'}$ stated here express the fact that the R matrix is symmetric in this representation. This is a consequence of time-reversal invariance discussed in the next section. The off-diagonal element $R^{JJ'}$ vanishes for the p - p system, as the antisymmetry of the wave function precludes states having the same orbital angular momentum L but different total spin. If isotopic spin is conserved, the $R^{JJ'}$ also vanishes for the neutron-proton system, since for the same L the two spin states have different isotopic spin.

By carrying out the arithmetic implied in 5.4 and 5.5 and using the abbreviations 5.6 through 5.9, one obtains the expressions for the M -matrix element given in Table II. Table II refers specifically to the n - p case. For the p - p case, only the antisymmetric states contribute, and in these a factor of two must be added, as discussed in Section 7. For the p - p case the Coulomb effects must also be included. Explicit p - p formulas are given in (14). An extensive discussion of relativistic Coulomb corrections is given by Breit (15).

Equations 5.4 and 5.5 give the decomposition of R into partial waves. However, the unitarity condition on $S = R + 1$ has not yet been invoked. By our choice of representation the only nondiagonal, nonvanishing matrix elements of R are the R^J and $R^{J'}$. Thus by grouping in pairs the two states $L = J \pm 1$ for $S = 1$ and the two states $S = \frac{1}{2} \pm \frac{1}{2}$ for $L = J$, the R matrix breaks into a series of two-by-two matrices, all other elements vanishing. The matrix $S = R + 1$ also must have this form, and the condition that S be unitary is equivalent to the condition that each of the two-by-two submatrices be unitary.

A symmetric, unitary two-by-two matrix has three degrees of freedom and can be expressed in terms of three real parameters in either of the forms

$$\begin{pmatrix} \cos \epsilon & -\sin \epsilon \\ \sin \epsilon & \cos \epsilon \end{pmatrix} \begin{pmatrix} e^{2i\delta_-} & 0 \\ 0 & e^{2i\delta_+} \end{pmatrix} \begin{pmatrix} \cos \epsilon & \sin \epsilon \\ -\sin \epsilon & \cos \epsilon \end{pmatrix}$$

or

$$\begin{pmatrix} e^{i\bar{\delta}_-} & 0 \\ 0 & e^{i\bar{\delta}_+} \end{pmatrix} \begin{pmatrix} \cos 2\bar{\epsilon} & i \sin 2\bar{\epsilon} \\ i \sin 2\bar{\epsilon} & \cos 2\bar{\epsilon} \end{pmatrix} \begin{pmatrix} e^{i\bar{\delta}_-} & 0 \\ 0 & e^{i\bar{\delta}_+} \end{pmatrix}.$$

Here the individual matrices are all unitary and the forms are obviously symmetric.

The first form has been used by Blatt and Biedenharn, and the real parameters δ_- , δ_+ , and ϵ are often called the Blatt and Biedenharn (type) phase shifts, or mixing parameter for the case of ϵ . The two matrices on the outside can be considered the transformation to the representation where S is diagonal. As the elements of a diagonal unitary matrix must be pure phase factors, they may be defined to be $e^{2i\delta_{\pm}}$.

The parameters of the second form are called "bar" phase shifts and are useful for several reasons (14). First, these phases are proportional to

TABLE II

M MATRIX ELEMENTS IN TERMS OF *R* MATRIX ELEMENTS

The *R*-matrix elements are defined in Section 5 with the added constraints that R_{lj} for $j < 0$ and R^j for $j \leq 0$ are zero. The $P_l^m(\theta)$ are the associated Legendre polynomials as defined in (13). The subscripts *s* and 1, 0, -1 designate the singlet and triplet states, respectively. Invariance under time reversal, space reflection and rotations, and isotopic spin rotations is assumed. The sign conventions in this table are in agreement with Equation 4.4 of the text. In (14) and (18) the R^j are defined to have the opposite sign from those of this table. In the tables and graphs of Part III the conventions of (14) are used, however.

$$\begin{aligned}
 M_{ss}(\theta, \phi) &= (ik)^{-1} \sum P_l(\theta) \left(\frac{2l+1}{2} \right) R_l \\
 M_{11}(\theta, \phi) &= (ik)^{-1} \sum P_l(\theta) \cdot \left\{ \left(\frac{l+2}{4} \right) R_{l,l+1} + \left(\frac{2l+1}{4} \right) R_{l,l} + \left(\frac{l-1}{4} \right) R_{l,l-1} \right. \\
 &\quad \left. + \frac{1}{4}[(l+1)(l+2)]^{1/2} R^{l+1} + \frac{1}{4}[(l-1)l]^{1/2} R^{l-1} \right\} \\
 M_{00}(\theta, \phi) &= + (ik)^{-1} \sum P_l(\theta) \cdot \left\{ \left(\frac{l+1}{2} \right) R_{l,l+1} + \left(\frac{l}{2} \right) R_{l,l-1} \right. \\
 &\quad \left. - \frac{1}{2}[(l+1)(l+2)]^{1/2} R^{l+1} - \frac{1}{2}[(l-1)l]^{1/2} R^{l-1} \right\} \\
 M_{01}(\theta, \phi) &= (ik)^{-1} e^{i\phi} \sum P_l^1(\theta) \left\{ -\frac{\sqrt{2}}{4} \left(\frac{l+2}{l+1} \right) R_{l,l+1} + \frac{\sqrt{2}}{4} \left(\frac{2l+1}{l(l+1)} \right) R_{l,l} \right. \\
 &\quad \left. + \frac{\sqrt{2}}{4} \left(\frac{l-1}{l} \right) R_{l,l-1} - \frac{\sqrt{2}}{4} \left(\frac{l+2}{l+1} \right)^{1/2} R^{l+1} + \frac{\sqrt{2}}{4} \left(\frac{l-1}{l} \right)^{1/2} R^{l-1} \right\} \\
 M_{10}(\theta, \phi) &= (ik)^{-1} e^{-i\phi} \sum P_l^1(\theta) \left\{ \left(\frac{\sqrt{2}}{4} \right) R_{l,l+1} - \left(\frac{\sqrt{2}}{4} \right) R_{l,l-1} \right. \\
 &\quad \left. - \frac{\sqrt{2}}{4} \left(\frac{l+2}{l+1} \right)^{1/2} R^{l+1} + \frac{\sqrt{2}}{4} \left(\frac{l-1}{l} \right)^{1/2} R^{l-1} \right\} \\
 M_{1-1}(\theta, \phi) &= (ik)^{-1} e^{-2i\phi} \sum P_l^2(\theta) \left\{ \left(\frac{1}{4(l+1)} \right) R_{l,l+1} - \left(\frac{2l+1}{4l(l+1)} \right) R_{l,l} \right. \\
 &\quad \left. + \left(\frac{1}{4l} \right) R_{l,l-1} + \frac{1}{4}[(l+1)(l+2)]^{-1/2} R^{l+1} + \frac{1}{4}[(l-1)l]^{-1/2} R^{l-1} \right\} \\
 M_{-1-1}(\theta, \phi) &= M_{11}(\theta, -\phi) \quad M_{01}(\theta, \phi) = -M_{0-1}(\theta, -\phi) \\
 M_{-11}(\theta, \phi) &= M_{1-1}(\theta, -\phi) \quad M_{10}(\theta, \phi) = -M_{-10}(\theta, -\phi)
 \end{aligned}$$

TABLE III

RELATIONS INVOLVING WOLFENSTEIN PARAMETERS

The Wolfenstein parameters are defined in Equations 2.10 and 2.10'. The subscripts s and 1 , 0 , -1 or M_{ij} designate singlet and triplet states respectively. The M -matrix elements are evaluated at $\phi=0$. Invariance under time reversal, space reflection and rotations, and isotopic spin rotations is assumed.

$$\begin{aligned}
 a &= \frac{1}{4} \text{Tr} M = \frac{1}{4} (2M_{11} + M_{00} + M_{ss}) \\
 c &= \frac{1}{4} \text{Tr} M \phi^{(1)} \cdot N = \frac{1}{4} \text{Tr} M \phi^{(2)} \cdot N = \frac{i\sqrt{2}}{4} (M_{10} - M_{01}) \\
 m &= \frac{1}{4} \text{Tr} M \phi^{(1)} \cdot N \phi^{(2)} \cdot N = \frac{1}{4} (-2M_{1-1} + M_{00} - M_{ss}) \\
 g &= \frac{1}{8} \text{Tr} M \{ \phi^{(1)} \cdot P \phi^{(2)} \cdot P + \phi^{(1)} \cdot K \phi^{(2)} \cdot K \} = \frac{1}{4} (M_{11} + M_{1-1} - M_{ss}) \\
 h &= \frac{1}{8} \text{Tr} M \{ \phi^{(1)} \cdot P \phi^{(2)} \cdot P - \phi^{(1)} \cdot K \phi^{(2)} \cdot K \} = \frac{1}{4 \cos \theta} (M_{11} - M_{1-1} - M_{00}) \\
 &= \frac{\sqrt{2}}{4 \sin \theta} (M_{10} + M_{01}) \\
 B &= M_{ss} \\
 C &= \frac{i\sqrt{2}}{4} (M_{10} - M_{01}) \\
 H &= \frac{-\sqrt{2}}{2 \sin \theta} (M_{10} + M_{01}) \\
 N &= \frac{1}{2} (M_{11} + M_{00} - M_{1-1}) \\
 (G - N) &= (M_{11} + M_{1-1}) \\
 a &= \frac{1}{4} (B + G + N) \\
 g &= \frac{1}{4} (G - B - N) \\
 m &= \frac{1}{4} (3N - B - G) \\
 c &= C \\
 h &= -\frac{1}{2} H
 \end{aligned}$$

the R -matrix elements in lowest order and approach zero as R goes to zero. Second, the parameter $\bar{\epsilon}$ gives a measure of the amount by which orbital angular momentum is not conserved, in the sense that a particle entering in one orbital state has a probability $\sin^2 2\bar{\epsilon}$ of being in the other state when it emerges. Third, in the Born approximation the phases are given by simple matrix elements of the interaction energy and hence obey simple interval rules. Fourth, Coulomb effects can be subtracted to lowest order by subtracting the Coulomb phases from the total bar phases. The essential difference between the two types of phases is that the mixing is in the asymptotic region for the Blatt and Biedenharn phases and at the core for bar phases. Equations relating the two types are given in (6) and (14).

The equations given above and in Table II allow the matrix elements of M in the single-triplet representation to be expressed in terms of phase shifts.

TABLE IV

EXPRESSIONS FOR THE WOLFENSTEIN PARAMETERS FOR THE
NEUTRON-NEUTRON SYSTEM

$$L_{\max} = 5$$

The conventions for the sign of R^j are the same as in (10) and (14). See these references for a description of the changes required for proton-proton scattering.

$$\begin{aligned}
 B &= + \frac{1}{8ik} \{ [8R_0 - 20R_2 + 27R_4] + [60R_2 - 270R_4] \cos^2 \theta + 315R_4 \cos^4 \theta \} \\
 C &= - \frac{\sin \theta}{64k} \{ [16R_{10} + 24R_{11} - 40R_{12} - 40R_{32} - 14R_{33} + 54R_{34} + 54R_{54} \\
 &\quad + 11R_{55} - 65R_{56}] \\
 &\quad + [200R_{32} + 70R_{33} - 270R_{34} - 756R_{54} - 154R_{55} + 910R_{56}] \cos^2 \theta \\
 &\quad + [1134R_{54} + 231R_{55} - 1365R_{56}] \cos^4 \theta \} \\
 H &= \frac{1}{32ik} \{ [16R_{10} - 24R_{11} + 8R_{12} - 8R_{32} + 14R_{33} - 6R_{34} + 6R_{54} - 11R_{55} \\
 &\quad + 5R_{56} - (32\sqrt{6})R^2 + (48\sqrt{5})R^4] \\
 &\quad + [40R_{32} - 70R_{33} + 30R_{34} - 84R_{54} + 154R_{55} - 70R_{56} + (80\sqrt{6})R^2 \\
 &\quad - (456\sqrt{5})R^4] \cos^2 \theta \\
 &\quad + [126R_{54} - 231R_{55} + 105R_{56} + (504\sqrt{5})R^4] \cos^4 \theta \} \\
 N &= + \frac{1}{32ik} \{ [16R_{10} + 24R_{11} + 56R_{12} - 136R_{32} - 14R_{33} - 186R_{34} + 294R_{54} \\
 &\quad + 11R_{55} + 355R_{56} + (16\sqrt{6})R^2 - (24\sqrt{5})R^4] \cos \theta \\
 &\quad + [200R_{32} + 70R_{33} + 290R_{34} - 1316R_{54} - 154R_{55} - 1610R_{56} + (56\sqrt{5})R^4] \cos^3 \theta \\
 &\quad + [1134R_{54} + 231R_{55} + 1407R_{56}] \cos^5 \theta \} \\
 G - N &= + \frac{1}{32ik} \{ [48R_{11} + 48R_{12} + 32R_{32} - 308R_{33} - 60R_{34} - 48R_{54} + 638R_{55} \\
 &\quad + 70R_{56} - (32\sqrt{6})R^2 + (48\sqrt{5})R^4] \cos \theta \\
 &\quad + [420R_{33} + 140R_{34} + 112R_{54} - 2772R_{55} - 420R_{56} - (112\sqrt{5})R^4] \cos^3 \theta \\
 &\quad + [-0R_{54} + 2310R_{55} + 462R_{56}] \cos^5 \theta \}.
 \end{aligned}$$

Since the observables are expressed in terms of the Wolfenstein parameters, the relationships between the M -matrix elements and the Wolfenstein parameters are still needed. These may be obtained by taking traces of the expression for M given in 2.10 to obtain explicit formulas for the Wolfenstein parameters. Carrying out the trace operations and using the well-known connection between the single-particle and the singlet-triplet representations, one obtains the results given in Table III. Intermediate steps are given in (6). In Table IV the expressions for the Wolfenstein parameters in terms of the R -matrix elements are given. A corresponding table in (10) contains several errors.

An alternative way of obtaining the connection between the Wolfenstein parameters and the phase shifts has been given by Wright (16) and by Bakke & Steck (17). The general phase-shift formalism for the neutron-proton

system is developed in a review article by Blatt & Biedenharn (18). General phase-shift formulas are also given by Breit & Hull (19).

The unitarity condition can also be introduced without using phase shifts. In particular the relation.

$$SS^* = 1 = (R + 1)(R^* + 1) = RR^* + R + R^* + 1$$

implies for all θ, ϕ , and all $\theta'\phi'$ the equation

$$- \langle \theta, \phi | R + R^* | \theta' \phi' \rangle = \langle \theta', \phi' | R | \theta'' \phi'' \rangle \langle \theta'' \phi'' | R^* | \theta' \phi' \rangle.$$

Using the relation 5.3 between R and M one obtains immediately

$$\left(\frac{2k}{4\pi}\right)^2 2 \operatorname{Im} M(\Omega, \Omega') = \left(\frac{2k}{4\pi}\right)^2 \int d\Omega'' M(\Omega, \Omega'') M^*(\Omega'', \Omega').$$

Multiplying this by $\sigma_{\mu}^{(1)} \sigma_{\nu}^{(2)}$ and taking one-quarter the trace, one finds

$$\operatorname{Im} M^{\nu\mu}(\Omega, \Omega') = \frac{2k}{4\pi} \int d\Omega'' \frac{1}{2} \operatorname{Tr}(M(\Omega \Omega'') M^*(\Omega'' \Omega') \sigma_{\mu}^{(1)} \sigma_{\nu}^{(2)}) \quad 5.10.$$

Although 5.10 contains 16 equations, only six of these (five for p - p) are independent. The same invariance conditions that allow M —and hence the left-hand side—to contain only six (five) degrees of freedom also constrain the right-hand side correspondingly. Since the phase enters in 5.10, and hence is no longer arbitrary, these unitary conditions reduce the number of arbitrary angle-dependent functions required to specify the M matrix to six (five) and thus, as pointed out by Puzikov, Ryndin & Smorodinskii (9), six (five) independent experiments, performed at all angles, are sufficient to determine M at all angles. If inelastic processes are considered, the unitarity condition involves the additional states, and the argument is no longer complete.

This result regarding the number of experiments needed to determine the scattering matrix, though often quoted, is rather academic. In practice, if data at many angles are to be analyzed simultaneously, a phase-shift analysis is used. A maximum angular momentum is usually chosen, and this fixes the number of powers of $\cos \theta$ in the various observables, and hence the number of parameters to be experimentally determined. The number of phases is also fixed. An analysis by Ypsilantis (10) shows that for $L_{\max} > 0$, three types of experiments—cross section, polarization, and one triple-scattering experiment—are more than sufficient to determine the phases in principle. For $L_{\max} = 0$, one experiment at one angle is evidently sufficient for the p - p or n - n case, since there is only one phase shift. For the proton-proton case, cross-section measurements involve interference with the approximately known Coulomb amplitude, and this circumstance also tends to reduce the number of types of experiments needed.

6. CONSEQUENCES OF TIME-REVERSAL INVARIANCE

The fundamental consequence of time-reversal invariance is (13, p. 529)

$$\langle a | S | b \rangle = \langle b_T | S | a_T \rangle \quad 6.1.$$

where a and b specify time-independent ($t=0$) basis vectors and a_T and b_T specify their respective time-inverse states. In the notation of Section 5, the time inverse of the state $|L, m\rangle$ is $(-1)^{L-m} |L, -m\rangle$; the $(-1)^L$ comes from the required complex conjugation of the radial part $i^L j_L(kr)$ and the remaining changes come from the relation (13) $Y_L^m(\theta, \phi)^* = (-1)^m Y_L^{-m}(\theta, \phi)$. For the case with spin, the time inverse of the state $|J, M\rangle$ is defined to be $(-1)^{J-M} |J, -M\rangle$. The spin is hereby reversed, as one requires for a time-reversed state, and the consistency of the definition with the composition law of angular momenta is guaranteed by the symmetry law for Clebsch-Gordan coefficients

$$C_{LS}(J, -M; -m, -m_s) = (-1)^{(J-M+L-m+S-m_s)} C_{LS}(J, M; m, m_s)$$

In some earlier treatments of time reversal this consistency condition was not maintained, as was pointed out by Huby (20). Inserting the definition for the time-reversed state in Equation 6.1, one obtains

$$\langle L, S, J, M | S | L', S', J, M \rangle = \langle L', S', J, -M | S | L, S, J, -M \rangle (-1)^{2J-2M} \quad 6.2.$$

Since the matrix element is independent of M and $(-1)^{2J-2M}$ is unity, the symmetry of the matrix follows.

It should be noted that a unitary transformation does not generally leave a symmetric matrix symmetric, and a change of basis, even by phase factors only, generally destroys the symmetry of S .

The time inverse of a Pauli spin state, $|\frac{1}{2}, \pm\frac{1}{2}\rangle$, is $\pm|\frac{1}{2}, \mp\frac{1}{2}\rangle$; that is, $|\chi_T\rangle = -i\sigma_2|\chi\rangle$. The condition of time-reversal invariance applied to the R matrix can therefore be written in the form

$$\begin{aligned} \langle k, \chi | R(\vartheta^{(1)}, \vartheta^{(2)}) | k', \chi \rangle &= \langle -k', \chi' | \sigma_2^{(1)} \sigma_2^{(2)} R(\vartheta^{(1)}, \vartheta^{(2)}) \sigma_2^{(1)} \sigma_2^{(2)} | -k, \chi \rangle \\ &= \langle -k', \chi' | R(\sigma_2^{(1)} \vartheta^{(1)} \sigma_2^{(1)}, \sigma_2^{(2)} \vartheta^{(2)} \sigma_2^{(2)}) | -k, \chi \rangle \\ &= \langle -k', \chi' | R(-\tilde{\vartheta}^{(1)}, \tilde{\vartheta}^{(2)}) | -k, \chi \rangle \\ &= \langle -k', \chi | R(-\vartheta^{(1)}, -\vartheta^{(2)}) | -k, \chi' \rangle \end{aligned}$$

Thus time-reversal invariance implies

$$\langle k | R(\vartheta^{(1)}, \vartheta^{(2)}) | k' \rangle = \langle -k' | R(-\vartheta^{(1)}, -\vartheta^{(2)}) | -k \rangle \quad 6.3.$$

as stated earlier. Equation 4.2 can be obtained by using similar methods. A discussion of time-reversal invariance and its consequences is given by Shirokov (21). Consequences of time irreversibility are discussed by Phillips (22).

7. SYMMETRIZATION

In the above, the two particles have been assumed to be distinguishable. If, as in proton-proton scattering, the Fermi particles are identical, the amplitudes in the symmetric states are zero and those in the antisymmetric states are twice those for nonidentical particles.

It is perhaps not immediately clear that this factor two should not be rather the square root of two. If one simply writes the familiar antisym-

metrized wave function $1/\sqrt{2}[\psi(\chi) - \psi(-\chi)]$, or its generalized version with spins, it is $\sqrt{2}$ that occurs. As the question involved here seems to arise often in practical work, a discussion of the problem seems warranted.

If identical particles are considered to differ from distinguishable particles only in that they happen to start in an antisymmetrized state and remain so because the interaction is symmetrical, then in an incident plane wave the amplitudes in the symmetrical and antisymmetrical spin-orbit partial wave states are 0 or $\sqrt{2}$ times their normal values, respectively, as indicated above. However, the detecting apparatus measures both particles, and this introduces an additional and independent factor of two in measured particle densities. The wave function can be normalized to the measured densities if an additional factor of $\sqrt{2}$ is supplied.

In a somewhat more sophisticated view, the identical nature of indistinguishable particles is ingrained more deeply in the mode of description. A wave function and a second wave function obtained from it by an interchange of particle co-ordinates are considered to represent not different states, but rather the same state multiplied by minus one. The effect of this is that in summing over a complete set of states care must be taken to include each state only once. For instance, the normalization condition becomes

$$\int |\psi(x_1, x_2)|^2 \theta(x_1, x_2) dx_1 dx_2 = 1$$

where $\theta(x_1, x_2)$ is zero for x_1 less than x_2 and one for x_1 not less than x_2 . This factor $\theta(x_1, x_2)$ ensures that a state contributes only once to the sum over states. The normalized plane wave is then $\exp(ikx) - \exp(-ikx)$, and the totally antisymmetric partial-wave amplitudes are twice normal. Since the particles are considered identical, there is no additional factor due to the counter's ability to detect either one. This second approach is the wave-function transcription of what happens in field theory.

The most satisfactory method of treating identical particles is to use quantum field theory. The formalism is completely defined and there is no question of interpretation or viewpoint. For $\mathbf{k} \neq 0$ the normalized plane wave state is given by $|\psi\rangle = a^*(\mathbf{k})a^*(-\mathbf{k})|0\rangle$, where $a^*(\mathbf{k})$ and $a^*(-\mathbf{k})$ are operators that create particles in states of momentum \mathbf{k} and $-\mathbf{k}$, respectively, and $|0\rangle$ represents the vacuum state. The wave function is $\langle 0|\psi(x_2)\psi(x_1)|\psi\rangle = \exp(ikx) - \exp(-ikx)$, where $x = x_1 - x_2$, and where the quantization volume is taken to be unity. When the Dyson-Wick (23) expansion of the S matrix is applied to this initial state, the scattering amplitude is found to be $f(\theta, \phi) = f_u(\theta, \phi) - f_u(\pi - \theta, \phi + \pi)$, where the two terms on the right-hand side come from the forward and backward scattered particle, respectively, for $\theta < \pi/2$.

The factor of two occurring for identical particles must evidently be included also for neutron-proton states if the isotopic spin formalism is used,

for in this approach the neutron and proton are considered different states of the same particle. However, this two is cancelled by a one-half if the formalism is applied consistently. For instance, the S matrix takes the form $P_0 A_0 + P_1 A_1$, where P_0 and P_1 are projection operators for the isotopic singlet and triplet states and A_0 and A_1 are the corresponding amplitudes, which include the factor two. The matrix element of P_1 between two p - p states is unity but between two n - p states is one-half.

The factor of two has been discussed in detail by Breit & Hull (19) and by the present author (6).

8. RELATIVISTIC FORMALISM

In the formalism described above, the nucleons are represented by two-component spin functions instead of the relativistic four-component spinors. The M matrix of the two-component formalism can be obtained from the relativistic formalism, by multiplying the relativistic scattering matrix by the free-particle spinors, provided that the center-of-the-mass frame is used. For a Dirac particle with momentum \mathbf{p} the spinors for the two possible spin state are $u_{\alpha 1}(\mathbf{p})$ and $u_{\alpha 2}(\mathbf{p})$, where α is the Dirac spinor index and 1 and 2 are indices labeling the two spin states. The $u_{\alpha i}(\mathbf{p})$ may be expressed as matrix elements of the matrix

$$u(\mathbf{p}) = (-i\mathbf{p} \cdot \boldsymbol{\gamma} + \beta M)\beta/[2M(p_0 + M)]^{1/2} \quad 8.1$$

where the spinor and spin indices run over rows and columns, respectively. Stated differently, the $u_i(\mathbf{p})$ are obtained by operating on the proper spin states $w_1 = (1, 0, 0, 0)$ and $w_2 = (0, 1, 0, 0)$ with the Lorentz transformation

$$\mathcal{L}^{-1}(\mathbf{p}) = (-i\mathbf{p} \cdot \boldsymbol{\gamma} + \beta M)\beta/[2M(p_0 + M)]^{1/2} \quad 8.2$$

which transforms spin state amplitudes from their values in the particle-rest frame to values in the frame where the particle has momentum \mathbf{p} . With these definitions it is not hard to see that if the center-of-mass frame is used, the reduced Pauli-type scattering matrix

$$M_{i,j;k,l} = \bar{u}_i^{(1)}(\mathbf{p}_1) \bar{u}_j^{(2)}(\mathbf{p}_2) \mathcal{M} u_k^{(1)}(\mathbf{p}_1') u_l^{(2)}(\mathbf{p}_2') \quad 8.3$$

where \mathcal{M} is the relativistic scattering matrix and where spinor indices are suppressed, possesses the same transformation properties under rotations, spatial reflections, and time reversal that it has in the nonrelativistic theory. Thus, the same group theoretical arguments may be applied and the non-relativistic theory is formally unchanged.

According to the above connection, the spin vector of the nonrelativistic treatment can be equated to the relativistic spin vector provided the latter is measured in the particle rest-frame related to the reaction center-of-mass frame by the inverse of the Lorentz transformation 8.2. Conversely, the relativistic spin vector, which, according to Michel & Wightman (24), is a pseudovector whose fourth component vanishes in the particle-rest frame can be obtained by applying the Lorentz transformation 8.2 to the spin

vector of the nonrelativistic treatment. The relativistic spin vector in the laboratory frame may then be obtained by a second Lorentz transformation.

If the outgoing particle for one reaction is the incident particle for a second reaction, the second reaction must be described in its own rest frame if the two-component formalism is to be applicable. The relativistic spin vector in this second center-of-mass frame may be obtained by a Lorentz transformation from the laboratory frame. Finally, the three-component spin vector needed for the two-component formalism is obtained by a transformation from this second center-of-mass frame back to the particle rest-frame. Although this sequence of four Lorentz transformations brings vectors back to their values in a particle rest-frame, the final rest-frame is rotated relative to the original one. This rotation is discussed in some detail in (25), where explicit formulae are given. Discussions of the connection between the relativistic and nonrelativistic formulations have also been given by Steck (26), Garren (27), and Breit (15). A more formal general approach to the question of the relativistic description of polarized particles is given by Chou & Shirokov (28).

II. EXPERIMENTAL DATA

BY MALCOLM H. MACGREGOR

1. INTRODUCTION

Elastic nucleon-nucleon scattering experiments are easier to analyze than nucleon-nucleon experiments in which both elastic and inelastic processes occur. Since in all analyses done to date it is assumed that only elastic processes are present, we will limit our summary of data to the energy range where inelastic processes (pion production) are unimportant. Strictly speaking, this is from 0 to 290 Mev; but Phillips has shown (29) that below 400 Mev, inelastic processes can safely be ignored. This summary therefore includes data from 0 to 400 Mev.

High-energy nucleons for nucleon-nucleon scattering experiments are obtained by accelerating protons in a linear accelerator or a cyclotron. For proton scattering, the proton beam is brought out of the accelerator and used directly. Energy variations are obtained either by varying the energy of the accelerator or, in the case of a fixed energy cyclotron, by degrading the beam in energy with an absorber. The inherent straggling of protons is small and the beam energy can be reduced to (say) one-third of its original value and still be reasonably monoenergetic. For neutron scattering at high energies, the internal proton beam is allowed to strike a target such as beryllium, producing neutrons by a proton-neutron reaction. The neutron beam formed in this manner has a considerable energy spread and has an effective energy somewhat lower than the original proton beam. For neutron scattering at lower energies of about 30 Mev and below, deuteron accelerators and

the deuterium-tritium reaction can be used to produce monoenergetic neutron beams.

Proton targets are generally liquid hydrogen, although many experiments have been carried out by taking the difference between hydrocarbon-target and carbon-target scattering. Neutron targets are obtained by taking the difference between deuterium and hydrogen scattering. At low bombarding energies the deuteron binding energy and the shadow effect caused by the spectator particle in the deuteron tend to obscure the results, but at high energies these effects become rather small. With a suitable combination of beam and target, p - p , p - n , n - p , and n - n scattering experiments can be carried out. Because of the ease in producing and detecting protons, p - p scattering experiments have been carried out in most detail.

This part of the review article consists chiefly of a list of references for the published reports on 0 to 400 Mev nucleon-nucleon scattering experiments and of graphs of some of the data. The latter are designed to give the reader a knowledge of the general features of the experimental situation. Since the older experiments (pre-1950) are mainly of historical interest, only occasional reference is made to them. The review article by Breit & Gluckstern (30) (1953) summarizes these early experiments. We have made no effort to present numerical data in tabular form. For these it will be necessary to consult the original papers. In this connection, the review article of Hess (31) (1958) is useful. Hess has collected (and in some cases renormalized) the nucleon-nucleon differential cross section and polarization measurements and has tabulated the data.

The experimental nucleon-nucleon field is an active one at the present time. For p - p scattering, accurate differential cross-section and polarization data exist at many energies. Some triple-scattering measurements have been carried out, and a few 90° spin correlation measurements exist. For n - p scattering, a large number of differential cross-section measurements and polarization measurements have been made, although these are not as accurate as the corresponding p - p cross-section measurements. There are no n - p triple-scattering measurements as yet, although experiments are in progress. For n - n scattering, a differential cross section at one energy and total cross sections at a number of energies have been measured.

2. TOTAL CROSS-SECTION MEASUREMENTS

Total cross sections are obtained by transmission measurements. Counting rates are determined with and without the absorbing sample in the beam, and the ratio of counting rates gives the cross section. The incident beam must be collimated to the diameter of the detector, or, alternately, the scattering sample must have a diameter just large enough to "shadow" the detector. Otherwise, particles not in the direct beam will be scattered into the detector, necessitating corrections to the data. In the ideal case (good geometry), the detector is a point, and all beam particles that are at all scattered are lost. If the detector has a large acceptance angle for scattered

particles (poor geometry), only those particles scattered at angles large enough to be outside of this cone will be lost and hence will be "measured" as part of the total cross section. At energies above 290 Mev, the total cross section is the sum of elastic plus inelastic scattering.

Total n - p and p - p cross sections are measured by determining the attenuation of a neutron and proton beam in liquid hydrogen. Total p - p cross-section measurements are complicated by Coulomb effects. Measurements are usually made in poor geometry, so that the (small angle) Coulomb-scattered protons are still counted. An extrapolation is then made to the good geometry case to give the total nuclear scattering cross section. Since accurate p - p differential cross sections exist, total cross sections are often calculated by simply integrating over the differential cross section with the forward Coulomb peak removed. Total p - n and n - n cross sections are determined by difference measurements, using deuterium and hydrogen targets.

Table V lists total cross-section measurements. There are also recent unpublished results from Harwell (32). The results of these measurements are

TABLE V
NUCLEON-NUCLEON TOTAL CROSS-SECTION MEASUREMENTS

Measurement	Energy (Mev)	Laboratory	Ref.
p - p , p - n	208, 315	Chicago	(33)
p - p , p - n	408	Chicago	(34)
p - p	225, 330	Berkeley	(35)
n - p	1.32	M.I.T.	(36)
n - p	4.75	Brookhaven	(37)
n - p	3-12	Los Alamos	(38)
n - p	13.9	Carnegie Tech.	(39)
n - p	14.1	Brookhaven	(40)
n - p	14.1	Los Alamos	(41)
n - p	7-14	Livermore	(42)
n - p	20	Los Alamos	(43, 44)
n - p	17-29	Livermore	(45)
n - p , n - n	42	Berkeley	(46)
n - p	47.5, 88	Harvard	(47)
n - p , n - n	95	Berkeley	(48)
n - p	93-107	Harvard	(49)
n - p	38-153	Harwell	(50 to 52)
n - n	153	Harwell	(50)
n - n	109-169	Uppsala	(53)
n - p	169	Uppsala	(54)
n - p	97-220	Rochester	(55)
n - p	160, 220	Berkeley	(56)
n - p , n - n	270	Berkeley	(57)
n - p , n - n	280	Berkeley	(58)
n - p , n - n	380	Moscow	(59, 60)
n - p , n - n	410	Chicago	(61)

summarized in Figure 1. Total n - n and p - p measurements are in good agreement, as are n - p and p - n measurements.

3. PROTON-PROTON DIFFERENTIAL CROSS-SECTION MEASUREMENTS

Early measurements of p - p differential cross sections have been summarized by Jackson & Blatt (62) (1950) and Breit & Gluckstern (30) (1953). Table VI summarizes the more recent measurements.

TABLE VI
PROTON-PROTON DIFFERENTIAL CROSS-SECTION MEASUREMENTS

Energy	Laboratory	Ref.
$\sim 0.4^\dagger$	M.I.T.	(63)
1.4-2.4	Wisconsin	(64 to 66)*
5.77	Illinois	(67)
9.68	Minnesota	(68)
9.73	Berkeley	(69)
18.2	Princeton	(70)
19.8	UCLA	(71, 72)
25.63	Minnesota	(73)
29.4-31.8	Berkeley	(74 to 77)
39.4	Minnesota	(78)
20-68 †	Minnesota	(79)
68.3	Minnesota	(80)
41-95 †	Harvard	(81)
70, 95	Harvard	(81)
75, 105	Harvard	(82)
134	Harwell	(83, 84)
147	Harwell	(85 to 87)
46-147	Harvard	(88)
240	Rochester	(89, 90)
170, 260	Berkeley	(91)
120-345	Berkeley	(92)
300-340	Berkeley	(35, 93, 94)
365-428	Carnegie Tech.	(95)
380	Liverpool	(96, 97)
419	Chicago	(98)

* The latest published data (64) still need slight corrections at 1.397 and 2.425 Mev. New data have been taken at 1.397, 2.425, and 3.037 Mev.

† 90° angle only.

The most striking feature about p - p differential cross sections is the flatness of the spectrum with angle outside of the Coulomb peak and Coulomb interference regions. Although many partial waves are present in the scattering (see the next chapter), these add up to give a cross section almost

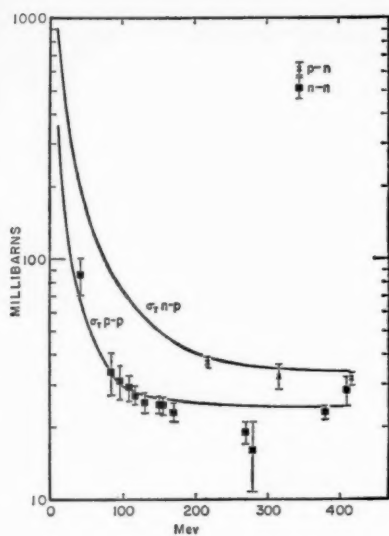


FIG. 1

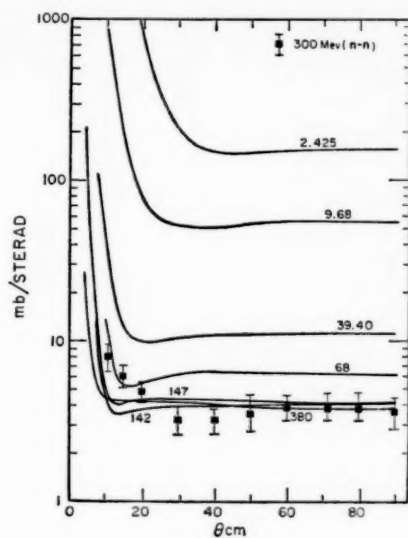


FIG. 2

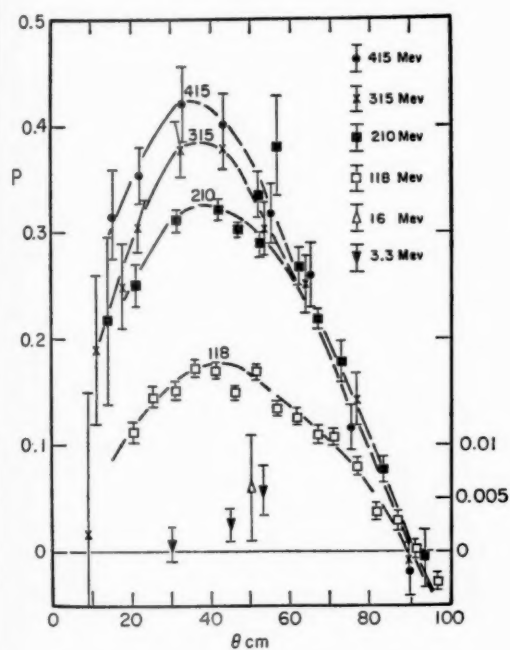


FIG. 3

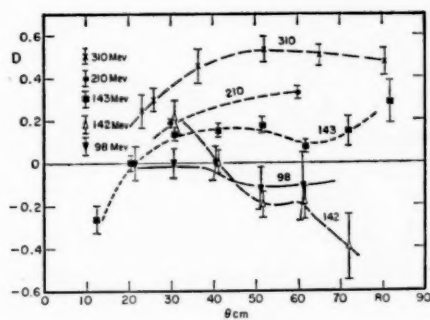


FIG. 4

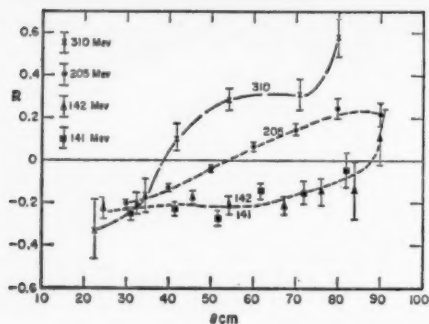


FIG. 5

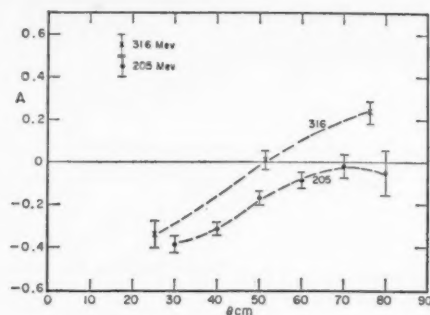


FIG. 6

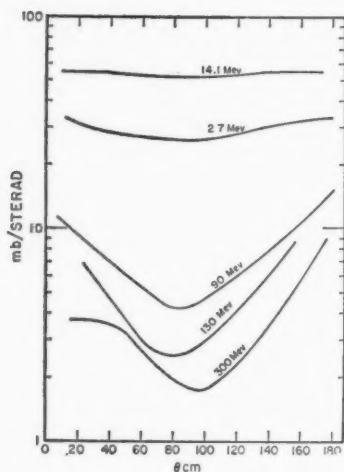


FIG. 7

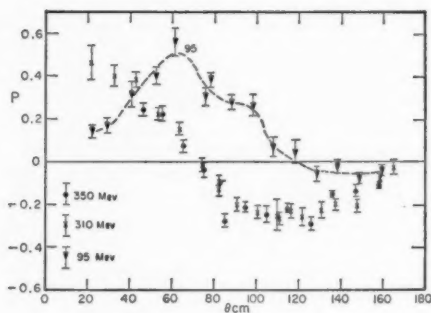


FIG. 8

DESCRIPTION OF FIGURES 1-8

FIG. 1. Total cross sections. For p - p and n - p , smooth curves were drawn to represent the experimental data. For p - n and n - n , the data are given. The p - n and n - n data are actually deuterium minus hydrogen difference measurements with the interference term assumed to be zero [see (31) for a more detailed discussion].

FIG. 2. Proton-proton and neutron-neutron differential-cross-section measurements. The references are: 380 Mev (96, 97); 147 Mev (88); 142 Mev (87); 68 Mev (80); 39.4 Mev (78); 9.68 Mev (68); 2.425 Mev (64). The experimental points are n - n data at 300 Mev (104). The constancy of the cross section with energy at the higher energies is well illustrated by the curves at 142, 147, and 380 Mev. Here, 142- and 147-Mev curves are both drawn normalized to the

independent of angle except for Coulomb effects. Figure 2 shows typical p - p angular distributions. At higher energies the p - p differential cross section is almost independent of energy.

The 400 Kev 90° differential cross sections (63) were measured to locate the minimum in the cross section due to the Coulomb-nuclear cancellation. New measurements on this are now being carried out at Los Alamos. The Wisconsin measurements from 1.4 to 4.2 Mev have been improved several times, and very precise cross sections have been obtained in the small scattering angles. This information has been very useful in studying vacuum-polarization corrections to the Coulomb scattering (99 to 102). The University of Minnesota proton linac has been used to measure a series of very accurate differential cross sections (68, 73, 78 to 80) with experimental errors of about 1 per cent except at very small angles. The Harvard group has recently measured a series of differential cross sections (88) in the 46 to 147-Mev range. As Figure 2 shows, the Harvard and Harwell differential cross sections around 145 Mev differ somewhat in shape. While this difference is not large, it is more than one would expect from the accuracy of the two experiments. New measurements have recently been made at Harwell of the relative shape of the cross section at 146 Mev (32).

Systematic phase-shift analyses of the p - p differential cross section data (103) suggest that the Berkeley data around 30 Mev (74 to 77) have systematic errors. There is also a question as to the correct normalization of the 240-Mev Rochester data (89, 90). These are all rather old measurements. New differential cross sections at 210 Mev are now being measured at Rochester.

same 90° value. As can be seen, there is a slight difference in the results at small angles. The n - n cross sections agree well with the high-energy p - p cross sections.

- FIG. 3. Proton-proton measurements of $P(\theta)$. The references are: 415 Mev (119); 315 Mev (116, 118); 210 Mev (111); 118 Mev (88); 16 Mev (105); 3.3 Mev (106). The low-energy data (105, 106) are plotted multiplied by 10 (right-hand ordinate).
- FIG. 4. Proton-proton measurements of $D(\theta)$. The references are: 310 Mev (118); 210 Mev (125); 143 Mev (123, 124); 142 Mev (122); 98 Mev (121). Harvard (123, 124) and Harwell (122) measurements do not agree.
- FIG. 5. Proton-proton measurements of $R(\theta)$. The references are: 310 Mev (118); 205 Mev (129); 142 Mev (128); 141 Mev (127).
- FIG. 6. Proton-proton measurements of $A(\theta)$. The references are: 316 Mev (131); 205 Mev (130).
- FIG. 7. Neutron-proton differential-cross-section measurements. The references are: 300 Mev (160); 130 Mev (154); 90 Mev (144 to 147, 149, 151, 152); 27 Mev (142, 143); 14.1 Mev (139, 140).
- FIG. 8. Neutron-proton measurements of $P(\theta)$. The references are: 350 Mev (167); 310 Mev (166); 95 Mev (153).

4. PROTON-PROTON POLARIZATION MEASUREMENTS

When an incident unpolarized proton beam scatters off an unpolarized proton target, it becomes polarized in a direction perpendicular to the plane of scattering. The measurement of this polarization requires a second scattering from a target with known analyzing power. Polarization measurements are inherently more difficult than cross-section measurements. At high energies the p - p polarization is large and positive, as shown in Figure 3. (The polarization is of course antisymmetric around 90° .) At low energies the polarization falls off rapidly, making accurate measurements very difficult. The Harvard group have speculated in their article (88) that perhaps there is even a sign change at low energies. However, the very low-energy data (105, 106) that have subsequently been published indicate that this is not the case. The sign remains positive.

The reports on p - p polarization that have been published are listed in Table VII. In addition to these references, the Harwell group is completing measurements at 40 Mev (32), and the Wisconsin group (107) is planning additional measurements up to 10 Mev.

TABLE VII
PROTON-PROTON POLARIZATION MEASUREMENTS

Energy (Mev)	Laboratory	Ref.
3.3	Wisconsin	(106)
16	Princeton	(105)
18	Princeton	(108)
133	Harwell	(109)
142	Harwell	(87)
46-147	Harvard	(88)
66, 95, 118, 147	Harvard	(88)
174	Berkeley	(110)
130, 170, 210	Rochester	(111, 112)
240	Rochester	(113)
314	Chicago	(114, 115)
276, 315	Berkeley	(35, 116 to 118)
415	Carnegie Tech.	(119)
439	Chicago	(120)

5. PROTON-PROTON TRIPLE-SCATTERING AND SPIN CORRELATION EXPERIMENTS

Triple-scattering experiments measure the change in polarization when a polarized nucleon scatters from an unpolarized nucleon. They are generally more difficult than polarization experiments, but this is not necessarily true at low energies, since here the polarization is very small, whereas the triple scattering parameters are still large (103). Spin correlation experiments

measure the polarization of both scattered particles after the collision of an unpolarized beam with an unpolarized target. Table VIII lists the triple-scattering experiments carried out to date.

Measurements of the scattering parameter $D(\theta)$ are shown in Figure 4. There is an unresolved discrepancy between the Harwell (122) and Harvard (123, 124) results at 142 Mev. The Harwell group (32) is remeasuring D using a different experimental arrangement, and the discrepancy may be solved by the time this article is in print. The Rochester group is presently making D measurements at 210 Mev (125).

The measurement of $D(\theta)$ involves three coplanar scatterings. The $R(\theta)$ measurement differs in having the second scattering in a plane perpendicular

TABLE VIII

PROTON-PROTON TRIPLE-SCATTERING AND SPIN CORRELATION EXPERIMENTS

Experiment	Energy	Laboratory	Ref.
D	98	Harvard	(121)
D	142	Harwell	(122)
D	143	Harvard	(123, 124)
D	210	Rochester	(125)
D	310	Berkeley	(118)
D	415	Carnegie Tech.	(126)
R	140	Harvard	(127)
R	142	Harwell	(128)
R	205	Rochester	(129)
R	310	Berkeley	(118)
A	210	Rochester	(130)
A	316	Berkeley	(131)
C_{nn}	320*	Liverpool	(132, 133)
C_{nn}	382*	Liverpool	(134, 133)
C_{kp}	382*	Liverpool	(136)

* 90° angle only.

to the first scattering plane. Figure 5 shows the existing R data. The Harvard (127) and Harwell (128) data around 142 Mev are in good agreement. In the Harvard measurement, a magnetic field was used to rotate the polarization vector of the incident proton in the second scattering so that all measurements could be kept in a single scattering plane.

Measurements of $A(\theta)$ are illustrated in Figure 6. Since these require a longitudinal component of the polarization vector in the incident beam for the nucleon-nucleon scattering, a magnetic field is used to rotate the polarization vector of this beam. In addition to the A measurements shown in Figure 6, both the Harwell and Harvard groups are planning measurements of A at 140 Mev.

The only measurements of the spin correlation parameters C_{nn} and C_{kp} were done at Liverpool and are listed in Table VIII. Allaby, Ashmore, Eades & Taylor (132) are planning a measurement of C_{kp} at 320 Mev and a scattering angle of 45° c.m. in order to choose between Stapp solutions 1 and 2 (135) (see the discussion in the final part of this article). This is a difficult experiment since the low-energy proton scattered out will have a mean energy of only 20 Mev. A carbon analyzer with a 40° scattering angle will be used for the low-energy proton, and a carbon analyzer with a 9° scattering angle will be used for the high-energy proton. Brolley and co-workers at Los Alamos (137) are working on equipment to measure proton-proton spin

TABLE IX
NEUTRON-PROTON DIFFERENTIAL CROSS-SECTION MEASUREMENTS

Energy (Mev)	Laboratory	Ref.
10.6	Carnegie Tech.	(138)
14.1	Los Alamos	(139, 140)
17.9	Oak Ridge	(141)
27.2	Los Alamos	(142)
13.7, 28.4	Illinois	(143)
90	Berkeley	(144 to 150)
93	Harvard	(151, 152)
127	Harvard	(153)
130	Harwell	(154)
105, 137	Harwell	(155)
96, 130, 137	London	(156)
156	Harwell	(157)
215	Rochester	(158)
260	Berkeley	(159)
308	Berkeley	(160)
353	Liverpool ¹	(161)
390	Carnegie Tech.	(95, 162)
400	Moscow	(104)

correlations at 20 Mev. The actual experiment will probably be carried out at Oak Ridge using an external proton beam from the Oak Ridge cyclotron.

6. NEUTRON-PROTON DIFFERENTIAL-CROSS-SECTION AND POLARIZATION MEASUREMENTS

Neutron-proton differential cross sections are determined by measuring the angular distribution of either the proton or neutron. Normalization is usually accomplished by integrating over angles and comparing to a total n - p cross-section measurement (Fig. 1). The n - p angular distribution is quite symmetric about 90° at low energies, but at higher energies the cross section tends to peak at large angles, showing that a charge-exchange type

of scattering is favored. Figure 7 illustrates typical n - p differential cross sections. The accuracy of the data points is typically 10 per cent, and the precise shapes of the smoothed curves shown in Figure 7 should not be taken too literally. A comparison with Figure 2 shows that n - p and p - p differential cross-section curves bear little resemblance to each other, even apart from Coulomb effects. Table IX summarizes the references. The Harwell group have additional measurements that have not been published as yet (32). Also, workers at Los Alamos (137) are building a bubble chamber for n - p differential cross-section measurements in the 25- to 35-Mev range.

7. NEUTRON-PROTON POLARIZATION MEASUREMENTS

A number of n - p polarization measurements have been carried out. These are summarized in Table X. Figure 8 shows typical measurements. Since the angular distribution of polarization is not (anti) symmetric about 90° , as in the p - p case, measurements are made over the whole 180° range.

TABLE X
NEUTRON-PROTON POLARIZATION MEASUREMENTS

Energy (Mev)	Laboratory	Ref.
77	Harwell	(163)
98	Harvard	(153)
127	Harwell	(164)
210	Rochester	(165)
310	Berkeley	(166)
350	Carnegie Tech.	(167)

8. NEUTRON-PROTON TRIPLE-SCATTERING MEASUREMENTS

To date no n - p or p - n triple-scattering measurements have been completed. However, the Harvard group is currently measuring D and R at 140 Mev for the p - n reaction by scattering protons on deuterium. Similar measurements are also being planned at 210 Mev by the Rochester group.

9. NEUTRON-NEUTRON DIFFERENTIAL CROSS SECTIONS

The only measurements of the n - n differential cross section in the 0 to 400-Mev range are the Moscow results at 300 Mev (104). These have been plotted on Figure 2 with the p - p results. As can be seen, the agreement is quite good, providing a verification of the charge symmetry of nuclear forces.

10. POLARIZED SOURCES AND TARGETS

Accurate experimental data on the scattering parameters in nucleon-nucleon scattering are essential for specification of the scattering matrix. These data have been slow in forthcoming because of the intrinsic difficulty of the experiments. A great simplification will be effected when polarized

beams and polarized targets are available. Polarized beams produced by scattering protons off nuclei such as carbon already exist. Proton accelerators featuring polarized ions from the accelerator ion source are being developed by several groups. References (168) and (169), respectively, give accounts of the production of polarized proton and polarized neutron beams. Several groups are also developing polarized targets. For example, the Harvard group is using the Overhauser effect with a deuterium target (170).

As a typical example of work now under way in the field of polarized sources and targets, we quote the following two paragraphs, kindly sent to us by Professor L. Johnston at the University of Minnesota. The first paragraph was written by H. G. Clausnitzer and the second by C. F. Hwang and T. M. Sanders.

A polarized proton ion source is being made at the University of Minnesota, with which it is hoped that a 68 Mev proton beam, at least 40% polarized, will be achieved in 1960. An average beam current of at least 10^{-12} amperes is anticipated. The method is basically that of passing a neutral atomic hydrogen beam through a 6-pole inhomogeneous magnetic field which focuses a desired polarization component along the beam axis [(171)]. The neutral polarized beam then drifts into the high voltage terminal of the 1/2 Mev injector accelerator, where it is ionized and injected into the proton linear accelerator.

At the University of Minnesota, efforts are being made to produce a polarized proton target. It has been shown by Abraham et al. [(172)], that nuclear polarization can be achieved via the saturation of the microwave electronspin resonance of paramagnetic centers in various materials. A polarized target, when used in conjunction with a polarized beam, will enable one to measure the various spin correlation coefficients by a single scattering process. High density polyethylene was chosen to be the target material and paramagnetic centers were introduced through radiation-damage of the target material. "X" band microwave radiation was utilized and both electron and proton resonances were observed at 1.2°K. A twenty-fold increase of the proton resonance signal strength was observed in the presence of the microwave radiation, corresponding to a 0.6% polarization of the protons at this temperature. By using "K" band microwave at 0.8°K, it should be possible to obtain a 10% reversible-spin polarized target.

III. PHENOMENOLOGICAL ANALYSIS

BY MICHAEL J. MORAVCSIK

The object of the study of nucleon-nucleon scattering is to acquire information on nuclear forces. It became evident quite early that the nuclear force law is sufficiently complicated that one cannot follow the simple procedure of taking a few measurements and then deducing from them the force law directly, as is possible, for instance, in the case of Coulomb's law. It is convenient, therefore, to establish a common meeting ground for experiments and theory, consisting of some formalism in terms of which experiments can be summarized with some ease and theory can be expressed quite directly. This formalism has so far been the partial wave analysis discussed in Part I.

At energies up to a few Mev, only S waves are important in the partial wave analysis of nucleon-nucleon scattering experiments of present accuracy. In this energy range the interest focuses therefore, on the energy dependence of the S wave phase shift. The description of this dependence is the object of the effective-range theory, which is discussed in Section 1. Effective-range considerations are also important at higher energies once the S wave is separated from the rest of the interaction, since the S wave explores the innermost regions of the interaction and hence can give information on the repulsive core that presumably exists in that region.

In Section 2, phase-shift analyses at higher energies are discussed. In these the contributions of a certain finite number of low angular-momentum states are included, and the contributions of the remaining states are taken to be zero.

Modified forms of phase-shift analysis are also discussed in which the contributions from the higher states are taken from meson theory. Finally, one can analyze data at all energies simultaneously, in which case coefficients describing the energy dependence of phase shifts are determined from the experiments. Some preliminary results of such an analysis, started only recently, are included at the end of Section 2.

1. EFFECTIVE-RANGE FORMALISM

The effective-range formalism was described in the last review (30) in these volumes. The formulae are

$$C^2 k \operatorname{ctg} \delta + 2k\eta h(\eta) = -\frac{1}{a} + \frac{1}{2} r_0 k^2 - P r_0^3 k^4 \quad 1.1.$$

for proton-proton scattering, and

$$k \operatorname{ctg} \delta = -\frac{1}{a} + \frac{1}{2} r_0 k^2 - P r_0^3 k^4 \quad 1.2.$$

for neutron-proton scattering, where k is the momentum of one nucleon in the center-of-mass system, and $\eta = e^2 \hbar^{-1} v^{-1}$, v being the velocity of a nucleon in the laboratory system.

$$h(\eta) = -0.57721 \dots - \log \eta + \eta^2 \sum_{n=1}^{\infty} \frac{1}{n(n^2 + \eta^2)} \quad 1.3.$$

$$C^2 = \frac{2\pi\eta}{e^{2i\eta} - 1} \quad 1.4.$$

and δ is the appropriate S phase shift.

The parameters a , r_0 , and P are called scattering length, effective-range, and shape parameter, respectively. The best presently known values of the effective-range parameters are given in Table XI. Those for the isotopic spin triplet state are from Heller (100) and from Noyes & Hafner (99), while others are from Gammel & Thaler (173) and from Hulthén & Sugawara (174). The neutron scattering lengths can be determined directly from

scattering experiments at very low energies, and the isotopic singlet effective range is then obtained from the scattering length and the binding energy of deuteron, assuming the shape-independent approximation, since the corresponding shape-parameter cannot be obtained from experiments of the present precision. The sign of the shape-parameter may be of importance in deciding the validity of potential models in the nucleon-nucleon interaction (175).

The difference between the scattering lengths in the isotopic spin triplet state for p - p and n - p scattering is partly due to Coulomb effects. After this correction is made, however, there is still a difference of some 25 per cent. It used to be claimed (176) that this difference can be explained in terms of

TABLE XI
VALUES OF THE EFFECTIVE RANGE FORMULA PARAMETERS AS DEFINED
BY EQUATIONS 1.1 AND 1.2

Isotopic spin	Spin	p - p or n - p	Scattering length in fermis	Effective range in fermis	Shape parameter
1	0	n - p	-23.74 ± 0.09	2.670 ± 0.023	0.017 ± 0.028
1	0	p - p	-7.77	2.77	0.047
0	1	n - p	5.39 ± 0.03	1.704 ± 0.028	0 by assumption

the difference in magnetic moments. It was shown, however, that if the nuclear forces are assumed to have a repulsive core (177) or if the measured form factors for magnetic moments are taken into account (178, 179), the magnetic moment corrections are much too small to account for the difference. It was also shown (178, 179), however, that the corrections due to the difference in mass between the neutral and charged pions, as well as between the corresponding pion-nucleon coupling constants, could certainly explain the difference, although this calculation, based on a model, does not permit unambiguous quantitative conclusions. The difference between the p - p and n - p isotopic triplet effective ranges is much smaller, and it is hoped that it can be explained in terms of Coulomb effects. Thus, at the present time, there is no evidence that the charge independence of nuclear forces is violated.

It was shown first by Foldy & Eriksen (180) that vacuum polarization corrections to p - p scattering are of appreciable magnitude. Vacuum polarization potentials extend out to about a half an electron Compton wave-

length, and hence a large number of partial waves (of the order of 20 or 30) make appreciable contributions to the scattering amplitude when it includes the vacuum polarization correction. Although individual phase shifts of the vacuum polarization contribution are small (of the order of $2e^2/3\pi\hbar c$), they carry the Coulomb phase factor $\exp 2i(\phi_l - \phi_0)$, and the sum over l contributes to both the real and the imaginary part of the scattering amplitude. Heller (100) therefore proposes to refer the nuclear scattering to the full electric amplitude (Coulomb plus vacuum polarization plus magnetic moments plus form factor) rather than just to the Coulomb wave functions as is done in the usual inclusion of Coulomb effects. His nuclear-electric phase shifts δ_l^E are related to the conventional phase shifts K_l referred to Coulomb wave functions by $K_l = \delta_l^E + \tau_l$ where τ_l is the phase shift produced by the departure from pure Coulomb scattering in the absence of any nuclear interaction. The δ_l^E should be distinguished from the phase shifts δ_l^C which are defined to be the values which the nuclear phase shifts [defined in (14)] would have if there were Coulomb scattering but no other electric interaction. Heller showed that the effective range expansion can be modified to give a model-independent energy parameterization for δ_l^E .

In practice, so far, the inclusion of vacuum polarization effects have been done only in an approximate way. Foldy & Eriksen (180, 181), for instance, assume that vacuum polarization effects were important only for the S wave. In their analysis, δ^C was computed using this assumption and the assumption that the nuclear force is of the Yukawa type. The difference between δ_l^C and δ_l^E is an almost energy-independent function above 0.5 Mev which depends on the assumed nuclear interaction.

Durand (102) pointed out the importance of the higher partial waves and that for experiments of high precision one must use the relativistic Coulomb parameter $e^2/\hbar v_{lab}$. In the procedure adopted by de Wit & Durand (101) for the analysis of the Wisconsin (65) experiments, an S wave is assumed known, and the interference between vacuum polarization and nuclear interaction for $l > 0$ are ignored. This is shown to be a good approximation at these energies. The analysis gives δ_l^N for the S wave and δ_l^E for the higher waves, as noted by Heller.

From a practical point of view, the vacuum polarization corrections, which amount to something of the order of 0.1° for each phase, are now of little importance at the higher energies where the experimental accuracy limits the determination of phases to an error of a degree or so. At low energies, however, the S phase can be determined to an accuracy of a few hundredths of a degree, and hence the vacuum polarization correction is of considerable importance. Finally, in an effective-range analysis, the vacuum polarization corrections are of vital importance in the determination of the effective range and, especially, of the shape-parameter.

A modification of the effective-range formula has been devised by Raphael (182) that has practical advantages, as will be shown. While this

modification was originally motivated by the boundary condition model of Feshbach & Lomon (183) it is independent of the details of that model. The relationship between this modified form and the conventional effective-range formulae can be discussed easily in terms of variational principles. Let us denote by $u(r)$ the S -state wave function satisfying the Schrodinger equation

$$u''(r) + [k^2 - \lambda(r)]u(r) = 0 \quad \lambda(r) = \frac{M}{\hbar^2} V(r) \quad 1.5.$$

and by $v(r)$ the asymptotic form of $u(r)$ satisfying

$$v''(r) + k^2 v(r) = 0 \quad 1.6.$$

Then, following Schwinger (176), let us consider

$$I = \lim_{R \rightarrow \infty} \left\{ \int_0^R \{u'^2(r) - [k^2 - \lambda(r)]u^2(r)\} dr - \int_0^R \{v'^2(r) - k^2 v^2(r)\} dr \right\} \quad 1.7.$$

It can easily be shown that I is stationary with respect to independent variations of u and v if

$$u(0) = 0 \quad u(r) - v(r) \rightarrow 0 \quad \text{when } r \rightarrow \infty \quad 1.8.$$

and if $u(r)$ and $v(r)$ satisfy Equations 1.5 and 1.6 respectively.

For small changes in energy, therefore, we have no alteration in the corresponding wave function. Hence, writing

$$I = k \cot(\delta + k\bar{r})v^2(r) \quad 1.9.$$

we have

$$\frac{d}{dk^2} [k \cot(\delta + k\bar{r})] = \frac{1}{v^2(r)} \left[\int_r^\infty v^2(r) dr - \int_0^\infty u^2(r) dr \right] \quad 1.10.$$

So far our expressions have been exact. If we now make an expansion in k^2 ,

$$\begin{aligned} u(r) &= u_0(r) + k^2 u_1(r) + \dots \\ v(r) &= v_0(r) + k^2 v_1(r) + \dots \end{aligned} \quad 1.11.$$

then, using the normalization of $v(\bar{r})$ we have

$$k \cot(\delta + k\bar{r}) = A + Bk^2 + \frac{1}{2}Ck^4 \dots \quad 1.12.$$

where

$$B = \int_{\bar{r}}^\infty v_0^2(r) dr - \int_0^\infty u_0^2(r) dr \quad 1.13.$$

$$C = 2 \int_{\bar{r}}^\infty v_0(v)r_1(r) dr - 2 \int_0^\infty u_0(r)u_1(r) dr \quad 1.14.$$

Letting $\bar{r}=0$ we get the usual effective-range relations where the coefficients are usually denoted by

$$A = -\frac{1}{a} \quad B = \frac{1}{2} r_0 \quad C = -2Pr_s^2 \quad 1.15.$$

The Raphael modification of these effective-range formulae can be obtained by choosing \bar{r} so that

$$B = \int_{\bar{r}}^{\infty} v_0^2(r) dr = \int_0^{\infty} u_0^2(r) dr = 0 \quad 1.16.$$

in which case one has

$$k \cot(\delta + k\bar{r}) = A_R + \frac{1}{2}C_R k^4 \quad 1.17.$$

with no quadratic term. The relationship between the two sets of parameters is as follows

$$\begin{aligned} -\frac{1}{a} &= \frac{A_R}{1 - A_R \bar{r}} = \frac{x}{\bar{r}} \\ \frac{1}{2} r_0 &= \bar{r} \left(1 + x + \frac{1}{3} x^2 \right) \\ -P &= \frac{1}{24} \left[(1+x)^2(1+\beta) + \frac{2}{5} x^2 + \frac{1}{3} x^3 \right] \left[1 + x + \frac{1}{3} x^2 \right] \end{aligned} \quad 1.18.$$

where

$$x = \frac{A_R \bar{r}}{1 - A_R \bar{r}} \quad \text{and} \quad \beta = \frac{3C_R}{\bar{r}^3} \quad 1.19.$$

The physical motivation behind this form is the idea that if the innermost region of the nuclear interaction is separated from the outer region by an appropriate choice of \bar{r} , the resulting expression involving the phase shift should be much less energy dependent than the usual effective-range formula whose range of validity is about 10 Mev. The reason is that for a strong interaction in the inner core the energy term in the Schrodinger equation will be negligible with respect to the potential term, and hence the logarithmic derivative of the wave function at \bar{r} will be a constant. Model calculations and comparisons with phenomenological potentials confirmed this, and the Raphael form appears to hold even at 300 Mev (175).

A similar effective-range formula can also be derived for p - p scattering, in which Coulomb effects also have to be included. It is

$$\frac{2\pi\eta}{e^{2\pi\eta} - 1} k \cot \delta - 2k\eta h(\eta) = \frac{A + Bk^4 + k \tan k\bar{r}}{1 - k^{-1}(A + Bk^4) \tan k\bar{r}} \quad 1.20.$$

where the quantities η and $h(\eta)$ are the same as those defined earlier for the conventional effective range formulae.

2. PHASE-SHIFT ANALYSES

Part I discussed the connection between phase shifts and the physical observables in nucleon-nucleon scattering. In practice, once one has phase shifts, it is trivial to calculate the observables, but the reverse procedure is not at all trivial. Given the experimental quantities, there is in general no feasible analytical procedure to obtain from them the phase shifts. There are some especially simple cases for which an analytic solution is possible, such

as the one treated by the method of Clementel, Villi, and their collaborators (184 to 188). This will be discussed later. In general, however, one can only guess at the phase shifts, calculate the fit, and then improve it by stepwise alteration of the phase shifts. In the early phase-shift analyses of nucleon-nucleon scattering data this procedure was carried out by hand computation. This was made possible by the relatively few phase shifts that were included in the analysis, as well as by the comparatively small number of data available on correspondingly few types of experiments. Later, when triple-scattering experiments became feasible and when experimental accuracy justified the inclusion of a larger number of phase shifts, the amount of computation became prohibitive, and electronic computers had to be used.

The goodness of a fit can, of course, be judged in a rough way by visual comparison between the experimental points and by prediction of the phase shift in question for the observable physical conditions. In more quantitative work, however, statistical criteria must be used. The quantity used in such criteria is called "chi squared" and is defined as

$$\chi^2 = \sum_i \frac{(E_i - O_i)^2}{\sigma_i^2} \quad 2.1.$$

where E_i is the experimental measurement, O_i is the value of the observable as calculated from the set of phase shifts in question, and σ_i is the standard deviation pertaining to the experimental measurement. The index i is to be carried over all the pieces of data included in the analysis. This quantity χ^2 is expected to be, for a good fit, equal to the number of pieces of data minus the number of parameters (in our cases, phase shifts). In general, the better the fit, the smaller χ^2 is. The mathematical procedure of fitting the phase shifts to the data is therefore the minimization of χ^2 as a function of the phase shifts. The geometrical picture is, in the case of N phase shifts, that of an $N+1$ dimensional space, with N dimensions representing the phase shifts and the $N+1$ th dimension being the value of χ^2 . The values of χ^2 as functions of the phase shifts form an N -dimensional surface in this space, and the minimization of the function corresponds to finding the "valleys" on this surface. There might be several such valleys, some of them deeper than others corresponding to several phase shift solutions, some better than others. If the value of χ^2 at the bottom of a valley is very much larger than the expected value, one might tend to disregard that solution as a spurious one. If the number of pieces of data minus the number of phase shifts is 30, for instance, the probability of a good fit resulting in a χ^2 of 60 or larger is less than 0.1 per cent.

The number of phase shifts to be included in an analysis depends on the energy at which the measurements were carried out as well as on the precision of the data. A very rough estimate of the maximum angular-momentum quantum number that ought to be important at a given energy can be made by equating the range of the nuclear force times the momentum

of the incident particle to h times the maximum angular-momentum quantum number. This impact-parameter argument gives, for instance, $L_{\max}=2$ at 40 Mev, and $L_{\max}=6$ at 350 Mev. The argument, however, is not only very rough but also semiclassical and hence is not at all valid for the lowest angular-momentum states, to which the correspondence principle cannot be applied at all.

In practice, the number of phase shifts considered in an analysis is limited by the maximum number of parameters that can be obtained from the data in question. In the modified analysis, the high angular-momentum states are represented by the prediction of meson theory. In this case, experiments are used to determine how many of the low angular-momentum states must be described in terms of phase shifts rather than represented by the theoretical prediction.

Part II of this article discussed the experimental status of nucleon-nucleon scattering and pointed out that p - p experiments are on a much better footing at the present time than n - p experiments. It is practical, therefore, to consider these two kinds of experiments separately.

Proton-proton scattering.—(a) *Ordinary phase shift analyses at fixed energies.* Early work on p - p scattering below 100 Mev was done by Clementel, Villi, and their collaborators (184 to 188). It was shown by them that if only differential cross-section measurements are available and if P waves are the only triplet states included, there are four sets of P waves for each given value of the singlet phases. They carried out an S - P - D analysis, using data at low as well as high energies, which took some account of the requirement that the phase shifts are continuous functions of energy. The result was far from unambiguous. Also, at high energies, F and higher waves were later shown to play an appreciable role, as will be mentioned below.

The method Clementel & Villi use is analytical. It consists of the determination of four bilinear combinations of the phases directly from the angular distribution, after which the phases can be obtained from the bilinear combinations. Their method is also amenable to graphical handling. Graphical methods were used also by the Yale group (189, 190) at higher energies.

The analytic method of Clementel, Villi, and collaborators was adapted to machine calculations by Noyes & MacGregor (191) for the analysis of low-energy experiments. Their most important finding is that rudimentary polarization measurements at 46 Mev are not consistent with the 40-Mev angular distribution unless F waves or mixing parameters are present. Further analysis of data up to 40 Mev by MacGregor (103) showed the data to be insufficient for a unique determination of the phases. He was able to map out solution regions within which all phase-shift sets gave equally good fits. He pointed out that certain of these sets were to be preferred if one requires the 1D_2 phases to be approximately those given by calculations from meson-theoretic models. It is evident from his predictions of the hitherto unmeasured observables (such as spin correlation and triple-

TABLE XII
SUMMARY OF ORDINARY PHASE-SHIFT ANALYSIS OF PROTON-PROTON AND
NEUTRON-PROTON SCATTERING EXPERIMENTS

Author(s) and reference	p - p or n - p	Energy or energies in Mev	Angular momentum states	Kind of data	Ref. for data
Garren (192)	p - p	240	$^1S_0, ^3P_0, ^3P_1, ^3P_2$	σ, P	(89, 92, 216)
Thaler & Bengston (189)	p - p and n - p	240	$^1S_0, ^3P_0, ^3P_1, ^3P_2, ^3S_1, ^3D_1 = ^3D_2 = ^3D_3$	σ	(89, 90, 159)
Thaler <i>et al.</i> (190)	p - p and n - p	240	$^1S_0, ^3P_0, ^3P_1, ^3P_2, ^3D_2, ^3F_2, ^3S_1, ^3P_1, ^3D_2$	σ	89, 90, 159)
Garren (217)	p - p	213	$^1S_0, ^3P_0, ^3P_1, ^3P_2$	σ, P	(109, 112, 218 to 220)
Garren (221)	p - p and n - p	213	$^1S_0, ^3P_0, ^3P_1, ^3P_2, ^3S_1, ^3P_1$	σ, P	(89, 92, 109, 112, 157 to 159, 218 to 225)
Klein (193)	p - p	170, 260, 330	$^1S_0, ^3P_0, ^3P_1, ^3P_2$	σ, P	(89, 94, 109, 112, 116, 216, 219)
Klein (215)	n - p	170, 260, 330	$^1S_0, ^3P_0, ^3P_1, ^3P_2, ^3S_1, ^3P_1, ^3D_2$	σ, P	(115, 157 to 159, 162, 226 to 232)
Beretta <i>et al.</i> (184)	p - p	18	$^1S_0, ^3P_0, ^3P_1, ^3P_2$	σ	(70)
Beretta <i>et al.</i> (185)	p - p	240	$^1S_0, ^3P_0, ^3P_1, ^3P_2$	σ	(90, 94, 219, 220)
Stapp (6)	p - p	310	$^1S_0, ^3P_0, ^3P_1, ^3P_2, ^3S_1, ^3D_2, ^3F_2, ^3F_3, ^3F_4$	σ, P, D, R	(94, 116, 233, 234)
Zimin (192a)	p - p	1-450	$^1S_0, ^3P_0$	σ	Averaging data collected in (235)
Garren (196)	p - p	213	$^1S_0, ^3P_0, ^3P_1, ^3P_2$	σ, P	(109, 112, 218 to 220, 222)
Ohnuma & Feldman (236)	p - p	150	$^1S_0, ^3P_0, ^3P_1, ^3P_2, ^1D_2, ^3F_2$	σ, P	(86, 89, 90, 92, 109, 110, 112, 219, 222, 237 to 239)
Hull <i>et al.</i> (195)	p - p	310	$^1S_0, ^3P_0, ^3P_1, ^3P_2, ^1D_2, ^3F_2, ^3F_3, ^3F_4$	σ, P	(109, 114, 116, 117, 218, 219, 232, 240)
Clementel <i>et al.</i> (188)	p - p	18, 30, 75, 95, 170, 260	$^1S_0, ^3P_0, ^3P_1, ^3P_2$	σ, P	(70, 75, 81, 82, 94, 109, 110, 112, 116, 219, 241)
Clementel & Villi (214)	n - p	27, 40, 90, 156, 172, 215, 260	$^1S_0, ^3P_0, ^3P_1, ^3P_2, ^3S_1, ^3P_1, ^3D_1 = ^3D_2 = ^3D_3$	σ, P	(142, 145, 147, 149, 157, 159, 242, 243)
Phillips (194)	p - p	150	$^1S_0, ^3P_0, ^3P_1, ^3P_2, ^1D_2, ^3F_2$ or 3F_4	σ, P	(83, 85, 86, 109, 244)
Phillips (191a)	p - p n - p	95	$^1S_0, ^3P_0, ^3P_1, ^3P_2, ^1D_2, ^3S_1, ^3P_1, ^3D_1, ^3D_2, ^3D_3, ^3F_2$	σ, P σ	(151, 155, 243, 245, 246)
Stapp <i>et al.</i> (14)	p - p	310	$^1S_0, ^3P_0, ^3P_1, ^3P_2, ^3S_1, ^3D_2, ^3F_2, ^3F_3, ^3F_4, ^3G_4, ^3H_4, ^3H_5, ^3H_6$	σ, P, D, R, A	(92, 118, 131)
Noyes & MacGregor (191)	p - p	40	$^1S_0, ^3P_0, ^3P_1, ^3P_2, ^1D_2, ^3S_1$	σ, P	(78, 247, 248)
MacGregor (103)	p - p	1.855, 4.203, 9.68, 9.73, 18.2, 19.8, 31.8, 39.4	$^1S_0, ^3P_0, ^3P_1, ^3P_2, ^1D_2$	σ, P	(65, 69, 70, 76, 78, 249 to 253)
Stabler & Lomon (199)	p - p	145	$^1S_0, ^3P_0, ^3P_1, ^3P_2, ^3S_1, ^3D_2, ^3F_2, ^3F_3, ^3F_4$	σ, P, D, R	(88, 170)

scattering parameters) that almost any of these experiments would be of great help in finding unique phase shifts in this region.

Other analyses below 100 Mev include that of Phillips (191a), who worked on the scattering and polarization data at 96 Mev. He included S , P , and D waves and found three solution regions, although no claim was made that these were the only reasonable solutions. He also showed that the effects of F waves are small.

In several of these analyses as well as in those at higher energies, the interference between the nuclear and Coulomb scattering has proven to be quite important (192).

At higher energies, above 100 Mev, a large number of analyses were carried out. They are tabulated, together with those at low energies and those for n - p scattering, in Table XII. Because of the scarcity of the data and because of the computational problems connected with a large number of parameters, these analyses were admittedly preliminary in nature up to about 1956. Usually, only S , P , and D waves were included (189, 192a to 193), although sometimes the 3F_2 state (194, 195) and its coupling to the 3P_2 state (190) were also considered. The experiments on which these analyses were based included mostly just differential cross-section and polarization measurements which turned out to be insufficient to determine even as few as half a dozen parameters.

Since no definite conclusions could be reached by trying to determine all phase shifts from experiments, constraints were often placed on some of the phases. For example, Phillips, at 150 Mev (194), considered only negative 3P_0 phases, and only 3P_2 phases between 6° and 12° , while Thaler, Bengston & Breit (190), at 240 Mev, used a fixed S phase calculated from theory. On account of the tentative nature of these analyses, no special effort was made to take advantage of the quantitative criteria for the goodness of fit, and therefore no values of χ^2 are given by these authors as a rule.

In spite of their tentative nature, these early analyses are of considerable value. They serve as a check on the compatibility of data and also help in determining the number of phase shifts needed for a complete and unique analysis at a given energy. Furthermore, sometimes even the qualitative features of the phase shifts can be used to draw conclusions. For instance, large differences among the three triplet phases for a given orbital angular-momentum state indicate the presence of noncentral forces. On a more practical level, these early phase-shift sets serve very well as starting points of more comprehensive analyses which can be carried out later using a more comprehensive set of data. For example, some of the solutions of Garren (196) and of Klein (193) for p - p scattering at 210 Mev are rather similar to the solutions recently obtained (197) from a much enlarged set of data.

The first really satisfactory analysis could be carried out only after a series of measurements at Berkeley resulted in a comprehensive set of data on p - p scattering at 310 Mev. These experiments were discussed in Part II,

where it was pointed out that five different types of experiments were carried out, yielding a total of 36 pieces of data. In the analysis of these data (14) it was assumed that S , P , D , F , G , and H waves are important. This was, to some extent, verified *a posteriori* by the value of χ^2 for the good solutions and by the small magnitude of the G and H phase shifts. Because of the variety of data and the large number (14) of phase shifts, the computation was carried out on an electronic computer. The calculation started with 420 randomly chosen initial sets of phase shift. Each of these random initial sets of phase shifts was then improved by changing their values until a minimum value of χ^2 was obtained. For details on the procedure used in these search processes, the original reference should be consulted.

In these 420 searches, 34 different solutions were found. Of these, eight had considerably smaller values of χ^2 than the others. For 36 pieces of data to be fitted with 14 parameters, one expects a χ^2 of about 22, and the probability of such a fit having a χ^2 of 52 (which is the χ^2 of the worst of the eight best solutions) or higher is less than 0.1 per cent. Thus, only the first eight solutions were published. They were numbered 1-8 in order of increasing χ^2 . Of these, solutions 5, 7, and 8 were eliminated on the basis of experiments on the reaction (198),



leaving five possible solutions, all of which had negative 3S_0 phases.

These five solutions can be classified into three groups, one containing solutions 1 and 3, the second solutions 2 and 4, and finally the third containing solution 6. Solutions in a given group are very similar to each other. Numerical tables of these solutions are given in Table XIII.

On the basis of data then available, it was not possible to select the right solution out of the five best ones obtained in the search. Plotting the predictions of these solutions for the physical observables in the angular range where experiments were not available, however, it appeared that additional experiments would make the selection possible. The modified analysis, to be discussed below, offered another way of distinguishing among the five solutions.

More recently, triple-scattering experiments were also carried out at 140 Mev. A description of these experiments can be found in Part II. An analysis of some of these data has been given by Stabler & Lomon (199). They used differential and polarization data as well as some preliminary data on D . They conclude that at this energy the Group III type of solution is vastly inferior to the Group I solution. They obtained a good Group I type solution, but their numerical values might be subject to change since the experimental data on D which they used have since undergone several corrections.

(b) *Modified phase-shift analysis at fixed energies.* The modified analysis scheme is a logical extension of the conventional phase-shift analysis formalism. The underlying idea goes back to the early days of meson theory [for a

TABLE XIII
PHASE SHIFTS FOR PROTON-PROTON SCATTERING

(As obtained by ordinary analysis at 310 Mev and by modified analyses at 310, 210, 145, 95, and 68 Mev.) The table gives nuclear bar phase shifts in degrees as defined in (14).

	1S_0	3P_0	3P_1	3P_2	1D_2	3F_2	3F_3	3F_4	1G_4	3H_4	3H_5	3H_6	Ref.
310 Mev #1	-10.1	-14.3	-26.6	16.1	12.9	-4.4	0.8	3.2	2.0	-1.2	0.1	1.3	(14)
310 Mev #2	-19.5	-36.0	-11.7	18.8	4.4	0.3	-0.5	2.5	2.6	-1.5	-1.4	1.4	(14)
310 Mev #6	-0.3	-64.7	-13.4	8.2	12.8	3.0	-2.1	3.2	-1.0	1.3	-2.0	0.3	(14)
310 Mev #1	-8.92	-11.27	-27.49	16.65	11.87	-3.53	1.21	3.54		OPEC*			—(206)
310 Mev #2	-28.99	-27.92	-8.71	21.05	4.78	-0.03	-0.49	3.33		OPEC			—(206)
210 Mev #1	5.9	2.1	-20.9	17.0	7.5	-2.0	-0.4	0.3		OPEC			—(197)
210 Mev #2	-15.7	-28.4	-2.1	17.9	2.8	-2.3	1.2	1.0		OPEC			—(197)
145 Mev	11.6	16.8	-16.7	14.2	7.4	1.0	-1.8	0.07		OPEC			—(208)
95 Mev	23.5	14.1	-12.9	10.1	4.0			OPEC					—(208)
95 Mev	21.1	18.1	-11.1	11.0	4.2			OPEC					—(209)
68 Mev	33.2	12.7	-10.2	7.7	2.7			OPEC					—(208)

* OPEC = one-pion exchange contribution.

summary see (200)] and was used in a rudimentary form (103) in narrowing down the number of solutions. The modified scheme consists of adding to the usual expression for the scattering amplitude, in terms of phase shift, a closed expression which represents all higher angular-momentum states. This expression originates in some very well-established general features of meson theory.

Phenomenological schemes are always based on a certain amount of theory. In fact, phenomenology should include as much generally valid theory as possible and should be formulated in terms of parameters which have theoretical significance. The modified analysis supplements the usual phase-shift formalism with the idea that in a scattering process, the highest angular-momentum states are dominated by that part of the force which has the longest range and, hence, by that contribution to the scattering process corresponding to the exchange of the particle or particles with the smallest total mass.

There are two ways of justifying this procedure. Semiclassically, one can argue that for a given incident momentum, the particles with a large impact parameter and hence a large angular momentum will feel only the long-range part of the force. In terms of the Yukawa model, the range of the force is inversely proportional to the mass of the particle being exchanged, the range being just the Compton wavelength corresponding to the exchanged mass.

An alternative way of saying the same thing uses the language of dispersion theory. In that approach, the scattering amplitude is considered a function of a complex variable, and the singularities of this function are studied. For our purpose, consider the nucleon-nucleon scattering amplitude at a fixed energy, as a function of x , the cosine of the scattering angle θ in the center-of-mass system. It may be shown that the singularities of the scattering amplitude are situated as shown in Figure 9 and that various singularities and cuts correspond to the exchange between nucleons of various particles, as is also indicated in Figure 9. As shown in the figure, the process with the smallest exchange mass is the one-pion exchange process which lies closest to the physical region. The physical region is where $\cos \theta$ is between $+1$ and -1 , and the distance of the singularities from the nearer end-point is proportional to the mass exchanged in the scattering process.

If the scattering amplitude is expressed as a contour integral, the x dependence comes wholly from the Cauchy denominator $(x-x_0)^{-1}$ where x_0 is the value of x at a singularity or along the cut. If $(x-x_0)^{-1}$ is expanded in powers of x , one sees that for a closer singularity one needs more powers of x for a given precision of approximation. Since higher powers of x represent high angular-momentum states, we arrive at the same conclusion as before; the one-pion exchange process should dominate the high angular-momentum states.

These arguments are based on the presumption that the processes with large exchange mass do not make an anomalously large contribution to some state, and this presumption must be checked *a posteriori*.

It is important for the dispersion theory argument that the contribution from the single near-by pole which describes the one-pion exchange process can be exactly calculated. This one-pion exchange contribution is in fact given, formally, by the lowest-order covariant Born approximation calculation for nucleon-nucleon scattering, if one considers the coupling constant appearing in the calculations as the physical, renormalized coupling constant. Unfortunately, there is no such simple recipe for calculating the contributions of the processes involving the exchange of more than one pion that are represented by cuts in the $\cos \theta$ plane. Hence the contribution of these processes, which are mostly important in the low angular-momentum states, can only be described in terms of the usual phenomenological parameters, the phase shifts.

The higher the energy, the closer all the singularities move to the physical region, but the ratio of the distances of the various singularities from the end of the physical region remains unchanged. This means that for higher energies more powers of x and hence more angular-momentum states are needed, but it remains true that the one-pion exchange process should dominate the higher angular-momentum states.

Summarizing, therefore, the modified analysis scheme (201 to 203) consists of adding to the usual phase-shift expression, which includes a certain finite number of angular-momentum states, a closed expression that is the contribution of the one-pion exchange process in all the higher angular-momentum states omitted in the usual phase-shift formalism.

Before writing down the appropriate formulae, a practical, calculational remark is in order. The closed expression for the one-pion exchange contribution that one gets, formally, by carrying out the Born approximation calculation, represents the one-pion exchange contribution in all angular-momentum states, including the lowest ones in which we want to use phase shifts to describe the scattering amplitude. But phase shifts always refer to the total scattering amplitude in a given angular-momentum state, thus including the part which comes from the one-pion exchange process. To avoid counting this part twice, therefore, one has to subtract the one-pion exchange contribution in the low angular-momentum states. Thus, the formula for the composite scattering amplitudes can be written as

$$M = M(\delta) + M^P - M^{PS}$$

where $M(\delta)$ is the part of the amplitude contributed by the phase-shift expressions for the angular-momentum states $0 \leq J \leq J_{\max}$, M^P is the total one-pion exchange contribution, and M^{PS} is this contribution in the momentum states $0 \leq J \leq J_{\max}$ that has to be subtracted.

The first part, $M(\delta)$, is discussed in Part I. The second part, M^P , is obtained by the direct application of the Feynman rules to the first-order diagram for nucleon-nucleon scattering. Finally, M^{PS} is obtained by applying a projection operator to M^P to separate out the contributions in the various

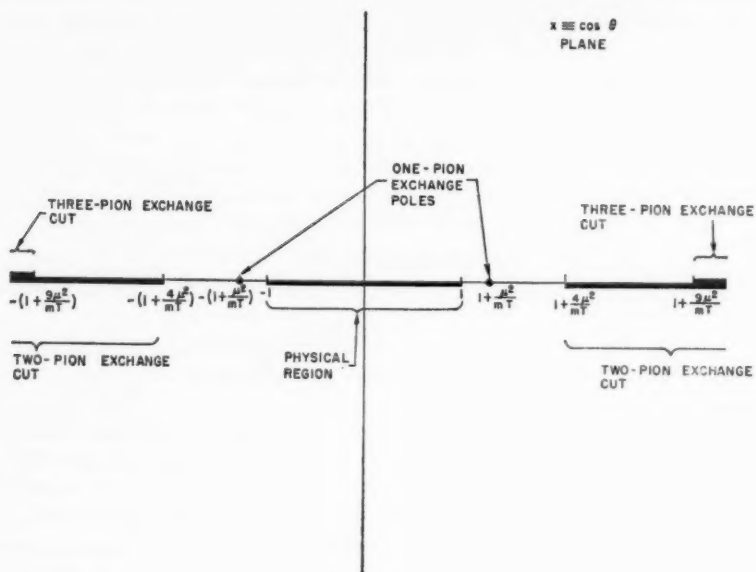


FIG. 9

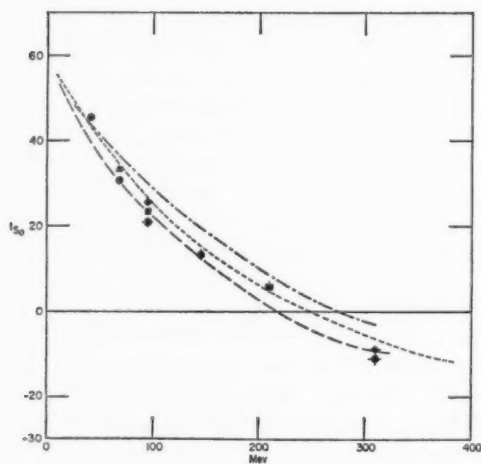


FIG. 10

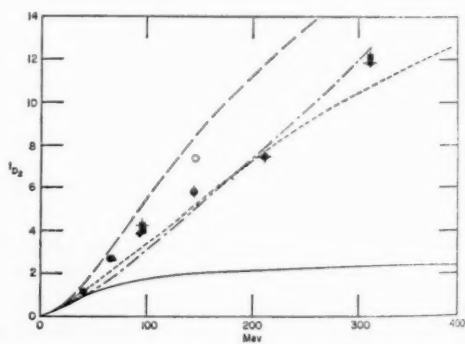


FIG. 11

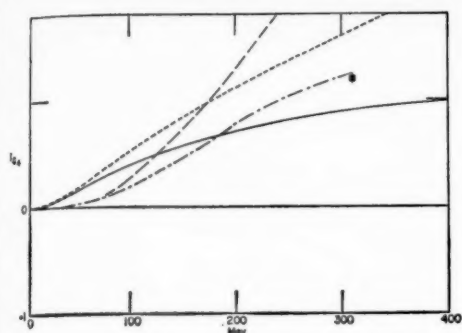


FIG. 12

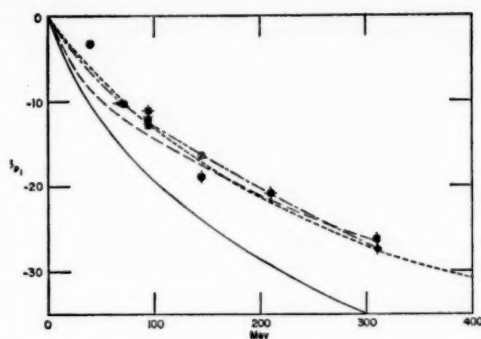


FIG. 14

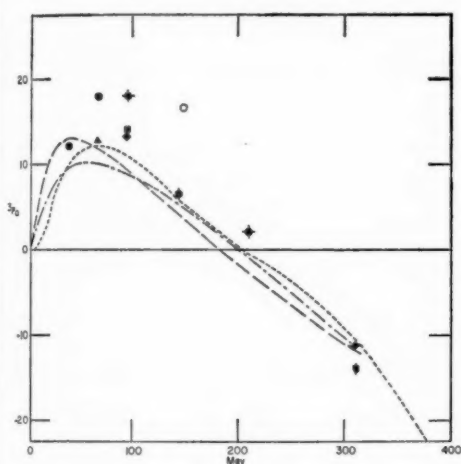


FIG. 13

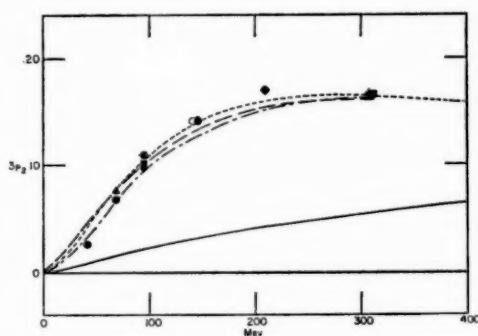


FIG. 15

DESCRIPTION OF FIGURES 9-23

FIG. 9. The complex scattering angle plane at a fixed energy for nucleon-nucleon scattering. Notations: μ = pion mass; m = nucleon mass; T = incident nucleon kinetic energy in the laboratory system.

FIG. 10-23. Proton-proton scattering phase shifts as functions of energy. The points are results of analyses at fixed energies; references are as follows: \bullet = (209); \blacktriangle = (208); \blacklozenge = (209); \blacksquare = (208); \blacklozenge = (209); \circ = (208); \odot = (199); \blacklozenge = (197); \blacklozenge = (206); \blacklozenge = (203). The dotted line is a preliminary result of an energy-dependent analysis by the California group. The dashed curve is from Gammel & Thaler (212), and the dash-dot curve is that of Bryan (213). The solid line is the one-pion exchange contribution with $g^2 = 14$. The figures give nuclear bar phase shifts in degrees as defined in (14).

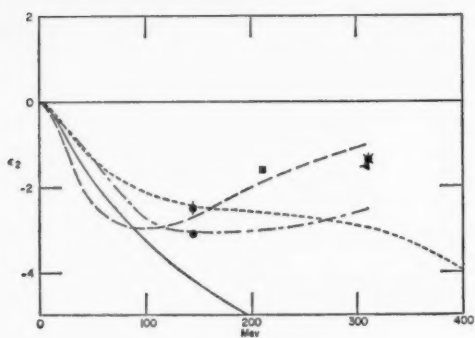


FIG. 16

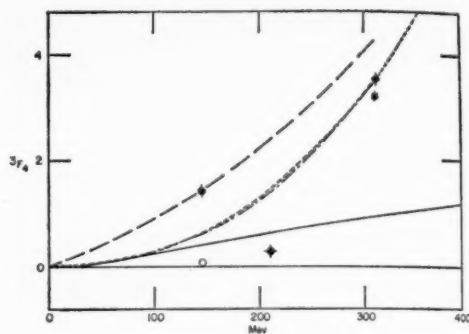


FIG. 19

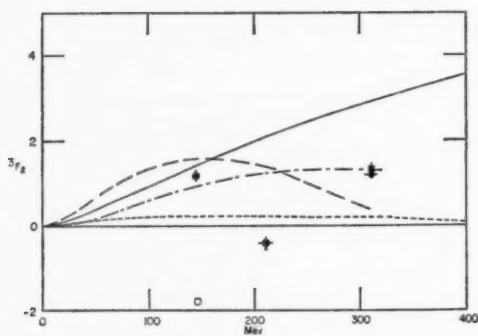


FIG. 17

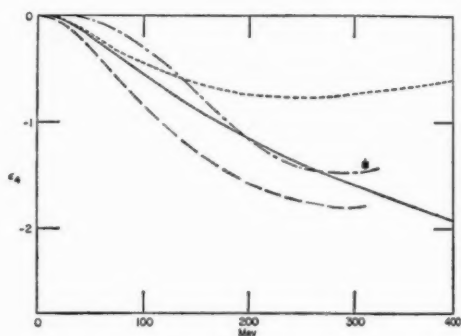


FIG. 20

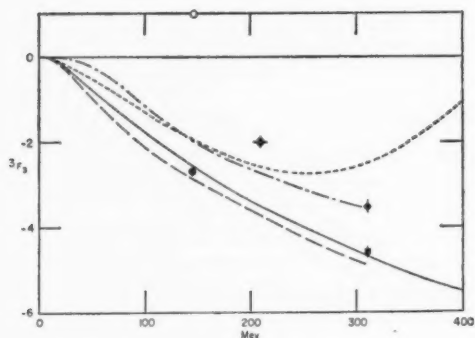


FIG. 18

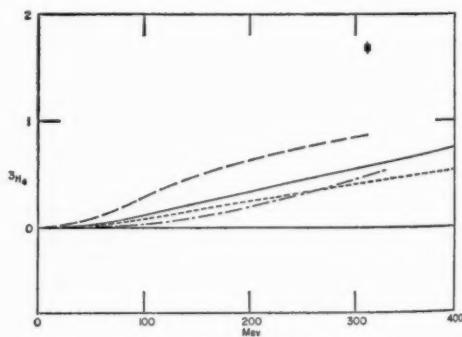


FIG. 21

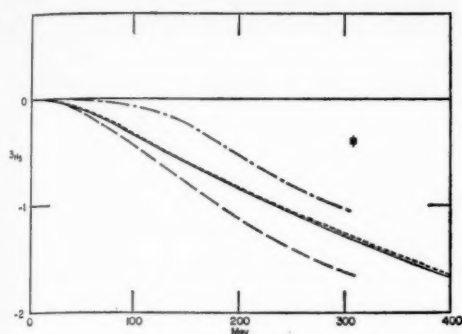


FIG. 22

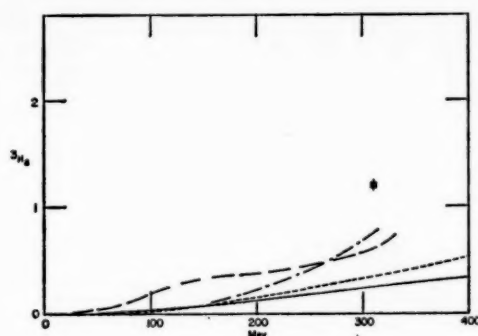


FIG. 23

partial wave states. Details are given in (202) and (203). The results, for M^P , are

$$\begin{aligned}
 M_{11}^P &= M_{-1-1}^P = -\frac{g^2}{8E} [A(1+x) - B(1-x)] \\
 M_{10}^P &= M_{01}^P = -M_{-10}^P = -M_{0-1}^P \\
 &= -\frac{g^2\sqrt{2}}{8E} (B+A) \sin \theta \\
 M_{1-1}^P &= M_{-11}^P = -\frac{g^2}{8E} [A(1-x) - B(1+x)] \\
 M_{00}^P &= \frac{g^2}{4E} (B+A)x \\
 M_{ss}^P &= \frac{g^2}{4E} (A+B)
 \end{aligned} \tag{2.3}$$

The M_i^{PS} 's are given by Table III of (14) if we substitute

$$\begin{aligned}
 \alpha_{J-1,J} &= -\frac{ik}{2E} \frac{Cg^2}{2J+1} \{Q_J(x_0) - Q_{J-1}(x_0)\} \\
 \alpha_{J,J} &= -\frac{ik}{2E} \frac{Cg^2}{2J+1} \{JQ_{J+1}(x_0) + (J+1)Q_{J-1}(x_0) - (2J+1)Q_J(x_0)\} \\
 \alpha_{J+1,J} &= -\frac{ik}{2E} \frac{Cg^2}{2J+1} \{Q_{J+1}(x_0) - Q_J(x_0)\} \\
 \frac{\alpha_J}{\sqrt{J(J+1)}} &= -\frac{ik}{2E} \frac{Cg^2}{2J+1} \{Q_{J+1}(x_0) - Q_{J-1}(x_0) - 2Q_J(x_0)\} \\
 \alpha_J &= -\frac{ik}{2E} \frac{Cg^2}{2J+1} \{-(J+1)Q_{J+1}(x_0) - JQ_{J-1}(x_0) + (2J+1)Q_J(x_0)\}
 \end{aligned} \tag{2.4}$$

for

$$L >$$

and

$$\alpha_0 = -\frac{ik}{2E} Cg^2[1 + Q_0(x_0)(1 - x_0)]$$

where

$$A = \lambda \frac{1+x}{x_0+x} \quad B = \gamma \frac{1-x}{x_0-x} \quad 2.5.$$

In these formulae the symbols are defined as follows:

μ	pion mass
m	nucleon mass
k	nucleon momentum in the center-of-mass system.
T	nucleon kinetic energy in the lab system
E	nucleon total energy in the center-of-mass system
$x_0 = 1 + \frac{\mu^2}{mT} = 1 + \frac{\mu^2}{2k^2}$	
g	pion-nucleon coupling constant, $g^2 \sim 14$
Y_L^{Lz}	spherical harmonics, as defined in Part I
Q_L^{Lz}	Legendre function of the second kind (204)
δ_{L0}	Kronecker delta
$C = \begin{cases} 1 & \text{isotriplet } p-p \\ 1/2 & \text{isotriplet } n-p \\ -3/2 & \text{isosinglet } n-p \end{cases}$	
$\gamma = \begin{cases} 1 & \text{isotriplet } p-p \\ +1/2 & \text{isotriplet } n-p \\ -3/2 & \text{isosinglet } n-p \end{cases}$	
$\lambda = \begin{cases} 1 & \text{isotriplet } p-p \\ +1/2 & \text{isotriplet } n-p \\ +3/2 & \text{isosinglet } n-p \end{cases}$	

where

$$M_j(n-p) = M_j(n-p, T=1) + M_j(n-p, T=0) \quad 2.6.$$

In general, the modified analysis can be expected to improve a phase-shift analysis in the following ways:

(a) The inclusion of all angular-momentum states at least in some approximation should lead to a more accurate representation of the scattering amplitude.

(b) Since the highest angular-momentum states included in the conventional phase-shift analysis might be adequately represented by the one-pion exchange contribution, fewer variable parameters may be needed.

(c) By treating the pion-nucleon coupling constant g^2 as a parameter to be fitted, its value can be determined from nucleon-nucleon scattering experiments.

(d) On the basis of their incompatibility with one-pion exchange contribution in the high angular-momentum states, some of the phase-shift solutions admissible in the ordinary phase-shift analysis might be eliminated.

The first case in which the modified analysis was used was a reanalysis of the Berkeley p - p data at 310 Mev, permitting a comparison with the ordinary analysis in (14). All four types of improvements listed above seemed to occur in this case (202, 205, 206). For solutions 1 and 2 of (14), the addition of the one-pion exchange contribution in the high angular momenta improved the fit; and, in fact, almost as good fits were obtained with nine parameters (plus the coupling constant) as were previously gotten with 14 parameters. The best values of the χ^2 were reasonably sensitive to changes in the value of the coupling constant, and the values of g^2 determined from the 310-Mev data were 12.0 ± 2.1 and 13.3 ± 3.3 for solutions 1 and 2, respectively. These values correspond to $f^2 = 0.062 \pm 0.011$ and $f^2 = 0.069 \pm 0.017$, respectively, and describe the interaction between a proton and a neutral pion.

Inclusion of the one-pion exchange contribution did not improve the fit of solution 6, and for the case where all but nine parameters were represented by this contribution the χ^2 was larger than 60, whereas for solutions 1 and 2 it was less than 30. This result was construed as rather strong evidence against solution 6. Since then, this solution has also been excluded on the basis of new spin correlation experiments at Liverpool (136).

The modified analysis also showed that solutions in a given group (as defined earlier) are basically identical solutions. In particular, inclusion of the one-pion exchange contribution resulted in solutions in a given group merging for certain ranges of the coupling constant. This effect could be interpreted in terms of, say, solution 3 being just a local minimum near the larger minimum corresponding to solution 1. Indeed, the local minimum disappears for certain values of g^2 . Thus the conclusion of the modified analysis of Berkeley p - p data at 310 Mev was that there are only two basically different good solutions, namely, those corresponding to solutions 1 and 2 of the ordinary analysis. (See Table XIII.)

Inclusion of the one-pion exchange contribution in the analysis of these data did not result in a clear preference for one of these two solutions over the other. The predictions, however, for c_{kp} at 45° are 0.7 and 0.0 for solutions 1 and 2, respectively. This experiment is now being carried out at Liverpool, but results are not yet available.

In the last few years, triple-scattering experiments have been performed at an increasing number of energies, as described in Part II. Various groups have been trying to interpret these data, using the modified analysis scheme. In particular, the data at 210 Mev have been analyzed using S , P , D , and F waves and the one-pion exchange contribution beyond that (197). Four solutions, named a , b , c , and d in order of increasing χ^2 , were found to be much better than others. Solution a seems to have no counterpart at 310 Mev, but solutions b , c , and d correspond, at 310 Mev, to solutions 1, 2, and

6, respectively. Solution *a* can apparently be ruled out on several grounds. It has no counterpart at 310 Mev, it runs counter to calculations on the photodisintegration of the deuteron (207), and it also disagrees with some preliminary measurements (125) of *D* at this energy. Solution *d*, like solution 6 at 310 Mev, has a quite high χ^2 . In addition, it disagrees even more than solution *a* with the preliminary data on *D*. Thus, as at 310 Mev, only two solutions remain, with solution *b* being slightly favored over solution *c*. As at 310 Mev, further experiments at 210 Mev should resolve this remaining ambiguity. Plots of the predicted values are given in (197).

Modified analyses have also been carried out for *p-p* scattering at 145 and 95 Mev. At 145 Mev, the situation is somewhat obscured by contradictory experimental data from Harwell and Harvard. One satisfactory solution has been reported (208), based on the use of the Harwell data on differential cross section, *P*, *D*, and *R*. Another solution was found by ordinary analysis by Stabler & Lomon (199), using some of the Harvard data. This work was discussed earlier in this article. Both of these solutions correspond to solution 1 at 310 Mev. At 95 Mev, differential cross sections and *P* are available from both Harvard and Harwell, and *D* measurements have been made at Harvard. Analyses (208, 209) of these data have uncovered only one solution with a good fit whose *S* and *D* phases are both positive, as one would expect from an interpolation between low- and high-energy results. This solution also seems to correspond to solution 1 at 310 Mev. That no solution corresponding to solution 2 has been found either at 145 or at 95 Mev is evidence supporting solution 1 over solution 2 at 310 and 210 Mev.

A phase-shift solution corresponding to solution 1 at 310 Mev has also been obtained at 68 Mev (208), using differential cross-section and polarization data, but more investigation is needed to establish whether this solution is discrete or part of a continuum.

Modified analyses have also been carried out on *p-p* data from 1 to 40 Mev (209), but the absence of triple-scattering data in this region did not permit any important conclusions that were not known before on the basis of ordinary analysis. At the lowest energies (1 to 3 Mev), additional information on polarization permitted a determination of the *S* and the effective *P* phases. The latter has been shown to depend on whether the one-pion exchange contribution is added or not; in fact, one-third of the effective *P* phase obtained in an ordinary *S-P* analysis turns out to be due to higher phases if such a contribution is added. In general, however, in the energy range up to 40 Mev, addition of the one-pion exchange contribution does not reduce the ambiguities, and so triple-scattering experiments are badly needed in this region.

(c) *Energy-dependent analysis.* Analyses discussed in the previous sections dealt with data at a given energy in terms of phase-shift parameters. It is logical to assume, however, that the energy dependence of phase shifts contains additional information on the interaction of nucleons which is wasted if the energies are considered individually. The simplest way to take

into account the relationship of phases at various energies is to demand that they be some smooth function of energy. Such argument was used by Clementel and his collaborators, as well as by Klein. A more quantitative approach is to write the phase shifts as some function of energy containing variable parameters and then to fit these parameters to data at several energies. Such a program was initiated at Yale and has also been undertaken more recently at the University of California.

In the Yale program (210, 211), the usual phase-shift expression in the low angular-momentum states is supplemented by phase shifts in a large but finite number of high angular-momentum states, calculated from a one-meson exchange potential with relativistic corrections. Both p - p data and n - p data have been considered. In the phase-shift parametrization, the chief aim has been to obtain a good fit, and hence various correction functions are used in energy intervals where the fits indicate room for improvement. Various starting points have been used in the search procedures.

In the work at the University of California, the one-pion exchange contribution is used in the high angular-momentum states. Only p - p data have been considered so far. Attention has also been concentrated on a solution 1 type solution. The objective of the California group is to use forms for the energy dependences having the analytic structures indicated by recent dispersion-theoretic investigations.

Results attained by both groups have been preliminary. The fits obtained so far have not been as good as one would expect, assuming only random distribution of experimental errors. On the other hand, the preliminary results obtained by the two groups for the energy dependence of the phase shifts appear to be similar. The best solution obtained to date at California is given in Figures 10 to 23, but the work is still at a very preliminary stage. Also shown are the phase shifts obtained at individual energies by various groups, as well as the phases calculated from the Gammel-Thaler potential (212) and from Bryan's work (213).

Neutron-proton scattering.—Experiments on n - p scattering lag considerably behind those for p - p scattering, as discussed in Part II of this article. As a result, phase-shift analyses of n - p scattering are few in number and rather preliminary. (See Table XII.)

The most ambitious of these analyses is that of Clementel & Villi (214). They consider data in the energy range from 27 to 260 Mev and make use of the requirement that the phase shifts be a smooth function of energy. One of their conclusions is that at 260 Mev a description including only S and P waves is inadequate, and they are forced to include D waves and S - D coupling. Charge independence is assumed, and so the isotopic triplet phases are taken from earlier work of the same group on p - p scattering (188). The solutions they obtain have a positive 3S_1 phase that decreases from 78° at 27 Mev to 10° at 215 Mev, and a negative 1P_1 phase which increases from -15° at 27 Mev to -53° at 215 Mev. The 3D phases, which for sake of simplicity are all taken to be the same, are small and negative, reaching -10° at 215

Mev. There is the usual fourfold ambiguity of the 3P phases.

Clementel & Villi's solutions correspond to some obtained by Phillips (191a), by Klein (215), and by the Yale group (190), while some other solutions obtained by these latter workers are rejected by Clementel & Villi on the basis that they exist only in the energy interval from 170 to 260 Mev. It seems that final decision has to await the time when more than just differential-cross-section and polarization data are available for n - p scattering.

In view of the limited amount of experimental information, it appears that one would have to assume charge independence in the analysis of n - p scattering for some time to come. Eventually, however, one would like to verify this assumption. A check of limited scope has already been made by the Yale group (211), who showed that it is consistent with the data to assume that the one-pion exchange contributions for p - p and n - p scattering have the same coupling constant.

As mentioned in Part II, triple-scattering experiments for n - p scattering are now in progress, which should greatly contribute in the coming years to a quantitative analysis of such scattering.

LITERATURE CITED

1. Wolfenstein, L., and Ashkin, J., *Phys. Rev.*, **85**, 947 (1952)
2. Dalitz, R. H., *Proc. Phys. Soc. (London)*, **A65**, 175 (1952)
3. Wolfenstein, L., *Phys. Rev.*, **96**, 1654 (1954)
4. Wolfenstein, L., *Ann. Rev. Nuclear Sci.*, **6**, 43 (1956)
5. Bargman, V., Michel, L., and Telegdi, V. L., *Phys. Rev. Letters*, **2**, 435 (1959)
6. Stapp, H. P., *Univ. Calif. Radiation Lab Repts.*, UCRL-2825 (1954) and 3098 (1955)
7. Oehme, R., *Phys. Rev.*, **98**, 147 (1955)
8. Oehme, R., *Phys. Rev.*, **98**, 216 (1955)
9. Puzikov, L. D., Ryndin, R., and Smorodinskii, Ia., *J. Exptl. Theoret. Phys. (U.S.S.R.)*, **32**, 592 (1956); *Soviet Phys. JETP*, **5**, 489 (1957)
10. Chamberlain, O., Segrè, E., Tripp, R. D., Wiegand, C., and Ypsilantis, T. J., *Phys. Rev.*, **105**, 288 (1957)
11. Golovin, B. M., Dzhelepov, V. P., Nadezhdin, V. S., and Satarov, I., *J. Exptl. Theoret. Phys. (U.S.S.R.)*, **36**, 433 (1959); *Soviet Phys. JETP*, **9**, 302 (1959)
12. Phillips, R. J. N., *Harwell Research Rept.*, AERE-R3141 (1960)
13. Blatt, J. M., and Weisskopf, V. F., *Theoretical Nuclear Physics*, App. A (John Wiley & Sons, Inc., New York, N. Y., 1952)
14. Stapp, H. P., Ypsilantis, T. J., and Metropolis, N., *Phys. Rev.*, **105**, 302 (1957)
15. Breit, G., *Phys. Rev.*, **106**, 314 (1957)
16. Wright, S. C., *Phys. Rev.*, **99**, 996 (1955)
17. Bakke, F., and Steck, B., *Z. Physik*, **144**, 219 (1956)
18. Blatt, J. M., and Biedenharn, L. C., *Revs. Mod. Phys.*, **24**, 258 (1952)
19. Breit, G., and Hull, M. H., Jr., *Phys. Rev.*, **97**, 1047 (1955)
20. Huby, R., *Proc. Phys. Soc. (London)*, **A67**, 1103 (1954)
21. Shirokov, M. I., *J. Exptl. Theoret. Phys. (U.S.S.R.)*, **33**, 975 (1957); *Soviet Phys. JETP*, **6**, 748 (1958)
22. Phillips, R. J. N., *Nuovo cimento*, **8**, 265 (1958)
23. Wick, G. C., *Phys. Rev.*, **80**, 268 (1950)
24. Michel, L., and Wightman, A. S., *Phys. Rev.*, **98**, 1190 (1955)
25. Stapp, H. P., *Phys. Rev.*, **103**, 425 (1956)
26. Steck, B., *Z. Physik*, **144**, 215 (1955)
27. Garren, A., *Phys. Rev.*, **96**, 1709 (1954)
28. Chou, K.-C., and Shirokov, M. I., *J. Exptl. Theoret. Phys. (U.S.S.R.)*, **34**, 1230 (1958); *Soviet Phys. JETP*, **7**, 851 (1958)
29. Phillips, R. N. J. (Preprint)
30. Breit, G., and Gluckstern, R. L., *Ann. Rev. Nuclear Sci.*, **2**, 365-98 (1953)
31. Hess, W. N., *Revs. Mod. Phys.*, **30**, 368 (1958)
32. Taylor, A. E. (Private communication)
33. de Carvalho, H. G., *Phys. Rev.*, **96**, 398 (1954)
34. Marshall, J., Marshall, L., and Nedzel, V. A., *Phys. Rev.*, **91**, 767 (1953)
35. Chamberlain, O., Pettengill, G., Segrè, E., and Wiegand, C., *Phys. Rev.*, **93**, 1424 (1953); Pettengill, G. H., *Measurement on Proton-Proton Scattering in the Energy Region 150 to 340 Mev* (Doctoral thesis, Univ. Calif., UCRL-2808, December 1954)
36. Storrs, C. L., and Frisch, D. H., *Phys. Rev.*, **95**, 1252 (1954)
37. Hafner, E. M., Hornyak, W. F., Falk, C. E., Snow, G., and Coor, T., *Phys. Rev.*, **89**, 204 (1953)
38. Nereson, N., and Darden, S., *Phys. Rev.*, **89**, 775 (1953)
39. Lasday, A. H., *Phys. Rev.*, **81**, 139 (1951)
40. Poss, H. L., Salant, E. O., Snow, G. A., and Yuan, L. C. L., *Phys. Rev.*, **87**, 11 (1952)
41. Los Alamos Physics and Cryogenics Groups, *Nuclear Phys.*, **12**, 291 (1959)
42. Bratenahl, A., Peterson, J. M., and Stoering, J. P., *Phys. Rev.*, **110**, 927 (1958)
43. Day, R. B., and Henkel, R. L., *Phys. Rev.*, **92**, 358 (1953)
44. Day, R. B., Mills, R. L., Perry, J. E., Jr., and Scherb, F., *Phys. Rev.*, **114**, 209 (1959)
45. Peterson, J. M., Bratenahl, A., and Stoering, J. P., *Phys. Rev.* (In press)
46. Hildebrand, R. H., and Leith, C., *Phys. Rev.*, **80**, 842 (1950)
47. Hillman, P., Stahl, R. H., and Ramsey, N. F., *Phys. Rev.*, **96**, 115 (1954)
48. De Juren, J., and Knable, N., *Phys. Rev.*, **77**, 606 (1950)
49. Culler, V., and Waniek, R. W., *Phys. Rev.*, **99**, 740 (1955)

50. Taylor, A. E., Pickavance, T. G., Cassels, J. M., and Randle, T. C., *Phil. Mag.*, **42**, 751 (1951)
51. Taylor, A. E., and Wood, E., *Phil. Mag.*, **44**, 95 (1953)
52. Taylor, A. E., Pickavance, T. G., Cassels, J. M., and Randle, T. C., *Phil. Mag.*, **42**, 328 (1951)
53. Alphonse, R., Johansson, A., Taylor, A. E., and Tibell, G., *Phil. Mag.*, **46**, 295 (1955)
54. Taylor, A. E., *Phys. Rev.*, **92**, 1071 (1953)
55. Mott, G. R., Guernsey, G. L., and Nelson, B. K., *Phys. Rev.*, **88**, 9 (1952)
56. De Juren, J., and Moyer, B. J., *Phys. Rev.*, **81**, 919 (1951)
57. De Juren, J., *Phys. Rev.*, **80**, 27 (1950)
58. Fox, R., Leith, C., Wouters, L., and MacKenzie, K. R., *Phys. Rev.*, **80**, 23 (1950)
59. Dzhelepov, V. P., Golovin, B. M., and Satarov, V. I., in report of *Inst. Nuclear Phys., Moscow* (1952)
60. Dzhelepov, V. P., Satarov, V. I., and Golovin, B. M., *Doklady Akad. Nauk S.S.S.R.*, **104**, 717 (1955)
61. Nedzel, V. A., *Phys. Rev.*, **94**, 174 (1954)
62. Jackson, J. D., and Blatt, J. M., *Revs. Mod. Phys.*, **22**, 77 (1950)
63. Cooper, D. I., Frisch, D. H., and Zimmerman, R. L., *Phys. Rev.*, **94**, 1209 (1954)
64. Knecht, D. J., Messelt, S., Berners, E. D., and Northcliffe, L. C., *Phys. Rev.*, **114**, 550 (1959)
65. Worthington, H. R., McGruer, J. N., and Findley, D. E., *Phys. Rev.*, **90**, 899 (1953)
66. Dahl, P. F. (Private communication)
67. Zimmerman, E. J., Kerman, R. O., Singer, S., Kruger, P. G., and Jentschke, W. K., *Phys. Rev.*, **96**, 1322 (1954)
68. Johnston, L. H., and Young, D. E., *Phys. Rev.*, **116**, 989 (1959)
69. Cork, B., and Hartsough, W., *Phys. Rev.*, **94**, 1300 (1954)
70. Yntema, J. L., and White, M. G., *Phys. Rev.*, **95**, 1226 (1954)
71. Burki, J. W., Richardson, J. R., and Schrank, G. E., *Phys. Rev.*, **113**, 290 (1959)
72. Royden, H. N., and Wright, B. T., *Phys. Rev.*, **113**, 294 (1959)
73. Jeong, T. H., Johnson, L. H., and Young, D. E., *Phys. Rev.*, **118**, 1080 (1960)
74. Panofsky, W. K. H., and Fillmore, F. L., *Phys. Rev.*, **79**, 57 (1950)
75. Fillmore, F. L., *Phys. Rev.*, **83**, 1252 (1951)
76. Cork, B., Johnson, L. H., and Richman, C., *Phys. Rev.*, **79**, 71 (1950)
77. Cork, B., *Phys. Rev.*, **80**, 321 (1950)
78. Johnston, L. H., and Swenson, D. A., *Phys. Rev.*, **111**, 212 (1958)
79. Johnston, L. H., and Tsai, Y. S., *Phys. Rev.*, **115**, 1293 (1959)
80. Young, D. E., and Johnston, L. H., *Phys. Rev.*, **119**, 313 (1960)
81. Kruse, U. E., Teem, J. M., and Ramsey, N. F., *Phys. Rev.*, **101**, 1079 (1956)
82. Birge, R. W., Kruse, U. E., and Ramsey, N. F., *Phys. Rev.*, **83**, 274 (1951)
83. Taylor, A. E., and Wood, E., *Proc. Phys. Soc. (London)*, **A69**, 645 (1956)
84. Taylor, A. E., and Wood, E., *Phil. Mag.*, **44**, 95 (1953)
85. Cassels, J. M., *Proc. Phys. Soc. (London)*, **A69**, 495 (1956)
86. Cassels, J. M., Pickavance, T. G., and Stafford, G. H., *Proc. Roy. Soc. (London)*, **214**, 262 (1952)
87. Bird, L., Wood, E., and Taylor, A. E. (Private communication)
88. Palmieri, J. N., Cormack, A. M., Ramsey, N. F., and Wilson, R., *Ann. Phys.*, **5**, 299 (1958)
89. Oxley, C. L., and Schamberger, R. D., *Phys. Rev.*, **85**, 416 (1952)
90. Fowler, O. A., *Phys. Rev.*, **85**, 1024 (1952)
91. Garrison, J. D., *Proton-Proton Scattering Experiments at 170 and 260 Mev* (Doctoral thesis, Univ. Calif., UCRL-2659, July 1954); Chamberlain, O., and Garrison, J. D., *Phys. Rev.*, **95**, 1350 (1954); **103**, 1860 (1956)
92. Chamberlain, O., Segrè, E., and Wiegand, C., *Phys. Rev.*, **83**, 923 (1951)
93. Chamberlain, O., and Wiegand, C., *Phys. Rev.*, **81**, 284 (1951)
94. Fischer, D., and Goldhaber, G., *Phys. Rev.*, **95**, 1350 (1954)
95. Hartzler, A. J., and Siegel, R. T., *Phys. Rev.*, **95**, 185 (1954)
96. Holt, J. R., Kluver, J. C., and Moore, J. A., *Proc. Phys. Soc. (London)*, **71**, 781 (1958)
97. Hartung, D., Holt, J. R., and Moore, J. A., *Proc. Phys. Soc. (London)*, **71**, 770 (1958)
98. Marshall, J., Marshall, L., and Nedzel, V. A., *Phys. Rev.*, **98**, 1513 (1955)
99. Noyes, H. P., and Hafner, E. M., *The ^{18}O Nucleon-Nucleon Effective*

- Range and Shape Parameter* (Preprint)
100. Heller, L., *Proton-Proton Effective Range Theory with Vacuum Polarization* (Preprint)
 101. de Witt, M., and Durand, L., *Phys. Rev.*, **111**, 1597 (1958)
 102. Durand, L., III, *Phys. Rev.*, **108**, 1597 (1957)
 103. MacGregor, M. H., *Phys. Rev.*, **113**, 1559 (1959)
 104. Dzhelepov, V. P., and Kazarinov, Ju. M., *Doklady Akad. Nauk S.S.S.R.*, **99**, 939 (1954); Dzhelepov, V. P., Golovin, B. M., and Satarov, V. I., *Doklady Akad. Nauk S.S.S.R.*, **99**, 943 (1954); Dzhelepov, V. P., Kazarinov, Ju. M., Golovin, B. M., Fljagin, V. B., and Satarov, V. I., *Izvest. Akad. Nauk S.S.S.R.*, **19**, 573 (1955); *Nuovo cimento, Suppl.*, **3** (X), 61 (1956)
 105. Blanpied, W. A., *Phys. Rev.*, **116**, 738 (1959)
 106. Alexeff, I., and Haeblerli, W., *Nuclear Phys.*, **15**, 609 (1960)
 107. Haeblerli, W. (Private communication)
 108. Brockman, K. W., Jr., *Phys. Rev.*, **110**, 163 (1958)
 109. Dickson, J. M., and Salter, D. C., *Nature*, **173**, 946 (1954)
 110. Fischer, D., and Baldwin, J., *Phys. Rev.*, **100**, 1445 (1955)
 111. Baskir, E., Hafner, E. M., Roberts, A., and Tinlot, J. H., *Phys. Rev.*, **106**, 564 (1957)
 112. Oxley, C. L., Cartwright, W. F., and Rouvina, J., *Phys. Rev.*, **93**, 806 (1954)
 113. Baskir, E., and Chestnut, W. G., *Proc. Ann. Rochester Conf. High-Energy Phys.*, **5th** (1955)
 114. Marshall, J., Marshall, L., and de Carvalho, H. G., *Phys. Rev.*, **93**, 1431 (1954)
 115. Marshall, J., Marshall, L., Nagle, D., and Skolnik, W., *Phys. Rev.*, **95**, 1020 (1954)
 116. Chamberlain, O., Pettengill, B., Segrè, E., and Wiegand, C., *Phys. Rev.*, **95**, 1348 (1954)
 117. Chamberlain, O., Segrè, E., Tripp, R., Wiegand, C., and Ypsilantis, T., *Phys. Rev.*, **93**, 1430 (1954)
 118. Chamberlain, O., Segre, E., Tripp, R., Wiegand, C., and Ypsilantis, T., *Phys. Rev.*, **105**, 288 (1957)
 119. Kane, J. A., Stallwood, R. A., Sutton, R. B., Fields, T. H., and Fox, J. G., *Phys. Rev.*, **95**, 1694 (1954)
 120. de Carvalho, H. G., Heiberg, E., Marshall, J., and Marshall, L., *Phys. Rev.*, **94**, 1796 (1954)
 121. Thorndike, E. H., and Ophel, T. R., *Phys. Rev.*, **119**, 362 (1960)
 122. Taylor, A. E., and Wood, E., *Ann. Intern. Conf. High-Energy Phys. CERN, Geneva, 1958*, **56** (1958)
 123. Hwang, C. F., Ophel, T. R., Thorndike, E. H., Wilson, R., and Ramsey, N. F., *Phys. Rev. Letters*, **2**, 310 (1959)
 124. Hwang, C. F., Ophel, T. R., Thorndike, E. H., and Wilson, R., *Phys. Rev.*, **119**, 352 (1960)
 125. Gotow, K., and Heer, E. (Private communication)
 126. Kane, J. A., "Polarization and depolarization in proton-proton collisions at 415 Mev," *Carnegie Inst. Tech. Rept., NYO-7110* (June 1956)
 127. Thorndike, E. H., Lefrancois, J., and Wilson, R., *Bull. Am. Phys. Soc.*, **115**, 282 (1960)
 128. Bird, L., Edwards, D. N., Rose, B., Taylor, A. E., and Wood, E., *Phys. Rev. Letters*, **4**, 302 (1960)
 129. Tinlot, J., Heer, E., England, A., and Gibson, W., *Bull. Am. Phys. Soc.*, **114**, 252 (1959)
 130. England, A., Gibson, W., Heer, E., and Tinlot, J. H., *Bull. Am. Phys. Soc.*, **115**, 76 (1960)
 131. Simmons, J. E., *Phys. Rev.*, **104**, 416 (1956)
 132. Allaby, J. V., Ashmore, A., Diddens, A. N., and Eades, J., *Proc. Phys. Soc. (London)*, **74**, 482 (1959)
 133. Allaby, J. V., Ashmore, A., Diddens, A. N., Eades, J., Huxtable, G. B., and Skarsvåg, K., *Proc. Phys. Soc. (London)* (To be published)
 134. Ashmore, A., Diddens, A. N., Huxtable, G. B., and Skarsvåg, K., *Proc. Phys. Soc. (London)*, **72**, 289 (1958)
 135. MacGregor, M. H., Moravcsik, M. J., and Stapp, H. P., *Fig. 6, Phys. Rev.*, **116**, 1248 (1959)
 136. Ashmore, A., Diddens, A. N., and Huxtable, G. B., *Proc. Phys. Soc. (London)*, **73**, 957 (1959)
 137. Day, R. B. (Private communication)
 138. Baldwin, E. M., *Phys. Rev.*, **83**, 495 (1951)
 139. Allred, J. C., Armstrong, A. H., and Rosen, L., *Phys. Rev.*, **91**, 90 (1953)
 140. Seagrave, J. D., *Phys. Rev.*, **97**, 757 (1955)
 141. Galonsky, A., and Judist, J. P., *Phys. Rev.*, **100**, 121 (1955)
 142. Brolley, J. E., Jr., Coon, J. H., and

- Fowler, J. L., *Phys. Rev.*, **82**, 190 (1951)
143. Remley, M. E., Jentschke, W. K., and Kruger, P. G., *Phys. Rev.*, **89**, 1194 (1953)
144. Chih, C. Y., and Powell, W. M., *Phys. Rev.*, **106**, 539 (1957)
145. Wallace, R., *Phys. Rev.*, **81**, 493 (1951)
146. Fox, R. H., *Neutron-Proton Scattering at 90 Mev* (Doctoral thesis, Univ. Calif., UCRL-867, August 1950)
147. Chamberlain, O., and Easley, J. W., *Phys. Rev.*, **94**, 208 (1954)
148. Easley, J. W., Small-Angle Neutron-Proton Scattering at 90 and 290 Mev (Doctoral thesis, Univ. Calif., UCRL-2693, September 1954)
149. Hadley, J., Kelly, E., Leith, C., Segrè, E., Wiegand, C., and York, H., *Phys. Rev.*, **75**, 351 (1949)
150. Brueckner, K., Hartsough, W., Hayward, E., and Powell, W. M., *Phys. Rev.*, **75**, 555 (1949)
151. Stahl, R. H., and Ramsey, N. F., *Phys. Rev.*, **96**, 1310 (1954)
152. Selove, W., Strauch, K., and Titus, F., *Phys. Rev.*, **92**, 724 (1953)
153. Hobbie, R. K., and Miller, D., *Bull. Am. Phys. Soc.*, **115**, 282 (1960)
154. Randle, T. C., Skyrme, D. M., Snowden, M., Taylor, A. E., Uridge, F., and Wood, E., *Proc. Phys. Soc. (London)*, **A69**, 760 (1956)
155. Thresher, J. J., Voss, R. G. P., and Wilson, R., *Proc. Roy. Soc. (London)*, **A229**, 492 (1955)
156. Griffith, T. C., Banford, A. P., Uppal, M. Y., and Williams, W. S. C., *Proc. Phys. Soc. (London)*, **A71**, 305 (1958)
157. Randle, T. C., Taylor, A. E., and Wood, E., *Proc. Roy. Soc. (London)*, **A213**, 392 (1952)
158. Guernsey, G. L., Mott, G. R., and Nelson, B. K., *Phys. Rev.*, **88**, 15 (1952)
159. Kelly, E., Leith, C., Segrè, E., and Wiegand, C., *Phys. Rev.*, **79**, 96 (1950)
160. De Pangher, J., *Phys. Rev.*, **99**, 1447 (1955)
161. Ashmore, A., Range, W. R., Taylor, A. E., and Townes, B. M. (Private communication)
162. Hartzler, A. J., Siegel, R. T., and Opitz, W., *Phys. Rev.*, **95**, 591 (1954)
163. Whitehead, C., Tornabene, S., and Stafford, G. H., *Proc. Phys. Soc. (London)*, **75**, 345 (1960)
164. Hillman, P., and Stafford, G. H., *Nuovo cimento*, **3**, 633 (1956); Stafford, G. H., Whitehead, C., and Hillman, P., *Nuovo cimento*, **5**, 1589 (1957)
165. Warner, R. E., and Tinlot, J. H., *Bull. Am. Phys. Soc.*, **115**, 282 (1960)
166. Ypsilantis, T. J., *Experiments on Polarization in Nucleon-Nucleon Scattering at 310 Mev* (Doctoral thesis, Univ. Calif., UCRL-3047, (1955); Chamberlain, O., Donaldson, R., Segrè, E., Tripp, R. D., Wiegand, C., and Ypsilantis, T. J., *Phys. Rev.*, **95**, 850 (1954); Chamberlain, O., Segrè, E., Tripp, R. D., Wiegand, C., and Ypsilantis, T. J., *Phys. Rev.*, **105**, 288 (1957)
167. Siegel, R. T., Hartzler, A. J., and Love, W. A., *Phys. Rev.*, **101**, 838 (1956)
168. Modansky, L., and Owen, G. E., *Phys. Rev. Letters*, **2**, 209 (1959)
169. Miller, D., and Hobbie, R. K., *Phys. Rev.*, **118**, 1391 (1960)
170. Wilson, R. (Private communication)
171. Clausnitzer, G., Fleischmann, R., and Schopper, H., *Z. Physik*, **144**, 336 (1956); Clausnitzer, G., *Z. Physik*, **153**, 609 (1958)
172. Abraham, M., McCausland, M. A. H., and Robinson, F. N. H., *Phys. Rev. Letters*, **2**, 449 (1959)
173. Gammel, J. L., and Thaler, R. M., *Elementary Particle and Cosmic Ray Physics* (To be published)
174. Hulthén, L., and Sugawara, M., *Encyclopedia Phys.*, **39**, 1 (1957)
175. Noyes, H. P., *Univ. Calif. Radiation Lab. Rept.*, UCRL-5521-T (1959)
176. Schwinger, J., *Phys. Rev.*, **78**, 135 (1950)
177. Salpeter, E. E., *Phys. Rev.*, **91**, 994 (1953)
178. Riazuddin, *Nuclear Phys.*, **7**, 217 (1958)
179. Riazuddin, *Nuclear Phys.*, **7**, 223 (1958)
180. Foldy, L., and Eriksen, E., *Phys. Rev.*, **95**, 1048 (1954)
181. Foldy, L., and Eriksen, E., *Phys. Rev.*, **98**, 775 (1955)
182. Raphael, R., *Phys. Rev.*, **102**, 905 (1956)
183. Feshbach, H., and Lomon, E. L., *Phys. Rev.*, **102**, 891 (1956)
184. Beretta, L., Clementel, E., and Villi, C., *Nuovo cimento*, **1**, 739 (1955)
185. Beretta, L., Clementel, E., and Villi, C., *Phys. Rev.*, **98**, 1526 (1955)
186. Clementel, E., and Villi, C., *Nuovo cimento*, **2**, 356 (1955)
187. Clementel, E., and Villi, C., *Nuovo cimento*, **2**, 1165 (1955)

188. Clementel, E., Villi, C., and Jess, L., *Nuovo cimento*, **5**, 907 (1957)
189. Thaler, R. M., and Bengtson, J., *Phys. Rev.*, **94**, 679 (1954)
190. Thaler, R. M., Bengtson, J., and Breit, G., *Phys. Rev.*, **94**, 683 (1954)
191. Noyes, H. P., and MacGregor, M. H., *Phys. Rev.*, **111**, 223 (1958)
- 191a. Phillips, R. N. J., *Proc. Phys. Soc. (London)*, **A70**, 721 (1957)
192. Garren, A., *Phys. Rev.*, **92**, 213 (1953)
[Erratum: **92**, 1587 (1953)]
- 192a. Zimin, A., *Dokl. Akad. Nauk S.S.S.R.*, **105**, 73 (1955)
193. Klein, C. A., *Nuovo cimento*, **1**, 581 (1955)
194. Phillips, R. N. J., *Nuovo cimento*, **5**, 1335 (1957)
195. Hull, M. H., Jr., Ehrman, J. B., Hatcher, R. D., and Durand, L., *Phys. Rev.*, **103**, 1047 (1956)
196. Garren, A., *Phys. Rev.*, **101**, 419 (1956)
197. MacGregor, M. H., and Moravcsik, M. J., *Phys. Rev. Letters*, **4**, 524 (1960)
198. Tripp, R., *Phys. Rev.*, **102**, 862 (1956)
199. Stabler, R. C., and Lomon, E. E., *Nuovo cimento*, **15**, 150 (1960)
200. *Progr. Theoret. Phys. (Kyoto)*, Suppl. III (1956)
201. Moravcsik, M. J., *Univ. Calif., Radiation Lab. Rept.*, UCRL-5317-T (1958)
202. Grashin, A. F., *J. Exptl. Theoret. Phys.*, **36**, 1717 (1959)
203. Czifra, P., MacGregor, M. H., Moravcsik, M. J., and Stapp, H. P., *Phys. Rev.*, **114**, 880 (1959)
204. Morse, P., and Feshbach, H., *Methods of Theoretical Physics* (McGraw-Hill Book Co., New York, N. Y., 1953)
205. Moravcsik, M. J., Czifra, P., MacGregor, M. H., and Stapp, H. P., *Bull. Am. Phys. Soc.*, **4**, 49 (1959)
206. MacGregor, M. H., Moravcsik, M. J., and Stapp, H. P., *Phys. Rev.*, **116**, 1248 (1959)
207. Kramer, G., *Nuclear Phys.*, **15**, 60 (1960)
208. Perring, J. (Private communication)
209. MacGregor, M. H., Moravcsik, M. J., and Noyes, H. P., *Phys. Rev.* (To be published)
210. Breit, G., *Proc. London Conf. Nuclear Forces and the Few-Nucleon Problem* (Pergamon Press, Ltd., London, Engl., 1959)
211. Breit, G., Hull, M. H., Jr., Lassila, K., and Pyatt, K. D., Jr., *Phys. Rev. Letters*, **4**, 79 (1960)
212. Gammel, J. L., and Thaler, R. M., *Phys. Rev.*, **107**, 291 (1957)
213. Bryan, R. A., *Univ. Rochester Rept.*, NYO-9028 (1960)
214. Clementel, E., and Villi, C., *Nuovo cimento*, **5**, 1166 (1957)
215. Klein, C. A., *Nuovo cimento*, **2**, 38 (1955)
216. Oxley, C. L., Cartwright, W. F., Rouvina, J., Baskir, E., Klein, D., Ring, J., and Skillman, W., *Phys. Rev.*, **91**, 419 (1953)
217. Garren, A., *Phys. Rev.*, **96**, 1709 (1954)
218. Chamberlain, O., Pettengill, G., Segrè, E., and Wiegand, C., *Phys. Rev.*, **93**, 1424 (1954)
219. Chamberlain, O., and Garrison, J. D., *Phys. Rev.*, **95**, 1349 (1954)
220. Towler, O. A., *Phys. Rev.*, **84**, 1262 (1951)
221. Garren, A., *Atomic Energy Commission Rept.*, UCAEC-NYO-7102 (Doctoral thesis, 1955)
222. Marshall, L., and Marshall, J., *Phys. Rev.*, **98**, 1398 (1955)
223. Guernsey, G., Mott, G., and Nelson, B. V., *Phys. Rev.*, **88**, 9 (1952)
224. De Pangher, J., *Phys. Rev.*, **92**, 1084 (1953)
225. De Pangher, J., *Univ. Calif. Radiation Lab. Rept.*, UCRL-2153 (1953)
226. Griffith, T. C., *Proc. Conf. Nuclear Meson Phys.*, Glasgow, 1954 (1955)
227. Dickson, J. M., and Salter, D. C., *Proc. Phys. Soc. (London)*, **A66**, 721 (1953)
228. Roberts, A., Tinlot, J., and Hafner, E. M., *Phys. Rev.*, **95**, 1099 (1954)
229. Dzhelepov, V. P., and Kazarinov, M., *Dokl. Akad. Nauk S.S.S.R.*, **99**, 939 (1954)
230. Bradner, H., and Donaldson, R., *Phys. Rev.*, **95**, 1701 (1954)
231. De Pangher, J., *Phys. Rev.*, **95**, 518 (1954)
232. Chamberlain, O., Donaldson, R., Segrè, E., Tripp, R., Wiegand, C., and Ypsilantis, T. J., *Phys. Rev.*, **95**, 850 (1954)
233. Ypsilantis, T. J., Wiegand, C., Tripp, R., Segrè, E., and Chamberlain, O., *Phys. Rev.*, **98**, 840 (1955)
234. Ypsilantis, T. J., *Univ. Calif. Radiation Lab. Rept.*, UCRL-3047 (Doctoral thesis, 1955)
235. *Suppl. Nuovo cimento*, Suppl. 12, 499 (1954)
236. Ohnuma, S., and Feldman, D., *Phys. Rev.*, **102**, 1641 (1956)
237. Dickson, J. M., Rose, B., and Salter, D. C., *Proc. Phys. Soc. (London)*, **A68**, 361 (1955)
238. Baskir, E. (Private communication)

239. Brinkworth, M. J., and Rose, B., *Proc. Rochester Conf. High-Energy Nuclear Phys.*, 5th, 159 (1955)
240. Fischer, D., and Goldhaber, G., *Phys. Rev.*, 99, 1350 (1955)
241. Kruse, U. E., Teem, J. M., and Ramsey, N. F., *Phys. Rev.*, 94, 1795 (1954)
242. Mott, G. R., Guernsey, G. L., and Nelson, B. K., *Phys. Rev.*, 88, 15 (1952)
243. Stafford, G. H., Whitehead, C., and Hillman, P., *Nuovo cimento* 5, 1589 (1957)
244. Taylor, A. E., *Proc. Rochester Conf. High-Energy Nuclear Phys.*, 6th (1956)
245. Taylor, A. E., and Wood, E. (Private communication)
246. Chih, C. Y., *Univ. Calif. Radiation Lab. Rept.*, UCRL-2575 (1954)
247. Johnston, L. A., and Swenson, D., *Univ. Minn. Rept.* (1957)
248. Johnston, L. A., and Swenson, D., *Bull. Phys. Soc.*, 112, 180 (1957)
249. Johnston, L. A., and Young, D. E., *Bull. Am. Phys. Soc.*, 113, 3, 501 (1958)
250. Johnston, L. A. (Private communication)
251. Knecht, D. J., Messelt, S., Berners, E. D., and Northcliffe, L. C., *Bull. Am. Phys. Soc.*, 113, 203 (1958)
252. Knecht, D. J. (Private communication)
253. Burkig, J. W., Schrank, G. E., and Richardson, J. R., *Phys. Rev.*, 100, 1805 (1955)
254. Phillips, R. N. J., *Repts. Progr. in Phys.*, 22, 562 (1959)

THEORETICAL INTERPRETATION OF ENERGY LEVELS IN LIGHT NUCLEI^{1,2,3}

BY I. TALMI AND I. UNNA

Department of Physics, The Weizmann Institute of Science, Rehovoth, Israel

I. INTRODUCTION

The atomic nucleus is a system of A particles (Z protons and N neutrons) the motion of which is governed by their mutual interactions. The exact description of the behavior of this system is equivalent to the solution of the n -body problem in quantum mechanics. Recently, several attempts have been made to obtain approximate solutions to the nuclear problem but we are still far from an accurate description. Although qualitative understanding was gained, exact eigenfunctions cannot be calculated for any given (finite) nucleus. In the past, various models were proposed, some very successful. These models replace the nuclei by greatly simplified systems which can be handled mathematically. The wave functions of the successful models can be used to calculate many properties of nuclei to a high degree of accuracy. Among these, the individual-particle model, better known as the shell model (1, 2, 3), and the collective model (4, 5) have given a qualitative understanding of many nuclear features and served as a very useful guide to the experimental work. Also, quantitative calculations of various nuclear data were successfully carried out, in the framework of these models.

There are regions in which the collective model gives a very accurate description of nuclear properties. In these regions, i.e. in the rare-earth and transuranium regions, there are many nucleons outside closed shells, and the nuclear deformations are large. On the other hand, in light nuclei, there are never enough nucleons outside closed shells, and the shell model is expected to give a good description of nuclear states. Since the present review deals with light nuclei, we shall make use only of the shell model; however, for the sake of completeness, we list, in addition to references (4) and (5), papers (60 to 67) dealing with light nuclei from the point of view of the collective model. We shall describe very briefly the mathematical framework of the shell model and shall concentrate on comparison of the theoretical predictions with the experimental data. We shall discuss the calculation of

¹ The survey of literature pertaining to this review was concluded May 1, 1960. As a service to the reader, the Editors are reproducing as an appendix to this article the Energy Levels of the Light Nuclei by F. Ajzenberg-Selove & T. Lauritsen from a forthcoming edition of the *American Institute Handbook* (McGraw-Hill Book Co., Inc., New York, N. Y., 1961).

² Among the abbreviations used in this chapter are: c.f.p. (coefficient of fractional parentage) and C.E. (Coulomb energy).

³ Work sponsored in part by the Aeronautical Research Laboratory, Wright Air Development Center of the Air Research and Development Command, United States Air Force, through its European Office.

energy levels of nuclei and transitions between nuclear states⁴ but will not go into the shell-model description of nuclear reactions. Although much information can be gathered from, say, stripping reactions (10), we shall not discuss them. This limitation is necessary to keep this review within reasonable bounds. Quantitative results will be mentioned wherever they were obtained. In regions where no quantitative calculations were carried out, we shall describe the predictions of the model only qualitatively.

II. THE SHELL MODEL

In the shell model, we consider the nucleons to move independently of each other in a central field. This field represents in some way the average interaction of every nucleon with all others. The Hamiltonian of such a central field obviously cannot be exactly equal to the real one. Therefore, there are residual interactions to be considered. These mutual interactions are taken as a perturbation. The interaction between two nucleons, as determined from scattering experiments and the deuteron, is still not very well known. However, it is clearly very strong at small distances and is believed to give rise to infinite repulsion (hard core) at distances of about 0.4 fermi (1 fermi = 10^{-13} cm.). It is therefore clear that this interaction cannot be treated in the usual perturbation theory with shell-model wave functions for the nucleons. It seems, however, that this strong nuclear interaction modifies strongly the nuclear wave function only where two nucleons are very close together. The real wave functions can thus be approximated by shell-model wave functions modified by two-particle short-range correlations (with the experimentally observed nuclear densities there is only a slight chance of three nucleons being very close together). Instead of using these modified wave functions with the real interaction, it is possible to keep using unmodified shell-model wave functions with interactions which are modified by the two-particle correlations. Similarly, if we calculate matrix elements of other operators with shell-model wave functions, we must use a modified form of these operators. We thus see that if we use the shell model, we must take a modified Hamiltonian which contains effective two-body interactions between nucleons. No reliable calculations of the effective interaction (known technically as the t matrix or reaction matrix) are available for finite nuclei. Preliminary results indicate, however, that the effective interaction obtained is nonlocal. There is evidence from nuclear spectra (as well as from scattering and deuteron data) that the interaction has a considerable noncentral part such as tensor forces and mutual spin-orbit interaction. A phenomenological simple interaction intended to replace the effective interaction must therefore contain many adjustable constants (sometimes more than experimental data to be accounted for). Also, the form of the radial parts of the single-nucleon wave functions can be chosen in many ways.

⁴ Experimental data are taken from references (6 to 9). Other references to experimental work will be made below.

A possible way out of this difficulty is to try to determine the effective interaction from the experimental data. At first sight it seems that this is a rather arbitrary procedure. However, if there are only effective two-body forces acting between nucleons, there appears a severe limitation. In this case, all energy levels of n -particle configurations are linear combinations of matrix elements in two-particle configurations. Using a definite scheme of wave functions, e.g. jj coupling, we can thus calculate the energies in the n -particle configurations in terms of the energies of two-nucleon configurations. We consider the experimental data taken from a group of nuclei in which the same configurations occur. If we assume that the matrix elements of the effective nuclear interaction are the same in all these nuclei, all energies can be expressed in terms of a small number of unknown parameters. These parameters are the matrix elements in the appropriate two-nucleon configuration. We now look for a set of values of these matrix elements that will accurately reproduce the experimental data. If the number of experimentally determined energies is bigger than the number of the parameters, this procedure is not arbitrary. Good agreement between experimental energies and those calculated with the best values of the matrix elements indicates that the underlying assumptions are justified. This agreement would also justify the configuration assignments made for the various levels. The matrix elements of the two-body effective nuclear interaction, thus obtained, can be used in further calculations where experimental data are not known.

This approach was first applied by Bacher & Goudsmit in the analysis of atomic spectra (11). Even in the atomic case, where for good reasons the shell model is a good approximation, there is evidence for effective forces between electrons. Even there, it is very difficult to calculate accurately the radial integrals of the Coulomb interaction. Hence the radial integrals are replaced by free parameters to be determined from the atomic spectra. In addition, there is evidence for an interaction of the type $(l_i \cdot l_k)$, far bigger than the magnetic orbit-orbit interaction. This term is probably a manifestation of the effective interaction (12). In most cases of atomic spectroscopy, many more levels than theoretical parameters are known experimentally, and thus the consistency of the model can be checked. In nuclear spectra this is not true, but there is a great simplification over the atomic case. One finds that the matrix elements of the effective nuclear interaction remain constant to a good degree from one nucleus to the next. This makes it possible to obtain information about the validity of the model and configuration assignment as well as about the values of matrix elements without prior knowledge of the effective nuclear interaction.

We can summarize the situation as follows. Because of the two-body interactions, every shell-model wave function is modified by admixtures of other configurations. This configuration interaction modifies the energy of the state considered. Even if the admixture is not large, the modification in interaction energy may be considerable (as in the case of a strong repulsive potential). The effect of configuration interaction may assume the form of a

modification of the two-body forces. In this case it gives rise to an effective nuclear interaction. Conventional second-order perturbation theory seems to indicate that, at least in some cases where the perturbing configurations are sufficiently far away, their effect is indeed a modification of the two-body interaction. However, in certain instances, such an effect appears even if the perturbing configurations lie rather low and the admixture is large. It is important to bear in mind these facts when considering the success of the shell model in actual cases. It should be remembered that even if very good agreement is obtained for the energies, the configurations may not be pure. This is manifested when other operators, like magnetic moments and transition probabilities, are considered. If the real operators are used in such calculations, it cannot be expected that the unmodified shell-model wave functions will give correct results. If, on the other hand, the shell-model wave functions are to be used, we should take modified forms of the single-particle operators. It may happen that these modified operators also can be expressed by effective single-particle operators.

We shall discuss some examples in which transition probabilities can be given in terms of effective (or modified) single-particle operators. However, there are situations in which such an approach is bound to fail. Let us consider, for example, an electromagnetic transition between two nuclear states. The operator which determines the transition probability is a single-particle operator so that only one nucleon changes its state while the γ quantum is emitted. If the radiation is a 2^l -pole, the sum of l and the spin of the initial state of the nucleon considered j_i must be equal to the final spin of this nucleon, $j_i + l = j_f$. In addition, the total initial and final spins of the nucleus must also satisfy $J_i + l = J_f$. This fact is expressed mathematically by the matrix element of the operator considered, being proportional to the Racah coefficient

$$\left\{ \begin{matrix} j_i & j_f & l \\ J_f & J_i & J_0 \end{matrix} \right\},$$

where J_0 is the spin of the rest of the nucleus which must remain unchanged. Usually the radiation emitted has the lowest possible l value. This minimum allowed value of l is, for a pure configuration, the bigger of the numbers $|J_i - J_f|$ and $|j_i - j_f|$ (if they do not both vanish; if both vanish the minimum value is $l = 1$). If $|j_i - j_f| \leq |J_i - J_f| = l$, the allowed transition can take place between the two shell-model wave functions characterized by j_i and j_f . Even if other shell-model wave functions are admixed to these two, no transition can occur between any of them with a lower value of l . Thus if the admixtures are slight (a few per cent in probability), the transition rate may be modified but is expected to have the same order of magnitude. In such cases the actual transition rate may be ascribed to an effective single-particle operator.

On the other hand, if $|j_i - j_f| > |J_i - J_f|$, slight admixtures to the shell-model wave functions may greatly enhance the transition rate. The transi-

tion between the two shell-model wave functions which are the major components of the initial and final state must be of order $|j_i - j_f|$. However, admixtures with other possible values of j_i and j_f may enable a transition with a smaller l , for which $|j_i - j_f| > l \geq |J_i - J_f|$, to take place between initial and final states. Such a change of l may give rise to a transition several orders of magnitudes faster. This transition rate must first be multiplied by the probability of admixture, but it may still be faster than the transition of order $|j_i - j_f|$. This is the reason why the transition rate is primarily determined by $|J_i - J_f|$ even if the major components of the states involved are given by the shell model. We shall consider this phenomenon in more detail; in cases where it occurs we shall specifically mention it.

We shall treat cases where transition probabilities can be adequately reproduced with shell-model wave functions and effective single-nucleon operators are those of electromagnetic transitions. We shall mention one case dealing with effective matrix elements of first-forbidden $\Delta J = 2$ beta transitions. However, the situation with respect to allowed beta transitions is far more complex. The main difficulty is the occurrence of unfavored transitions. The allowed Fermi transitions take place only between states with the same isospin T (and the same value of J). The sums of matrix elements squared are then simply given by $T(T+1 - M_T M'_T)$ where M_T and M'_T are the initial and final eigenvalues of T_z . To the extent that charge independence holds, the Fermi matrix elements are independent of the details of the wave functions involved, i.e. of the configuration assignment, coupling scheme, etc. Actually, we find that pure Fermi ($J=0 \rightarrow J=0$) transitions with $\Delta T=0$ are always favored (even as high as in Co^{54}), and the matrix elements have practically their full value. Another class of favored transitions is that of transitions between mirror nuclei, to which also the Gamow-Teller matrix elements contribute. If the Fermi contribution, calculated from $0 \rightarrow 0$ transitions, is subtracted from the mirror transitions, we find that the Gamow-Teller matrix elements are very different in the various nuclei. This is also true in the pure Gamow-Teller transitions (with $\Delta T=1$) of which some are favored (e.g., in He^6 and F^{19}) and others are highly unfavored (e.g. in C^{14}). The Gamow-Teller matrix elements should be rather sensitive to small changes in the wave functions (particularly in the jj -coupling scheme); the actual data support this statement.

The Gamow-Teller matrix elements are always reduced in the case of transitions of odd nuclei with $\Delta T=1$. Such transitions are found to be unfavored. This may be connected with the fact, to be discussed later, that the shell-model description of $T=3/2$ states is much better than that of $T=1/2$ states. However, there is no known simple way to take into account the unfavoredness factor. In view of the existence of both favored and unfavored Gamow-Teller transitions in the same shell, it is not clear whether it will be possible to describe beta decays by effective matrix elements. We shall therefore not consider beta decay of nuclear levels here. The beta-transition rates

are a great help for the rough determination of external properties of states, like spins and parities. However, they cannot yet be used for studying the details of nuclear states like the shell-model configurations involved. We shall thus consider only electromagnetic transitions. Since these occur between initial and final states of the same nucleus, they are probably easier to treat theoretically. In several instances such transitions can furnish detailed information about nuclear states.

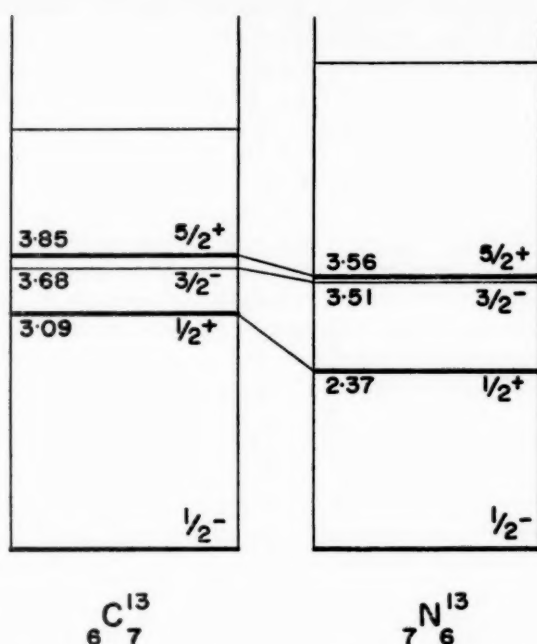
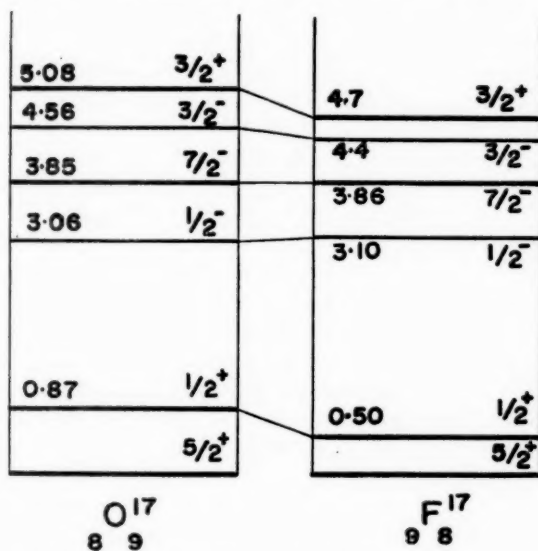
III. SINGLE-PARTICLE STATES

Let us consider a nucleus which contains nucleons in closed shells only. The excitations in this case involve raising one of the nucleons to the next higher orbit. Therefore, the excitation energy is composed of the difference in the energy of single-nucleon orbits as well as the change in interaction energy. It is thus rather difficult to excite closed shells from their state with $J=0$. If one nucleon is added to a closed-shell nucleus, it occupies the lowest available orbit. The nucleus obtained has a series of levels in which the single extra nucleon is excited to higher orbits. The excitation energies depend on the proximity of available orbits. The states of the nucleus obtained this way may be called single-nucleon states since the wave function can be approximated by that of the single nucleon in a central field.

The order of single-nucleon levels is usually taken to be essentially that of a three-dimensional harmonic oscillator. The lowest is the $1s$ orbit and the next higher the $1p$ orbit. As a result of spin-orbit interaction, we can distinguish between the $1p_{3/2}$ orbit for which $j=l+1/2=3/2$ and the higher $1p_{1/2}$ orbit. The next oscillator shell has the $1d$ and $2s$ orbits and their order is $1d_{5/2}$, $2s_{1/2}$ and $1d_{3/2}$. The $1f_{7/2}$ is the next shell beginning after proton (or neutron) number 20. The higher orbits will not be considered in the present article.

We present here the single-particle spectra of C^{13} and N^{13} (Fig. 1) and also of O^{17} and F^{17} (Fig. 2). As is well known, the spectra of mirror nuclei are almost identical, indicating that charge symmetry is a good approximation. Thus, apart from electrostatic repulsion, the interaction between two protons is the same as between two neutrons. It is interesting to see how the single-nucleon levels differ from the idealized picture. We first notice that the order of the single-particle levels is not necessarily the order of filling of the orbits. In other words, as more nucleons are added, the order of levels changes. This change is due to the mutual effective interaction and will be discussed later. Thus, in C^{13} and N^{13} the $2s_{1/2}$ level is below the $1d_{5/2}$ level whereas in O^{17} and F^{17} their order is reversed. Also in O^{17} (and F^{17}) the $1f_{7/2}$ level is below the $1d_{3/2}$ level. However, the $1d_{3/2}$ orbit becomes lower as more nucleons are added and is filled before the $1f_{7/2}$ orbit.

Another important feature is the behavior of the energy spacings of the single-nucleon states. In the harmonic oscillator spectrum, the distance between oscillator shells is $\hbar\omega$. The angular frequency ω of the oscillator determines the radial parts of the single-nucleon wave functions. It can therefore

FIG. 1. Single-particle levels of C^{13} and N^{13} (in Mev).FIG. 2. Single-particle levels of O^{17} and F^{17} (in Mev).

be determined from the Coulomb energies, calculated with these functions. The parameter $e^2\sqrt{\nu}/\pi$ of the oscillator wave functions was determined to be 0.3–0.35 Mev (13 to 15). Here ν is given by $\nu = m\omega/(2\hbar)$, and one obtains for $\hbar\omega$ values around 11 to 13 Mev. Experimentally we find a spacing of 3 to 4 Mev only between the $1p_{1/2}$ shell and the $2s_{1/2}$, $1d_{5/2}$ shell and the same distance between the $1d_{5/2}$, $2s_{1/2}$ levels and the $1f_{7/2}$ level. These facts should be borne in mind when considering actual nuclei.

The magnitude of the splitting between the $j=l+1/2$ and $j=l-1/2$ levels can be obtained from the observed single-nucleon spectra. This splitting is due to a spin-orbit (effective) interaction of the single nucleon. The bigger the splitting, the better the approximation offered by jj coupling. If the spin-orbit interaction is more important than the mutual (effective) interaction between nucleons, the states with $j=l+1/2$ and $j=l-1/2$ can be taken as two different orbits. In this jj -coupling scheme, nucleons fill one of these orbits first so that the values of their total spins j are good quantum numbers. As is well known, it was found empirically by M. G. Mayer and by Haxel, Jensen, and Suess that the single-nucleon orbits have definite j values. The orbit with $j=l+1/2$ has lower energy than the $j=l-1/2$ orbit.

In O^{17} (and F^{17}) the splitting between the $1d_{5/2}$ ground state and the $1d_{3/2}$ level amounts to 5.08 (and 4.7) Mev. This energy difference is rather large and even bigger than the difference between the ground state and the $1f_{7/2}$ level which belongs to the next oscillator shell. Only when more $1d_{5/2}$ nucleons are added does the $1d_{3/2}$ level become lower than the $1f_{7/2}$ level. It would be interesting to have the exact splitting between the $1f_{7/2}$ and the $1f_{5/2}$ orbits. The $1f_{5/2}$ level was looked for but has not yet been found in Ca^{41} up to 4 Mev above the ground state. Recently, results on the single-nucleon states of Sc^{41} were published (16). According to this reference, the $f_{7/2}-f_{5/2}$ splitting amounts to 6.4 Mev. This is even bigger than the $f_{7/2}-g_{9/2}$ difference which is given there as 5.6 Mev. The value of 6.4 Mev should not be surprising in view of the 5-Mev $d_{5/2}-d_{3/2}$ splitting. Evidence will be given that jj coupling is a good approximation in the $1f_{7/2}$ shell. This already points to a large $1f_{7/2}-1f_{5/2}$ splitting. On the other hand, the value obtained for the $2p_{3/2}-2p_{1/2}$ splitting in Sc^{41} is much smaller, being only 2.2 Mev. Also, the order of filling indicates that when more $1f_{7/2}$ nucleons are added, the $1f_{5/2}$ orbit becomes lower than both the $1g_{9/2}$ and $2p_{1/2}$ orbits.

As we shall see, the coupling scheme in the first p shell changes from LS coupling to jj coupling when more nucleons are added. Such an effect may occur if the single-particle spin-orbit splitting is small at the beginning of the shell. As more nucleons are added, the spin-orbit splitting is increased and the scheme may go over into jj coupling. Such behavior is expected if the spin-orbit splitting is due to mutual spin-orbit (effective) interaction between the nucleons (17).

We can obtain some information on the behavior of the spin-orbit interaction by comparing the $p_{3/2}-p_{1/2}$ splitting for one p nucleon and for one p -nucleon hole, i.e. one nucleon missing from the closed p shell. It is possible

to treat such a configuration by considering the wave function of the missing p nucleon. In N^{15} (and O^{15}) we interpret the $3/2^-$ level as due to one $p_{3/2}$ nucleon missing from the closed shells of O^{16} . Thus the $p_{3/2}-p_{1/2}$ splitting (which has the opposite sign in this case) turns out to be 6.33 (and 6.15) Mev. This value is rather large and indicates that jj coupling may be a good approximation for the last nuclei before O^{16} . Unfortunately, the first nucleon in the p shell is not bound either in He^5 or Li^5 ; therefore, it is doubtful whether the $p_{3/2}-p_{1/2}$ splitting in these two nuclei has a direct meaning in terms of a spin-orbit interaction. Some information can be obtained by considering Li^7 and Be^7 if we assume a certain coupling scheme for them. In LS coupling, taking the ground state to be 2P with $L=1$ $S=1/2$ and with maximum symmetry in the space co-ordinates (lowest supermultiplet), we can calculate the splitting between the two states $^2P_{3/2}$ and $^2P_{1/2}$. We find that the single-nucleon spin-orbit splitting is reduced in this case by a factor 3. The observed splitting is 0.478 Mev in Li^7 (0.431 Mev in Be^7). Thus, a reasonable value of the $p_{3/2}-p_{1/2}$ splitting for one p nucleon would be about 1.4 Mev. This value is indeed considerably smaller than the value of 6.3 Mev found for a single p hole.

Single-particle states present another interesting feature. We can calculate the wave function of the single nucleon by assuming that it moves in an effective potential well. If the separation energy is large, we can approximate the wave function by using an infinite potential well (e.g. the harmonic oscillator well). For smaller values of the separation energy, we have to take into account that the potential goes rapidly to zero beyond the nuclear radius and that hence the wave functions can be much influenced.

This effect of the finite potential well is important in calculating Coulomb energy differences of mirror nuclei. The Coulomb energy difference calculated with a finite well is smaller than the value calculated with an infinite potential well. The smaller the separation energy, the bigger this effect. Also, it is more pronounced for $l=0$ states since for higher l values there is always the centrifugal barrier which acts to decrease the change in the proton wave function. This change in the Coulomb energy difference in the case of a small separation energy, particularly pronounced for s states, is called the Thomas-Ehrman effect (18, 19).

The Thomas-Ehrman effect is found experimentally in many cases. It is clearly demonstrated in the single-nucleon spectra of mass 17 (Fig. 2) and mass 13 (Fig. 1) nuclei. In these nuclei the separation energies of the excited states are small, and in some cases the single nucleons are not even bound. The much larger shift of the $s_{1/2}$ level is rather pronounced. This situation should be compared to that in N^{15} and O^{15} . There is a shift in the position of the $1/2^+$ level (5.31 Mev above the ground state in N^{15} and 5.20 Mev in O^{15}) which is bigger than that of the $5/2^+$ level (5.28 Mev in N^{15} and 5.25 Mev in O^{15}). Still, this shift is very small because the separation energy is 5 Mev in N^{15} (and 2 Mev in O^{15}). We shall see that this effect appears also in configurations with several extra nucleons in which one nucleon is excited into an $s_{1/2}$

orbit. It thus can serve as a guide indicating, in some cases, where single nucleons are excited to $s_{1/2}$ orbits.

Some properties of single-particle states can be calculated with the single-nucleon wave functions and compared with the experimental data. The single-nucleon excitation energies are, naturally, the most difficult to calculate. As explained, we shall discuss only the agreement between many-nucleon energies calculated with shell-model wave functions without specifying the effective interaction. In such calculations we determine the single-nucleon energies from the experiment along with the matrix elements of the nuclear interaction. In regions where good agreement is obtained, we can correlate single-nucleon energies in different nuclei. For example, we can calculate the single-nucleon energies in O^{17} in terms of these energies in C^{13} and the effective mutual interactions. Since such calculations involve the interaction between several particles, they will be described later. Rates of electromagnetic transitions will be discussed in detail in Section VI. Here we shall briefly mention magnetic moments of nuclei with one nucleon outside closed shells.

The closed shells have always $J=0$ and thus do not contribute to the magnetic moment. The magnetic moment due to a single nucleon is given in nuclear magnetons by the well-known Schmidt formula

$$\begin{aligned}\mu &= g_l j = g_l l + \frac{1}{2} g_s \quad \text{for } j = l + 1/2 \\ \mu &= g_l j = \frac{j}{j+1} \left[g_l(l+1) - \frac{1}{2} g_s \right] \quad \text{for } j = l - 1/2\end{aligned}\tag{1}$$

In these expressions $g_l = 1$ for a single proton and $g_l = 0$ for a single neutron, whereas $\frac{1}{2}g_s = 2.793$ for a single proton and $\frac{1}{2}g_s = -1.913$ for a single neutron. The Schmidt values for the magnetic moments of nuclei are expected to hold only if the shell-model wave functions (of closed shells plus an extra nucleon) are a very good approximation. Slight changes in the wave functions, like those due to configuration interaction, can change the magnetic moments considerably. The formulae are also applicable to nuclei in which only one nucleon is missing from closed shells. Stable nuclei with closed shells plus or minus a single nucleon are not numerous. We can take C^{13} as such a case, N^{15} , O^{17} , and K^{39} . If we consider the $2s_{1/2}$ shell to begin after Si^{28} and the $d_{3/2}$ shell to begin after S^{32} , we can add to the list Si^{29} , P^{31} , S^{33} , S^{35} , and Cl^{37} .

It is interesting that the magnetic moments of C^{13} , N^{15} , and O^{17} agree remarkably well with the above formula. These nuclei have a single $p_{1/2}$ neutron, a single $p_{1/2}$ proton hole, and a single $d_{5/2}$ neutron, respectively. The experimental magnetic moments in nuclear magnetons are 0.702, -0.283 , and -1.894 to be compared with Schmidt's values 0.638, -0.264 , and -1.913 , respectively. In all other cases the agreement is not as good. The experimental moments of Si^{29} and P^{31} with a single $s_{1/2}$ neutron and a single $s_{1/2}$ proton hole are -0.555 and 1.132 while Schmidt's values are -1.913 and 2.793 , respectively. The single $d_{3/2}$ neutron S^{33} and single $d_{3/2}$ neutron

hole S^{35} have measured moments of 0.643 and 1.00 ± 0.14 as compared to the calculated value of 1.146 nuclear magnetons. The measured magnetic moments of the single $d_{3/2}$ proton and $d_{3/2}$ proton-hole nuclei Cl^{37} and K^{39} are 0.684 and 0.391 while the Schmidt value is 0.124. It could be argued that in Si^{29} to S^{36} there is configuration interaction and that they are not nuclei with proper closed shells plus or minus one. However, we shall present some evidence that for energy calculations, the states of Cl^{37} and K^{39} are well approximated by jj coupling. The discrepancy of the magnetic moments indicates that single-particle operators also must be modified or "quenched" if they are to be used with shell-model wave functions. We shall discuss examples in which the modification can be expressed as giving rise to effective single-particle operators that have approximately the same values in several nuclei.

If there are several nucleons outside closed shells, the shell-model wave functions represent a many-nucleon system. Nevertheless, the ground states for an odd number of spin j nucleons have, in many cases, a total spin equal to that of the single nucleon, $J=j$. However, this state is not simply a single-nucleon state. For example, the (unmodified) magnetic moment is no longer given by the Schmidt formulae. If one nucleon is raised into the j' orbit, we may obtain a state with $J=j'$ and a parity which is the same as that of the j' nucleon. This state also is a many-nucleon state and the coupling scheme may be rather involved. Sometimes such states are described by the single-nucleon notation with the l and j of the odd nucleon. It should be remembered that this is an oversimplification which has only a qualitative meaning. A more accurate description of shell-model wave functions with several nucleons outside closed shells is given in the next section.

IV. MANY-NUCLEON STATES

There is much evidence in favor of charge independence of nuclear forces. This assumption means that the nuclear forces between two protons are the same as between two neutrons or a proton-neutron pair. This equality holds if the pair of nucleons are in the same state. Since in light nuclei the Coulomb field which acts only on the protons is not so important, we usually consider protons and neutrons together. The proton and neutron are taken to be two states of the same particle which are distinguished by the eigenvalues $+1$ and -1 of the isospin operator τ_3 (20). Under these conditions, the symmetry of the wave function with respect to the isospin co-ordinates of the nucleons is determined by the value of the total isospin of the state T . Here, T is defined in terms of the eigenvalues of the square of the total isospin vector

$$T = \frac{1}{2} \sum \tau_i = \sum t_i \quad \text{by} \quad T^2 = T(T+1).$$

The higher the T value, the higher the symmetry in the isospin co-ordinates. The exclusion principle operates now with respect to all co-ordinates of the nuclear wave functions. Therefore, the higher the symmetry in the isospin co-ordinates, the lower the symmetry in the space and spin co-ordinates of

the nucleons. The eigenvalues of T_3 will be denoted by M_T . These are uniquely and definitely determined by the proton and neutron numbers in the nucleus, $M_T = \frac{1}{2}(Z - N)$.

In the stable heavier nuclei, because of the effect of the Coulomb energy, there are more neutrons than protons. Charge independence can still be a good approximation and the isospin T a good quantum number. However, once protons and neutrons occupy different unfilled shells, there is no need to use the isospin formalism explicitly in the ground states. The smallest possible value of T is given by $\frac{1}{2}|Z - N|$, which is also the maximum possible T for the ground configuration in this case. Thus, the isospin T continues to be a good quantum number even when protons and neutrons are in different shells; it is, however, not required for specifying the ground state.

Next to single-nucleon states, the simplest nuclei are those in which one kind of nucleon, either protons or neutrons, is in closed shells. Closed shells have always $J=0$ which indicates spherical symmetry; thus, the interaction of an extra nucleon with them is independent of the orientation of its spin. The interaction of a single nucleon with closed shells is the same as an interaction with a central field. We can therefore consider only the extra nucleons outside closed shells. We limit the discussion to the more important case of jj coupling. Even in cases where jj coupling does not give a good approximation, it is a well-defined scheme of wave functions with which it is possible to discuss better wave functions. We shall consider first the states of several identical nucleons in the same j shell and later generalize to configurations of both protons and neutrons.

The wave function of several identical nucleons must be antisymmetric with respect to exchange of the space and spin co-ordinates of any two nucleons. If there are two nucleons present, i.e. in the j^2 configuration, states with definite J have a definite symmetry. States with even values of J ($J=0, 2, 4, \dots, 2j-1$) are antisymmetric (and are symmetric in the isospin co-ordinates, $T=1$) whereas states with odd J ($J=1, 3, \dots, 2j$) are symmetric (and thus belong to $T=0$). Therefore, for identical nucleons, only even values of J appear in the j^2 configuration. If the interaction is short range and attractive (δ -function potential), the bigger the overlap between the wave functions of the interacting nucleons, the stronger the interaction. Here, therefore, $J=0$ is the ground state and the other levels have $J=2, J=4$ in this order (at least for small values of j). This is actually the observed order of levels in even-even nuclei, also in nuclei with more than two extra nucleons. We shall see that the lower levels of nuclear spectra of even-even nuclei strongly resemble those of the j^2 configuration.

In order to construct wave functions for three identical nucleons, we couple two of them to an even spin J_0 and couple the spin $j_3=j$ of the third nucleon to J_0 to give the total J . All these couplings are carried out by constructing linear combinations of products of wave functions with vector addition (Clebsch-Gordan) coefficients. The resulting function will be denoted by $\psi(j^2(J_0)j_3JM)$. We now antisymmetrize the function and recouple the

spins so that nucleons 1 and 2 are always coupled first to a J_1 and $j_3=j$ is coupled to it. The antisymmetric function obtained has the form (after proper normalization)

$$\psi(j^3\alpha JM) = \sum_{J_1, \text{ even}} (j^2(J_1)jJ | \{j^3\alpha J\} \psi(j^2(J_1)j_3 JM) \quad 2.$$

The coefficients in this expansion are the fractional parentage coefficients (21) or, in short, c.f.p. The α are the additional quantum numbers necessary to define the state uniquely if there are several states of the j^3 configuration with the same J (this does not happen for $j \leq 7/2$). Similarly, normalized antisymmetric wave functions of n nucleons can be expressed in terms of the j^{n-1} states by

$$\psi(j^n\alpha JM) = \sum_{\alpha_1 J_1} (j^{n-1}(\alpha_1 J_1)jJ | \{j^n\alpha J\} \psi(j^{n-1}(\alpha_1 J_1)j_n JM) \quad 3.$$

where $j_n=j$ represents the spin of the n th nucleon.

This form of the antisymmetric functions, in which the n th nucleon is always coupled to various antisymmetric states of the j^{n-1} configuration, is very convenient. Matrix elements of single-particle operators $F = \sum_{i=1}^n f_i$ are given in terms of c.f.p. by calculating f_n (all the f contribute equally with antisymmetric wave functions!) and multiplying the result by n

$$\begin{aligned} \langle j^n\alpha JM | F | j^n\alpha' J' M' \rangle &= n \sum_{\alpha_1 J_1} \langle j^{n-1}(\alpha_1 J_1)jJ | \{j^n\alpha J\} \langle j^{n-1}(\alpha_1 J_1)jJ' | \{j^n\alpha' J'\} \\ &\cdot \langle j^{n-1}(\alpha_1 J_1)j_n JM | f_n | j^{n-1}(\alpha_1 J_1)j_n J' M' \rangle \end{aligned} \quad 4.$$

If F is a tensor operator of degree k (22), $F^{(k)} = \sum f_i^{(k)}$, the result can be further simplified. It is only necessary to write the result of the reduced matrix element of $F^{(k)}$ defined by the Wigner-Eckart theorem⁵

$$\langle JM | F_{\kappa}^{(k)} | J' M' \rangle = (-1)^{J-M} \langle J || F^{(k)} || J' \rangle \begin{pmatrix} J & k & J' \\ -M & \kappa & M' \end{pmatrix} \quad 5.$$

where the 3- j symbol is related to the Clebsch-Gordan coefficient.⁵ Equation 4 can now be written as

$$\begin{aligned} \langle j^n\alpha J || F^{(k)} || j^n\alpha' J' \rangle &= n(j || f^{(k)} || j) \sum_{\alpha_1 J_1} (j^{n-1}(\alpha_1 J_1)jJ | \{j^n\alpha J\} \cdot \\ &\cdot (j^{n-1}(\alpha_1 J_1)jJ' | \{j^n\alpha' J'\} \left\{ \begin{matrix} J & J' & k \\ j & j & J_0 \end{matrix} \right\} \end{aligned} \quad 6.$$

In Equation 6 the symbol in curly brackets is a Racah coefficient. Some tables are available for this coefficient in which a slightly different definition is used, i.e.,

$$W(abcd; ef) = (-1)^{a+b+c+d} \left\{ \begin{matrix} a & b & e \\ d & c & f \end{matrix} \right\}.$$

The closed expression in Equation 6 can be used in the calculation of single-particle tensor operators like those giving the transition rate of various electromagnetic multipole fields, to be considered in Section VI.

⁵ The algebra of tensors and their matrix elements is given in (23 to 26).

Some operators, like the interaction energy, are the sum of two-nucleon operators

$$G = \sum_{i < k}^n g_{ik}.$$

We shall consider only scalar operators, like the mutual interaction. Their matrix elements vanish between states with different values of J or M , and the diagonal elements are independent of M . In this case it is more convenient to calculate the contribution of

$$\sum_{i < k}^{n-1} g_{ik}$$

and multiply it by $n/n-2$. We thus obtain

$$\begin{aligned} \langle j^n \alpha J M | G | j^n \alpha' J M \rangle &= \frac{n}{n-2} \sum_{\alpha_1 \alpha'_1 J_1} (j^{n-1}(\alpha_1 J_1) j J | \{ j^n \alpha J \} (j^{n-1}(\alpha'_1 J_1) j J | \{ j^n \alpha' J \} \\ &\cdot \langle j^{n-1} \alpha_1 J_1 | \sum_{i < k}^{n-1} g_{ik} | j^{n-1} \alpha'_1 J_1 \rangle \end{aligned} \quad 7.$$

In this way, matrix elements in the j^n configuration are expressed in terms of matrix elements in the j^{n-1} configuration. By continuing the process, we obtain these matrix elements in terms of those in the j^2 configuration.

We shall now turn to the additional quantum numbers α . For identical nucleons, no such α are necessary for j^n configurations with $j \leq 5/2$. Nevertheless, we consider them here not only for the case of the $f_{7/2}$ shell but also for mixed proton and neutron configurations where they are necessary for $j \geq 3/2$. We therefore discuss the seniority scheme, which is very useful in nuclei. Let us start from the j^n configuration and consider a state with a given J . We can try to obtain from it a state with the same J of the j^{n+2} configuration by coupling to its wave function the wave function of two nucleons coupled to $J_0=0$ and antisymmetrizing. If the wave function obtained does not vanish, we obtain a state which is said to have the same seniority as the corresponding state in the j^n configuration. Similarly, we can see whether that state can be obtained by the same procedure from a state with the same J in the j^{n-2} configuration and so on. We finally arrive at a state with the same J (and seniority) of a configuration j^v , which cannot be obtained from any state of the j^{v-2} configuration, by adding a nucleon pair coupled to $J_0=0$ and antisymmetrizing. The number of nucleons v is the seniority of that state in the j^v configuration and of all states obtained from it by adding pairs coupled to $J_0=0$ and antisymmetrizing. States with different seniorities are orthogonal to each other. The seniority v can distinguish between states with the same value of J (we shall not consider more complicated cases where there are several states with the same J and the same v).

A two-body operator intimately connected with the seniority scheme was defined by Racah (20). This is a scalar operator, and its eigenvalues are given by

$$\langle j^2 J | q_{12} | j^2 J \rangle = (2j+1)\delta_{J0} \quad 8.$$

It vanishes for $v=2$ and is different from zero only in the state $J=0$ ($v=0$). The factor $2j+1$ is for normalization. The operator

$$Q = \sum_{i < k}^n q_{ik}$$

is diagonal in the seniority scheme, and its eigenvalues which depend only on n and v (but not on J) are given by

$$Q(n, v) = \langle j^n v J | Q | j^n v J \rangle = (n - v)(2j + 3 - n - v)/2 \quad 9.$$

As can be seen, the normalization factor $2j+1$ was introduced to make $Q(n, v)$ have integral eigenvalues. The quantity Q measures the extent to which nucleons are paired in $J=0$ states. It is not simply equal to $(n-v)(2j+1)/2$ when there are $(n-v)/2$ pairs because of the Pauli principle which does not allow several pairs to be independent of each other. In the following we shall make use of this operator.

The state with $J=0$ of the j^2 configuration has, by definition, $v=0$. Such a state appears in all j^n configurations with n even. Other states with $J=0$ may occur, but they have higher v ; e.g., a $J=0, v=4$ state appears in the $g_{7/2}^4$ configuration. The states $J=2, 4, 6 \dots$ of the j^2 configuration have $v=2$. The state $J=j$ of a single nucleon has $v=1$; such a state (with $J=j, v=1$) appears in all j^n configurations with n odd. We shall see that states with $J=j, v=1$ have in some way a single-nucleon character in contrast to other states with $J=j$ (like the $J=9/2, v=3$ state of the $g_{7/2}^3$ configuration). We can thus summarize Mayer's finding (27) on the ground state spins by saying that ground states have the lowest seniorities. The seniority scheme is a very good one for calculations of the c.f.p. of the wave functions and thus of energies. In the next section we shall discuss the results of such calculations in more detail. First, we have to consider the coupling scheme for the case of protons and neutrons outside closed shells.

The next simple case of many-nucleon configurations is that in which protons and neutrons occupy different unfilled shells. The states can be uniquely defined by specifying the states of the proton configuration and the neutron configuration. If the m protons are in the j shell and the n neutrons in the j' shell, the states of the system can be built up by coupling a state of the j^m -proton configuration, with a definite J_p (and v_p), to a state of the j'^n -neutron configuration, with J_n (and v_n), to give a state with a definite J . This gives a well-defined eigenstate of T only if the neutron j shell is closed. Excited states, where a spin- j neutron is excited to a higher orbit, need more careful handling. It should be further remembered that a state built up with definite J_p and J_n need not be an eigenstate of the Hamiltonian. Mutual interactions between spin- j protons and spin- j' neutrons will admix such states. An eigenstate of the Hamiltonian with a definite J will thus be, in general, a linear combination of several states defined by their J_p and J_n , the amplitudes of which are determined by the interaction. In Section V we shall see examples of such cases.

In the general case of protons and neutrons outside closed shells, the situation is more complicated. The proton configuration and the neutron configuration are not defined in a state with a given T , the wave function of which is antisymmetrized. We can construct well-defined states only by coupling antisymmetric states of the various j configurations involved with given J and T (and other quantum numbers α which may be necessary). Thus, a state with a total J and total T will be defined in the case of two j configurations $j_1^{n_1}$ and $j_2^{n_2}$ by giving the $\alpha_1 J_1 T_1$ quantum numbers of the $j_1^{n_1}$ configurations and $\alpha_2 J_2 T_2$ of the $j_2^{n_2}$ configurations. The J_1 and J_2 should be coupled to J , as well as T_1 and T_2 to T . States thus obtained may not be eigenstates of the Hamiltonian, but they furnish a well-defined scheme to work with. The wave functions should now be antisymmetrized between nucleon numbers between the two j configurations, but this will not change the situation. Every state constructed from antisymmetric states in the two j configurations will be an allowed state. Moreover, matrix elements of single-particle operators have the same value whether calculated with the antisymmetrized wave functions or with the wave functions before the antisymmetrization between the two j configurations (provided, of course, that the wave functions of the $j_1^{n_1}$ configuration and the $j_2^{n_2}$ configuration are properly antisymmetrized). Also, two-particle operators

$$\sum_{i=1}^{n_1} \sum_{k=1}^{n_2} g_{ik}$$

which connect nucleons from the two j configurations can be obtained without the antisymmetrization between the two j configurations. The matrix elements can be first expressed as matrix elements in the two-nucleon jj' configuration, but the two-nucleon wave functions used in calculating these matrix elements should be antisymmetrized. We shall see that the only case where the definition and the construction of antisymmetric states is more involved is the j^n configuration of equivalent nucleons (i.e. protons and neutrons in the same j orbit). We turn now to this case.

The wave functions in the two-nucleon j^2 configuration are very simple. As mentioned already, the states with even J are antisymmetric in the space and spin co-ordinates. Therefore, they should be multiplied by the symmetric $T=1$ wave function of the isospin co-ordinates. On the other hand, the states with odd values of J are symmetric in the space and spin co-ordinates. These wave functions should be multiplied by the antisymmetric $T=0$ isospin function. In the case of three or more nucleons, the wave functions are no longer products of ordinary and isospin functions. To build antisymmetric wave functions in the j^n configurations, we can proceed as in the case of identical nucleons. Using c.f.p., we can write down the normalized antisymmetric wave function with a definite J and T as follows

$$\psi(j^n \alpha T J) = \sum_{\alpha_1 T_1 J_1} (j^{n-1}(\alpha_1 T_1 J_1) j T J | j^n \alpha T J) \psi(j^{n-1}(\alpha_1 T_1 J_1) j_n T J) \quad 10.$$

In this expansion the states of the j^{n-1} configuration are antisymmetric and characterized by $T_1 J_1$ and additional quantum numbers α_1 if necessary. The

n th nucleon spin vector j_n is coupled to J_1 to give the total J , and its isospin t_n is coupled to T_1 to give the total isospin T . It should be remembered that the n th nucleon is generally not in a well-defined state of charge. These wave functions are easy to work with if used for calculation of matrix elements of single-particle as well as two-body operators. Equations 6 and 7 hold here with the necessary modifications and therefore we shall not repeat them.

We shall now briefly describe the seniority scheme in the present case. As for identical nucleons, this is a very useful scheme which furnishes some of the additional quantum numbers α that are necessary to define the various states uniquely. Also, we here consider states of the j^n configuration obtained from corresponding states in the j^{n-2} configuration by adding a pair of nucleons coupled to $J=0$ and antisymmetrizing. Such states obtained one from the other will be defined to have the same seniority. A state with a definite J and T of the j^n configuration, which cannot be obtained by adding a pair with $J=0$ of the j^{n-2} configuration, is defined to have the seniority v . A pair with $J=0$ does not change the total spin J of the state; so all states with the same seniority, built by consecutive additions of pairs coupled to $J=0$ and antisymmetrizations, have the same spins J . However, now the isospin has to be considered also. A pair with $J=0$ must have $T=1$, and the adding of such a pair may change the value of T . Therefore, states with the same v (and J) need not have the same isospin T . At least one other quantum number is necessary. This is the value of the isospin in the state of the j^n configuration from which the state considered in the j^n configuration (specified by T and by the same J) was obtained by successively coupling $(n-v)/2$ pairs with $J=0$ (and $T=1$). This isospin of the state in the j^n configuration is called the reduced isospin (28) and is denoted by t .

The specific cases discussed for identical nucleons will now be given definite values of t . First, the $J=0, v=0, T=1$ state of the j^2 configuration has also, by definition, $t=0$. The other states of the j^2 configuration with even values of $J, v=2, T=1$, have $t=1$ (in general, if $v=n, T$ must be equal to t , by definition). Similarly, the j^2 states with odd J have $T=t=0$. The j state with $v=1$ has $T=t=1/2$. In the j^3 configuration there are generally two states with $J=j, v=1, t=1/2$, one with $T=3/2$, and one with $T=1/2$.

We conclude this section by considering the operator Q defined above. In the present case it still does not depend on J but depends on T and t , naturally. Thus, Q is diagonal in the seniority scheme and its eigenvalues are given (15, 29) by

$$Q(n, v, t, T) = \langle j^n v t T J | Q | j^n v t T J \rangle \\ = (n-v)(4j+8-n-v)/8 - T(T+1) + t(t+1) \quad 11.$$

In the following, we shall use Q also in j^n configurations with protons and neutrons.

V. ENERGIES OF NUCLEAR STATES

The total energy of the nucleus (its binding energy) is the sum of the following terms. First, we have the kinetic and interaction energy of nucleons

in the closed shells. This energy is, according to our assumptions, independent of the extra nucleons outside closed shells. It is equal to the same constant in the groups of nuclei to be considered and can be omitted from our considerations. The kinetic energy of an extra nucleon is obviously independent of the orientation of its spin in space. Also, the interaction of an extra nucleon with nucleons in closed shells has this property because of the spherical symmetry of the closed shells. Thus, the sum of kinetic energies of the extra nucleons and their interaction with the closed shells depends only on the occupation of the various orbits. It is the same in all states of the same configuration of extra nucleons, obtained by the different couplings of the spins. In other words, this is a sum of single-nucleon energies. The last term in the total energy is the mutual interaction of the extra nucleons. The calculation of this interaction energy is the subject of this section.

We first consider protons and neutrons in different unfilled shells. Let us assume, for the sake of simplicity, that there is only one neutron in the j' orbit whereas there are m protons in the j orbit (the neutron j shell is taken to be completely filled). The j^m -proton configuration can be in a certain state with spin J_1 which must be coupled with j' to form the state with the total spin J . There may be another state with the same spin J obtained by coupling to j' the spin J'_1 of another proton state. The proton-neutron interaction will generally have a nonvanishing matrix element between these two states. Therefore, the eigenstates of the Hamiltonian will be linear combinations of these two states, determined by diagonalizing the energy matrix. For example, in the ground configuration of $^{18}\text{A}_{21}^{39}$, the protons outside closed shells are in the $d_{3/2}^2$ configuration whereas the extra neutron is in the $f_{7/2}$ shell. The ground state spin is $J = 7/2$. This spin value can be obtained either by coupling the proton state $J_1 = 0$ with $j' = 7/2$ or by coupling the other proton state $J'_1 = 2$ with $j' = 7/2$.

The diagonal as well as the nondiagonal matrix elements of the proton-neutron interaction in the scheme of wave functions defined by the proton spin J_1 are given as follows in terms of c.f.p. of the proton configuration (30)

$$\begin{aligned}
 & \langle j^m(\alpha_1 J_1) j' J | \sum_{k=1}^m V_{k,m+1} | j^m(\alpha'_1 J'_1) j' J \rangle \\
 &= m \sum_{\alpha_2 J_2 J_0} (j^{m-1}(\alpha_2 J_2) j J_1 | j^m \alpha_1 J_1) (j^{m-1}(\alpha_2 J_2) j J'_1 | j^m \alpha'_1 J'_1) [(2J_1 + 1)(2J'_1 + 1)]^{1/2} \\
 & \cdot \begin{Bmatrix} J_2 & j & J_1 \\ j' & J & J_0 \end{Bmatrix} \begin{Bmatrix} J_2 & j & J'_1 \\ j' & J & J_0 \end{Bmatrix} (2J_0 + 1) \langle jj' J_0 | V | jj' J_0 \rangle
 \end{aligned} \tag{12}$$

Here $V_{k,m+1}$ is the effective interaction between the k th proton and the neutron, which is the $(m+1)$ th particle. The matrix element on the right-hand side of Equation 12 is the effective interaction between a proton in the j orbit and the neutron in the j' orbit. If we know the interaction energy within the proton configuration, we can write down, with the help of Equation 12, the complete interaction matrix and diagonalize it. In more complicated cases, when n neutrons are in the j' orbit, there are similar expressions

for the matrix elements of the interaction in the scheme where the protons are in a state with a definite J_1 and the neutrons in a state with a definite J_2 . We shall not present here the analogous expressions but refer the reader to (30).

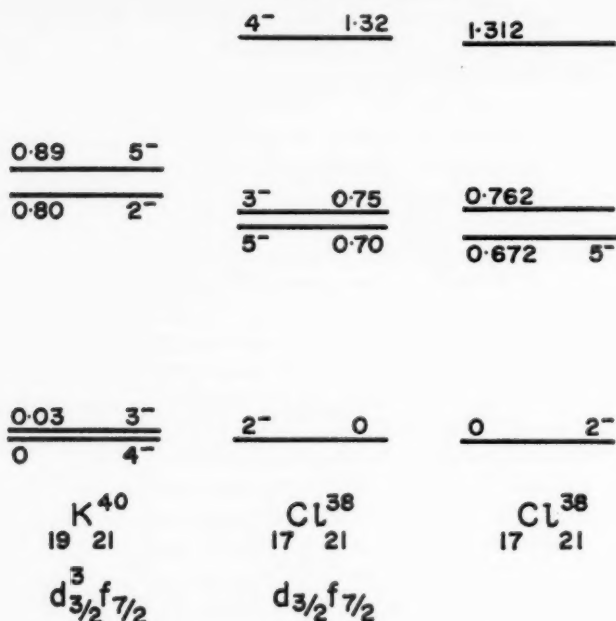
We shall now illustrate this method by a simple example. Consider the nuclei $^{17}\text{Cl}_{21}^{38}$ and $^{19}\text{K}_{21}^{40}$. In the first, there is only one $d_{3/2}$ proton so that there is only one state with $J_1=3/2$ in the proton configuration. In the other nucleus the situation is very similar. Three $d_{3/2}$ protons can couple only to one state with $J_1=3/2$ since four $d_{3/2}$ protons form a closed shell. The resultant spins in the two cases, obtained by coupling $J_1=3/2$ to $J_2=7/2$, are $J=2, 3, 4, 5$. Using Equation 12, we can express the interaction energies in the various states of K^{40} in terms of those in Cl^{38} (and vice versa). Since the configuration is the same in these states, the level spacings in each case are equal to differences of the interaction energies. We can thus obtain from the known levels of K^{40} the level spacings in Cl^{38} (31, 32). The results obtained are shown in Figure 3. It is seen that the agreement obtained is very good. No further assumptions were made in this calculation other than using jj coupling with two-body forces and taking the same values for the matrix elements in the two cases. The agreement obtained indicates that not only in K^{40} but even in Cl^{38} jj coupling is very good, presumably since the proton configuration in the latter nucleus is of closed $d_{5/2}$ and $s_{1/2}$ shells and a single $d_{3/2}$ proton. A more detailed discussion of $d_{3/2}^m f_{7/2}^n$ configurations is given in (30).

This case may serve to illustrate a general feature of nuclear spectra. In Cl^{38} we have a $d_{3/2}$ proton and an $f_{7/2}$ neutron configuration whereas in K^{40} we have a $d_{3/2}$ proton "hole" and an $f_{7/2}$ neutron configuration. With a potential (non-exchange) interaction (Wigner force), the level spacings in a proton-hole neutron configuration are the same as in the corresponding proton-neutron configuration, but the order is reversed. We see in Figure 3 that this is not the case. The order is drastically changed but is not exactly reversed. This shows how arbitrary are general coupling rules which give the ground state spin of an odd-odd nucleus. The exact relation between particle-hole and particle-particle interaction energies is given in (32) by

$$\langle j^{-1}J | V | j^{-1}J \rangle = K - \sum_{J_0} \begin{Bmatrix} j & j' & J \\ j & j' & J_0 \end{Bmatrix} (2J_0 + 1) \langle jj'J_0 | V | jj'J_0 \rangle \quad 13.$$

where K is a constant independent of J . The level order and spacings in a proton-hole neutron-hole configuration are the same as in the corresponding proton-neutron configuration.

These relations between special configurations can be used to give results in a very simple case. In $^{18}\text{P}_{17}^{32}$ there is an $s_{1/2}$ proton and a $d_{3/2}$ neutron. The levels of this configuration have $J=1$ and $J=2$. The ground state of P^{32} has $J=1$, and a $J=2$ level is found 0.077 Mev above it which probably belongs to the same configuration. In $^{18}\text{P}_{19}^{34}$ there is an $s_{1/2}$ proton and a $d_{3/2}$ neutron hole. However, since $s_{1/2}^2$ is a closed proton shell, an $s_{1/2}$ proton is at the same



EXPERIMENTAL CALCULATED EXPERIMENTAL

FIG. 3. Energy levels of Cl³⁸ and K⁴⁰ (in Mev).

time an $s_{1/2}$ proton hole. Thus, the ground-state configuration of P³⁴ can be described as having an $s_{1/2}$ proton hole and a $d_{3/2}$ neutron hole. It should therefore have the $J=1$ and $J=2$ levels in the same order and with the same spacing as in P³². The ground state spin of P³⁴ is indeed known to be $J=1$. Since there is some evidence (from stripping, etc.) that jj coupling provides a good description of P³², it is very interesting to find out whether a $J=2$ level is really there about 0.077 Mev above the ground state of P³⁴.

We consider next the energy levels of the j^n configuration of identical nucleons. In the case $j=1/2$ there are only the single-nucleon and the two-nucleon configurations, each with only one level. In the case $j=3/2$ there are only two levels in the $(3/2)^2$ configuration, with $J=0$ and $J=2$. However, the $(3/2)^3$ configuration is a hole configuration and the $(3/2)^2$ configuration is a closed shell.

We consider in detail the case of $j=5/2$. If we denote by C the single j -nucleon energy (its kinetic energy plus its interaction with the closed shells), the contribution of the single-nucleon energies to all states of the j^n configuration is the same and is equal to nC . The interaction energies in the J states of the $(5/2)^2$ configuration will be denoted by V_J . There are only three states, with $J=0$, $J=2$ and $J=4$. The interaction energy in the $(5/2)^n$ con-

figuration is a linear combination of the V_J . These linear combinations can be calculated in terms of the c.f.p. by using Equation 7. However, we shall make use here of a simpler method designed by Racah (33). It is clear that the interaction energy can be calculated with any form of the two-body interaction provided its eigenvalues in the $(5/2)^2$ configuration are equal to the given V_0 , V_2 , and V_4 . We can write down such a simple interaction whose eigenvalues are simple and known in the j^n configuration. Consider the two-body interaction

$$a + b2(j_1 \cdot j_2) + cq_{12} \quad 14.$$

where q_{12} has been defined in Equation 8. Its eigenvalues in the states of the j^n configuration with definite J and v are simply

$$an(n-1)/2 + b[J(J+1) - n_j(j+1)] + cQ(n, v) \quad 15.$$

The constants a , b , and c must be determined so that they will give in the j^2 configuration the values V_J . Thus, in the case $j=5/2$, the equations

$$a - (35/2)b + 6c = V_0$$

$$a - (23/2)b = V_2$$

$$a + (5/2)b = V_4$$

determine a , b , and c . The total energy (apart from that of the closed shells) of every state of the $(5/2)^n$ configuration is given, according to Equation 9, by

$$E[(5/2)^n v J] = nC + an(n-1)/2 + b[J(J+1) - (35/4)n] + c(n-v)(8-n-v)/2 \quad 16.$$

The energy differences of the levels are obviously given only by the last two terms. We see that in this case we do not need the c.f.p. to calculate the energies.

As an example, we shall consider the first $1d_{5/2}$ shell in the oxygen isotopes. In O^{18} there are 2^+ and 4^+ levels at 1.98 and 3.55 Mev above the 0^+ ground state. We assume, for the sake of simplicity, that this is the level scheme of the pure neutron $d_{5/2}^2$ configuration. We can then determine the constants b and c from $-14b = V_2 - V_4$ and $-6b + 6c = V_0 - V_2$. Taking the binding energy to be a positive number, b turns out negative and has the value $b = -0.112$ Mev. For the other constant we obtain $c = 0.218$ Mev. The energy differences in the $d_{5/2}^3$ configuration, expected for O^{19} , are given by

$$b[J(J+1) - 105/4] + c(3-v)(5-v)/2 \quad 17.$$

There are three states, one with $v=1$, $J=5/2$, and two $v=3$ states with $J=3/2$ and $J=9/2$. One finds that the ground state has $J=5/2$, the $J=3/2$ level should be 0.31 Mev and the $J=9/2$ level 2.66 Mev above it. No levels are known in O^{19} above 1.5 Mev, but there is a $3/2^+$ level 0.10 Mev above the $5/2^+$ ground state. We can thus identify the ground and first excited states of O^{19} as the $J=5/2$ and $J=3/2$ states of the $d_{5/2}^3$ configuration. We see that starting from O^{18} and making the simplest possible assumptions, we can

predict a low-lying $3/2^+$ level in O^{19} and even calculate fairly well its energy above the ground state. In O^{20} there should be the $d_{5/2}^4$ configuration which has two holes in the closed $d_{5/2}$ shell. The level order and spacings should then be equal to the $d_{5/2}^2$ case of O^{18} . Hence a 2^+ level is expected in O^{20} about 2 Mev and a 4^+ level about 3.5 Mev above the ground state. A 2^+ level has recently been found in O^{20} at 1.7 Mev above the ground state (34).

The trick we used in the case of $j=5/2$ cannot work for higher j values. If j is bigger than $5/2$ there are more than three even- J levels in the j^2 configuration whereas the interaction in Equation 14 has only three independent constants. Still, by using a similar method, we can calculate averages of groups of states with the same seniority v (33). We define such averages as

$$\sum_J (2J+1) \langle j^n v J | V | j^n v J \rangle / \sum_J (2J+1)$$

where the summation is over all states with the same seniority v . It turns out that such averages can be obtained by using, instead of the real interaction in the j^2 configuration with eigenvalues V_J , another two-body interaction. This other interaction has the same eigenvalues in all states of the j^2 configuration with seniority $v=2$. The eigenvalues are equal to the average of the original interaction in the states with $v=2$. Thus, the eigenvalue in the state $v=0, J=0$ is V_0 whereas for $v=2, J$ even, the eigenvalue is

$$\bar{V}_2 = \sum_{J=2, \text{ even}}^{2j-1} (2J+1) V_J / \sum_{J=2, \text{ even}}^{2j-1} (2J+1).$$

Such an interaction is given simply by

$$a + b q_{12} \quad 18.$$

where $a + (2j+1)b = V_0$ and $a = \bar{V}_2$. Therefore, the averages in the j^n configuration are given by

$$\bar{E}(j^n v) = nC + an(n-1)/2 + b(n-v)(2j+3-n-v)/2 \quad 19.$$

This expression is not yet of much help since it gives only positions of "centers of mass" of groups of levels. However, it gives all the information for states with seniority $v=0$ since there is only one such state with $J=0$ in the j^n configuration with n even. Similarly, there is only one state with $v=1$ (and $J=j$) in the j^n configuration with n odd. In these cases, Equation 19 gives directly the total energy of the state considered (apart from the energy of the closed shells).

The states with $v=0, J=0$ and $v=1, J=j$ are generally the ground states of nuclei, and so Equation 19 gives the binding energy of the nucleus considered (minus the binding energy of a nucleus with the closed shells only). Equation 19 becomes in the case of $v=0$

$$E(j^n v=0 J=0) = nC + \frac{n(n-1)}{2} (a-b) + (2j+2)b \frac{n}{2}$$

In the case of $v=1$ it becomes

$$E(j^n v=1 J=j) = nC + \frac{n(n-1)}{2}(a-b) + (2j+2)b \frac{n-1}{2}$$

We see that the last term is a step function or a pairing term. We introduce the function $[n/2]$ which is equal to $n/2$ for even n and to $(n-1)/2$ for odd n . The binding energy of a nucleus (minus that of the closed shells) with only protons (or neutrons) outside closed shells can now be written in the more general form

$$nC + \alpha n(n-1)/2 + \beta[n/2] \quad 20.$$

where C , α , and β are constants over the shell [$\alpha=a-b$ and $\beta=(2j+2)b$]. This form of the energy is independent of the particular choice of the two-body interaction. Only the constants can have different values, but there are always a linear term, a quadratic term, and a pairing term with constant coefficients. It is worthwhile to mention that if the single-nucleon energy C is not a constant but varies slightly with n , the part of its change which is linear in n is absorbed into the coefficient α . On the basis of agreement with experiment, it is practically impossible to distinguish this effect if it happens. The expression in Equation 20 is exact if the seniority is a good quantum number in the j shell (this is true for any interaction if $j \leq 7/2$). If the seniority is not a good quantum number, Equation 20 is only the expectation value in the state of lowest seniority.

We make use here of Equation 20 to analyze the binding energies in the $1f_{7/2}$ shell (35). We try to fit the binding energies of the calcium isotopes minus the binding energy of Ca^{40} with this expression. We do the same also for nuclei in which the protons are in the $f_{7/2}$ shell and the neutrons form the closed shell of 28. In each case we determine the parameters C , α , and β so as to reproduce the measured binding energies best. Having obtained these best values (by a least square fit), we insert them into Equation 20 and obtain the calculated values. These should be compared to the experimental energies in order to see the agreement obtained. The results are presented in Table I. It is obvious that the agreement is very good. The parameters which give the best fit (with their statistical errors) are the following:

For the neutron configurations

$$C = 8.379 \pm 0.048, \quad \alpha = -0.230 \pm 0.008, \quad \beta = 3.330 \pm 0.119 \text{ Mev}$$

For the proton configurations

$$C = 9.695 \pm 0.043, \quad \alpha = -0.781 \pm 0.007, \quad \beta = 3.114 \pm 0.093 \text{ Mev}$$

The single-nucleon energy C in the two cases is positive since a single neutron outside Ca^{40} and a single proton outside Ca^{48} are actually bound. The constant β can be described as the pairing energy or pairing term (the interaction energy of the $f_{7/2}^2$ configuration is $\alpha+\beta$). It turns out to be considerable in magnitude and positive (attractive). Its magnitude is the

TABLE I
BINDING ENERGIES IN $f_{7/2}^n$ CONFIGURATIONS

Nucleus	Binding energy*		Nucleus	Binding Energy†	
	Experi- mental	Calculated		Experi- mental	Calculated
$^{20}\text{Ca}_{21}^{41}$	8.36	8.38	$^{21}\text{Sc}_{28}^{40}$	—	9.65
$^{20}\text{Ca}_{22}^{42}$	19.83	19.86	$^{22}\text{Ti}_{28}^{50}$	21.78	21.72
$^{20}\text{Ca}_{23}^{43}$	27.75	27.78	$^{23}\text{V}_{28}^{51}$	29.82	29.86
$^{20}\text{Ca}_{24}^{44}$	38.89	38.80	$^{24}\text{Cr}_{28}^{52}$	40.34	40.32
$^{20}\text{Ca}_{25}^{45}$	46.31	46.26	$^{25}\text{Mn}_{28}^{53}$	46.90	46.90
$^{20}\text{Ca}_{26}^{46}$	56.72	56.82	$^{26}\text{Fe}_{28}^{54}$	55.75	55.80
$^{20}\text{Ca}_{27}^{47}$	—	63.81	$^{27}\text{Co}_{28}^{55}$	60.85	60.81
$^{20}\text{Ca}_{28}^{48}$	73.95	73.93	$^{28}\text{Ni}_{28}^{56}$	—	68.17

* From these the binding energy of Ca^{40} was subtracted. All energies are in Mev.

† From these the binding energy of Ca^{48} was subtracted.

same, within the statistical errors, for protons and neutrons. The parameter α turns out to be negative. This is in agreement with the well-known fact that nuclei to which more and more nucleons of the same kind are added become less and less stable. It is a requirement of any effective interaction that the parameter α must be negative. Although it is rather small in absolute magnitude, it is very effective since it is multiplied by the large factor $n(n-1)/2$. The values of α in the case of protons and neutrons are rather different. This difference probably arises from the electrostatic repulsion of the protons which tends to increase the absolute magnitude of the negative α . From the point of view of the "mass surface," the expression in Equation 20 describes very accurately two parabolas, one for odd A and the other for even A . These parabolas are obtained, as we saw, from the shell model with no additional assumptions.

As already mentioned, the parameter α does not give any information about level spacings in the j^2 configuration. The parameter β , on the other hand, is related to the position of the center of mass of the levels with $J=2, 4, \dots, 2j-1$ above the $J=0$ ground state. Denoting the average interaction energy in these $v=2$ levels by \bar{V}_2 we readily obtain

$$V_0 - \bar{V}_2 = \beta(2j+1)/(2j+2) \quad 21.$$

In the $f_{7/2}$ shell we obtained, for β , roughly 3.2 Mev. Therefore, the center of mass of the $J=2, 4, 6$ levels must be about 2.84 Mev above the ground state. This is in good agreement with the detailed level schemes found in that region (36, 37).

We consider now the j^n configuration of protons and neutrons. The energies of the various states can be calculated in terms of the appropriate

c.f.p. according to the analogue of Equation 7. However, we shall also use here techniques similar to those for identical nucleons (33). To consider a definite case, let us take $j=3/2$. The $(3/2)^2$ configuration has four states with $J=0, 1, 2, 3$. The state with $J=0$ has $v=0, t=0, T=1$, the one with $J=2$ has $v=2, t=T=1$, whereas those with $J=1, 3$ have $v=2$ and $t=T=0$. All interaction energies in the $(3/2)^n$ configuration are linear combinations of the interaction energies V_J in the $(3/2)^2$ states. Thus, we can replace the effective interaction by any two-body interaction with the eigenvalues V_J . In analogy to Equation 14 we consider the interaction

$$a + b2(t_1 \cdot t_2) + cq_{12} + d2(j_1 \cdot j_2) \quad 22.$$

Its eigenvalues in the states of the j^n configuration with definite v, t, T , and J are given by

$$an(n-1)/2 + b[T(T+1) - 3n/4] + cQ(n, v, t, T) + d[J(J+1) - nj(j+1)] \quad 23.$$

The constants a, b, c , and d are determined by the eigenvalues V_J of the $(3/2)^2$ configuration. If C denotes the single-nucleon energy, the total energies of the states of the $(3/2)^n$ configuration (apart from that of the closed shells) are given by

$$\begin{aligned} E((3/2)^n v t T J) = nC + an(n-1)/2 + b[T(T+1) - 3n/4] \\ + c[(n-v)/4(14-n-v) - T(T+1) + t(t+1)] \\ + d[J(J+1) - 15n/4] + C.E. \end{aligned} \quad 24.$$

The last term is the Coulomb energy due to the protons. We shall not go in detail into the calculation of this term. The best way to obtain its value is from mirror nuclei (13, 15). We can bring this expression to a more compact form as follows

$$\begin{aligned} nC + \frac{n(n-1)}{2} \alpha + \left[T(T+1) - \frac{3}{4} n \right] \beta + \left[\frac{v(v-4)}{4} + t(t+1) + \frac{5}{2} (n-v) \right] c \\ + \left[J(J+1) - \frac{15}{4} n \right] d + C.E. \end{aligned} \quad 25.$$

where $\alpha = a - c/2$ and $\beta = b - c$. This expression is exact for any type of two-body interaction (with $j=3/2$ the seniority is a good quantum number). It is clear that only β, c , and d determine the level spacings of the various configurations. The parameters C and α enter only into binding energy calculations (14).

It is rather difficult to find immediate use for the explicit formula in Equation 25. In the $d_{3/2}$ shell there is not enough information about level spacings. In the other possible case, the $p_{3/2}$ shell, there is the difficulty that jj coupling becomes good only towards the end of the shell. Still, if more information becomes available, Equation 25 relates all energy levels in the $d_{3/2}^n$ configurations and therefore can be very useful. We shall now obtain rough values for the interaction parameters in the $p_{3/2}$ shell in order to examine the predictions of the model at least about the level order in the various nuclei.

Since jj coupling is only approximately good in the $p_{3/2}$ shell, we shall use only tentative values of the V_J , all taken directly from the $p_{3/2}^{-2}$ configuration of B^{10} . This yields (in Mev) $V_3 - V_1 = 10d = 0.72$, $V_3 - V_0 = -2\beta - 6c + 12d = 1.74$, and $V_3 - V_2 = -2\beta - 2c + 6d = 5.16$. From these equations we obtain

$$\beta = -3.29, \quad c = 0.95, \quad \text{and} \quad d = 0.07 \text{ Mev} \quad 26.$$

The $p_{3/2}^n$ spectra of Be^{10} and C^{10} are the same as the $T=1$ spectrum of B^{10} . The $V_0 - V_2$ separation in Be^{10} and C^{10} is equal with a good accuracy to that of B^{10} . This fact indicates the validity of charge independence for those nuclei. The ground state of B^{11} (or C^{11}) must have $J=3/2$ since there is one hole in the closed $p_{3/2}$ shell. For $n=5$ (Be^9 and B^9), using the values of β , c , and d of Equation 26, it becomes clear from Equation 25 that the ground state will have $T=1/2$. Of the four states with $T=1/2$, the one with $J=3/2$ is the lowest (as observed) since it has $v=1$, $t=1/2$ whereas the states with $J=1/2, 5/2, 7/2$ have $v=3$, $t=3/2$. More interesting are the nuclei with $n=4$, i.e. Li^8 and Be^8 . The ground state isospin of Li^8 is $T=1$ (the term with β contributes more than 13 Mev difference between states with $T=1$ and $T=2$). There are three states with $T=1$ with spins $J=2$, $J=3$, and $J=1$. Since the $J=2$ state has $t=1$, the term with c in Equation 25 contributes 1.9 Mev difference between the $J=2$ state and the other two which have $t=0$. This difference is much bigger than the contribution of the term with d , so that the state $J=2$ is obtained as the ground state of Li^8 . Using Equation 25 and only the information from B^{10} , we can thus understand why the ground state spin of Li^8 is $J=2$. In Be^8 the ground state has the minimum value of isospin which is $T=0$. Of the states with $T=0$, the ground state has $J=0$, $v=0$. It follows from Equation 25 that the first excited $T=0$ state should be the $J=2$, $v=2$ level at the same height above the $J=0$ state as in B^{10} . Actually a 2^+ level is observed in Be^8 at 2.90 Mev above the ground state (as compared to 3.37 Mev in B^{10}). There are two more states with $T=0$ with spins $J=4$ and $J=2$. These states, however, should lie much higher than the $J=2$, $v=2$ level since they have $v=4$ and $t=0$. The term with c in Equation 25 contributes 9.5 Mev to the separation of these levels and the ground state. Experimentally, a 4^+ level is found in Be^8 at ~ 11.7 Mev above the ground state. It is questionable whether these simple considerations are applicable to a nucleus like Be^8 which is unstable against emission of a large fraction of its constituent particles. Nevertheless, the semiquantitative agreement obtained with the simple shell-model calculations is interesting.

As with identical nucleons, a simple expression, analogous to Equation 25, can be obtained even for higher values of j , which, however, gives only the average positions of groups of states with the same T , v , and t . These averages, or rather centers of mass, can be obtained with a simplified two-body interaction. It is defined as having in the j^2 configuration with $J=0$ the eigenvalue V_0 ; in all states with even $J>0$ (and $v=2$, $t=1$) the same eigenvalue

$$\bar{V}_2 = \sum_{J=2, \text{ even}}^{2j-1} (2J+1)V_J / \sum_{J=2, \text{ even}}^{2j-1} (2J+1)$$

and in all states with odd $J(v=2, t=0)$ the same eigenvalue

$$\bar{V}_1 = \sum_{J=1, \text{ odd}}^{2j} (2J+1)V_J / \sum_{J=1, \text{ odd}}^{2j} (2J+1)$$

Such an interaction can be written simply as

$$a + b 2(t_1 \cdot t_2) + cq_{12} \quad 27.$$

where $a + (1/2)b + (2j+1)c = V_0$, $a + (1/2)b = \bar{V}_2$ and $a - (3/2)b = \bar{V}_1$. The averages in the j^n configuration are thus given by

$$\begin{aligned} \bar{E}(j^n v t T) = nC + \frac{n(n-1)}{2} a + \left[T(T+1) - \frac{3}{4} n \right] b \\ + \left[\frac{n-v}{4} (4j+8-n-v) - T(T+1) + t(t+1) \right] c + \text{C.E.} \end{aligned}$$

We rewrite this expression in a more compact form

$$\begin{aligned} nC + \frac{n(n-1)}{2} \alpha + \left[T(T+1) - \frac{3}{4} n \right] \beta \\ + \left[\frac{v(v-4)}{4} + t(t+1) + \frac{2j+2}{2} (n-v) \right] c + \text{C.E.} \quad 28. \end{aligned}$$

Where $\alpha = a - c/2$ and $\beta = b - c$.

The interaction energy is diagonal in the seniority scheme for $j \leq 3/2$ for any form of the interaction. With higher j , the seniority may still be a good quantum number for the effective interaction. In these cases, Equation 28 gives the actual positions of the centers of mass. If the seniority is not a good quantum number, the positions of levels may shift because of matrix elements which are nondiagonal in the seniority scheme. As with identical particles, there are cases in which there is only one state of lowest seniority in the j^n configuration with a given T . If n is even, this is the state with $J=0$, $v=0$, $t=0$; if it occurs for the value of T considered, and if n is odd, this is the state with $J=j$, $v=1$ and $t=1/2$. The expression in Equation 28 gives directly the energies of these states.

The states of lowest seniority are generally the ground states of even-even and even-odd nuclei. Therefore, Equation 28 gives a closed formula for the binding energy of nuclei (if the seniority is a good quantum number). In such cases, the term with c in Equation 28 has the simple form $cn(2j+2)/2$ for even n and $c(n-1)(2j+2)/2$ for odd n . This pairing term has the same form of a step function as in the case of identical particles. We present here the results of a least-squares analysis which gives the best values of the parameters C , α , β , and c in the $d_{3/2}$ shell (14). The calculated values in Table II were obtained from Equation 28 by substituting the best values of the parameters. These best values are found to be

$$C = 8.66, \quad \alpha = 0.12, \quad \beta = -1.82, \quad (2j+2)c = 3.52 \text{ Mev}$$

TABLE II
BINDING ENERGIES IN THE $d_{3/2}^n$ CONFIGURATIONS

Nucleus	Binding energy*		Nucleus	Binding energy*	
	Experi- mental	Calculated		Experi- mental	Calculated
$^{16}\text{S}_{17}^{33}$	8.65	8.66	$^{18}\text{A}_{17}^{35}$	19.69	19.58
$^{16}\text{S}_{18}^{34}$	20.05	20.04	$^{18}\text{A}_{18}^{36}$	34.96	34.83
$^{16}\text{S}_{19}^{35}$	27.07	27.12	$^{18}\text{A}_{19}^{37}$	43.79	43.96
$^{16}\text{S}_{20}^{36}$	36.97	36.97	$^{18}\text{A}_{20}^{38}$	55.54	55.82
$^{17}\text{Cl}_{16}^{33}$	2.42	2.38	$^{19}\text{K}_{18}^{37}$	36.88	37.00
$^{17}\text{Cl}_{17}^{34}$	13.75	13.77	$^{19}\text{K}_{19}^{38}$	48.88	48.86
$^{17}\text{Cl}_{18}^{35}$	26.46	26.29	$^{19}\text{K}_{20}^{39}$	61.96	61.85
$^{17}\text{Cl}_{19}^{36}$	35.03	35.10	$^{20}\text{Ca}_{19}^{39}$	54.32	54.44
$^{17}\text{Cl}_{20}^{37}$	45.39	45.23	$^{20}\text{Ca}_{20}^{40}$	70.29	70.17

* From these the binding energy of S^{32} was subtracted. All energies are in Mev.

As we see, the agreement obtained is quite good. It seems that ground states of nuclei between S^{32} and Ca^{40} can be adequately described as belonging to the $d_{3/2}^n$ configuration with effective two-body interactions. It is not clear, however, whether excited levels of the $d_{3/2}^n$ configurations can be obtained with the same effective forces. The pairing energy $(2j+2)c$ gives the position of the center of mass of the $J>0$ even levels above the $J=0$ ground state in the j^2 configurations. In the case $j=3/2$ there is only one such level, i.e., $J=2$. Therefore the V_0-V_2 spacing should be given according to Equation 21 by $\frac{4}{3}3.5=2.8$ Mev. In S^{34} and A^{38} , where the $d_{3/2}^2$ (or $d_{3/2}^{-2}$) configurations appear, there is a 2^+ level at 2.15 Mev above the ground state. Also, in A^{36} where according to Equation 25 the $J=2, v=2$ level should be at the same position as in the $d_{3/2}^2$ configuration, there is a 2^+ level at 2 Mev above the ground state. If these levels actually belong to the $d_{3/2}^n$ configuration, the agreement between 2.8 and 2.15 Mev is not very good. No definite conclusions can yet be drawn, but it may well happen that all $d_{3/2}^n$ states are subject to configuration interaction. In this case, a more detailed analysis is required to obtain quantitative agreement for ground states as well as for excited levels.

The last case to be described is that of excited configurations. We start from the configuration j^n of protons and neutrons outside closed shells and consider the configuration obtained by exciting one or more j nucleons into higher order orbits. For example, we consider the $j^m j'$ configuration. This is similar to the situation described at the beginning of this section where the m spin- j nucleons were protons and the j' nucleon a neutron. In the present case the j' nucleon can be either a proton or a neutron, and the states must be characterized by the values of the total isospin T (in addition to the total spin J). Still, matrix elements of the interaction are given by a formula

very similar to Equation 12 (38). The states with definite T and J are written down in a scheme where the j^m configuration is in a state with definite T_1 and J_1 . Equation 12 should only be augmented with the quantum numbers T , T_1 and T'_1 . These appear in the c.f.p. and also in Racah coefficients, etc., for the isospin part.

Several such excited configurations were analyzed. Among these are the $p_{1/2}^m s_{1/2}$ and the $p_{1/2}^m d_{5/2}$ configurations which occur in nuclei beyond C^{12} . These cases will be described in detail. We would like to present here the matrix elements of the interaction obtained from that analysis. The interaction parameters are defined by

$$\begin{aligned} V'_J &= \langle jj'T=1J | V | jj'T=1J \rangle, \\ V_J &= \frac{1}{2} [\langle jj'T=0J | V | jj'T=0J \rangle + \langle jj'T=1J | V | jj'T=1J \rangle] \end{aligned} \quad 29.$$

where V is the effective two-nucleon interaction. In the $p_{1/2}d_{5/2}$ configuration, J can have the values $J=2$ and $J=3$, whereas in the $p_{1/2}s_{1/2}$ configuration, only $J=0$ and $J=1$ appear. The values obtained for the various parameters (with their statistical errors) are

$$\begin{aligned} p_{1/2}d_{5/2}: V_2 &= 1.750 \pm 0.041, & V_3 &= 1.604 \pm 0.035, \\ V'_2 &= -0.486 \pm 0.048, & V'_3 &= 0.067 \pm 0.039 \text{ Mev} \\ p_{1/2}s_{1/2}: V_0 &= 1.115 \pm 0.050, & V_1 &= 0.972 \pm 0.035, \\ V'_0 &= -0.835 \pm 0.062, & V'_1 &= -0.172 \pm 0.032 \text{ Mev} \end{aligned} \quad 30.$$

The physical meaning of the V_J is the interaction between a j proton and a j' neutron (when the j -neutron shell is closed). These interactions are attractive. On the other hand, the interaction between two identical particles (two protons or two neutrons) is given by the V'_J and is generally repulsive. This feature is also clear from the qualitative behavior of nuclear binding energies. It seems that the only strong and attractive interaction between identical nucleons is the pairing term in Equation 20. We see the great similarity between the interaction constants in the two cases. The V_J with the even value of J is slightly more attractive than V_J with the odd value of J . On the other hand, V'_J with the even value of J is more repulsive than the V'_J with the odd value of J .

VI. ELECTROMAGNETIC TRANSITIONS AND MAGNETIC MOMENTS

The operator which couples the nucleons to the electromagnetic field is a single-particle (F -type) operator. Therefore, no electromagnetic transitions can occur between states of two configurations different by the orbits of more than one particle. The transition probability (inverse mean life) for a 2^l -pole transition (magnetic or electric) is given (2, 20) by

$$T(l) = \frac{1}{\hbar} \frac{8\pi(l+1)}{l[2l+1]!!^2} \left(\frac{E}{\hbar c} \right)^{2l+1} \frac{1}{2J+1} \sum_{\lambda MM'} |\langle \alpha T J M | \Omega_\lambda^{(l)} | \alpha' T' J' M' \rangle|^2 \quad 31.$$

Here $\Omega_\lambda^{(l)} = \sum_i \Omega_\lambda^{(l)}(i)$, and the summation extends over all particles. Explicit expressions for Ω are given below. The α, α' denote all other quantum

numbers which are necessary to define the states uniquely. The summation in Equation 31 can be carried out to give

$$\sum_{\lambda MM'} |\langle \alpha T J M | \Omega_{\lambda}^{(l)} | \alpha' T' J' M' \rangle|^2 = \langle \alpha T J || \Omega^{(l)} || \alpha' T' J' \rangle^2 \quad 32.$$

where the reduced or double-barred matrix element is defined in (22). The radiative width of a level is given by

$$\Gamma_{\gamma}(I) = \hbar T(I) = \frac{8\pi(l+1)}{l[(2l+1)!!]^2} \left(\frac{E}{\hbar c}\right)^{2l+1} \frac{1}{2J+1} \langle \alpha T J || \Omega^{(l)} || \alpha' T' J' \rangle^2 \quad 33.$$

The single-particle operator for magnetic 2^l -pole radiation is given (2) by

$$\Omega_{\lambda}^{(l)(\text{mag})} = \sqrt{l(2l+1)} \left\{ \frac{2}{l+1} g_l [Y_{l-1} \times l]_{\lambda}^{(l)} + g_s [Y_{l-1} \times s]_{\lambda}^{(l)} \right\} \left(\frac{e\hbar}{2mc}\right) r^{l-1} \quad 34.$$

Electric 2^l -pole transitions are determined by the simpler expression

$$\Omega_{\lambda}^{(l)(e1..)} = e r^l Y_{\lambda} \quad 35.$$

In Equation 34 and Equation 35, Y_{λ} are the ordinary spherical harmonics, and $[Y_{l-1} \times l]_{\lambda}^{(l)}$ is the λ component of the tensor product of Y_{λ} and l . In particular, for electric dipole transitions, Equation 35 reduces to

$$\Omega(E1) = e \sqrt{\frac{3}{4\pi}} \sum_i \frac{1}{2} (1 - \tau_{3i}) r_i \quad 36.$$

where, as well as in the rest of this section, τ_{3i} denotes the 3-component of the isospin operator of the i th nucleon. For electric quadrupole transitions, the corresponding expression is slightly more complicated. The zero component of the second-degree tensor operator is given by

$$\Omega_0^{(2)}(E2) = e \sqrt{\frac{5}{16\pi}} \sum_i \frac{1}{2} (1 - \tau_{3i}) (3z_i^2 - r_i^2) \quad 37.$$

Magnetic dipole transitions are given by the operator

$$\Omega(M1) = \frac{e\hbar}{2mc} \sqrt{\frac{3}{4\pi}} (g_l l + g_s s) \quad 38.$$

where for protons $g_l = 1$, $g_s = 2 \times 2.793 = 5.59$ and for neutrons $g_l = 0$, $g_s = 2 \times (-1.914) = -3.83$. Using the notation of reference (39), we introduce the transition strength

$$\Lambda(I) = [1/(2J+1)] \langle \alpha T J || \Omega^{(l)} || \alpha' T' J' \rangle^2 \quad 39.$$

and obtain for the radiative width

$$\Gamma_{\gamma}(M1) = 2.76 \times 10^{-3} E_{\gamma}^3 \Lambda(M1) \text{ ev} \quad 40.$$

Here $\Lambda(M1)$ is in units of nuclear magnetons, squared, and E_{γ} is the energy of the emitted γ ray in Mev. Similarly, we obtain

$$\Gamma_{\gamma}(E1) = 2.5 \times 10^{-1} E_{\gamma}^3 \Lambda(E1) \text{ ev} \quad 41.$$

where $\Delta(E1)$ is in units of $[e\langle r \rangle]^2$ and $\langle r \rangle$ is measured in units of 10^{-13} cm. (E_γ is in Mev). For electric quadrupole transitions, we obtain

$$\Gamma_\gamma(E2) = 8.02 \times 10^{-8} E_\gamma^5 \Delta(E2) \text{ ev} \quad 42.$$

Here, $\Delta(E2)$ is in units of $[e\langle r^2 \rangle]^2$ where $\langle r^2 \rangle$ is measured in units of 10^{-25} cm.² and E_γ is in Mev.

The $E1$ transition is forbidden in self-conjugate nuclei for transitions with $\Delta T=0$. In fact, $\Omega(E1)$ can be written as a sum of two terms

$$\Omega(E1) = \frac{e}{2} \sqrt{\frac{3}{4\pi}} \sum_i r_i - \frac{e}{2} \sqrt{\frac{3}{4\pi}} \sum_i \tau_{3i} r_i \quad 43.$$

The first term in Equation 43 is the center-of-mass co-ordinate of the system. This term has vanishing matrix elements between two orthogonal states of internal motion (neglecting the recoil of the nucleus during the photon emission). The second term is the 3-component of a vector in the isospin space. According to the Wigner-Eckart theorem, its matrix elements for $\Delta T=0$ are proportional to $\langle TM_T | T_3 | TM_T \rangle = M_T$. This vanishes in a self-conjugate nucleus for which $M_T=0$ (40).

In pure jj coupling, the matrix elements of the magnetic dipole operator within the j^n configuration are given by

$$\Omega(M1) = \sqrt{\frac{3}{4\pi}} \frac{e\hbar}{2mc} \sum_i [\frac{1}{2}(1 - \tau_{3i})g_{j_i}^{(p)} + \frac{1}{2}(1 + \tau_{3i})g_{j_i}^{(n)}] j_i \quad 44.$$

Here $g_{j_i}^{(p)}$ is the g factor of a proton in the j_i orbit, and $g_{j_i}^{(n)}$ is the corresponding g factor of a neutron. These g factors are given by the Schmidt values, Equation 1. It can be seen from Equation 44 that no $M1$ transitions can occur between states of the j^n configuration of identical nucleons, because then $\Omega(M1)$ is proportional to J and, therefore, only diagonal elements are different from zero.

Also, in the j^n configuration in a self-conjugate nucleus, $M1$ transitions are forbidden if $\Delta T=0$. According to Equation 44, $\Omega(M1)$ is the sum of two terms, one of which is proportional to J and the other to $\sum \tau_{3i} j_i$. The first term has no nonvanishing matrix elements between two orthogonal states. According to the Wigner-Eckart theorem, the second term is proportional to $\langle TM_T | T_3 | TM_T \rangle = M_T$ and vanishes for $M_T=0$.

This last selection rule has a more general validity (41). Transition strengths of $M1$ transitions between levels with the same T in self-conjugate nuclei are expected to be on the average smaller by a factor 100 than in other $M1$ transitions. We do not repeat here Morpurgo's arguments (41) leading to this rule. Rather, we present, as an illustration, the calculation for a concrete case.

Let us consider a two-nucleon configuration of a self-conjugate nucleus (e.g. N^{14} to be discussed later). From Equations 39 and 44 we obtain for $\Delta T=1$

$$\Lambda(M1) = \frac{2J' + 1}{4} \left[\sqrt{j_1(j_1 + 1)(2j_1 + 1)} \begin{Bmatrix} j_1 & J & j_2 \\ J' & j_1 & 1 \end{Bmatrix} (g_{l_{j_1}^{(n)}} - g_{l_{j_1}^{(p)}}) \right. \\ \left. + (-1)^{J+J'} \sqrt{j_2(j_2 + 1)(2j_2 + 1)} \begin{Bmatrix} j_2 & J & j_1 \\ J' & j_2 & 1 \end{Bmatrix} (g_{l_{j_2}^{(n)}} - g_{l_{j_2}^{(p)}}) \right]^2 \quad 45.$$

and for $\Delta T = 0$

$$\Lambda(M1) = \frac{2J' + 1}{8} \left\{ \sqrt{j_1(j_1 + 1)(2j_1 + 1)} \begin{Bmatrix} j_1 & J & j_2 \\ J' & j_1 & 1 \end{Bmatrix} (g_{l_{j_1}^{(n)}} + g_{l_{j_1}^{(p)}}) \right. \\ \left. + (-1)^{J+J'} \sqrt{j_2(j_2 + 1)(2j_2 + 1)} \begin{Bmatrix} j_2 & J & j_1 \\ J' & j_2 & 1 \end{Bmatrix} (g_{l_{j_2}^{(n)}} + g_{l_{j_2}^{(p)}}) \right\}^2 \quad 46.$$

Comparing Equation 45 with Equation 46, it is seen that the transition rates for $\Delta T = 0$ are weaker by a factor of about 250 than those of the $\Delta T = 1$ transitions for $p_{1/2}s_{1/2}$ and $p_{1/2}d_{1/2}$ configurations in N^{14} . This is so because μ_n and μ_p have opposite signs so that $\mu_p + \mu_n = 0.9$, whereas $\mu_p - \mu_n = 4.7$.

The above mentioned selection rules are confirmed by experimental data. $E1$ transitions with $\Delta T = 0$ in self-conjugate nuclei are very much retarded as compared to $E1$ transitions with $\Delta T = 1$ in the same nuclei and in other nuclei [(42); earlier papers are also mentioned here].

The $M1$ transition strength between the $5/2^-$ level (at 0.32 Mev) and the $7/2^-$ ground state in ${}^{23}\text{V}_{28}^{51}$ is retarded by a factor of about 300. Here, both levels belong to the proton $f_{7/2}^3$ configuration. This retardation agrees, therefore, with the selection rule for $M1$ transitions in j^n configurations of identical particles. The same situation exists in the $3/2^+ (0.096 \text{ Mev}) \rightarrow 5/2^+$ (ground state) transition in O^{19} with the neutron $d_{5/2}^3$ configuration. The retardation is by a factor 36. Very small contaminations of other configurations are sufficient to explain the very slow existing transitions.

The selection rule for $\Delta T = 0$ $M1$ transitions in self-conjugate nuclei can be seen to hold in various cases. A good example is the case of N^{14} . The branching in the γ decay of the $1^+ T = 0$ level at 3.95 Mev is 96 per cent to the $0^+ T = 1$ level at 2.31 Mev and only 4 per cent to the $1^+ T = 0$ ground state, although the latter transition has the higher energy. Only one $M1$ transition with $\Delta T = 0$ between odd-parity levels was observed in N^{14} . This is the transition between the $3^- T = 0$ level at 5.83 Mev and the $2^- T = 0$ level at 5.10 Mev. It is, however, very weak ($\Gamma_\gamma \sim 10^{-3} \text{ ev}$), in agreement with Morpurgo's selection rule.

The $E1$ and $M1$ selection rules for $\Delta T = 0$ discussed above are due to general properties of the initial and final states and are therefore expected to have general validity. There are other selection rules which depend on the details of the states, like the configurations. One such selection rule states that $M1$ transitions require a spin flip of the particle whose orbit is changed in the transition ($\Delta l = 0$). Similarly, for $E1$ transitions, $\Delta l = \pm 1$. When these conditions are not satisfied, the situation is referred to as "forbiddenness." Specially striking is the absence of $M1$ transitions with $\Delta T = 1$ in N^{14} be-

tween the $p_{1/2}s_{1/2}J=1$ and $p_{1/2}d_{5/2}J=2$ states (43). These transitions would have been allowed but for the l forbiddenness; further details will be given later.

As already mentioned, it may be possible to treat transition probabilities in the same manner as energies by introducing effective matrix elements. Even in $M1$ transitions, where there are no radial integrals involved, the g factors which appear in the matrix element may be taken as adjustable parameters. This has been done successfully for $M1$ transitions in N^{14} and will be discussed in Section IX. Also, use of an effective matrix element ($p_{1/2}||\Omega(E1)||s_{1/2}$) reproduces fairly accurately several $E1$ transitions in C^{12} , N^{13} , N^{14} , and O^{16} (Sec. IX).

Another example of such an approach is the comparison between $E2$ transitions in N^{16} and O^{17} . According to the usual theory, $E2$ transitions in which a neutron goes from one orbit to another are very much attenuated. However, one effective matrix element ($d_{5/2}||\Omega(E2)||s_{1/2}$) for neutrons reproduces the transition between the 0^- level at 0.12 Mev and the 2^- ground states in N^{16} as well as the transition between the $s_{1/2}$ level at 0.87 Mev and the $d_{5/2}$ ground state in O^{17} . It would be desirable to have an accurate measurement of the corresponding transition between the $d_{5/2}$ level (at 3.86 Mev) and the $s_{1/2}$ level (at 3.09 Mev) in C^{13} for comparison. This transition involves the same parameter and thus could provide another check to the usefulness of the concept of effective operators. All these transitions exist, although they are between configurations differing by a neutron orbit. The lifetimes of the transitions from the first excited $1/2^+$ states to the ground $5/2^+$ states in Mg^{25} and Al^{25} were recently measured by Ferguson, Grace & Newton (43a). Taking the ground states to belong to the $d_{5/2}^9$ configuration with $v=1$, $t=1/2$ and the $1/2^+$ states as $d_{5/2}^8(v=0, t=0)s_{1/2}$, the lifetimes agree with those calculated from the corresponding transitions in O^{17} and F^{17} .

The same methods that are used to calculate $M1$ transitions may be used to calculate static magnetic moments. The only difference is that in this case diagonal matrix elements must be calculated. The magnetic moment of the ground state of the j^n (n -odd) configuration is shown to be (44).

$$\mu = \beta\mu_e + (1 - \beta)\mu_o \quad 47.$$

Here, μ_o is the Schmidt value for a nucleon of the odd group and μ_e the value of a nucleon of the other kind. The factor β is given by

$$\beta = \begin{cases} \frac{N_o}{(2j+2)(2T+2)} & \text{for } N_o > N_e \\ \frac{2j+1-N_e}{(2j+2)(2T+2)} & \text{for } N_e > N_o \end{cases} \quad 48.$$

Here, N_o is the odd number of nucleons in the odd group, and N_e is the number of nucleons of the other kind. Although Equation 48 is qualitatively in agreement with the trend observed in nuclear moments, it gives far too

small corrections and cannot explain the large deviations from the Schmidt values.

Also, in the case of nuclear magnetic moments we can try to correlate data by the use of effective magnetic moments. An example of analyzing data by this method is offered by the potassium isotopes (45). The ground states of all these nuclei belong to $d_{3/2}^{-1}f_{7/2}^n$ configurations with a proton hole in the $d_{3/2}$ shell and n neutrons in the $f_{7/2}$ shell. Within these configurations

$$\psi(d_{3/2}^{-1}f_{7/2}^n J) = \sum_{J'} a_{J'} \psi(d_{3/2}^{-1}f_{7/2}^n(J') J) \quad 49.$$

In the functions on the right-hand side of Equation 49, the neutrons are coupled to a definite angular momentum J' . The $a_{J'}$ can be determined from experimental values of nuclear energies (30, 46).

Magnetic moments were calculated using these wave functions and effective g factors for protons and neutrons. These two g factors were taken to be the same for all nuclei and were determined by a least-squares fit with experimental data. The results are tabulated in Table III. The agreement is seen to be good. The effective g factors are different from the corresponding single-particle (Schmidt) values. The effective $d_{3/2}$ proton moment obtained is 0.335 n.m. as compared to the Schmidt value 0.124 n.m. Similarly, the effective $f_{7/2}$ neutron magnetic moment is -1.569 n.m. whereas the Schmidt value is -1.913 n.m.

TABLE III
MAGNETIC MOMENTS OF K ISOTOPES

Nucleus	K ³⁹	K ⁴⁰	K ⁴¹	K ⁴²	K ⁴³
Experimental	0.391	-1.30	0.215	-1.14	0.163
Calculated	0.335	-1.256	0.208	-1.199	0.187

Configuration admixtures are not expected to be large in these nuclei. Therefore the observed quenching of the moments may be due to interaction with many highly excited configurations, and may be the same for all the nuclei considered.

This analysis is closely related to an earlier work dealing with beta decay. We mention it here only briefly. Using the wave functions given in Equation 49, in the $d_{3/2}^{-1}f_{7/2}^n$ region, Oquidam & Jancovici (46) made a successful analysis for $\Delta J = 2$, yes beta transitions. They find good agreement with experimental data by taking in all cases the same single nucleon matrix element for the $f_{7/2} \rightarrow d_{3/2}$ transition. The value of this effective matrix element is, however, smaller by about a factor 4 than the one calculated from beta-decay theory. The $M2$ transitions in A³⁹ and K⁴¹ involve the same matrix element. Oquidam & Jancovici (46) find that the values of these matrix elements calculated from the experimental half lives are reduced by about

the same factor. This reduction may also be due to configuration mixing with many highly excited configurations.

VII. THE FIRST p SHELL

The nuclei in the $\text{He}^4\text{--O}^{16}$ region are the lightest nuclei that we consider. In these nuclei, the first p shell is being filled. Although the jj coupling approximation is usually good, it seems that in the very light nuclei, LS coupling is a better approximation. This is probably why an analysis based on pure jj coupling fails to reproduce accurately the binding energies of nuclei with masses 5, 6, and 7 (14). Hence it is difficult to obtain significant quantitative agreement, and our description of the p^n configuration will be rather brief and qualitative.

Intermediate coupling calculations by Kurath (47, 48) demonstrate these facts. In the calculations a special form of the interaction is chosen (a mixture of central forces and a single-particle spin-orbit interaction). Range and strength of the central forces, radius of the nucleus, and strength of the spin orbit interaction are adjustable parameters. The results are sensitive only to changes in strength of the spin-orbit interaction. Best agreement with experimental data is obtained with values of this parameter that increase as one goes from lighter to heavier nuclei. Accordingly, the mode of coupling changes from LS coupling towards jj coupling.

Li^6 , He^6 , and Be^6 are the first nuclei in the $1p$ shell that are stable against particle emission. The second excited level of Li^6 at 3.560 Mev above ground state with $T=1$, $J^\pi=0^+$, is the $M_T=0$ member of the isospin triplet of two p nucleons outside the closed shell of He^4 . The other two members of this triplet are the ground states of He^6 and Be^6 . If jj coupling were valid for both Li^6 and B^{10} , the lower parts of both spectra should have been identical. One nucleus would have a two-nucleon $p_{3/2}^2$ configuration and the other a two-hole $p_{3/2}^{-2}$ configuration. This is, however, not the case. The level order and spacings in Li^6 are different from those in B^{10} . This difference in the spectra may be understood by the fact that in Li^6 , LS coupling is a better approximation whereas in B^{10} , jj coupling is better.

According to Wigner's supermultiplet theory (49), two states belong to the supermultiplet $(1, 0, 0)$ in the p^2 configuration. These are the $^{13}\text{S}_1$ and the $^{13}\text{D}_{3,2,1}$ levels. The ground state of Li^6 is a 1^+ $T=0$ state. It is very probably the $^{13}\text{S}_1$ state. The levels with $T=0$, $J^\pi=3^+$, 2^+ , 1^+ (at 2.18, 4.52, and 5.5 Mev, respectively) may well be due to the $^{13}\text{D}_{3,2,1}$ triplet. In jj coupling the spectrum looks quite different, as we shall see in B^{10} . In He^6 , like most even-even nuclei, the ground state has 0^+ and the first excited state has 2^+ . The 0^+ (3.56 Mev) and 2^+ (5.35 Mev) levels in Li^6 are their analogues (differing only in M_T). The spacing between these two levels is 1.71 Mev, which is smaller than the corresponding spacing in B^{10} .

In Li^7 and Be^7 , two mirror nuclei, LS coupling is apparently a good approximation. The ground state is a $3/2^-$ state, and a $1/2^-$ state lies 0.478

Mev (0.431 Mev in Be^7) above it. There is another pair of rather close-lying levels with $7/2^-$ (4.63 Mev) and $5/2^-$ (7.47 Mev). These two pairs can be qualitatively explained in LS coupling as the two doublets $^{22}\text{P}_{3/2,1/2}$ and $^{22}\text{F}_{7/2,5/2}$. These two doublets are the only members of the lowest supermultiplet ($1/2, 1/2, -1/2$). The relatively small spin-orbit interaction separates the two levels in each doublet. The state with the greater J in each pair is the lower-lying member of the doublets. It is interesting that four levels with the same spins would appear also in jj coupling. The $3/2^-$ level would again be the ground state (it has the lowest seniority), but the order of the other levels and the spacings would be quite different. The spacings of the $1/2^-$, $5/2^-$, and $7/2^-$ levels, which have the same T and the same seniority, would be proportional to $J(J+1)$ as mentioned in Section V. Such spacings are, however, very different from the observed ones. Levels with parity opposite to that of the ground state result from excitation of a p nucleon into a higher shell with even l . These states will be considered in Section VIII.

In Be^8 , Li^8 , and B^8 , jj coupling begins to be a better approximation. The ground configuration in these nuclei is the $p_{3/2}^4$ configuration. As already mentioned, this configuration has four states with $T=0$. One such state has $J=0$ and $v=0$, one state has $J=2$ and $v=2$, whereas the other two states have $J=2$ and $J=4$ and $v=4$. Therefore, the second excited state (which has $J=4$) in Be^8 lies much higher (about 11.7 Mev) than the first excited 2^+ state (2.90 Mev). Only in configurations with $j > 3/2$ are there lower-lying $J=4$ states with seniority $v=2$. The high position of the 4^+ level does not, however, indicate the validity of jj coupling. It was shown (33) that in the supermultiplet theory the heights of the 0^+ , 2^+ , and 4^+ levels should be proportional to $L(L+1)$ since these are the ^{11}S , ^{11}D , and ^{11}G levels belonging to the supermultiplet (0, 0, 0). The positions of the 2^+ (2.90 Mev) and 4^+ (11.7 Mev) levels do indeed fit this law.

There are three possible $T=1$ states in the $p_{3/2}^4$ configuration, a 1^+ and a 3^+ level, both with $v=2$, $t=0$, and a 2^+ level with $v=2$, $t=1$. Such levels are found in Li^8 (and also in Be^8 and B^8), the ground state (2^+), the 0.98 (1^+), and the 2.26 (3^+) states. However, there is no quantitative agreement with jj coupling. From Equations 24 and 25 in Section V it follows that the spacing and order of the $J=3$ and $J=1$ levels should be the same as in B^{10} , which is not the case.

In Be^9 and B^9 very little is known experimentally. These nuclei have the ground $p_{3/2}^{-3}$ configuration in pure jj coupling. It is, however, clear that pure jj coupling would not give rise to the $J=5/2$ first excited (odd-parity) state (compare the discussion for Li^7). Kurath (47), on the other hand, finds rough agreement for the $5/2$ level as well as for dipole and quadrupole moments of Be^9 .

B^{10} , Be^{10} , and C^{10} are in the middle of the $1p$ shell and should, therefore, have the most complicated spectra. As already mentioned, the differences

in the spectra of Li^6 and B^{10} possibly arise from the difference in coupling schemes. In these nuclei there are two $p_{3/2}$ nucleons missing from the closed shells of C^{12} . The ground configuration is therefore equivalent to the $p_{3/2}^2$ configuration. The $T=1$ levels observed in these nuclei correspond to this picture. In addition to the $J=0$ ground state, there is only one $T=1$ excited state in the $p_{3/2}^2$ configuration which has $J=2$. A 2^+ level is indeed observed in each of the three nuclei at 3.4 Mev above the $J=0$, $T=1$ state. Other $T=1$ levels are observed only at ~ 6 Mev (above that state). On the other hand, the situation for $T=0$ is not as clear cut. The two lowest $T=0$ states have spins $J=3$ and $J=1$ as expected for the $p_{3/2}^2$ configuration. However, there is another 1^+ $T=0$ state only 1.43 Mev above the lowest 1^+ $T=0$ state. Such other $T=0$ levels should lie higher since they require the excitation of a $p_{3/2}$ nucleon into the $p_{1/2}$ subshell. That there is another low-lying 1^+ state suggests that the 1^+ $T=0$ states do not belong to pure jj -coupling configurations.

Kurath's calculations (47) give a fair fit with the lower part of the B^{10} spectrum. Kurath also calculated (48) transition probabilities in B^{10} with the wave functions used for the energy calculations. The results, however, do not agree with the experimental data. Intermediate coupling calculations, using effective interactions and taking into account most of the experimentally known $1p^n$ levels (50), give an approximate fit between calculated levels and the low-lying levels of B^{10} .

In B^{11} and C^{11} only one level, the $3/2^-$ level, belongs to the jj -coupling ground configuration, which is the one-hole $p_{3/2}^{-1}$ configuration. Other levels result from excitations of $p_{3/2}$ nucleons into the $p_{1/2}$ subshell. The ground state of B^{11} has, indeed, $3/2^-$. However, a $1/2^-$ state lies only 2.13 Mev above it. The addition of a $p_{1/2}$ nucleon to the B^{10} nucleus gives rise to many states. Three $1/2^-$ states with $T=0$ can be obtained by its coupling to the two 1^+ states (at 0.72 and 2.15 Mev) and the 0^+ (at 1.74 Mev) of B^{10} . Coupling the $p_{1/2}$ nucleon to the 3^+ ground state of B^{10} gives rise to two states with $5/2^-$ and $7/2^-$. Levels with $5/2^-$ and $7/2^-$ are observed in B^{11} at 4.46 and 6.76 Mev above the ground state of B^{11} . Other states with spins $3/2^-$, $5/2^-$, etc., can similarly be obtained. However, each state observed in B^{11} has, generally, no well-defined "parent state" in B^{10} from which it is obtained by adding a $p_{1/2}$ nucleon. The $p_{3/2}-p_{1/2}$ interaction, as well as nondiagonal elements of the two-nucleon interaction, gives rise to admixtures of such states.

Calculations by Kurath (47) give fair agreement for the low-lying levels up to about 7 Mev. Transition probabilities and branching ratios calculated with Kurath's wave functions agree with experimental values. The branching of the 5.03-Mev and 7.30-Mev states agrees with the assignments $3/2^-$ and $5/2^-$, respectively (51). Fair agreement is also obtained by Kurath (47) for magnetic dipole and electric quadrupole moments calculated with the same wave functions. Calculations (50) of the B^{11} levels with effective interactions also give agreement with the data. The three $3/2^-$ levels (ground state,

5.03 Mev, and 6.81 Mev) are found to belong mainly to the $p_{3/2}^7$ and $p_{3/2}^6 p_{1/2}^2$ configurations. The $1/2^-$ (2.13 Mev), $5/2^-$ (4.46 and 7.30 Mev), and $7/2^-$ (6.76 Mev) levels are admixtures of the $p_{3/2}^6 p_{1/2}$ and $p_{3/2}^5 p_{1/2}^2$ configurations with appreciable amounts of the $p_{3/2}^4 p_{1/2}^3$ configuration.

In C^{12} the $p_{3/2}$ subshell is closed. This results in greater stability of this nucleus as compared to neighboring nuclei. Also, the first excited (2^+) state is higher than usual. To obtain any excited state, the subshell has to be broken up, which requires extra energy.

Kurath's calculated energies (47) agree with the experimental spacings of the ground state (0^+), the first excited state at 4.43 Mev (2^+), and the two $T=1$ levels at 15.11 (1^+) and 16.11 Mev (2^+). There is not enough experimental information on the other expected levels. The $M1$ transitions from these two $T=1$ levels to the two lowest levels are also reproduced by Kurath's calculations (48). Calculations with effective interactions (50) show that the two 0^+ states (ground state and 7.66 Mev) are mixtures of the $p_{3/2}^8$ and $p_{3/2}^6 p_{1/2}^2$ configurations. The $T=0$ levels at 4.43 (2^+) and 12.73 (1^+) and the $T=1$ levels at 15.11 (1^+) and 16.11 Mev (2^+) are mainly $p_{3/2}^7 p_{1/2}$ levels. The same holds for the analogous levels in B^{12} , the 1^+ ground state, and the 2^+ level at 0.95 Mev.

In B^{13} only five states are possible for $(1p)^9$ configurations. Rough estimate shows that only two of these should lie below 7 Mev. The $3/2^-$ ground state is mainly the $p_{3/2}^7 p_{1/2}^2$ state. A $1/2^-$ state belongs to the $p_{3/2}^6 p_{1/2}^3$ configuration and should lie at about 5 Mev above ground state. One of the four known excited levels in B^{13} may be this $1/2^-$ level.

From C^{13} and N^{13} on, the $1p_{1/2}$ shell is regularly filled. If the binding energies (including the 0^+ $T=1$ 2.31-Mev state in N^{14}) are calculated by assuming pure $p_{1/2}^n$ configurations, the results are straightforward (14). The energies of the states of the $p_{1/2}^n$ configuration, with isospin T , are given as a special case of Equation 28 obtained by putting $c=0$ in Equation 27. We thus obtain for the energies in the $p_{1/2}^n$ configurations

$$nC + (1/2)n(n-1)a + [T(T+1) - (3/4)n]b + \text{C.E.} \quad 50.$$

Here, the constants a and b are given by

$$\begin{aligned} \langle p_{1/2}^3 T=0 J=1 | V_{12} | p_{1/2}^3 T=0 J=1 \rangle &= a - (3/2)b \\ \langle p_{1/2}^3 T=1 J=0 | V_{12} | p_{1/2}^3 T=1 J=0 \rangle &= a + (1/2)b \end{aligned}$$

The Coulomb energy, C.E., for the above isotopes is taken from the binding energies of mirror nuclei. The values of the parameters as determined by a least-squares calculation are $C=5.34$ Mev, $a=2.91$ Mev, $b=-1.09$ Mev. The agreement obtained between experimental and calculated binding energies is displayed in Table IV.

The lower levels of C^{13} and N^{13} include the single-particle excitations already discussed in Section III. The ground state is the $1p_{1/2}$ state. The $3/2^-$ state (at 3.68 Mev in C^{13} , 3.51 Mev in N^{13}) results from an excitation of a $1p_{3/2}$ nucleon into the $1p_{1/2}$ subshell.

TABLE IV
BINDING ENERGIES IN THE FIRST $p_{1/2}$ SUBSHELL

Nucleus	Binding energy*	
	Experimental	Calculated
${}^6\text{C}_7^{13}$	4.95	5.34
${}^6\text{C}_8^{14}$	13.11	13.04
${}^7\text{N}_6^{13}$	1.95	2.31
${}^7\text{N}_7^{14} (J=0)$	10.18	10.02
${}^7\text{N}_7^{14} (J=1)$	12.49	12.19
${}^7\text{N}_8^{15}$	23.33	23.35
${}^8\text{O}_6^{14}$	6.55	6.48
${}^8\text{O}_7^{15}$	19.84	19.81
${}^8\text{O}_8^{16}$	35.44	35.51

* From these the binding energy of C^{12} was subtracted. All energies are in Mev.

N^{14} , C^{14} , and O^{14} provide an especially great variety of experimental data, which may be correlated and calculated. A detailed analysis of these nuclei has been carried out by Warburton & Pinkston (43). The many odd-parity levels in these nuclei belong to the $p_{1/2}s_{1/2}$ and $p_{1/2}d_{5/2}$ configurations and will be considered in Section VIII.

The similarity between the spectra of C^{14} and Be^{10} is interesting. In both nuclei the odd-parity levels begin at the same height (about 6 Mev above the ground states) and are lower than the even-parity states of excited configurations. The main difference between these spectra is the absence of the 2^+ level in C^{14} . In C^{14} , a 2^+ level can be obtained only by raising a $1p_{3/2}$ nucleon from the closed C^{12} core into the $1p_{1/2}$ subshell. Still, it is interesting to see why the 2^+ level due to an excitation of a $p_{3/2}$ nucleon into the $p_{1/2}$ subshell should lie so high. States which result from a similar mechanism in N^{15} (6.33, $3/2^-$) and C^{13} (3.68, $3/2^-$) lie lower. It is possible to calculate the height of these levels by considering the energy necessary for the excitation in each case. The amount necessary to excite N^{15} from its $p_{3/2}^8 p_{1/2}^3$ ground configuration ($p_{1/2}^{-1}$ state) to the $p_{3/2}^7 p_{1/2}^4$ configuration ($p_{3/2}^{-1}$ state) is equal to

$$E(p_{3/2}^8 p_{1/2}^3) - E(p_{3/2}^7 p_{1/2}^4) \\ = [E(p_{3/2}^8) - E(p_{3/2}^7)] - [E(p_{1/2}^4) - E(p_{1/2}^3)] + 6(V + V') - 7(V + V'')$$

Here E stands for the total energy of the configuration. V is defined by $V = (3V_1 + 5V_2)/4$ and V' is defined by $V' = (3V'_1 + 5V'_2)/4$. The V_j and V'_j are defined by Equation 29, with $j = p_{3/2}$, $j = p_{1/2}$. The amount necessary to excite C^{14} from its ground $p_{3/2}^8 p_{1/2}^2 T=1 J=0$ state to the excited $p_{3/2}^7 p_{1/2}^3 T=1 J=2$ state (still not known experimentally) is equal to

$$\begin{aligned}
 E(p_{3/2}^8 p_{1/2}^8 T=1 J=0) - E(p_{3/2}^7 p_{1/2}^3 T=1 J=2) \\
 = [E(p_{3/2}^8) - E(p_{3/2}^7)] - [E(p_{1/2}^3) - E(p_{1/2}^2 T=1 J=0)] \\
 + 4(V + V') - [5(V + V') + V'_2]
 \end{aligned}$$

The excitation energy in C^{14} is, therefore, bigger than that of N^{15} by (using Equation 50 for the energies of $p_{1/2}^n$ configurations)

$$\begin{aligned}
 V_0(p_{1/2}) - V'_2(p_{3/2} p_{1/2}) \\
 = \langle p_{1/2}^2 T=1 J=0 | V | p_{1/2}^2 T=1 J=0 \rangle - \langle p_{3/2} p_{1/2} T=1 J=2 | V | p_{3/2} p_{1/2} T=1 J=2 \rangle
 \end{aligned}$$

The first term can be taken from Equation 50 to be 2.37 Mev. The second term is known to be negative or at least very small (cf. end of Sect. V). Thus, the height of the 2^+ level above the ground state in C^{14} should be bigger by about 2 Mev than the height of the $3/2^-$ level above the ground state of N^{15} (6.33 Mev). In C^{13} the situation is a little more complicated. It is found that the excitation energy in C^{13} is about 3 Mev smaller than in N^{15} . Thus, the $3/2^-$ level should lie at about 3.5 Mev above ground state of C^{13} as compared to 6.33 Mev in N^{15} .

An analysis of the even-parity levels in N^{14} in terms of effective interactions gives the following results on the $1p^{-2}$ configuration. The $1^+ T=0$ ground state has a strong admixture of the $p_{1/2}^{-1} p_{3/2}^{-1}$ configuration. The 2.31-Mev ($0^+ T=1$) state has an almost pure $p_{1/2}^{-2}$ configuration and corresponds to the ground states of C^{14} and O^{14} . The 3.95-Mev ($1^+ T=0$) state interacts with the ground state and is, therefore, an admixture of the $p_{1/2}^{-1} p_{3/2}^{-1}$ configuration and the ground $p_{1/2}^{-2}$ configuration. The 7.03- ($2^+ T=0$) and 10.43-Mev ($2^+ T=1$) levels belong to the $p_{3/2}^{-1} p_{1/2}^{-1}$ configuration. The 11.38 ($3^+ T=0$) level is very probably a $p_{3/2}^{-2}$ level. These assignments, determined by the use of effective interactions, agree with those made by Warburton & Pinkston (43), who used transition probabilities and reduced widths for inelastic scatterings on N^{14} .

It can be simply understood that the first excited $T=0$ state in N^{14} has $J^\pi=1^-$ although the first excited $T=0$ state in C^{12} has $J^\pi=2^+$. The configuration of that state in N^{14} is the $p_{3/2}^{-1} p_{1/2}^{-1}$ configuration.⁶ In C^{12} it is the $p_{3/2}^{-1} p_{1/2}$ configuration. The simple relations between particle-hole and hole-hole-interaction (Eq. 13) give rise to the relation

$$\Delta(N^{14} T=0) = (3/2)\Delta(C^{12} T=1) - (1/2)\Delta(C^{12} T=0) \quad 51.$$

In Equation 51, Δ denotes the difference between the binding energies in the 1^+ and the 2^+ states. First, $\Delta(C^{12} T=1)$ is known to be positive (about 1 Mev). On the other hand, $\Delta(C^{12} T=0)$ is known to be negative (although the exact value is not known). As a result, $\Delta(N^{14} T=0)$ must be positive, i.e., the $1^+ T=0$ (excited) level should lie lower than the $2^+ T=0$ level. By the same method it follows that

⁶ Even in case of a strong mixing between the $p_{3/2}^{-1} p_{1/2}^{-1}$ and the $p_{1/2}^{-2}$ configurations, our considerations still hold. The pure $p_{3/2}^{-1} p_{1/2}^{-1}$ $1^+ T=0$ level then lies lower by about 1.5 Mev.

$$\Delta(N^{14} T=1) = (1/2)\Delta(C^{12} T=1) + (1/2)\Delta(C^{12} T=0) \quad 52.$$

This expression turns out to be negative, and the $1^+ T=1$ level in N^{14} should be higher than the $2^+ T=1$ level.

In N^{15} and O^{15} there are two levels which belong to the $1p^{11}$ configuration. The ground state ($1/2^-$) has the pure $p_{3/2}^8 p_{1/2}^3$ or $p_{1/2}^{-1}$ configuration. The $3/2^-$ state (at 6.33 Mev in N^{15} and 6.15 Mev in O^{15} above ground states) has the pure $p_{3/2}^7 p_{1/2}^4$ or $p_{3/2}^{-1}$ configuration.

The configuration assignments mentioned above may give rise to predictions on transition probabilities which agree more or less with the experimental data. However, it should be kept in mind that, unlike energies, transition probabilities are sensitive to small changes in the wave functions. Therefore, even wave functions which reproduce the energies of states may fail in giving the correct transition probabilities.

VIII. EXCITED CONFIGURATIONS IN THE FIRST p SHELL

A few levels with parity opposite to that of the ground state are found in nuclei in which the $1p_{3/2}$ subshell is being filled. Many of these levels are due to excitation of a $1p_{3/2}$ nucleon into the $2s_{1/2}$ orbit. These levels lie lower than levels with $1d_{5/2}$ nucleons although the $1d_{5/2}$ orbit is filled first after the completion of the $1p$ shell. As we shall see, the interactions of the $2s_{1/2}$ and $1d_{5/2}$ nucleons with the $1p_{1/2}$ shell change the order of the single-nucleon levels. There is not enough experimental information on such levels, obtained by exciting a $1p_{3/2}$ nucleon into the $2s_{1/2}$ orbit. Therefore, the analysis to be presented is only tentative.

In C^{12} and B^{12} two $T=1$ levels are known to have negative parity. These are the 2^- level (at 16.58 Mev) and the 1^- level (at 17.23 Mev) in C^{12} . The corresponding levels in B^{12} are respectively at 1.67 and 2.62 Mev above the ground state. These levels belong to the $p_{3/2}^{-1}s_{1/2}$ configuration, i.e., to the configuration in which one $1p_{3/2}$ nucleon is excited into the $2s_{1/2}$ shell. It is convenient to consider the separation energy of the $2s_{1/2}$ nucleon, i.e., the energy required to remove it from the nucleus. It is simply the difference between the total energy of B^{12} (or C^{12}) in the excited state and the binding energy of B^{11} (or C^{11}).

We start from the separation energy of the $2s_{1/2}$ neutron in C^{13} . We denote it by C_s and find from the experimental data $C_s = 1.86$ Mev. Removing one proton from C^{13} we obtain B^{12} with two odd-parity levels with $J=1$ and $J=2$. The center of mass of these two levels has the separation energy of 1.32 Mev. The separation energy of the center of mass in B^{12} is equal to C_s minus the average particle-particle interaction. We thus obtain

$$C_s - V/2 = 1.32 \text{ Mev}$$

where $V = (3V_1 + 5V_2)/4$. The V_J are defined in Equation 29 for $j \equiv p_{3/2}$ and $j' \equiv s_{1/2}$. The same analogous equation for the corresponding two $T=1$ levels

in C^{12} is obtained if C_s is replaced by $\frac{1}{2}(C_s + C'_s)$. C'_s is the separation energy of the $2s_{1/2}$ proton in N^{13} .

Removing another proton from B^{12} we obtain Be^{11} . Considering the state obtained by adding a $2s_{1/2}$ neutron to the ground state of Be^{10} , its separation energy is given simply by $C_s - V$. Extrapolating from C^{13} and B^{12} we obtain $C_s - V = 0.78$ Mev. This value should be compared with the separation energy of the Be^{11} ground state found experimentally to be 0.54 ± 0.15 Mev. This suggests that the ground state of Be^{11} may well be an $s_{1/2}$ state. In fact, a similar linear extrapolation indicates that the $2s_{1/2}$ orbit may be lower than the $1p_{1/2}$ orbit in Be^{11} (52), as suggested by experimental data (53).

In Be^{10} there are two negative-parity levels, a 1^- level at 5.96 Mev and a 2^- level at 6.26 Mev (the corresponding $2^- T=1$ level is also observed in B^{10} at 7.48 Mev). Using the separation energies of these levels, as well as the data previously mentioned, we can obtain tentative values for all four $p_{3/2}s_{1/2}$ (particle-particle) interaction parameters. These tentative values are, in Mev,

$$\begin{array}{lll} V_2 = 0.90 & V_1 = 0.25 & V = 1.32 \\ V'_2 = -0.26 & V'_1 = 0.12 & V' = -0.24 \end{array}$$

We can compare these parameters with those of the $p_{1/2}d_{5/2}$ and $p_{1/2}s_{1/2}$ interactions given in Section V. Also, here the V_J with the even value of J is more attractive than the one with an odd J value (although the difference between the two is here rather large). Similarly, the V'_J with the even value of J is more repulsive than V'_J with the odd value of J .

We can try to calculate with these parameters the position of the 2^- and 1^- levels with $T=0$ in B^{10} . Assuming also that these levels are obtained by exciting an $1p_{3/2}$ nucleon into the $2s_{1/2}$ orbit, we calculate their separation energies into $B^9 + n$ to be 3.05 Mev and 1.78 Mev, respectively. These two values agree fairly well with the values of 3.33 Mev and 1.56 Mev obtained from the experimentally known 2^- level (at 5.11 Mev) and 1^- level (at 6.88 Mev) in B^{10} .

The situation is not so clear in B^{11} . The two even-parity $7/2^+$ (at 9.19 Mev) and $5/2^+$ (at 9.28 Mev) levels may be due to coupling of a $2s_{1/2}$ neutron to the 3^+ ground state of B^{10} (54). Using our interaction parameters, we obtain roughly the correct spacing between the two levels, but their separation energy turns out to be about 1 Mev less than the experimental value. This discrepancy is not too big in view of the tentative nature of the analysis and the restriction to pure $p_{3/2}n s_{1/2}$ configurations.

The experimental situation is very much better where the $1p_{3/2}$ subshell is already closed and the $1p_{1/2}$ subshell is being filled. Excitations of $1p_{1/2}$ nucleons into both $2s_{1/2}$ and $1d_{5/2}$ orbits are observed and can be easily distinguished by the parities and spins of the resulting states. On the other hand, the $1d_{3/2}$ orbit lies much higher (about 5 Mev above the $1d_{5/2}$ orbit in O^{17}), and excitations to it need not be taken into account.

Let us first consider configurations in which one $p_{1/2}$ nucleon has been

excited into the $s_{1/2}$ or $d_{5/2}$ orbits (38, 55). In the even nuclei it is possible to distinguish between levels of $p_{1/2}^{n-1}s_{1/2}$ configurations and levels of $p_{1/2}^{n-1}d_{5/2}$ configurations. In the first case, the levels have spins 0^- and 1^- whereas in the second case the resulting levels have 2^- and 3^- . Inasmuch as the $d_{3/2}$ orbit is ignored, these odd-parity states of even nuclei belong to pure configurations.

In C^{13} and N^{13} the $1/2^+$ levels (at 3.09 and 2.37 Mev, respectively) and the $5/2^+$ levels (at 3.85 and 3.56, respectively) are taken to be the single $2s_{1/2}$ and single $1d_{5/2}$ levels.

In N^{14} the 0^- , 2^- , 1^- , and 3^- $T=0$ levels at 4.91, 5.10, 5.69, and 5.83 Mev, respectively, belong to the $p_{1/2}d_{5/2}$ and $p_{1/2}s_{1/2}$ configurations. The same assignment is made for the 1^- , 0^- , 3^- , and 2^- $T=1$ levels at 8.06, 8.71, 8.90, and 9.50 Mev, respectively. The corresponding $T=1$ levels in C^{14} lie at 6.09 (1^-), 6.72 (3^-), 6.89 (0^-), and 7.35 (2^-) Mev above the ground state. All these levels are shown in Figure 4. That the $T=1$ levels are due to a single-particle excitation can be recognized by the Thomas-Ehrman shift (discussed in Sect. III) between C^{14} and N^{14} . This shift is particularly big for the states with a $2s_{1/2}$ nucleon.

In O^{16} the 0^- , 2^- , 1^- , and 3^- levels at 12.78, 12.96, 13.09, and 13.25 Mev, respectively, belong to the $p_{1/2}^3s_{1/2}$ and $p_{1/2}^3d_{5/2}$ configurations. The corresponding ($T=1$) levels in N^{16} are the 2^- ground state and the levels at 0.120 (0^-), 0.295 (3^-), and 0.392 (1^-) Mev. These $T=1$ levels in O^{16} and N^{16} are shown in Figure 5. In this figure, the position of the N^{16} ground state is determined by its binding energy. It was calculated by adding to the O^{16} - N^{16} mass difference the N^{16} - O^{16} mass difference. In this way, the Coulomb energy and the proton neutron mass difference were eliminated. The Thomas-Ehrman shifts of these states are clearly seen. The states with a $2s_{1/2}$ nucleon are easily recognized by their much larger shift.

In O^{17} and F^{17} the ground states belong to the $p_{1/2}^4d_{5/2}$ configuration. The $p_{1/2}^4s_{1/2}$ states lie at 0.871 and 0.500 Mev, respectively.

All these levels are used to obtain the interaction constants as well as to check the validity of the model and configuration assignments. From the total energies of the levels mentioned, the binding energy of C^{12} is subtracted. The remaining energy in the $p_{1/2}^m s_{1/2}$ (or $p_{1/2}^m d_{5/2}$) configuration can be written as the sum of the following terms. The first term is the kinetic energy and interaction with the C^{12} closed shells of the m $p_{1/2}$ nucleons, as well as their mutual interaction. This term is known from the analysis of Section VII (Table IV) and is taken from there. The second term is the kinetic energy and interaction with the C^{12} closed shells of the single $2s_{1/2}$ or $1d_{5/2}$ nucleon. These single-particle energies are taken as unknown parameters and are denoted by C_s and C'_s for a $2s_{1/2}$ neutron and proton, respectively. Similarly, C_d and C'_d are the single $1d_{5/2}$ neutron and single $1d_{5/2}$ proton energies. The third term is the interaction between the $p_{1/2}$ nucleons and the $s_{1/2}$ or $d_{5/2}$ nucleon. This last term can be expressed as a linear combination of the parameters V_J and V'_J . In the case with a $s_{1/2}$ nucleon these are the four

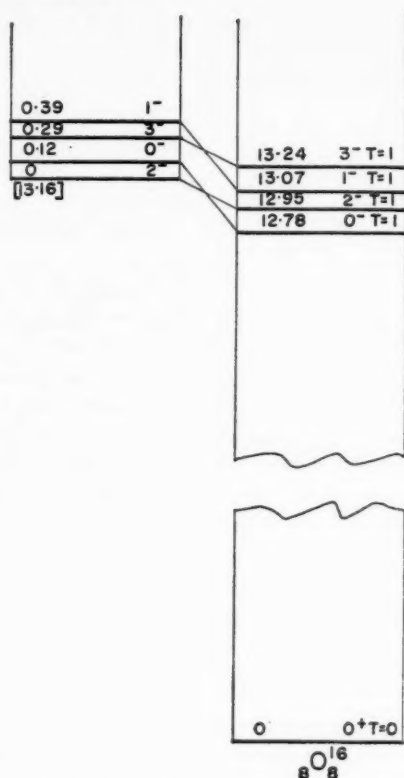
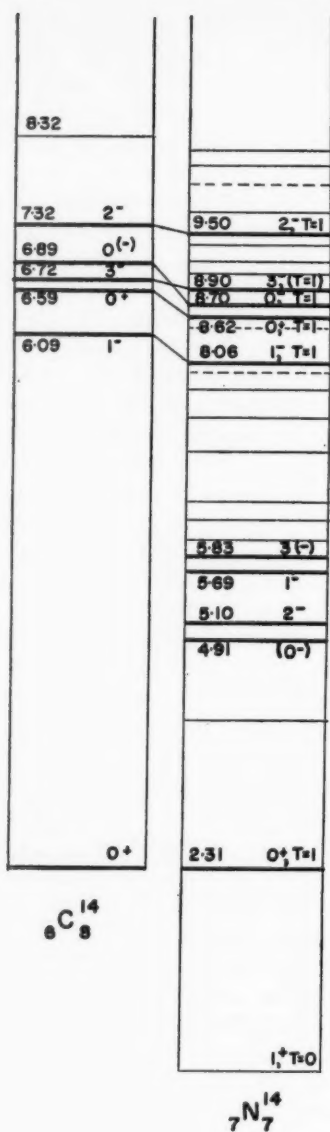


FIG. 5. Odd-parity $T=1$ levels in N^{16} and O^{16} (in Mev.).

FIG. 4. Odd-parity levels in C^{14} and N^{14} (in Mev.).

parameters V_0 , V_1 , V'_0 , and V'_1 , whereas for a $d_{5/2}$ nucleon these are V_2 , V_3 , V'_2 , and V'_3 . Most of the Coulomb energy is included in the difference between the constants C and C' . The remaining Coulomb energy is between the $2s_{1/2}$ (or $1d_{3/2}$) proton and the $1p_{1/2}$ protons. It is calculated using the harmonic oscillator wave functions (13).

There are, altogether, six theoretical parameters for $p_{1/2}^m s_{1/2}$ configurations and six such parameters for the $p_{1/2}^m d_{5/2}$ configurations. The levels listed above furnish 14 experimental energies for each case. A least-squares fit is made to find the values of the parameters that will best reproduce the experimental energies. The values obtained for the V_J and V'_J were given in Equation 30 at the end of Section V. The single-nucleon energies obtained are (with the statistical errors), in Mev,

$$C_s = 1.860 \pm 0.048 \quad C'_s = -0.372 \pm 0.062$$

$$C_d = 0.979 \pm 0.044 \quad C'_d = -1.639 \pm 0.057$$

Putting these best values of the parameters into the theoretical expressions, we obtain the calculated energies to be compared with the experimental data. This comparison is made in Table V for the $p_{1/2}^m s_{1/2}$ configurations and in Table VI for the $p_{1/2}^m d_{5/2}$ configurations. The agreement is seen to be very good. Therefore, it seems worth-while to calculate positions of other levels with the interaction parameters obtained in this analysis.

In C^{16} two possible states belong to the $p_{1/2}^2 s_{1/2}$ and $p_{1/2}^2 d_{5/2}$ neutron configurations. These two states are essentially single-nucleon states since there is one $2s_{1/2}$ (or $1d_{5/2}$) neutron outside the closed shells of C^{14} . The interaction constants obtained above give very good agreement between the calculated $p_{1/2}^2 s_{1/2}$ energy and the binding energy of C^{16} . The calculated energy of

TABLE V
ENERGIES OF $p_{1/2}^m s_{1/2}$ CONFIGURATIONS

Nucleus	Level	J^π	T	Configura- tion	Total energy*	
					Experi- mental	Calculated
${}^6C_7^{13}$	3.09	$1/2^+$	$1/2$	$s_{1/2}$	1.86	1.86
${}^7N_6^{13}$	2.37	$1/2^+$	$1/2$	$s_{1/2}$	-0.42	-0.37
${}^6C_8^{14}$	6.89	0^-	1	$p_{1/2} s_{1/2}$	6.23	6.37
	6.09	1^-	1	$p_{1/2} s_{1/2}$	7.03	7.03
${}^7N_7^{14}$	8.70	0^-	1	$p_{1/2} s_{1/2}$	3.79	3.74
	8.06	1^-	1	$p_{1/2} s_{1/2}$	4.43	4.40
	4.91	0^-	0	$p_{1/2} s_{1/2}$	7.58	7.47
	5.69	1^-	0	$p_{1/2} s_{1/2}$	6.80	6.86
${}^6C_9^{15}$	g.s.	$1/2^+$	$3/2$	$p_{1/2}^2 s_{1/2}$	14.33	14.23
${}^7N_9^{16}$	0.12	0^-	1	$p_{1/2}^2 s_{1/2}$	25.87	25.83
	0.39	1^-	1	$p_{1/2}^2 s_{1/2}$	25.60	25.69
${}^8O_8^{16}$	12.78	0^-	1	$p_{1/2}^2 s_{1/2}$	22.66	22.55
	13.09	1^-	1	$p_{1/2}^2 s_{1/2}$	22.35	22.39
${}^8O_9^{17}$	0.87	$1/2^+$	$1/2$	$p_{1/2}^2 s_{1/2}$	38.72	38.73
${}^9F_8^{17}$	0.51	$1/2^+$	$1/2$	$p_{1/2}^2 s_{1/2}$	35.53	35.58

* From these the binding energy of C^{12} was subtracted. All energies are in Mev.

TABLE VI
 ENERGIES OF $p_{1/2}^m d_{5/2}$ CONFIGURATION

Nucleus	Level	J^π	T	Configura- tion	Total energy*	
					Experi- mental	Calculated
${}^6\text{C}^{12}$	3.86	$5/2^+$	1/2	$d_{5/2}$	1.09	0.98
${}^7\text{N}^{13}$	3.56	$5/2^+$	1/2	$d_{5/2}$	-1.61	-1.64
${}^8\text{C}^{14}$	7.35	2^-	1	$p_{1/2}d_{5/2}$	5.77	5.83
	6.72	3^-	1	$p_{1/2}d_{5/2}$	6.40	6.39
${}^7\text{N}^{14}$	9.50	2^-	1	$p_{1/2}d_{5/2}$	2.99	3.01
	8.90	3^-	1	$p_{1/2}d_{5/2}$	3.59	3.61
	5.10	2^-	0	$p_{1/2}d_{5/2}$	7.39	7.48
	5.83	3^-	0	$p_{1/2}d_{5/2}$	6.66	6.64
${}^8\text{C}^{15}$	0.66	$5/2^+$	3/2	$p_{1/2}^3d_{5/2}$	13.67	13.76
${}^7\text{N}^{16}$	g.s.	2^-	1	$p_{1/2}^3d_{5/2}$	25.99	25.93
	0.30	3^-	1	$p_{1/2}^3d_{5/2}$	25.71	25.79
${}^8\text{O}^{16}$	12.95	2^-	1	$p_{1/2}^3d_{5/2}$	22.49	22.46
	13.24	3^-	1	$p_{1/2}^3d_{5/2}$	22.20	22.32
${}^8\text{O}^{17}$	g.s.	$5/2^+$	1/2	$p_{1/2}^4d_{5/2}$	39.59	39.51
${}^9\text{F}^{17}$	g.s.	$5/2^+$	1/2	$p_{1/2}^4d_{5/2}$	36.04	35.98

* From these the binding energy of C^{12} was subtracted. All energies are in Mev.

the $p_{1/2}^2d_{5/2}$ state agrees very well with the energy of the first excited state in C^{15} . Thus, on the basis of the above analysis it is possible to predict the spins of the ground state and first excited level in C^{15} . There are now experimental indications that the predicted assignments are correct. The energies of these two states of C^{15} are included in Table V and Table VI. The same good agreement is obtained for the $1/2^+ T=3/2$ level at 11.61 Mev in N^{15} .

Another simple case which can be treated is that of the odd-parity $T=0$ levels in O^{16} . The 0^- and 1^- levels of the $p_{1/2}^3s_{1/2}$ configuration are calculated to lie at 11.41 and 9.95 Mev, respectively. Similarly, the calculated 2^- and 3^- levels of the $p_{1/2}^3d_{5/2}$ configuration lie at 10.17 and 8.84 Mev, respectively, above the O^{16} ground state. Of all energies of these four calculated levels, there seems to be only one that agrees with the experimental energy. The lowest $0^- T=0$ level observed in O^{16} lies at 10.94 Mev above the ground state as compared with the predicted value of 11.41 Mev. However, the lowest 1^- , 2^- , and $3^- T=0$ levels lie at 7.12, 8.88, and 6.14 Mev above the O^{16} ground state. The discrepancy between the calculated and experimental energies is thus about 1-3 Mev! It is clear that these levels have no simple shell-model description. We see that the simple model, which gives good results for the $T=1$ states, is not sufficient for the $T=0$ states in O^{16} . This seems to be a rather general feature (56). We shall see more examples of this behavior in

the following. Possibly this effect is ascribable to a much larger configuration interaction in $T=0$ levels as compared to $T=1$ levels. In fact, levels with $T=0$ are, on the average, much closer than $T=1$ levels. It is significant that much better agreement is obtained for the 0^- $T=0$ level. Such $J=0$ states are much more scarce than the others. For example, we can consider only one-nucleon excitation from the $p_{3/2}$, $p_{1/2}$ shell into the $d_{3/2}$, $s_{1/2}$, $d_{5/2}$ shell. Only one 0^- state can be obtained in addition to the one discussed above. It is caused by excitation of a $p_{3/2}$ nucleon into the $d_{3/2}$ orbit. Such an excitation has a large energy difference and can probably be neglected. On the other hand, there are several such 1^- , 2^- , and 3^- states which can interact.

The case of the $T=1/2$ levels in N^{16} and O^{16} is also significantly different from the $T=3/2$ case (of C^{16} and N^{16}). The $1/2^+$ and $5/2^+$ $T=0$ levels in N^{16} and O^{16} are not single-nucleon levels. They can be built by coupling the $2s_{1/2}$ or $1d_{5/2}$ nucleon to either the $J=0$, $T=1$ (2.31 Mev) state or the $J=1$, $T=0$ ground state of N^{14} . Therefore, the two-by-two matrix built with the interaction parameters V_J and V'_J should be diagonalized. The lowest $1/2^+$ and $5/2^+$ states are thus calculated to lie at 7.33 and 6.76 above the ground state of N^{16} . The lowest levels known experimentally are found in N^{16} at 5.31 and 5.28 Mev, respectively. Also, in this case the discrepancy is about 2 Mev in contrast to the good agreement obtained for the $T=3/2$ levels. Configuration interaction may well be important. In the present calculation, the pure jj -coupling $p_{1/2}^2$ configuration is assumed for N^{14} . Since this is not actually correct, the present calculation is not fully adequate. For example, the actual $1/2^+$ and $5/2^+$ states may be strongly admixed with states built by coupling the $2s_{1/2}$ (or $1d_{5/2}$) nucleon to the second 1^+ $T=0$ (3.95 Mev) state of N^{14} .⁷

A nice check for the assignments to the odd-parity levels considered is obtained from $M1$ -transition probabilities, particularly in N^{14} (43). In Figure 6 all the relevant $M1$ transitions are shown.

The most striking fact is the absence of transitions between the 2^- $T=1$ level (at 9.50 Mev) to the 1^- $T=0$ level (at 5.69 Mev) and between the 1^- $T=1$ level (at 8.06 Mev) to the 2^- $T=0$ level (at 5.10 Mev). From spin, isospin, parity, and energy considerations, $M1$ transitions should occur in these cases. These transitions are, however, between states of the $p_{1/2}s_{1/2}$ and $p_{1/2}d_{5/2}$ configurations and thus have vanishing matrix elements of the $M1$ operator (Eq. 38). That no such (l -forbidden) transitions are found is in full agreement with our configuration assignments.

Thus, every $M1$ transition occurring between odd-parity levels in N^{14} is within a certain configuration. Only one $M1$ transition with $\Delta T=0$ was observed. It is, however, very weak in agreement with Morpurgo's selection rule (41) on $M1$ transitions with $\Delta T=0$. All other $M1$ transitions between odd-parity states in N^{14} are given in Table VII.

The quantity presented is the reduced matrix element

$$(j_1 j_2 T_1 J_1 || \Omega(M1) || j_1 j_2 T_2 J_2)$$

⁷ We are grateful to Prof. J. B. French for pointing out this possibility.

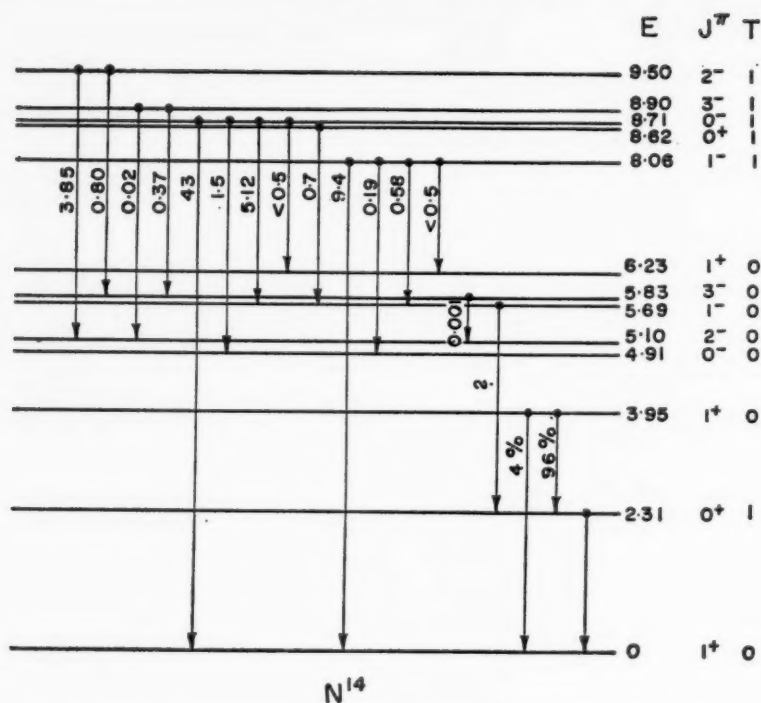


FIG. 6. $M1$ and $E1$ transitions in N^{14} . Energies are given in Mev. Radiative widths (Γ_γ , in ev) of the various transitions are indicated. Also given is the percentage branching of the transitions from the 3.95-Mev level.

TABLE VII
REDUCED MATRIX ELEMENTS FOR $M1$ TRANSITIONS IN N^{14}

Configuration	Transition		Reduced matrix elements	
	$E_i(T_i J_i)$	$E_f(T_f J_f)$	Experimental	Calculated
$p_{1/2} s_{1/2}$	8.71(1 0)	5.69(0 1)	$\leq 7.95^*$	5.41
$p_{1/2} s_{1/2}$	8.06(1 1)	4.91(0 0)	2.57	5.41
$p_{1/2} s_{1/2}$	8.06(1 1)	5.69(0 1)	-6.76	-4.76
$p_{1/2} d_{5/2}$	9.50(1 2)	5.10(0 2)	9.05	8.21
$p_{1/2} d_{5/2}$	9.50(1 2)	5.83(0 3)	5.42	3.92
$p_{1/2} d_{5/2}$	8.90(1 3)	5.10(0 2)	0.96*	3.92
$p_{1/2} d_{5/2}$	8.90(1 3)	5.83(0 3)	-5.70	-6.73

* These values are highly uncertain and were excluded from the analysis.

whose square, according to Equation 39, is equal, to $(2J+1)\Delta(M1)$. The experimental values of the reduced matrix elements given in Table VII were

obtained from the experimental transition strengths Λ . The sign of these experimental reduced matrix elements is obviously not given by the transition rates and was chosen according to the theoretical expectation. The two experimental values with an asterisk are highly uncertain and were excluded from the analysis. The theoretical formula for the reduced matrix elements is given by Equation 45 in terms of the various $g_{ji}^{(n)} - g_{ji}^{(p)}$. In the present case, there are altogether three such differences for $j \equiv 1p_{1/2}$, $j \equiv 2s_{1/2}$, and $j \equiv 1d_{5/2}$. We take these three quantities as undertermined parameters and try to find values of these that will best reproduce the experimental reduced matrix elements. A least-squares fit gives these best values which are listed in Table VIII. When these values are introduced into the theoretical expressions, we

TABLE VIII
EFFECTIVE VS. SCHMIDT g FACTORS

Difference of g factors	Effective value	Schmidt value
$g_{p_{1/2}}^{(n)} - g_{p_{1/2}}^{(p)}$	2.36	1.805
$g_{s_{1/2}}^{(n)} - g_{s_{1/2}}^{(p)}$	-10.13	-9.414
$g_{d_{5/2}}^{(n)} - g_{d_{5/2}}^{(p)}$	-2.23	-2.683

obtain the calculated values of the reduced matrix elements listed in the last column of Table VII. There seems to be a fair agreement between experimental and calculated values. This agreement is, however, less complete than that in many energy calculations. It was already pointed out that transition probabilities are more sensitive to small changes in the wave functions. Furthermore, the experimental data are not very accurate. For example, in Figure 6 an experimental γ -transition rate is quoted between two 0^- levels. This is strictly forbidden (because of angular momentum conservation).

It is of interest to compare the effective values of the differences of g factors with those obtained from Schmidt values (Eq. 1) (last column of Table VIII). It can be seen that the effective values are rather close to Schmidt values. The deviations are rather small but agree only in one case of the three with the trend observed for nuclear (static) magnetic moments. This should not be surprising in view of the tentative nature of the analysis described above. More accurate experimental data are required before it can be concluded whether the approach of using effective g factors is successful.

The other nucleus in which relevant $M1$ transitions are observed is N^{16} . Unfortunately, no $M1$ lifetimes were measured. The only experimental fact of interest is the branching of the transitions from the 1^- level at 0.392 Mev. It decays 75 per cent to the 0^- level (at 0.120 Mev) and 25 per cent to the 2^- ground state. If the configurations were 100 per cent pure, the $1^- \rightarrow 2^-$ transition could be only an $E2$ transition since the $M1$ transition would be l forbidden. If this were true, the $1^- \rightarrow 2^-$ branch would be far smaller. However, small admixtures of, say, the $p_{1/2}^3 d_{3/2}$ configuration in the 1^- state

enable it to decay to the 2^- state with the $p_{1/2}^3 d_{3/2}$ configuration by $M1$ transition. It was already mentioned that in this case such a transition cannot be adequately described by an effective $E2$ operator since the admixture allows the much faster $M1$ transitions. Still, the $1^- \rightarrow 2^-$ branch is considerably smaller than the $1^- \rightarrow 0^-$ branch, although the energy difference is bigger in the first transition. The ratio between the two rates multiplied by the cube of the energies ratio is 9. A more detailed calculation shows that in order to obtain this ratio, the probability of the $p_{1/2}^3 d_{3/2}$ configuration in the 1^- state should be less than 5 per cent.

IX. CONFIGURATIONS OF $s_{1/2}$ AND $d_{5/2}$ NUCLEONS

After the $1p$ shell is closed (beyond O^{16}), the $1d_{5/2}$ and $2s_{1/2}$ orbits are being filled. As soon as the $1p$ shell is full, the $1d_{5/2}$ orbit becomes lower than the single $2s_{1/2}$ -nucleon level. These two subshells are almost degenerate. On the other hand, the $1d_{3/2}$ subshell, which belongs to the same harmonic oscillator shell, lies much higher. This situation is clearly demonstrated in the single-particle spectrum of O^{17} (or F^{17}) in Figure 2. We have seen in Section VIII that the $p_{1/2}s_{1/2}$ and $p_{1/2}d_{5/2}$ configurations overlap whereas the $p_{1/2}d_{3/2}$ configurations are not observed in the same region. It can therefore be assumed that, to a certain approximation, $d_{3/2}$ nucleons are not involved in the low-lying states of nuclei beyond O^{16} . On the other hand, strong mixing may take place between the possible configuration involving $d_{5/2}$ and $s_{1/2}$ nucleons.

Let us first consider the oxygen isotopes. Here, only the neutron shell is being filled. The following analysis of the low-lying levels with effective interactions shows that they can be described, to a good approximation, by pure $d_{5/2}^n$ configurations. The total energies of states of $d_{5/2}^n$ configurations were given in Section V by the closed expression in Equation 16. The analysis is thus straightforward.

The ground state of O^{17} provides the energy of a single $d_{5/2}$ neutron (above the O^{16} binding energy). In O^{18} the 0^+ (ground state), 2^+ (1.98 Mev), and 4^+ (3.55 Mev) levels are taken to belong to the $d_{5/2}^2$ configuration. In O^{19} the $5/2^+$ ground state is taken to belong to the $d_{5/2}^3$ configuration. The same assumption is made on the first excited $3/2^+$ state (at 0.096 Mev) of O^{19} . We saw in Section V that using the levels spacings of O^{18} with Equation 17, the spacing between the $J=5/2$ and $J=3/2$ of the $d_{5/2}^3$ configuration agrees well enough with the observed $5/2^+ - 3/2^+$ spacing in O^{19} . The $1/2^+$ level at 1.47 Mev above the ground state of O^{19} cannot belong to the $d_{5/2}^3$ configuration which has only three states with $J=5/2$, $J=3/2$, and $J=9/2$; it must belong to the $d_{5/2}^2 s_{1/2}$ configuration and is thus not considered here. In O^{20} the ground state, as well as the first excited 2^+ level (at 1.7 Mev), is taken to belong to the $d_{5/2}^4$ configuration; and their energies are included in the analysis. The 0—2 separation in O^{20} should be equal on this assumption to that in O^{18} , since the $d_{5/2}^4$ configuration is equivalent to the two-hole $d_{5/2}^{-2}$ configuration. Actually it is slightly smaller (1.70 Mev as compared to 1.98 Mev). Also, the 4^+ level in O^{20} is expected to be at the same height as the one in O^{18} .

The total energies of all these levels can be best reproduced by Equation 16 with the following values (in Mev) of the interaction parameters

$$C = 4.37 \quad a = 0.08 \quad b = -0.12 \quad c = 0.21$$

The sign of b is negative since the $J=2$ level is below the $J=4$ level in the $d_{5/2}^2$ configuration. The signs and magnitudes of a and c are such that the factor α multiplying the quadratic term in Equation 20 is equal in the present case to $a-c = -0.13$ Mev and is thus repulsive, as it should be. When these values of the interaction constants are inserted in Equation 16, we obtain the calculated values to be compared with the experimental energies. This comparison is made in Table IX. We see that the agreement is quite good.

The $J=9/2$ state of the $d_{5/2}^3$ configuration in O^{19} is calculated with our parameters to lie 2.6 Mev above the $5/2^+$ ground state. It would be interesting to establish experimentally the position of this $9/2^+$ level. As seen from Table IX, the $J=3/2$ state in O^{19} is calculated to be very close to the $J=5/2$ ground state. The existence of a very low-lying state with $J=j-1$ in j^3 configurations (of identical nucleons) is a general feature of nuclear spectra. It can be traced to the properties of the effective two-body nuclear interaction. In the $d_{5/2}$ orbit this property causes the spacing between the levels with $J=4$ and $J=2$ to be almost equal to the $0-2$ spacing. For configurations with higher values of j , the behavior is essentially the same. With δ -type interactions, the $0-2$ spacing is much bigger than the spacings between the $v=2$ levels with $J=2, 4, \dots$ in the j^2 configuration. In this case, there is also a large spacing between the $v=1, J=j$ state and all $v=3$ levels. However, actual nuclear spectra of j^2 configurations are very different from those obtained with δ forces (or other short-range forces). The $2-4$ separation,

TABLE IX
ENERGIES OF $d_{5/2}^n$ -NEUTRON CONFIGURATIONS

Nucleus	E	J^* of state	Theoretical expression (Eq. 16)	Total energy*	
				Experi- mental	Calculated
$^8O^{17}$	g.s. †	$5/2^+$	C	4.14	4.37
$^8O^{18}$	g.s.	0^+	$2C+a-(35/2)b+6c$	12.21	12.18
	1.982	2^+	$2C+a-(23/2)b$	10.23	10.20
	3.55	4^+	$2C+a+(5/2)b$	8.66	8.52
$^{11}O^{19}$	g.s.	$5/2^+$	$3C+3a-(35/2)b+4c$	16.16	16.29
	0.096	$3/2^+$	$3C+3a-(45/2)b$	16.06	16.05
$^8O^{20}$	g.s.	0^+	$4C+6a-35b+8c$	23.82	23.84
	1.70	2^+	$4C+6a-29b+2c$	22.12	21.86

* From these the binding energy of O^{16} was subtracted. All energies are in Mev.

† Ground state.

for example, is in general not much smaller than the 0—2 separation. This is true in the $1d_{5/2}^2$ configuration just discussed, as well as in the $1f_{7/2}^2$ configuration (36, 37) and the $1g_{9/2}^2$ configuration (57). In fact, a low-lying $5/2^-$ state is found in nuclei with $f_{7/2}^3$ configurations (Ca^{43} , Ca^{45} , V^{51} , and Mn^{53}). Similarly, a low-lying $7/2^+$ state is found in Sr^{85} with the $g_{9/2}^{-3}$ neutron configuration.

It has been shown in Section VI that in pure jj coupling, $M1$ transitions between any two states of the j^3 configuration are forbidden. The $M1$ transition found in O^{19} between the $3/2^+$ (0.096 Mev) level and the $5/2^+$ ground state is in fact very much retarded. This transition can take place because of a small admixture of the $d_{5/2}^2 d_{3/2}$ configuration in the $3/2^+$ state. The probability of admixture necessary to give the experimentally found transition probability (with a measured radiative width of about 4×10^{-7} ev) can be calculated and turns out to be about 3 per cent.

The situation becomes different when both protons and neutrons are present (more accurately, for states with T smaller than the maximum). This fact is illustrated by comparing the spectrum of F^{18} to that of Al^{26} . If no configuration interaction were present, certain parts of these two spectra should be the same since in F^{18} there is the $d_{5/2}^2$ configuration and in Al^{26} the $d_{5/2}^{-2}$ configuration. Indeed, certain similarities are observed between the two spectra. In both nuclei, the separation between the $T=1$ levels with $J=0$ and $J=2$ is about the same (1.84 Mev in Al^{26} , 1.97 Mev in F^{18}). The $T=1$, $J=4$ level is not known experimentally in Al^{26} . There are, however, also other similarities between the two spectra. The 5^+ and 3^+ $T=0$ levels and 0^+ $T=1$ level are close together in both cases. In F^{18} the 3^+ level is at 0.94, the 0^+ at 1.09, and the 5^+ at 1.13 Mev. In Al^{26} the order is 5^+ , ground state, 0^+ at 0.23 and 3^+ at 0.42 Mev. The main difference between the two spectra is in the positions of the 1^+ $T=0$ states. One such state lies 1.13 Mev below the 5^+ state in F^{18} , another 1^+ $T=0$ state lies 0.57 Mev above the 5^+ state. On the other hand, the one known 1^+ $T=0$ state in Al^{26} lies 1.05 Mev above the 5^+ ground state. This shows that configuration interaction must be present and is particularly important for the $J=1$ states. It is clear that no simple configuration interaction can affect the 5^+ level in F^{18} , which must be a pure $d_{5/2}^2$ state. Rough estimates on the relative importance of the configuration interaction parameters can, therefore, be achieved by comparing the spacings between the 5^+ level and the other levels in F^{18} and Al^{26} . The 3^+ state is shifted down by 0.61 Mev in F^{18} as compared to Al^{26} . There must, therefore, be some interaction between the $d_{5/2}^2$ $T=0$, $J=3$ state and the $d_{5/2} s_{1/2}$ $T=0$, $J=3$ state. The 0^+ state is shifted only by 0.27 Mev and the 2^+ only by 0.14 Mev. In these states there is probably only very slight configuration interaction, in agreement with our analysis of the oxygen isotopes. Far worse is the situation in the $T=0$, $J=1$ states. Obviously they are most strongly affected by configuration interaction. Furthermore, it can be seen that it may not be sufficient to take into account only the two $T=0$, $J=1$ states of the $d_{5/2}^2$ and $s_{1/2}^2$ configurations.

It is necessary to assume configuration interaction not only for explaining the spectrum of F^{18} ; the spectra of F^{19} (and Ne^{19}) and Ne^{20} are much more difficult to understand without configuration interaction. Only by assuming configuration mixing can one understand the very high binding energies of F^{19} (and Ne^{19}) and Ne^{20} and the fact that the $1/2^+$ and $5/2^+$ states in F^{19} (and Ne^{19}) are almost degenerate (58). As the $1d_{5/2}$ subshell is being filled, configuration interaction may become less important. In fact, the Al^{26} spectrum has fewer low-lying levels than that of F^{18} . If this trend is really true, it may still be possible that the shell-model description in terms of $d_{5/2}^n$ configurations will be more valid beyond Ne^{20} . We shall point out here only a few simple features of some spectra which can be understood on this basis.

The $T=1/2$ ground state of Ne^{21} with the $d_{5/2}^5$ configuration has $J=3/2$, and there is a $J=5/2$ state at 0.35 Mev above it. A very similar spectrum is observed also in nuclei where the equivalent $d_{5/2}^7$ ($d_{5/2}^{-5}$) configuration is expected. In Na^{23} the ground state has $J=3/2$, and a $J=5/2$ state lies 0.44 Mev above it (the corresponding spacing in the mirror nucleus Mg^{23} is 0.45 Mev). The level order and spacing are almost the same in the two cases.

Mg^{25} and Al^{25} are very interesting nuclei. Their ground states have $J=5/2$ which could belong to the $d_{5/2}^{-3}$ configuration. The first excited $1/2^+$ state (at 0.58 in Mg^{25} and at 0.45 in Al^{25}) is far lower than the $J=1/2$ state of the $d_{5/2}^{-3}$ configuration (with tentative interaction parameters taken from the Al^{26} and F^{18} spectra). We may assume that this $1/2^+$ state is obtained by coupling a $2s_{1/2}$ nucleon to the ground state of Mg^{24} . It is then interesting to see whether $3/2^+$ and $5/2^+$ states could be found in Mg^{25} (and Al^{25}) which are similarly obtained from the first excited 2^+ state in Mg^{24} (at 1.37 Mev). If both ground state and 2^+ state in Mg^{24} belong to the $d_{5/2}^{-4}$ configuration, a simple relation exists between the energies of the states involved. This relation is known as the "center-of-mass theorem" (59) and will now be briefly discussed.

Let us consider, for simplicity, one j' neutron coupled to a state with a given J of the j^n -proton configuration (with the neutron j shell closed). We look at all states with spins J' obtained by coupling j' to J . It can be shown that the average interaction between the j' neutron and the j protons in all these states is independent of the state (with spin J) of the j^n -proton configuration. In particular, if n is even, this "center-of-mass interaction" is equal to the interaction energy in the single state with $J=0$ and $J'=j'$. If, now, H is the complete shell-model Hamiltonian, containing single-particle energies as well as mutual two-body interactions, it follows from this property that

$$\frac{\sum (2J' + 1) \langle j^n(J)j'J' | H | j^n(J)j'J' \rangle}{\sum (2J' + 1)} - \langle j^n(0)j' | H | j^n(0)J' \rangle \\ = \langle j^nJ | H | j^nJ \rangle - \langle j^nJ=0 | H | j^nJ=0 \rangle \quad 53.$$

The summation in Equation 53 extends over the J' values of all possible

states. It should be remembered that the interaction energy has nonvanishing elements $\langle j^n(J_1)j'J' | H | j^n(J_2)j'J' \rangle$ which contribute to the energy. Therefore, Equation 53 cannot generally be used with the experimental energies of the $j^n j'$ configuration. However, in certain cases, notably for $j' = 1/2$, the center-of-mass theorem may become more useful.

We can apply Equation 53 also in the case of the $2s_{1/2}$ neutron coupled to the $T=0$ states of Mg^{24} . According to this equation, the spacing between the center of mass of the $5/2^+$ and $3/2^+$ of Mg^{25} , built on the $T=0$, $J=2$ state of Mg^{24} , and the $1/2^+$ state, built on the 0^+ ground state, should be equal to the 0—2 spacing in Mg^{24} . The center of mass of the $5/2^+$ level at 1.96 Mev and the $3/2^+$ level at 0.98 Mev lies 1.57 Mev above the Mg^{25} ground state. It is therefore separated by 0.99 Mev from the $1/2^+$ level (at 0.58 Mev). The corresponding spacing in the mirror Al^{25} nucleus is 1.02 Mev. This spacing should be compared to the 1.37 Mev 0—2 separation in Mg^{24} . The agreement is not very good, but it may still indicate the major components of the configurations in the states considered.

Although the $1d_{5/2}$, $2s_{1/2}$ shell begins to fill beyond O^{16} , there are several levels in lighter nuclei in which the extra nucleons are probably in these orbits. In Section VIII we discussed excited configuration with one $1d_{5/2}$ or $2s_{1/2}$ nucleon. There are, however, some cases which may be interpreted as having two such nucleons. There are, for instance, two levels in N^{14} in which the two nucleons outside C^{12} are in the $2s_{1/2}$ or the $1d_{5/2}$ orbits (43). The 0^+ $T=1$ state at 8.62 Mev is probably an admixture of the $s_{1/2}^2$ and $d_{5/2}^2$ configurations. This can be seen right away from the large Thomas-Ehrman shift of this level in C^{14} and N^{14} (Fig. 4). A preliminary calculation with the tentative interaction parameters obtained from the analysis of F^{18} (and Al^{26}) shows that in N^{14} the admixture should be much larger than in O^{18} . Another such case is the 1^+ $T=0$ state at 6.23 Mev in N^{14} .

In the region C^{12} — O^{16} there are a number of $E1$ transitions, all of which involve a transition of a nucleon from $2s_{1/2}$ to $1p_{1/2}$ state. All these transitions can be expressed in terms of one (effective) reduced matrix element, namely $\langle s_{1/2} || \Omega(E1) || p_{1/2} \rangle$. These transitions occur between states of configurations of the $p_{1/2}^m$, $p_{1/2}^{m-1}s_{1/2}$ and $p_{1/2}^{m-2}s_{1/2}^2$. These $E1$ transitions can all be roughly calculated with one value of the effective matrix element.

It is clear that to have a better shell-model description of the $1d_{5/2}$, $2s_{1/2}$ shell, much more theoretical work is required as well as many more experimental data.

LITERATURE CITED

1. Mayer, M. G., and Jensen, J. H. D., *Elementary Theory of Nuclear Shell Structure* (John Wiley & Sons, Inc., New York, N. Y., 269 pp., 1955)
2. Elliott, J. P., and Lane, A. M., *Handbuch der Physik*, 39, 241 (1957)
3. Elliott, J. P., in *Nuclear Reactions*, 42-85 (Endt, P. M., and Demeur, M., Eds., North Holland Publishing Co., Amsterdam, Netherlands, 502 pp., 1959)
4. Bohr, A., and Mottelson, B. R., *Kgl. Danske Videnskab. Selskab, Mat.-fys. Medd.*, 27, (16) (1953)
5. Kerman, A. K., in *Nuclear Reactions*, 427-93 (Endt, P. M., and Demeur, M., Eds., North Holland Publishing Co., Amsterdam, Netherlands, 502 pp., 1959)
6. Aizenberg-Selove, F., and Lauritsen, T., *Nuclear Phys.*, 11, 1 (1959)
7. Endt, P. M., and Braams, C. M., *Revs. Mod. Phys.*, 29, 683 (1957)
8. *Nuclear Level Schemes $A=40-A=92$* , Compiled by Way, K., King, R. W., McGinnis, C. L., and van Lieshout, R., *U. S. Atomic Energy Commission Rept.*, TID-5300 (1955)
9. *Nuclear Data Sheets*, Compiled by McGinnis, C. L., Ed., Anderson, G., Fullwer, G. H., Marion, J. B., Way, K., and Yamada, M. (National Research Council, Washington, D. C.)
10. Macfarlane, M. H., and French, J. B., *NYO Rept.*, 2846, *Univ. Rochester* (Preprint, 1959) (To be published)
11. Bacher, R. F., and Goudsmit, S., *Phys. Rev.*, 46, 948 (1934)
12. Racah, G., *Phys. Rev.*, 85, 381 (1952)
13. Carlson, B. C., and Talmi, I., *Phys. Rev.*, 96, 436 (1954)
14. Talmi, I., and Thieberger, R., *Phys. Rev.*, 103, 718 (1956)
15. Unna, I., *Nuclear Phys.*, 8, 468 (1958)
16. Class, C. M., Davis, R. H., and Johnson, J. H., *Phys. Rev. Letters*, 3, 4 (1959)
17. Lane, A. M., and Elliott, J. P., *Phys. Rev.*, 96, 1160 (1954)
18. Thomas, R. G., *Phys. Rev.*, 81, 148 (1951)
19. Ehrman, J. B., *Phys. Rev.*, 81, 412 (1951)
20. Blatt, J. M., and Weisskopf, V. F., *Theoretical Nuclear Physics* (John Wiley & Sons, Inc., New York, 864 pp., 1952)
21. Racah, G., *Phys. Rev.*, 63, 367 (1943)
22. Racah, G., *Phys. Rev.*, 62, 438 (1942)
23. Edmonds, A. R., *Angular Momentum in Quantum Mechanics* (Princeton Univ. Press, Princeton, N. J., 146 pp., 1957)
24. Rose, M. E., *Elementary Theory of Angular Momentum* (John Wiley & Sons, Inc., New York, N. Y., 248 pp., 1957)
25. Fano, U., and Racah, G., *Irreducible Tensorial Sets* (Academic Press, Inc., New York, N. Y., 171 pp., 1959)
26. de-Shalit, A., and Talmi, I., *Nuclear Shell Theory* (Academic Press, Inc., New York, N. Y., to be published)
27. Mayer, M. G., *Phys. Rev.*, 78, 16, 22 (1950)
28. Flowers, B. H., *Proc. Roy. Soc. (London)*, A212, 248 (1952)
29. Edmonds, A. R., and Flowers, B. H., *Proc. Roy. Soc. (London)*, A214, 515 (1952)
30. Goldstein, S., and Talmi, I., *Phys. Rev.*, 105, 995 (1957)
31. Goldstein, S., and Talmi, I., *Phys. Rev.*, 102, 589 (1956)
32. Pandya, S. P., *Phys. Rev.*, 103, 956 (1956)
33. Racah, G. in *L. Farkas Memorial Volume*, 294-304 (Research Council of Israel Publication, Jerusalem, Israel, 1952)
34. Jarmie, N., and Silbert, M. G., *Phys. Rev. Letters*, 3, 50 (1959)
35. Talmi, I., *Phys. Rev.*, 107, 326 (1957)
36. Lawson, R. D., and Uretsky, J. L., *Phys. Rev.*, 106, 1369 (1957)
37. Talmi, I., in *Proc. Rehovoth Conf. Nuclear Structure, 1957*, 31-45 (1958)
38. Unna, I., and Talmi, I., *Phys. Rev.*, 112, 452 (1958)
39. Lane, A. M., and Radicati, L. A., *Proc. Phys. Soc. (London)*, A67, 167 (1954)
40. Radicati, L. A., *Phys. Rev.*, 87, 521 (1952)
41. Morpurgo, G., *Phys. Rev.*, 110, 721 (1958)
42. Wilkinson, D. H., in *Proc. Rehovoth Conf. Nuclear Structure, 1957*, 175-201 (1958)
43. Warburton, E. K., and Pinkston, W. T., *Phys. Rev.*, 118, 733 (1960)
- 43a. Ferguson, A. T. G., Grace, M. A., and Newton, J. O., *Nuclear Phys.*, 17, 1 (1960)
44. Teitelbaum, P., *Bull. Research Council Israel*, 3, 299 (1954)
45. Talmi, I. (To be published)

46. Oquidam, B., and Jancovici, B., *Nuovo cimento*, **11**, 578 (1959)
47. Kurath, D., *Phys. Rev.*, **101**, 216 (1956)
48. Kurath, D., *Phys. Rev.*, **106**, 975 (1957)
49. Wigner, E. P., *Phys. Rev.*, **51**, 106 (1937)
50. Amit, D. (Private communication)
51. Ferguson, A. J., Gove, H. E., Kuehner, J. A., Litherland, A. E., Almqvist, E., and Bromley, D. A., *Phys. Rev. Letters*, **1**, 414 (1958)
52. Talmi, I., and Unna, I., *Phys. Rev. Letters*, **4**, 469 (1960)
53. Wilkinson, D. H., and Alburger, D. E., *Phys. Rev.*, **113**, 563 (1959)
54. Bilaniuk, O. M., and French, J. B., *NYO Rept.*, 2853, *Univ. Rochester* (Preprint, 1959) (To be published)
55. Unna, I., and Talmi, I., *Energies of Ground and Excited Nuclear Configurations in the First $p_{1/2}$ Region*, **II** (To be published)
56. Elliott, J. P., and Flowers, B. H., *Proc. Roy. Soc. (London)*, **A242**, 57 (1957)
57. Talmi, I., and Unna, I., *Nuclear Phys.* (To be published)
58. Elliott, J. P., and Flowers, B. H., *Proc. Roy. Soc. (London)*, **A229**, 536 (1955)
59. Lawson, R. D., and Uretsky, J. L., *Phys. Rev.*, **108**, 1300 (1957)
60. Bohr, A., and Mottelson, B. R., in *Beta and Gamma Spectroscopy*, 468-93 (Siegbahn, K., Ed., North Holland Publishing Co., Amsterdam, Netherlands, 959 pp., 1955)
61. Nilsson, S. G., *Kgl. Danske Videnskab. Selskab, Mat.-fys. Medd.*, **29**(16) (1955)
62. Litherland, A. E., Paul, E. B., Bartholomew, G. A., and Gove, H. E., *Phys. Rev.*, **102**, 208 (1956)
63. Bromley, D. A., Gove, H. E., and Litherland, A. E., *Can. J. Phys.*, **35**, 1057 (1957)
64. Litherland, A. E., McManus, H., Paul, E. B., Bromley, D. A., and Gove, H. E., *Can. J. Phys.*, **36**, 378 (1958)
65. Bromley, D. A., in *Proc. Rehovoth Conf. Nuclear Structure, 1957*, 108-17 (1958)
66. Sheline, R. K., *Nuclear Phys.*, **2**, 382 (1956-57)
67. Paul, E. B., *Phil. Mag.*, **2**, 311 (1957)

APPENDIX: ENERGY LEVELS OF THE LIGHT NUCLEI

BY F. AJZENBERG-SELOVE AND T. LAURITSEN

*Haverford College, Haverford, Pennsylvania, and California Institute of
Technology, Pasadena, California*

Foreword

The following isobaric level schemes of the light nuclei are presented here as a service to the reader of the preceding article. Coulomb-energy differences and neutron-proton mass differences have been removed in accordance with the method described in (1, 2) in order to exhibit the correspondence of levels comprising isotopic-spin multiplets. Remaining mass differences are indicated in square brackets. Level energies in Mev, total angular momentum and parity J^π , and isobaric spin T are indicated. Uncertain values are enclosed in parentheses; uncertain, but probable, levels are shown by dashed lines. Further explanations are given in (3). Detailed references on which these compilations are based can be found in (4, 5). Atomic mass values have been taken from (6).

Acknowledgments

The material is reproduced here by permission of the McGraw-Hill Book Co. from a forthcoming edition of the *American Institute of Physics Handbook* (McGraw-Hill Book Co., Inc., New York, N. Y., 1961). The Editors are most grateful to the McGraw-Hill Book Company for this permission and to Drs. Ajzenberg-Selove and Lauritsen for furnishing the figures prior to publication in the *Handbook*.

The compilation of this material was supported in part by the joint program of the Office of Naval Research and the U. S. Atomic Energy Commission, and by the National Science Foundation.

References to Appendix

1. Lauritsen, T., *Ann. Rev. Nuclear Sci.*, **1**, 67 (1952)
2. Lauritsen, T., and Ajzenberg-Selove, F., *American Institute of Physics Handbook*, **8**, 56 (Gray, D. E., Ed., McGraw-Hill Book Co., Inc., New York, N. Y., 1957)
3. Ajzenberg-Selove, F., and Lauritsen, T., *American Institute of Physics Handbook* (Gray, D. E., Ed., McGraw-Hill Book Co., Inc., New York, N. Y., 1961)
4. Ajzenberg-Selove, F., and Lauritsen, T., *Nuclear Phys.*, **11**, 1 (1959)
5. *Landolt-Börnstein Tables*, 6th Ed., *Supplementary Volume on Nuclear Physics* (Springer-Verlag, Berlin, Germany, 1961)
6. Everling, F., König, L. A., Mattauch, J. H. E., and Wapstra, A. H., *Nuclear Phys.*, **15**, 342 (1960)

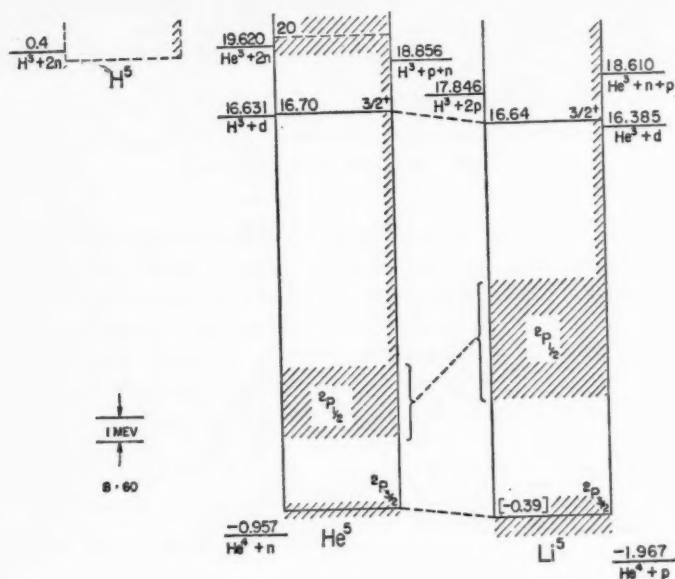


FIG. 1

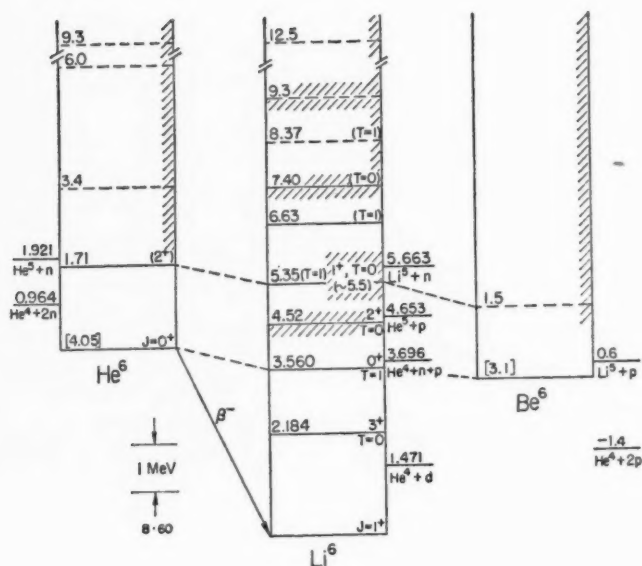


FIG. 2

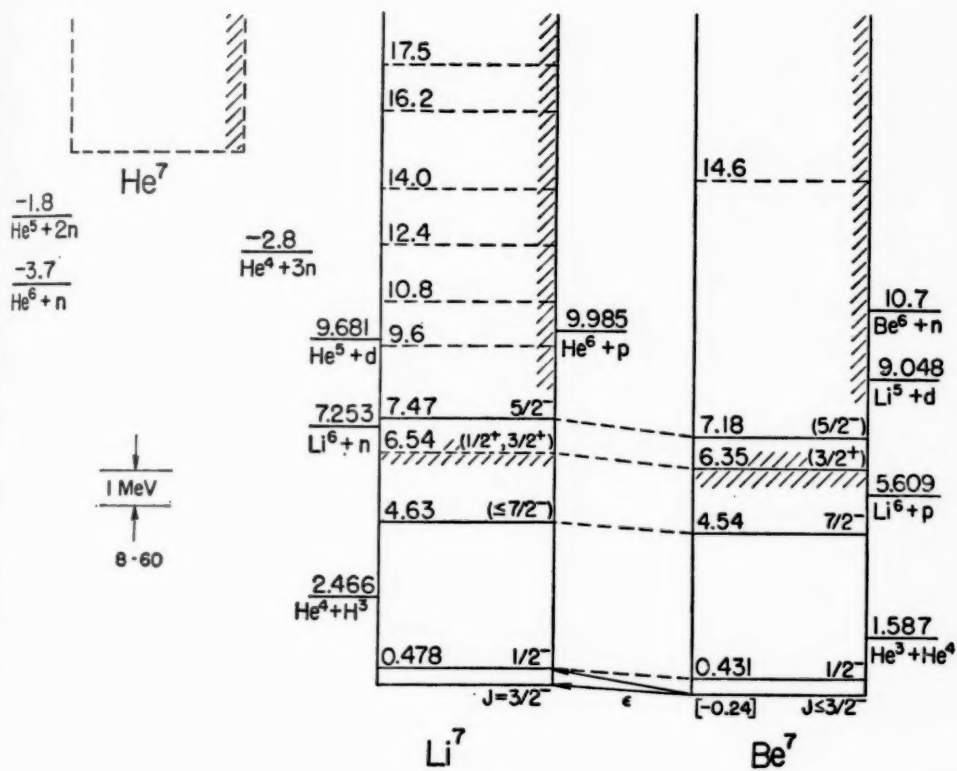


FIG. 3

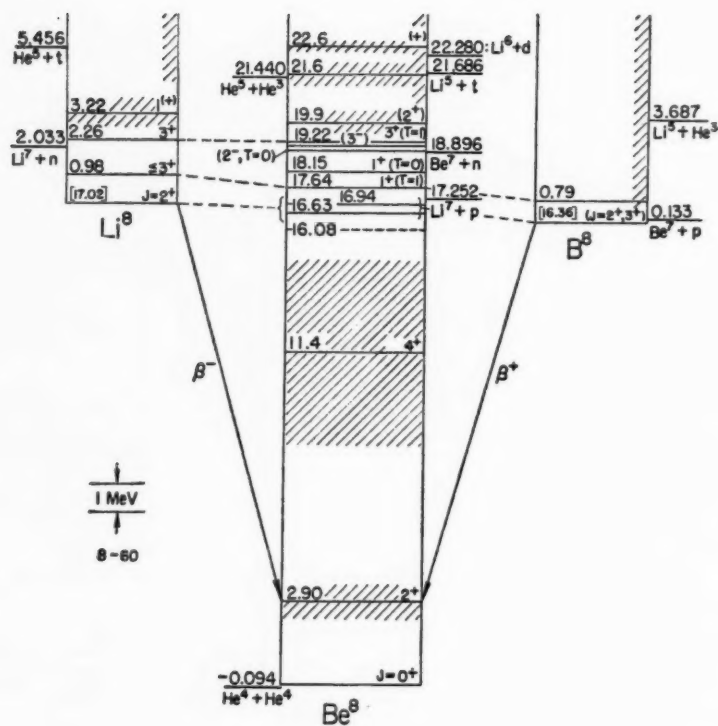


FIG. 4

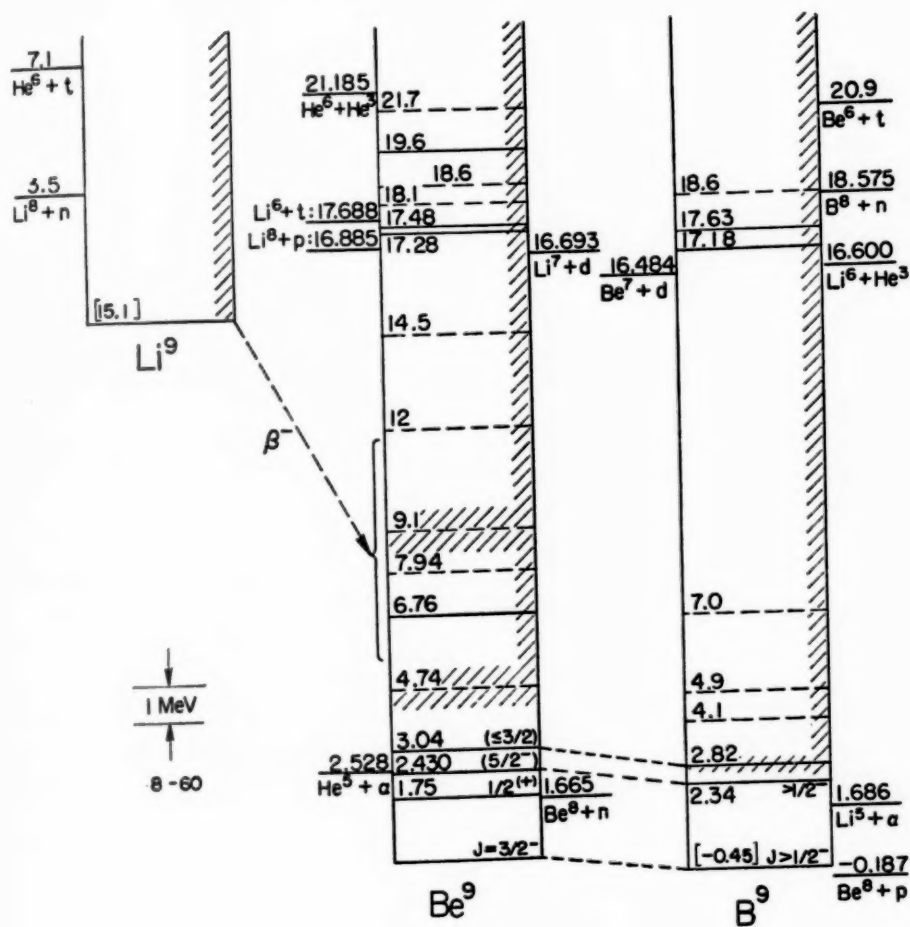


FIG. 5

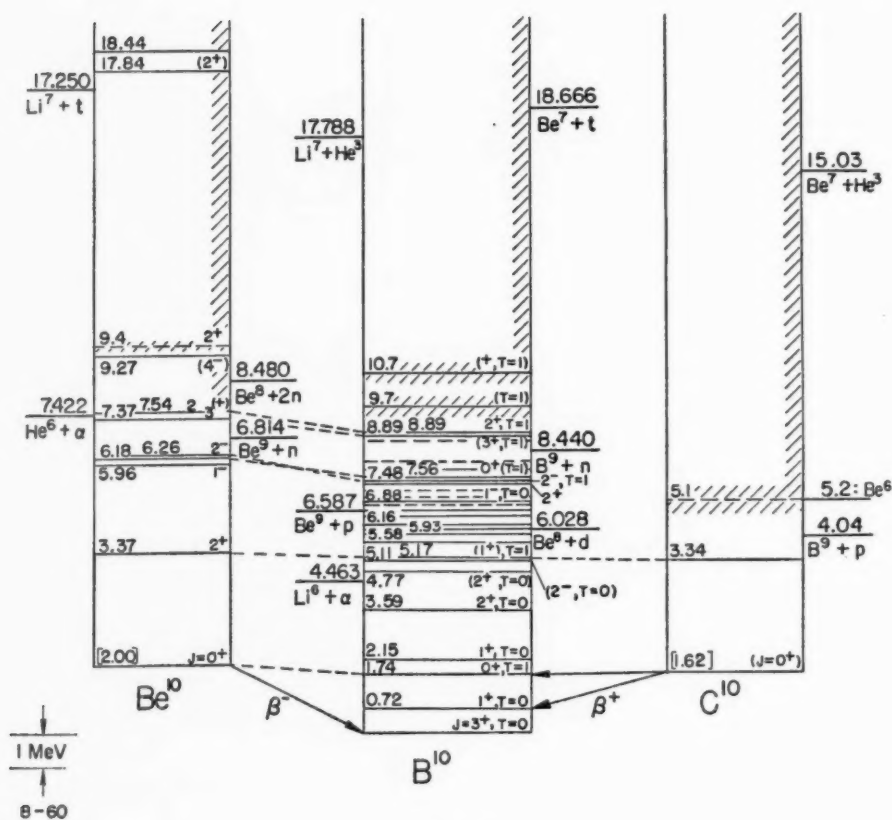


FIG. 6

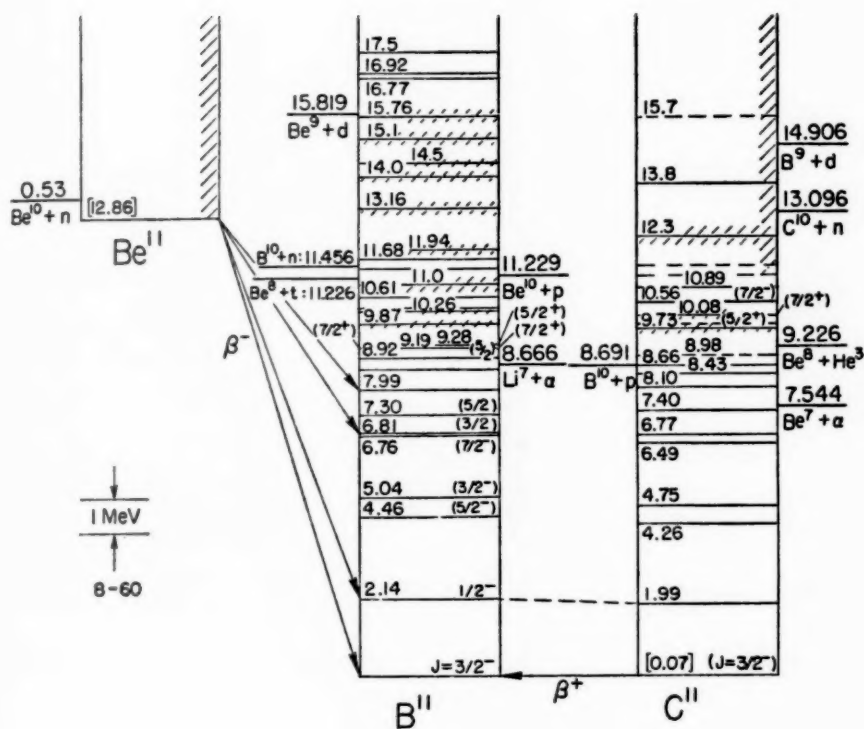


FIG. 7

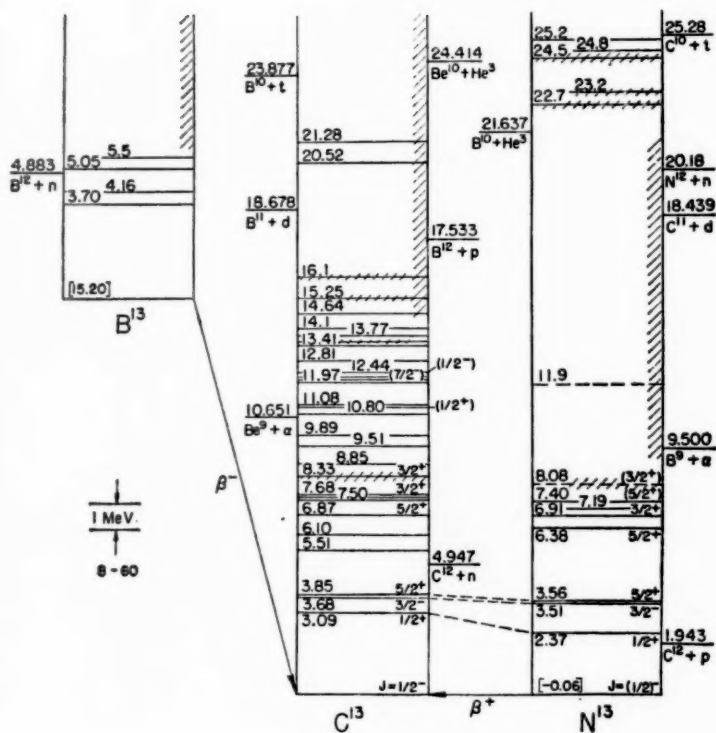


FIG. 9

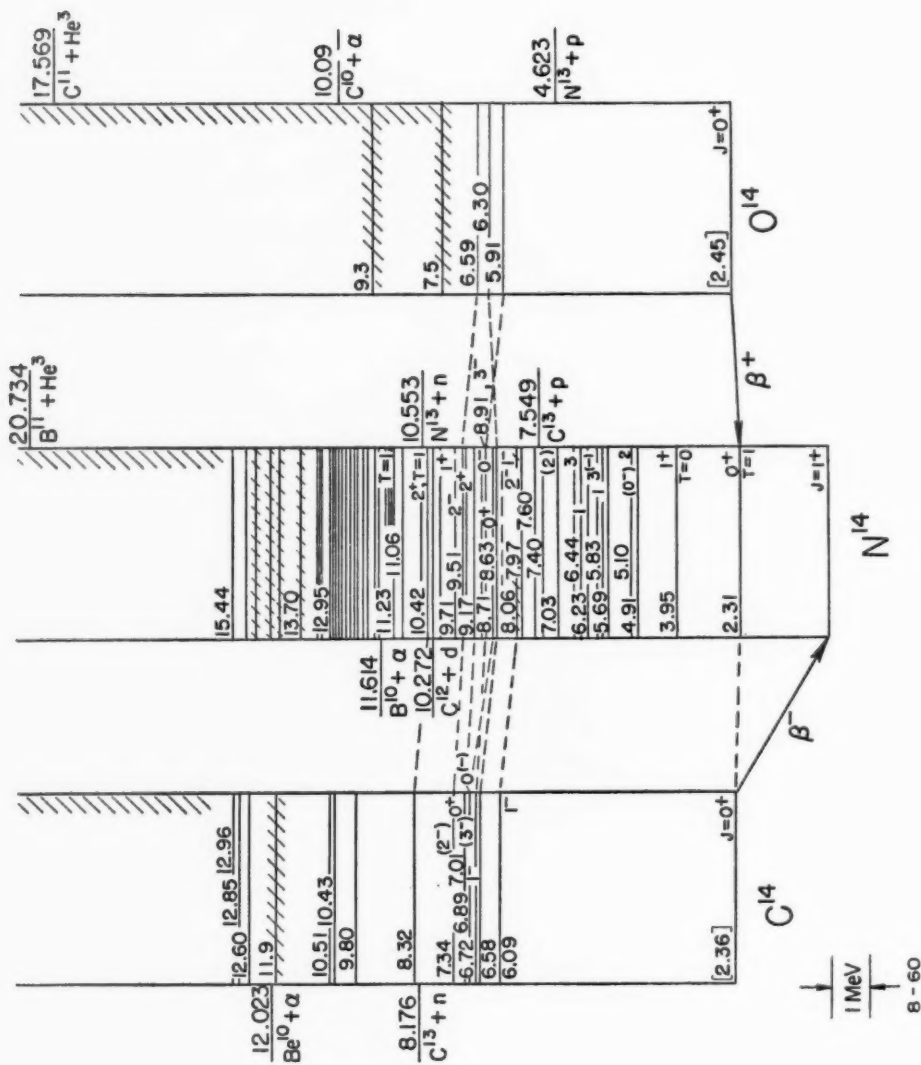


FIG. 10

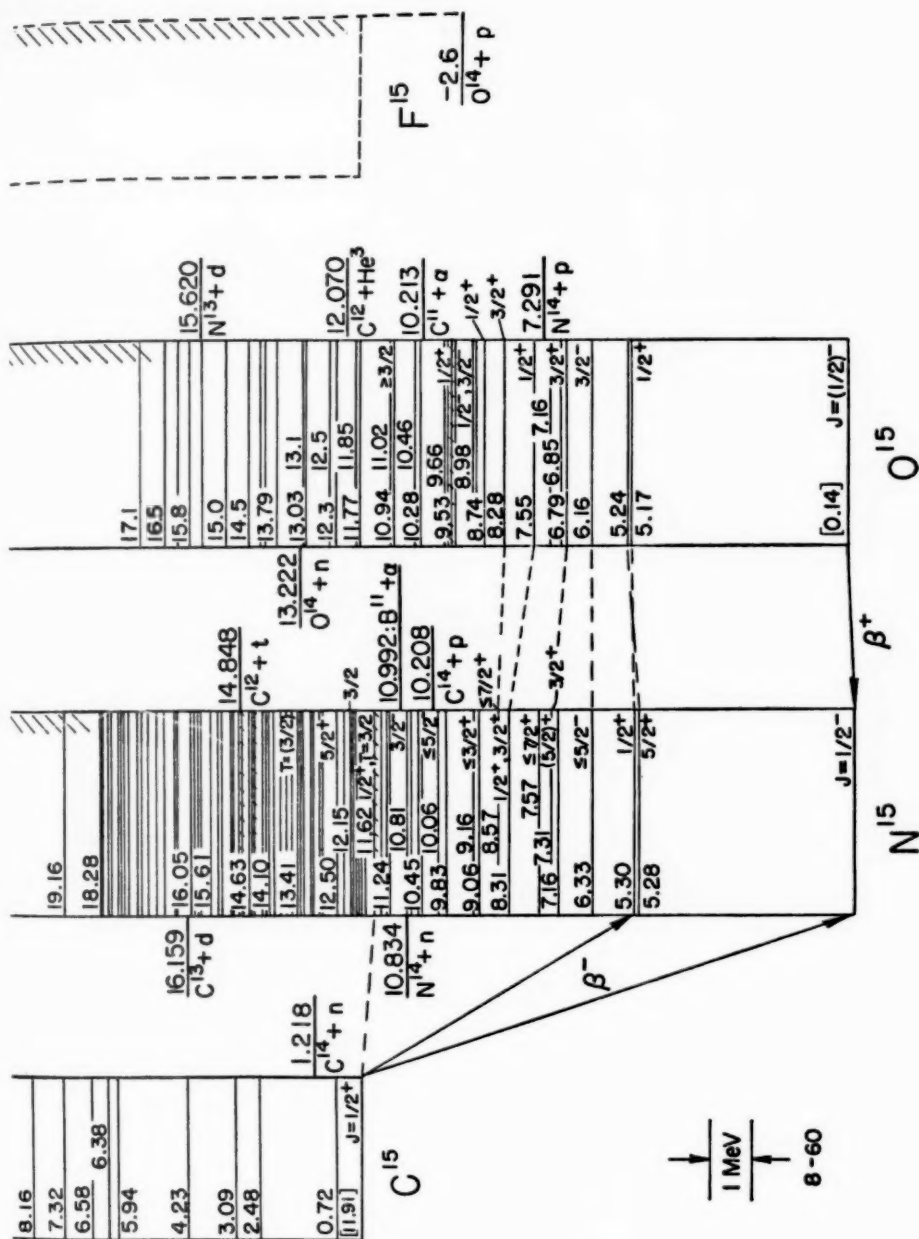


FIG. 11

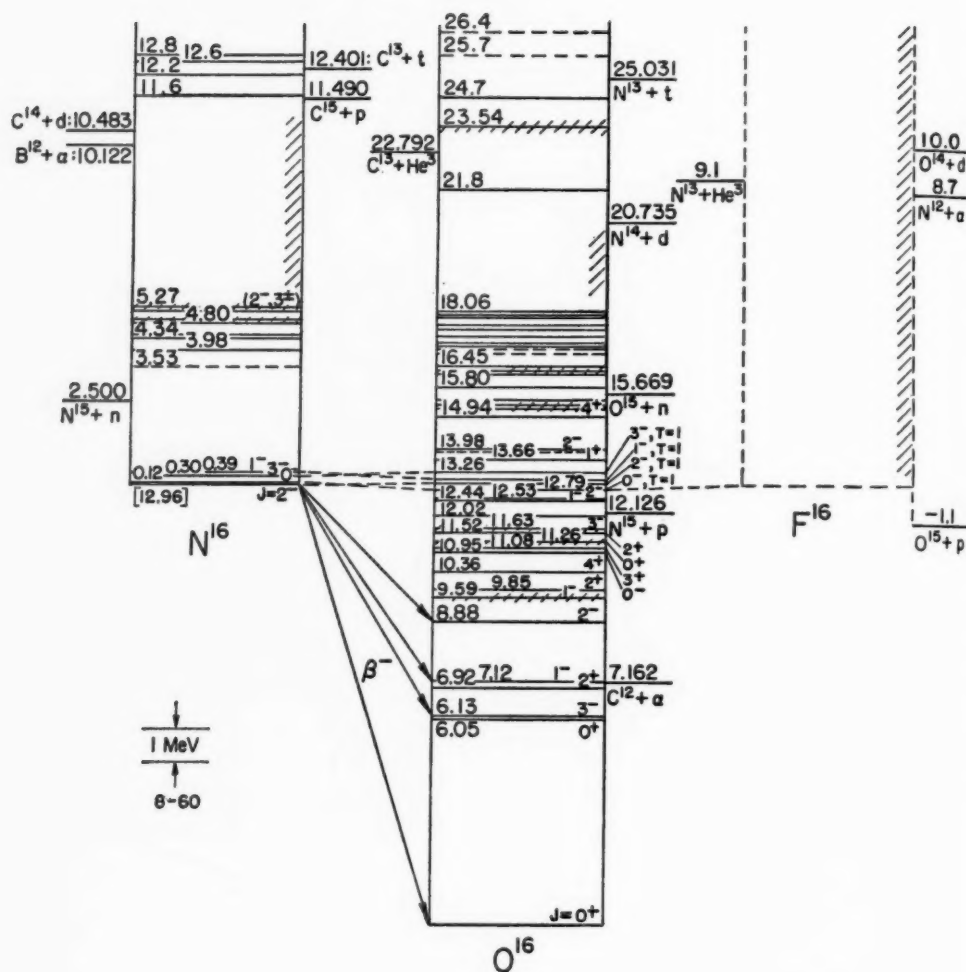
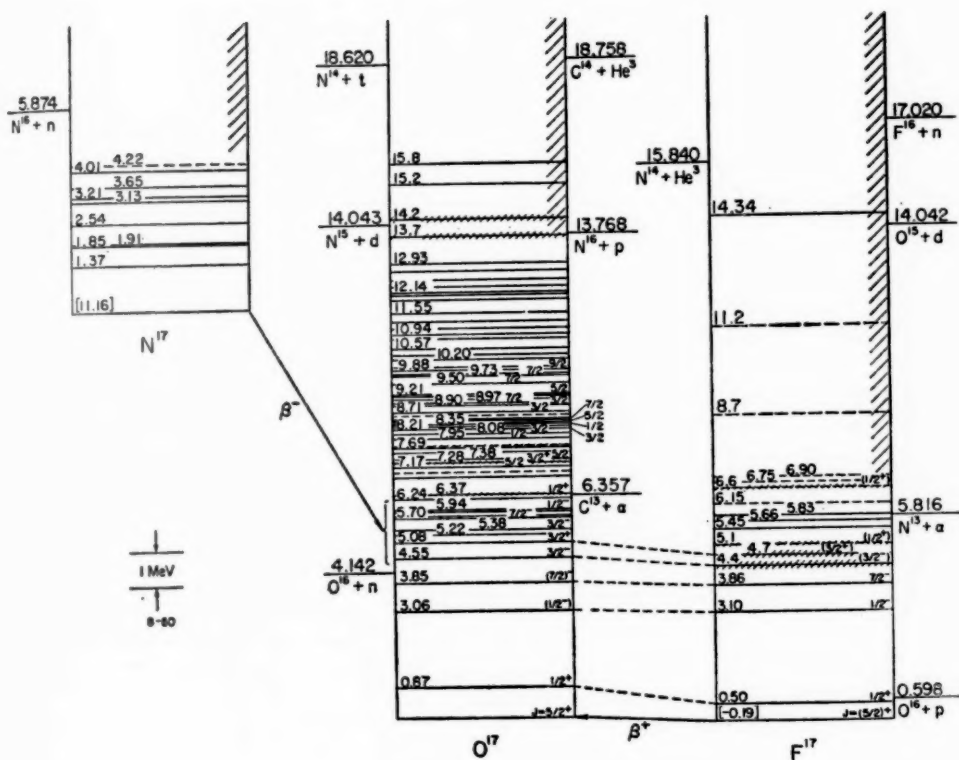


FIG. 12



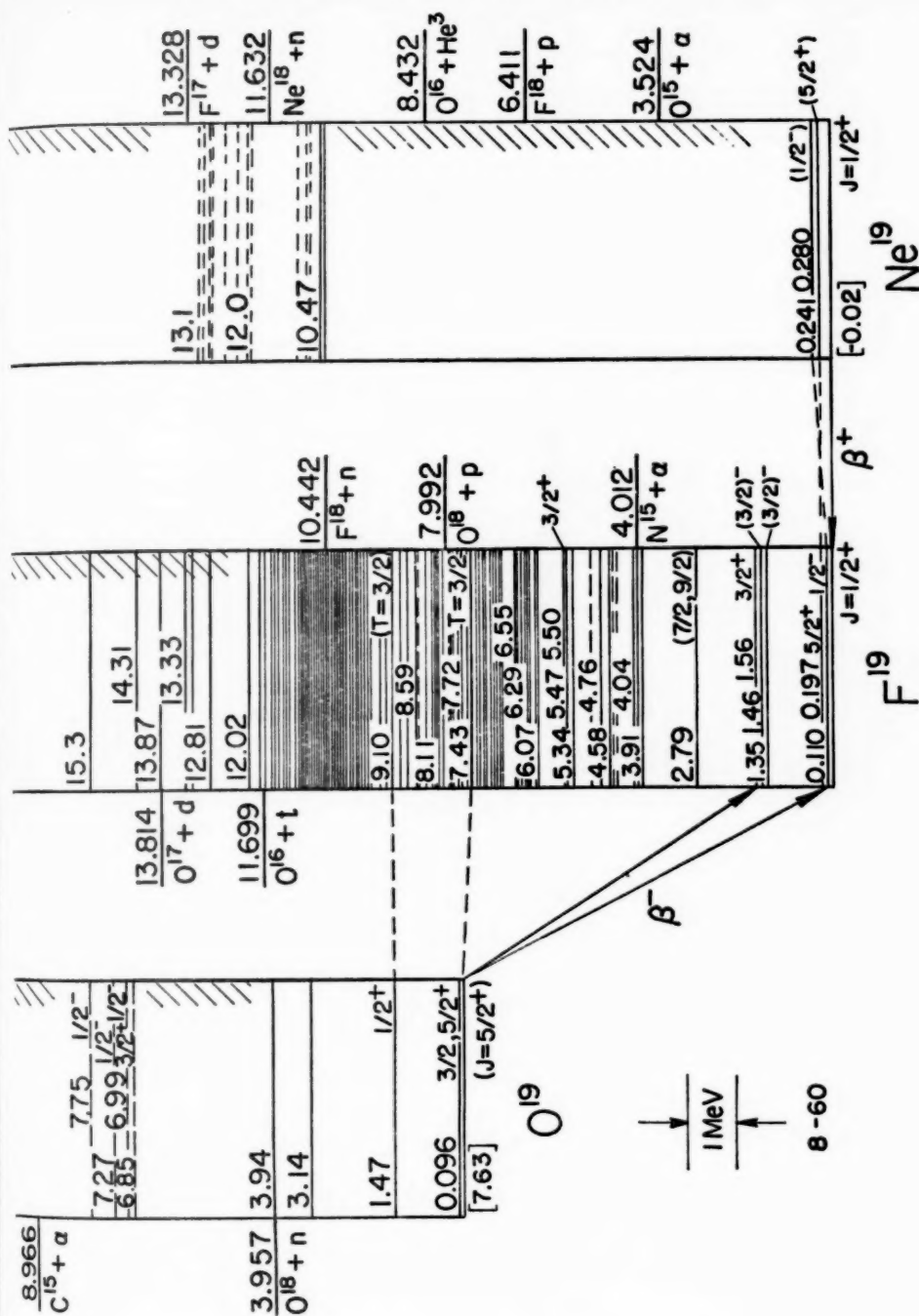


FIG. 15

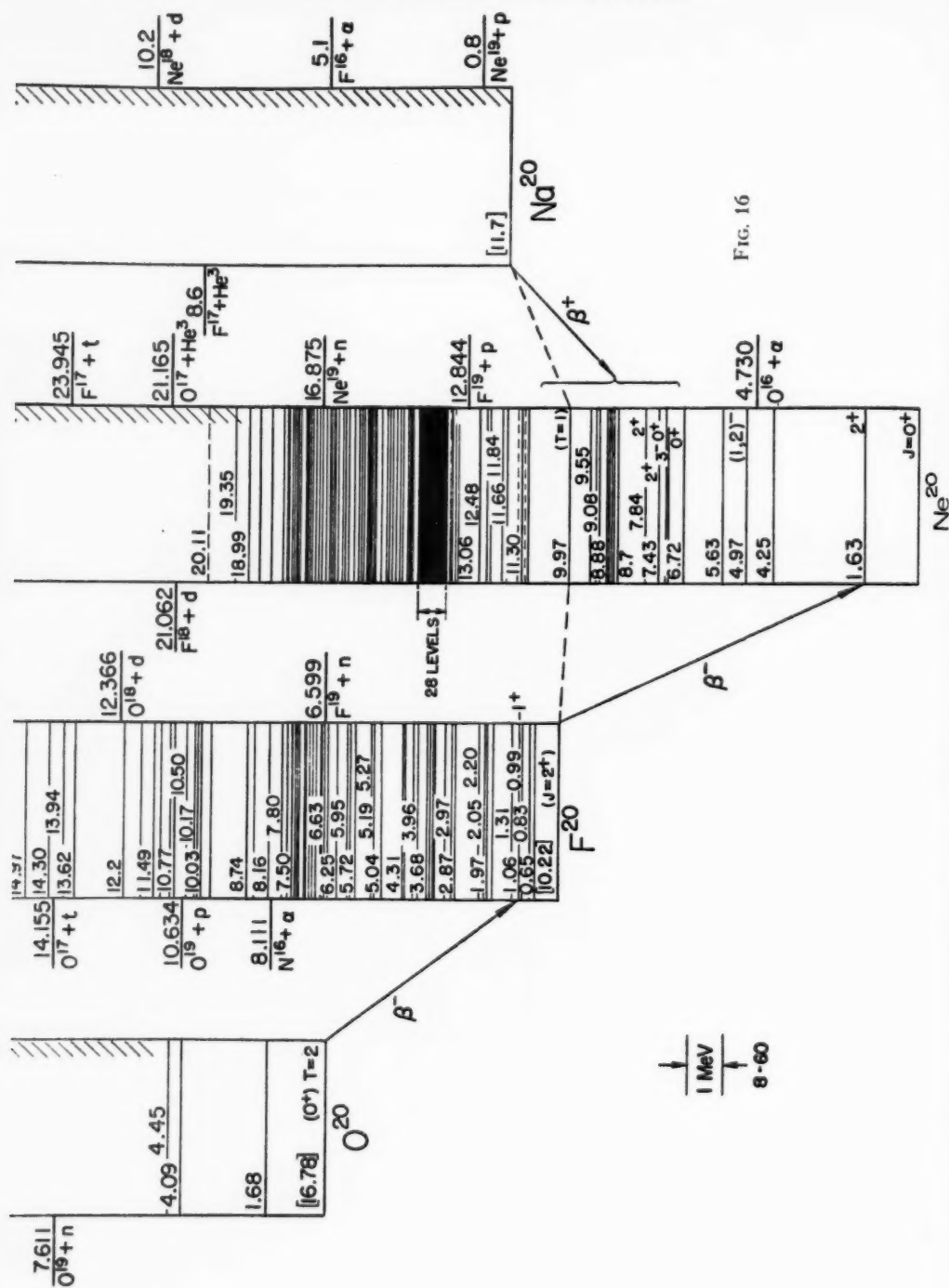


FIG. 16

NUCLEAR METHODS FOR SUBSURFACE PROSPECTING¹

By J. G. BECKERLEY

International Atomic Energy Agency, Vienna I, Austria

INTRODUCTION

Nuclear research began more than sixty years ago with the detection of the effects of nuclear radiations from a mineral specimen. This association of nuclear research and the earth sciences has broadened over the intervening years so that now the origin of the earth itself, as well as the sources of the earth's heat energy, is described in terms of nuclear phenomena. The nature of many important geological processes is revealed by studies of radioisotope and stable isotope distributions in minerals and rocks (1 to 4). Just as radio-carbon measurements have greatly improved the precision of the chronology of archeology, so will isotope measurements transform geochronology. In fact, the number of aspects of geology which are concerned with nuclear phenomena has increased to the point where nuclear geology is a recognized field of study (5, 6).

In the present review we will consider the use of nuclear techniques for measuring *in situ* the properties of subsurface formations.² To complete the account, we will also review briefly in an introductory section the use of nuclear techniques in aerial and surface prospecting. Then the economic importance of subsurface prospecting and the fundamental limitations of nuclear techniques will be indicated. After a discussion of existing "boundary conditions" in subsurface prospecting methods, we will consider the status of each nuclear method in turn. The review will be concluded by identifying the major gaps in the art and by commenting on the future course of development of nuclear methods for subsurface prospecting.

AERIAL AND SURFACE PROSPECTING

Nuclear techniques are now used in aerial prospecting almost entirely for locating uranium and thorium deposits, as well as a few economically valuable minerals (e.g., niobium and vanadium) associated with such deposits. The same is generally true for nuclear methods in surface prospecting.

¹ The survey of literature pertaining to this review was concluded in November 1959.

² "Nuclear" methods are defined in this review as those in which (a) geological formations are irradiated with neutrons and/or gamma rays and the response of the formations (by emission of neutrons and/or gamma rays, prompt or delayed) observed and (b) the natural or spontaneous emission of gamma rays and/or neutrons by geological formations is observed.

In a typical airborne surveying operation, the total gamma-ray flux (gamma-ray energy ≥ 50 kev) is measured and recorded continuously in successive aircraft or helicopter transits across a selected area of the earth's surface. Thus profiles are obtained which show the variation in gamma radiation emitted from the earth's surface and from the local atmosphere. From these profiles and other data on surface conditions, such as weathering, vegetation, drainage, recent rainfall, and fall-out, plus any other information on the nature of the surface formations themselves, it is possible to identify and locate the existence of radioactivity anomalies. High activities are associated with uranium, thorium, or potassium deposits. Anomalously low activities appear, in some instances at least, to be associated with aquifers (7) or with petroleum occurrences (8, 9).

The development of large, rugged scintillation detectors has made it quite practical to measure gamma-radiation levels with airborne equipment; that is, the contribution of earth-emitted gammas to the observed total counting rate is adequate even at appreciable transit speeds (approximately 100 km./hr.). Even so, in many areas the anomalies can be identified only by careful statistical analysis of the data. So-called "eyeballing" of the radioactivity profiles is not adequate for identifying anomalies. Depending on the terrain and on the desired area resolution of the survey, the counter may be located at about 500 ft. (~ 150 m.) above the ground for regional surveys and at 100 ft. (~ 30 m.) for "low-level" surveys.

Boyle of the United States Atomic Energy Commission has reviewed the results of an extensive low-level surveying program (10) in which about 80,000 square miles ($\sim 200,000$ km.²) were surveyed in 500,000 linear miles of flight at a cost of about \$7 per square mile or about \$1 per flight mile. During about 14,000 hours of flight time, more than 1000 anomalies were discovered. The cost of these surveys was small compared to the value of the discovered ore. In a typical case, ore reserves of 100,000 tons of 0.25 per cent U_3O_8 were located in aerial surveys costing about \$25,000, which means a cost of \$0.05 per lb. of contained U_3O_8 . The value of U_3O_8 is of the order of \$10 per lb. (11). Similar experiences have been reported in aerial prospecting in French Africa, in the United Kingdom, and elsewhere (12, 13, 14).

Moxham of the United States Geological Survey has reviewed the results of extensive regional aerial surveys (7). In these the detector elevation was about 500 ft. above the ground. Interpretation of results, as in low-level surveys, is not simple, and care had to be taken to reduce the effect of radon outgassing. Thus, surveys were not made after heavy rainfalls or when atmospheric conditions tend to produce abnormal radon concentrations, e.g. at midday. In surveys over farm areas, the effect of potassium-bearing fertilizers had to be considered. In spite of all the possible perturbations, aerial surveys at higher detector elevations are extremely useful in locating radioactivity anomalies which warrant further investigation.

After aerial radiometric surveying, the anomalies must be investigated at the surface. In its simplest form, this examination consists in observing

the total gamma emission from rock samples, outcrops, etc., using a hand-carried detector. The information is precise but the area covered per man-hour of surveying is small. The techniques of surface radioactive surveying have been covered in a number of books [e.g. the reference list on p. 171 of (15)].

In areas where it is feasible, prospecting with a small truck permits substantial improvements in the nuclear techniques. Not only is it possible to carry much more sensitive detectors and even provide directional sensitivity (16), but it is also possible to analyze the energy distribution of the gamma radiation whenever an important anomaly is located. Energy discrimination permits a preliminary identification of the radiation source, that is, it determines whether uranium, thorium, or potassium minerals predominate. This method has been used in car-borne prospecting by the French Commissariat à l'Énergie Atomique (14) and in India (17). The method is similar to that used in subsurface gamma-spectral logging, to be discussed below. It is likely that this method will become commonplace, particularly now that commercial transistorized multichannel pulse-height analyzers are available. With suitable precautions, particularly the use of calibrated sources of U, Th, and K, gamma spectrometry can be sufficiently accurate and not too time-consuming (about 10 min. per spectrum) for regular field use.

One basic limitation in aerial and surface radioactivity prospecting should be pointed out. The limited range in the rock of the gamma radiations from U, Th, and K minerals (and the products of some of these minerals) means that aerial or surface surveys will scarcely "feel" more than the first few feet of the materials on the earth's surface. Of course, a large high-grade deposit might be detected through a thicker overburden; however, such an increase in depth of investigation will be as rare as the large, rich deposits. In one example of this limitation, an experimental aerial survey was made over a large deposit (estimated as more than 10^6 tons of uranium ore) in the Panangana Salt Dome in Texas. The survey revealed no evidence of the ore deposit, because the deposit was covered by several hundred feet of cap rock (7, 18). The only possibility of detecting deeper deposits by radiometric surveys occurs where radium transport from the ore body results in radon anomalies. Such effects have been exploited successfully in some uranium prospecting activities (19, 20).

The scale of effort in developing new nuclear techniques for aerial and surface prospecting is more likely to decrease than increase in the immediate future, since the interest in finding new uranium deposits has generally decreased. The rate of consumption of uranium in power-generating nuclear reactors is presently rather small and the prospects for immediate increased consumption are not bright. There is ample uranium on hand, and known reserves are substantial (11). Of course, this situation will not last indefinitely; moreover, nuclear power will in time become economically competitive with fossil fuel power in many locations.

These facts are mentioned because, in contrast, there are strong incentives, economic and strategic, for the discovery of new sources of petroleum, which incentives have encouraged substantial efforts in the development of nuclear methods for subsurface prospecting.

INCENTIVES FOR SUBSURFACE PROSPECTING

Subsurface prospecting is based almost entirely on the search for petroleum. The position of petroleum as a primary source of energy for human activities will be maintained for some decades (21). Even if the importance of petroleum as a fuel has diminished, there will still be a large demand based on its chemical value. Moreover, because of defense considerations in present day civilization, each nation has an incentive to develop domestic petroleum resources independent of the supplies available elsewhere.

These factors have made the search for petroleum a substantial and increasing effort. In the United States the number of wells drilled per year is approaching the 60,000 mark. Although many wells are drilled in the neighborhood of other wells that have previously been investigated by various subsurface techniques, nevertheless about one-fourth are exploratory holes which warrant careful subsurface prospecting. In fact, more than half of these exploratory holes are considered "new-field wildcats" of importance in the development of new petroleum-producing fields (22).

Thus, in round numbers we can see that in the United States there must be about 10,000 holes drilled (average depth around 4500 ft.) each year which merit careful subsurface measurements.³ These figures are incomplete as they do not include the need for further measurements on existing wells or in holes drilled in known producing fields.

To define the economic incentives for developing improved subsurface prospecting methods, we must consider the costs associated with this drilling activity. It is expensive to drill the average well because the shallower pools of petroleum have already been exploited. To go deeper is technically more difficult and correspondingly costlier. Drilling costs vary from more than \$750,000 average cost per hole for an off-shore operation to roughly \$50,000 average cost for a 5000-ft. hole in reasonable terrain. This means as far as subsurface prospecting is concerned it is possible to justify the expenditure of at least a few thousand dollars per hole drilled for subsurface measurements or "logging." The cost of drilling, in a sense, fixes the economic scale-factor for the permissible expenditures on logging: the total cost of making subsurface measurements should be between one and two orders of magnitude below the cost of drilling the hole.

This reckoning has been confirmed by a number of studies. Nuclear well-logging services, which constitute only one class of subsurface prospecting

³ Radioactivity logging in the U.S.S.R. has been reported as 3500 km. of drill hole in 1954 (40, p. 731). Comparisons are not possible without details of the method of reporting. However, the U.S.S.R. figure appears to indicate a nuclear logging activity of less than one-fourth that of the U.S.A.

methods, brought an estimated income of over \$25,000,000 per year to United States service companies and their foreign affiliates, during the period 1955-57 (23). From the figures noted above, i.e. around $5 \cdot 10^4$ wells per year, costing about $\$5 \cdot 10^4$ per well, one finds that for every \$100 spent in putting a hole in the ground about \$1 is spent in nuclear logging. An appreciable part of this income is available for the development of new nuclear prospecting techniques.

In addition to the economic factors, we must note the geological fact that petroleum is least abundant (or better concealed) where it is in the greatest demand. Thus there is a strong incentive for developing new subsurface prospecting methods. For example, petroleum production of a single well in the Near East fields is frequently limited by the diameter of the hole drilled or by the ability to handle the flow at the surface. In contrast, the production of the average well in the United States is more than an order of magnitude smaller (frequently two to three orders of magnitude smaller). The petroleum production per man-hour of exploratory effort is correspondingly much smaller in the United States. Thus there is a premium for developing better exploration techniques. The pattern is a familiar one in all exploration for important raw materials, namely: the scarcer and leaner the deposits are, the more sophisticated must the exploration techniques become.

We have cited only petroleum exploration in the above, whereas subsurface nuclear techniques can be used in exploration for other raw materials such as potassium (e.g. detected by its natural gamma radiation), heavy minerals (e.g. detected by strong absorption of gamma radiation), or sulfur (e.g. detected by neutron capture gammas). These uses are limited. For economic and technical reasons, any raw material which can not be made to flow (in contrast to gas, oil, water, molten sulfur, etc.) must be found reasonably near to the earth's surface. There are exceptions such as deep coal mines and gold-bearing minerals. Nevertheless, the searches for most other mineral resources are "shallow" activities when compared to petroleum exploration. For shallow deposits it is normally easier and less expensive to extract a core and study the core at the surface. When core extraction is difficult, the desirability of *in situ* measurements increases. Thus, for example, a Polish nuclear research group has reported conditions in prospecting for potassium salts where nuclear logging methods were used (24). As will be noted later, shallow subsurface measurements can be more easily made because of the less rigorous physical conditions, i.e. no high temperatures, high pressures, and no risk of cave-in. Consequently the instrumentation problems are generally simpler. Although in some instances the equipment developed for petroleum exploration is technically suitable for shallower subsurface prospecting for other minerals, such use is not a common practice, primarily because equipment developed for deep exploration is too expensive. In spite of this factor, it is very likely that those nuclear techniques developed for petroleum exploration will find increasing application to the search for other minerals.

INCENTIVES FOR DEVELOPMENT OF NUCLEAR TECHNIQUES

In addition to the economic and strategic incentives noted above, the development of specifically nuclear techniques for subsurface evaluation of formations is stimulated by the technical fact that nuclear measurements can be made on formations even behind steel casing. Neutrons and gamma radiation can penetrate the casing and the associated cement. What this means is that the formations adjacent to existing wells which have been cemented and cased and, normally, put into production can be reinvestigated without drilling a new hole. Examination of formations behind casing is extremely valuable in situations where open-hole measurements (made before completion of the well) are insufficient or inconclusive or in those instances where it may be desirable to produce more than one oil-bearing zone. In the latter instance, the use of nuclear techniques permits not only the identification and partial evaluation of the formation of interest but also its precise location with respect to the casing.

The possibility of formation evaluation through casing is essentially unique to nuclear methods. Electrical techniques are subject to the severe short-circuiting action of the metallic casing. Acoustic (Sonic or Continuous Velocity) logging is impeded by the transmission of sound through the casing. A reduction in signal-to-noise ratio is also experienced in nuclear techniques, as the nuclear measurements must be made on a formation that is farther from the instrument and through materials of indeterminate geometry which absorb and degrade nuclear radiations. On the other hand, there are some important and favorable aspects of nuclear logging through casing which help increase signal-to-noise ratio. First, the formations back of the casing are usually in equilibrium, i.e., gas, oil, and water interfaces are no longer disturbed by the invasion of the drilling mud filtrate. In addition, the fluid in the well itself is subject to some control—in contrast to open-hole logging where the drilling mud is fixed by considerations of hole stability, etc. Finally, when logging in casing, it is often possible to increase the measurement time (see discussion below).

Although it might be presumed that the ability of nuclear radiations to penetrate casing and cement would assure the supremacy of nuclear methods in cased-hole formation evaluation, this may not always be true. The recent development and commercial availability of devices for sampling formation fluids through casing by puncture could result in some competition with nuclear techniques in cased holes, although the basic advantages of *in situ* and nondestructive measurements are rather compelling.

BASIC "BOUNDARY CONDITIONS" IN SUBSURFACE PROSPECTING

There are many "boundary conditions" imposed on all subsurface prospecting techniques. Some of these constitute severe restrictions on certain nuclear methods. While it is possible that some of the boundary conditions will change as a consequence of new technical developments, others are likely to remain.

The nature of these conditions is readily appreciated by considering a typical subsurface situation. Figure 1 shows schematically the physical set-up in using a typical subsurface prospecting method for open-hole (i.e., before cementing and casing) formation evaluation. A series of sedimentary formations, F_1, F_2, \dots roughly perpendicular to the borehole axis is penetrated by a borehole of diameter D , which may vary appreciably. The borehole is filled with a mud M . Some mud filtrate has penetrated the porous and permeable formations F_1, F_2 , forming an "invaded zone" I of variable

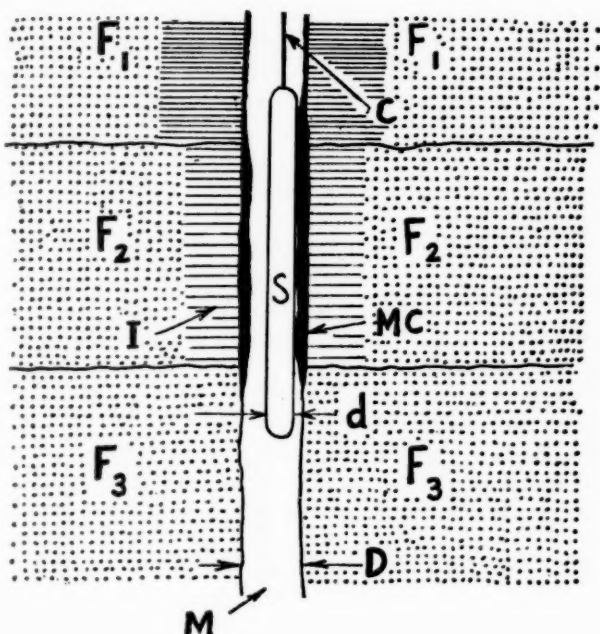


FIG. 1. Typical subsurface situation. S denotes sonde; F_1, F_2, \dots are formations; M , drilling mud; C , logging cable; D , diameter of borehole; d , diameter of sonde. The invaded zone (I) is shown with horizontal cross hatching, mud cake (MC) in black, while virgin formation is dotted.

depth. A mudcake MC has formed on the permeable intervals. The sonde S of diameter d has been lowered by a cable C into the borehole. The voids of the formations F_1, F_2 are filled with either water (of variable salinity), oil, or gas or a combination of these. The filtrate from the mud has a salinity normally different from the salinity of formation water. In some situations the mud may have a base of oil in which case there may be no invasion. It should be understood that this figure is presented only as "typical." There are many possible variations of the situation sketched.

Borehole geometry variations.—One boundary condition is immediately apparent. The geometry in which the subsurface sonde finds itself is neither simple nor controllable. Variation of the borehole diameter D is dependent on the mechanical complexities of drilling and on the stability of the hole. Hole stability is a complex function of composition of the formations, of the time during which the drilling mud has been in contact with the formations, and of the nature of the mud itself.

In principle one can determine the borehole profile by independent measurements, preferably made at the same time as the sonde measurements, and thus take its variations into account. However, this is an extremely difficult technical problem which has only partially been solved. Essentially all calipering devices developed to date measure the variation of a diameter, but whether the diameter measured is a reliable average diameter is not determined. For example, a two-armed calipering device can follow a spiral groove which is certainly not an average diameter. A practical multi-armed (three arms or more) calipering device suitable for open-hole use is presently not available in the petroleum industry.

Even if one knew the borehole geometry, there would still be the problem of finding where the sonde was located with respect to this geometry. Normally the sonde rides on the "low" side of the borehole.⁴ Recently there has been a tendency to supply eccentricizing (or centralizing) devices for those sondes which are relatively sensitive to borehole geometry thus assuring that the sonde does ride on one side, or in the center, of the borehole. Obviously, when an eccentricized sonde passes by a caved-in section of length less than the length of the sonde (which is somewhat more than 10 ft.), the sonde is not going to maintain contact with all the adjacent formation and the measurement is inaccurate if it is sensitive to borehole size or "stand-off."

The borehole geometry problem varies for different geological regions. In so-called "hard" formation areas, hole stability is no real problem, and with reasonably good drilling practices the borehole should be an approximate cylinder. On the other hand, boreholes drilled through unconsolidated or moderately consolidated formations may have great (e.g. more than 100% increase in diameter opposite caved-in sections) variations in borehole diameter and shape.

Any subsurface prospecting method must be devised to cope with this boundary condition. One way, which is feasible for some electrical and acoustic techniques, is to devise methods that are relatively insensitive to borehole geometry variations. This is difficult with nuclear methods. The density contrast between borehole fluid and formation densities (formation density is approximately equal to twice mud density) makes some gamma ray techniques sensitive to borehole geometry variations. Similarly, the

⁴ As the borehole axis is normally not precisely vertical, gravity causes the sonde to ride on the edge of the borehole.

hydrogen concentration contrast between borehole fluid and formation introduces difficulties in neutron techniques. The small sonde diameter (less than about 4 in. or 10 cm.) available for the collimation of nuclear radiations makes directional techniques, which are usually less sensitive to borehole size variation, essentially impossible with neutrons and very difficult with gammas.

Another approach to the borehole geometry problem is through improvement of drilling techniques. Efforts are being made to understand the basic causes of well-bore instability and to develop muds and other fluids which will accomplish all the necessary tasks, such as transport of rock chips to the surface, prevention of fluid losses into permeable formations, prevention of loss of formation fluids or gas, etc., and still not contribute to degradation of the borehole wall. These efforts appear to be progressing (25). It is not within the scope of this review to consider the various important changes that would probably be introduced by the development and use of greatly improved muds. Suffice it to note that control of borehole geometry and reduction or elimination of interaction of mud and formation would reduce the number of unknowns encountered in subsurface prospecting methods. This action would, in turn, reduce the number of measurements required. As far as nuclear methods are concerned, such developments would greatly increase the reliability of nuclear measurements, primarily because, as available nuclear radiations have a relatively short range of investigation any reduction of perturbations in formation and geometry adjacent to the borehole would be extremely important. For example, neutron capture-gamma spectroscopy of formations and formation fluids in open holes would become very attractive.

Borehole fluid variations.—As noted above, the mud used in the borehole is designed to perform many tasks. None of these has any relation to the logging technique itself, so that the mud could have properties which would make some logging techniques impossible or very difficult. Thus, for example, in some areas it has been found essential to use oil-based muds. As a result, some electrical logging techniques have become almost impossible, and other techniques have to be used.

For those nuclear logging techniques which depend on the transmission of gamma rays through the borehole fluid, the important physical quantity is the mud density.⁶ It is relatively easy to determine; in fact, it is one of the variables which is closely controlled by the driller. Of course, in the event that gas is escaping into the mud, there can be significant and not entirely known variations in subsurface mud density.

For those techniques which depend on neutron transmission and absorption, the situation is not as straightforward. The variation of hydrogen (water) or of neutron absorbers in the borehole can greatly vary the pattern

⁶ The ratio of atomic number to mass number is more or less constant, except for muds heavily loaded with barium or for very low-density muds.

of thermal neutrons and the associated pattern of capture-gamma rays. Fortunately, the usefulness of appreciable concentrations of such elements as boron, lithium, or the rare earths in drilling muds appears to be rather limited, so that perturbations attributable to the presence of these elements do not occur often. Of more importance is the presence of salt. The absorption of neutrons by chlorine and the associated high-energy capture-gamma rays are important. Consequently, it is necessary in some neutron logging techniques to know the mud salinity. This is not difficult to determine and, in fact, is usually measured for other reasons.

Though knowledge of mud density and salinity usually suffices for nuclear techniques, the situation is not entirely satisfactory. In some techniques it would be very desirable to know more about the nuclear properties of the drilling mud in which the nuclear logging device finds itself. The basic difficulty is that, for various reasons, there are a great variety of recipes for drilling muds and many local variations (26). As one reviewer (27) has put it, "normal muds are as difficult to find as they are to define." It would therefore seem desirable to measure the nuclear properties of mud or to make a chemical analysis of a sample for those techniques which are sensitive to borehole fluid properties. This is just not practical, nor considered necessary, at the present time.

In recent years there has been an increase in use of gas or air as the drilling fluid (28, 29). This is possible in some regions and has the advantage that drilling is faster and cheaper; in addition, the technique is very valuable where producing formations plug up upon contact with water. The principal difficulty is that whenever a water-bearing formation is encountered, there are great difficulties in coping with the water. Consequently, in some situations conventional drilling (using muds) is employed through intervals where water is encountered, the well is cased past these intervals, and the drilling is resumed using gas or air. It is difficult to predict the course of such developments. Insofar as nuclear methods are concerned, subsurface prospecting in an "empty" borehole presents substantial problems for some techniques (conventional neutron logging) and none for others (natural gamma logging). At the present time, however, the practice is not widespread.

Time available for measurements.—One of the most important boundary conditions on all subsurface prospecting methods is the limited time available for measurements, since every hour taken by the logging operation costs tens of dollars and even hundreds in deep offshore wells. There is no easy way to define the time limit except to point out that when measurements are made on a continuous basis, that is, with the sonde moving continually in one direction up or down the borehole, for a 5000-ft. open hole the measurements should take no more than a few hours. Logging speeds are, therefore, normally 10 ft./min. or greater. Slower speeds, or even point-by-point measurements, can be permitted only if the formations to be studied are known to be of limited vertical extent or if the data obtained are of ex-

treme practical value. At times, low speeds may not be permitted because of the hazard of having the sonde stick.

The importance of this boundary condition is obvious. There are nuclear techniques which are technically feasible and which might yield useful data on subsurface formations but which are ruled out as commercial operations because they take too long. It should be understood that this condition does not always hold for experimental or research measurements: in such cases the goodwill of the well owner or his agreement to permit longer surveying times (e.g. in return for the experimental data or in return for a nominal fee) may make it possible to conduct lengthy measurements. Even this latter possibility may be ruled out when the drilling is through loose or unconsolidated formations or when the borehole is unstable.

Another consequence of limitations on the time available for subsurface prospecting is the premium placed on going into the borehole in a minimum time. Because the sonde may meet obstructions such as mud bridges en route to the formations of interest, this requirement is equivalent to demanding extreme ruggedness of the sonde. Entry rates in excess of 150 ft./min. (~ 3 km./hr.) are commonplace. In recent years the increasing use of miniaturized, rugged electronic components (normally developed in connection with military defense work) has helped improve the reliability of subsurface prospecting equipment and meet the demand for reducing the entry time.

Rigors of temperature, pressure, and confinement.—If all the wells drilled were shallow, the temperature and pressures experienced by the subsurface prospecting device could be considered difficult but reasonable. The requirements might be simply that the subsurface device be capable of operating at temperatures up to about 230°F. (110°C.) and under pressures up to about 5000 lb./in.² (about 300 atm.). Unfortunately, the deeper the hole, the more valuable or desirable is the information derived from subsurface measurements. As a consequence, minimum conditions are usually more like 125°C. and 600 atm. There is general agreement that during the next decade at least, the worst condition that might be encountered is about 250°C. and 1500 atm. (30, 31). If the so-called "Moho" experimental hole (through the oceanic crust to the Mohorovičić discontinuity) is attempted, there will be a requirement that the prospecting tools be operable at pressures up to 2000 atm. (32); temperatures will be lower than in deep wells on continental crusts.

The difficulties in meeting even the minimum of these boundary conditions are apparent when the limitation on prospecting tool diameters is noted. Present day drilling practices make it very difficult to use any subsurface prospecting device which has an outer diameter greater than about 4 in. (10 cm.). The usual maximum diameter is taken as $3\frac{5}{8}$ in. (9.2 cm.) for nuclear logging devices. In some quarters (33, 34), "slim-hole" drilling (borehole diameter about $3\frac{1}{4}$ to $4\frac{1}{2}$ in.) is being advocated; this practice, if it became widespread, could make it necessary to reduce the diameter of the "standard" open-hole logging tool to less than 3 in. It should be understood

that these are outer dimensions; the diameter of the inner volume which is available for nuclear detectors, electronics, etc., is an inch or so smaller, because of the pressure requirement.

In connection with the temperatures noted above, it should be remarked that these are the temperatures of the surroundings; the internal temperatures within the instrument housing might be higher if there are heat sources, such as vacuum tubes, present in the circuits.

The pressure limitation has a further constraint: mechanical design of the housing must minimize entry problems. In other words, windows or slits or external electrical connections require careful consideration. The simpler the external sheath, the more likely it will be able to stand up under downhole pressure. This is important in connection with nuclear logging devices because enclosing detectors in thick steel housings is often not desirable from a nuclear physics point of view. Nevertheless, the rigors of downhole conditions frequently require one to adopt a "nuclear-wise" poor design.

Laboratory simulation of subsurface formations.—One of the most important boundary conditions in the development of subsurface prospecting techniques is imposed by the great difficulty in laboratory simulation of subsurface formations. For almost all nuclear techniques, the only available models are samples of the formations themselves. For techniques which depend only on the properties of gamma radiation, e.g. density logging by gamma-ray scattering, simulation is not as difficult. What is required is a reasonable match in density and in ratio of atomic number to mass number.

However, for techniques in which neutrons are used, the problem is extremely difficult. Not only are large (about 1 m.³) samples of formations required, but the samples must be uniform and with no cracks or voids. There are substantial problems associated with securing representative pieces of the sample for analysis (calibration): pieces must be taken from the surface of the sample formation and it is precisely the surface which is most likely to have been rendered "unrepresentative" in quarrying, transporting, etc. Moreover, large samples of formations covering a range of important formation variables (principally porosity) are not available. This will be illustrated in later discussion of neutron logging calibration. Finally, it should be noted that simulation of porous and permeable formations requires that the samples be filled with water of known salinity; all the original water must be removed and the block reimpregnated in such a way that no voids remain. All this must be done without altering the basic sample or affecting its presumed homogeneity.

Laboratory simulation is further made difficult by the variability of borehole geometry. Consequently, it is desirable to have formations in the laboratory with variable borehole diameter and to simulate variation of borehole fluid and of the fluid content of the formation. Hence, laboratory setups are unable to simulate a reasonable range of field conditions except in a crude and preliminary way. As a consequence, the development of new nuclear techniques depends strongly on experiments in actual wells, a very

slow, expensive, and not entirely satisfactory procedure. The impossibility of reasonably conclusive laboratory testing of new nuclear techniques also means that every new experimental device must be engineered sufficiently to withstand the rigors of testing in the field and this must be done before the feasibility or value of the device is established. "Sealing wax and string" experiments are impossible.

The situation is somewhat different for electrical surveying techniques. While it is not possible to simulate the wide range of formations (resistivities from about 10^{-1} to 10^4 ohm meters) in practical laboratory setups, theoretical methods exist for reducing the number of necessary laboratory experiments. Moreover, analogue computing can be used.

Theoretical techniques are now available which could reduce the problem of laboratory simulation of subsurface geometry and formations in nuclear logging also. Whether these are being used is not apparent from the literature. Except for a basic theoretical paper on neutron distributions in borehole geometry (35), there are no significant publications on this important problem. (This situation is to be compared with the large number of publications on simulating subsurface formations in connection with studies of formation fluid transport problems, e.g. water-flooding.)

One important consequence of the laboratory simulation problem is that no technique for subsurface prospecting is considered developed until it has undergone extensive field testing and until the measurements it makes have been studied and found to be useful to the petroleum geologist. This careful analysis results in long delays in development of new techniques. Some techniques which have been abandoned, because the resulting measurements could not be used, may be revived at a future date when the geologic interpretation of the measurements becomes apparent. This feedback between technique development and field results is another aspect of the great difficulty, or even impossibility, of realistically simulating subsurface situations in the laboratory.

Nuclear versus molecular measurements.—Enthusiasts for nuclear methods in subsurface prospecting often forget the fundamental limitations of nuclear measurements. In searching for petroleum the interest lies in finding certain kinds of molecules, not nuclei. For example, many neutron prospecting techniques are sensitive to variations in hydrogen concentration, whereas the petroleum geologist is not interested in hydrogen, but in the molecule CH_2 . Most neutron techniques cannot distinguish between CH_2 and OH_2 , nor between the oxygen in carbonate, the oxygen in silica, and the oxygen in water. Yet from a geological point of view these differences are of critical importance. What is wanted, for example, is not a "hydrogen log" or a "carbon log" or an "oxygen log," but rather a "hydrocarbon log" or a "carbonate log" or a "water log."

This basic limitation could, in principle, be overcome by developing molecule-sensitive techniques using nuclear radiations. Low-energy gamma-ray scattering or transmission offers a possibility, but the depth of penetra-

tion would be too small to be reliable. Molecular effects can be detected with neutrons in the laboratory, but no practical application of such techniques for subsurface prospecting has been presented in the literature. The prospects for the development of essentially molecule-sensitive nuclear techniques are not bright.

Thus nuclear prospecting methods may remain of secondary importance, in open-hole situations, to other methods which measure quantities more directly related to the petroleum geologists' interest; electrical techniques—sensitive to the kind of fluid (oil or saline water) and to its concentration and distribution—may always be more widely and frequently used in open-hole prospecting than nuclear techniques.

Cable transmission limitations.—Another boundary condition in the development of nuclear techniques for subsurface prospecting is imposed by the cable between the surface logging truck and the subsurface sonde. Logging cables are steel-armored, multiconductor (one to seven conductors) and are normally 10,000 ft. (3000 m.) or more in length. The electrical properties of the cable are far from ideal.

The most important limitation is that imposed on the transmission of information from the downhole sonde to the surface recording equipment. If the information is transmitted by slowly varying direct current or by alternating current of reasonably low frequency (less than about 10^3 sec.^{-1}), communication difficulties are not large. On the other hand, if sharp pulses are to be transmitted, the great attenuation of the higher frequencies can smear out the pulses received at the surface and degrade the information. For simpler devices, where counting losses are of principal concern it is possible to incorporate a downhole scaler or an integrating circuit or to resort to other tricks. This complicates the sonde somewhat. However, for more sophisticated techniques, such as pulse-height analysis (for capture-gamma-ray spectrometry devices), the accurate transmission of the detector information to the surface may be impossible so that other ways, such as downhole sorting of the pulses and transmission of simpler signals, must be used. This involves a great increase in the complexity and reliability of the sonde, especially when it is considered that the downhole circuits must fit in a small space and be subjected to rather high temperatures.

The cable also imposes limitations on the number of control circuits available and on the number of circuits for checking or calibrating the downhole sonde, which can be partially overcome by use of relays and other complexities. These problems are encountered in all remotely operated devices, but very little has been published, as the solutions are considered trade secrets. Any improvements in logging cables will have an important effect on the scope of feasible subsurface prospecting equipment.

There are other limitations imposed by the cable, such as its temperature-dependent properties (and any borehole has a temperature gradient) and the practical limits of power which can be transmitted. The latter limitation usually rules out techniques which require more than 1 kw. for operation of

the downhole sonde; the limit is lower for small diameter cable. The effect of this constraint has been eased in recent years by the use of semiconductor devices and other low power-consumption components.

Requirement for absolute measurements.—In all subsurface prospecting the measurements must be absolute. Thus any device which simply records the relative variation of some measurement as a function of sonde position is generally not acceptable. The reason is that the basic interest in subsurface data is directed not only toward the variation in one borehole but also toward the variation from one borehole to another. If, for example, in a borehole survey a formation is found to have a certain total natural gamma activity, the same formation when penetrated in drilling another well in the same region may have the same radioactivity; or if a difference appears, there should be some geological significance in the difference. The petroleum geologist needs to know whether the observed difference is real or just attributable to calibration errors.

The requirement for absolute measurements means that all nuclear techniques must include precise calibration practices. The calibrations must be done, for the most part, at the well-head. This is not easy in the rigorous physical conditions of petroleum prospecting. Only in recent years has the calibration problem been solved satisfactorily. As will be noted later, the comparison of nuclear calibrations between service companies has been established.

SPECIFIC NUCLEAR TECHNIQUES

In the following, the status of each specific class of nuclear technique now used in subsurface prospecting will be reviewed. A prognosis for each method will be included. For convenience, the various nuclear logging techniques will be grouped into five categories; see Table I. Of these five, only the first three are in common use. The last two have been used in commercial operations but are not really established techniques.

There are other techniques in commercial use which do not fit into the five groups as well as a few techniques which have had very limited commercial use and which are not established, e.g. natural gamma spectrometry. These will be discussed under the technically related category. The patent literature is cluttered with other concepts of nuclear prospecting methods which we will not mention here simply because most of these methods will probably not be exploited.

Before discussing the individual categories of nuclear techniques, we should note the state of the general literature on nuclear subsurface prospecting methods. An excellent basic reference is Tittman's lectures at the University of Kansas Petroleum Logging Conference in April 1956 (36). For general references concerned with all logging techniques, Wyllie's book (37) and the Schlumberger Document No. 8 (38) are recommended. Caldwell has written a comprehensive review of the use of nuclear methods (39). Tittle's chapter in "Nuclear Geology" (5) is brief but informative. The Fourth

TABLE I
NUCLEAR TECHNIQUES FOR SUBSURFACE PROSPECTING

Category	Source	Detector	Source-detector spacing	Geological quantity usually measured
1. Natural gammas	None	Low-energy γ detector	—	Total natural radioactivity (U, Th, K concentration)
2. Density (gamma scattering)	Radioisotope γ emitter	Scintillation γ detector	≥ 20 cm.	Formation density (related to porosity)
3. Neutron	Ra-Be, Po-Be, Ac-Be, Pu-Be	γ Detector (capture), neutron detector for thermal or epithermal neutrons	≥ 40 cm.	"Hydrogen index," related to porosity
4. Neutron activation	d,t accelerator (14-Mev neutrons) or Ra-Be, Po-Be, Ac-Be, Pu-Be	Scintillation γ detector	—	O, Al in formation; Na (in brine-oil interface location)
5. Neutron capture, inelastic gammas	d,t accelerator (14-Mev neutrons) or Ra-Be, Po-Be, Ac-Be, Pu-Be	Scintillation γ detector	—	Cl, C, O, etc., in formation

World Petroleum Congress (40) included a symposium on well logging; the discussion of nuclear methods is rather brief and not entirely satisfactory. There are many other general accounts of nuclear methods in the various petroleum geology texts and in review articles in the various petroleum journals; some of the latter are not entirely reliable and reflect a lack of understanding of basic nuclear physics. The *Proceedings of the First United Nations International Conference on the Peaceful Uses of Atomic Energy* (1955) and the *Proceedings* for the 1958 Conference include a number of review articles relevant to nuclear logging. The *Proceedings of the Conference of the Academy of Sciences of the U.S.S.R. on the Peaceful Uses of Atomic Energy* (Moscow, July 1-5, 1955) also includes papers on nuclear well logging in the U.S.S.R.

Natural gamma logging.—This technique consists in measuring the gamma activity of subsurface formations by observing the gamma-ray intensity in the borehole. Scintillation detection is preferred because it is possible to secure better vertical definition of the formation. Field calibration of the equipment is performed with small radioisotope gamma sources (41). Until recently the various service companies used a variety of units for reporting the gamma intensity observed in subsurface formations (42). There has been consistency within each company's measurements (assuming proper and frequent calibration of each sonde), but comparisons between companies have been difficult.

To improve intercomparison, the American Petroleum Institute convened a subcommittee on gamma-ray and neutron logging standardization which recommended the establishment of a calibration facility at the University of Houston in Texas (43), completed in 1959.⁶ It seems very likely that this facility will improve the intercomparison of gamma logs and that differences found between measurements by different service companies will, in fact, be real and not just calibration differences. It is interesting to note that a similar pit arrangement has been used elsewhere for standardization of gamma logging in uranium prospecting (44).

⁶ For standardization of gamma-ray surveys, a 25-ft. deep cylindrical pit (diameter 4 ft.) was constructed with three 8-ft. layers of "formations" and a 1-ft. layer of water on the top. A "borehole" with 5½-in. casing penetrates the axis of the cylinder and continues for 15 ft. below the bottom layer. The borehole is normally filled with fresh water. The three formations are cement loaded with potassium, thorium, and uranium. The gamma activity on the axis of the middle formation is about twice that observed for an average midcontinent shale. Any gamma logging tool which transmits the calibration arrangement will show 8 ft. of "low" radioactivity and 8 ft. of "high" radioactivity followed by another 8 ft. of "low." The deflection of the counting-rate recorder observed between "high" and "low" layers is arbitrarily set equal to "200 A.P.I. Units." Obviously the facility can not be used for precise calibration of devices with radically different spectral responses; however, it appears that, for practical reasons (e.g. everyone faces about the same boundary conditions in subsurface prospecting technique development), these differences are not large.

In addition to the general improvement in calibration of gamma-ray equipment, gamma-ray sondes have been combined with a number of other subsurface techniques. In principle, it would be desirable to record a gamma log simultaneously with all other subsurface measurements because the gamma-ray pattern constitutes a depth fiduciary that is essentially permanent and that can be observed even after a well is cased. Simultaneous gamma-ray logs are run as a standard practice when a neutron log is run; the same is becoming true for acoustic logs (Sonic, etc.). Simultaneous gamma-ray logs with perforating guns are also used in some areas (45, 46).

To date the primary analytical use of gamma-ray logs has been in the identification of shales. This use is based on the empirical observation that the gamma activities of shales are greater than the activities of potential petroleum-bearing formations, i.e. sandstones and limestones (47, 48). It should be noted that the activities of the latter are independent of fluid content.

There have been many attempts to use the gamma log as a quantitative indicator of the shale content of subsurface formations. Shale content has substantial geological importance, and for quantitative interpretation of certain electrical logs it must be known. In some regions where the cementing material of permeable formations is mostly clay, it has been found possible to correlate gamma radiation and permeability (49). Measurements for different wells were normalized by reference to the activity of a characteristic bentonite bed several feet thick and with an apparently consistent and high level of activity over this region. In another area it has been found that the observed gamma activity correlates closely with formation porosity (50).

As pointed out in the discussion of aerial and surface techniques, gamma logging is important in prospecting for uranium or thorium minerals. Stead (51) has reported on gamma logging of holes drilled in connection with uranium exploration. About 23 million ft. (~ 7000 km.) were surveyed in the period 1949-58. Gamma logging was the basis for about 85 per cent of the newly developed ore reserves. The shale-identifying ability of the gamma logs was also found to be valuable in placement of mine workings. Knowledge of the location of the mechanically weaker shale masses permits placing mine workings in the stronger sandstone portions of the ore bodies.

The standard gamma logging technique now used in the petroleum industry only measures total gamma activity. The source of activity is not identified. To identify the relative contributions of uranium, thorium, or potassium (and the daughters of U), a spectral analysis of the gamma radiation is required. As basic theoretical (52) and experimental studies (53) of gamma transmission through typical subsurface formations show, the higher-energy gamma flux (i.e. the unscattered gammas from the radioactive minerals) in the borehole is about two orders of magnitude lower in intensity than the degraded gamma flux (about 50 kev). The latter flux is virtually independent of the gamma source identity. A subsurface device for natural gamma spectroscopy using a detector of size and efficiency comparable to

those presently available in downhole equipment therefore will require long periods to make useful measurements. If continuous logging is attempted at a speed of 10 ft./min., with typical counting rates around 100 cps, only about 10 counts of high-energy gammas would be detected in 10 sec. (corresponding to about 2-ft. vertical transit). Analyzing this into two or three components as a function of depth would be impractical. Hence, the surveying must be done at lower speeds or point-by-point. Brannon & Osaba (54) have reported field experiments in spectral gamma-ray logging. Using a shorter cable to reduce high-frequency attenuation (see earlier discussion), the pulses were brought to the surface and analyzed. The relative contributions of uranium, thorium, and potassium to the total gamma flux were determined. Logging was at 1 ft./min. and stationary measurements were made for 15 min. at each level.

The value of the subsurface gamma spectral information in geological research on sedimentary processes has been shown, e.g., in Adams' studies of the variation of the Th/U ratio (55). In the sedimentary formations of interest in the search for petroleum, it would be extremely valuable if a specific relationship were established between the spectral data and some quantity of practical interest, e.g., petroleum or connate water content, porosity, permeability, shale content. However, such relationships, if they exist, have not yet been established. Unfortunately, until a relationship is found, the accumulation of experimental field data will be very slow, because of the difficulties of the technique as well as the previously mentioned cost of logging time. This is a typical situation in subsurface prospecting: one needs to make many expensive surveys in order to show whether or not it was useful to have made the surveys in the first place.

With respect to the spectral logging technique itself, there do not seem to be any obvious ways to reduce drastically the time required for measurements. Increasing detector sensitivity while retaining reasonable energy resolution is possible; a multiplicity of detectors could be used. The pulse-height and sonde-depth data might be recorded on magnetic tape (56) and then analyzed extensively in the laboratory; this method would increase the useful information derived from each borehole survey and presumably reduce the number of surveys necessary. The radiometric study of cores (57, 58) could be increased, although core data are always subject to question because of leaching, exposure to drilling mud, etc., during the removal of the core to the surface. All of these possibilities are expensive in time and money—and it isn't apparent what value the data have to petroleum exploration. Consequently, it is likely that gamma logging will continue to measure total gamma activity and, unless there is a real breakthrough in gamma energy detection techniques, spectral logging will be scarce in petroleum exploration.⁷

⁷ If it is found that the natural gamma spectra of shales can be used for correlation of shale intervals, this would provide an incentive for further development and use of gamma spectral logging.

Density or "gamma-gamma" logging.—In the density or "gamma-gamma" logging technique for subsurface prospecting, a sonde consisting of a gamma-ray source and a gamma-ray detector is used (59). A beam of gamma radiation from a radioisotope source (e.g. Co^{60} , Cs^{137}) is directed at the formation, and the intensity of scattered gamma radiation is measured with a detector located about 20 cm. or more vertically above or below the source. Both source and detector are collimated by suitable shielding. The sonde is used as a sidewall device, that is, it is pressed against the formation by a backup spring and the source and detector apertures are oriented towards the formation. The detector is biased to be insensitive to the lower-energy (degraded) gamma radiation, as there is a substantial probability that such radiation has interacted with the borehole fluid. If the low counting rates could be tolerated, the detector would be used to detect only the once or twice scattered gammas, as these are only responsive to formation properties.

Under laboratory conditions the gamma-gamma technique has been shown to yield reliable density measurements in general accord with theoretical analysis (60, 61). For the geometry used, the detector counting rates decrease exponentially with the increase in density. Counting rates are adequate for continuous logging. Actually, as the range of density encountered in subsurface formations is normally in the limited range of 2.0 to 2.8 gm./cm.³, a linear counting rate versus density calibration is usually satisfactory. Laboratory simulation of subsurface formations for gamma transmission and scattering is, as noted earlier, fairly easy and straightforward. From simulated formations it has been shown for a specific tool that the radial depth of penetration is less than about 6 in. (15 cm.). The vertical range will be comparable to the source-detector spacing or greater than about 30 cm. Sensitivity to variation in borehole fluid density has been demonstrated; however, the effect can be reasonably compensated.

The formation density per se is of geological interest, particularly in interpretation of seismic or acoustic measurements. In petroleum prospecting the predominant interest in density arises from its relationship to formation porosity. The bulk density ρ_b of a porous formation is $\rho_b = (1 - \phi)\rho_g + \phi\rho_f$ where ρ_g is the density of the grains (matrix density), ρ_f the fluid density, and ϕ the formation porosity (fraction of the volume which is porous). As the quantities ρ_f and ρ_g can be estimated⁸ for specific situations, the measurement of the bulk density with the gamma-gamma log permits the calculation of the formation porosity.

From a physics point of view, the technique should be accurate and, because the properties of gamma radiation are well known and amenable to precise laboratory measurement, the results should be unambiguous. In spite of this, the technique has not been adopted by the petroleum industry to any great extent. Other porosity measuring tools (neutron, acoustic,

⁸ The grain matrix density (ρ_g) varies from 2.65 gm./cm.³ for silica, 2.71 gm./cm.³ for limestones, to 2.85 gm./cm.³ for dolomites (45).

electrical) are more generally used. The reason for this situation is apparent when one considers the basic boundary conditions discussed earlier. The relatively short range of radial penetration makes the gamma-gamma log especially sensitive to borehole geometry variations. If a relatively small volume of borehole fluid or mud cake is interposed in the region near gamma source or detector, the device will not measure formation density. Hence there must be good contact over the face of the tool between the source and detector and somewhat beyond each, i.e. over a distance of more than 30 cm. This is not easy to accomplish, especially in areas such as the Gulf Coast where there is a need for better porosity measurements. If the sonde were short and were able to make a continuously good contact, spurious measurements would be minimized.

Unfortunately the designers of gamma-gamma equipment do not appear to have solved the problem. They recommend (45) simultaneous caliper logging to determine borehole size correction and to locate intervals where wall contact is not good. There are at least two drawbacks in this solution: first, the addition of a caliper makes the sonde longer and more complicated mechanically, thus aggravating the problem of wall contact; and second, because of the limitations of presently available calipers, the caliper data will provide reliable indications only for the worst spots in the borehole and will not show the small geometry disturbances in front of the source-detector arrangement. The use of bowsprings to assure wall contact is also a debatable solution. The possibility of getting stuck with a bowspring device is very real and undoubtedly makes many well operators reluctant to use a gamma-gamma device. Moreover, the usual bowspring only provides a strong backup spring for a limited range of borehole sizes.

In sum, the gamma-gamma technique measures an important formation parameter, density, and, provided the geometrical perturbations are absent, does so in an unambiguous way. Calibration is straightforward and can be performed in the field. The basic difficulty is that existing tools do not seem to operate reliably under less-than-ideal borehole conditions. If the designers of such tools will exert the same efforts and ingenuity as those who have designed other successful wall-contact subsurface prospecting equipment, the technique will undoubtedly be more widely used.

Neutron logging.—The basic principle of neutron logging is to place a neutron source in the borehole and by detecting the capture-gamma flux (" n, γ technique"), or the thermal-neutron flux (" n, n_{th} technique"), or the epithermal-neutron flux⁹ (" n, n_{epi} technique"), to deduce the fluid content of the adjacent formation (62, 63). Under borehole conditions it is possible to measure the flux in one axial position only, usually above the neutron source, as the latter is attached to the bottom of the sonde. The detector is usually separated from the source by more than 30 cm. for n, γ , and n, n_{th} techniques;

⁹ The term "epithermal-neutron detector" as used in nuclear logging refers to a detector having a maximum sensitivity to neutrons in the energy range of about 0.1 to 100 electron-volts.

for n, n_{epi} technique the separation is decreased. The borehole geometry, the borehole fluid,¹⁰ and the sonde position should be known for reasonably reliable interpretation of the flux measurement.

Tittman has described the fundamentals of the technique (36). A basic theoretical paper has been published on neutron flux distributions in a borehole geometry (35). This study does not include the effect of sonde volume nor asymmetrical placement of the source.

Laboratory studies of the n, γ method, have been reported in the literature (64, 65) and in pamphlets issued by the various well logging service companies. For fixed borehole diameter and borehole fluid, the response appears to be such that the counting rate decreases linearly with the logarithm of the formation porosity. Such a semilog plot is commonly used, although a good case can be made for reversing the variables, that is, the logarithm of the counting rate decreases linearly with increasing formation porosity (66). That both plots are defensible indicates that the range of variables which can be checked in the laboratory, as well as the number of different (and reliably known) sample formations which can be used in laboratory test pits, is very limited. Neither method for plotting the variables has a theoretical basis. The laboratory studies provide means for correcting for different borehole sizes, mud densities, sonde position, and bed thickness.

The other neutron techniques, n, n_{th} and n, n_{epi} , exhibit the same general character. The n, n_{th} technique is generally considered the least reliable, as the thermal-neutron flux is subject to many perturbations, such as salinity variations in borehole and formation fluids. The n, γ technique also is perturbed by salinity variations although to a much smaller degree—the salt depresses the neutron flux but the associated increase in high-energy chlorine capture gammas tends to compensate.

The n, n_{epi} technique should, in principle, be the most reliable because the epithermal neutron flux is hardly affected by salinity variations, or variations of thermal-neutron absorbers. Unfortunately, the epithermal-neutron technique is affected very strongly by the degree of contact between sonde and formation. A few millimeters of water or borehole fluid are an effective shield against epithermal neutrons in contrast to thermal neutrons and capture gammas. This means that the epithermal sonde should have a wall-contact capability comparable to the gamma-gamma sonde. Consequently, the remarks made in connection with the latter at the end of the

¹⁰ Unless it is otherwise specified, we assume in this section that the borehole is filled with mud or other fluid with appreciable hydrogen density. In the event the borehole is gas or air filled, the value of the conventional neutron logging technique is debatable. The leakage of neutrons up and down the borehole distorts the neutron- and gamma-flux pattern considerably. Unless the source-to-detector distance is increased, the porosity sensitivity of the device may vanish. Empty boreholes require the development of special neutron tools; to date, this apparently has not been considered necessary. The various service companies have provided curves for use of standard (or slightly modified) sondes in empty boreholes.

last section are apropos, namely, that mechanical ingenuity is required (and apparently has not been applied) to solve the problem of good sonde wall contact.

From a basic physics point of view, the differences between the neutron techniques can be appreciated. The epithermal-neutron technique measures the varying ability of the formations, and the borehole, in slowing down neutrons. Slowing down is essentially a function of fluid (H_2O or CH_4) content as the matrix effect usually is not large.¹¹ The thermal-neutron technique measures both slowing-down and diffusion characteristics (i.e. migration length variations). The capture gamma technique measures slowing-down, diffusion, and capture-gamma emission characteristics. It is not at all obvious which of these techniques is "best" nor even what "best" means under actual field conditions.

It is unfortunate that the logging literature reveals no scientific analysis and discussion of the relative merits of the three basic neutron logging systems. In the laboratory, where geometry can be controlled, the epithermal technique should provide the most unambiguous results in measuring the porosity of simulated formations. Even in the laboratory one should note that the various formation matrices (silica, calcium carbonate, etc.) do affect the slowing-down pattern (67). This is true for all three techniques. Although the n, n_{epi} technique is superior in the laboratory, this does not mean that it is superior in the field, particularly where there are unknown geometry perturbations.

As noted earlier, logging time is an important consideration in any subsurface prospecting technique. Counting rates must be high enough to permit meaningful measurements (reasonable statistics) in the time scale demanded by oil-field conditions. One practical effect of this condition is to keep the source-detector spacing in the n, γ technique less than 50 cm., even though for larger spacing the porosity resolution (fractional change in counting rate per unit porosity change) increases. Counting rates can be increased by using stronger neutron sources; however, transport and safe field use limit the source strength to about 10^7 neutrons/sec. In commercial epithermal-neutron logging, the counting rates are lower than for n, γ techniques simply because the epithermal-neutron population is smaller than the capture-gamma flux at a given distance from the source and one can not reduce the source-detector distance in the epithermal technique sufficiently to compensate for this. However, the differences in counting rates and porosity resolution between the two techniques do not appear to be considered as important as the differences in sensitivity to variations in sonde position and to variations in borehole geometry.

Because of the requirements for intercomparison of logs for different wells, each service company provides some at-the-well calibration. This can

¹¹ As shales contain hydrogen (bound), the neutron technique responds to shaliness as if there were connate water present. This results in a spuriously higher indication of formation porosity.

vary from a detector check using a small calibrated radioactive source to a systems check (i.e., an integrated check of source strength, source-detector geometry, and detector) in which the neutron sonde is immersed in a calibrated synthetic formation. The latter is either a sleeve of plastic material (68) or a tank of water; in both of these arrangements the radiation leakage is sufficient to make the flux level at the detector correspond to a formation of some average porosity. The technique of using a synthetic formation at the well has an advantage in being a complete systems check; it has disadvantages in bringing a possible radiation hazard to the rig and in conducting a calibration experiment under unfavorable conditions. Some companies now favor a detector calibration check at the well and a systems calibration at the nearest service company location. Both calibrations are technically desirable. As the source strength and the source-detector geometry essentially can not be changed without opening the tool (assuming parts are bolted down inside the sonde), a systems check is not essential at the well-head. However, detector calibration at the well is essential. It should be remarked that this does not guarantee accuracy, as the detector response may vary with downhole temperature, particularly if scintillation detection equipment is used (69). Temperature effects obviously can not be carefully checked at the well, although logging a given formation interval at the beginning of the survey and repeating at the end of the survey should show up instrumental drifts.

The intercomparison of neutron logs made by different companies and with different techniques has been partially solved in the United States by the establishment of an industry-wide neutron calibration facility (43). This facility, sponsored by the American Petroleum Institute, is located in the University of Houston, in conjunction with the gamma calibration facility described earlier.¹²

¹² The neutron calibration pit consists of three cylindrical synthetic formations (porous limestone blocks with porosity values 2%, 19% and 26%) each formation 6 ft. (180 cm.) high and 6 ft. in diameter. These have been impregnated with fresh water and placed at the bottom of a pit filled with fresh water to a depth of about 7 ft. above the topmost formation. The axis of the arrangement is penetrated by a $7\frac{1}{8}$ -in. (20.6 cm.) borehole which goes through the formation and extends 15 ft. below the bottom of the pit. The sonde to be calibrated is lowered into the borehole and positioned against one side of the borehole. Readings are taken throughout the vertical length of the formations. The observed deflection (from instrument zero) in the 19 per cent porosity formation is designated as "1000 A.P.I. units," providing the scale in which to express the deflections observed when the sonde is opposite the other formations or in the top layer of water. The resulting graph of porosity versus A.P.I. units of deflection is the basic calibration curve of the neutron device. Corrections for borehole size, salinity, and mud density variations have to be made by each service company from its own experimental data. In effect, the facility provides for intercomparison of all neutron logging tools under a very limited (but somewhat "average") set of laboratory conditions. One can hope that more facilities will be added to the calibration facility, for example, test arrangements similar to those provided in some service company laboratories (65, 70).

The neutron pattern set up by a neutron logging sonde will vary in dimensions according to the porosity of the formation and the composition of the borehole fluid. For a borehole filled with water, the radial range of investigation of an n,γ sonde extends about 6 in. (15 cm.) into a highly porous formation and about four times that distance for a hard nonporous formation (38). The vertical range of investigation with the sonde stationary is slightly larger than the source-detector spacing, that is, about 2 ft. (60 cm.). When a transit of the sonde is made over thin beds, the reading opposite each bed is affected by the presence of adjacent beds. Such thin-bed effects have been computed, and correction factors are available.

The effective radius of investigation can be increased by increasing the source-detector spacing. The outer fringes of the neutron pattern are affected by events deeper in the formation. However, the counting rate decreases roughly exponentially as the source-detector spacing is increased so that there are very definite limits to spacing increase. In Venezuela, it was found in 1953 that comparison of measurements made with two different source-detector spacings yielded definite indications of gas sands, the effect being associated with the peripheral distortion of the neutron pattern by limited invasion of the borehole fluid in a gas sand. The shapes of the logs obtained with the two different source-detector spacings differed. As the papers reporting the results of "multispaced neutron logging" indicate, the technique is not easy and seems to be valuable only under rather special conditions (71, 72). Variable geometry devices will probably never become as important in nuclear prospecting techniques as in electrical techniques.

The trend in all subsurface prospecting is to combine devices. In nuclear techniques this has resulted in the almost industry-wide combination of neutron logging devices with natural gamma logging devices. (In addition, casing-collar-locators are combined for surveying cased wells.) As the natural gamma radiation is very weak, it is necessary to make the survey at speeds of about 10 to 30 ft./min. The counts of both neutron and gamma detectors are separately recorded and each is integrated over an arbitrary "time constant." The time constant is chosen so that the formation structure may not be obscured (e.g., a 6-sec. time constant when logging at 20 ft./min. means the sonde averages measurements over about a 2-ft. interval). There are other practical considerations, such as log appearance (36).

Outside the trends towards better calibration practices and increased combination with other subsurface prospecting equipment, the general direction of neutron logging development in recent years has been simply general improvement of equipment. In the United States the relaxation of restrictions on the use of plutonium has resulted in increasing use of plutonium-beryllium neutron sources. This will reduce somewhat the gamma shielding problem but will do nothing with respect to the neutron hazard. In view of the very close similarity of the neutron emission from all α,n sources, the resulting subsurface measurements will be unchanged.

Neutron activation logging.—The possibility of using a neutron source to activate nuclei in subsurface formations and then identifying the activated nuclei probably occurred to the first workers in the field of neutron logging.

As long as the source available is an α, n source (Ra-Be, Po-Be, Ac-Be, Pu-Be), the prospect is discouraging. The thermal-neutron intensity from the sonde source is too small, and the number of geologically interesting and readily activated nuclei is essentially zero.

The principal elements occurring in sedimentary formations encountered in subsurface petroleum prospecting are:

H, C, O, Na, Mg, Al, Si, P, S, Cl, K, Ca, Fe.

Assuming that the product of thermal-neutron activation must have a half life of 10 min. or less, from Meinke's sensitivity chart (73) it follows that only Al (2.3-min. Al^{28} activity), Mg (10-min. Mg^{27} activity), Ca (8.7-min. Ca^{49} activity), and S (5-min. S^{37} activity) are possibilities. On closer examination, only aluminum activation has any conceivable interest in short-time subsurface irradiation using a conventional neutron source. It is possible to correlate aluminum concentration with the shaliness of some formations but this has not proved practical with a standard neutron logging source. (There is also some interference from the $\text{Si}^{28}(n, p)\text{Al}^{28}$ reaction produced by the fast-neutron component of the source acting on silica.) To date the only practical application of thermal neutron activation has been the determination of the brine-oil interface position in a cased hole (74). In this technique the irradiation time is long (about 5 hrs.), and the observation of the Na^{24} (15.1 hr.) activity must be made 10 to 12 hr. after irradiation, to eliminate the interference of short-lived activities. This is obviously a very specialized technique and, because of the time involved, can only be used in very special situations.

The development of borehole neutron generators based on deuterium-tritium accelerators alters the prospect somewhat. Now one has 14-Mev neutrons which can activate a number of nuclei by n, γ , n, p , and n, α reactions. In a recent report on research in activating core samples with 14-Mev neutrons, Caldwell & Mills (75) point out that 14-Mev activation analysis is most promising for O (7.3-sec. N^{16}), Si (2.3-min. Al^{28} , 6.6-min. Al^{29} , 9.5-min. Mg^{27}), P (2.3-min. Al^{28}), Al (9.5-min. Mg^{27} , 15-hr. Na^{24}) and Mg (1.0-min. Na^{25} , 15-hr. Na^{24}) in decreasing order. As far as the use of these 14-Mev neutrons in actual field situations, only oxygen logging has been reported (76, 79).

In oxygen logging a borehole accelerator is used to produce 14-Mev neutrons by the d, t reaction. There have been a number of brief, semi-informative descriptions of borehole accelerators in the literature (76, 78, 79). Obviously the production of an accelerator device which will operate under the difficult subsurface conditions described earlier is quite a technical achievement and is regarded by the various service companies as a trade secret. Unfortunately it is not possible to evaluate the usefulness of borehole accelerators without further numerical information such as yield, pulsing data, effect of temperature, and stability (i.e., variation in neutron output). Presumably such information will become available in the future,

especially as those responsible for interpreting subsurface measurements will require the data for evaluating the technique.

The oxygen-activation technique is straightforward. The accelerator is turned on steadily and the logging tool (3½ in. diam., 22 ft. long) is drawn upward past the formation. A detector responding to the 6.3-Mev gammas emitted by the 7.3-sec. N^{16} is located several feet below the accelerator neutron source. Logging speed is about 20 ft./min., which is slow enough to permit adequate irradiation of the formation and not so slow that the formation activity has decayed by the time the detector is opposite the irradiation formation.

The physical basis of the device is firm; however, the usefulness is not at all clear, especially in open holes. In open-hole logging there are many oxygen nuclei which are unaffiliated with the fluid of interest (formation water). The oxygen atoms in SiO_2 , $CaCO_3$, and the borehole fluid all will contribute to the signal. A simple calculation shows that the oxygen activation technique, as described in the literature, even under ideal conditions, may have value in open-hole logging only where the formations are very porous. In such situations other logging techniques would undoubtedly be superior. For air- or gas-filled boreholes, the borehole fluid interference is eliminated. However, highly porous formations are not likely to be encountered.

For cased-hole logging the situation might be different. At the oil-water interface the oxygen concentration has a sharp discontinuity. However, the signal will again be diluted with the oxygen component of the formation matrix as well as the oxygen in the cement and borehole fluid. Moreover, the presence of iron (and usually some manganese) will increase the gamma background substantially. If the neutron source can be pulsed, it may be possible to reduce some of these last interfering effects by discriminating against all but the 7.3-sec. activity. It is too early to assess the future value of oxygen-logging. One can only be skeptical on the basis of what has been published to date.

Capture and inelastic gamma techniques.—When a neutron source is located in a prospecting sonde adjacent to a subsurface formation, the resulting neutron inelastic-scattering and capture processes generate gamma radiation of various energies. Before the gamma radiation reaches the detector in a sonde, most of it is degraded in the usual manner. That radiation which is only slightly degraded in the transit from formation to sonde detector can be analyzed to identify the nucleus in which the scattering or capture took place. However, the identification is by no means simple and unambiguous. The capture-gamma signal itself is usually complicated, as a thermal-neutron capture-gamma-ray atlas (80) shows. The detector contributes to the "smearing," and the system of transmitting the information to the surface may also contribute to loss of resolution. Measurements have to be made over an appreciable interval of time to eliminate statistical effects.

In the laboratory, complete spectral curves have been obtained for a

Po-Be source in several simulated high-porosity (35 to 50%) formations (81, 82). The arrangement was similar to that of a neutron sonde in a borehole, except that the sonde did not, apparently, have a high pressure housing. Under the very special conditions of the laboratory arrangement it was possible to secure qualitative analyses for H, Cl, Ca, Si, S, and Mg. However, when one examines the published experimental surveys and speculates on how far these experiments deviated from the realities of a subsurface prospecting situation, it is difficult to believe that such qualitative analyses would be possible in most field situations.

In other experiments using a Po-Be source (77), it was noted that the unique high-energy thermal-neutron capture gammas from chlorine could be used in locating oil-water contacts.¹³ This technique is simpler in that one searches within a single formation interval for a discontinuity in the count rate of all capture gammas above 6 Mev. In order to know where to look, it is necessary to know the porous intervals and the boundaries; this information can be secured, e.g., from a standard neutron survey. In open (uncased) holes where the mud filtrate invades the formation, the technique usually will not work. However, in cased holes where the brine-oil interface is established up to the edge of the formation, the technique has a reasonable chance for success. This technique of surveying for the high-energy capture gammas has been exploited in a number of quarters; "chlorine" or "salinity" logs are now being run experimentally and commercially (83). In this connection, reference to a capture-gamma atlas (80) shows that iron capture gammas will tend to interfere with the chlorine gammas, as will the gammas from the 7.3-sec. oxygen activity. Both of these latter may be constant backgrounds in many field situations, so the effect may not be disastrous.

With Po-Be (or Ac-Be, Pu-Be, etc.) sources, the principal gammas are those resulting from thermal-neutron capture and, to a much lesser extent, from decay of some induced radioactivities. (The latter may be important when the exposure of the formation is long.) If, on the other hand, a 14-Mev neutron source is used, i.e., a deuterium-tritium accelerator, both capture gammas and gammas from inelastic events are produced (77, 79). Some of these latter are of unique interest, e.g., the 4.4-Mev gamma from carbon excitation. A carbon-oxygen ratio technique has been studied in the laboratory (77) and shown to be a possible brine-oil differentiator. The possibility of detecting magnesium as a means for distinguishing between limestone and dolomite has been noted, although the relatively low energy of the prominent magnesium gamma ray (1.37 Mev) makes the practical field use of the technique dubious.

The basic difficulty in all gamma-spectroscopy techniques, where the gammas are induced by various neutron processes, is that the signal-to-noise ratio is low. The "noise" consists of contributions from other capture

¹³ In some field situations, the interfering effect of halite in the formation matrix (85, 86) may be significant.

gammas plus all the degraded gammas. As a general rule, the higher the energy of the gamma being measured, the higher the signal-to-noise ratio. High-energy gammas include relatively fewer degraded gammas and, if the detector has directional sensitivity towards the formation, the high-energy gamma component has relatively fewer gammas which have originated outside the formation and have been scattered into the detector.

Clearly what is needed is some way to separate the various gamma-producing processes. One possibility has been described by Tittman & Nelligan (79). They have performed laboratory studies in simulated formations using a borehole accelerator as a pulsed neutron generator. The 14-Mev neutron generator was turned on for 15 to 20 μ sec., then turned off for several hundred μ sec. before repeating the cycle. The gamma detector system was gated in two ways: "burst gate" in which the detector was on only during the first 15 μ sec. of the neutron burst; "delayed gate" in which the detector was on at all times except the first 25 μ sec. after the initiation of each neutron burst. In the burst gate most of the detected gammas are from inelastic-scattering processes; in the delayed gate most are from thermal-neutron captures. The spectra obtained with a laboratory multichannel pulse-height analyzer are presented for experiments with a laboratory sonde in an 8-in. (20-cm.) diam. borehole through three synthetic formations: 40 per cent porous clean silica sand filled with fresh water, with 15 per cent salt solution, and with Number 2 fuel oil. The carbon and oxygen inelastic gammas can be identified on the burst gate detection and not on the delayed gate detection. Similarly the hydrogen, silicon, and chlorine thermal-neutron capture gammas show up on the delayed gate detection, while with burst gate detection they are greatly reduced. The inelastic spectra for salt water and fresh water formations are nearly identical, leading to the conclusion that one can distinguish between salt and fresh water by comparison of inelastic and thermal spectra. Similarly, the oil sand exhibits no chlorine peaks in the thermal spectra. In addition to the separate inelastic and thermal spectra, the paper presents the measurements with the detector on all the time. Examination of the latter spectra for the three laboratory formations studied shows that a substantial improvement in the analytical capabilities of the technique has been achieved. Whether such time discrimination can be used successfully under average field conditions is not clear. The laboratory experiments reported are somewhat idealized; for example, an aluminum sleeve is used instead of an iron pressure housing; moreover, the highly porous silica formations and the good geometry are certainly optimistic. Nevertheless, it seems clear from the results quoted that capture-gamma or inelastic-gamma spectrometry using a pulsed neutron source is a promising approach.

Assuming that the instrumentation problems are solved—and these are certainly difficult—and that thermal capture and inelastic gamma spectra can be obtained in routine field operations, the question is: will the information be of sufficient geological significance to warrant the effort? There is

little doubt that the pulsed accelerator plus gamma spectrometer technique will detect brine-oil interfaces in a cased hole for formations with silica matrices and reasonable porosity, as even cruder capture-gamma techniques can often do this. In an air- or gas-drilled empty hole, the technique may have similar capabilities; the same is probably true for open holes drilled with oil-based muds, assuming negligible invasion. However, for the normal open hole with salt-water muds the prospect is not encouraging. In the latter, and most common, situations it will be necessary to run a large number of field experiments before one can find the geological significance, if any, of the data. In this respect the technique will face the same hurdle as the natural-gamma spectrometer technique. Fortunately, unlike the natural-gamma spectrometer approach, there are at least some situations in which the pulsed accelerator plus gamma spectrometer technique is likely to have immediate practical value.

The future of all subsurface prospecting techniques which use neutron sources with gamma spectrometry is promising, but probably not such as to be characterized as "a new era in well logging," to quote an early sales-inspired paper on this subject. Quantitative analysis by detection of neutron-induced gamma radiation is an established technique in very specialized laboratory situations. In specific instances the technique can be competitive with chemical analytical methods [e.g. (75, 84)]. However, in subsurface prospecting the technique is subject to the many severe boundary conditions discussed in detail earlier in this review. Many of these conditions are not likely to be altered in the near future. Consequently, quantitative analysis is going to be extremely difficult to achieve, especially under open-hole conditions. In cased holes, the method of identifying brine-oil interfaces by qualitative analysis appears to be the only technique which is encouraging.

FUTURE OF NUCLEAR SUBSURFACE PROSPECTING METHODS

Inasmuch as nuclear techniques are relatively short-range (distance usually less than 50 cm.) investigative methods, there could be a "new era" in nuclear logging in open holes if changes in drilling techniques bring about a drastic improvement in borehole geometry and an elimination of invasion by the borehole fluid. In other words, if drilling techniques improve so that the sonde is surrounded by virgin formation and is located in a known geometry, the possibilities of meaningful and unambiguous interpretation of the nuclear measurements will be greatly improved. Of course, all other logging techniques would benefit by such improvements in drilling techniques so that it is not a necessary consequence that the relative value of nuclear methods in open-hole logging would improve.

In cased holes the difficulties of coping with the effects of iron casing and cement will probably always exist. However, improved drilling and cementing practices would benefit nuclear techniques by making the geometry of the cement annulus more certain. As noted earlier, nuclear methods have

a unique advantage in cased-hole logging, being the only technique at present for *in situ*, nondestructive formation analysis. Because of this it is obvious that any "improvement" in cased-hole practices (e.g., improved centralizing of casing, improved cementing practices, elimination of sonde-restricting hardware) and in cased-hole operations (e.g., willingness and capability to replace salt water or other fluid in casing with fresh water or diesel oil) will improve the prospect of securing reliable analytical information with nuclear techniques.

It is safe to predict that those oil-field practices which handicap nuclear logging techniques are not likely to change rapidly. As a consequence it is essential that laboratory experiments be realistic. Although, quite properly, preliminary studies should be made in idealized arrangements, no technique should be characterized as the "seventh sense" (quoted from a "technical" article on a not-completely-cooked technique) or similar superlative until it has been checked out in the laboratory with respect to the effect of variation of borehole diameter, sensitivity to stand-off (distance from the borehole wall), effect of borehole fluid density and salinity variations, effect of matrix variation (silica versus calcium carbonate), and any other significant variables which can be simulated in the laboratory. There are many nuclear techniques presented in sales-oriented papers which are based on too few experiments—for example, based on putting the experimental device in a barrel of water and in a barrel of oil and reporting the difference in response. There is nothing objectionable in presenting the results of such experiments as experiments, but presenting such results as if the data established a new logging technique is essentially dishonest. It is not appropriate to cite specific references to such practices; however, one does not have to search the literature very extensively to find examples.

There are some nuclear techniques, the improvement of which will probably not require further laboratory studies with simulated formations. As noted earlier, natural gamma spectroscopy faces primarily a "measurement time" problem; better and more rapid detecting and analyzing techniques are required. The density (gamma-gamma) technique is handicapped by geometry, so that the most urgently needed improvement is to make a sonde which maintains a reliable and continuous wall contact over the source-detector interval.

On the other hand, other nuclear techniques definitely need more laboratory studies in simulated formations. The standard neutron (porosity) method has never been studied in the detail that it requires, or at least such studies have not been reported in the literature. The standard neutron log is a very complex technique whether an epithermal-neutron, a thermal-neutron, or a capture-gamma detector is used. The universal use of empirical semilog graphs is indicative of the primitive state of the technique; each petroleum geologist has his own preferred graphs, usually different ones for each district. The situation has been improved in the past several years by increasing the reliability of tools and better calibration. Still, the published

technical data are not complete, and those who must interpret the measurements do not have available sufficient laboratory information on the devices being used in the field. Unless the various groups in the service companies and in the oil companies do the experiments and report the results fully, it is safe to predict that in open-hole logging the standard neutron technique will be gradually replaced by other techniques (e.g., gamma-gamma, acoustic) which have been better reported in the literature.¹⁴

The newer techniques, neutron activation and capture- (and/or inelastic-)gamma techniques, certainly require more laboratory studies. The former does not seem to have as much promise as the latter in view of the measurement time required for activation analysis of those elements of possible geological interest. The latter technique, particularly with time-discrimination, appears promising and should be completely explored in the laboratory and the results reported in the open literature.

There is one problem common to all laboratory studies, namely, how to simulate subsurface formations. This problem must be faced. For example, there is almost nothing in the literature to indicate whether more readily fabricated composite structures of formation matrix and fluid (laminated or otherwise) can be used to simulate subsurface formations. Obviously such synthetic structures will not respond to nuclear radiations in the same way as actual formations; however, it may be possible to infer from measurements with a synthetic structure what a specific nuclear technique may do in a real formation. The present practice of relying on the limited number of different kinds of blocks obtained from various quarries is certainly not desirable.

CONCLUSION

During the twenty years since the first use of nuclear methods for subsurface prospecting, there have been remarkable advances. Gamma and neutron detectors of all sizes and shapes, capable (with their associated circuits and mechanical components) of measuring nuclear radiations, natural or induced, at depths to about $4\frac{1}{2}$ miles (7 km.) below the earth's surface and at temperatures up to about 400°F. (200°C.), are now available to those searching for petroleum. The measurements are quantitative and, with the steady improvement in calibration and standardization procedures, the measurements are reproducible.

The development of borehole accelerators represents a significant technical achievement. From information published it is not clear that the presently available borehole neutron generators can survive the difficult subsurface environment nor that the present cost and complexity are com-

¹⁴ The gamma-gamma technique per se has not been adequately reported in the literature, but the basic data on gamma-ray transmission through extended media is available in many publications (52). The technique has also been analyzed in theoretical studies (60, 61).

patible with routine commercial use. The important problems of calibration and standardization have not been solved and will require attention and effort in the future. It is unlikely that sondes using accelerator neutron generators will replace standard neutron devices. The use of 14-Mev neutrons for conventional porosity measurements does not offer any apparent advantages; the disadvantages can be readily appreciated by comparing cost and reliability of a Po-Be (or Ra-Be, Ac-Be, or Pu-Be) source with neutron generator (*d,t* tube, high-voltage supply, control electronics, etc.). The borehole accelerator will be valuable if it can measure some formation property which can not be measured by any other logging device and which has appreciable significance for the petroleum geologist. As noted earlier, there are some promising possibilities, but further laboratory and field studies are needed before the practical value of borehole accelerators can be assessed.

The interpretation of nuclear measurements in subsurface prospecting has improved, but there is still much room for further improvement. Some of the ambiguity in interpretation is attributable to natural causes (e.g., the hydrogen in a shale "looks" the same as the hydrogen in connate water or hydrocarbon); some is attributable to sonde design inadequacies (e.g. borehole, wall-contact devices which can not always contact the wall). In addition, individuals called on to interpret the measurements do not have available all the necessary nuclear-logging physics to make proper use of the measurements. This last situation can be improved by a change of attitude on the part of the oil companies and the logging service companies. It is common knowledge that many studies of nuclear logging techniques are made simultaneously and independently in many laboratories. Some duplication of effort is bound to occur in a competitive activity. However, it is apparent that with respect to the development of nuclear methods for subsurface prospecting there are too much duplication and too little publication of results. Many of the reports that are published are either strictly sales talk or technical papers with great gaps in the data presented. For example, a recent paper concerning a new nuclear logging technique does not identify the borehole fluid although this is a critical parameter in the experiments discussed. In addition, papers written for petroleum geologists often waste substantial space re-explaining—and incorrectly at times—nuclear physics when a reference to any one of the many standard textbooks would suffice.

There seems to be a widespread belief in the petroleum industry that nuclear methods may provide a "breakthrough" in subsurface prospecting and, because of this, extreme trade secrecy in nuclear work is practiced. The technical facts do not support this belief. Actually, a careful study of all subsurface prospecting techniques reveals that nuclear methods are important but by no means more important than other methods. There is no reason to assume that the "glamor" and future promise of nuclear processes as concentrated and abundant energy sources are transferable to the use of nuclear processes in prospecting for petroleum.

Nuclear techniques are indeed important additions to the continually growing stockpile of subsurface prospecting techniques, but they are only additions to the stockpile, not replacements of the stockpile.

ACKNOWLEDGMENTS

The author would like to express appreciation to his former colleagues in the Schlumberger Well Surveying Corporation, especially to Jay Tittman of Ridgefield, Connecticut, and John Dewan of Houston, Texas. Although they did not participate in the preparation of this review, the technical content reflects many stimulating discussions with them. The opinions expressed in this paper are, however, the author's sole responsibility.

LITERATURE CITED

1. Truman, T. P., and Saito, N., *Ann. Rev. Nuclear Sci.*, **4**, 401 (1954)
2. Abelson, P. H., Ed., *Researches in Geochemistry* (John Wiley & Sons, Inc., New York, N. Y., 511 pp., 1959)
3. Adler, H. H., *Proc. Intern. Conf. Peaceful Uses Atomic Energy*, **2nd**, Geneva, 1958, **2**, 224 (1958)
4. Merrill, J. R., Honda, M., and Arnold, J. R., *Proc. Intern. Conf. Peaceful Uses Atomic Energy*, **2nd**, Geneva, 1958, **2**, 251 (1958)
5. Faul, H., Ed., *Nuclear Geology* (John Wiley & Sons, Inc., New York, N. Y., 414 pp., 1954)
6. Rankama, K., *Isotope Geology* (McGraw-Hill Book Co., New York, N. Y., 535 pp., 1954)
7. Moxham, R. M., *Proc. Intern. Conf. Peaceful Uses Atomic Energy*, **2nd**, Geneva, 1958, **2**, 815 (1958)
8. Crews, W. D., *Oil Gas J.*, **57**(21), 391 (1959)
9. Bisir, D. P., *Proc. Intern. Conf. Peaceful Uses Atomic Energy*, **2nd**, Geneva, 1958, **2**, 837 (1958)
10. Boyle, T. L., *Proc. Intern. Conf. Peaceful Uses Atomic Energy*, **2nd**, Geneva, 1958, **2**, 820 (1958)
11. Johnson, J. C., *Proc. Intern. Conf. Peaceful Uses Atomic Energy*, **2nd**, Geneva, 1958, **2**, 3 (1958)
12. Lecoq, J. J., Bigotte, G., Hinault, J., and Leconte, J. R., *Proc. Intern. Conf. Peaceful Uses Atomic Energy*, **2nd**, Geneva, 1958, **2**, 744 (1958)
13. Bowie, S. H. U., Miller, J. M., Pickup, J., and Williams, D., *Proc. Intern. Conf. Peaceful Uses Atomic Energy*, **2nd**, Geneva, 1958, **2**, 787 (1958)
14. Berbezier, J., Blangy, B., Guitton, J., and Lallemand, C., *Proc. Intern. Conf. Peaceful Uses Atomic Energy*, **2nd**, Geneva, 1958, **2**, 799 (1958)
15. Nininger, R. D., *Minerals for Atomic Energy*, **2nd** ed. (D. Van Nostrand Co., Inc., Princeton, N. J., 399 pp., 1956)
16. Takahashi, K., Kakayama, N., and Sato, M., *Proc. Intern. Conf. Peaceful Uses Atomic Energy*, **2nd**, Geneva, 1958, **3**, 77 (1958)
17. Bhatnagar, A. S., *Proc. Intern. Conf. Peaceful Uses Atomic Energy*, **2nd**, Geneva, 1958, **3**, 71 (1958)
18. Russell, R. T., *Proc. Intern. Conf. Peaceful Uses Atomic Energy*, **2nd**, Geneva, 1958, **2**, 358 (1958)
19. Bulashevich, Iu. P., *Proc. Intern. Conf. Peaceful Uses Atomic Energy*, **2nd**, Geneva, 1958, **2**, 825 (1958)
20. Grammakov, A. G., Kvashnevskaya, N. V., Nikonov, A. I., Sokolov, M. M., Sochevanov, N. M., Suppe, S. H., and Tafeyev, G. P., *Proc. Intern. Conf. Peaceful Uses Atomic Energy*, **2nd**, Geneva, 1958, **2**, 732 (1958)
21. Phelps, T. W., *J. Petrol. Technol.*, **11**, (7), 22 (1959)
22. Blanpied, B. W., *Bull. Am. Assoc. Petrol. Geologists*, **43**(6), 1117 (1959)
23. Mott, W. E., *World Petrol. Congr. Proc.*, **5th**, New York, June 1959
24. Czubek, J., Dziunikowski, B., Jurkiewicz, L., Krzok, J., Niewodniczański, J., Owsiak, T., Przewlocki, K., and Zuber, A., *Proc. Intern. Conf. Peaceful Uses Atomic Energy*, **2nd**, Geneva, 1958, **3**, 83 (1958)
25. Weiss, W. J., Graves, R. H., and Hall, W. L., *Petrol. Engr.*, **30**(4), B-43 (1958)
26. Gray, G. R., *Oil Gas J.*, **56**(50), 90 (1958)
27. Barrett, H. M., *The Fundamentals of Rotary Drilling* (The Petroleum Engineer, Publ., Dallas, Texas, 152 pp., 1955)
28. Smith, F. W., *Oil Gas J.*, **57**(18), 169 (1959)
29. Adams, J. H., *Petrol. Engr.*, **29**(5), B-30 (1957)
30. ASME panel discussion reported in *Oil Gas J.*, **56**(2), 62 (1958)
31. Gardner, F. J., *Oil Gas J.*, **55**(27), 185 (1957)
32. Lill, G., and Bascom, W., *Nature*, **184** (4681), 140 (1959)
33. Keen, R. E., *Petrol. Engr.*, **31**(3), B-30 (1959)
34. Cannon, G. E., and Watson, R. A., *Petrol. Engr.*, **29**(5), B-82 (1957)
35. Glauberman, A. E., and Talianskyi, I. I., *Atomnaya Energ.*, **3**(7), 23 (1957)
36. Tixier, M. P., Martin, M., and Tittman, J., *Fundamentals of Logging* (Univ. of Kansas, Lawrence, Kansas, 169 pp., 1956)
37. Wyllie, M. R. J., *The Fundamentals of Electric Log Interpretation* (Academic Press, Inc., New York, N. Y., 2nd Ed., 1957)
38. *Introduction to Schlumberger Well Logging* (Doc. No. 8) (Schlumberger Well Surveying Corp., Houston, Texas, 176 pp., 1958)

39. Caldwell, R. L., *Nucleonics*, 16(12), 58 (1958)
40. *World Petrol. Congr. Proc.*, 4th, Rome, 1955
41. Blanchard, A., and Dewan, J. T., *Petrol. Engr.*, 25(8), B-76 (1953)
42. Tittle, C. W., and Wyllie, M. R. J., *Oil Gas J.*, 53(47), 159 (1955)
43. Anonymous, *Oil Gas J.*, 57(29), 82 (1959)
44. Drouillard, R. F., and Dodd, P. H., *Proc. Intern. Conf. Peaceful Uses Atomic Energy*, 2nd, Geneva, 1958, 3, 46 (1958)
45. Wilson, J. C., and Marquis, G. L., *Ann. Petrol. Conf. New Developments and Techniques*, 2nd (McMurry College, Abilene, Texas, 1957)
46. Anonymous, *Oil Gas J.*, 57(27), 79 (1959)
47. Russell, W. L., *Geophysics*, 9, 180 (1944)
48. Kokes, F. P., *Oil Gas J.* (July 26, 1951)
49. Rabe, C. L., *J. Petrol. Technol.*, 9(2), 65 (1957)
50. Cutmore, T. P., *Oil Gas J.*, 56(5), 97 (1958)
51. Stead, F. W., *Proc. Conf. Peaceful Uses Atomic Energy*, 2nd, Geneva, 1958, 3, 32 (1958)
52. Goldstein, H., *Fundamental Aspects of Reactor Shielding* (Addison-Wesley Publ. Co., Reading, Mass., 416 pp., 1959); see especially Chap. 5
53. Matveev, V. V., Sokolov, A. D., and Shlyapnikov, R. S., *Atomnaya Energ.*, 1(4), 57 (1956)
54. Brannon, H. R., Jr., and Osoba, J. S., *J. Petrol. Technol.*, 8(2), 30 (1956)
55. Adams, J. A. S., and Weaver, C. E., *Bull. Am. Assoc. Petrol. Geologists*, 42, 387 (1958)
56. Bird, J. R., and Waters, J. R., *Nuclear Phys.*, 14, 212 (1959)
57. Jenkins, R. E., and Meurer, M. C., *Petrol. Engr.*, 30(2), 8-64 (1958)
58. Hurley, P. M., *Bull. Geol. Soc. Am.*, 67, 406 (1956)
59. Baker, P. E., *J. Petrol. Technol.*, 9(10), 289 (1957)
60. Ochkur, A. P., *Vses. nauchno-issled. inst. razved. geofiz. Voprosy rudnoy geofiz.*, *Sbornik Statei*, 1, 62-68 (1957)
61. Voskoboynikov, G. M., *Izvest. Akad. Nauk S.S.S.R., Ser. Geofiz.*, No. 3, 351 (1957)
62. Russell, W. L., *Bull. Am. Assoc. Petrol. Geologists*, 36, 312 (1952)
63. Guerrero, E. T., and Stewart, F. M., *Oil Gas J.*, 57(2), 100 (1959)
64. Dewan, J. T., and Allaud, L. A., *Petrol. Engr.*, 25(9), B-49 (1953)
65. Dewan, J. T., *J. Petrol. Technol.*, 8(2), 50 (1956)
66. Brown, A. A., and Bowers, B., *Petrol. Engr.*, 30(5), B-30 (1958)
67. Tittman, J., *J. Appl. Phys.*, 26, 394 (1955)
68. Hamilton, R. G., and Charrin, P., *Oil Gas J.*, 55(20), 199 (1957)
69. Youmans, A., and Monaghan, R., *J. Petrol. Technol.*, 9(8), 231 (1957)
70. Widmyer, R. H., and Wood, G. M., *J. Petrol. Technol.*, 10(5), 57 (1958)
71. Swift, G., and Norelius, R. G., *Oil Gas J.*, 54(76), 109 (1956)
72. Grosman, M., and Walker, E. B., *J. Petrol. Technol.*, 9(5), 140 (1957)
73. Meinke, W. W., *Anal. Chem.*, 31, 792 (1959)
74. Kukharensko, N. K., Odinkov, V. P., and Shimelevich, Yu. S., *Proc. Conf. Acad. Sciences U.S.S.R. Peaceful Uses Atomic Energy* (Moscow, July 1-5, 1955)
75. Caldwell, R. L., and Mills, W. R., Jr., *Nuclear Instr. & Methods*, 5, 312 (1959)
76. Youmans, A. H., and Zimmerman, C. W., *Oil Gas J.*, 57(24), 139 (1959)
77. Caldwell, R. L., and Sippel, R. F., *Bull. Am. Assoc. Petrol. Geologists*, 42(1), 159 (1958)
78. Anonymous, *Nucleonics*, 15(9), 192 (1957)
79. Tittman, J., and Nelligan, W. B., *Soc. Petrol. Engrs., AIME Paper No. 1227-G* (Meeting in Caspar, Wyoming, April 2, 1959)
80. Groshev, L. V., Demidov, A. M., Lutsenko, V. N., and Pelekhov, V. I., *Atlas of Gamma Ray Spectra from Radiative Capture of Thermal Neutrons* (Sykes, J. B., Transl. Pergamon Press, London, Engl., 198 pp., 1959)
81. Baker, P. E., *J. Petrol. Technol.*, 9(3), 97 (1957)
82. Muench, N. L., and Osoba, J. S., *Trans. Am. Inst. Mining, Met. Petrol. Engrs.*, 210, 89 (1957)
83. Rabson, W. R., *Petrol. Engr.*, 31(3), B-103 (1959)
84. Tittman, J., and Nelligan, W. B., *IRE Trans. on Nuclear Sci.*, NS-5(3), 187 (1958)
85. Waldschmidt, W. A., *Bull. Am. Assoc. Petrol. Geologists*, 42, 871 (1958)
86. Martinez, S. J., and Hurst, R. E., *Petrol. Engr.*, 28(12), B-68 (1956)

EXPERIMENTS ON COSMIC RAYS AND RELATED SUBJECTS DURING THE INTERNATIONAL GEOPHYSICAL YEAR¹

By E. P. NEY

School of Physics, University of Minnesota, Minneapolis, Minnesota

INTRODUCTION

In his conclusion to the article on primary cosmic radiation in the *Annual Review*, H. V. Neher (1) made the statement, "The present problems in the field of cosmic rays divide themselves into two categories: (a) those having to do with solar influences and (b) those having to do with their origin." The International Geophysical Year has given cosmic ray physicists an opportunity to answer many questions concerning the solar influences on cosmic rays, and also to throw some light on the origin of cosmic rays, at least those of solar origin. In studying the effect of solar activity on cosmic rays, new and interesting radiation phenomena in space have been discovered, the most outstanding being the discovery by Van Allen and his collaborators of radiation belts surrounding the earth. The advent of the Russian and American satellite launchings suddenly created a new tool for the study of extraterrestrial radiation and provided new impetus for these experiments. Not only have scientists studied the natural phenomena existing in the vicinity of the earth with radiation detectors, but the understanding of these phenomena led to a series of experiments (the Argus explosions) in which energetic nuclear particles were injected into the magnetic field of the earth and this man-made radiation shell was studied in detail with earth-circling satellites.

The Geophysical Year was conceived at a very opportune time from the standpoint of cosmic ray experiments. For the last two solar cycles, cosmic rays at sea level and mountain altitudes have been monitored with ionization chambers by Forbush (2) and at balloon altitudes by Neher (3, 4). These experiments have shown that a solar cycle dependence of cosmic ray intensity does exist. They also demonstrated that several days following strong solar disturbances, cosmic rays suffered abrupt decreases, now called Forbush decreases, recovering to their predecrease intensity in a matter of weeks. The techniques for more extensive studies of the incoming particles existed at the beginning of IGY. These used such devices as high-altitude plastic balloons capable of monitoring cosmic rays at the top of the atmosphere. In the period just before IGY the neutron monitor was invented by Simpson and his collaborators (5) and has served as an extremely useful instrument for determining the instantaneous value of sea level nucleonic

¹ The survey of literature pertaining to this chapter was concluded February 29, 1960.

cosmic rays. The radiation phenomena observed during the Geophysical Year were perhaps more intense than in the last 200 years during which solar activity has been observed. Late in 1957 the sun reached the highest recorded level of sunspot numbers (6). The counting of sunspots has been carried out as a crude measure of solar activity since 1749, and of all the cycles of solar activity the one which reached its maximum in 1957-58 appears to be the most intense. In this review, we will discuss the kinds of radiation detected at the earth and in space and affected by solar activity.

THE SOFT RADIATION AND AURORAL X-RAYS

The Stoermer theory of the motion of charged particles in the magnetic dipole field was developed in an attempt to understand the properties of the aurora borealis. This theory has proved remarkably successful in predicting cutoff energies for cosmic ray particles. However, Stoermer and others almost immediately realized that it did not, in fact, account for the aurora in terms of vacuum trajectories of charged particles in the earth's magnetic field. The principal difficulty in explaining the aurora by Stoermer theory arises from the fact that very low-energy particles are able to enter at latitudes where the cutoff energy as predicted by Stoermer theory would not allow them to come in. For example, at a geomagnetic latitude of 55° , aurora is frequently seen overhead. The primary particles responsible for the aurora have energies considerably less than one million electron volts. The Stoermer cutoff energy, on the other hand, for vertical incidence at this latitude is 1.5 Bev for electrons and 850 Mev for protons. To account for this fact and for other observations in connection with magnetic storms, Chapman, Alfvén and others introduced the concept of solar beams, consisting of positive and negative particles which together represent a highly conducting plasma approaching the earth. This plasma is able to distort the earth's magnetic field and allow the entry of the aurora-producing particles. The first evidence that large numbers of low-energy particles did indeed exist at high altitude was obtained by the State University of Iowa group in the summer of 1953 (7). That these soft particles were present predominantly in the auroral zone was shown by Van Allen and his collaborators in the period from 1953 to 1958. Further clarification of this problem was obtained through the experiments of Winckler and his collaborators who established in the early period of the Geophysical Year that energetic x-rays could be observed coincident with visible aurorae at balloon altitudes. The two types of experiments will be briefly described.

The experiments of the Iowa group consisted of flying a rocket experiment in or near the auroral zone. The detectors were Geiger counters, shielded and unshielded, and scintillators. They were carried to high altitude by a rocket launched from a floating balloon, a system developed by the Iowa group and called the Rockoon technique. Figure 1 shows an example of the response of shielded and unshielded radiation detectors as the rocket ascends. It can be seen that at balloon altitudes no detectable soft radiation is present,

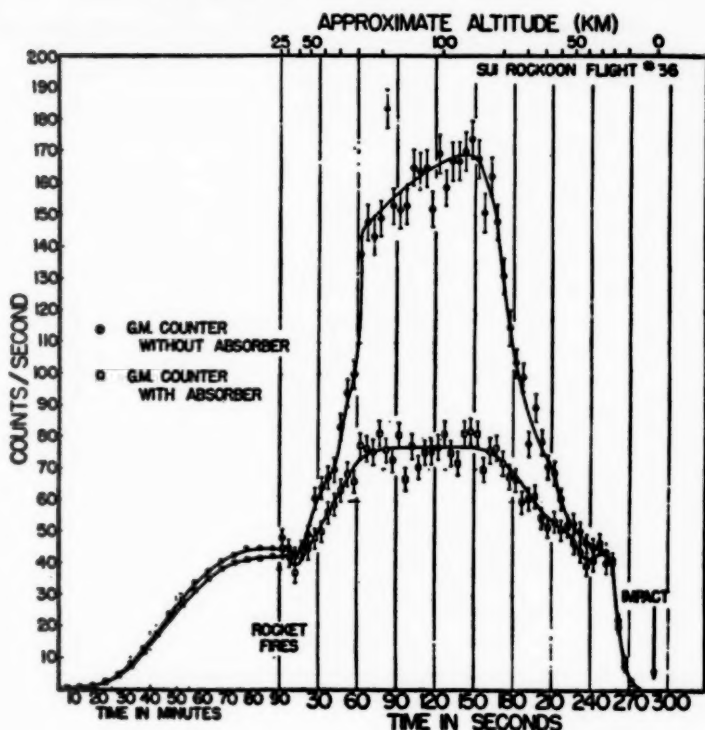


FIG. 1. A typical set of raw flight data observed with two Geiger tubes, one without absorber and one incased in an absorber of 150 mg./cm.^2 of aluminum. The normal cosmic ray counting rate is about 39 counts/sec. at altitudes above 50 km. The additional counts are due to the soft radiation. (From J. A. Van Allen, "Rocket Measurement of Soft Radiation," *IGY Rocket Rept. No. 1*, July 30, 1958, p. 159.)

but shortly after the rocket fires and reaches altitudes in excess of 150,000 ft. the counting rate of both detectors increases greatly due to the presence of low-energy electrons and ions. Subsequent experiments by McIlwain (8) and Meredith *et al.* (9) have shown that the soft radiation detected at auroral latitudes consists of low-energy electrons and ions. The energies of the charged particles detected were below 1 Mev. Although these energies are low by nuclear physics standards, they are extremely high in terms of auroral particles, and the particles were referred to by Van Allen as the "millionaires of the auroral spectrum."

The first discovery of IGY was that electrons above the atmosphere produce x-rays detectable at balloon altitudes. On July 1, 1957, Winckler and his collaborators discovered that radiation detectors flying at a geomagnetic latitude of 55° detected strong bursts of x-rays coincident with the appearance at the zenith of visible aurorae (10). It is now believed that the x-rays

associated with visible aurorae at latitudes as low as 55° are produced by the release of electrons trapped in the great radiation belts. Therefore, the understanding of auroral x-rays had to await the discovery of these radiation belts. The auroral x-rays were observed many times during the IGY period (11), and Figure 2 shows an example of this phenomenon in the great storm of

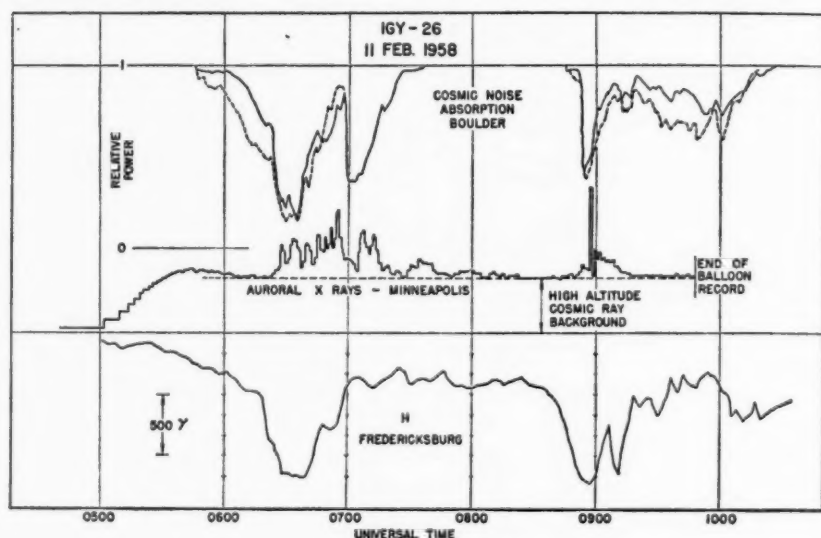


FIG. 2. Comparison of the horizontal magnetic field—at Fredericksburg, auroral x-rays at Minneapolis, and cosmic noise absorption at Boulder. Two cases of intense ionospheric ionization apparently occurred, reaching maxima at approximately 0630 and 0900. The ionization was very widespread as shown by this correlation and by the all-sky camera photographs. [From J. R. Winckler *et al.*, *J. Geophys. Research*, 64, 597 (1959).]

February 11, 1958. It is clear from this figure that the occurrence of auroral x-rays over Minneapolis is accompanied by a great disturbance of the horizontal magnetic field of the earth and by the appearance of the absorption of cosmic noise in the ionosphere as detected at Boulder, Colorado. The interpretation of the auroral x-rays is that they arise by bremsstrahlung of electrons high in the atmosphere and far above the balloon altitudes. The x-rays which are produced by electron bremsstrahlung have energies up to 100 kev. That at least some of these x-rays must arise from the release of trapped electrons in the earth's magnetic field was established by earth satellites during the storm of August 16–17, 1958. This will be discussed in a later section.

MODULATION OF GALACTIC COSMIC RAYS

It was discovered by Forbush (2), in the solar cycle which had its minimum in 1944 and its maximum in 1947, that there was an inverse relation-

ship between the counting rate of ion chambers at sea level and the sunspot numbers. In other words, increased solar activity is associated with decreases in cosmic ray intensity at the earth. The balloon flights of Neher (4) and his collaborators showed that the changes in intensity at the top of the atmosphere were much larger than those at sea level. To give the orders of magnitude, the ion chamber at Huancayo shows a solar cycle effect of 4 per cent and the neutron monitor at the same station, about 12 per cent whereas the change observed at the top of the atmosphere is approximately a factor of two in total ionization. An extensive series of balloon flights was made at the University of Minnesota during the recent period of solar maximum to determine the extent of the solar modulation of galactic cosmic rays and its effect on the various components of the primaries. It has now been established that the maximum change occurring in this solar cycle, between solar minimum in 1954 and solar maximum in 1957-58, amounted to almost a factor of three in the total ionization at the top of the atmosphere. The total ionization is changed periodically by the Forbush-decrease type of event, but the overall level of cosmic ray intensity began depressing in late 1956 and reached its lowest value in late 1958. This result agrees with the indications of sea level neutron monitors which, however, show a much smaller solar cycle modulation.

Detailed studies of the primary cosmic rays showed that in addition to the decrease in intensity there was a change in the form of the energy spectrum of the primaries. For various experimental reasons it is difficult to separate cleanly the proton component of cosmic rays from the other diluting singly-charged components. It is possible, however, with primary alpha particles, to eliminate the background of secondaries; and a detailed study of the alpha-particle spectrum has shown that the total flux of primary alpha particles decreased at sunspot maximum (1958) by a factor of two from its sunspot minimum value in 1954 (12). The decrease is more pronounced at lower energies and is therefore reflected in a somewhat flatter energy spectrum at sunspot maximum than at sunspot minimum. The effect on the integral energy spectrum of alpha particles is shown in Figure 3. Here we have plotted the spectra obtained at sunspot minimum in 1954 and at sunspot maximum in 1957. The fluxes of alpha particles are measured in nuclear emulsion packages carried aloft by balloons, and the alpha particles are identified by a combination of ionization and scattering measurements. The integral spectra at kinetic energies E greater than 500 Mev/nucleon may be represented by an expression of the form

$$n(>E) = \frac{C}{(m_0c^2 + E)^n}$$

where C and n are constant. The values of C and n found at sunspot maximum are $C = 185 \pm 30$, and $n = 1.17 \pm 0.14$. These values can be compared with those of $C = 360 \pm 40$ and $n = 1.48 \pm 0.12$ found during the sunspot minimum over the same range of energies. It can be seen that the slope of the

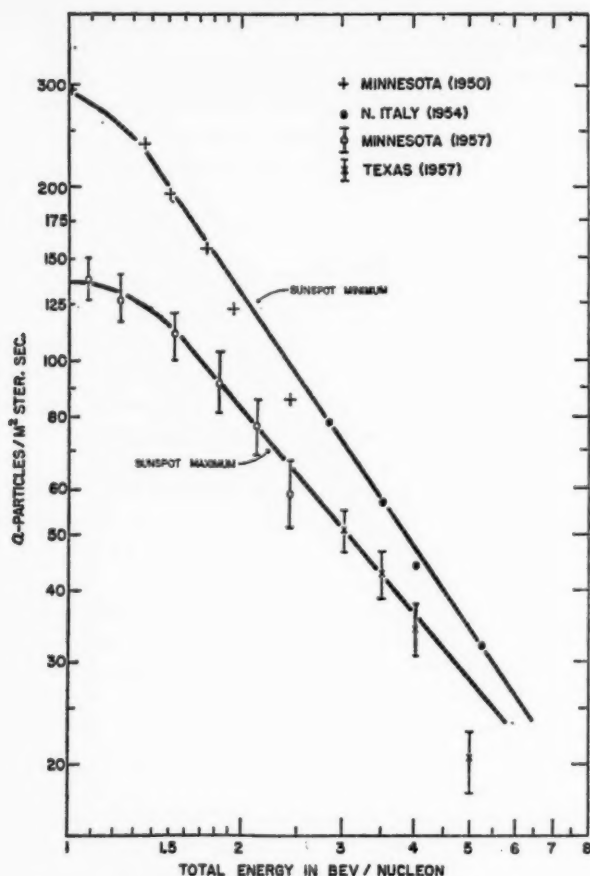


FIG. 3. The integral energy spectrum of alpha particles obtained from scattering measurements.

integral energy spectrum measured at sunspot maximum is appreciably smaller than that observed at sunspot minimum. This result agrees with the evidence from neutron monitors (13). The study of the sunspot minimum and maximum alpha-particle fluxes for this solar cycle, and in particular the investigation of the differential energy spectra, has shown that the solar cycle modulation is produced by a depression of all cosmic rays and not by the imposition of a sharp cutoff, as sometimes suggested. The so-called "knee" in the cosmic ray spectrum at high altitude is produced by the form of the incoming galactic cosmic ray spectrum which has a maximum in its differential energy spectrum at about 300 Mev/nucleon at sunspot minimum and about 500 Mev/nucleon at sunspot maximum. Although the reason for

the maximum in the differential spectrum is not yet understood, it is quite clear that it is not produced by a sharp magnetic cutoff such as would be effected by non-time-varying magnetic fields.

McDonald has measured both protons and alpha particles with a combination Cerenkov scintillation counter detector (14). He finds that the rigidity spectra of protons and alpha particles are alike both at sunspot minimum and sunspot maximum. His results are shown in Figure 4. Note that in this

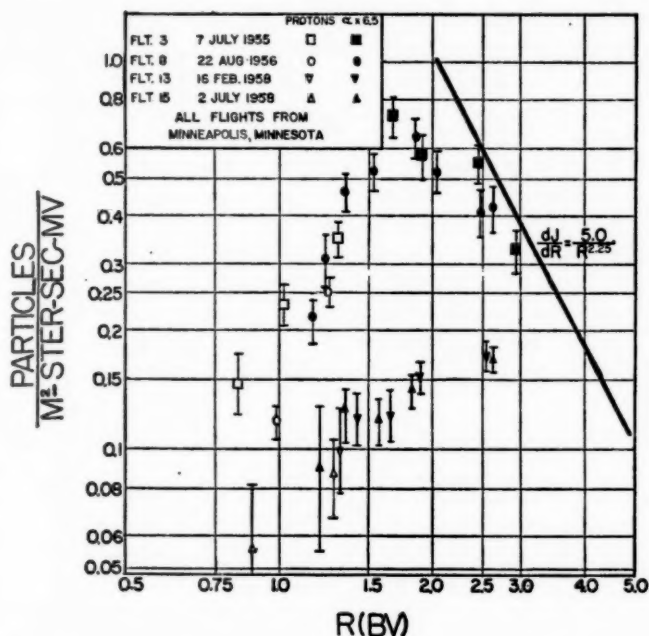


FIG. 4. The differential flux of protons and alpha particles, at times of sunspot maximum (lower symbols) and minimum (upper symbols). Note that the open symbols refer to protons and the other to alpha particles (flux multiplied by 6.5—see text). Note: 1 BV = $\frac{1}{3} \times 10^7$ gauss-cm.

figure, proton and alpha differential spectra are the same if the alpha-particle fluxes are multiplied by 6.5, the ratio of protons to alpha particles in primary cosmic rays. Since particles of the same rigidity are modulated in the same way, a magnetic modulating mechanism is suggested to account for his data.

An ingenious technique for monitoring the total flux of cosmic rays has been developed by Waddington (15). It consists of measuring the density of ending particles in nuclear emulsions exposed on balloon flights at various times. Waddington has shown that the measurement is insensitive to balloon

altitude at pressures less than about 10 gm./cm.^2 . His measurement of the flux of ending particles at sunspot maximum and minimum as a function of magnetic rigidity is shown in Figure 5. The total flux of cosmic rays as measured by Waddington shows the same variation with solar activity as does the alpha-particle flux. This is shown in Figure 6. In these figures h is the time of exposure at ceiling altitude.

The solar cycle modulation of cosmic rays is probably produced by the cloud of magnetic plasma ejected by the sun at high levels of solar activity. This magnetic cloud can fill the solar system and by deflecting out primary cosmic rays can cause a depression in measured cosmic ray intensity in the

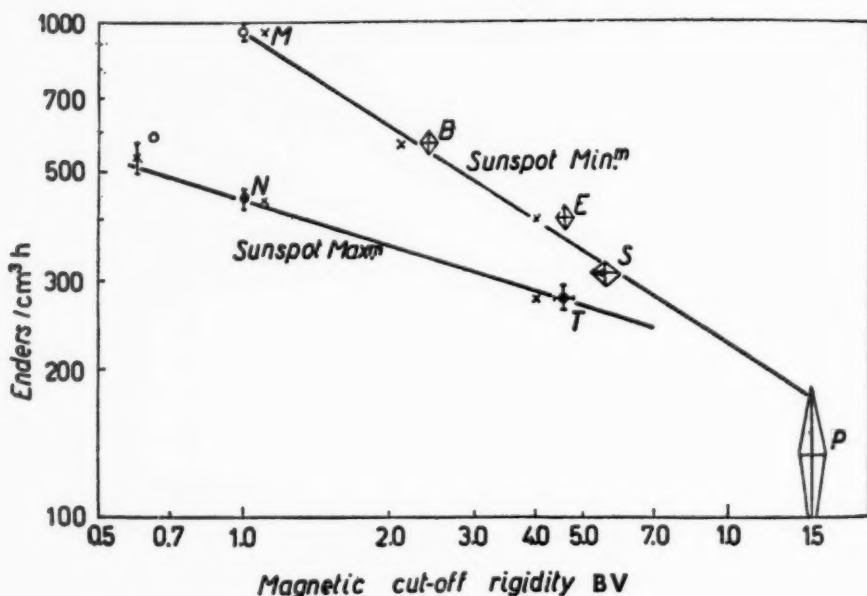


FIG. 5. The variation of the rate of production of stopping particles, ρ , expressed in ends/cm.²h, with R , the magnetic cutoff rigidity in BV. Crosses mark the rigidity values calculated by Quenby and Webber.

vicinity of the earth. This depression in galactic cosmic rays presumably occurs throughout the solar system. In order to understand the phenomenon it will be of some interest to see in detail which components of the primary cosmic rays recover first as the next sunspot minimum is approached. It appears that the depression of cosmic rays occurs rather abruptly in the year or two preceding sunspot maximum, and the depression of the level of cosmic rays persists for some years after sunspot maximum. As of March 1960, the intensity of cosmic rays still remained at its depressed value. It is possible that some other mechanism than magnetic clouds may be responsible for the solar cycle modulation. For example, electrostatic modulation of cosmic

rays could occur if the conductivity of the space surrounding the solar system changed with the solar cycle. The known current of 10,000 amp. of positive cosmic rays flowing to the sun would charge the solar system to a potential the value of which would depend on the conductivity of the interstellar space. If the cosmic ray modulation were electrostatic, the depression of positively charged cosmic ray intensities would be accompanied by an increased flux of primary electrons. Unfortunately, the primary electron flux at high energies is so low that it has not yet been successfully measured. It has been shown (16) that during a period intermediate between sunspot

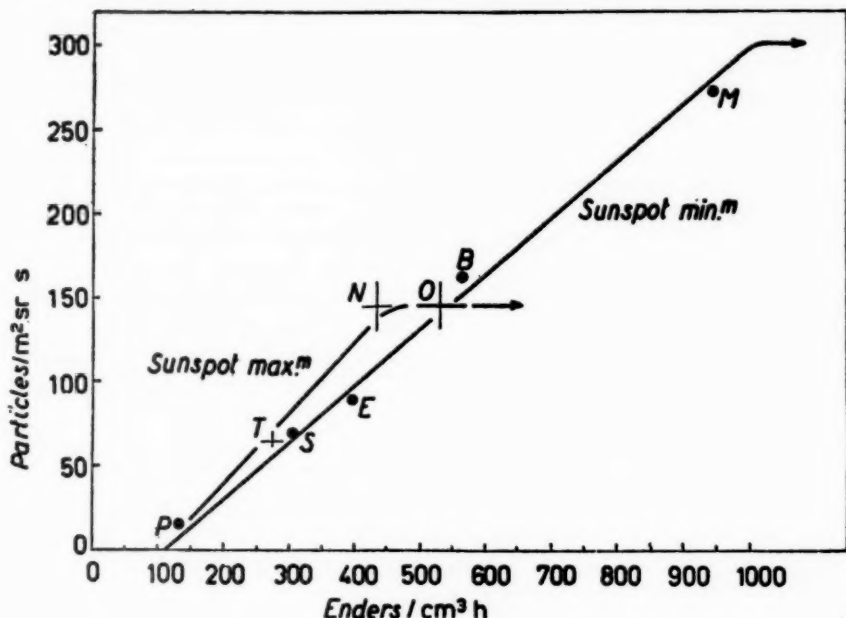


FIG. 6. The relationship between the flux of primary alpha particles and ρ , the rate of production of ending particles.

maximum and sunspot minimum, the primary electron flux represents less than half of one per cent of the incoming flux of positive particles above the same magnetic rigidity, namely 1 BV ($=\frac{1}{3} \times 10^7$ gauss-cm.).

The fact that cosmic ray intensity varies so widely throughout the solar cycle leads to interesting speculation in related fields. For example, the carbon-14 dating of ancient objects assumes, among other things, the constancy of cosmic rays and the consequent production of carbon-14 throughout past history. It seems remarkable that the carbon-14 dating gives values in such good agreement with the known ages of ancient objects, unless the solar cycle modulation is such that the average intensity of cosmic rays over a solar cycle varies very little from one cycle to another. This, of course, may be true, but many decades will be required to answer this question.

THE EARTH'S RADIATION BELTS AND THE ARGUS NUCLEAR EXPLOSION

The first scientifically successful United States satellite was called Explorer I, or 1958 Alpha. The radiation-detecting equipment on this satellite, and on Explorer III (1958 Gamma), was supplied by the State University of Iowa group under Professor J. A. Van Allen. In these flights, in particular that of Explorer III, the inner radiation belt surrounding the earth was first discovered (17). The instrumentation of the satellite was not designed to encounter counting rates as high as those experienced in the radiation belt, and the discovery of the existence of the trapped radiation layers represents an outstanding piece of detective work. The presence of the radiation belt was confirmed with the Russian satellite observations of Vernov (18). Later satellite and lunar probes made further measurements of the two great radiation belts. The mechanism of trapping the cosmic rays in the geomagnetic field is now well understood, but the loss mechanism and the process of injection are still not definitely established.

In order to understand the trapping phenomenon, one needs to consider an almost degenerate case of Stoermer orbits. This is the case in which the energy of the particle moving in the magnetic field is so low that its radius of curvature is very small compared with the radius of the earth. Under these circumstances it is easy to show that the particle undergoes a helical orbit oscillating from one hemisphere to the other between reflection points called mirror points. The reflection points are places at which the earth's magnetic field has increased as the tube of force approaches the surface. The motion is completely determined by specifying the pitch angle of the orbit as it crosses the equatorial plane, and this pitch angle will determine the distance along the tube of force which the particle must travel in order to be reflected. To understand this motion in a simple way, one could compare it with the motion of a compass needle lined up antiparallel to a magnetic field, which varies in space. The antiparallel compass needle will move back and forth being reflected at mirror points. The quantity which remains constant in the particle's motion is the magnetic moment of the particle due to its circular motion. The constant magnetic moment may be written as follows:

$$\frac{1}{2} \frac{mv^2 \sin^2 \psi}{\sqrt{1 - \beta^2}} \frac{1}{B}$$

where m is the mass of the particle, v its velocity, and ψ its instantaneous pitch angle with the magnetic field of induction B . Since $v \cos \psi$ is the component of velocity parallel to the magnetic field, particles are reflected from regions where

$$\frac{1}{B} = \frac{\sin^2 \psi_0}{B_0}$$

where B_0 is the magnetic field at the equator and ψ_0 is the equatorial pitch angle. It is clear from this picture that the particles spend a large fraction of their time at the mirror points and complete the passage from one hemi-

sphere to the other in a matter of seconds, the time of transit depending on the pitch angle of the orbit at the equator. Incidentally, it is easy to show that the locus of the particle's trajectory traces out the outline of a magnetic tube of force. There is another important property of the motion of the charged particles. Because the magnetic field of the earth drops off with distance as $1/r^3$, it is clear that the magnetic field on the inner side of the tube of force is stronger than it is on the outer edge of the tube of force. This means that the particle will have a somewhat tighter radius of curvature on the portion of its orbit close to the earth than that at larger radius from the earth. This effect produces precessional motion, in which the particles travel along the tube of force to a first approximation but precess east or west because of the gradient of the magnetic field. The precessional velocity of the guiding center caused by the field gradient is given by

$$\frac{mc}{eB\sqrt{1-\beta^2}} v^3 \cos^2 \psi \frac{1}{2B} |\nabla_{\perp} B|$$

The negative particles precess toward the east and the positive particles toward the west. The precessional velocity constitutes the ring current required to explain magnetic storms. It can be shown that the precessional velocity is proportional to the average energy of the trapped particles (19). For example, a 1-Mev electron requires approximately 30 min. to make a complete precessional circuit around the earth whereas a 10-Mev electron requires 3 min. for the same circuit. It can be seen, therefore, that a group of particles injected into the earth's field rapidly spreads out into a shell which surrounds the whole earth. The loss of particles from this shell will be determined by small angle Coulomb scattering and magnetic irregularities which will change the geometry and cause the particles to enter more deeply into the atmosphere before they can be reflected. The deeper entry into the atmosphere can then remove the particles by ionization.

The question of the origin of these trapped particles is of some interest. Almost immediately after the discovery of the intense radiation belts, two alternate modes of injection of particles were discussed. The first is the injection of cosmic ray protons and electrons from the decay of albedo neutrons produced by cosmic ray interactions in the atmosphere. This model was suggested by Kellogg (20), Singer (21), and Vernov (22), independently. The initial calculations for the number of protons and electrons in the inner Van Allen belt because of neutron albedo seem to show that it is difficult to obtain the required density of electrons assuming reasonable lifetimes for trapping. Detailed calculations on the flux of electrons and protons obtainable from cosmic ray albedo are given by Kellogg (20). The other possibility for injecting the trapped radiation consists of the incoming particles in solar streams. It now appears that at least a large fraction of the particles in the outer radiation belt arises in this way, since this outer radiation belt varies in intensity at least by a factor of 10 over relatively short periods of time. This has been demonstrated by comparing the initial measurements of the

outer radiation belt of Van Allen with the more recent measurement made by Winckler in Explorer VI (23). The Russian satellite experiments and those of Van Allen also demonstrated the variability of the intensity of the outer radiation belt. Figure 7 shows meridional projections of the radiation belts as

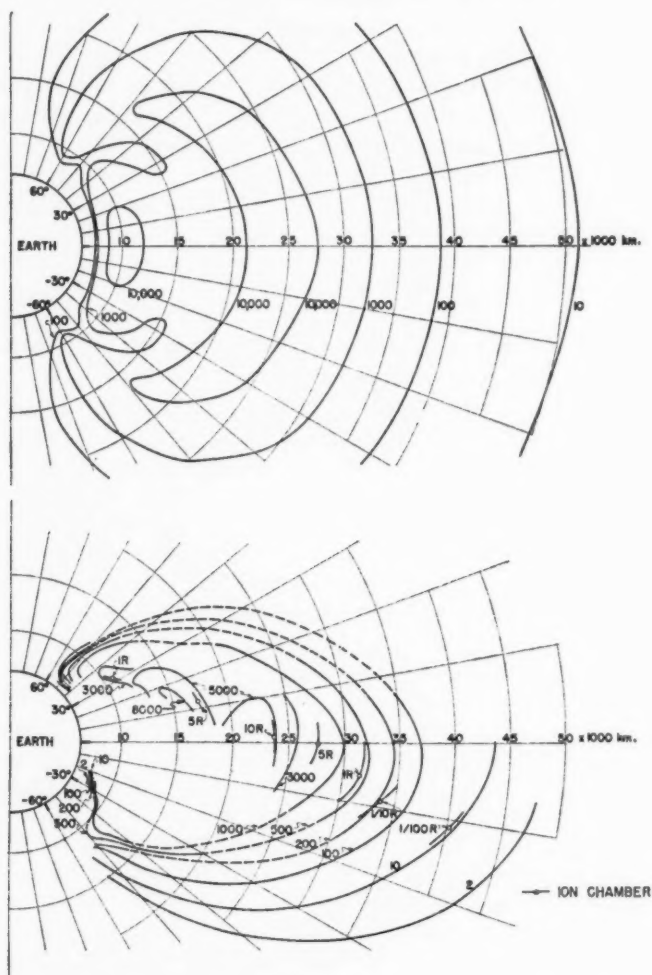


FIG. 7. Comparison of the counting rate contours in the radiation zone as given by Van Allen (upper) and as given by analysis of Explorer VI (lower) shown on a polar plot. It is apparent that the radiation zones during the time of Explorer VI have shrunk considerably and changed form since those inferred from the Explorer IV and Pioneer III and IV data. (From J. R. Winckler *et al.*, "Observations of the Van Allen Radiation Regions during August and September 1959, Part I," *J. Geophys. Research*, in press for May 1960.)

measured by Van Allen and by Winckler. Winckler's curves also show the intensity in roentgens per hour experienced by his ionization chamber in the radiation belt. For example, at the peak intensity of the outer belt, the radiation observed within the ionization chamber corresponds to 10 r/hr. The radiation detected in the outer radiation belt, with its maximum intensity occurring at about three earth radii, consists predominantly of electrons, with the electron spectrum peaked at very low energies so that the detectors flown in the satellite actually respond to bremsstrahlung x-rays produced by the stopping of these electrons in the shell of the satellite and in the counting equipment. It is interesting that the trapping of charged particles is not effective at latitudes above about 65° . In other words, trapping is confined to latitudes somewhat south of the auroral zone, and the maximum of the outer belt corresponds to a line of force which re-enters the earth at about 55° geomagnetic latitude. Probably the lines of force which enter at higher latitudes go so far into space that they are perturbed by random interplanetary fields and are not able to trap particles except for a short time.

It seems very probable that radiation in the outer belt is injected by the sun during periods of solar activity although it is possible that slow solar particles may somehow be accelerated during a magnetic storm and subsequent to the storm become trapped in the radiation belt. It has been shown by Rothwell (24) and by Winckler (23) that it is possible for a magnetic storm to release radiation already trapped in the outer Van Allen belt. This "dumping" of radiation was observed during the geomagnetic storm of August 16-17, 1958, when successive passes of the satellite Explorer VI allowed measurements of the intensity of the radiation before and after the arrival of the magnetic storm. Integration of the counting rates along the lines of force allows a determination of the latitudes at which the "dumped" radiation should appear at the surface of the earth. This is shown in Figure 8, and it is quite clear in this case that the dumped radiation coincides precisely with the position of the visible aurora observed during the course of this storm. One of the outstanding problems in connection with the outer radiation belt will be the competition between injection of particles, local acceleration, and dumping of radiation during periods of magnetic activity.

In contrast with the variability of the intensity measured in the outer radiation belt, it is now established that the inner belt undergoes no such violent changes in intensity, and presumably is of a different nature. The inner belt has its maximum intensity at about 10,000 km. over the equator. (See top of Figure 7.) Counting equipment flown through the inner belts indicates that the particles there are predominantly high-energy protons and electrons with much greater penetrating power than the soft electrons of the outer radiation belt. A great contribution to understanding the nature of the particles in the inner belt has come from the experiments of Freden & White (25) who have succeeded in recovering photographic emulsions exposed in the inner Van Allen region. They have measured the energy spectrum of protons found in the inner belt and report that

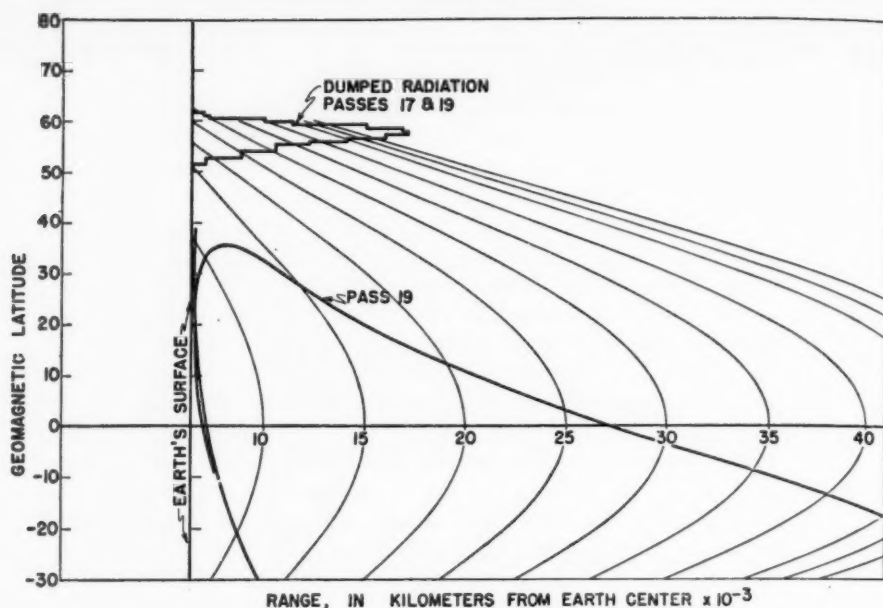


FIG. 8. Estimate of the precipitation of electronic radiation from the outer regions of the trapped radiation onto the surface of the earth inferred from the measurements before and during the geomagnetic storm of August 16 and 17, 1959. Note that the electrons stroke the earth's surface at about 57° geomagnetic latitude and, at least with the profile of radiation intensity observed in August and September 1959, are not discharged into the auroral zone. (From J. R. Winckler *et al.*, "Observations of the Van Allen Radiation Regions during August and September 1959, Part I", *J. Geophys. Research*, in press for May 1960.)

this spectrum has the same form as the cosmic ray energy spectrum. Their result is shown in Figure 9. Since it is well known that all of the secondary components of cosmic rays in general show an energy spectrum like those of the primaries, this seems to be very strong evidence that the inner belt consists of particles injected by cosmic ray neutron albedo. Freden & White have also shown that the proton content of the inner belt was not affected by the exceedingly strong solar flare event of May 10th. During this solar flare a large flux of solar protons was observed at the earth and will be discussed in the next section. That these protons did not enter the inner belt seems a cogent argument against an appreciable fraction of this radiation layer having solar origin. The composition and intensity changes of the inner and outer radiation belts will form an interesting study during the next solar cycle. If the outer belt is indeed supplied by solar beams, it would be expected to decrease in intensity as the sun approaches its minimum of activity. During this time, however, the solar

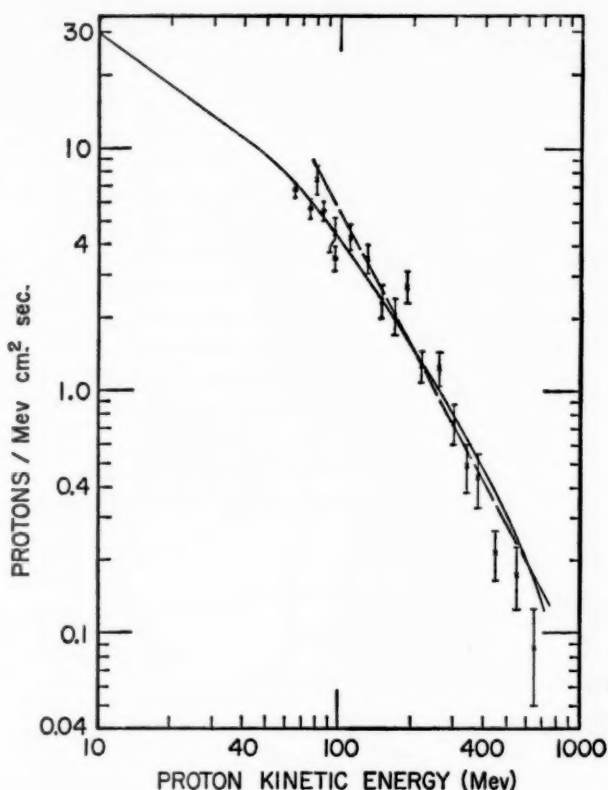


FIG. 9. The differential flux of protons observed by Freden & White in the inner belt. Dots and crosses represent experimental data. Curves are based on the trapping theory, assuming neutron injection.

cycle modulation of cosmic rays should lead to an increase in the cosmic ray flux; and if the inner belt is truly injected by cosmic ray neutron decays, the inner belt may be expected to increase in intensity as sunspot minimum is approached. In any event, the measurements of the constitution of the two radiation belts during the next few years should help to decide the origin of this terrestrial corona.

Because of the very effective coupling of a magnetohydrodynamic plasma with the magnetic field of the earth at altitudes in excess of 100 miles, nuclear explosions at high altitudes should be expected to distort the earth's magnetic field and release and inject particles into this field. Apparently, several groups have independently considered the possibility of injection and release of particles from the trapping region around the earth. The first of these was Christofilos (26) whose ideas, however, were not declassified until early 1959. His suggestion was to detonate a small nuclear explosion

at high altitude and to observe with satellites the trapped radiation so produced and study its decay and its properties. This was the experiment known as the "Argus" experiment which ultimately consisted of three detonations of kiloton atomic bombs at altitudes of about 300 miles in late August and early September 1958. Prior to the Argus shots, however, the Defense Department detonated two atomic explosions at altitudes of approximately 100 miles at Johnston Island near Hawaii. These detonations have subsequently been identified as megaton hydrogen bombs, and they produced enormous geophysical effects. The effect of the artificial aurora at Apia produced at the other end of the magnetic line of force connecting with Johnston Island was reported first by Cullington (27), and its interpretation was discussed by Fowler & Waddington (28) and by Kellogg, Ney & Winckler (29).

Figures 10 and 11 show the geometry of the Johnston Island explosion together with the line of force which acted as a guiding center for the par-

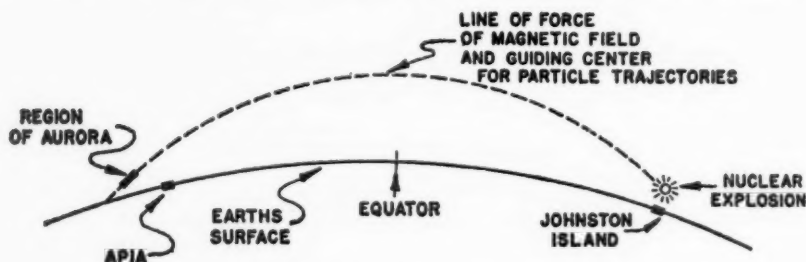


FIG. 10. Geometry of the Johnston Island nuclear explosion.

ticle trajectories. At the southern end of the line of force, a pronounced aurora and magnetic storm were observed, although at this latitude magnetic storms are rare or nonexistent. The aurora and magnetic storm occurred within seconds of the time of detonation of the nuclear explosion. The principal effects were rather immediate, although there seems to be some indication from the scientific data released concerning the Argus shots, made a month later, that some radioactive remains of the Johnston Island explosions still existed at high altitude. Because the line of force in the Johnston Island explosion rises only about 400 miles above the surface of the earth at the equator and because the nuclear explosions were carried out at a relatively low altitude, the lifetime of the trapped particles would be very short. It is possible, however, in the Johnston Island explosions, that neutrons injected decay products higher in the atmosphere and these decay products would therefore be able to persist for a long time.

The Argus explosions themselves were carried out at such a high altitude, 480 km., that the lifetime of the trapped particles was of the order of weeks. The region of injection of the Argus electrons was between the earth's two great radiation belts. (See Fig. 12.) In this region the natural radiation was at low enough intensity so that the Argus shell could be detected. It was

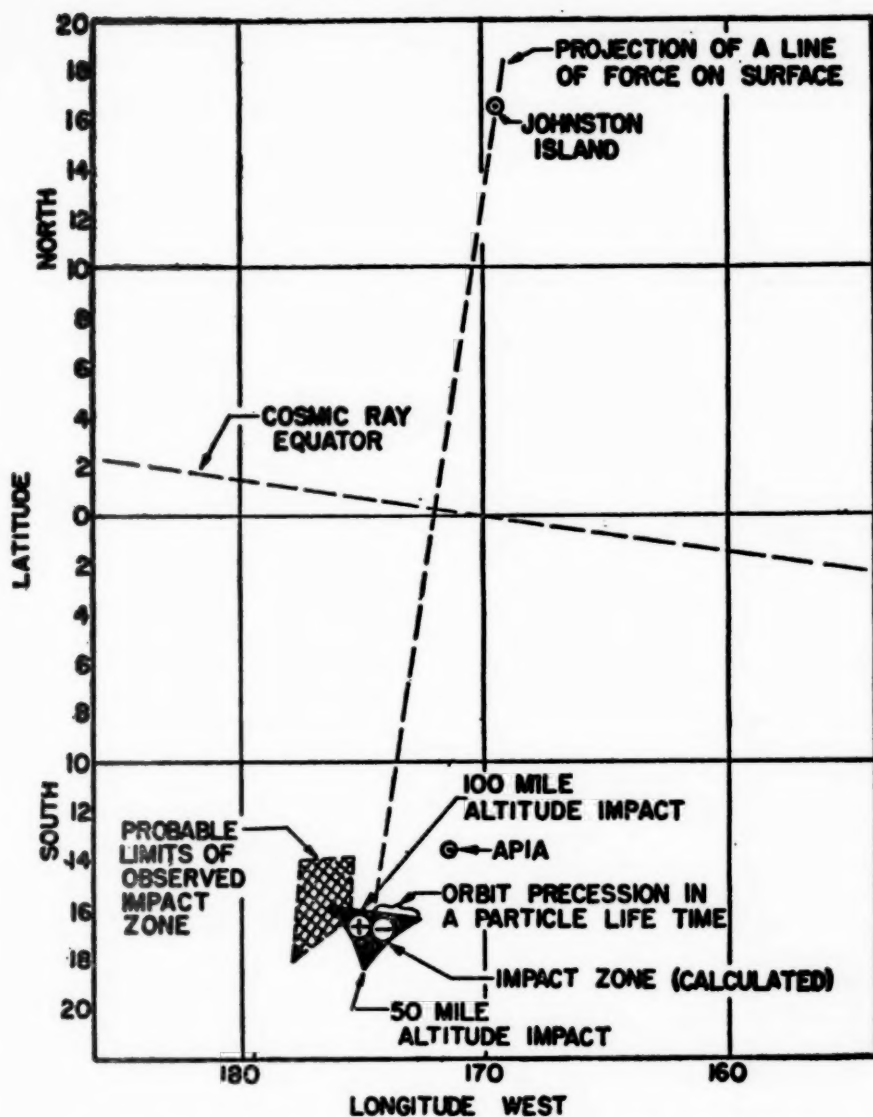
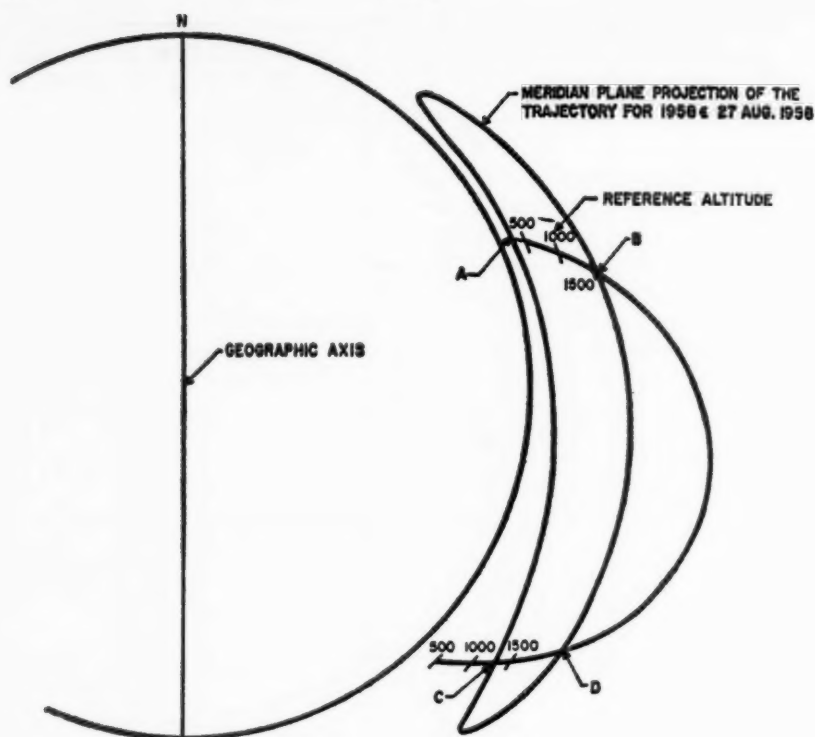


FIG. 11. Predicted and observed impact zones for the Johnston Island nuclear explosion. Signs + and - refer to calculated impact zones for positive and negative particles respectively.

measured on Explorer IV by Van Allen, and Figure 13 shows the counting rates of the unshielded and shielded Geiger counters carried in Explorer IV as they pass through the relatively thin Argus shell. The measurements



INTERSECTION OF SATELLITE ORBIT WITH A GEOMAGNETIC SHELL

FIG. 12. Illustrative diagram showing a sample geometric relationship between the orbit of satellite 1958 epsilon and a chosen magnetic shell at a given longitude. (Van Allen *et al.*, "Satellite Observations of Electrons Artificially Injected into the Geomagnetic Field," *IGY Satellite Rept. No. 9*, September 15, 1959.)

demonstrated that the Argus shell decayed rather rapidly with time. The number of trapped electrons is inversely proportional to the time. In the second Argus shot, the intensity had been reduced by a factor of 10 in 10 hr. after the detonation and by a factor of 100 after 100 hr. In the third Argus experiment, the Argus electrons were still detectable after a period of several hundred hours. The first and second Argus explosions were detonated just before a strong magnetic storm on September 4, and there seems to be good evidence that this magnetic storm produced enough perturbation of the earth's magnetic field to increase greatly the rate of loss from the Argus shells. This is in agreement with the observation of Winckler on the natural radiation in the outer belt which also appears to be released by magnetic perturbations.

It should be pointed out that a nuclear explosion at high altitude will couple the kinetic energy of the expanding plasma with the earth's magnetic

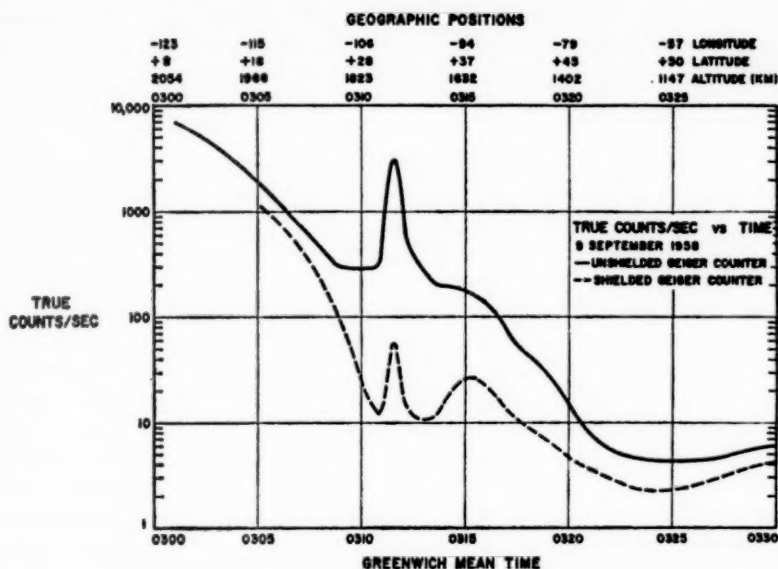


FIG. 13. A plot of radiation observations with Explorer IV on September 9, 1958, showing the Argus III peak at about 0312 U.T. (Van Allen *et al.*, "Satellite Observations of Electrons Artificially Injected into the Geomagnetic Field," *IGY Satellite Rept.*, No. 9, September 15, 1959.)

field. This distortion of the earth's magnetic field will release the trapped natural radiation already present. However, it is relatively easy to show that with a nuclear explosion the radioactive decays of the bomb products will ultimately inject more particles into the earth's field than were originally there. To see the effect of the simple release of the natural radiation, it would be necessary to carry out a high altitude explosion with a chemical bomb rather than a nuclear weapon. The principal result of the Argus explosions was the determination of the trapping time of charged particles in the earth's magnetic field, and the demonstration of magnetohydrodynamic interaction of the bomb plasma with the magnetic field of the earth. In evaluating the effects of high-altitude explosions which can effectively couple kinetic energy to the earth's magnetic field, it is worth pointing out that the entire energy stored as $B^2/8\pi$ in the magnetic field of the earth external to the surface is 10^{28} ergs. This is approximately equal to the energy release in a 20-megaton atomic weapon. It should therefore be possible to distort the external field of the earth greatly with very high altitude nuclear explosions of large weapons.

SOLAR COSMIC RAYS

During the past ten years, there have been four very large recorded increases of cosmic ray intensity at sea level. These increases were detected with ionization chambers or with neutron monitors. In the most spectacular

of these events, February 23, 1956, the neutron monitor network of Simpson recorded intensity variations throughout the latitude range from the equator to high geomagnetic latitudes (30). Study of these records and those obtained by the Russians has led to the belief that a class 3+ flare² on the limb of the sun had injected a large flux of high-energy cosmic rays into the interplanetary medium. The analysis of the February 23 event led to the conclusion that the integral energy spectrum of the solar-injected cosmic rays was very steep, given approximately by the expression $N(>E) = K/E^6$ where E is the kinetic energy, and that the decrease of intensity with time, T , following the flare, approximately obeyed the law $I = C/T^n$ where n was between 3/2 and 2. Previous activity on the sun had led to a magnetic storm and a Forbush decrease in February, and the large intensity increase in cosmic rays observed on February 23 occurred after the beginning of this Forbush decrease which was presumably caused by magnetic clouds in the solar system. A good discussion of this event is given by Dorman (31). No adequate explanation has been proposed for the acceleration of cosmic rays accompanying a large flare, but a number of attempts were made to understand the persistence of the intensity after the flare. The models proposed were the diffusion model of Simpson and Parker (30) and the magnetic tongue suggested by Gold and others (32). Whether either of these models is the correct one is still in doubt. However, it is quite clear that in this very large event some mechanism is required to store particles accelerated during the flare for long periods of time. It was unfortunate that in this event no photographic emulsions were exposed at high altitude. It was therefore impossible to state whether the incoming beam from the sun contained pure protons or a mixture of protons and heavier nuclei. The effects at sea level quite clearly indicate that the incoming stream from space is principally nucleonic, but the composition of this stream could not be determined. Because of the occurrence of intensity increases at sea level associated with the large solar flare effects observed in the February 23 flare and the other large cosmic ray flares, it was believed that sea level neutron monitors or ion chambers would give adequate warning of the arrival of solar-produced cosmic rays.

The discovery in 1957 of solar proton beams of low energy, however, has shown that the neutron monitor usually does not indicate the arrival at the top of the atmosphere of solar cosmic rays. Bailey (33) seems to have been the first to realize that incoming solar streams of heavy ions would produce, and did produce in the February 1956 case, great ionization of the ionospheric D -layer and consequent absorption of radiowaves. In discussing the February 23 event, Bailey makes the following statement,

... it seems necessary to recognize a new class of signal-intensity enhancement for waves propagated by ionospheric scattering and a new kind of high-altitude absorption phenomenon. It would seem inappropriate to identify the observed absorption

² Solar observers classify flares on an increasing scale which runs from 1- to 3+. The classification is based on size, brightness, and duration of the flare area.

effects as merely a special case of the well-known polar blackout absorption. It is clear that an event such as that reported is rare. To the extent that such events are associated generally with outbursts of solar cosmic rays, they may on the basis of very meager statistics be expected to occur about once in four years. Actually smaller events may occur more frequently, but are likely to be associated with important flares. The particle velocities thought necessary to account for the absorption effects are of the order of a tenth of cosmic-ray particle velocities, and the associated particle energies are correspondingly lower. The sun is, therefore, more likely to eject absorption-producing particles than particles having cosmic-ray energies.

Bailey's speculations of the preceding paragraph have now been amply verified by subsequent experiments.

Leinbach & Reid (34) obtained the most clear-cut evidence of the arrival of heavy particles at high latitude in the event following the flare of July 29, 1958. Their measurements were made at College, Alaska, and other points over the polar cap using a device called the riometer, which is short for "relative ionospheric opacity meter." This device is essentially a 27-Mc. radio receiver fed by a Yagi antenna which looks at the sky over a rather wide angular interval. The meter normally, therefore, measures the intensity of galactic radio emission as it arrives at the earth, and on normal days such a meter can be calibrated in terms of the measured and known cosmic noise sources that exist. In the July 29 event, Leinbach & Reid observed a large attenuation of the incoming cosmic noise, and they ascribe this attenuation to excess ionization in the *D*-layer produced by incoming solar particles presumably accelerated in the class 3+ flare² which had occurred. The characteristic feature of the cosmic noise absorption events is that, in contrast to auroral-produced cosmic noise absorption, these produce absorption throughout the polar cap but not at lower latitudes. They were believed, therefore, as Bailey and Little & Leinbach (35) had previously suggested, to have been caused by the arrival of ions from the sun able to penetrate into the atmosphere to altitudes of approximately 60 km. This requires incoming protons from the sun of energy approximately 20–30 Mev.

The confirmation of the nature of the solar particles arriving at the earth came rather soon, through the work of Anderson (36); Rothwell & McIlwain (37); and Freier, Ney & Winckler (38). These investigators detected, at balloon and satellite altitudes, streams of particles associated with large solar flares. The first balloon event to be properly interpreted was that of Anderson and his collaborators, who measured an increase in charged particle intensity above Churchill, Canada, and Fairbanks, Alaska, on August 22 and 23, 1957. They measured with ion chambers the variation in counting rate as a function of altitude following the solar flare and compared this counting rate with normal ones on days of no solar activity. The variation of counting rate with altitude allowed them to infer a proton energy spectrum and to set some limits on the flux of primary electrons. Anderson deduced a differential number energy spectrum $N(E)dE = KE^{-5}dE$ and found that their results were consistent with protons arriving in the energy

range from 100–400 Mev. Rothwell & McIlwain (37), in experiments with Explorer IV, found large solar flare increases occurring at 0432 UT on August 16 and at 0005 UT on August 22. They measured the counting rates in shielded and unshielded Geiger counters during the period of the increases and concluded that the incoming beam must consist largely of protons.

The first observations of the incoming solar cosmic rays in emulsions were made by Freier *et al.* (38) in the event which occurred on March 26, 1958. The most detailed information concerning the solar cosmic rays has come from the analysis of events which occurred on May 12, 1959 (39), and during July 1959 (40 to 42). It should be pointed out that the balloon observations of the solar cosmic rays were made possible because of the realization that cosmic noise absorption as indicated by the riometer was an indication that particles were arriving at high latitudes. Arrangements were made between the people carrying out the balloon experiments and H. Leinbach at College, Alaska, which allowed the launching of high-altitude balloons shortly following the onset of the cosmic noise absorption. Such balloon experiments have been carried out by Brown (40); Ney, Winckler & Freier (39); Anderson (41); and Charakhchian (42), during the spectacular events of May and July 1959. These measurements have been made at latitudes ranging from that of Minneapolis to Thule, Greenland, in the summer of 1959 series of solar events. The most spectacular characteristic of both the May and the July events was that the intensity of protons at the top of the atmosphere was several thousand times the normal intensity of cosmic rays. Figure 14 shows a photomicrograph taken during the May event at an altitude of 100,000 ft. In this photomicrograph, enlarged approximately 500 times, there are of the order of 100 protons passing through the emulsion. A corresponding cosmic ray exposure would have required 10 times this area to show an individual track.

The following general features of the solar proton events have now been established:

(a) The atmospheric effects are produced by protons primarily in the energy range from 30 Mev to something in excess of 500 Mev.

(b) Alpha particles appear to be present with approximately the same rigidity spectrum as the incoming protons.

(c) The arrival of the proton beam heralded by the onset of cosmic noise absorption may occur within hours of the onset of the solar flare. The longest delay observed was the case of the storm of March 28, 1958, in which the arrival of the proton beam was coincident with the Forbush decrease and the magnetic storm. This occurred 20 hr. after the flare. In contrast to this long delay, half of the events have delay times less than 5 hr.

(d) The measurements at high latitudes of incoming particle fluxes confirm the suspicion that the cosmic noise absorption shown by the riometer is a good measure of the intensity of arrival of the incoming beam and that the incoming protons die off quasiexponentially with a time constant of the order of several days.

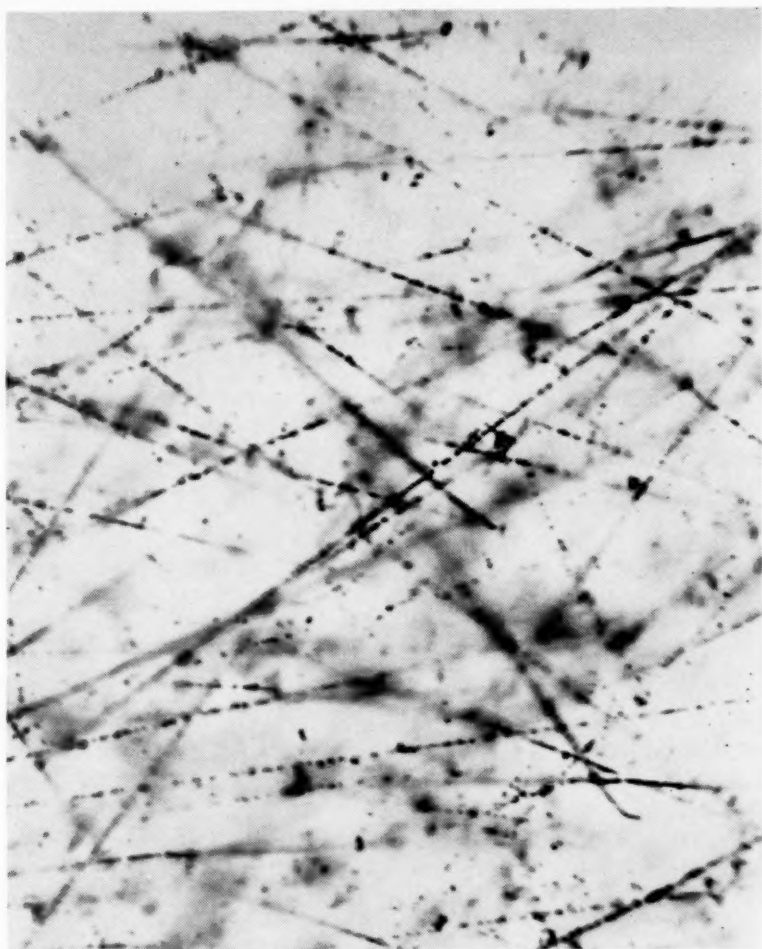


FIG. 14. Photomicrograph enlarged 500 times showing solar protons observed at an altitude of 1000 ft. on May 12, 1959. Normal cosmic ray exposure would require 10 times this area to show one track.

(e) At latitudes as far south as Minneapolis, the events are very much more complicated. Even though particles may be arriving at high latitude, as shown by balloon measurements as well as riometer indications, the particles do not enter the atmosphere at Minnesota until the onset of the geomagnetic storm. The reason for this is that the normal cosmic ray cutoffs at Minnesota exclude the majority of the protons of the energies contained in the solar beam. It is, therefore, impossible for these particles to enter at this latitude without a perturbation of the earth's magnetic field. Although the cutoff energy for protons at Minnesota is of the order of 300 Mev, during the

magnetic storm the solar particles with energies down to 50 Mev are able to enter. The time decay of the particle intensity at this low latitude, however, seems to be entirely governed by the behavior of the magnetic field as affected by the incoming solar stream. In the event in May 1959, the particle intensities persisted at their very high value for only several hours although the riometer showed that they continued to persist at high latitude for a number of days. Direct observations of the high latitude cosmic rays and the corresponding protons at Minnesota were made in the July event during which it became quite clear that the particle fluxes could arrive at Minnesota in essentially full intensity as long as the magnetic field was perturbed, but when the earth's magnetic field returned to normal the particles were not allowed to enter in Minnesota but were still arriving at the latitude of Churchill, Canada (43).

(f) The incoming solar beams appear to be almost entirely positively charged. Certainly less than 10 per cent of the particles in these beams are electrons. Since alphas of the same rigidity appear to be present, the question arises as to whether electrons accelerated with the positive particles can lose their energy in some specific way and therefore not be allowed to reach the earth. One possible explanation for the absence of the electrons would be that these electrons are trapped in the magnetic field of the solar corona and lose their energy by synchrotron radiation, thereby emitting radio waves. It has been established now by Thompson & Maxwell (44) and by Kundu & Haddock (45) that the radio emission from the sun at the time of the flare acceleration of the cosmic rays is of a particular kind which could, in fact, be attributed to synchrotron radiation of electrons. This will be discussed briefly in the following.

(g) The incoming proton beams, several hours after the beginning of the event, seem to be isotropic at the top of the atmosphere. This conclusion must be taken with some reservation, however, until direct measurements are made simultaneously at satellite altitudes and at balloon altitudes.

(h) The measured radiation doses at 30 km. during the arrival of an incoming proton beam are of the order of 0.2 r/hr. If the particles are indeed isotropic outside the atmosphere, this would lead to an extraterrestrial intensity of the order of 5-10 r/hr. and would represent a serious hazard to space travel.

It is extremely important, therefore, to determine the intensities of the proton beams with satellite measurements. No high-flying satellite has yet been up during the arrival of such a beam. Since the solar beams are presumed to fill the entire solar system, it would be impossible to avoid an exposure in such a beam for a satellite in space. At present, it is impossible to predict the time of emission of such a beam from the sun, although one would be inclined to believe that these beams must be more prevalent at sunspot maximum than sunspot minimum. Post-mortem analysis of riometer absorption data at high latitude indicates that during the period of high solar activity (1957, 1958), Type III cosmic noise absorption appar-

ently occurred on the average of once a month. Type III absorption is polar cap absorption now known to be coincident with the proton beam arrival. These low-energy proton beams, therefore, are very much more frequent than the sorts of cosmic ray increases that are detected by cosmic ray monitors at sea level. In fact, in the series of low-energy solar cosmic ray events described here, the neutron monitors at sea level did not show any effect except the Forbush decrease associated with the arrival of the magnetic cloud. The balloon experiments indicate that the intensity rises above normal at altitudes in excess of 50,000 ft., reflecting the steepness of the energy spectrum in these events. Although the energy spectra seem to vary from event to event, they all appear to be somewhat steeper than the cosmic ray spectrum. The exponents in the integral energy spectrum $N(>E) = C/E^n$ vary from $n=2$ to $n=5$ in the solar proton events. The exponent in the spectrum for cosmic rays is $n=1.5$.

Figure 15 shows the counting rates during the series of three July events as observed at Minneapolis and Churchill, Canada. In this figure are also plotted the planetary magnetic indices and the neutron monitor counting rate at Deep River, Canada. It can be seen from this figure that the intensity of the particles at Churchill is constant during a period when it changes violently at Minnesota. It is clear from this figure that the particles arrive at Minneapolis when the magnetic field of the earth is perturbed as shown by the planetary magnetic index and that in these three events the arrival of the cloud of gas which perturbs the magnetic field also produces sharp Forbush decreases of intensity. These decreases are presumably caused by the modulation of galactic cosmic rays by the magnetic cloud, and their importance here is that the magnetic cloud is necessary to allow entry of the solar cosmic rays at low latitude. Although the experimental facts about the solar-accelerated protons are now fairly well established, there is as yet no satisfactory mechanism for either the acceleration process which produces the cosmic rays at the sun or the trapping of these cosmic rays in the solar system. It is certainly significant, however, that of the 28 polar cap absorption events which have been observed to date, all but two have been associated with flares observable on this side of the sun. In this respect the low-energy proton events are like the high-energy solar cosmic ray events, such as February 23, in that all four of these high-energy cosmic ray increases are associated with visible flares.

The prediction of the occurrence of these events is of some importance, not only for their study but in connection with sending men into space when the radiation intensity may be lethal. Thompson & Maxwell (44) and Kundu & Haddock (45) have shown that certain types of radio emission from the sun are characteristic of solar flare events which subsequently give rise to polar cap absorption and to cosmic rays incident on the earth. The best correlation with subsequent cosmic ray events seems to be the outbursts of centimeter wave radiation from the sun. These centimeter wave outbursts have a very wide radio spectrum extending to meter waves, and the burst

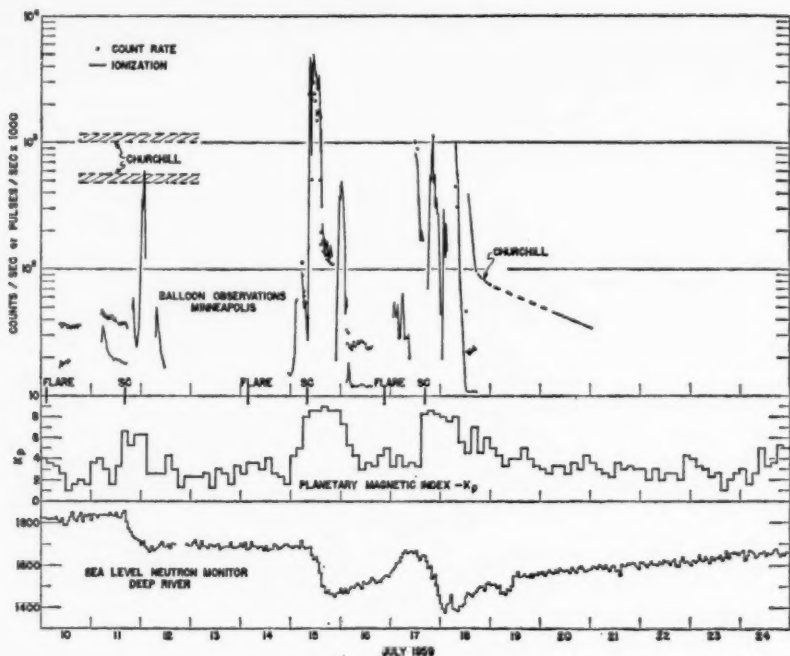


FIG. 15. Intensity of solar cosmic rays, planetary magnetic indices, and sea-level neutron monitor data during the July series of solar events. (This figure is from data collected by J. R. Winckler.) SC indicates the sudden commencement of a magnetic storm.

radiation on centimeter waves is always partially polarized and usually lasts more than ten minutes. All of the 28 polar cap absorption events previously referred to are associated with centimeter wave outbursts. If only intense outbursts are considered, 83 per cent are associated with polar cap absorption and solar cosmic rays arriving at the earth. A centimeter wave outburst is detected at the earth an hour or more in advance of the arrival of the fastest particles accelerated in the flare events. It seems very probable, therefore, that either centimeter wave outbursts or continuum radiation from the sun will represent a good means for predicting those solar flares which have led to the acceleration of cosmic rays.

CONCLUSION

In the past several years, a great deal has been learned about the relationship between solar activity and radiation phenomena in space. In particular, the decrease of galactic cosmic rays at sunspot maximum has been verified in detail and studied for the proton and alpha components of the primary cosmic rays. The great radiation belts around the earth have been recently

discovered and shown to be at least partially fed by solar streams and by albedo from cosmic rays. A man-made explosion has, in addition, injected particles into the trapping region around the earth and has been studied with earth satellites. Frequent high-intensity beams of low-energy solar cosmic rays have been discovered associated with solar flares and radio outbursts on the sun. Since it is now known that cosmic rays can come from the sun, it will be of interest during the coming years to try to determine what fraction of cosmic rays are solar and which are truly galactic. There are many questions about the earth's radiation belts and their injection and loss which also can be studied as the sun goes from its maximum activity toward the coming minimum. Through more frequent use of satellites with more sophisticated equipment, it should also be possible in the coming years to measure the cosmic radiation and the solar effects throughout a large region of the solar system, perhaps even almost up to the surface of the sun itself.

LITERATURE CITED

1. Neher, H. V., *Ann. Rev. Nuclear Sci.*, **8**, 217 (1958)
2. Forbush, S. E., *J. Geophys. Research*, **59**, 525 (1954)
3. Neher, H. V., *Phys. Rev.*, **107**, 558 (1957)
4. Neher, H. V., and Anderson, H., *Phys. Rev.*, **109**, 608 (1958)
5. Simpson, J. A., Fonger, W., and Trieman, S. B., *Phys. Rev.*, **90**, 934 (1953)
6. *Bulletin CRPL-F186, Part B, Solar-Geophysical Data* (U. S. Dept. Commerce, Natl. Bur. Standards, Boulder, Colo., 1960)
7. Meredith, L. H., Gottlieb, M. B., and Van Allen, J. A., *Phys. Rev.*, **97**, 201 (1955)
8. McIlwain, C. E., "Direct Measurement of Radiation Associated with Visible Aurorae," *Fifth General Assembly CSAGI, Moscow* (July-August, 1958) (in *IGY Rocket Rept. No. 1*, 164, Natl. Acad. Sci., 1958)
9. Meredith, L. H., Davis, L. R., Hepner, J. P., and Berg, O. E., *Fifth General Assembly CSAGI, Moscow* (July-August, 1958) (in *IGY Rocket Rept. No. 2*, 169, Natl. Acad. Sci., 1958)
10. Winckler, J. R., and Peterson, L., *Phys. Rev.*, **108**, 903 (1957)
11. Winckler, J. R., "Balloon Study of High Altitude Radiations during the International Geophysical Year," *J. Geophys. Research* (In press for May 1960)
12. Freier, P. S., Ney, E. P., and Waddington, C. J., *Phys. Rev.*, **114**, 365 (1959)
13. Meyer, P., and Simpson, J. A., *Phys. Rev.*, **106**, 568 (1957)
14. McDonald, F. B., *Phys. Rev.*, **116**, 462 (1959); McDonald, F. B., and Webber, W. R., *Phys. Rev.*, **115**, 194 (1959)
15. Waddington, C. J., *Nuovo cimento*, **14**, 1205 (1959)
16. Critchfield, C. L., Ney, E. P., and Oleksa, S., *Phys. Rev.*, **85**, 461 (1952)
17. Van Allen, J. A., Ludwig, G. H., Ray, E. C., and McIlwain, C. E., *Jet Propulsion*, **28**, 588 (1958)
18. Vernov, S. N., Chudakov, A. Ye., Valulov, P. V., and Logachev, Yu. I., *Doklady Akad. Nauk S.S.S.R.*, **125**, 304 (1959)
19. Welch, J. A., and Whitaker, W. A., *J. Geophys. Research*, **64**, 909 (1959)
20. Kellogg, P. J., *Nuovo cimento*, **11**, 48 (1959)
21. Singer, S. F., *Phys. Rev. Letters*, **1**, 181 (1958)
22. Vernov, S. N., Special Lecture, *Fifth General Assembly CSAGI, Moscow* (July-August 1958)
23. Arnoldy, R. L., Hoffman, R. A., and Winckler, J. R., "Observations of the Van Allen Radiation Regions during August and September 1959, Part I," *J. Geophys. Research* (In press for May 1960)
24. Rothwell, P., and McIlwain, C. E., *J. Geophys. Research*, **65**, 799 (1960)
25. Freden, S. C., and White, R. S., *Phys. Rev. Letters*, **3**, 9 (1959)
26. Christofilos, N. C., *J. Geophys. Research*, **64**, 869 (1959)

27. Cullington, A. L., *Nature*, **182**, 1365 (1958)
28. Fowler, P. H., and Waddington, C. J., *Nature*, **182**, 1728 (1958)
29. Kellogg, P. J., Ney, E. P., and Winckler, J. R., *Nature*, **183**, 358 (1959)
30. Meyer, P., Parker, E. N., and Simpson, J. A., *Phys. Rev.*, **104**, 768 (1956)
31. Dorman, L. I., *Cosmic Ray Variations* (State Publishing House for Technical and Theoretical Literature, Moscow, U.S.S.R., 726 pp., 1957)
32. Cocconi, G., Greisen, K., Morrison, P., Gold, T., and Hayakawa, S., *Nuovo cimento*, **10**, Suppl. 8, 161 (1958)
33. Bailey, D. K., *J. Geophys. Research*, **62**, 431 (1957)
34. Leinbach, H., and Reid, G. C., *Phys. Rev. Letters*, **2**, 61 (1959)
35. Little, C. G., and Leinbach, H., *Proc. I.R.E. (Inst. Radio Engrs.)*, **46**, 334 (1958)
36. Anderson, K. A., *Phys. Rev. Letters*, **1**, 335 (1958)
37. Rothwell, P., and McIlwain, C. E., *Nature*, **184**, 138 (1959)
38. Freier, P. S., Ney, E. P., and Winckler, J. R., *J. Geophys. Research*, **64**, 685 (1959)
39. Ney, E. P., Winckler, J. R., and Freier, P. S., *Phys. Rev. Letters*, **3**, 183 (1959)
40. Brown, R. R., and D'Arcy, R. G., *Phys. Rev. Letters*, **3**, 390 (1959)
41. Anderson, K. A., and Enemark, D. C., "Observations of Solar Cosmic Rays Near the North Magnetic Pole," *Preprint SUI-60-3* (Dept. of Physics and Astronomy, State Univ. of Iowa, Iowa City, 1960); *Proc. 1st Intern. Conf. Space Science, Nice* (In press, 1960)
42. Charakhchian, A. N., Tulinov, V. F., and Charakhchian, T. N., "Cosmic Rays Emitted by the Sun," *Preprint, Lebedev Physical Institute* (January 1960); *J. Exptl. Theoret. Phys. (U.S.S.R.)* (In press, 1960); *Proc. 1st Intern. Conf. Space Science, Nice* (In press, 1960)
43. Earl, J. A., *Solar Cosmic Rays at Ft. Churchill during July 1959* (Report to Midwest Cosmic Ray Colloquium, Iowa City, October 1959)
44. Thompson, A. R., and Maxwell, A., *Nature*, **185**, 89 (1960)
45. Kundu, M. R., and Haddock, F. T., "A Relation between Solar Radio Emission and Polar Cap Absorption of Cosmic Noise," *Nature* (In press, 1960)

CELLULAR RADIOBIOLOGY^{1,2,3}

BY TIKVAH ALPER

*Medical Research Council, Experimental Radiopathology Research Unit,
Hammersmith Hospital, London, England*

A review on this topic becomes increasingly concerned with almost everything published on the effects of radiation on living things, as radiation damage to tissues and to whole organisms becomes more and more clearly associated with damage to the reproductive ability of specific cells [e.g. Quastler (1, 2); Scott (3); Puck (4); Oakberg (5)]. In order to deal adequately with the great volume of relevant literature, it has been necessary to interpret the title of this review literally. It will therefore be less concerned than its predecessors with the radiation chemistry of biological molecules, or with effects on viruses and other subcellular units. Investigations carried out with UV will be referred to only insofar as they have an obvious bearing on effects of ionizing radiation.

The subject of molecular biology, which attracts the attention of many radiobiologists, now has a journal devoted to it (6). Two numbers of *Reviews of Modern Physics* were devoted to a Biophysical Study program, and one contained a series of five papers by well-known radiobiologists [Zirkle (7); Pollard (8); Wood (9); Tobias (10); Puck (4)]. Developments in target theory since 1946 were comprehensively reviewed by Sommermeyer (11). The oxygen effect was reviewed by Gray (12), and by four Russian authors who published a book giving a very full account of the literature up to about the beginning of 1956 [Shchepot'eva *et al.* (13)]. The genetic effects of small doses of ionizing radiation were discussed in a review by Shapiro (14). A book on the radiobiology of *Vicia faba* by Read (15) is a detailed account which includes some hitherto unpublished results of the author and which also reviews some related work with other test systems.

ELECTRON SPIN RESONANCE

The books of Lea (16) and of Timoféeff-Ressovsky & Zimmer (17) were based on the concept that radiobiological effects are directly related to ionizations taking place within certain structures in the cell which are vital to the function under test. The current revival of interest in this concept is extended to the techniques of microwave spectroscopy, which can be used to detect and to measure concentrations of free radicals. The relevance of the

¹ The survey of literature was completed for the most part in January 1960.

² The following abbreviations are used: e.s.r. (electron spin resonance); LET (Linear Energy Transfer); RBE (Relative Biological Effectiveness); UV (ultraviolet light).

³ I wish to acknowledge my indebtedness to Drs. J. W. Boag and M. Ebert for translating certain papers from Russian.

subject to quantitative radiobiology has been discussed by Müller & Zimmer (18). At present, the signals derived from miscellaneous cellular material cannot be related to paramagnetic resonance spectra obtained with pure substances; furthermore, the number of radicals required to produce detectable signals is very much greater than appears to be needed for producing profound biological effects in many cells. However, a few papers have claimed correlation between electron-spin-resonance (e.s.r.) phenomena and the radiobiology of the same material. So far these have dealt with dry seeds, which require doses of several kilorads to produce measurable biological effects and which have the advantage that they can be used as samples in e.s.r. studies in conditions of humidity which are normal to them.

Sparrman *et al.* (19) used small grass seeds in a parallel investigation on biological damage and magnetic centres with the seeds stored before and after irradiation in nitrogen, air, or nitric oxide. The biological effects of radiation were studied with seeds at various humidities; magnetic centres were observed in irradiated seeds with a moisture content of 4.5 per cent and were followed for 75 hr. after irradiation. The derivative amplitude of the e.s.r. absorption was initially about the same for the seeds irradiated and stored in air and those irradiated and stored in nitric oxide. With the latter, however, the amplitude decreased with time, and by 24 hr. it had become about half as great. In the biological experiments the seeds were stored for 24 hr. before and 24 hr. after irradiation in air, N₂, or NO, and when the moisture content was 4.5 per cent the doses required to produce the same effect were respectively 8, 11, and 62 kr. These results therefore demonstrate a qualitative correspondence between the extent of biological damage and the concentration of magnetic centres. However, it is known that the longer seeds are stored in contact with oxygen, the more effect of radiation they demonstrate (20, 21), and it should not be overlooked that in the experiments of Sparrman *et al.* (19) there was no change in the amplitude of the e.s.r. signal, within 75 hr., from seeds irradiated and stored in air. Conger & Randolph (22), working with barley and wheat embryos ground into powder, found that the signals decayed with storage both in air and in nitrogen, although the rate of decay was slower in the latter. The rate of decay of signals from "wet" material (i.e. at 33 per cent humidity) was greater than from "dry" material. Curtis *et al.* (21) had previously shown that irradiated seeds containing 24 per cent moisture did not demonstrate a change in biological effect on storage whereas dry seeds showed an increasing effect of radiation, the longer they were stored. It would therefore seem premature at this time to attempt to correlate the extent of biological damage with concentration of magnetic centres, since in some cases a decay in signal amplitude is correlated with conditions which increase biological damage, while in others the reverse is true.

An interesting observation of Conger & Randolph (22) was that highly purified calf-thymus DNA or bovine-liver RNA failed to give detectable signals even when doses of 6.10^8 rads were given. This result conflicts with other reports which have appeared; and Pai-gen *et al.* (23) and Shields &

Gordy (24), using commercially prepared samples, described signals from both types of nucleic acid and their degradation products. The admission of oxygen after irradiation did not change the signals, according to Shields & Gordy (24). This may be contrasted with its action on the signals from many other biological substances, such as cholesterol (25) and haemoglobin (26). Boag & Müller (27) used a laboratory preparation of calf-thymus DNA which contained 0.7 per cent by weight of protein. They observed signals in very dry material, whether it was irradiated (with doses up to 10^8 rads) *in vacuo*, in air, or in NO, and without any appreciable decrease in the signal over a week. They failed to find signals, even with 10^8 rads, if moisture was present, and suggest that the decay observed by other workers may have been due to traces of moisture in the samples.

Klingmüller & Saxena (28) reported a difference in the concentration of magnetic centres per unit dose of radiation delivered to embryos and cotyledons of *Vicia faba*; they estimated that 83 and 45 ev respectively were required to produce one detectable radical, when the water content was 4.6 per cent. With 12 per cent moisture the yield was much reduced. They detected magnetic centres with 10 kr, a dose which they claim is low compared with those used by other authors. [See also Klingmüller *et al.* (29).]

An ingenious technique was used by Smaller & Avery (30) to study the interaction of cysteamine with the e.s.r. of yeast irradiated with 150 kr of γ -rays. The signals were normally 25 gauss in width, but were reduced to only 9 gauss when the yeast had been grown in deuterium oxide. It was therefore possible to study the signals from yeast in suspension, these being still further enhanced, relative to the doublet resonance from water, by reducing the radiofrequency power. The presence of cysteamine in concentration 0.06 M left the yeast signal unchanged, 0.3 M reduced it to one half, and 1.3 M reduced it to a small "pip," while signals from the cysteamine increased correspondingly. These observations were carried out with suspensions at 77°K. After annealing them for 1 min. at 125°K, the water signals disappeared, while the others were left unchanged. The authors concluded that water radicals did not react with yeast radicals or with cysteamine radicals and that the change in the signal from yeast was due to interaction of the cysteamine with cellular constituents, probably protein.

DOSE-EFFECT RELATIONSHIPS

"LETHAL" EFFECT OF RADIATION: DEFINITION

Throughout this review, the terms "lethal effect," "cell death," and "killing" will be defined in the restricted sense of causing loss of the ability to originate a clone of viable daughter cells. "Survival" will imply the retention of this ability.

SIGMOID SURVIVAL CURVES

When plotted semilogarithmically, a sigmoid survival curve will have an initial shoulder, and it may then gradually assume an exponential form. If the exponential portion is extrapolated back to zero dose, the intercept with

the ordinate will represent a multiple of the control population, and it is proposed to call this the "extrapolation number," in order to avoid the implications of such terms as "multiplicity," "target-number," or "hit-number."

Interpretations of sigmoid survival curves were exhaustively discussed by Timoféeff-Ressovsky & Zimmer (17). The difficulties and fallacies involved in identifying ploidy with extrapolation numbers were discussed by Atwood (31) with particular reference to yeast. In recent years, certain experiments have suggested strongly that it may be fallacious to interpret extrapolation numbers as necessarily representing specific numbers of targets in the morphological sense. Hollaender, Stapleton & Martin (32) showed that different methods of culture of the strain *Escherichia coli* B/r, before irradiation, resulted in survival curves which differed only, but very greatly, in the extrapolation numbers, which were said by Zelle & Hollaender (33) to correspond to the numbers of "nuclear bodies" observed in the cells. However, Deering (34) examined the mode of killing of filamentous cells of *E. coli* B, in which the numbers of "nuclear bodies" are roughly proportional to their length, and found that the survival curves were exponential, in confirmation of an earlier report of Lea *et al.* (35). It follows from a previous paper of Deering (36) that the radiosensitivity must also have been in direct proportion to the amount of DNA per filament. Shekhtman *et al.* (37) found that *E. coli communis* grown on peptone agar gave exponential survival curves, both with x-rays and α -rays. If glucose had been used in the culture medium, the survival curves with both types of radiation had extrapolation numbers of about ten. The bacteria grown in glucose were much larger, but, as the authors pointed out, it is difficult to envisage morphological sites which present the same degree of multiplicity to these two types of radiation.

The postulate that extrapolation numbers necessarily represent a multiplicity of like morphological sites becomes even less tenable in the light of certain experiments in which radiation effects have been modified by treatments after irradiation. Alper & Gillies (38) have found that the shapes of the survival curves for the strains *E. coli* B/r and *E. coli* B may be considerably changed by various treatments after irradiation. When logarithmic-stage cells of *E. coli* B/r were exposed to UV, the survival curve was exponential, if they were cultured after irradiation on minimal medium; if nutrient agar was used, the survival curve had an equal slope, but an extrapolation number of 50. Survival curves for the parent strain, *E. coli* B, were initially of exponential form, in normal conditions of growth after irradiation. If they were treated with chloramphenicol, however, which effected considerable rescue of the cells, the survival curves became sigmoid, with extrapolation numbers of five after UV and after x-rays delivered in anoxic conditions. The sigmoid nature of the curves sometimes obtained with these two strains must therefore depend upon the interaction between the damaged cells and the metabolic conditions after irradiation; i.e., the "multiplicity" cannot be due solely to the morphology of the cells at the time of irradiation. A different type of study by Elkind & Sutton (39) throws doubt on the concept that in mammalian cells the extrapolation number is correlated with ploidy or with

sites of damage which can be referred to morphological structures. The survival curve for cells of the Chinese hamster, cultured *in vitro*, had an extrapolation number of 5.2. Cells were given a dose of radiation sufficient to reduce the viable count to a level at which the curve was of exponential form; on the conventional multiple target view, the surviving cells must have had all but one of the multiple targets damaged. If the cells were then left on the culture medium for various times after the initial dose, though for less than the time to the next division, survival curves again demonstrated a shoulder, so that it was once more necessary to score more than one effective "hit" per cell in order to kill it. After 18 hr. the original survival curve, with extrapolation number 5.2, was reproduced exactly. It seems implausible that if all but one of a number of morphological sites in a cell are damaged at random, all will recover completely as long as any one site remains undamaged; and it is particularly implausible that the postulated damage should all be in the form of actual or even potential chromosome breaks [see Puck (4)].

LETHAL EFFECTS ON MICRO-ORGANISMS

Woese (40) made a further report on data obtained by irradiating various species of *Bacillus*, both as resting and as germinating spores. Some gave survival curves of exponential form for both; when the survival curves were sigmoid, the extrapolation numbers were higher for the resting than for the germinating spores. Hill & Phillips (41) found that spores of *B. subtilis* exposed to γ -rays in solutions of penicillin were killed exponentially; the 37 per cent dose was 80 kilorads.

Elkind & Sutton (42) carried out a careful examination of the survival curves obtained when mixed populations of single and budding yeast cells ("interdivisional" and "dividing" cells) were exposed to UV. Hitherto the well-marked differentiation in sensitivity to ionizing radiation exhibited by these two types of cell has not been demonstrated with UV, and it might have been supposed that the UV killed both types of cell at random, as if they were uniformly sensitive. These authors have now shown that the UV survival curves for both haploid and diploid yeast do indeed have points of inflection. With some strains these could be detected only by a very high degree of accuracy in determining surviving fractions. The evidence that the interdivisional cells were preferentially killed by UV was securely based, however, on experiments in which cells which had been exposed to low doses of UV were then exposed to x-rays, since the response was characteristic of populations in which a proportion of the sensitive interdivisional cells had been killed, the resistant dividing cells being unaffected. X-rays had much the more clearly differential effect on the two types of cell, but the dividing cells demonstrated markedly sigmoid survival curves with both types of radiation.

LETHAL EFFECTS OF IONIZING RADIATIONS ON MAMMALIAN CELLS

Somatic cells.—The first "survival curves" for mammalian cells were published by Puck & Marcus in 1956 (43), the cells having been irradiated

and cultured *in vitro*. A dramatic development during 1959 has been the first appearance of comparable results for cells irradiated and cultured *in vivo*. Hewitt & Wilson (44, 45) used an elegant technique for estimating the sensitivity of liver leukemia cells irradiated *in vivo* in leukemic mice. The survival curves were of exponential form from 0.2 survivors down to 10^{-5} . Like the curves for human tumour (HeLa) cells irradiated *in vitro* (43), those pertaining to mouse leukemia cells demonstrated an extrapolation number of about two. The slope of the survival curve established by Hewitt & Wilson lies within the range of those published by Puck *et al.* (43, 46), 200 to 300 rads being required to reduce the viable population by 90 per cent. It should be noted that doses given in the papers from Puck's laboratory before 1959 should be multiplied by a factor of 1.45 [Morkovin & Feldman (47)].

Other techniques for examining the radiosensitivity of mammalian cells *in vivo* and *in vitro* have given similar estimates. Simpson (48) estimated the dose-effect relationship for undifferentiated blood cells in rats by counting the numbers of megakaryocytes per unit volume of blood, seven days after whole-body irradiation by various doses of x-rays. She constructed a survival curve which is of exponential form, about 250 rads being required to reduce the population of megakaryocytes to 10 per cent of normal. Till *et al.* (49) estimated that it required the injection of 10^4 bone-marrow cells to rescue mice which had been exposed to the otherwise 100 per cent lethal dose of 950 rads. They then irradiated samples of bone-marrow cells *in vitro* and found that a dose of 250 to 300 rads reduced the number of effective cells by a factor of 10. The exponential portion of the survival curve for Chinese hamster cells shows that the sensitivity of these, too, is about the same [Elkind & Sutton (39)].

The remarkable uniformity of all estimates of the sensitivity of somatic mammalian cells, irradiated *in vitro* and *in vivo*, and deriving from different species, encourages a belief in their relevance to tumour therapy. Morkovin & Feldman (47) calculated that a dose of about 2600 rads should be sufficient to kill every cell in a tumour weighing 0.1 g., while 3200 rads would be needed if the tumour weighed 10 g. Doses of this order are commonly used in radiotherapy, and it is striking that a factor of 100 in tumour size can be accommodated within the comparatively small range of 600 rads. These figures apply to well-oxygenated cells. By contrast, the effect of having even part of a tumour anoxic can be very much greater, as has been pointed out by Gray (12) and by Scott (3). Hewitt & Wilson (50) used the ingenious device of irradiating leukemic mice soon after killing them, in order to determine the sensitivity of the leukemia cells irradiated *in vivo* in anoxic conditions. The enhancement ratio for oxygen was found to be 2.3, so that a dose of 6000 rads would be required to kill every cell in a tumour weighing only 0.1 g., if all the cells were anoxic. Thus the effect of having only 1 per cent of cells anoxic, in a 10-g. tumour, would be to double the dose required for a cure.

Lymphatic cells.—Using induction of nuclear pyknosis and of intranuclear vacuoles as a test of damage, Hjort (51) examined the effect of graded

doses of whole-body irradiation on lymph-node cells. Observations of the fraction of normal cells in nodes from animals killed at 6 hr. show that 10 per cent of cells were normal after 400 r. The fraction of normal cells decreased exponentially with time after irradiation, and it may be inferred that 10 per cent of normal cells would have been observed 8 hr. after a dose of 300 r.

Germinal cells.—The uniformity so far observed in the radiosensitivity of somatic mammalian cells does not extend to the germinal cells; spermatogonia at least appear to be considerably more sensitive. Oakberg (5) reported an extensive morphological investigation on mouse spermatogonia after exposures to doses in the range 20 to 600 r. Types A and B cells were examined for necrosis and for mitotic index, and data were given for the ratios of normal cells seen in irradiated and control animals at times ranging from 1 hr. to 54 days after irradiation. The times at which ratios were at a minimum were longer, the greater the dose. In terms of these minimum ratios, it required only 20 to 25 r to reduce the ratios of both types to 50 per cent, corresponding to a 37 per cent dose of 30 to 35 r.

The combined study of cell morphology and of mitotic index confirmed Oakberg's view that depletion of spermatogonia was due to the killing of cells by radiation. An attempt to distinguish between the roles of inhibition of mitosis and of cell death was also made by Sharman (52) who used the marsupial *Potorous tridactylus*. He observed chromosomal aberrations after 50 and 150 r, the highest fraction of abnormal cells being about 50 per cent with the higher dose, two days after irradiation. He also concluded that inhibition of mitotic divisions in spermatogonia could not be the cause of their depletion. The course of meiosis continued until it was stopped by the absence of primary spermatocytes ready to begin meiotic division.

An estimate of the sensitivity of rat oocytes may be based on data of Mandl (53). Rats were exposed to doses of 29 to 4400 r and sacrificed from 3 hr. to 30 days after irradiation. Degenerative changes in primordial oocytes appeared early. Dose-effect curves were given for total numbers of oocytes seen at 24 hr., and when plotted semilogarithmically they are seen to have a steep component, which refers to the primordial oocytes, with a 37 per cent dose of about 180 r. Data for the doses 50 r and 100 r, giving total counts at 100 and 1000 hr., indicate that the sensitivity would appear higher in terms of the counts made at those times.

RADIOSENSITIVITIES OF DIFFERENT FUNCTIONS IN THE SAME CELL

Chick fibroblasts were found by Rubin & Temin (54) to vary in the extent to which radiation damaged their ability to support the growth of Rous sarcoma virus (a tumour virus) and Newcastle disease virus, which is cytocidal: capacity to initiate the growth of the latter was many times more resistant both to UV and to x-rays, while the capacity for Rous sarcoma virus had about the same sensitivity as the clone-forming ability of the fibroblasts. In the free form, the Rous sarcoma virus was the less sensitive to radiation. Once the cells had started to produce Rous sarcoma virus, much

larger doses were required to destroy the ability of the cell to produce it than to destroy the cell's ability to divide. The authors concluded that some radio-sensitive process other than DNA synthesis was required in the early stages of infection.

Woese (55, 56) used lysogenic strains of *B. megaterium* to compare the "sensitive volume" for plaque-forming ability with that of the phage in the free form. With three different strains, the sensitivity of the phage was three times that of the plaque-forming ability, and the survival curves were of different shape. The capacity of the cells to support the growth of virulent phage was less sensitive still. Strains which were noninducible in the vegetative state could be induced if the resting spores were irradiated. Shapiro *et al.* (57) compared two different tests of damage in an investigation with an unspecified strain of *E. coli*. Loss of ability to form visible colonies was called "genetic death," and failure of cells to elongate was called "physiological death." The ratio of the sensitivities for these two tests was about five to one.

Very interesting comparisons were made by Stuy (58) between the UV sensitivities of Transforming Principle (TP) *in vivo*, i.e. within the cells, and *in vitro*, and between the sensitivities of the TP and the ability of the cells (*Haemophilus influenzae*) to form colonies. With irradiation *in vivo*, the dose required to reduce the transforming ability was about 4.5 times greater than that required to reduce colony-forming ability of the host cells. Stuy also made important observations on the increase in cellular DNA and in TP activity after irradiation, the latter increasing at a rate equal to that in the control cells, even after the largest dose used, which reduced the viable cell population to less than 10^{-4} . More recent work of Stuy with x-rays has yielded essentially the same results (personal communication).

GENETIC EFFECTS

The production of new types of visible mutations by x-rays in the mosquito is of interest because, according to Pal & Krishnamurthy (59), no spontaneous mutations other than micromutations are known in this insect. Ives (60) carried out studies on sex-linked mutations arising in mature spermatozoa of *Drosophila*, using doses up to 12.5 kr. His results were compatible with the interpretation that a Poisson-like accumulation of lethal mutations occurs throughout the dose range, with an average increase of 2 per cent lethal mutations per kr.

The induction of reverse mutations in *Drosophila melanogaster* was examined by Green (61) with two forked pseudoalleles in which reverse mutations occur spontaneously. A dose of 4000 r significantly increased back mutations of f^n but not of f' . No associated chromosome aberration was detected.

Variations to radiation resistance, either spontaneous or as a result of irradiation, were reported for a few organisms. Schabinski *et al.* (62) derived resistant mutants from the survivors of irradiated populations of an unspecified *E. coli* strain. Increased resistance to γ -radiation was paralleled by in-

creased resistance to H_2O_2 . Wichterman (63) attempted to breed radiation-resistant mutants from a strain of *Paramecium* by exposing them to large doses of x-rays, but the descendants of survivors showed changes, persisting in subculture, which were generally concomitant with decreased vitality and which made them more sensitive to x-radiation than the parent strain. Banić (64) described a neat technique for isolating radiation-resistant mutants of *E. coli* by replica plating.

VARIABILITY OF EFFECTS WITH DOSE RATE AND DOSE FRACTIONATION

In radiobiological experiments there appear to be two ways in which dose rate may affect the result: on the one hand, a dose spread over a time which is long, compared with the division stage of the cell, may be less damaging than the same dose given in a shorter time; on the other hand, a dose given in a time which is short, compared with that necessary for diffusion of oxygen to or within a cell, may be less effective than one given in a longer time.

Examples of the first type of dose-rate effect have occurred in recent genetic studies. Russell *et al.* (65) reported that a single dose of radiation induced a significantly higher mutation rate in mouse oogonia than the same dose spread over several weeks, supporting a similar result with spermatogonia. In both males and females the dose-rate effect applied only to the gametogenic stage. In an abstract, Oster *et al.* (66) reported comparable results for female *Drosophila*. A dose of 4000 r delivered in 31 sec. induced 3.4 per cent recessive lethals in oogonia whereas 1.3 per cent were induced by the same dose delivered over two weeks. They noted the same trend with spermatogonia, but the results were not so conclusive.

An influence of dose rate on the impairment of fertility in female mice was observed by Mole (67). The total number of offspring produced was halved, if C57 Bl. females were given a single dose of 25 r of γ -rays at 10 to 12 weeks; the same effect was produced by about 80 r given at 2.2 r per day. Damage to mouse testes was assessed by Nuzhdin *et al.* (68) in terms of alteration in testis weight. They compared the effects of single and fractionated doses of 100, 400, and 1600 r. No effect of fractionation was observed after 100 r or 400 r, these doses being fractionated in various ways, up to a spread of the total dose over ten days. With 1600 r, however, less damage was observed from four equal doses, either at two-day or four-day intervals, than from a single dose.

The work of Elkind & Sutton (39) with Chinese hamster cells was reviewed in a previous section. They established the important fact that the reduced effectiveness of a second dose was related to metabolic processes, which restored to the cells the property of requiring a threshold dose before survival curves followed an exponential course. Abrahamson (69) examined the effect of fractionation on chromosome rearrangements in *Drosophila* oocytes. If the dose was split into two, with an hour between irradiations, the effect was significantly less than that of a single dose. He also examined the effect of anoxia during the hour between doses; this will be discussed in a

later section. The effect of fractionation on induction of recessive lethals in *Drosophila* sperm was examined by Luning & Henriksson (70). A first dose of 2750 r was delivered in anoxic conditions and was followed at varying intervals by a dose of 1650 r, the flies apparently having been kept in air between doses. The frequency of recessive lethals was greater if the interval between doses was less than 40 min.

Alteration in dose rate over a much smaller range (3200 rads in 30 to 900 sec.) was reported by Yanders (73) to be without effect on the mutation rate in mature *Drosophila* sperm. Tobias (10) quoted experiments of Welch, who set up a continuous culture of yeast cells as a model for a multicellular organism containing dividing cells. The lower the dose rate, the greater was the number of mitotic divisions the cell could undergo before reproductive ability was lost.

A linear accelerator was designed by Boag & Miller (71) to irradiate samples with one or a few pulses of electrons, and this technique makes it possible to study the effects of radiation delivered at a very high rate. Dewey & Boag (72), working with *Serratia marcescens*, were able to deliver 10 to 20 kilorads of 1.5 Mev electrons in single pulses of 2 μ sec. duration. When the bacterial suspension was in equilibrium with a gas mixture of 1 per cent oxygen in nitrogen, the sensitivity of the bacteria was the same as if they had been irradiated in anoxic conditions, whereas the 1 per cent oxygen was sufficient to enhance by a ratio of 2.5 the effect of radiation delivered at 1000 rads/min. The result was ascribed to local removal of dissolved oxygen within the bacteria during the first few kilorads of the pulse, the duration of which was too short to allow its replacement by diffusion from outside. The effect was not observed when the oxygen concentration in the suspension was raised to 5 per cent.

EFFECTS ON GROWTH AND COURSE OF DEVELOPMENT

Bacteria.—An unusual effect of x-rays on *E. coli* B was observed by Laser & Thornley (74). The bacteria had been maintained for many years on a salts medium, with glucose and NH_4Cl as sources of carbon and nitrogen, and viable counts on irradiated cells cultured in this medium showed an initial lag, followed by a period of shorter generation time than the controls, and finally a period in which the generation times were the same [see Alper & Gillies (38) for similar observations with *E. coli* B in nutrient broth after irradiation]. The more unusual situation arose when maltose was used as a carbon source in the postirradiation culture medium. Unirradiated cells could utilize the maltose only in the presence of glutamate or other organic nitrogen source; irradiated cells, on the other hand, could utilize maltose in the absence of glutamate and showed a higher rate of oxygen uptake than the unirradiated cells, whether glutamate was present or not. The generation time of the irradiated bacteria was considerably less than that of controls, in the glutamate-maltose medium, and the final count was somewhat higher. It was established that the unirradiated control cells could utilize maltose, if it

got into the cells, and that the increased utilization of maltose by irradiated cells could not be due to increased uptake by way of a damaged cell membrane, since the response to maltose was inhibited by chloramphenicol. It was concluded that radiation induced the formation, or destroyed an inhibitor, of the permease necessary for maltose transport.

Hermier (75) reported that high doses of γ -rays, like heat treatment, caused spores of *B. subtilis* to germinate on unfavourable media. Doses of 2 or 3 megarads had about the same effect as about 3 hr. exposure to 100°C., in synthetic salts media with valine, alanine, or glucose as supplements. If the medium contained both glucose and alanine, the fraction of spores germinating after 0.01 megarads equaled that in untreated controls (4.5 per cent), and it decreased with increasing dose, while heat treatment for 30 min. increased the number germinating to 52 per cent.

Yeast.—Effects of ^{60}Co γ -radiation on the budding of diploid and haploid strains were investigated by Korogodin *et al.* (76) and by Korogodin & Liu Ah-Shen (77). Viable counts were made in the usual way, and microcolony formation was also observed. Results were in essential agreement with earlier work, e.g. Beam *et al.* (78); Latarjet (79); Burns (80). Haploid cells were more resistant to radiation when they were budding; diploid cells which failed to form macrocolonies after irradiation might still bud several times whereas killed haploid cells infrequently budded more than once. Increased survival was observed with diploid, but not with haploid cells, if they were maintained in nonnutrient medium after irradiation [see also Korogodin & Malumina (81), reviewed below]; the corresponding diminution in numbers of cells reaching only the one-to-two-bud or the three-to-seven-bud stage was about equal.

Budding of *Saccharomyces cerevisiae* during and after continuous irradiation at 2.85 kr/hr. was investigated by Spoerl & Looney (82). Cultures were irradiated while growing exponentially, and cell counts increased exponentially until the accumulated dose was about 4.3 kr. No further budding was observed during the 3-hr. irradiation period. After this, the cells budded in more and more synchronous fashion, so that budding was observed to occur in two steps within a 4-hr. period; the newly-formed buds grew to the size of cells but did not separate from the mother cell, even when centrifuged and resuspended in fresh medium. Concurrent biochemical investigations showed a higher uptake of ^{32}P per unit dry weight in cells inhibited from budding than in those ready to bud. Insoluble polyphosphates of inhibited cells showed accelerated uptake of ^{32}P , but uptake in soluble polyphosphates was reduced. Uptake in nucleic acid was unchanged in the irradiated cells.

SOME EFFECTS OF LOW DOSES

A high incidence of spontaneous lymphoid leukemia occurs in mice of strain AkR, and Rudali & Reverdy (83) exposed newborn mice to a dose of 5 r. This reduced the average latent period in males from 334 to 278 days but did not affect the latent period in females or the incidence in either sex. Doses

of 50 r delivered to mice in the eighth day of pregnancy were sufficient to produce some exencephalics (cerebral hernias) in the offspring; after 200 r, the incidence was 26 per cent [Rugh & Grupp (84)]. This was only one form of congenital abnormality indicative of gross damage to the central nervous system. Responses to doses of 50 and 100 r in amphibian erythrocytes were observed by Lessler (85). He noted changes in morphology, some hemolysis, and changes in the cell membranes demonstrated by increased uptake of $^{42}\text{K}_2\text{CO}_3$, followed by increased loss of potassium. The capacitance of the membrane increased, and was at a maximum half an hour after irradiation. Visual sensitization by doses of 1 to 25 r were found by Dawson & Smith (86) to occur in the single visual receptor in the lateral eye of *Limulus*. Complete adaptation to light canceled the effects of the ionizing radiation. Blum (87) reported data from studies on tumour induction with ultraviolet light which showed that there was no threshold for the response. He argued from this that a similar response to ionizing radiation could be expected, and should be assumed, unless contrary evidence was provided. The papers of Oakberg (5) and of Mole (67), who observed destruction of 50 per cent of germinal cells with doses of about 25 r, were reviewed in previous sections.

RADIATIONS OF DIFFERENT QUALITY

SPECIFICATION OF QUALITY AND DOSIMETRY

In recent years the term "Linear Energy Transfer," coined by Zirkle (88), has gained acceptance in the place of "density of ionization" as a measure for specifying radiation quality. This concept, too, has presented difficulties. One of these was highlighted by the experiments of Conger *et al.* (89), who found that very different results were obtained, depending on whether the "energy-average" or "track-average" LET of 14-Mev neutrons was used. Rossi (90) has examined once more the specification of radiation quality and has proposed a new method which, he claims, will dispose of some difficulties such as the lack of knowledge of δ -ray energies and distribution. He has therefore proposed the term *Y*, the definition being: "the energy imparted in an event, divided by the sphere diameter"—an event being essentially the instantaneous passage of a charged particle through or near the volume. Some idealized *Y* distributions were given, and it was claimed that representation of a dose in *Y* for a range of diameters would yield information on the spatial distribution of energy, as well as the local dose and the frequency with which it was delivered. In a further paper, Rosenzweig & Rossi (91) described determinations of *Y* spectra for mono-energetic neutrons of different energies, using a spherical proportional counter.

A theoretical analysis of the relationship between radiation quality and yield of Fe^{3+} or Ce^{4+} ions in aqueous solution was made by Burch (92). His treatment is particularly relevant to investigations such as that of Sinclair *et al.* (93), in which the radiations being compared (200 kvp x-rays, ^{60}Co γ -rays, and 22 Mevp x-rays) vary in their biological effectiveness by only 10 or 20 per cent. In this type of work accurate dosimetry is crucial. Sinclair

et al. used air-ionization measurements, based on a calibrated Victorian chamber, but depended also on ferrous dosimetry, so that it was necessary to adopt G values applicable to the three radiations used. Problems of dosimetry as well as specification of quality were a formidable part of the investigation of Birge & Sayeg (94), who provided the physical basis of the investigation by Sayeg *et al.* (95) into the biological effects of beams of particles, including stripped carbon nuclei, from the Berkeley 60-inch cyclotron. Each run required elaborate preliminary physical measurements on range, Bragg ionization curve, and intensity distribution, on the basis of which the apparatus was aligned. The biological samples were irradiated only in those portions of the particle ranges in which average LET's were uniform. Dosimetry during irradiations of the biological samples was carried out by means of a specially designed quadrant electrometer to measure the dose and to indicate the highly critical beam alignment.

An analysis of photon spectra for five different qualities of x-rays, ranging from 130 kvp to 25 Mevp, was made by Danzker *et al.* (96) who made their calculations without assuming "space-independence," i.e. that spectra remain constant in a medium (such as mammalian tissue) which varies in its composition. Krokowski (97) described a scintillation dosimeter which he claimed to be wavelength-independent within 3 per cent for x-rays between 30 and 250 kv and direction-independent between 0 and 325°. Sodium silicate was judged to be the optimum material for attaining both high sensitivity and wavelength independence; the scintillator was incorporated into Plexiglass, the thickness being 0.04 cm. and the volume 0.1 cc. Changes in the optical properties of glass were used by Brustad & Henriksen (98) to estimate doses of the order of 10^4 to 10^6 rads. The method was thought to be particularly useful when small biological objects were suspended in a thin water-layer between two coverslips.

Ardashnikov & Chetverikov (99) gave an extensive theoretical treatment concerning doses due to point sources of α - and β -rays. They calculated doses absorbed in bodies which are figures of rotation irradiated by point sources lying on the rotation axis, the solution applying also to doses at points lying on the rotation axes of sources in the form of bodies of rotation. The authors promised tables of numerical solutions for specific radiations and geometries.

In trying to distinguish between the mutagenic effects due to radiation from the transmutation of ^{32}P , ingested by *Drosophila melanogaster*, Oftedal (100) was faced with extremely complicated problems of dosimetry. He used comparative studies with ^{91}Y , which has a similar β -ray spectrum to ^{32}P but is of no importance metabolically. With reservations, because of the difficulties in estimating doses, Oftedal concluded that only 1 in 100 transmutations of ^{32}P was mutagenically effective.

VARIATIONS IN BIOLOGICAL EFFECTS

Only the paper of Sayeg *et al.* (95) has been concerned with the effects of several different types of radiation. These authors tested colony formation

by haploid yeast after exposure in aerobic conditions to x-rays, to ^{210}Po α -particles, and to particle radiations of various types and energies from the Berkeley cyclotron. The ^{210}Po α -particles were the most effective form of radiation, the RBE being about two. With radiations of higher LET (stripped carbon nuclei of energies 24 to 65 Mev) the RBE decreased. A maximum in the RBE/LET curve has been observed also with other cellular systems [cf. Read (15, p. 142 ff.)]. It should be noted that the yeast cells used in the experiments of Sayeg *et al.* had been starved for 48 hr. Elkind & Beam (101) showed that whereas the RBE for haploid yeast irradiated in this condition is greater with α -rays than with x-rays, the reverse is true for the nonbudding cells in a freshly harvested population.

A series of papers by Neary, Evans and co-workers compared the effectiveness of 3-Mev neutrons, derived from 900-keV deuterons on lithium-6 deuteride, with ^{60}Co γ -rays. They tested the RBE for inducing mitotic delay [Neary *et al.* (102)], chromosome damage [Evans *et al.* (103)], and reduction in growth rate in roots of *Vicia faba* [Neary *et al.* (104)]. In their experimental conditions the meristematic cells were probably at or near an oxygen concentration which was sufficient to give maximum effectiveness to the radiation. The RBE values differed somewhat from test to test and also with the dosage levels, since some dose-effect curves for the two radiations were of different shape. Nevertheless, there is sufficient agreement between various workers with plant material [see Read (15)], and between the results of different tests of damage, to justify the tentative suggestion that the pattern observed by Conger *et al.* (89) is generally true for plant cells: RBE reaches a maximum of the order of 10, for radiations of LET average energy about 60 keV/ μ , and thereafter decreases [see also Spalding *et al.* (105)]. Curve A of Figure 1 indicates this over-all picture.

Data for animal cells are not so extensive. Vogel & Jordan (106) compared the effectiveness of fission neutrons to ^{60}Co γ -rays in killing 4-day chick embryos. The RBE ranged from 2.2 to 2.8, depending on whether the LD₅₀ was assessed at 6 hr. or 6 days. Hornsey *et al.* (107) examined the effectiveness of fast neutrons relative to that of 1.5 MeV x-rays in inducing chromosome aberrations in ascites tumour cells, and they found the RBE in aerobic conditions to lie between 2.5 and 3.6, depending on the level of damage. If data on "bone-marrow death" can be regarded as an indication of the lethal effects of radiation in well-oxygenated primitive blood cells, it may tentatively be concluded that the RBE for fast neutrons is between 2.5 and 4. Furthermore, the data of Edington & Randolph (108) and of Storer *et al.* (109), as calculated by Read (15), suggest that there may be a peak in the RBE/LET curve for animal cells, as there is with starved yeast and plant cells. Curve B of Figure 1 has been sketched on the basis of these assumptions.

Brustad *et al.* (110) have reported, so far only in an abstract, that in aerobic conditions there is a continuous decrease in RBE with LET for the killing of *Shigella flexneri*. This confirms observations of Howard-Flanders &

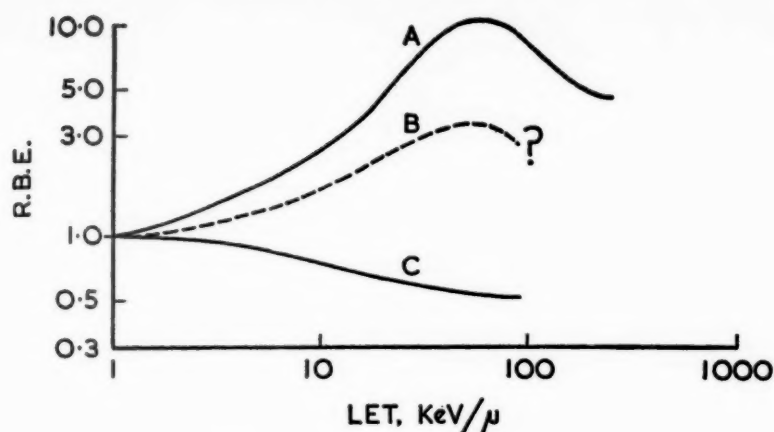


FIG. 1. Variation in RBE with LET, for biological materials irradiated in aerobic conditions. A: plant cells (15, 89, 102 to 105). B: animal cells (15, 106 to 109). C: two strains of bacteria (110 to 112).

Alper (111) with neutrons and x-rays and agrees with the much earlier results of Lea *et al.* (112) for *E. coli*. Curve C of Figure 1 presents the variation of RBE with LET for at least these two strains of vegetative bacteria irradiated in aerobic conditions. There seem to be some grounds, therefore, for concluding that the three types of cell, plant, animal, and vegetative bacteria, demonstrate different patterns in the variation of RBE with LET, the implication being that there are important differences in the mechanism by which radiation affects the viability of these three cell types. This is all the more striking in view of phenomena which are common to all: induction by radiation of giant cell formation and of delay in division, and enhancement by oxygen of radiation effects.

Dose-effect curves obtained with radiations of different quality are frequently dissimilar in shape [e.g. (104, 107)]. Instances have been reported of effects which are seen with one type of radiation and not at all with another. Ehrenberg (113) quoted a type of mutation induced in barley seeds by x-rays which has never been observed after neutron irradiation. Fabergé (114) found that α -rays produced stable free chromosome ends in maize, a phenomenon never observed after UV or x-irradiation.

MODIFICATION OF RADIATION RESPONSE BY TREATMENT BEFORE OR DURING IRRADIATION

CONDITIONS OF GROWTH BEFORE IRRADIATION

The observations of Shekhtman *et al.* (37) have been discussed in a previous section. Billen (115, 116) incubated cells of *E. coli* B/r and *E. coli* 15 T⁻ (thymine-requiring) with chloramphenicol before exposing them to x-rays.

Survival curves show that there was an alteration in the extrapolation number only, which increased from about 2.2 for the untreated cells to 4.5 for those treated with chloramphenicol. The slopes remained the same. This alteration in the dose-response curve occurred only with cells treated in the logarithmic stage. The thymine-requiring cells which had been incubated with chloramphenicol before irradiation survived to a greater extent, provided thymine had been present in the medium. With this strain, too, the change appears to have been mainly in the extrapolation number.

PRE-TREATMENT BY NON-IONIZING RADIATION

Moh & Withrow (117, 118) reported that if bean roots were exposed for 3 hr. to radiation in the region 715 to 940 $m\mu$, they demonstrated 40 per cent more chromosome abnormality after subsequent exposure to 100 or 120 r of x-rays. Treatment with light in the range 620 to 680 $m\mu$ nullified or reversed this potentiating effect. The authors postulate that the far red light reduces the level of oxidative phosphorylation, thereby reducing the repair of chromosomes, and that the light of shorter wavelength counteracts this effect.

Three papers dealing with different test systems have demonstrated that exposure to UV may reduce the effect of a subsequent exposure to x-rays. Swaminathan & Natarajan (119), using wheat seeds, examined chromosome abnormalities in the root tips of the germinated seeds and also the number of mutants appearing in the second generation. The UV pre-treatment (dose not stated) reduced by a factor of nearly two the effectiveness of the x-rays in inducing chromosome abnormalities, which were not seen after UV alone. The dose-effect curves for mutation induction by x-rays alone show a peak at about 20 kr. With doses below this level, the UV pre-treatment again acted in the sense of reducing the effectiveness of the x-rays. With higher doses, however, in the region in which mutations produced by x-rays alone decreased with increasing dose, the number of mutants in the progeny of seeds pre-treated with UV continued to increase with increasing x-ray dose.

An effect which appears to be to some extent analogous was observed with spores of *Streptomyces aureofaciens*. Gol'dat & Alikhanyan (120) found that doses of 4000 ergs/mm.² of UV and 36 kr of 60 kv x-rays given separately reduced the surviving populations respectively to 3.7×10^{-3} and to 0.15. If the effects of successive exposures to the two types of radiation were additive, the expected surviving fraction would be 5.5×10^{-4} , provided the killing followed an exponential law. However, it was found that if the x-ray exposure followed the UV treatment, the number of survivors was considerably higher than expected on the basis of the two irradiations acting independently. The extent of the increase depended on the time interval separating the exposures, the maximum effect being observed when the x-ray exposure was given one hour after the UV, the surviving fraction then being 3.3×10^{-3} .

Elkind & Sutton (121) reported an extensive series of experiments with

various strains of yeast. The cells were exposed to UV either before or after x-rays. If the x-ray survival curves pertaining to the UV-treated cells were plotted from the survival level to which the original population had been reduced, and as if they had received the x-ray dose required to reduce them to this level, the UV could in most of the examples shown be regarded as having had a protective action. When large doses of UV were used, it was most effective as an agent for reducing subsequent damage by x-rays if a period of exposure to visible light intervened. This is particularly well illustrated by one experiment with the strain SC-7. The preliminary UV treatment reduced the surviving population to 7.6×10^{-5} , and treatment with visible light increased the surviving fraction to 2.2×10^{-3} . This treatment was more effective in protecting the cells against subsequent x-ray exposure than doses of UV alone which reduced the surviving population to 3.4×10^{-3} , 1.4×10^{-3} , or 1.5×10^{-3} . This is a neat demonstration of the fact that "reactivation" by visible light after UV does not necessarily bring about a true reversal of UV effects.

THE EFFECT OF OXYGEN

New data on oxygen enhancement ratios.—Results have been reported with a few test systems and criteria of damage which have not hitherto been examined from this point of view. Data on oxygen enhancement ratios with radiations other than x- or γ -rays have hitherto been rather sparse, and several papers during 1959 have dealt with this aspect of the oxygen effect. The new data on oxygen enhancement ratios are collected in Table I.

A point of interest in Wright & Batchelor's paper (122) was that they were able to complete their irradiations within 1 or 2 sec. when they used electrons from an 8 Mev linear accelerator. This enabled them to make the observation that the thymus attained its anoxic level of sensitivity within 10 sec. of the start of nitrogen treatment. Loiseleur & Petit (126) succeeded in making rats anoxic by the simple method of keeping them in an enclosed space for half an hour; they were able to survive anoxia induced in this way.

Detailed investigations.—An expression suggested by Alper & Howard-Flanders (127) to describe variation in radiosensitivity with oxygen concentration contained two constants which they called m and k : m may be defined as the maximum ratio of sensitivities in oxygenated and anoxic conditions, this "maximum enhancement ratio" being approached asymptotically as the oxygen concentration increases; while k is that oxygen concentration at which the sensitivity, relative to that in anoxic conditions, is $(m+1)/2$. The results of three different investigations reported in 1959 were well fitted by the suggested hyperbolic form of this equation, and these have all confirmed the observation, made by Alper & Howard-Flanders (127) with micro-organisms in controlled gas conditions, that k is considerably lower than had been suggested by earlier work. Deschner & Gray (128) used ascites tumour cells, their test of damage being the induction of chromosome aberrations. They paid particular attention to equilibration of the gas mixtures with the

TABLE I
NEW DATA ON OXYGEN ENHANCEMENT RATIOS

Biological Material	Criterion of Damage	Type of Radiation	Oxygen Enhancement Ratio	Authors	Ref.
Thymus of mouse	Weight loss	250 kvp x-rays 8 Mev electrons	~3	Wright & Batchelor	(122)
Ascites tumour cells	Anaphase abnormalities	1.5 Mev x-rays Fast neutrons (D→Be)	2.6 1.4	Hornsey <i>et al.</i>	(107)
Ascites tumour cells	Inhibition of anaerobic glycolysis	x-rays	>1*	Warburg <i>et al.</i>	(123)
Root tips, <i>Vicia faba</i>	Chromosome damage (micronuclei)	Fast neutrons (D→ ³ LD)	1.4	Evans <i>et al.</i>	(103)
Root tips, <i>Vicia faba</i>	Reduction in growth rate	Fast neutrons (D→ ³ LD)	~1.4	Neary <i>et al.</i>	(104)
Root tips, <i>Vicia faba</i>	Mitotic delay	Fast neutrons ⁶⁰ Co γ-rays	1.0 2.0	Neary <i>et al.</i> Evans <i>et al.</i>	(102) (124)
<i>Rhodnius prolixus</i>	Burn, epidermis	x-rays	2-3	Baldwin & Salthouse	(125)

* Ratio not stated.

suspensions of actively respiring cells. Their values for m and k were respectively 3.1 ± 0.27 and $5 \pm 2 \mu\text{M/l}$. Kihlman (129) reported fully on his investigation with roots of *Vicia faba*, aberrant cell morphology again being the test of damage. He found that if he used respiratory inhibitors to diminish the oxygen gradient through the layers of respiring cells, the value of k was in the range 3.3 to $5.2 \mu\text{M/l}$, i.e. the same, within experimental error, as had been observed for micro-organisms (111).

The remarkable similarity in the values of k for micro-organisms, ascites tumour cells, and bean-root cells is all the more striking in that, by chance, three test systems had been chosen which differ very widely in their response to radiations of different quality (Fig. 1) and presumably, therefore, also in the mechanism by which radiation affects them. The close agreement may, of course, be fortuitous, since the somewhat higher value of $k = 10 \pm 2.8 \mu\text{M/l}$ has been reported by Evans & Neary (130) to apply to *Tradescantia* pollen-tube chromosomes. The errors in all the measurements of k have been in the range 10 per cent to 40 per cent, and it is not possible therefore to say whether k is really the same for all four types of test material which have been used, or whether the higher value for *Tradescantia* pollen tubes is evidence that a range of values of k exists. In any event, there seems little doubt of the order of magnitude of the oxygen concentration required to double the radio-sensitivity of this wide range of cell types.

Low temperature and hypoxia.—Lowered temperature before or during irradiation has been variously reported to enhance and to protect against radiation effects [e.g. Crabtree & Cramer (131); Hornsey (132)]. The work already reported makes it clear that when blocks of tissue, unstirred cell suspensions, or organized tissues such as plant inflorescences are used, a lower temperature will diminish oxygen gradients and will therefore enhance radiation effects if even a small trace of oxygen is present. On the other hand, whole animals at low temperatures cease to breathe, and Hornsey (132) postulated that hypothermia acted protectively on mice by inducing anoxia in the tissues as a whole. This has been well substantiated by a group of three papers: Cater & Weiss (133) showed that the oxygen tension in the spleens of mice was drastically lowered as they became hypothermic; Weiss (134) induced anoxia in mouse spleens by ligature and found that when irradiated in this condition they were protected against weight loss induced by 800 r whole-body irradiation, whereas spleens ligated after the irradiation suffered the same weight loss as unligated spleens; lastly, Weiss (135) showed that if mice were exposed to 800 r (whole-body) in hypothermic conditions, the spleens were protected, as judged by weight change, to the same extent as the ligated spleens, which could be assumed to have been anoxic during irradiation.

Variability and modifications of the oxygen effect.—Gillies & Alper (136) confirmed a previous report that the oxygen enhancement ratio observed with *E. coli* strain B depended on conditions of culture after irradiation. Chloramphenicol treatment considerably reduced the lethal effects of radiation, the

extent of the "rescue" after x-rays being much greater if these had been delivered in anoxic conditions. Thus survival curves of chloramphenicol-treated cells demonstrated a larger oxygen enhancement ratio than those of untreated cells [Alper & Gillies (38)]. As previously shown (137), the component of damage which came to light in rapidly growing cells could be differentiated from the over-all damage, and this component was equal for irradiations given in anoxic and oxygenated conditions, i.e. it was not enhanced by the presence of oxygen. The number of lethal mutations induced in *Paramecium* has been found by Kimball and his co-workers to be reduced if inhibitory conditions are applied after irradiation. This system has many analogies with the effects of such conditions on the survival of *E. coli*. B. Kimball, Gaither & Wilson (138) reported that streptomycin was effective in this way whether x-irradiation had been given anoxically or not; significance of the difference between treated and untreated animals was greater for irradiation in anoxic conditions.

An interdependence of temperature and oxygen effect was reported by Powers, Webb & Ehret (139), who used dry spores of *B. megaterium*. If these were irradiated at temperatures below -150°C . no dependence of sensitivity on temperature or on oxygen was detected. Above this, sensitivity increased linearly with temperature, but the coefficient of increase was greater if the spores were irradiated in oxygen. Thus there was a linear increase in oxygen enhancement ratio to 1.25 at 37° . At still higher temperatures, the anoxic sensitivity decreased sharply, while in oxygen it remained the same or increased slightly. The oxygen enhancement ratio therefore increased from 1.25 to over 2.2 in the temperature range 37° to 82°C .

Haploid yeast cultures when freshly harvested contain single and budding cells, which are very different in their sensitivity to ionizing radiation. Alper (140) reported that they also differed markedly in the extent to which oxygen affected their radiosensitivity: oxygen enhancement ratios measured with 8 Mev electrons were respectively 3.4 and 1.7 for the single and budding cells.

MODIFYING ACTION OF GASES OTHER THAN OXYGEN

Nitric oxide.—An enhancing action of NO, which seemed similar to that of oxygen, was first reported by Howard-Flanders (141), and this was followed by confirmatory reports [Gray *et al.* (142); Kihlman (143)]. Dissimilarities in the action of the two gases have now appeared in relation to materials irradiated in the dry state. Sparrman *et al.* (19) examined the effect of irradiating and then storing small grass seeds in NO, using reduction in seedling height as the criterion. The effect of NO was more protective than that of anoxia if the moisture content of the seeds was less than 8 per cent. At 12 per cent humidity the effect of NO was between that of air and anoxia, and at 14 per cent it had about the same effect as irradiation and storage in air, or perhaps slightly more. In an abstract, Powers *et al.* (144) reported that NO protected dry bacterial spores, whether it was present during irradiation

or not applied until afterwards, provided the irradiation had been carried out in anoxic conditions.

Gases under pressure.—Various gases applied under pressure were reported by Ebert *et al.* (145) to suppress the enhancing action of O_2 ; the criteria of damage were reduction of growth rate in *Vicia faba* roots and induction of anaphase abnormalities in Ehrlich ascites tumour cells. Chang *et al.* (146) looked for comparable effects in the induction by 1000 r of recessive lethals in *Drosophila melanogaster* and dominant lethals in *Drosophila virilis*. The modifying action of the gas mixtures varied somewhat with the stage at which the flies were mated; for the ensuing brief account, effects on the two most sensitive stages, i.e. spermatids, have been considered together (C and D in *melanogaster*, D and E in *virilis*). In the experiment on recessive lethals, 9 atm. of N_2 added to 1 of O_2 had slightly more protective action than 9 atm. of argon added to 1 of air. Nitrogen was thus more effective than argon in suppressing the effect of O_2 . This is a very different result from that of Ebert *et al.*, who found that six times as high a pressure of N_2 as of argon was needed to suppress the oxygen effect to the same extent. Chang *et al.* used a different range of gas mixtures in the experiments on *virilis*. In these, methane at 10 atm., with no oxygen present, was the most protective; 9 atm. of argon added to 1 of O_2 had about the same protective effect as 9 atm. of methane added to 1 of air.

MODIFICATION OF DAMAGE BY TREATMENT AFTER IRRADIATION

Methods of changing the response of cells by treatment after irradiation are often also methods of increasing or decreasing the rate of metabolic processes. Several papers have dealt with anoxia, and it is possible in some cases to distinguish clearly between the effects of anoxia during and after the irradiation. The imposition of anoxia on metabolizing cells after irradiation has been shown in some cases to reduce the damage [e.g. Pahl & Bachofer (147)] and in others to increase it [e.g. Wolff & Luippold (148)]. In such experiments, the effectiveness of the postirradiation treatment depends on the length of time it is applied, and the times necessary for effective action are comparable with the division stages of the cells under test. By contrast, the generally enhancing effect of oxygen during irradiation of wet cells has been as closely identified with the actual period of irradiation as experimental techniques have permitted [Howard-Flanders & Moore (149)].

The effect of UV (254 $m\mu$) on bacteria is not influenced by the presence of oxygen; but if UV-irradiated cells of *E. coli* B are inoculated into nutrient broth and held anoxic at 37°C., the lethal effect of the radiation is considerably reduced, as it is by other agents or conditions which act as metabolic inhibitors [Alper & Gillies (38)]. Anoxia after x-irradiation acted as an enhancing agent in the experiments of Abrahamson (69), who observed translocations in *Drosophila* oocytes, using a genetic test. If radiation was given

in a single exposure, the frequency of the translocations was greater when the flies were kept anoxic for about an hour thereafter. The enhancing effect of the anoxia was more than sufficient to counteract the mitigating effect of fractionation: if the dose was separated into two, and the flies kept in air between doses, the effect was less than that of a single dose; but if the flies were kept anoxic for the hour between doses, the effect was greater than that of a single dose.

Shapiro *et al.* (150) used mouse ascites tumour cells in an investigation on effects of oxygen, their test being the frequency of chromosome abnormalities. No data were given on the time of incubation in the mouse required to demonstrate the maximum effect; their time of fixation, 24 hr., seems long compared with the 14 hr. which Deschner & Gray (128) found to be the optimum. Shapiro *et al.* irradiated the ascites tumour cells in ampoules, which were either open at the time of irradiation (in ice) or opened to the air immediately thereafter and left for 2 hr. before reinoculation. They found that cells kept anoxic after irradiation demonstrated even less damage than those irradiated while anoxic but later exposed to air. The same authors also reported an experiment with barley seeds which was essentially the same as that carried out by Caldecott *et al.* (20), except that chromosome abnormalities, observed at the first anaphase, were the test of damage. Seeds with a moisture content of 4 per cent were irradiated with a dose of 10^4 r, and were then soaked in either well-oxygenated or deoxygenated water; less damage was observed with the latter. Shapiro *et al.* (150) consider that the effects of post-irradiation anoxia on mammalian cells and on seeds are illustrative of the same phenomenon, but Caldecott *et al.* (20), and others who have confirmed their results, take the view that with the dry and presumably nonmetabolizing seeds the effect of oxygen introduced after irradiation is akin rather to the enhancing effect of oxygen during irradiation of wet cells [e.g. Curtis *et al.* (21)].

Data on the effect of oxygen after irradiation of seeds were presented also by Sparrman *et al.* (19), who used small grass seeds in biological experiments conducted in parallel with observations on e.s.r. Seeds irradiated and stored in air showed more damage than those irradiated and stored in nitrogen; the largest enhancement ratio, nearly three, was observed for seeds irradiated with 8 per cent humidity. The effects of anoxia at the time of irradiation and during postirradiation storage were not separately assessed. Sire & Nilan (151) irradiated seeds of *Crepis capillaris* at 8 per cent humidity, subsequently storing them in oxygen at 100 p.s.i., for periods up to 42 days. The fraction of root tip cells with abnormalities in the first mitotic division increased from 24.9 per cent, for seeds soaked immediately, to 90.6 per cent. Roots from unirradiated seeds also showed an increase in abnormalities with oxygen under pressure, from 1.2 to 4.2 per cent during 42 days.

Postirradiation treatments affecting cellular metabolism have been used by Kimball, Gaither & Wilson (152) to reduce the frequency of recessive lethal mutations in *Paramecium*. Stationary-phase animals were irradiated

in an exhausted culture medium and transferred to fresh medium at various times thereafter. The longer they were kept in starvation medium, the smaller the frequency of recessive lethals, and after 100 hr. starvation this was only half as great as after immediate transfer. Starvation before irradiation was without effect. Streptomycin and chloramphenicol had an effect similar to that of starvation after exposure, but this was not observed if the treatment was delayed for 24 hr. In another paper (138) the same authors compared the action of metabolic inhibitors after UV, x-rays, and α -particles; the modifying action of the metabolic inhibitors was greatest after UV. Temperature after irradiation was used as a variable by Litvinova (153, 154), who observed division delay and viability in *Paramecium* after doses of 100, 150, and 300 kr. The higher the temperature, the more nearly did the division time approximate that observed in the controls; at the same time, incubation at higher temperatures increased the lethal effect of a given dose. The results are in good agreement with those of Powers (155).

Effects of nutrients and of metabolic inhibitors on *E. coli* B, and its resistant mutant B/r, were reported by Alper & Gillies (38). For strain B it was confirmed that nutritional conditions which increased the rate of growth (of both control and irradiated cells) were those in which most radiation damage came to light; treatment by metabolic inhibitors after irradiation reduced the effects of both ionizing radiation and UV. With strain B/r, on the other hand, the reverse was true, so that the strains became more nearly alike in sensitivity if growth inhibitory culture conditions were used. When logarithmic-stage cells of both strains were exposed to UV and then plated on minimal medium, the survival curves were identical and of exponential form. Immediate treatment of both strains with chloramphenicol, followed by incubation on nutrient agar, produced a similar end result: the survival of strain B was increased, that of B/r decreased, so that surviving fractions after the same doses were equal. It was concluded that the parent and mutant strains differed in radiosensitivity by virtue of differences in response to metabolic conditions after irradiation. Doudney (156) reported that treatment with 6-aza-uracil after UV irradiation achieved as much rescue of *E. coli* B as chloramphenicol treatment; the effect could be reversed by adding uridine to the medium. He differed from Gillies & Alper (136) in being unable to effect chloramphenicol rescue of this strain without preliminary incubation in chloramphenicol-free medium. Doudney, however, treated the irradiated cells for a maximum time of 160 min., and his results are therefore not in conflict with those of Gillies & Alper, since they had observed a drop in the viable counts, from UV-irradiated logarithmic-stage cells, after short periods of chloramphenicol treatment; the maximum rescue could be achieved only by treatment times of about 8 hr., after the higher UV doses used.

Korogodin & Malumina (81) observed that if diploid yeast (*Saccharomyces vini*) was maintained in sterile tap-water for 24 to 48 hr. after x-irradiation, many more colonies were formed; effectiveness of the radiation was reduced by a factor of about 2.5. They controlled the possibility that viable

cells may have been stimulated to divide in the water because of the release of nutrients from lysed cells. With a haploid strain, *Zygosaccharomyces Bailii*, postirradiation incubation in water did not increase the fraction of cells able to form colonies (76, 77).

In recent years the modification of UV-induced mutations in micro-organisms has aroused considerable interest. Doudney & Haas (157, 158) concluded that two processes were involved in establishing reversions in a tryptophan-requiring strain of *E. coli*. "Mutation fixation" corresponded in its time relationships to RNA synthesis, while "mutation expression," an event occurring later in time, was correlated with DNA syntheses [Haas & Doudney (159)]. These results, as well as previous work on the postirradiation modification of UV-induced mutation, were reviewed by Catcheside (160).

Klingmüller (161) failed to find any alteration, by soaking seeds in 2.5 per cent cysteine or 0.8 per cent cysteamine, in the effect of x-rays on viability, root growth, mitotic index, or differentiation in root tips. His results are therefore at variance with those of Künkel & Schubert (162). It should be noted, however, that Klingmüller delayed soaking the seeds for 41 hr. after irradiation whereas Künkel & Schubert had reported a decreasing activity of cysteine, the longer application was delayed. An investigation of the action of cysteine applied to pea seeds after irradiation was carried out by Luchnik & Tsarapkin (163). The seeds were exposed to 15,000 r and then soaked for 24 hr. Half the seeds were treated with cysteine for 4 to 6 hr. during this period; the concentration of cysteine and the timing of the treatment were not stated. Chromosomal aberrations in root tips were counted in anaphase, at the first mitosis, and classified according to type. For all types, more than twice as many abnormalities per anaphase cell were seen in the untreated material. A further difference was seen in the ratio of bridges to fragments, which was twice as great in the cysteine-treated material. Engelhard *et al.* (164) reported that cysteine added to suspensions of *Saccharomyces cerevisiae* after irradiation decreased the lethal effect and also the effect on diffusion of sodium ions across the membrane. Inhibition of anaerobic glycolysis, which resulted from irradiation, was not modified by cysteine. Examples were given earlier of the modification of radiation effects by anoxia after irradiation, and cysteine can act as an efficient means for removing oxygen from aqueous solutions [Gray (165)]. In this connection, the striking effects obtained by Luchnik & Tsarapkin (163) may perhaps be compared with those of Shapiro *et al.* (150) and the earlier observations of Adams & Nilan (166). It should be noted that Luchnik & Tsarapkin observed no effect of cysteine applied after irradiation to pea seedlings, in contrast to the effect with seeds.

Daniels & Vogel (167) found that amoebae exposed to 15 kilorads of fission neutrons died within 10 days. Nonirradiated amoebae were separated by centrifugation into three fractions, and fusion with the lightest and heaviest thirds enabled 13 and 96 per cent respectively of the irradiated amoebae to survive and to originate clones. It is interesting that treatment which gave the highest survival was associated with the longest delay to the first division.

The lethal effect of x-rays on yeast was reduced by subsequent exposure to UV [Elkind & Sutton (121)]. In the examples they gave, the x-ray exposures were large enough to kill effectively all the sensitive interdivisional cells, so that the effects of subsequent UV exposure were on the resistant dividing cells. The most effective doses were of the order of 400 ergs/mm², which increased the fraction of cells surviving the x-rays by a factor of 3 or 4 and was thus tantamount to reducing the effectiveness of the x-ray dose by about one-fourth. Gol'dat & Alikhanyan (120) observed an analogous effect with spores of *Streptomyces aureofaciens*. A restoring action of UV was noted both for lethal effects and for mutation induction. The extent of the effect varied with the time lapse between the x-ray and the UV exposures.

It is common practice to refer to a diminution in damage caused by post-irradiation treatment as "recovery." Unless there is evidence of repair mechanisms, however, it appears equally valid to consider that radiation damage may be latent, and may or may not be brought to light, depending on the conditions imposed on the cell. Luchnik & Tsarapkin (163) referred to the latent damage in dormant seeds, which later manifested itself as chromosome aberrations. The development of latent damage in cells has been very well illustrated in a paper of Shapiro (168), who examined chromosome aberrations in regenerating livers of rats which had received 500 r to the whole body. In a series of experiments, hepatectomies were performed one day, two months, and four months after irradiation. In another experiment, a dose of 500 r was given in two halves, separated by seven days, and hepatectomy performed one day after the second exposure. Finally, a hepatectomy was performed one day after irradiation, and a second one 30 days later. Animals were sacrificed 30 hr. after hepatectomy, and the abnormal anaphases and telophases counted. In all series of experiments except the one involving the double hepatectomy, about 60 per cent of the cells showed abnormalities, the results being the same, within experimental error, at whatever time hepatectomy had been performed. The rats which were killed after the second hepatectomy showed 26 per cent of anaphase cells with abnormalities. This study has put on a quantitative basis an observation of Koller [reported by Holmes & Mee (169)] that regenerating rat livers showed high numbers of cells with abnormalities, if the animals had been irradiated before hepatectomy. An analogous observation on thyroid tissue was made by Doniach & Logothetopoulos (170). It is of very great interest that the law of Bergonié & Tribondeau [whose paper of 1906 was recently translated by Fletcher (171)] should apply to tissues which are classed as "insensitive."

Latent damage was the subject also of two papers by Baldwin & Salthouse (172, 173) on radiation effects in the blood-sucking insect *Rhodnius prolixus*. Normally the cells of the epidermis start to enlarge within a day or two after feeding; mitosis begins on about the fifth day. An area of the abdomen 1.6 mm. in diameter was exposed to 50,000 r, and after the insects had been fed it was observed that there was an excess of cells in prophase and metaphase; evidence of cell destruction appeared in the ninth and tenth days. Even when the insects were kept without food for three months, the course of develop-

ment of x-ray damage was the same. An interesting form of latency in radiation effects was demonstrated by Cather (174), who studied cleavage delay in eggs of a snail, *Ilyanassa obsoleta*. Radiation induced a delay in the time to first cleavage, which became smaller, the nearer to first cleavage the radiation was given; correspondingly, the delay until second and third cleavages was prolonged. For example, if irradiation took place in early interphase, about 95 min. before first cleavage normally occurred, there was 25 min. delay in the time to first cleavage, 5 min. to the second, and 15 min. to the third. If the eggs were irradiated in metaphase, 30 min. before the normal first cleavage, the corresponding delays were respectively 0 min., 22 min., and 15 min. The metaphase stage would have been judged as "insensitive," if the test was delay to first cleavage, but when second and third cleavage delays were taken into account, the over-all damage was approximately the same at all division stages.

BIOCHEMICAL INVESTIGATIONS

LEAKAGE THROUGH CELL WALLS AND RELATED EFFECTS

Cellular metabolism after high doses (10 to 200 kilorads) was studied by Bresciani *et al.* (175), who used isolated rat diaphragm, rat liver, and frog heart. They measured changes in oxygen consumption, in the rate of anaerobic glycolysis, and in electrolyte balance of the cell and concluded that the metabolic changes observed were due mainly to alterations in the K/Na ratios. Anaerobic glycolysis was thought to be inhibited mainly because of loss of K. They disagreed with the mechanism proposed by Maass *et al.* (176), who had related inhibition of anaerobic glycolysis to a reduction in concentration of diphosphopyridine nucleotide, with consequent effects on carbohydrate metabolism and protein synthesis. Bresciani *et al.* (175) considered that a reduction in diphosphopyridine nucleotide concentration could not account for the increase in oxygen consumption which they observed within the first hour after doses in the range 10 to 200 kilorads; they ascribed all the metabolic effects rather to the alteration in the electrolyte balance within the cell.

The effect of x-rays on Na diffusion out of yeast cells was investigated by Engelhard *et al.* (164) by growing *Saccharomyces cerevisiae* in such a way that the K normally present was replaced by Na. In such cells the Na readily diffuses out in a solution of KCl, and irradiation increases the rate of loss of Na. This was found to be a less sensitive test than inhibition of cell division, about four times the dose increment being required to produce the same relative change in the effect. The inhibition of anaerobic glycolysis, unlike the other two effects studied, was not affected by the addition of cysteine after irradiation. No attempt to control the gas phase was mentioned, and the results suggest the possibility that both killing and increase in rate of ion transport were affected by oxygen depletion, whereas inhibition of anaerobic

glycolysis was not. Trinchler (177) subjected erythrocytes to doses up to 300 kilorads and observed alkaline hemolysis thereafter. Only the latent period preceding hemolysis was dose-dependent, the time before onset varying between 100 min. after 300 kilorads to 400 min. in the control cells. The results suggested to the author that the erythrocyte membrane contained a number of radiosensitive sites which acted as separate targets. A different type of cell-wall effect, the adsorption of colloidal ^{110}Ag , was found by Ivanitzkaia (178) to be affected at much lower doses. Both erythrocytes and ascites tumour cells, given 1000 r in suspension, demonstrated reduced uptake of the colloid at about 4 hr. after irradiation, the effect increasing with time to 24 hr. The effect was due to the irradiation of the cells, and not of the suspending medium. Comparison of irradiated cells with controls maintained at 0°C . led the author to conclude that the change in adsorption was related to a metabolic change in the cells.

EFFECTS ON ENZYMES IRRADIATED WITHIN THE CELL

A new method of looking at effects of radiation on enzyme systems was described by Pauly (179). In the strain *Bacterium cadaveris*, lysine decarboxylase could be induced in nongrowing cells by treatment with *L*-lysine, the activity increasing linearly with time until a maximum was reached. X-rays reduced both the rate of increase in enzyme activity and the final level, dose-effect curves for both types of damage being exponential in form. Pauly explained the results by postulating that cells contain one or several synthetic centres, each capable of producing a limited number of enzyme molecules. The dose required to reduce the rate of increase, or the final activity, by 37 per cent was 70 kilorads, and conventional target-size calculations yielded a target of molecular weight 20×10^6 . Pauly postulated that this referred to a nucleic acid structure on which the enzyme system was dependent. The inactivation dose for the enzyme molecule itself was quoted as 14 megarads. Similar relationships between the radiosensitivity of induction of β -galactosidase and of the enzyme molecule itself were quoted as a personal communication from Novick. A paper by Pollard & Barrett (180) gave the inactivation dose for β -galactosidase by ^{60}Co γ -rays as four megarads. The object of the investigation, carried out by irradiating cells of *E. coli* with radiations of various qualities, was to determine by this means the molecular weight of the enzyme. The result agreed well with determinations by other methods. A very interesting aspect of the work was the result that the inactivation dose for the enzyme was the same, whether the cells were irradiated in the wet or the dry state. [See also Laser & Thornley (74), reviewed in a previous section.]

NUCLEIC ACID SYNTHESIS AND RELATED TOPICS

Atwood (31) quoted some experiments with various cell types in which radiation did not affect DNA synthesis in the dose range that left only very

small surviving fractions. Another such report has been made by Whitfield & Rixon (181), who worked with L-strain (mouse fibroblast) cells in liquid culture. DNA synthesis proceeded when cell division was inhibited, whether by radiation or by simple dilution into fresh medium. When the premitotic level of DNA was reached, synthesis stopped until cell division had taken place. In one series of experiments DNA, RNA, and protein content, as well as cell counts, were measured 72 hr. after graded doses of radiation and compared with nonirradiated controls. Cell counts in liquid culture include non-viable as well as viable cells, and the dose-effect curve cannot therefore demonstrate as great a sensitivity as conventional "survival curves." Nevertheless, the effect of the radiation on cell counts made in this way was greater than on DNA or RNA synthesis, while protein synthesis was the least affected. After a dose of 4000 r all cell division was stopped, but DNA synthesis was only temporarily inhibited; it was resumed again, and the average DNA content per cell increased until premitotic level was reached, whereafter no more synthesis took place. [See also Stuy (58), reported in a previous section.]

Lymphatic cells and Ehrlich ascites tumour cells were used by Sibatani (182) to follow DNA and RNA synthesis after irradiation, uptake of ^{32}P being the index. The effects of 800 r of x-rays were not so pronounced as those of specific inhibitors of nucleic acid synthesis, such as arsenate, and could not be observed so soon after treatment. Jaffe *et al.* (183) assayed deoxyribose, deoxyribonucleosides, and deoxyribonucleotides in regenerating liver and followed DNA synthesis by ^{32}P uptake, doses of 200 and 400 r having been given 12 hr. after partial hepatectomy. Irradiation produced a rise in deoxyribonucleoside level for the first 12 hr., associated with delay in the appearance of deoxyribonucleotides. It was concluded that DNA synthesis was inhibited through an effect on induction of thymidilic kinase, rather than by inactivation of the existing enzyme. Okada & Hempelmann (184), using the same test system, found some increase in the enzymes concerned with thymidine degradation 24 hr. after irradiation, and an almost complete block in the DNA-synthesizing system. Thymidine phosphorylase in the irradiated regenerating liver was reduced to the level found in normal (non-regenerating) liver.

The observations of Lajtha *et al.* (185), made on bone-marrow cells in culture, have been roughly confirmed for *in vivo* conditions by Uyeki *et al.* (186), using Feulgen microspectrometric measurements of DNA in rabbit bone-marrow nuclei. They based their adopted standard for the "diploid" amount of DNA, 6.10^{-9} mg./nucleus, on observations on liver cells, in which the great majority of cells contained that amount of DNA or less. Bone-marrow nuclei showed a normal distribution of DNA, up to values about twice the diploid value; those which contained more than 6.10^{-9} mg./nucleus were considered to be synthesizing DNA in preparation for division. Effects of 800 r were assessed by irradiating half the animal and comparing DNA contents of nuclei from irradiated and control femurs at various times after

irradiation. The first measurable differences were observed 24 hr. after irradiation; there was then an increase in the proportion of nuclei containing only the diploid amount of DNA, which the authors interpreted as indicating a decrease in the number of synthesizing nuclei. They observed no differences in the DNA content of erythroblasts from control and irradiated limbs, although the DNA in the nuclei was in the diploid-tetraploid range.

Recently, techniques have been developed for handling isolated cell nuclei in such a way that they are able to carry out a variety of biochemical functions [see Allfrey *et al.* (187)]; such material has obvious advantages for the radiobiological investigator. Errera *et al.* (188) and Logan *et al.* (189) used autoradiographic methods for estimating uptake of adenine and phenylalanine labeled with ^{14}C , as guides to the synthesis of nucleic acids and proteins. Doses of 50, 300, and 900 r to thymus nuclei had about the same effect, in that RNA synthesis was 40 per cent less than in the controls 2 hr. after irradiation. Protein synthesis was affected from the earliest time of measurement, and incorporation of the phenylalanine had ceased by 30 min. The effects of 300 r on rat-liver nuclei were somewhat different, uptake of both adenine and phenylalanine being inhibited. The addition of microsomes to the preparation of nuclei enhanced the uptake of the labeled compounds: irradiation had the same effect, whether it was delivered to microsomes, to nuclei, or to both together. The relevance of these results to biological effects such as chromosome aberration and cell death cannot be assessed, since neither of the types of nuclei used lends itself to examination of these particular effects. Logan (190) measured the uptake of various nucleic acid precursors, all labeled with ^{14}C , in irradiated and control nuclei. A dose of 300 r suppressed the uptake of precursors, but at 2 hr. after irradiation no differences were detected in the DNA or RNA content of irradiated and control preparations.

A nuclear enzyme system first described by Osawa *et al.* (191), nuclear phosphorylation, was found by Creasey & Stocken (192) to be very sensitive to radiation. Animals were irradiated, and nuclei isolated as soon as possible from lymph node or bone marrow suffered complete inhibition in the formation of labile phosphates after 25 r; from spleen, after 50 r; and from thymus gland, after 100 r. Preparations of nuclei were irradiated also *in vitro*, in which state the sensitivity was even higher. Nuclei from thymus glands of rats injected with cysteamine (150 mg./kg. body weight) and exposed to 100 r showed less inhibition of nuclear phosphorylation after 1 hr. than nuclei from unprotected rats, and more rapid recovery. No protection by cysteamine or glutathione of preparations irradiated *in vitro* could be demonstrated with concentrations low enough not to inhibit the enzyme system, but some protection was afforded by anoxia. The authors made a point of the clear separation between "radiosensitive" and "radio-insensitive" tissues in demonstration of this type of enzyme action. For example, it was not observed with nuclei of normal liver cells. However, the observations of Koller

(169) and of Shapiro (168) with regenerating liver, and of Doniach & Logothetopoulos (170) with thyroid tissue show that, at least as far as radiosensitivity is concerned, the distinction is rather between nondividing and dividing cells, since "insensitive" cells may carry latent damage for months and will prove to have been "sensitive" if they are induced to divide. It seems debatable whether nuclear oxidative phosphorylation is in fact characteristic of radiosensitive cells or whether both the enzyme system and the radiosensitivity are characteristic of dividing cells.

Rappoport & Sewell (193) proposed that mammalian erythrocytes might be used as an indicator of radiation effects, since they were able to observe changes in utilization of various nucleic acid precursors after 500 and 1000 r whole-body irradiation. Katchman *et al.* (194) and Spoerl *et al.* (195) studied changes in phosphorus metabolism of yeast cells undergoing continuous irradiation. Katchman *et al.* found that nitrogen mustards as well as irradiation caused a decrease in orthophosphate, insoluble polyphosphate, and DNA-P, whereas RNA-P and lipid P showed no changes. Spoerl *et al.* found that ^{32}P uptake into insoluble phosphates was greater in irradiated than in nonirradiated cells, while uptake into soluble polyphosphates was decreased; transfer of the cells to fresh medium before irradiation caused these effects to be reversed. [See also Spoerl & Looney (82), reviewed in a previous section.]

On the whole, RNA has received less attention than DNA in its relationship to radiation effects. Drakulić (196) described the effects of UV (900 ergs/mm.²) on the synthesis of RNA in cells of *E. coli* B. Synthesis was followed by uptake of ^{14}C -adenine; at given times, samples were taken from the culture, and protoplasts formed which were subjected to osmotic shock. After irradiation, adenine incorporation was decreased in the particulate fraction of the RNA but increased in the soluble RNA. It was suggested that some of the particulate RNA synthesized early during the postirradiation period became soluble, perhaps because a conjugated protein failed to be synthesized. Results with a promising new technique were described in abstract by Pollard & Kennedy (197). Products of irradiated cells of *E. coli* B were analysed by ion exchange; 60 kr reduced the amount of phosphate uptake in the fraction corresponding to the larger ribosomes. There were indications that the ribosomes were capable of partial but not final protein synthesis and that the most sensitive mechanism was that which transformed phosphate into RNA and incorporated it into the particulate fraction.

EVIDENCE AND SPECULATIONS ON RADIOBIOLOGICAL MECHANISMS

RADIOSENSITIVITY AND DIVISION STAGE

Although there is evidence demonstrating variation in radiosensitivity with cell cycle in higher organisms, it is perhaps not always appreciated that

this rests on experiments performed with specialized germ cells, which are particularly suitable material for investigating this parameter. The assumption is frequently made that such evidence applies also to somatic cells and is independent of criterion of damage. Observations on the effect of radiation on DNA synthesis have led experimenters [e.g. Lajtha *et al.* (185)] to deduce that the extent of the effect is very dependent on division stage, but the attribution of a similar dependence of "radiosensitivity," in general, seems unwarranted, particularly since Lajtha *et al.* noted that their test of radiation effects was not related to cell death. Some recent results suggest that in fact lethal effects of radiation on somatic cells, and perhaps also morphological effects, are independent of the division stage at which the cells are irradiated. Hewitt & Wilson (50) found that survival curves for mouse leukemia cells were exponential to surviving fractions of less than 10^{-6} ; their data would have permitted detection of a resistant fraction of less than 10^{-3} of the original population. By the test of Lajtha *et al.* (185) only the cells in the pre-synthetic period were "sensitive"; about 40 per cent were not in this stage and were therefore "resistant." Simpson's (48) methods allowed her to observe failure of mast cells to reproduce, and survival curves were exponential to a level of 4 per cent surviving cells, which was as far as dose effects could be followed. Other survival curves taken on somatic mammalian cells have also revealed no evidence of resistant fractions of the population [Puck *et al.* (46); Elkind & Sutton (39)]; yet all these varied types of mammalian cells were heterogeneous as regards division stage when they were irradiated.

If, as many believe, higher cells lose their ability to reproduce mainly because the radiation induces chromosomal defects, then the evidence quoted in respect of the one test should apply also to the other. However, there is more direct evidence that the response of somatic cells is independent of the stage in the cell cycle, in regard to chromosomal aberrations observed at the mitosis following irradiation. Revell's (198) examination of the effects of 50 r on root-tip cells of *Vicia faba* led him to conclude that there are "no appreciable fluctuations in the incidence of any real chromatid aberrations," i.e. with the stage of cell development before mitosis. Deschner & Gray (128) presented timing curves showing the incidence of abnormal anaphases in irradiated ascites tumour cells during the period 6 hr. to 24 hr. after irradiation; particularly when the cells were irradiated at 37°, the curves were rather flat, with a variation in incidence of at most 2 to 1 over the period 6 hr. to 24 hr.

Revell (198) found that no abnormal anaphases appeared in the bean-root cells for the first 2 hr. after irradiation; and a dose of 50 r to the roots did not lower the rate of progress of cells which were within 2 hr. of going into metaphase. He concluded that chromatid aberrations could not be induced in cells in which prophase had begun. Various investigations with microbeams, exemplified by those of Munro (199) and of Smith (200), have shown that very large doses of radiation can be delivered to mitotic chromosomes with-

out affecting their ability to proceed from one phase to the next. According to Munro, cells in anaphase, in which chromosomes were exposed to as much as 16 to 117 α -particles/ μ^2 , did not suffer inhibition of nuclear reconstruction, and the first nuclear membrane appeared at the normal time. It might be argued from such experiments that the cell is indeed very "insensitive," once it has entered prophase, regardless of the evidence relating to cell survival. However, no experiments appear to have been done in which individual somatic cells irradiated while already in mitosis have been followed through to the next one. It is relevant to recall the experiments of Cather (174), in which snails' eggs irradiated in prophase showed little or no delay until the first cleavage, and were therefore "insensitive," by that test. However, they showed a considerably greater delay to second cleavage than eggs irradiated at earlier stages.

CHEMICAL PROTECTION

It has long been recognized that at least some of the chemical protective agents exercise their effects by inducing anoxia in cells by one means or another, and the realization that radiosensitivity may be affected by what were previously regarded as negligible amounts of oxygen has underlined the desirability of rigorous control of this aspect of protection, wherever possible. The pitfalls of using actively respiring cell suspensions without careful precautions for equilibration with an oxygen-containing gas phase were described by Deschner & Gray (128), and the pitfalls of working with organized tissues in "anoxic" conditions which are in fact not rigorously anoxic were described by Kihlman (129). All work in the chemical protection field which controls the possibilities of hidden oxygen effects is therefore to be welcomed.

The difficult task of measuring oxygen tension in mouse spleens was undertaken by van der Meer & van Bekkum (201) in an attempt to elucidate the protective action of certain biological amines. They had found protective and pharmacological action to be related but could not correlate protective activity with an effect on blood pressure. When they measured the effect on spleen oxygen tension of the ten drugs they used, however, they found very good correlation between protective ability and induction of anoxia in the mouse spleens. Thus, epinephrine was a good radiation protective agent, while norepinephrine was not. Both drugs increased the arterial blood pressure to the same extent, but epinephrine markedly reduced spleen oxygen tension, while norepinephrine did not. Another aspect of the same phenomenon was illustrated by strain differences: histamine exerted a smaller protective effect on C57 *Bl.* than on CBA mice, and it required 10 mg. histamine to reduce spleen oxygen tension in C57 *Bl.* to the same extent as was observed with 0.1 mg. in the CBA mice. Reducing the oxygen content of the inspired air, which exerted a radioprotective action, also caused a fall in spleen oxygen tension. The hypothesis that 5-hydroxytryptamine acts protectively by inducing hypoxia was favoured by van den Brenk & Moore

(202). They exposed protected rats to radiation under an oxygen pressure of 4 to 5 atm. and found that the drug was then no longer protective. On the other hand, the high oxygen pressure failed to reverse the action of cysteamine. It was suggested briefly by van der Meer & van Bekkum (201) that cysteine and cysteamine may act protectively in the animal by a somewhat different mechanism from drugs which are now known to induce spleen hypoxia, and the same suggestion comes from a reference by Ardashnikov (203) to work of Graevskii, who measured the oxygen tension in organs and tissues (animal not stated): this was lower than normal under the action of carbon monoxide, epinephrine, and heroin but not under cysteine and cysteamine.

Studies on the interrelationship between these two drugs and oxygen concentration are still at variance, as far as work with cell suspensions is concerned. Salerno & Friedell (204), in an abstract, reported that the protection afforded to U12 fibroblasts by cysteine could be abolished by simultaneous exposure to oxygen under pressure. They quoted an oxygen enhancement ratio of 4.5 for these cells. On the other hand, co-workers Kohn & Gunter (205) found that 0.1 M *L*-cysteine reduced the effectiveness of radiation (delivered to aerobic but unstirred suspensions of *E. coli* B/r) by a factor of five, and considered that the protection was greater than could be accounted for by induced anoxia, since an enhancement ratio of three for this strain had been measured by other investigators. It was necessary to follow a rigorous procedure for incubating the cells with the cysteine in order to attain the protective effect. Kohn & Gunter (206) reported later on the results of irradiating *E. coli* B/r under different oxygen concentrations, in the presence and absence of *L*-cysteine; it increased the 37 per cent dose in anoxic and also in well-oxygenated conditions.

Earlier investigations have also given conflicting results on the question whether the protective effect of cysteamine on cells in suspension is more than can be attained by anoxia alone. Hollaender & Stapleton (207) reported that it did; Wood (208) quoted preliminary results with haploid yeast giving dose reductions factor of 1.8 ± 0.1 by anoxia and of 2.2 ± 0.1 by anoxia plus cysteamine, so the additional effect is of doubtful significance; Marcovich (209) and Alper (unpublished) found that anoxia plus cysteamine did not protect *E. coli* B/r to a greater extent than anoxia alone. It might be relevant that Smaller & Avery (30) found e.s.r. signals from yeast to be changed by the presence of cysteamine, but in concentration 0.06 M it did not affect the signals, and 0.3 M was required to reduce them by one-half. Concentrations of much less than 0.06 M are toxic to bacteria [Baldini & Ferri (210)], to suspensions of cell nuclei [Creasey & Stocken (192)], and to freshly harvested yeast (Alper, unpublished); and Hollaender & Doudney (211) found that the maximum level of protection of *E. coli* B/r is attained with cysteamine at 0.006 M. The mechanism of cysteamine protection of cells in suspension must therefore be regarded as unsettled. Todorov & Robev (212) reported investi-

gations with a variety of substances as protective agents for a strain of *E. coli*. There was no attempt at gas control, and survival curves are suggestive of gradual oxygen depletion in the unprotected suspensions.

Lycopene, a substance with some interesting properties, was reported as a protective agent for mice by Forssberg *et al.* (213). It is insoluble and is injected as a suspension. It acted as a protective agent if given 24 hr. before or after irradiation but as an enhancing agent if given after 7 hr. It was suggested that part of its protective effect might be by prevention of bacteraemia, but it was also found to accelerate haemopoietic recovery. In another paper it was reported to confer on mice resistance to bacteria and to the growth of ascites tumour cells, and also to protect growing tumours [Lingen, Ernster & Lindberg (214)].

Cysteine protects against the induction of cataract, and Pirie & Lajtha (215) proposed a mechanism of action which was based on two observations: an injection of 1 gm./kg. of cysteine, without irradiation, inhibited mitosis in the epithelial cells of the rabbit lens; and cysteine in a concentration of 1 mM (which was calculated to be that reached in the aqueous humour of the eye) depressed DNA synthesis in bone-marrow cultures by 60 to 80 per cent. It was suggested that cysteine prevents the cells from reaching a radiosensitive stage by depressing DNA synthesis before that stage is reached. This hypothesis depends on the assumption that cells vary in their sensitivity to the lethal effects of radiation as they proceed through the cell cycle; data on other somatic cell types make such a variation unlikely (see previous section). The mechanism proposed by Pirie & Lajtha would also imply that only a small fraction (less than 1 per cent) of cells could be affected in this way by the cysteine, since it is protective if given 0.5 hr. before irradiation whereas the whole cell cycle takes several days. It would follow that, at any given time, the total number of radiosensitive cells, on which cataract induction depends, must also be rather small, otherwise cysteine could not have a significantly protective effect. Such a conclusion appears inconsistent with the results of Pirie & Drance (216), who were able to map the irradiated area of a partly shielded lens by observing cell depletion and numerous fragmental nuclei, even 28 days after irradiation. Unshielded lenses showed more damage still.

MECHANISM OF CHROMOSOME BREAKAGE

The main purpose of Revell's investigation (198) was to test the hypothesis that true chromatid exchanges are structurally established at a stage which is later in time than the crossing of the chromosomes by an ionizing particle. On this hypothesis, chromosome abnormalities are a consequence of interaction between parts of the same or of neighbouring chromatids, which are in contact at or near the point where the particle crosses. Revell believes that some aberrations conventionally classed as chromatid or isochromatid breaks can be shown to be "intrachanges," i.e. exchanges between neigh-

bouring points on the same chromosome; by Revell's hypothesis, all true aberrations must be due either to this type of exchange or to "complete" exchanges between chromatids of different chromosomes.

According to Revell, the most striking difference in prediction between his hypothesis and the conventional "breakage first" hypothesis would lie in the ratio of breaks to exchanges, which should be much lower by the former hypothesis. By Revell's method of scoring, this was indeed the case, and he attributed contrary results in the literature to the scoring at metaphase of unstained "gaps" which, he maintained, were not true discontinuities in the chromatid. When he excluded these, the number of "real" chromatid breaks was lower than the number of isochromatid breaks, minutes, or interchanges throughout the period of 6 hr. after irradiation during which aberrations were observed. On the other hand, the numbers of "gaps" scored both at metaphase and at anaphase were considerably higher than any other type of aberration. Revell considered that the distinction he drew between gaps and real breaks was supported by the large excess of metaphase gaps over chromatid fragments seen at anaphase and by the fact that gaps were visible at anaphase in obviously unbroken chromosomes. Previously, Neary & Evans (217) had stated that their results supported Revell's hypothesis.

Sire & Nilan (151) examined the effect of storing seeds of *Crepis capillaris* in O₂ under pressure, assessing this by scoring aberrations at metaphase in the first mitotic division. This material is very favourable for morphological observation, since there are only 6 chromosomes in the diploid cell, and one of them has a long arm of 6 μ . The large majority of breaks leading to dicentric chromosomes occurred in or near the heterochromatic regions; "simple" breaks, on the other hand, were found mostly in the euchromatin. With increasing exposure of the seeds to oxygen the pattern remained the same, all types of aberration being increased uniformly. The authors suggested that the original breakage occurred at random, but the broken ends in the euchromatin "healed," so the rejoining was differentially inhibited.

LETHAL ACTIONS OF RADIATIONS ON CELLS

As in previous years, several authors have been inclined to attribute the lethal effects of ionizing radiations to lesions in genetically important DNA [e.g. Puck (4); Woese (40); Billen (116)]. Difficulties in sustaining this postulate have been discernible for some time [see Alper (218)] and have been emphasized by some of last year's results. Stuy (58), for example, demonstrated a clear-cut separation between the effects of radiation on cell death and on the inactivation of functional DNA. It is an important part of his investigation that replication of Transforming Principle could continue even after doses which left only a very small fraction of cells able to originate colonies. Deering's experiments (34) also are difficult to reconcile with the concept that cell death results primarily from lesions in the genetically important DNA. If the increased DNA content of the filamentous cells resulted

from reduplication of genetically important DNA, the exponential nature of the survival curves, as well as the increased sensitivity of the filaments, is in conflict with the view that such reduplication should confer increased resistance. If the increased DNA content is genetically unimportant but is still implicated in the cell killing, it is difficult to see why sensitivity should ordinarily be related to genetically important DNA.

In the course of the symposium on yeast held at the First International Congress of Radiation Research, Magni (219) showed that factors other than dominant or recessive lethals must be involved in cell death. Beam (220) had found that the radiosensitivity of yeast cells decreased markedly when mitotic prophase had begun. His discussion was based on the point of view that the sensitivity of the interdivisional cell implicates the nucleus, i.e. the genetic apparatus, and that the nucleus of the dividing cell is relatively "invulnerable." Alper (140) inferred that there must be a change in the nature of the main target of damage, once budding has begun, since the oxygen enhancement ratio changes markedly, and at the same time, according to Elkind & Beam (101), the relative effectiveness of α -particles and x-rays changes.

It is widely postulated that, in higher cells, death occurs as a result of defects induced in chromosomes. The data of Neary *et al.* (104) and Evans *et al.* (103) support the existence of a close link between cell death and chromosomal aberrations, since RBE values and oxygen enhancement ratios were similar for the two criteria of damage. On the other hand, the observations of Elkind & Sutton (39), discussed in a previous section, suggest that there may be a primary lesion for cell death which is not specifically chromosomal. It is also apparent from their results that the shape of the survival curve is not necessarily determined by the ploidy of the cell.

The question whether diffusing intermediates, particularly the radiolysis products of water, play an important part in the lethal effects of radiation has not been much discussed in 1959. Mookerjee (221) published survival curves for yeast irradiated dry and in aqueous suspension, and attributed the higher sensitivity of the wet yeast to "indirect action." Wood (9, 208), in two review papers, stated that this postulate appears to him the only one capable of explaining why sensitivity is reduced when cells are frozen or why it should be correlated with decreased water content of yeast cells. Such a correlation does not hold for all types of cell [see Alper (218) for references]; it is now well known that the reverse is true for seeds (222), an observation which was confirmed in 1959 by Sparrman *et al.* (19) and by Sicard & Schwartz (223). However, Wood's thesis that an increase in radiosensitivity is due to radiolysis products of water presents a grave difficulty, even if it is regarded as being applicable only to haploid yeast. As used by him, these cells appear to have the same radiobiological characteristics as the starved cells used in the experiments of Sinclair *et al.* (93) and of Sayeg *et al.* (95). Irradiations were carried out in aerobic conditions, in both instances; and Sinclair *et al.* found

the sensitivity to ^{60}Co γ -rays to be less than to 200 kvp x-rays, while Sayeg *et al.* found ^{210}Po α -particles to be the most effective of the different radiations used. The G_{OH} for these three radiations, as quoted by Burch (92), are respectively 2.85, 1.76, and 0.67, while the G_{H} values are 3.66, 3.33, and 0.77. In aerobic conditions, the yield of H_2O_2 decreases with increasing LET (224). If diffusible intermediates deriving from water are the agents of "indirect effects," it is difficult to see which species can be responsible for mediating the lethal action of radiation on starved haploid yeast.

LITERATURE CITED

1. Quastler, H., *Radiation Research*, **4**, 303-20 (1956)
2. Quastler, H., *Radiology*, **73**, 161-65 (1959)
3. Scott, O. C. A., *Advances in Biol. and Med. Phys.*, **6**, 121-73 (1958)
4. Puck, T. T., *Revs. Mod. Phys.*, **31**, 433-48 (1959)
5. Oakberg, E. F., *Radiation Research*, **11**, 700-19 (1959)
6. *Journal of Molecular Biology* (Academic Press, Inc., London and New York)
7. Zirkle, R. E., *Revs. Mod. Phys.*, **31**, 269-71 (1959)
8. Pollard, E., *Revs. Mod. Phys.*, **31**, 273-81 (1959)
9. Wood, T. H., *Revs. Mod. Phys.*, **31**, 282-88 (1959)
10. Tobias, C. A., *Revs. Mod. Phys.*, **31**, 289-96 (1959)
11. Sommermeyer, K., *Strahlenbiologie, Nuklearmedizin, Strahlentherapie und Krebsforschung*, 1-65 (Georg Thieme Verlag, Stuttgart, Germany, 1959)
12. Gray, L. H., *Lectures on the Scientific Basis of Medicine*, **VII**, 314-47 (Athlone Press, London, England, 496 pp., 1959)
13. Shchepot'eva, E. S., Ardashnikov, S. N., Lurie, G., and Rachmanova, T. B., *The Oxygen Effect in the Action of Ionizing Radiations* (Medgiz, Moscow, U.S.S.R., 185 pp., 1959)
14. Shapiro, N. I., *Med. Radiol.*, No. 2, 67-77 (1959)
15. Read, J., *Radiation Biology of Vicia Faba in Relation to the General Problem* (Blackwell Scientific Publications, Oxford, England, 270 pp., 1959)
16. Lea, D. E., *Actions of Radiations on Living Cells*, 2nd ed. (Cambridge University Press, Cambridge, England, 416 pp., 1955)
17. Timoféeff-Ressovsky, N. W., and Zimmer, K. G., *Das Trefferprinzip in der Biologie* (S. Hirzel Verlag, Leipzig, Germany, 317 pp., 1947)
18. Müller, A., and Zimmer, K. G., *Strahlentherapie*, **109**, 192-99 (1959)
19. Sparrman, B., Ehrenberg, L., and Ehrenberg, A., *Acta Chem. Scand.*, **13**, 199-200 (1959)
20. Caldecott, R. S., Johnson, E. B., North, D. T., and Konzak, C. F., *Proc. Natl. Acad. Sci. U. S.*, **43**, 975-83 (1957)
21. Curtis, H. J., Delihias, N., Caldecott, R. S., and Konzak, C. F., *Radiation Research*, **8**, 526-33 (1958)
22. Conger, A. D., and Randolph, M. L., *Radiation Research*, **11**, 54-66 (1959)
23. Pai-gen, Shen, Blumenfeld, L. A., Kalmanson, A. E., and Passinsky, A. G., *Biofizika*, **4**, 263-74 (1959)
24. Shields, H., and Gordy, W., *Proc. Natl. Acad. Sci. U. S.*, **45**, 269-81 (1959)
25. Rexroad, H. N., and Gordy, W., *Proc. Natl. Acad. Sci. U. S.*, **45**, 256-69 (1959)
26. Gordy, W., *Radiation Research*, Suppl. **1**, 491-510 (1959)
27. Boag, J. W., and Müller, A., *Nature*, **183**, 831-32 (1959)
28. Klingmüller, W., and Saxena, M. C., *Naturwissenschaften*, **46**, 475-76 (1959)
29. Klingmüller, W., Lane, G. R., Saxena, M. C., and Ingram, D. J. E., *Nature*, **184**, 464-65 (1959)
30. Smaller, B., and Avery, E. C., *Nature*, **183**, 539-40 (1959)
31. Atwood, K. C., *Ann. Rev. Nuclear Sci.*, **9**, 533-92 (1959)
32. Hollaender, A., Stapleton, G. E., and Martin, F. L., *Nature*, **167**, 103-4 (1951)
33. Zelle, M. R., and Hollaender, A., in *Radiation Biology*, **II**, 365-430 (McGraw-Hill Book Co., Inc., New York, N. Y., 593 pp., 1955)
34. Deering, R. A., *Biochim. et Biophys. Acta*, **31**, 11-19 (1959)
35. Lea, D. E., Haines, R. B., and Coulson, C. A., *Proc. Roy. Soc. (London)*, **B123**, 1-21 (1937)
36. Deering, R. A., *J. Bacteriol.*, **76**, 123-30 (1958)
37. Shekhtman, Ia. L., Plokhov, V. I., and Filippova, G. V., *Biofizika*, **3**, 479-86 (1958)
38. Alper, T., and Gillies, N. E., *J. Gen. Microbiol.*, **22**, 113-28 (1960)
39. Elkind, M. M., and Sutton, H., *Nature*, **184**, 1293-95 (1959)
40. Woese, C., *J. Bacteriol.*, **77**, 38-42 (1959)
41. Hill, E. C., and Phillips, G. O., *J. Appl. Bacteriol.*, **22**, 8-13 (1959)
42. Elkind, M. M., and Sutton, H., *Radiation Research*, **10**, 283-95 (1959)
43. Puck, T. T., and Marcus, P. I., *J. Exptl. Med.*, **103**, 653-66 (1956)
44. Hewitt, H. B., and Wilson, C. W., *Nature*, **183**, 1060-61 (1959)

45. Hewitt, H. B., and Wilson, C. W., *Brit. J. Cancer*, **13**, 69-75 (1959)
46. Puck, T. T., Morkovin, D., Marcus, P. I., and Cieciora, S. J., *J. Exptl. Med.*, **106**, 485-500 (1956)
47. Morkovin, D., and Feldman, A., *Brit. J. Radiol.*, **32**, 282 (1959)
48. Simpson, S. M., *Intern. J. Radiation Biol.*, **1**, 181-88 (1959)
49. Till, J. E., McCulloch, E. A., and Hall, A. E. D., *Radiation Research*, **11**, 473 (1959)
50. Hewitt, H. B., and Wilson, C. W., *Brit. J. Cancer*, **13**, 675-84 (1959)
51. Hjort, G. H., *Acta Radiol.*, **52**, 315-20 (1959)
52. Sharman, G. B., *Intern. J. Radiation Biol.*, **1**, 115-30 (1959)
53. Mandl, A., *Proc. Roy. Soc. (London)*, **B150**, 53-71 (1959)
54. Rubin, H., and Temin, H. M., *Virology*, **7**, 75-91 (1959)
55. Woese, C. R., *Arch. Biochem. Biophys.*, **79**, 55-66 (1959)
56. Woese, C., *Radiation Research*, **10**, 370-79 (1959)
57. Shapiro, N. G., Nenarokova, I. F., and Suslikov, V. I., *Biofizika*, **4**, 559-66 (1959)
58. Stuy, J. H., *J. Bacteriol.*, **78**, 49-58 (1959)
59. Pal, R., and Krishnamurthy, B. S., *Nature*, **184**, 658 (1959)
60. Ives, P. T., *Proc. Natl. Acad. Sci. U. S.*, **45**, 188-92 (1959)
61. Green, M. M., *Proc. Natl. Acad. Sci. U. S.*, **45**, 16-18 (1959)
62. Schabinski, G., Ahlendorf, W., and Schwabe, F., *Naturwissenschaften*, **46**, 268 (1959)
63. Wichterman, R., *Science*, **129**, 207-8 (1959)
64. Banić, S., *Caryologia*, **11**, 404-6 (1959)
65. Russell, W. L., Russell, L. B., and Cupp, M. B., *Proc. Natl. Acad. Sci. U. S.*, **45**, 18-23 (1959)
66. Oster, I. I., Zimmering, S., and Muller, H. J., *Science*, **130**, 1423 (1959)
67. Mole, R. H., *Intern. J. Radiation Biol.*, **1**, 107-14 (1959)
68. Nuzhdin, N. N., Shapiro, N. I., Pomerantzeva, M. D., and Kuznetsova, N. N., *J. Gen. Biol. (U.S.S.R.)*, **Ser. 3**, **20**, 216-29 (1959)
69. Abrahamson, S., *Genetics*, **44**, 173-86 (1959)
70. Lüning, K. G., and Henriksson, H. O., *Nature*, **183**, 1211-12 (1959)
71. Boag, J. W., and Miller, C. W., *Proc. Intern. Conf. Peaceful Uses Atomic Energy*, **2nd**, Geneva, 1958, **14**, 437-44 (1959)
72. Dewey, D. L., and Boag, J. W., *Nature*, **183**, 1450-51 (1959)
73. Yanders, A. F., *Radiation Research*, **10**, 30-36 (1959)
74. Laser, H., and Thornley, M. J., *Proc. Roy. Soc. (London)*, **B150**, 539-53 (1959)
75. Hermier, J., *Compt. rend.*, **249**, 195-97 (1959)
76. Korogodin, V. I., Malinowskii, O. V., Poryadkeva, N. A., and Izmozherov, N. A., *Cytologia*, **1**, 306-15 (1959)
77. Korogodin, V. I., and Ah-Shen, Liu, *Cytologia*, **1**, 379-86 (1959)
78. Beam, C. A., Mortimer, R. K., Wolfe, R. G., and Tobias, C. A., *Arch. Biochem. Biophys.*, **49**, 110-22 (1954)
79. Latarjet, R., in *Symposium on Radiobiology, The Basic Aspects of Radiation Effects on Living Systems*, 241-57 (John Wiley & Sons Inc., New York, N. Y., 465 pp., 1952)
80. Burns, V. W., *Radiation Research*, **4**, 394-412 (1956)
81. Korogodin, V. I., and Malumina, T. S., *Priroda*, 82-85 (1959)
82. Spoerl, E., and Looney, D., *Exptl. Cell Research*, **17**, 320-27 (1959)
83. Rudali, G., and Reverdy, J., *Compt. rend.*, **248**, 1248-49 (1959)
84. Rugh, R., and Grupp, E., *Am. J. Roentgenol., Radium Therapy Nuclear Med.*, **81**, 1026-47 (1959)
85. Lessler, M. A., *Science*, **129**, 1551-52 (1959)
86. Dawson, W. W., and Smith, J. C., *Science*, **129**, 1670-71 (1959)
87. Blum, H. F., *Science*, **130**, 1545-47 (1959)
88. Zirkle, R. E., in *Radiation Biology*, **I**, 315-50 (McGraw-Hill Book Co. Inc., New York, N. Y., 626 pp., 1954)
89. Conger, A. D., Randolph, M. L., Sheppard, C. W., and Luippold, H. J., *Radiation Research*, **9**, 525-47 (1958)
90. Rossi, H. H., *Radiation Research*, **10**, 522-31 (1959)
91. Rosenzweig, W., and Rossi, H. H., *Radiation Research*, **10**, 532-44 (1959)
92. Burch, P. R. J., *Radiation Research*, **11**, 481-97 (1959)
93. Sinclair, W. K., Gunter, S. E., and Cole, A., *Radiation Research*, **10**, 418-32 (1959)

94. Birge, A. C., and Sayeg, J. A., *Radiation Research*, **10**, 433-48 (1959)
95. Sayeg, J. A., Birge, A. C., Beam, C. A., and Tobias, C. A., *Radiation Research*, **10**, 449-61 (1959)
96. Danzker, M., Kessar, N. D., and Laughlin, J. S., *Radiology*, **72**, 51-61 (1959)
97. Krokowski, E., *Z. Naturforsch.*, **14b**, 304-6 (1959)
98. Brustad, T., and Henriksen, T., *Am. J. Roentgenol., Radium Therapy Nuclear Med.*, **81**, 509-11 (1959)
99. Ardashnikov, S. N., and Chetverikov, N. S., *Biofizika*, **3**, 494-515 (1958)
100. Oftedal, P., *Hereditas*, **45**, 245-331 (1959)
101. Elkind, M. M., and Beam, C. A., *Radiation Research*, **3**, 88-104 (1955)
102. Neary, G. J., Evans, H. J., Tonkinson, S. M., and Williamson, F. S., *Intern. J. Radiation Biol.*, **1**, 230-40 (1959)
103. Evans, H. J., Neary, G. J., and Williamson, F. S., *Intern. J. Radiation Biol.*, **1**, 216-29 (1959)
104. Neary, G. J., Tonkinson, S. M., and Williamson, F. S., *Intern. J. Radiation Biol.*, **1**, 201-15 (1959)
105. Spalding, F. J., Strang, V. G., and Sayeg, J. A., *Radiation Research*, **10**, 176-79 (1959)
106. Vogel, H. H., Jr., and Jordan, D. L., *Radiation Research*, **11**, 607-83 (1959)
107. Hornsey, S., Howard-Flanders, P., and Moore, D., *Intern. J. Radiation Biol.*, **2**, 37-44 (1960)
108. Edington, C. W., and Randolph, M. L., *Genetics*, **43**, 715-25 (1958)
109. Storer, J. B., Harris, P. S., Furchner, J. E., and Langham, W. H., *Radiation Research*, **6**, 188-288 (1957)
110. Brustad, T., Ariotti, P., and Barr, J., *Radiation Research*, **11**, 432 (1959)
111. Howard-Flanders, P., and Alper, T., *Radiation Research*, **7**, 518-40 (1957)
112. Lea, D. E., Haines, R. B., and Bretscher, E., *J. Hyg.*, **41**, 1-16 (1941)
113. Ehrenberg, L., *Radiation Research*, Suppl. **1**, 102-23 (1959)
114. Fabergé, A. C., *Genetics*, **44**, 279-85 (1959)
115. Billen, D., *Nature*, **184**, 174-76 (1959)
116. Billen, D., *Biochim. et Biophys. Acta*, **34**, 110-16 (1959)
117. Moh, C. C., and Withrow, R. B., *Radiation Research*, **10**, 13-19 (1959)
118. Moh, C. C., and Withrow, R. B., *Radiation Research*, **11**, 18-23 (1959)
119. Swaminathan, M. S., and Natarajan, A. T., *Science*, **130**, 1407-9 (1959)
120. Gol'dat, S. Yu., and Alikhanyan, S. I., *Soviet Phys. "Doklady,"* **4**, 286-88 (1959)
121. Elkind, M. M., and Sutton, H., *Radiation Research*, **10**, 296-312 (1959)
122. Wright, E. A., and Batchelor, A. L., *Brit. J. Radiol.*, **32**, 168-72 (1959)
123. Warburg, O., Gawehn, K., Geissler, A.-W., Schröder, W., Gewitz, H.-S., and Völker, W., *Naturwissenschaften*, **46**, 25-29 (1959)
124. Evans, H. J., Neary, G. J., and Tonkinson, S. M., *Exptl. Cell Research*, **17**, 144-59 (1959)
125. Baldwin, W. T., and Salthouse, T. N., *Nature*, **183**, 974 (1959)
126. Loiseleur, J., and Petit, M., *Compt. rend.*, **249**, 323-25 (1959)
127. Alper, T., and Howard-Flanders, P., *Nature*, **178**, 978-79 (1956)
128. Deschner, E. E., and Gray, L. H., *Radiation Research*, **11**, 115-46 (1959)
129. Kihlman, B. A., *J. Biophys. Biochem. Cytol.*, **5**, 481-90 (1959)
130. Evans, H. J., and Neary, G. J., *Radiation Research*, **11**, 636-41 (1959)
131. Crabtree, H. G., and Cramer, W., *Sci. Rept., Imperial Cancer Research Fund*, **11th**, 89-101; 103-17 (1934)
132. Hornsey, S., *Advances in Radiobiol.*, 248-54 (Oliver & Boyd, Edinburgh, Scotland, 500 pp., 1957)
133. Cater, D. B., and Weiss, L., *Nature*, **183**, 1521-22 (1959)
134. Weiss, L., *Nature*, **184**, 1156-57 (1959)
135. Weiss, L., *Brit. J. Radiol.*, **33**, 32-35 (1959)
136. Gillies, N. E., and Alper, T., *Nature*, **183**, 237-38 (1959)
137. Alper, T., and Gillies, N. E., *Nature*, **181**, 961-63 (1958)
138. Kimball, R. F., Gaither, N., and Wilson, S. M., *Radiation Research*, **10**, 490-97 (1959)
139. Powers, E. L., Webb, R. B., and Ehret, C. F., *Exptl. Cell Research*, **17**, 550-54 (1959)
140. Alper, T., *Intern. J. Radiation Biol.*, **1**, 414-19 (1959)
141. Howard-Flanders, P., *Nature*, **180**, 1191-92 (1957)
142. Gray, L. H., Green, F. O., and Hawes, C. A., *Nature*, **182**, 952-53 (1958)

143. Kihlman, B. A., *Exptl. Cell Research*, **17**, 588-90 (1959)
144. Powers, E. L., Kaleta, B. F., and Webb, R. B., *Radiation Research*, **11**, 461 (1959)
145. Ebert, M., Hornsey, S., and Howard, A., *Nature*, **181**, 613-16 (1958)
146. Chang, T.-H., Wilson, F. D., and Stone, W. S., *Proc. Natl. Acad. Sci. U. S.*, **45**, 1397-1404 (1959)
147. Pahl, G., and Bachofer, C. S., *Biol. Bull.*, **112**, 383-89 (1957)
148. Wolf, S., and Luippold, H. E., *Genetics*, **43**, 493-501 (1958)
149. Howard-Flanders, P., and Moore, D., *Radiation Research*, **9**, 422-37 (1958)
150. Shapiro, N. I., Bocharova, E. M., and Belitzina, N. V., *Doklady Akad. Nauk S.S.S.R.*, **126**, 191-94 (1959)
151. Sire, M. W., and Nilan, R. A., *Genetics*, **44**, 124-36 (1959)
152. Kimball, R. F., Gaither, N., and Wilson, S. M., *Proc. Natl. Acad. Sci. U. S.*, **45**, 833-39 (1959)
153. Litvinova, I. B., *Soviet Phys. "Doklady,"* **4**, 246-48 (1959)
154. Litvinova, I. B., *Soviet Phys. "Doklady,"* **4**, 249-51 (1959)
155. Powers, E. L., *Ann. N. Y. Acad. Sci.*, **59**, 619-37 (1955)
156. Doudney, C. O., *Nature*, **184**, 189-90 (1959)
157. Doudney, C. O., and Haas, F. L., *Proc. Natl. Acad. Sci. U. S.*, **45**, 709-22 (1959)
158. Doudney, C. O., and Haas, F. L., *J. Mol. Biol.*, **1**, 81-83 (1959)
159. Haas, F. L., and Doudney, C. O., *Proc. Natl. Acad. Sci. U. S.*, **45**, 1620-24 (1959)
160. Catcheside, D. G., *Phys. in Med Biol.*, **4**, 117-25 (1959)
161. Klingmüller, W., *Z. Naturforsch.*, **14b**, 268-72 (1959)
162. Künkel, H. A., and Schubert, G., *Progr. in Nuclear Energy, Ser. VI*, **2**, 217-24 (1959)
163. Luchnik, N. V., and Tsarapkin, L. S., *Soviet Phys. "Doklady,"* **4**, 236-39 (1959)
164. Engelhard, H., Schneewis, K. E., and Bülow, H., *Z. Naturforsch.*, **14b**, 152-57 (1959)
165. Gray, L. H., in *Progress in Radiobiology*, 267-73 (Oliver & Boyd, Edinburgh, Scotland, 557 pp., 1956)
166. Adams, J. D., and Nilan, R. A., *Radiation Research*, **8**, 111-22 (1958)
167. Daniels, E. W., and Vogel, H. H., Jr., *Radiation Research*, **10**, 584-96 (1959)
168. Shapiro, M., *Soviet Phys. "Doklady,"* **4**, 252-54 (1959)
169. Holmes, B. E., and Mee, L. K., in *Radiobiology Symposium 1954*, 220-24 (Butterworths Scientific Publications, London, England, 362 pp., 1955)
170. Doniach, I., and Logothetopoulos, J. H., *Brit. J. Cancer*, **9**, 117-27 (1955)
171. Bergonié, J., and Tribondeau, L. (Fletcher, G. H., transl.), *Radiation Research*, **11**, 587-88 (1959)
172. Baldwin, W. F., and Salthouse, T. N., *Radiation Research*, **10**, 387-96 (1959)
173. Baldwin, W. F., and Salthouse, T. N., *Radiation Research*, **10**, 397-99 (1959)
174. Cather, J. N., *Radiation Research*, **11**, 720-31 (1959)
175. Bresciani, F., Dose, K., and Rajewsky, B., *Z. Naturforsch.*, **14b**, 158-68 (1959)
176. Maass, H., Rathgen, G. H., Künkel, H. A., and Schubert, G., *Z. Naturforsch.*, **13b**, 735-41 (1958)
177. Trincer, K. S., *Biofizika*, **4**, 78-83 (1959)
178. Ivanitzkaia, E. A., *Biofizika*, **4**, 71-77 (1959)
179. Pauly, H., *Nature*, **184**, 1570 (1959)
180. Pollard, E., and Barrett, N., *Radiation Research*, **11**, 781-92 (1959)
181. Whitfield, J. F., and Rixon, R. H., *Exptl. Cell Research*, **18**, 126-37 (1959)
182. Sibatani, A., *Exptl. Cell Research*, **17**, 131-43 (1959)
183. Jaffe, J. F., Lajtha, L. G., Lascelles, J., Ord, M. D., and Stocken, L. A., *Intern. J. Radiation Biol.*, **1**, 241-46 (1959)
184. Okada, S., and Hempelmann, L. H., *Intern. J. Radiation Biol.*, **1**, 305-11 (1959)
185. Lajtha, L. G., Oliver, R., Kumatori, T., and Ellis, F., *Radiation Research*, **8**, 1-16 (1958)
186. Uyeki, E. M., Leuchtenberger, C., and Salerno, P. R., *Exptl. Cell Research*, **17**, 405-13 (1959)
187. Allfrey, V. G., Mirsky, A. E., and Osawa, S., *The Chemical Basis of Heredity*, 200-31 (Johns Hopkins Press, Baltimore, Md., 847 pp., 1957)
188. Errera, M., Ficq, A., Logan, R., Skreb, Y., and Vanderhaeghe, F.,

- Exptl. Cell Research*, Suppl. 6, 268-76 (1959)
189. Logan, R., Errera, M., and Ficq, A., *Biochim. et Biophys. Acta*, **32**, 147-55 (1959)
 190. Logan, R., *Biochim. et Biophys. Acta*, **35**, 251-53 (1959)
 191. Osawa, S., Allfrey, V. G., and Mirsky, A. E., *J. Gen. Physiol.*, **40**, 491-513 (1957)
 192. Creasey, W. A., and Stocken, L. A., *Biochem. J.*, **72**, 519-23 (1959)
 193. Rappoport, D. A., and Sewell, B. W., *Nature*, **184**, 846-49 (1959)
 194. Katchman, B. J., Fetty, W. O., and Busch, K. A., *J. Bacteriol.*, **77**, 331-37 (1959)
 195. Spoerl, E., Looney, D., and Kazmierczak, J. E., *Radiation Research*, **11**, 793-803 (1959)
 196. Drakulić, M., *Biochim. et Biophys. Acta*, **36**, 172-76 (1959)
 197. Pollard, E., and Kennedy, J., *Radiation Research*, **11**, 460 (1959)
 198. Revell, S. H., *Proc. Roy. Soc. (London)*, **B150**, 564-89 (1959)
 199. Munro, T. R., *Exptl. Cell Research*, **18**, 76-99 (1959)
 200. Smith, C. L., *Proc. Roy. Soc. (London)*, **B150**, 372-80 (1959)
 201. van der Meer, C., and van Bekkum, D. W., *Intern. J. Radiation Biol.*, **1**, 5-23 (1959)
 202. van den Brenk, H. A. S., and Moore, R., *Nature*, **183**, 1530-31 (1959)
 203. Ardashnikov, S. N., *Med. Radiol.*, **4**, 92-96 (1959)
 204. Salerno, P. R., and Friedell, H. L., *Radiation Research*, **11**, 465 (1959)
 205. Kohn, H. I., and Gunter, S. E., *Radiation Research*, **11**, 732-44 (1959)
 206. Kohn, H. I., and Gunter, S. E., *Univ. Calif. School of Med. Radiol. Lab. Progr. Rept.*, **UCSF-19**, 23 (September 1959)
 207. Hollaender, A., and Stapleton, G. E., *Proc. Intern. Conf. Peaceful Uses Atomic Energy*, Geneva, 1955, **11**, 311-14 (1956)
 208. Wood, T. H., *Radiation Research*, Suppl. 1, 332-46 (1959)
 209. Marcovich, H., *Ann. inst. Pasteur*, **93**, 456-62 (1957)
 210. Baldini, G., and Ferri, L., *Brit. J. Radiol.*, **29**, 623-24 (1956)
 211. Hollaender, A., and Doudney, C. O., in *Radiobiology Symposium 1954*, 112-15 (Butterworths Scientific Publications, London, England, 362 pp., 1955)
 212. Todorov, S., and Robev, St., *Z. Naturforsch.*, **14b**, 383-85 (1959)
 213. Forssberg, A., Lingen, C., Ernster, L., and Lindberg, O., *Exptl. Cell Research*, **16**, 7-14 (1959)
 214. Lingen, C., Ernster, L., and Lindberg, O., *Exptl. Cell Research*, **16**, 384-93 (1959)
 215. Pirie, A., and Lajtha, L. G., *Nature*, **184**, 1125-27 (1959)
 216. Pirie, A., and Drance, S. M., *Intern. J. Radiation Biol.*, **1**, 293-304 (1959)
 217. Neary, G. J., and Evans, H. J., *Nature*, **182**, 890-91 (1958)
 218. Alper, T., *Mechanisms in Radiobiology*, **I**, Chap. V (Academic Press, New York, N. Y., 1960)
 219. Magni, G. E., *Radiation Research*, Suppl. 1, 347-56 (1959)
 220. Beam, C. A., *Radiation Research*, Suppl. 1, 372-90 (1959)
 221. Mookerjee, A., *Nature*, **184**, 1502-3 (1959)
 222. Caldecott, R. S., *Radiation Research*, **2**, 339-50 (1955)
 223. Sicard, M. A., and Schwartz, D., *Radiation Research*, **10**, 1-5 (1959)
 224. Ebert, M., Howard-Flanders, P., and Moore, D., *Radiation Research*, **4**, 110-16 (1956)

VERTEBRATE RADIOBIOLOGY: METABOLISM OF INTERNAL EMITTERS^{1,2}

BY ROY C. THOMPSON

*Biology Operation, Hanford Laboratories, General Electric Company,
Richland, Washington*

INTRODUCTION

A review of the metabolism of internal emitters has not previously appeared in these volumes. One might, indeed, question whether the subject is properly classified as nuclear science, or radiobiology. There can be no question, however, of the significance of the subject for the radiobiologist concerned with the evaluation of hazards from internally deposited radioisotopes. Radiobiological significance will, then, be the criterion for selection of material for this review. Radiation damage from internal emitters will not be considered, except to the extent that studies in this area may be cited to support the significance of, or need for, information of a metabolic nature. The toxicity of internal emitters has been recently reviewed by Foreman (1) and has received much attention with regard to radioisotopes present in the fall-out from nuclear weapons tests [e.g. (2, 3, 4)]. Also excluded are considerations of therapeutic measures for removal of internally deposited radioisotopes—a field recently reviewed by Schubert (5). Even with these limitations, the subject can be covered in the space allotted only by severe selection of material. Preference will, in general, be given to the more comprehensive and accessible references without regard to historical precedence. Studies in the fields of industrial toxicology and mineral nutrition contribute a very extensive background of information often pertinent to problems of internal emitter hazards, and standard works in these fields may be consulted to advantage (6 to 10). Ellinger (11) has reviewed the metabolism of a number of radioisotopes in connection with their medical applications.

Certain aspects of the internal emitter problem are periodically brought into focus in publications of the International Commission on Radiological Protection (ICRP) (12, 13) and the National Committee on Radiation Protection (NCRP) (14, 15). These bodies are charged with the responsibility for recommending permissible limits for radioisotopes in the human body, and in water and air. The most recent report of the ICRP (13) is particularly comprehensive, with detailed consideration of approximately 240 radionuclides. Included are tabulations of the physical and biological parameters

¹ The survey of literature pertaining to this review was concluded in January 1960.

² Among the abbreviations used in this chapter are: ICRP (International Commission on Radiological Protection); MPC (maximum permissible concentrations [of isotopes]); mrem (milliroentgen equivalent man); and NCRP (National Committee on Radiation Protection).

for calculation of the recommended limits. The biological data include such information as average daily ingestion, and concentrations in organs and tissues of the stable elements; the biological and effective half lives of the radioisotopes in various organs and tissues; and the distribution of these radioisotopes after ingestion or inhalation. These tabulated data were selected on the basis of their applicability to a particular hazard evaluation procedure and represent in many cases gross oversimplification of the actual physiologic behavior. Many of the listed parameters may be expected to vary widely, depending upon a host of circumstances. Of particular value is the extensive bibliography which lists and indexes, by author and element, over 2000 references for the data on which the ICRP has based its considerations.

This discussion will take up first those general considerations pertinent to all radioisotopes or to substantial groups of radioisotopes. This will be followed by a review of the metabolism of specific radioelements considered in relation to their grouping in the Periodic Table. Frequent reference to the ICRP will be understood to refer to reference (13).

GENERAL CONSIDERATIONS

Methods of radioisotope detection.—The same radiations which constitute the hazard of radioisotopes provide a very sensitive means of studying their metabolic behavior. The general methods and theories of radioisotope tracer studies are well documented [see (16, 17)]. Certain recent advances in radioisotope detection procedures will be singled out, however, because of their probable impact on future developments. Of particular interest are the methods, mainly of an autoradiographic nature, which permit a microdelineation of radioisotope distribution. As our understanding of radioisotope metabolism improves, we are increasingly faced with the need for information on the events in smaller and smaller volumes of tissue.

For general information on autoradiography, reference can be made to the treatise of Boyd (18) and to more recent bibliographies compiled by Johnston (19, 20). The most up-to-date account of techniques and applications of autoradiography is contained in the proceedings of a conference held in Rye, New York, in 1958 (21). Of particular interest are the remarkable studies of radioisotope distribution in bone made possible through the simultaneous application of autoradiographic, microradiographic, and histologic techniques. Such studies were pioneered by Engström and co-workers in Sweden (22) and by Owen, Jowsey & Vaughan in England (23). Marshall *et al.* in the United States have made extensive use of the techniques (24 to 26). Application of these methods to estimation of the radiation dose to bone in cases of human radium exposure has been reported by Hindmarsh *et al.* (27, 28) and by Rowland & Marshall (29). Methods for calculation of radiation dose to bone have been described by Spiers (30) and Kononenko (31) for alpha particles and by Engström *et al.* (22) and Hindmarsh *et al.* (27) for beta particles.

These approaches to dosimetry of internal emitters still involve the

measurement of radioisotope concentration in thin tissue sections, from which the radiation dose is calculated. Direct measurement of radiation dose by thick-section autoradiography has been evaluated by Blackett, Kember & Lamerton (32) for P^{32} ; the method has also been applied by Sinclair *et al.* (33) to I^{131} dosage to thyroid and by Owen & Vaughan (34) to Sr^{90} — Y^{90} dosage to bone. Another promising direct approach to the dosimetry problem involves miniature glass dosimeters [Schulman & Etzel (35)], which are as small as 1×6 mm. and are suitable for implantation *in vivo*. Studies with these dosimeters by Hodara, Friedman & Hine (36) indicate that the dose rate from at least the more energetic beta emitters can be accurately measured at levels of the order of 100 rad. A recent general discussion of dosimetry of internal emitters has been presented by Loevinger, Holt & Hine (37). Bertinchamps & Cotzias (38) have published a useful nomogram for the estimation of tissue doses of internally deposited beta and gamma emitters.

Coincident with advances in methods for determining the fine structure of radioisotope distribution, there have been notable advances in the gross estimation of total-body radioisotope content by direct counting procedures. The number of "total-body counter" installations has greatly increased during the past several years, but data are as yet available from only a few. The best general account of the various types of instruments is contained in the proceedings of a conference on the measurement of body radioactivity, held at Leeds, England, in 1956 (39). A somewhat more recent account of what appears to be the most versatile type of facility, employing a large sodium iodide (thallium activated) scintillation crystal in a heavily shielded room, has been published by Miller (40). The usefulness of these counters is not limited to study of gamma-emitting radioisotopes since the bremsstrahlung from beta emitters may also be detected [Liden (41); Mays *et al.* (42)]. These instruments have been used for study of the normal radioisotope content in man [Sievert (43); Anderson & Langham (44)], for detection of accumulated fall-out radioisotopes [Miller & Marinelli (45)], and for the detection of radioactive contaminants in wounds [Gustafson *et al.* (46); Roesch & Baum (47)]. Their use in many tracer studies employing radioisotopes in man and experimental animals will be considered in later discussions of individual elements.

Routes of radioisotope entry to the body.—The inhalation of radioisotopes has been the subject of much recent study because it represents a likely route of entry, which is difficult to control and about which relatively little is known. This problem was reviewed by a committee of the National Academy of Sciences (48). It has also been considered by Stannard (49) who emphasizes the importance of insoluble radioisotope accumulation in pulmonary lymph nodes. In the absence of detailed physiological data for most radioisotopes, the NCRP and ICRP base calculations of permissible concentrations in air on a hypothetical lung model [Langham (50)] which assumes that 25 per cent of inhaled particles are exhaled without deposition and that 50 per cent deposit in the upper respiratory tract and are removed by ciliary action and

swallowed. Of the remaining 25 per cent of initially inhaled material, if readily soluble, all is absorbed rapidly into the body—if insoluble, half is assumed to be excreted via the trachea and the remainder retained in the lung with a biological half life of 120 days.

In the case of many poorly absorbed radioisotopes, irradiation of the gastrointestinal tract may be the critical factor in limiting radioisotope ingestion. The ICRP has published data on the mass of contents of various sections of the gastrointestinal tract of the "standard man" and on the time food remains in these sections (13). From these data, calculations can be made of the radiation dose to various portions of the tract by radioisotopes in transit. Studies of the rate of passage of nonabsorbed radioisotopes through the gastrointestinal tract of rats were reported by Thompson & Hollis (51). With these measurements as a basis, the dose to the tract from ingested alpha and beta emitters was calculated and related to the incidence of acute radiation damage. It was shown that an ingested alpha emitter Pu^{239} was completely ineffective in eliciting symptoms of radiation damage [Sullivan *et al.* (52, 53)], while an ingested beta emitter Y^{91} damaged the intestine in a manner and to an extent comparable to that from similar doses of x-radiation (53). In the latest recommendations of the ICRP it is assumed that only 1 per cent of the energy from alpha emission will be effective in damaging the intestine.

Retention of radioisotopes in the body.—Of particular concern in evaluation of internal emitter hazards is the mathematical formulation of radioisotope retention or excretion [Robertson (54)]. Retention has most frequently been represented as an exponential function. This is convenient, since loss of radioisotope by physical decay is also an exponential process, and by analogy with radioactive half life one may speak of a biological half life for loss of the radioisotope through biological processes. While an admitted oversimplification, a single exponential function is assumed to govern the loss of radioisotopes from the critical organ in calculations of maximum permissible concentrations of radioisotopes (MPC's) by the NCRP and ICRP. However, more complex models are considered in arriving at the MPC, and the value of the single biological half life employed in the final calculation is "... selected to produce in 50 years of constant level exposure the retention indicated by the more detailed model, ..." (13). Of the more detailed models, the multiple exponential formulation has been most frequently employed. Such a model assumes that the radioisotope is distributed among several compartments, from each of which it is lost with a characteristic half life. The retention equation will take the form:

$$R = Ae^{-\lambda_1 t} + Be^{-\lambda_2 t} + Ce^{-\lambda_3 t} + \dots$$

where R is the amount retained at time t , and A , B , C —and λ_1 , λ_2 , λ_3 —are constants characteristic of the various compartments.

Another expression, used with particular success in the case of bone-

deposited radioisotopes, relates biological retention to a power function of time:

$$R = At^{-b}$$

where R is the amount retained at time t , and A and b are constants. The application of the power function to hazard evaluation problems has been discussed by Healy (55) and by Norris, Tyler & Brues (56). With a sufficient number of terms, a multiple exponential expression can give as good a fit to experimentally obtained retention data as can the power function. When extrapolated beyond the data on which they were based, however, the two forms of expression can lead to widely varying conclusions. Stewart *et al.* (57), for example, fit excretion data on Sr^{90} obtained from two human subjects over a period of approximately 500 days to multiple exponential and power function curves. Either expression gave an equally satisfactory fit to the data, but the extrapolated 40-year bone dose calculated from the power function model was in one case 60 times, and in the other case 18 times, the dose calculated from the exponential model. The exponential model has been preferred by some on the grounds that it bears a rational relationship to probable physiological compartments, while the power function is a purely empirical relation in which one can place no confidence beyond the range of the experimental data [Robertson (54)]. On the other hand, it can also be argued that the relationship between exponential components and physiological compartments is often more fancied than real. [See Solomon (58) for a discussion of the difficulties.] Some success has been attained in providing a theoretical physiologic basis for the power function as applied to bone, in terms of the diffusion of radioactive atoms within individual bone crystals [Reynolds (59)].

Derivation of permissible limits for radioisotopes.—Consideration of the many factors leading to the choice of permissible radiation dose limits for exposure from internal emitters is beyond the scope of this review. Once they are established, the application of these dose limits to a particular organ or tissue must be based on a knowledge of the metabolic behavior of the radioelement involved. Present practice of the NCRP and ICRP is to choose values for the permissible body burdens and for MPC's such that exposure of the "critical organ" never exceeds the permissible dose limit. Procedures employed are described at length in the ICRP report (13) and have been discussed by Morgan (60). Problems involved in the choice of a critical organ have been discussed by Stannard (61).

As the localization of radioisotopes in the body is defined with increasing precision, it becomes possible to delimit more and more precisely the distribution of radiation dose. Graul (62), employing autoradiographic techniques, has illustrated the cellular localization of a number of radioisotopes in soft tissues. In studying the distribution of radiation dose in the bones of victims of radium poisoning, Hindmarsh *et al.* (28) found areas which received as

much as 14 times the average radiation dose to the whole bone, and in similar studies Rowland & Marshall (29) estimated the dose to certain microscopic volumes of bone at as much as 100 times the average bone dose. Should one then choose some portion of the bone, rather than total bone, as the "critical organ"? This approach could lead with a little refinement of technique to "critical cells" or even "critical molecules." Yet, as Stannard has pointed out (61), toxicity sometimes seems to be more closely related to total body burden than to organ distribution. There is clearly a need for further study relating radioisotope distribution to biological effect.

The permissible body burdens and MPC's established by the NCRP and ICRP are concerned with chronic lifetime exposure. They should ideally be based on lifetime experience with radioisotopes in humans. In the absence of such experience, reliance must be placed in most instances on animal data, and most frequently on single dose studies rather than on chronic administration studies. Under such circumstances the methods of extrapolation become of critical importance. In a few instances it has been shown that the extrapolation of small-animal single dose studies has agreed well with the results of chronic administration studies [Cook, Morgan & Barkow (63); Ballou & Thompson (64)]. In other cases, however, the choice of function employed in the extrapolation process was shown to make very substantial differences in the results obtained [Stewart *et al.* (57); Healy (55); ICRP (13)]. In view of the necessity for applying animal data to man, there is need for comparative gross metabolic data in several species, including man, such as can be obtained quite readily with suitable isotopes in whole-body counters. Richmond & Langham (65, 66) have reported such comparative retention and excretion data for the alkali metals, in mice, rats, dogs, monkeys, and man. Recent extensive data on the elemental composition of human organs and tissues obtained by spectrographic analysis [Tipton *et al.*, results summarized in (13)] have been extensively utilized in the most recent ICRP revision of MPC's when human or animal radioisotope data were lacking.

Evaluation of environmental contamination hazards.—The environmental contamination problem of major concern has been that resulting from the testing of nuclear weapons. While the establishment of permissible limits for radioisotope deposition in, or ingestion by, man requires only a knowledge of the metabolic fate of the radioisotope in the human, the evaluation of environmental contamination hazards involves the metabolism of the radioisotope through all of the plant and animal stages in the food chain, plus the physical factors affecting the distribution and availability of the radioisotope in the environment. The complexity of the problem and the approaches which have been utilized in its study are well summarized in the annex on environmental contamination of the United Nations Report (4). A more concise presentation of the biological aspects of the problem has been given by Comar, Russell & Wasserman (67).

The movement of Sr^{90} through the food chain has usually been studied in

terms of its relation to calcium; because of the chemical similarity of the two elements, it is assumed that the ratio Sr^{90}/Ca would vary in a more regular and predictable manner than any other expression of Sr^{90} concentration that might be used. Palmer, Thompson & Kornberg (68, 69) have called attention to a variety of nutritional factors influencing the relative behavior of strontium and calcium, and Kornberg (70) has discussed the limitations imposed by the use of ratios of two elements in hazard evaluation procedures. This problem also applies to evaluation of Cs^{137} contamination levels which are now being expressed in terms of Cs^{137}/K ratios. In view of the considerable disparity in the biological behavior of cesium and potassium, there would seem to be very little justification for such a practice.

In terms of a practical assessment of Sr^{90} and Cs^{137} contamination levels in man, methods of direct measurement have already provided a fairly detailed picture that can probably be empirically extrapolated to future times or conditions with as much accuracy as can be presently derived from a theoretical assessment of the biological and physical factors involved. Results of the world-wide program of bone collection and analysis were most recently reviewed by Kulp, Schulert & Hodges (71). The analysis for Sr^{90} is technically difficult and can be applied only to gross samples of bone. Estimation of Cs^{137} content, on the other hand, is a very simple and rapid operation, with suitable total-body counting equipment. Since such equipment is relatively immobile and available in only a few areas of the world, data for human Cs^{137} content are geographically more limited than the Sr^{90} data, but more extensive for certain areas and, for these areas, more readily correlated with environmental factors [Anderson (72); Langham & Anderson (73)].

A very interesting group, from the standpoint of the relationship between environmental contamination and internal deposition of radioisotopes, is composed of the inhabitants of the Rongelap Atoll which was heavily contaminated in 1954 by close-in fall-out from a large thermonuclear device. While internal deposition of radioisotopes accounted for a rather insignificant fraction of the total exposure of these people, the change in their deposited radioisotope burden as a function of time and continued environmental exposure has been, and could continue to be, most informative [Conard *et al.* (74)].

Estimation of human radioisotope deposition.—The estimation of significantly hazardous quantities of gamma-emitting radioisotopes such as Cs^{137} or Zn^{65} , in man, is a relatively simple matter with low background total-body counting equipment. For other isotopes with unsuitable radiation characteristics, or in the absence of sensitive counting equipment, recourse must often be had to the analysis of excreta for an indication of the body radioisotope content. Langham (50) has reviewed the methods and assumptions involved in such procedures, and Healy (75) has considered, more specifically, the estimation of lung burdens of inhaled radioisotopes. Some of the problems encountered with specific radioisotopes will be considered later in this review.

CONSIDERATION OF SPECIFIC RADIOELEMENTS

Hydrogen (tritium).—The physiology and toxicology of tritium in man have been reviewed by Pinson & Langham (76). Tritium oxide is one of the few radioactively hazardous materials readily absorbed through the skin. In tritiated water vapor atmospheres, as much tritium will enter the body through the skin as through the lung [DeLong, Thompson & Kornberg (77)]. Tritium oxide equilibrates rapidly with total body water. Its loss from the body is determined by the turnover rate of body water which can vary within wide limits depending upon fluid intake. The ICRP assumes an average biological half life of 12 days. The incorporation of a small fraction of the body water tritium into organic compounds and its retention in this form for long periods of time have been considered in a series of papers by Thompson & Ballou (78). This retention of tritium in organic compounds cannot significantly affect the chronic exposure hazard, nor can the fractionation of hydrogen isotopes which occurs in biological systems [Thompson & Ballou (79)]. Because of its uniform distribution throughout the body, permissible exposure to tritium oxide is limited by the 100 mrem/week limit for gonad or total-body exposure.

The noble gases.—Of the noble gases, only radon has received prominent consideration as a hazardous internal emitter. The physiological behavior of these gases is characterized by preferential solubility in body fats [Nussbaum & Hursh (80)] and by the absence of chemical reactions with body constituents. The uptake and elimination of these elements have been studied in connection with their use as anesthetics [see Pittinger *et al.* (81)]. From a radiation hazard standpoint, the most significant recent developments are concerned with the retention of radon formed from internally deposited radium. Norris, Speckman & Gustafson (82) found that in long-standing cases of human radium poisoning an average of 70 per cent of the radon produced in the body was exhaled. The use of this value, in place of the earlier assumed value of 45 per cent, accounts for recent changes in permissible body burdens and MPC's for a number of bone-seeking radioisotopes, limits for which are set with reference to radium (13). Mays *et al.* (83) have measured radon retention in radium-injected beagles and find that the fraction retained increases with time after radium injection. For the same length of time after injection, retention was similar in rat, dog, and man, and independent of radium dose level. These findings were consistent with a proposed theory relating radon retention to bone mineral density, crystal size, and diffusion coefficient. The very complex problem of radiation dosage to the respiratory system from inhaled radon and thoron and their decay products has been studied by Chamberlain & Dyson (84) and by Shapiro (85).

The alkali metals.—Of the alkali metals, two are of particular interest as internal emitters: potassium, because of its naturally occurring radioisotope K^{40} which is the major natural source of internal irradiation; and cesium, because of the prominence of its radioisotope Cs^{137} among the long-lived products of nuclear fission. In a very interesting interspecies comparison of the

gross retention of four alkali metals, Richmond *et al.* (65, 66), using total-body counting techniques, measured the time for loss from the body of half the administered radioisotope. Values of 11.0 days, 35 days, 80 days, and 110 days were obtained for sodium, potassium, rubidium, and cesium, respectively, in man. Half-retention times for sodium in the mouse, rat, monkey, dog, and man were, respectively, 1.7, 2.9, 7.5, 9.5, and 11.0 days. Species differences were even greater for rubidium and cesium. Such data emphasize the uncertainties in the extrapolation of animal data to man and in the sometimes unavoidable assumptions based on the chemical similarity of elements.

Lithium has no known radioisotope of half life longer than one second and is therefore of no concern as an internal emitter. Sodium metabolism has been extensively studied, using either the short-lived Na^{24} (half life, 15 hr.) or the longer-lived Na^{22} (half life, 2.6 yr.). These studies have shed much light on the role of bone in sodium metabolism [Nichols & Nichols (86)]. The possibility of very long-term retention of a small fraction of bone-deposited sodium is suggested by recent studies of Na^{22} retention in the bones of growing rats [Kellerman (87)].

The content of potassium in the human body is probably more accurately known, and certainly more easily measured, than that of any other element, owing to total-body gamma-scintillation counting techniques. Anderson & Langham (44) have published the results of nearly 1600 K^{40} measurements which show clearly defined sex differences and age trends in potassium concentration and which correlate directly with the ratio of lean, oxidizing, protoplasmic mass to total body mass. The body content of K^{40} is responsible for an estimated dose of about 20 mrem/year to gonads and other soft tissues and for a dose perhaps half this great to bone [United Nations (4)]. Aside from K^{40} there is no known radioisotope of potassium with a half life as long as one day.

The metabolism of rubidium has been studied recently, primarily in connection with the possible use of Rb^{86} as a tracer for potassium; there is no radioisotope of potassium suitable for studies of more than a relatively few days' duration. Extensive investigations by Burch, Ray & Threefoot are summarized in a Geneva Conference paper (88). Kilpatrick *et al.* (89) compared the distribution of K^{42} and Rb^{86} in rabbit and man; there was a somewhat more selective distribution of rubidium with substantial differences in urinary excretion of the two radioisotopes by man. A slight preferential concentration of rubidium in pancreas, spleen, and liver has been noted by Zipser & Freedberg (90) in studies with Rn^{86} in mouse, guinea pig, dog, and man, and by Tipton *et al.* [results summarized in (13)] in studies of the stable element distribution in man. Loss of one-half of administered Rb^{86} from the mouse, rat, monkey, dog, and man was accomplished, respectively, in 3.8, 8.6, 15, 20, and 80 days [Richmond & Langham (65, 66)].

Cesium and rubidium are probably more alike in their metabolic behavior than any other pair of the alkali metals. The times for loss of one-half of administered Cs^{134} or Cs^{137} from the mouse, rat, monkey, dog, and man

were, respectively, 1.2, 6.5, 19, 25, and 110 days, values very similar to those for rubidium [Richmond & Langham (65, 66)]. Earlier studies by Hood & Comar (91) compared the distribution and retention of Cs^{137} in rats, cattle, sheep, swine, and poultry. Placental transfer of the radioisotope occurred in rats, but with no tendency for preferential concentration in the fetus. The excretion of cesium by the dog and its retention in blood plasma and erythrocytes have been studied in detail by Threefoot, Burch & Ray (92). Ballou & Thompson (64) followed the accumulation of cesium in rats over a period of 300 days' chronic feeding. They found no evidence in any tissue for cesium retention with a biological half life longer than 17 days. The effects of dietary constituents, particularly other alkali metals and various adsorptive agents, in laboratory and farm animals have been reported by Mraz, Patrick *et al.* [see (93)]. While there are substantial interactions between certain of the alkali metals in their metabolic behavior, the chances of employing these characteristics in any practical scheme for dietary control of radiocesium deposition seem very remote.

Cesium-137, in 92 per cent of its disintegrations, decays by beta emission to metastable Ba^{137m} , which has a half life of 2.6 min. and decays by gamma emission to stable Ba^{137} . The energy of the Ba^{137m} gamma is conventionally included with that of the Cs^{137} beta in calculating permissible limits for Cs^{137} . It has been recently shown, however [Wasserman, Twardock & Comar (94)], that Ba^{137m} is very significantly concentrated, relative to its Cs^{137} parent in certain tissues. The significance of this finding in terms of radiation dose distribution and permissible exposure limits cannot be completely evaluated on the basis of data thus far reported; however, it may have relatively little effect since Ba^{137m} emits only gamma photons, and concentrates in blood and bone, tissues which normally contain the lowest concentrations of Cs^{137} .

The deposition of fall-out Cs^{137} in man has been measured in a number of laboratories, equipped with total-body counting equipment. The most extensive data have been reported from the Los Alamos laboratory, where, since 1956, some 2000 subjects have been studied [Anderson (72); Langham & Anderson (73); Hardy & Klein (95)]. These data indicate a close correlation between body Cs^{137} content and milk Cs^{137} content, which in turn is related to the rate of precipitation in the area. The average level of Cs^{137} in people in the United States in 1957 was $44 \mu\text{mc./gm. potassium}$ (72); in 1959, individual values were occasionally exceeding $100 \mu\text{mc./gm. potassium}$ (95). These levels represent less than 1/1000 of the present permissible burden in the total body for persons occupationally exposed and will contribute only a few per cent of the average total radiation dose from all nonmedical sources.

The establishment of permissible body burdens and maximum permissible concentrations for radioisotopes of the alkali metals is perhaps as straightforward and uncomplicated as that for any group of elements. They are all readily absorbed from the intestinal tract, their retention appears to follow relatively uncomplicated patterns, with no cumulative buildup over very long time periods, and their distribution is sufficiently uniform so that the

critical organ, in the case of nearly every isotope, becomes the total body (because of the lower permissible limit for total-body exposure).

Transition elements of group I.—The biological role of copper has been very extensively investigated, chiefly from the standpoint of nutritional deficiencies in domestic animals and metabolic disorders in man [Underwood (9)]. The metabolism of silver has received relatively little attention. Studies with radiosilver in the rat have been reported by Scott & Hamilton (96). Biological interest in gold has centered around its use in the treatment of arthritis [Bertrand, Waive & Tobias (97)] and the use of colloidal radioactive gold for radiotherapy [Root *et al.* (98)]. For all of the commonly available radioisotopes of these elements, the ICRP has considered irradiation of the intestinal tract as critical because of limited absorption and, in most cases, relatively short physical half life.

The alkaline earths.—Radioisotopes of the three lighter alkaline earths, beryllium, magnesium, and calcium, have been used extensively in studies of their biological behavior, but there is no particular hazard concern in the case of any of these isotopes. The metabolism of beryllium is of interest because of its extreme chemical toxicity, and Be^7 has been employed to advantage in tracing its distribution and retention in the rat [e.g., Crowley, Hamilton & Scott (99); Van Cleave & Kaylor (100)]. Magnesium-28, the longest-lived radioisotope of magnesium (half life, 21.3 hr.), has been available for only a few years but has been employed in experiments reported in at least a dozen papers during the past two years. Aikawa and associates have been notably active in this field (101). A comparison of magnesium and calcium metabolism in the rat has been reported by Lengemann (102). Much additional use of this radioisotope may be anticipated in view of limited present knowledge concerning the metabolic significance of magnesium. Study of calcium metabolism has been greatly stimulated in recent years by the availability of Ca^{45} , a pure beta emitter of 160-day half life. The availability of Ca^{47} , with a half life of about 5 days and a gamma suitable for external counting, is eagerly awaited. Studies with Ca^{45} are of interest from an internal emitter hazard point of view mainly for the light which they shed upon the metabolism of bone, since so many radioisotopes deposit preferentially in bone. Recent developments in this field have been reviewed by Neuman & Neuman (103). Marshall, Rowland, and associates (24 to 26; 104, 105) have emphasized the important role of long-term exchange of calcium between blood and bone as opposed to the more conventionally considered processes of bone accretion and resorption. Much recent work on calcium metabolism has, of course, been stimulated by interest in the Sr^{90} fall-out hazard and has involved the comparison of strontium with calcium.

The gamma emitter Sr^{85} (half life, 65 days) has been employed in a number of experiments with humans. In a recent paper, Laszlo and his associates (106) describe the distribution and retention of Sr^{85} and Ca^{45} in 10 terminal patients who came to autopsy after periods extending to 124 days after

radioisotope administration. For the period studied, retention appeared to level off at about 60 per cent for Ca^{45} and 25 per cent for Sr^{85} , with more than 99 per cent of both isotopes present in bone. There was an apparent decrease in the $\text{Sr}^{85}/\text{Ca}^{45}$ ratio in bone with time. The filterability of Sr^{85} in human blood sera was shown to be greater (60 per cent ultrafilterable) than that of Ca^{45} (40 per cent ultrafilterable) [Samachson & Lederer (107)]. The potentialities for external counting of Sr^{85} in man over short intervals of time have been explored by Bauer & Ray (108) and by MacDonald (109). Hasterlik, Druyan & Fink (110), using total-body counting techniques, observed a retention, after 8 days, of 8 per cent or less of an orally administered dose of Sr^{85} in 11 of 12 patients studied; the twelfth retained 14 per cent after 48 days. Not more than 20 per cent of the orally administered dose was excreted in the urine.

Studies of inert strontium have also contributed to our knowledge of strontium metabolism in man. The most extensive series of analyses on human bone ash indicates strontium levels usually in the range from 100 to 300 p.p.m. [Thurber *et al.* (111)]. No age effect was noted among adults, although Sowden & Stich (112) report a lower strontium concentration in young children. Thurber *et al.* (111) find the average Sr/Ca ratio in human bone to be about 1/15 of the Sr/Ca ratio in average rock or soil. Alexander & Nusbaum (113), comparing strontium content of human bone with the strontium content of milk and dairy cattle feed from the same locality, find the Sr/Ca ratio in bone to be about 0.18 times that in the diet, and the Sr/Ca ratio in milk to be about 0.13 times the Sr/Ca ratio in the cattle feed. These quantitative measures of the metabolic discrimination against stable strontium relative to calcium are in reasonable agreement with estimates based on radioisotope studies of the various discriminatory processes in animals. The stable element studies are of particular interest since they reflect the cumulative effects of lifelong exposure

Quite extensive data are now available on the measured Sr^{90} content of human bone [Kulp, Schulert & Hodges (71)]. As of January 1958, the average adult burden of Sr^{90} was estimated at $0.19 \mu\text{c. Sr}^{90}/\text{gm. Ca}$; average levels in young children generally ranged between 1 and $2 \mu\text{c.}/\text{gm. Ca}$. The variation in Sr^{90} content of bone as a function of age was consistent with predictions based on estimates of the dietary Sr^{90} levels, the rate of bone growth and turnover, and the metabolic discrimination against strontium. The distribution of Sr^{90} among different bones of the skeleton has been studied by Schulert *et al.* (114), who find a quite uniform distribution in the newborn and young children, but a pronounced and consistent nonuniformity in adults.

The rather extensive human data on strontium metabolism must still be supplemented in many areas by small-animal data. This is particularly true with regard to detailed distribution data and studies of the mechanisms involved in the metabolism of strontium and calcium. Only a sampling of recent developments in this area can be attempted. The field was reviewed in 1956 by Comar & Wasserman (8). Extensive *in vitro* studies of strontium and

calcium deposition in bone have been summarized by Harrison *et al.* (115) and Boyd, Neuman & Hodge (115a) who stress the importance of ion-exchange mechanisms and predict that skeletal processes should discriminate against strontium. That such discrimination is apparently not effective *in vivo* is attributed to the dynamic nature of the *in vivo* process, in which the equilibrium achieved in bone powder experiments is not approached. The more significant discrimination against strontium seems to occur in the processes of absorption from the intestine and excretion by the kidney [Comar, Russell & Wasserman (67)]. Schachter & Rosen (116) presented evidence which suggests that strontium is not absorbed by the same mechanism that is responsible for the active transport of calcium through the intestinal wall. The enhanced absorption of Sr^{90} from milk diets has received much attention and appears to be related in some manner to the influence in the intestinal tract of certain amino acids and lactose present in milk [Wasserman & Comar (117)]. Placental transmission of strontium has been shown to occur with only about half the efficiency of calcium [Wasserman *et al.* (118)]. The long-term retention of Sr^{90} in dogs has been studied by Stover & Atherton (119) who found simple power functions of time adequate to describe retention in total body, and concentration in plasma, over a two-year period. The retention function was very similar to that for radium. The problem of strontium distribution within bone has been studied experimentally in small animals [Owen & Vaughan (34)]; theoretical formulations were discussed previously under General Considerations. The uniformity of Sr^{90} distribution in bone will be influenced by exposure conditions, and it has been proposed that a higher permissible body burden should be allowable if accumulated through chronic rather than through infrequent acute exposures [Björnerstedt & Engström (120)].

Much of the total energy release in the decay of the $\text{Sr}^{90}-\text{Y}^{90}$ pair is due to the daughter Y^{90} which has a half life of 64 hr. That Y^{90} produced by decay of skeletally fixed Sr^{90} is not lost from the bone was shown by Arnold, Stover & Van Dilla (121). The possible significance of dissociation of the Y^{90} from its parent Sr^{90} in other tissues is indicated by the finding of much higher than equilibrium concentrations of Y^{90} in the retina of the rabbit's eye [Mole, Pirie & Vaughan (122)].

The ICRP arrives at an MPC for Sr^{90} in water by assuming a deposition in bone of 9 per cent of the Sr^{90} ingested and an effective half life of 6400 days. This is a quite different procedure from that usually employed in predicting human exposure from fall-out. According to this latter procedure, the ratio of Sr^{90}/Ca in man would be expected to attain a value about one-fourth of the Sr^{90}/Ca ratio in the ingested material. On this basis, the MPC for Sr^{90} in water would be about four times that recommended by the ICRP and in rather close agreement with the values calculated (but not recommended) by the ICRP on the assumption that Sr^{90} retention is best expressed as a power function of time.

The longest-lived radioisotope of barium, Ba^{140} (half life, 12.8 days), is

one of the more abundant fission products. Its presence has been reported in foods but not, thus far, in people [Anderson (72)]. Because of its short half life, there is no concern over possible long-term retention. Except for the early and limited studies of Hamilton (123), small-animal experiments have been reported only for short time periods after administration [e.g. Bauer, Carlsson & Lindquist (124)]. Data on the distribution of inert barium in human tissues have been obtained using neutron-activation techniques [Sowden & Stitch (112); Sowden (125)]. The very high concentration of barium observed in certain eye tissues of animals [Garner (126)] is not observed in man. The metabolic behavior of barium appears very similar to that of strontium.

The central position of radium in considerations of internal emitter hazards is the result of some hundreds of human exposures in which the metabolism and biological effects of radium may be studied. Efforts to identify victims of radium poisoning and to obtain the greatest possible information from them have been greatly intensified in recent years. Probably the most informative studies in this area are those of Norris, Speckman & Gustafson (82) and Looney *et al.* (127) on a group of mental patients injected with fixed amounts of radium of known purity. The radium content of these patients was measured in 1931-32 during the first year following radium injection and again with more refined techniques in 1951 and 1953. These data provide the best estimate of radium retention in man and appear to be expressed best as a power function of time. After 22 years, an average of 0.6 per cent of the original intravenously administered dose remained in these patients. The ICRP employs a biological half life of 1.64×10^4 days for radium in bone, which leads to an approximately tenfold lower MPC for Ra^{226} in water than would be calculated using the power function derived from the available human data.

It has been possible to study the detailed distribution of radium in bone, 20 or more years after initial deposition. Rowland & Marshall (29), studying bones from 12 such individuals, found about half of the radium uniformly distributed throughout cortical bone. The remainder was concentrated in "hotspots" with an average radium concentration 90 times as great as that in the areas of uniformly distributed radium. The hotspots were considered to have lost nine-tenths of their original activity during the 26-year period following injection. Other studies of radium distribution in human bone have been reported by Hindmarsh *et al.* (27, 28).

The normal radium content of the body now seems fairly well established. The most recent of a number of closely agreeing studies is that of Walton, Kologrivov & Kulp (128) who analyzed bones collected from all over the world. The weighted world-wide average concentration was about 1×10^{-14} gm. Ra/gm. ash with a range of area averages from 0.3 to 3.0×10^{-14} gm. Ra/gm. ash. There was no marked variation among different bones of the skeleton or as a function of age or sex. Muth *et al.* (129) have recently reported a surprisingly high normal radium content of soft tissues, which, in view of much contrary evidence, should be carefully rechecked.

Detailed information on the metabolism of radium is being obtained from long-term toxicity studies in dogs [Van Dilla *et al.* (130)]. The retention of radium in dogs is described by a power function of time. About 20 per cent of the intravenous dose was retained after three years. Radium was retained to approximately the same degree as calcium over a 100-day period, although this would appear to be due to a canceling of substantial differences in renal clearance rates, plasma levels, and skeletal binding.

Transition elements of group II.—The biochemistry, physiology, and pathology of zinc have been recently reviewed by Vallee (131). While not a fission product, Zn^{65} (half life, 245 days) is produced as a neutron activation product in nuclear weapons tests, and it was a prominent component of the internal contamination of the exposed Marshallese [Conard *et al.* (74)]. It is also produced in the cooling water in the Hanford plutonium production reactors and has been detected in persons deriving their drinking water from the Columbia River below these reactors or deriving food from lands irrigated with this water [Perkins & Nielsen (132)]. Because the radiation from Zn^{65} consists predominantly of photons, its distribution within the body is of less significance than with most radioisotopes, and permissible limits are calculated by the ICRP in terms of the total body as the critical organ. The tissue of highest concentration is probably the prostate, although data in man are limited [Prout, Sierp & Whitmore (133)]. Long-term retention studies in both small animals [Ballou (134)] and man [Richmond & Langham (135)] indicate major retention of zinc in bone and skin, with effective half lives in excess of 100 days.

Neither cadmium nor mercury is presently of particular concern as an internal emitter. Cadmium is quite selectively retained in liver and kidney [Durbin, Scott & Hamilton (136); Burch & Walsh (137)]; however, since it is so slightly absorbed after ingestion, the gastrointestinal tract is considered by the ICRP as the critical organ. Mercury is similarly distributed in tissues but is absorbed to a much greater extent than cadmium [Durbin *et al.* (136)]. In this instance, the kidney is the critical organ for calculations of permissible limits.

Elements of group III.—Boron, aluminum, and scandium have excited no particular interest as internal emitters. Gallium has been studied in both animals and terminal cancer patients to determine the usefulness of Ga^{72} or Ga^{67} for selective irradiation of bone tumors [Brucer, Andrews & Bruner (138)]. While bone appears to be the tissue of ultimate retention, there are early high levels of gallium in liver, kidney, and other visceral tissues. Deposition of indium-114 occurs principally in liver, kidney, spleen, and bone [Durbin *et al.* (136)]. Elimination was slight over the 16-day period studied. Less than 0.1 per cent of an oral dose was absorbed by rats. Experiments of longer duration, including inhalation studies, have been conducted by Smith, Thomas & Scott (139). Radiothallium is readily absorbed following oral administration and fairly uniformly distributed [Durbin *et al.* (136)]. Concentration of thallium in the thyroid was noted by Truhaut, Blanquet & Capot (140) who studied autoradiographically the distribution of Tl^{204} in the rabbit.

Yttrium and lanthanum are very similar in chemical and metabolic behavior to the rare earths and will be considered later with these elements.

Elements of group IV.—Of the group-IV elements, only carbon is of particular interest as an internal emitter. Initial concern centered around the hazard involved in the use of C^{14} as a tracer in laboratory and clinical studies. Reference may be made to the most recent of a series of papers on this subject by Skipper and co-workers (141). Distribution and retention of C^{14} will of course be influenced by the compound in which it is contained. More recently, interest has centered on the increased C^{14} level in the biosphere resulting from nuclear tests [Broecker & Walton (142)]. By January 1959, C^{14} levels in man had increased by as much as 10 per cent over pretesting levels [Broecker, Schulert & Olson (143)]. Levels of C^{14} in the atmosphere and in man (assuming no further testing) should drop off much faster than would be indicated by the half life of C^{14} , because of continuing equilibration of the newly formed C^{14} with the total carbon of the biosphere. Natural C^{14} contributes less than 2 per cent of the total radiation dose from natural sources [United Nations (4)].

In studies with rats, rabbits, and dogs, Dudley & Wallace (144) found no selective tissue localization of germanium-71. Elimination was rapid, chiefly via the urine. Absorption from the gastrointestinal tract is reported as less than 1 per cent, and irradiation of the intestinal tract is considered the principal hazard of ingested radiogermanium [ICRP (13)]. Bone would appear to be the principal site of deposition of zirconium, but because of very slight absorption, the intestine is considered the critical organ for ingestion [Hamilton (123); ICRP (13)]. A recent study with carrier-free Zr^{89} in man showed excretion during a seven-day period of less than 10 per cent of an intravenously injected dose [Mealey (145)]. This retention of carrier-free zirconium radioisotope contrasts with the rapid elimination of macro quantities of zirconium administered for therapeutic purposes [Schubert (5)]. The metabolism of hafnium-181 in the rat has been studied by Kittle *et al.* (146). While both tin and lead have been extensively studied for their biochemical effects, little interest attaches to their effects as internal emitters. Durbin *et al.* (136) have described recent radioisotope studies with tin and lead in rats and have also reviewed the earlier literature.

Elements of group V.—Detailed consideration of the extensive clinical use of radiophosphorus as an internal emitter is beyond the scope of this review. One might have hoped that such medical use would lead to a rather complete understanding of the kinetics of phosphorus distribution in man. Such has not been the case, however, and the 1952 estimates of human dosage from intravenously administered P^{32} by Low-Beer, Blais & Scofield (147) still appear to be the most extensive data on the subject. Wyard (148), however, has questioned the assumption of early concentration of intravenously injected P^{32} in bone. Basing his conclusions on external counting of bremsstrahlung and an evaluation of autopsy data, he feels that concentration of P^{32} throughout the body is reasonably uniform with at most a twofold con-

centration in bone and a somewhat higher concentration in liver. Although bone is the ultimate site of deposition of 90 per cent of phosphorus, the short-term concentration in various soft tissues is important from a hazard standpoint in view of the short physical half life of P^{32} (14.5 days). Recent studies by Kawin (149) point to the possible hazard of localized concentrations of P^{32} within the ovary.

The ICRP employs a value of 0.75 for the fraction of ingested phosphorus absorbed from the intestinal tract, based on experiments in rats reported by Kawin & Palmer (150). The fraction of ingested phosphorus deposited in bone is given as 0.375. Both of these numbers are probably maximum values and certainly may be expected to vary widely with age [Bonner (151)]. The very extensive applications of P^{32} in studies of bone metabolism have been most recently reviewed by Neuman & Neuman (103). Autoradiographic studies of the distribution of P^{32} in bone have been reported [Leblond *et al.* (152)], but recent advances in autoradiographic and microradiographic techniques that have been so profitably employed with the alkaline earths have not yet been applied in studies with P^{32} . Studies of the placental transmission of P^{32} in the rat, with estimates of the resulting radiation dose to embryonic tissues at various stages of gestation, have been reported by Sikov & Lofstrom (153).

The metabolism of radioisotopes of niobium and tantalum has been studied by Durbin *et al.* (136) who also review the earlier literature concerning these elements. The toxicology and biochemistry of arsenic have been reviewed by Vallee, Ulmer & Wacker (154). Studies of the deposition and retention in man of inhaled As^{74} have been reported by Holland, McCall & Lanz (155).

Elements of group VI.—Sulfur, like phosphorus, has been extensively employed in radioisotope studies, but few of the data obtained are directly applicable to hazard evaluation. Sulfur ingested as inorganic sulfate or sulfide is concentrated primarily in the mucopolysaccharides of connective and cartilaginous tissue; if ingested as a radiosulfur-labeled amino acid, such as methionine, it will concentrate in tissues with active protein synthesis [Nuñez & Mancini (156)]. There have been no comprehensive long-term studies of S^{35} retention in any animal species. Denko & Priest (157) report autopsy data on a terminal cancer patient, injected with S^{35} 13 days previous to death, which indicates highest S^{35} concentrations in the tumor (carcinoma of the breast) and in bone marrow. High levels were also found in gastrointestinal mucosa, tracheal cartilage, and kidney, although the range for most tissues did not exceed a factor of five. Some rather fragmentary data on human tissue distribution of S^{35} , reported by Gottschalk, Alpert & Miller (158), also indicate a relatively high concentration in tumor tissue (chondrosarcoma) and bone marrow and a rather rapid turnover in most tissues. From 30 to 90 per cent of intravenously administered radiosulfate was excreted by humans, in urine, within 48 hours [Siegel, Sachs & Graig (159)]. Studies with orally administered radiosulfate in baby pigs indicated a 60 per cent excretion

in urine during the first four days with highest concentrations in ear cartilage and red bone marrow [Kulwich, Struglia & Pearson (160)]. The choice by the ICRP of testis as a critical organ for S^{35} deposition, and the long biological half lives assumed, do not seem in accord with the best available biological data. Among the many autoradiographic studies of S^{35} distribution in tissues, some of the more pertinent for hazard considerations include the observations of Boström & Odeblad (161) on the female genital organs; of Kent *et al.* (162) on cortical bone; and Odell, Tausche & Gude (163) on bone marrow.

Of the analogues of sulfur, only polonium has been extensively studied. Selenium appears to have attracted no recent attention. Supplementing the early data of Hamilton (123), a comparative study of the metabolism of tellurium-132 in mice, rats, guinea pigs, and rabbits has been reported by Barnes *et al.* (164). Early studies of polonium metabolism in small animals and man were summarized by Fink (165) and by Anthony *et al.* (166). More recent studies have been partially reviewed by Stannard (61). Distribution and retention studies in the mouse have been reported by Finkel *et al.* (167), who direct attention to the possible criticalness of the ovaries. Spleen and kidney are the organs which retain the highest concentrations of polonium and on which the ICRP bases its permissible limits. Retention of polonium in the red blood cell, where it is combined with the globin portion of hemoglobin, is also of potential concern [Campbell & Talley (168)]. Experience with two accidents involving the inhalation of polonium, and including urinary and fecal excretion data, has been reported by Foreman, Moss & Eustler (169).

Radioisotopes of the transition elements of group VI, chromium, molybdenum, and tungsten, have all been employed in biological studies although none would seem to present an important internal emitter hazard. The metabolism of chromium presents quite a complex picture since different valence states are handled in different manners [Visek *et al.* (170)]. Under most circumstances, chromium appears to behave as a colloid and is retained in the reticuloendothelial system. Retention was noted particularly in the spleen of rats [MacKenzie *et al.* (171)]. Irradiation of the intestine by unabsorbed Cr^{61} is considered the critical factor in the establishment of permissible limits for ingestion. However, the ICRP assumption of a fraction of 0.005 absorbed is lower by a factor of 10 than recently measured values for absorption of hexavalent chromium in the rat [MacKenzie *et al.* (171)].

The metabolism of molybdenum and tungsten has been recently studied and the earlier literature reviewed by Durbin *et al.* (136). These elements seem to be characterized by rapid elimination, although small amounts of tungsten are retained rather tenaciously in spleen and bone [Ballou, private communication]. The high value of 0.8 assumed by the ICRP for the fraction of molybdenum absorbed from the gastrointestinal tract would appear to be based on data from ruminants and is much higher than has been observed in rats.

Elements of group VII.—Although biological studies have been performed employing radioactive isotopes of fluorine, chlorine, and bromine [ICRP

(13)], iodine is the halogen of primary concern as an internal emitter. Radioisotopes of iodine are prominent among the shorter-lived fission products and have appeared in human thyroids as a result of nuclear weapons tests [Comar *et al.* (172)]. Lewis (173) estimates that the natural background dose of radiation to the thyroids of children was for several years, on the average, at least doubled as a consequence of radioiodine ingestion, primarily in milk. Radioiodine levels in the biosphere are maintained only under conditions of frequent testing, since I^{131} , the longest-lived of the iodine fission product isotopes, has a half life of only about 8 days.

As the most widely used radioisotope in clinical practice, I^{131} has received much recent attention. For summaries of this work and bibliographies one may refer to the monograph on the thyroid edited by Werner (174) and to the comprehensive volume on the thyroid hormones by Pitt-Rivers, Tata & Trotter (175). Although much of the available human data is concerned with diseased states of the thyroid, recent studies of Rosenberg (176) on healthy males have provided data on the thyroidal uptake and biological half life of I^{131} as a function of age. Of the many autoradiographic studies of I^{131} in the thyroid, that of Sinclair *et al.* (33) is of particular interest in that it endeavors to quantitate both the irregularity of radioisotope deposition and the irregularity of radiation dose distribution.

Of the many animal experiments performed with I^{131} , the continuing studies of Bustad *et al.* (177) with sheep are noteworthy for the lifetime periods of exposure involved and the comprehensive nature of the observations. It would appear from these studies that the most critical tissue for radioiodine exposure is the late fetal thyroid, which may accumulate two to three times the concentration of I^{131} present in the thyroid of the dam. With a clearly defined critical organ, a short physical half life, and extensive human and animal data on both metabolism and biological effect, the internal exposure hazard from I^{131} is perhaps as well understood as that of any radioelement.

The metabolism of astatine has been studied in animals [Hamilton, Durbin & Parrott (178); Shellabarger & Godwin (179)] and in man [Hamilton, Durbin & Parrott (180)], chiefly from the standpoint of its potential usefulness as a radiotherapeutic agent. Astatine, like iodine, is markedly concentrated in the thyroid. It also concentrates in other tissues, however, to an extent not matched by iodine, and its concentration in the ovary might be of critical hazard significance [Durbin *et al.* (181)].

The metabolism of manganese has been recently reviewed by Cotzias (182). The absorption of manganese is sufficiently low, and its turnover in tissues is sufficiently rapid, so that irradiation of the intestinal tract becomes the principal hazard of ingestion [ICRP (13)]. Technetium and rhenium appear to be more readily absorbed than manganese, but the limited information available indicates a rapid elimination [Durbin *et al.* (136)] and the intestinal tract is considered by the ICRP to be the critical organ for ingestion. In many respects the metabolism of technetium and rhenium seems to resemble most closely that of iodine.

Elements of group VIII.—The general subject of iron metabolism was

reviewed by Gubler (183) in 1956. Recent papers by Finch and co-workers (184 to 186) are especially pertinent to evaluation of the gross turnover of iron in man. Absorption of iron from the intestinal tract varies inversely with iron stores and directly with the degree of erythropoiesis. It is also dependent upon the form in which the iron is fed. The figure of 0.1 employed by the ICRP for fraction absorbed is probably higher than the average for normal individuals, but is certainly within the range of normal variation (185). The choice of critical organ is somewhat difficult in the case of radioiron. The highest concentrations of iron are found in erythrocytes, and blood was earlier considered the critical organ [ICRP (12)]. Any cumulative damage from low-level irradiation of erythrocytes is difficult to envisage, however, and the most recent recommendations of the ICRP assume spleen to be the critical organ for Fe^{55} (half life, 2.9 yr.) and the lower large intestine to be the critical organ for Fe^{59} (half life, 45 days). A detailed study of the time-distribution of radioiron in rats, as a function of age, has been reported by Garcia (187). Shoden & Sturgeon (188) studied the redistribution of storage iron in rabbits among liver, spleen, and bone marrow. The half life for retention of iron in man is longer than anticipated from the life span of the erythrocyte, because of efficient reutilization of hemoglobin iron. Finch (186) finds the half life of red cell iron to be about eight years in men and nonmenstruating women and three to four years in menstruating women. This should represent the turnover of most, but apparently not all, of the iron in the body; it is a considerably greater value than the 800-day half life for total body iron calculated by the ICRP from inert iron turnover.

Radioisotopes of cobalt, like those of iron, were among the first available for biological experiments. The rather extensive early work was reviewed by Comar (189). More recently, emphasis has centered on the use of radiocobalt in studies of vitamin B_{12} . Cook, Morgan & Barkow (63) studied the metabolism of Co^{60} in the rat from the specific standpoint of internal emitter hazards. Greatest accumulation of Co^{60} during chronic feeding was noted in the contents of the gastrointestinal tract, which is considered by the ICRP to be the critical organ. The possibility of cobalt accumulation in bone has evidently received inadequate consideration. Joelson *et al.* (190) recently directed attention to radiocobalt uptake by the ovary. That the value of 0.3 employed by the ICRP for fraction absorbed from the intestinal tract may be somewhat low is suggested by studies of Harp & Scoular (191) who found that most of their human subjects absorbed better than 90 per cent of dietary cobalt. Although iron and nickel are excreted predominantly via the feces, cobalt is excreted principally in the urine. Nickel has not been of concern as an internal emitter, and very little is known of its metabolic behavior [Underwood (9)].

The remaining elements of group VIII, the so-called "platinum metals," have been studied as a group by Durbin *et al.* (136). Of the group, only ruthenium is of present concern as an internal emitter. Ruthenium-103 (half life, 40 days) is prominent among the short-lived fission products, and Ru^{106} (half life, 1 yr.) is one of the more abundant of the longer-lived fission

products. Thompson *et al.* (192) have reported a comprehensive study of the absorption, distribution, and retention of radioruthenium in the rat after administration by various routes. Ruthenium is absorbed from the intestine to the extent of only a few per cent, at most, and the intestinal tract is considered by the ICRP to be the critical organ for ingested ruthenium. The chronic feeding experiments of Thompson *et al.* (192) indicate retention of ruthenium in the rat with much longer half lives than those assumed by the ICRP. Although initial deposition of ruthenium is highest in kidney and liver, the skeleton and gonads accumulate concentrations of possible concern.

Rare-earth and actinide elements.—The rare earths, elements of atomic number 58 to 71, are very similar in their chemical properties. They are also similar to the "second rare-earth" or "actinide" series of elements (atomic number 90 to 103). Yttrium, lanthanum, and actinium are also similar to these elements in chemical behavior, and yttrium has frequently been employed as a prototype for the whole group. Intestinal absorption of all of these elements is very limited. For all except the longer-lived alpha emitters, the gastrointestinal tract is, with little doubt, the critical organ for ingestion. The distribution of these elements appears to be particularly sensitive to the quantity of material involved; thus the carrier-free radioisotopes are concentrated to a greater or lesser degree in bone while, with the addition of quantities of the inert element, there is an increasing tendency for deposition in liver and other organs of the reticuloendothelial system.

The metabolic relationships between Y^{90} and its parent Sr^{90} have been considered in the previous discussion of strontium. The metabolism of yttrium radioisotopes in man has received attention particularly from the standpoint of its possible usefulness as a radiotherapeutic agent [Hart *et al.* (193); Dudley & Greenberg (194)]. In such applications, advantage is taken of the ability to influence the site of yttrium deposition, or its localization at the injection site, by addition of inert-carrier yttrium to the injection solution. Recent studies by Graul & Hundeshagen (195) that indicate a preferential deposition of Y^{90} in many visceral organs, rather than bone, may perhaps be explained as an effect of inert-carrier yttrium. The report by these authors of an approximately 50 per cent absorption of orally administered Y^{90} is startling in view of the less than 0.01 per cent absorption consistently reported by other investigators. A great deal of interest attaches to the question of how yttrium is deposited and retained in bone, particularly since the behavior of all rare-earth and actinide elements is probably similar. This problem is discussed by Jowsey, Rowland & Marshall (196), who present evidence from studies with yttrium-91, cerium-144, and thulium-170 to indicate that deposition of these isotopes occurs on highly calcified, nongrowing bone surfaces, usually in areas undergoing active resorption and probably by a process of surface adsorption. This interpretation is at variance with earlier suggestions that these elements were associated in some manner with the organic fraction of bone [e.g. Durbin *et al.* (197)]. MacDonald, Lorick & Petriello (198) have compared the deposition rates of Y^{91} , Ca^{45} , and S^{35} in

healing bone fractures. The behavior of Y^{91} was distinctly different from that of S^{35} , which presumably reflected the synthesis of sulfated mucopolysaccharides in the organic matrix of bone, and also different from that of Ca^{45} which reflected the mineralization process. Whatever the exact mechanism of yttrium deposition in bone, it is clearly quite different from that of the alkaline earth metals.

All of the rare earths, and lanthanum, have been studied under comparable conditions in rats by Durbin *et al.* (197). Radioisotopes of high specific activity were used, and determinations of organ distribution were made at fixed intervals following intramuscular injection. The results afford an unequaled example of the regular variation of metabolic behavior as a consequence of very minor changes in chemical properties. With increasing atomic number there is an increased tendency for deposition in bone and a decreased tendency for deposition in liver. Fecal excretion predominates with the lighter rare earths, and urinary excretion with the heavier rare earths. Loss of a major portion of the liver-deposited radioisotope is fairly rapid, while that deposited in bone is much more tenaciously retained. Absorption from the gastrointestinal tract of cerium, europium, terbium, and thulium was found to be less than 0.1 per cent. Comparative studies of the metabolism of several rare-earth elements and yttrium in rats have also been reported by Foreman & Finnegan (199) who observed trends in organ content similar to those discussed above. Spode and co-workers have reported on distribution and retention in the mouse, as a function of injection route, of lanthanum (200), cerium (201), holmium (202), and lutetium (203). Certain aspects of the metabolism of lanthanum were studied in man by Hart *et al.* (193). The possible use of radiolutetium as a radiotherapeutic agent, particularly for lymph nodes, has been rather thoroughly investigated by Kyker *et al.* (204, 205).

Actinium, which may be considered the prototype of the actinide group of elements, has received little study from the standpoint of its hazard as an internal emitter. Campbell, Robajdek & Anthony (206) have reported studies in the rat, which point to bone as the critical organ. Over a period of a year there was no significant turnover of Ac^{227} from bone. Daughter products, whose radiations are much more hazardous than the weak beta of Ac^{227} , were retained in the bone. Absorption of orally administered Ac^{227} was less than 0.1 per cent.

Extensive experience with thorium and its compounds in industrial and medical applications indicates a considerably lower degree of toxicity than one would estimate from the little that is known of its metabolic behavior [ICRP (13)]. Boone *et al.* (207) found the distribution and excretion of Th^{230} , after intravenous administration in the rat, to be similar to that of plutonium except for relatively lower levels (25 to 30 per cent of retained dose) in bone and higher levels in soft tissues. The wider distribution of thorium seemed attributable to its greater degree of association with the reticuloendothelial system. Heavy concentrations in bone marrow were of particular interest

from a hazard standpoint. Studies with Th^{232} in dogs show a quite general distribution of thorium throughout the soft tissues [Stover, Atherton & Buster (208)]. Thorium has been administered to humans as a thorium dioxide preparation known as "thorotrast," which until recently was widely employed in diagnostic radiology for visualization of the liver and spleen. When administered in relatively massive quantities in this insoluble form, thorium is deposited almost entirely in the reticuloendothelial tissues and is not excreted to any appreciable degree [Hursh *et al.* (209)]. The distribution of thorotrast within the liver is such that much of the energy of the alpha disintegrations is absorbed within the thorium dioxide aggregates [Rotblat & Ward (210)]. The pattern of thorotrast distribution contrasts sharply with that seen in the rat after oral administration of thorium nitrate, where of the 0.06 per cent absorbed, essentially all is deposited in the skeleton [Salerno & Mattis (211)]. The problem of the retention and metabolic redistribution of the daughter products of deposited thorium isotopes is a complex one which has been studied by Hursh *et al.* (209) and by Rundo (212), among others.

Uranium has probably received more attention as an industrial toxic agent than any other element. Studies in this field conducted during and immediately following the Second World War have been published in volumes edited by Tannenbaum (213) and by Voegtlin & Hodge (214). The biological hazard of natural uranium is a chemical rather than a radiological one. Although the long-term retention of uranium is primarily in bone, it concentrates in kidney during early periods following administration and causes fatal damage to this organ after doses much lower than would be expected to produce radiation effects in bone. For specific isotopes of uranium, radiation effects may, of course, be significant. Kisielski *et al.* (215) have reported on the metabolism of U^{233} in mice. The distribution in kidney, liver, spleen, and bone was studied autoradiographically. Over a period of 120 days, there was a sharp decrease in kidney uranium but little change in bone-deposited uranium. In man this distinction in turnover rates between bone and kidney appears to be less clear cut. Bernard (216) has recently reviewed the human experimental data on uranium, with particular reference to the establishment of permissible limits for its ingestion or inhalation.

Of the transuranium elements, only plutonium has been extensively studied. The physiology and toxicology of Pu^{239} were recently reviewed by Langham (217). Plutonium metabolism is similar to that typical of the rare-earth and actinide elements with less than 0.01 per cent normally absorbed from an ingested dose [Weeks *et al.* (218)], with deposition predominantly in liver and skeleton [Stover, Atherton & Keller (219)] and with virtually total retention [Langham (50)]. Of particular recent interest are the studies of plutonium metabolism in dogs reported by Stover *et al.* (219). These are long-term continuing studies which should serve to extend in detail the limited data on the retention of plutonium in man [Langham (50)]. Although radiation effects in these dogs were seen predominantly in the skeletons, the average radiation dose to the liver was essentially the same as that to bone. This

long-term retention of plutonium in the liver is not observed in rats, but is probably typical of the behavior to be anticipated in man.

Plutonium, presumably arising from the inhalation of fall-out material, has recently been detected in a number of soft tissues from humans, notably in lymph nodes, but was not found in bone [Hardy & Klein (95)]. There is evidence, also, from studies with pigs that bone may not be the site of highest plutonium concentration [Clarke *et al.* (220)]. In studies with dogs, inhaled plutonium oxide was found to concentrate in tracheobronchial lymph nodes, with very little translocation to bone [Bair, private communication]. Undoubtedly the physical and chemical nature of the material inhaled, injected, or ingested plays an important role in determining the site of deposition. From a hazard point of view, the degree of uniformity of plutonium distribution may be of much greater significance than average concentrations. Arnold & Jee (221) have reported autoradiographic studies of the comparative distribution of Pu^{239} and Ra^{226} in the bones of dogs, correlating these distribution patterns with the radiation effects noted at various levels of administration.

The remaining actinide elements have received only sufficient study to indicate their general similarities to each other and to the actinide and rare-earth elements in general. Studies in rats with protactinium, neptunium, americium, and curium are described by Hamilton (123). Scott *et al.* present a more detailed account of the metabolism of americium (222) and curium (223), including autoradiographic studies of distribution in bone. A case of human internal contamination with americium has been described by Foreman, Moss & Eustler (169).

ADDENDUM

Too late for consideration in the preparation of this review, Durbin (224) published a most interesting paper on the comparative metabolic characteristics of 70 elements in rats. This paper is a useful index to the extensive work of the University of California group, much of which is published only in Atomic Energy Commission documents. The data presented by Durbin and the correlations she is able to make between chemical state and metabolic properties are an impressive achievement representing many years of effort by many people. Without detracting in any way from this achievement, one is nevertheless aware that these data represent only a very limited aspect of the total problem. Thus, the data are limited to a single animal, the rat; to studies with carrier-free radioisotopes administered in soluble form; and, for the most part, to a single mode of administration, intramuscular injection. The metabolic criteria are gross distribution among a very limited number of tissues at a single time interval following injection, and cumulative excretion in urine and feces. Clearly, we are still a long way from a "unified theory" of the metabolism of the elements. The employment by the NCRP and ICRP of a standard metabolic model in terms of which the metabolism of any element is defined by a few constants can be defended

as a practical necessity in the case of many elements for which very meager information is available. In the case of an increasing number of elements, however, the information available has already outgrown the model, and a rather more individualized approach to the evaluation of hazard and the establishment of limits seem called for. One would hope that the future will see more studies specifically directed at the evaluation of internal emitter hazards, and less necessity for the insertion of inapplicable data into generalized formulae.

LITERATURE CITED

1. Foreman, H., *Ann. Rev. Med.*, **9**, 369-86 (1958)
2. *Report of the Committee on Pathologic Effects of Atomic Radiation* (Natl. Acad. Sci.—Natl. Research Council, Washington, D. C., 1956)
3. *The Hazards to Man of Nuclear and Allied Radiations* (Med. Research Council, London, Engl., 1956)
4. *Report of the United Nations Scientific Committee on the Effects of Atomic Radiation* (United Nations, New York, N. Y., 1958)
5. Schubert, J., *Ann. Rev. Nuclear Sci.*, **5**, 369-412 (1955)
6. Fairhall, L. T., *Industrial Toxicology* (Williams & Wilkins Co., Baltimore, Md., 1949)
7. Goodman, L. S., and Gilman, A., *The Pharmacological Basis of Therapeutics*, 2nd Ed. (The Macmillan Co., New York, N. Y., 1955)
8. Comar, C. L., and Wasserman, R. H., *Prog. in Nuclear Energy, Ser. VI*, **1**, 153-96 (1956)
9. Underwood, E. J., *Trace Elements in Human and Animal Nutrition* (Academic Press, Inc., New York, N. Y., 1956)
10. Monier-Williams, G. W., *Trace Elements in Food* (John Wiley & Sons, Inc., New York, N. Y., 1949)
11. Ellinger, F. P., *Medical Radiation Biology* (Charles C Thomas, Springfield, Ill., 1957)
12. "Recommendations of the International Commission on Radiological Protection," *Brit. J. Radiol.*, Suppl. **6** (1955)
13. *Report of Committee II International Commission on Radiological Protection on Permissible Dose for Internal Radiation—1959 Revision* (Published as Vol. 3 of *Health Phys.*, 1960)
14. National Committee on Radiation Protection, *Natl. Bur. Standards (U. S.), Handbook No. 52* (1953)
15. National Committee on Radiation Protection, *Natl. Bur. Standards (U. S.), Handbook No. 69* (1959)
16. Comar, C. L., *Radioisotopes in Biology and Agriculture* (McGraw-Hill Book Co., New York, N. Y., 1955)
17. Kamen, M. D., *Isotopic Tracers in Biology* (Academic Press, Inc., New York, N. Y., 1957)
18. Boyd, G. A., *Autoradiography in Biology and Medicine* (Academic Press, Inc., New York, N. Y., 1955)
19. Johnston, M. E., *U. S. Atomic Energy Comm. Document, UCRL-8400* (1958)
20. Johnston, M. E., *U. S. Atomic Energy Comm. Document, UCRL-8901* (1959)
21. "Conference on Autoradiography," *Lab. Invest.*, **8**, 59-333 (1959)
22. Engström, A., Björnerstedt, R., Clemenson, C. J., and Nelson, A., *Bone and Radiostrontium* (John Wiley & Sons, Inc., New York, N. Y., 1958)
23. Owen, M., Jowsey, J., and Vaughan, J., *J. Bone and Joint Surg.*, **37B**, 324-42 (1955)
24. Marshall, J. H., White, V. K., and Cohen, J., *Radiation Research*, **10**, 197-212 (1959)
25. Marshall, J. H., Rowland, R. E., and Jowsey, J., *Radiation Research*, **10**, 213-33 (1959)
26. Rowland, R. E., Jowsey, J., and Marshall, J. H., *Radiation Research*, **10**, 234-42 (1959)
27. Hindmarsh, M., Owen, M., Vaughan, J., Lamerton, L. F., and Spiers, F. W., *Brit. J. Radiol.*, **31**, 518-33 (1958)
28. Hindmarsh, M., Owen, M., and

- Vaughan, J., *Brit. J. Radiol.*, **32**, 183-87 (1959)
29. Rowland, R. E., and Marshall, J. H., *Radiation Research*, **11**, 299-313 (1959)
 30. Spiers, F. W., *Brit. J. Radiol.*, **26**, 296-301 (1953)
 31. Kononenko, A. M., *Biophysics*, **2**, 98-117 (1957)
 32. Blackett, N. M., Kember, N. F., and Lamerton, L. F., *Lab. Invest.*, **8**, 171-80 (1959)
 33. Sinclair, W. K., Abbatt, J. D., Farran, H. E. A., Harris, E. B., and Lamerton, L. F., *Brit. J. Radiol.*, **29**, 36-41 (1956)
 34. Owen, M., and Vaughan, J., *Brit. J. Radiol.*, **32**, 714-24 (1959)
 35. Schulman, J. H., and Etzel, H. W., *Science*, **118**, 184-86 (1953)
 36. Hodara, M., Friedman, M., and Hine, G. J., *Radiology*, **73**, 693-706 (1959)
 37. Loevinger, R., Holt, J. G., and Hine, G. J., in *Radiation Dosimetry*, 801-73 (Hine, G. J., and Brownell, G. L., Eds., Academic Press, Inc., New York, N. Y., 1956)
 38. Bertinchamps, A. J., and Cotzias, G. C., *Science*, **128**, 988-90 (1958)
 39. "Proceedings of Conference on the Measurement of Body Radioactivity," *Brit. J. Radiol.*, Suppl. 7 (1957)
 40. Miller, C. E., *Proc. Intern. Conf. Peaceful Uses Atomic Energy*, 2nd, Geneva, 1958, **23**, 113-22 (1958)
 41. Liden, K., *Proc. Intern. Conf. Peaceful Uses Atomic Energy*, 2nd, Geneva, 1958, **23**, 133-39 (1958)
 42. Mays, C. W., Taysum, D. H., Fisher, W., and Glad, B. W., *Health Phys.*, **1**, 282-87 (1958)
 43. Sievert, R. M., *Strahlentherapie*, **99**, 185-95 (1956)
 44. Anderson, E. C., and Langham, W. H., *Science*, **130**, 713-14 (1959)
 45. Miller, C. E., and Marinelli, L. D., *Science*, **124**, 122-23 (1956)
 46. Gustafson, P. F., Marinelli, L. D., and Hathaway, E. A., *Radiology*, **68**, 358-65 (1957)
 47. Roesch, W. C., and Baum, J. W., *Proc. Intern. Conf. Peaceful Uses Atomic Energy*, 2nd, Geneva, 1958, **23**, 142-43 (1958)
 48. "Report of the Subcommittee on Acute and Chronic Effects of Radioactive Particles on the Respiratory Tract," in *Pathologic Effects of Atomic Radiation* (Natl. Acad. Sci.—Natl. Research Council, Washington, D. C., 1956)
 49. Stannard, J. N., *Proc. Intern. Conf. Peaceful Uses Atomic Energy*, 2nd, Geneva, 1958, **23**, 306-12 (1958)
 50. Langham, W. H., *Am. Ind. Hyg. Assoc. Quart.*, **17**, 305-18 (1956)
 51. Thompson, R. C., and Hollis, O. L., *Am. J. Physiol.*, **194**, 308-12 (1958)
 52. Sullivan, M. F., and Thompson, R. C., *Nature*, **180**, 651-52 (1957)
 53. Sullivan, M. F., Hackett, P. L., George, L. A., and Thompson, R. C., *Radiation Research* (In press)
 54. Robertson, J. S., *Physiol. Revs.*, **37**, 133-54 (1957)
 55. Healy, J. W., *Radiation Research*, **4**, 367-72 (1956)
 56. Norris, W. P., Tyler, S. A., Brues, A. M., *Science*, **128**, 456-62 (1958)
 57. Stewart, C. G., Vogt, E., Hitchman, A. J. W., and Jupe, N., *Proc. Intern. Conf. Peaceful Uses Atomic Energy*, 2nd, Geneva, 1958, **23**, 123-32 (1958)
 58. Solomon, A. K., *Advances in Biol. and Med. Phys.*, **3**, 65-97 (1953)
 59. Reynolds, J. C., *U. S. Atomic Energy Comm. Document*, ANL-5967, 81-98 (1958)
 60. Morgan, K. Z., *Health Phys.*, **1**, 125-34 (1958)
 61. Stannard, J. N., *Proc. Intern. Conf. Peaceful Uses Atomic Energy*, 1st, Geneva, 1955, **13**, 205-9 (1956)
 62. Graul, E. H., *Atompraxis*, **5**, 173-82 (1959)
 63. Cook, M. J., Morgan, K. Z., and Barkow, A. G., *Am. J. Roentgenol., Radium Therapy Nuclear Med.*, **75**, 1177-87 (1956)
 64. Ballou, J. E., and Thompson, R. C., *Health Phys.*, **1**, 85-89 (1958)
 65. Richmond, C. R., and Langham, W., *Health Phys.*, **1**, 223-24 (1958)
 66. Richmond, C. R., *U. S. Atomic Energy Comm. Document*, LA-2207 (1958)
 67. Comar, C. L., Russell, R. S., and Wasserman, R. H., *Science*, **126**, 485-92 (1957)
 68. Palmer, R. F., Thompson, R. C., and Kornberg, H. A., *Science*, **127**, 1505-6 (1958)
 69. Palmer, R. F., Thompson, R. C., and Kornberg, H. A., *Science*, **128**, 1505-6 (1958)
 70. Kornberg, H. A., *U. S. Atomic Energy Comm. Document*, HW-60127 (1959)
 71. Kulp, J. L., Schulert, A. R., and

- Hodges, E. J., *Science*, **129**, 1249-55 (1959)
72. Anderson, E. C., *Science*, **128**, 822-86 (1958)
73. Langham, W. H., and Anderson, E. C., *Health Phys.*, **2**, 30-48 (1959)
74. Conard, R. A., Meyer, L. M., Robertson, J. S., Sutow, W. W., Wolins, W., and Hechter, H., *Radiation Research*, Suppl. 1, 280-95 (1959)
75. Healy, J. W., *Am. Ind. Hyg. Assoc. Quart.*, **18**, 261-66 (1957)
76. Pinson, E. A., and Langham, W. H., *J. Appl. Physiol.*, **10**, 108-26 (1957)
77. DeLong, C. W., Thompson, R. C., and Kornberg, H. A., *Am. J. Roentgenol., Radium Therapy Nuclear Med.*, **71**, 1038-45 (1954)
78. Thompson, R. C., and Ballou, J. E., *J. Biol. Chem.*, **223**, 795-809 (1956)
79. Thompson, R. C., and Ballou, J. E., *J. Biol. Chem.*, **206**, 101-7 (1954)
80. Nussbaum, E., and Hurah, J. B., *Science*, **125**, 552-53 (1957)
81. Pittinger, C. B., Featherstone, R. M., Gross, E. G., Stickley, E. E., and Levy, L., *J. Pharmacol. Exptl. Therap.*, **110**, 458-62 (1954)
82. Norris, W. P., Speckman, T. W., and Gustafson, P. F., *Am. J. Roentgenol., Radium Therapy Nuclear Med.*, **73**, 785-802 (1955)
83. Mays, C. W., VanDilla, M. A., Floyd, R. L., and Arnold, J. S., *Radiation Research*, **8**, 480-89 (1958)
84. Chamberlain, A. C., and Dyson, E. D., *Brit. J. Radiol.*, **29**, 317-25 (1956)
85. Shapiro, J., *Arch. Ind. Health*, **14**, 169-77 (1956)
86. Nichols, G., Jr., and Nichols, N., *Metabolism, Clin. and Exptl.*, **5**, 438-46 (1956)
87. Kellerman, G. M., *Nature*, **181**, 914-15 (1958)
88. Burch, G. E., Ray, C. T., and Threefoot, S. A., *Proc. Intern. Conf. Peaceful Uses Atomic Energy, 1st, Geneva, 1955*, **10**, 458-68 (1956)
89. Kilpatrick, R., Renschler, H. E., Munro, D. S., and Wilson, G. M., *J. Physiol.*, **133**, 194-201 (1956)
90. Zipser, A., and Freedberg, A. S., *Cancer Research*, **12**, 867-70 (1952)
91. Hood, S. L., and Comar, C. L., *Arch. Biochem. Biophys.*, **45**, 423-33 (1953)
92. Threefoot, S. A., Burch, G. E., and Ray, C. T., *J. Lab. Clin. Med.*, **45**, 313-22 (1955)
93. Mraz, F. R., *J. Nutrition*, **68**, 655-62 (1959)
94. Wasserman, R. H., Twardock, A. R., and Comar, C. L., *Science*, **129**, 568-69 (1959)
95. Hardy, E. P., Jr., and Klein, S., Eds., *U. S. Atomic Energy Comm. Document, HASL-77* (1960)
96. Scott, K. G., and Hamilton, J. G., *Univ. Calif. (Berkeley), Publs. Pharmacol.*, **2**, 241-62 (1950)
97. Bertrand, J. J., Waine, H., and Tobias, C. A., *J. Lab. Clin. Med.*, **33**, 1133-38 (1948)
98. Root, S. W., Andrews, G. A., Knisely, R. M., and Tyor, M. P., *Cancer*, **7**, 856-66 (1954)
99. Crowley, J. F., Hamilton, J. G., and Scott, K. G., *J. Biol. Chem.*, **177**, 975-84 (1949)
100. Van Cleave, C. D., and Kaylor, C. T., *Arch. Ind. Health*, **11**, 375-92 (1955)
101. Aikawa, J. K., Rhoades, E. L., Harms, D. R., and Reardon, J. Z., *Am. J. Physiol.*, **197**, 99-101 (1959)
102. Lengemann, F. W., *Arch. Biochem. Biophys.*, **84**, 278-85 (1959)
103. Neuman, W. F., and Neuman, M. W., *The Chemical Dynamics of Bone Mineral* (Univ. of Chicago Press, Chicago, Ill., 1958)
104. Marshall, J. H., Jowsey, J., and Rowland, R. E., *Radiation Research*, **10**, 243-57 (1959)
105. Marshall, J. H., Rowland, R. E., and Jowsey, J., *Radiation Research*, **10**, 258-70 (1959)
106. Schultert, A. R., Peets, E. A., Laszlo, D., Spencer, H., Charles, M., and Samachson, J., *Intern. J. Appl. Radiation and Isotopes*, **4**, 144-53 (1959)
107. Samachson, J., and Lederer, H., *Proc. Soc. Exptl. Biol. Med.*, **98**, 867-70 (1958)
108. Bauer, G. C. H., and Ray, R. D., *J. Bone and Joint Surg.*, **40A**, 171-86 (1958)
109. MacDonald, N. S., *J. Lab. Clin. Med.*, **52**, 541-58 (1958)
110. Hasterlik, R. J., Druyan, R., and Fink, D. L., *J. Lab. Clin. Med.*, **48**, 815-16 (1956)
111. Thurber, D. L., Kulp, J. L., Hodges, E., Gast, P. W., and Wampler, J. M., *Science*, **128**, 256-57 (1958)
112. Sowden, E. M., and Stitch, S. R., *Biochem. J.*, **67**, 104-9 (1957)
113. Alexander, G. V., and Nusbaum, R. E., *J. Biol. Chem.*, **234**, 418-21 (1959)
114. Schultert, A. R., Hodges, E. J., Len-

- hoff, E. S., and Kulp, J. L., *Health Phys.*, **2**, 62-68 (1959)
115. Harrison, G. E., Lumsden, E., Raymond, W. H. A., and Sutton, A. (Part I), *Arch. Biochem. Biophys.*, **80**, 97-113 (1959)
- 115a. Boyd, J., Neuman, W. F., and Hodge, H. C. (Part II), *Arch. Biochem. Biophys.*, **80**, 97-113 (1959)
116. Schachter, D., and Rosen, S. M., *Am. J. Physiol.*, **196**, 357-62 (1959)
117. Wasserman, R. H., and Comar, C. L., *Proc. Soc. Exptl. Biol. Med.*, **101**, 314-17 (1959)
118. Wasserman, R. H., Comar, C. L., Nold, M. M., and Lengemann, F. W., *Am. J. Physiol.*, **189**, 91-97 (1957)
119. Stover, B. J., and Atherton, D. R., *Proc. Soc. Exptl. Biol. Med.*, **99**, 201-5 (1958)
120. Björnerstedt, R., and Engström, A., *Science*, **129**, 327-28 (1959)
121. Arnold, J. S., Stover, B. J., Van Dilla, M. A., *Proc. Soc. Exptl. Biol. Med.*, **90**, 260-63 (1955)
122. Mole, R. H., Pirie, A., and Vaughan, J. M., *Nature*, **183**, 802-7 (1959)
123. Hamilton, J. G., *Radiology*, **49**, 325-43 (1947)
124. Bauer, G. C. H., Carlsson, A., and Lindquist, B., *Biochem. J.*, **63**, 535-42 (1955)
125. Sowden, E. M., *Biochem. J.*, **70**, 712-15 (1958)
126. Garner, R. J., *Nature*, **184**, 733-34 (1959)
127. Looney, W. B., Hasterlik, R. J., Brues, A. M., and Skirmont, E., *Am. J. Roentgenol., Radium Therapy Nuclear Med.*, **73**, 1006-37 (1955)
128. Walton, A., Kologrivov, R., and Kulp, J. L., *Health Phys.*, **1**, 409-16 (1959)
129. Muth, H., Schraub, A., Aurand, K., and Hantke, H. J., *Brit. J. Radiol., Suppl.* **7**, 54-66 (1957)
130. Van Dilla, M. A., Stover, B. J., Floyd, R. L., Atherton, D. R., and Taysum, D. H., *Radiation Research*, **8**, 417-37 (1958)
131. Vallee, B. L., *Physiol. Revs.*, **39**, 443-90 (1959)
132. Perkins, R. W., and Nielsen, J. M., *Science*, **129**, 94-95 (1959)
133. Prout, G. R., Sierp, M., and Whitmore, W. F., *J. Am. Med. Assoc.*, **169**, 1703-10 (1959)
134. Ballou, J. E., *Health Phys.*, **1**, 232 (1958)
135. Richmond, C. R., and Langham, W. H., *Health Phys.*, **2**, 97 (1959)
136. Durbin, P. W., Scott, K. G., and Hamilton, J. G., *Univ. Calif. (Berkeley) Publ. Pharmacol.*, **3**, 1-34 (1957)
137. Burch, G. E., and Walsh, J. J., *J. Lab. Clin. Med.*, **43**, 66-72 (1959)
138. Brucer, M., Andrews, G. A., and Bruner, H. D., *Radiology*, **61**, 534-613 (1953)
139. Smith, G. A., Thomas, R. G., and Scott, J. K., *U. S. Atomic Energy Comm. Document, UR-554* (1959)
140. Truhaut, R., Blanquet, P., and Capot, L., *Compt. rend.*, **245**, 116-19 (1957)
141. Skipper, H. E., Simpson, L., and Bell, M., *Proc. Soc. Exptl. Biol. Med.*, **92**, 549-50 (1956)
142. Broecker, W. S., and Walton, A., *Science*, **130**, 309-14 (1959)
143. Broecker, W. S., Schuler, A., and Olson, E. A., *Science*, **130**, 331-32 (1959)
144. Dudley, H. C., and Wallace, E. J., *Arch. Ind. Hyg. Occupational Med.*, **6**, 263-70 (1952)
145. Mealey, J., *Nature*, **179**, 673-74 (1957)
146. Kittle, C. F., King, E. R., Bahner, C. T., and Brucer, M., *Proc. Soc. Exptl. Biol. Med.*, **76**, 278-84 (1951)
147. Low-Beer, B. V. A., Blais, R. S., and Scofield, N. E., *Am. J. Roentgenol., Radium Therapy Nuclear Med.*, **67**, 28-41 (1952)
148. Wyard, S. J., *Brit. J. Radiol.*, **29**, 576 (1956)
149. Kavin, B., *Health Phys.*, **2**, 53-56 (1959)
150. Kavin, B., and Palmer, R. F., *Nature*, **181**, 127-28 (1958)
151. Bonner, J. F., Jr., in *Pharmacology and Toxicology of Uranium Compounds*, 1970-91 (Voegtlin, C., and Hodge, H. C., Eds., McGraw-Hill Book Co., New York, N. Y., 1953)
152. Leblond, C. P., Wilkinson, G. W., Belanger, L. F., and Robichon, J., *Am. J. Anat.*, **86**, 289-341 (1950)
153. Sikov, M. R., and Lofstrom, J. E., *Phys. in Med. Biol.*, **2**, 157-68 (1957)
154. Vallee, B. L., Ulmer, D. D., and Wacker, W. E. C., *Arch. Ind. Health*, **21**, 132-51 (1960)
155. Holland, R. H., McCall, M. S., and Lanz, H. C., *Cancer Research*, **19**, 1154-56 (1959)
156. Nunez, C., and Mancini, R. E., *Proc. Intern. Conf. Peaceful Uses Atomic*

- Energy, 1st, Geneva, 1955, 12, 461-65 (1956)*
157. Denko, C. W., and Priest, R. E., *J. Lab. Clin. Med.*, **50**, 107-12 (1957)
 158. Gottschalk, R. G., Alpert, L. K., and Miller, P. O., *Cancer Research*, **19**, 1078-85 (1959)
 159. Siegel, E., Sachs, N. A., and Graig, F. A., *Proc. Soc. Exptl. Biol. Med.*, **101**, 53-56 (1959)
 160. Kulwich, R., Struglia, L., and Pearson, P. B., *Proc. Soc. Exptl. Biol. Med.*, **97**, 408-10 (1958)
 161. Boström, H., and Odeblad, E., *Acta Endocrinol.*, **10**, 89-96 (1952)
 162. Kent, P. W., Jowsey, J., Steddon, L. M., Oliver, R., and Vaughan, J., *Biochem. J.*, **62**, 470-76 (1956)
 163. Odell, T. T., Tausche, F. G., and Gude, W. D., *Am. J. Physiol.*, **180**, 491-94 (1955)
 164. Barnes, D. W. H., Cook, G. B., Harrison, G. E., Loutit, J. F., and Raymond, W. H. A., *J. Nuclear Energy*, **1**, 218-30 (1955)
 165. Fink, R. M., *Biological Studies with Polonium, Radium and Plutonium* (McGraw-Hill Book Co., New York, N. Y., 1950)
 166. Anthony, D. S., Davis, R. N., Cowden, R. N., and Volley, W. P., *Proc. Intern. Conf. Peaceful Uses Atomic Energy, 1st, Geneva, 1955*, **13**, 215-18 (1956)
 167. Finkel, M. P., Norris, W. P., Kisielski, W. E., and Hirsch, G. M., *Am. J. Roentgenol., Radium Therapy Nuclear Med.*, **70**, 477-85 (1953)
 168. Campbell, J. E., and Talley, L. H., *Proc. Soc. Exptl. Biol. Med.*, **87**, 221-23 (1954)
 169. Foreman, H., Moss, W., and Eustler, B. C., *Am. J. Roentgenol., Radium Therapy Nuclear Med.*, **79**, 1071-79 (1958)
 170. Visek, W. J., Whitney, I. B., Kuhn, U. S. G., III, and Comar, C. L., *Proc. Soc. Exptl. Biol. Med.*, **84**, 610-15 (1953)
 171. MacKenzie, R. D., Anwar, R. A., Byerrum, R. U., and Hoppert, C. A., *Arch. Biochem. Biophys.*, **79**, 200-5 (1959)
 172. Comar, C. L., Trum, B. F., Kuhn, U. S. G., III, Wasserman, R. H., Nold, M. M., and Schooley, J. C., *Science*, **126**, 16-18 (1957)
 173. Lewis, E. B., *Proc. Natl. Acad. Sci.*, **45**, 894-97 (1959)
 174. Werner, S. C., Ed., *The Thyroid* (Paul B. Hoeber, Inc., New York, N. Y., 1955)
 175. Pitt-Rivers, R., Tata, J. R., and Trotter, W. R., *The Thyroid Hormones* (Pergamon Press, Inc., New York, N. Y., 1959)
 176. Rosenberg, G., *J. Clin. Endocrinol. and Metabolism*, **18**, 516-21 (1958)
 177. Bustad, L. K., George, L. A., Jr., Marks, S., Warner, D. E., Barnes, C. M., Herde, K. E., and Kornberg, H. A., *Radiation Research*, **6**, 380-413 (1957)
 178. Hamilton, J. G., Durbin, P. W., and Parrott, M. W., *J. Clin. Endocrinol. and Metabolism*, **14**, 1161-78 (1954)
 179. Shellabarger, C. J., and Godwin, J. T., *J. Clin. Endocrinol. and Metabolism*, **14**, 1149-60 (1954)
 180. Hamilton, J. G., Durbin, P. W., and Parrott, M. W., *Proc. Soc. Exptl. Biol. Med.*, **86**, 366-69 (1954)
 181. Durbin, P. W., Asling, C. W., Johnston, M. E., Parrott, M. W., Jeung, N., Williams, M. H., and Hamilton, J. G., *Radiation Research*, **9**, 378-97 (1958)
 182. Cotzias, G. C., *Physiol. Revs.*, **38**, 503-32 (1958)
 183. Gubler, C. J., *Science*, **123**, 87-90 (1956)
 184. Bothwell, T. H., Pirzio-Biroli, G., and Finch, C. A., *J. Lab. Clin. Med.*, **51**, 24-36 (1958)
 185. Pirzio-Biroli, G., Bothwell, T. H., and Finch, C. A., *J. Lab. Clin. Med.*, **51**, 37-48 (1958)
 186. Finch, C. A., *J. Clin. Invest.*, **38**, 392-96 (1959)
 187. Garcia, J. F., *Am. J. Physiol.*, **190**, 31-36 (1957)
 188. Shoden, A., and Sturgeon, P., *Am. J. Pathol.*, **34**, 1139-47 (1958)
 189. Comar, C. L., *Nucleonics*, **3**, No. 4, 30-42 (1948)
 190. Joelson, I., Meurman, L., Odeblad, E., and Westin, B., *Nuclear Med.*, **1**, 59-61 (1959)
 191. Harp, M. J., and Scoular, F. I., *J. Nutrition*, **47**, 67-72 (1952)
 192. Thompson, R. C., Weeks, M. H., Hollis, O. L., Ballou, J. E., and Oakley, W. D., *Am. J. Roentgenol., Radium Therapy Nuclear Med.*, **79**, 1026-44 (1958)
 193. Hart, H. E., Greenberg, J., Lewin, R., Spencer, H., Stern, K. G., and Laszlo, D., *J. Lab. Clin. Med.*, **46**, 182-92 (1955)
 194. Dudley, H. C., and Greenberg, J., *J. Lab. Clin. Med.*, **52**, 533-40 (1958)
 195. Graul, E. H., and Hundeshagen, H.,

- Intern. J. Appl. Radiation and Isotopes*, **5**, 243-52 (1959)
196. Jowsey, J., Rowland, R. E., and Marshall, J. H., *Radiation Research*, **8**, 490-501 (1958)
 197. Durbin, P. W., Williams, M. H., Gee, M., Newman, R. H., and Hamilton, J. G., *Proc. Soc. Exptl. Biol. Med.*, **91**, 78-85 (1956)
 198. MacDonald, N. S., Lorick, P. C., and Petriello, L. I., *Am. J. Physiol.*, **191**, 185-88 (1957)
 199. Foreman, H., and Finnegan, C., *J. Biol. Chem.*, **226**, 745-49 (1957)
 200. Spode, E., and Gensicke, F., *Naturwissenschaften*, **45**, 135-36 (1958)
 201. Spode, E., and Gensicke, F., *Naturwissenschaften*, **45**, 117 (1958)
 202. Spode, E., Gensicke, F., and Glaser, R., *Strahlentherapie*, **108**, 97-101 (1959)
 203. Spode, E., Gensicke, F., and Glaser, R., *Experientia*, **14**, 456-57 (1958)
 204. Kyker, G. C., Christopherson, W. M., Berg, H. F., and Brucer, M., *Cancer*, **9**, 489-98 (1956)
 205. Christopherson, W. M., Kyker, G. C., Berg, H. F., Brucer, M., and Meyer, J., *Proc. Soc. Exptl. Biol. Med.*, **95**, 750-54 (1957)
 206. Campbell, J. E., Robajdek, E. S., and Anthony, D. S., *Radiation Research*, **4**, 294-302 (1956)
 207. Boone, I. U., Rogers, B. S., White, D. C., and Harris, P. S., *Am. Ind. Hyg. Assoc. J.*, **19**, 285-95 (1958)
 208. Stover, B. J., Atherton, D. R., and Buster, D. S., *Radiation Research*, **11**, 470 (1959)
 209. Hursh, J. B., Steadman, L. T., Looney, W. B., and Colodzin, M., *Acta Radiol.*, **47**, 481-98 (1957)
 210. Rotblat, J., and Ward, G. B., *Nature*, **172**, 769-70 (1953)
 211. Salerno, P. R., and Mattis, P. A., *J. Pharmacol. Exptl. Therap.*, **101**, 31-32 (1951)
 212. Rundo, J., *Phys. in Med. Biol.*, **1**, 138-46 (1956)
 213. Tannenbaum, A., Ed., *Toxicology of Uranium* (McGraw-Hill Book Co., New York, N. Y., 1951)
 214. Voegtlin, C., and Hodge, H. C., Eds., *Pharmacology and Toxicology of Uranium Compounds* (McGraw-Hill Book Co., New York, N. Y. 1949-1953)
 215. Kisilewski, W. E., Faraghan, W. G., Norris, W. P., and Arnold, J. S., *J. Pharmacol. Exptl. Therap.*, **104**, 459-67 (1952)
 216. Bernard, S. R., *Health Phys.*, **1**, 288-305 (1958)
 217. Langham, W. H., *Health Phys.*, **2**, 172-85 (1959)
 218. Weeks, M. H., Katz, J., Oakley, W. D. Ballou, J. E., George, L. A., Bustad, L. K., Thompson, R. C., and Kornberg, H. A., *Radiation Research*, **4**, 339-47 (1956)
 219. Stover, B. J., Atherton, D. R., and Keller, N., *Radiation Research*, **10**, 130-47 (1959)
 220. Clarke, W. J., McKenney, J. R., Horstman, V. G., Seigneur, L. J., Terry, J. L., and Bustad, L., *U. S. Atomic Energy Comm. Document, HW-59500*, 54-60 (1959)
 221. Arnold, J. S., and Jee, W. S. S., *Lab. Invest.*, **8**, 194-204 (1959)
 222. Scott, K. G., Copp, D. H., Axelrod, D. J., and Hamilton, J. G., *J. Biol. Chem.*, **175**, 691-704 (1948)
 223. Scott, K. G., Axelrod, D. J., and Hamilton, J. G., *J. Biol. Chem.*, **177**, 325-36 (1949)
 224. Durbin, P. W., *Health Phys.*, **2**, 225-38 (1960)

VERTEBRATE RADIOBIOLOGY: LATE EFFECTS^{1,2}

By J. B. STORER

Roscoe B. Jackson Memorial Laboratory, Bar Harbor, Maine

AND

D. GRAHN

*Biology Branch, Division of Biology and Medicine, U. S. Atomic
Energy Commission, Washington, D. C.*

The purpose of this review is to examine recent data on the late effects of ionizing radiations on man and experimental animals. Topics to be covered include life shortening and a limited amount of material on the induction of leukemia, genetic defects, congenital abnormalities, and neonatal death. The most recent articles in this review series which discussed some of these topics were those of Bond & Robertson on lethal actions and associated effects (1) and of Rugh on vertebrate embryology (2).

In the past several years, there has been an increasing preoccupation on the part of the scientific and lay public with the potentially deleterious late effects of low levels of radiation exposure on man. This preoccupation is reflected in the increased number of experimental studies dealing with late effects; by the relatively large number of pertinent review articles; by comprehensive public hearings on the subject held before the Special Subcommittee on Radiation, Joint Committee on Atomic Energy, Congress of the United States; by a number of committee statements and reports such as those sponsored by the National Academy of Sciences—National Research Council, the United Nations, and the British Medical Research Council; and finally, by the number of lively scientific controversies.

Recent reviews on life shortening by irradiation include those by Comfort (3); Yockey (4); Strehler (5); Upton (6); Mole (7); and Alexander (8). Radiation carcinogenesis, especially leukemogenesis, has been covered by Glucksmann *et al.* (9); Upton (10); Schwartz & Upton (11); Brues (12, 13); Mole (14); Furth & Upton (15, 16); Law (17); and Kaplan (18). Excellent summaries of the status of our knowledge concerning the role of radiation as a leukemogenic agent for man have been presented by Burnet (19) and Hempelmann (20). Late pathologic sequelae have been reviewed by Furth *et al.* (21) and Tullis (22). Somewhat more general reviews of late somatic effects have included those by Brues (23) and Mole (24). Evaluations of the hazards to man have been made by Kaplan (25); Webster (26); Hodges (27); Schull (28); and Neel & Schull (29). Russell & Russell (30) and Carter (31) have discussed genetic effects in mammals. Publication of the *Proceedings of*

¹ The survey of literature pertaining to this review was concluded in February 1960.

² Among the abbreviations used in this review is RBE (relative biological effectiveness).

the Second United Nations Conference on the Peaceful Uses of Atomic Energy (32) has provided a valuable collection of papers concerning late effects. The records of the hearings on the effects of fall-out from nuclear weapons tests held before a special subcommittee of the United States Congress in June 1957 and in May 1959 have been published (33, 34). These records, along with that of the hearings on biological and environmental effects of nuclear war (35), provide lucid statements of many of the problems associated with evaluating late effects, as well as considerable information on the current state of knowledge. Eminently qualified committees and study groups operating under the auspices of the United States National Academy of Sciences—National Research Council, the British Medical Research Council, the United Nations, and the World Health Organization have issued reports (36 to 39) which summarize and evaluate the long-term hazards of exposure to low radiation dosages. Volumes on radiation biology edited by Bugher, Coursaget & Loutit (40); Claus (41); deHevesy, Forssberg & Abbatt (42); and Mitchell, Holmes & Smith (43) provide additional valuable reference material.

It would appear from the above noted review and summarizing articles that such reviews appear with a frequency nearly equal to that of articles presenting new and original research. Certainly the ratio is much higher than that found in other areas of biological research, which reflects the fact that many vital decisions and recommendations are being demanded in an area where there are insufficient data and where research studies are large, costly, and time consuming.

The remainder of this review will be devoted to consideration of some of the recent pertinent data on late effects in man and experimental animals.

LIFE SHORTENING

MAN

Although there is no doubt that exposure of rodents to reasonably high doses of total-body radiation results in a shortening of their life span, such an effect has not been demonstrated unequivocally for man. Warren (44), drawing on data from the obituary column of the *Journal of the American Medical Association*, reported that radiologists as a group died at a somewhat earlier mean age than did other physicians not exposed occupationally to x-rays. Seltser & Sartwell (45), however, found that when these data were corrected for the age distribution of the groups at risk, there was no difference in the life span of radiologists and other physicians. The United Nations report (38) presents an additional analysis which indicates that mortality ratios for various medical specialties range from 0.79 to 1.26 and that dermatologists and roentgenologists have ratios of 1.25 and 1.16, respectively. Though these ratios do not differ significantly from 1.00 (the value for all specialties combined), they do suggest that this form of occupational exposure may induce an increase in the mortality rate from all causes and thus

some measure of life shortening. Court-Brown & Doll (46, 47), however, have reported on the life expectancy of British radiologists and have concluded that they do now show evidence of life shortening.

Kohn (48) has compared the survival time of women with stage II cancer of the breast treated with x-rays at levels in excess of 1500 r with that of women with the same disease who did not receive x-ray treatment, and he found no differences. Newell (49) has followed the survival of women cured of cancer of the uterine cervix by local radium treatment and those cured by a combination of radium and heavy pelvic x-irradiation. He has estimated the radiation doses at 3 megagram rads for the former group and at 25 megagram rads for the latter. At present both groups appear to show the same age-corrected mortality rate. The four year follow-up on the 82 Marshallese exposed to fall-out on Rongelap Atoll has not suggested evidence of life shortening or premature aging (50), although the time interval would be much too short to detect such effects unless the magnitude of effect was substantially greater than would be predicted from animal experimentation.

All the above studies suffer from certain limitations that seem to be inevitably associated with evaluations of data for human beings. The radiation dosages received by the radiologists are not known and any estimate would appear to be largely an educated guess. The distribution of dosage must have been far from homogeneous with the hands, arms, and upper body receiving considerably more than the lower body. The low energy of the radiation further confuses the picture since much of the total dose must have been absorbed superficially. There is also, of course, the problem as to a suitable control group, since there are undoubtedly differences in environment and working conditions, other than an increased radiation background, that could confound interpretations. Despite these uncertainties, the data on radiologists and other medical specialists represent one of the best available means for studying late effects of radiation on man, and, at the moment, it must be concluded that life shortening has not been unequivocally demonstrated. From the study of the survivors of the Hiroshima and Nagasaki bombings, the most complete information on irradiated human beings will eventually be provided. Though many years will be required for that study to reach completion, it is virtually inevitable that some life shortening will be observed since the Japanese survivors have shown a significantly greater rate of mortality from leukemia than their controls over the past 10 or 12 years.

The studies of Kohn (48) and Newell (49) contribute appreciably to the available data for man, but both were made on women already suffering from serious disease processes. Radiation was restricted to relatively small areas of the body, and animal experiments demonstrate very well that irradiation of a limited area is far less effective in shortening life span than is total-body exposure (51 to 56). Sample sizes in all the reported human studies were relatively small; only in the case of the radiologists has sufficient time elapsed to make a final evaluation. It is unlikely that man is refractory to the life

shortening effects demonstrated in rodents although, as noted above, it may be necessary to await the final evaluation of the Hiroshima and Nagasaki data to define man's relative sensitivity.

EXPERIMENTAL ANIMALS

Single-dose exposures.—Recent data on the life shortening effect of single, total-body, x- or gamma-ray exposures to mice are included in papers by Alexander & Connell (57); Lindop & Rotblat (58); Curtis *et al.* (59, 60); Grahn & Sacher (61); Grahn (62, 63), Storer *et al.* (64, 65); Kallman & Kohn (51); Kohn & Guttman (66); Boone (52); and Gowen & Stadler (67). Data from studies with rats are included in reports by Lamson *et al.* (53); Maisin *et al.* (54, 55); and Dunjic *et al.* (56). The data confirm the well-established fact that moderately high doses of radiation shorten the life span of rodents. Since these studies were done primarily to investigate other facets of the life shortening problem, and the irradiated groups served as a baseline for comparison, little new information was presented which bears directly on the problem of the dose-response relationship. While there are several studies in progress (58, 68, 69) which promise to yield extensive data on life shortening as a function of a wide range of dosages, it appears that the data from Operation Greenhouse (70) remain the most extensive in this respect. Sacher's (71) conclusion, based on Furth's (70) and his own data, that life shortening is a nonlinear function of dose, with an accelerating rate of loss of life with increasing dose, has not been seriously challenged. The data of Gowen & Stadler (67) that cover a wide dose range are compatible with a curvilinear relationship; and the data of Storer & Sanders (64) and of Duhig & Warren (72) that are compatible with a linear hypothesis are not sufficiently discriminating to permit a choice between the alternatives. Extensive preliminary data of Noble & Doull (69) tend to support the curvilinear hypothesis.

None of the studies reported to date give direct evidence for or against the existence of a threshold dose below which radiation exposure is ineffective. This, of course, is not surprising. If the true dose-response curve is curvilinear and passes through the intercept, then an apparent threshold would be demonstrated in studies in which the sample size is not large enough to detect very small differences between control and irradiated groups. As sample sizes are increased, the apparent threshold should shift to smaller and smaller dosage values. On the other hand, if a true threshold exists it would be impossible to demonstrate it to everyone's satisfaction. If it were demonstrated in a large sample that a particular low dose of radiation did not produce an observable effect, the proponents of the "no-threshold" hypothesis could rightfully argue that the true effect was too small to be shown by the particular sample size utilized. This argument can be repeated *ad nauseam*. Consequently, the threshold versus no-threshold argument for life shortening and other radiation effects may be rather pointless. As others have pointed out repeatedly, until we have a detailed understanding of the cellular basis of late radiation effects it may be impossible to resolve this controversy. An

excellent discussion of this problem appears in a recent statement of the Ad Hoc Committee of the National Committee on Radiation Protection and Measurements (73).

It is our conclusion that existing data on life shortening in rodents by single total-body exposures to x- or gamma-radiation strongly support the hypothesis of a curvilinear dose-response relationship. Problems and pitfalls in attempts to extrapolate to man are beyond the scope of this review. It might be noted, however, that the problem of extrapolation is rendered more complex by the present lack of data on life shortening for large animals whose life spans are intermediate between rodents and man.

Partial-body exposures.—Partial-body exposure of mice and rats is far less effective in shortening life span than is total-body exposure [Kallman & Kohn (51); Boone (52); Lamson *et al.* (53); Maisin *et al.* (54, 55); and Dunjic *et al.* (56)]. The extent of life shortening depends on the area irradiated, the size of the field, and total dose. Generally, partial-body irradiation is only about 10 to 50 per cent as effective as total-body irradiation, depending on the body region irradiated. Maisin and co-workers (55) found that in rats the after-survival curves had distinctly different shapes depending on the region of the body exposed. They concluded that the total-body survival curve is a composite of the partial body curves and that injury to the various body regions summates to produce the observed total-body effects. Lamson *et al.* (53) found that life shortening was roughly proportional to the per cent of the body irradiated. It is not clear that this is the general case, and there is no apparent clear-cut relationship that would allow direct extrapolation of information for total-body irradiation to the partial-body exposure situation.

Age effects.—Kohn & Guttman (66) have investigated the important problem of the effect of age at the time of radiation exposure on reduction of life span in mice. When mice were given single x-ray exposures at ages of 160, 435, or 535 days there was significantly less life shortening when the irradiations were performed at the later ages. Curiously enough, the total gross tumor incidence was also depressed. In another study Kohn (48) found that exposure of mice at 730 days of age did not produce a detectable reduction in life span. The explanation for this decrease in effect with age is perhaps found in Kohn's experiments (66) in which mice were exposed to 500 r of total-body radiation at an age of 435 days. An increase in the death rate of the irradiated mice as compared to controls was not detected until 24 weeks later in male mice and 16 weeks later in the females. This finding suggests that the damage which results in premature death may evolve slowly. Since 24 weeks are an appreciable fraction of the normal life span, it might be postulated that irradiation of animals late in their life does not allow sufficient time for the damage to express itself since many of the mice will die from natural causes before the radiation damage can contribute.

Continuous exposure.—The observation that continuous or greatly protracted radiation exposures are considerably less effective than the same dose given in a single rapid exposure has been amply confirmed by recent work

[Neary, Munson & Mole (74); Noble & Doull (69); Grahn (62, 63); Upton (75)]. The precise factor relating effectiveness of single and protracted exposures varies somewhat, depending on dosage level and conditions of the experiment. Generally, single exposures in the acute-lethal dose range have about five times the life shortening effect of the same total dose given as a protracted exposure. Apparently the dose-response curve for protracted exposures is less distinctly curvilinear than for single exposures and, for accumulated doses below about 2000 r, may be indistinguishable from a linear function. At higher total doses the curvilinearity becomes apparent [Grahn (62); Noble & Doull (69)].

Carlson & Jackson (76) have reported an increased median survival time for rats exposed for one year to low levels of gamma radiation. This result, still to be explained adequately, was previously reported for mice by Lorenz *et al.* (77) and confirmed by Sacher & Grahn (78). Animals continuously exposed to dose rates below 5 to 10 r/day tend to show a lower death rate than their controls early in the irradiation period when infectious diseases are primarily responsible for death. It can, therefore, be argued that the continuous low radiation exposure is in some way altering the responses to infection. Further studies of this phenomenon would be highly desirable.

Fractionated exposure.—Data on the effect of a limited number of fractionated exposures on life span have not demonstrated an entirely clear-cut relationship between life shortening and the exposure variables. In general, small dosages of less than 50 r given in a large number of fractions tend to result in life shortening similar to that seen with continuous exposures to the same total dose [Hursh *et al.* (79); Mole (80); Sacher (71)].

Larger dosages delivered in a small number of fractions with relatively short intervals between exposures tend to give a result similar to that seen with single exposures to the same total dose (71, 80, 81). It is unlikely that there is a sharply defined point in fractionated dose schedules on one side of which the response is similar to that seen with a single dose and on the other side of which the response simulates that for continuous exposure. Intermediate results between that for single and continuous exposure have been demonstrated (71). At present, however, there are insufficient data to enable the formulation of empirical equations that will predict the response for all conceivable fractionation schedules. One confounding factor in studies of this type is the variability in the response of mice as a function of strain. For certain strains with a high susceptibility to radiation-induced lymphatic leukemia, fractionated exposures are clearly more leukemogenic than single exposures (81, 82). If leukemia is a major cause of death, then the life table will reflect this effect; and fractionated exposures will appear more potent in the shortening of life than single exposures (81), even though the incidence of degenerative diseases, such as nephrosclerosis, decreases with increasing fractionation. Such data can be corrected for the perturbations introduced by a high incidence of leukemia, or other strain or sex specific tumors; and life shortening from other causes can be evaluated (62). Such corrected data, unfortunately, are not usually reported.

Relative biological effectiveness.—The effectiveness of single doses of neutrons relative to x- or gamma-rays in the production of life shortening in mice or rats has been studied recently by a number of investigators (60, 64, 65, 81). There is a surprising agreement that the relative biological effectiveness (RBE) of single-neutron exposures is about the same for life shortening as for acute effects, or, in other words, that neutrons are roughly 2 to 3 times as effective in shortening life span as x- or gamma-rays. Cole and co-workers (81) have also reported a neutron RBE of about unity for production of nephrosclerosis in mice and an RBE of 2 to 3 for production of intestinal adenomas. The earlier observations by other workers that neutrons are far more effective in the production of lens opacities (RBE of 5 to 10) have not been challenged.

The determination of RBE for shortening of life span by neutrons under continuous or fractionated exposure presents a far more complex problem. Earlier workers, notably Henshaw *et al.* (83) and Evans (84), felt that the effectiveness of neutrons relative to gamma rays was increased over that for a single exposure when dosages were protracted. It would follow from this conclusion that the RBE for neutrons would also vary as a function of dose rate or fractionation schedule since, presumably, dose-response curves intermediate between that for single exposures and extreme protraction could be demonstrated by proper fractionation schedules. If the RBE for neutrons is low for single exposures but high for extremely protracted exposures, then intermediate values should result when the dose schedules lie between the two extremes. Neary, Munson & Mole (74) suggested that the conclusion that protracted neutron exposures are relatively more effective may be erroneous since it depended on a questionable method of interpretation. Unfortunately, their own work does not resolve this problem since their baseline data were obtained for a single dose level of gamma rays and, as they point out, "... only one method [of calculating the RBE] is permissible, the comparison of dose rates which produce the same degree of damage in the same time after the onset of irradiation." On the basis of their own data and that of Evans (84), Henshaw *et al.* (83), and Lorenz *et al.* (77), Neary and colleagues concluded that the RBE for protracted neutron exposures must be about 10. This value is somewhat higher than their other reported values for the RBE for acute and subacute effects such as organ weight loss and fertility. Interestingly enough, they did not find a shift in the RBE with protraction of exposure when testicular atrophy was used as the endpoint. The question of whether neutrons have a higher RBE for life shortening when exposures are protracted can probably not be settled until subsamples from the same initial animal population are exposed to graded protracted and graded single doses of neutrons and gamma rays. Tentative evaluations of two as yet unpublished studies on life shortening by protracted neutron and gamma-ray exposures strongly suggest that the RBE of neutrons is higher for protracted than for single doses [Noble & Doull (69); Upton (75)]. It will be of interest to see if these studies also demonstrate a variation in RBE with various systems of fractionation.

Other environmental stresses.—Ionizing radiation is undoubtedly the most extensively studied of various environmental and occupational hazards. The question has been raised whether the administration of other toxic agents to experimental animals will also result in an observable reduction in life span. The question takes on additional importance in view of the "somatic mutation" and "accumulation of stresses" theories of aging and radiation effects (discussed in a later section), since certain chemical compounds are known mutagens and should simulate radiation effects if the latter are mediated by alteration of the genetic material of cells. Curtis & Healy (59) tested single large doses of a variety of toxic agents including one of the nitrogen mustards, a known mutagen, for effectiveness in reducing the life span of mice. No life shortening was demonstrable, although x-ray exposures of similar physiologic effectiveness (in terms of fraction of the median lethal dose for acute mortality) produced a marked reduction of life span. Curtis & Gebhard (60) then tested these agents (turpentine, tetanus toxin and toxoid, typhoid vaccine, and nitrogen mustard) further by giving repeated injections. The dosage levels used were, in some cases, sufficiently high so that an appreciable fraction of the treated group died from the acute toxic effects. Injections were then discontinued and after-survival measured. Curtis & Gebhard concluded that these treatments did not result in life shortening. It is clear from their data that the effect was not as great as would result from comparable doses of x-rays. It is not clear, however, that there was no effect on the life span. If allowances are made for the size of the sample at risk at the later time intervals, it appears that the death rate may have been higher in certain of the stressed groups than in the control groups. The reported data are not sufficiently detailed to allow an independent evaluation in this respect. Recently, Alexander & Connell (57) reported significant life shortening in mice repeatedly injected with the nitrogen mustard chlorambucil or with busulfan (Myleran), a related alkylating agent. It appears, then, that ionizing radiation may not be unique in its ability to shorten life span and that certain other toxic agents share this property. It has not been established whether only radiomimetic agents, such as the nitrogen mustards, produce the effect or whether other nonspecific stressing agents are also effective. The tissue distribution of the agents in question must also be accurately determined since it is not appropriate to compare the effects of radiation damage that has occurred randomly in all tissues with that produced by metabolically active chemical agents in a few selective tissues.

Prophylaxis and therapy.—The question whether protective and therapeutic agents which markedly alter the acute response to radiation are also effective in reducing life shortening has not been entirely answered. Hol-laender *et al.* (85) have reported that β -aminoethylthiouronium bromide hydrobromide (AET), a potent prophylactic agent with respect to acute effects, also reduces radiation-induced life shortening in mice. On the other hand, Mewissen (86) reported that cysteamine and cystamine, which are considered to protect by the same mechanisms as AET, did not alter life

shortening in mice. Maisin and co-workers (55) found a similar lack of effect with cysteamine administration in rats. Hollcroft and colleagues (87) found that cysteine or hypoxia was effective in mice, while spleen shielding was not. Maisin *et al.* (55) reported marrow transplantation to be ineffective in rats, while Hollaender reported it to be effective in mice. Since in certain strains, the inoculation of marrow (88) or spleen (89) has been shown to lower the incidence of radiation-induced leukemia, it follows that such treatment would also reduce life shortening in strains where leukemia is a major cause of death. There is the possibility that these various treatments may protect against one or more, but not all, of the late lesions produced by irradiation and that the conflicting reports may be due to the use of animal material that differs considerably in the incidence of these lesions. If this were the case, then different species or even different strains within a species might show entirely different life-table data, depending on principal causes of death. Additional studies are necessary. The over-all problem of genetic variation in long-term responses to irradiation has been studied in some detail by Grahm and is reported elsewhere (62).

Nature of the lesion.—The primary histopathologic or physiologic lesion(s) responsible for nonspecific life shortening in irradiated animals has not been identified with any degree of certainty. Perhaps this is not too surprising, as the primary lesions or defects responsible for normal aging have not yet been identified. Casarett and co-workers (90, 91) are inclined to the view that arteriolocapillary fibrosis may play a major role in the production of late radiation effects. If this viewpoint is correct, it should be possible to demonstrate functional deficits in the circulation to various organs and to evaluate whether these deficits run a parallel course in normal aging. Such findings would be most stimulating but would not, of course, prove a cause and effect relationship, but would rather demonstrate an association of effects. The various hypotheses and models advanced to explain aging and life shortening by radiation have not been particularly helpful in pointing out promising areas for histologic or physiologic studies. Theories based on information theory and somatic mutations (92 to 98) do not specify any areas for investigation of primary lesions other than the cell nucleus. Statistical theories based on fluctuations in the mean physiologic state (71, 99) point to all metabolic and physiologic variables as potential areas for investigation. Theories based on irreparable levels of injury (100, 101) point out methods for measuring the level without attempting its identification, and similarly the hypothesis of progressive loss of ability to repair damage (102) does not specify the nature of the repair function. It is possible, and perhaps even likely, that life shortening represents such a complexity of physiologic deficits that it would not be possible to identify any particular lesions or deficits of primary importance. This pessimistic view should not discourage attempts at identification of the deficiencies, however.

Theoretical research.—In the past several years, a number of theoretical approaches have been made to the problem of natural aging and radiation-

induced life shortening. These theories may be grouped roughly into four categories as follows: (a) the theory of additive irreparable injury, (b) the statistical theory of fluctuations in mean physiologic state or magnitude of physiologic stresses, (c) the theory of progressive disruption of biological organization, and (d) the theory of spontaneously occurring and radiation-induced mutations in somatic cells. Certain of these theories have obvious similarities, and the differences are primarily in the approach to the problem. For this reason the above grouping is arbitrary and not intended to indicate that the categories are mutually exclusive. An extensive evaluation of these theoretical studies will not be attempted here; the reader is referred to the original papers and a recent critical, summarizing review by Strehler (5).

The irreparable injury theory was first advanced by Blair (100, 101). In essence, he postulates that radiation-induced injury is linearly related to dose and is additive with all previous and succeeding injury. A constant proportion of the damage is assumed to be irreparable, while the reparable component repairs exponentially. It is also postulated that natural aging is equivalent to a linear accumulation of injury and that radiation-induced injury adds with aging injury to produce a predictable degree of life shortening that is proportional to dose.

The stochastic theory advanced by Sacher (71, 99) holds that the physiologic state of an individual varies about some mean value and that homeostatic mechanisms tend to correct deviations from the mean. The probability of deviations of various magnitudes from the mean is assumed to show a Gaussian distribution. When fluctuations exceed a critical magnitude, death occurs. Radiation exposure causes an unfavorable displacement of the mean physiologic state relative to control animals. It is further assumed that the mean physiologic state of a population decreases linearly with age. Strehler (5) has modified Sacher's theory primarily by assuming that the logarithmically increasing probability of death with increasing age is a consequence of the interaction between a linearly decreasing size of the minimum stress necessary to kill and a distribution of stresses which increases logarithmically in number. Radiation damage is assumed to add with aging in decreasing the size of the stress that can be survived.

Sacher's and Strehler's theories both lead to the Gompertzian equation (103) which states that the probability of death increases exponentially with age. The Gompertz analysis is applicable in general terms to the life tables of populations following single exposures (61, 71), fractionated exposures (71), and continuous exposures (71, 104). Briefly, it has been observed that a single exposure in early adult life causes the Gompertz plot or age-specific mortality rate curve to undergo a parallel displacement above (to the left of) the compared control plot. Thus, a given dose will cause the mortality rate to be increased by a constant multiple for most of the postirradiation period. In the immediate postirradiation period, there is a transitional state that has not been completely quantitated. There is also the possibility that the mortality rate of irradiated animals may decline slightly at advanced ages, at least

for populations initially exposed at later ages (66). Fine details of the life-table analysis techniques thus remain to be satisfactorily worked out since there are some recognized exceptions to parallel displacement. For example, it has been recognized that a moderate incidence of leukemia in the irradiated population will cause deviations from parallelism to occur (105, 106). Other causes of death also act in this manner (107), but the value of the life-table analysis lies in its ability to permit separate evaluation of all factors contributing to the dying out of the populations under study. The factor of increase in the mortality rate of irradiated groups over that of controls is definitely a function of dose (71). Increasing single doses cause an accelerating increase in this factor, while increasing daily doses cause a progressive increase in the slope of the Gompertz function and thus a greater divergence from the control with increasing age. It is hoped that, eventually, the life-table analysis will form the basis of a sound predictive theory of chronic radiation injury and the diverse individual manifestations of such injury.

Jones (108, 109), using the above approach, has suggested that susceptibility to further stress is conditioned by previous stress and that the death rate is a function of accumulated damage. He further suggests that the rate of accumulation of damage is proportional to the amount previously accumulated and is thus, in a sense, autocatalytic. In this scheme, radiation damage would add with other stressful experiences.

Yockey (92, 93) and Quastler (94), drawing on information theory, have pointed out that biological systems are highly ordered and that aging and life shortening by radiation could result from a progressive loss of orderliness (information) until a critical level is reached that is incompatible with life. Since, presumably, the information content resides in deoxyribonucleic acid (DNA), this theory overlaps those proposed by Muller (95); Henshaw (96); Failla (97, 98); and Szilard (110) who assume, in effect, that the progressive accumulation of gene mutations and chromosomal aberrations with age or radiation exposure leads ultimately to death by disruption of essential functions, the induction of neoplasia, etc.

All the above theories are now more descriptive than predictive. They point out clearly, however, that our present state of experimental knowledge is inadequate and, in some cases, indicate the areas in which some of the deficiencies lie. In this respect they have been extremely valuable in stimulating additional research.

LEUKEMOGENESIS

MAN

There can be no question that ionizing radiation is a potent leukemogenic agent for man. A number of studies have shown that American radiologists occupationally exposed to x-rays had a higher incidence of leukemia than other physicians [Henshaw & Hawkins (111); Warren (44); March (112)]. Court-Brown & Doll (46, 47) reported a high incidence of leukemia in pa-

tients given radiotherapy to the spine for ankylosing spondylitis. Studies of the atomic bomb survivors in Hiroshima and Nagasaki have shown an increased incidence of leukemia among those exposed to significant doses of radiation [Folley *et al.* (113); Lange *et al.* (114); Moloney & Kastenbaum (115); Wald (116)]. Children given therapeutic radiation to the thymus to reduce its size have, in some studies, subsequently shown a higher incidence of leukemia than would be expected on the basis of standard-experience, age-specific leukemia incidence rates for the population under consideration [Simpson *et al.* (117, 118); Simpson (119); Polhemus & Koch (120); Hempelmann (20)]. Other studies have been negative in this respect [Snegireff (121); Conti *et al.* (122)].

The issue, then, is not whether radiation is leukemogenic, but whether the increased levels of environmental radiation are an important etiologic factor in the rising leukemia incidence rate (123) and whether a dose-response curve of predictive value can be constructed. The first of these issues can be disposed of rather more easily than the second. While there have been suggestions that an increased radiation level (primarily from the increased medical use of x-rays) may play a major role in leukemia incidence, to our knowledge no qualified scientist has seriously proposed that natural background radiation is responsible for the majority of spontaneously occurring leukemias (or that the increasing incidence rate is primarily due to the increased uses of radiation). Burnet (19), using the most pessimistic assumptions about dose-response relationships, concluded that only a small fraction of the total leukemia incidence could be reasonably ascribed to radiation exposure. Lewis (124), using similar assumptions, suggested that perhaps 10 to 20 per cent of spontaneously occurring leukemias might be due to background radiation, and Schubert (125) estimated that 5 per cent of all childhood neoplasms were due to natural background radiation. If leukemia is caused by environmental agents, agents other than radiation must play a major role in the etiology of this disease.

The second question, that of construction of the dose-response relationship, has resulted in lively controversies and discussions. Lewis (124), drawing on leukemia incidence in four exposed groups: namely, the American radiologists, the atom bomb survivors, the ankylosing spondylitis patients, and the children irradiated for thymic enlargement, concluded that the "best" estimate of the probability of an individual developing leukemia per rad of exposure per year was $1 \text{ to } 2 \times 10^{-6}$. On the basis of his analysis of the available data, Lewis suggested that a linear relationship exists between dose and leukemia incidence. Court-Brown (126) has also indicated that he favors the linearity hypothesis. This hypothesis has been vigorously questioned on statistical grounds by Kimball (127) and on more general grounds by Brues (13), Hempelmann (20), and Law (17). The basis of these dissenting opinions is not that the dose-response relationship is of a definite type other than linear, but that there are too many uncertainties in the human data to permit choice of a specific type of regression line. There is no

great likelihood that the data will be sufficiently refined in the immediate future to enable the establishment of a definitive dose-response relationship. The Ad Hoc committee of the National Committee on Radiation Protection and Measurement discussed this dilemma and concluded that in considering human hazards it would be prudent to utilize the linearity hypothesis since it represents the conservative point of view (73).

Of the various objections to assigning an increase in leukemia incidence rate per rad of exposure, perhaps the most serious is the uncertainty in radiation dosages. Because of the great variations in type of equipment used and the differences in work practices of the American radiologists, it is, as Hempelmann (20) points out, "... almost impossible to make any sensible statements about the relationship of dose and leukemia frequency." The uncertainties in dosages received by the atomic bomb survivors have been discussed in detail by Hempelmann (20), Wald (116), and Brues (13), and include questions of the exact distance of survivors from the hypocenter, the nature and extent of shielding, and the RBE of the neutron component of the radiation.

In human studies in which radiation dosages are reasonably well established, there are other confounding variables. In the series of patients with ankylosing spondylitis, the exposures were essentially partial body in type. The factors for relating partial-body exposure to total-body exposure are not known. The shape of the dose-response curve can be shown to vary whether radiation dose to the spinal marrow is considered or whether the total integral dose is used (13, 20, 47, 126). The studies of children irradiated for thymic enlargement provide valuable information on leukemogenesis, but again the exposure was to a limited region and to patients who were abnormal at least in size of the thymus. In a study of children who received radiation to a normal-sized thymus, Conti *et al.* (122) did not find an increased incidence of leukemia; however, the radiation port size was smaller than in the other reported series and minor increases would not be detected because of the small sample size. On the other hand, Murray and co-workers (128) reported that thymic enlargement is not a necessary prerequisite for leukemia induction since children given therapeutic radiation for other benign diseases also showed increased incidence of leukemia.

Faber (129), using tumor registry data, did a retrospective study of the history of radiation exposure in patients dying from leukemia. Of those dying from lymphatic leukemia, only 18 per cent had received diagnostic or therapeutic irradiation, while 30.2 per cent of patients with chronic myelogenous leukemia and 31.9 per cent of those with "acute" leukemia had histories of exposure. Faber considered that lymphatic leukemia is not radiation induced and used this group for his controls. Radiation doses, of course, were not well established and it is not clear that the control group was suitably chosen.

Perhaps the lowest dose range yet studied is represented in the work of Stewart *et al.* (130) and Ford *et al.* (131). These workers did retrospective studies of radiation exposure history in two groups of children. One of the

groups represented children dead from leukemia or other malignancies and the other represented live children (130) or children dead from other causes (131). The groups were roughly matched for age, sex, and locality. In both these studies, the frequency of *in utero* diagnostic x-ray exposure was about twice as high in the leukemic groups as in the control groups. Since the exposure doses were extremely small, this finding would suggest a remarkable sensitivity of the human fetus to the leukemogenic effects of x-rays. It should be noted, however, that in studies by Polhemus & Koch (120) and by Murray *et al.* (128), a significant difference in frequency of prenatal exposure between the leukemic and control groups was not found. Kaplan (25), doing a similar study, found that the detection of differences depended on the method of selecting the control group. When the controls were siblings there was an increased frequency of prenatal exposure in the leukemic group. This difference disappeared, however, when playmates were used as the control. The picture is further confused by an earlier study by Manning & Carroll (132) who were not specifically looking for a history of radiation exposure in leukemic children but were attempting to identify other possible etiological factors. They found hypersensitivities of various sorts were more common in the mothers of leukemic children, and about twice as many of these mothers used "cold" tablets (usually antihistamines) as did mothers of control children.

These studies on leukemia incidence in children exposed neonatally to diagnostic x-ray exposures or in early life for thymic enlargement suggest that radiation may be an etiologic factor in the production of leukemia, but it has not been possible to rule out a contributing effect of the medical condition for which the exposures were given [Hempelmann (20)]. A similar comment may also apply to the ankylosing spondylitis patients since Abbatt & Lea (133) have shown an association between arthritis and leukemia. Until such associated factors can be fully evaluated, any predictions for normal populations which are based on these studies must be considered cautiously.

In summary, it must be concluded that a linear relationship between radiation dose and leukemia incidence has not been firmly established for man; but, for that matter, neither has any alternative relationship been satisfactorily substantiated. In passing it might be pointed out that proponents of the linear relationship have suggested on *a priori* grounds that linearity would be the logical result if somatic mutations were responsible. If it is assumed that somatic mutations are responsible for leukemia, there is still no compelling reason to believe a single hit event is always responsible for the "critical" mutation. If multihit chromosome aberrations contribute, then there would be a nonlinear component which would be dose-rate dependent.

EXPERIMENTAL ANIMALS

The mouse has been the most extensively utilized animal in studies of radiation leukemogenesis, because of the ease of leukemia induction and the variety of forms characteristic of various inbred strains. A number of reviews

have appeared recently, and no attempt will be made to cover the extensive current literature. Rather, only those aspects with an apparent direct bearing on the problem of human radiation leukemogenesis will be considered. Law (17), in his extensive review of radiation carcinogenesis, has again emphasized with admirable clarity that murine leukemia is not a single disease and that much of the confusion in interpreting experimental studies arises because precise classification is often lacking. The most extensively studied mouse leukemia appears to be the lymphocytic type originating in the thymus, which is variously classified as thymic leukemia, thymic lymphosarcoma, malignant lymphoma, and, unfortunately, as "mouse leukemia." Extensive studies by Upton and co-workers (134) have shown clearly that factors which influence the induction of this type of neoplasm may differ markedly from those which influence the induction of myeloid or granulocytic leukemia. Since the majority of radiation-induced leukemias in man are of the myeloid type, at least in adults, the thymic leukemia of mice may bear the least analogous relationship to the human situation. Further, Law (17) points out that since thymic lymphomas are "probably special and unique to the mouse" great caution should be exercised in attempting to extrapolate from them to man. The myeloid form of leukemia in mice, which may possibly be more analogous to human radiation-induced leukemia, has been less extensively studied.

In spite of these considerations of noncomparability of human and murine leukemias, it is worth noting that the leukemia responses of the two species show certain common qualities (104). Both species demonstrate a phasic incidence of excess leukemia mortality following single-dose whole-body exposure. In mice, it is not uncommon to observe the leukemia death rate of irradiated groups to fall back to or near control levels 18 to 20 months after exposure (61, 105). The same general phenomenon can be seen among the Hiroshima and Nagasaki survivors (116) although, by 1957, they still showed some excess mortality over their unirradiated controls. By a shifting of time scales, the human and murine experiences can be made to superimpose; and, for comparable radiation exposures, the factor of increase in age-specific leukemia mortality over the control is nearly identical for the two species (104).

Radiation-induced, murine lymphatic leukemia shows the following characteristics. In certain strains of mice the presence of the thymus is necessary for induction [Kaplan (135)] although the thymus itself need not be irradiated. There is strong evidence that the mechanism of induction is indirect since a normal thymus transplanted to an irradiated host may become neoplastic [Kaplan & Brown (136)]. In other strains, the removal of the thymus shifts the site of origin of the tumor to other lymphoid tissue (134). Repeated radiation exposures given in the proper sequence result in a higher incidence than do single exposures to the same total dose [Kaplan (137); Upton *et al.* (134); Cole *et al.* (81)]. Inoculations of normal bone marrow (88) or spleen (89), partial shielding (134, 138, 139), and certain of the radiation-protective agents (140) decrease the incidence. There is a striking dose-rate dependence

in response [Mole (80, 141, 142)] that, together with the incidence following various sized radiation dosages (134), strongly suggests a curvilinear relationship between dose and response.

Radiation-induced myeloid leukemias, on the other hand, are uninfluenced by the presence or absence of the thymus but are reduced by splenectomy (134). They are induced by lower radiation dosages than is the thymic form. Fractionation of exposure appears not to increase the incidence (134). Partial shielding reduces the incidence (134), as does the prophylactic administration of mercaptoethyl guanidine (140), a radioprotective agent. The incidence appears to reach a plateau at radiation doses above 150 r (134). The shape of the dose-response curve is not definitely known, but data for the incidence following doses of 16 and 32 r (143) and following 128 or more roentgens (134, 143) suggest curvilinearity in the low dose range.

There are a large number of variables other than radiation dose that contribute to the probability of an animal's developing leukemia. For example, strain, sex, and endocrine status are known to play major roles. Leukemia incidence can be increased or decreased by experimental modification of the endocrine status and genetic inheritance (by selection, hybridization, etc.), or by removal or implantation of tissues. The importance of a number of physiological variables has been emphasized in reviews by Law (17, 144); Furth & Baldini (145); Furth (146); Kaplan (147); Gardner *et al.* (148); and Upton & Furth (16). Recent research has also emphasized the role of filterable agents (viruses) in the induction of certain murine leukemias. Among recent review and summarizing articles are those by Gross (149, 150); Gross *et al.* (151); Dmochowski *et al.* (152); Furth & Baldini (145); Friend (153), and Graffi (154). Implication of viruses as possible etiologic agents, as well as the clear demonstration of the role of the animal's physiologic state, indicates that leukemia induction in mice is a complex phenomenon. This complexity should be considered in the formulation of models and hypotheses which attempt to account for radiation leukemogenesis.

GENETICS

Normally, a review of this type does not concern itself with genetic effects of radiation. However, increased concern over low-dose effects has focused attention on questions of both genetic and somatic damage and, as will be noted below, there is a point where the two become nearly inseparable. In addition, a better understanding of low-dose genetic effects may well clarify our understanding of low-dose somatic responses at the cellular level. Consequently, a brief discussion is given on what might be called studies of opportunity on progeny of groups of humans known to have been exposed to penetrating radiations.

MAN

Although there are no quantitative data for man on increases in mutation rate at specific loci as a function of radiation dose, there are several ways in

which genetic effects may be studied. One of the more direct methods is the study of sex ratio in offspring of irradiated parents. According to genetic theory, exposure of the female parent should result in a decreased proportion of male offspring (since the unpaired X chromosome in male children is inherited from the female parent), and exposure of the male parent should result in an increased proportion of male offspring since sex-linked lethals would be transmitted only to the female children. Schull (28) and Schull & Neel (155) have reviewed the available data on sex ratios in the offspring of irradiated parent. These data include the study by Kaplan (156) on offspring of women receiving ovarian radiation to correct an apparent sterility, the work of Macht & Lawrence (157) on sex ratios in the offspring of American radiologists, the data of Turpin *et al.* (158) on offspring of patients receiving therapeutic radiation to the pelvic area, and their own extensive information on offspring of atomic bomb survivors. In 14 of the 18 comparisons that could be set up, the shift in sex ratio was in the direction predicted by theory. This finding suggests that in spite of the many complicating factors inherent in this type of study, the response is at least qualitatively in accord with expectation.

The incidence of congenital abnormalities in the children of radiologists has been studied by Macht & Lawrence (157). Of 5461 children, 5.99 per cent showed defects (many of them minor) whereas 4.84 per cent of 4484 control children showed defects. While this difference may be significant, Neel & Schull (29) have questioned its validity because of the method of scoring the data and the types of defects included. In their own extensive studies in Hiroshima and Nagasaki, Neel & Schull were not able to show that radiation exposure had increased the incidence of congenital defects in the first generation. This finding is not, however, necessarily in conflict with theory (29). Gentry *et al.* (159) have studied the variation in incidence of congenital malformations in New York State as a function of geographical area. The hypothesis under test was that those areas likely to show a high radiation background on the basis of geological data (type of rock formations) would also show an elevated incidence of congenital malformation. The results appeared to indicate that there was an association between these factors. The lack of information as to the actual radiation exposures to the populations under consideration, as well as an apparent lack of detailed investigation of consanguinity of matings, precludes definitive consideration of the results in terms of potential radiation effects. A preliminary report by Kratchman & Grahn (160) has also attempted to relate variation in the incidence of death from malformations to certain characteristics of the geologic environment with particular reference to the major uranium-ore-bearing regions. They concluded that those areas which might be expected to show an elevated level of background radiation appear to show a higher incidence of death from congenital malformations. They emphasize, however, that their data are uncorrected for a number of factors known to have a bearing on the incidence of malformations and that the radiation levels have not been measured di-

rectly. For these reasons, they caution against drawing any definitive conclusions.

There is, at present, an increasing interest in epidemiologic investigations of the above type, since comparatively large human populations can be observed. Potentially, such studies can be of great assistance in evaluation of the effects of very low levels of radiation exposure. Unfortunately, there is some tendency to conclude that these studies only measure the effects of an increased mutation rate, thus ignoring the possibility that a portion of any observed differences could be the result of direct irradiation damage to the developing embryo. Since the effects of both genetic and somatic radiation damage are undoubtedly being measured along with all other confounded environmental and biological variants in the population, the real problem becomes one of separating the effects of the various contributing factors. In this respect, congenital malformations may not be the most critical endpoint and, wherever possible, other measures should be made concurrently, i.e., sex ratio, fetal death rate, birth weight, neonatal, infant, and childhood death rate, and the incidence of neoplastic diseases.

Fetal death, one of the predicted consequences of induced mutations, has not been shown to be significantly higher in the offspring of radiologists (157, 161) or atomic bomb survivors (29). This statement, of course, does not apply to those cases of direct irradiation of the fetus where death is presumably the result of somatic damage. Once again, this negative finding does not refute genetic theory because only those fetuses that have survived to a relatively late stage in development would be scored as stillbirths and early lethal effects would be missed. Additionally, if the mutations were predominantly recessive they would not be expected to become manifest in the first generation.

Crow (161) did not find an increased incidence of neonatal death among children of radiologists, nor did Neel & Schull (29) find an increased death rate in the first week of life for children born to survivors of the Hiroshima and Nagasaki bombings. There is, however, a suggestion of an increased mortality between birth and nine months of age for the children of exposed parents in both cities (29) though, statistically, the differences are not significant.

EXPERIMENTAL ANIMALS

The literature on experimental radiation genetics is too voluminous to review here and the reader is referred to other sources (38, 39, 41). No review of late effects would seem complete, however, without mention of the recent finding of Russell *et al.* (30, 162, 163) that the mutation rate in mouse spermatogonia shows an apparent dose-rate dependence with protracted exposures being about one-fourth as effective as single exposures. This finding, which necessitates revision of much of the previous thinking on both germinal and somatic radiation-induced mutations, may prove to be one of the most highly significant in the field of radiation biology in recent years.

LITERATURE CITED

1. Bond, V. P., and Robertson, J. S., *Ann. Rev. Nuclear Sci.*, **7**, 135-62 (1957)
2. Rugh, R., *Ann. Rev. Nuclear Sci.*, **9**, 493-522 (1959)
3. Comfort, A., *Radiation Research*, Suppl. 1, 216-34 (1959)
4. Yockey, H. P., *Health Phys.*, **1**, 427-41 (1959)
5. Strehler, B. L., *Quart. Rev. Biol.*, **34**, 117-42 (1959)
6. Upton, A. C., *J. Gerontol.*, **12**, 306-13 (1957)
7. Mole, R. H., *Nature*, **180**, 456-60 (1957)
8. Alexander, P., *Gerontologia*, **1**, 174-93 (1957)
9. Glucksmann, A., Lamerton, L. F., and Mayneord, W. V., in *Cancer*, **1**, 497-539 (Raven, R. W., Ed., Butterworth and Co. Ltd., London, Engl., 1957)
10. Upton, A. C., *Federation Proc.*, **17**, 698-713 (1958)
11. Schwartz, E. E., and Upton, A. C., *Blood*, **13**, 845-64 (1958)
12. Brues, A. M., *Radiation Research*, **3**, 272-80 (1955)
13. Brues, A. M., *Science*, **128**, 693-99 (1958)
14. Mole, R. H., *Brit. Med. Bull.*, **14**, 184-89 (1958)
15. Furth, J., and Upton, A. C., *Acta Radiol.*, Suppl. 116, 469-76 (1954)
16. Upton, A. C., and Furth, J., *Proc. Natl. Cancer Conf.*, 3rd, 1956, 312-24 (1957)
17. Law, L. W., in *Fallout from Nuclear Weapons Tests. Hearings before Special Subcommittee on Radiation of Joint Committee on Atomic Energy, Congr. of the U. S., May 27-29 and June 3-7, 1957*, **2**, 1421-36 (1959)
18. Kaplan, H. S., *Cancer Research*, **19**, 791-803 (1959)
19. Burnet, M., *New Engl. J. Med.*, **259**, 423-31 (1958)
20. Hempelmann, L. H., *Cancer Research*, **20**, 18-27 (1960)
21. Furth, J., Upton, A. C., and Kimball, A. W., *Radiation Research*, Suppl. 1, 243-64 (1959)
22. Tullis, J. L., *Arch. Pathol.*, **66**, 403-17 (1958)
23. Brues, A. M., *Publ. Am. Assoc. Advance Sci.*, No. 59, 73-86 (1959)
24. Mole, R. H., *Radiation Research*, Suppl. 1, 124-48 (1959)
25. Kaplan, H. S., *Am. J. Roentgenol.*, *Radium Therapy Nuclear Med.*, **80**, 696-706 (1958)
26. Webster, E. W., *Radiology*, **72**, 493-507 (1959)
27. Hodges, P. C., *Radiology*, **72**, 481-88 (1959)
28. Schull, W. J., *Radiology*, **72**, 522-28 (1959)
29. Neel, J. V., and Schull, W. J., *Natl. Acad. Sci.—Natl. Research Council*, Publ. No. 461 (1956)
30. Russell, W. L., and Russell, L. B., *Radiation Research*, Suppl. 1, 296-305 (1959)
31. Carter, T. C., *Lancet*, **I**, 216-17 (1960)
32. *Proc. Intern. Conf. Peaceful Uses Atomic Energy*, 2nd, Geneva, 1958, **22**, 23 (1958)
33. *The Nature of Radioactive Fallout and Its Effects on Man. Hearings before Special Subcommittee on Radiation of Joint Committee on Atomic Energy, Congr. of the U. S., May 27-29 and June 3-7, 1957*, **1**, 2 (U. S. Govt. Printing Office, Washington, D. C., 1959)
34. *Fallout from Nuclear Weapons Tests. Hearings before Special Subcommittee on Radiation of Joint Committee on Atomic Energy, Congr. of the U. S., May 5-8, 1959*, **1**, 2, 3 (U. S. Govt. Printing Office, Washington, D. C., 1959)
35. *Biological and Environmental Effects of Nuclear War. Hearings before Special Subcommittee on Radiation of Joint Committee on Atomic Energy, Congr. of the U. S., June 22-26 (1959)*
36. *The Biological Effects of Atomic Radiation. Summary Repts.* (U. S. Natl. Acad. Sci.—Natl. Research Council, Washington, D. C., 1956)
37. *The Hazards to Man of Nuclear and Allied Radiation, Rept. of Med. Research Council* (Her Majesty's Stationery Office, London, Engl., 1956)
38. *Report of the U.N. Committee on Effects of Atomic Radiation*, Suppl. No. 17 (A/3838) (United Nations, New York, N. Y., 1958)
39. *Effect of Radiation on Human Heredity* (World Health Organization, Geneva, 1957)
40. Bugher, J. G., Coursaget, J., and Loutit, J. F., Eds., *Progr. in Nuclear Energy, Ser. VI, Biol. Sci.*, **2** (1959)
41. Claus, W. D., Ed., *Radiation Biol.*

- ogy and Medicine (Addison-Wesley Publ., Reading, Mass., 1958)
42. deHevesy, J., Forssberg, A. G., and Abbott, J. D., Eds., *Advances in Radiobiology* (Oliver and Boyd, Ltd., Edinburgh, Scotland, 1957)
 43. Mitchell, J. S., Holmes, B. E., and Smith, C. L., Eds., *Progress in Radiobiology* (Charles C Thomas, Springfield, Ill., 1956)
 44. Warren, S., *J. Am. Med. Assoc.*, **162**, 464-68 (1956)
 45. Seltser, R., and Sartwell, P. E., *J. Am. Med. Assoc.*, **166**, 585-87 (1958)
 46. Court-Brown, W. M., and Doll, R., *Brit. Med. J.*, **II**, 181-87 (1958)
 47. Court-Brown, W. M., and Doll, R., *Proc. Intern. Conf. Peaceful Uses Atomic Energy*, 2nd, Geneva, 1958, **23**, 179-82 (1958)
 48. Kohn, H. I., *Radiol. Lab., Univ. Calif., San Francisco, Progr. Rept. UCSF-19* (1959)
 49. Newell, R. R., *Biological and Environmental Effects of Nuclear War. Hearings before Special Subcommittee on Radiation of Joint Committee on Atomic Energy, Congr. of the U. S., June 22-26*, 307 (1959)
 50. Conard, R. A., Meyer, L. M., Robertson, J. S., Sutow, W. W., Wolins, W., and Hechter, H., *Radiation Research*, Suppl. 1, 280-95 (1959)
 51. Kallman, R. F., and Kohn, H. I., *Science*, **128**, 301-2 (1958)
 52. Boone, I. U., *Radiation Research*, **11**, 434 (1959)
 53. Lamson, B. G., Billings, M. S., and Bennett, L. R., *J. Natl. Cancer Inst.*, **22**, 1059-75 (1959)
 54. Maisin, J., Maldague, P., Dunjic, A., and Maisin, H., *J. belge radiol.*, **40**, 347-98 (1957)
 55. Maisin, J., Dunjic, A., Maldague, P., and Maisin, H., *Proc. Intern. Conf. Peaceful Uses Atomic Energy*, 2nd, Geneva, 1958, **22**, 57-64 (1958)
 56. Dunjic, A., Maisin, J., Maldague, P., and Maisin, H., *Radiation Research*, **12**, 155-66 (1960)
 57. Alexander, P., and Connell, D. I., *Radiation Research*, **12**, 38-48 (1960)
 58. Lindop, P., and Rotblat, J., *Proc. Intern. Conf. Peaceful Uses Atomic Energy*, 2nd, Geneva, 1958, **22**, 46-52 (1958)
 59. Curtis, H. J., and Healy, R., in *Advances in Radiobiology*, 261-65 (Oliver and Boyd, Ltd., Edinburgh, Scotland, 1956)
 60. Curtis, H. J., and Gebhard, K., *Radiation Research*, **9**, 278-84 (1958)
 61. Grahn, D., and Sacher, G. A., *Radiation Research*, **8**, 187-94 (1958)
 62. Grahn, D., *Radioisotopes in the Biosphere* (Center for Continuation Study, Univ. of Minn., Minneapolis, Minn., in press, 1960)
 63. Grahn, D., *Proc. Intern. Conf. Peaceful Uses Atomic Energy*, 2nd, Geneva, 1958, **22**, 394-99 (1958)
 64. Storer, J. B., and Sanders, P. C., *Radiation Research*, **8**, 64-70 (1958)
 65. Storer, J. B., Rogers, B. S., Boone, I. U., and Harris, P. S., *Radiation Research*, **8**, 71-76 (1958)
 66. Kohn, H. I., and Guttman, P. H., *Nature*, **184**, Suppl. 10, 735-36 (1959)
 67. Gowen, J. W., and Stadler, J., *J. Exptl. Zool.*, **132**, 133-55 (1956)
 68. Storer, J. B. (In progress, 1960)
 69. Noble, J. F., and Doull, J. (Personal communication)
 70. Furth, J., Upton, A. C., Christenberry, K. W., Benedict, W. H., and Moshman, J., *Radiology*, **63**, 562-70 (1954)
 71. Sacher, G. A., *Radiology*, **67**, 250-57 (1956)
 72. Duhig, J. T., and Warren, S., *Arch. Pathol.* (In press)
 73. "Report of the Ad Hoc Committee of the National Committee on Radiation Protection and Measurements," *Science*, **131**, 482-86 (1960)
 74. Neary, G. J., Munson, R. J., and Mole, R. H., *Chronic Radiation Hazards: An Experimental Study with Fast Neutrons* (Pergamon Press, London, Engl, 1957)
 75. Upton, A. C. (Personal communication)
 76. Carlson, L. D., and Jackson, B. H., *Radiation Research*, **11**, 509-19 (1959)
 77. Lorenz, E., Jacobson, L. O., Heston, W. E., Shimkin, M., Eschenbrenner, A. B., Deringer, M. K., Doniger, J., and Schweisthal, R., in *Biological Effects of External X and Gamma Radiation*, 1-242 (McGraw-Hill Publishing Co., New York, N. Y., 1954)
 78. Sacher, G. A., and Grahn, D. (Unpublished observations)
 79. Hursh, J. B., Noonan, T. R., Casarett, G., and Van Slyke, F., *Am. J. Roentgenol., Radium Therapy Nuclear Med.*, **74**, 130-34 (1955)
 80. Mole, R. H., *Brit. J. Radiol.*, **32**, 497-501 (1959)
 81. Cole, L. J., Nowell, P. C., and Arnold,

- J. S., *Radiation Research*, 12, 173-85 (1960)
82. Kaplan, H. S., and Brown, M. B., *J. Natl. Cancer Inst.*, 13, 185-208 (1952)
83. Henshaw, P. S., Riley, E. F., and Stapleton, G. E., *Radiology*, 49, 349-59 (1947)
84. Evans, T. C., *Radiology*, 50, 811-33 (1948)
85. Hollaender, A., Congdon, C. C., Doherty, D. G., Makinodan, T., and Upton, A. C., *Proc. Intern. Conf. Peaceful Uses Atomic Energy*, 2nd, Geneva, 1958, 23, 3-9 (1958)
86. Mewissen, D. J., *Compt. rend. soc. biol.*, 153, 183-87 (1959)
87. Hollcroft, J., Lorenz, E., Miller, E., Congdon, C. C., Schweisthal, R., and Uphoff, D., *J. Natl. Cancer Inst.*, 18, 615-40 (1957)
88. Kaplan, H. S., Brown, M. B., and Paul, J., *J. Natl. Cancer Inst.*, 14, 303-16 (1953)
89. Cole, L. J., Nowell, P. C., and Ellis, M. E., *J. Natl. Cancer Inst.*, 17, 435-47 (1956)
90. Casarett, G. W., *Univ. of Rochester Rept. UR-492* (1956)
91. Hursh, J. B., Casarett, G. W., Carsten, A. L., Noonan, T. R., Michaelson, S. M., Howland, J. W., and Blair, H. A., *Proc. Conf. Peaceful Uses Atomic Energy*, 2nd, Geneva, 1958, 22, 178-83 (1958)
92. Yockey, H. P., *Radiation Research*, 5, 146-55 (1956)
93. Yockey, H. P., in *Radiation Biology and Medicine*, 250-82 (Addison-Wesley Pub. Co., Cambridge, Mass., 1958)
94. Quastler, H., *Ann. Rev. Nuclear Sci.*, 8, 387-400 (1958)
95. Muller, H. J., *J. Cellular Comp. Physiol.*, 35, Suppl. 1, 9-70 (1950)
96. Henshaw, P. S., *Radiology*, 69, 30-36 (1957)
97. Failla, G., *Proc. Gallinburg Conf. Biol. Aspects of Aging* (Am. Inst. Biol. Sci., Washington, D. C., 1957)
98. Failla, G., *Proc. N. Y. Acad. Sci.*, 71, 1124-40 (1958)
99. Sacher, G. A., in *Symposium on Information Theory in Biology*, 317-30 (Pergamon Press, New York, N. Y., 1958)
100. Blair, H. A., *Intern. Conf. Peaceful Uses Atomic Energy*, 1st, Geneva, 1955, 11, 118-20 (1956)
101. Blair, H. A., *Univ. Rochester Rept. U.R.-206* (1958)
102. Storer, J. B., *Radiation Research*, 10, 180-96 (1959)
103. Gompertz, B., *Phil. Trans. Roy. Soc. London, Ser. A*, 115, 513-89 (1825)
104. Sacher, G. A., *Proc. Intern. Congr. Radiol.* (In press, 1959)
105. Brues, A. M., and Sacher, G. A., in *Symposium on Radiobiology* (John Wiley & Sons, New York, N. Y., 1952)
106. Grahn, D., Hamilton, K. F., and Sacher, G. A., *Proc. Intern. Congr. Genet.*, 10th, 2, 102-3 (1958)
107. Leshner, S., Grahn, D., and Sallesse, A., *J. Natl. Cancer Inst.*, 19, 1119-27 (1957)
108. Jones, H. B., *Advances in Biol. and Med. Phys.*, 4, 281-337 (1956)
109. Jones, H. B., *Trans. N. Y. Acad. Sci.*, 18, 298-333 (1956)
110. Szilard, L., *Proc. Natl. Acad. Sci., U. S.*, 45, 30-45 (1959)
111. Henshaw, P. S., and Hawkins, J. W., *J. Natl. Cancer Inst.*, 4, 339-46 (1944)
112. March, H. C., *Am. J. Med. Sci.*, 220, 282-86 (1950)
113. Folley, J. H., Borges, W., and Yamawaki, T., *Am. J. Med.*, 13, 311-21 (1952)
114. Lange, R. D., Moloney, W. C., and Yamawaki, T., *Blood*, 9, 574-85 (1954)
115. Moloney, W. C., and Kastenbaum, M. A., *Science*, 121, 308-9 (1955)
116. Wald, N., *Science*, 127, 699-700 (1958)
117. Simpson, C. L., Hempelmann, L. H., and Fuller, L. M., *Radiology*, 64, 840-45 (1955)
118. Simpson, C. L., and Hempelmann, L. H., *Cancer*, 10, 42-56 (1957)
119. Simpson, C. L., in *Radiation Biology and Cancer*, 336-46 (University of Texas Press, Austin, Texas, 1959)
120. Polhemus, D. W., and Koch, D., *Pediatrics*, 23, 453-61 (1959)
121. Snegireff, L. S., *Radiology*, 72, 508-17 (1959)
122. Conti, E. A., Patton, G. B., Conti, J. E., and Hempelmann, L. H., in *Hempelmann, L. H., Cancer Research*, 20, 18-27 (1960)
123. Gilliam, A. G., and Walter, W. A., *Public Health Repts.*, 73, 773-84 (1958)
124. Lewis, E. B., *Science*, 125, 965-72 (1957)
125. Schubert, J., in *Fallout from Nuclear Weapons Tests. Hearings before Special Subcommittee on Radiation of Joint Committee on Atomic*

- Energy, Congr. of the U. S., May 5-8, 1959, 2, 1657 (1959)*
126. Court-Brown, W. M., *Brit. Med. Bull.*, **14**, 168-73 (1958)
 127. Kimball, A. W., *J. Natl. Cancer Inst.*, **21**, 383-91 (1958)
 128. Murray, R., Heckel, P., and Hempelmann, L. H., *New Engl. J. Med.*, **261**, 585-89 (1959)
 129. Faber, M., in *Advances in Radiobiology*, 397-404 (deHevesy, G., Forssberg, A. G., and Abbott, J. D., Eds., Oliver & Boyd, Ltd., Edinburgh, Scotland, 1957)
 130. Stewart, A., Webb, J., and Hewitt, D., *Brit. Med. J.*, **1**, 1495-1508 (1958)
 131. Ford, D. D., Paterson, J. C. S., and Treuting, W. L., *J. Natl. Cancer Inst.*, **22**, 1093-1104 (1959)
 132. Manning, M. D., and Carroll, B. E., *J. Natl. Cancer Inst.*, **19**, 1087-94 (1957)
 133. Abbott, J. D., and Lea, A. J., *Lancet*, **II**, 880-83 (1958)
 134. Upton, A. C., Wolff, F. F., Furth, J., and Kimball, A. W., *Cancer Research*, **18**, 842-48 (1958)
 135. Kaplan, H. S., *J. Natl. Cancer Inst.*, **11**, 83-90 (1950)
 136. Kaplan, H. S., and Brown, M. B., *Science*, **119**, 439-40 (1954)
 137. Kaplan, H. S., *J. Natl. Cancer Inst.*, **13**, 185-208 (1952)
 138. Lorenz, E., Congdon, C. C., and Up-hoff, D. J., *J. Natl. Cancer Inst.*, **14**, 291-301 (1953)
 139. Kaplan, H. S., *Cancer Research*, **12**, 441-44 (1952)
 140. Upton, A. C., Doherty, D. G., and Melville, G. S., Jr., *Acta Radiol.*, **51**, 379-84 (1959)
 141. Mole, R. H., *Brit. Med. Bull.*, **14**, 174-77 (1958)
 142. Mole, R. H., *Proc. Intern. Conf. Peaceful Uses Atomic Energy*, 2nd, Geneva, 1958, **22**, 145-48 (1958)
 143. Upton, A. C., Furth, J., and Christen-bery, K. W., *Cancer Research*, **14**, 682-90 (1954)
 144. Law, L. W., *Ann. N. Y. Acad. Sci.*, **68**, 616-35 (1957)
 145. Furth, J., and Baldini, M., in *The Phys-iopathology of Cancer*, 2nd Ed., 364-468 (Hoebner-Harper, New York, N. Y., 1959)
 146. Furth, J., *Cancer Research*, **19**, 241-58 (1959)
 147. Kaplan, H. S., in *Radiation Biology and Cancer*, 289-302 (Univ. of Texas, Austin, Texas, 1959)
 148. Gardner, W. U., Pfeiffer, C. A., and Trentin, J. J., in *The Physio-pathology of Cancer*, 2nd Ed., 152-237 (Hoebner-Harper, New York, N. Y., 1959)
 149. Gross, L., *Cancer Research*, **18**, 371-81 (1958)
 150. Gross, L., *Ann. N. Y. Acad. Sci.*, **68**, 501-21 (1957)
 151. Gross, L., Roswit, B., Mada, E. R., Dreyfuss, Y., and Moore, L. A., *Cancer Research*, **19**, 316-20 (1959)
 152. Dmochowski, L., Grey, C. E., and Gross, L., in *Radiation Biology and Cancer*, 382-99 (University of Texas Press, Austin, Texas, 1959)
 153. Friend, C., *Ann. N. Y. Acad. Sci.*, **68**, 522-32 (1957)
 154. Graffi, A., *Ann. N. Y. Acad. Sci.*, **68**, 540-58 (1957)
 155. Schull, W. J., and Neel, J. V., *Science*, **128**, 343-48 (1958)
 156. Kaplan, I. I., *Radiology*, **72**, 518-21 (1959)
 157. Macht, L. H., and Lawrence, P. L., *Am. J. Roentgenol., Radium Ther-apy Nuclear Med.*, **73**, 446-66 (1955)
 158. Turpin, R., Lejeune, J., and Rethore, M. O., *Proc. Intern. Congr. Human Genetics, 1st, Copenhagen, 1956*, (1957)
 159. Gentry, J. T., Parkhurst, E., and Bulin, E. V., Jr., *Am. J. Public Health*, **49**, 457-513 (1959)
 160. Kratchman, J., and Grahn, D., *U. S. Atomic Energy Commission Rept. TID-8204* (1959)
 161. Crow, J. F., *Am. J. Roentgenol., Ra-dium Therapy Nuclear Med.*, **73**, 467-71 (1955)
 162. Russell, W. L., Russell, L. B., and Kelley, E. M., *Science*, **128**, 1546-50 (1958)
 163. Russell, W. L., and Russell, L. B., *Proc. Intern. Conf. Peaceful Uses Atomic Energy*, 2nd, Geneva, 1958, **22**, 360-65 (1958)

AUTHOR INDEX

A

Abbatt, J. D., 533, 549, 574
 Abraham, M., 324
 Abrahamson, S., 497, 509
 Adams, J. A. S., 443
 Adams, J. D., 512
 Adams, J. H., 434
 Adler, H. H., 425
 Agnew, L., 182
 Ahlendorf, W., 496
 Ahrens, R. W., 281
 Ah-Shen, L., 512, 599
 Aikawa, J. K., 541
 Aizu, H., 102
 Ajzenberg-Selove, F., 409-24; 354, 409
 Akopian, G. M. T., see Ter-Akopian, G. M.
 Alaga, G., 231, 233
 Alburger, D. E., 394
 Alder, K., 231, 233
 Alexander, G. V., 542
 Alexander, J. M., 241, 242, 246, 247, 248, 249, 251, 252, 253, 254, 255
 Alexander, P., 561, 564, 568
 Alexeff, I., 319, 320
 Alichanyan, A. I., 126
 Alikhanyan, S. I., 504, 513
 Alimarin, I. P., 264, 269
 Aliprandi, B., 285
 Alkhazov, D. G., 43
 Allaby, J. V., 321, 322
 Allaud, L. A., 446
 Allen, C. W., 24
 Allen, J., 2
 Allfrey, V. G., 517
 Allred, J. C., 319, 322
 Almqvist, E., 58, 389
 Alper, T., 489-530; 491, 498, 502, 503, 505, 507, 508, 509, 511, 523, 524
 Alpert, L. K., 547
 Alpher, R. A., 24
 Alphonse, R., 315
 Alston, M., 157
 Alvarez, L. W., 15, 116, 140
 Alyea, E. D., 117
 Amery, A., 131, 133, 139
 Amiot, P., 109, 128, 135, 147
 Amit, D., 389
 Anderson, C. E., 44, 45, 53, 55, 60
 Anderson, E. C., 533, 537, 539, 540, 544
 Anderson, H., 461, 465

Anderson, K. A., 481, 482
 Anderson, R. C., 260, 265, 269, 270, 271, 275, 276, 277, 284
 Andrews, G. A., 541, 545
 Andronikashvili, E. L., 78
 Anfinsen, C. B., 281
 Anthony, D. S., 548, 552
 Anwar, R. A., 548
 Ardashnikov, S. N., 489, 501, 521
 Ariotti, P., 502, 503
 Armstrong, A. H., 319, 322
 Arnold, J. R., 425
 Arnold, J. S., 538, 543, 553, 554, 566, 567, 575
 Arnoldy, R. L., 472, 473
 Aronovich, P. M., 272
 Arrée, O. H., 252
 Asaro, F., 229
 Ashburn, A. G., 131, 133, 139
 Ashkin, J., 293, 296, 298
 Ashmore, A., 321, 322, 343
 Asling, C. W., 549
 Atherton, D. R., 543, 545, 553
 Atkinson, J. H., 152
 Atterling, H., 244, 246, 247, 250
 Atwood, K. C., 492, 515
 Auger, P., 97
 Aurand, K., 544
 Avery, E. C., 491
 Axelrod, D. J., 554

B

Bach, G. R., 44, 45, 55
 Bacher, R. F., 355
 Bachofer, C. S., 509
 Bahner, C. T., 546
 Bailey, D. K., 480
 Bainbridge, K. T., 169, 186
 Baker, P. E., 444, 452
 Baker, S. D., 33
 Bakke, F., 308
 Baldini, G., 521
 Baldini, M., 576
 Baldwin, J., 320, 332
 Baldwin, W. F., 513
 Baldwin, W. T., 505, 506
 Ball, E. G., 284
 Ball, J. B., 242
 Ballou, J. E., 536, 538, 540, 545, 551, 553
 Band, I. M., 195, 199, 201, 203, 204, 210, 231
 Banford, A. P., 322
 Banit, S., 497
 Baraboshkin, S. A., 45, 50
 Barbieri, R., 270, 271, 276, 277
 Bardwell, D. C., 259
 Barford, N. C., 109, 125, 131, 133, 135, 138, 139, 140
 Bargman, V., 298
 Barkas, W. H., 60, 151, 152, 154
 Barkow, A. G., 536, 550
 Barnes, C. M., 549
 Barnes, D. W. H., 548
 Barr, J., 502, 503
 Barrett, H. M., 434
 Barrett, N., 515
 Barrett, P. H., 78
 Bartholomew, G. A., 353
 Bascom, W., 435
 Bashkin, S., 60
 Baskin, S., 25
 Baskir, E., 319, 320, 332
 Bassel, R. H., 36
 Bassi, P., 115, 116, 123
 Batchelor, A. L., 505, 506
 Bauer, G. C. H., 542, 544
 Baulch, D. L., 239, 241, 246, 249
 Baum, J. W., 533
 Beam, C. A., 499, 501, 502, 524
 Becker, L. C., 33
 Beckerley, J. G., 425-60
 Beer, B. V. A. L., see Low-Beer, B. V. A.
 Beer, J. F. de, 81
 Bekkum, D. W. van, 520, 521
 Belanger, L. F., 547
 Belenki, S. Z., 94
 Belitzina, N. V., 510
 Bell, G. I., 244
 Bell, M., 546
 Belluco, U., 270, 271, 276, 277
 Belonogov, A. V., 131, 138
 Belsky, N. K., 272
 Benedict, W. H., 564
 Bengston, J., 331, 332, 333, 346
 Bennett, L. R., 563, 564, 565
 Bennett, S., 78, 79, 80
 Berbezier, J., 426, 427
 Beretta, L., 329, 331, 332
 Berg, H. F., 552
 Berg, O. E., 463
 Bergoniè, J., 513
 Bergström, S., 281
 Bernard, S. R., 553

- Berners, E. D., 316, 318, 332
 Bertanza, L., 122
 Bertinchamps, A. J., 533
 Bertrand, J. J., 541
 Bethe, H. A., 1, 2
 Beydon, J., 52
 Bhatnagar, A. S., 427
 Bibilashvili, M. F.,
 Biedenbarn, L. C., 306, 309
 Bigotte, G., 426
 Bilaniuk, O. M., 394
 Billen, D., 503, 523
 Billings, M. S., 563, 564, 565
 Bird, J. R., 443
 Bird, L., 316, 318, 319, 320, 321
 Birge, A. C., 501, 524
 Birge, R. W., 154, 316, 332
 Birkhoff, G., 115
 Biroll, G. P., see Pirzio-Biroll, G.
 Birss, I. R., 115
 Bisir, D. P., 426
 Bivins, R., 255
 Björnerstedt, R., 532, 543
 Blackett, N. M., 533
 Bladwin, E. M., 322
 Blair, H. A., 569, 570
 Blair, J. S., 31
 Blais, R. S., 546
 Blanchard, A., 441
 Blangy, B., 426, 427
 Blankenship, J. L., 60
 Blanpied, B. W., 428
 Blanpied, W. A., 319, 320
 Blanquet, P., 545
 Blatt, J. M., 47, 303, 304, 306, 309, 310, 316, 363, 366, 381
 Bleuler, E., 195, 231
 Blewett, J. P., 190
 Blinov, G. A., 115, 145
 Block, M. M., 116, 122
 Blum, H. F., 500
 Blumberg, R., 157
 Blumenfeld, L. A., 490
 Boag, J. W., 491, 498
 Bocharova, E. M., 510
 Bøggild, J. K., 245, 252
 Bohr, A., 196, 215, 219, 220, 231, 233, 353
 Bohr, N., 46, 244, 245, 247
 Bollinger, L. M., 78
 Bond, V. P., 561
 Bonner, J. F., Jr., 547
 Bonner, N. A., 259
 Boone, I. U., 552, 563, 564, 565, 567
 Booth, E. T., 252
 Borelli, V., 116, 123
 Borges, W., 572
 Boström, H., 548
 Bothwell, T. H., 550
 Bowers, B., 446
 Bowie, S. H. U., 426
 Boyd, G. A., 532
 Boyd, J., 543
 Boyle, T. L., 426
 Braams, C. M., 354
 Bradlow, H. L., 279, 280
 Bradner, H., 109-60; 111, 140, 143, 147, 332
 Brannon, H. R., Jr., 443
 Bratenahl, A., 315
 Breit, G., 29, 38, 41, 42, 46, 291, 305, 309, 312, 314, 316, 331, 332, 333, 345, 346
 Brenk, H. A. S. van den, 521
 Bresciani, F., 514
 Bretscher, E., 503
 Brinkworth, M. J., 332
 Britton, E. C., 284
 Brockman, K. W., Jr., 320
 Broda, E., 259
 Broecker, W. S., 546
 Brolley, J. E., Jr., 319, 322
 Bromley, D. A., 58, 353, 389
 Brooks, H., 259
 Brostrom, K. J., 245
 Brown, A. A., 446
 Brown, J. L., 117
 Brown, M. B., 566, 569, 575
 Brown, R. R., 482
 Brown, W. G., 279, 280
 Brown, W. M. C., see Court-Brown, W. M.
 Browne, C. P., 182
 Brucer, M., 545, 546, 552
 Brueckner, K., 322
 Brues, A. M., 534, 544, 561, 571, 572, 573, 575
 Brunello, C., 271, 275, 276
 Bruner, H. D., 545
 Brunnings, J. H. M., 244
 Bruno, M., 270, 271, 276, 277
 Brustad, T., 501, 502, 503
 Bryan, B. L. F., see Ferrell-Bryan, B. L.
 Bryan, R. A., 339, 345
 Bryant, H. C., 117
 Bryak, N., 204
 Buechner, W. W., 169, 182
 Bugg, D. V., 109, 116, 117, 120, 122, 134
 Bulashevich, Iu. P., 427
 Bull, E. V., Jr., 577
 Bülow, H., 512, 514
 Bunker, M. E., 232
 Burch, G. E., 539, 540, 545
 Burch, P. R. J., 500, 525
 Burcham, W. E., 60
 Burkig, J. W., 316, 332
 Burnet, M., 561, 572
 Burns, V. W., 499
 Burnstein, R. A., 117
 Busch, K. A., 518
 Bustad, L., 554
 Bustad, L. K., 549, 553
 Buster, D. S., 553
 Butler, C. C., 131, 133, 139
 Buttery, R. G., 278
 Buu Hoi, Ng. Ph., 284
 Byerrum, R. U., 548
- C
- Cacace, F., 270, 271, 275, 276, 285
 Cachon, A., 97
 Caldecott, R. S., 490, 510, 524
 Caldwell, R. L., 439, 450, 452, 454
 Calvin, M., 286
 Cameron, A. G. W., 55
 Campbell, I. G., 284
 Campbell, J. E., 548, 552
 Campos, M., 243
 Cannon, G. E., 435
 Capot, L., 545
 Capron, P. C., 260
 Carlson, B. C., 360, 377, 396
 Carlson, L. D., 566
 Carlson, R. R., 60
 Carlson, T. A., 284
 Carlsson, A., 544
 Carroll, B. E., 574
 Carsten, A. L., 569
 Carter, R. E., 3
 Carter, T. C., 561
 Cartwright, W. F., 292, 320, 332
 Carvalho, H. G. de, 315, 320, 332
 Casarett, G., 566
 Casarett, G. W., 569
 Cassels, J. M., 315, 316, 332
 Catcheside, D. G., 512
 Cater, D. B., 507
 Cather, J. N., 514, 520
 Chackett, K. F., 38, 45
 Chalmers, T. A., 259
 Chalvet, O., 259
 Chamberlain, A. C., 538
 Chamberlain, O., 161-92; 182, 292, 300, 308, 309, 315, 316, 319, 320, 321, 322, 323, 332
 Chaminade, R., 52
 Champion, W. R., 283
 Chandhuri, N., 278
 Chang, S. C., 270, 271
 Chang, T.-H., 509
 Charakhchian, A. N., 482
 Charakhchian, T. N., 482
 Charles, M., 541
 Charrin, P., 448
 Chastel, R., 252

Chestnut, W. G., 320
 Chetverikov, N. S., 501
 Chien, J. C. W., 263, 264, 266, 269
 Chih, C. Y., 319, 322, 332
 Chou, K.-C., 313
 Chretien, M., 180
 Christenbery, K. W., 564, 576
 Christofilos, N. C., 475
 Christopherson, W. M., 552
 Chuan Chen-Niang, 145
 Chudakov, A. E., 86, 88
 Chudakov, A. Ye., 470
 Church, E. L., 193-234; 195, 203, 208, 217, 230, 231, 232
 Chuvilo, I. V., 117
 Cieciura, S. J., 494, 519
 Cleri, L., 269, 270, 271, 275, 276, 285
 Clok, P., 94, 102
 Ciranni, G., 285
 Citron, A., 97
 Clark, G., 79
 Clarke, W. J., 554
 Class, C. M., 232, 360
 Clausnitzer, G., 324
 Clemedson, C. J., 532
 Clementel, E., 329, 330, 331, 332, 345
 Clermont, Y. G., see Goldschmidt-Clermont, Y.
 Cocconi, G., 21, 78, 94, 102, 480
 Coelho, F. P., 284
 Coffin, C. T., 244
 Coghen, T., 94, 102
 Cohen, A. F., 237, 244
 Cohen, B. L., 46, 50, 51, 237, 244
 Cohen, J., 532, 541
 Coish, H. R., 196
 Cole, A., 500, 524
 Cole, L. J., 566, 567, 569, 575
 Coley, C. D., 237, 244
 Collinson, E., 269
 Colodzin, M., 553
 Comar, C. L., 532, 536, 540, 542, 543, 548, 549, 550
 Comfort, A., 561
 Conard, R. A., 537, 545, 563
 Congdon, C. C., 568, 569, 575
 Conger, A. D., 490, 500, 502, 503
 Connell, D. I., 564, 568
 Conti, E. A., 572, 573
 Conti, J. E., 572, 573
 Conversi, M., 116, 123
 Cook, G. B., 548
 Cook, M. J., 536, 550
 Cool, R. L., 190
 Coombe, D. J., 244

Coombes, C. A., 187
 Coon, J. H., 319, 322, 332
 Cooper, D. I., 316, 319
 Cooper, O., 284
 Coor, T., 315
 Copp, D. H., 554
 Cork, B., 184, 187, 316, 319, 332
 Cormack, A. M., 316, 318, 319, 320, 332
 Cornman, W. R., Jr., 271
 Corson, D. R., 252
 Cotzias, G. C., 533, 549
 Coulson, C. A., 492
 Courant, E. D., 163
 Court-Brown, W. M., 563, 571, 572, 573
 Cowan, C. L., Jr., 2, 3, 9, 12
 Cowden, R. N., 548
 Crabtree, H. G., 507
 Cramer, W., 507
 Cranshaw, T. E., 81
 Crawford, F. S., 154
 Creasey, W. A., 517, 521
 Crew, A. V., 181, 182
 Crews, W. D., 426
 Critchfield, C. L., 469
 Croatto, U., 270, 271, 275, 276
 Cross, W. G., 169
 Crow, J. F., 578
 Crowley, J. F., 541
 Crut, M., 52
 Culler, V., 315
 Cullington, A. L., 476
 Cupp, M. B., 497
 Curtis, H. J., 490, 510, 564, 567, 568
 Cutmore, T. P., 442
 Cziffra, P., 337, 339, 341, 343
 Czubek, J., 429

D

Dahl, P. F., 316
 Dalitz, R. H., 293, 300
 Dancoff, S., 200
 Daniels, E. W., 512
 Danzker, M., 501
 D'Arcy, R. G., 482
 Darden, S., 315
 Daudel, R., 259, 284
 Daudin, A., 97
 Davies, G. E., 138
 Davies, J. A., 246, 247
 Davies, T. H., 259
 Davis, L. R., 463
 Davis, R., 15, 24
 Davis, R. H., 360
 Davis, R. N., 548
 Davison, R. J., 104
 Dawson, W. W., 500
 Day, R. B., 315, 322, 323
 de Beer, J. F., see Beer, J. F. de

de Carvalho, H. G., see Carvalho, H. G. de
 Deering, R. A., 492, 523
 De Juren, J., 315
 Delabarre, Y., 284
 Delhas, N., 490, 510
 DeLong, C. W., 538
 Delvaille, J., 74, 81, 94, 103
 Demers, P., 245, 252
 Demidov, A. M., 451, 452
 Denko, C. W., 547
 De Pangher, J., 319, 322, 332
 Deringer, M. K., 566, 567
 Deschner, E. E., 505, 510, 519, 520
 de-Shalit, A., see Shalit, A. de-
 Deutch, B. I., 222
 Dewan, J. T., 441, 446, 448
 Dewey, D. L., 498
 de Witt, M., see Witt, M. de
 Dickson, J. M., 320, 332
 Diddens, A. N., 321, 322, 343
 Dmitriyev, V. A., 76, 83
 Dmochowski, L., 576
 Dodd, C., 115
 Dodd, P. H., 441
 Dodson, R. W., 260, 266, 284
 Doering, W. von E., 278
 Doherty, D. G., 568, 575, 576
 Doll, R., 563, 571, 573
 Donaldson, R., 145, 319, 323, 332
 Doniach, I., 513, 518
 Doniger, J., 566, 567
 Donovan, P. F., 237, 238, 241, 242, 246, 249, 255
 Dorfman, L. M., 282
 Dorman, L. I., 480
 Dosc, K., 514
 Dostrovsky, I., 52, 255
 Doudney, C. O., 511, 512, 521
 Douglas, R. A., 60
 Doull, J., 564, 566, 567
 Douthett, E. M., 238
 Dovzenko, O. I., 83
 Drakulic, M., 518
 Drance, S. M., 522
 Dreyfuss, Y., 576
 Drisko, R. M., 36
 Dropesky, B. J., 232
 Drouillard, R. F., 441
 Druin, V. A., 56, 57
 Druyan, R., 542
 Dudley, H. C., 546, 551
 Duhig, J. T., 564
 Duncan, J. F., 239, 241, 246, 249
 Dunjic, A., 563, 564, 565, 569
 Dunning, J. R., 252

- Durand, L., 319, 327, 332, 333
 Durbin, P. W., 546, 548, 549, 550, 551, 552, 554
 Durham, F. E., 232
 Dutton, H. J., 281, 282
 Dyson, E. D., 538
 Dzhelepov, V. P., 300, 303, 315, 318, 322, 323, 332
 Dziunikowski, B., 429
- E
- Eades, J., 321, 322
 Earl, J., 79
 Earl, J. A., 484
 Easley, J. W., 319, 322, 332
 Eaton, W., 134
 Ebel, M. E., 41
 Eberhard, P., 189, 190
 Ebert, M., 509, 525
 Edington, C. W., 502, 503
 Edmonds, A. R., 365, 369
 Edwards, D. N., 319, 321
 Edwards, R., 271
 Edwards, R. R., 259
 Ehrenberg, A., 490, 510, 524
 Ehrenberg, L., 490, 503, 510, 524
 Ehret, C. F., 508
 Ehrman, J. B., 332, 333, 361
 Eigner, J., 279
 Eisberg, R. M., 33
 Eisenberg, Y., 78
 Eisinger, J., 196
 Eisler, F., 116, 123
 Elioff, T., 182
 Elkind, M. M., 492, 493, 494, 497, 502, 504, 513, 519, 524
 Ellinger, F. P., 531
 Elliott, J. P., 353, 360, 381, 382, 398, 405
 Ellis, F., 516, 519
 Ellis, M. E., 569, 575
 El Sayed, M. A., 259, 265, 279, 281, 282
 Endt, P. M., 354
 Enemark, D. C., 482
 Enge, H. A., 182
 Engelhard, H., 512, 514
 England, A., 319, 321
 Engström, A., 532, 543
 Eriksen, E., 327
 Erlykin, A. D., 76
 Ernster, L., 522
 Errera, M., 517
 Eschenbrenner, A. B., 566, 567
 Estrup, P. J., 259, 265, 279, 281, 282
 Etzel, H. W., 533
 Eustler, B. C., 548, 554
 Evans, H. J., 502, 503, 505, 506, 507, 523, 524
 Evans, J. B., 259, 265, 266, 279, 281, 282, 283
 Evans, T. C., 567
 Evans, W. H., 131, 133, 139
 Everling, F., 409
- F
- Faber, M., 573
 Fabergé, A. C., 503
 Failla, G., 569, 571
 Fairbank, W. M., 116, 122
 Fairhall, A. W., 242
 Fairhall, L. T., 531
 Falk, C. E., 315
 Fano, U., 365
 Faraggi, H., 52, 262
 Faraghan, W. G., 553
 Farran, H. E. A., 533, 549
 Featherstone, R. M., 538
 Fechter, H. R., 182
 Feldman, A., 494
 Feldman, D., 332
 Ferguson, A. J., 389
 Ferguson, A. T. G., 385
 Fermi, E., 1, 3, 18, 94, 168
 Ferrell, B. L., 244
 Ferrell-Bryan, B. L., 244
 Ferri, L., 521
 Feshbach, H., 196, 328, 342
 Petty, W. O., 518
 Feynman, R. B., 2, 13
 Ficq, A., 517
 Fields, T. H., 319, 320
 Filippova, G. V., 492, 503
 Fillmore, F. L., 316, 319, 332
 Finch, C. A., 550
 Findley, D. E., 316, 327, 332
 Fink, D. L., 542
 Fink, R. M., 548
 Finkel, B., 238
 Finkel, M. P., 548
 Finnegan, C., 552
 Fischer, D., 316, 320, 332
 Fisher, D. E., 39, 51
 Fisher, W., 533
 Fisk, J. B., 194
 Flanders, P. H., see Howard Flanders, P.
 Fleischmann, R., 324
 Flerov, G. N., 38, 45, 50, 56, 60
 Fletcher, N. R., 182
 Fljagin, V. B., 318, 322, 323
 Flowers, B. H., 369, 398, 405
 Floyd, R. L., 538, 545
 Foldy, L., 327
 Folley, J. H., 572
 Follin, J. W., 24
 Fomichev, V. A., 55
 Fonger, W., 461
 Forbush, S. E., 461, 464
 Ford, D. D., 573, 574
 Ford, K. W., 31, 34
 Foreman, H., 531, 548, 552, 554
 Forssberg, A., 522
 Fowler, E. C., 115
 Fowler, J. L., 319, 322, 332
 Fowler, O. A., 316, 319, 332
 Fowler, P. H., 476
 Fowler, W. A., 25, 182
 Fox, J. G., 319, 320
 Fox, M. S., 261, 262, 263, 264
 Fox, R., 315
 Fox, R. H., 319, 322
 Fraenkel, Z., 52, 255
 Franca, E. P., see Penna-Franca, E.
 Franck, J. F., 149
 Franck, J. V., 128, 129
 Frank, P. W., 248, 252
 Frankel, S., 215, 217, 218
 Franzini, P., 116, 123
 Fraser, J. S., 252
 Freden, S. C., 473
 Freedberg, A. S., 539
 Freedman, M. S., 252
 Freier, P. S., 465, 481, 482
 Fremlin, J. H., 38, 45, 52
 French, J. B., 354, 394
 Fretter, W. B., 109, 147
 Friedell, H. L., 521
 Friedlander, G., 52, 255
 Friedman, M., 533
 Friend, C., 576
 Frisch, D. H., 315, 316, 319
 Fujimoto, Y., 102
 Fukui, S., 99
 Fukushima, D. K., 279, 280
 Fuller, L. M., 572
 Fulmer, C. B., 252
 Funabashi, K., 260
 Fung, S. C., 243
 Furchner, J. E., 502, 503
 Furth, J., 561, 564, 575, 576
- G
- Gaither, N., 508, 510, 511
 Galbraith, W., 21, 86, 187
 Gallagher, C. J., Jr., 232
 Gallagher, L. R., 117
 Galonsky, A., 322
 Galper, A. M., 126
 Gammel, J. L., 291, 325, 345
 Gangraskil, Iu. P., 43
 Gant, P. L., 282
 Garcia, J. F., 550
 Gardner, F. J., 435
 Gardner, W. U., 576
 Garner, R. J., 544

Garnett, J. L., 279, 280
 Garren, A., 313, 332, 333
 Garrison, J. D., 316, 332
 Gast, P. W., 542
 Gavoret, G., 284
 Gawehn, K., 505, 506
 Gazdik, M. R., 241, 242, 248, 252, 253, 254
 Gebhard, K., 564, 567, 568
 Gee, M., 551, 552
 Geissler, A.-W., 505, 506
 Geissler, P. R., 263, 264
 Gell-Mann, M., 2, 13
 Gensicke, F., 552
 Gentry, J. T., 577
 Geoffrion, C., 186
 George, L. A., 534, 553
 George, L. A., Jr., 549
 Gerholm, T. R., 232
 Gerlit, Yu. B., 50
 Gewitz, H.-S., 505, 506
 Ghorso, A., 239
 Giacomello, G., 270, 271, 275, 276, 285
 Gibson, W., 319, 321
 Gierula, J., 94, 102
 Gilliam, A. G., 572
 Gillies, N. E., 507, 508, 511
 Gilman, A., 531
 Gimmi, F., 217, 218
 Giranni, G., 285
 Glad, B. W., 533
 Glaser, D. A., 109, 110, 111, 113, 115, 117
 Glaser, R., 552
 Glashow, S., 16
 Glauberman, A. E., 437, 446
 Glucksmann, A., 561
 Gluckstern, R. L., 29, 291, 314, 316
 Glueckauf, E., 259, 283
 Godwin, J. T., 549
 Goertzel, G. H., 194, 196, 199, 201
 Gold, T., 480
 Goldansky, V. I., 41, 42
 Gol'dat, S. Yu., 504, 513
 Goldberg, E., 32, 33
 Goldberg, N., 222
 Goldhaber, G., 316, 332
 Goldhaber, G. S., see Scharff-Goldhaber, G.
 Goldhaber, M., 23
 Goldschmidt-Clermont, Y., 148, 150
 Goldstein, H., 442, 456
 Goldstein, S., 371, 386
 Golovin, B. M., 300, 303, 315, 318, 322, 323
 Gompertz, B., 570
 Gonzalez-Vidal, J., 255
 Good, M. L., 142, 189, 190
 Good, W. M., 239
 Goodman, C. D., 53, 55
 Goodman, L. S., 531
 Gordon, B., 270, 271, 277

Gordus, A. A., 266, 279, 281, 284
 Gordy, W., 490, 491
 Gorry, J., 281
 Goryunov, N. N., 76, 83
 Gotow, K., 319, 321, 344
 Gottlieb, M. B., 462
 Gottschalk, R. G., 547
 Goudsmit, S., 355
 Gove, H. E., 353, 389
 Gow, J. D., 116, 128
 Gowen, J. W., 564
 Grabowski, Z., 232
 Grace, M. A., 385
 Graff, A., 576
 Grahn, D., 561-82; 564, 566, 570, 571, 575, 577
 Graig, F. A., 547
 Grammakov, A. G., 427
 Grashin, A. F., 337, 341, 343
 Graul, E. H., 535, 551
 Graves, R. H., 433
 Gray, G. R., 434
 Gray, L. H., 489, 494, 505, 508, 510, 512, 519, 520
 Green, F. O., 508
 Green, J. H., 259
 Green, L. L., 252
 Green, M. M., 496
 Green, T. A., 212, 222, 223, 225
 Greenberg, J., 551, 552
 Greisen, K., 63-108; 74, 78, 81, 87, 97, 103, 104, 480
 Grey, C. E., 576
 Griffith, T. C., 322, 332
 Grobbs, N. S., see Salomons-Grobbs, N.
 Gropp, A., 39, 51
 Groshev, L. V., 451, 452
 Grosmangin, M., 449
 Gross, E. G., 538
 Gross, L., 576
 Grupp, E., 500
 Gryder, J. W., 260
 Guarino, A., 285
 Gubler, C. J., 550
 Gude, W. D., 548
 Guernsey, G. L., 315, 322, 332
 Guerrero, E. T., 445
 Guillaume, M., 285
 Guitton, J., 426, 427
 Gunter, S. E., 500, 521, 524
 Gustafson, P. F., 533, 538, 544
 Gutmann, J. R., 244
 Guttman, P. H., 564, 565, 571

H

Haas, F. L., 512
 Hackett, P. L., 534

Haddock, F. T., 485
 Hadley, J., 319, 322, 332
 Haeblerl, W., 319, 320
 Hafner, E. M., 315, 319, 320, 325, 332
 Hahn, B., 122
 Hahn, O., 259
 Haines, R. B., 492, 503
 Haissinsky, M., 259
 Halbert, M. L., 31, 32, 33, 35, 36, 38, 39, 41, 50, 52, 53, 55, 60
 Hall, A. E. D., 494
 Hall, W. L., 433
 Halpern, I., 236, 242, 244
 Hamill, W. H., 263, 264
 Hamilton, J. G., 541, 544, 546, 548, 549, 550, 551, 552, 554
 Hamilton, K. F., 571
 Hamilton, R. G., 448
 Hand, L. N., 177
 Handley, T. H., 38, 39, 50
 Hanngren, A., 281
 Hansen, M. F., 270, 271
 Hantke, H. J., 544
 Harbottle, G., 259, 260, 262, 265, 266
 Harmer, D. S., 15, 24
 Harms, D. R., 541
 Harp, M. J., 550
 Harr, J., 194, 199, 201
 Harris, E. B., 533, 549
 Harris, P. S., 502, 503, 552, 564, 567
 Harrison, F. B., 2, 3
 Harrison, G. E., 543, 548
 Hart, H. E., 551, 552
 Harth, E. M., 116, 122
 Hartsough, W., 316, 322, 332
 Hartung, D., 316, 318
 Hartung, R. W., 117
 Hartzler, A. J., 316, 319, 322, 332
 Harvey, B. G., 235-58; 236, 237, 238, 242, 246, 249, 255
 Hasegawa, H., 99, 102
 Hasegawa, S., 102
 Hasterlik, R. J., 542, 544
 Hatcher, R. D., 332, 333
 Hathaway, E. A., 533
 Hawes, C. A., 508
 Hawkins, J. W., 571
 Hayakawa, S., 480
 Hayward, E., 322
 Healy, J. W., 535, 537
 Healy, R., 564, 568
 Hechter, H., 537, 545, 563
 Heckel, P., 573, 574
 Heckman, H. H., 60
 Heer, E., 217, 218, 319, 321, 344
 Heiberg, E., 320
 Hein, R. E., 270, 271
 Heller, L., 319, 325, 327
 Hempelmann, L. H., 516,

- 561, 572, 573, 574
Henderson, C., 126
Henkel, R. L., 315
Henriksen, T., 501
Henriksson, H. O., 498
Henshaw, P. S., 567, 569, 571
Hepner, J. P., 463
Herde, K. E., 549
Hermann, R. C., 24
Hermier, J., 499
Hernandez, H. P., 134
Herr, W., 284
Hess, D. C., 259
Hess, W. N., 314, 318
Heston, W. E., 566, 567
Hewitt, D., 573, 574
Hewitt, H. B., 494, 519
Hildebrand, R. H., 22, 116, 117, 139, 315
Hill, E. C., 493
Hillman, P., 315, 323, 332
Hilsdorf, G. J., 263, 264
Hinault, J., 426
Hindmarsh, M., 532, 535, 544
Hine, G. J., 533
Hirsch, G. M., 548
Hitchman, A. J. W., 535, 536
Hjort, G. H., 494
Hoagland, E. J., 238
Hobbie, R. K., 319, 322, 323, 324
Hock, A., 284
Hodara, M., 533
Hodge, H. C., 543
Hodges, E., 542
Hodges, E. J., 537, 542
Hodges, P. C., 561
Hoff, W. J., Jr., 279, 280
Hoffman, R. A., 472, 473
Hofstadter, R., 182, 207, 233
Hoï, Ng. Ph. B., see Buu
Hoï, Ng. Ph.
Hollaender, A., 492, 521, 568
Holland, R. H., 547
Hollander, J. M., 215, 229
Hollcroft, J., 569
Hollis, O. L., 534, 551
Holmes, B. E., 513, 517, 518
Holmes, D. K., 204
Holt, J. G., 533
Holt, J. R., 316, 318
Holynski, R., 94, 102
Honda, M., 425
Hood, S. L., 540
Hoppert, C. A., 548
Hornig, J. F., 265
Horning, W. A., 115
Hornsey, S., 502, 503, 506, 507, 509
Hornyak, W. F., 315
Horstman, V. G., 554
Horwitz, N., 189
Howard, A., 509
Howard-Flanders, P., 502, 503, 505, 506, 507, 508, 509, 525
Howland, J. W., 569
Hubbard, E. L., 58
Huby, R., 310
Hudis, J., 236
Huizenga, J. R., 221
Hull, M. H., Jr., 29, 309, 312, 332, 333, 345, 346
Hullings, M. K., 244
Hulme, H. R., 194
Hultberg, S., 232
Hulthén, L., 291, 325
Hummel, O., 284
Hundeshagen, H., 551
Hunting, C. E., 32, 36
Hurley, P. M., 443
Hursh, J. B., 538, 553, 566, 569
Hurst, R. E., 452
Huxtable, G. B., 321, 343
Hwang, C. F., 319, 321
- I
- Iakovlev, V. I., 83
Igo, G., 33
Imaeda, K., 102
Ingram, D. J. E., 491
Ishii, Y., 102
Ivanitzkaia, E. A., 515
Ivanoff, N., 284
Ives, P. T., 496
Izmozherov, N. A., 499, 512
- J
- Jaccarino, V., 196
Jackson, B. H., 566
Jackson, J. D., 50, 316
Jacobi, R. B., 259, 283
Jacobs, J. A., 60
Jacobson, L. O., 566, 567
Jaffe, J. F., 516
Jancovici, B., 386
Jarmie, N., 374
Jean, M., 231
Jee, W. S. S., 554
Jelley, J. V., 86
Jenkins, R. E., 443
Jensen, J. H. D., 353
Jentschke, W. K., 316, 319, 322
Jeong, T. H., 316, 319
Jess, L., 330, 331, 332, 345
Jeung, N., 549
Jobes, F. C., 38, 40, 41
Joelson, L., 550
Johansson, A., 315
Johnson, E. B., 490, 510
Johnson, J. C., 426, 427
Johnson, J. H., 360
Johnston, L. A., 332
Johnston, L. H., 316, 318, 319, 332
Johnston, M. E., 532, 549
Jones, E. P., 281, 282
Jones, H. B., 571
Jones, T. O., 259, 263
Jones, W. H., 244
Jordan, D. L., 502, 503
Jowsey, J., 532, 541, 544, 548, 551
Judd, D. L., 169
Judist, J. P., 322
Jupe, N., 535, 536
Jurak, A., 94, 102
Jurkiewicz, L., 429
- K
- Kadyk, J. A., 117
Kakayama, N., 427
Kaleta, B. F., 508
Kallman, R. F., 563, 564, 565
Kalmanson, A. E., 590
Kalmus, G. E., 122, 128
Kamarek, T. I., 117
Kamata, K., 71
Kameda, T., 76
Kamen, M. D., 532
Kammuri, T., 46
Kamnev, A. B., 76
Kane, J. A., 319, 320, 321
Kaplan, H. S., 561, 566, 569, 574, 575, 576
Kaplan, I. I., 577
Karamian, A. S., 45, 49, 50, 55
Karnaikhov, V. A., 42, 43, 45
Kasarov, R. E., 78
Kastenbaum, M. A., 572
Katchman, B. J., 518
Katcoff, S., 238, 239, 247, 248, 252
Katz, J., 553
Kaufmann, R., 43, 44, 45
Kavanagh, R. W., 25
Kawin, B., 547
Kay, J. G., 279, 280, 282
Kaylor, C. T., 541
Kazarinov, Ju. M., 318, 322, 323, 332
Kazmierczak, J. E., 518
Kazuno, M., 102
Keen, R. E., 435
Keller, H., 259, 265, 279, 280
Keller, N., 553
Kellerman, G. M., 539
Kelley, E. M., 578
Kellogg, P. J., 471, 476
Kelly, E., 319, 322, 332
Kember, N. F., 533
Kendzioriski, F., 74, 81, 97, 103
Kennedy, J., 518

- Kent, P. W., 548
 Kerlee, D. D., 32, 33
 Kerman, A. K., 353
 Kerman, R. O., 316
 Kerwin, L., 186
 Kessaris, N. D., 501
 Khalizov, V. L., 42, 43, 45
 Christiansen, G. B., 76, 83
 Khwan Shen-Nian, 145
 Kihlman, B. A., 507, 508, 520
 Kikuchi, K., 50, 51
 Kikuchi, T., 116, 122
 Kilpatrick, R., 539
 Kim, Y. B., 154
 Kimball, A. W., 561, 572, 575, 576
 Kimball, R. F., 508, 510, 511
 Kinchin, G. H., 260, 261, 262, 265
 King, E. R., 546
 Kinoshita, T., 16
 Kirillov-Ugrumov, W. G., 126
 Kisteleksi, W. E., 548, 553
 Kisslinger, L. S., 221
 Kitt, G. P., 259, 283
 Kittle, C. F., 546
 Klein, C. A., 332, 333, 346
 Klein, D., 332
 Klingmüller, W., 491, 512
 Kluyver, J. C., 316, 318
 Knable, N., 315
 Knecht, D. J., 316, 318, 332
 Knie, J., 259
 Knight, J. D., 232
 Knipp, J. K., 244
 Knisely, R. M., 541
 Knox, W. J., 44, 45, 53, 55, 60
 Knudsen, A. W., 122
 Koch, D., 572, 574
 Koehler, J. S., 260, 262
 Kofsky, L. L., 99
 Kohn, H. I., 521, 563, 564, 565, 571
 Kokesch, F. P., 442
 Kolganov, V. Z., 131, 138
 Kologrivov, R., 544
 König, L. A., 409
 Kononenko, A. M., 532
 Konopinski, E. J., 1, 3
 Konzak, C. F., 490, 510
 Kornberg, H. A., 537, 538, 549
 Korogodin, V. I., 499, 511, 512
 Koski, W. S., 284
 Kotenko, L. P., 126
 Kowald, J., 283
 Kramer, G., 200, 201, 344
 Kratchman, J., 577
 Kraushaar, W., 79
 Krestnikov, Iu. S., 115
 Krishnamurthy, B. S., 496
 Krokowski, E., 501
 Kropschot, R. H., 134
 Kruger, P. G., 316, 319, 322
 Kruse, H. W., 2, 3
 Kruse, U. E., 316, 332
 Krutov, V. A., 196
 Krzúk, J., 429
 Kuehner, J. A., 58, 389
 Kuhn, U. S. G., III, 548, 549
 Kukharensko, N. K., 450
 Kulikov, G. V., 76, 83
 Kulp, J. L., 537, 542, 544
 Kulwich, R., 548
 Kumatori, T., 516, 519
 Kundu, M. R., 485
 Kunkel, H. A., 512, 514
 Kurath, D., 387, 388, 389, 390
 Kusin, L. A., 126
 Kuznetsov, E. P., 126
 Kuznetsov, E. V., 145
 Kuznetsova, N. N., 497
 Kvashnevskaya, N. V., 427
 Kyker, G. C., 552
- L
- Lagarrigue, A., 116
 Lajtha, L. G., 516, 519, 522
 Lallemand, C., 426, 427
 Lamb, W. E., 244
 Lambertson, G. R., 184, 187
 Lamerton, L. F., 532, 533, 544, 561
 Lamson, B. G., 563, 564, 565
 Landau, L. D., 2, 94
 Landsberg, L. G., 131, 138
 Lane, A. M., 353, 360, 381, 382
 Lane, G. R., 491
 Lang, D. W., 48
 Lang, J. M. B., 48
 Lange, R. D., 572
 Langham, W., 536, 539, 540
 Langham, W. H., 502, 503, 532, 533, 537, 538, 539, 540, 545, 553
 Lanz, H. C., 547
 Lascelles, J., 516
 Lasday, A. H., 315
 Laser, H., 498
 Lassen, N. O., 244, 252
 Lassila, K., 345, 346
 Laszlo, D., 541, 551, 552
 Lataret, R., 499
 Laughlin, J. S., 501
 Laughlin, R. G., 278
 Lauritsen, C. C., 182
 Lauritsen, T., 409-24; 245, 354, 409
 Law, L. W., 561, 572, 575, 576
 Lawrence, P. L., 577, 578
 Lawson, R. D., 376, 405
 Lea, A. J., 574
 Lea, D. E., 489, 492, 502, 503
 Leachman, R. B., 244, 246, 247, 250, 252
 Lebedev, A. V., 131, 138
 Leblond, C. P., 547
 Leconte, J. R., 426
 Lecoq, J. J., 426
 Le Couteur, K. J., 48
 Lederer, H., 542
 Lee, J. K., 279, 281, 282, 283
 Lee, T. D., 1, 16, 17, 18, 19, 20
 Lefrançois, J., 319, 321
 Lehrer, S., 99
 Leighton, R. B., 23
 Leinbach, H., 481
 Leith, C., 315, 319, 322, 332
 Leitner, J., 116, 122, 180
 Lejeune, J., 577
 Lemberg, I. Kh., 43
 Lemmon, R. M., 282, 286
 Lengemann, F. W., 541, 543
 Lenhoff, E. S., 542
 Lesher, S., 571
 Lessler, M. A., 500
 Leuchtenberger, C., 516
 Levey, G., 265
 Levy, L., 538
 Lewin, R., 551, 552
 Lewis, E. B., 549, 572
 Libby, W. F., 260, 261, 262, 263, 264, 270, 271, 276
 Liden, K., 533
 Liess, M., 285
 Lifshitz, E., 41, 42
 Lill, G., 435
 Lille, J. S., 52
 Lind, S. C., 259
 Lindberg, O., 522
 Lindhard, J., 244, 247
 Lindop, P., 564
 Lindquist, B., 544
 Lindstedt, S., 281
 Lingen, C., 522
 Linsley, J., 79
 Lint, V. A. J. van, 246, 250
 Lipp, M., 284
 Listengarten, M. A., 195, 199, 203, 204, 209, 230, 231
 Litherland, A. E., 353, 389
 Little, C. G., 481
 Litvinova, I. B., 511
 Livak, J. E., 284
 Livesey, D. L., 252
 Livingston, M. S., 163

- Lobonov, Yu. V., 56, 57
 Loevinger, R., 533
 Lofstrom, J. E., 547
 Logachev, Yu. I., 470
 Logan, R., 517
 Logothetopoulos, J. H., 513, 518
 Loiseleur, J., 505
 Lomanov, M. F., 115, 145
 Lomon, E. E., 332, 334, 339, 344
 Looney, D., 499, 518
 Looney, W. B., 544, 553
 Lorenz, E., 566, 567, 569, 575
 Loria, A., 115
 Lorick, P. C., 551
 Loutit, J. F., 548
 Lovati, A., 182
 Love, W. A., 319, 323
 Low-Beer, B. V. A., 546
 Lozhkin, O. V., 252
 Luchnik, N. V., 512
 Ludwig, G. H., 470
 Luebke, R. H., Jr., 259, 263
 Luippold, H. J., 500, 502, 503, 509
 Lumsden, E., 543
 Luning, K. G., 498
 Lurie, G., 489
 Lutsenko, V. N., 451, 452
 Lutz, I., 180
- M
- Maass, H., 514
 McCall, M. S., 547
 McCauley, C. E., 259, 263, 264, 265
 McCausland, M. A. H., 324
 McCormick, G. M., 244
 McCulloch, E. A., 494
 McDonald, F. B., 467
 MacDonald, N. S., 542, 551
 McFarland, R. H., 270, 271
 Macfarlane, M. H., 354
 McGowan, F. K., 209, 220
 MacGregor, M. H., 291-352 (313-24); 319, 320, 322, 331, 332, 333, 335, 336, 337, 339, 341, 343, 344
 McGruer, J. N., 316, 327, 332
 McGuire, A. D., 2, 3
 Macht, L. H., 577, 578
 McIlwain, C. E., 463, 470, 473, 481, 482
 McIntosh, J. S., 36
 McIntyre, J. A., 33, 38, 40, 41, 182, 184
 MacKay, C. F., 270, 271, 276, 281
 McKay, H. A. C., 259, 282
- McKenney, J. R., 554
 MacKenzie, K. R., 315
 MacKenzie, R. D., 548
 McManas, H., 353
 McMillan, E. M., 252
 McMullan, D., 131, 133, 139
 Mada, E. R., 576
 Maddock, A. G., 259, 270, 271, 275, 276, 284
 Madsen, B. S., 245, 252
 Maeda, T., 76
 Magee, J. L., 260
 Magnac-Valette, D., 285
 Magni, G. E., 524
 Maisin, H., 563, 564, 565, 569
 Maisin, J., 563, 564, 565, 569
 Makinodan, T., 568
 Maldague, P., 563, 564, 565, 569
 Mallinowski, O. V., 499, 512
 Malsan, R. P., 279, 280, 282
 Maltsev, E. I., 117
 Malumina, T. S., 511, 599
 Mancini, R. E., 547
 Mandl, A., 495
 Manelli, I., 116, 123
 Mann, M. G., see Gell-Mann, M.
 Manning, M. D., 574
 March, H. C., 571
 Marcovich, H., 521
 Marcus, P. I., 493, 494, 519
 Margulies, R. S., 115
 Marinelli, L. D., 15, 533
 Marklund, I., 232
 Marks, S., 549
 Marquis, G. L., 442, 444, 445
 Marshak, R. E., 2, 13
 Marshall, J., 315, 316, 320, 332
 Marshall, J. H., 532, 536, 541, 544, 551
 Marshall, L., 315, 316, 320, 332
 Martelli, G., 122
 Martin, F. L., 492
 Martin, M., 439, 446, 449
 Martinez, S. J., 452
 Masi, I., 270, 271
 Masironi, R., 285
 Mason, L. H., 281, 282
 Matano, T., 99
 Mathieu, R., 245, 252
 Mattauch, J. H. E., 409
 Mattis, P. A., 553
 Matumoto, Z., 204
 Matveev, V. V., 442
 Maurer, W., 284
 Maxwell, A., 485
 May, S., 259, 284
- Mayer, M. G., 353, 387
 Mayneord, W. F., 561
 Mays, C. W., 533, 538
 Mazzetti, F., 286
 Meadows, J. W., 244
 Mealey, J., 546
 Mee, L. K., 513, 517, 518
 Meer, C. van der, 520, 521
 Meier, O., Jr., 182
 Meinke, W. W., 450
 Meitner, L., 259
 Melkanoff, M. A., 36
 Meltzer, C., 116, 122
 Melville, G. S., Jr., 575, 576
 Meredith, L. H., 462, 463
 Merkel, G., 58
 Merrill, J. R., 425
 Messelt, S., 316, 318, 332
 Metcalf, R. P., 252
 Metropolis, N., 255, 305, 306, 307, 308, 327, 332, 334, 335
 Meurer, M. C., 443
 Meurman, L., 550
 Mewissen, D. J., 568
 Meyer, J., 552
 Meyer, J. A., 115
 Meyer, L. M., 537, 545, 563
 Meyer, P., 466, 480
 Michaelson, S. M., 569
 Michel, L., 298, 312
 Miesowicz, M., 94, 102
 Mikesell, R. P., 134
 Mikhailov, B. M., 272
 Miller, C. E., 15, 533
 Miller, C. W., 498
 Miller, D., 189, 319, 322, 323, 324
 Miller, E., 569
 Miller, J. M., 236, 255, 260, 266, 426
 Miller, P. O., 547
 Mills, R. L., 315
 Mills, W. R., Jr., 450, 454
 Milman, M., 263, 264, 265
 Milton, J. C. D., 252
 Minakawa, O., 102
 Minhagen, L., 252
 Minozzi, G., 269, 271, 275
 Mirsky, A. E., 517
 Miskel, J. A., 238, 239, 247, 248, 252
 Misra, A. L., 281
 Mittner, P., 115
 Miura, I., 99
 Modansky, L., 324
 Moh, C. C., 504, 523
 Mole, R. H., 497, 500, 543, 561, 566, 567, 576
 Moloney, W. C., 572
 Monaghan, R., 448
 Monchick, L., 260
 Monier-Williams, G. W., 531

Montefinale, S., 271, 275
 Mookerjee, A., 524
 Moore, D., 502, 503, 506, 509, 525
 Moore, J. A., 316, 318
 Moore, L. A., 576
 Moore, M. J., 131, 133, 139
 Moore, R., 521
 Moravcsik, M. J., 291-352 (324-46); 322, 333, 335, 337, 339, 341, 343, 344
 Morgan, K. Z., 535, 536, 550
 Mori, H., 102
 Morkovin, D., 494, 519
 Morpurgo, G., 383, 399
 Morris, T. W., 190
 Morrison, P., 104, 200, 480
 Morse, P., 342
 Morse, P. M., 196
 Mortimer, R. K., 499
 Morton, J. R., 241
 Moshman, J., 564
 Moss, W., 548, 554
 Mott, G. R., 315, 322, 332
 Mott, N. F., 194, 196
 Mott, W. E., 429
 Mottelson, B. R., 215, 216, 217, 219, 220, 230, 353
 Moxham, R. M., 426, 427
 Moyer, B. J., 315
 Mráz, F. R., 540
 Muehlhaue, C. O., 15
 Muench, N. L., 452
 Mullen, R., 286
 Müller, A., 490, 491
 Muller, H. J., 497, 569, 571
 Muller, K., 196
 Mullins, J. H., 117
 Munro, D. S., 539
 Munro, T. R., 519
 Munson, R. J., 566, 567
 Murray, J. J., 189
 Murray, M. F., 284
 Murray, R., 573, 574
 Murzina, E. A., 83
 Musgrave, B., 279, 281, 282, 283
 Musset, P., 116
 Muth, H., 544
 Muxart, R., 259, 260, 271, 275, 276, 277
 Myasoedov, B. F., 50

N

Nadezhdin, V. S., 300, 303
 Nagel, D. E., 116, 139
 Nagle, D., 320, 332
 Nagy, J., 117
 Nagy, T., 117
 Nahmias, M. E., 2
 Nakasima, R., 50, 51
 Natarajan, A. T., 504

Nathan, O., 232
 Neary, G. J., 502, 503, 505, 506, 507, 523, 524, 566, 567
 Nechin, Yu. A., 76, 83
 Nedzel, V. A., 315, 316
 Need, J. L., 53
 Neel, J. V., 561, 577, 578
 Neher, H. V., 461, 465
 Neidigh, R. V., 244
 Nelligan, W. B., 452, 453, 454
 Nelson, A., 532
 Nelson, B. K., 315, 322, 332
 Nelson, B. V., 332
 Nenarokova, I. F., 496
 Nereson, N., 315
 Nesmeyanov, A. N., 259
 Nesterova, N. M., 86, 88
 Neuman, M. W., 541, 547
 Neuman, W. F., 541, 543, 547
 Newell, R. R., 563
 Newman, E., 60
 Newman, R. H., 551, 552
 Newton, J. O., 385
 Newton, T. D., 48
 Ney, E. P., 461-88; 465, 469, 476, 481, 482
 Nichols, G., Jr., 539
 Nichols, N., 539
 Niday, J. B., 248, 252
 Nielsen, J. M., 545
 Nielsen, K. O., 244, 245
 Nielsen, O. B., 252
 Niewodniczański, J., 429
 Nijgh, G. J., 220, 221
 Nikitin, S. Ia., 131, 138
 Nikolsky, S. I., 83, 84
 Nikonov, A. I., 427
 Nilan, R. A., 510, 512
 Nilsson, S. G., 215, 216, 217, 219, 223, 228, 229, 230, 353
 Nininger, R. D., 427
 Nishikawa, K., 102
 Nishimura, J., 71, 102
 Nishimura, Y., 102
 Niu, K., 102
 Noble, J. F., 564, 566, 567
 Nold, M. M., 543, 549
 Noonan, T. R., 566, 569
 Norellus, R. G., 449
 Norris, T. H., 271
 Norris, W. P., 535, 538, 544, 548, 553
 North, D. T., 490, 510
 Northcliffe, L. C., 60, 316, 318, 332
 Nowell, P. C., 566, 567, 575
 Noyes, H. P., 319, 325, 326, 329, 331, 332, 335, 339, 344
 Nullens, G., 135

Numerof, P., 284
 Nuñez, C., 547
 Nusbaum, R. E., 542
 Nussbaum, E., 538
 Nuzhdin, N. N., 497
 Nystrom, R. F., 281, 282

O

Oae, S., 270, 273, 274
 Oakberg, E. F., 489, 495, 500
 Oakley, W. D., 551, 553
 Ochkur, A. P., 444, 456
 Oda, M., 99
 Odeblad, E., 548, 550
 Odell, T. T., 548
 Odinovsk, V. P., 450
 Oehme, R., 300
 Oftedal, P., 501
 Oganesian, Yu. Ts., 60
 Ogdén, B. K., 109, 128, 147
 Ogita, N., 99
 Ohnuma, S., 332
 Okada, S., 516
 Oleksa, S., 15, 469
 Oliver, R., 516, 519, 548
 Olkowsky, J., 52
 Olson, E. A., 546
 Oltman, A., 268
 Oort, J. H., 105
 Ophel, T. R., 319, 321
 Optiz, W., 322, 332
 Oquidam, B., 386
 Ord, M. D., 516
 Ornstein, L. Th. M., 221
 Osawa, S., 517
 Oshima, Y., 260
 Osoba, J. S., 443, 452
 Oster, I. I., 497
 Owen, G. E., 324
 Owen, M., 532, 533, 535, 543, 544
 Owsiak, T., 429
 Oxley, C. L., 292, 316, 319, 320, 332

P

Pahl, G., 509
 Pal-gen, S., 490
 Pal, R., 496
 Palmer, R. F., 537, 547
 Palmieri, J. N., 316, 318, 319, 320, 332
 Pandya, S. P., 371
 Panofsky, W. K. H., 177, 184, 190, 316, 319
 Pany, J., 281
 Papineau, A., 52
 Parfanovich, D. M., 45, 52, 60
 Parham, A. G., 81
 Park, S. C., 36
 Parker, E. N., 480
 Parker, P. D., 25

- Parkhurst, E., 577
 Parrott, M. W., 549
 Pasiuk, A. S., 38
 Passinsky, A. G., 490
 Pate, B. D., 238
 Paterson, J. C. S., 573, 574
 Patton, G. B., 572, 573
 Paul, E. B., 353
 Paul, J., 569, 575
 Pauli, W., 1
 Pauli, W., Jr., 1
 Pauly, H., 515
 Pearson, P. B., 548
 Pease, R. S., 260, 261, 262, 265
 Peets, E. A., 541
 Peterls, R. E., 1
 Peker, L. K., 231
 Pelekhov, V. I., 451, 452
 Penna-Franca, E., 271
 Perfilov, N. A., 244, 252
 Perkins, B. L., 60
 Perkins, R. W., 545
 Perlman, I., 229, 232, 243
 Perring, J., 335, 339, 344
 Perry, J. E., Jr., 315
 Peters, B., 100
 Peterson, J. M., 315
 Pettit, M., 505
 Petriello, L. I., 551
 Pettengill, B., 319, 320, 332
 Pettengill, G., 315, 316, 320
 Pettersson, B. G., 232
 Peyrou, C., 131, 135, 137, 139
 Pfeiffer, C. A., 576
 Phelps, T. W., 428
 Phillips, R. J. N., 300, 301, 310, 313, 331, 332, 333, 346
 Phillips, G. O., 493
 Piccioni, O., 182, 184
 Pickavance, T. G., 315, 316, 332
 Pickup, J., 426
 Pike, C., 180
 Pinajian, J. J., 38, 39, 42, 43, 52
 Pine, J., 104
 Pinkston, W. T., 385, 391, 392, 399
 Pinson, E. A., 538
 Pinte, G., 271, 275, 277
 Pirie, A., 522, 543
 Pirzio-Biroli, G., 550
 Pittinger, C. B., 538
 Pitt-Rivers, R., 549
 Plano, R., 116, 123, 126, 140
 Plano, R. J., 139
 Pleasonton, F., 259
 Pless, I., 126
 Plessett, M. S., 115
 Pleve, A. A., 49, 50
 Plokhov, V. I., 492, 503
 Poczynajlo, A., 284
 Polak, P., 131, 133, 139
 Polhemus, D. W., 572, 574
 Polikanov, S. M., 56, 57
 Pollard, E., 489, 515, 518
 Pomerantzeva, M. D., 497
 Pontecorvo, B., 1, 15, 16, 17
 Popov, U. S., 126
 Porges, K. G., 49
 Porile, N. T., 243, 256
 Porter, C. E., 36
 Poryadkeva, N. A., 499, 512
 Poss, H. L., 315
 Possagno, E., 285
 Powell, W. M., 122, 126, 319, 322
 Powers, E. L., 508, 511
 Pratt, T., 285
 Priest, R. E., 547
 Primak, W., 262
 Prodell, A., 116, 123
 Prokes, A., 117
 Prokofiev, A. Y., 5
 Prout, G. R., 545
 Przewlocki, K., 429
 Puck, T. T., 489, 493, 494, 519, 523
 Puppi, G., 116, 123
 Putten, J. D. van, 117
 Puzikov, L. D., 300, 301, 309
 Pyatt, K. D., Jr., 345, 346
- Q
- Quastler, H., 489, 569, 571
 Quinlan, J. E., 259, 265, 266, 279, 281, 282, 283
 Quinton, A. R., 44, 45, 53, 55, 60
- R
- Rabe, C. L., 442
 Rabin, N. V., 45, 52
 Rabinowitz, P., 255
 Rabson, W. R., 452
 Racah, G., 355, 364, 365, 373, 374, 377, 382, 388
 Rachmanova, T. B., 489
 Radicati, L. A., 382, 383
 Rahm, D. C., 110, 115, 125, 131
 Rajewsky, B., 514
 Ramaniah, M. V., 244
 Ramsey, N. F., 315, 316, 318, 319, 320, 321, 322, 332
 Rancon, P., 116
 Randle, T. C., 315, 319, 322, 332
 Randolph, M. L., 490, 500, 502, 503
 Range, W. R., 322
 Rankama, K., 425
 Rankin, B., 164
 Raphael, R., 327
 Rappoport, D. A., 518
 Rasetti, F., 143
 Rasmussen, J. O., 223, 228, 229, 232
 Rathgen, G. H., 514
 Rau, R. R., 190
 Rauth, A. M., 60
 Ray, C. T., 539, 540
 Ray, E. C., 470
 Ray, R. D., 542
 Raymond, W. H. A., 543, 548
 Read, J., 489, 502, 503
 Reardon, J. Z., 541
 Redvanly, C. S., 260, 265, 269, 270, 271, 275, 276, 277
 Rees, J. R., 31
 Reid, A. F., 259
 Reid, G. C., 481
 Reiner, A. S., 203, 220, 231, 232
 Reines, F., 1-26; 2, 3, 9, 12
 Remley, M. E., 319, 322
 Renschler, H. E., 539
 Resegotti, L., 126
 Ressonovsky, N. W. T., see Timofeef-Ressonovsky, N. W.
 Rester, D. H., 232
 Rethore, M. O., 577
 Revell, S. H., 519, 522
 Reverdy, J., 499
 Rexroad, H. N., 491
 Reynolds, F. L., 286
 Reynolds, H. L., 32, 33, 36, 38, 43, 45, 50, 51, 60
 Reynolds, J. C., 535
 Rhoades, E. L., 541
 Riazuddin, 326
 Richardson, J. R., 316, 332
 Richman, C., 316, 319, 332
 Richmond, C. R., 536, 539, 540, 545
 Riddiford, L., 131, 133, 139
 Riepe, G., 122
 Riesz, P., 281, 282
 Riley, E. F., 587
 Ring, J., 332
 Rivers, R. P., see Pitt-Rivers, R.
 Rixon, R. H., 516
 Robajdek, E. S., 552
 Roberts, A., 319, 320, 332
 Robertson, J. S., 533, 534, 537, 545, 561, 563
 Robev, S., 521
 Robichon, J., 547
 Robinson, F. N. H., 324

Roesch, W. C., 533
 Rogers, B. S., 552, 564, 567
 Roll, P. G., 60
 Rollefson, G. K., 271
 Ronzak, C. F., 490, 510
 Root, S. W., 541
 Rose, B., 319, 321, 332
 Rose, J. E., 15
 Rose, M. E., 194, 195, 196, 199, 201, 202, 203, 204, 211, 212, 217, 222, 223, 225, 226, 231, 365
 Rosen, S. M., 543
 Rosenberg, G., 549
 Rosenblum, C., 281, 282, 284
 Rosenbluth, M., 18
 Rosendorff, S., 2
 Rosenfeld, A. H., 128, 141, 150, 151, 152, 154
 Rosenzweig, W., 500
 Ross, M., 215
 Ross, R., 138
 Rossi, B., 74, 75, 79, 97, 103, 116
 Rossi, H. H., 500
 Roswit, B., 576
 Rotblat, J., 553, 564
 Rothwell, P., 473, 481, 482
 Rousset, A., 116, 126
 Rouvina, J., 292, 320, 332
 Roux, M., 284
 Rowland, F. S., 259, 260, 265, 279, 280, 281, 282, 283, 285
 Rowland, R. E., 15, 532, 536, 541, 544, 551
 Roy, J. C., 263, 264
 Royden, H. N., 316
 Rubin, A. G., 46
 Rubin, H., 495
 Rubin, S., 182
 Rudall, G., 499
 Rugh, R., 500, 561
 Rundo, J., 553
 Rusinov, L. I., 55
 Russell, L. B., 497, 561, 578
 Russell, R. S., 536, 543
 Russell, R. T., 427
 Russell, W. L., 442, 445, 497, 561, 578
 Rydberg, J., 281
 Ryndin, R., 300, 301, 309

S

Sacher, G. A., 564, 566, 569, 570, 571, 575
 Sachs, N. A., 547
 Sachs, R. G., 215
 Saito, N., 425
 Salam, A., 2
 Salant, E. O., 315
 Salerno, P. R., 516, 521, 553
 Sallese, A., 571
 Salomons-Grobbe, N., 221
 Salpeter, E. E., 326
 Salter, D. C., 320, 332
 Salthouse, T. N., 505, 506, 513
 Samachson, J., 541, 542
 Samios, N. P., 116, 123, 180
 Sanders, P. C., 564, 567
 Saniewska, T., 94, 102
 Santangelo, R., 116, 123
 Santoro, V., 269, 271, 275
 San-Tsiang, T., 252
 Sartwell, P. E., 562
 Satarov, V. I., 315, 318, 322, 323
 Sato, M., 427
 Sauer, M. C., Jr., 259, 265, 266, 279, 281, 282
 Sauteron, X., 116
 Saxena, M. C., 491
 Sayeg, J. A., 501, 502, 503, 524
 Sazonov, L. A., 259
 Sazonova, I. S., 259
 Schabinski, G., 496
 Schachter, D., 543
 Schamberger, R. D., 316, 319, 332
 Schambra, P. E., 60
 Scharff, M., 244, 247
 Scharff-Goldhaber, G., 231
 Scharpenseel, H. W., 279, 281
 Scherb, F., 79, 315
 Scherrer, P., 217, 218
 Schiavon, G., 271, 276, 277
 Schlüssel, H., 284
 Schmidt, F., 284
 Schmitt, H. W., 252
 Schmitt, R. A., 246, 250
 Schneeweis, K. W., 512, 514
 Schooley, J. C., 549
 Schopper, H., 324
 Schrank, G. E., 316, 332
 Schraub, A., 544
 Schröder, W., 505, 506
 Schrod, A. G., 270, 271, 276
 Schubert, G., 512, 514
 Schubert, J., 531, 546, 572
 Schuler, R. H., 259, 263, 264, 265
 Schulert, A., 546
 Schulert, A. R., 537, 541, 542
 Schull, W. J., 561, 577, 578
 Schulman, J. H., 533
 Schwabe, F., 496
 Schwartz, D., 524
 Schwartz, E. E., 561
 Schwartz, M., 1, 17, 116, 123, 180
 Schweisthal, R., 566, 567, 569
 Schwemin, A. J., 141
 Schwinger, J., 326
 Scofield, N. E., 546
 Scotoni, I., 115
 Scott, D. W., 38, 43, 60
 Scott, J. K., 545
 Scott, K. G., 541, 546, 548, 549, 550, 554
 Scott, O. C. A., 489, 494
 Scoular, F. I., 550
 Seaborg, G. T., 215
 Seagrave, J. D., 319, 322
 Segrè, E., 182, 238, 252, 292, 300, 308, 309, 315, 316, 319, 320, 321, 322, 323, 332
 Selgneur, L. J., 554
 Seltz, F., 114, 260, 262
 Selove, F. A., see Ajzenberg-Selove, F.
 Selove, W., 319, 322
 Seltzer, R., 562
 Semchnova, A. M., 45, 52, 60
 Senftle, F. E., 283
 Setser, D. W., 270, 271
 Sewell, B. W., 518
 Shalit, A. de-, 365
 Shamov, V. P., 252
 Shapiro, J., 538
 Shapiro, M., 513, 518
 Shapiro, M. M., 48, 51
 Shapiro, N. G., 496
 Shapiro, N. I., 489, 497, 510
 Sharman, G. B., 495
 Sharp, R. A., 246, 250
 Shaw, D., 131, 133, 139
 Shaw, P. F. D., 263, 265
 Shchepot'eva, E. S., 489
 Shekhtman, Ia. L., 503, 592
 Sheline, R. K., 353
 Shellabarger, C. J., 549
 Sheppard, C. E., 500, 502, 503
 Shields, H., 490, 491
 Shimelevich, Yu. S., 450
 Shimkin, M., 566, 567
 Shirokov, M. I., 310, 313
 Shlyapnikov, R. S., 442
 Shoden, A., 550
 Sibatani, A., 516
 Sicard, M. A., 524
 Siegel, E., 547
 Siegel, R. T., 316, 319, 322, 323, 332
 Siekierska, K. E., 284
 Sierp, M., 545
 Sievert, R. M., 533
 Sigurgeirsson, T., 252
 Sikkeland, T., 239
 Sikov, M. R., 547
 Silbert, M. G., 374
 Silvestrini, V., 116, 123
 Simmons, J. E., 319,

- 321, 332
 Simon, W. G., 60
 Simpson, C. L., 572
 Simpson, I. B., 265
 Simpson, J. A., 461, 466, 480
 Simpson, L., 546
 Simpson, S. M., 494, 519
 Sinclair, D., 117
 Sinclair, W. K., 500, 524, 533, 549
 Singer, S., 316
 Singer, S. F., 471
 Sippel, R. F., 452
 Sire, M. W., 510
 Sitte, K., 99
 Siuda, A., 284
 Six, J., 116
 Skarsvag, K., 321
 Skhobin, U. N., 117
 Skillman, W., 332
 Skinner, H. W. B., 131, 133, 139
 Skipper, H. E., 546
 Skirmont, E., 544
 Skolnik, W., 320, 332
 Skreb, Y., 517
 Skyrme, D. M., 319, 322
 Slack, F., 252
 Slätis, H., 109, 122
 Sliv, L. A., 195, 199, 201, 203, 204, 210, 231
 Smaller, B., 491
 Smith, C. L., 519
 Smith, E. R., 248, 252
 Smith, F. M., 60
 Smith, F. W., 434
 Smith, G. A., 545
 Smith, J. C., 500
 Smollankin, V. I., 131, 138
 Smorodinskii, La., 300, 301, 309
 Snegireff, L. S., 572
 Snell, A. H., 259
 Snow, G., 315
 Snow, G. A., 315
 Snowden, M., 131, 133, 139, 319, 322
 Snyder, C. W., 182
 Snyder, E. S., 215, 217, 218
 Snyder, H. S., 163
 Sochevanov, N. M., 427
 Sokolev, A. P., 131, 138
 Sokoloff, V. S., 5
 Sokolov, A. D., 442
 Sokolov, M. M., 427
 Sokolowska, A., 284
 Solmitz, F., 147
 Solmitz, F. T., 141
 Solomon, A. K., 284, 535
 Soloviera, V. I., 76
 Sommermeyer, K., 469
 Sordelli, D., 270, 271
 Sosnosky, A. N., 5
 Sowden, E. M., 542, 544
 Spalding, F. J., 502, 503
 Sparrman, B., 490, 510, 524
 Speckman, T. W., 538, 544
 Spencer, H., 541, 551, 552
 Spiers, F. W., 532, 544
 Spinrad, B. I., 194, 199, 201
 Spivak, P. E., 5
 Spode, E., 552
 Spoerl, E., 499, 518
 Spondlin, R., 135
 Stabler, R. C., 332, 334, 339, 344
 Stadler, J., 564
 Stafford, G. H., 316, 323, 332
 Stahl, R. H., 315, 319, 322, 332
 Stallwood, R. A., 319, 320
 Stanis, O., 94, 102
 Stanley, C. W., 238, 239, 247, 248, 252
 Stannard, J. N., 533, 535, 536, 548
 Stapleton, G. E., 492, 521, 567
 Stapp, H. P., 291-352 (292-313); 299, 300, 302, 305, 306, 307, 308, 312, 313, 322, 327, 332, 334, 335, 337, 339, 341, 343
 Starner, J. W., 232
 Stashkov, G. M., 117
 Stead, F. W., 442
 Steadman, L. T., 553
 Stech, B., 231, 233
 Steck, B., 308, 313
 Steddon, L. M., 548
 Steigert, F. E., 60
 Stein, W. E., 252
 Steinberg, D., 281
 Steinberger, J., 116, 123, 180
 Steiner, H., 182
 Stelson, P. H., 209, 220
 Stephens, F. S., 229
 Stern, K. G., 551, 552
 Sternheimer, R. M., 169, 177
 Stewart, A., 573, 574
 Stewart, C. G., 535, 536
 Stewart, F. M., 445
 Stickley, E. E., 538
 Stierwalt, D. L., 99
 Stiller, G., 97
 Stitch, S. R., 542, 544
 Stocken, L. A., 516, 517, 521
 Stöcklin, G., 284
 Stoering, J. P., 315
 Stone, W. S., 509
 Storer, J. B., 561-82; 502, 503, 564, 567, 569
 Stork, D. H., 171
 Storm, M., 255
 Storrs, C. L., 315
 Stover, B. J., 543, 545, 553
 Strang, V. G., 502, 503
 Strauch, K., 319, 322
 Strehler, B. L., 561, 570
 Strohmeier, W., 282
 Strominger, D., 215
 Strong, P., 194, 199, 201
 Strugalsky, Z. S., 76
 Struglia, L., 548
 Sturgeon, P., 550
 Stuy, J. H., 496, 516, 523
 Sudarshan, G., 2, 13
 Suga, K., 99
 Sugarman, N., 238, 243, 244, 248, 252, 256
 Sugawara, M., 291, 325
 Sullivan, M. F., 534
 Suppe, S. H., 427
 Suryanarayana, B., 259, 265, 271, 275, 284
 Suslikov, V. I., 496
 Sutin, N., 259, 260, 262, 265, 266, 284
 Sutton, A., 543
 Sutton, H., 492, 493, 494, 497, 504, 513, 519, 524
 Sutton, R. B., 319, 320
 Sutow, W. W., 537, 545, 563
 Suzor, F., 242, 248, 252
 Svoboda, K. F., 264, 269
 Swallow, A. J., 269
 Swaminathan, M. S., 503
 Swenson, D., 332
 Swenson, D. A., 316, 318, 319, 332
 Swift, G., 449
 Szilard, L., 259, 571
- T
- Tafeyev, G. P., 427
 Takahashi, K., 427
 Talianskyi, I. I., 437, 446
 Talley, L. H., 548
 Talmi, I., 353-408; 360, 371, 375, 376, 377, 379, 381, 386, 387, 390, 394, 395, 396, 404
 Tamers, M. A., 50
 Tanahashi, G., 99
 Tanaka, H., 116, 123
 Tanaka, Y., 50, 51, 99
 Tang, Y. C., 223
 Tata, J. R., 549
 Tausche, F. G., 548
 Tausk, K., 99
 Taylor, A. E., 315, 316, 318, 319, 320, 321, 322, 323, 332
 Taylor, H. M., 194, 196
 Taysum, D. H., 533, 545
 Teem, J. M., 117, 316, 332
 Teitelbaum, P., 385

- Telegdi, V. L., 298
 Teller, E., 244
 Temin, H. M., 495
 Templeton, D. H., 238
 Ter-Akopian, G. M., 42, 43, 45
 Terhaar, C. J., 270, 271
 Terry, J. L., 554
 Thaler, R. M., 291, 325, 331, 332, 333, 345, 346
 Thetford, A., 131, 133, 139
 Thieberger, R., 360, 377, 379, 387, 390
 Thieme, M. T., 195, 231
 Thomas, D. B., 131, 133, 139
 Thomas, R. G., 361, 545
 Thomas, T. D., 232
 Thompson, A. R., 485
 Thompson, R. C., 531-60; 534, 536, 537, 538, 540, 551, 553
 Thorndike, A. M., 190
 Thorndike, E. H., 319, 321
 Thornley, M. J., 498, 515
 Thornton, R. L., 252
 Threefoot, S. A., 539, 540
 Thresher, J. J., 322, 332
 Thurber, D. L., 542
 Tibell, G., 315
 Ticho, H. K., 189, 190
 Till, J. E., 494
 Timofëef-Ressovsky, N. W., 489, 492
 Tinlot, J., 321, 332
 Tinlot, J. H., 319, 320, 321, 323
 Tiomno, J., 18
 Tittle, C. W., 441
 Tittman, J., 439, 446, 447, 449, 452, 453, 454
 Titus, F., 319, 322
 Tixier, M. P., 439, 446, 449
 Tobias, C. A., 489, 498, 499, 501, 524, 541
 Todorov, S., 521
 Tokunaga, S., 102
 Tolbert, B. M., 282
 Tonkinson, S. M., 502, 503, 505, 506, 524
 Tornabene, S., 323
 Towler, O. A., 332
 Townes, B. M., 322
 Toth, K. S., 40, 41
 Toyoda, Y., 76
 Tralli, N., 196
 Trentin, J. J., 576
 Treuting, W. L., 573, 574
 Tribondeau, L., 513
 Trieman, S. B., 461
 Trilling, G. H., 117
 Trinchler, K. S., 515
 Tripp, R., 319, 320, 321, 332
 Tripp, R. D., 189, 292, 300, 308, 309, 319, 323, 332, 334
 Trotter, W. R., 549
 Truhaut, R., 545
 Trum, B. F., 549
 Truman, T. P., 425
 Tsai, Y. S., 316, 319
 Tsarapkin, L. S., 512
 Tsiang, T. S., see San-Tsiang, T.
 Tsutsui, M., 279, 280
 Tsuzuki, M., 102
 Tukish, E. I., 84, 86, 88
 Tulinov, V. F., 482
 Tullis, J. L., 561
 Tumanov, K. A., 281
 Turkevich, A., 255
 Turner, J. E., 36
 Turpin, R., 577
 Turton, C. N., 279, 280, 285
 Twardock, A. R., 540
 Tyler, S. A., 535
 Tyor, M. P., 541
 Tyrén, H., 182
- U
- Ugrumov, W. G. K., see Kirillov-Ugrumov, W. G.
 Ulmer, D. D., 547
 Underwood, E. J., 531, 541, 550
 Unna, I., 353-408; 360, 369, 377, 381, 394, 395, 404
 Uphoff, D., 569, 575
 Uppal, M. Y., 322
 Upton, A. C., 561, 564, 566, 567, 568, 575, 576
 Urch, D. S., 279, 281, 282
 Uretsky, J. L., 376, 405
 Uridge, F., 319, 322
 Ustenko, E. P., 117
 Uyeki, E. M., 516
- V
- Valette, D. M., see Magnac-Valette, D.
 Vallee, B. L., 545, 547
 Valulov, P. V., 470
 Valyocsk, E. W., 240, 241, 246, 247, 248
 Van Allen, J. A., 462, 470
 van Bakkum, see Bakkum, D. W. van
 Van Cleave, C. D., 541
 van den Brenk, H. A. S., see Brenk, H. A. S. van den
 Van de Raay, H. B., 131, 133, 139
 Vanderhaeghe, F., 517
 van der Meer, C., see Meer, C. van der
- Vander Weele, J. C., 284
 Vande Velde, J. C., 117
 VanDilla, M. A., 538, 543, 545
 van Lint, V. A. J., see Lint, V. A. J. van
 Van Nootjen, B., 232
 van Putten, J. D., see Putten, J. D. van
 Van Slyke, F., 566
 Vaughan, J., 532, 533, 535, 543, 544, 548
 Vaughan, J. D., 270, 281
 Vaughan, J. M., 543
 Velde, J. C. V., see Vande Velde, J. C.
 Veremeev, M. M., 126
 Vernov, S. N., 76, 83, 470, 471
 Vidal, J. G., see Gonzalez-Vidal, J.
 Vigneron, L., 252
 Villi, C., 329, 330, 331, 332, 345
 Visek, W. J., 548
 Vogel, H. H., Jr., 502, 503, 512
 Vogt, E., 535, 536
 Volkhanskii, M. E., 230
 Völker, W., 505, 506
 Volkov, V. V., 38
 Volley, W. P., 548
 Voskoboinikov, G. M., 444, 456
 Voss, R. G. P., 322, 332
- W
- Wacker, W. E. C., 547
 Waddington, C. J., 465, 467, 476
 Wade, W. H., 237, 238, 242, 246, 249, 255
 Wagner, J. J., 3
 Wahl, A. C., 259
 Waine, H., 541
 Wald, M., 270, 273, 274
 Wald, N., 572, 573, 575
 Waldschmidt, W. A., 452
 Walker, D., 45
 Walker, E. B., 449
 Wall, N. S., 31
 Wallace, E. J., 546
 Wallace, R., 319, 322, 332
 Waloschek, P., 116, 123
 Walraven, Th., 105
 Walsh, J. J., 545
 Walter, W. A., 572
 Walton, A., 544, 546
 Walton, G. N., 236
 Wampler, J. M., 542
 Wang, K. H., 33
 Waniek, R. W., 315
 Wapstra, A. H., 220, 221, 409
 Warburg, O., 505, 506
 Warburton, E. K., 385,

- 391, 392, 399
 Ward, G. B., 553
 Warner, D. E., 549
 Warner, R. E., 323
 Warren, B., 232
 Warren, S., 561, 562, 564
 Wasserman, R. H., 532,
 536, 540, 542, 543, 549
 Wataghin, A., 99
 Waters, J. R., 443
 Watson, R. A., 435
 Watt, R., 145
 Watts, T. L., 38, 40, 41
 Weaver, C. E., 443
 Webb, J., 573, 574
 Webb, R. B., 508
 Webb, W. H., 38, 39, 45,
 60
 Webber, W. R., 467
 Webster, E. W., 561
 Weeks, M. H., 551, 553
 Weele, J. C. V., see
 Vander Weele, J. C.
 Wegner, H. E., 33
 Wei, H. Z., see Zah-Wei, H.
 Weigel, H., 284
 Weiss, L., 507
 Weiss, W. J., 433
 Weisskopf, V. F., 47, 48,
 50, 196, 303, 304, 306,
 309, 310, 363, 366, 381
 Welch, J. A., 471
 Welford, W. T., 131, 133,
 139, 143
 Weneser, J., 193-234; 195,
 203, 208, 217, 230, 231,
 232
 Wenzel, W. A., 184, 187,
 190
 Westin, B., 550
 Wexler, S., 259
 Wheeler, J. A., 18, 34
 Whetstone, S. L., 252
 Whitaker, W. A., 471
 White, D. C., 552
 White, H., 151
 White, M. G., 316, 332
 White, R. M., 279, 280, 283
 White, R. S., 473
 White, V. K., 532, 541
 Whitehead, C., 323, 332
 Whitfield, J. F., 516
 Whitmore, W. F., 545
 Whitney, I. B., 548
 Whittemore, I. M., 282
 Whittemore, W. L., 190
 Wichterman, R., 497
 Wick, G. C., 311
 Widmyer, R. H., 448
 Wiegand, C., 182, 236, 252,
 292, 300, 308, 309, 315,
 316, 319, 320, 321, 322,
 323, 332
 Wielgoz, K., 243
 Wightman, A., 2
 Wightman, A. S., 312
 Wigner, E. P., 46, 387
 Wilets, L., 231
 Wilkinson, D. H., 384, 394
 Wilkinson, G. W., 547
 Willard, J. E., 259, 262,
 263, 264, 265, 266, 269,
 279, 281, 282, 283, 284
 Williams, D., 426
 Williams, G. W. M., see
 Monier-Williams, G. W.
 Williams, M. H., 549,
 551, 552
 Williams, P. R., 131, 133,
 139
 Williams, R. R., Jr., 259,
 263, 264
 Williams, R. W., 109, 117,
 122, 154
 Williams, W. S. C., 322
 Williamson, F. S., 502,
 503, 506, 524
 Williamson, R. M., 182
 Willis, B. H., 152
 Willis, W. J., 115
 Wilson, C. W., 494, 519
 Wilson, F. D., 509
 Wilson, G. M., 539
 Wilson, J. C., 442, 444,
 445
 Wilson, J. G., 142
 Wilson, J. R., 259, 263
 Wilson, R., 316, 318, 319,
 320, 321, 322, 324, 332
 Wilson, S. M., 508, 510,
 511
 Winbach, K. E., 281, 282
 Winckler, J. R., 464, 472,
 473, 476, 481, 482
 Winhold, E. J., 244
 Winsberg, L., 243, 246,
 247, 249, 251, 255
 Winther, A., 231, 233
 Wisseman, W. R., 182
 Withrow, R. B., 504, 523
 Witt, M. de, 319
 Woese, C. R., 493, 496, 523
 Wolf, A. P., 259-90; 259,
 260, 265, 268, 269, 270,
 271, 275, 276, 277, 278,
 279, 284
 Wolfe, R. G., 499
 Wolfenstein, L., 293, 296,
 297, 298, 302
 Wolff, F. F., 575, 576
 Wolff, S., 509
 Wolfgang, R., 43, 44, 45,
 50, 59, 259, 260, 265,
 279, 280, 281, 282, 285
 Wolins, W., 537, 545, 563
 Wolke, R. L., 244
 Wollan, E. O., 239
 Wood, E., 315, 316, 318,
 319, 320, 321, 322, 332
 Wood, G. M., 448
 Wood, J. G., 111
 Wood, T. H., 489, 521,
 524
 Woodbury, D. T., 284
 Woods, L. A., 281
 Worthington, H. R., 316,
 327, 332
 Wouters, L., 315
 Wright, B. T., 316
 Wright, E. A., 505, 506
 Wright, S. C., 308
 Wyard, S. J., 546
 Wyllie, M. R. J., 439,
 441
 Wyman, M. E., 3

 Y
 Yaffe, L., 238
 Yamada, M., 204
 Yamanouchi, H., 102
 Yamawaki, T., 572
 Yanders, A. F., 498
 Yang, C. N., 1, 2, 16,
 17, 18, 19, 20
 Yang, J., 269, 270, 271,
 278
 Yang, K., 282
 Yankwich, P. E., 260, 262,
 270, 271
 Yntema, J. L., 316, 332
 Yockey, H. P., 561
 York, H., 319, 322, 332
 Youmans, A., 448
 Youmans, A. H., 450
 Young, D. E., 316, 318,
 319, 332
 Ypsilantis, T. J., 182, 292,
 300, 305, 306, 307, 308,
 309, 319, 323, 327, 332,
 334, 335, 339, 341, 343
 Yuan, L. C. L., 315
 Yukawa, H., 16

 Z
 Zacutti, A., 122
 Zah-Wei, H., 252
 Zatsepin, G. T., 76,
 83
 Zatsepin, V. I., 86, 88
 Zeldovich, A. G., 131, 138
 Zelle, M. R., 492
 Zifferero, M., 269, 270,
 271, 275, 276, 285
 Zimin, A., 332, 333
 Zimmer, K. G., 489, 490,
 492
 Zimmering, S., 497
 Zimmerman, C. W., 450
 Zimmerman, E. J., 316
 Zimmerman, R. L., 316,
 319
 Zipser, A., 539
 Zirkle, R. E., 489, 500
 Zobel, V., 116, 123
 Zuber, A., 429
 Zucker, A., 27-62; 30, 31, 32,
 33, 35, 36, 38, 39, 41, 43,
 45, 50, 51, 53, 54, 55, 60
 Zwick, S. A., 115

SUBJECT INDEX

A

- Acceleration of ions
 - in labeling techniques, 285-86
- Actinide elements
 - in vertebrate radiobiology, 551-54
- Actinium
 - in vertebrate radiobiology, 551-52
- Aerial and surface prospecting
 - by nuclear means, 425-28
- Age effects
 - in vertebrate radiobiology, 555
- Alkali metals
 - in vertebrate radiobiology, 538-41
- Alkaline earths
 - in vertebrate radiobiology, 541-45
- Aluminum
 - in vertebrate radiobiology, 545
- Alvarez 72-inch hydrogen bubble chamber, 127-31
- Americium
 - in vertebrate radiobiology, 554
- Angular distributions
 - of fission products, 243-44
 - of recoils measured with thick targets, 243-44
 - of spallation products, 6, 242, 243
- Anomalies
 - in magnetic hyperfine structure, 195-96
- Antineutrinos
 - absorption by deuterons, 13-14
 - distinguishability from neutrinos, 15
 - energy spectrum
 - from fission, 3-4, 11
 - predicted absorption cross section
 - by free protons, 3-5
 - upper limits on cosmic flux of, 24-25
 - see also Neutrinos
- Argus nuclear explosion, 470-79
 - see also IGY cosmic ray experiments
- Arsenic
 - in vertebrate radiobiology, 547

- Astatine
 - in vertebrate radiobiology, 549
- Auroral x-rays, 462-64
- Autoradiographic methods
 - in vertebrate radiobiology, 532-33
 - see also Vertebrate radiobiology

B

- Barium
 - in vertebrate radiobiology, 543-44
- Barometric effect
 - in extensive air showers, 95-96
 - see also Extensive air showers
- "Bar" phase shifts
 - in nucleon-nucleon scattering, 305-9, 335
 - see also Nucleon-nucleon scattering
- Beryllium
 - in vertebrate radiobiology, 541
- "Billiard-ball" collisions
 - in nuclear recoil labeling, 261
 - see also Recoil labeling
- Bohr-Mottelson unified model
 - in internal conversion, 215-22, 228-32
- Boron
 - in vertebrate radiobiology, 545
- Boundary condition model
 - of nucleon-nucleon scattering, 327-29
 - see also Nucleon-nucleon scattering
- Bromide and iodide retention
 - in recoil labeling, 264
 - see also Recoil labeling
- Bromine
 - in vertebrate radiobiology, 548-49
- Bubble chambers, 109-60
 - analysis of events in, 146-51
 - bubble formation, 111, 113-16
 - design, construction, and operation of, 122, 131
 - hydrogen, 125-31
 - large heavy liquid, 125, 126

- large hydrogen
 - design considerations of, 131-44
 - see also Hydrogen
- bubble chambers, large
 - number of bubbles
 - per unit track length, 115
 - rate of bubble growth, 115-16
 - track distortion, 145
 - use of lead plates, 117
- Bubble chamber liquids
 - comparative characteristics of, 122, 152-53
- deuterium, 116
- freons, 117
- helium, 116
- hydrogen, 116
- operating parameters, 122
- propane, 116-17
- radiation lengths, 122
- thermal properties of, 111
- tungsten hexafluoride, 117
- xenon, 117

C

- Cadmium
 - in vertebrate radiobiology, 545
- Caging effects
 - in nuclear recoil labeling, 261
- Calcium
 - in vertebrate radiobiology, 541-43
- Carbon
 - in vertebrate radiobiology, 546
- Carbon-14
 - replacement of an asymmetric carbon by, 276
- Carbon-14⁺ ion beam
 - used in labeling of organic compounds, 285-86
- Carbon-14 labeled compounds, 270-71
- Carbon-14 labeling, 260, 267-79
 - active nitrogen used in, 272
 - addition complexes used in, 269
 - application of recoil-labeled compounds
 - in the oil industry and in biogenesis studies, 278-79
 - carrier methods, 277
 - clathrates
 - use in, 269

- difficulty with use of thermal neutron columns for irradiation, 267
 effect of phase
 on yield of re-entry and synthesis products, 275
 fragmentation products, 272-73
 gamma heating, 267
 gas-liquid chromatography techniques, 277
 isolation and purification of recoil products, 276-77
 isolation of synthesis products, 277
 mechanisms involved
 in product formation from recoils, 278-79
 neutron fluxes required for, 267-69
 nitrogen sources for, 269
 paper chromatographic techniques, 277
 rearranged activity, 274
 re-entry compound purification, 277
 re-entry products, 272-73, 275
 relation of availability of hydrogen
 to yield of synthesis products, 275
 replacement of ring carbons, 273
 ring expansion of compounds, 272
 specific labeling, 274
 specificity and randomness, 273
 statistical replacement, 274-75
 of hydrogen, 276, 278
 synthesis compounds, 274
 synthesis products, 272-73, 275
 temperature ranges used, 267
 use of neutron flux monitoring foils, 268
 yield of carbon-14, 267-71
 yields of
 aliphatic synthesis products, 275
 aromatic synthesis products, 275
 see also Recoil labeling
 Carbon-14 recoils
 in inorganic compounds, 271
 Carrier methods
 in carbon-14 labeling, 277
 Cataract induction, 522
 see also Vertebrate radiobiology
- Cellular radiobiology, 489-530
 biochemical investigations, 514-18
 cataract induction, 522
 chemical protection, 520-22
 chromosome breakage mechanisms of, 522-23
 cysteamine
 electron-spin resonance studies of, 491
 DNA
 studies of, 490, 492, 512, 515-24
 dose-effect relationships, 491-500
 dosimetry, 500-1
 effects on enzymes irradiated within the cell, 515, 517-18
 electron spin resonance phenomena, 489-91
 "extrapolation number" in survival curves, 491-92
 gases under pressure
 effects of, 509
 genetic effects, 496-97
 growth and development
 effects of radiation on, 498-99
 hypoxia
 effects of, 507
 latent damage, 513-14
 leakage through cell walls and related effects, 514-15
 lethal actions of radiations
 on cells, 493-95, 523-28
 on mammalian cells, 493-95
 on micro-organisms, 493
 "linear energy transfer," 500-3
 low doses
 effects of, 499-500
 low temperatures
 effects of, 507
 magnetic centers
 in electron spin resonance studies, 490-91
 mechanisms of, evidence, and speculation on, 518-25
 modification of damage
 by treatment after irradiation, 509-14
 modification of radiation response
 by treatment, 503-9
 modifying action of gases other than oxygen, 508-9
 "multiplicity" in survival curves, 491-92
 nitric oxide
- effect of, 508-9
 nucleic acid synthesis and related topics, 515-18
 nutrients and metabolic inhibitors
 effects of after irradiation, 510-11
 oxygen
 effect of after irradiation, 509-10
 effects of, 505-8, 520-22
 enhancement ratios, 505-8
 pre-treatment
 by non-ionizing radiation, 504-5
 "quality" of radiations, 500-1
 radiations of different quality
 significance of, 500-3
 radiosensitivity of different functions in the same cell, 495-96
 radiosensitivity and the division stage, 518-20
 "recovery"
 from radiation damage, 513
 RNA
 studies of, 491-91, 512, 515-18
 sigmoid curves, 491-93
 survival curves
 for germinal cells, 495
 for lymphatic cells, 494-95
 for mammalian cells, 493-95
 tumor therapy, 494
 ultraviolet irradiation, 492-93, 495-96, 504-5, 509-14
 variability
 of the oxygen effect, 507-8
 of radiation effects with dose rate and dose fractionation, 497-98
 variations
 in biological effects, 501-3
 in RBE, 501-3
 water
 effect of after irradiation, 511-12
 water radicals, 424-25, 491
 Y distributions, 500
 Cerium
 in vertebrate radiobiology, 551-52
 Cesium
 in vertebrate radiobiology, 538-40
 Charge independence
 of nuclear forces, 326,

363-64
 Charge states
 of fission fragments, 244
 Cherenkov light
 in extensive air showers,
 86-89
 lateral distribution of
 light in, 87, 88
 Chi-squared test for phase
 shift analysis
 of nucleon-nucleon scat-
 tering, 330
 see also Nucleon-nucleon
 scattering
 Chloride retention
 in recoil labeling, 264
 Chlorine
 in vertebrate radiobiology,
 548-49
 Chromium
 in vertebrate radiobiology,
 548
 Cobalt
 in vertebrate radiobiology,
 550
 Coefficients of fractional
 parentage, 364-69
 Compound nucleus
 heavy-ion reactions
 comparison of calculated
 and measured cross
 sections in, 50-52
 shape of excitation func-
 tions for, 48-50
 spectra and angular dis-
 tribution of products
 of, 52-55
 see also Heavy-ion reac-
 tions
 Continuous exposure effects
 in vertebrate radiobiology,
 565-66
 Copper
 in vertebrate radiobiology,
 541
 Correlation experiments
 in nucleon-nucleon scatter-
 ing, 300-2, 343
 see also Nucleon-nucleon
 scattering
 Cosmic ray experiments
 during the International
 Geophysical Year,
 461-88
 Cosmic rays
 Forbush decreases, 464-
 69
 interaction lengths of
 primaries, 99, 100
 interactions in space,
 104, 105
 isotropy of, 65-66, 97-98,
 102-4
 maximum energy of, 98,
 102-4
 modulation of
 by solar activity, 464-69

 pion spectrum produced by,
 104, 105
 primary neutrinos, 22,
 67, 104, 106-7
 primary photon spectrum,
 67, 104-6
 source of greatest energy
 component, 98
 time lag of, 66, 67
 volume occupied by, 98
 see also Extensive air
 showers and IGY cos-
 mic ray experiments
 Cosmic ray showers, 63-
 108
 Coulomb scattering formula
 multiple, 152, 154
 Counters
 total-body, 533, 537, 540
 see also Particle detectors
 Curium
 in vertebrate radiobiology,
 554
 Cysteamine
 protective effects
 in vertebrate radiobiology,
 568-69
 radiobiology of, 491, 512,
 521-22

D

Dancoff-Morrison "gauge
 transformation," 200-1
 Deformed nuclei
 in internal conversion, 232
 see also Bohr-Mottelson
 unified model
 Delta rays, 154
 Density logging, 444-45
 see also Subsurface nuclear
 prospecting
 Density matrix and statisti-
 cal mixtures
 in nucleon-nucleon scatter-
 ing, 293-96
 see also Nucleon-nucleon
 scattering
 Density spectrum
 in extensive air showers,
 89-92
 Differential cross-section
 measurements
 in nucleon-nucleon scat-
 tering, 314, 316-19,
 322, 323
 Dispersion theory
 in nucleon-nucleon scat-
 tering, 336-43
 Displacement collisions,
 261-62
 DNA
 radiobiological studies of,
 490, 492, 512, 515-24
 Dosimetry
 in radiobiology, 500-1
 internal emitters, 532-

 33
 see also Vertebrate
 radiobiology
 Dynamical effects
 in magnetic transitions,
 210-22
 see also Internal conversion

E

Earth's radiation belts,
 470-79
 see also IGY cosmic ray
 experiments
 Effective range theory
 in nucleon-nucleon scat-
 tering, 325-29
 Electric monopole
 mode of nuclear de-exci-
 tation, 196
 transitions in internal
 conversion, 230-33
 Electric multipoles
 in internal conversion,
 199-203
 Electric penetration coeffi-
 cients
 in internal conversion, 224-
 30
 Electric transitions
 dynamical effects
 in internal conversion,
 222-33
 Electron-nuclear interaction
 multipole expansion of,
 191-203
 see also Internal conversion
 Electron spin resonance
 cysteamine
 studies with, 491
 nucleic acid
 studies of, 490-91
 phenomena in cellular
 radiobiology, 489-91
 see also Cellular radio-
 biology
 Elements of group III
 in vertebrate radiobiology,
 545-46
 Elements of group IV
 in vertebrate radiobiology,
 546
 Elements of group V
 in vertebrate radiobiology,
 546-47
 Elements of group VI
 in vertebrate radiobiology,
 547-48
 Elements of group VII
 in vertebrate radiobiology,
 548-49
 Elements of group VIII
 in vertebrate radiobiology,
 549-51
 Energy balance
 of nuclear interacting com-
 ponents

- in extensive air showers, 85-86
- Energy dependence
 - of S-wave phase shifts
 - in nucleon-nucleon scattering, 325-29
- Energy level diagrams for light nuclei, 409-24
- Energy levels of light nuclei, 353-424
- Energy loss per ion pair formed by nuclear recoils, 245
- Energy loss of recoils and ionization, 244-45
 - by nuclear stopping, 245
- Extensive air showers, 63-108
 - absorption length of, 93-95
 - barometric effect, 95-96
 - charge ratio of mesons, 81
 - Cherenkov light, 86-89
 - density spectrum, 89-92
 - energy balance, 80-81, 85-86
 - energy spectrum
 - of electromagnetic component, 75-77
 - of mu-mesons, 78-80
 - evolution of, 69-70
 - fluctuations, 86, 99
 - genetic relations of particles, 69-70
 - growth and absorption of, 92-97
 - heavy nuclei, 96, 99-100
 - lateral distribution
 - of charged particle density, 70-75
 - of mu-mesons, 78-79
 - methods of observation, 67-69, 81-82
 - muon component of, 77-81
 - nuclear interacting components, 81-86
 - altitude variation of, 82-83
 - average energy of, 85
 - energy spectrum of, 84-85
 - lateral variations of, 82-84
 - methods of study of, 81-82
 - number spectrum of, 90-92
 - primaries
 - interaction length of, 99-100
 - structure near axis, 74-75
 - theoretical models
 - of nuclear interactions used in analysis, 94
 - track length of electrons, 89, 95
 - transverse momentum of nuclear interacting component, 101-2
 - ultra-high-energy nuclear
 - interactions, 64-65, 101-2
 - zenith angle distribution, 95
- Extraneous radiation
 - effect of
 - in recoil labeling, 264
 - "Extrapolation number" in
 - in cellular radiobiology, 491-92
- F
- Fission
 - induced by heavy ions, 55-57
 - recoil techniques
 - in study of, 237-38
- Fission fragments
 - charge status of, 244
 - range-velocity curves for, 252-58
 - see also Heavy-ion reactions
- Fluctuations
 - in extensive air showers, 99
- Fluorine
 - in vertebrate radiobiology, 548-49
- Forbush decrease
 - in cosmic rays, 464-69
 - see also IGY cosmic ray experiments
- Fractionated exposure
 - in vertebrate radiobiology, 566
- Fragmentation products
 - produced by carbon-14 labeling, 272-73
- G
- Galactic cosmic rays
 - modulation
 - by solar activity, 464-69
 - see also IGY cosmic ray experiments
- Gallium
 - in vertebrate radiobiology, 245
- "Gamma-gamma" logging, 444, 445
- Gamma logging, 441-43
 - see also Subsurface nuclear prospecting
- Gamma-ray matrix elements, 210-22, 226-27
 - see also Internal conversion
 - see also Light nuclei
- Gammel-Thaler potential
 - in nucleon-nucleon scattering analysis, 345
- Gas bubble chambers, 117, 120
 - see also Bubble chambers
- Genetic effects
 - in cellular radiobiology, 496-97
 - in vertebrate radiobiology, 576-78
- "Geometry" of transmission experiments
 - in nucleon-nucleon scattering, 314-16
- Germanium
 - in vertebrate radiobiology, 546
- Germinal cells
 - radiosensitivity of, 495
- Gold
 - in vertebrate radiobiology, 541
- H
- Hafnium
 - in vertebrate radiobiology, 546
- Halogen isotope recoil labeling, 284
- Harmonic nuclei
 - internal conversion in, 231-32
- Heavy-ion elastic scattering, 30-37, 58
 - optical model of, 36-37
 - rainbow angle, 34
 - rainbow scattering model of, 34-36
 - sharp-cutoff model, 30-34
- Heavy-ion-induced fission
 - excitation function for, 56-57
 - fission fragments in
 - angular distribution of, 57
 - mass distribution of, 57
- Heavy-ion reactions, 27-60, 247-52, 255
 - compound nucleus formation, 46-55
 - comparison of calculated and measured cross sections for, 50-52
 - level density formula for, 48, 51, 53-55
 - shape of excitation functions for, 48-50
 - spectra and angular distribution of reaction products for, 52-55
 - statistical model treatment of, 46-55
- effects of high angular momenta, 55
- nuclear temperature
 - in statistical model of, 48, 53-55
- quasimolecular state
 - of two carbon nuclei, 58
- transfer reactions, 37-

46, 58-59
 see also Heavy-ion elastic scattering
 Heavy ions
 elastic scattering of, 30-37, 58
 fission induced by, 55-57
 laboratories engaged in study of, 29
 range-energy data for, 60-260-61
 see also Range-energy relations, etc.
 response of scintillators and surface barrier layer counters to, 60
 Heavy ion scattering, 30-37, 58
 see also Heavy-ion elastic scattering
 Heavy-ion transfer reactions
 "backshot" mechanism, 45
 complex transfer, 37, 42-46
 contact transfer, 44
 exchange transfer, 37, 42
 fragmentation reaction mechanism, 45
 multiple transfer, 37, 42-46
 single transfer, 37-42
 Heavy nuclei
 in extensive air showers, 96, 99-100
 High-energy beams
 magnetic focusing of, 165-79
 optics of, 161-92
 High-energy de-excitation
 in recoil labeling, 262
 High-energy nuclear interactions
 angular distribution, 102
 theoretical models of, 102
 see also Extensive air showers
 Holmium
 in vertebrate radiobiology, 552
 Hot reactions
 in recoil labeling, 262, 265
 Human radioisotopic deposition
 estimation of, 537
 see also Vertebrate radiobiology
 Hydrogen bubble chambers
 large
 chamber materials, 134
 chamber windows, 134, 136-37
 dark field illumination of, 139
 expansion mechanisms for, 134-36
 gaskets for, 129, 134
 illumination of, 137-41

magnets for, 133-34
 photography for, 141-45
 single-window illumination of, 139-41
 some tentative parameters of, 133
 I
 Impact parameter
 in nucleon-nucleon scattering analysis, 330-31
 Indium
 in vertebrate radiobiology, 245
 Interaction energy operator
 for shell-model analysis of light nuclei, 366, 369-71
 Internal conversion
 accidental cancellation in rotational transitions, 219-22
 β -vibrational states
 effects of, 232
 Bohr-Mottelson unified model, 215-22, 228-32
 Dancoff-Morrison "gauge transformation," 200-1
 deformed nuclei, 232
 see also Bohr-Mottelson unified model
 dynamical effects
 in electric transitions, 222-33
 in magnetic transitions, 210-22
 dynamical penetration effects, 195-96
 EL gamma-ray matrix elements, 226-27
 electric monopole conversion effect
 on directional correlation experiments, 231-32
 electric monopole mode, 196, 202-3, 231
 electric monopole strength parameter of, 231
 electric monopole transitions, 230-33
 electric monopole transition probability, 231
 electric multipoles, 199-203
 electric penetration coefficients, 224-30
 electric penetration matrix elements
 formulae for, 226
 and nuclear models, 228-30
 two types of, 222-30
 electric penetration weight-

ing functions, 222-23
 electron wave function for nucleus of finite extent, 205-8
 gamma-gamma directional correlation, 215-22
 gamma-K conversion electron directional correlation, 217-22
 gamma-ray matrix elements, 210-22
 harmonic nuclei, 231-32
 see also Internal conversion, rotational transitions
 isotope shift effect, 195-96
 $j \cdot \nabla$ type of penetration matrix elements, 229-30
 $j \cdot \hat{r}$ type of penetration matrix elements, 229-30
 "knitting-needle" nucleus, 229
 magnetic hyperfine structure anomalies, 195-96
 magnetic monopole effects
 absence of, 202
 magnetic multipoles, 198-99
 magnetic penetration coefficients, 211-22
 magnetic penetration matrix elements
 for nuclear models, 210-22
 monopole mode
 for harmonic nuclei, 231
 "no-penetration" model, 169, 201-2
 nuclear charge distribution
 effect of, 203-8
 nuclear magnetic moments
 effect of, 208
 nuclear size effects, 203-6
 nuclear structure effects, 193-234
 penetration coefficients
 magnetic and electric, 211-33
 penetration matrix elements, 210-33
 penetration weighting functions, 211, 222-23
 point nucleus approximations, 198-99, 201
 realistic charge distribution
 effect of, 207
 rotational transitions, 219-22, 228-32
 spin and convection nuclear currents, 214-15
 static effects, 194-95
 static nuclear moments

- effect of, 208-10
static nuclear quadrupole moment
effect of, 208-10
strength parameter, 231
"surface current" model, 199, 201-2
uniform charge distribution
effect of, 207
vector spherical harmonics
use of, 196-203
see also Penetration matrix elements, etc.
- Internal conversion coefficients, 194
- International Geophysical Year cosmic ray experiments, 461-88
- Argus nuclear explosion, 470-79
- artificial aurora, 475-79
- auroral x-rays and soft radiation, 462-64
- change in cosmic ray energy spectra
with solar activity, 465-68
- comparison of α -particle and proton momentum spectra
for solar cosmic rays, 482
- composition of solar cosmic rays, 481-84
- constancy
of inner radiation belt intensity, 473-75
- distortions of earth's magnetic field
by high-altitude nuclear explosions, 478-79
- "dumping" of radiation
from outer radiation belt, 473
- electrons associated with auroral radiation, 463-64
- electron-synchrotron radiation
from the sun, 484-86
- energy spectrum
of solar cosmic rays, 480, 482, 484, 485
- Forbush decreases, 464-69
- injection mechanism
for the Van Allen belts, 471-79
- injection into radiation belts
from decay of neutrons, 471, 473-75
- ion trapping
in earth's magnetic field, 470-71
- magnetic plasma
as modulation mechanism
originating from solar activity, 468-69
- modulation of cosmic rays
by solar activity, 464-69
- precession of charged particle orbits, 471
- radiation intensity
due to solar cosmic rays, 484-85
- solar cosmic rays, 479-87
- Van Allen radiation belts, 470-79
- variation in outer radiation belt intensity, 471-73
- Iodine
in vertebrate radiobiology, 549
- Ionization and energy loss
of recoils, 244-45
see also Range-energy relations; Recoil labeling
- Ionization methods
in isotopic labeling, 285
- Iron
in vertebrate radiobiology, 549-50
- Isobaric level diagrams
for light nuclei, 409-24
- Isomerization processes
in recoil labeling, 264
- Isospin formalism
for the shell model of light nuclei, 363-64, 368
- Isotope shift, 195-96
- Isotopes of interest in recoil labeling other than carbon-14 and tritium, 283
- Isotopic labeling
by acceleration of ions
into organic materials, 285-86
- carbon-14⁺ ion beams
use of, 285-86
- ionization methods, 285
see also Recoil labeling
- K
- K-conversion electron-gamma ray directional correlation, 217-22
see also Internal conversion
- L
- Labeling of organic compounds
by recoil methods, 259-90
see also Recoil labeling
- Lanthanum
in vertebrate radiobiology, 551-52
- Late effects in vertebrate radiobiology, 561-82
- Latent damage
in biological irradiation, 513-14
see also Vertebrate radiobiology
- Lead
in vertebrate radiobiology, 546
- Lesions
in vertebrate radiobiology
nature of, 569
- Lethal actions
of radiations
on cells, 523-25
see also Cellular Radiobiology
- Leukemogenesis
in experimental animals, 574-76
in man, 571-74
in vertebrate radiobiology, 571-76
- L-forbiddenness in electromagnetic transitions
in light nuclei, 384-85
- Light nuclei - appendix
isobaric level schemes
for mass 5 to mass 20, inclusive, 409-24
- calculated energies
in the $d\ 3/2\ n$ configuration, 380
- in the $d\ 5/2\ n$ neutron configuration, 403
- in the $f\ 7/2\ n$ configuration, 376
- in the $p\ 1/2\ n\ d_{5/2}$ configuration, 398
- of the $p_{1/2}\ n\ s_{1/2}$ configuration, 397
- charge independence
of nuclear forces, 326, 363-64
see also Nucleon-nucleon scattering
- collective model, 353
see also Bohr-Mottelson unified model
- configurations of $s_{1/2}$ and $d_{5/2}$ nucleons, 402-8
- Coulomb energy differences
in mirror nuclei, 360-61
- coupling scheme transition
in the first p shell, 360-61, 378
- effective nuclear two-body interaction
in shell-model analysis, 354-63, 369-81
- effective single-particle operators, 356
- electric multipole radiation, 382-83
- electromagnetic transition rates, 356-57, 381-85,

399-402, 404, 406
 energies of nuclear states, 369-81
 energy level diagrams for, 409-24
 energy level structure of, 353-424
 energy splitting
 between shells, 358, 360
 excited configurations
 in the first p shell, 393-402
 Fermi-beta transitions, 357
 Gamow-Teller beta transitions, 357-58
 general case of neutrons and protons outside closed shells, 368-69
 identical nucleons
 in the 1^n configuration, 372-81
 interaction energy operator, 366, 369-81
 jj coupling scheme, 355-63, 378
 l-forbiddennness
 in gamma-ray transitions, 384-85
 LS coupling scheme, 360-61, 378
 magnetic dipole gamma-ray transitions, 382-85, 399-402, 404
 magnetic moments, 362-63, 385-87, 401-2
 many-nucleon states, 363-69
 modified shell-model wave functions, 354-56
 non-locality of effective nuclear interactions, 354
 ordering of single-nucleon levels, 358
 reduced matrix elements for M1 transitions in nitrogen 14, 400
 Schmidt formula
 for magnetic moments, 362-63
 seniority scheme, 366-67, 375, 377, 379
 several identical nucleons in one configuration, 364-67
 shell model of, 354-408
 "center of mass" of groups of levels, 374, 378-79, 405-6
 energy levels for protons and neutrons in different unfilled shells, 370-72
 shell model results
 for the first p shell, 387-

93
 single-particle states, 358-63
 spin-orbit splitting, 360-61
 theoretical interpretations of energy levels, 353-424
 Thomas-Ehrman effect, 361-62
 two-particle correlations in modified shell-model wave functions, 354
 Wigner-Eckart theorem in shell-model analysis, 365, 383
 Lithium
 in vertebrate radiobiology, 539
 Lutetium
 in vertebrate radiobiology, 552

M

Magnesium
 in vertebrate radiobiology, 541
 Magnetic hyperfine structure anomalies, 195, 196
 Magnetic moments
 effects on nucleon-nucleon scattering, 326
 of light nuclei, 362-63, 385-87, 401-2
 nuclear effects on internal conversion, 198, 199
 Magnetic multipoles in internal conversion, 198, 199
 Magnetic penetration coefficients, 211-22
 Magnetic penetration matrix elements, 210-22
 Magnetic quadrupole lenses
 aberrations of, 186-87
 Magnetic spectrometers and spectrographs, 180-84
 Magnetic transitions
 dynamical effects in internal conversion, 210-22
 Magnets
 optics of
 see High-energy beams, optics of
 Manganese
 in vertebrate radiobiology, 549
 Maximum angular momentum quantum number in phase shift analysis of nucleon-nucleon scattering, 330-31,

336
 Maximum permissible concentration of radioisotopes, 533-55
 see also Vertebrate radiobiology
 Measurement of recoil ranges, 237-42
 in plastic films, 237-38
 see also Range-energy relations, etc.; Recoil ranges, measurement of
 Mercury
 in vertebrate radiobiology, 545
 Metabolism of internal emitters
 in vertebrate radiobiology, 531-60
 see also Vertebrate radiobiology
 Mixing parameters in nucleon-nucleon scattering, 331
 Modified phase shift analysis
 in nucleon-nucleon scattering, 331, 334-45
 Molybdenum
 in vertebrate radiobiology, 548
 Mu mesons
 energy spectrum in extensive air showers, 78, 79, 80
 in extensive air showers, 77-81
 lateral distribution in, 78, 79
 Multiple Coulomb scattering formula, 152, 154
 "Multiplicity"
 in cellular radiobiology, 491-92
 Multipole expansion of electron-nuclear interaction, 196-203
 see also Internal conversion

N

Natural gamma logging, 441-43
 see also Subsurface nuclear prospecting
 Neptunium
 in vertebrate radiobiology, 554
 "Nest" or "brush heap" of radicals
 in recoil labeling, 262
 Neutrino component of primary cosmic rays, 22, 67, 104, 106-7
 Neutrinos

- detection of, 5-10
- detection of high-energy machine-produced, 21-22
- effect of neutral lepton currents on scattering of, 17-18
- elastic scattering
 - by electrons, 13-15
 - by nucleons, 17-18
- extraterrestrial cosmic ray production of, 22
- flux from stellar energy sources, 24, 25, 105-6
- high-energy interactions of, 16-26
- high-energy machine production of, 19-22
- interactions of, 1-26
- limits on electromagnetic moments of, 2
- low-energy interactions of, 1-16
- non-local interactions of, 16, 17
- possible sources of, 15, 16
- production
 - by antimatter in the universe, 23-24
 - in atmosphere by cosmic rays, 23
 - by supernovae, 105-6
- significance in cosmology, 23-25
- solar production of, 25
- Neutron activation logging, 449-51
 - see also Subsurface nuclear prospecting
- Neutron capture and inelastic gamma logging, 451-54
 - see also Subsurface nuclear prospecting
- Neutron logging, 445-49
 - see also Subsurface nuclear prospecting
- Neutron-neutron differential cross sections, 323
- Neutron-proton differential cross sections, 322-323
- Neutron-proton polarization measurements, 322-323
 - see also Nucleon-nucleon scattering
- Niobium
 - in vertebrate radiobiology, 547
- Noble gases
 - in vertebrate radiobiology, 538
- Non-central forces
 - in nucleon-nucleon scattering, 333
- Non-ionizing pre-treatment in radiobiology, 504-5
- "No-penetration" model
 - in internal conversion, 199, 201-2
- Nuclear charge distribution
 - effect on internal conversion, 203-8
- Nuclear currents, j_n
 - connection with penetration matrix elements, 214
 - spin and convection parts, 214-15
- Nuclear de-excitation
 - electric monopole mode of, 96, 202-3
 - see also Internal conversion
- Nuclear interacting component
 - in extensive air showers, 81-86
 - altitude variation in, 82, 83
 - average energy in, 85
 - energy balance in, 85-86
 - energy spectrum in, 84-85
 - lateral variation in, 82-84
- Nuclear interactions
 - transverse momentum, 101-2
- Nuclear magnetic moment
 - effects on internal conversion, 208
- Nuclear methods
 - for subsurface prospecting, 425-60
 - see also Subsurface nuclear prospecting
- Nuclear models
 - calculation of magnetic penetration matrix elements for, 210-22
 - see also Internal conversion
- Nuclear moments, static
 - effects on internal conversion, 208-10
- Nuclear quadrupole moments, static
 - effects on internal conversion, 208-10
- Nuclear reaction mechanisms
 - deduction from recoil measurements, 255-56
 - see also Recoil techniques
- Nuclear reaction products
 - charge states of, 237
- Nuclear reactions
 - elasticity of, 101
 - recoil techniques in study of, 235-58
- Nuclear recoils
 - "billiard ball" collision effects, 261
 - caging effects, 211
 - displacement collision in, 261
 - energy loss of, 260-62
 - replacement collisions in, 261-62, 265
 - terminal hot spot effect in, 261
 - see also Recoil labeling
- Nuclear shell model
 - see Shell model analysis of light nuclei
- Nuclear size
 - effect on internal conversion, 203-6
- Nuclear stopping
 - contribution to energy loss of recoils, 245
- Nuclear structure effects in internal conversion, 193-234
- Nucleic acids
 - electron spin resonance studies of, 490-91
 - radiobiology of, 490-91, 512, 515-24
- Nucleic acid synthesis
 - radiation effects of, 515-18
- Nucleon-nucleon scattering
 - accelerators
 - for production of nucleon beams, 313-14, 319
 - boundary condition model, 327-29
 - correlation experiments, 300-2, 343
 - correlation parameters, 298
 - density matrix
 - use of, 293-96
 - depolarization experiments, 299
 - deuterium-tritium reaction
 - for neutron production, 314
 - difference in mass between the neutral and charged pions
 - effect on, 326
 - differential cross-section measurements, 314, 316-19, 322-23
 - dispersion theory, 336-43
 - effective range theory in, 325-29
 - effect of magnetic moments on, 326
 - energy-dependent phase shift analysis, 344-45
 - experimental data, 313-24
 - experimental observables
 - in terms of the Wolfenstein parameters, 301
 - higher partial waves
 - importance of, 327
 - inelastic processes, 313
 - maximum angular momentum quantum number

in phase shift analysis, 330-31
 mixing parameters, 331
 modified phase shift analysis
 using some results of meson theory, 325
 neutron-neutron differential cross sections, 323
 neutron-proton differential cross sections, 322-323
 neutron-proton polarization measurements, 322-23
 neutron-proton triple-scattering measurements, 314, 323
 non-central forces
 effects of, 333
 nuclear-Coulomb interference, 333
 phase shift analysis of, 329-46
 phase shift solutions for proton-proton scattering, 334-35
 phenomenological analysis of, 291-352
 pion production, 313
 polarization experiments, 292
 polarization measurements, 314, 318-20, 322-23
 polarized beams
 use of, 323-24
 polarized targets
 use of, 324-25
 polarizing and analyzing powers, 298
 polarizing function, 298
 possible experiments, 297-300
 potential models, 326
 proton-proton differential cross sections, 316-19
 proton-proton polarization measurements, 320
 relativistic Coulomb parameter, 327
 relativistic formalism, 312, 313
 repulsive core, 325
 "shadow" effect, 314
 space-reflection and time-reversal invariances, 296, 302, 309-10
 spin correlation in proton-proton scattering, 320-22, 343
 S-wave phase shifts, 325-29, 331-36
 targets used, 314
 theoretical relations be-

 tween experiments, 300-3
 total cross section in, 314-16
 triple-scattering experiments, 292, 299, 320-23, 330
 vacuum polarization effect, 326, 327
 Nucleon-nucleon scattering analysis
 "bar" phase shifts, 305-9, 335
 Blatt and Biedenharn phase shifts, 305-9
 effective range, 325-29
 Feynman rules
 use of, 337
 Gammel-Thaler potential, 345
 general formalism for, 292-313
 identical particles
 treatment of, 310-12
 one-meson exchange potential, 331, 334-45
 phase shifts, 303-9, 325-41
 photodisintegration of the deuteron
 use of, 344
 projection operators
 use of, 337, 341, 342
 symmetrization of wave functions, 310-12
 unitarity requirement, 303-9
 Wolfenstein parameter, 296, 300-3, 307-8, 321-22
 Nucleon-nucleon scattering
 effective range theory
 scattering length, 325-29
 shape parameter, 325-29
 Nucleon-nucleon scattering experiments
 "geometries" used in, 314-16
 Nucleon-nucleon scattering phase shift analysis
 D waves, 331-35, 345-46
 F waves, 331-35
 G waves, 332, 334-35
 H waves, 334
 P waves, 331-35, 345-46
 tests of goodness of fit, 330

O

One-meson exchange potential
 in nucleon-nucleon scattering analysis, 331, 344-45
 Optics of high-energy beams,

 161-92
 formation of separated beams, 187-90
 highly collimated beams, 190-91
 transmission of magnetic beam-forming systems, 184-86
 see also High-energy beams
 Oxygen enhancement ratios in cellular radiobiology, 505-8

P

Partial-body exposure in vertebrate radiobiology, 565
 Particle detectors
 comparative characteristics of, 112
 scintillation and surface barrier counters
 response to heavy ions, 60
 Penetration coefficients, 212-33
 electric, 224-30
 magnetic, 211-22
 see also Internal conversion
 Penetration matrix elements, 33, 210
 accidental cancellation effects, 214
 electric, 222-30
 l-forbiddenness, 214-15
 magnetic, 210-11
 radial selection rules for, 214
 see also Internal conversion
 Penetration parameter, 210-33
 Penetration terms for electric conversion, 222-33
 Penetration weighting function, 211
 see also Internal conversion
 Permissible limits for radiolotope concentration
 derivation of, 535-36
 see also Vertebrate radiobiology
 Phase shift analysis of nucleon-nucleon scattering, 329-46
 Phenomenological analysis of nucleon-nucleon scattering experiments, 291-352
 see also Nucleon-nucleon scattering

- Phosphorus
in vertebrate radiobiology,
546-47
- Photodisintegration
of the deuteron
use in nucleon-nucleon
scattering analysis,
344
- Photon component
of primary cosmic rays,
104-5
- Pi-meson spectrum
produced by cosmic rays,
104-5
- Plutonium
in vertebrate radiobiology,
553-54
- Point nucleus approximation
in internal conversion,
198-99, 201
- Polarization experiments
and measurements,
292, 314, 318, 320,
322-23
see also Nucleon-nucleon
scattering
- Polarization of nucleons
see Nucleon-nucleon scat-
tering
- Polarized beams
use in nucleon-nucleon
scattering, 323-24
- Polarized targets
use in nucleon-nucleon
scattering, 298, 323-
24
- Polarizing and analyzing
powers
in nucleon-nucleon scat-
tering, 298
- Polarizing functions
for nucleon-nucleon scat-
tering, 298
- Polonium
in vertebrate radiobiology,
548
- Potassium
in vertebrate radiobiology,
538-39
- Pre-treatment by non-
ionizing radiation
in radiobiology, 504-5
- Primary cosmic rays
photon component of, 67,
104-5
neutrino component of, 22,
67, 104, 106-7
- Protoactinium
in vertebrate radiobiology,
554
- Proton-proton polarization
measurements
in nucleon-nucleon scat-
tering, 320
- Proton-proton scattering
differential cross
sections, 316-19
- Proton-proton scattering
phase shift solutions,
334-35
see also Nucleon-nucleon
scattering
- Q**
- Quadrupole lenses
see High-energy beams,
optics of; Magnetic
quadrupole lenses
- Quadrupole magnets, 163-
64, 169-79, 186-87
see also High-energy
beams, optics of
- Quadrupole moments
static nuclear effects
in internal conversion,
208-10
- R**
- Radial selection rule
in gamma-ray matrix ele-
ments, 214
- Radiation
contamination hazards in
the environment,
536-37
see also Vertebrate
radiobiology
- damage
in recoil labeling proc-
esses, 264, 267, 269,
271-72
life shortening induced by,
and natural aging
theoretical research on,
569-71
see also Vertebrate
radiobiology
- Radical scavenger effect
in recoil labeling, 262-
64, 266
- Radiobiology, 489-582
of vertebrates
metabolism of internal
emitters, 531-60
see also Vertebrate radio-
biology
- "Radiochemical yield,"
263, 267
- Radioisotope detection meth-
ods
in vertebrate radiobiology,
532-33
- Radioisotopes
maximum permissible
concentrations of,
533-55
see also Vertebrate radio-
biology
- in vertebrate radiobiology,
545-46
actinide elements, 551-
54
- alkali metals, 538-41
alkaline earths, 541-45
elements of group IV,
546
elements of group V,
546-47
elements of group VI,
547-48
elements of group VII,
548-49
elements of group VIII,
549-51
noble gases, 538
rare-earth elements,
551-52
transition elements of
group I, 541
transition elements of
group II, 545
tritium, 538
- Radiosensitivity
of different functions in
the same cell, 495-
96
of germinal cells, 495
- Radium
in vertebrate radiobiology,
544-45, 554
- Radon
in vertebrate radiobiology,
538
- Range distribution of recoils
gaussian nature of,
245-47, 251-52
- Range-energy data
for heavy ions, 60,
252-55, 260-61
- Range-energy and range-
momentum relations
in hydrogen and propane
bubble chambers,
154, 156-57
- Range-energy relations
for ions, 210-11
see also Recoil ranges
theory of, 244-47
- Range of fission fragments
measurement of, 241-42
- Range of high-energy re-
coils
experimental results,
252-55
- Range of low-energy recoils
experimental results,
247-52
- Range of recoils
measurement of, 237-42
see also Recoil ranges
- Range-straggling param-
eter, 245, 247,
251-52
- Range-velocity curves
for light and heavy fission
fragments, 252-55
- Range-velocity equations
for fission fragments,
254

Range-velocity relations
see Range-energy relations
Rare-earth elements
in vertebrate radiobiology,
551-52

RBE
in cellular radiobiology,
501-3

Recoil ions
see Nuclear recoils; Recoil
labeling

Recoil-labeled compounds
applications
in the oil industry and
in biogenesis studies,
278-79

Recoil labeling
carbon-14, 260
see also Carbon-14 la-
beling
displacement collisions,
261-62

halogen isotopes in, 284
high-energy de-excitation,
262

hot reaction, 262-65
hot region in, 265
isomerization processes in,
264

isotopes of interest other
than carbon-14 and
tritium, 283

labeling by elements other
than carbon and tri-
tium, 283-85

"nest" or "brush heap" of
radicals, 262

radiation damage, 267, 269,
276, 279
effects, 264, 267, 269,
271-72

radical scavenging effect,
262-64, 266

radical traps
effects of, 266

radiochemical purity, 277,
281

radiochemical yields, 263-
67

replacement collisions,
261-65

"retention," 263-64

sulfur-35 labeling, 284

thermal or "diffusive"
products, 262-63

thermal radicals, 266

thermal reaction, 265-66

thermal region, 265

tritium, 260, 279, 283
see also Tritium recoil
labeling

tritons, 279, 283
see also Carbon-14 labeling;
Nuclear recoils

Recoil measurements
use of
to determine nuclear re-

action mechanisms,
255-56

Recoil methods
in the labeling of organic
compounds, 259-90

Recoil nuclei
average energy loss
per ion pair, 245
energy loss of, 260-61

Recoil ranges
measurements of, 237-42
in air, 238-39
in gases, 239-41
in plastic films, 238
from thick targets, 242-43
see also Range-energy re-
lations

Recoils
measurement of ranges of
low-energy particles,
247-52
range-straggling param-
eter for, 245-47, 251-52

Recoil techniques
in nuclear reaction and fis-
sion studies, 235-58
in study of spallation,
236-37

Relative biological effective-
ness
in vertebrate radiobiology,
567

Relativistic Coulomb param-
eter
in nucleon-nucleon scat-
tering, 327

Relativistic formalism
in nucleon-nucleon scat-
tering, 312, 313

Replacement collisions,
261-62, 265

Repulsive core
in nucleon-nucleon scat-
tering, 325

"Retention" of activity
in recoil labeling, 263

Retention of radioisotopes
in the body, 534-35
see also Vertebrate radio-
biology

Rhenium
in vertebrate radiobiology,
549

Ring expansion of compounds
in carbon-14 labeling,
272

RNA
radiobiological studies of,
490-91, 512, 515-
24

Rotational transitions
in internal conversion,
219-22

Rubidium
in vertebrate radiobiology,
539

Ruthenium

in vertebrate radiobiology,
550-51

S

Scandium
in vertebrate radiobiology,
545

Scattering
in heavy-ion processes
see Heavy-ion scattering
nucleon-nucleon
see Nucleon-nucleon
scattering

Scattering lengths
in nucleon-nucleon scat-
tering analysis, 325-
29

Schmidt formula for magnetic
moments, 362-63

Seniority scheme of classi-
fication
of shell-model wave func-
tions, 366-67, 375,
377, 379

see also Light nuclei
"Shadow" effect
in nucleon-nucleon scat-
tering, 314

Shape parameter
in nucleon-nucleon scatter-
ing analysis, 325-29

Shell-model analysis
of light nuclei, 354-408
effective single-particle
operators, 356

see also Light nuclei

Shell-model calculations
reduced matrix elements,
365

see also Light nuclei, shell-
model theory of

Shell-model of light nuclei
coefficients of fractional
parentage, 364-69

Shell-model theory for light
nuclei

isospin formalism for,
363-64, 368

Sigmoid survival curves
in cellular radiobiology,
491-93

Silver
in vertebrate radiobiology,
541

Single-dose exposure
in vertebrate radiobiology,
564-65

Single-particle states
in the shell model of light
nuclei, 358-63

Sodium
in vertebrate radiobiology,
539

Soft radiation and auroral
x-rays, 462-64

Solar cosmic rays, 479-87

- see also IGY cosmic ray experiments
 Solar effect
 upon cosmic rays, 464-69
 see also IGY cosmic ray experiments
 Sources of tritium
 for tritium recoil labeling, 279-80
 Space-reflection invariance
 in nucleon-nucleon scattering, 302
 Spallation
 recoil techniques in study of, 236-37
 Spallation products
 angular distribution of, 242
 Specific radioisotopes
 in vertebrate radiobiology, 538-54
 Spectrographs
 magnetic, 180-84
 Spectrometers
 magnetic, 180-84
 Spin-correlation experiments
 in nucleon-nucleon scattering, 320-22, 343
 Static nuclear moments
 effects on internal conversion, 208-10
 Static nuclear quadrupole moments
 effects on internal conversion, 208-10
 Statistical mixtures and the density matrix
 in nucleon-nucleon scattering, 293-96
 see also Nucleon-nucleon scattering
 Statistical model
 see Heavy-ion reactions
 Statistical replacement
 in carbon-14 labeling, 274-75
 Strength parameter
 in internal conversion, 231
 Strong focusing magnets, 163-64, 169-79
 Strontium
 in vertebrate radiobiology, 541-43
 Subsurface nuclear prospecting
 activities of significance for neutron activation logging, 450
 basic "boundary conditions," 430-39
 borehole fluid variations, 433-34
 borehole geometry variations, 432-33
 cable transmission limitations, 438-39
 density or "gamma-gamma" logging, 444-45
 deuterium-tritium accelerators
 for neutron activation logging, 450-51
 effective radius of investigation
 in neutron logging, 449
 future of methods, 454-56
 gamma logging
 for petroleum, 442-43
 for uranium and thorium, 442
 gamma spectral logging, 442-43
 general techniques (tabulated), 440
 incentives for, 428-29
 incentives for development of nuclear techniques, 430
 laboratory simulation of subsurface formations, 436-37
 limitations
 from temperature, pressure, and confinement, 435-36
 natural gamma logging, 441-43
 neutron activation logging, 449-51
 neutron capture and inelastic gamma logging, 451-54
 neutron-gamma technique, 445-49
 (neutron-epithermal neutron) technique in, 445-47
 neutron logging, 445-49
 (neutron-thermal neutron) technique, 445-49
 nuclear methods of, 425-60
 nuclear versus molecular measurements, 437-38
 oxygen logging, 450-51
 requirements for absolute measurements, 439
 specific nuclear techniques, 439-58
 standardization of gamma-ray surveys, 441-42
 time available for measurements, 434-35
 total gamma activity logging, 442-43
 use of pulsed deuterium-tritium neutron sources, 453
 Sulfur
 in vertebrate radiobiology, 547-48
 Sulfur-35-labeled cystine
 by recoil methods, 284
 Supernovae
 electrons, neutrinos, and high-energy photons from, 105-6
 "Surface current" model
 in internal conversion, 199, 201-2
 S-wave phase shift
 in nucleon-nucleon scattering, 325-29, 331-36
 Symmetrization of wave functions
 in the nucleon-nucleon scattering analysis, 310-12
- T
- Tantalum
 in vertebrate radiobiology, 547
 Targets
 used in nucleon-nucleon scattering, 314
 Technetium
 in vertebrate radiobiology, 549
 Terminal hot spot
 in nuclear recoils, 261
 see also Recoil labeling
 Thallium
 in vertebrate radiobiology, 545
 Theoretical interpretations
 of energy levels of light nuclei, 353-424
 Thermal or "diffusive" products, 262-63
 Thermal reaction
 in recoil labeling, 265-66
 Thomas-Ehrman effect
 in light nuclei, 361-62
 Thorium
 in vertebrate radiobiology, 552-53
 Thulium
 in vertebrate radiobiology, 551-52
 Time-reversal invariances
 in the nucleon-nucleon scattering analysis, 296, 302, 309-10
 Tin
 in vertebrate radiobiology, 546
 Total-body counters, 533, 537, 540
 Total cross sections
 in nucleon-nucleon scattering, 314-16
 Track length
 of electrons
 in extensive air showers, 89
 Transition elements of group I
 in vertebrate radiobiology, 541

- Transition elements of group II
in vertebrate radiobiology, 545
- Transmission of magnetic beam-forming systems, 184-86
- Transmission measurements of total cross section in nucleon-nucleon scattering, 314-16
see also Nucleon-nucleon scattering
- Transverse momentum in nuclear interactions, 101-2
- Triple-scattering experiments, 292, 299, 320-23, 330
see also Nucleon-nucleon scattering
- Tritium recoil-labeled compounds, 280
- Tritium recoil labeling, 260, 279, 283
connection of the exposure to tritium gas to labeling yield, 281
discharge method, 282
gas phase work, 281
labile tritium, 280
mechanisms of gas-phase reactions, 282, 283
reduction of double bonds, 281
use of slurries and other heterogeneous mixtures, 280
see also Recoil labeling
- Tritium
in vertebrate radiobiology, 538
- Tumor therapy, 494
- Tungsten
in vertebrate radiobiology, 548
- U
- Ultra-high-energy nuclear interaction
in cosmic ray showers, 101-2
- Ultraviolet irradiation
in radiobiology, 492-93, 495-96, 504-5, 509-14
- Unitarity
in nucleon-nucleon scattering, 303-9
- Uranium
in vertebrate radiobiology, 553
- V
- Vacuum polarization
effect on nucleon-nucleon scattering, 326-27
- Van Allen radiation belts, 470-79
see also IGY cosmic ray experiments
- Variations
in biological effects of radiation, 501-3
- Vector spherical harmonics in internal conversion, 196-203
- Vertebrate radiobiology, 531-82
age effects, 565
alkali metals, 538-41
alkaline earths, 541-45
autoradiographic methods, 532-33
continuous exposure effects of, 565-66
cysteamine protective effects of, 568-69
derivation of permissible limits
for radioisotopic concentrations, 535-36
dose dependence of mutation rate, 578
dose-rate dependence of leukemogenesis, 575-76
dose-response relation in leukemogenesis
in man, 572-74
dosimetry
of internal emitters, 532-33
effects
of heavy x-ray dosage, 563
of some non-radiative stresses on life span, 568
elements of group III, 545-46
elements of group IV, 546
elements of group V, 546-47
elements of group VI, 547-48
elements of group VII, 548-49
elements of group VIII, 549-51
environmental contamination hazards
evaluation of, 536-37
fractionated exposure effects of, 566
genetics of animals
effects of irradiation on, 578
genetics of man
effects of irradiation on, 576-78
human radioisotopic deposition
estimation of, 537
late effects, 561-82
leukemia
comparison of in man and animals, 575-76
leukemogenesis, 571-76
life shortening
in experimental animals, 564-71
in man, 562-64
maximum permissible concentration
of radioisotopes, 533-55
metabolism
of internal emitters, 531-60
methods of radioisotope detection, 535-33
mortality
from induced leukemia, 563, 566
see also Leukemogenesis
multiple exponential model of radioisotope retention, 534-35
nature of the lesion, 569
noble gases, 538
partial-body exposures
effects of, 565
power-law model of radioisotope retention, 535
question of threshold
in dosage-response relationships, 564-65
radioelements, specific discussions of, 538-54
radiologists
life shortening of, 562-63
rare-earth elements, 551-52
relative biological effectiveness
of different radiations, 567
retention of radioisotopes
in the body, 534-35
routes of radioisotopes to the body, 533-34
single-dose exposures
effects of, 564-65
theoretical research
on problem of natural aging and radiation-induced life shortening, 569-71
therapy and prophylaxis
against irradiation effects, 568-69
"total-body counters," 533, 537, 540
transition elements of group I, 541

transition elements of
 group II, 545
 tritium, 538
 Vibrational nuclei
 see Bohr-Mottelson unified
 model: Harmonic
 nuclei

W

Water radicals, 424-25,
 491
 Weak interactions
 intermediate boson hypothe-
 sis of, 16-17
 Wigner-Eckart theorem
 365, 383

Wire orbits
 use in testing magnetic
 components, 179-
 81
 Wolfenstein parameters,
 296, 300-3, 307-8,
 321-22

X

X-rays
 in the aurora, 462-64

Y

Y-distributions
 in radiobiology, 500

Yields of synthesis products
 in carbon-14 labeling
 aliphatic, 275
 aromatic, 275

Yttrium
 in vertebrate radiobiol-
 ogy, 543, 551-
 52

Z

Zinc
 in vertebrate radiobiology,
 545

Zirconium
 in vertebrate radiobiology,
 546

CUMULATIVE INDEX OF CHAPTER TITLES

Volumes 1 to 10

ACCELERATORS

High-Energy Accelerators
(Standard Cyclotron)
(Synchrocyclotron)
(Synchrotrons)

(Linear Accelerators)
(Proton Synchrotron)

Recent Progress in Accelerators

Recent Developments in Proton

Synchrotrons

Conceptual Advances in Accelerators

Optics of High-Energy Beams

CHEMISTRY, NUCLEAR AND RADIO-

Chemistry of the Actinide Elements

Analytical Nuclear Chemistry

Separation Techniques Used in

Radiochemistry

Fission Radiochemistry (Low-Energy
Fission)

Radiochemical Separation Techniques

Generalized Acidity in Radiochemical
Separations

Applications of Oxygen Isotopes in
Chemical Studies

Radiochemical Separations by Ion
Exchange

Equipment for High Level Radio-
chemical Processes

Technetium and Astatine Chemistry

Solvent Extraction in Radiochemical
Separations

Labeling of Organic Compounds
by Recoil Methods

COSMIC RAYS

Nuclear Interactions of Cosmic Rays
Origin and Propagation of Cosmic
Rays

Mesons and Heavy Unstable Particles

in Cosmic Rays

Time Variations of Primary Cosmic

Rays

The Primary Cosmic Radiation

Cosmic Ray Showers

Experiments on Cosmic Rays and
Related Subjects during the

International Geophysical Year

DETECTORS

Nuclear Particle Detection

(Fast Electronics)

(Characteristics of Scintillators)

(Characteristics of Cerenkov

Counters)

(Cloud Chambers and Bubble

Chambers)

Photographic Emulsions

The Fundamentals of Radioautography

M. S. Livingston

1:157-62

M. S. Livingston

1:163-68

J. E. Thomas, Jr., W. L.

Kraushaar, I. Halpern

1:175-98

J. C. Slater

1:199-206

M. S. Livingston

2:169-74

E. L. Chu, L. I. Schiff

2:79-92

J. P. Blewett

4:1-12

D. L. Judd

8:181-216

O. Chamberlain

10:161-92

J. J. Katz, W. M. Manning

1:245-62

C. J. Rodden

1:343-62

P. C. Stevenson, H. G.

Hicks

3:221-34

L. E. Glendenin, E. P.

Steinberg

4:69-80

H. L. Finston, J. Miskel

5:269-96

R. A. Horne, C. D. Coryell,

L. S. Goldring

6:163-78

H. Taube

6:277-302

K. A. Kraus, F. Nelson

7:31-46

N. B. Garden, E. Nielsen

7:47-62

E. Anders

9:203-20

H. Freiser, G. H. Morrison

9:221-44

A. P. Wolf

10:259-90

R. V. Adams

1:107-36

L. Biermann

2:335-64

L. Leprince-Ringuet

3:39-66

V. Sarabhai, N. W. Nerurkar

6:1-42

N. V. Neher

8:217-42

K. Greisen

10:63-108

E. P. Ney

10:461-88

W. H. Jordan

1:207-44

R. E. Bell

4:93-110

R. K. Swank

4:111-40

J. Marshall

4:141-56

W. B. Fretter

5:145-78

Y. Goldschmidt-Clermont

3:141-70

W. P. Norris, L. A. Woodruff

5:297-326

Recent Advances in Low Level Counting Techniques	E. C. Anderson, F. N. Hayes	6:303-16
Gamma-Ray Spectroscopy by Direct Crystal Diffraction	J. W. M. DuMond	8:163-80
Electronics Associated with Nuclear Research	H. W. Kendall	9:343-66
Bubble Chambers	H. Bradner	10:109-60
FISSION (REACTORS)		
High-Energy Fission	R. W. Spence, G. P. Gord	2:399-410
Design Comparison of Nuclear Reactors for Research	L. B. Borst	5:179-96
Nuclear Reactors for Electric Power Generation	L. Davidson, W. A. Loeb, G. Young	6:317-52
Nuclear Fission	I. Halpern	9:245-342
High-Temperature Research and Controlled Fusion	R. F. Post	9:367-436
Fast Reactors	L. J. Koch, H. C. Paxton	9:437-72
Economics of Nuclear Power	J. A. Lane	9:473-92
INTERACTION OF NUCLEAR RADIATIONS AND MATTER		
Radiation Effects in Solids	G. J. Dienes	2:187-220
Extranuclear Interactions of Electrons and Gamma Rays	D. R. Corson, A. O. Hanson	3:67-92
Radiation Chemistry	J. L. Magee	3:171-92
Chemical Effects of Nuclear Transformations	J. E. Willard	3:193-220
Penetration of Heavy Charged Particles in Matter	E. A. Uehling	4:315-50
Radiation Chemistry	F. S. Dainton	5:213-40
Nuclear Radiation Effects in Solids	H. Brooks	6:215-76
Nuclear Methods for Subsurface Prospecting	J. G. Beckerley	10:425-60
LOW TEMPERATURES		
Low-Temperature Phenomena	C. T. Lane	1:413-40
MESONS AND ELEMENTARY PARTICLES		
Meson Physics	R. E. Marshak	1:1-42
Subnuclear Particles	J. S. Blair, G. F. Chew	2:163-86
Reactions of π -Mesons with Nucleons	E. M. Henley, M. A. Ruderman, J. Steinberger	3:1-38
Positronium	S. DeBenedetti, H. Corben	4:191-218
The Interaction Between π -Mesons and Nucleons	M. Gell-Mann, K. M. Watson	4:219-70
Heavy Mesons	C. Dilworth, G. P. S. Occhialini, L. Scarsi	4:271-314
Mu-Meson Physics	J. Rainwater	7:1-30
Hyperons and Heavy Mesons (Systematics and Decay)	M. Gell-Mann, A. H. Rosenfeld	7:407-78
Invariance Principles of Nuclear Physics	G. C. Wick	8:1-48
Hyperfragments	W. F. Fry	8:105-26
Antinucleons	E. Segrè	8:127-62
The Pion-Nucleon Interaction and Dispersion Relations	G. F. Chew	9:29-60
Strange Particles	L. Okun	9:61-98
Neutrino Interactions	F. Reines	10:1-26
METALLURGY		
Progress in Metallurgy	B. A. Rogers, F. H. Spedding	1:441-64
NEUTRONS (SEE ALSO REACTORS)		
Neutron Optics	D. J. Hughes	3:93-118
The Standardization of Neutron Measurements	A. Wattenberg	3:119-40
NUCLEAR GEOLOGY, COSMOLOGY		
Geochemistry	M. Fleischer, J. C. Rabbitt	1:465-78
Origin and Abundance Distribution of the Elements	R. A. Alpher, R. C. Herman	2:1-40
Energy Production in Stars	E. E. Salpeter	2:41-62
Production and Distribution of Radiocarbon	E. C. Anderson	2:63-73

Radioactivity in Geology and Cosmology	T. P. Kohman, N. Saito	4:401-62
Radioactivity of the Atmosphere and Hydrosphere	H. E. Suess	8:243-56
Geochronology by Radioactive Decay	L. T. Aldrich, G. W. Wetherill	8:257-98
Nuclear Astrophysics	A. G. W. Cameron	8:299-326
NUCLEAR MOMENTS, NUCLEAR MODELS AND STRUCTURE		
Recent Developments in the Theory of Nuclear Structure	E. Feenberg	1:43-66
Energy Levels of Light Nuclei	T. Lauritsen	1:67-96
Nuclear Moments	N. Ramsey	1:97-106
	B. T. Feld	2:239-60
Radiofrequency and Microwave Spectroscopy of Nuclei	G. E. Pake	4:33-50
Distribution of Charge in the Nucleus	K. W. Ford, D. L. Hill	5:25-72
Isotope Shift in Atomic Spectra	J. E. Mack, H. Arroe	6:117-28
Properties of Medium-Weight Nuclei	K. Way, D. N. Kundu, C. L. McGinnis, R. van Lieshout	6:129-62
	F. Villars	7:185-230
Collective Model of Nuclei		
Measurement of the Nuclear Spins and Static Moments of Radioactive Isotopes	W. A. Nierenberg	7:349-406
Optical Model and Its Justification	H. Feshbach	8:49-104
The Experimental Clarification of the Laws of β -Radioactivity	E. J. Konopinski	9:99-158
Theoretical Interpretation of Energy Levels of Light Nuclei	I. Talmi, I. Unna	10:353-408
Appendix: Energy Levels of the Light Nuclei	F. Ajzenberg-Selove, T. Lauritsen	10:409-24
Nuclear Effects in Internal Conversion	E. L. Church, J. Wenner	10:193-234
NUCLEAR REACTIONS		
Nuclear Reactions Induced by High-Energy Particles	D. H. Templeton	2:93-104
Recent Studies of Photoneuclear Reactions	K. Strauch	2:105-28
Advances in Nucleon-Nucleon Scattering Experiments and Their Theoretical Consequences	G. Breit, R. L. Gluckstern	2:365-98
Theories of Photoneuclear Reactions	J. S. Levinger	4:13-32
Nuclear Reactions of Intermediate-Energy Heavy Particles	D. C. Peaslee	5:99-144
Polarization of Fast Nucleons	L. Wolfenstein	6:43-76
Excitation of Nuclei by Charged Particles	N. P. Heydenburg, G. M. Temmer	6:77-116
Nuclear and Nucleon Scattering of High-Energy Electrons	R. Hofstadter	7:231-316
Collision of \geq Bey Particles (Excluding Electrons and Photons) with Nuclei	S. J. Lindenbaum	7:317-48
Nuclear Photodisintegration	D. H. Wilkinson	9:1-28
High-Energy Nuclear Reactions	J. M. Miller, J. Hudis	9:159-202
High-Temperature Plasma Research and Controlled Fusion	R. F. Post	9:367-436
Nuclear Interactions of Heavy Ions	A. Zucker	10:27-62
Recoil Techniques in Nuclear Reaction and Fission Studies	B. G. Harvey	10:235-58
Nucleon-Nucleon Scattering Experiments and Their Phenomenological Analysis		10:291-352
General Formalism	H. P. Stapp	10:292-313
Experimental Data	M. H. MacGregor	10:313-24
Phenomenological Analysis	M. J. Moravcsik	10:324-46
POSITRONIUM, ANTIPARTICLES		
Positronium	S. DeBenedetti, H. C. Corben	4:191-218
Invariance Principles of Nuclear Physics	G. C. Wick	8:1-48

Antinucleons	E. Segrè	8:127-82
RADIATION EFFECTS AND HAZARDS		
Radiation Dosimetry and Protection	L. D. Marinelli	3:249-70
Practical Aspects of Radiation Injury	L. H. Hempelmann, J. G. Hoffman	3:369-92
Removal of Radioelements from the Mammalian Body	J. Schubert	5:369-412
Biochemical Effects of Ionizing Radiation	B. E. Holmes	7:89-134
	M. G. Ord, L. A. Stocken	9:523-52
Practical Control of Radiation Hazards in Physics Research	B. J. Moyer	8:327-42
RADIOACTIVITY		
Angular Correlation of the Theory of Nuclear Radiation	H. Frauenfelder	2:129-62
Experimental Clarification of the Theory of Beta Decay	E. J. Konopinski, L. M. Langer	2:261-304
Beta-Decay Energetics	C. D. Coryell	2:305-34
Alpha Radioactivity	I. Perlman, F. Asaro	4:157-90
Electromagnetic Transitions in Nuclei	M. Goldhaber, J. Weneser	5:1-24
Neutrino Interactions	F. Reines	10:1-26
RADIOBIOLOGY		
Genetic Effects of Radiation	R. F. Kimball	1:479-94
Some Aspects of the Biological Action of High-Energy Radiations	H. M. Patt	1:495-524
Cellular Radiobiology	A. H. Sparrow, F. Forro, Jr.	3:339-68
	R. K. Mortimer, C. A. Beam	5:327-68
	L. H. Gray	6:353-422
	E. L. Powers	7:63-88
	T. H. Wood	8:343-86
	K. C. Atwood	9:553-92
	T. Alper	10:489-530
Biochemical Effects of Radiation	K. P. DuBois, D. F. Petersen	4:351-76
Information Theory in Radiobiology	H. Quastler	8:387-400
Vertebrate Radiobiology		
Embryology	R. Rugh	3:271-302
	J. P. O'Brien	6:423-53
	R. Rugh	9:493-522
	J. Furth, A. C. Upton	3:303-38
Histopathology and Carcinogenesis	J. F. Thomson	4:377-400
Lethal Actions and Associated Effects	V. P. Bond, J. S. Robertson	7:135-62
	A. Edelmann	5:413-24
Physiology	C. C. Lushbaugh	7:163-84
Pathology of Radiation Exposure	R. C. Thompson	10:531-60
Metabolism of Internal Emitters	J. B. Storer, D. Grahn	10:561-82
Late Effects		
RADIOISOTOPES		
Isotopic Tracers in Chemical Systems	R. R. Edwards	1:301-42
Radioisotopes in Biochemical and Medical Research	C. A. Villee	1:525-68
Radioisotopes in Soils Research and Plant Nutrition	S. B. Hendricks, L. A. Dean	1:597-610
Isotopes	J. Bigeleisen	2:221-38
Standardization of Radioactive Sources	G. Manov	4:51-68
SHIELDING		
Nuclear Radiation Shielding (See also RADIATION HAZARDS)	E. P. Blizard	5:73-98
SPECTROSCOPY		
Atomic and Molecular Spectroscopy	G. H. Dieke	1:363-412
Isotope Shift in Atomic Spectra	J. E. Mack, H. Arroe	6:117-28
Gamma-Ray Spectroscopy by Direct Crystal Diffraction	J. W. M. DuMond	8:163-80
STABLE ISOTOPES, MASS SPECTROMETRY		
Mass and Relative Abundance of Isotopes	A. O. Nier	1:137-56
Electromagnetic Separation of		

INDEX OF CHAPTER TITLES

615

Stable Isotopes	C. P. Keim	1:263-92
Chemical Separation of Stable Isotopes	G. H. Clewett	1:293-300
Stable Isotopes in Biochemical Research	D. Rittenberg, T. D. Price	1:569-96
Isotope Effects in Chemical Reactions	P. E. Yankwich	3:235-48
Stable Isotope Dilution as an Analytical Tool	M. G. Inghram	4:81-92
Industrial Applications (Mass Spectrometry)	C. E. Berry, J. K. Walker	5:197-212
Mass Spectra and the Chemical Species Produced by the Impact of Low-Energy Electrons	M. Krauss, A. L. Wahrhaftig, H. Eyring	5:241-68
The Masses of Light Nuclides	J. Mattauch, L. Waldmann, R. Bieri, F. Everling	6:179-214

CUMULATIVE INDEX OF CONTRIBUTING AUTHORS

Volumes 1 to 10

A

Adams, R. V., 1:107
Ajzenberg-Selove, F., 10:
409
Aldrich, L. T., 8:257
Alper, T., 10:489
Alpher, R. A., 2:1
Anders, E., 9:203
Anderson, E. C., 2:63;
6:303
Arroe, H., 6:117
Asaro, F., 4:157
Atwood, K. C., 9:553

B

Beam, C. A., 5:327
Beckerley, J. G., 10:425
Bell, R. E., 4:93
Berry, C. E., 5:197
Bieri, R., 6:179
Biermann, L., 2:335
Bigeleisen, J., 2:221
Blair, J. S., 2:163
Blewett, J. P., 4:1
Blizard, E. P., 5:73
Bond, V. P., 7:135
Borst, L. B., 5:179
Bradner, H., 10:109
Brett, G., 2:365
Brooks, H., 6:215

C

Cameron, A. G. W., 8:
299
Chamberlain, O., 10:161
Chew, G. F., 2:163; 9:29
Chu, E. L., 2:79
Church, E. L., 10:193
Clewett, G. H., 1:293
Corben, H. C., 4:191
Corson, D. R., 3:67
Coryell, C. D., 2:305; 6:
163

D

Dainton, F. S., 5:213
Davidson, L., 6:317
Dean, L. A., 1:597
DeBenedetti, S., 4:191
Dieke, G. H., 1:363
Dienes, G. J., 2:187
Dilworth, C., 4:271
DuBois, K. P., 4:351
DuMond, J. W. M., 8:163

E

Edelmann, A., 5:413
Edwards, R. R., 1:301
Everling, F., 6:179
Eyring, H., 5:241

F

Feenberg, E., 1:43
Feld, B. T., 2:239
Feshbach, H., 8:49
Flinston, H. L., 5:269
Fleischer, M., 1:465
Ford, G. P., 2:399
Ford, K. W., 5:25
Forro, F., Jr., 3:339
Frauenfelder, H., 2:129
Freiser, H., 9:221
Fretter, W. B., 5:145
Fry, W. F., 8:105
Furth, J., 3:303

G

Garden, N. B., 7:47
Gell-Mann, M., 4:219; 7:
407
Glendenin, L. E., 4:69
Gluckstern, R. L., 2:365
Goldhaber, M., 5:1
Goldring, L. S., 6:163
Goldschmidt-Clermont, Y.,
3:141
Grahn, D., 10:561
Gray, L. H., 6:353
Greisen, K., 10:63

H

Halpern, I., 1:175; 9:245
Hanson, A. O., 3:67
Harvey, B. G., 10:235
Hayes, F. N., 6:303
Hempelmann, L. H., 3:369
Hendricks, S. B., 1:597
Henley, E. M., 3:1
Herman, R. C., 2:1
Heydenburg, N. P., 6:77
Hicks, H. G., 3:221
Hill, D. L., 5:25
Hoffman, J. G., 3:369
Hofstadter, R., 7:231
Holmes, B. E., 7:89
Horne, R. A., 6:163
Hudis, J., 9:
159
Hughes, D. J., 3:93

I

Inghram, M. G., 4:81

J

Jordan, W. H., 1:207
Judd, D. L., 8:181

K

Katz, J. J., 1:245
Keim, C. P., 1:263
Kendall, H. W., 9:343
Kimball, R. F., 1:479
Koch, L. J., 9:437
Kohman, T. P., 4:401
Konopinski, E. J., 2:261;
9:99
Kraus, K. A., 7:31
Kraushaar, W. L., 1:175
Krauss, M., 5:241
Kundu, D. N., 6:129

L

Lane, C. T., 1:413
Lane, J. A., 9:473
Langer, L. M., 2:261
Lauritsen, T., 1:67;
10:409
Leprince-Ringuet, L., 3:
39
Levinger, J. S., 4:13
Lieshout, R. van, 6:129
Lindenbaum, S. J., 7:
317
Livingston, M. S., 157,
163, 169
Loeb, W. A., 6:317
Lushbaugh, C. C., 7:163

M

Mack, J. E., 6:117
McGinnis, C. L., 6:129
MacGregor, M. H., 10:
317
Magee, J. L., 3:171
Manning, W. M., 1:245
Manov, G., 4:51
Marinelli, L. D., 3:249
Marshak, R. E., 1:1
Marshall, J., 4:141
Mattauch, J., 6:179
Miller, J. M., 9:159
Miskel, J., 5:269

Moravcsik, M. J., 10:
324

Morrison, G. H., 9:221
Mortimer, R. K., 5:327
Moyer, B. J., 8:327

N

Neher, H. V., 8:217
Nelson, F., 7:31
Nerurkar, N. W., 6:1
Ney, E. P., 10:461
Nielsen, E., 7:47
Nier, A. O., 1:137
Nierenberg, W. A., 7:
349
Norris, W. P., 5:297

O

O'Brien, J. P., 6:423
Occhialini, G. P. S., 5:
271
Okun', L., 9:61
Ord, M. G., 9:523

P

Pake, G. E., 4:33
Patt, H. M., 1:495
Paxton, H. C., 9:437
Peaslee, D. C., 5:99
Perlman, I., 4:157
Petersen, D. F., 4:
351
Post, R. F., 9:367
Powers, E. L., 7:63
Price, T. D., 1:569

Q

Quastler, H., 8:387

R

Rabblitt, J. C., 1:465
Rainwater, J., 7:1
Ramsey, N., 1:97
Reines, F., 10:1
Rittenberg, D., 1:569
Robertson, J. S., 7:135
Rodden, C. J., 1:343
Rogers, B. A., 1:441
Rosenfeld, A. H., 7:407
Ruderman, M. A., 3:1
Rugh, R., 3:371; 9:493

S

Saito, N., 4:401
Salpeter, E. E., 2:41
Sarabhai, V., 6:1
Scarsi, L., 4:271
Schiff, L. I., 2:79
Schubert, J., 5:369
Segrè, E., 8:127
Slater, J. C., 1:199
Sparrow, A. H., 3:339
Spedding, F. H., 1:441
Spence, R. W., 3:399
Stapp, H. P., 10:292
Steinberg, E. P., 4:69
Steinberger, J., 3:1
Stevenson, P. C., 3:221
Stocken, L. A., 9:523
Storer, J. B., 10:561
Strauch, K., 2:105
Suess, H. E., 8:243
Swank, R. K., 4:111

T

Talmi, I., 10:353
Taube, H., 6:277
Temmer, G. M., 6:77

Templeton, D. H., 2:93
Thomas, J. E., Jr., 1:175
Thompson, R. C., 10:531
Thomson, J. F., 4:377

U

Uehling, E. A., 4:315
Unna, I., 10:353
Upton, A. C., 3:303

V

Villee, C. A., 1:525
Villars, F., 7:185

W

Wahrhaftig, A. L., 5:241
Waldmann, L., 6:179
Walker, J. K., 5:197
Watson, K. M., 4:219
Wattenberg, A., 3:119
Way, K., 6:129
Weneser, J., 5:1; 10:193
Wetherill, G. W., 8:257
Wick, G. C., 8:1
Wilkinson, D. H., 9:1
Willard, J. E., 3:193
Wolf, A. P., 10:259
Wolfenstein, L., 6:43
Wood, T. H., 8:343
Woodruff, L. A., 5:297

Y

Yankwich, P. E., 3:235
Young, G., 6:317

Z

Zucker, A., 10:27